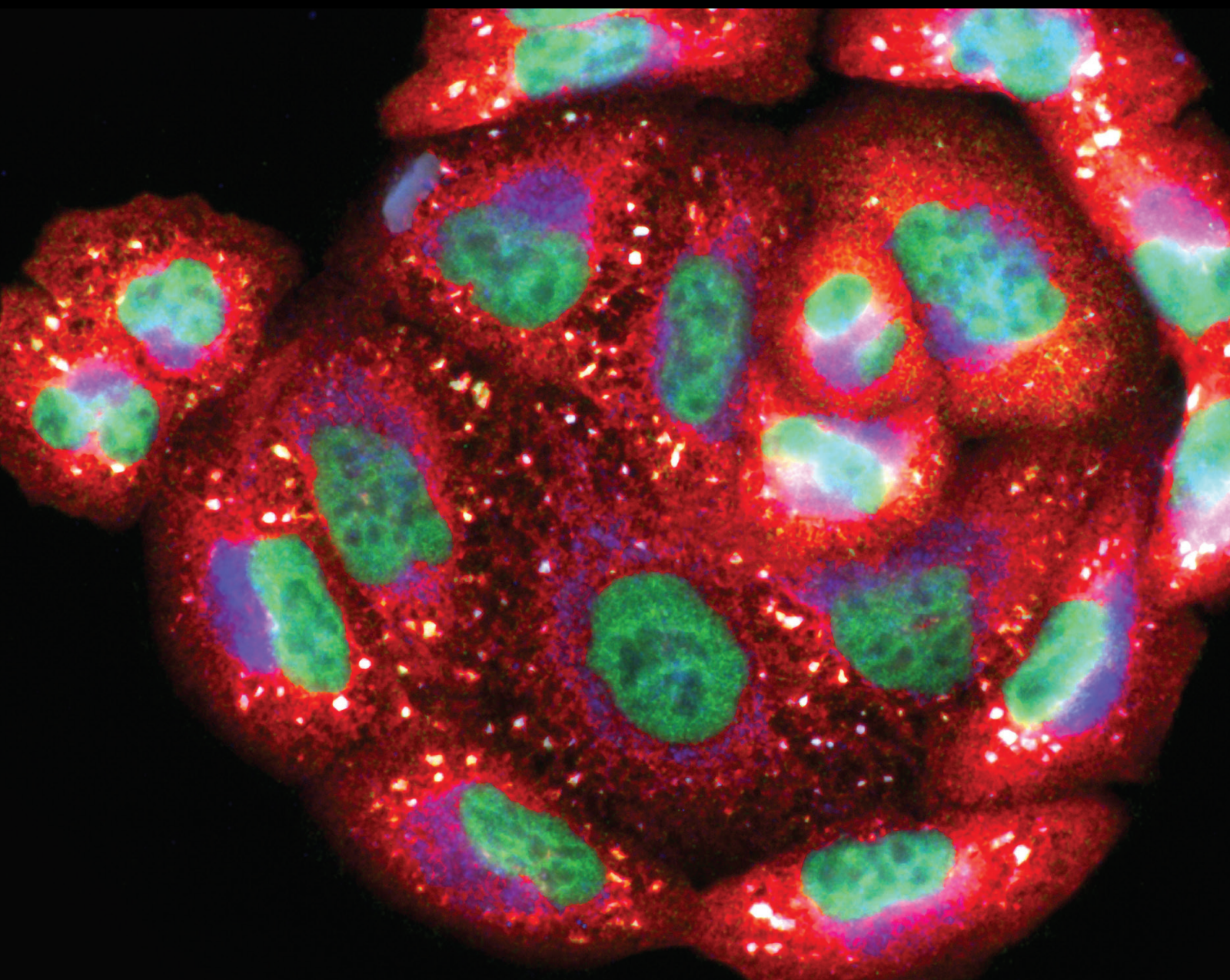


Molecular Mechanisms of Dietary Bioactive Compounds in Redox Balance and Metabolic Disorders

Lead Guest Editor: Si Qin

Guest Editors: De-Xing Hou, Hua Xu, and Wuquan Deng





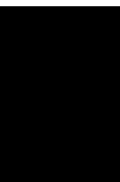
**Molecular Mechanisms of Dietary Bioactive
Compounds in Redox Balance and Metabolic
Disorders**

Oxidative Medicine and Cellular Longevity

**Molecular Mechanisms of Dietary
Bioactive Compounds in Redox Balance
and Metabolic Disorders**

Lead Guest Editor: Si Qin

Guest Editors: De-Xing Hou, Hua Xu, and Wuquan
Deng



Copyright © 2022 Hindawi Limited. All rights reserved.

This is a special issue published in "Oxidative Medicine and Cellular Longevity" All articles are open access articles distributed under the Creative Commons Attribution License, which permits unrestricted use, distribution, and reproduction in any medium, provided the original work is properly cited.

Chief Editor

Jeannette Vasquez-Vivar, USA

Associate Editors

Amjad Islam Aqib, Pakistan
Angel Catalá , Argentina
Cinzia Domenicotti , Italy
Janusz Gebicki , Australia
Aldrin V. Gomes , USA
Vladimir Jakovljevic , Serbia
Thomas Kietzmann , Finland
Juan C. Mayo , Spain
Ryuichi Morishita , Japan
Claudia Penna , Italy
Sachchida Nand Rai , India
Paola Rizzo , Italy
Mithun Sinha , USA
Daniele Vergara , Italy
Victor M. Victor , Spain

Academic Editors

Ammar AL-Farga , Saudi Arabia
Mohd Adnan , Saudi Arabia
Ivanov Alexander , Russia
Fabio Altieri , Italy
Daniel Dias Rufino Arcanjo , Brazil
Peter Backx, Canada
Amira Badr , Egypt
Damian Bailey, United Kingdom
Rengasamy Balakrishnan , Republic of Korea
Jiaolin Bao, China
Ji C. Bihl , USA
Hareram Birla, India
Abdelhakim Bouyahya, Morocco
Ralf Braun , Austria
Laura Bravo , Spain
Matt Brody , USA
Amadou Camara , USA
Marcio Carcho , Portugal
Peter Celec , Slovakia
Giselle Cerchiaro , Brazil
Arpita Chatterjee , USA
Shao-Yu Chen , USA
Yujie Chen, China
Deepak Chhangani , USA
Ferdinando Chiaradonna , Italy

Zhao Zhong Chong, USA
Fabio Ciccarone, Italy
Alin Ciobica , Romania
Ana Cipak Gasparovic , Croatia
Giuseppe Cirillo , Italy
Maria R. Ciriolo , Italy
Massimo Collino , Italy
Manuela Corte-Real , Portugal
Manuela Curcio, Italy
Domenico D'Arca , Italy
Francesca Danesi , Italy
Claudio De Lucia , USA
Damião De Sousa , Brazil
Enrico Desideri, Italy
Francesca Diomede , Italy
Raul Dominguez-Perles, Spain
Joël R. Drevet , France
Grégory Durand , France
Alessandra Durazzo , Italy
Javier Egea , Spain
Pablo A. Evelson , Argentina
Mohd Farhan, USA
Ioannis G. Fatouros , Greece
Gianna Ferretti , Italy
Swaran J. S. Flora , India
Maurizio Forte , Italy
Teresa I. Fortoul, Mexico
Anna Fracassi , USA
Rodrigo Franco , USA
Juan Gambini , Spain
Gerardo García-Rivas , Mexico
Husam Ghanim, USA
Jayeeta Ghose , USA
Rajeshwary Ghosh , USA
Lucia Gimeno-Mallench, Spain
Anna M. Giudetti , Italy
Daniela Giustarini , Italy
José Rodrigo Godoy, USA
Saeid Golbidi , Canada
Guohua Gong , China
Tilman Grune, Germany
Solomon Habtemariam , United Kingdom
Eva-Maria Hanschmann , Germany
Md Saquib Hasnain , India
Md Hassan , India


Tim Hofer , Norway
John D. Horowitz, Australia
Silvana Hrelia , Italy
Dragan Hrnčić, Serbia
Zebo Huang , China
Zhao Huang , China
Tariq Hussain , Pakistan
Stephan Immenschuh , Germany
Norsharina Ismail, Malaysia
Franco J. L. , Brazil
Sedat Kacar , USA
Andleeb Khan , Saudi Arabia
Kum Kum Khanna, Australia
Neelam Khaper , Canada
Ramoji Kosuru , USA
Demetrios Kouretas , Greece
Andrey V. Kozlov , Austria
Chan-Yen Kuo, Taiwan
Gaocai Li , China
Guoping Li , USA
Jin-Long Li , China
Qiangqiang Li , China
Xin-Feng Li , China
Jialiang Liang , China
Adam Lightfoot, United Kingdom
Christopher Horst Lillig , Germany
Paloma B. Liton , USA
Ana Lloret , Spain
Lorenzo Loffredo , Italy
Camilo López-Alarcón , Chile
Daniel Lopez-Malo , Spain
Massimo Lucarini , Italy
Hai-Chun Ma, China
Nageswara Madamanchi , USA
Kenneth Maiese , USA
Marco Malaguti , Italy
Steven McAnulty, USA
Antonio Desmond McCarthy , Argentina
Sonia Medina-Escudero , Spain
Pedro Mena , Italy
V́ctor M. Mendoza-Núñez , Mexico
Lidija Milkovic , Croatia
Alexandra Miller, USA
Sara Missaglia , Italy

Premysl Mladenka , Czech Republic
Sandra Moreno , Italy
Trevor A. Mori , Australia
Fabiana Morroni , Italy
Ange Mouithys-Mickalad, Belgium
Iordanis Mourouzis , Greece
Ryoji Nagai , Japan
Amit Kumar Nayak , India
Abderrahim Nemmar , United Arab Emirates
Xing Niu , China
Cristina Nocella, Italy
Susana Novella , Spain
Hassan Obied , Australia
Pál Pacher, USA
Pasquale Pagliaro , Italy
Dilipkumar Pal , India
Valentina Pallottini , Italy
Swapnil Pandey , USA
Mayur Parmar , USA
Vassilis Paschalis , Greece
Keshav Raj Paudel, Australia
Ilaria Peluso , Italy
Tiziana Persichini , Italy
Shazib Pervaiz , Singapore
Abdul Rehman Phull, Republic of Korea
Vincent Pialoux , France
Alessandro Poggi , Italy
Zsolt Radak , Hungary
Dario C. Ramirez , Argentina
Erika Ramos-Tovar , Mexico
Sid D. Ray , USA
Muneeb Rehman , Saudi Arabia
Hamid Reza Rezvani , France
Alessandra Ricelli, Italy
Francisco J. Romero , Spain
Joan Roselló-Catafau, Spain
Subhadeep Roy , India
Josep V. Rubert , The Netherlands
Sumbal Saba , Brazil
Kunihiro Sakuma, Japan
Gabriele Saretzki , United Kingdom
Luciano Saso , Italy
Nadja Schroder , Brazil

Anwen Shao , China
Iman Sherif, Egypt
Salah A Sheweita, Saudi Arabia
Xiaolei Shi, China
Manjari Singh, India
Giulia Sita , Italy
Ramachandran Srinivasan , India
Adrian Sturza , Romania
Kuo-hui Su , United Kingdom
Eisa Tahmasbpour Marzouni , Iran
Hailiang Tang, China
Carla Tatone , Italy
Shane Thomas , Australia
Carlo Gabriele Tocchetti , Italy
Angela Trovato Salinaro, Italy
Rosa Tundis , Italy
Kai Wang , China
Min-qi Wang , China
Natalie Ward , Australia
Grzegorz Wegrzyn, Poland
Philip Wenzel , Germany
Guangzhen Wu , China
Jianbo Xiao , Spain
Qiongming Xu , China
Liang-Jun Yan , USA
Guillermo Zalba , Spain
Jia Zhang , China
Junmin Zhang , China
Junli Zhao , USA
Chen-he Zhou , China
Yong Zhou , China
Mario Zoratti , Italy

Contents

Studies on the Mechanism of the Volatile Oils from Caoguo-4 Decoction in Regulating Spleen Deficiency Diarrhea by Adjusting Intestinal Microbiota

Li Mei, Fang Wang , Ming Yang, Zhiyong Liu , Liangfeng Wang, Qingyao Chen, Fengqin Li, and Xiaofei Zhang 


Research Article (13 pages), Article ID 5559151, Volume 2022 (2022)

Serum Fetuin-B Levels Are Elevated in Women with Metabolic Syndrome and Associated with Increased Oxidative Stress

Shiyao Xue , Hongdong Han , Shunli Rui, Mengliu Yang , Yizhou Huang, Bin Zhan, Shan Geng , Hua Liu, Chen Chen , Gangyi Yang, and Ling Li 

Research Article (17 pages), Article ID 6657658, Volume 2021 (2021)

Croctin Exerts Its Anti-inflammatory Property in LPS-Induced RAW264.7 Cells Potentially via Modulation on the Crosstalk between MEK1/JNK/NF- κ B/iNOS Pathway and Nrf2/HO-1 Pathway

Yi-Ling Wen, Ziyu He, De-Xing Hou, and Si Qin 

Research Article (18 pages), Article ID 6631929, Volume 2021 (2021)

The Neuroprotective Effects of Moderate and Regular Caffeine Consumption in Alzheimer's Disease

Xiangyu Zhou  and Lin Zhang 

Review Article (18 pages), Article ID 5568011, Volume 2021 (2021)

L-Theanine Ameliorates D-Galactose-Induced Brain Damage in Rats via Inhibiting AGE Formation and Regulating Sirtuin1 and BDNF Signaling Pathways

Li Zeng , Ling Lin, Ling Chen, Wenjun Xiao , and Zhihua Gong 

Research Article (13 pages), Article ID 8850112, Volume 2021 (2021)

Roles of Dietary Bioactive Peptides in Redox Balance and Metabolic Disorders

Qinqin Qiao , Liang Chen, Xiang Li , Xiangyang Lu, and Qingbiao Xu 

Review Article (27 pages), Article ID 5582245, Volume 2021 (2021)

Dietary Bioactive Peptide Alanyl-Glutamine Attenuates Dextran Sodium Sulfate-Induced Colitis by Modulating Gut Microbiota

Qingbiao Xu , Mingyang Hu, Min Li, Jinxiu Hou , Xianghua Zhang, Ya Gao, Bahram Chachar, and Xiang Li 


Research Article (17 pages), Article ID 5543003, Volume 2021 (2021)

Emodin-Induced Oxidative Inhibition of Mitochondrial Function Assists BiP/IRE1 α /CHOP Signaling-Mediated ER-Related Apoptosis

Li-zhen Qiu , Lan-xin Yue, Yu-hao Ni, Wei Zhou , Cong-shu Huang, Hui-fang Deng, Ning-ning Wang, Hong Liu, Xian Liu, Yong-qiang Zhou, Cheng-rong Xiao, Yu-guang Wang, and Yue Gao 







Research Article (13 pages), Article ID 8865813, Volume 2021 (2021)

Vinegar/Tetramethylpyrazine Induces Nutritional Preconditioning Protecting the Myocardium Mediated by VDAC1

Huan He, Liang Wang, Yang Qiao, Qing Zhou, Bin Yang, Lu Yin, Dong Yin , and Ming He 



Research Article (17 pages), Article ID 6670088, Volume 2021 (2021)

Bacteriocins: Potential for Human Health

Fuqing Huang , Kunling Teng , Yayong Liu , Yanhong Cao, Tianwei Wang , Cui Ma , Jie Zhang , and Jin Zhong 





Review Article (17 pages), Article ID 5518825, Volume 2021 (2021)

Dietary Fiber: An Opportunity for a Global Control of Hyperlipidemia

Ying Nie  and Feijun Luo 




Review Article (20 pages), Article ID 5542342, Volume 2021 (2021)

Dietary Beta-Hydroxy Beta-Methyl Butyrate Supplementation Alleviates Liver Injury in Lipopolysaccharide-Challenged Piglets

Yehui Duan , Bo Song , Changbing Zheng , Yinzhao Zhong, Qiuping Guo, Jie Zheng, Yulong Yin, Jianjun Li , and Fengna Li 



Research Article (9 pages), Article ID 5546843, Volume 2021 (2021)

Gut Immunity and Microbiota Dysbiosis Are Associated with Altered Bile Acid Metabolism in LPS-Challenged Piglets

Xiao Xiao , Yuanzhi Cheng, Jie Fu, Zeqing Lu, Fengqin Wang, Mingliang Jin, Xin Zong , and Yizhen Wang 







Research Article (15 pages), Article ID 6634821, Volume 2021 (2021)

The Role of lncRNA AF117829.1 in the Immunological Pathogenesis of Severe Aplastic Anaemia

Yang Li , Ling Deng , Xiaofeng Pan, Chunyan Liu, and Rong Fu 



Research Article (19 pages), Article ID 5587921, Volume 2021 (2021)

***Eurotium cristatum* Fermented Loose Dark Tea Ameliorates Cigarette Smoke-Induced Lung Injury by MAPK Pathway and Enhances Hepatic Metabolic Detoxification by PXR/AhR Pathway in Mice**

Xiang-Xiang Huang , Shuai Xu , Li-Jun Yu , Yu-Fei Zhou , Ying Zhou , and Zhong-Hua Liu 






Research Article (17 pages), Article ID 6635080, Volume 2021 (2021)

Ca²⁺-Dependent Glucose Transport in Skeletal Muscle by Diphlorethohydroxycarmalol, an Alga Phlorotannin: *In Vitro* and *In Vivo* Study

Hye-Won Yang, Yun-Fei Jiang, Hyo-Geun Lee, You-Jin Jeon , and BoMi Ryu 








Research Article (15 pages), Article ID 8893679, Volume 2021 (2021)

Chlorogenic Acid Alleviates Colon Mucosal Damage Induced by a High-Fat Diet via Gut Microflora Adjustment to Increase Short-Chain Fatty Acid Accumulation in Rats

M. Gui Xie , Y. Quan Fei , Y. Wang , W. Yan Wang , and Z. Wang 

Research Article (18 pages), Article ID 3456542, Volume 2021 (2021)

The Role of Oxidative Stress and Antioxidants in Diabetic Wound Healing

Liling Deng , Chenzhen Du , Peiyang Song , Tianyi Chen , Shunli Rui , David G. Armstrong , and Wuquan Deng 




Review Article (11 pages), Article ID 8852759, Volume 2021 (2021)

Contents



Bixin Attenuates High-Fat Diet-Caused Liver Steatosis and Inflammatory Injury through Nrf2/PPAR α Signals

Shasha Tao , Youjing Yang , Jianzhong Li , Hongyan Wang , and Yu Ma 
Research Article (17 pages), Article ID 6610124, Volume 2021 (2021)

The Landscape of Interactions between Hypoxia-Inducible Factors and Reactive Oxygen Species in the Gastrointestinal Tract

Yirui Shao , Kexing Wang, Xia Xiong , Hongnan Liu, Jian Zhou, Lijun Zou, Ming Qi, Gang Liu , Ruilin Huang, Zhiliang Tan, and Yulong Yin
Review Article (9 pages), Article ID 8893663, Volume 2021 (2021)





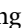


Ophiopogonin D Increases SERCA2a Interaction with Phospholamban by Promoting CYP2J3 Upregulation

Jia Wang, Wenting You, Ningning Wang, Wei Zhou, Yunxuan Ge, Zengchun Ma, Hongling Tan, Yuguang Wang , and Yue Gao 
Research Article (22 pages), Article ID 8857906, Volume 2020 (2020)





Alanylglutamine Relieved Asthma Symptoms by Regulating Gut Microbiota and the Derived Metabolites in Mice

Shao-Kun Liu , Li-Bing Ma, Yu Yuan, Xiao-Ying Ji, Wen-Jin Sun, Jia-Xi Duan, Qing-Ping Zeng, Binaya Wasti, Bing Xiao, Jian-Fei Zheng, Ping Chen, and Xu-Dong Xiang 
Research Article (18 pages), Article ID 7101407, Volume 2020 (2020)



Inhibitory Effect of *Lactobacillus plantarum* CCFM8724 towards *Streptococcus mutans*- and *Candida albicans*-Induced Caries in Rats

Qiuxiang Zhang , Sujia Qin , Xianyin Xu , Jianxin Zhao , Hao Zhang , Zhenmin Liu , and Wei Chen 
Research Article (10 pages), Article ID 4345804, Volume 2020 (2020)



The Associated Regulatory Mechanisms of Zinc Lactate in Redox Balance and Mitochondrial Function of Intestinal Porcine Epithelial Cells

Wenjie Tang, Jing Long, Tiejun Li, Lingyuan Yang, Jianzhong Li , Liuqin He , Shuwei Li, Shengyao Kuang , Yanzhong Feng, Heshu Chen, Fenglan Li, Zhiliang Du, and Yulong Yin 
Research Article (15 pages), Article ID 8815383, Volume 2020 (2020)

Bisphenol A and Its Analogues in Chinese Total Diets: Contaminated Levels and Risk Assessment

Kai Yao, Jing Zhang, Jie Yin, Yunfeng Zhao, Jianzhong Shen, Haiyang Jiang , and Bing Shao 
Research Article (14 pages), Article ID 8822321, Volume 2020 (2020)

Differences in the Hemolytic Behavior of Two Isomers in *Ophiopogon japonicus* *In Vitro* and *In Vivo* and Their Risk Warnings





Huan-Hua Xu , Zhen-Hong Jiang, Yu-Ting Sun, Li-Zhen Qiu, Long-Long Xu, Xiang-Lin Tang, Zeng-Chun Ma, and Yue Gao 
Research Article (16 pages), Article ID 8870656, Volume 2020 (2020)

Effects of Fasting-Mimicking Diet and Specific Meal Replacement Foods on Blood Glucose Control in Patients with Type 2 Diabetes: A Randomized Controlled Trial

Fang Tang  and Xuan Lin 


Research Article (8 pages), Article ID 6615295, Volume 2020 (2020)

Mitochondria-Targeted Antioxidants: A Step towards Disease Treatment

Qian Jiang , Jie Yin , Jiashun Chen, Xiaokang Ma, Miaomiao Wu, Gang Liu , Kang Yao, Bie Tan , and Yulong Yin


Review Article (18 pages), Article ID 8837893, Volume 2020 (2020)

Protective Effect of Quercetin against H₂O₂-Induced Oxidative Damage in PC-12 Cells: Comprehensive Analysis of a lncRNA-Associated ceRNA Network

Zheyu Zhang, Pengji Yi, Min Yi, Xiaoliang Tong, Xin Cheng, Jingjing Yang, Yang Hu, and Weijun Peng 


Research Article (22 pages), Article ID 6038919, Volume 2020 (2020)

Diazepam and Its Disinfection Byproduct Promote the Early Development of Nervous System in Zebrafish Embryos

Xiaole Zhao, Xiaoyong Huang, Jiachen Shi, Kui Zhu, and Bing Shao 

Research Article (10 pages), Article ID 8878143, Volume 2020 (2020)

Inhibitory Effect of Delphinidin on Oxidative Stress Induced by H₂O₂ in HepG2 Cells

Jingjing Xu, Yanwei Zhang, Guofeng Ren , Rengui Yang, Jingfang Chen, Xiaojing Xiang, Hong Qin , and Jihua Chen 

Research Article (12 pages), Article ID 4694760, Volume 2020 (2020)

Research Article

Studies on the Mechanism of the Volatile Oils from Caoguo-4 Decoction in Regulating Spleen Deficiency Diarrhea by Adjusting Intestinal Microbiota

Li Mei,^{1,2} Fang Wang ,¹ Ming Yang,¹ Zhiyong Liu ,¹ Liangfeng Wang,^{1,3} Qingyao Chen,¹ Fengqin Li,¹ and Xiaofei Zhang ^{1,4}

¹Jiangxi University of Chinese Medicine, 1688 Meiling Avenue, Wanli District, Nanchang 330004, China

²Inner Mongolia Minzu University, No. 536 West Huolinhe Street, Horqin District,

Tongliao Inner Mongolia Autonomous Region 028000, China

³College of Pharmacy, Shanghai University of Chinese Medicine, Shanghai 201203, China

⁴Shaanxi University of Chinese Medicine, Xixian Avenue, Xixian District, Xianyang 712046, China

Correspondence should be addressed to Fang Wang; wangfang09421@126.com and Xiaofei Zhang; 84964547@qq.com

Received 7 October 2021; Accepted 13 December 2021; Published 27 January 2022

Academic Editor: Wuquan Deng

Copyright © 2022 Li Mei et al. This is an open access article distributed under the Creative Commons Attribution License, which permits unrestricted use, distribution, and reproduction in any medium, provided the original work is properly cited.

Background. The Caoguo-4 decoction, a classical Mongolian medicine formula, is widely used to treat spleen deficiency diarrhea (SDD) in Mongolian for decades. Previously, the Caoguo-4 decoction volatile oil has been confirmed to be effective in ameliorating symptoms of spleen deficiency diarrhea in an animal model. However, the underlying mechanism of the Caoguo-4 decoction volatile oil is yet to be established. The aim of the current study was to investigate the antidiarrheal effects and mechanism of the Caoguo-4 decoction volatile oil. **Method.** Wistar rats were randomly divided into 5 groups of 10 animals including control, model, positive, Caoguo-4 decoction, and Caoguo-4 decoction volatile oil groups (10 rats in each group). All the rats, besides those in the control group, were induced to develop SDD by a bitter-cold purgation method with Xiaochengqi decoction. The antidiarrheal effect of Caoguo-4 decoction volatile oil was evaluated by pathological section, serum D-xylose and AMS content, plasma MTL content, and gut microbiota analysis via 16S rRNA sequencing. **Results.** The results showed that the developed SDD rat model (model group) had decreased food intake, increased weight loss, soft stool, and bad hair color. When compared with the control group, serum was significantly reduced serum D-xylose and AML but increased MTL levels in the model group ($p < 0.05$). However, after treatment with either the Caoguo-4 decoction (the decoction group) or Smecta (the positive group) or volatile oil from the Caoguo-4 decoction (the volatile oil group), a significant increase in the serum D-xylose levels was observed. Additionally, AML levels significantly increased in the positive and volatile oil groups, and MTL levels significantly decreased in the decoction and volatile oil groups, when compared with the model group ($p < 0.05$). The pathological changes of the intestinal mucosa showed that the structure of the epithelium in the villi of the small intestine was affected, deformed, and incomplete in the model group when compared with the control group. However, either the decoction group or the volatile oil group recovered the villous morphology. The results of OTU analysis and alpha diversity analysis of intestinal bacteria showed that the intestinal microbiota of the SDD model rats showed an obvious decrease in richness and diversity of intestinal microbiota. But the intervention treatment of decoction and volatile oil could significantly recover the richness and diversity of intestinal microbiota. **Conclusion.** The intestinal microbiota destroyed in SDD modelling could be significantly improved by the Caoguo-4 decoction volatile oils, which provides reference for clinical medication.

1. Introduction

Spleen deficiency diarrhea (SDD) is a common disease of traditional Chinese medicine (TCM). The main cause of

SDD according to TCM is considered to be spleen deficiency, endophytic dampness, Qi consumption, and stomach disharmony, resulting in conductive dysfunction of the intestines [1, 2]. The deficient spleen fails to transport and the weak

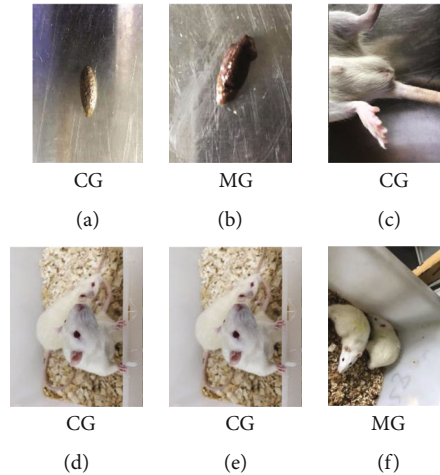


FIGURE 1: Microcosmic indexes of rats in the control group and the model group. Note: CG: control group; MG: model group: (a) stool from the control group; (b) stool from the model group; (c) anal area of the control group; (d) anal area of the model group; (e) posture of the control group; (f) posture of the model group.

stomach fails to digest and process foods; thus, the water and foods are then retained to affect the ascent of spleen yang; consequently, it collapses to cause diarrhea [3]. At present, the specific pathogenesis of SDD remains unknown: immune dysfunction, intestinal barrier dysfunction, mental factors, etc. [4]. With the deepening of research, gut microbiota has become one of the most critical factors in SDD progression, accompanied by diarrhea induced by dysfunctional or infection intestinal environment [5, 6]. Related research also confirmed that the quantity of beneficial physiological bacteria such as *Lactobacillus* and *Bifidobacterium* in the intestine of mice is negatively correlated with the severity of the symptoms of SDD in mice; that is, the more severe the symptom of SDD in mice, the smaller the quantity of *Lactobacillus* and *Bifidobacterium* in the intestine of mice, leading to disorder of gut microbiota [7]. Therefore, a better understanding of the gastrointestinal microflora in SDD has been of great significance. Acupoint application therapy is the application of Chinese herbal medicine to the corresponding points to regulate meridians, yin and yang, and qi as well as the blood of the human body [8]. The Shenque point has a thin cuticle making it conducive to rapid drug absorption, and its location close to the intestinal tract strengthens the spleen and stomach by promoting the flow of Qi and relaxing the bowels [9]. Increasing evidence suggests that TCM achieved a good therapeutic effect for SDD for its less toxicity and equal or even better antidiarrheal efficacy [10]. Caoguo-4 decoction is a kind of traditional Mongolian medicine formula, originated from the medical classic of “Yi Fang Feng Ji.” It has long been used clinically for the maintenance of “Heyi” and upward “Heyi” disease and specifically has been identified to have a significant effect on spleen deficiency diarrhea. “Mongolian Medicine Prescription” [11]: “Used for the treatment of stomach “Heyi” syndrome, head tingling, spleen disease, etc.” “Chinese Medical Encyclopedia (Mongolian version)” recorded [12]: “Indications for head stabbing pain, abdominal distension and bowel rumbling caused by Ascending “Heyi” and “Siming Heyi.” “It is composed of *Amomum tsao-ko* Crevost et Lemarie, *Eugenia caryophyllata*

TABLE 1: The contents of D-xylose, AML, and MTL in blood of rats with spleen deficiency diarrhea.

Group	D-Xylose	AMS	MTL
CG	1.66 ± 0.30	4294 ± 848	167.58 ± 25.73
MG	0.81 ± 0.37*	2469 ± 929*	196.34 ± 23.47*
TG	2.52 ± 1.20 [#]	2880 ± 371	160.47 ± 28.68 [#]
HG	2.15 ± 0.41 ^{##}	3862 ± 559 [#]	145.20 ± 17.99 ^{##}
YXG	2.07 ± 0.54 ^{##}	3712 ± 740 [#]	202.03 ± 62.39

Note: CG: control group; MG: model group; TG: soup group; HG: oil group; YXG: positive group. Compared with the control group, * $p < 0.05$, ** $p < 0.01$; compared with the model group, [#] $p < 0.05$, ^{##} $p < 0.01$.

Thunb., *Aucklandia lappa* Decne., and *Foeniculum vulgare* Mill., which all belong to the “warm-natured” category of the Mongolian medicine, with a role specifically in dispelling the spleen and stomach chill. However, Caoguo-4 decoction has a curative clinical effect on SDD, but with limited development due to being short of defined pharmacodynamics and mechanisms.

Volatile oils refer to the active components from TCM. Valuable properties of volatile oils have been confirmed experimentally or empirically. Examples include [13] *Eugenia caryophyllata* Thunb. (strengthening the spleen and resisting bacteria), *Aucklandia lappa* Decne. (moving Qi and relieving pain), *Amomum tsao-ko* Crevost et Lemarie (invigorating the stomach and dispelling dampness), *Foeniculum vulgare* Mill. (regulating Qi flowing for strengthening the spleen), etc. In the previous study from this group, the Caoguo-4 decoction volatile oil has been confirmed to be effective in ameliorating symptoms of the SDD rat model, which is comparable to the effect of the Caoguo-4 decoction. However, the underlying mechanisms by which the Caoguo-4 decoction volatile oil exhibits antidiarrheal activity remains poorly understood. Hence, the aim of this study was to investigate the antidiarrheal effect and mechanism of the Caoguo-4 decoction volatile oil through regulation of intestinal microbiota.

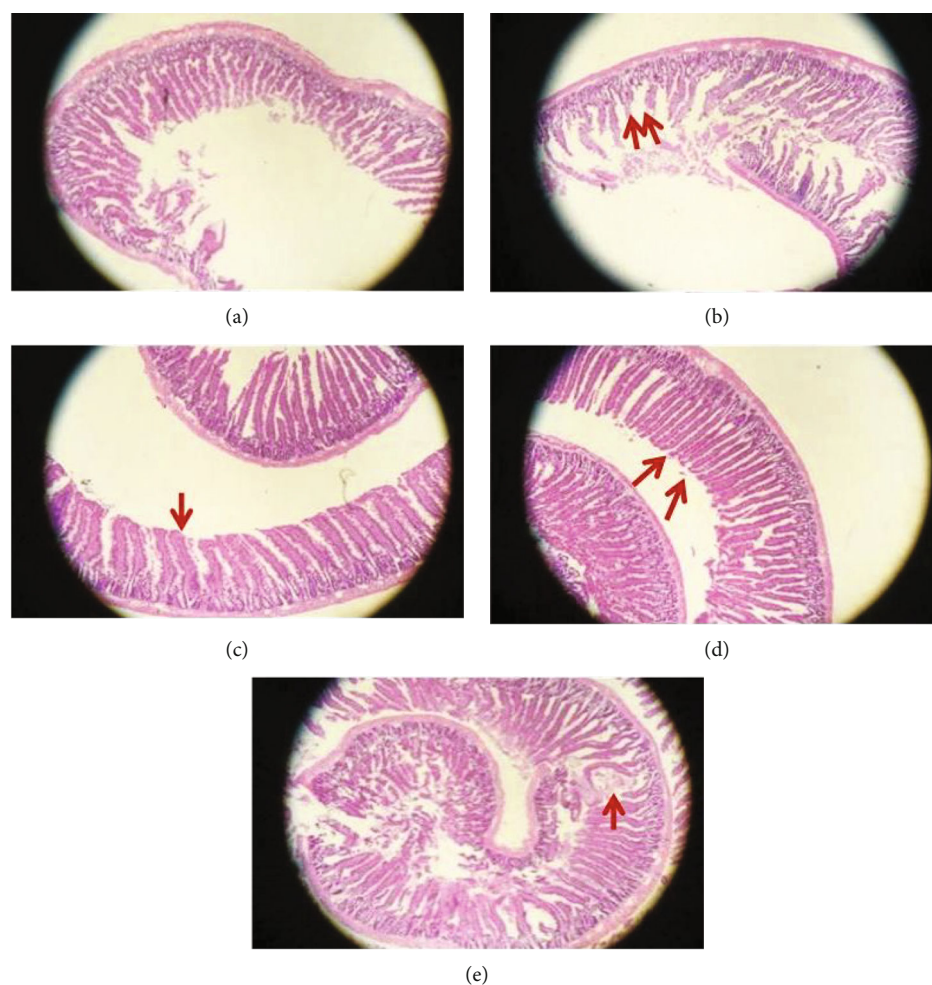


FIGURE 2: Effect of each group on small intestinal mucosa histopathology in rats with spleen deficiency diarrhea (hematoxylin-eosin; 40x magnification): (a) CG group, (b) MG group, (c) TG group, (d) HG group, and (e) YXG group.

2. Materials and Methods

2.1. Materials and Chemicals. Amomum tsao-ko (batch number: 1709009), cloves (batch number: 1710004), fennel (batch number: 1711009), Costustoot (batch number: 1703003), Rheum officinale (batch number: 1806007), fructus aurantii immaturus (batch number: 1806008), and *Magnolia officinalis* (batch number: 1805003) were purchased from Jiangxi Zhangshu Tianqitang Chinese Herbal Slices Co., Ltd. (Jiangxi, China). The commercial enzyme-linked immunosorbent assay (ELISA) kits for D-xylose, serum motilin (MTL), and amylase were purchased from Jiancheng Enzymatic Immunity Co., Ltd. (Nanjing, China). Jojoba oil was purchased from Dimei Biotechnology Co., Ltd. (Guangzhou, China).

2.2. Plant Materials and Volatile Oil Extraction. Caoguo-4 decoction, a kind of traditional Mongolian medicine formula, contains the following ingredient: *Amomum tsao-ko* Crevost et Lemarie (also known as CaoGuo in China), *Eugenia caryophyllata* Thunb. (also known as DingXiang in China), *Aucklandia lappa* Decne. (also known as MuXiang in China), and *Foeniculum vulgare* Mill. (also known as

HuiXiang in China). All the herbs were purchased from Chengdu Huichu Technology Co., Ltd. (Chengdu, China), which were authenticated by Professor Fei Ge (Jiangxi University of Traditional Chinese Medicine, Nanchang, China). According to the ratio of CG : MX : DX : HX = 5 : 5 : 3 : 3, the dried Chinese herbs were crushed into coarse powder.

Caoguo-4 decoction was prepared as follows: 100 g crude Caoguo-4 decoction was made into powder and put in 10 times of water for 15 minutes, boiled for 30 minutes, filtered, and collected. Repeat such procedures. Puted the two liquid together, concentrated them to 0.256 g/ml.

Caoguo-4 decoction volatile oil was extracted by the steam distillation method. The steam distillations were carried out according to the Chinese Pharmacopoeia (2020). Briefly, 360 g of Caoguo-4 decoction medicinal powder was completely immersed in Milli-Q water in proportion of 1:10 (W/V) for 30 min. The mixture was submitted to hydrodistillation in a Clevenger-type apparatus at temperature of 100°C for 240 minutes. Volatile oil was dried over Na₂SO₄. The yield of volatile oil was 5% (V/W), and the oil was stored at -20°C until analysis. For animal experiment, the volatile oil was diluted with jojoba oil with the dilution ratio of 1:10 (V/V).

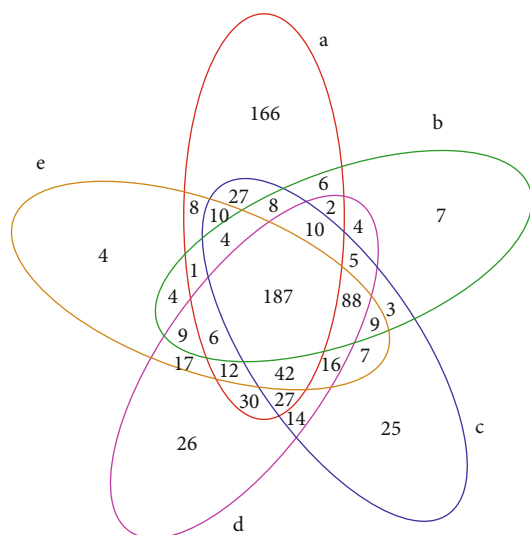


FIGURE 3: OTU Venn figure: a—CG group, b—MG group, c—TG group, d—HG group, and e—YXG group.

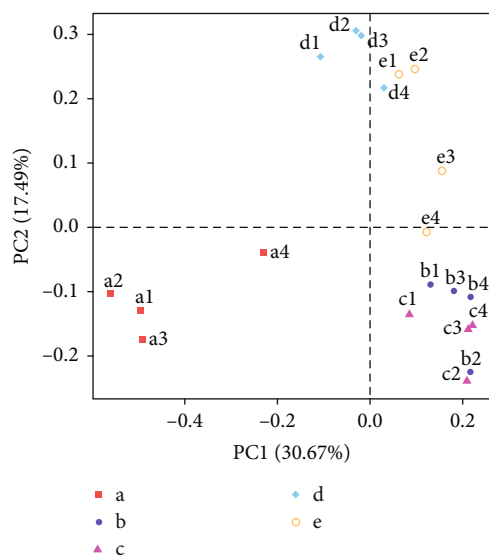


FIGURE 4: PCA based on OTU level: a—CG group, b—MG group, c—TG group, d—HG group, and e—YXG group.

2.3. Animal Experimental Design

2.3.1. Animal. SPF Wistar rats weighing ~200–220 g were purchased from Lai-Ke-Jing-Da Experimental Animal Co. Ltd. (Hunan, China) and consisted of both genders at a proportion of 1 : 1. The animals were housed individually in the Experimental Animal Center of Jiangxi University of Chinese Medicine (Jiangxi, China). Standard tap water and rat food were available. After acclimation for 7 days, all rats were randomly divided into 5 groups of 10 animals each as follows: the normal control group (CG), the spleen deficiency diarrhea model group of treatment groups (MG), the positive group of treatment groups (YXG), the Caoguo-4 decoction group of treatment groups (TG), and the Caoguo-4 decoction volatile oil group of treatment groups (HG). The spleen deficiency diarrhea model was induced

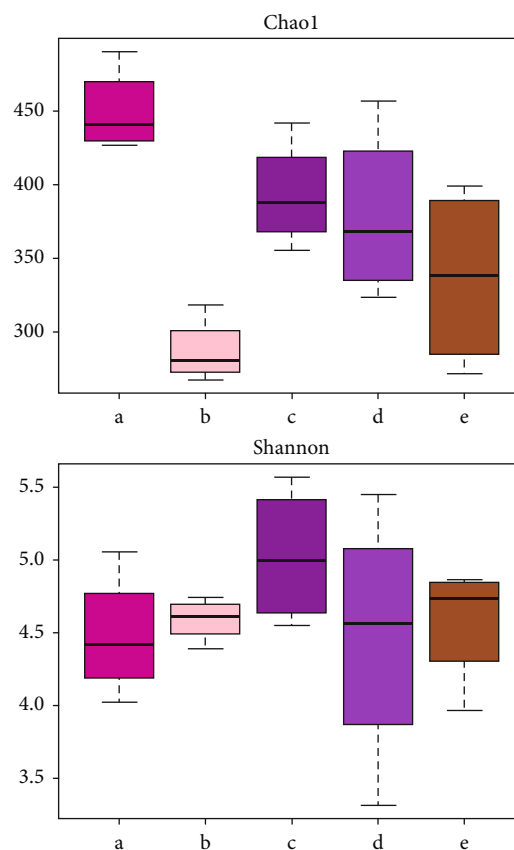


FIGURE 5: Alpha diversity index box figure: a—CG group, b—MG group, c—TG group, d—HG group, and e—YXG group.

in the MG group, the YXG group, the TG group, and the HG group.

During all experiments, water and food were available ad libitum. All animal procedures were conducted in accordance with the institutional guidelines approved by the Ethics Committee of the Jiangxi University of Chinese Medicine (no. JZLLSC2018-0086).

2.3.2. Spleen Deficiency Diarrhea Model and Group Treatments. The spleen deficiency diarrhea (SDD) model was established using a bitter-cold purgation method with Xiaochengqi decoction [14, 15]. Briefly, the rats were intragastrically administered with 3 ml/100 g Xiaochengqi decoction for 21 days once every other day. Meanwhile, the rats were not fed with any chow but drinking water freely on gavage day and were fed ad libitum on the next day. The CG group was intragastrically administered with the same volume of double-distilled water with food and water ad libitum. The YXG group was intragastrically administered with Smecta, prepared in 40 mg/ml suspension with distilled water (equivalent to 10 times the clinical dosage). The TG group was given the Caoguo-4 decoction with a mass concentration of 0.256 g/ml (the amount of 10 ml/kg/day was applied). The HG group was given the Caoguo-4 decoction volatile oil through the umbilical cord and stimulating the Shenque acupoint with 1.92 ml (the yield of volatile oil was 5% (V/W), 10 times of the oral dose). The modelling was

TABLE 2: Comparison of OTUs and diversity of samples between groups.

Groups	A	Observed species	PD-whole tree	B	Recovery rate
CG	449.86 ± 28.72	351.50 ± 10.64	34.48 ± 0.31	4.47 ± 0.43	>0.99
MG	286.88 ± 22.05**	233.80 ± 13.62**	24.40 ± 1.89**	4.59 ± 0.15	>0.99
TG	393.16 ± 36.37##	311.08 ± 34.21##	30.42 ± 3.02#	5.03 ± 0.47	>0.99
HG	379.11 ± 58.53#	312.05 ± 55.76#	30.79 ± 4.18#	4.47 ± 0.89	>0.99
YXG	337.04 ± 61.82	274.28 ± 39.38	28.17 ± 3.04	4.57 ± 0.42	>0.99

Note: CG: control group; MG: model group; TG: soup group; HG: oil group; YXG: positive group. Compared with the control group, * $p < 0.05$, ** $p < 0.01$; compared with the model group, # $p < 0.05$, ## $p < 0.01$.

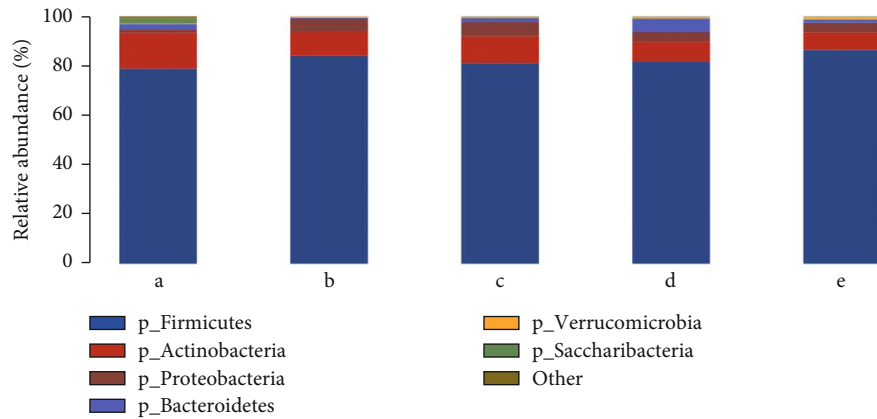


FIGURE 6: Profiling histograms of species at different groups of phylum classification levels. The horizontal coordinate is the sample name, and the longitudinal coordinates are the relative abundance of the species in the sample: a—CG group, b—MG group, c—TG group, d—HG group, and e—YXG group.

TABLE 3: Species at different groups of phylum classification levels (%).

Phylum	CG group	MG group	TG group	HG group	YXY group
<i>Cyanobacteria</i>	0.12%	0.00%**	0.03%	0.01%	0.01%
<i>Saccharibacteria</i>	2.30%	0.00%*	0.10%#	0.07%#	0.14%
<i>Proteobacteria</i>	1.36%	5.24%**	5.89%	3.97%#	3.96%
<i>Tenericutes</i>	0.42%	0.05%**	0.10%	0.15%	0.09%
<i>Bacteroidetes</i>	2.17%	0.64%	1.57%	5.47%	1.24%
<i>Firmicutes</i>	78.76%	84.05%	80.95%	81.78%	86.42%
<i>Euryarchaeota</i>	0.04%	0.00%*	0.01%	0.01%	0.01%
<i>Verrucomicrobia</i>	0.21%	0.37%	0.36%	0.64%	1.09%
<i>Actinobacteria</i>	14.54%	9.61%	10.96%	7.90%	7.03%
Other	0.07%	0.03%	0.02%	0.02%	0.01%

Note: compared with the control group, * $p < 0.05$, ** $p < 0.01$; compared with the model group, # $p < 0.05$, ## $p < 0.01$.

considered successful if the following criteria were met: (a) slow weight gain or weight loss, (b) less eating amount and more drinking volume, (c) loose stools, (d) lassitude or irritating, (e) yellow and dry hair, (f) curling up for fear of cold, and (g) D-xylose and amylase (AMS) levels measured once per week for 3 weeks.

Xiaochengqi decoction, a kind of traditional Chinese formula, contains the following ingredient: *Radix et Rhizoma*

Rhei, *Fructus Citri aurantii immaturus*, and *Cortex Magnoliae officinalis* with the amount ratio of 2:3:3 for SDD modelling. All the herbs were purchased from Jiangzhong Chinese Medicine Yinpian Co. Ltd. (Jiangxi, China) as crude herbs. Xiaochengqi decoction was prepared as follows: the herbs were soaked in 10 times the amount of water for 30 minutes and heated for 1 hour each time, and the filtrate was combined twice and then condensed to 1 g/ml.

2.4. Sample Collection. At the 21th day, after fasting for 24 hours, the rats were sacrificed by intraperitoneal injection of 1% pentobarbital sodium (50 mg pentobarbital/kg rat body weight). Blood was harvested from the abdominal aorta into tubes with ethylene diamine tetra acetic acid. Plasma was isolated by centrifugation at 4000 rpm for 15 min at 4.0°C. The supernatant was collected and stored at -80°C for later analysis. The small intestine was put into 4% buffered formalin solution and embedded in paraffin. These sections were stained with hematoxylin and eosin (HE) and periodic acid-Schiff (PAS), respectively, in accordance with the standard procedures for histopathological analysis. The intestinal feces were taken under sterile conditions and then put into sterile tubes in liquid nitrogen for further analysis. The amounts of spleen deficiency-associated cytokines including D-xylose, AMS, and MTL were determined using ELISA kits according to the manufacturers' instructions.

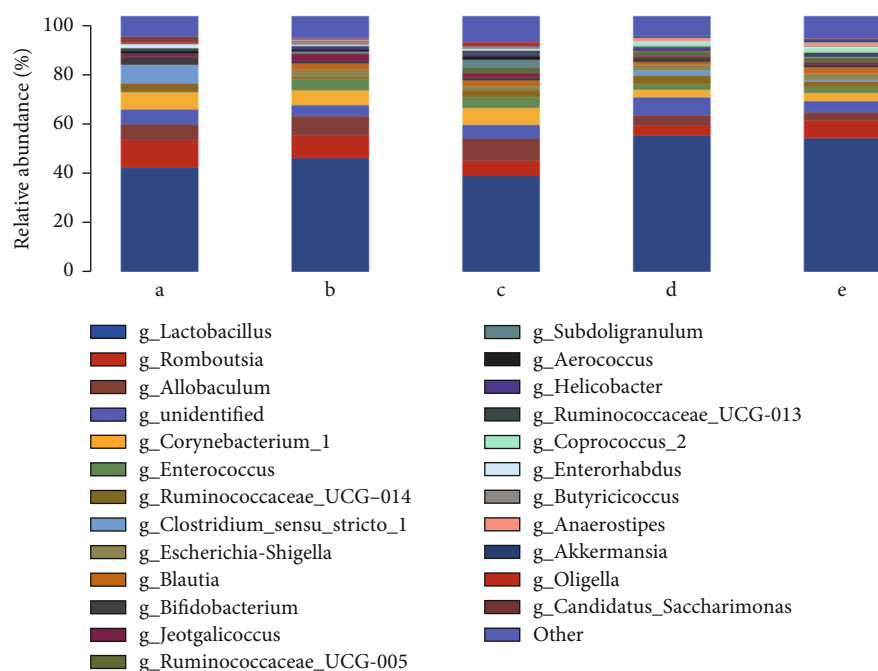


FIGURE 7: Profiling histograms of species at different groups of genus classification levels: a—CG group, b—MG group, c—TG group, d—HG group, and e—YXG group.

2.5. ELISA. The rats were sacrificed by intraperitoneal injection of 1% pentobarbital sodium (50 mg pentobarbital/kg rat body weight). Serum was stored at -80°C for analysis of D-xylose and AMS content using the enzyme-linked immunosorbent assay (D-xylose ELISA kit provided by Nanjing Jiancheng Bioengineering Institute Co., Ltd., no.20180621; AMS ELISA kit provided by Nanjing Jiancheng Bioengineering Institute Co., Ltd., no. 20180612). Plasma was stored at -80°C for analysis of MTL content using the enzyme-linked immunosorbent assay (MTL ELISA kit provided by Nanjing Jiancheng Bioengineering Institute Co., Ltd., no. 20180901).

2.6. Histopathological Observation. The jejunum tissues were isolated, rinsed with ice PBS, fixed in 4% paraformaldehyde solution for 24 hours, removed, cut well into the dewatering box, and dehydrated in 75% alcohol for 4 h, 85% alcohol, and 90% alcohol for 2 hours each; anhydrous ethanol I and anhydrous ethanol II for 30 min; alcohol benzene, xylene I, and xylene II for 5-10 min; and wax I, wax II, and wax III for 1 h. The tissue was soaked in wax and embedded. The paraffin tissues were cut into $4\ \mu\text{m}$ thick sections with a cryotome and were stained with hematoxylin and eosin (H&E), periodic acid-Schiff (PAS), or Masson's trichrome (M-T). The morphological changes in the stained tissues were observed under a light microscope.

2.7. Gut Microbiota Analysis. The feces samples collected from all groups on the third week were used for the microbial community analysis. Total genomic DNAs from the feces of mice were extracted using the E.Z.N.A.[®] stool DNA-Kit (Omega Bio-Tek, Norcross, GA, U.S.) according to the manufacturer's instruction. The quality of extracted DNA

was checked by 1% agarose gel electrophoresis and spectrophotometry (optical density at the 260 nm/280 nm ratio). All extracted DNA samples were stored at -20°C for further analysis.

The V3-V4 hypervariable regions of the 16s rRNA gene were subjected to high-throughput sequencing by Beijing Allwegene Tech, Ltd. (Beijing, China) using the Illumina MiSeq PE300 sequencing platform (Illumina, Inc., CA, USA). The V3-V4 regions of the bacterial 16s rRNA gene were amplified with the universal primers of the forward 338F ($5'$ -ACTCCTACGGGAGGCAGCAG-3') and the reverse 806R ($5'$ -GACTACHVGGGTWTCTAAT-3'). The PCR program was as follows: 95°C for 5 min and 25 cycles at 95°C for 30 s, 55°C for 30 s, and 72°C for 30 s with the final extension of 72°C for 10 min. PCR reactions were performed in triplicate: $25\ \mu\text{l}$ mixture containing $2.5\ \mu\text{l}$ of $10\times$ Pyrobest Buffer, $2\ \mu\text{l}$ of 2.5 mM dNTPs, $1\ \mu\text{l}$ of each primer ($10\ \mu\text{M}$), 0.4 U of Pyrobest DNA Polymerase (TaKaRa), and 15 ng of template DNA. The amplicon mixture was applied to the MiSeq Genome Sequencer (Illumina, San Diego, CA, USA).

2.8. Illumina MiSeq Sequencing. Amplicons were extracted from 2% agarose gels and purified using the AxyPrep DNA Gel Extraction Kit (Axygen Biosciences, Union City, CA, U.S.) according to the manufacturer's instructions and quantified using QuantiFluor[™]-ST (Promega, U.S.). Purified amplicons were pooled in equimolar and paired-end sequenced (2×300) on an Illumina MiSeq platform according to the standard protocols.

The extraction of high-quality sequences was firstly performed with the QIIME package (Quantitative Insights Into Microbial Ecology) (v1.2.1). Raw sequences were selected

TABLE 4: Species at different groups of genus classification levels (%).

Genus	GC	MC	TJG	HFYG	YXZ
<i>Collinsella</i>	0.01%	0.55%**	0.07%##	0.64%	0.74%
<i>Phascolarctobacterium</i>	0.00%	0.65%*	0.08%##	0.19%	0.17%
<i>Bifidobacterium</i>	3.10%	1.14%	1.20%	1.80%	1.16%
<i>Akkermansia</i>	0.21%	0.37%	0.36%	0.64%	1.09%
<i>Ruminococcaceae_UCG-014</i>	3.32%	0.95%*	2.49%	3.35%##	2.09%
<i>Anaerostipes</i>	0.00%	0.33%	0.09%	1.27%	1.21%##
<i>Acinetobacter</i>	0.00%	0.11%*	0.73%	0.03%	0.30%
<i>Ruminococcaceae_UCG-013</i>	0.87%	0.13%*	1.15%	0.55%	0.78%#
<i>Ruminococcus_torques_group</i>	0.00%	0.42%*	0.19%	0.11%	0.74%
<i>Escherichia-Shigella</i>	0.00%	2.43%**	1.71%	2.16%	2.31%
<i>Aerococcus</i>	1.36%	0.85%	1.55%	0.21%#	0.23%#
<i>Anaerotruncus</i>	0.01%	0.54%	0.19%	0.37%	0.15%
<i>Bacteroides</i>	0.00%	0.20%**	0.07%#	0.78%	0.25%
<i>Faecalibaculum</i>	0.42%	0.02%**	0.17%	0.13%	0.05%
<i>Butyricoccus</i>	0.01%	1.80%*	0.79%	0.12%#	0.53%
<i>Staphylococcus</i>	0.83%	0.44%	0.19%	0.02%#	0.10%
<i>Desulfovibrio</i>	0.49%	0.22%	0.34%	0.11%	0.06%
<i>Jeotgalicoccus</i>	1.10%	2.79%	1.72%	0.53%#	0.77%#
<i>Eubacterium_coprostanoligenes_group</i>	0.23%	0.11%	0.52%	0.67%	0.65%
<i>Romboutsia</i>	10.56%	8.65%	6.03%#	3.83%##	6.92%
<i>Blautia</i>	0.03%	2.52%*	2.23%##	1.15%	2.48%
<i>Subdoligranulum</i>	0.00%	0.62%*	2.91%#	0.27%	0.66%
<i>Lachnospiraceae_NK4A136_group</i>	0.27%	0.09%	1.00%	0.05%	0.06%
<i>Lactobacillus</i>	40.83%	44.49%	37.52%	53.23%	52.16%
<i>Candidatus_Saccharimonas</i>	2.28%	0.00%**	0.05%	0.07%#	0.12%
<i>Oligella</i>	0.52%	0.20%	1.44%#	0.10%	0.37%
<i>Allobaculum</i>	6.17%	7.75%	8.52%	4.09%	3.27%#
<i>Enterococcus</i>	0.23%	4.47%	4.30%	2.21%	2.42%
<i>Facklamia</i>	0.48%	0.43%	0.85%#	0.10%#	0.25%#
<i>Ruminococcus_2</i>	0.05%	0.11%	0.15%	0.91%#	0.79%#
<i>Adlercreutzia</i>	0.93%	0.22%	0.13%	0.12%	0.17%
<i>Enterorhabdus</i>	1.55%	0.27%*	0.54%#	0.42%	0.48%#
<i>Helicobacter</i>	0.00%	1.25%**	0.97%	1.09%	0.56%
<i>Eubacterium_hallii_group</i>	0.00%	0.34%*	0.51%	0.08%	0.31%
<i>Parasutterella</i>	0.00%	0.74%	0.15%	0.42%	0.13%
<i>Corynebacterium_1</i>	6.67%	5.78%	6.60%	2.95%	3.19%
<i>Ruminococcaceae_UCG-005</i>	0.08%	0.17%	2.22%	1.64%	1.74%
<i>Clostridium_sensu_stricto_1</i>	7.27%	0.07%	0.01%	1.97%#	0.67%#
Other	10.08%	7.77%	9.66%	11.04%	9.24%

Note: CG: control group; MG: model group; TG: soup group; HG: oil group; YXG: positive group. Compared with the control group, * $p < 0.05$, ** $p < 0.01$; compared with the model group, # $p < 0.05$, ## $p < 0.01$.

based on sequence length, quality, primer, and tag. The raw sequences were selected, and the low-quality sequences were removed; specific information is as follows: (i) the 300 bp reads were truncated at any site receiving an average quality score < 20 over a 50 bp sliding window, discarding the truncated reads that were shorter than 50 bp. (ii) Exact

barcode matching, 2 nucleotide mismatches in primer matching, and reads containing ambiguous characters were removed. (iii) Only sequences that overlap longer than 10 bp were assembled according to their overlap sequence. Reads which could not be assembled were discarded. The unique sequence set was classified into operational

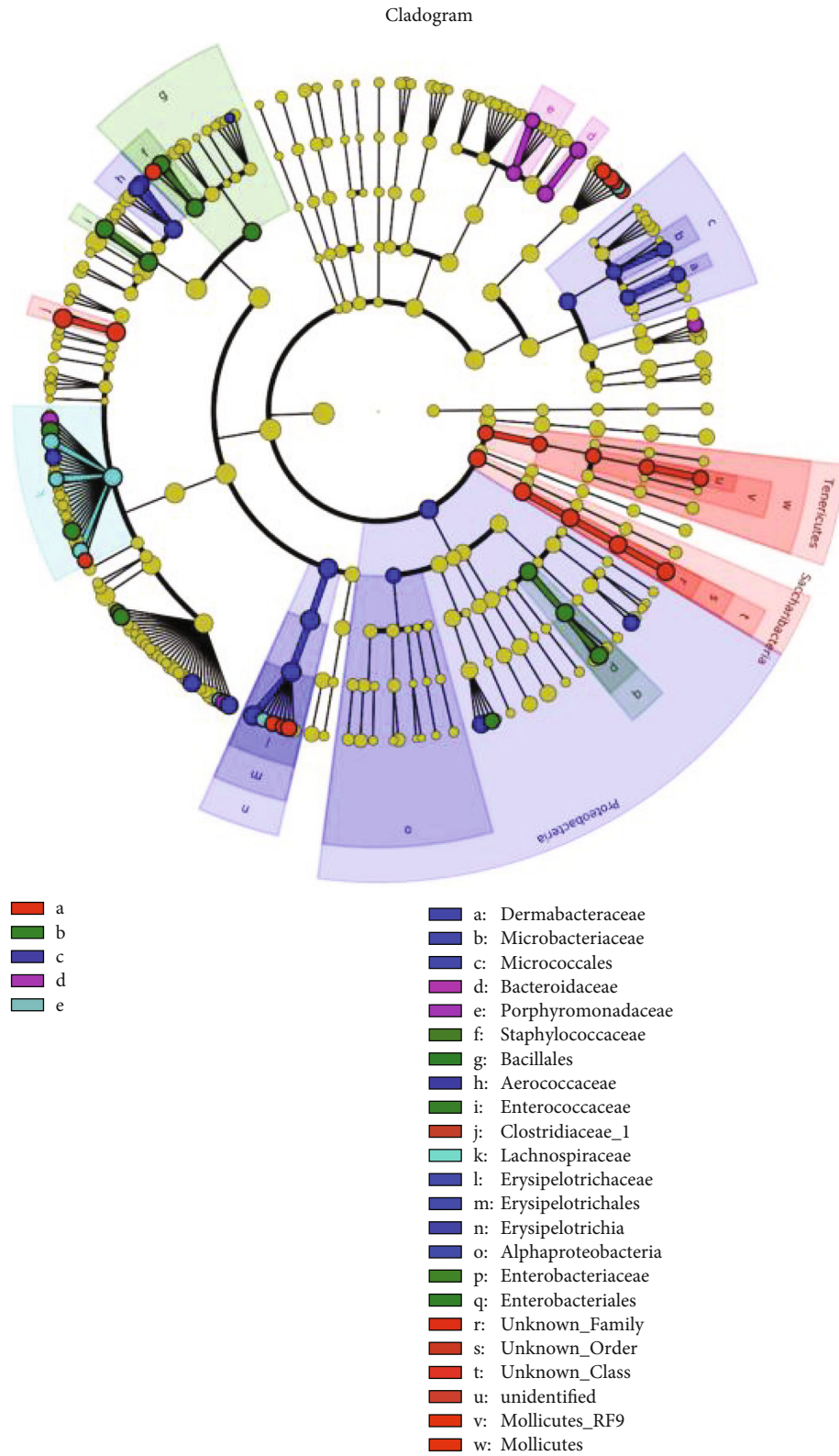


FIGURE 8: Cladogram: analysis of significant difference between samples: a—CG group, b—MG group, c—TG group, d—HG group, and e—YXG group.

taxonomic units (OTUs) under the threshold of 97% identity using UCLUST. Chimeric sequences were identified and removed using USEARCH (version 8.0.1623). The tax-

onomy of each 16S rRNA gene sequence was analyzed by UCLUST against the Silva119 16S rRNA database using confidence threshold of 90%.

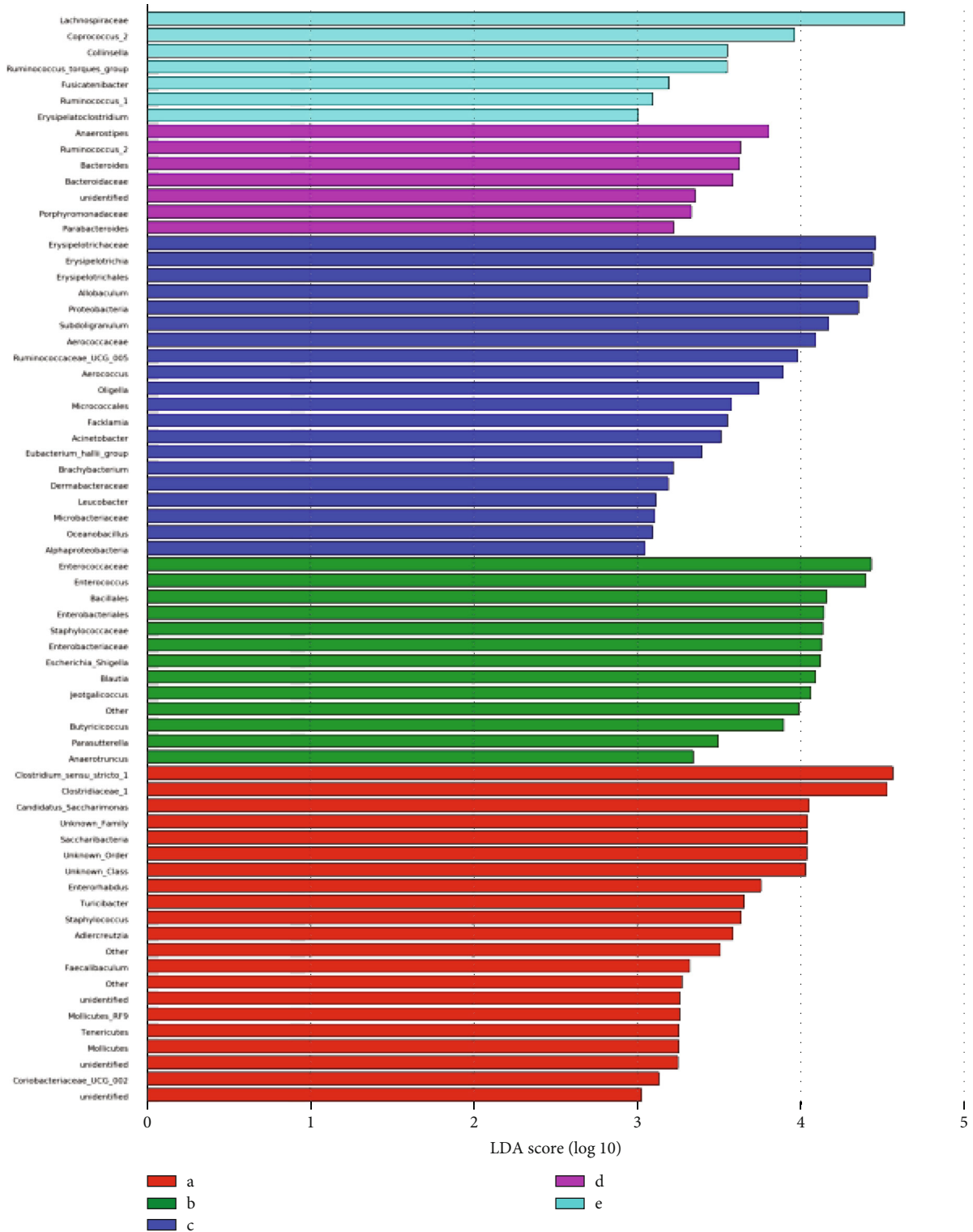


FIGURE 9: LDA score of significantly different bacteria in each group: a—CG group, b—MG group, c—TG group, d—HG group, and e—YXG group.

2.9. Statistical Analysis. Statistical analysis was performed using SPSS 24.0. The graphs were made using GraphPad Prism 6.0. One-way analysis of variance (ANOVA) and two-tail Student's *t*-test were conducted for comparisons among the multiple groups. $p < 0.05$ was considered to be statistically significant.

3. Results

3.1. Macro Characterization. Throughout the experiment, the physiological status between the CG group and the other four groups (MG, TG, HG, and YXG group) is significant. The CG group displayed flexible reaction, smooth coat, controlled food intake, and granular stool. The spleen deficiency model in the other four groups (MG, TG, HG, and YXG group) was developed using Xiaochengqi decoction as previously described. The rats in other groups began to have diarrhea on the 3rd day after the establishment of the model. The water content in their stools increased markedly. On the 7th day, the diarrhea was more obvious. The stools were thin, and there was dirt around the anal area. They squinted visually, crouched obviously, piled up, arched back, were tired and sleepy, fed less, reacted slowly, and defecated many times, and their fur was dark and glossy (Figure 1).

3.2. Effect of Caoguo-4 Decoction Volatile Oil on Serum D-Xylose and AMS Content and Plasma MTL Content in Spleen Deficiency Rats. Table 1 shows that the plasma MTL content in the MC group was higher than that in the CG group ($p < 0.05$). The plasma MTL content in the TG and MG groups was lower than that in the MG group ($p < 0.05$). The serum D-xylose and AMS content in the MG group was lower than that in the CG group ($p < 0.05$), but for the TG, MG, and YXG groups, serum was significantly increased in the serum D-xylose and AMS levels ($p < 0.01$ or $p < 0.05$). This result indicated that Caoguo-4 decoction and Caoguo-4 decoction volatile oil could upregulate the content of D-xylose, AML, and MTL in rats.

3.3. The Histopathological Changes in the Intestinal Mucosa. The histopathological changes of the intestinal mucosa of mice in all groups were analyzed by HE staining (Figure 2). Mice in the CG group showed integrity of the intestinal epithelium and no inflammatory cell infiltration in interstitial cells. But in the MC group, mucosal lesions with a massively destructed epithelium and a mass of glands were decreased with disorder and inflammatory cell infiltration. In the TG and HG group, with a little inflammatory cell infiltration, the structure of the epithelium in the villi of the small intestine was almost complete, only partially broken. This result indicated that Caoguo-4 decoction and Caoguo-4 decoction volatile oil could significantly protect intestinal mucosa structure and reduce histologic inflammation.

3.4. OTU Analysis. Figure 3 shows the operational taxonomic unit (OTU) number of all the bacteria in the gut. When compared with the CG group, the MG group had 224 identical species, the TG group had 315 identical species, the HG group had 316 identical species, and the TYG group had 270 identical species. Further, when compared with the

MG group, the TG group had 314 identical species, the HG group had 311 identical species, and the YXG group had 308 identical species. Between the TG group and the HG group, there were 389 identical species. It can be seen that after the treatment using the Caoguo-4 decoction volatile oil, the number of bacterial OTUs in the HG group is the same as that in the TG group; further, there was similar number of bacterial OTUs in the TG group and the CG group. The results indicate that the simultaneous use of the Caoguo-4 decoction volatile oil and the Caoguo-4 decoction can effectively restore intestinal microbiota and restore intestinal microecological environment.

In Figure 4, we find that the YXG group points are more dispersed, indicating that the intestinal microbial community in this group of rats is the most different. However, the TG group and the HG group points are relatively concentrated, indicating that the difference between the two groups of rat's intestinal microbial community is small. Interestingly, in the HG group, the difference was minimal.

3.5. Alpha Diversity Analysis. The good coverage value for each group was greater than 0.99, indicating that the results of this sequencing can reflect the actual situation of microorganisms in the sample. The results of alpha diversity analysis between groups (Figure 5) indicated that compared with the CG group, the intestinal microbiota richness index (Figure 5, chao1 and observed species) (Table 2) in the MG group was significantly reduced ($p < 0.01$) and the diversity index (PD whole tree) significantly decreased ($p < 0.05$). Further, compared with the MG group, the intestinal microbiota richness index (Figure 5, chao1 and observed species) of rats in the TG group and HG group was significantly increased ($p < 0.01$) and the diversity index (whole tree) increased significantly ($p < 0.05$). There was no significant difference in the YXG group ($p > 0.05$). Further, there was no significant difference in the Shannon index (Figure 5, Shannon) in each experimental group ($p > 0.05$), which indicated that the intestinal microbiota of spleen deficiency diarrhea rats had been well recovered posttreatment with Caoguo-4 decoction.

3.6. Species Annotation Analysis. According to the OTUs obtained from the sample sequencing and the species represented by OTUs, the corresponding columnar diagrams of the species were drawn for each sample (Figure 6) at the phylum and belonging to the classification grade.

The distribution of phylum horizontal species is shown in Table 3. The results show that the intestinal structure of rats at the phylum level is mainly thick-walled fungus, *Actinomyces* phylum, and deformed fungus phylum, in which the proportion of deformed bacteria phylum is the lowest, the proportion of thick-walled fungus is the highest, and *Actinomyces* phylum is the second most dominant flora. Compared to the control group, in the model group, *Saccharibacteria* ($p < 0.05$), *Tenericutes* ($p < 0.01$), *Euryarchaeota* ($p < 0.05$), and *Cyanobacteria* significantly decreased ($p < 0.01$). However, *Proteobacteria* significantly increased ($p < 0.01$). Compared with the model group, the *Saccharibacteria* of the decoction group increased significantly ($p < 0.05$). And *Proteobacteria* of the volatile oil group

decreased significantly ($p < 0.05$), *Saccharibacteria* significantly increased ($p < 0.05$), and there was no significant difference in the positive group.

Figure 7 and Table 4 show the distribution of horizontal species; the results show that when compared with the control group, in the model group, *Enterorhabdus* ($p < 0.05$), *Candidatus_Saccharimonas* ($p < 0.01$), and *Ruminococcaceae_UCG-013/UCG-014* ($p < 0.05$) significantly decreased. However, *Escherichia-Shigella* and *Helicobacter* significantly increased ($p < 0.01$). Compared with the model group, the decoction group had significantly decreased *Romboutsia* ($p < 0.05$) and significantly increased *Subdoligranulum* ($p < 0.05$), *Enterorhabdus* ($p < 0.05$), and *Oligella* ($p < 0.05$). In the volatile oil group, *Candidatus_Saccharimonas* ($p < 0.05$) and *Ruminococcaceae_UCG-014* ($p < 0.01$) significantly increased and *Aerococcus* ($p < 0.05$), *Butyricoccus* ($p < 0.05$), and *Romboutsia* ($p < 0.01$) significantly decreased. In the positive group, *Aerococcus* ($p < 0.01$), *Ruminococcaceae_UCG-013* ($p < 0.01$), and *Jeotgalicoccus* ($p < 0.01$) significantly decreased, whereas *Anaerostipes* ($p < 0.01$) and *Enterorhabdus* ($p < 0.05$) significantly increased.

3.7. Analysis of Significant Difference between Samples. The circle radiating from the inside to the outside represents the classification level from the door to the genus (or species). Each small circle at different levels represents a classification at this level, and the diameter size of the small circle is proportional to the relative abundance size of each genus or species (Figure 8). With coloring principle, the species without significant difference is colored yellow; the different species biomarkers follow the group coloring: the red node represents the microbial group that plays an important role in the “red group” and the green node represents the microbial group that plays an important role in the “green group.” The name of the species is represented in the English alphabet in the figure and is shown in the legend on the right.

Figure 9 shows the species in which the linear discriminant analysis (LDA) score is greater than the set value, that is, the biomarker with statistically significant differences. This figure indicates species with significant differences in abundance in different groups, and the length of the histogram represents the size of the significantly different species. The longer the column, the greater the LDA value. *Clostridium*, *Clostridiaceae*, *Enterorhabdus*, *Staphylococcus*, soft-wall fungus door *Tenericutes*, and *Coriobacteriaceae* had the highest abundance in the control group. *Enterococcaceae*, *Bacillales*, *Enterobacteriales*, *Escherichia*, *Blautia*, and the genus *Anaerotruncus* were the most abundant in the model group. *Erysipelotrichia*, *Erysipelotrichaceae*, *Erysipelotrichiales*, *Allobaculum*, *Proteobacteria*, *Aerococcaceae*, *Ruminococcaceae*, *Aerococcus*, *Oligella*, *Micrococcales*, *Eubacterium Hallii*, *Brachy bacterium*, *Dermabacteraceae*, *Microbacteriaceae*, marine *Oceanobacillus*, and α -*Proteobacteria* had the highest abundance in the decoction group. *Anaerostipes*, *Ruminococcus 2*, *Bacteroides*, *Bacteroidaceae*, *Porphyromonadaceae*, and *Parabacteroides* had the highest abundance in volatile oil groups. The different species with the highest abundance in the positive group were *Lachnospiraceae*, *Coprococcus*, and *Ruminococcaceae*.

4. Discussion

To test our hypothesis that regulation of intestinal microbiota by the Caoguo-4 decoction volatile oil is related to its antidiarrheal efficacy, we established the SDD model in rats demonstrated by indices of diarrhea and clinical symptoms, which is consistent with previous studies. Its main function is to affect the power of the gastrointestinal tract and can stimulate the secretion of pepsin and pancreatic fluid along with gallbladder contraction. The effect on gastrointestinal movement is manifested in increasing the tension of the lower esophageal sphincter, promoting the movement of the stomach, small intestine, and gallbladder, and contributing to the absorption of food. The experimental results showed that the plasma motilin in the model group was significantly higher than that in the control group, which was consistent with the previous studies such as Lu [16] and Li and Zhen [17], but the results are inconsistent with studies from groups such as Song et al. [18] and Shao et al. [19]; hence, there is a need to further study its mechanism. After administration with either the decoction group or volatile oil group, there is significant decrease in motilin, and the decrease in the volatile oil group was more obvious thus proving that this group was most efficient for the treatment of SDD. Results also showed that there was some damage to the intestinal mucosal structure in the model group, and the Caoguo-4 decoction and the Caoguo-4 decoction volatile oil group could improve the damaged epithelial structure and reduce inflammation.

The results of OTU analysis and alpha diversity analysis showed that the intestinal microbiota of spleen deficiency model rats changed significantly. With the increase in the number of samples and their corresponding grade values, the number of bacteria and relative abundance tend to be more towards a certain constant value. This indicates that the sequencing depth is sufficient to reflect the level of community richness, the number of OTUs is close to the actual situation, and the uniformity of community composition is higher. Additionally, the coverage value is the coverage of the sample library in the experiment, with 10% as the upper limit; the higher the value, the higher the probability of the sequence being detected in the sample, which means that the sequencing results can reflect the real situation of the sample.

Further, the richness and diversity of intestinal microbiota also decreased significantly. Through intervention with decoction and volatile oil, the richness and diversity of intestinal flora recovered significantly, but there was no significant change in the positive group. This shows that the intestinal microbiota in rats with SDD has been destroyed, and both decoction and volatile oil can restore the unbalanced intestinal microbiota, and it can be speculated that decoction and volatile oil are superior to Smecta in the treatment of spleen deficiency diarrhea.

Intestinal microbiota are the most important and diverse microbial community living in the human body [20], and in order to maintain the body function in a stable state, intestinal microbiota will restrict each other to achieve dynamic balance. Intestinal microbiota disorders in the TCM are

considered important biological basis for “spleen deficiency” [21]. Further, the intestinal microecological changes of the SDD model are closely related to spleen inactivation. In this study, the thick-wall fungus door accounted for a large proportion in the gut, but there was no significant difference between the groups in this experiment. The change of the main intestinal microbiota caused by SDD is the decrease in the number of bacteria and *Saccharibacteria* in the intestinal tract (Bacteroidetes), but the number of bacteria in the deformed fungus door (Proteobacteria) increased correspondingly. This change was mainly due to the high nutritional requirements of the anaerobic bacteria Gram-negative *Bacillus* (mostly *Bacillus*-gate bacteria) caused by intestinal microenvironment destruction and the proliferation of lactobacillus bacteria with strong antibiotic resistance and lower nutritional requirements [22]. In this experiment, the *Proteobacteria* in the diarrhea model group of SDD was significantly increased, and the treatment of volatile oil in Caoguo-4 decoction inhibited the *Proteobacteria* in rats, and the bacteria of *Bacillus* were recovered. In this paper, the number of *Mycobacterium* doors in the model group was lower than that in the control group, and the number of *Bacillus* in the volatile oil group was the best to recover.

At the level of diarrhea, the genus *Escherichia coli*, *Enterococcus*, and *pylori* were observed to be increased, but the genus *Bifidobacterium* and rumen were reduced. *Escherichia coli* is the main pathogen causing the global epidemic of infectious diarrhea and outbreak of local diarrhea. The genus *Enterococcus* is a gram-positive coccus, which is aerobic or anaerobic and is in control of the host. Under controlled circumstances, it will not endanger the health of the host, but in the lack of nutrients, high alkaline and other harsh environment for a prolonged time can cause pathological changes, leading to infection disease [23, 24]. *Bifidobacterium* is a probiotic in the gut of humans and animals. It participates in a series of physiological processes, such as immunity, nutrition, digestion, and protection, and has the function of maintaining the balance of controlling intestinal microbiota, inhibiting the growth of pathogenic bacteria, and preventing and controlling constipation, dysentery, and gastrointestinal disorders [20]. In this study, each drug group had a conditioning effect on lactic acid bacilli in the gut of rats in the model group.

In addition, the regulation degree of the Caoguo-4 decoction agent and volatile oil on intestinal microbiota of SDD model rats was different. Compared with decoction, volatile oil had a conditioning effect on rumen fungus, pseudo-rod bacteria, and *Saccharibacteria*. Compared with the volatile oil group, decoction has a conditioning effect on *Bacillus*, *Enterococcus*, *Romboutsia*, *Subdoligranulum*, *Enterorhabdus*, and *Oligella*. The results show that the potential mechanism of the Caoguo-4 decoction agent and volatile oil on the SDD rat model is different, which may suggest the unique regulation mechanism of volatile oil on intestinal microbiota. In short, the two intervention groups changed the structure of intestinal microbiota and increased the beneficial bacteria such as the *Bifidobacterium* genus, rumen fungus, *Arabidopsis* bacteria, and *Saccharibacteria* and reduced harmful bacteria such as deformed fungus

doors, *Escherichia coli*, *Romboutsia*, and *Blautia*. Further, by analyzing the species or communities with significant differences between the groups, it was found that the changes of *Enterococcus*, *Enterobacter*, and *Escherichia coli* may be related to the diarrhea index of spleen deficiency.

5. Conclusion

In summary, Caoguo-4 decoction and volatile oils are beneficial against diarrhea, which reduced the incidence of diarrhea and improved stool. Our research proved that Caoguo-4 decoction and volatile oils can upregulate the content of D-xylose, AML, and MTL in rats, changing the structure of intestinal microbiota by increasing the beneficial bacteria such as the *Bifidobacterium* genus, rumen fungus, *Arabidopsis* bacteria, and *Saccharibacteria* and reducing harmful bacteria such as deformed fungus doors, *Escherichia coli*, *Romboutsia*, and *Blautia*. To achieve treatment of spleen deficiency diarrhea with its mechanism being still unknown, further research is needed.

Data Availability

All data used to support the findings of this study are available from the corresponding author upon request.

Ethical Approval

The animal study was reviewed and approved by the Animal Ethics Committee of Jiangxi University of Traditional Chinese Medicine.

Conflicts of Interest

The authors declare that there is no conflict of interests regarding the publication of this paper.

Authors' Contributions

MY and FW cosupervised the study. LM, XFZ, and FW codesigned the study based on the sequenced data. FW, YZG, and QYC codesigned and implemented the therapeutic measures and sampling. LFW, ZYL, and FQL analyzed the data and made the plots and tables of the result. LM, YM, and FW wrote and revised the manuscript, and all authors proofread and improved the manuscript. Fang Wang is the co-first author.

Acknowledgments

This study was supported by grants from the Project of National Natural Science Foundation of China (81960714), the Jiangxi Province Science and Technology Major Projects (20194ABC28009), the funding from Jiangxi University of Traditional Chinese Medicine (JXSYLXK-ZHYAO083, JXSYLXKZHYAO084), the “Double First-Rate” Construction Program of the Inner Mongolia University for Nationalities (NMDGJ0012), and the Natural Science Foundation of Inner Mongolia Autonomous Region of China (2020BS08008).

References

- [1] J. Wang, W. Feng, S. Zhang et al., "Ameliorative effect of *Atractylodes macrocephala* essential oil combined with *Panax ginseng* total saponins on 5-fluorouracil induced diarrhea is associated with gut microbial modulation," *Journal of Ethnopharmacology*, vol. 238, article 111887, 2019.
- [2] Q. Liu and C. J. Wang, "Treatment of chronic diarrhea due to intestinal microbiota imbalance according to the theory of "spleen deficiency"," *Clinical Journal of Traditional Chinese Medicine*, vol. 29, no. 12, pp. 2032-2033, 2017.
- [3] W. Ruan, Z. H. W. Chen, and J. T. Yan, "Four-step massage" in treating childhood spleen-deficiency diarrhea," *Journal of Acupuncture and Tuina Science*, vol. 4, no. 5, pp. 271-273, 2006.
- [4] C. A. Lozupone, J. I. Stombaugh, J. I. Gordon, J. K. Jansson, and R. Knight, "Diversity, stability and resilience of the human gut microbiota," *Nature*, vol. 489, no. 7415, pp. 220-230, 2012.
- [5] B. Y. Xu, Y. Q. Yan, J. C. Huang, B. Q. Yin, Y. X. Pan, and L. B. Ma, "Cortex Phellodendri extract anti-diarrhea effect in mice related to its modification of gut microbiota," *Biomedicine & Pharmacotherapy*, vol. 3, no. 123, pp. 63-63, 2020.
- [6] G. Solano-Aguilar, K. Fernandez, H. Ets et al., "Characterization of fecal microbiota of children with diarrhea in 2 locations in Colombia," *Journal of Pediatric Gastroenterology and Nutrition*, vol. 56, no. 5, pp. 503-511, 2013.
- [7] J. Ma, Z. G. Yang, J. C. Wei et al., "Effects of different processed products of *Radix Codonopsis* on intestinal microbiota of rats with spleen deficiency," *Medicinal Plant*, vol. 11, no. 1, pp. 63-63, 2020.
- [8] R. Wang, Y. Shi, X. Xie et al., "Use of Shenhuang paste on Shenque point improves chemotherapy induced gastrointestinal toxicity in breast cancer: a protocol for randomized controlled trial," *Medicine*, vol. 100, no. 15, article e25097, 2021.
- [9] W. B. Han, "Clinical observation of acupoint application for slow transit constipation due spleen deficiency and intestine dryness," *Shanghai Journal of Acupuncture and Moxibustion*, vol. 37, no. 12, pp. 1359-1362, 2018.
- [10] K. X. Guo, M. J. Peng, X. X. Peng, H. Y. Hui, and Z. J. Tan, "Effects of Qiweibaizhu powder on the intestinal bacterial diversity in dysbacteriotic diarrhea mice," *Wei Sheng Wu Hsueh T'ung Pao Microbiology*, vol. 45, no. 7, pp. 1470-1479, 2018.
- [11] Inner Mongolia Autonomous Region Hospital, *Mongolian Medicine Verification Prescription (Mongolian Version)*, Ancient Xinhua Printing of Inner Mongolia, Hohhot, Mongolia, 1971.
- [12] The Editorial Board of Chinese Medical Encyclopedia, *Chinese Medical Encyclopedia (Mongolian Edition)*, Shanghai Science and Technology Press, Shanghai, China, 1992.
- [13] Y. Q. Wang, Y. Z. Yang, Z. F. Wang, Y. K. Xiong, and M. Yang, "Traditional function and modern research progress on volatile oil in Chinese materia medica," *Chinese Traditional and Herbal Drugs*, vol. 49, no. 2, pp. 455-457, 2018.
- [14] Y. H. Li, D. M. Zhang, S. Y. Wang et al., "Development of animal model of spleen deficiency syndrome," *Guiding Journal Of Traditional Chinese Medicine*, vol. 25, no. 1, pp. 100-103, 2019.
- [15] W. Zhang, H. Y. Zhang, and S. P. Huang, "The study of composite factors make spleen-deficient model in rats," *Lishizhen Medicine and Materia Medica Research*, vol. 26, no. 4, pp. 1022-1023, 2015.
- [16] Z. Lu, *Mouse Gut Microbiota Composition and Metabolites Change Caused by Inulin Addition in High Fat Diet*, Tsinghua University, 2017.
- [17] B. F. Li and C. H. Zhen, "The influence of Smeta on serum motilin and gastrin levels in rats with sp," *Zhejiang Clinical Medical Journal*, vol. 10, pp. 841-843, 2004.
- [18] Y. P. Song, H. F. Chen, Y. X. Hu, S. S. Tan, X. Q. Luo, and W. L. Yang, "Effect of *Pericarpium Citri Reticulatae* and its main active ingredients on gastrin in serum, acetylcholine, motilin, substance P and vasoactive intestinal peptide in plasma of rats," *Pharmacology and Clinics of Chinese Materia Medice*, vol. 33, no. 3, 2017.
- [19] N. J. Shao, X. Ma, X. X. Zhu, H. D. Wang, and Q. Gao, "Effects of Yunpiwenyang granule on MTL, SS and VIP in the blood of mouse with splenic deficiency diarrhea," *Journal of Changchun University of Traditional Chinese Medicine*, vol. 30, no. 6, 2014.
- [20] Y. Y. Chen, R. Wang, J. H. Zhang et al., "Effects of intestinal microflora on drug metabolism," *Chinese Pharmacological Bulletin*, vol. 35, no. 2, pp. 168-175, 2019.
- [21] G. Yuan and S. Qinglong, "Advances in pharmacology research of Shenqi Baizhu powder based on intestinal microecology," *Lishizhen Medicine and Materia Medica Research*, vol. 29, no. 3, 2018.
- [22] H. Yao, Z. Lv, H. F. Xu, and J. R. Su, "The study of regulation of berberine to gut microflora in mouse model with *Clostridium difficile* associated diarrhea," *The Chinese Medical Journal*, vol. 53, no. 1, pp. 77-77, 2018.
- [23] V. Shetty, S. H. Kumar, A. K. Shetty, I. Karunasagar, and I. Karunasagar, "Prevalence and characterization of diarrheagenic *Escherichia coli* isolated from adults and children in Mangalore, India," *Journal of Laboratory Physicians*, vol. 4, no. 1, pp. 24-029, 2012.
- [24] S. Patzi-Vargas, M. B. Zaidi, Perez-Martinez et al., "Diarrheagenic *Escherichia coli* carrying supplementary virulence genes are an important cause of moderate to severe diarrhoeal disease in Mexico," *PLoS Neglected Tropical Diseases*, vol. 9, no. 3, 2015.

Research Article

Serum Fetuin-B Levels Are Elevated in Women with Metabolic Syndrome and Associated with Increased Oxidative Stress

Shiyao Xue ^{1,2}, Hongdong Han ², Shunli Rui,^{1,3} Mengliu Yang ^{2,4}, Yizhou Huang,² Bin Zhan,⁵ Shan Geng ², Hua Liu,⁶ Chen Chen ⁴, Gangyi Yang,² and Ling Li ¹

¹Key Laboratory of Diagnostic Medicine (Ministry of Education) and Department of Clinical Biochemistry, College of Laboratory Medicine, Chongqing Medical University, 400016 Chongqing, China

²Department of Endocrinology, The Second Affiliated Hospital, Chongqing Medical University, Chongqing 400010, China

³Department of Endocrinology, Multidisciplinary Diabetic Foot Medical Center, Chongqing Emergency Medical Center, Chongqing University Central Hospital, Chongqing University, Chongqing, China

⁴Endocrinology, SBMS, Faculty of Medicine, University of Queensland, Brisbane 4072, Australia

⁵The Thirteenth People's Hospital of Chongqing, Chongqing 400016, China

⁶Department of Pediatrics, University of Mississippi Medical Center, 2500 North State Street, Jackson, Mississippi, MS 39216-4505, USA

Correspondence should be addressed to Ling Li; liling@cqmu.edu.cn

Received 23 December 2020; Revised 27 March 2021; Accepted 31 August 2021; Published 4 October 2021

Academic Editor: Colin Murdoch

Copyright © 2021 Shiyao Xue et al. This is an open access article distributed under the Creative Commons Attribution License, which permits unrestricted use, distribution, and reproduction in any medium, provided the original work is properly cited.

Previous studies on serum fetuin-B (fetuin-like protein IRL685) have investigated its association with T2DM; however, the reason for the variation in serum fetuin-B and its regulatory factors in metabolic disease remain unclear. Here, we evaluated serum fetuin-B levels in women with newly diagnosed MetS and performed multiple interventions to investigate the role of fetuin-B in the pathogenesis of MetS. Serum fetuin-B levels were assessed using ELISA. Bioinformatics analysis was performed to analyze fetuin-B-related genes and signaling pathways. Additionally, oxidative stress parameters were measured in the *in vitro* study. For subgroup analyses, we performed EHC, OGTT, and treatment with a GLP-1RA to investigate the regulatory factors of serum fetuin-B. We found that in comparison with healthy subjects, serum fetuin-B levels were markedly increased in women with MetS. Further, serum fetuin-B showed a positive correlation with WHR, FAT%, TG, FBG, HbA1c, FIns, HOMA-IR, VAI, and LAP. Bioinformatics analysis revealed that most fetuin-B-related core genes were involved in cholesterol metabolism and fat decomposition. Consistent with this finding, multivariate regression analysis showed that triglyceride content and WHR were independently associated with serum fetuin-B. We also observed that serum fetuin-B levels were markedly elevated in healthy subjects after glucose loading and in women with MetS during EHC. *In vitro*, overexpression of fetuin-B promoted oxidative stress in HepG2 cell. After 6 months of treatment with a GLP-1RA, serum fetuin-B levels in women with MetS decreased following an improvement in metabolism and insulin sensitivity. Therefore, serum fetuin-B is associated with MetS, which may serve as a biomarker of oxidative stress. This trial is registered with ChiCTR-OCC-11001422.

1. Introduction

Metabolic syndrome (MetS) is characterized by several symptoms, including insulin resistance (IR), abdominal obesity, hypertension, and dyslipidemia [1]. Over the past few decades, MetS and obesity have developed into global epidemics, attributable to high-fat diet and sedentary lifestyle, placing an enormous economic burden on healthcare sys-

tems [2]. The risk of cardiovascular disease and type 2 diabetes mellitus (T2DM) has been reported to increase by 2- and 5-fold in patients with MetS, respectively [3, 4]. Furthermore, MetS increases all-cause mortality from 1.30- to 1.70-fold, with women showing a higher incidence than men [5]. Therefore, the pathogenesis of MetS and how its components interact remain uncertain, and there is a lack of consistent treatment recommendation. For the optimal

management of patients with MetS, it is thus critical to identify biomarkers that can accurately predict outcomes and therapeutic responses.

Fetuin-like protein IRL685 (fetuin-B) was first identified as the second member of the cystatin superfamily of cysteine protease inhibitors in 2000. It shows 22% homology with fetuin-A [6]. Fetuin-B is encoded by the FETUB gene, which has a chromosomal localization of 3q27.3 with eight exons, and mutations in this region have previously been confirmed to be prone to MetS and diabetes [6]. Further, fetuin-B expression levels have been reported to be higher in hepatocytes from mice with liver steatosis, impairing insulin action in myotubes and hepatocytes. In addition, fetuin-B silencing improved glucose tolerance in obese mice but did not affect their body weight, which suggests that fetuin-B regulates blood glucose levels via an insulin-independent mechanism, possibly through glucose effectiveness [7, 8]. In clinical studies, serum fetuin-B was found to be strongly associated with triglyceride (TG) content in the liver and early insulin secretion stimulated by glucose [9, 10]. It has also been reported that in comparison with healthy controls, fetuin-B levels are substantially increased in patients with nonalcoholic fatty liver disease, T2DM, polycystic ovary syndrome, and gestational diabetes mellitus [11–13]. Therefore, previous studies have suggested that fetuin-B, as an adipokine or hepatokine, is closely related to glucose and lipid metabolism. However, the association between fetuin-B and MetS and its mechanism remain unclear.

In this study, we measured serum fetuin-B levels in healthy individuals and women newly diagnosed with MetS. A preprint for this part of the study has been published [14]. To investigate the association between serum fetuin-B and MetS as well as IR, we performed multiple intervention experiments, including euglycemic-hyperinsulinemic clamps (EHCs), oral glucose tolerance tests (OGTTs), and treatment with a glucagon-like peptide-1 receptor agonist (GLP-1RA). Furthermore, we investigated the effect of fetuin-B on FFA-induced oxidative stress *in vitro*.

2. Materials and Methods

2.1. Participants and Inclusion/Exclusion Criteria. Overall, 377 Chinese women (192 with MetS, 185 healthy subjects; age, 38 ± 15 years; body mass index (BMI), 23.7 ± 4.2 kg/m²) were recruited from outpatients attending the Department of Endocrinology at the Second Affiliated Hospital, Chongqing Medical University, as well as from the community or universities via advertisements or routine medical examinations performed between December 2016 and December 2018. The diagnostic criteria of MetS were based on the United States National Cholesterol Education Program Expert Panel Adult Treatment Panel III criteria [15]. Participants were diagnosed with MetS if they showed ≥ 3 of the following: (1) central obesity (waist circumference (WC): Asian women, ≥ 80 cm), (2) hypertension ($\geq 130/85$ mmHg), (3) hyperglycemia (fasting glucose ≥ 5.6 mmol/L or T2DM), (4) elevated plasma TG levels (≥ 1.69 mmol/L), and (5) low levels of high-density lipoprotein-cholesterol (HDL-C: women, < 1.29 mmol/L). The participants were classified as those hav-

ing normal glucose tolerance, impaired glucose tolerance, or T2DM, using the diagnostic criteria of the American Diabetes Association [16]. The exclusion criteria included heart, hepatic, or renal failure; presence of malignant tumors, type 1 diabetes, acute infection, or other chronic metabolic diseases; pregnancy; and long-term use of steroids. In this study, all participants with MetS were newly diagnosed, and there was no involvement of any drug treatment, physical exercise, or diet control. The healthy subjects had no history of other diseases, hypertension, or family history of diabetes, and their blood glucose levels were normal. All study protocols were approved by the Human Research Ethics Committee of Chongqing Medical University, and all experiments were performed in accordance with the Declaration of Helsinki. Written informed consent was obtained from all participants.

2.2. Anthropometric Examinations and Biochemical Measurements. After an overnight fast for at least 12 h, anthropometric measurements were made and blood samples were obtained by professionals from all participants. Body measurements (weight, height, WC, hip circumference (HC), blood pressure, and fat percentage *in vivo* (FAT%)) and biochemical indices, including levels of fasting blood glucose (FBG), 2 h post-OGTT glucose (2 h-BG), insulin, glycosylated hemoglobin (HbA1c), TG, total cholesterol (TC), HDL-C, low-density lipoprotein cholesterol (LDL-C), and free fatty acids (FFA), were measured, as previously reported [17]. We also subjected all women to a 75 g, 2 h OGTT, according to the American Diabetes Association criteria [16].

2.3. Measurement of Serum Fetuin-B Levels. Serum fetuin-B levels were determined using a commercial enzyme-linked immunosorbent assay kit (RayBiotech, Inc., Norcross, GA, USA), as the manufacturer's instructions. The detection limit of this kit was 4.0 ng/mL; the intra- and interassay coefficient of variation was 10% and 12%, respectively.

2.4. Bioinformatic Analysis

2.4.1. Protein-Protein Interaction (PPI) Network Construction and REACTOME Analysis. The Search Tool for the Retrieval of Interacting Genes (STRING) database was used to construct the PPI network [18]. An interaction score of 0.4 was used as the cut-off standard, and the PPI network was visualized. The STRING database was used for REACTOME enrichment analysis to screen out signal pathways and genes related to metabolism [19]. The false discovery rate (FDR) < 0.01 indicated statistical significance in REACTOME analysis.

2.4.2. Gene Ontology (GO) and Kyoto Encyclopedia of Genes and Genomes (KEGG) Analysis. We used the clusterProfiler package to perform GO and KEGG pathway analyses [20]. A list of GO and KEGG annotation terms was thus obtained. Further, we categorized all genes to the biological processes (BP), cellular components (CC), and molecular functions (MF) of GO categories. $p < 0.05$ indicated statistical significance in the case of GO and KEGG terms.

2.5. In Vitro Study

2.5.1. Cell Culture and Treatment. HepG2 cells were cultured in DMEM supplemented by 10% fetal bovine serum as previously reported [21]. The cells were transfected with plasmid expressing fetuin-B (pcDNA3.1-fetuin-B, GenePharma, Inc. Shanghai, China) or control plasmid (pcDNA3.1) for 24 h. To induce oxidative stress, HepG2 cells were exposed to 1 mM fatty acid mixtures (FFAs, oleic acid: palmitate, 2:1) for another 24 h as previously reported [21].

2.5.2. Determination of Oxidative Stress Parameters. The activities of antioxidant enzymes including superoxide dismutase (SOD), glutathione (GSH), and malondialdehyde (MDA) were measured by their specific assay kits (Beyotime, Inc., Shanghai, China), according to the manufacturer's instructions. To investigate intracellular reactive oxygen species (ROS) formation, FFA-treated HepG2 cells were incubated with 10 μ M dichloro-dihydro-fluorescein diacetate (DCFH-DA) at 37°C for 20 min. Fluorescence of ROS in the cells was recorded with a fluorescence microscope (Olympus Corporation, Tokyo, Japan), and intensity was analyzed using ImageJ software.

2.6. EHC. For subgroup analysis, EHC was performed in 16 women with MetS and 27 healthy subjects as previously reported [17]. A venous channel was established in the antecubital vein to infuse insulin and glucose, and another catheter was implanted into the dorsal vein of the contralateral hand for blood sampling. Regular human insulin (1 mU/kg/min) was infused for 2 h, and 20% glucose was infused to maintain blood glucose levels at the primary level. The blood glucose level was measured every 15 min during EHC to guide the glucose infusion rate. During the steady state of the clamp, the glucose infusion rate was equal to the glucose disposal rate and related to body weight (*M* value). Blood samples were collected at 0, 80, 100, and 120 min to analyze serum fetuin-B levels and other parameters. The blood samples were centrifuged to separate serum and stored at -80°C until analysis.

2.7. Intervention Therapy with Liraglutide (GLP-1RA). Twenty-four obese women with MetS were recruited from outpatients attending the Department of Obesity at the Second Affiliated Hospital, Chongqing Medical University. The inclusion criteria were age 18–35 years, BMI of 25–35 kg/m², and meeting the diagnostic criteria of MetS which have been described previously [15]. The exclusion criteria included the presence of medullary thyroid carcinoma or severe gastrointestinal diseases, family history of thyroid tumor, pregnancy, and recent history of medication. These individuals have voluntarily participated in the GLP-1RA intervention study for 6 months. The initial dose of liraglutide taken before breakfast was 0.6 mg/d; the dose was increased by 0.6 mg/d every week until it reached 1.8 mg/d. All participants provided informed consent and were aware of the potential side effects of liraglutide before treatment. Anthropometric measurements, biochemical examinations, OGTTs, and EHCs were performed as described above before treatment and also at weeks 12 and 24.

2.8. Calculations. BMI (kg/m²) was calculated as weight (kg) divided by height squared (m²). Waist-to-hip ratio (WHR) was calculated as follows: WC (cm)/HC (cm). The *M* value was calculated as glucose infusion rate divided by body weight, as previously described [17]. Homeostasis model assessment of insulin resistance (HOMA-IR) was calculated as follows: [fasting insulin (FIns, mU/L) \times FBG (mmol/L)]/22.5. The cut-off value of IR was HOMA-IR > 3 [22]. Visceral adiposity index (VAI) was calculated as [WC (cm)/(36.58 + BMI (kg/m²) \times 1.89)] \times [TG (mmol/L)/0.81] \times [1.52/HDL-C (mmol/L)]. Finally, lipid accumulation product (LAP) in women was calculated as follows: [WC (cm) - 58] \times TG (mmol/L) [23, 24].

2.9. Statistical Analysis. SPSS v24.0 (SPSS, Chicago, IL) was used for statistical analyses. Values are expressed as the mean \pm SD or SME, or median with interquartile range. Before analysis, logarithmic conversion was conducted for variables with nonnormal distribution. Student's *t*-test, non-parametric tests, or analysis of variance was used to compare differences between groups. Simple and partial correlation analyses were conducted to explore the relationships between variables and serum fetuin-B. The variables that showed an independent association with serum fetuin-B levels were evaluated using multiple linear regression. Binary logistic regression analysis was used to examine the association between serum fetuin-B and MetS. The change in fetuin-B levels in women with MetS was analyzed using the row mean score and Cochran–Armitage trend test. When data were compared with the control group, *p* < 0.05 indicated a significant difference.

3. Results

3.1. Anthropometric and Biochemical Parameters and Serum Fetuin-B Levels. In this cross-sectional study, the distribution range of serum fetuin-B levels was 1.08–10.30 mg/L for most healthy subjects (83.2%, Figure 1(a)). Table 1 shows the main clinical features and metabolic parameters of all participants (average age, 37.9 \pm 15.6 years). In comparison with healthy subjects (6.01 \pm 3.94 mg/L), women with MetS showed a significant increase in serum fetuin-B levels (8.03 \pm 3.75 mg/L, *p* < 0.001, Table 1, Figure 1(b)). After adjustment for age and BMI, this increase remained significant. In comparison with healthy subjects, age, BMI, FAT%, WHR, blood pressure, blood lipids (including TG, TC, LDL-C, and FFA), FBG, 2 h-BG, FIns, 2 h insulin after glucose overload (2 h-Ins), HbA1c, HOMA-IR, VAI, and LAP were significantly higher in women with MetS, while HDL-C was lower (*p* < 0.001 for all, Table 1). In addition, there was a statistically significant increase in serum fetuin-B levels in overweight/obese women (*n* = 161, BMI \geq 24 kg/m²) than in lean women (*n* = 216, BMI < 24 kg/m²; 7.52 \pm 4.01 vs. 6.68 \pm 3.91 mg/L, *p* < 0.05; Figure 1(c)). To assess the association between serum fetuin-B levels and IR, we classified all subjects into IR (HOMA-IR > 3) and no IR (HOMA-IR \leq 3) groups. In comparison with the no IR group (6.33 \pm 3.95 mg/L), serum fetuin-B levels were

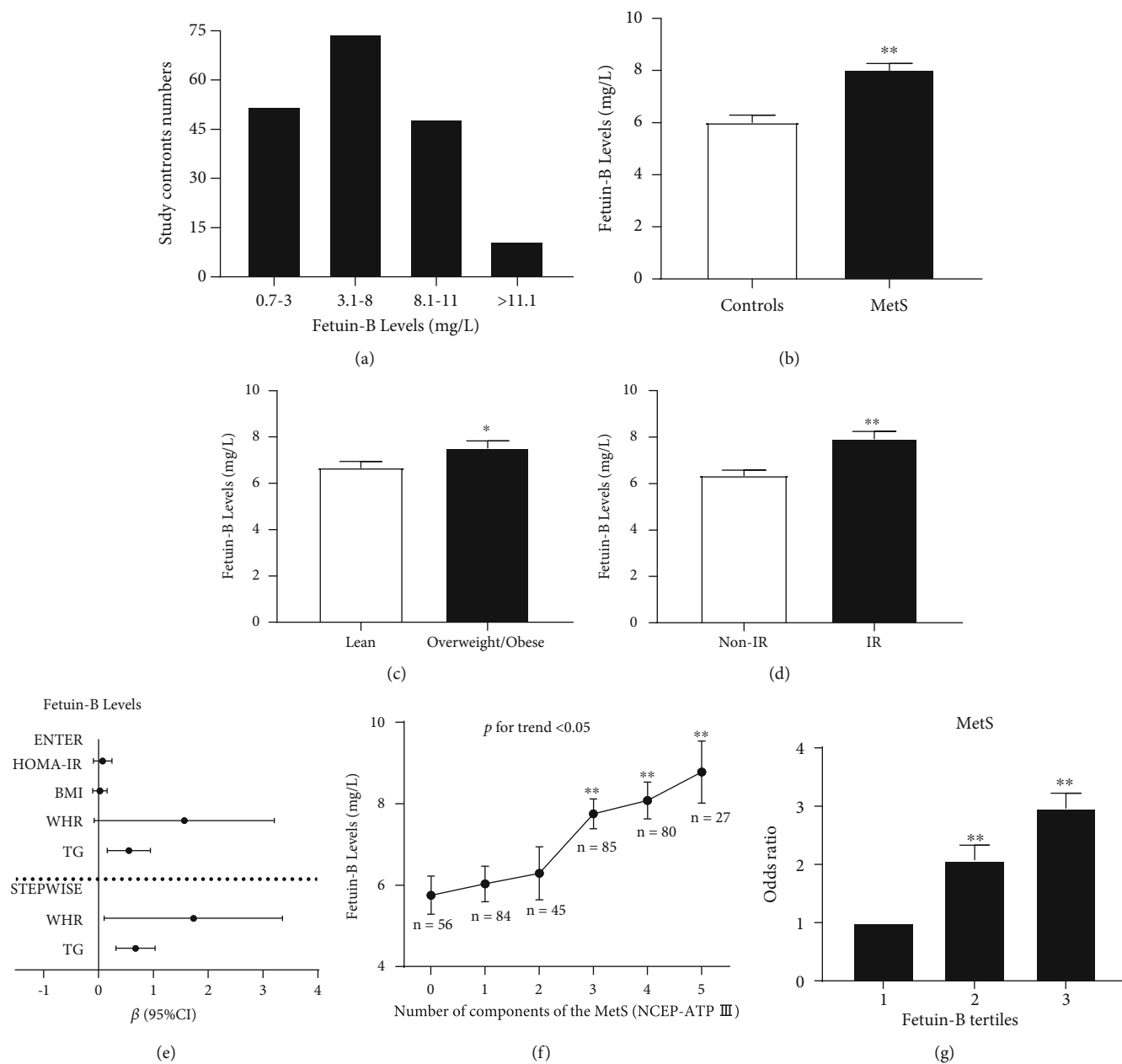


FIGURE 1: Serum fetuin-B levels in the study population. (a) Distribution of serum fetuin-B in 185 healthy women. (b) Serum fetuin-B levels in MetS and healthy subjects. (c) Serum fetuin-B levels according to BMI (lean: BMI < 24 kg/m²; overweight/obese: BMI ≥ 24 kg/m²). (d) Serum fetuin-B levels, according to HOMA-IR (IR: HOMA-IR > 3; non-IR: HOMA-IR ≤ 3). (e) All factors and stepwise multiple regression analyses of the serum fetuin-B and MetS in study individuals. (f) Serum fetuin-B levels in relation to the number of MetS components. (g) The odds ratio of having MetS in different tertiles of serum fetuin-B (tertile 1, ≤5.49 mg/L; tertile 2, 5.49-8.58 mg/L; tertile 3, >8.58 mg/L). Data were means ± SME. * p < 0.05 or ** p < 0.01 vs. controls, lean, no IR, or tertile 1.

markedly elevated in the IR group (7.92 ± 4.04 mg/L, $p < 0.01$; Figure 1(d)).

3.2. Association between Fetuin-B and Other Variables. Linear correlation analysis showed that there was a significant positive correlation between fetuin-B and obesity- and lipid-related (BMI, WHR, FAT%, TG, LAP, and VAI) as well as glucose-related (HbA1c, FBG, 2 h-BG, FIns, 2 h-Ins, and HOMA-IR) ($p < 0.05$ or $p < 0.01$) parameters in all subjects,

but no correlation was observed between fetuin-B and HDL-C or FFA (Table S1). Moreover, TG and WHR were independently associated with serum fetuin-B, as evident via multiple regression analysis (Figure 1(e), Table S1). The multiple regression equation was $Y_{\text{fetuin-B}} = 4.381 + 0.674 X_{\text{TG}} + 1.731 X_{\text{WHR}}$.

3.3. Relationship between Serum Fetuin-B and MetS. Logistic regression analysis demonstrated that serum fetuin-B was

TABLE 1: Main clinical features and serum fetuin-B levels in MetS and control subjects.

Variable	Controls ($n = 185$)	MetS ($n = 192$)	p
Age (years) [‡]	33.4 ± 13.1	42.2 ± 16.5	<0.001
BMI (kg/m ²)	20.9 ± 2.7	26.3 ± 3.6	<0.001
FAT (%)	26.8 ± 5.3	37.3 ± 6.1	<0.001
WHR [‡]	0.80 ± 0.07	0.98 ± 0.34	<0.001
SBP (mmHg)	112.0 ± 13.3	129.4 ± 18.9	<0.001
DBP (mmHg)	73.3 ± 10.2	81.2 ± 12.1	<0.001
TC (mmol/L)	4.18 ± 1.01	4.79 ± 1.15	<0.001
TG (mmol/L) [†]	1.02 ± 0.58	2.27 ± 1.23	<0.001
HDL-C (mmol/L) [†]	1.35 ± 0.36	1.18 ± 0.34	<0.001
LDL-C (mmol/L)	2.37 ± 0.82	2.86 ± 0.88	<0.001
FFA (μmol/L)	0.51 ± 0.23	0.63 ± 0.27	<0.001
HbA1c (%) [‡]	5.2 ± 0.3	6.2 ± 1.5	<0.001
FBG (mmol/L) [‡]	4.73 ± 0.52	6.55 ± 2.19	<0.001
2 h-BG (mmol/L) [†]	5.57 (4.85-6.44)	9.46 (7.55-12.02)	<0.001
FIns (mU/L) [†]	6.79 (5.70-8.28)	17.94 (11.46-27.51)	<0.001
2 h-Ins (mU/L) [†]	41.09 (26.13-60.29)	124.10 (67.76-221.90)	<0.001
HOMA-IR [†]	1.43 (1.16-1.78)	5.13 (3.42-7.51)	<0.001
LAP [†]	11.50 (5.36-20.71)	65.84 (48.29-89.02)	<0.001
VAI [†]	1.23 (0.85-1.74)	3.55 (2.58-4.81)	<0.001
Fetuin-B (mg/L)	6.01 ± 3.94	8.03 ± 3.75	<0.001
Fetuin-B (mg/L) [§]	6.07 ± 0.35	8.09 ± 0.33	<0.001

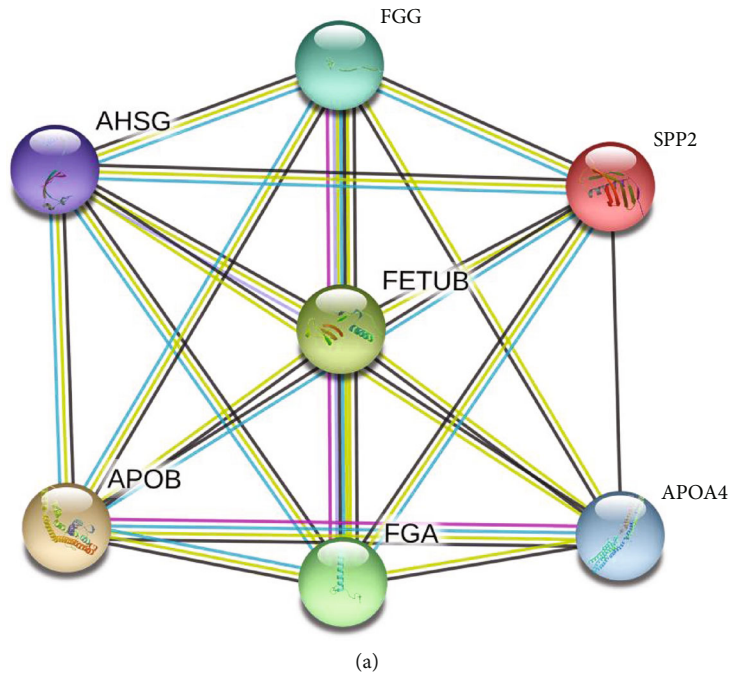
Values are given as mean ± SD or median (interquartile range). Abbreviations: BMI: body mass index; FAT%: the percentage of fat *in vivo*; WHR: waist-hip ratio; SBP: systolic blood pressure; DBP: diastolic blood pressure; TG: triglyceride; TC: total cholesterol; HDL-C: high-density lipoprotein cholesterol; LDL-C: low-density lipoprotein cholesterol; FFA: free fatty acid; FBG: fasting blood glucose; 2 h-BG: 2 h blood glucose after glucose overload; FIns: fasting plasma insulin; 2 h-Ins: 2 h plasma insulin after glucose overload; HbA1c: glycosylated hemoglobin; HOMA-IR: homeostasis model assessment of insulin resistance; LAP: lipid accumulation product; VAI: visceral adiposity index. [†]Log transformed before analysis; [‡]nonparametric tests; [§]mean ± standard error by general linear model with adjustment of age and BMI.

related to MetS (odds ratio OR, 1.150; 95% confidence interval (CI), 1.086–1.217; $p < 0.01$). This relationship persisted even after age, BMI, FAT%, HbA1c, FIns, TC, LDL, and FFA, and other possible confounding factors were controlled (Table S2). Further, the row mean score and Cochran–Armitage trend test showed a significant linear trend and independent correlation between serum fetuin-B levels and MetS (Table S3). Moreover, according to MetS components, we divided the mean levels of serum fetuin-B into six grades. Figure 1(f) shows that with an increase in MetS components, serum fetuin-B levels progressively increased (p for trend < 0.05). Individuals with 0, 1, 2, 3, 4, and 5 MetS components showed increasing serum fetuin-B levels (5.75 ± 3.49 , 6.03 ± 4.00 , 6.29 ± 4.38 , 7.75 ± 3.39 , 8.08 ± 4.05 , and 8.78 ± 3.97 mg/L, respectively). Furthermore, we divided serum fetuin-B levels into tertile 1 (≤ 5.49 mg/L), 2 (5.49 – 8.58 mg/L), and 3 (> 8.58 mg/L). The OR was calculated as an estimate of developing MetS. The risk of developing MetS in tertiles 2 and 3 was higher than that in tertile 1 (OR, 2.07; 95% CI, 1.25–3.43 for tertile 2; OR, 2.96; 95% CI, 1.78–4.94 for tertile 3; vs. tertile 1, $p < 0.01$ for all, Figure 1(g)).

3.4. Bioinformatic Analysis of Fetuin-B-Related Genes and Signaling Pathways

3.4.1. PPI Network Construction. We ranked the degree of genes enriched in metabolic pathways from high to low. The top six genes (fibrinogen alpha chain (FGA), apolipoprotein B-100 (APOB), apolipoprotein A-IV (APOA4), fibrinogen gamma chain (FGG), alpha-2-HS-glycoprotein (AHSG), and secreted phosphoprotein 24 (SPP2)) were used as the core genes for another round of enrichment (Figure 2(a)). Metabolic pathways were screened *via* REACTOME enrichment analysis, and the core genes enriched in those pathways were ranked (Figure 2(b)).

3.4.2. GO Analysis. We used $p < 0.05$ as the screening condition and arranged the results from large degree to small degree. In the case of biological processes, proteins were mainly involved in posttranslational protein modification, toll-like receptor signaling pathway, chylomicron assembly, and TG-rich lipoprotein particle remodeling. In the case of cellular components, proteins were mainly enriched in the endoplasmic reticulum lumen, endoplasmic reticulum part,



REACTOME PATHWAYS

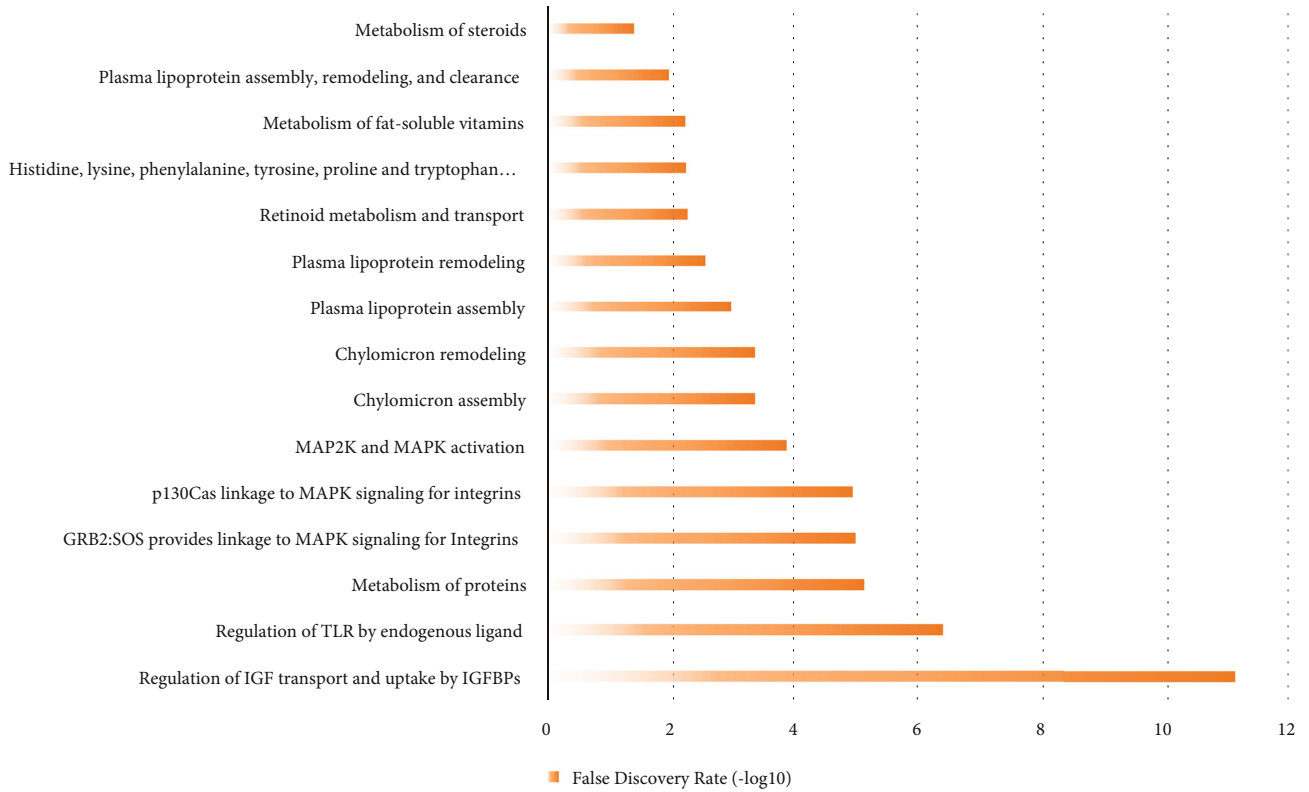


FIGURE 2: Continued.

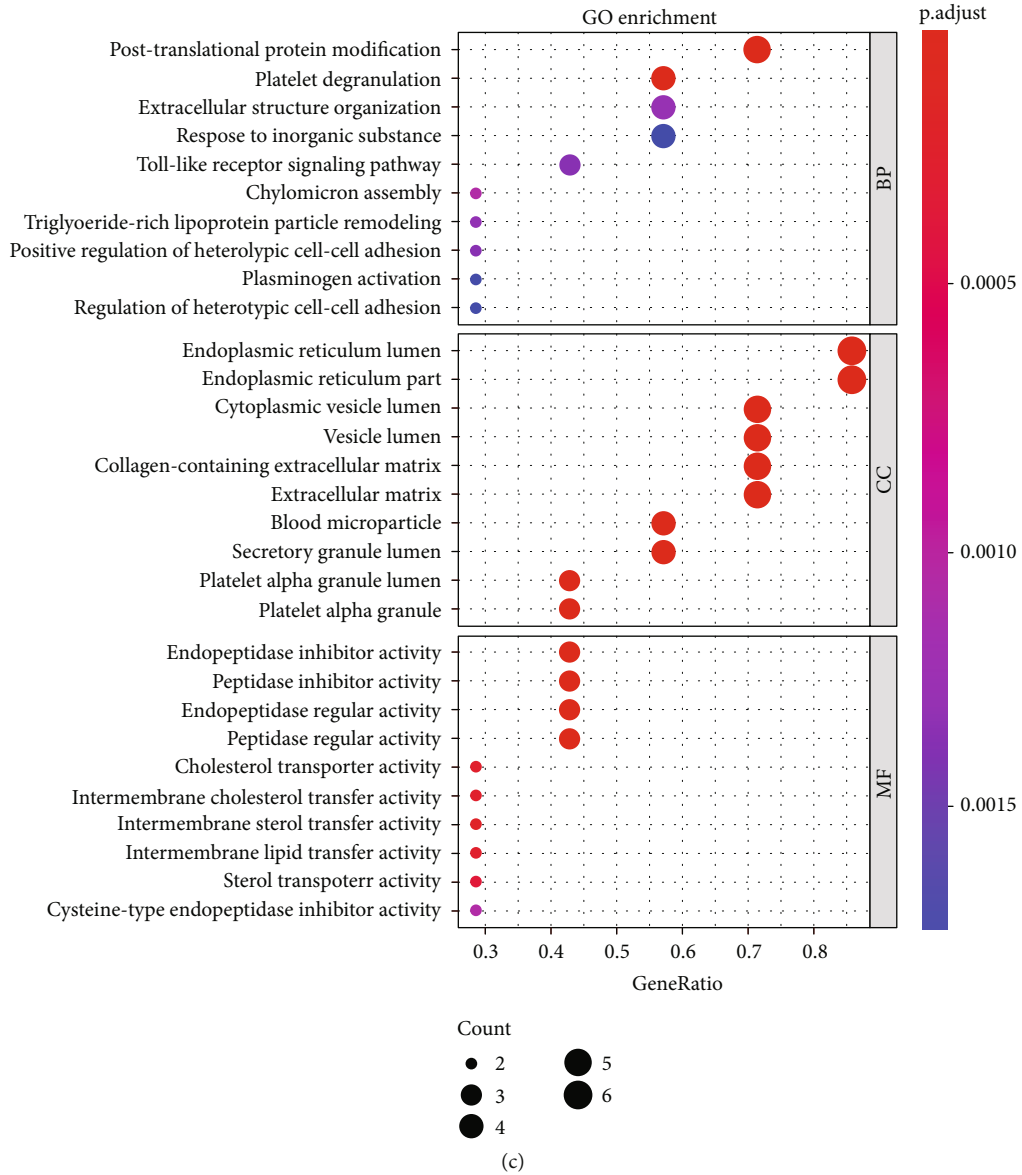


FIGURE 2: Continued.

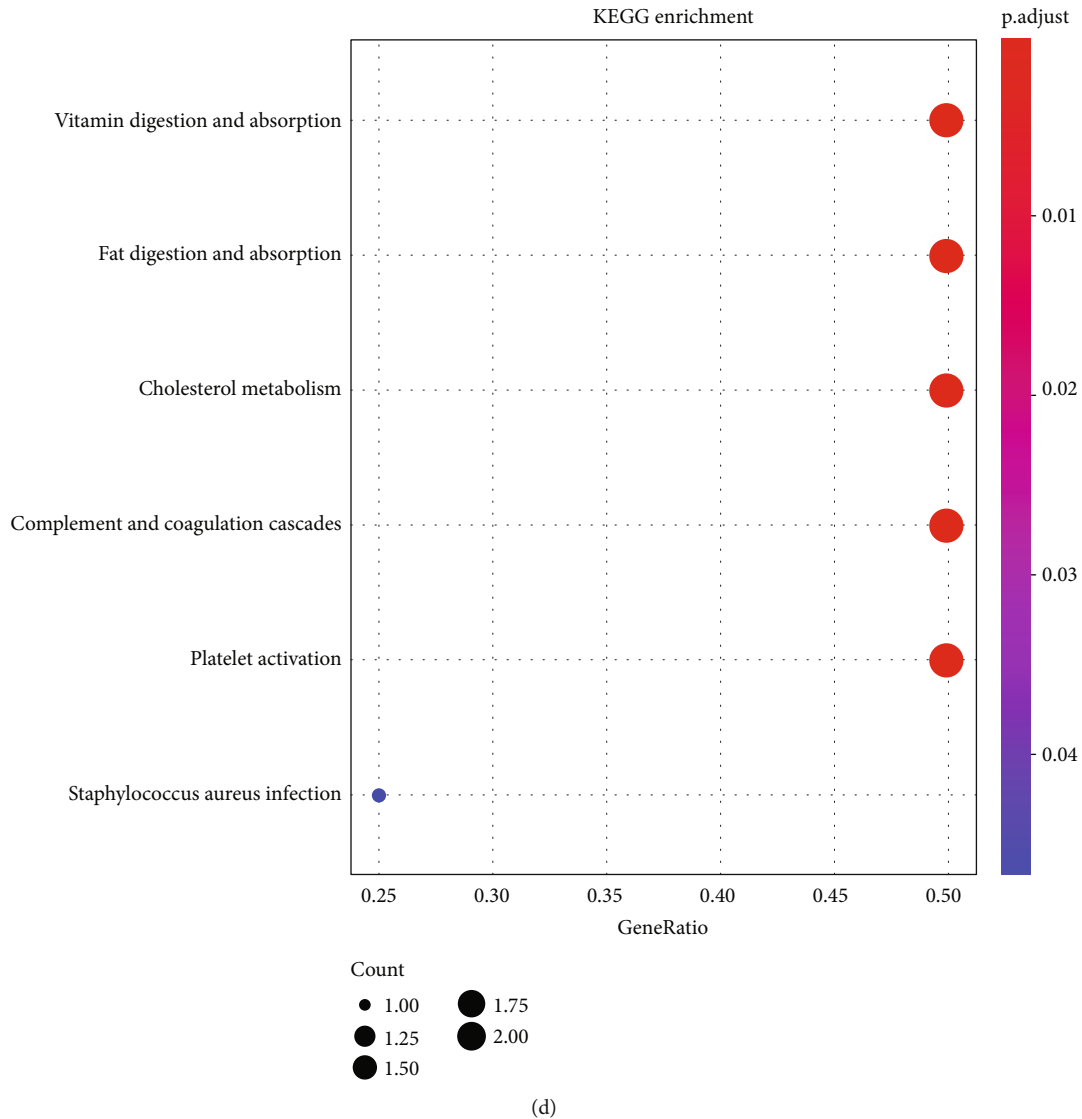


FIGURE 2: Bioinformatics analysis related to fetuin-B. (a) The PPI network through the keyword FETUB related to metabolism. (b) The enriched pathways of the REACTOME. The X-axis represents FDR. The Y-axis represents the pathway terms. The longer the bar means the more reliable the pathways. (c, d) The results of GO and KEGG analysis. The X-axis represents the ratio of involved genes, and the Y-axis represents GO and KEGG terms. The size of the bubbles indicates the number of genes involved, and each bubble represents a term. The darker the color, the smaller the p value.

and cytoplasmic vesicle lumen. Finally, in the case of molecular function, proteins were mainly involved in endopeptidase inhibitor and regulator activity, cholesterol transporter activity, and intermembrane cholesterol transfer activity (Figure 2(c)).

3.4.3. KEGG Pathway Analysis. We used $p < 0.05$ as the screening condition and ranked the p values from large to small. We found that proteins were predominantly enriched in pathways associated with vitamin digestion and absorption, fat digestion and absorption, cholesterol metabolism, complement and coagulation cascades, platelet activation, and staphylococcus aureus infection (Figure 2(d)).

3.5. Overexpression of Fetuin-B Aggravated Oxidative Stress in HepG2 Cells. It has been reported that metabolic disorder

is related to oxidative stress [25]. Therefore, we investigated the effect of fetuin-B on FFA-induced oxidative stress in HepG2 cells.

As expected, the expression of fetuin-B protein and mRNA was significantly increased in HepG2 cells transfected with pcDNA3.1-fetuin-B (Figures 3(a) and 3(b)). As shown in Figure 2(c), overexpression of fetuin-B in HepG2 cells significantly increased intracellular ROS production induced by FFAs, compared with that in control cells. Furthermore, in FFA-treated HepG2 cells, overexpression of fetuin-B significantly decreased SOD and GSH levels but increased MDA levels (Figures 3(d)–3(f)). These results indicated that fetuin-B increases oxidative stress in HepG2 cells.

3.6. Effects of Hyperglycemia and Hyperinsulinemia on Serum Fetuin-B. To understand the effects of glucose load

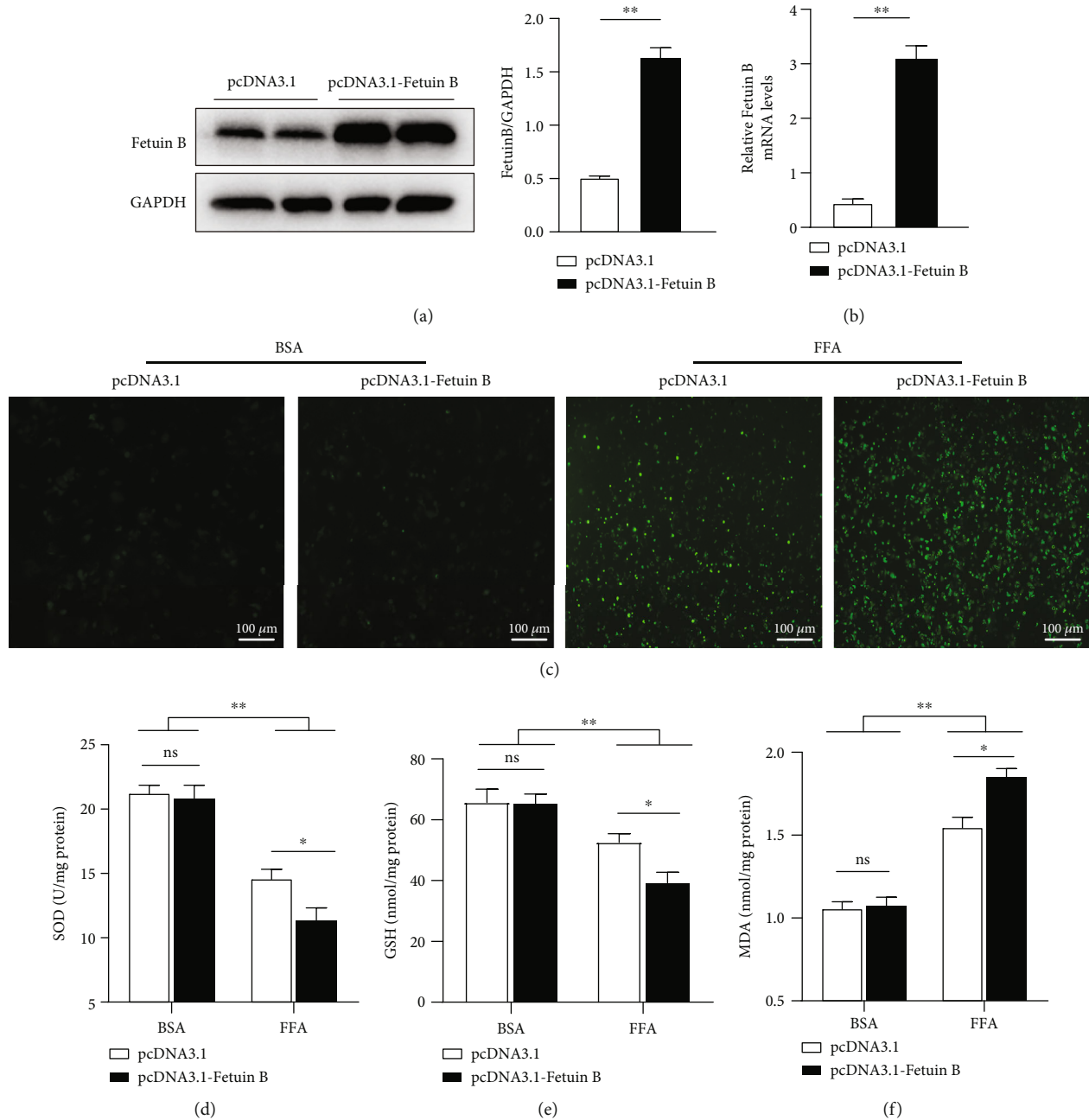
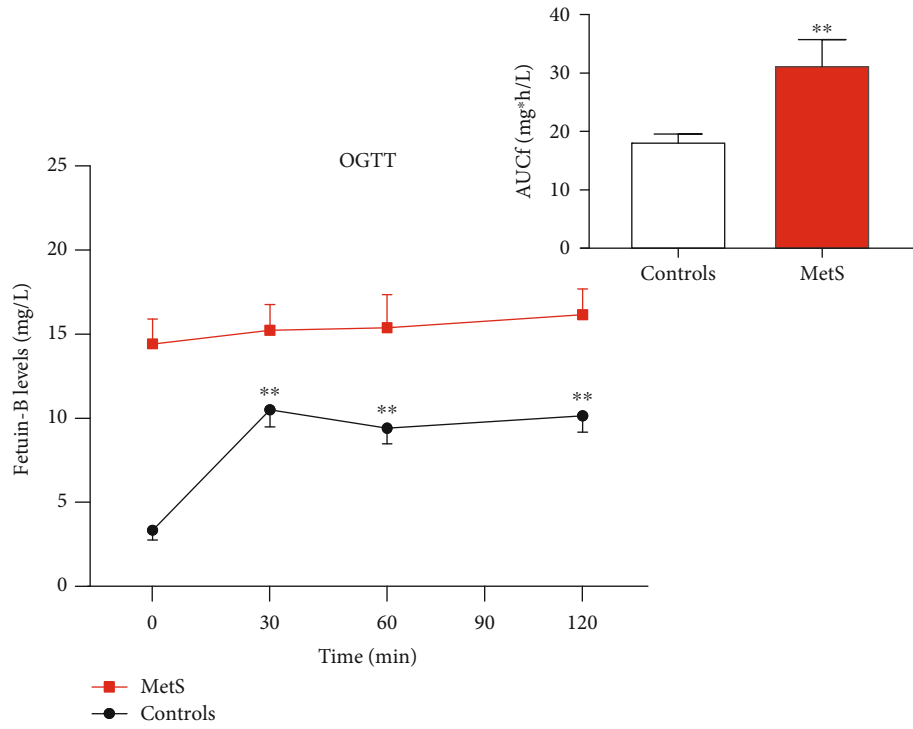


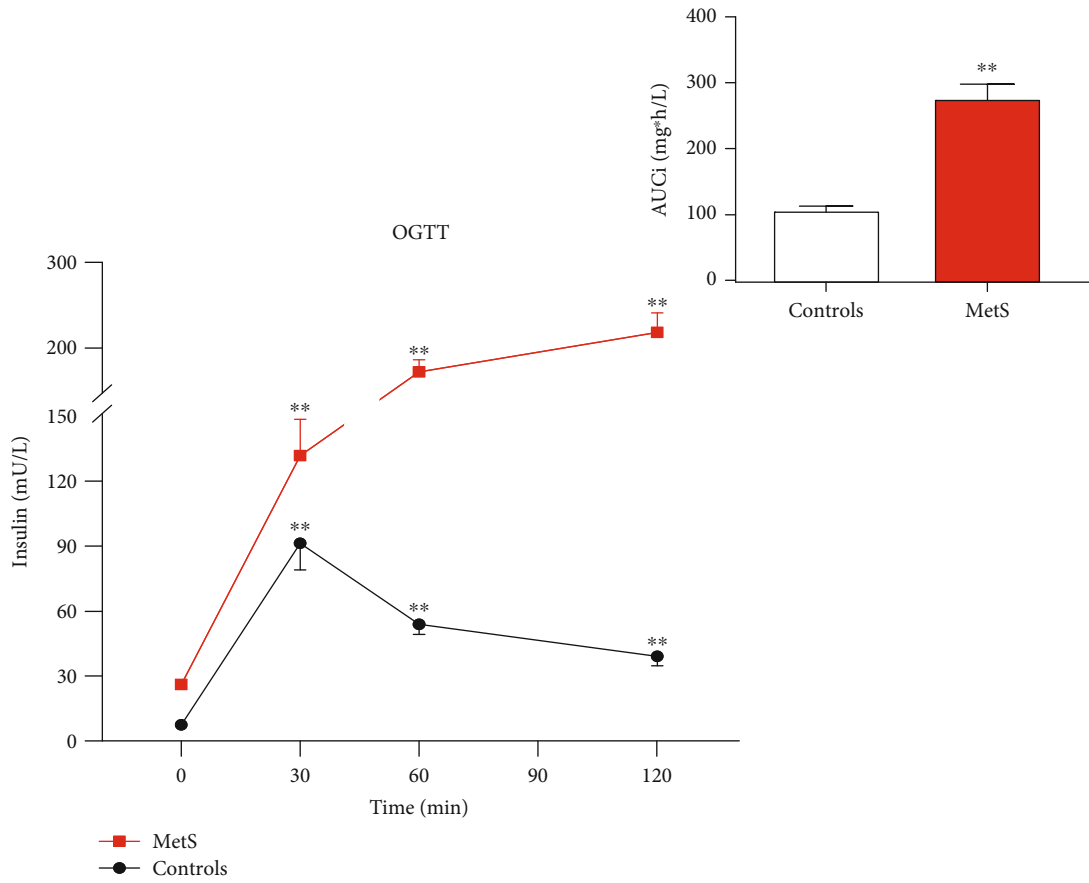
FIGURE 3: Fetuin-B exacerbated FFA-induced oxidative stress in HepG2 cells. HepG2 cells were transfected with pcDNA3.1-fetuin-B or pcDNA3.1 for 24 h and treated as indicated in the methods. (a) Fetuin-B protein expression. (b) Fetuin-B mRNA expression. (c) The level of intracellular ROS production. (d) The SOD activity. (e) The GSH production. (f) The MDA production. ROS: reactive oxygen species; SOD: superoxide dismutase; GSH: glutathione; MDA: malondialdehyde. The results were presented as the mean \pm SD. * $p < 0.05$ and ** $p < 0.01$.

on the circulating levels of fetuin-B, we performed OGTTs. In healthy women, serum fetuin-B levels were significantly higher after glucose challenge compared with the basal value, peaking at 30 min (from 3.34 ± 2.96 to 10.15 ± 5.17 mg/L) and remaining stable until the end of the experiment (Figure 4(a)). However, in patients with MetS, glucose load did not cause any significant changes in serum fetuin-B levels (Figure 4(a)). In comparison with healthy subjects, the area under the curve for fetuin-B (AUC_f) was signifi-

cantly increased in women with MetS (Figure 4(a)). During OGTTs, glucose-stimulated insulin secretion curves showed that the level of insulin secretion in women with MetS was significantly higher than that in healthy subjects and showed a peak delay; moreover, the area under the curve for insulin (AUC_i) was increased in comparison with healthy subjects, which also confirmed the existence of IR in patients with MetS (Figure 4(b)). We then performed EHCs to further explore the factors affecting the secretion of serum fetuin-B



(a)



(b)

FIGURE 4: Continued.

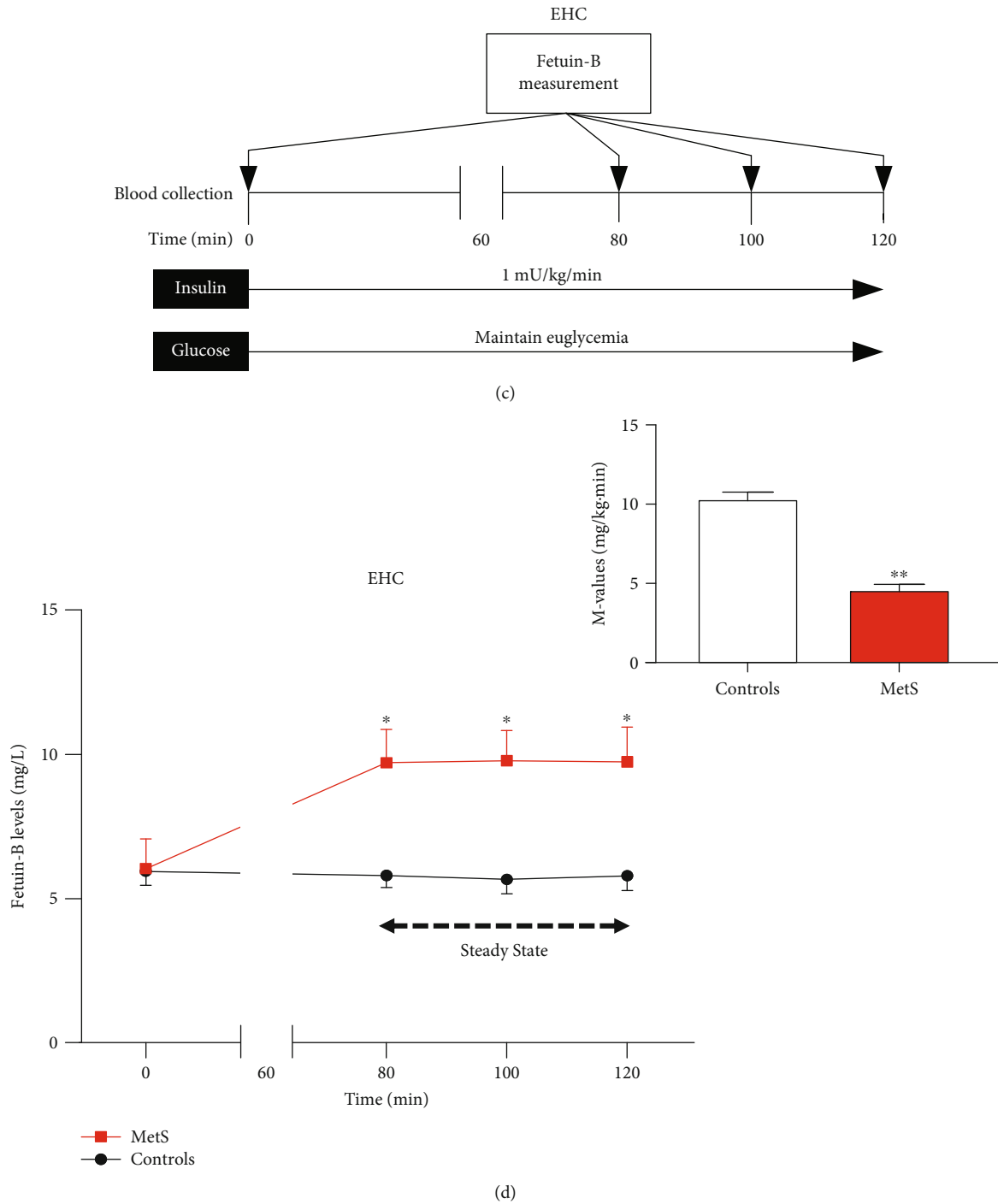
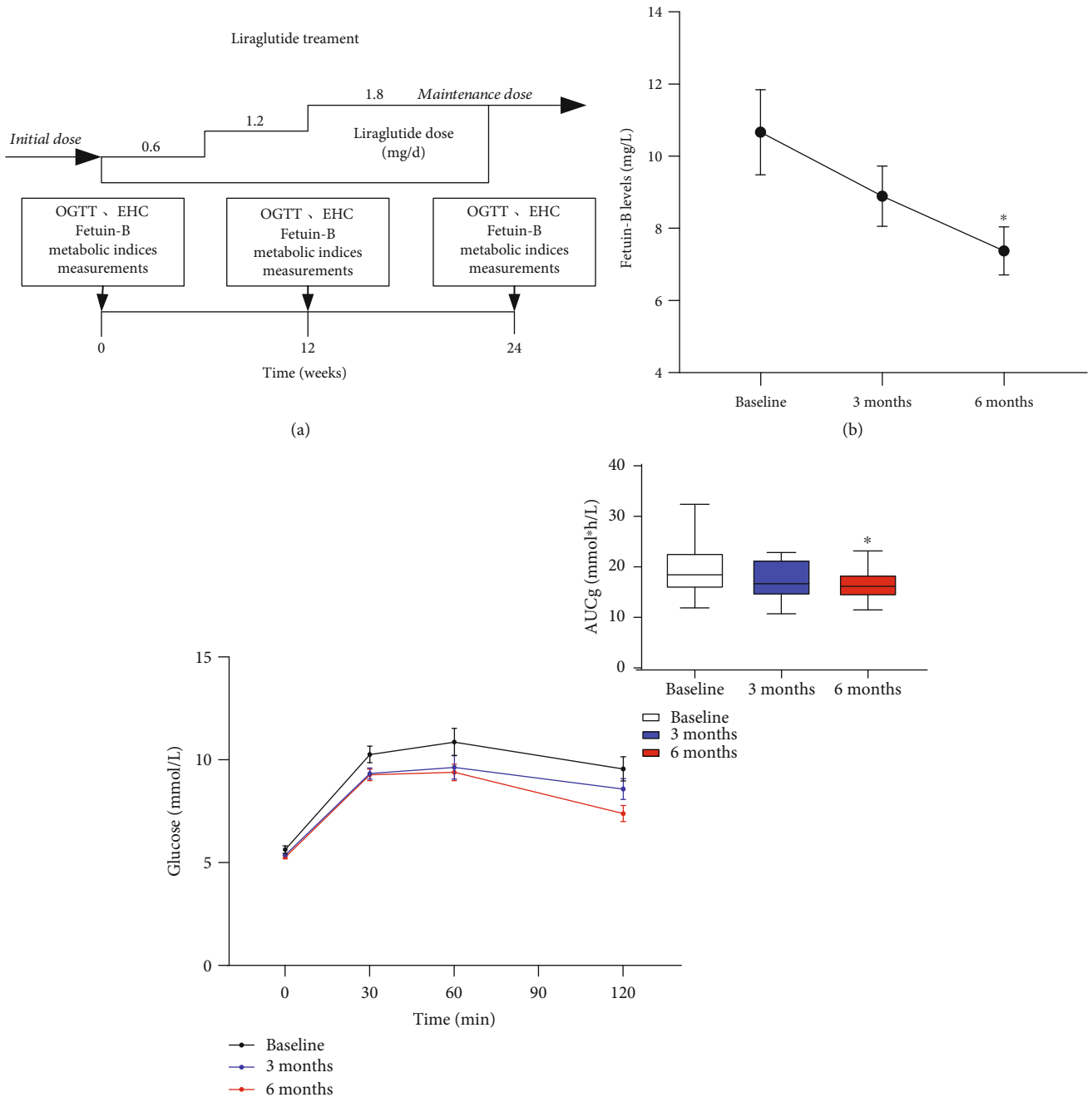


FIGURE 4: Serum fetuin-B levels in interventional studies. (a) Time course of changes in serum fetuin-B levels in healthy ($n = 15$) and MetS subjects ($n = 28$) during the OGTT and the area under the curve for serum fetuin-B (AUC_f). (b) Glucose-stimulated insulin secretion curve in healthy ($n = 15$) and MetS ($n = 28$) subjects during the OGTT and the area under the curve for insulin (AUC_i). (c) EHC protocol. (d) Time course of serum fetuin-B changes and the M values in healthy ($n = 16$) and MetS subjects ($n = 27$) during the EHC. Data were means \pm SME. * $p < 0.05$ or ** $p < 0.01$ vs. control or baseline.

(Figure 4(c)). In response to hyperinsulinemia, serum fetuin-B levels significantly increased in patients with MetS, whereas there was no change in healthy subjects (Figure 4(d)). Meanwhile, women with MetS showed lower M values than healthy women (4.47 ± 1.88 vs. 10.23 ± 2.79 mg/kg/min, $p < 0.01$; Figure 4(d)). These results indicated

that patients with MetS showed IR and that serum fetuin-B secretion might be regulated by circulating insulin levels *in vivo*.

3.7. Effects of GLP-1RA Intervention on Serum Fetuin-B Levels. Twenty-four patients with MetS participated in a



(c)

FIGURE 5: Continued.

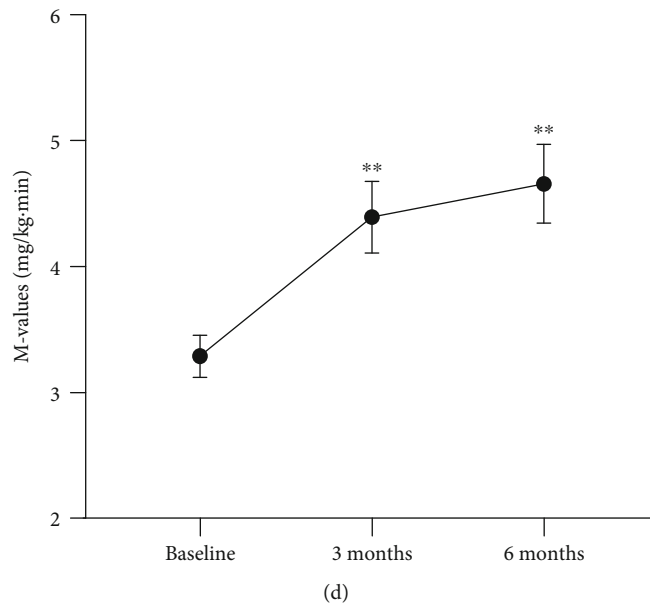


FIGURE 5: Effects of GLP-1RA treatment on serum fetuin-B and insulin sensitivity in MetS women. (a) Liraglutide treatment protocol. (b) Serum fetuin-B levels in MetS subjects after GLP-1RA treatment. (c) Blood glucose levels and the area under the curve for blood glucose (AUC_g) in MetS subjects during the OGTT after GLP-1RA treatment. (d) Changes of *M* value in MetS subjects during the EHC after GLP-1RA treatment. Data were means \pm SME. * $p < 0.05$ or ** $p < 0.01$ vs. baseline.

GLP-1RA intervention study for 6 months (Figure 5(a)). Table S4 shows the main clinical features and metabolic parameters pre- and posttreatment. In comparison with pretreatment data, markers of lipid metabolism and obesity (BMI, FAT%, TG, TC, HDL-C, LDL-C, and LAP) and parameters associated with glucose metabolism and IR (HbA1c, FIns, and HOMA-IR) were significantly ameliorated 3 months posttreatment in patients with MetS ($p < 0.01$ or $p < 0.05$). Furthermore, 6 months posttreatment, FBG, 2h-BG, and VAI also showed a significant decline ($p < 0.01$). A noticeable decline was observed in serum fetuin-B levels from 10.67 ± 4.87 mg/L pretreatment to 8.90 ± 3.45 mg/L 3 months posttreatment and 7.38 ± 2.74 mg/L 6 months posttreatment (Figure 5(b)). In addition, blood glucose levels at 120 min and the area under the curve for glucose (AUC_g, 16.68 ± 2.79 vs. 19.46 ± 4.74 mmol/h/L, $p < 0.05$) during OGTTs were significantly lower than before GLP-1RA intervention (Figure 5(c)). In comparison with pretreatment data, *M* values during EHCs were significantly higher at both 3 and 6 months posttreatment (4.39 ± 1.30 and 4.66 ± 1.53 vs. 3.29 ± 0.82 , $p < 0.01$ for all; Figure 5(d)). These data further confirmed that fetuin-B levels decreased *in vivo* with an improvement in IR.

4. Discussion

Fetuin-B, which is believed to be a hepatokine and/or adipokine, is mainly expressed in the liver and white adipose tissue, placenta, and heart, and it is evidently strongly associated with energy metabolism [6]. Several case-controlled and cross-sectional studies have reported that serum fetuin-B levels are markedly elevated in patients with nonalcoholic fatty liver disease, T2DM, gestational diabetes mellitus, and polycystic ovary syndrome [11–13]. However,

only a few studies have explored the relationship between fetuin-B and MetS in humans, and the pathophysiological mechanism remains unclear. In this study, women were selected for eliminating the interference of gender differences. Serum fetuin-B levels were significantly elevated in women with MetS. In addition, fetuin-B was positively related to lipid- and glucose-related parameters and independently associated with MetS. As expected, in addition, fetuin-B overexpression aggravated oxidative stress *in vitro*. Therefore, our results suggest that fetuin-B impacts glucose and lipid metabolism and antioxidant stress, which is closely related to the occurrence and development of MetS. However, the cause of elevated fetuin-B levels in patients with MetS remains unknown. We believe that an increase in serum fetuin-B levels in patients with MetS can be attributed to elevated metabolic stress, involving, for example, hyperinsulinemia, dyslipidosis, and antioxidative disorder. These disorders stimulate fetuin-B release and secretion; nevertheless, further studies are warranted.

Meex et al. recently reported that fetuin-B silencing in obese mice improved glucose tolerance but did not affect body weight. In the case of humans, they found that serum fetuin-B was positively associated with fasting insulin and HOMA-IR, but no correlation was observed between serum fetuin-B and markers of obesity, inflammation, and blood fat [7]. Another study in women with gestational diabetes mellitus reported that serum fetuin-B had no association with obesity, hypertension, and dyslipidemia [13]. In addition, Qu et al. found that serum fetuin-B in patients with T2DM showed a significant positive association with TG, but no association was observed with other lipids or BMI [10]. However, herein, serum fetuin-B levels were noticeably elevated in overweight/obese women compared with lean women, and they were associated with BMI, LAP, and

VAI; furthermore, TG and WHR were independently associated with serum fetuin-B. These data suggest that serum fetuin-B is associated with lipid metabolism and obesity. The precise reason for the discrepancy in our results and those reported by previous studies is unknown, but we believe that the discrepancy could be due to the higher BMI of patients with MetS included in this study. The association between fetuin-B and obesity thus remains ambiguous.

To further explore the association between fetuin-B and glucose and lipid metabolism, we performed bioinformatics analysis to identify related core genes and signaling pathways. Through the construction of a PPI network, we identified six fetuin-B-related proteins; they were enriched in pathways related to glucose and lipid metabolism, which formed the core of the PPI network. Among the identified proteins, alpha-2-HS-glycoprotein is reportedly associated with IR and diabetes [26, 27]; fibrinogen alpha chain with chronic inflammation, lipid metabolism, and diabetic complications [28]; and fibrinogen gamma chain and secreted phosphoprotein 24 with lipid metabolism and obesity [29]. Secreted phosphoprotein 24 is also involved in glucose and lipid metabolism [30]. Apolipoprotein A-IV and apolipoprotein B-100 are closely related to glucose and lipid metabolism, IR, and polycystic ovary syndrome [31–34]. Based on GO and KEGG pathway analysis, fetuin-B-related proteins were found to be involved in, for example, fat absorption and cholesterol metabolism. Therefore, consistent with the results of our population-based study, bioinformatics analysis revealed that fetuin-B is closely related to lipid metabolism and IR, ultimately leading to occurrence and development of MetS.

It has been well established that oxidative stress induced by lipid metabolism disorder is one of the important causes of IR [35]. However, whether fetuin-B promotes IR is related to oxidative stress remains unknown. In this experiment, we investigated the effect of fetuin-B on FFA-induced oxidative stress *in vitro*. The results demonstrated that fetuin-B overexpression aggravated oxidative stress by increasing ROS and MDA production and inhibiting SOD activity and GSH production. Meanwhile, Zhou et al. reported that hepatic knockdown of fetuin-B activated the AMP-activated protein kinase (AMPK) pathway to inhibit lipogenesis [21]. Fetuin-B silencing in obese mice improved glucose tolerance and IR [7]. This further supported our hypothesis that fetuin-B may aggravate metabolic disorder and IR in MetS individuals by promoting oxidative stress.

To evaluate whether blood glucose and insulin affect fetuin-B secretion, we performed OGTTs to observe changes in serum fetuin-B levels *in vivo*. A significant increase in serum fetuin-B levels was observed in healthy subjects, but patients with MetS showed no change. These results indicated that hyperglycemia and/or hyperinsulinemia promote fetuin-B secretion in healthy individuals.

EHC is the gold standard technique for evaluating IR in both humans and animals. During EHC, under the conditions of hyperinsulinemia and euglycemia, serum fetuin-B levels did not change in healthy subjects; however, a significant increase in serum fetuin-B levels was observed in

patients with MetS. Therefore, we believe that hyperglycemia, not hyperinsulinemia, is the main factor affecting serum fetuin-B levels in healthy individuals. In patients with MetS, elevated insulin levels led to an increase in serum fetuin-B levels, while hyperglycemia inhibited fetuin-B release. Therefore, serum fetuin-B levels did not change during OGTTs under the conditions of hyperglycemia and hyperinsulinemia. However, the cause of this phenomenon is unknown. Meex et al. suggested that fetuin-B might regulate glucose metabolism by reducing glucose effectiveness or by another unknown insulin-independent mechanism [7]. Similar results were reported by another study [8]. In contrast, our human studies demonstrated that hyperglycemia may lead to an increase in fetuin-B levels in healthy women but inhibit fetuin-B release in patients with MetS. It remains unclear whether feedback regulation exists between fetuin-B and glucose. Moreover, as evident from our EHC results, *M* values showed significant differences between the groups. The difference between our results and those of previous studies could be attributed to long-term metabolic disorders and IR in women with MetS, but further studies need to be conducted to validate such findings.

Liraglutide is a GLP-1RA and is used for treatment of T2DM and obesity; it has beneficial effects on various metabolic parameters and is one of the preferred drugs for improving IR [36, 37]. In previous studies, we found that liraglutide promotes the secretion of some adipokines, such as adiponectin and visfatin *in vivo* [38, 39]. In this study, we found that GLP-1RA treatment for 6 months led to a significant decrease in serum fetuin-B levels, which was accompanied by ameliorated glucose metabolism and IR, as indicated by increased *M* values. Therefore, it is possible that chronic hyperinsulinemia related to IR results in an increase in fetuin-B levels. This indicates that the effect of liraglutide on fetuin-B levels is at least partially mediated by GLP-1RA-induced changes in insulin levels, which is secondary to the role of GLP-1RA in enhancing insulin sensitivity. These results further suggest that fetuin-B is associated with IR and MetS and also demonstrate a beneficial role of GLP-1RA in affecting fetuin-B secretion and release *in vivo*. Based on these data, it is apparent that fetuin-B levels tend to be lower in the state of insulin sensitivity and higher in the state of IR. Previous studies have found that GLP-1RA regulated the expression of lipid metabolism-related genes and delayed the cellular senescence by alleviating oxidative stress and inflammatory reaction [40]. A recent study has shown that liraglutide significantly reduced ROS production but increased SOD activity in high fat-treated HepG2 cells [41]. We found for the first time that the decrease of fetuin-B in MetS patients after liraglutide treatment may also be related to its antioxidation. However, more studies were needed to confirm our conjecture.

Our study has some limitations: (1) considering the cross-sectional design of this study, our results do not prove causal relationships; (2) we included a relatively small sample size, particularly in intervention experiments; therefore, our data may be affected by outliers; (3) this cohort included only Chinese women and did not include men. Therefore, our findings should be applied cautiously to other ethnic

populations; and (4) the study failed to investigate the specific signal pathways by which fetuin-B affects hepatocytes. However, we included patients who were newly diagnosed with MetS and those without any lifestyle intervention and drug treatments, thereby avoiding the interference of disease course and other confounding factors. In addition, we performed various intervention experiments *in vivo* and *in vitro*, including EHC, to evaluate the association between fetuin-B and metabolism and IR. Thus, our data provide sufficient evidence to confirm that an association is present between fetuin-B and MetS in women.

5. Conclusions

We report that serum fetuin-B levels are elevated in women with MetS and that is related to glucose and lipid metabolism and IR. Using multiple interventions, including EHCs, OGTTs, and treatment with a GLP-1RA, we also found that serum fetuin-B was affected by blood glucose, insulin, and GLP-1RA *in vivo*. Additionally, fetuin-B overexpression aggravated oxidative stress *in vitro*. Therefore, we believe that fetuin-B can serve as a biomarker for screening MetS in women.

Abbreviations

T2DM:	Type 2 diabetes mellitus
MetS:	Metabolic syndrome
OGTT:	Oral glucose tolerance test
EHC:	Euglycemic-hyperinsulinemic clamp
GLP-1RA:	Glucagon-like peptide-1 receptor agonists
WHR:	Waist-to-hip ratio
FAT%:	Fat percentage <i>in vivo</i>
TG:	Triglyceride
FBG:	Fasting blood glucose
FIns:	Fasting plasma insulin
HbA1c:	Glycosylated hemoglobin
HOMA-IR:	Homeostasis model assessment of insulin resistance
LAP:	Lipid accumulation product
VAI:	Visceral adiposity index
SOD:	Superoxide dismutase
GSH:	Glutathione
MDA:	Malondialdehyde
ROS:	Reactive oxygen species.

Data Availability

All the data used to support the findings of this study are available from the corresponding author upon request.

Conflicts of Interest

The authors declare that there is no conflict of interest regarding the publication of this paper.

Authors' Contributions

S.X., H.H., S.R., M.Y., and S.G. researched and analyzed data. B.Z., Y.H., and H.L. reviewed and edited the manu-

script. C.C. revised English. L.L. and G.Y. wrote and edited the manuscript. L.L. is the guarantor of this work and, as such, had full access to all of the data in the study and take responsibility for the integrity of the data and the accuracy of the data analysis. Shiyao Xue, Hongdong Han, and Shunli Rui contributed equally to this project.

Acknowledgments

This work was supported by research grants from the National Natural Science Foundation of China (81300670) and from the Science and Technology Program of Health Bureau of Chongqing (2019ZDXM039). We thank patients and healthy individuals who made this study possible.

Supplementary Materials

Table S1: correlation analysis of variables associated with circulating fetuin-B levels in study population. Table S2: association of serum fetuin-B levels with MetS in fully adjusted models. Table S3: row mean scores and Cochran-Armitage trend test of the impact of circulating fetuin-B levels on MetS individuals. Table S4: main clinical and metabolic features pre- and posttreatment with GLP-1RA in MetS women. (*Supplementary Materials*)

References

- [1] R. H. Eckel, K. G. M. M. Alberti, S. M. Grundy, and P. Z. Zimmet, "The metabolic syndrome," *The Lancet*, vol. 375, no. 9710, pp. 181–183, 2010.
- [2] M. G. Saklayen, "The global epidemic of the metabolic syndrome," *Current Hypertension Reports*, vol. 20, no. 2, p. 12, 2018.
- [3] J. B. Meigs, M. K. Rutter, L. M. Sullivan, C. S. Fox, R. B. D'Agostino Sr., and P. W. Wilson, "Impact of insulin resistance on risk of type 2 diabetes and cardiovascular disease in people with metabolic syndrome," *Diabetes Care*, vol. 30, no. 5, pp. 1219–1225, 2007.
- [4] S. M. Grundy, B. Hansen, S. C. Smith, J. I. Cleeman, R. A. Kahn, and for Conference Participants, "Clinical management of metabolic syndrome," *Circulation*, vol. 109, no. 4, pp. 551–556, 2004.
- [5] E. Ford, "Risks for all-cause mortality, cardiovascular disease, and diabetes associated with the metabolic syndrome: a summary of the evidence," *Diabetes Care*, vol. 28, no. 7, pp. 1769–1778, 2005.
- [6] E. Olivier, E. Soury, P. Ruminy et al., "Fetuin-B, a second member of the fetuin family in mammals," *The Biochemical Journal*, vol. 350, no. 2, pp. 589–597, 2000.
- [7] R. C. Meex, A. J. Hoy, A. Morris et al., "Fetuin B is a secreted hepatocyte factor linking steatosis to impaired glucose metabolism," *Cell Metabolism*, vol. 22, no. 6, pp. 1078–1089, 2015.
- [8] A. Peter, M. Kovarova, H. Staiger et al., "The hepatokines fetuin-A and fetuin-B are up-regulated in the state of hepatic steatosis and may differently impact on glucose homeostasis in humans," *American Journal of Physiology-Endocrinology and Metabolism*, vol. 314, no. 3, pp. E266–E273, 2018.
- [9] D. Wang, Y. Liu, S. Liu et al., "Serum fetuin-B is positively associated with intrahepatic triglyceride content and increases the risk of insulin resistance in obese Chinese adults: a cross-

- sectional study," *Journal of Diabetes*, vol. 10, no. 7, pp. 581–588, 2018.
- [10] H. Qu, Y. Qiu, Y. Wang, Y. Liao, Y. Zheng, and H. Zheng, "Plasma fetuin-B concentrations are associated with insulin resistance and first-phase glucose-stimulated insulin secretion in individuals with different degrees of glucose tolerance," *Diabetes & Metabolism*, vol. 44, no. 6, pp. 488–492, 2018.
- [11] Z. Li, M. Lin, C. Liu et al., "Fetuin-B links nonalcoholic fatty liver disease to type 2 diabetes via inducing insulin resistance: association and path analyses," *Cytokine*, vol. 108, pp. 145–150, 2018.
- [12] A. Adamska, A. M. Polak, A. Krentowska et al., "Increased serum fetuin-B concentration is associated with homa-beta and indices of liver steatosis in women with polycystic ovary syndrome: a pilot study," *Endocrine Connections*, vol. 8, pp. 1159–1167, 2019.
- [13] S. Kralisch, A. Hoffmann, U. Lössner et al., "Regulation of the novel adipokines/hepatokines fetuin A and fetuin B in gestational diabetes mellitus," *Metabolism*, vol. 68, pp. 88–94, 2017.
- [14] S. Xue, Y. Ren, M. Yang et al., "High serum fetuin-B levels are associated with the presence of metabolic syndrome in women: a case-controlled study and interventional studies," *Researchsquare*, 2020.
- [15] S. M. Grundy, J. I. Cleeman, S. R. Daniels et al., "Diagnosis and management of the metabolic Syndrome," *Circulation*, vol. 112, no. 17, pp. 2735–2752, 2005.
- [16] D. A. American, "Diagnosis and classification of diabetes mellitus," *Diabetes Care*, vol. 35, Supplement_1, pp. S64–S71, 2012.
- [17] M. Yang, R. Liu, S. Li et al., "Zinc-2-Glycoprotein is associated with insulin resistance in humans and is regulated by hyperglycemia, hyperinsulinemia, or liraglutide Administration: Cross-sectional and interventional studies in normal subjects, insulin-resistant subjects, and subjects with newly diagnosed diabetes," *Diabetes Care*, vol. 36, no. 5, pp. 1074–1082, 2013.
- [18] D. Szklarczyk, J. H. Morris, H. Cook et al., "The STRING database in 2017: quality-controlled protein–protein association networks, made broadly accessible," *Nucl Acids Research*, vol. 45, pp. D362–D3D8, 2017.
- [19] B. Jassal, L. Matthews, G. Viteri et al., "The reactome pathway knowledgebase," *Nucleic Acids Research*, vol. 48, pp. D498–D503, 2019.
- [20] G. Yu, L. G. Wang, Y. Han, and Q. Y. He, "clusterProfiler: an R package for comparing biological themes among gene clusters," *OMICS*, vol. 16, no. 5, pp. 284–287, 2012.
- [21] W. Zhou, J. Yang, J. Zhu et al., "Fetuin B aggravates liver X receptor-mediated hepatic steatosis through AMPK in Hep G2 cells and mice," *American Journal of Translational Research*, vol. 11, pp. 1498–1509, 2019.
- [22] A. Valsesia, W. H. M. Saris, A. Astrup, J. Hager, and M. Masoodi, "Distinct lipid profiles predict improved glycemic control in obese, nondiabetic patients after a low-calorie diet intervention: the diet, obesity and genes randomized trial," *The American Journal of Clinical Nutrition*, vol. 104, no. 3, pp. 566–575, 2016.
- [23] M. C. Amato, C. Giordano, M. Galia et al., "Visceral adiposity index: a reliable indicator of visceral fat function associated with cardiometabolic risk," *Diabetes Care*, vol. 33, no. 4, pp. 920–922, 2010.
- [24] G. Bedogni, H. Kahn, S. Bellentani, and C. Tiribelli, "A simple index of lipid overaccumulation is a good marker of liver steatosis," *BMC Gastroenterology*, vol. 10, no. 1, p. 98, 2010.
- [25] S. Spahis, J. Borys, and E. Levy, "Metabolic syndrome as a multifaceted risk factor for oxidative stress," *Antioxidants & Redox Signaling*, vol. 26, no. 9, pp. 445–461, 2017.
- [26] Y. Wang, W. Koh, M. Jensen, J. Yuan, and A. Pan, "Plasma fetuin-A levels and risk of type 2 diabetes mellitus in a Chinese population: a nested case-control study," *Diabetes and Metabolism Journal*, vol. 43, no. 4, pp. 474–486, 2019.
- [27] J. I. Heo, D. W. Yoon, J. H. Yu et al., "Melatonin improves insulin resistance and hepatic steatosis through attenuation of alpha-2-HS-glycoprotein," *Journal of Pineal Research*, vol. 65, no. 2, article e12493, 2018.
- [28] M. Zhang, G. Fu, and T. Lei, "Two urinary peptides associated closely with type 2 diabetes mellitus," *PLoS One*, vol. 10, no. 4, article e0122950, 2015.
- [29] M. Insenser, R. Montes-Nieto, N. Vilarrasa et al., "A nontargeted proteomic approach to the study of visceral and subcutaneous adipose tissue in human obesity," *Molecular and Cellular Endocrinology*, vol. 363, no. 1–2, pp. 10–19, 2012.
- [30] P. Hebbar, R. Nizam, M. Melhem et al., "Genome-wide association study identifies novel recessive genetic variants for high TGs in an Arab population," *Journal of Lipid Research*, vol. 59, no. 10, pp. 1951–1966, 2018.
- [31] Z. Wang, L. Wang, Z. Zhang, L. Feng, X. Song, and J. Wu, "Apolipoprotein A-IV involves in glucose and lipid metabolism of rat," *Nutrition & Metabolism*, vol. 16, no. 1, p. 41, 2019.
- [32] Y. S. Kim, B. H. Gu, B. C. Choi et al., "Apolipoprotein A-IV as a novel gene associated with polycystic ovary syndrome," *International Journal of Molecular Medicine*, vol. 31, no. 3, pp. 707–716, 2013.
- [33] V. Lamantia, S. Bissonnette, H. Wassef et al., "ApoB-lipoproteins and dysfunctional white adipose tissue: Relation to risk factors for type 2 diabetes in humans," *Journal of Clinical Lipidology*, vol. 11, no. 1, pp. 34–45.e2, 2017.
- [34] D. F. Vine, Y. Wang, M. M. Jetha, G. D. C. Ball, and S. D. Proctor, "Impaired Apo B-lipoprotein and triglyceride metabolism in obese adolescents with polycystic ovary syndrome," *The Journal of Clinical Endocrinology and Metabolism*, vol. 102, pp. 970–982, 2017.
- [35] J. Meigs, M. Larson, C. Fox, J. Keaney, R. Vasani, and E. Benjamin, "Association of oxidative stress, insulin resistance, and diabetes risk phenotypes: the Framingham Offspring Study," *Diabetes Care*, vol. 30, no. 10, pp. 2529–2535, 2007.
- [36] M. Rizzo, A. A. Rizvi, A. M. Patti et al., "Liraglutide improves metabolic parameters and carotid intima-media thickness in diabetic patients with the metabolic syndrome: an 18-month prospective study," *Cardiovascular Diabetology*, vol. 15, no. 1, p. 162, 2016.
- [37] A. Astrup, S. Rössner, L. van Gaal et al., "Effects of liraglutide in the treatment of obesity: a randomised, double-blind, placebo-controlled study," *The Lancet*, vol. 374, no. 9701, pp. 1606–1616, 2009.
- [38] L. Li, G. Yang, Q. Li et al., "Exenatide prevents fat-induced insulin resistance and raises adiponectin expression and plasma levels," *Diabetes, Obesity & Metabolism*, vol. 10, no. 10, pp. 921–930, 2008.
- [39] L. Li, Z. Miao, R. Liu, M. Yang, H. Liu, and G. Yang, "Liraglutide prevents hypo adiponectinemia-induced insulin resistance

and alterations of gene expression involved in glucose and lipid metabolism,” *Molecular Medicine*, vol. 17, no. 11-12, pp. 1168–1178, 2011.

- [40] Y. Oh and H. Jun, “Effects of glucagon-like peptide-1 on oxidative stress and Nrf 2 signaling,” *International Journal of Molecular Sciences*, vol. 19, 2018.
- [41] C. Zhu, Y. Luo, H. Wang et al., “Liraglutide ameliorates lipotoxicity-induced oxidative stress by activating the NRF2 pathway in HepG2 cells,” *Hormone and Metabolic Research*, vol. 52, no. 7, pp. 532–539, 2020.

Research Article

Crocetin Exerts Its Anti-inflammatory Property in LPS-Induced RAW264.7 Cells Potentially via Modulation on the Crosstalk between MEK1/JNK/NF- κ B/iNOS Pathway and Nrf2/HO-1 Pathway

Yi-Ling Wen,¹ Ziyu He,² De-Xing Hou,² and Si Qin ^{1,2}

¹Key Laboratory for Food Science and Biotechnology of Hunan Province, College of Food Science and Technology, Hunan Agricultural University, Changsha 410128, China

²The United Graduate School of Agricultural Sciences, Faculty of Agriculture, Kagoshima University, Korimoto 1-21-24, Kagoshima 890-0065, Japan

Correspondence should be addressed to Si Qin; qinsiman@hunau.edu.cn

Received 26 November 2020; Revised 17 July 2021; Accepted 13 August 2021; Published 10 September 2021

Academic Editor: Alin Ciobica

Copyright © 2021 Yi-Ling Wen et al. This is an open access article distributed under the Creative Commons Attribution License, which permits unrestricted use, distribution, and reproduction in any medium, provided the original work is properly cited.

Crocetin is a main bioactive component with a carotenoid skeleton in *Gardenia jasminoides*, a typical traditional Chinese medicine with a long history in Southeast Asia. Crocetin is being commonly consumed as spices, dyes, and food colorants. Recent pharmacological studies had implied that crocetin may possess potent anti-inflammatory properties; however, the underlying molecular mechanism is not fully elucidated. In the present study, the regulatory effect of crocetin on redox balance was systematically investigated in lipopolysaccharide- (LPS-) stimulated RAW264.7 cells. The results showed that crocetin dose-dependently inhibited LPS-induced nitric oxide production and inducible nitric oxide synthase (iNOS) expression in RAW264.7 cells. Molecular data revealed that crocetin exerted its anti-inflammatory property by inhibiting the MEK1/JNK/NF- κ B/iNOS pathway and activating the Nrf2/HO-1 pathway. The shRNA-knockdown (KD) of MEK1 and ERK1 confirmed that the activation of MEK1 and inhibition of JNK mediated the anti-inflammatory effect of crocetin. Moreover, the pull-down assay and computational molecule docking showed that crocetin could directly bind to MEK1 and JNK1/2. It is noticed that both KD and knockout (KO) of *HO-1* gene blocked this action. More detailed data have shown that *HO-1*-KO blocked the inhibition of p-I κ B- α by crocetin. These data indicated that crocetin exerted its anti-inflammatory property via modulating the crosstalk between the MEK1/JNK/NF- κ B/iNOS pathway and the Nrf2/HO-1 pathway, highlighting HO-1 as a major player. Therefore, the present study reveals that crocetin can act as a potential candidate for redox-balancing modulation in charge of its anti-inflammatory and chemopreventive effect, which strengthens its potency in the subsequent clinic application in the near future.

1. Introduction

Gardenia jasminoides is widely planted in China, Japan, Korea, India, and North America [1]. As a traditional and crucial herbal medicine, *Gardenia jasminoides* is recorded in Chinese Pharmacopoeia, with multiple functions on clearing heat and detoxifying, reducing fever and headache, causing diuresis, cooling blood, and eliminating swelling [2, 3]. Plenty of pharmacological studies had found that *Gardenia jasminoides* can possess various pharmacological activities

in hepatochemoprevention [4, 5], neuroprotection [6], anti-inflammatory regulation [7, 8], and antithrombotic and cardiovascular intervention [1, 9, 10]. In addition, it is also widely applied as an excellent natural colorant. Crocetin, as the major natural colorant in *Gardenia jasminoides*, has been used in many fields, such as cotton, textiles, beverages, and food. The beneficial characteristics and pharmacological activities of crocetin have also been reported previously, including the chemopreventive effect on tumors [11–13], neurodegeneration [14–16], cardiovascular disease [17, 18],

hepatic damage [19, 20], diabetes [21–23], and colitis diseases [24]. Molecular mechanism studies suggested that crocetin's biological activity may be attributed to its anti-inflammatory ability [14, 25]. However, the underlying molecular mechanism of its anti-inflammatory ability has not been fully elucidated.

Nitric oxide (NO), a highly reactive gas signal molecule, is involved in various physiological and pathological processes in many organ systems including nervous, immune, and cardiovascular [26, 27]. The production of NO is precisely regulated by nitric oxide synthase (NOS). There are three isozymes of NOS: the two constitutively expressed forms, endothelial NOS (eNOS) and neuronal NOS (nNOS), and the inducible form (iNOS) [28]. Significantly, high-level iNOS expression is associated with various inflammations and chronic diseases, such as stroke, demyelinating diseases, cancer, and neurodegenerative diseases [28, 29]. Thus, identification of iNOS inhibitors is considered to be a promising approach to prevent acute and chronic inflammatory states.

The nuclear factor erythroid 2 related factor 2 (Nrf2)/heme oxygenase 1 (HO-1) signaling pathway plays a critical role in protecting cells against excess oxidative stress stimuli, and it can maintain intracellular redox homeostasis via regulation on a variety of pathways such as autophagy, ferroptosis, pyroptosis, and apoptosis [30]. Recent molecular evidence shows that the Nrf2/HO-1 signaling pathway plays important role on the anti-inflammatory property of bioactive compounds [31], and overexpression of HO-1 in macrophages can significantly inhibit the production of proinflammatory cytokines by LPS stimulation and increase the anti-inflammatory response [32]. Further *in vivo* data shows that IL-10-mediated protection against LPS-induced septic shock in mice was significantly attenuated by cotreatment with the HO-1 inhibitor, zinc protoporphyrin [33], and both mice and humans lacking HO-1 expression have a phenotype that develops a chronic inflammatory state [34, 35]. These data imply that there exists a key link between antioxidation and anti-inflammation, and activation of Nrf2/HO-1 may be the potent and promising new molecular target for the treatment of inflammation-related disorders. Moreover, the crosstalk between the Nrf2/HO-1 pathway and the inflammatory pathway has been investigated in several studies, and HO-1 is a candidate to connect these pathways [36, 37]. However, this crosstalk is not well studied and lacks in-depth molecular evidence.

Therefore, in the present study, the molecular mechanism underlying the anti-inflammatory and antioxidant effect of crocetin is fully investigated by the application of shRNA-KD and CRISPR-Cas9-KO technologies in LPS-induced inflammatory RAW264.7 cells, especially the role of crocetin on modulation of redox balance, the crosstalk between the Nrf2/HO-1 pathway and the inflammatory pathway, and its targeted extracellular receptors.

2. Materials and Methods

2.1. Materials and Cell Culture. Crocetin is donated by Tairui Biotechnology Co., Ltd (Nanyang, Henan, China).

Crocetin was purified by HPLC with 98% purity, and it can be dissolved in DMSO (0.1% final concentration in culture medium). LPS (*Escherichia coli* Serotype 055:B5) was purchased from Sigma (St. Louis, MO, USA). AZD6244, SB202190, SP600125, and U0126 were from MedChemExpress (Monmouth Junction, NJ, USA). Antibodies against iNOS, phospho-ERK1/2, phospho-p38 kinase, phospho-JNK, ERK1/2, p38 kinase, JNK, and $\text{I}\kappa\text{B-}\alpha$ were purchased from Cell Signaling Technology (Beverly, MA, USA). GAPDH and p65 were from Santa Cruz Biotechnology, Inc. (Santa Cruz, CA, USA). Antibodies against HO-1 and Nrf2 were from Abcam (Cambridge, MA, USA); 2',7'-dichlorofluorescein diacetate (DCFH-DA) was from Beyotime Institute of Biotechnology (Beyotime, Guangzhou, China). Fetal bovine serum (FBS) was from Biological Industries (Kibbutz Beit Haemek, Israel). Murine macrophage-like RAW264.7 cells were purchased from ATCC (Rockville, MD, USA) and cultured at 37°C in a 5% CO₂ atmosphere in Dulbecco's modified Eagle's medium (DMEM) containing 10% FBS. Because FBS contains numerous compounds, such as LPS and growth factors, which influence the biological characteristics of macrophages [38–41], we performed all of the experiments under serum-free conditions.

2.2. Cell Viability Assay. The cell viability was measured by an MTT assay. Briefly, RAW264.7 cells were seeded in a 96-well plate and treated with various concentrations of crocetin for 24 h. Subsequently, the supernatant was discarded, and 50 μl of MTT solution was added to each well. Cells were incubated at 37°C for an additional 4 h in the dark. The acidic isopropanol was added to dissolve the formazan crystals, and the optical density (OD) was measured at 570 nm with a microplate reader (Thermo Scientific, MA, USA). Viability was determined by comparing the OD of sample-treated cells with those of the untreated cells.

2.3. Pull-Down Assay. Crocetin-Sepharose 4B beads were prepared as described previously [42]. Briefly, crocetin (5 mg) was coupled to CNBr-activated Sepharose 4B beads (75 mg) in a coupling buffer overnight at 4°C according to the manufacturer's instructions. The mixture was washed in 5 volumes of coupling buffer and then centrifuged at 110 g for 3 min at 4°C. The precipitate was resuspended in 5 volumes of 0.1 M Tris-HCl buffer (pH 8.0) with 2 h rotation at room temperature. After washing three times with 0.1 M acetate buffer (pH 4.0) containing 0.5 M NaCl, the mixture was further washed with 0.1 M Tris-HCl (pH 8.0) buffer containing 0.5 M NaCl. The RAW264.7 cell lysate (500 g/mL) was incubated at 4°C overnight with Sepharose 4B beads or Sepharose 4B crocetin-coupled beads (100 μl , 50% slurry) in reaction buffer (NP-40). The beads were then washed five times with a washing buffer. The proteins were detected by Western blotting with each specific antibody.

2.4. Molecular Modeling. The modeling of crocetin to TLR4-MD2, MEK1, JNK1/2, and Keap1-Nrf2 proteins (PDB codes: 5IJB, 1S9J, 3V3V, and 3WN7) was performed using Molecular Operating Environment™ software (MOE, Version

2012.10, Chemical Computing Group Inc.) [43]. Hydrogen atoms were first added, and force field atomic charges were assigned. Docking of crocetin to protein kinases was done by using MOE-AS EDock 2013 software [42].

2.5. Construction and Transfection of Short Hairpin RNA (shRNA). Three short hairpin RNA (shRNA) interference sequences targeting mouse HO-1, MEK1, ERK1, Nrf2, and a negative control sequence (NC) were designed, synthesized, and cloned into the pLKO.1 vector. After DNA sequencing, a three-plasmid-based lentiviral packaging system (vector plasmid-psPAX2-pMD2.G) was used to transfect HEK293T cells to package lentiviruses. Plasmids were transiently transfected into HEK293T cells using the Lipofectamine 3000 DNA Transfection Reagent (Thermo Scientific, MA, USA). The supernatants containing viruses were harvested and added with PGE8000 at a final concentration of 5% for incubation overnight and then were centrifuged at 7000 g for 20 min at 4°C by ultracentrifugation (Thermo Scientific, MA, USA). RAW264.7 cells were incubated with lentivirus for at least 36 h for successful infection. Puromycin was added for screening living cells, and the interference efficiency was detected by Western blotting.

2.6. Construction of HO-1 Knockout Gene by CRISPR System. Single-guide RNA (sgRNA) targeting mouse HO-1 gene (NM_010442.2) was designed using the CRISPR design website (<http://crispr.mit.edu>, in the public domain). The control sgRNA sequence (5'-TGCGAATACGCCACGCGA TGGG-3') was designed to target the lacZ gene from *Escherichia coli* [44]. The lentiCRISPR-v2 vector was purchased from Addgene (Cat. 52961; Cambridge, MA, USA). To express sgRNA in the RAW264.7 cells, the oligos of top oligos 5'-CACCG-20 nt and bottom oligos 5'-AAAC-20 nt-C-3' were annealed and cloned into the lentiCRISPR-v2 vector by BsmB1 (New England Biolabs, Boston, MA, USA). The flowing steps (virus packaging, virus infection, and puromycin screening) were done as described in shRNA-KD. Subsequently, the monoclonal cells were picked out and cultured into clumps, and the knockout efficiency was detected by Western blotting.

2.7. Measurement of Nitric Oxide (NO) and Intracellular ROS Assay. Nitric oxide in the culture medium is stably present as nitrite (NO₂⁻) which can be assayed by using the Griess reagent (Madison, WI, USA). According to the manufacturer's manual, RAW264.7 cells (1.0 × 10⁶ cells) were seeded into each well of 12-well plates. After preculture for 24 h, cells were starved by being cultured in serum-free medium for another 2.5 h to eliminate the influence of FBS. The cells were then treated with or without crocetin for 1.5 h before exposure to 40 ng/ml LPS for 12 h. The level of nitric oxide released into the culture medium was determined by measuring absorbance at 530 nm in a microplate reader.

The intracellular reactive oxygen species (ROS) generation of cells was investigated using DCFH-DA as a well-established compound to detect and quantify intracellular-produced hydrogen peroxide [45]. In brief, RAW264.7 cells

were plated in a 96-well plate and pretreated with crocetin for 2 h before exposure to LPS (40 ng/ml) for 12 h. DCFH-DA was added to the medium with a final concentration of 20 μM for an additional 30 min. The fluorescence intensity was then measured at an excitation (485 nm) and emission (530 nm) wavelength using a fluorescent Multilabel Counter (Perkin-Elmer) and was expressed as the percentage of DMSO vehicle control in the absence of LPS. Data are the mean ± SD of three separate experiments.

2.8. Nuclear Protein Extraction and Western Blot Analysis. Nuclear extracts were prepared according to the manufacturer's manual (Sigma, St. Louis, MO, USA). Harvested cells were lysed in buffer A on ice for 10 min and then centrifuged at 17000 g for 10 min at 4°C. The nuclear pellets were resuspended in buffer B on ice for 40 min and then centrifuged at 17000 g for 10 min at 4°C. The supernatants containing nuclear extracts were stored at -80°C until use.

Protein concentration was determined by using a dye-binding protein assay kit (Beyotime, Guangzhou, China). Protein extracts were separated by 10% SDS-PAGE and transferred to PVDF membranes (Amersham Pharmacia Biotech, Little Chalfont, UK). The membranes were blocked at room temperature for 1 h with 5% nonfat dry milk and then incubated with each primary antibody at 4°C overnight and further incubated for 1 h with HRP-conjugated secondary antibody. Bound antibodies were detected by the ECL system with a Lumi Vision PRO machine.

2.9. Statistical Analyses. ImageJ and Prism 5.0 were utilized to perform quantitative analysis. All of the results from three independent experiments and data were expressed as the mean ± standard error of the mean (SEM) for the number of experiments. A statistical probability of $p < 0.05$ was considered statistically significant.

3. Results

3.1. Crocetin Suppresses LPS-Induced NO Release and iNOS Expression. Crocin and crocetin are the main natural pigments that coexisted in Gardenia Yellow with functional potency. It was reported that crocin exerted powerful anti-inflammatory properties by the inhibition of iNOS expression [46]. Therefore, it is necessary to clarify the anti-inflammatory activity of crocetin (the structure is shown in Figure 1(a)). Firstly, the effect of crocetin on the viability of RAW264.7 cells was conducted with the MTT assay. As shown in Figure 1(b), it was found that there is no significant difference in the cell viability when treated with crocetin at the concentrations of 0, 10, 20, and 40 μg/ml, while the number of living cells was significantly reduced at 80 μg/ml ($p < 0.05$). Thus, the concentrations of 10 and 20 μg/ml were selected to proceed in the following study. In Figure 1(c), 40 ng/ml of LPS successfully stimulated the expressions of NO in RAW264.7 cells; pretreatment with 10 or 20 μg/ml of crocetin inhibited the LPS-induced NO release. Moreover, the expression of iNOS, the rate-limiting enzymes of NO, was also detected. As shown in Figure 1(d), dose-dependent inhibition of iNOS expression was found in

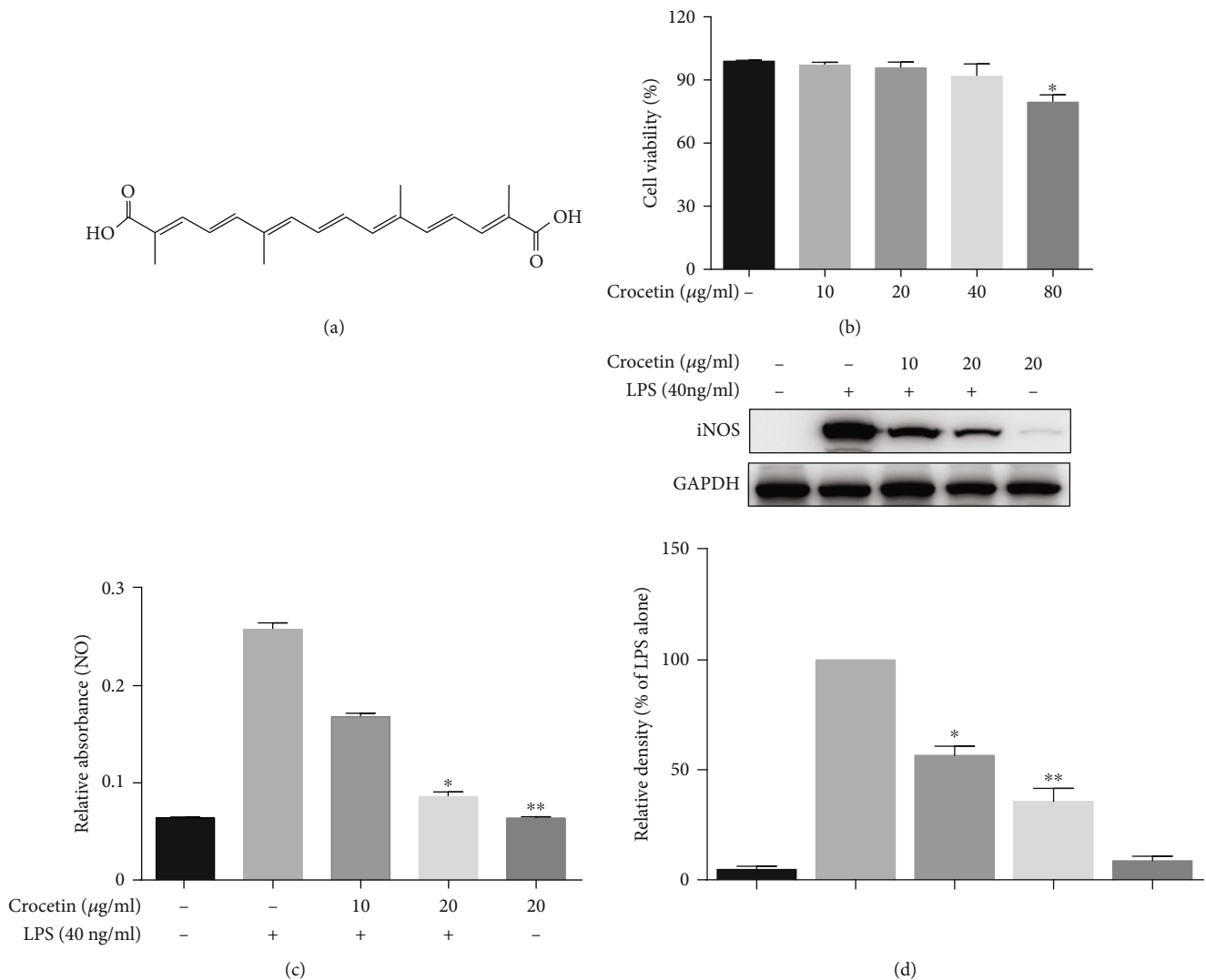


FIGURE 1: The effects of crocetin on nitric oxide production and iNOS expression. (a) The structure of crocetin. (b) The cytotoxicity assay of crocetin in RAW264.7 cells. Cytotoxicity assay was performed as described in Materials and Methods. (c) Crocetin inhibits LPS-induced NO release. RAW264.7 cells were treated with crocetin (10–20 $\mu\text{g/ml}$) for 1 h before starvation in serum-free medium for another 2.5 h and then exposed to 40 ng/ml LPS for an additional 12 h. The amount of NO in medium was measured as described in Materials and Methods. (d) Crocetin suppresses LPS-induced iNOS expression. RAW264.7 cells were pretreated with crocetin (10–20 $\mu\text{g/ml}$) for 1 h before starvation in serum-free medium for 2.5 h and then exposed to 40 ng/ml LPS for an additional 12 h of treatment. The expressions of proteins were detected by Western blot analysis using their corresponding antibodies. Data are presented as the mean \pm SD of at least triplicate tests. * $p < 0.05$ and ** $p < 0.01$ vs. LPS-treated cells.

LPS-stimulated cells after crocetin treatment ($p < 0.01$). These results indicated that crocetin possessed inhibitory activity on NO production and iNOS expression.

3.2. Crocetin Inhibits the Activation of the Nuclear Factor kappaB ($\text{NF-}\kappa\text{B}$). To date, transcription factor nuclear factor kappaB ($\text{NF-}\kappa\text{B}$) is frequently reported to directly bind to the conserved sequence in the promoter region of *iNOS* gene and can regulate its transcription efficiently [28, 29, 47–49]. Thus, $\text{NF-}\kappa\text{B}$ was selected in the subsequent study to find which transcriptional factor is the target for crocetin. Firstly, the time course of treatment with 20 $\mu\text{g/ml}$ of crocetin was performed to investigate its effect on the expression of $\text{I}\kappa\text{B-}\alpha$ and p65. As shown in Figure 2(a), 40 ng/ml of LPS was

found to significantly reduce the expression of $\text{I}\kappa\text{B-}\alpha$ at 30 min and 60 min ($p < 0.05$) and restore to the basal expression at 120 min; cotreatment with 20 $\mu\text{g/ml}$ of crocetin maintains the high expression of cytoplasm $\text{I}\kappa\text{B-}\alpha$ at 30 min, but not at 60 min and 120 min. Moreover, the expressions of nuclear p65 were inhibited significantly at 60 min by crocetin treatment, compared with LPS stimulation only, while this action disappeared at 120 min. The time course result of LPS treatment only and cotreatment of crocetin indicated that the time points of LPS stimulation in the cell model and the action of the transcription factor are consistent with the previous studies.

To verify the inhibitory effect of crocetin on the $\text{NF-}\kappa\text{B}$ pathway, the dose course of crocetin treatment was

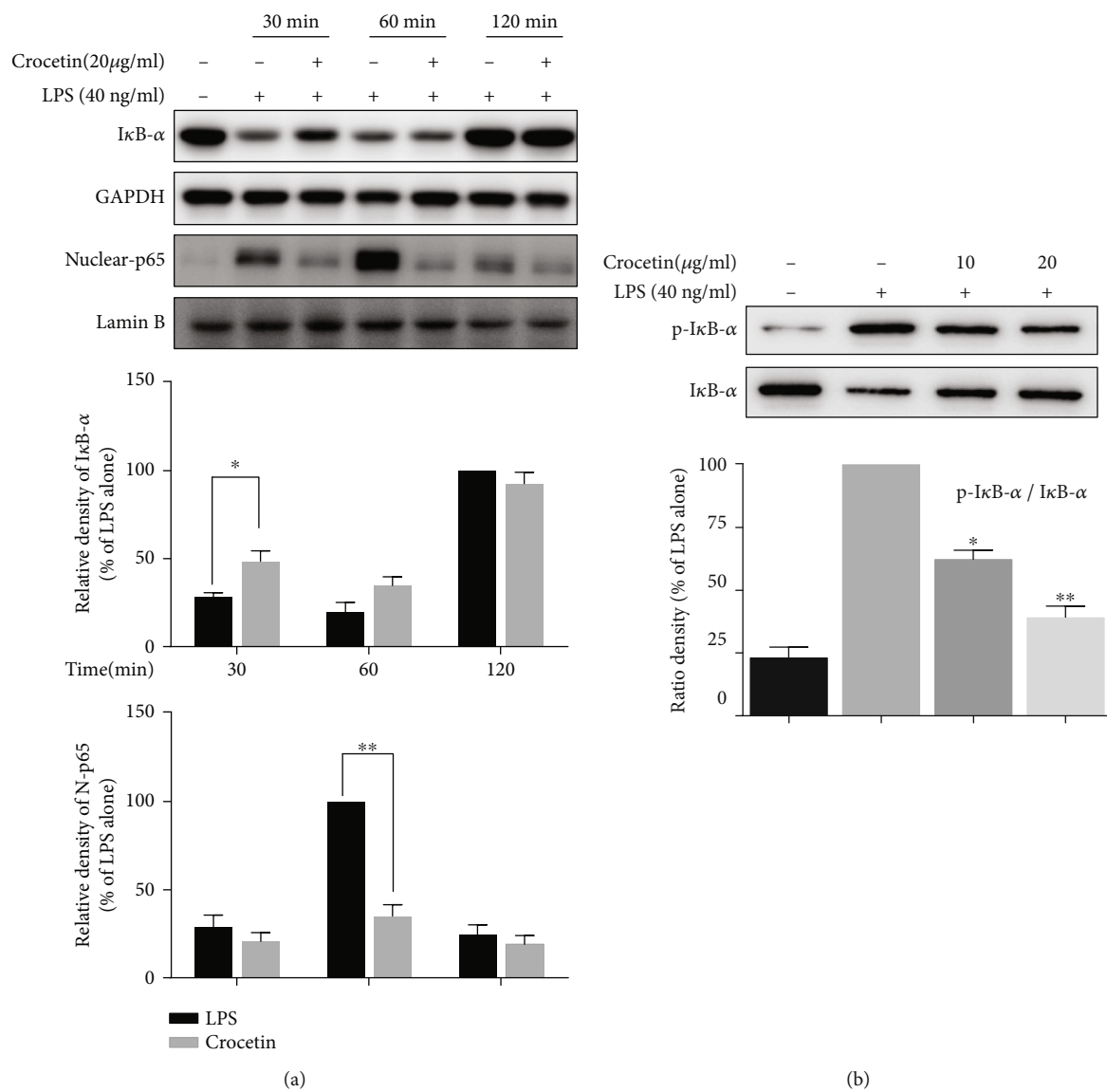


FIGURE 2: Continued.

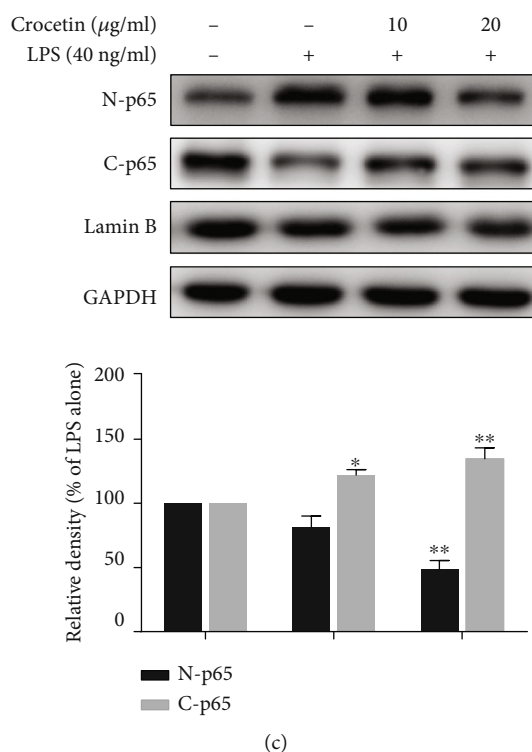


FIGURE 2: The effect of crocetin on the key nuclear transcription factors of *iNOS* gene. (a) The effect of crocetin on $\text{I}\kappa\text{B-}\alpha/\text{p65}$ expression at an indicated time. RAW264.7 cells were pretreated with crocetin (20 $\mu\text{g/ml}$) for 1 h before starvation in serum-free medium for 2.5 h and then exposed to 40 ng/ml LPS for an indicated time. The level of protein was detected by Western blot analysis using their corresponding antibodies. (b) Crocetin dose-dependently inhibits LPS-induced degradation of $\text{I}\kappa\text{B-}\alpha$. RAW264.7 cells were pretreated with crocetin (10–20 $\mu\text{g/ml}$) for 1 h before starvation in serum-free medium for 2.5 h and then exposed to 40 ng/ml LPS for an additional 30 min. The total and phosphorylation of $\text{I}\kappa\text{B-}\alpha$ were detected by Western blot analysis using their corresponding antibodies. (c) Crocetin inhibits LPS-induced nuclear translocation of p65. Cell culture and crocetin (10–20 $\mu\text{g/ml}$) treatment were done as described in (b). Extraction of nuclear and cytosolic p65 was performed as described in Materials and Methods. Lamin B and GAPDH were used as a control for nuclear and cytosolic protein, respectively. Data are presented as the mean \pm SD of at least triplicate tests. * $p < 0.05$ and ** $p < 0.01$ vs. LPS-treated cells.

conducted to confirm its effect on the key factor of this pathway, the expressions of cytoplasm $\text{I}\kappa\text{B-}\alpha$ and p- $\text{I}\kappa\text{B-}\alpha$. The results obtained in Figure 2(b) showed that LPS increased the phosphorylation of $\text{I}\kappa\text{B-}\alpha$ and decreased the protein level of $\text{I}\kappa\text{B-}\alpha$ ($p < 0.01$), and cotreatment with crocetin dose-dependently blocked this process. To further confirm the nuclear translocation of the transcription factor p65, the nuclear translocations of them were both detected. According to the action time point for these two transcription factors in Figure 2(a), the result showed that pretreatment with crocetin can dose-dependently inhibit the LPS-induced nuclear translocation of p65 (Figure 2(c)). All of these results revealed that crocetin inhibited the expression of *iNOS* by blocking LPS-induced $\text{I}\kappa\text{B-}\alpha$ phosphorylation and p65 translocation.

3.3. Crocetin Blocks LPS-Induced *iNOS* Expression by Increasing MEK1/ERK1 Phosphorylation but Inhibiting JNK Phosphorylation. MAPKs play essential roles in LPS or phytochemical stimulated *iNOS* expression in RAW264.7 cells; thus, it is necessary to detect the protein kinase cascades and their activities in the crocetin-induced NO inhibitory effect to better elucidate the underlying mechanism. Firstly,

several typical protein kinase inhibitors were selected to be applied in the following experiment, including AZD6244, SB202190, and SP600125, which are the inhibitors for MEK1/2, p38 kinase, and JNK, respectively. As shown in Figure 3(a), pretreatment of JNK inhibitor can markedly reduce LPS-induced *iNOS* expression ($p < 0.001$), MEK inhibitor only slightly reduce that, and p38 has no effect, which implied that only JNK is essential in LPS-induced *iNOS* expression. To further investigate the coefficient of crocetin on this process, 20 $\mu\text{g/ml}$ crocetin was coadded in the cells with protein kinase inhibitor treatment. Surprisingly, as shown in Figure 3(b), pretreatment with MEK inhibitor eliminated the inhibitory effect of crocetin on *iNOS* expression ($p < 0.01$). These results indicated that crocetin may inhibit the expression of *iNOS* by regulating the phosphorylation of MEK and JNK.

Moreover, to investigate the actual effect of crocetin on the protein kinase pathways of JNK, MEK, and p38, a series of immune blots were detected. As shown in Figure 3(c), crocetin only showed a dose-dependent inhibitory effect on LPS-induced phosphorylation of JNK ($p < 0.01$), but there is no significant effect on phosphorylation of MEK and p38. This result aroused our curiosity, and we speculate that

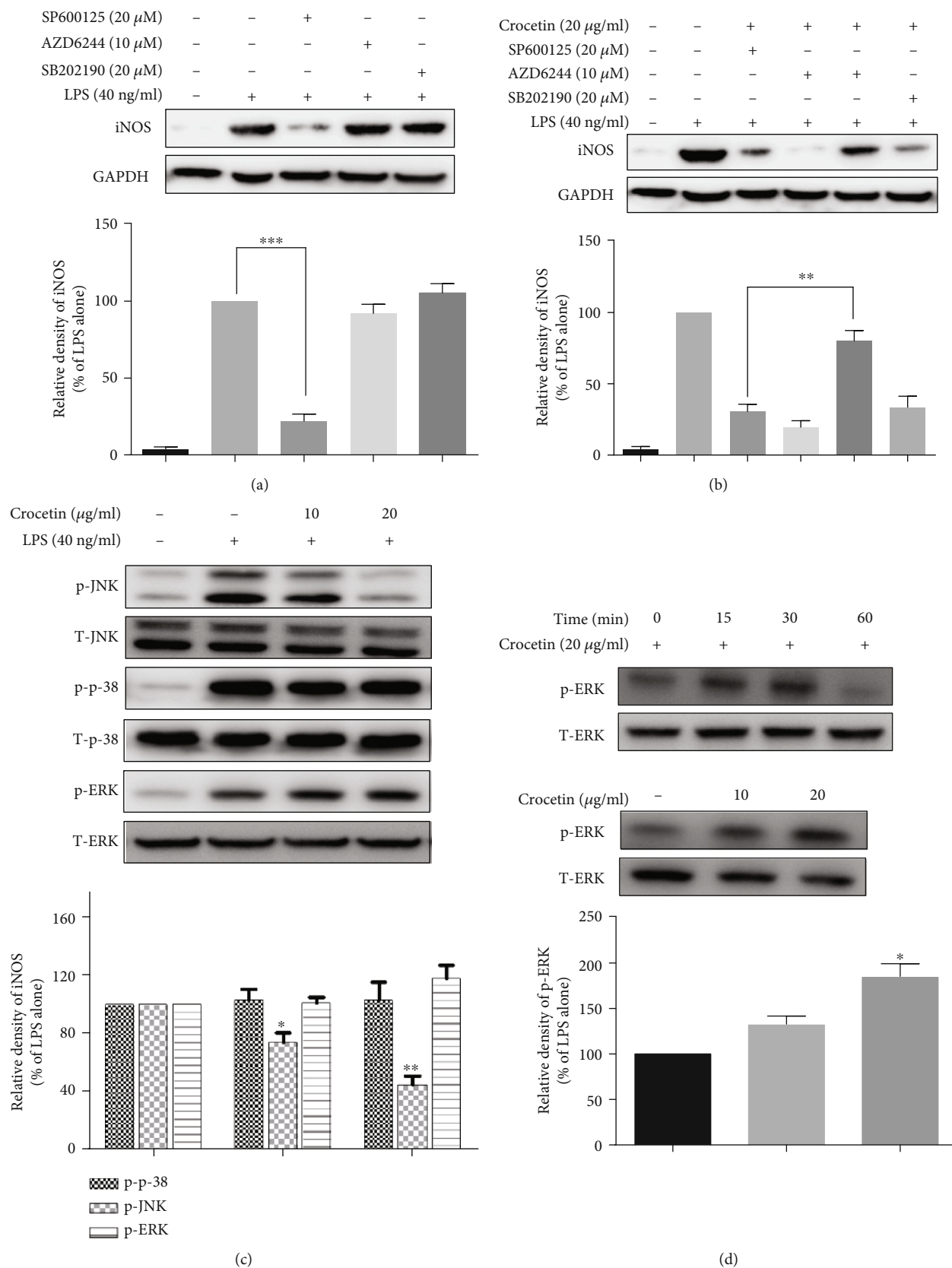


FIGURE 3: Continued.

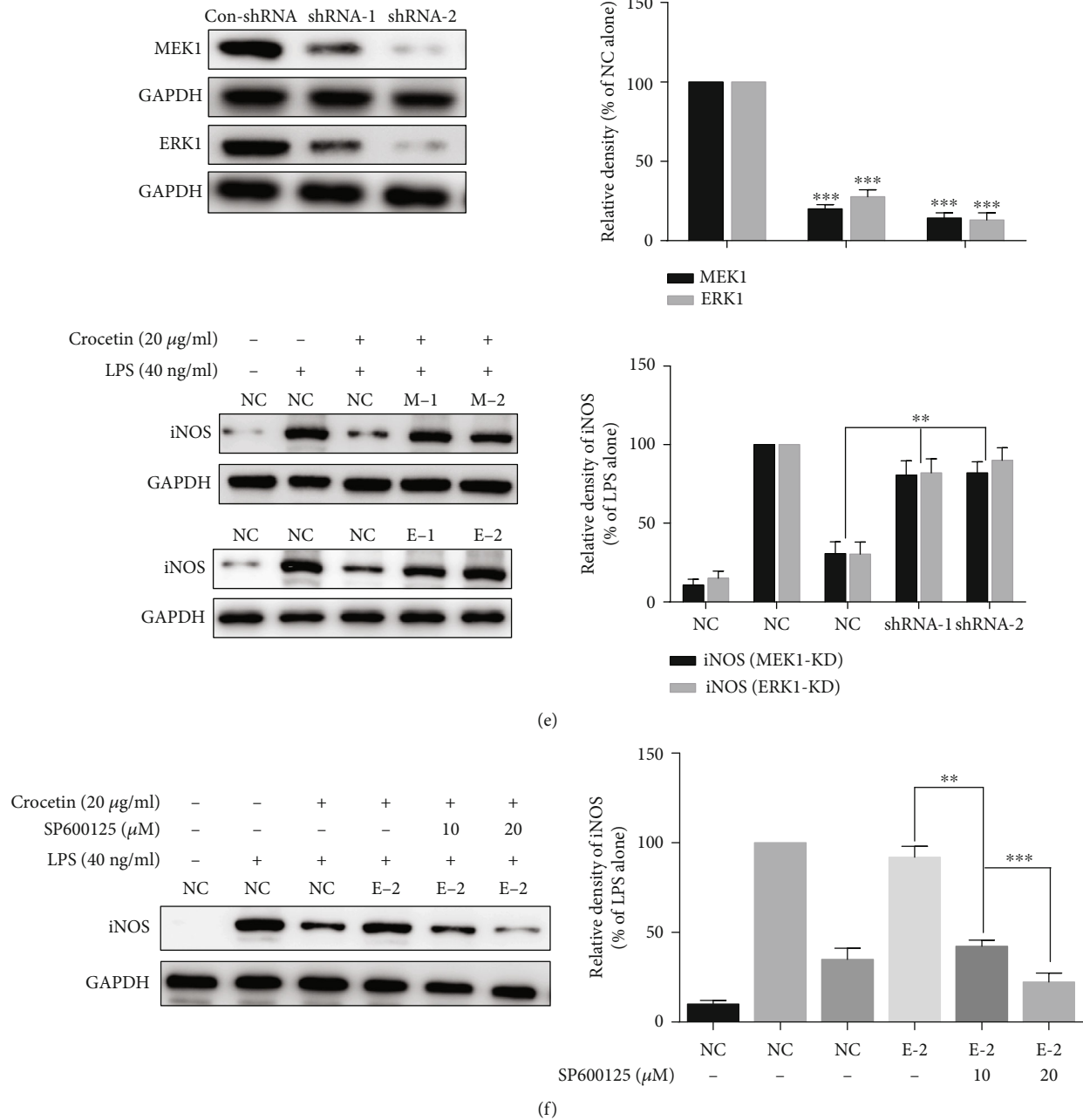
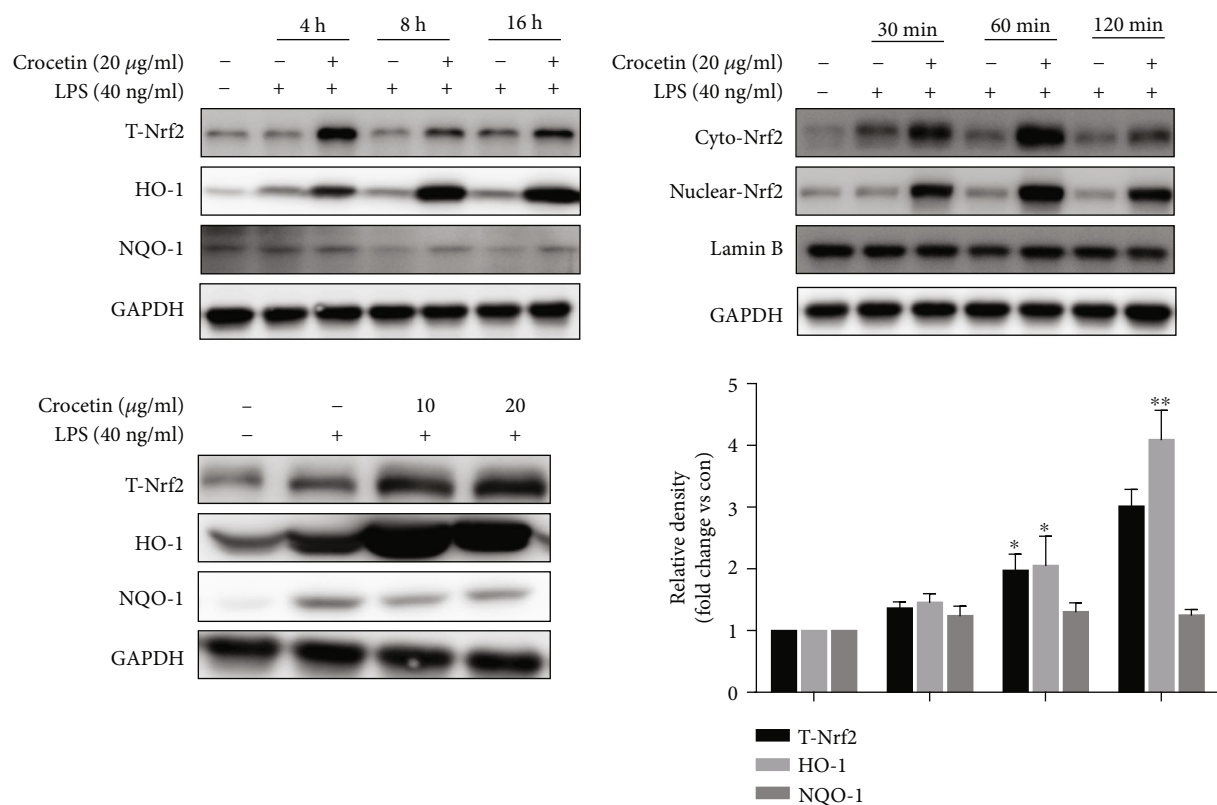


FIGURE 3: The effect of crocetin on the phosphorylation of protein kinases. (a) JNK inhibitor suppressed LPS-induced iNOS expression. RAW264.7 cells were pretreated for 1 h with AZD6244, SB202190, or SP600125 alone and then exposed to 40 ng/ml LPS for 12 h. The expression of iNOS was detected by Western blot analysis. (b) MEK inhibitor reversed the effect on crocetin-mediated iNOS inhibition. RAW264.7 cells were treated with MAPK inhibitors for 1 h, subsequently added crocetin for another 1 h, and then exposed to 40 ng/ml LPS for 12 h. Western blot was applied to detect iNOS expression. (c) Crocetin inhibited LPS-induced phosphorylation of JNK but has no significant effect on MEK and p38. RAW264.7 cells were pretreated with crocetin (10-20 $\mu\text{g/ml}$) for 1 h and then exposed to 40 ng/ml LPS for 0.5 h. The total and phosphorylated protein kinases were detected with their antibodies, respectively. (d) MEK1-KD and ERK1-KD relieved the crocetin-induced iNOS inhibition. Selecting RAW264.7 cells with scramble shRNA as blank controls (NC), MEK1-KD cell lines or ERK1-KD cell lines were treated with crocetin for 1 h and then exposed to 40 ng/ml LPS for 12 h. The iNOS expression was detected by Western blot analysis. (e) Crocetin increased the phosphorylation of MEK. RAW264.7 cells were pretreated with crocetin (20 $\mu\text{g/ml}$) at the indicated time or pretreated with crocetin (10-20 $\mu\text{g/ml}$) for 30 min, and then, total and phosphorylated protein levels of MEK were detected with their antibodies, respectively. (f) JNK is critical for LPS-induced iNOS expression. ERK1-KD (shRNA-2) cells were pretreated with SP600125 (10-20 μM) for 1 h, and the following steps were done as described in (a). The expressions of iNOS were detected by Western blot analysis. Each value represents the mean \pm SD of triplicate tests. * $p < 0.05$ and ** $p < 0.01$ vs. LPS-treated cells.



(a)

FIGURE 4: Continued.

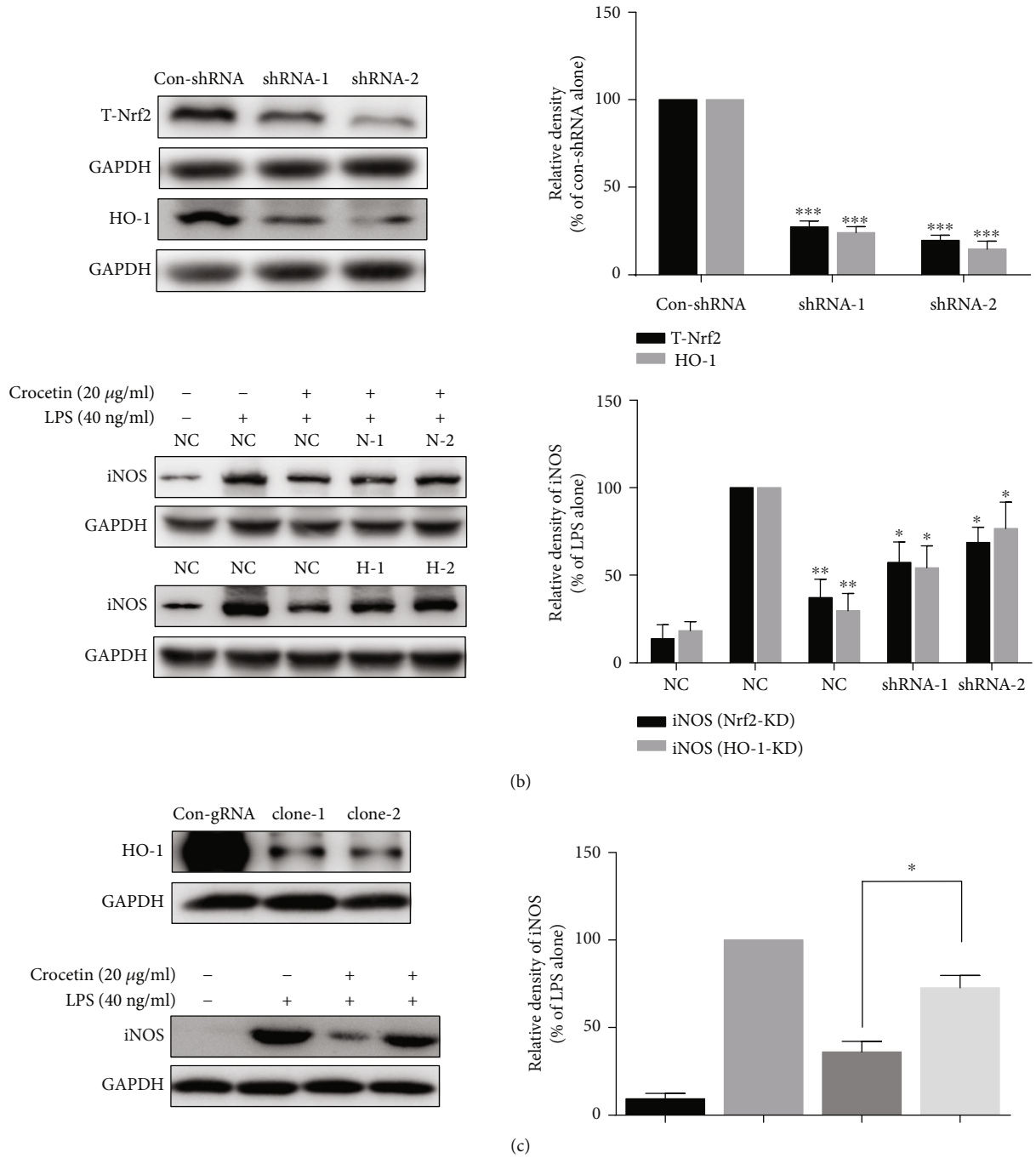


FIGURE 4: Continued.

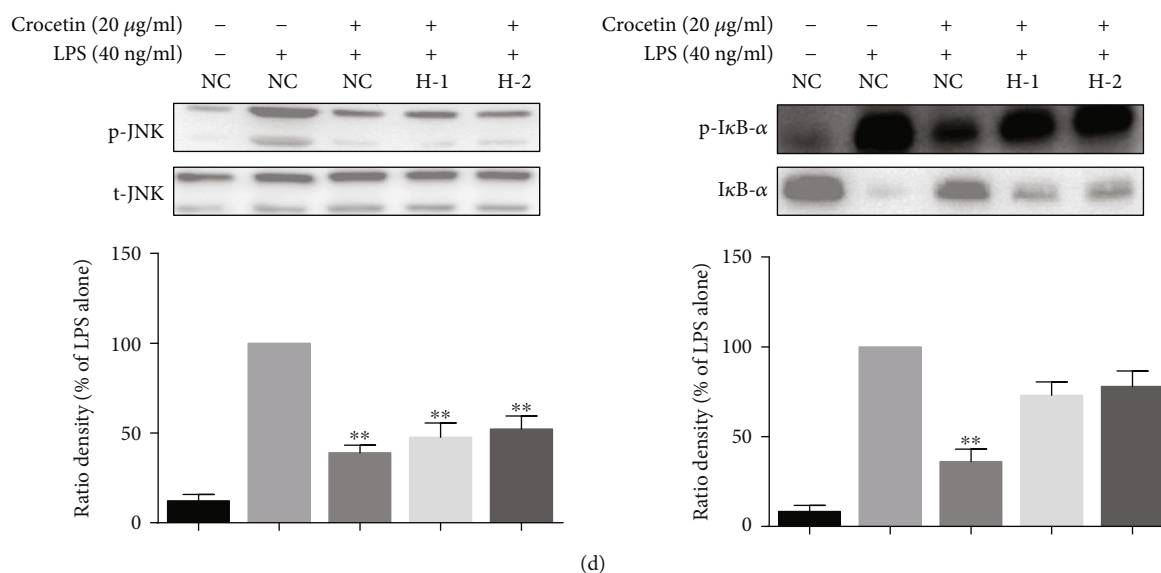


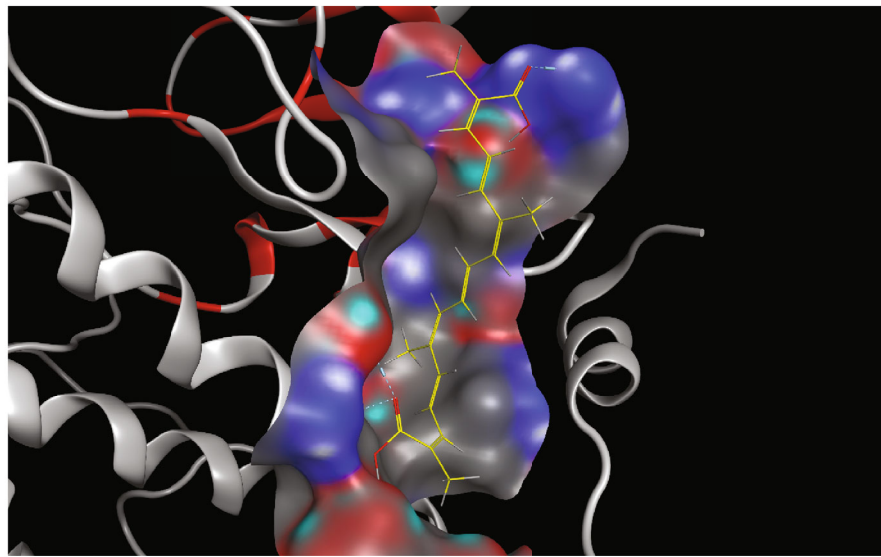
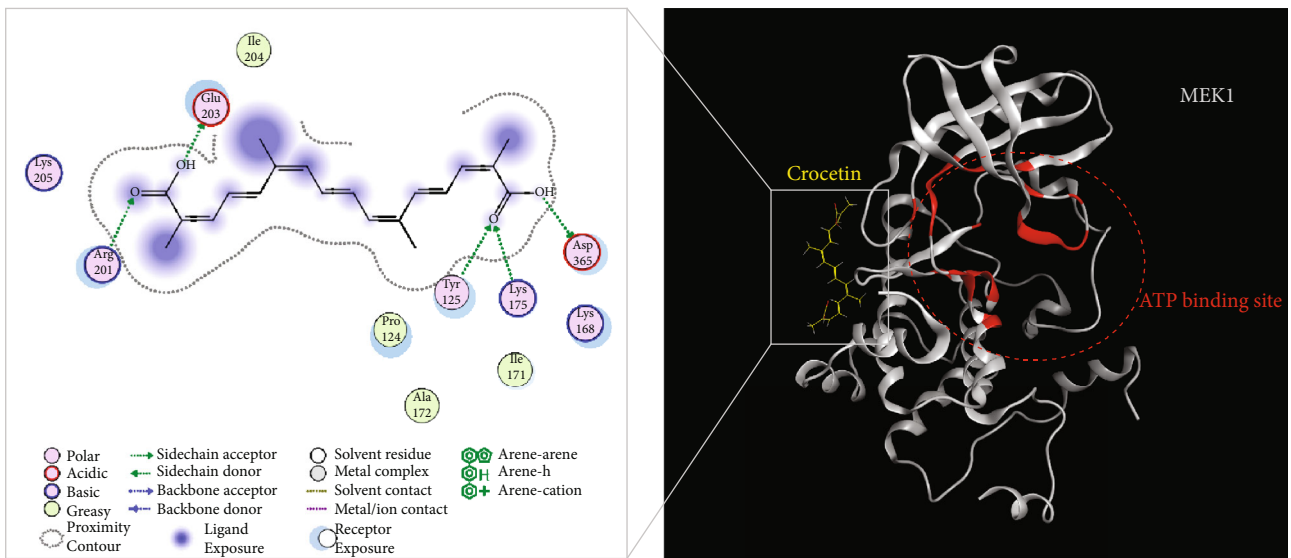
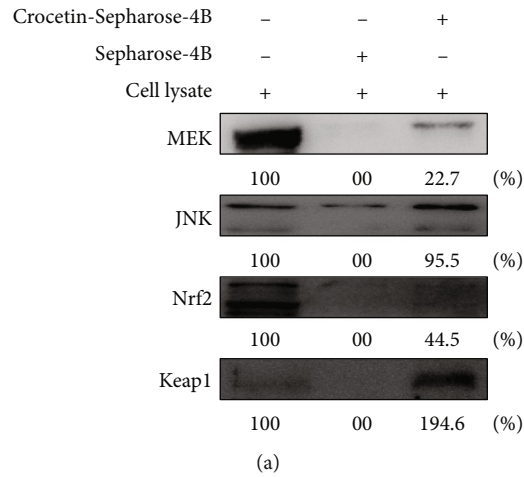
FIGURE 4: The involvement of the Nrf2/HO-1 pathway in the crocetin-induced inhibitory activity on iNOS expression. (a) Crocetin increased the expressions of Nrf2 and HO-1 and the nuclear translocation of Nrf2. For Nrf2 and HO-1 expressions, RAW264.7 cells were pretreated with the indicated dose of crocetin for 1 h before starvation in serum-free medium for 2.5 h and then exposed to 40 ng/ml LPS for an indicated time. For Nrf2 nuclear translocation, cell culture and crocetin (20 μg/ml) treatment were done as described in Figure 2(c). The expressions of proteins were detected by Western blot analysis using their corresponding antibodies. (b) Nrf2-knockdown (Nrf2-KD) and HO-1-knockdown (HO-1-KD) blocked crocetin-dependent iNOS inhibition. Detection of the knockout efficiency of two monoclonal cells (top). NC and HO-1-KO cell treatment was done as described in (b). (c) HO-1-knockout (HO-1-KO) blocked crocetin-dependent iNOS inhibition. The total and phosphorylated protein kinases were detected with their antibodies, respectively. (d) HO-1-KO blocked crocetin-dependent p-IκB-α inhibition. NC and HO-1-KO cell treatment was done as described in Figure 2(b). Data are presented as the mean ± SD of triplicate tests. * $p < 0.05$ and ** $p < 0.01$ vs. LPS-treated cells.

the reason for this phenomenon is that the MEK inhibitor has diverse targets or mutual antagonism competing with crocetin. Subsequently, shRNA technology was applied to knock down (KD) the gene expression of *MEK1* and *ERK1* to eliminate these potential possibilities. Interestingly, the same result was obtained as MEK inhibitor treatment (Figure 3(b)); both MEK1 knockdown (MEK1-KD) and ERK knockdown (ERK1-KD) restored LPS-induced iNOS expression which is inhibited by crocetin treatment, $p < 0.01$ (Figure 3(e)). These results indicated that the above possibilities are not the reason for the not significant effect of crocetin on the MEK pathway; maybe the treatment time of its inhibitor for a long time is the cause. Therefore, pretreatment with crocetin for 15-60 min was selected for immunoblot, instead of the previous 90 min (Figure 3(c)). As shown in Figure 3(d), it was found that the phosphorylation of ERK was increased significantly within 30 minutes after crocetin treatment, and crocetin also increased the expressions of p-ERK in a dose-dependent manner ($p < 0.05$).

Furthermore, to investigate the relationship between MEK1/ERK1 and JNK, the JNK inhibitor was used in ERK1-KD cells. The result showed that the JNK inhibitor can still significantly inhibit the expression of iNOS in the ERK1-KD cell line in a dose-dependent manner, $p < 0.001$ (Figure 3(f)), which indicated that JNK played a crucial role in LPS-stimulated iNOS expression, and crocetin exerted its anti-inflammatory effect via induction of MEK1/ERK1 phosphorylation and subsequent inhibition of JNK phosphorylation.

3.4. Crocetin Exerts Its Anti-inflammatory Effect via Activation of Nrf2/HO-1 Signaling Pathway. It has been reported that the activation of the Nrf2/HO-1 pathway is involved in the attenuation of NF-κB translocation and iNOS expression [50, 51]. To investigate the effect of crocetin on the crosstalk between Nrf2/HO-1 and NF-κB/iNOS pathway and whether this crosstalk is essential for its anti-inflammatory property, gene knockdown and knockout technologies had been performed. As shown in Figure 4(a), the time course result of 4-16 h showed that the expressions of total Nrf2 and its downstream antioxidant protein HO-1 were increased significantly by crocetin treatment ($p < 0.01$), but not that by NQO1, compared with LPS treatment only; the time course result of 30-120 min showed that the expressions of both cytoplasm and nuclear Nrf2 were induced significantly by crocetin treatment ($p < 0.01$). Besides, crocetin was found to activate the Nrf2/HO-1 pathway significantly in a dose-dependent manner.

To verify the essential role of the Nrf2/HO-1 pathway in crocetin-inhibited iNOS expression, both *Nrf2* and *HO-1* genes were knocked down. As shown in Figure 4(b), two repeated KD genes for *Nrf2* and *HO-1* had been constructed ($p < 0.001$), and the results showed that knockdown of *HO-1* and *Nrf2* genes could largely diminish the inhibitory effect of crocetin on LPS-induced iNOS overexpression, $p < 0.05$ (Figure 4(b)). Moreover, the CRISPR/Cas9 system was used to construct the *HO-1* gene knockout (KO) cell model to further confirm this action. As shown in Figure 4(c), the results of *HO-1*-KO cells displayed are similar to that of *HO-1*-KD cells



(b)

FIGURE 5: Continued.

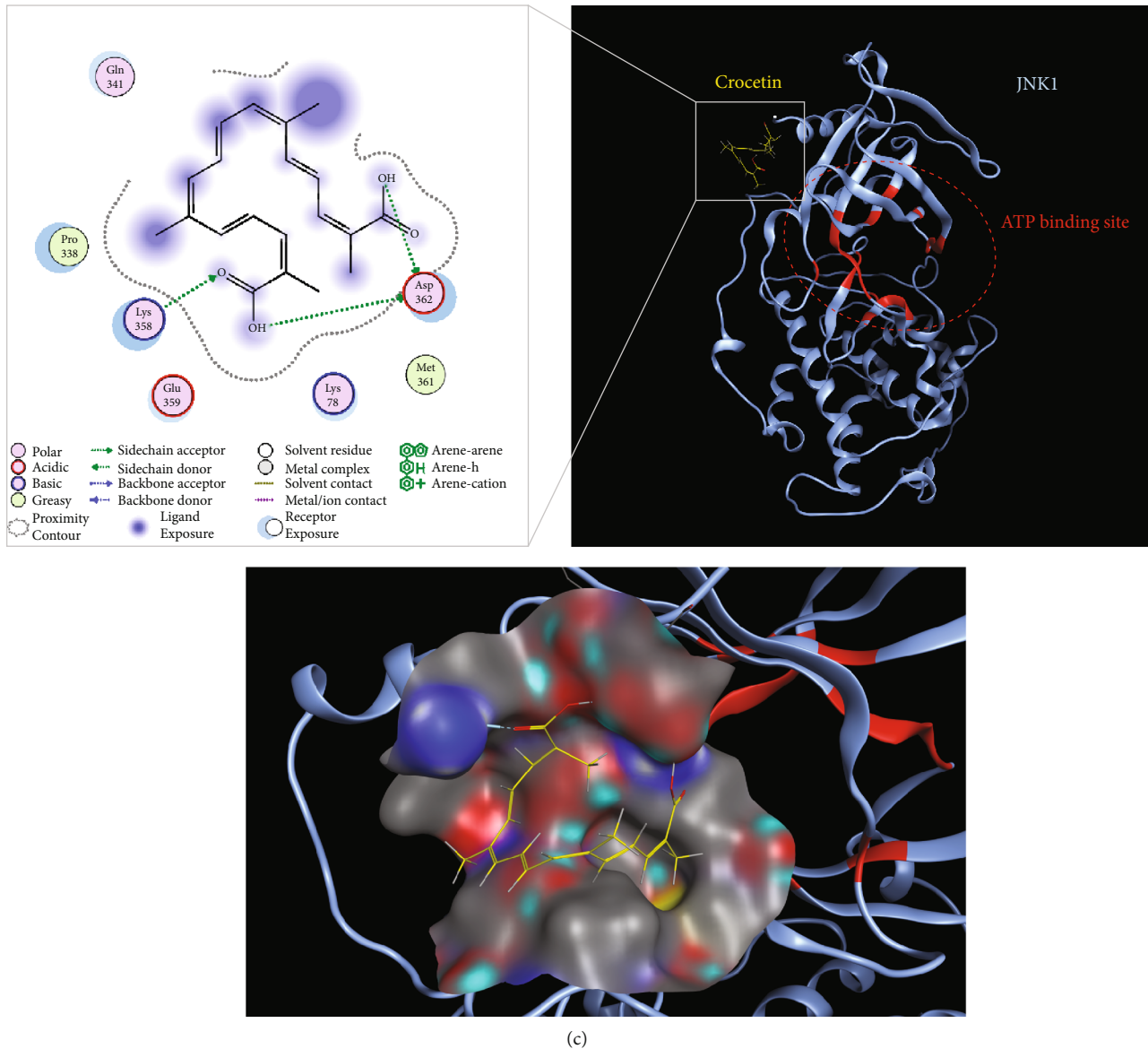


FIGURE 5: The direct binding proof and computational docking model for the action of crocetin. (a) Binding abilities of crocetin to MEK1, JNK1/2, and Keap1-Nrf2. Whole cell lysate (input control, lane 1), lysate precipitation with Sepharose 4B beads (negative control, lane 2), and Sepharose 4B-crocetin-coupled beads (lane 3) were applied to SDS-PAGE and then detected with MEK1, JNK1/2, Nrf2, or Keap1 antibody, respectively. The binding efficiency to crocetin was presented as the ratio of input control. (b, c) The docking models of crocetin to MEK1 and JNK1/2. Electrostatic potential surface is indicated in a close-up figure of the upper side, and hydrogen bonds are indicated by blue and green lines in the lower figure. White, blue ribbon: protein kinase; red ribbon: ATP-binding site; yellow: crocetin.

(Figure 4(b)). Further, the role of HO-1 in the inflammatory signaling pathway was determined. As shown in Figure 4(d), crocetin significantly inhibited the expression of p-I κ B- α ($p < 0.01$), but this effect can be reversed in HO-1-KO cells. In addition, crocetin significantly inhibited the phosphorylation of JNK, and this effect can also be detected in HO-1-KO cells ($p < 0.01$). These results strengthen the direct crosstalk between the Nrf2/HO-1 and NF- κ B/iNOS pathways and highlight the essential role of HO-1 in this crosstalk.

The above data indicated that crocetin may exert its anti-inflammatory effect via activation of the Nrf2/HO-1 signaling pathway, and HO-1 is a vital link to regulate the redox balance in RAW264.7 cells treated with crocetin.

3.5. The Direct Binding Proof and Docking Model of Crocetin to MEK1, JNK1/2, Keap1-Nrf2, and TLR4-MD2. Our data suggest that MEK1, JNK1/2, Keap1, and Nrf2 are potential targets for crocetin to inhibit inflammatory signaling. Thus, we investigated whether the crocetin directly binds to them, using the bead-bound pull-down assay, which has been validated as an effective screening tool in our previous study [42]. In brief, crocetin is coupled with CNBr-Sepharose 4B beads and then incubated with protein lysate extracted from RAW264.7 cells. The bound protein was extracted by centrifuge and detected by Western blotting with respective antibodies after washing out. As shown in Figure 5(a), MEK1 and JNK1/2 were detected in the complex of Sepharose 4B

beads-crocetin-proteins, with 22.7% and 95% binding rates compared to the cell lysate control, while only JNK1/2 was slightly detected in the Sepharose 4B beads alone. Meanwhile, Keap1, the major Nrf2 endogenous inhibitor, has shown a powerful combination with Crocetin-Sepharose 4B beads with a 194.6% binding rate, and only 12.5% binding rate was detected with Nrf2 antibody, while both Keap1 and Nrf2 were not detected in the Sepharose 4B beads alone. These data showed that crocetin could bind directly with protein kinases of MEK1 and JNK1/2. Moreover, Keap1 had stronger binding activity than Nrf2, which is suggested that crocetin may directly combine with Keap1 for modification and then release Nrf2 from the Keap1-Nrf2 complex.

As shown in Supplementary Fig. 3A, the computational docking analysis data showed that there are 3 hydrogen bonds for the binding of crocetin to the TLR4-MD2 complex, which is not the same binding region of LPS. This result suggested that crocetin may not bind competitively with LPS to block the LPS-induced inflammation. To know how crocetin binds to MEK1, JNK1/2, and Keap1-Nrf2 complex, the computer modeling of crocetin bound to these proteins was performed, using the software as described in Materials and Methods. The results provided interesting information that five hydrogen bonds were formed between crocetin and Arg201, Glu201, Tyr125, Lys175, and Asp635 residues of MEK1, which are configured nearby ATP-binding pocket (Figure 5(b)). As shown in Figure 5(c), three hydrogen bonds were formed between crocetin and Lys358 and Asp362 residues of JNK1/2, which configured a part of the ATP-binding pocket. Further analysis data suggested that crocetin can directly bind to MEK1 on the ATP-binding site 145 and 146 and bind to JNK1/2 by hydrogen bond 358. For the Keap1-Nrf2 complex, three hydrogen bonds were formed between crocetin and His552, Asp579, and Asp573 residues of Keap1, which did not configure a part of the Keap1 catalytic domain (Supplementary Fig. 3B). These docking results further support our pull-down binding data between crocetin and MEK1 and JNK1/2.

4. Discussion

Crocetin is previously reported as an effective anti-inflammatory agent in other studies [25, 52]. However, the molecular mechanism underlying this action has not been fully elucidated, especially the effect of crocetin on the extracellular receptor and the crosstalk between inflammatory pathways and other pathways. In the present study, the molecular mechanism of the anti-inflammatory property of crocetin in the LPS-stimulated RAW264.7 cell model had been investigated in depth. The results showed that crocetin exerts its anti-inflammatory property mainly via the MEK1/ERK1/JNK/NF- κ B/iNOS pathway (Figure 1). Further molecular data by application of shRNA-KD and CRISPR-Cas9 KO technologies confirmed the anti-inflammatory effect of crocetin, and what is more interesting, KD and KO of *HO-1* gene both inhibited this action (Figure 4). Coupled with the molecular data of Nrf2 activation by crocetin, the present study discovers the crosstalk between the Nrf2/HO-1 pathway and the MEK1/ERK1/JNK/NF- κ B/i-

NOS pathway, and HO-1 plays an essential role in the regulatory effect of crocetin on keeping the redox balance (Figures 3 and 4). The molecular mechanism in detail is summarized in Figure 6.

NO, as a major inflammatory mediator, has played a significant role in the expansion of oncogenesis and inflammatory reaction, and it is suggested that the inhibition of NO overproduction or downregulation of iNOS is an imperative target for the prevention and treatment of inflammation and its related complications. Up to now, several studies, both in vitro and in vivo, have shown that crocetin has strong anti-inflammatory activity via inhibition of NO or iNOS in cancer cells [46, 53]. However, the effect of crocetin on the above two inflammatory mediators in the RAW cell model has not been fully investigated [25]. In the present study, it was found that the anti-inflammatory property of crocetin depends on its inhibition of NO and iNOS.

Mitogen-activated protein kinase activation induces the expression of multiple inflammatory genes by regulating nuclear transcription factor NF- κ B [54, 55]. In the present study, specific inhibitors of these protein kinases were used, and it was found that only JNK and MEK1/ERK1 are associated with the anti-inflammatory activity of crocetin (Figure 3). Further data by using MEK1/ERK1-KD cells and JNK inhibitor implied that phosphorylation of JNK is essential for the action of crocetin, and JNK is downstream of MEK1/ERK1, which is consistent with other previous studies [54, 56, 57]. In brief, it was reported that dual-specificity protein phosphatases (DUSP) can dephosphorylate both the threonine and tyrosine residues in the activation loop of MAPKs, thereby inactivating them [56]. Activation of MEK1/ERK1 can increase the transcription of DUSP2 which can limit JNK phosphorylation [57]. More powerful evidences have been shown by using Sepharose 4B beads and pull-down assay to find out the direct binding proof of crocetin to MEK1 and JNK1/2. Our result (Figure 5(a)) suggested that crocetin may directly bind to MEK1 and JNK1/2. Besides, computational docking of crocetin to MEK1 and JNK1/2 (Figures 5(b) and 5(c)) was also analyzed, and the results provided some interesting binding information between the hydroxyl groups of crocetin and amino acid residues of MEK1 and JNK1/2.

As is well known, the Nrf2/HO-1 antioxidant signaling pathway plays a crucial role in the anti-inflammatory process. LPS can stimulate a higher level of ROS generation, cytokines, and chemokines in Nrf2-KO cells [58, 59]. Several studies have reported the crosstalk between Nrf2/HO-1 with NF- κ B/iNOS. Nrf2-knockout mice showed increased mRNA and protein levels of iNOS, and the activation of Nrf2 leads to the reduction of iNOS [58, 60]. Nrf2 or HO-1 gene-deficient mice with pneumococcal meningitis showed significantly higher levels of HMGB1 and iNOS [61]. Here, the data showed that crocetin can activate the Nrf2/HO-1 pathway (Figure 4(a)) which may be attributed to the direct binding between crocetin and Keap1-Nrf2 complex (Supplementary Fig. 3B). Nrf2-KD, HO-1-KD, and HO-1-KO inhibition can attenuate crocetin-mediated iNOS inhibitory activity (Figures 4(b) and 4(c)). More detail is shown in Figure 4(d) that crocetin had increased the expression of

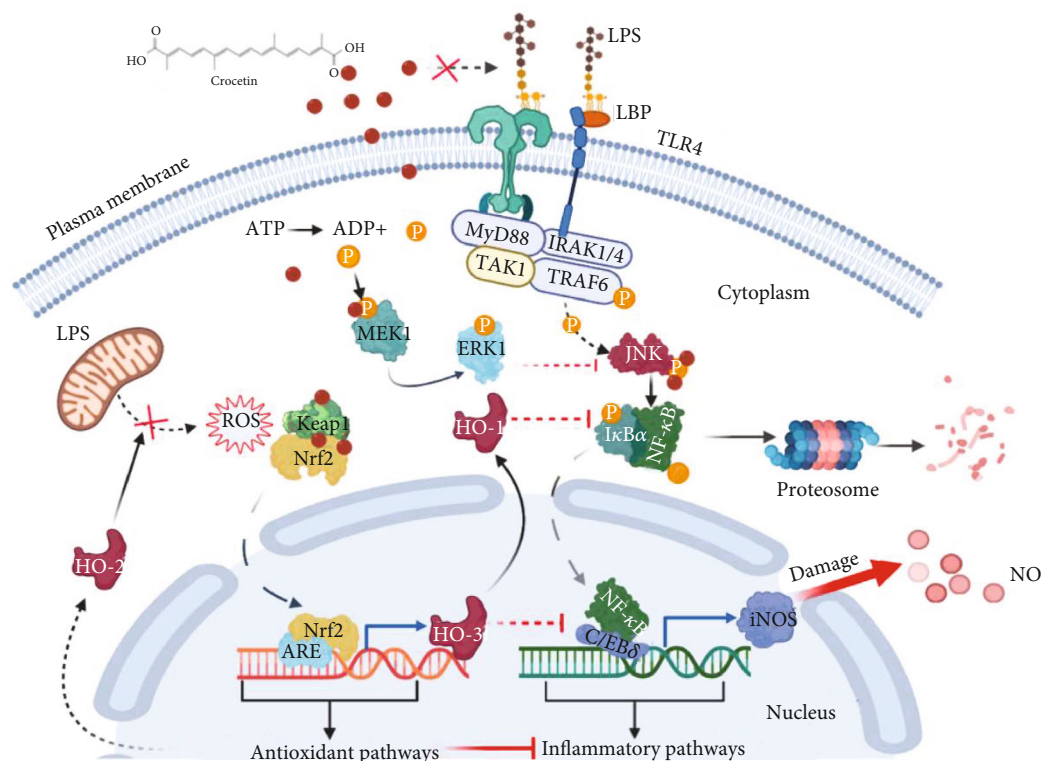


FIGURE 6: Schematic diagram of the molecular mechanism underlying the anti-inflammatory effect of crocetin on LPS-induced RAW264.7 cells. LPS can stimulate the activation of the TLR4/NF- κ B/iNOS inflammatory pathway in RAW264.7 cells. Crocetin treatment effectively inhibits LPS-induced iNOS expression by inhibition of the MEK1/ERK1/JNK/NF- κ B/iNOS pathway and activation of the Nrf2/HO-1 pathway. HO-1 is the link point for the crosstalk between these two pathways, and KD or KO of *HO-1* gene can eliminate the potent anti-inflammatory effect of crocetin. In addition, crocetin treatment significantly inhibits the LPS-induced ROS production, while this protective mechanism involved is not clarified, which is involved in protected effects.

HO-1 which is contributed to the stability of I κ B- α (Figure 4(d)). This result was also well replicated in another study [62]. These data implied that this action of crocetin is partially attributed to the activation of the Nrf2/HO-1 pathway, especially the induction of HO-1. Moreover, a series of studies speculate that the regulation of iNOS by the Nrf2/HO-1 antioxidant signaling pathway stems from its ability to inhibit the production of ROS which can effectively activate MAPKs [63]. However, as shown in Supplementary Fig. 1, crocetin was found to dose-dependently inhibit LPS-induced ROS production, but treatment with different concentrations of NAC, a common ROS scavenger [64], has no effect on LPS-induced iNOS expression. These results suggested that there was no significant correlation between the crocetin-mediated iNOS inhibitory activity and the reduction of crocetin-mediated ROS production. Thus, further research is needed to elucidate the molecular mechanism in depth underlying the relationship between ROS, Nrf2/HO-1, and NF- κ B/iNOS.

A previous review suggests that the immunomodulatory activity of crocetin may be caused by direct targeting Toll-like receptors (TLRs) and the subsequent regulation of various transcription factors such as NF- κ B and AP-1 [65]. Thus, to confirm whether crocetin competes with LPS for binding to TLR4 to exert its anti-inflammatory property, computational docking analysis based on the structure of the TLR4-MD2

complex (PDB ID: 5IJB) and crocetin was performed. The data (Supplementary Figure 3A) showed that crocetin is docked in the different domains of the TLR4-MD2 complex with LPS, suggesting that crocetin might have no competitive binding to the TLR4-MD2 complex with LPS. Moreover, another piece of evidence is that knockdown of TLR-4 has no effect on crocetin-caused induction of HO-1 (Supplementary Fig. 2). These data further confirmed that crocetin exerts its anti-inflammatory effect by not targeting TLR-4, and which potent extracellular receptors crocetin targets require more detailed exploration.

5. Conclusion

In the present study, it was found that crocetin exerted its anti-inflammatory property by inhibiting the MEK1/JNK/NF- κ B/iNOS pathway and activating the Nrf2/HO-1 pathway; the direct crosstalk between the MEK1/JNK/NF- κ B/iNOS pathway and the Nrf2/HO-1 pathway is existing in crocetin-treated cells, which is essential for the anti-inflammatory effect of crocetin; HO-1 is the key link point of the above crosstalk. Therefore, crocetin can act as a redox balance modulator to orchestrate precisely its anti-inflammatory and chemopreventive effect via its regulatory action on the crosstalk between the NF- κ B/iNOS pathway and the Nrf2/HO-1 pathway.

Data Availability

The authors confirm that all data underlying the findings are available. All relevant data are within the paper and its supporting information files.

Conflicts of Interest

The authors declare that there are no conflicts of interest regarding the publication of this paper.

Acknowledgments

This work was partially supported by the National Key Research and Development Program of China (2019YFC1604903), Natural Science Foundation of China (31101268), Natural Science Foundation of Hunan Province (2019JJ40132), and Double First-Class Construction Project of Hunan Agricultural University (SYL201802025) to Si Qin.

Supplementary Materials

Supplementary 1. Supplementary Figure 1: the role of ROS in LPS-induced iNOS expression. (A) Crocetin inhibits LPS-induced ROS production. Cell culture and treatment were done as described in Materials and Methods. (B) NAC (ROS scavengers) cannot inhibit LPS-induced iNOS expression. RAW264.7 cells were treated with NAC (5–15 μ M) for 1 h before starvation in serum-free medium for another 2.5 h and then exposed to 40 ng/ml LPS for an additional 12 h. The expressions of iNOS were detected by Western blot analysis. Data are presented as the mean \pm SD of at least triplicate tests. * p < 0.05 and ** p < 0.01 vs. LPS-treated cells.

Supplementary 2. Supplementary Figure 2: the involvement of TLR-4 in iNOS and HO-1 expressions. (A) RT-qPCR test of gene knockdown efficiency. (B) TLR-4 is involved in LPS-induced iNOS inhibition but not involved in crocetin-induced HO-1 overexpression. NC and TLR-4-KD cells were pretreated with crocetin (20 μ g/ml) for 1 h and then exposed to 40 ng/ml LPS for an additional 12 h. The HO-1 and iNOS expression was detected by Western blot analysis using their corresponding antibodies. Data are presented as the mean \pm SD of triplicate tests. * p < 0.05 and ** p < 0.01 vs. LPS-treated cells.

Supplementary 3. Supplementary Figure 3: the docking models of crocetin to TLR4-MD2 and Keap1-Nrf2 complex. (A) There are 3 hydrogen bonds for the binding of crocetin to the TLR4-MD2 complex, which is not the same binding region of LPS. (B) For the Keap1-Nrf2 complex, three hydrogen bonds were formed between crocetin and His552, Asp579, and Asp573 residues of Keap1, which did not configure a part of the Keap1 catalytic domain.

References

- [1] S. Higashino, Y. Sasaki, J. C. Giddings et al., "Crocetin, a carotenoid from gardenia jasminoides Ellis, protects against hypertension and cerebral thrombogenesis in stroke-prone

spontaneously hypertensive rats," *Phytotherapy Research*, vol. 28, no. 9, pp. 1315–1319, 2014.

- [2] M. Hashemi and H. Hosseinzadeh, "A comprehensive review on biological activities and toxicology of crocetin," *Food and Chemical Toxicology*, vol. 130, pp. 44–60, 2019.
- [3] M. Rameshrad, B. M. Razavi, and H. Hosseinzadeh, "Saffron and its derivatives, crocin, crocetin and safranal: a patent review," *Expert Opinion on Therapeutic Patents*, vol. 28, no. 2, pp. 147–165, 2018.
- [4] L. C. Dong, Y. X. Fan, Q. Yu et al., "Synergistic effects of rhubarb-gardenia herb pair in cholestatic rats at pharmacodynamic and pharmacokinetic levels," *Journal of Ethnopharmacology*, vol. 175, pp. 67–74, 2015.
- [5] H. Chen, X. Huang, J. Min et al., "Geniposidic acid protected against ANIT-induced hepatotoxicity and acute intrahepatic cholestasis, due to Fxr-mediated regulation of Bsep and Mrp2," *Journal of Ethnopharmacology*, vol. 179, pp. 197–207, 2016.
- [6] H. Zhang, Q. Lai, Y. Li, Y. Liu, and M. Yang, "Learning and memory improvement and neuroprotection of *Gardenia jasminoides* (*Fructus gardenia*) extract on ischemic brain injury rats," *Journal of Ethnopharmacology*, vol. 196, pp. 225–235, 2017.
- [7] X. Song, W. Zhang, T. Wang et al., "Geniposide plays an anti-inflammatory role via regulating TLR4 and downstream signaling pathways in lipopolysaccharide-induced mastitis in mice," *Inflammation*, vol. 37, no. 5, pp. 1588–1598, 2014.
- [8] Y. Xiaofeng, C. Qinren, H. Jingping et al., "Geniposide, an iridoid glucoside derived from *Gardenia jasminoides*, protects against lipopolysaccharide-induced acute lung injury in mice," *Planta Medica*, vol. 78, no. 6, pp. 557–564, 2012.
- [9] C. Zhang, Y. T. Li, Y. Q. Xiao, D. R. Yu, Y. L. Ma, and X. Z. Gu, "Content comparison of main chemical compositions in *Gardenia jasminoides* roasted with ginger juice," *China Journal of Chinese Materia Medica*, vol. 38, no. 7, pp. 962–965, 2013.
- [10] C. Zhao, H. Zhang, H. Li et al., "Geniposide ameliorates cognitive deficits by attenuating the cholinergic defect and amyloidosis in middle-aged Alzheimer model mice," *Neuropharmacology*, vol. 116, pp. 18–29, 2017.
- [11] F. Soltani, M. Ramezani, S. Amel Farzad, A. Mokhtarzadeh, and M. Hashemi, "Comparison study of the effect of alkyl-modified and unmodified PAMAM and PPI dendrimers on solubility and antitumor activity of crocetin," *Artificial Cells, Nanomedicine, and Biotechnology*, vol. 45, no. 7, pp. 1356–1362, 2017.
- [12] A. Zhang and J. Li, "Crocetin shifts autophagic cell survival to death of breast cancer cells in chemotherapy," *Tumor Biology*, vol. 39, 2017.
- [13] S. Li, Y. Qu, X. Y. Shen et al., "Multiple signal pathways involved in crocetin-induced apoptosis in KYSE-150 cells," *Pharmacology*, vol. 103, no. 5-6, pp. 263–272, 2019.
- [14] K. N. Nam, Y.-M. Park, H.-J. Jung et al., "Anti-inflammatory effects of crocin and crocetin in rat brain microglial cells," *European Journal of Pharmacology*, vol. 648, no. 1-3, pp. 110–116, 2010.
- [15] M. Lautenschläger, J. Sendker, S. Hüwel et al., "Intestinal formation of *trans*-crocetin from saffron extract (*Crocus sativus*L.) and *in vitro* permeation through intestinal and blood brain barrier," *Phytomedicine*, vol. 22, no. 1, pp. 36–44, 2015.
- [16] X. Wang, X. Jiao, Z. Liu, and Y. Li, "Crocetin potentiates neurite growth in hippocampal neurons and facilitates functional

- recovery in rats with spinal cord injury,” *Neuroscience Bulletin*, vol. 33, no. 6, pp. 695–702, 2017.
- [17] S. Li, “A corpus-based study of vague language in legislative texts: strategic use of vague terms,” *English for Specific Purposes*, vol. 45, pp. 98–109, 2017.
 - [18] L. Song, C. Kang, Y. Sun, W. Huang, W. Liu, and Z. Qian, “Crocin inhibits lipopolysaccharide-induced inflammatory response in human umbilical vein endothelial cells,” *Cellular Physiology and Biochemistry*, vol. 40, no. 3–4, pp. 443–452, 2016.
 - [19] P. Chen, Y. Chen, Y. Wang et al., “Comparative evaluation of hepatoprotective activities of geniposide, crocins and crocetin by CCl₄-induced liver injury in mice,” *Biomolecules & Therapeutics*, vol. 24, no. 2, pp. 156–162, 2016.
 - [20] R. Yang, K. Vernon, A. Thomas, D. Morrison, N. Qureshi, and C. W. van Way III, “Crocin reduces activation of hepatic apoptotic pathways and improves survival in experimental hemorrhagic shock,” *Journal of Parenteral and Enteral Nutrition*, vol. 35, no. 1, pp. 107–113, 2011.
 - [21] M. Xiang, R. Yang, Y. Zhang et al., “Effect of crocetin on vascular smooth muscle cells migration induced by advanced glycosylation end products,” *Microvascular Research*, vol. 112, pp. 30–36, 2017.
 - [22] S. Mahdavi, S. Z. Bathaie, M. Nakhjavani, and M. Taghikhani, “The synergistic effect of antiglycating agents (MB-92) on inhibition of protein glycation, misfolding and diabetic complications in diabetic- atherosclerotic rat,” *European Journal of Medicinal Chemistry*, vol. 121, pp. 892–902, 2016.
 - [23] L. Yang, Z. Qian, H. Ji et al., “Inhibitory effect on protein kinase C θ by Crocetin attenuates palmitate- induced insulin insensitivity in 3T3-L1 adipocytes,” *European Journal of Pharmacology*, vol. 642, no. 1–3, pp. 47–55, 2010.
 - [24] E. Inoue, Y. Shimizu, M. Shoji, H. Tsuchida, Y. Sano, and C. Ito, “Pharmacological properties of N-095, a drug containing red ginseng, polygala root, saffron, antelope horn and aloe wood,” *American Journal of Chinese Medicine*, vol. 33, no. 1, pp. 49–60, 2005.
 - [25] B. Chen, Z. H. Hou, Z. Dong, and C. D. Li, “Crocin Downregulates the Proinflammatory Cytokines in Methylcholanthrene- Induced Rodent Tumor Model and Inhibits COX-2 Expression in Cervical Cancer Cells,” *BioMed Research International*, vol. 2015, Article ID 829513, 5 pages, 2015.
 - [26] L. J. Ignarro, “Nitric oxide as a unique signaling molecule in the vascular system: a historical overview,” *Journal of Physiology and Pharmacology*, vol. 53, 4, Part 1, pp. 503–514, 2002.
 - [27] H. Prast and A. Philippu, “Nitric oxide as modulator of neuronal function,” *Progress in Neurobiology*, vol. 64, no. 1, pp. 51–68, 2001.
 - [28] N. R. Bhat, D. L. Feinstein, Q. Shen, and A. N. Bhat, “p38 MAPK-mediated Transcriptional activation of inducible nitric-oxide synthase in glial cells,” *Journal of Biological Chemistry*, vol. 277, no. 33, pp. 29584–29592, 2002.
 - [29] R. N. Saha and K. Pahan, “Regulation of inducible nitric oxide synthase gene in glial cells,” *Antioxidants & Redox Signaling*, vol. 8, no. 5–6, pp. 929–947, 2006.
 - [30] X. Zhang, M. Ding, P. Zhu et al., “New insights into the Nrf-2/HO-1 signaling axis and its application in pediatric respiratory diseases,” *Oxidative Medicine and Cellular Longevity*, vol. 2019, Article ID 3214196, 9 pages, 2019.
 - [31] D. Willis, A. R. Moore, R. Frederick, and D. A. Willoughby, “Heme oxygenase: a novel target for the modulation of inflammatory response,” *Nature Medicine*, vol. 2, no. 1, pp. 87–90, 1996.
 - [32] T. Minamino, H. Christou, C.-M. Hsieh et al., “Targeted expression of heme oxygenase-1 prevents the pulmonary inflammatory and vascular responses to hypoxia,” *Proceedings of the National Academy of Sciences of the United States of America*, vol. 98, no. 15, pp. 8798–8803, 2001.
 - [33] T. S. Lee and L. Y. Chau, “Heme oxygenase-1 mediates the anti-inflammatory effect of interleukin-10 in mice,” *Nature Medicine*, vol. 8, no. 3, pp. 240–246, 2002.
 - [34] K. D. Poss and S. Tonegawa, “Heme oxygenase 1 is required for mammalian iron reutilization,” *Proceedings of the National Academy of Sciences of the United States of America*, vol. 94, no. 20, pp. 10919–10924, 1997.
 - [35] A. Yachie, Y. Niida, T. Wada et al., “Oxidative stress causes enhanced endothelial cell injury in human heme oxygenase-1 deficiency,” *Journal of Clinical Investigation*, vol. 103, no. 1, pp. 129–135, 1999.
 - [36] K. Tsoyi, I. T. Nizamutdinova, H. J. Jang et al., “Carbon monoxide from CORM-2 reduces HMGB1 release through regulation of IFN- β /JAK2/STAT-1/INOS/NO signaling but not COX-2 in TLR-activated macrophages,” *Shock*, vol. 34, no. 6, pp. 608–614, 2010.
 - [37] E. J. Park, Y. M. Kim, H. J. Kim, and K. C. Chang, “Luteolin activates ERK1/2- and Ca²⁺-dependent HO-1 induction that reduces LPS-induced HMGB1, iNOS/NO, and COX-2 expression in RAW264.7 cells and mitigates acute lung injury of endotoxin mice,” *Inflammation Research*, vol. 67, no. 5, pp. 445–453, 2018.
 - [38] T. Kirikae, H. Tamura, M. Hashizume et al., “Endotoxin contamination in fetal bovine serum and its influence on tumor necrosis factor production by macrophage-like cells J774.1 cultured in the presence of the serum,” *International Journal of Immunopharmacology*, vol. 19, no. 5, pp. 255–262, 1997.
 - [39] Z. Yang, L. S. Khemlani, D. F. Dean, C. D. Carter, D. O. Slau-son, and P. N. Bochsler, “Serum components enhance bacterial lipopolysaccharide-induced tissue factor expression and tumor necrosis factor- α secretion by bovine alveolar macrophages in vitro,” *Journal of Leukocyte Biology*, vol. 55, no. 4, pp. 483–488, 1994.
 - [40] Z. J. Jian, Z. Yang, G. L. Mason, D. O. Slau-son, and P. N. Bochsler, “Regulation of superoxide anion generation in bovine alveolar macrophages by bacterial lipopolysaccharide, serum proteins, and modulators of signal transduction,” *Inflammation*, vol. 19, no. 6, pp. 637–650, 1995.
 - [41] T. Uto, M. Fujii, and D. X. Hou, “Inhibition of lipopolysaccharide-induced cyclooxygenase-2 transcription by 6-(methylsulfinyl) hexyl isothiocyanate, a chemopreventive compound from *Wasabia japonica* (Miq.) Matsumura, in mouse macrophages,” *Biochemical Pharmacology*, vol. 70, no. 12, pp. 1772–1784, 2005.
 - [42] A. Hisanaga, R. Mukai, K. Sakao, J. Terao, and D.-X. Hou, “Anti-inflammatory effects and molecular mechanisms of 8-prenyl quercetin,” *Molecular Nutrition and Food Research*, vol. 60, no. 5, pp. 1020–1032, 2016.
 - [43] T. Kumamoto, M. Fujii, and D. X. Hou, “Akt is a direct target for myricetin to inhibit cell transformation,” *Molecular and Cellular Biochemistry*, vol. 332, no. 1–2, pp. 33–41, 2009.
 - [44] L. Swiech, M. Heidenreich, A. Banerjee et al., “In vivo interrogation of gene function in the mammalian brain using CRISPR-Cas9,” *Nature Biotechnology*, vol. 33, no. 1, pp. 102–106, 2015.

- [45] C. P. Lebel, H. Ischiropoulos, and S. C. Bondy, "Evaluation of the probe 2',7'-dichlorofluorescein as an indicator of reactive oxygen species formation and oxidative stress," *Chemical Research in Toxicology*, vol. 5, no. 2, pp. 227–231, 1992.
- [46] Y. J. Hong and K. S. Yang, "Anti-inflammatory activities of crocetin derivatives from processed *Gardenia jasminoides*," *Archives of Pharmacal Research*, vol. 36, no. 8, pp. 933–940, 2013.
- [47] P. Baeuerle and D. Baltimore, "I kappa B: a specific inhibitor of the NF-kappa B transcription factor," *Science*, vol. 242, no. 4878, pp. 540–546, 1988.
- [48] J. Lekstrom-Himes and K. G. Xanthopoulos, "Biological role of the ccaat/enhancer-binding protein family of transcription factors," *Journal of Biological Chemistry*, vol. 273, no. 44, pp. 28545–28548, 1998.
- [49] J. S. Won, Y. B. Im, L. Key, I. Singh, and A. K. Singh, "The involvement of glucose metabolism in the regulation of inducible nitric oxide synthase gene expression in glial cells: possible role of glucose-6-phosphate dehydrogenase and CCAA T/enhancing binding protein," *Journal of Neuroscience*, vol. 23, no. 20, pp. 7470–7478, 2003.
- [50] W. Lee, S. Yang, C. Lee et al., "Aloin reduces inflammatory gene iNOS via inhibition activity and p-STAT-1 and NF- κ B," *Food and Chemical Toxicology*, vol. 126, pp. 67–71, 2019.
- [51] D. Luo, Y. Guo, Y. Cheng, J. Zhao, Y. Wang, and J. Rong, "Natural product celastrol suppressed macrophage M1 polarization against inflammation in diet-induced obese mice via regulating Nrf2/HO-1, MAP kinase and NF- κ B pathways," *Aging*, vol. 9, no. 10, pp. 2069–2082, 2017.
- [52] R. Yang, X. Tan, A. M. Thomas et al., "Crocetin inhibits mRNA expression for tumor necrosis Factor- α , Interleukin-1 β , and inducible nitric oxide synthase in hemorrhagic shock," *Journal of Parenteral & Enteral Nutrition*, vol. 30, no. 4, pp. 297–301, 2006.
- [53] Y. Li, R. Kakkar, and J. Wang, "In vivo and in vitro approach to anti-arthritis and anti-inflammatory effect of crocetin by alteration of nuclear factor-E2-related factor 2/hem oxygenase (HO)-1 and NF- κ B expression," *Frontiers in Pharmacology*, vol. 9, 2018.
- [54] J. S. Arthur and S. C. Ley, "Mitogen-activated protein kinases in innate immunity," *Nature Reviews Immunology*, vol. 13, no. 9, pp. 679–692, 2013.
- [55] Y. Li, L. Zou, T. Li, D. Lai, Y. Wu, and S. Qin, "Mogroside V inhibits LPS-induced COX-2 expression/ROS production and overexpression of HO-1 by blocking phosphorylation of AKT1 in RAW264.7 cells," *Acta Biochimica et Biophysica Sinica*, vol. 51, no. 4, pp. 365–374, 2019.
- [56] C. J. Caunt and S. M. Keyse, "Dual-specificity MAP kinase phosphatases (MKPs): shaping the outcome of MAP kinase signalling," *The FEBS Journal*, vol. 280, no. 2, pp. 489–504, 2013.
- [57] K. L. Jeffrey, T. Brummer, M. S. Rolph et al., "Positive regulation of immune cell function and inflammatory responses by phosphatase PAC-1," *Nature Immunology*, vol. 7, no. 3, pp. 274–283, 2006.
- [58] R. K. Thimmulappa, C. Scollick, K. Traore et al., "Nrf2-dependent protection from LPS induced inflammatory response and mortality by CDDO-Imidazole," *Biochemical and Biophysical Research Communications*, vol. 351, no. 4, pp. 883–889, 2006.
- [59] J.-F. Luo, X.-Y. Shen, C. K. Lio et al., "Activation of Nrf2/HO-1 pathway by Nardochinoid C inhibits inflammation and oxidative stress in lipopolysaccharide-stimulated macrophages," *Frontiers in Pharmacology*, vol. 9, 2018.
- [60] F. M. Ho, H. C. Kang, S. T. Lee et al., "The anti-inflammatory actions of LCY-2-CHO, a carbazole analogue, in vascular smooth muscle cells," *Biochemical Pharmacology*, vol. 74, no. 2, pp. 298–308, 2007.
- [61] Z. Li, Q. Q. Ma, Y. Yan et al., "Edaravone attenuates hippocampal damage in an infant mouse model of pneumococcal meningitis by reducing HMGB1 and iNOS expression via the Nrf2/HO-1 pathway," *Acta Pharmacologica Sinica*, vol. 37, no. 10, pp. 1298–1306, 2016.
- [62] R. K. Thimmulappa, H. Lee, T. Rangasamy et al., "Nrf2 is a critical regulator of the innate immune response and survival during experimental sepsis," *Journal of Clinical Investigation*, vol. 116, no. 4, pp. 984–995, 2006.
- [63] I. Rahman and I. M. Adcock, "Oxidative stress and redox regulation of lung inflammation in COPD," *The European Respiratory Journal*, vol. 28, no. 1, pp. 219–242, 2006.
- [64] M. Suzuki, C. Bandoski, and J. D. Bartlett, "Fluoride induces oxidative damage and SIRT1/autophagy through ROS-mediated JNK signaling," *Free Radical Biology and Medicine*, vol. 89, pp. 369–378, 2015.
- [65] M. Zeinali, M. R. Zirak, S. A. Rezaee, G. Karimi, and H. Hosseinzadeh, "Immunoregulatory and anti-inflammatory properties of *Crocus sativus* (Saffron) and its main active constituents: a review," *Iranian Journal of Basic Medical Sciences*, vol. 22, no. 4, pp. 334–344, 2019.

Review Article

The Neuroprotective Effects of Moderate and Regular Caffeine Consumption in Alzheimer's Disease

Xiangyu Zhou ¹ and Lin Zhang ²

¹School of Food Science and Nutrition, University of Leeds, Leeds, West Yorkshire LS2 9JT, UK

²The Key Laboratory for Special Medical Food Process in Hunan Province, Central South University of Forestry and Technology, Changsha, Hunan 410004, China

Correspondence should be addressed to Lin Zhang; 29415441@qq.com

Received 21 January 2021; Revised 27 June 2021; Accepted 19 July 2021; Published 17 August 2021

Academic Editor: Si Qin

Copyright © 2021 Xiangyu Zhou and Lin Zhang. This is an open access article distributed under the Creative Commons Attribution License, which permits unrestricted use, distribution, and reproduction in any medium, provided the original work is properly cited.

The increasing numbers of elderly Alzheimer's disease (AD) patients because of a steady increase in the average lifespan and aging society attract great scientific concerns, while there were fewer effective treatments on AD progression due to unclear exact causes and pathogenesis of AD. Moderate (200-500 mg/d) and regular caffeine consumption from coffee and tea are considered to alleviate the risk of AD and have therapeutic potential. This paper reviewed epidemiological studies about the relationship of caffeine intake from coffee or/and tea with the risk of AD and summarized the caffeine-related AD therapies based on experimental models. And further well-designed and well-conducted studies are suggested to investigate the optimal dosages, frequencies, and durations of caffeine consumption to slow down AD progression and treat AD.

1. Introduction

AD is the most common cause of dementia, which is associated with the physical deterioration of the brain tissue, leading to greater cognitive malfunctions than those of normal brain aging [1]. The incident rate of AD increases dramatically with age, only 2% among 65 years of age, 12.7% among 90 years of age, and 21.2% among 95 years of age, respectively [2]. And cognitive impairment, characterized by rapid memory and attention decline, is the high-risk factor for AD [1]. Because cognitive impairment is likely to progress to AD at a rate of 10% quicker than normal cognitive people at the same age [3], cognitive decline is regarded as a preclinical marker for early dementia. Thus, lowering cognitive decline also indicates a reduction of the risk of AD [4]. Furthermore, cognitive disorders include dementia, cognitive impairment, and cognitive decline [5].

AD is the consequence of the complex interplay between the genetic and environmental factors, including medical history of diseases and dietary habits [6]. Currently, there are limited efficient pharmacological therapies in reversing the

cognitive deterioration and slowing down the progression of AD [7]. And the permitted six drugs only provide temporary and incomplete symptomatic relief accompanied by severe side effects [8]. Therefore, clinicians considered modifiable risk factors for brain function preservation, such as lifestyle, obesity, diabetes, and hypertension [5]. Because those nonpharmacological interventions are easy to achieve, acceptable, cheap, and without negative consequences at routine levels, they could help reduce healthcare costs at population levels as good prophylaxis of AD [9]. Concerning aspects relating to lifestyle, multiple studies have examined the potential role of phytochemicals in preventing and slowing down progressive pathogenic changes in AD, including flavonoids, phenolic acids, carotenoids, curcumin, resveratrol, and some alkaloids (in the comprehensive reviews [10, 11]). Among them, the effects of caffeine seem to be well researched and documented [12].

Caffeine (1,3,7-trimethylxanthine), a purine alkaloid, is one of the most common and widely consumed psychoactive stimulants daily, exerting its functions on CNS to help antifatigue, increase concentration, and trigger the arousal of

neurons after short-term consumption [13]. Because chronic low doses of caffeine have been reported to protect against CNS hypoxia and ischemia in rats [14] and gerbils [15, 16], whereas acute caffeine administration exacerbated ischemic neuronal damage in rats with forebrain ischemia produced by bilateral carotid occlusion plus hypotension [14], caffeine may have neuroprotective effects; thus, it is reasonably hypothesized that regular caffeine consumption at a low dose for the long term could help prevent AD.

This article is initially aimed at examining the potential role of constant caffeine consumption in AD development based on human studies and treating AD based on experimental studies. The second aim is to recommend caffeine dosages, frequencies, and durations that may be beneficial.

2. Caffeine in AD: Human Study

Coffee and tea are the two most popular drinks worldwide and are the leading global dietary sources of caffeine [13]. Although caffeine contents vary in a cup of coffee in different studies due to various serving sizes (50–190 ml), types of coffee beans (Arabica or Robusta), preparation methods (boiled or filtered), and serving types (decaffeinated or Italian), the mean caffeine content is generally 90 mg per 230 ml of coffee (a regular cup of coffee is 230 ml) [17]. Caffeine amounts also vary in a cup of different types of tea. Fresh tea leaves should undergo the diverse degree of fermentation and oxidation of polyphenols during manufacturing; therefore, 100 ml of non-fermented green tea has 15 mg of caffeine on average, and semifermented oolong tea and fermented black tea have 17 mg of caffeine per 100 ml on average (a regular cup of tea is 100 ml) [18]. If coffee or/and tea consumption could provide appropriate dosages of caffeine to modify the progression of a neurodegenerative disorder that may evolve many years before the emergence of visible clinical symptoms, as appears to be the case with AD, without side effects, they may be recommended as a daily natural complementary therapy for lowering the risk of AD and slowing down the progression of AD.

This article summarizes 15 human studies including case-control studies, cohort studies, cross-sectional studies, and meta-analyses in Table 1, to access the possible effects of caffeine from coffee or/and tea on AD and suggest optimal dosages, frequencies, and durations of coffee and tea consumption.

2.1. Method. (1) If the selected human studies defined neither the exact caffeine doses in a cup of coffee and tea nor the exact volume of a cup, the caffeine amounts were determined by 90 mg caffeine per cup of coffee (a regular cup of coffee is 230 ml) [17], 15 mg caffeine per cup of green tea, and 17 mg caffeine per cup of black/oolong tea (a regular cup of tea is 100 ml) [18]. (2) The average amounts of daily coffee and tea consumption by Canadians were determined by Conway [19] and Lindsay et al. [20], respectively. (3) Because Westerners consume more black tea and rarer green tea than Easterners [21], if the particular types of tea were not identified in the study from the West, tea consumption refers to the mean caffeine amounts of black tea. (4) Tea consumption based on the Eastern study refers to the majority of consumed tea types.

2.2. Caffeine. A retrospective and matched-pair case-control study reported that AD patients only consumed an average of 73.9 ± 97.9 mg/d caffeine as compared to healthy control cases who had 198.7 ± 135.7 mg/d during the last 20 years preceding AD diagnosis. And caffeine exposure during this period could lower the risk of AD significantly with an OR of 0.40 (95% CI = 0.25–0.67). Daily caffeine intake was sourced from instant coffee (60 mg caffeine/142 ml), decaffeinated coffee (3 mg caffeine/142 ml), tea leaf (30 mg caffeine/142 ml), instant tea (20 mg caffeine/142 ml), and cola drinks (18 mg caffeine/170 ml) [22]. However, another nested case-control study observed that midlife caffeine intake from coffee (137 mg/227 ml), tea (47 mg/227 ml), and cola (46 mg/340 ml) was not significantly associated with the risk of late-life AD (25 years later). But the highest levels of caffeine consumption (411.0–1872.5 mg/d) were related to a lower OR of having any of the neuropathological lesion types at autopsy as compared to lower caffeine intake (≤ 137.0 mg/d) (multivariable-adjusted OR = 0.45, 95% CI = 0.23–0.89, and $P = 0.04$). And the adjusted mean caffeine intake among decedents with AD lesions was 279 mg as compared to 333 mg among those without lesions ($P = 0.10$) [23]. The 2010 meta-analyses of 11 studies reported that caffeine intake could reduce the risk of AD, with the summary RR of 0.83 (95% CI = 0.32–2.15, $I^2 = 40.5\%$) [24].

2.3. Coffee. After a 21-year-long period of follow-up observations, the Finnish cohort study reported that participants who consumed 690 to 1150 mg/d of coffee (270 to 450 mg/d caffeine) at midlife had a decreased risk of late-life AD by 58% significantly compared with those drinking 0 to 460 mg/d of coffee (0 to 180 mg/d caffeine, reference). Tea consumption was not associated with a decreased risk of AD later in life, partially because the majority of participants (60.5%) in this study did not drink tea, making statistical power low [25]. A large-scale population-based prospective cohort study among Canadians aged above 65 years consistently reported that daily coffee consumption (243 mg/d caffeine [26]) reduced the risk of AD by 31% during a 5-year follow-up, while daily tea drinking (64 mg/d caffeine [19]) was not associated with lowering AD risk (OR = 1.12, 95% CI = 0.78–1.61) [20]. Furthermore, a multiethnic cohort study among persons aged above 45 years old reported that, during an average of 16.2 years of follow-up, higher coffee intake (above 2 cups/d, above 180 mg/d caffeine) lowered the risk for all-cause death, with an HR of 0.82, as compared to 1 cup/d (HR = 0.88, 95% CI = 0.85–0.91). But only lower coffee consumption (1 cup/d, 90 mg/d caffeine) had a marginally positive association with the risk of AD (HR = 0.90, 95% CI = 0.71–1.14) as compared to a negative effect by higher coffee consumption (above 2 cups/d, 180 mg/d caffeine) [27]. Another large population-based cohort study of old Swedish adults (mean age of 83.2 years) reported that there were no associations of coffee consumption (177 mg/d caffeine) and risk of dementia during a mean follow-up of 12.6 years [28]. However, the 2007 meta-analyses of 4 observational studies reported that coffee consumption could significantly reduce AD risk in comparison with nonconsumers with a pooled risk estimate of 0.73 (95% CI

TABLE 1: The characteristics of selected human clinical trials (N = 15).

Author (year)	Country	Study design	Follow-up period (years)	Population	Caffeine intake, source	Outcome measure	OR, HR, or RR (95% CI)	Covariates
<i>Caffeine</i>								
Maia and De Mendonça (2002) [22]	Portugal	Case-control study	N/A	54 cases and 54 controls (matched for age and sex) Caucasians aged above 50 years	Daily caffeine consumption during the last 20 years preceded the diagnosis of AD 198.7 ± 135.7 mg per day consumed by healthy cases as compared to 73.9 ± 97.9 mg per day consumed by AD patients	AD (NINCDS-ADRD)	Caffeine: 0.40 (0.25-0.67)	Age, sex, smoking habits (nicotine consumption), alcohol consumption, nonsteroidal anti-inflammatory drugs, heart diseases, family history of dementia, education, head trauma, stroke, diabetes, vitamin E, hypertension, gastric disorder
Gelber et al. (2011) [23]	USA	Case-control study Data derived from HAAS Programme	N/A	118 AD cases among 3494 Japanese American participants aged from 71 to 93 years	Caffeine: >115.5-188.0 mg/d vs. 0-115.5 mg/d >188.0-277.5 mg/d vs. 0-115.5 mg/d >277.5-415.0 mg/d vs. 115.5 mg/d >415.0-2673.0 mg/d vs. 0-115.5 mg/d	AD (NINCDS-ADRD) Cognitive decline: CASI < 74	Caffeine: 1.20 (0.65-2.23) 1.15 (0.62-2.11) 1.07 (0.57-2.00) 0.95 (0.46-1.95)	Age, BMI, physical activity index, cigarette smoking, alcohol consumption, education, hypertension, education, elevated cholesterol, ApoE ε4 status, number of childhood years spent in Japan, history of diabetes mellitus, CVD, occupational complexity, and marital status
Santos et al. (2010) [24]	Europe, Australia, North America, Asia	Meta-analyses 11 selected studies (2 case-control, 9 cohort studies)	N/A	19,928 participants aged above 50 years	Caffeine intake	AD (NINCDS-ADRD) and cognitive impairment (MMSE or Benton Visual Retention Test scores)	Cognitive impairment: 0.84 (0.72-0.99)	N/A
<i>Coffee</i>								
Eskelinen et al. (2009) [25]	Finland	Cohort study Data from the CAIDE study is within the North Karelia Project and the FINMONICA study	21	48 cases among 1409 Finns aged from 65 to 79 years	Coffee: 270-450 mg/d vs. 0-180 mg/d caffeine (3-5 cups/d vs. 0-2 cups/d) >450 mg/d vs. 0-180 mg/d caffeine (>5 cups/d vs. 0-2 cups/d) 17 mg/d caffeine (≥1 cup/d vs. none)	AD (NINCDS-ADRD) and MMSE ≤ 24	Coffee: 0.42 (0.12-1.46) 1.01 (0.33-3.08) Tea: 0.91 (0.48-1.71)	Age, sex, education, the community of residence, follow-up time, midlife smoking, BMI, SBP, total serum cholesterol, ApoE ε4, physical activity, presence of late-life MI/strokes/DM, and Beck Depression Scale

TABLE 1: Continued.

Author (year)	Country	Study design	Follow-up period (years)	Population	Caffeine intake, source	Outcome measure	OR, HR, or RR (95% CI)	Covariates
Lindsay et al. (2002) [20]	Canada	Cohort study Data from CSHA	5	194 AD cases among 4615 Canadians aged above 65 years	Daily coffee (243 mg/d caffeine) [26] and tea (64 mg/d caffeine) consumption [19] as compared to no drinking	AD (NINCDS-ADRDA criteria and 3MS score < 78/100), <i>Diagnostic and Statistical Manual of Mental Disorders</i> , Fourth Edition, criteria	Coffee: 0.69 (0.50-0.96) Tea: 1.12 (0.78-1.61)	Age, sex, and education
Park et al. (2017) [27]	USA	Cohort study Data from the MEC study	16.2	1404 AD deaths among 185,855 Americans aged from 45 to 75 years Americans (African Americans, Native Hawaiians, Japanese Americans, Latinos, and whites)	Coffee: 90 mg/d vs. 0 mg/d caffeine (1 cup/d vs. none) 180-270 mg/d vs. 0 mg/d caffeine (2-3 cups/d vs. none) ≥360 mg/d vs. 0 mg/d caffeine (≥4 cups/d vs. none)	Death ascertainment by annual linkage to files of state death certificates in California and Hawaii and periodic linkage to the National Death Index AD death is defined as follows: ICD-9: 331.0 ICD-10: G30	Coffee: 0.90 (0.71-1.14) 1.16 (0.90-1.49) 1.33 (0.86-2.04)	Age, sex, race/ethnicity, education, cigarette smoking, preexisting chronic diseases, BMI, physical activity, alcohol consumption, total energy intake, and energy from fat
Larsson and Wolk (2018) [28]	Sweden	Cohort study Data from the National Research Infrastructure SIMPLER	12.6 years	1299 AD cases among 28,775 Swedish participants aged from 65-83 years	Coffee: 59-171 mg/d vs. <59 mg/d caffeine (1-2.9 cups/d vs. <1 cup/d) 177-289 mg/d vs. <59 mg/d caffeine (3-4.9 cups/d vs. <1 cup/d) ≥295 mg/d vs. <59 mg/d caffeine (≥5 cups/d vs. <1 cup/d) (1 cup = 150 ml)	N/A	Coffee: 0.90 (0.70-1.17) 1.01 (0.78-1.30) 0.93 (0.70-1.24)	Age, sex, education, smoking, BMI, exercise, walking or bicycling, history of hypertension, hypercholesterolemia, diabetes, sleep duration, alcohol
Quintana et al. (2007) [29]	Europe, North America, Australia	Meta-analyses 4 selected studies (2 case-control and 2 cohort studies)	N/A	5951 participants aged above 50 years	Coffee consumers vs. nonconsumers	AD (NINCDS-ADRDA)	AD: 0.73 (0.58-0.92)	N/A

TABLE 1: Continued.

Author (year)	Country	Study design	Follow-up period (years)	Population	Caffeine intake, source	Outcome measure	OR, HR, or RR (95% CI)	Covariates
<i>Tea</i>								
Chen et al. (2012) [30]	China	Case-control study Data from the third wave (2002) and fourth wave (2005) of CLHLS	N/A	1489 cases and 4822 Chinese controls aged above 65 years	Tea drinking habits	Cognitive decline: MMSE-r \leq 18	Tea: 0.82 (0.69-1.00)	Age, gender, marital status, financial status, residential area, BMI, hypertension, diabetes, smoking, alcohol, exercise habits, eating legumes and vegetables, fish, eggs, meat, and sugar consumption
					Green tea: \leq 45 mg/wk (\leq 3 cups/wk) 60-90 mg/wk or 15 mg/d (4-6 cups/wk or 1 cup/d) \geq 30 mg/d (\geq 2 cups/d) Black or oolong tea: \leq 51 mg/wk (\leq 3 cups/wk)		Green tea: 1.0 (reference) 0.62 (0.33-1.19) 0.46 (0.30-0.72) Black or oolong tea: 1.0 (reference) 0.60 (0.35-1.02) 0.87 (0.55-1.38)	
Kuriyama et al. (2006) [31]	Japan	Cross-sectional study	N/A	1003 Japanese participants aged above 70 years	68-102 mg/wk or 17 mg/d (4-6 cups/wk or 1 cup/d) \geq 34 mg/d (\geq 2 cups/d) Coffee: \leq 117 mg/wk (\leq 3 cups/wk) 156-234 mg/wk or 39 mg/d (4-6 cups/wk or 1 cup/d) \geq 78 mg/d (\geq 2 cups/d) (1 cup = 100 ml)	Cognitive impairment: MMSE < 26	0.87 (0.55-1.38) Coffee: 1.0 (reference) 1.16 (0.78-1.73) 1.03 (0.59-1.80)	Age, sex, education, social activities, smoking, alcohol, physical activities, medical history, myocardial infarction, regular intake of supplements, self-rated health
	Singapore		N/A					

TABLE 1: Continued.

Author (year)	Country	Study design	Follow-up period (years)	Population	Caffeine intake, source	Outcome measure	OR, HR, or RR (95% CI)	Covariates
Ng et al. (2008) [4]		Cross-sectional study Data from SLAS		2194 Chinese living in Singapore aged above 55 years	<p>Coffee:</p> <p>Never or rarely ≥ 84 mg/d caffeine (≥ 1 cups/d)</p> <p>Habitual tea intake (sum of English black tea, Chinese black or oolong tea, green tea): Low, medium, and high levels vs. no drinking</p> <p>Low: < 37 mg/d caffeine (< 1 cup/d)</p> <p>Medium: 37-185 mg/d caffeine (1-5 cups/d)</p> <p>High: ≥ 222 mg/d caffeine (≥ 6 cups/d) (1 cup = 215 ml)</p> <p>Tea (include English black tea, Chinese black/oolong tea, and green tea):</p> <p>Never or rarely < 37 mg/wk (< 1 cup/wk)</p> <p>37-222 mg/wk (1-6 cups/wk)</p> <p>37-74 mg/d (1-2 cups/d)</p> <p>≥ 111 mg/d (≥ 3 cups/d)</p> <p>Coffee:</p> <p>Never or rarely < 84 mg/wk caffeine (< 1 cup/wk)</p> <p>84-504 mg/wk caffeine (1-6 cups/wk)</p> <p>84-168 mg/d (1-2 cups/d)</p> <p>≥ 252 mg/d (≥ 3 cups/d) (1 cup = 215 ml)</p>	<p>Cognitive impairment: MMSE-r ≤ 23</p>	<p>Coffee: 0.99 (0.69-1.45)</p> <p>Tea: Low: 0.56 (0.40-0.78) Medium: 0.45 (0.27-0.72) High: 0.37 (0.14-0.98)</p>	Age, sex, education, cigarette smoking, alcohol consumption, vegetable and fruit consumption, fish consumption, BMI, hypertension, diabetes, heart disease, stroke, depression, ApoE $\epsilon 4$, physical activities, social and productive activities, tea consumption (for coffee), and coffee consumption (for tea)
Feng et al. (2010) [32]	Singapore	Cross-sectional study Data came from SLAS	N/A	716 Chinese participants aged from 55 to 88 years	<p>37-74 mg/d (1-2 cups/d)</p> <p>≥ 111 mg/d (≥ 3 cups/d)</p> <p>Coffee:</p> <p>Never or rarely < 84 mg/wk caffeine (< 1 cup/wk)</p> <p>84-504 mg/wk caffeine (1-6 cups/wk)</p> <p>84-168 mg/d (1-2 cups/d)</p> <p>≥ 252 mg/d (≥ 3 cups/d) (1 cup = 215 ml)</p>	Neuropsychological and cognitive test battery: MMSE < 24	N/A	Age, sex, education, cigarette smoking, alcohol consumption, vegetable and fruit consumption, fish consumption, coffee consumption, medical conditions, blood pressure, fasting blood glucose, weight and height, ApoE $\epsilon 4$, physical activities, social activities, productive activities

TABLE 1: Continued.

Author (year)	Country	Study design	Follow-up period (years)	Population	Caffeine intake, source	Outcome measure	OR, HR, or RR (95% CI)	Covariates
Nurk et al. (2009) [21]	Norway	Cross-sectional study Part of population-based HUSK	N/A	2031 Norwegians aged from 70 to 74 years	Habitual tea intake during the previous year (mean value: 222 ml/d) vs. none	Cognitive impairment: m-MMSE score < 10	Tea: 0.95 (0.68–1.33)	Sex, history of CVD, diabetes, education, smoking status, use of vitamin supplements, and total energy intake
Ma et al. (2016) [33]	Asia, Europe, Australia, and North America	Meta-analyses 26 selected studies (10 case-control, 4 cohort, and 12 cross-sectional studies)	N/A	52,503 participants aged above 50 years	Daily tea consumption vs. nonconsumers/rare consumers	AD (NINCDS-ADRDA) and cognitive impairment (MMSE) Cognitive disorders include AD and cognitive impairment	Cognitive disorders: 0.65 (0.58–0.73) AD: 0.88 (0.65–1.12) Cognitive impairment: 0.52 (0.43–0.62)	N/A
Kim et al. (2015) [5]	Asia, Europe, Australia, North America	Meta-analyses 20 selected studies (5 case-control, 9 cohort, and 6 cross-sectional studies)	N/A	31,479 participants aged above 49 years	Caffeine intake	AD (NINCDS-ADRDA) and cognitive impairment (MMSE)	Cognitive disorders: 0.82 (0.67–1.01) AD: 0.78 (0.50–1.22) Cognitive impairment: 0.79 (0.61–1.04)	N/A

= 0.58–0.92), in a highly significant heterogeneity (chi-squared: 13.6, $P < 0.01$) [29].

2.4. Tea. A national population-based prospective nested case-control study on illiterate elderly Chinese subjects reported a significant inverse relationship between dietary habits of tea drinking and cognitive decline (OR = 0.82, 95% CI = 0.68–1.00, and $P = 0.0468$) [30]. And the community-based cross-sectional study among elderly Japanese subjects aged above 70 years also reported an inverse dose-dependent response between green tea consumption and prevalence of cognitive impairment. Subjects who consumed over 200 ml/d green tea (30 mg/d caffeine) and 100 ml/d (15 mg/d caffeine) had a significantly lower cognitive impairment risk by 54% and by 38%, respectively, as compared to below 300 ml/wk (45 mg/wk caffeine, reference) ($P = 0.0006$). However, a weaker association was observed for black or oolong tea consumption with the risk of cognitive impairment, and there was a null association between coffee consumption and the risk of cognitive impairment [31]. On the contrary, in the Singaporean cross-sectional study, participants habitually consumed vastly more black or oolong tea than green tea. Thus, the more inverse relation of black or oolong tea consumption with cognitive impairment was found as compared to green tea. And a higher intake corresponded to a lower risk of cognitive impairment, with an OR of 0.46 (95% CI = 0.31–0.68) for above 215 ml/d (37 mg/d caffeine) and an OR of 0.55 (95% CI = 0.38–0.79) for occasional intake. No significant associations were found between coffee intake and cognitive status [4]. And another Singaporean cross-sectional study among Chinese elders aged above 55 years reported that total tea consumption (34 mg/d caffeine) was related to better performance on global cognition (MMSE) ($B = 0.055$, $SE = 0.026$, and $P = 0.03$) and memory improvement ($B = 0.031$, $SE = 0.012$, and $P = 0.01$). The neuroprotective effects of tea consumption on cognitive function were not limited to a particular tea type. As 45.8% of participants consumed Chinese black/oolong tea, 37.6% consumed English black tea and 21.6% had green tea. However, no association was found between coffee intake and cognitive function, as well as a decrease in AD risk [32]. Another cross-sectional study among elderly Norwegians (aged 70–74 years) observed that habitual tea consumers who consumed a mean value of 222 ml/d (37 mg/d caffeine) black tea during the previous years had better cognitive performance than nonconsumers, examined by cognitive tests other than MMSE. And the sharpest dose-response effect of tea was up to 200 ml/d on cognitive performance, after which it tended to plateau [21]. Meanwhile, a meta-analysis of 26 studies (predominately Chinese studies) showed that tea drinking was significantly associated with a decreased risk of cognitive disorders in the elders (OR = 0.65, 95% CI = 0.58–0.73, and $I^2 = 78.8\%$) as compared to nonconsumers or rare consumers, partially owing to neuroprotective effects of caffeine components in tea. There were elusive findings of the relationship between tea intake and AD in the subgroup analysis (OR = 0.88, 95% CI = 0.65–1.12) due to the lack of included studies, especially non-Chinese studies [33]. On the contrary, a meta-analysis

of 20 studies concluded 5 AD-related studies, which reported that caffeine intake from coffee or tea was not significantly associated with the risk of AD in the random-effects model among elderly participants, with a subtotal OR/RR of 0.78 (95% CI = 0.50–1.22, $I^2 = 71.0\%$) [5].

2.5. Discussions on Human Studies. The current studies suggested that caffeine intake may be associated with a lower risk of cognitive disorders including AD, cognitive impairment, and cognitive decline, despite the presence of some inconsistent results. And the neuroprotective effects of caffeine were closely tied to the appropriate frequencies and dosages of consumption. According to Cappelletti et al., low caffeine intake is less than 200 mg/d, moderate caffeine intake is between 200 and 500 mg/d, and high caffeine intake is above 500 mg/day [34]. And the definitions of drinking frequency are regular intake (every day and above 5 times per week) and rare intake (below 2 times per week and never drinking). In line with data from included research showing an inverted U-shaped caffeine dose-response curve [20, 22, 25, 27], regularly intaking moderate caffeine had a better cognitive function and a lower AD risk. However, low caffeine intake levels had a borderline positive or null relationship with AD risk [27, 28], and high caffeine consumption may increase the risk of AD and decrease cognitive performance, especially from coffee intake [27].

Additionally, as the long-term follow-up observations were commonly used in the cohort design. And coffee drinking habits may alter over time, possibly after a significant interval, if the cognitive state or other environmental influences such as lifestyle changes occur. The more obvious protective effects of caffeine from coffee against AD were more likely to be reported in studies with shorter follow-up as cognition-impaired patients would reduce their daily coffee intake compared to healthy participants, just like the study conducted by Lindsay et al. of 5 years [20] compared with that by Larsson and Wolk of 12.3 years [28].

Coffee, which is more frequently consumed in Western countries than tea as a more popular beverage in Eastern countries, contains much higher amounts of caffeine than any type of tea [25]. Studies in Western countries consistently reported that coffee had neuroprotective effects but null associations of tea consumption, while Eastern countries found the opposite. The neuroprotective effects of tea consumption may be more related to the abundant tea flavonoids (catechins), especially EGCG in green tea and theaflavins in black tea, rather than the stimulant effect of scarce caffeine contents [32]. Furthermore, diversities connected to the ratio of tea leaves to hot water (the boiling way) and the reuse habits of the same tea leaves several times in East Asia in comparison with single-use coffee also make a difference in the analysis between the exact dosage of caffeine and positive neuroprotective effects [35]. And the amounts of caffeine intake from tea also depend on social and cultural diversities. For example, Japanese subjects consume vastly green tea (2 cups of green tea per day; one cup is 100 ml) as a social activity, while Chinese subjects consume a range of tea (more black/oolong tea) [4], resulting in inconsistent results about protective effects of different types of tea among

Japanese and Chinese subjects. Furthermore, because Westerners consume more black tea and rarer green tea than Easterners, a European study observed that habitual black tea consumption could lower the risk of AD but the plateau effects were up to 200 ml/d, even corresponding to the neuroprotective effects of lower caffeine amounts but in a habitual intake. And, by meta-analysis, which predominately had summarized Chinese studies, partially due to neuroprotective effects of caffeine in tea, tea consumption could reduce the risk of cognitive disorders in elders compared to nonconsumers or rare consumers [33]. It is thus reasonably assumed that the true association and interplay of flavonoids and caffeine with neuroprotection effects were underestimated. And all the studies on the neuroprotective effects of tea but not coffee were cross-sectional studies, with the results confined by the inference of a temporal causal relation between coffee and tea consumption and prevalence of AD, but the cognition in the old adults is shaped by long-term exposures [4]. Furthermore, the exact neuroprotection of tea for the old adults has also been affected by ambiguous drinking history and durations of tea before the involvement of studies. Further studies are needed to gather data from the long-term consumption of caffeinated coffee and tea to confirm the dose- and frequency-dependent association and the exact time of caffeine when its neuroprotective benefits begin [24]. And more well-defined studies are thus needed to be conducted on different racial/ethnic groups to achieve greater biological plausibility.

Findings of human epidemiological studies may also be influenced by various residual confounders, including smoking and physical activities, as a result of measurement errors or complementary effects of other active substances in coffee or/and tea, including magnesium [36], EGCG [37], and theaflavins [38], indicating human studies did not support the role of caffeine isolation in AD prophylactics.

Additionally, observational studies focusing on data from the self-reported questionnaires easily introduced biases and created incorrect information, especially in the long-term study. For example, the variability of daily doses of caffeine is increased through occasionally intaking other sources of caffeine like cola without informing the researchers. These exposure misclassifications undermine the methodological approach in particular in recalling it in the long term [24].

Further, different meta-analyses applied different searching strategies, inclusion criteria, and methods to select data for quantitative analysis, resulting in inconsistent findings [24]. And the quality of primary studies is the validity of meta-analysis. None of the double-blind placebo-controlled trials was selected in the meta-analysis that could provide more robust evidence [29], while observationally epidemiological studies were included, which recruited various participants, used different sample sizes, and applied different diagnostic criteria and methods of data analysis. For example, CSHA was a nationwide population-based study [20] while the study of Maia and De Mendonça [22] was a small hospital-based study with only 108 participants. Kuriyama et al. [31] utilized a cutoff value of MMSE of 26 for cognitive impairment diagnosis compared with 23 in Ng et al. [4]. And

meta-analysis has evened up a cup of coffee or tea among all studies, even though there were discrepancies in the definition of caffeine volumes in a cup, making it difficult to validate the dosages of neuroprotective effects of caffeine.

Besides, the main methodological limitation of this study was to neglect the effects of the coffee and tea preparation method, as well as specific coffee and tea types such as decaffeinated coffee and tea. Instead, it used 90 mg caffeine per 230 ml coffee, 15 mg caffeine per 100 ml green tea, and 17 mg caffeine per 100 ml black/oolong tea directly.

In conclusion, it is reasonably suggested that caffeine from moderate and regular caffeine consumption from coffee could impede AD progression but may not for tea intake. And it is required to conduct further well-defined studies on the exact optimal dosages, frequencies, and durations of caffeine from various tea types to minimize the risk of AD.

3. Caffeine: Pharmacokinetic Profile

The pharmacokinetic profile of caffeine may be linked to the favorable effects of caffeine on reducing the risk of AD.

After consuming caffeine, caffeine can be absorbed quickly and completely by the gastrointestinal tract, especially in the small intestine, with very high bioavailability (99%-100%) [39]. 96.34 mg of caffeine resulted in a maximal plasma concentration of 2.47 $\mu\text{g/ml}$ [40], in the following 30 to 60 minutes [41]. Due to the hydrophobic properties of caffeine, it can also cross through BBB quickly, and then, the brain achieves similar caffeine concentrations as blood, proposing mechanisms of neuroprotection against cognitive dysfunction by oral caffeine intake [41]. Long-term caffeine consumption leads to adaptive changes in the brain, indicating greater betterment on cognitive performance that occurred among the older adults with continuous and regular caffeine consumption [42]. And chronic caffeine treatments could protect against seizures and maintain spatial memory in the mouse model, which was greater than acute caffeine administration [42].

The elimination half-life of moderate amounts of caffeine in systemic circulation has been reported about 5 hours, indicating a quick metabolic rate of caffeine [43]. But the high doses of caffeine over 500 mg have lower elimination rates and thus may affect the cardiovascular system with their positive inotropic and chronotropic effects and the central nervous system with their locomotor activity stimulation and anxiogenic-like effects, accountable for tremor, tachycardia, and anxiety, respectively [34]. But in the habitual caffeine consumers with moderate amounts of caffeine consumption, the acute proarrhythmic effect even caused by high caffeine intake was somewhat attenuated [44]. But regularly intaking high amounts of caffeine leads to caffeine abuse and dependence and can result in caffeine intoxication, which puts individuals at risk for premature and unnatural death [34]. Consequently, caffeine is a central nervous stimulant and should not be used in excess. When used to treat AD, it may require controlling the doses of caffeine below 500 mg/d.

4. Pathogenesis of Alzheimer's Disease and Mechanisms of Caffeine Therapies

AD progressively causes neuronal damage and leads to dementia, which is commonly related to cognitive dysfunction and mental decline, being the third biggest cause of old disabilities and death [45]. This age-related problem is further influenced by population aging and leads to substantial growth in the AD patient population from 32.5 million in 2021 to 53.3 million by 2030 [46].

The neuropathological hallmarks of AD are the cerebral extracellular deposition of diffuse and neuritic senile plaques made by $A\beta$ peptides, the intracellular aggregation of flame-shaped NFTs composed of hyperphosphorylated aggregates of the microtubule-associated tau protein, and the selectively large-scale neuronal loss [47]. In understanding the pathology, neurobiological mechanisms underlying AD have been the key. And the most important changes identified can be explained currently by $A\beta$ theory, tau protein theory, oxidative stress theory, ApoE4 theory, and adenosine theory.

Meanwhile, human studies do not allow concluding on the role of caffeine itself in the modulation of AD risk. This article has concluded some experimental studies, especially in the transgenic mouse models of AD, based on the biological alternations observed in these human pathologies, to further investigate the effects of caffeine on AD development and potential therapeutic effects and dosages.

4.1. $A\beta$ Theory. $A\beta$ theory is related to the imbalance between the production of $A\beta$ through proteolysis of APP by β -secretase and γ -secretase and the clearance of produced $A\beta$, which is the triggering event and the most important factor [47].

Newly produced $A\beta$ comes into a dynamic equilibrium between isoforms soluble $A\beta_{1-40}$ and deposited $A\beta_{1-42}$ [48]. And the soluble $A\beta_{1-40}$ can be cleared out of the brain and entered into plasma down a concentration gradient [48], while the deposited toxic $A\beta_{1-42}$ is more difficult to be cleared due to greater hydrophobicity, which leads to acquiring the configuration of a β -pleated sheet and easily clumping themselves together to cause depositions of amyloid neuritic plaques, which disrupt cell functions and lead to AD [49]. By targeting β -secretase and γ -secretase to reduce $A\beta$ production or increasing the clearance speed of deposited $A\beta_{1-42}$, the progression of AD might be relieved.

APPsw mice, which were the most prominent transgenic AD models in animals, can develop substantial levels of brain $A\beta$ and widespread cognitive impairment with age [50]. The 4-5 weeks of treatment of 1.5 mg/d caffeine with the human equivalent of 500 mg/d caffeine in aged APPsw mice (18-19 months old) could stimulate PKA activity which would decrease the hyperactive form of c-Raf-1. This would correct dysregulation of the c-Raf-1 inflammatory pathway, inactivating the NF- κ B pathway and suppressing β -secretase expression (Figure 1, Pathway 1). Therefore, the evident $A\beta$ deposition was reduced by 46% and 40% within the entorhinal cortex and hippocampus of Tg caffeine-treated mice compared to Tg controls in total, respectively, at 20-21 months of age [51]. Among them, soluble $A\beta_{1-40}$ and insoluble

$A\beta_{1-42}$ levels of aged caffeine-treated Tg mice were reduced by 25% and 51% in the cortex and by 37% and 59% in the hippocampus, respectively, when compared with Tg controls [51]. Also, 1.5 mg/d caffeine treatment to aged 4-month-old APPsw Tg mice for 5.5 months could reduce β -secretase by 50% when following completion of behavioral testing at 9.5 months, then significantly lowering soluble $A\beta_{1-40}$ production by 37% ($P < 0.05$) and insoluble $A\beta_{1-42}$ production by 32% ($P < 0.05$) as compared to Tg control mice [41]. GSK-3 α dysregulation is known to $A\beta$ production by enhancing PS1 mutation which increases the γ -secretase cleavage of APP activity [52]. Caffeine (1.5 mg/d)-treated Tg mice had normalized PS1 band density ratios, compared with the significantly elevated Tg control group, after 5.5 months [41]. When treating cultured SweAPP N2a cells with caffeine in a dose-response manner (0-20 μ M), the maximal effects of decreasing active GSK-3 α levels were achieved at 20 μ M (the human equivalent of 100-200 mg of caffeine) by 90 minutes [51] (Figure 1, Pathway 1).

4.2. Tau Protein Theory. Although $A\beta$ theory is regarded to be the beginning of AD progression, however, it cannot fully explain the etiopathogenesis of AD. Tau protein is the secondary pathogenic event, subsequently leading to neurodegeneration [53]. $A\beta$ exposure promotes GSK-3 β overexpression, connected to neurodegeneration-related tau hyperphosphorylation [54]. Indeed, a study reported that chronic lithium (GSK-3 β inhibitor) treatment prevented tau hyperphosphorylation in the GSK-3 β transgenic mice [55].

Tau is a highly soluble protein whose biological activities are related to microtubules and are regulated by the degree of phosphorylation [56]. Under normal phosphorylation conditions, tau supports stabilizing the functions of microtubules on neuronal growth and axonal nutrient transport, while hyperphosphorylated tau loses its interactions with microtubules and prefers to aggregate with other tau molecules, forming neurofibrillary tangles inside neurons [56]. These neurofibrillary tangles consequently lead to microtubule dysfunction and blockage of the neuronal transport system, which damages the synaptic communications between neurons and AD-related brain changes [56]. And neurofibrillary tangles firstly found in the EC and hippocampus can extend to the amygdala and cortical areas (temporal, frontal, and parietal), causing more damage [57, 58].

The changes in $A\beta$ oligomers and tau protein are reported by studies to be the most important factors for neuronal dysfunction in AD pathology [59, 60]. And the strategies refer to decreasing phosphorylation degrees of tau.

In SweAPP N2a cells, the best caffeine treatment for suppression of GSK-3 β levels was 20 μ M for 30 minutes, and a lower phosphorylation degree of tau was proposed [51] (Figure 1, Pathway 2). 0.3 g/l of chronic caffeine delivery through drinking water (4 μ M plasma caffeine) to THY-Tau22 mice (aged 2 months old) for 10 months was significantly associated with an increase in dephosphorylated tau protein at Tau1 pathologic epitopes by 36.4% ($\pm 7.4\%$), as well as mitigated levels of proteolytic fragments of tau protein by reducing N-terminal fragments by 40.9% ($\pm 5.2\%$) and C-terminal fragments by 54.8% ($\pm 3.5\%$), as compared to

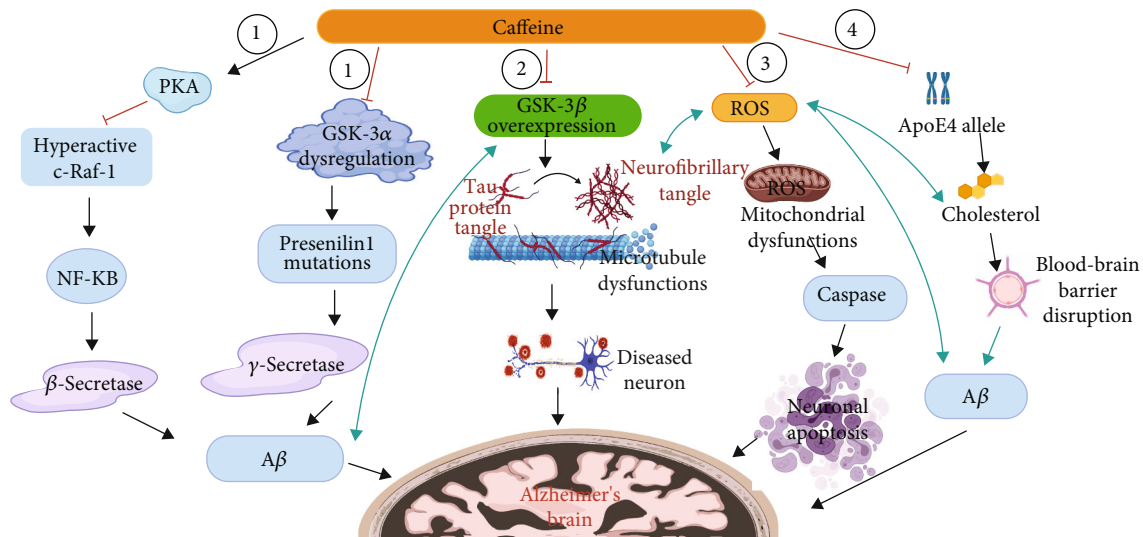


FIGURE 1: Caffeine neuroprotective mechanisms. (1) A β theory contains two routes. Firstly, caffeine stimulates PKA activity that decreases the hyperactive form of c-Raf-1. This abnormal c-Raf-1 form supports AD progression by activating the NF- κ B pathway and β -secretase expression. Secondly, caffeine lowers the GSK-3 α dysregulation which increases PS1 mutation and γ -secretase expression. (2) Tau protein theory relates to the caffeine deactivating GSK-3 β expression which can also be triggered by A β that expedites tau hyperphosphorylation and neurofibrillary tangle formation inside neurons. (3) Oxidative stress theory shows that caffeine inhibits ROS formation which can be promoted by A β . ROS can impair the mitochondrial electron transport system, further triggering caspase and neuronal apoptosis. (4) ApoE4 theory shows that caffeine can decrease high plasma and astrocyte cholesterol levels induced by high ApoE4 levels and reduce BBB disruptions by hypercholesterolemia (¹Adapted from "Pathology of Alzheimer's Disease", by BioRender.com (2021). Retrieved from <https://app.biorender.com/biorender-templates/t-5d8baeb4f7e1a5007dd46b18-pathology-of-alzheimers-disease/>).

untreated THY-Tau22 mice [61]. Reduction of tau phosphorylation by caffeine is consistent with an *in vitro* model of cultured cortical neurons (SH-SY5Y cells) in the non-pathogenic context, with dosages of 20 mM [62], which has been far higher than those achieved following habitual caffeine consumption (>10 mM) [63].

4.3. Oxidative Stress Theory. It is well understood that AD is strongly linked to extensive cellular OS [64]. OS is related to ROS accumulation in the brain because of inequality between ROS generation and antioxidant clearance activity [65]. The ROS could react quickly to biological components like lipid, leading to malfunction of the brain because the brain is mostly made up of a lipid that is easy to oxidize [65]. In addition, ROS could impair the mitochondrial electron transport system by disrupting its antioxidant enzyme functions, SOD1 and SOD2, causing a further increase in ROS levels that finally activate caspase and subsequently neuronal apoptosis [66] (Figure 1, Pathway 3). Also, OS could augment A β production and aggregation and facilitate tau hyperphosphorylation, which, in turn, further promotes ROS formation [67]. Thus, treatment with antioxidant properties could protect neurons from oxidative stress and A β toxicity.

Caffeine can be the antioxidant to inhibit lipid peroxidation and mitigate OS by suppressing the production of ROS [65]. The use of 10 μ M caffeine treatment might reduce intracellular ROS by 40.36%, increase SOD activity by 48.55%, and decrease malondialdehyde by 44.29% of the SH-SY5Y cells which have been exposed to the combination of A β ₂₅₋₃₅ and AlCl₃ for 48 h, and antiapoptotic Bcl-2 protein levels for the prevention of neuronal death has been rescued

[68]. Furthermore, the number of caspase-3-positive neurons was reduced by 48% after 1.84 mg/d caffeine treatment (equivalent to daily human consumption of 4.86 mg/kg body weight of caffeine) as compared to cultures treated with only 20 μ M of A β ₂₅₋₃₅ for 48 h, concurring the neuroprotective effects of caffeine against A β ₂₅₋₃₅-induced neuronal death [69].

4.4. ApoE4 Theory. ApoE4 is considered the largest genetic risk factor for AD, with a prevalence of about 14%, conferring a drastically elevated risk of AD with an earlier age of onset in a gene dose-dependent manner [70]. ApoE4 promotes the accumulation, aggregation, and deposition of A β in the brain. ApoE4 might be less efficient for clearing A β in the BBB due to a lower affinity to A β than other ApoE isoforms (ApoE2, ApoE3) [70].

Besides, ApoE4 also generates aberrant brain cholesterol metabolism which can further increase A β generation and contribute to the AD risk [70]. ApoE is mainly produced by brain astrocytes, which account for up to 40% of all brain cells, and could carry the lipoprotein-bound cholesterol from circulating plasma to the brain, which has been regulated by the presence of BBB [70]. ApoE4 is less efficient in transporting cholesterol from astrocytes to neurons and has a low binding capacity to plasma cholesterol [70]. Thus, high ApoE4 levels may lead to elevated cholesterol levels in the plasma and astrocytes [71]. And 2% cholesterol-enriched diets could induce hypercholesterolemia in rabbits; 3 times higher levels of insoluble A β ₁₋₄₀ were achieved by increasing γ -secretase activity to cleave APP on the hippocampus [72]. Hypercholesterolemia has been associated with OS by

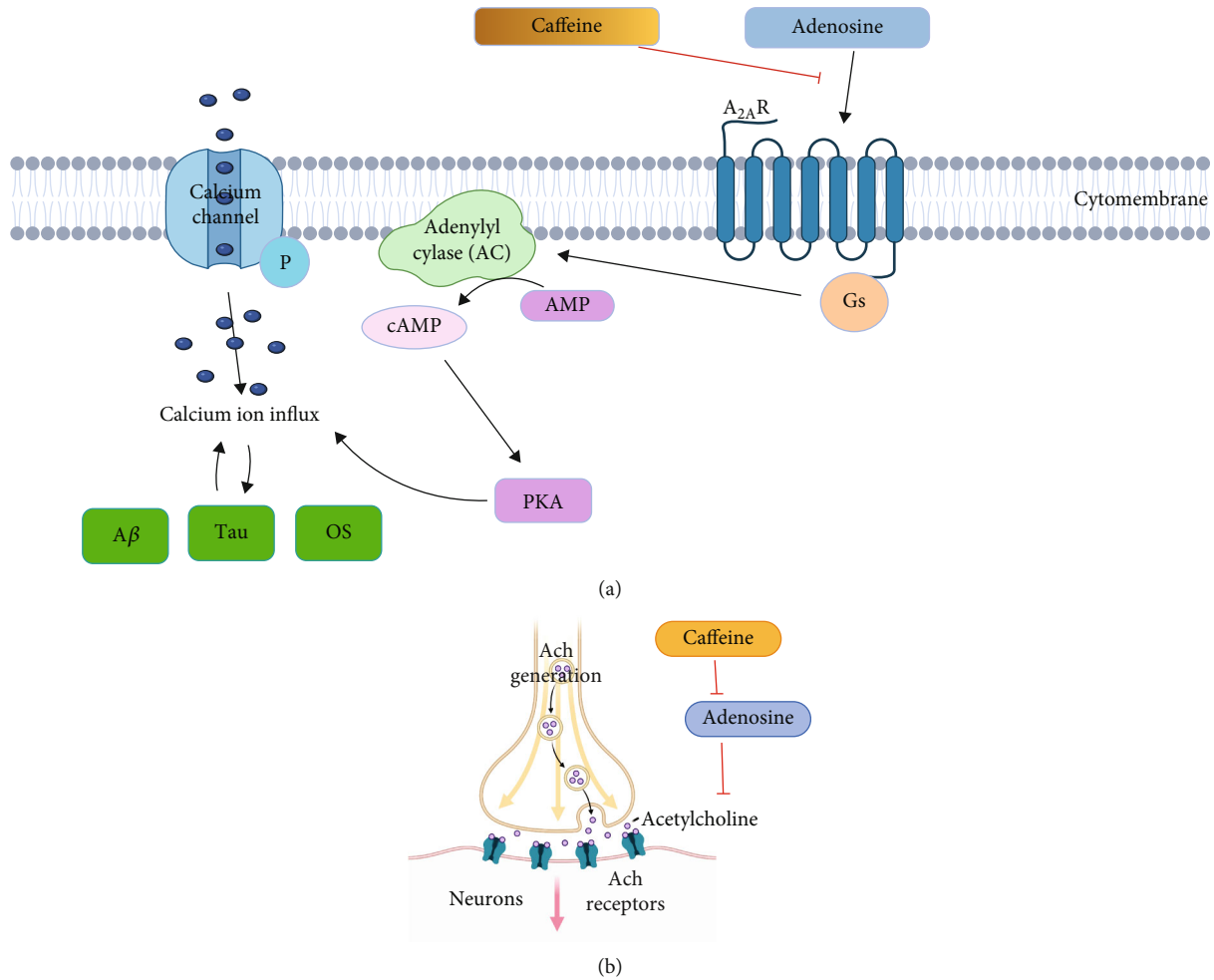


FIGURE 2: Caffeine intervenes with adenosine theory related to (a) lowering $A\beta$ production by antagonizing $A_{2A}R$ which can increase AC levels, cAMP and PKA activities, and overload of intracellular Ca^{2+} (²BioRender.com (2021). [Online]. Available from: <https://app.biorender.com/user/signin/>) and (b) inhibit adenosine functions on the decrease of neurotransmitter Ach expression (created with <https://biorender.com/> Created with BioRender.com.³ Adapted from "Neuromuscular Junction", by BioRender.com (2021). Retrieved from <https://app.biorender.com/biorender-templates/t-5ed6b2d243ee8200b0135913-neuromuscular-junction/>).

increasing ROS levels [72], and it could also disrupt BBB, increasing brain cholesterol levels further [73] (Figure 1, Pathway 4). Thus, strategies refer to reducing brain cholesterol accumulation.

0.5 mg/d and 30 mg/d caffeine treatments for 12 weeks decreased cholesterol-induced $A\beta$ accumulation and increased the phosphorylated tau and active form of enzyme GSK-3 β , as well as ROS generation in the hippocampus of rabbits (1.5-2 years old) which were daily fed a 2% cholesterol-enriched diet for 12 weeks. But the low caffeine dose (0.5 mg/d) was more efficient than the high dose (30 mg/d) in reducing $A\beta_{40}$ and $A\beta_{42}$ levels (-33.64% compared with -22.62%; -58.65% compared with -45.46%, respectively), which were reduced to similar levels as the control [72]. 12 weeks of 3 mg/d caffeine was given to rabbits aged 1.5 to 2 years, blocking the increased disruptions of BBB induced by the daily 2% cholesterol-enriched diet [73]. This was characterized by stabilization of the tight junctions between adjacent endothelial cells which involved an increase in expression of tight junction proteins includ-

ing occludin and zonula occludens by 72.71% and 50.37%, respectively [73].

4.5. Adenosine Theory. Aside from the common molecular pathogenesis of AD and associated theories, where many distinct factors interrelate, caffeine is largely linked to adenosine theory, which also interacts with other theories.

Adenosine is an endogenous neuroprotectant abundant in the CNS, and its extracellular concentrations rise considerably in response to brain damage, neuroinflammation, and aging [74]. Adenosine effects are mediated by interactions with G protein-coupled receptors called adenosine receptors, such as inhibitory A_1R and excitatory $A_{2A}R$ [75].

A_1R is found in abundance in the neocortex, cerebellum, hippocampus, and dorsal horn of the spinal cord [76]. $A_{2A}R$ is extensively expressed in the striatopallidal neurons and olfactory bulb, with lesser levels in other brain regions like the hippocampus [76]. Because low concentrations of adenosine prefer to act on the A_1R , while greater levels prefer to act on the $A_{2A}R$, aging causes an imbalance in the expression of

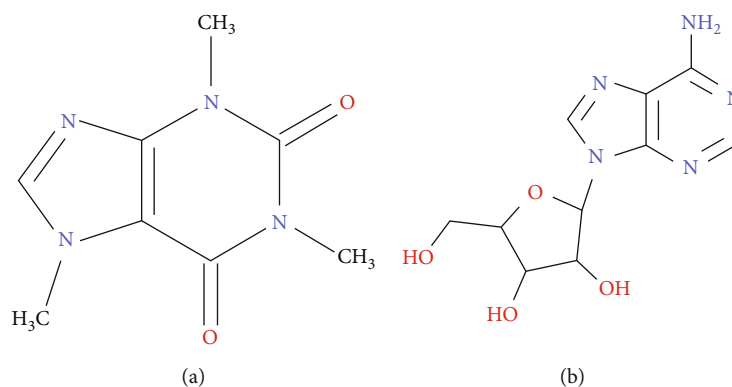


FIGURE 3: The chemical structure of caffeine (a) and adenosine (b) (⁴KingDraw (2021). [Online]. Available from <http://www.kingdraw.cn/en/index.html/>).

A₁R and A_{2A}R, contributing to cognitive impairment and an increased risk of AD [77, 78]. Meanwhile, adenosine lacks its inhibitory A₁R-mediated neuroprotective effects and ATP/adenosine metabolism in the aged brain but is modified to favor neurotransmission concerning stimulatory A_{2A}R; a physiological cost may be suggested by an increased vulnerability of senescent neurons to excitatory amino acid toxicity and a decrease in the number of functioning synapses [79]. Of high interest, A_{2A}R antagonists, in particular, have been proposed to protect against cognitive and memory dysfunction evoked in experimental models of AD [41], independent of A₁R-mediated responses [80].

Furthermore, the activations and increased numbers of A_{2A}R increase their coupling to G protein and efficacy in increasing AC levels, leading to AMP being converted to cAMP and higher levels of PKA. The calcium channels are more phosphorylated, resulting in an overload of intracellular Ca²⁺ [74], which stimulates A β and tau protein production and increases OS and neuroinflammation, ultimately contributing to increasing AD risk (Figure 2(a)) [64]. Also, the A β may promote overload of cellular calcium by inducing membrane-related OS and forming pores in the membrane [81]. Furthermore, the cholinergic and adenosinergic systems in the aged brain have an inverse relationship, with key neurotransmitter Ach levels in the brain declining with age while adenosine levels rise [82]. And because adenosine inhibits the release of Ach [83], adenosine accumulation has been linked to the progression of age-related cognitive deficits, making it an attractive target for pharmaceutical intervention (Figure 2(b)).

Caffeine, a well-known neuromodulator with an associative effect on cognitive performance, is structurally similar to adenosine due to purine backbones (Figure 3), which compete with the actions of adenosine as a nonselective A_{2A}R antagonist [84].

Subchronic administration of daily 30 mg/kg caffeine for 4 days to mice (3-4 months old, 35-45 g) (the equivalent of 360-540 mg of caffeine) prevented A β ₂₅₋₃₅-induced amnesic effects [84], extending the finding that 25 μ M caffeine fully prevented the death of cultured cerebellar granule neurons of rats caused by the A β ₂₅₋₃₅ through stimulating the cholinergic neurotransmission [85]. Chronic administration of

high amounts of caffeine (100 mg/kg/d) to mice (25-30 g) for 4 days resulted in a 40-50% increase in the density of cholinergic, muscarinic, and nicotinic receptors in the brain and may also have augmented cholinergic activity, which facilitated disruptions in the progression of AD [86].

Based on data collected from animal models and cell lines, chronic caffeine administration or other pharmacological agents that mimic caffeine in moderate amounts (200-500 mg/d) at midlife would have therapeutic potential in the AD treatment later in life according to five theories, especially attenuating the A β burden and A β -induced neurotoxicity. Even experimental studies indicate rather favorable effects of caffeine; such benefits may not be fully relevant to AD in humans, particularly when high dosages were used, necessitating us to carefully analyze and conduct more well-defined human studies to evaluate the role of caffeine on AD treatment. Meanwhile, a meta-analysis of diverse animal models also found that the effects of caffeine and A_{2A}R antagonists are mostly determined by the dose, the schedule and time of administration, and the method of administration [87]. Moderate dosages of caffeine have been shown to increase memory function in mice [88-90], whereas greater doses of caffeine have been shown to damage memory acquisition [91, 92].

5. Conclusions

In conclusion, based on the results of epidemiological and experimental studies, moderate and regular caffeine consumption may help to prevent or delay the onset of AD and may be a viable therapeutic approach. However, before conducting rigorous preclinical and clinical research on its therapeutic potential in terms of precise neuroprotective dosages, frequencies, and durations, this recommendation would be premature. And to answer conflicting results in some human studies, the future study is required to set international consensual criteria for outcome measure, apply multivariate analyses to manage various confounding risk factors, clarify the drinking history of coffee and tea in the self-reported questionnaires, recruit a large number of participants from multiethnic backgrounds, and conduct a long follow-up period.

Meanwhile, as long as caffeine intake is maintained daily (e.g., tolerance), moderate usage of caffeine is usually not associated with harmful side effects. Although caffeine has been suspected of causing hypertension, there is no association between caffeine consumption in coffee or/and tea and blood pressure. Given the already widespread use and acceptance of coffee in moderate amounts, long-term coffee intake could be a viable strategy for reducing the risk of AD. However, more research into the effects of tea consumption on the risk of AD is needed.

Abbreviations

AD:	Alzheimer's disease
CNS:	Central nervous system
mg/d:	Milligram per day
wk:	Week
OR:	Odds ratio
CI:	Confidence interval
RR:	Relative risk
I^2 :	Heterogeneity
HR:	Hazard ratio
MMSE:	Mini-Mental State Examination (higher MMSE scores mean higher cognitive function), which measures global cognition including memory, attention, language, praxis, and visuo-spatial ability [24]
MMSE-r:	The Chinese revised version of MMSE
m-MMSE:	A modified version of the Mini-Mental State Examination
B:	Regression coefficient
SE:	Standard error
NINCDS-ADRDA:	National Institute of Neurological and Communicative Disorders and Stroke and the Alzheimer's Disease and Related Disorders Association
BMI:	Body mass index
HAAS Programme:	Honolulu-Asia Aging prospective cohort Study Programme
CLHLS:	Chinese Longitudinal Health Longevity Study
CAIDE:	Cardiovascular Risk Factors, Aging and Dementia
SBP:	Systolic blood pressure
MI:	Myocardial infarction
DM:	Diabetes mellitus
CSHA:	Canadian Study of Health and Aging
MEC:	Multiethnic cohort
SIMPLER:	Swedish Infrastructure for Medical Population-based Life-course Environmental Research, previously the Swedish Mammography Cohort and the Cohort of Swedish Men
SLAS:	Singapore Longitudinal Aging Study
HUSK:	Hordaland Health Study
CASI:	Cognitive Abilities Screening Instrument
ICD:	Codes from the International Classification of Diseases

ICD-9:	Ninth revision
ICD-10:	Tenth revision
3MS:	Modified Mini-Mental State Examination
d:	Day
USA:	The United States of America
N/A:	None/anonymity
CVD:	Cardiovascular disease
BBB:	Blood-brain barrier
Ca ²⁺ :	Calcium ions
EGCG:	Epigallocatechin gallate
A β peptides:	Amyloid beta peptides
NFTs:	Neurofibrillary tangles
ApoE:	Apolipoprotein E
APP:	Amyloid precursor protein
β -Secretase:	Beta-secretase
γ -Secretase:	Gamma-secretase
APPsw:	Swedish mutation
PKA:	Protein kinase A
NF- κ B:	Nuclear factor kappa-light-chain-enhancer of activated B cells
GSK-3:	Glycogen synthase kinase-3
EC:	Entorhinal cortex
OS:	Oxidative stress
ROS:	Reactive oxygen species
SOD1:	Superoxide dismutase 1
SOD2:	Superoxide dismutase 2
Ach:	Acetylcholine
A ₁ R:	Adenosine A ₁ receptor
A _{2A} R:	Adenosine A _{2A} receptor
AC:	Adenylyl cyclase
cAMP:	Cyclic AMP
Tg:	Transgenic
PS1:	Presenilin 1
THY-Tau22:	Characterized by a significant tau expression in the hippocampal formation with a small cortex pathology and no significant spinal cord pathology, making it a reliable model for assessing the modeling effects on hippocampal tau pathology and their associated effects on behavior and plasticity [61]
Malondialdehyde:	A marker of oxidative stress.

Data Availability

After electronic searches on databases PubMed and ScienceDirect, potential eligible studies from 2000 up until 2020 have been identified. According to instructions in Boolean operators and wildcards, the searches applied the following terms to clarify dietary risk factors (coffee OR tea OR caffeine) combined with terms of interested results (cognit* AND (declin* OR damag*)) or (neurodegenerat* OR Alzheimer*). The range of obtained results is around 2000 records. After scanning titles, keywords, and the gist of abstracts in each article, the articles were retained for close reading and analysis of details if all of the following inclusion criteria are met: (1) the published paper had full length and was in a peer-reviewed source; (2) it evaluated caffeine which was sourced

from caffeine, coffee, or tea; and (3) it mentioned AD, cognitive impairment, or cognitive decline. And a study was excluded if it met one or more of the following exclusion criteria: (1) the published paper was in a non-peer-reviewed source (i.e., website, magazines); (2) it was in the abstract form; (3) the investigational product was not caffeine, coffee, or tea; (4) it investigated diseases which were not related to cognitive disorders; and (5) it was a duplicate publication. In addition, the present article included several secondary research papers (i.e., narrative review, systemic review, and meta-analysis studies) which could recommend other relevant research studies with the same topics after looking through their reference lists as key clues. Articles in which caffeine was not studied were excluded. Articles, where sources of caffeine were not from coffee or tea, were excluded. Also, articles in which cognitive decline or Alzheimer's disease was not mentioned were excluded as well. Researchers paid deliberate attention to papers which concluded human studies or animal studies for neuroprotective effects of caffeine for approving arguments as well as theories behind the pathogenesis of neurodegenerative diseases. This paper focused on the prevention and postponement of progression of age-related neurodegenerative diseases; thus, analyses ignored cognitive decline within the normal range. And articles concerning the dosage and frequency of coffee and tea consumption were selected to have a deep analysis for comparing the difference between coffee and tea. This article includes both single studies like longitudinal studies and meta-analyses for more prudent considerations.

Conflicts of Interest

This study does not have any conflicts of interest.

Authors' Contributions

Xiangyu Zhou and Lin Zhang contributed equally to this work.

Acknowledgments

This study was supported by the Hunan Key Laboratory for Processing of Special Medicine Food (2017TP1021) and Hunan key research and development plan project (2020NK2020). Figures 1 and 2 are created with <https://biorender.com/>. Figure 3 is created with <http://kingdraw.com/>.

References

- [1] S. Ray and S. Davidson, "Dementia and cognitive decline. A review of the evidence," *Age UK*, vol. 27, pp. 10–12, 2014.
- [2] B. D. James and J. A. Schneider, "Increasing incidence of dementia in the oldest old: evidence and implications," *Alzheimer's Research & Therapy*, vol. 2, no. 3, pp. 9–12, 2010.
- [3] R. C. Petersen, G. E. Smith, S. C. Waring, R. J. Ivnik, E. G. Tangalos, and E. Kokmen, "Mild cognitive impairment: clinical characterization and outcome," *Archives of Neurology*, vol. 56, no. 3, pp. 303–308, 1999.
- [4] T.-P. Ng, L. Feng, M. Niti, E. H. Kua, and K. B. Yap, "Tea consumption and cognitive impairment and decline in older Chinese adults," *The American Journal of Clinical Nutrition*, vol. 88, no. 1, pp. 224–231, 2008.
- [5] Y.-S. Kim, S. M. Kwak, and S.-K. Myung, "Caffeine intake from coffee or tea and cognitive disorders: a meta-analysis of observational studies," *Neuroepidemiology*, vol. 44, no. 1, pp. 51–63, 2015.
- [6] C. Patterson, J. W. Feightner, A. Garcia, G. Y. R. Hsiung, C. MacKnight, and A. D. Sadovnick, "Diagnosis and treatment of dementia. 1. Risk assessment and primary prevention of Alzheimer disease," *CMAJ*, vol. 178, no. 5, pp. 548–556, 2008.
- [7] K. Deckers, M. P. J. van Boxtel, O. J. G. Schiepers et al., "Target risk factors for dementia prevention: a systematic review and Delphi consensus study on the evidence from observational studies," *International Journal of Geriatric Psychiatry*, vol. 30, no. 3, pp. 234–246, 2015.
- [8] X. Du, X. Wang, and M. Geng, "Alzheimer's disease hypothesis and related therapies," *Translational neurodegeneration*, vol. 7, no. 1, pp. 1–7, 2018.
- [9] J. A. Watt, Z. Goodarzi, A. A. Veroniki et al., "Comparative efficacy of interventions for aggressive and agitated behaviors in dementia: a systematic review and network meta-analysis," *Annals of Internal Medicine*, vol. 171, no. 9, pp. 633–642, 2019.
- [10] M. J. R. Howes, N. S. L. Perry, C. Vázquez-Londoño, and E. K. Perry, "Role of phytochemicals as nutraceuticals for cognitive functions affected in ageing," *British Journal of Pharmacology*, vol. 177, no. 6, pp. 1294–1315, 2020.
- [11] N. Scarmeas, C. A. Anastasiou, and M. Yannakoulia, "Nutrition and prevention of cognitive impairment," *The Lancet Neurology*, vol. 17, no. 11, pp. 1006–1015, 2018.
- [12] P. Londzin, M. Zamora, B. Kałkol, A. Taborek, and J. Folwarczna, "Potential of caffeine in Alzheimer's disease—a review of experimental studies," *Nutrients*, vol. 13, no. 2, p. 537, 2021.
- [13] M. A. Heckman, J. Weil, and E. G. De Mejia, "Caffeine (1, 3, 7-trimethylxanthine) in foods: a comprehensive review on consumption, functionality, safety, and regulatory matters," *Journal of Food Science*, vol. 75, no. 3, pp. R77–R87, 2010.
- [14] G. Sutherland, J. Peeling, H. J. Lesiuk et al., "The effects of caffeine on ischemic neuronal injury as determined by magnetic resonance imaging and histopathology," *Neuroscience*, vol. 42, no. 1, pp. 171–182, 1991.
- [15] K. Rudolphi, M. Keil, J. Fastbom, and B. B. Fredholm, "Ischaemic damage in gerbil hippocampus is reduced following upregulation of adenosine (A₁) receptors by caffeine treatment," *Neuroscience Letters*, vol. 103, no. 3, pp. 275–280, 1989.
- [16] K. A. Rudolphi and P. Schubert, "Modulation of neuronal and glial cell function by adenosine and neuroprotection in vascular dementia," *Behavioural Brain Research*, vol. 83, no. 1–2, pp. 123–128, 1997.
- [17] A. Nehlig, "Are we dependent upon coffee and caffeine? A review on human and animal data," *Neuroscience & Biobehavioral Reviews*, vol. 23, no. 4, pp. 563–576, 1999.
- [18] C. Cabrera, R. Artacho, and R. Giménez, "Beneficial effects of green tea—a review," *Journal of the American College of Nutrition*, vol. 25, no. 2, pp. 79–99, 2006.
- [19] J. Conway, *Number of cups of tea Canadian consumers drink on an average day 2019*, Statista, 2020.
- [20] J. Lindsay, D. Laurin, R. Verreault et al., "Risk factors for Alzheimer's disease: a prospective analysis from the Canadian

- Study of Health and Aging,” *American Journal of Epidemiology*, vol. 156, no. 5, pp. 445–453, 2002.
- [21] E. Nurk, H. Refsum, C. A. Drevon et al., “Intake of flavonoid-rich wine, tea, and chocolate by elderly men and women is associated with better cognitive test performance,” *The Journal of Nutrition*, vol. 139, no. 1, pp. 120–127, 2009.
- [22] L. Maia and A. De Mendonça, “Does caffeine intake protect from Alzheimer’s disease?,” *European Journal of Neurology*, vol. 9, no. 4, pp. 377–382, 2002.
- [23] R. P. Gelber, H. Petrovitch, K. H. Masaki, G. W. Ross, and L. R. White, “Coffee intake in midlife and risk of dementia and its neuropathologic correlates,” *Journal of Alzheimer’s Disease*, vol. 23, no. 4, pp. 607–615, 2011.
- [24] C. Santos, J. Costa, J. Santos, A. Vaz-Carneiro, and N. Lunet, “Caffeine intake and dementia: systematic review and meta-analysis,” *Journal of Alzheimer’s Disease*, vol. 20, Supplement 1, pp. S187–S204, 2010.
- [25] M. H. Eskelinen, T. Ngandu, J. Tuomilehto, H. Soininen, and M. Kivipelto, “Midlife coffee and tea drinking and the risk of late-life dementia: a population-based CAIDE study,” *Journal of Alzheimer’s Disease*, vol. 16, no. 1, pp. 85–91, 2009.
- [26] J. Conway, *Number of cups of coffee consumed per day among coffee drinkers in Canada 2008–2020*, Statista, 2021.
- [27] S.-Y. Park, N. D. Freedman, C. A. Haiman, L. le Marchand, L. R. Wilkens, and V. W. Setiawan, “Association of coffee consumption with total and cause-specific mortality among non-white populations,” *Annals of Internal Medicine*, vol. 167, no. 4, pp. 228–235, 2017.
- [28] S. C. Larsson and A. Wolk, “The role of lifestyle factors and sleep duration for late-onset dementia: a cohort study,” *Journal of Alzheimer’s Disease*, vol. 66, no. 2, pp. 579–586, 2018.
- [29] J. L. B. Quintana, M. F. Allam, A. S. del Castillo, and R. F. C. Navajas, “Alzheimer’s disease and coffee: a quantitative review,” *Neurological Research*, vol. 29, no. 1, pp. 91–95, 2007.
- [30] X. Chen, Y. Huang, and H. Cheng, “Lower intake of vegetables and legumes associated with cognitive decline among illiterate elderly Chinese: a 3-year cohort study,” *The Journal of Nutrition, Health & Aging*, vol. 16, no. 6, pp. 549–552, 2012.
- [31] S. Kuriyama, A. Hozawa, K. Ohmori et al., “Green tea consumption and cognitive function: a cross-sectional study from the Tsurugaya Project,” *The American Journal of Clinical Nutrition*, vol. 83, no. 2, pp. 355–361, 2006.
- [32] L. Feng, X. Gwee, E. H. Kua, and T. P. Ng, “Cognitive function and tea consumption in community dwelling older Chinese in Singapore,” *The Journal of Nutrition, Health & Aging*, vol. 14, no. 6, pp. 433–438, 2010.
- [33] Q.-P. Ma, C. Huang, Q. Y. Cui et al., “Meta-analysis of the association between tea intake and the risk of cognitive disorders,” *PLoS One*, vol. 11, no. 11, article e0165861, 2016.
- [34] S. Cappelletti, P. Daria, G. Sani, and M. Aromatario, “Caffeine: cognitive and physical performance enhancer or psychoactive drug?,” *Current Neuropharmacology*, vol. 13, no. 1, pp. 71–88, 2015.
- [35] S. Kakutani, H. Watanabe, and N. Murayama, “Green tea intake and risks for dementia, Alzheimer’s disease, mild cognitive impairment, and cognitive impairment: a systematic review,” *Nutrients*, vol. 11, no. 5, p. 1165, 2019.
- [36] G. S. Watson and S. Craft, “The role of insulin resistance in the pathogenesis of Alzheimer’s disease,” *CNS Drugs*, vol. 17, no. 1, pp. 27–45, 2003.
- [37] S. Molino, M. Dossena, D. Buonocore et al., “Polyphenols in dementia: from molecular basis to clinical trials,” *Life Sciences*, vol. 161, pp. 69–77, 2016.
- [38] Y. Kataoka, K. Utsunomiya, A. Kimbara et al., “Preventive effect of green tea containing theanine at a high concentration on dementia in aged volunteers,” *The Journal of Japan Mibyou System Association*, vol. 15, pp. 17–23, 2009.
- [39] M. Arnaud, “The pharmacology of caffeine,” *Progress in drug research/Fortschritte der Arzneimittelforschung/Progress des recherches pharmaceutiques*, vol. 31, pp. 273–313, 1987.
- [40] S. Teekachunhatean, N. Tosri, N. Rojanasthien, S. Srichairatanakool, and C. Sangdee, “Pharmacokinetics of caffeine following a single administration of coffee enema versus oral coffee consumption in healthy male subjects,” *International Scholarly Research Notices*, vol. 2013, Article ID 147238, 7 pages, 2013.
- [41] G. Arendash, W. Schleif, K. Rezai-Zadeh et al., “Caffeine protects Alzheimer’s mice against cognitive impairment and reduces brain β -amyloid production,” *Neuroscience*, vol. 142, no. 4, pp. 941–952, 2006.
- [42] B. B. Fredholm, “Adenosine, adenosine receptors and the actions of caffeine,” *Pharmacology & Toxicology*, vol. 76, no. 2, pp. 93–101, 1995.
- [43] T. C. Theoharides, *Essentials of Pharmacology*, Little Brown & Company, 1996.
- [44] M. Cheng, Z. Hu, X. Lu, J. Huang, and D. Gu, “Caffeine intake and atrial fibrillation incidence: dose response meta-analysis of prospective cohort studies,” *Canadian Journal of Cardiology*, vol. 30, no. 4, pp. 448–454, 2014.
- [45] A. D. Gitler, P. Dhillon, and J. Shorter, *Neurodegenerative disease: models, mechanisms, and a new hope*, The Company of Biologists Ltd, 2017.
- [46] M. Prince, A. Wimo, M. Guerchet, G. C. Ali, Y. T. Wu, and M. Prina, *The global impact of dementia: an analysis of prevalence, incidence, cost and trends*, World Alzheimer Report, 2015, 2015.
- [47] M. P. Murphy and H. LeVine III, “Alzheimer’s disease and the amyloid- β peptide,” *Journal of Alzheimer’s Disease*, vol. 19, no. 1, pp. 311–323, 2010.
- [48] P. Rajendran, A. Bhatt, S. Manthuruthil, and S. Pericherla, “Caffeine and Alzheimer’s disease,” *International Journal of Biological and Medical Research*, vol. 3, pp. 3513–3514, 2013.
- [49] E. Mohandas, V. Rajmohan, and B. Raghunath, “Neurobiology of Alzheimer’s disease,” *Indian Journal of Psychiatry*, vol. 51, no. 1, pp. 55–61, 2009.
- [50] G. W. Arendash, M. F. Garcia, D. A. Costa, J. R. Cracchiolo, I. M. Wefes, and H. Potter, “Environmental enrichment improves cognition in aged Alzheimer’s transgenic mice despite stable β -amyloid deposition,” *Neuroreport*, vol. 15, no. 11, pp. 1751–1754, 2004.
- [51] G. W. Arendash, T. Mori, C. Cao et al., “Caffeine reverses cognitive impairment and decreases brain amyloid- β levels in aged Alzheimer’s disease mice,” *Journal of Alzheimer’s Disease*, vol. 17, no. 3, pp. 661–680, 2009.
- [52] C. J. Phiel, C. A. Wilson, V. M. Y. Lee, and P. S. Klein, “GSK-3 α regulates production of Alzheimer’s disease amyloid- β peptides,” *Nature*, vol. 423, no. 6938, pp. 435–439, 2003.
- [53] P. Fuentes G and A. Slachevsky Ch, “Enfermedad de Alzheimer: Actualización en terapia farmacológica,” *Revista Médica de Chile*, vol. 133, no. 2, pp. 224–230, 2005.

- [54] W.-H. Zheng, S. Bastianetto, F. Mennicken, W. Ma, and S. Kar, "Amyloid β peptide induces tau phosphorylation and loss of cholinergic neurons in rat primary septal cultures," *Neuroscience*, vol. 115, no. 1, pp. 201–211, 2002.
- [55] J. J. Lucas, F. Hernández, P. Gómez-Ramos, M. A. Morán, R. Hen, and J. Avila, "Decreased nuclear beta-catenin, tau hyperphosphorylation and neurodegeneration in GSK-3beta conditional transgenic mice," *The EMBO Journal*, vol. 20, no. 1, pp. 27–39, 2001.
- [56] K. Iqbal, F. Liu, C. X. Gong, and I. Grundke-Iqbal, "Tau in Alzheimer disease and related tauopathies," *Current Alzheimer Research*, vol. 7, no. 8, pp. 656–664, 2010.
- [57] M. Goedert and M. G. Spillantini, "A century of Alzheimer's disease," *Science*, vol. 314, no. 5800, pp. 777–781, 2006.
- [58] M. S. Rafiq and P. S. Aisen, "Recent developments in Alzheimer's disease therapeutics," *BMC Medicine*, vol. 7, no. 1, pp. 1–4, 2009.
- [59] W. H. Stoothoff and G. V. Johnson, "Tau phosphorylation: physiological and pathological consequences," *Biochimica et Biophysica Acta (BBA)-Molecular Basis of Disease*, vol. 1739, no. 2–3, pp. 280–297, 2005.
- [60] B. De Strooper, "Proteases and proteolysis in Alzheimer disease: a multifactorial view on the disease process," *Physiological Reviews*, vol. 90, no. 2, pp. 465–494, 2010.
- [61] C. Laurent, S. Eddarkaoui, M. Derisbourg et al., "Beneficial effects of caffeine in a transgenic model of Alzheimer's disease-like tau pathology," *Neurobiology of Aging*, vol. 35, no. 9, pp. 2079–2090, 2014.
- [62] A. Currais, K. Kato, L. Canuet et al., "Caffeine modulates tau phosphorylation and affects Akt signaling in postmitotic neurons," *Journal of Molecular Neuroscience*, vol. 43, no. 3, pp. 326–332, 2011.
- [63] B. B. Fredholm, K. Bättig, J. Holmén, A. Nehlig, and E. E. Zvartau, "Actions of caffeine in the brain with special reference to factors that contribute to its widespread use," *Pharmacological Reviews*, vol. 51, no. 1, pp. 83–133, 1999.
- [64] M. T. Lin and M. F. Beal, "Mitochondrial dysfunction and oxidative stress in neurodegenerative diseases," *Nature*, vol. 443, no. 7113, pp. 787–795, 2006.
- [65] W. J. Huang, X. Zhang, and W. W. Chen, "Role of oxidative stress in Alzheimer's disease," *Biomedical Reports*, vol. 4, no. 5, pp. 519–522, 2016.
- [66] P. I. Moreira, C. Carvalho, X. Zhu, M. A. Smith, and G. Perry, "Mitochondrial dysfunction is a trigger of Alzheimer's disease pathophysiology," *Biochimica et Biophysica Acta (BBA)-Molecular Basis of Disease*, vol. 1802, no. 1, pp. 2–10, 2010.
- [67] G. F. Makhaeva, S. V. Lushchekina, N. P. Boltneva et al., "Conjugates of γ -carboline and phenothiazine as new selective inhibitors of butyrylcholinesterase and blockers of NMDA receptors for Alzheimer disease," *Scientific Reports*, vol. 5, no. 1, pp. 1–11, 2015.
- [68] S. Giunta, V. Andriolo, and A. Castorina, "Dual blockade of the A_1 and A_{2A} adenosine receptor prevents amyloid beta toxicity in neuroblastoma cells exposed to aluminum chloride," *The International Journal of Biochemistry & Cell Biology*, vol. 54, pp. 122–136, 2014.
- [69] Y.-F. Chu, W. H. Chang, R. M. Black et al., "Crude caffeine reduces memory impairment and amyloid β_{1-42} levels in an Alzheimer's mouse model," *Food Chemistry*, vol. 135, no. 3, pp. 2095–2102, 2012.
- [70] C.-C. Liu, C. C. Liu, T. Kanekiyo, H. Xu, and G. Bu, "Apolipoprotein E and Alzheimer disease: risk, mechanisms and therapy," *Nature Reviews Neurology*, vol. 9, no. 2, pp. 106–118, 2013.
- [71] E. Boerwinkle and G. Utermann, "Simultaneous effects of the apolipoprotein E polymorphism on apolipoprotein E, apolipoprotein B, and cholesterol metabolism," *American Journal of Human Genetics*, vol. 42, no. 1, pp. 104–112, 1988.
- [72] J. R. Prasanthi, B. Dasari, G. Marwarha et al., "Caffeine protects against oxidative stress and Alzheimer's disease-like pathology in rabbit hippocampus induced by cholesterol-enriched diet," *Free Radical Biology and Medicine*, vol. 49, no. 7, pp. 1212–1220, 2010.
- [73] X. Chen, J. W. Gawryluk, J. F. Wagener, O. Ghribi, and J. D. Geiger, "Caffeine blocks disruption of blood brain barrier in a rabbit model of Alzheimer's disease," *Journal of Neuroinflammation*, vol. 5, no. 1, pp. 12–14, 2008.
- [74] R. B. Dias, D. M. Rombo, J. A. Ribeiro, J. M. Henley, and A. M. Sebastião, "Adenosine: setting the stage for plasticity," *Trends in Neurosciences*, vol. 36, no. 4, pp. 248–257, 2013.
- [75] S. Moro, F. Deflorian, G. Spalluto et al., "Demystifying the three dimensional structure of G protein-coupled receptors (GPCRs) with the aid of molecular modeling," *Chemical Communications*, vol. 24, no. 24, pp. 2949–2956, 2003.
- [76] J. Sawynok, "Adenosine receptor targets for pain," *Neuroscience*, vol. 338, pp. 1–18, 2016.
- [77] T. Almeida, R. J. Rodrigues, A. de Mendonça, J. A. Ribeiro, and R. A. Cunha, "Purinergetic P2 receptors trigger adenosine release leading to adenosine A_{2A} receptor activation and facilitation of long-term potentiation in rat hippocampal slices," *Neuroscience*, vol. 122, no. 1, pp. 111–121, 2003.
- [78] R. A. Cunha, P. Correia-de-Sá, A. M. Sebastião, and J. A. Ribeiro, "Preferential activation of excitatory adenosine receptors at rat hippocampal and neuromuscular synapses by adenosine formed from released adenine nucleotides," *British Journal of Pharmacology*, vol. 119, no. 2, pp. 253–260, 1996.
- [79] R. A. Cunha, T. Almeida, and J. Ribeiro, "Parallel modification of adenosine extracellular metabolism and modulatory action in the hippocampus of aged rats," *Journal of Neurochemistry*, vol. 76, no. 2, pp. 372–382, 2001.
- [80] L. V. Lopes, R. A. Cunha, and J. Ribeiro, "Increase in the number, G protein coupling, and efficiency of facilitatory adenosine A_{2A} receptors in the limbic cortex, but not striatum, of aged rats," *Journal of Neurochemistry*, vol. 73, no. 4, pp. 1733–1738, 1999.
- [81] A. Sanabria-Castro, I. Alvarado-Echeverría, and C. Monge-Bonilla, "Molecular pathogenesis of Alzheimer's disease: an update," *Annals of Neurosciences*, vol. 24, no. 1, pp. 46–54, 2017.
- [82] B. Sperlágh, G. Zsilla, M. Baranyi, A. Kékes-Szabó, and E. S. Vizi, "Age-dependent changes of presynaptic neuromodulation via A_1 -adenosine receptors in rat hippocampal slices," *International Journal of Developmental Neuroscience*, vol. 15, no. 6, pp. 739–747, 1997.
- [83] C. Corsi, M. Pazzagli, L. Bianchi, L. D. Corte, G. Pepeu, and F. Pedata, "In vivo amino acid release from the striatum of aging rats: adenosine modulation," *Neurobiology of Aging*, vol. 18, no. 2, pp. 243–250, 1997.
- [84] O. P. Dall'Igna, P. Fett, M. W. Gomes, D. O. Souza, R. A. Cunha, and D. R. Lara, "Caffeine and adenosine A_{2a} receptor

- antagonists prevent β -amyloid (25-35)-induced cognitive deficits in mice," *Experimental Neurology*, vol. 203, no. 1, pp. 241–245, 2007.
- [85] O. P. Dall'igna, L. O. Porciúncula, D. O. Souza, R. A. Cunha, and D. R. Lara, "Neuroprotection by caffeine and adenosine A2A receptor blockade of β -amyloid neurotoxicity," *British Journal of Pharmacology*, vol. 138, no. 7, pp. 1207–1209, 2003.
- [86] D. Shi, O. Nikodijević, K. A. Jacobson, and J. W. Daly, "Chronic caffeine alters the density of adenosine, adrenergic, cholinergic, GABA, and serotonin receptors and calcium channels in mouse brain," *Cellular and Molecular Neurobiology*, vol. 13, no. 3, pp. 247–261, 1993.
- [87] R. N. Takahashi, F. A. Pamplona, and R. Prediger, "Adenosine receptor antagonists for cognitive dysfunction: a review of animal studies," *Frontiers in Bioscience*, vol. 13, no. 13, pp. 2614–2632, 2008.
- [88] M. Angelucci, C. Cesário, R. H. Hiroi, P. L. Rosalen, and C. D. Cunha, "Effects of caffeine on learning and memory in rats tested in the Morris water maze," *Brazilian Journal of Medical and Biological Research*, vol. 35, no. 10, pp. 1201–1208, 2002.
- [89] M. Costa, P. H. Botton, S. Mioranza, D. O. Souza, and L. O. Porciúncula, "Caffeine prevents age-associated recognition memory decline and changes brain-derived neurotrophic factor and tyrosine kinase receptor (TrkB) content in mice," *Neuroscience*, vol. 153, no. 4, pp. 1071–1078, 2008.
- [90] R. D. Prediger, L. C. Batista, and R. N. Takahashi, "Caffeine reverses age-related deficits in olfactory discrimination and social recognition memory in rats," *Neurobiology of Aging*, vol. 26, no. 6, pp. 957–964, 2005.
- [91] M. E. Angelucci, M. A. B. F. Vital, C. Cesário, C. R. Zadusky, P. L. Rosalen, and C. da Cunha, "The effect of caffeine in animal models of learning and memory," *European Journal of Pharmacology*, vol. 373, no. 2-3, pp. 135–140, 1999.
- [92] K. P. Corodimas, J. M. Stieg, and J. C. Pruitt, "Acute exposure to caffeine selectively disrupts context conditioning in rats," *Psychopharmacology*, vol. 152, no. 4, pp. 376–382, 2000.

Research Article

L-Theanine Ameliorates D-Galactose-Induced Brain Damage in Rats via Inhibiting AGE Formation and Regulating Sirtuin1 and BDNF Signaling Pathways

Li Zeng ^{1,2,3}, Ling Lin,^{1,3} Ling Chen,^{1,3} Wenjun Xiao ^{1,3} and Zhihua Gong ^{1,3}

¹Key Lab of Tea Science of Ministry of Education, Hunan Agricultural University, Changsha, Hunan 410128, China

²School of Pharmacy, Shaoyang University, Shaoyang 422000, China

³National Research Center of Engineering and Technology for Utilization of Botanical Functional Ingredients, Hunan Agricultural University, Changsha 410128, China

Correspondence should be addressed to Wenjun Xiao; xiaowenjun88@sina.com and Zhihua Gong; gzh041211@163.com

Received 25 September 2020; Revised 2 December 2020; Accepted 6 January 2021; Published 20 July 2021

Academic Editor: Nadja Schroder

Copyright © 2021 Li Zeng et al. This is an open access article distributed under the Creative Commons Attribution License, which permits unrestricted use, distribution, and reproduction in any medium, provided the original work is properly cited.

The maintenance of homeostasis is essential for mitigating stress and delaying degenerative diseases such as Alzheimer's disease (AD). AD is generally defined as the abnormal production of β -amyloid ($A\beta$) and advanced glycation end products (AGEs). The effects of L-theanine on $A\beta$ and AGE generation were investigated in this study. Decreased AGEs and $A\beta_{1-42}$ levels were reflected by increased acetylcholine (ACh) concentration and acetylcholinesterase (AChE) activity inhibition compared to model rats. L-Theanine also inhibited nuclear factor- κ B (p65) protein expression by activating sirtuin1 (SIRT1), reducing inflammatory factor expression, and downregulating the mRNA and protein expression of AGE receptors (RAGE). Superoxide dismutase 2 and catalase protein expressions were markedly upregulated by L-theanine, whereas oxidative stress-related injury was alleviated. The expression of peroxisome proliferator-activated receptor- γ coactivator 1 α (PGC-1 α) was also found to be increased. H&E staining showed that the apoptosis of hippocampal neurons was mitigated by decreased Bax and cleaved-caspase-3 protein expression and the increase of Bcl-2 protein expression. Moreover, L-theanine increased the gene and protein expression of brain-derived neurotrophic factor (BDNF). These findings suggest that the potential preventive effects of L-theanine against AD may be attributed to its regulation of SIRT1 and BDNF proteins and its mitigation of AGEs/RAGE signaling pathways in the brain tissue of AD model rats.

1. Introduction

Advanced glycation end products (AGEs) accumulate in human and animal serum or tissues with age [1, 2]. Clinical studies have found that the amount of AGE-modified β -amyloid protein ($A\beta$) in the cerebrospinal fluid of patients with Alzheimer's disease (AD) is three times higher than that in healthy individuals [3]. AD is a progressive neurodegenerative disease associated with abnormal deposition of $A\beta$ in the brain [4]. Under normal conditions, the production and clearance of $A\beta$ in the body are in dynamic equilibrium. When $A\beta$ metabolism is dysfunctional, this balance is disrupted, and $A\beta$ accumulates, resulting in neurotoxicity [5]. Oxidative stress, mitochondrial dysfunction, inflammation,

and neuronal cell apoptosis are closely related to AD pathogenesis [6]. Receptor for AGEs (RAGE), a multiligand membrane receptor primarily expressed in neurons and immune cells [7], binds AGEs and $A\beta$, thus activating various signaling pathways in brain tissues, resulting in oxidative damage, mitochondrial dysfunction, chronic inflammation, protein degeneration, and apoptosis [7–9]. These mechanisms can disrupt brain cell homeostasis, ultimately leading to a degeneration of the normal brain structure and function [9, 10].

Since excess D-galactose exceeds the body glucose metabolism capacity, the Maillard reaction can occur between the aldehyde and protein free amino groups, resulting in the formation of AGEs [11, 12]. In addition, in the presence of oxidative stress, glucose produced by D-galactose metabolism is

oxidized to produce active carbonyl compounds (such as methylacetaldehyde), which also promote the formation of AGEs [1]. Studies have shown that the brain tissue is unable to metabolize excess D-galactose and that the gradual decrease in brain function induced by D-galactose positively correlates with AGE formation, A β deposition, decrease in acetylcholine (ACh) levels, neuronal apoptosis, and loss of brain-derived neurotrophic factor (BDNF) in brain tissues [13]. Sirtuin1 (SIRT1) is an important functional protein in various mammalian metabolic tissues and can regulate the biological processes involved in neurodegenerative diseases, such as inflammation, oxidative stress, mitochondrial function, cell senescence, and apoptosis [14]. Sirtuin1 elicits its effects by activating downstream transcription factors and has shown the potential to attenuate D-galactose-induced brain aging in rats [15, 16]. BDNF is a key factor that promotes neuronal survival and development and improves learning and memory [17, 18]. Additionally, SIRT1 and BDNF may be key factors in AGE production and cognitive impairment in D-galactose-induced glycosylation model rats [19, 20].

Food nutrition intervention aimed at inhibiting the production of AGEs, reducing the accumulation of A β in brain tissue, downregulating the expression of RAGE protein, and maintaining homeostasis in brain tissue may be an effective approach to treat and prevent AD [7, 21]. Epidemiological studies have shown that daily tea drinking can reduce the risk of neurodegenerative diseases, such as cognitive decline and cognitive impairment in the elderly [22, 23]. L-Theanine from tea can increase the amount of glutathione (GSH) and ACh and the activities of antioxidant enzymes, such as superoxide dismutase (SOD), catalase (CAT), and GSH-peroxidase (Px); promote the synthesis and secretion of BDNF; decrease the amount of malondialdehyde (MDA); and maintain a balance expression of inflammatory factors in brain tissue, thereby reducing mitochondrial damage induced by external stress, such as cadmium, A β_{1-42} , and polychlorinated biphenyls (e.g., Aroclor1254), and inhibiting apoptosis in brain neuronal cells [23, 24]. At the same time, *in vitro* studies have shown that L-theanine reduces AGE formation [25]. We have previously reported that L-theanine can protect the liver, promote AGE metabolism, and reduce the amount of AGEs in the liver and serum by maintaining the balance between oxidative stress and inflammation in the liver tissues of D-galactose-induced model rats [26, 27]. However, D-galactose can circulate in the blood, therefore reaching various tissues and organs and form AGEs [1, 8]. To the best of our knowledge, no reports have described the effects of L-theanine on AGE formation in brain tissues.

Therefore, D-galactose-induced glycosylated model rats were used to explore the mechanisms underlying L-theanine maintenance of homeostasis in brain tissues in this study. We further investigated the role of L-theanine in mitigating the effects of adverse factors, such as brain inflammation, oxidative stress, mitochondrial function, cell senescence, and apoptosis mediated by AGEs/RAGE. Our findings may provide a scientific basis for the development of functional products based on L-theanine to promote healthy aging.

2. Materials and Methods

2.1. Materials and Reagents. Healthy male Sprague-Dawley rats (6 weeks old, specific pathogen-free, weighing 180–200 g) were obtained from Hunan Slack Jingda Experimental Animal Co., Ltd. (China) (animal quality certificate number: 43004700043916). L-Theanine (cat. no. G5388) and D-galactose (cat. no. SMB00395; purity \geq 99%) were purchased from Sigma (St. Louis, MO, USA). Enzyme-linked immunosorbent assay (ELISA) kits for AGEs (cat. no. CSB-E09413r), A β_{1-42} (cat. no. CSB-E10786r), tumor necrosis factor- (TNF-) α (cat. no. CSB-E11987r), interleukin- (IL-) 1 β (cat. no. CSB-E08055r), IL-6 (cat. no. CSB-E04640r), and neuronal nitric oxide synthase (nNOS; cat. no. CSB-E14034r) were purchased from Wuhan Huamei Biological Engineering Co., Ltd. (China). Kits for evaluation of the expression or activity of SOD (cat. no. A001-3), CAT (cat. no. A007-1), GSH-Px (cat. no. A005), NOS (cat. no. A014-2), total antioxidant capacity (T-AOC; cat. no. A015-2), MDA (cat. no. A003-1), ACh (cat. no. A105-1), and acetylcholinesterase (AChE; cat. no. A024-1-1) were purchased from Nanjing Jiancheng Institute of Bioengineering (China). Antibodies targeting β -actin (cat. no. 60008-1-Ig), RAGE (cat. no. 16346-1-AP), SOD2 (cat. no. 24127-1-AP), CAT (cat. no. 14195-1-AP), SIRT1 (cat. no. 13161-1-AP), peroxisome proliferator-activated receptor- γ coactivator- (PGC-) 1 α (cat. no. 66369-1-Ig), nuclear factor- (NF-) κ B (p65) (cat. no. 10745-1-AP), Bcl-2 (cat. no. 26593-1-AP), Bax (cat. no. 50599-2-Ig), cleaved-caspase-3 (cat. no. 19677-1-AP), and BDNF (cat. no. 66292-1-Ig), as well as horseradish peroxidase (HRP) goat anti-mouse IgG (cat. no. SA00001-1) and HRP goat anti-rabbit IgG (cat. no. SA00001-2) were purchased from Proteintech Company (USA). Anti-Ace-NF- κ B antibodies (p65; cat. no. ab19870) were purchased from Abcam (Cambridge, UK).

2.2. Experimental Animal Design. Rats were housed in separate cages in a room with a constant temperature ($25 \pm 2^\circ\text{C}$) and humidity (50–60%), with a light cycle set to 14 h of light/10 h of darkness. Before the experiment, all 30 rats were provided with standard rat chow and water ad libitum. After 1 week for acclimation, the rats were divided into five groups ($n = 6$ rats/group) according to different treatment methods, as follows: (1) control group (CON), rats were fed the corresponding dose of normal saline according to their body weight, and the corresponding volume of normal saline was injected into the back of the neck; (2) model group (MOD), rats were fed the corresponding dose of physiological saline according to body weight and were injected with 200 mg/kg body weight (BW) of D-galactose physiological saline solution subcutaneously into the back of the neck; (3) low-dose L-theanine group (L-LT), rats were fed 100 mg/kg BW of L-theanine physiological saline solution and were injected with 200 mg/kg BW of D-galactose subcutaneously into the back of the neck; (4) medium-dose L-theanine group (M-LT), rats were fed 200 mg/kg BW of L-theanine physiological saline solution and simultaneously injected with 200 mg/kg BW of D-galactose into the back of the neck; and (5) high-dose L-theanine group (H-LT), rats were fed 400 mg/kg BW of

L-theanine physiological saline solution and injected with 200 mg/kg BW of D-galactose subcutaneously into the back of the neck.

The rats were treated once a day for 56 days. After 8 weeks, all rats fasted but were allowed free access to water *ad libitum*. Rats were anesthetized by intraperitoneal injection of 3% pentobarbital sodium, and rat brain tissues were harvested and stored in a cryogenic refrigerator at -80°C (Thermo Corporation, USA). The experimental animal program was approved by the Animal Experiment Ethics Committee of Hunan Agricultural University (No: 015063506, Changsha, China) and was strictly implemented in accordance with the 8th edition of the US Guidelines for the Care and Use of Laboratory Animals.

2.3. Sample Analysis

2.3.1. Histopathological Detection and Analysis of Hippocampal Tissue in Experimental Rats. With reference to the methods reported by Zeng et al. [26], the same part of the hippocampal tissue from three rats in each group was embedded in paraffin and stained with hematoxylin-eosin (H&E), and pathological changes in the hippocampal tissue were observed under a 400x light microscope (Leica Microsystems AG, Wetzlar, Germany).

2.3.2. Detection of AGEs and $A\beta_{1-42}$ in the Brain Tissues of Experimental Rats Using ELISA. Approximately 0.02 g tissue was collected from the same part of the brain in each rat, and the amount of AGEs and $A\beta_{1-42}$ in the brain tissue was detected according to the manufacturer's instructions.

2.3.3. Biochemical Detection of ACh and AChE in Experimental Rat Brain Tissue. Approximately 0.02 g tissue was collected from the same part of the brain in each rat, and the contents of ACh and AChE in the brain tissues were detected using an enzyme labeling instrument according to the manufacturer's instructions.

2.3.4. Detection of Oxidative Stress in the Brain Tissues of Experimental Rats. Approximately 0.02 g tissue was collected from the same part of the brain in each rat. The levels of SOD, CAT, GSH-Px, NOS, T-AOC, and MDA in the brain tissues of each group were detected using an enzyme labeling instrument according to the instructions provided by the kit manufacturer.

2.3.5. Detection of Inflammatory Cytokines in the Brain Tissues of Experimental Rats Using ELISA. Approximately 0.02 g tissue was collected from the same part of the brain in each rat. According to the manufacturer's instructions, the protein contents of TNF- α , IL-1 β , IL-6, and nNOS were measured using an enzyme labeling instrument.

2.3.6. Real-Time Quantitative Polymerase Chain Reaction (qPCR). The mRNA expression levels of RAGE, SIRT1, PGC-1 α , and BDNF in brain tissues were measured using qPCR. Approximately 0.05 g tissue was collected from the same part of the brain in each rat, and total RNA was extracted using TRIzol reagent (Invitrogen, Carlsbad, CA, USA). The RNA was then reverse transcribed into cDNA,

and an ABIQuantStudio3 fluorescence qPCR instrument was used for PCR amplification. The PCR cycle parameters were as follows: predenaturation at 95°C for 10 min, followed by 40 cycles of denaturation at 95°C for 15 s, and annealing at 60°C for 60 s. The $2^{-\Delta\Delta C_t}$ method was used to calculate the expression level of each gene in each sample relative to that in the control group. The sequences of the target genes were obtained from NCBI, and primers were designed using PrimerPremier5. All primers were synthesized by Shanghai Shengggong Biological Engineering Co., Ltd. (Table 1).

2.3.7. Western Blotting. With reference to the methods reported by Zeng et al. [26], homogenates from 0.05 g hippocampal tissue from three rats in each group were randomly selected, and protein was extracted after cleavage. Protein concentrations were then determined. Samples were boiled and denatured, and proteins were separated by electrophoresis and transferred to membranes. Membranes were then incubated with appropriate primary antibodies, washed, and incubated with secondary antibodies. Protein bands were detected using enhanced chemiluminescence. The molecular weight and optical density of target bands for RAGE, SOD2, CAT, SIRT1, PGC-1 α , NF- κB (p65), Ace-NF- κB (p65), BDNF, Bcl-2, Bax, and cleaved-caspase-3 were analyzed using a gel image processing system (Media Cybernetics, Inc., Rockville, MD, USA).

2.4. Statistical Analysis. The data were processed using the GraphPadPrism6 software (GraphPad Software, Inc., USA), and the results are expressed as means \pm standard deviations. Single-factor analysis of variance and least significant difference tests were used to compare the significance of differences between groups. Differences with P values <0.05 were considered significant.

3. Results

3.1. Pathological Changes in the Hippocampal Tissues of Rats in Each Group. Hippocampal neurons in the MOD group, which were induced by D-galactose, were arranged in a more disordered manner and showed higher shrinkage or apoptosis (black arrow) in comparison with the CON group (Figure 1). With the L-theanine treatment, the damage was substantially reduced, resulting in a neat arrangement of the cells. The effects obtained with the highest concentration of L-theanine were similar to the CON group, which indicate a potential protective effect of L-theanine in the hippocampal tissues.

3.2. Effects of L-Theanine on AGEs and $A\beta_{1-42}$ in the Brain Tissues of Experimental Rats. As shown in Figure 2, the concentrations of AGEs and $A\beta_{1-42}$ in the brain tissues of the MOD group were significantly ($P < 0.01$) higher than those of the CON group. Additionally, following the administration of medium (200 mg/kg) and high-dose (400 mg/kg) of L-theanine, the concentration of AGEs and $A\beta_{1-42}$ in the brain tissues significantly decreased in a dose-dependent manner. However, there was no significant decrease in the L-LT group.

TABLE 1: Primers used for qPCR.

Gene	Forward and reverse primer (5'-3')	Product size (bp)
β -Actin	F: ACATCCGTAAAGACCTCTATGCC R: TACTCCTGCTTGCTGATCCAC	223
RAGE	F: CTGCCTCTGAACTCACAGCCAATG R: GTGCCTCCTGGTCTCCTCCTTC	155
SIRT1	F: AAAGGAAATATATCCCGGACA R: TTTGGATTCTGCAACCTG	134
PGC-1 α	F: AATCAAGCCACTACAGACACC R: TCTCTGCGGTATTCTGTCCTC	148
BDNF	F: GTCCCGGTATCAAAAGCCAAC R: AGTGCCTTTTGTCTATGCCCT	103

3.3. Effects of L-Theanine on ACh and AChE in the Brain Tissues of Experimental Rats. The amounts of ACh and AChE in the brain tissues are shown in Figure 3. Compared with the CON group, the amounts of ACh and AChE were significantly decreased and increased, respectively, in the brain tissues of the MOD group ($P < 0.01$). Following L-theanine treatment, the level of ACh and AChE in brain tissues significantly improved and decreased, respectively, in a dose-dependent manner ($P < 0.05$ and $P < 0.01$, respectively).

3.4. Effects of L-Theanine on Oxidative Stress in Brain Tissues of Experimental Rats. Evaluation of oxidative stress response to L-theanine is shown in Figure 4. SOD, CAT, GSH-Px, and T-AOC activities were significantly decreased, whereas NOS activity and MDA concentration were significantly increased in brain tissues after D-galactose exposure ($P < 0.01$). After administration of medium and high-dose of L-theanine, SOD, CAT, and T-AOC activities were significantly increased, whereas NOS activity and MDA concentration significantly decreased ($P < 0.05$ and $P < 0.01$). Similarly, there were no significant changes in oxidative stress levels in brain tissues treated with a low concentration of L-theanine ($P > 0.05$).

3.5. Effects of L-Theanine on Inflammatory Cytokines in Brain Tissues from Experimental Rats. Inflammatory cytokines play important roles in age-related degenerative diseases [28]. As shown in Figure 5, inflammatory factors, including IL-1 β , IL-6, TNF- α , and nNOS, in the brain tissues of the MOD group were significantly higher than those of the CON group ($P < 0.01$). Compared with the MOD group, the levels of IL-1 β , IL-6, TNF- α , and nNOS in the brain tissues of the L-theanine-treated groups were significantly decreased ($P < 0.01$).

3.6. Effects of L-Theanine on RAGE, SIRT1, PGC-1 α , and BDNF mRNA Levels in the Brains of Experimental Rats. As shown in Figure 6, compared with the CON group, RAGE mRNA levels in the brain tissues of the MOD group were significantly increased, whereas those of PGC-1 α and BDNF mRNA significantly decreased ($P < 0.01$). Compared with the MOD group, RAGE mRNA levels in the brain tissues of the L-theanine-treated groups significantly decreased

($P < 0.01$). In contrast, the levels of SIRT1, PGC-1 α , and BDNF mRNAs were significantly increased in the M-LT and H-LT groups ($P < 0.01$).

3.7. Effects of L-Theanine on the Expression of Key Proteins in the Brain Tissues of Experimental Rats. As shown in Figure 7, the protein expression levels of RAGE, SIRT1, Ace-NF- κ B (p65), and BDNF in the brain tissues of the MOD group were significantly altered in comparison with the CON group ($P < 0.01$). Significant changes in those protein expression levels were observed in the M-LT and H-LT groups ($P < 0.05$ or $P < 0.01$), whereas no significant change was observed in brain tissues ($P > 0.05$).

As shown in Figure 8, the expression levels of PGC-1 α , SOD2, and CAT proteins in the brain tissues of rats in the MOD group were significantly lower than those of the CON group ($P < 0.01$). Compared with the MOD group, the protein expression levels of SOD2 in the brain tissues of rats in the L-LT group did not significantly change ($P > 0.05$), whereas those of PGC-1 α and CAT significantly increased ($P < 0.05$). The expression levels of PGC-1 α , SOD2, and CAT proteins in the brain tissues of rats in the M-LT and H-LT groups were significantly increased ($P < 0.01$).

As shown in Figure 9, compared with the CON group, the significant changes in protein expression levels of Bcl-2, Bax, and cleaved-caspase-3 were observed in the brain tissues of rats in the MOD group ($P < 0.01$). Compared with the MOD group, the protein expression levels of cleaved-caspase-3 in the brain tissues of rats in the L-LT group did not significantly change ($P > 0.05$), whereas the protein expression levels of Bcl-2 and Bax were significantly changed ($P < 0.01$). Additionally, significant changes in the protein expression levels of Bcl-2, Bax, and cleaved-caspase-3 were observed in the brain tissues of rats in the M-LT and H-LT groups ($P < 0.01$).

4. Discussion

A β is a transmembrane protein that abnormally accumulates in the brains of patients with AD and can penetrate the cell membrane of neurons, alter the cell osmotic balance, induce neurotoxicity, and lead to memory impairment and neuronal loss [29]. Notably, AGE concentration positively correlates with the degree of pathological changes in patients with cognitive impairment [3, 30]. Long-term exposure to a high concentration of D-galactose significantly increases AGEs and A β ₁₋₄₂ levels in the brain of mice and results in cognitive impairment [31, 32]. Reducing AGEs and A β ₁₋₄₂ levels in the brain is essential for the prevention of cognitive impairment. A β ₁₋₄₂ concentration in the cerebral cortex and hippocampus was reportedly significantly decreased in mice fed L-theanine for 5 weeks [33]. We found that the concentrations of AGEs and A β ₁₋₄₂ were significantly increased when induced with D-galactose and then decreased after L-theanine treatment, which is consistent with the fact that nutritional intervention with L-theanine effectively reduced the amount of AGEs and A β ₁₋₄₂ in brain tissues [33, 34].

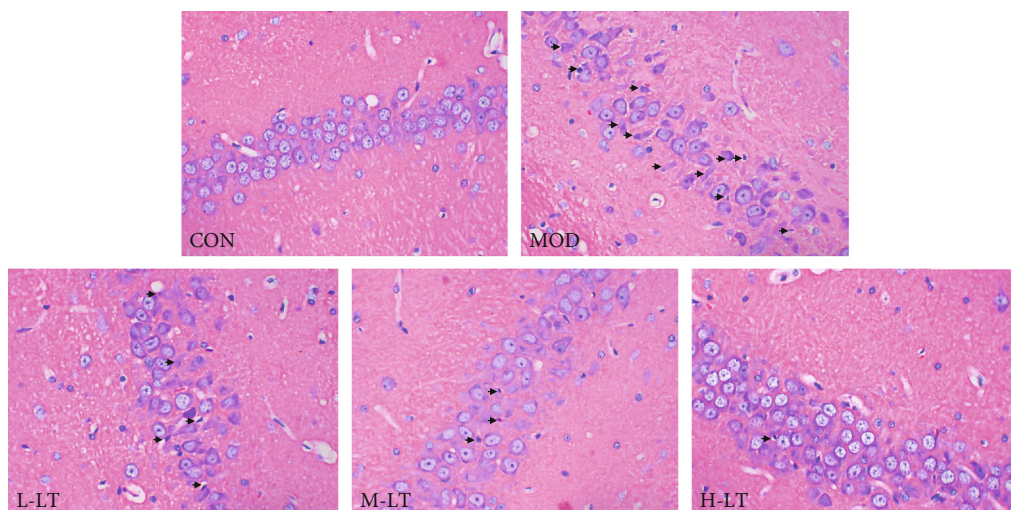


FIGURE 1: Pathological changes in rats' hippocampal tissues of each group (400x; $n = 3$). The black arrows indicate shrinkage or apoptosis of nerve cells. L-LT: low-dose (100 mg/kg) L-theanine group; M-LT: medium-dose (200 mg/kg) L-theanine group; H-LT: high-dose (400 mg/kg) L-theanine group.

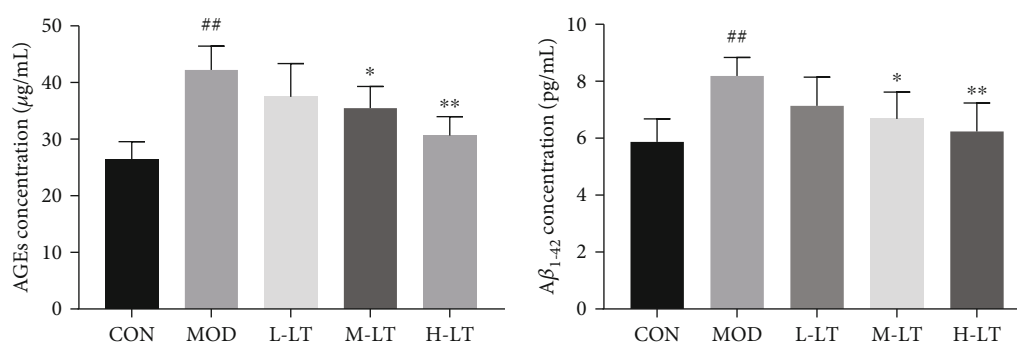


FIGURE 2: AGEs and Aβ₁₋₄₂ concentrations in rats' brain tissues of each group ($n = 6$). Compared with the CON group: [#] $P < 0.05$, ^{##} $P < 0.01$; compared with the MOD group: ^{*} $P < 0.05$, ^{**} $P < 0.01$. L-LT: low-dose (100 mg/kg) L-theanine group; M-LT: medium-dose (200 mg/kg) L-theanine group; H-LT: high-dose (400 mg/kg) L-theanine group.

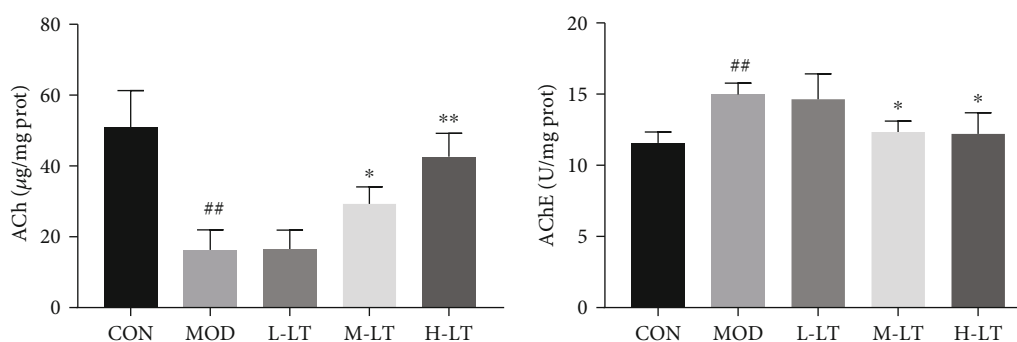


FIGURE 3: The concentration of ACh and AChE in rats' brain tissues of each group ($n = 6$). Compared with the CON group: [#] $P < 0.05$, ^{##} $P < 0.01$; compared with the MOD group: ^{*} $P < 0.05$, ^{**} $P < 0.01$. L-LT: low-dose (100 mg/kg) L-theanine group; M-LT: medium-dose (200 mg/kg) L-theanine group; H-LT: high-dose (400 mg/kg) L-theanine group.

Progressive cognitive impairment is also related to dynamic changes in ACh and AChE activity [35]. In this study, when induced by D-galactose, the activity of AChE was significantly increased in rat brains. L-Theanine can inhibit ACh degradation by decreasing the activity of AChE

in brain damage induced by scopolamine (1 mg/kg, i.p.) [36]. Similarly, our results showed that L-theanine inhibited the AChE activity and restored normal levels of ACh in brain tissues, thereby repressing the damage caused by AGEs and Aβ₁₋₄₂. These findings were consistent with the fact that

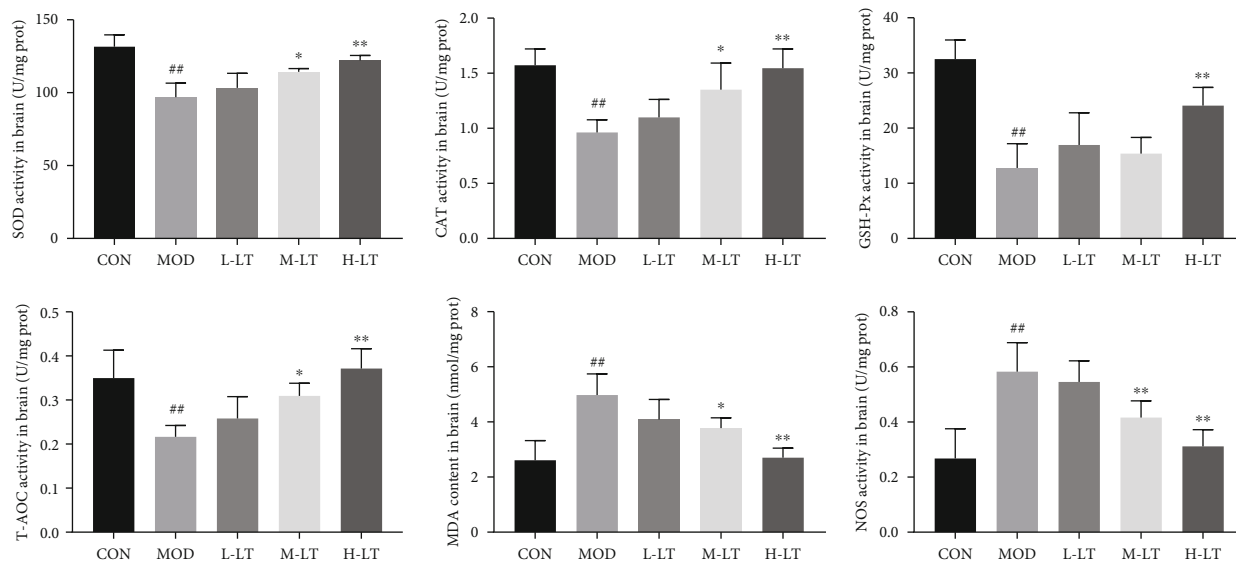


FIGURE 4: Activities and concentrations of oxidative stress-associated markers in rats' brain tissues of each group ($n = 6$). Compared with the CON group: # $P < 0.05$, ## $P < 0.01$; compared with the MOD group: * $P < 0.05$, ** $P < 0.01$. L-LT: low-dose (100 mg/kg) L-theanine group; M-LT: medium-dose (200 mg/kg) L-theanine group; H-LT: high-dose (400 mg/kg) L-theanine group.

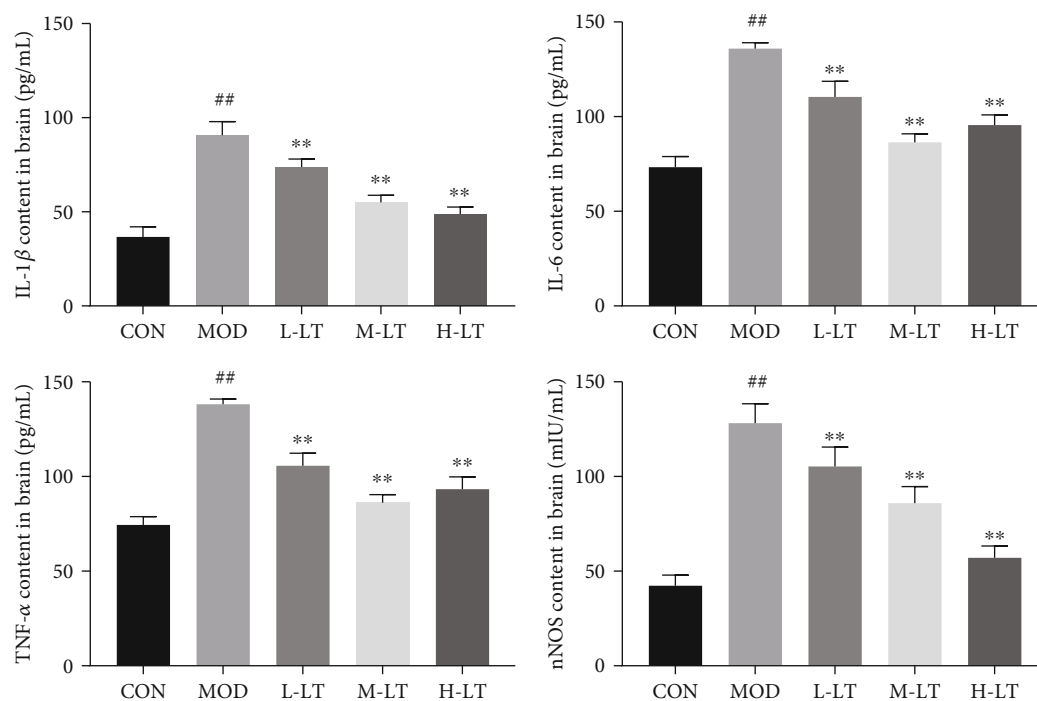


FIGURE 5: Concentrations of IL-1 β , IL-6, TNF- α , and nNOS in rats' brain tissues of each group ($n = 6$). Compared with the CON group: # $P < 0.05$, ## $P < 0.01$; compared with the MOD group: * $P < 0.05$, ** $P < 0.01$. L-LT: low-dose (100 mg/kg) L-theanine group; M-LT: medium-dose (200 mg/kg) L-theanine group; H-LT: high-dose (400 mg/kg) L-theanine group.

L-theanine blocked the increase in $A\beta_{1-42}$ content and AChE activity induced by external stress and prevented AD [33, 34, 36].

AGEs and $A\beta_{1-42}$ can bind to RAGE and promote intracellular oxidative stress production, with the activation of the RAGE signal pathway [8, 37]. The brain is the most vulnerable organ to oxidative stress due to its high metabolic activity,

high lipid content, and limited antioxidant defense capacity [13]. According to the theory of free radical aging, maintaining the balance of oxidative stress contributes to preventing or delaying age-related diseases [38]. Previous studies have shown that D-galactose induces oxidative stress damage and mitochondrial dysfunction and promotes the production of AGEs [13, 39]. In this study, we found that the gene and

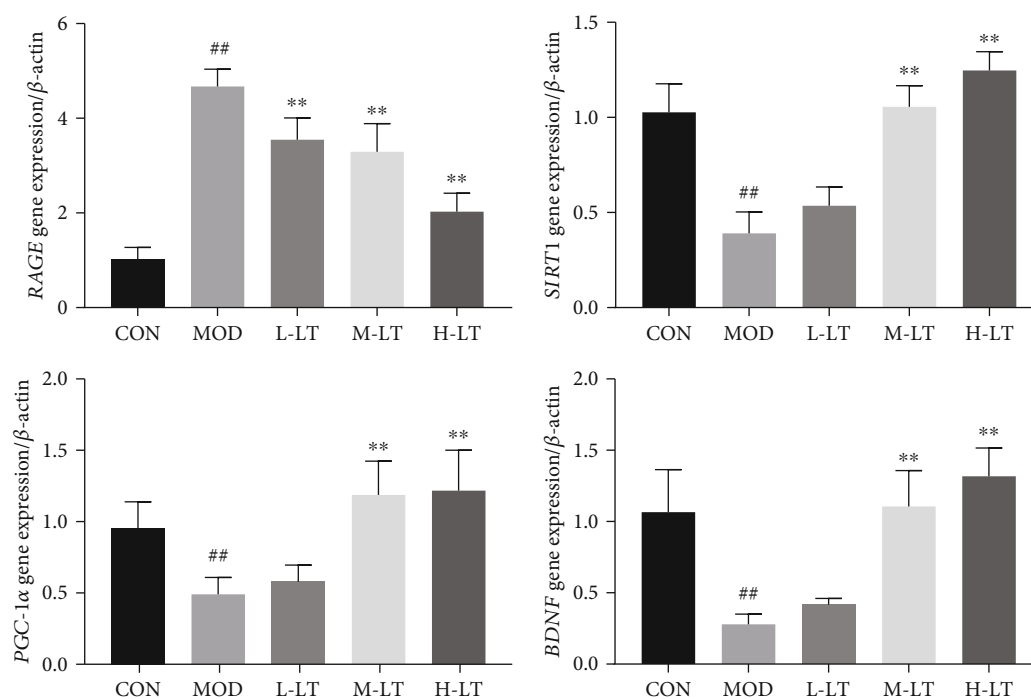


FIGURE 6: Expression levels of *RAGE*, *SIRT1*, *PGC-1α*, and *BDNF* mRNAs in rats' brain tissues of each group ($n = 6$). Compared with the CON group: # $P < 0.05$, ## $P < 0.01$; compared with the MOD group: * $P < 0.05$, ** $P < 0.01$. L-LT: low-dose (100 mg/kg) L-theanine group; M-LT: medium-dose (200 mg/kg) L-theanine group; H-LT: high-dose (400 mg/kg) L-theanine group.

protein expression levels of RAGE were increased in the brains of D-galactose-induced glycosylated model rats, and significant changes were observed in various oxidative stress indexes. Mitochondria are the primary energy production site for normal cell physiological activities and enhance brain cognitive ability [40]. However, excessive production of active oxidative stress products leads to mitochondrial damage and dysfunction, a key factor in the occurrence of neurodegenerative diseases, such as AD [41]. Studies have shown that PGC-1 α is a key regulator of mitochondrial biosynthesis and function [40, 42], whereas antioxidant enzymes such as SOD2 and CAT protect the mitochondria from oxidative stress, exerting neuroprotective effects [43]. L-Theanine increased SOD2 and CAT protein levels in the brains of rats exposed to D-galactose, thereby alleviating the imbalances in oxidative stress components, inhibiting the production of AGEs, and preventing AGE-induced neurotoxicity in brain tissues. L-Theanine also upregulated PGC-1 α mRNA and protein in the brains of D-galactose-treated rats, contributing to normal biosynthesis of mitochondria in rat brain tissues and positively regulating oxidative metabolism. In addition, L-theanine recalibrated the redox balance in the mitochondria to resist the occurrence and development of neurodegenerative diseases [44]. This may be attributed to the antioxidant activity of L-theanine, as reported by Ben and Jo; indeed, L-theanine maintains the normal biological function of mitochondria, thereby reducing neurotoxicity to protect nerve cells [45, 46].

Chronic inflammation, which is also highly related with AD, is a pathological condition characterized by a continuous active inflammatory response and tissue destruction [47].

Persistent oxidative stress injury is also a signal of chronic inflammation and is closely associated with the pathological and physiological changes of many age-related degenerative diseases [48]. Inflammation can mitigate abnormalities and promote tissue healing in acute cases at low levels. However, a long-term high level of inflammation could seriously damage host tissues [49]. The transcription factor NF- κ B is a key factor regulating inflammation. Of note, NF- κ B acetylation activates its regulatory ability. Continuous increases in Ace-NF- κ B (p65) protein levels promote the secretion of downstream proinflammatory factors, such as IL-1 β , IL-6, and TNF- α , and induce systemic inflammation [50]. In addition, activated NF- κ B (p65) positively correlates with high expression of RAGE [51]. Activated NF- κ B, RAGE, and proinflammatory factors form a vicious circle, causing a state of persistent pathological inflammation in the brain. As an effective immunomodulator [24, 52, 53], L-theanine was found to inhibit the activation of NF- κ B (p65) and the expression of proinflammatory factors, such as TNF- α , IL-1 β , and IL-6 in the rat brain, thereby promoting resistance to nerve cell damage. Accordingly, L-theanine inhibited Ace-NF- κ B protein expression in rat brains exposed to D-galactose and downregulated RAGE mRNA and protein expression, thus preventing an increase in proinflammatory markers, such as IL-1 β , nNOS, TNF- α , and IL-6. These findings suggest that L-theanine could be used to regulate the persistent pathological inflammatory state in the brain tissues of D-galactose-treated model rats and restore inflammatory balance in brain tissues.

Apoptosis is an active form of programmed cell death, which is closely related to AD lesions and is regulated by

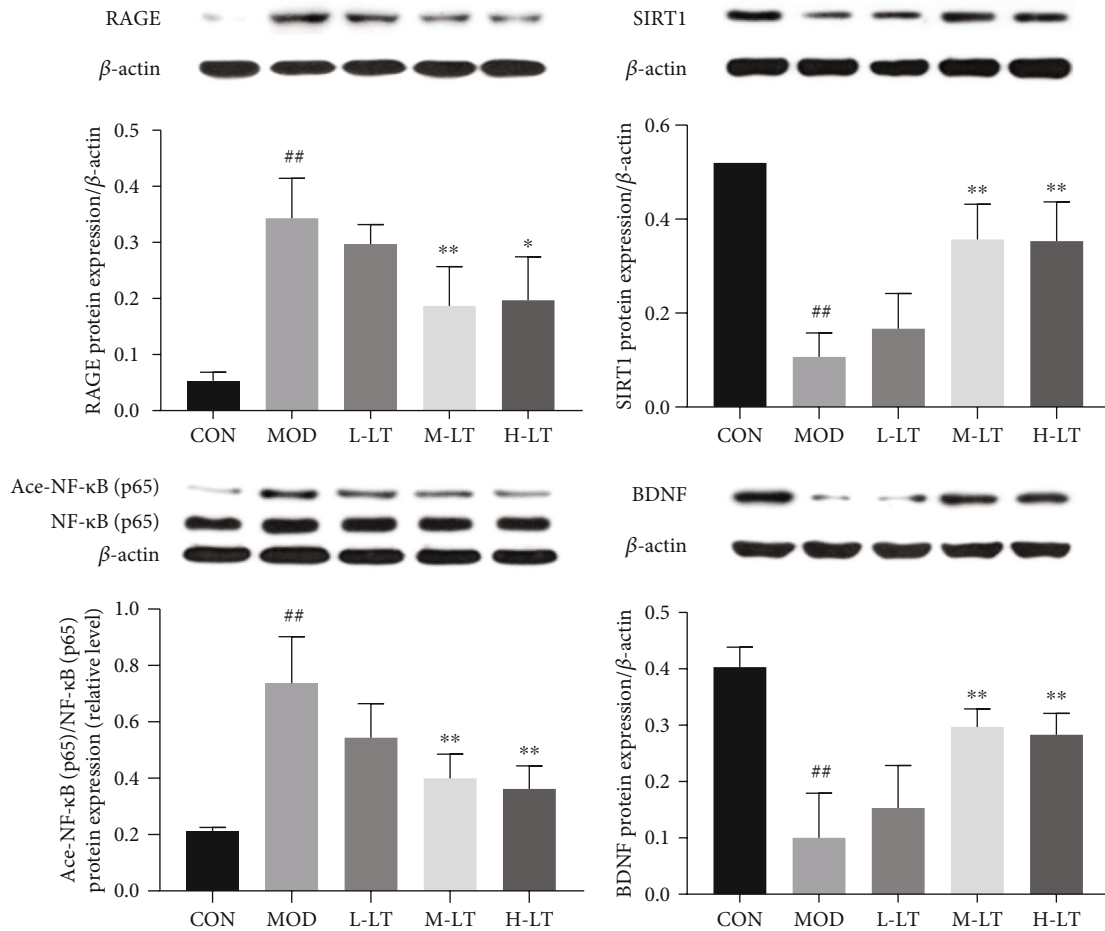


FIGURE 7: Protein expression of RAGE, SIRT1, Ace-NF-κB (p65), and BDNF in rats' brain tissues of each group ($n = 3$). Compared with the CON group: $^{\#}P < 0.05$, $^{##}P < 0.01$; compared with the MOD group: $^*P < 0.05$, $^{**}P < 0.01$. L-LT: low-dose (100 mg/kg) L-theanine group; M-LT: medium-dose (200 mg/kg) L-theanine group; H-LT: high-dose (400 mg/kg) L-theanine group.

specific proteins, including Bcl proteins and caspases [54]. Cho and Di reported that L-theanine has antineuronal apoptosis effects, suggesting applications in the prevention and treatment of neurodegenerative diseases [34, 55]. L-Theanine inhibited the expression of the apoptotic proteins, including Bax and cleaved-caspase-3. Furthermore, L-theanine promoted the expression of the antiapoptotic protein Bcl-2, which controls the level of neuronal apoptosis in brain tissues and maintains brain environment stability. Additionally, H&E staining of hippocampal rat tissues confirmed that L-theanine blocked D-galactose-induced neuronal apoptosis.

Impairment of neuronal plasticity due to normal aging is paralleled by neuronal damage, apoptosis, and reduced cognitive ability [17]. Neurotrophins and their receptors, particularly BDNF, are expressed in highly malleable brain regions (e.g., the hippocampus and cerebral cortex), which are considered molecular mediators of functional and morphological synaptic plasticity. These molecules are also essential for neuronal proliferation, excitability, synaptic transmission, and plasticity [56, 57]. In addition, BDNF plays a vital role in supporting the survival and growth of sensory and motor neurons, all of which are vital factors for learning and memory [58]. Moreover, some exogenous substances enhance

BDNF expression, thereby inhibiting neuronal apoptosis and reducing neurodegenerative changes [59, 60]. We found that D-galactose inhibited the expression of BDNF, whereas L-theanine enhanced the expression of BDNF mRNA and protein in the brains of D-galactose-treated rats, thereby preventing D-galactose-induced hippocampal neuron dysfunction. These findings are consistent with a report that L-theanine increases BDNF content in the serum or hippocampal tissue and inhibits the effects of neurotoxicity caused by exogenous stress on neurodegenerative diseases [55]. Furthermore, it has been reported that PGC-1 α overexpression can reverse the inhibition of BDNF mRNA expression in neurons of APP/PS1 transgenic mice [61]. More importantly, the increased expression of upstream PGC-1 α can upregulate the BDNF expression and counteract the effect of A β_{1-42} on neuronal apoptosis [61, 62]. Collectively, these findings indicate that PGC-1 α plays a pivotal role in BDNF upregulation. Our results suggest that L-theanine may also upregulate the level of PGC-1 α protein in rat hippocampus exposed to D-galactose, recover the level of BDNF, and improve the D-galactose-induced brain damage.

Homeostasis of the internal environment is essential for promoting healthy aging of the body [28]. SIRT1 is a highly

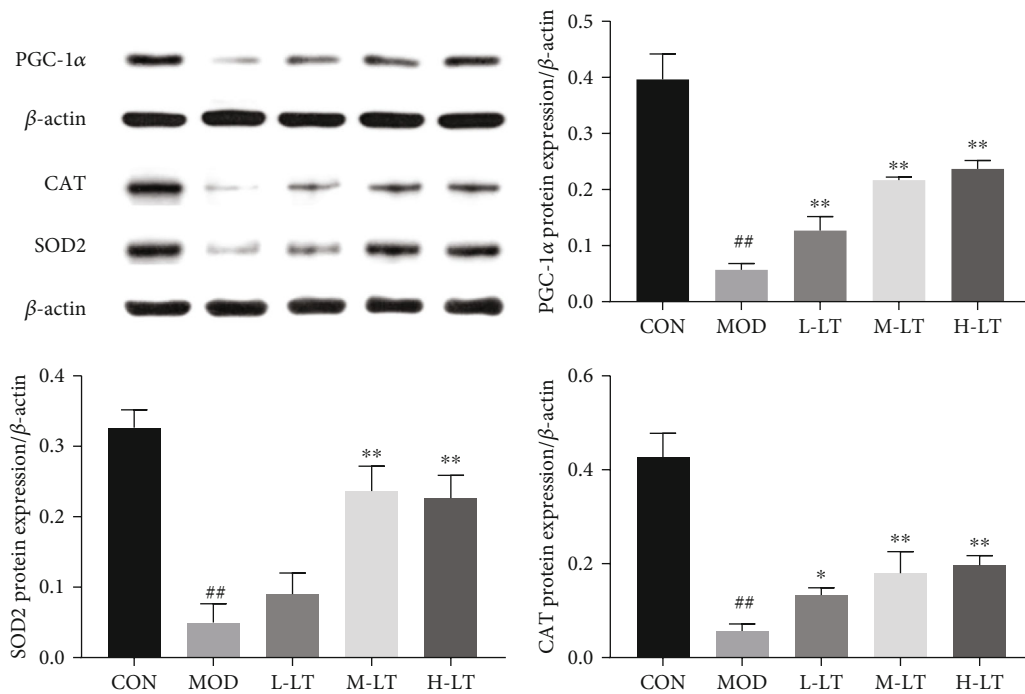


FIGURE 8: Protein expression of PGC-1α, SOD2, and CAT in rats' brain tissues of each group ($n = 3$). Compared with the CON group: $^{\#}P < 0.05$, $^{\#\#}P < 0.01$; compared with the MOD group: $^*P < 0.05$, $^{**}P < 0.01$. L-LT: low-dose (100 mg/kg) L-theanine group; M-LT: medium-dose (200 mg/kg) L-theanine group; H-LT: high-dose (400 mg/kg) L-theanine group.

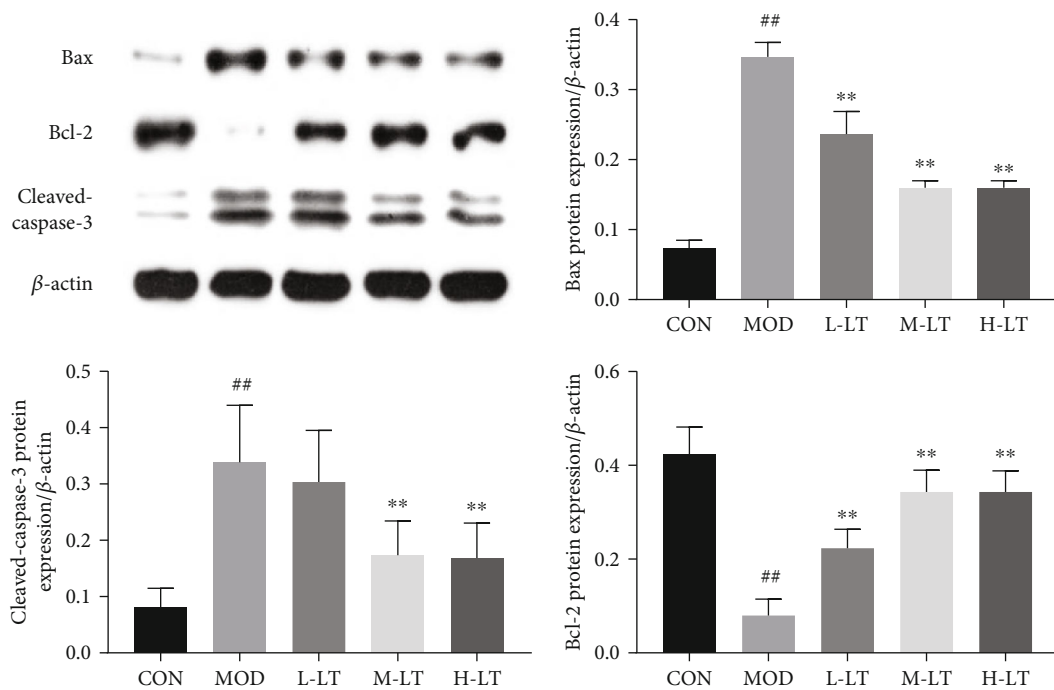


FIGURE 9: Protein expression of Bcl-2, Bax, and cleaved-caspase-3 in rats' brain tissues of each group ($n = 3$). Compared with the CON group: $^{\#}P < 0.05$, $^{\#\#}P < 0.01$; compared with the MOD group: $^*P < 0.05$, $^{**}P < 0.01$. L-LT: low-dose (100 mg/kg) L-theanine group; M-LT: medium-dose (200 mg/kg) L-theanine group; H-LT: high-dose (400 mg/kg) L-theanine group.

conserved protein that functions in deacetylation and maintenance of the homeostasis of the internal environment [28, 63]. SIRT1 is involved in several biological pro-

cesses, such as oxidative stress, inflammatory reactions, apoptosis and senescence, mitochondrial biosynthesis, glucose and lipid metabolism, and oxidative metabolism

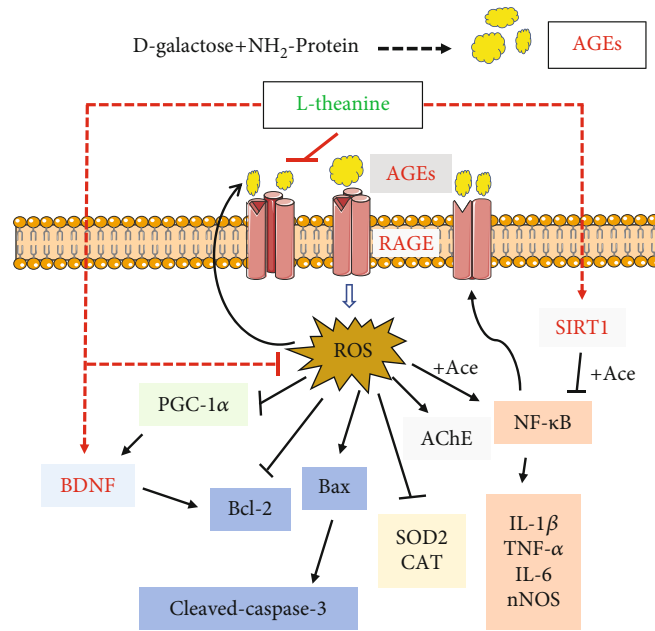


FIGURE 10: Potential alleviation mechanisms of L-theanine on brain injury in D-galactose-induced glycosylation model rats.

mediated by downstream RAGE factors, such as SOD2, CAT, NF- κ B, Bax, and PGC-1 α [63, 64]. Moreover, SIRT1 plays important roles in inhibiting the occurrence and development of neurodegenerative diseases, protecting nerve cells, and maintaining normal nerve function [14]. Abnormal increases in AGEs and $A\beta_{1-42}$ induced by D-galactose can mediate inflammation, oxidative stress injury, mitochondrial dysfunction, and apoptosis and decrease BDNF and ACh levels, resulting in induction of the pathological processes of neurodegenerative diseases [13, 65, 66]. Therefore, reducing the concentrations of AGEs and $A\beta_{1-42}$ and the RAGE expression in brain tissue is critical for preventing and treating neurodegenerative diseases. In our study, we showed that L-theanine inhibited the accumulation of AGEs and $A\beta_{1-42}$ in the brains of model rats exposed to D-galactose and facilitate the maintenance of normal BDNF and ACh levels. Additionally, L-theanine blocked NF- κ B acetylation and downregulated RAGE mRNA and protein levels by activating SIRT1 [67]. Furthermore, L-theanine maintained the balance of inflammatory responses, modulated redox balance and mitochondrial biosynthesis, and reduced neuronal apoptosis in the hippocampus, thereby facilitating homeostasis of brain tissue and alleviating brain injury induced by D-galactose.

Prevention and treatment of D-galactose-induced brain injury by L-theanine could apply to other tissues besides the brain. For example, previous studies have shown that age-related degenerative diseases can be controlled or attenuated by activating the energy metabolite adenylate-activated protein kinase (AMPK) [68]. The longevity protein SIRT1 is required for AMPK activity [69]. We have previously shown that L-theanine has protective effects in the livers of D-galactose-treated rats and promotes glucose metabolism through the AMPK signaling pathway, resulting in reduced sugar concentrations in the body [26, 27]. Therefore, we speculate that L-theanine can inhibit the positive reaction of Schiff base

formation between D-galactose and free amino groups, along with its reduction of AGEs and $A\beta_{1-42}$ concentrations, thereby alleviating D-galactose-induced damage in rats' brain tissues.

Thus, the potential alleviation mechanism of L-theanine on brain injury induced by D-galactose is presented in Figure 10. Treatment with L-theanine decreased $A\beta_{1-42}$ and mitigated AGEs/RAGE-induced brain damage by upregulating SIRT1 and BDNF proteins.

5. Conclusion

L-Theanine was found to mitigate brain damage via inhibiting AGEs/RAGE signaling pathways and upregulating SIRT1 and BDNF, which indicate that L-theanine may be a potential functional food to prevent AD and promote healthy aging. For future work, studies of further mechanisms of L-theanine on different tissues of rats will be required. It would also be desirable to examine the metabolism of L-theanine in a rat model of D-galactose-induced brain damage.

Abbreviations

A β :	β -Amyloid
ACh:	Acetylcholine
AChE:	Acetylcholinesterase
AD:	Alzheimer's disease
AGEs:	Advanced glycation end products
AMPK:	AMP-activated protein kinase
BDNF:	Brain-derived neurotrophic factor
CAT:	Catalase
CON:	Control group
GSH:	Glutathione peroxidase
H-LT:	High-dose L-theanine group
IL:	Interleukin

L-LT:	Low-dose L-theanine group
MDA:	Malondialdehyde
M-LT:	Medium-dose L-theanine group
MOD:	Model group
NF- κ B (p65), nNOS:	Neuronal nitric oxide synthase
NOS:	Nitric oxide synthase
PGC-1 α :	Peroxisome proliferator-activated receptor- γ coactivator-1 α
RAGE:	Receptor for AGEs
ROS:	Reactive oxygen species
SD:	Sprague-Dawley
SIRT1:	Sirtuin1
SOD:	Superoxide dismutase
T-AOC:	Total antioxidant capacity
TNF- α :	Tumor necrosis factor- α .

Data Availability

The data used to support the findings of this study are included within the article.

Conflicts of Interest

The authors declare no competing financial interest.

Acknowledgments

This work was financially supported by the National Natural Science Foundation of China (No. 31871804), the Natural Science Foundation of Hunan Province, China (No. 2019JJ40272 and 2020JJ4036), and the Scientific Research Foundation of Shaoyang College, China (No. 2020HX122). We would like to thank Editage (<http://online.editage.cn/>) for English language editing.

References

- [1] M. Frimat, M. Daroux, R. Litke, R. Nevière, F. J. Tessier, and E. Boulanger, "Kidney, heart and brain: three organs targeted by ageing and glycation," *Clinical Science*, vol. 131, no. 11, pp. 1069–1092, 2017.
- [2] S. A. Palma-Duran, M. D. Kontogianni, A. Vlassopoulos et al., "Serum levels of advanced glycation end-products (AGEs) and the decoy soluble receptor for AGEs (sRAGE) can identify non-alcoholic fatty liver disease in age-, sex- and BMI-matched normo-glycemic adults," *Metabolism*, vol. 83, pp. 120–127, 2018.
- [3] J. N. Fawver, H. E. Schall, R. D. Petrofes Chapa, X. Zhu, and I. V. J. Murray, "Amyloid- β metabolite sensing: biochemical linking of glycation modification and misfolding," *Journal of Alzheimers Disease*, vol. 30, no. 1, pp. 63–73, 2012.
- [4] B. A. Yankner, T. Lu, and P. Loerch, "The aging brain," *Annual Review of Pathology: Mechanisms of Disease*, vol. 3, no. 1, pp. 41–66, 2008.
- [5] S. Kawanishi, K. Takata, S. Itezo et al., "Bone-marrow-derived microglia-like cells ameliorate brain amyloid pathology and cognitive impairment in a mouse model of Alzheimer's disease," *Journal of Alzheimer's Disease*, vol. 64, no. 2, pp. 563–585, 2018.
- [6] S. W. Pimplikar, R. A. Nixon, N. K. Robakis, J. Shen, and L. H. Tsai, "Amyloid-independent mechanisms in Alzheimer's disease pathogenesis," *The Journal of Neuroscience*, vol. 30, no. 45, pp. 14946–14954, 2010.
- [7] V. Srikanth, A. Maczurek, T. Phan et al., "Advanced glycation endproducts and their receptor RAGE in Alzheimer's disease," *Neurobiology of Aging*, vol. 32, no. 5, pp. 763–777, 2011.
- [8] K. Byun, Y. Yoo, M. Son et al., "Advanced glycation end-products produced systemically and by macrophages: a common contributor to inflammation and degenerative diseases," *Pharmacology & therapeutics*, vol. 177, pp. 44–55, 2017.
- [9] C. Ott, K. Jacobs, E. Haucke, A. Navarrete Santos, T. Grune, and A. Simm, "Role of advanced glycation end products in cellular signaling," *Redox Biology*, vol. 2, pp. 411–429, 2014.
- [10] R. D. Semba, E. J. Nicklett, and L. Ferrucci, "Does accumulation of advanced glycation end products contribute to the aging phenotype?," *The Journals of Gerontology. Series A, Biological Sciences and Medical Sciences*, vol. 65, no. 9, pp. 963–975, 2010.
- [11] F. Ledl and E. Schleicher, "New aspects of the Maillard reaction in foods and in the human body," *Angewandte Chemie International Edition*, vol. 29, no. 6, pp. 565–594, 1990.
- [12] X. Song, M. Bao, D. Li, and Y. M. Li, "Advanced glycation in d-galactose induced mouse aging model," *Mechanisms of Ageing and Development*, vol. 108, no. 3, pp. 239–251, 1999.
- [13] T. Shwe, W. Pratchayasakul, N. Chattipakorn, and S. C. Chattipakorn, "Role of D-galactose-induced brain aging and its potential used for therapeutic interventions," *Experimental gerontology*, vol. 101, pp. 13–36, 2018.
- [14] A. Z. Herskovits and L. Guarente, "SIRT1 in neurodevelopment and brain senescence," *Neuron*, vol. 3, no. 81, pp. 471–483, 2014.
- [15] J. Gao, R. Zhou, X. You et al., "Salidroside suppresses inflammation in a D-galactose-induced rat model of Alzheimer's disease via SIRT1/NF- κ B pathway," *Metabolic Brain Disease*, vol. 31, no. 4, pp. 771–778, 2016.
- [16] Q. Li, J. Zeng, M. Su, Y. He, and B. Zhu, "Acetylshikonin from Zicao attenuates cognitive impairment and hippocampus senescence in D-galactose-induced aging mouse model via upregulating the expression of SIRT1," *Brain Research Bulletin*, vol. 137, pp. 311–318, 2018.
- [17] L. Tapia-Arancibia, E. Aliaga, M. Silhol, and S. Arancibia, "New insights into brain BDNF function in normal aging and Alzheimer disease," *Brain Research Reviews*, vol. 59, no. 1, pp. 201–220, 2008.
- [18] C. Molinari, V. Morsanuto, S. Ruga et al., "The Role of BDNF on Aging-Modulation Markers," *Brain Sci*, vol. 10, no. 5, p. 285, 2020.
- [19] H. Jeong, D. E. Cohen, L. Cui et al., "Sirt1 mediates neuroprotection from mutant huntingtin by activation of the TORC1 and CREB transcriptional pathway," *Nature Medicine*, vol. 18, no. 1, pp. 159–165, 2011.
- [20] C. Harrison, "A neuroprotective role for sirtuin 1," *Nature Reviews Drug Discovery*, vol. 11, no. 2, p. 108, 2012.
- [21] X. Peng, J. Ma, F. Chen, and M. Wang, "Naturally occurring inhibitors against the formation of advanced glycation end-products," *Food & Function*, vol. 2, no. 6, pp. 289–301, 2011.
- [22] M. I. Prasanth, B. S. Sivamaruthi, C. Chaiyasut, and T. Tencomnao, "A review of the role of green tea (*Camellia sinensis*) in antiphotaging, stress resistance, neuroprotection, and autophagy," *Nutrients*, vol. 11, no. 2, p. 474, 2019.

- [23] S.-Q. Chen, Z.-S. Wang, Y.-X. Ma et al., “Neuroprotective effects and mechanisms of tea bioactive components in neurodegenerative diseases,” *Molecules*, vol. 23, no. 3, 2018.
- [24] E. Sharma, R. Joshi, and A. Gulati, “L-Theanine: an astounding sui generis integrant in tea,” *Food Chemistry*, vol. 242, pp. 601–610, 2018.
- [25] A. Culetu, B. Fernandez-Gomez, M. Ullate, M. D. del Castillo, and W. Andlauer, “Effect of theanine and polyphenols enriched fractions from decaffeinated tea dust on the formation of Maillard reaction products and sensory attributes of breads,” *Food Chemistry*, vol. 197, no. 197, pp. 14–23, 2016.
- [26] L. Zeng, L. Lin, Y. Peng et al., “L-Theanine attenuates liver aging by inhibiting advanced glycation end products in D-galactose-induced rats and reversing an imbalance of oxidative stress and inflammation,” *Experimental Gerontology*, vol. 131, article 110823, 2020.
- [27] L. Lin, L. Zeng, A. Liu et al., “L-Theanine regulates glucose, lipid, and protein metabolism via insulin and AMP-activated protein kinase signaling pathways,” *Food & Function*, vol. 11, no. 2, pp. 1798–1809, 2020.
- [28] C. López-Otín, M. A. Blasco, L. Partridge, M. Serrano, and G. Kroemer, “The hallmarks of aging,” *Cell*, vol. 153, no. 6, pp. 1194–1217, 2013.
- [29] L. Pastorino and K. P. Lu, “Pathogenic mechanisms in Alzheimer’s disease,” *European Journal of Pharmacology*, vol. 545, no. 1, pp. 29–38, 2006.
- [30] V. Srikanth, B. Westcott, J. Forbes et al., “Methylglyoxal, cognitive function and cerebral atrophy in older people,” *The Journals of Gerontology Series A: Biological Sciences and Medical Sciences*, vol. 68, no. 1, pp. 68–73, 2013.
- [31] H. Zhao, N. Li, Q. Wang, X. J. Cheng, X. M. Li, and T. T. Liu, “Resveratrol decreases the insoluble A β 1-42 level in hippocampus and protects the integrity of the blood-brain barrier in AD rats,” *Neuroscience*, vol. 310, pp. 641–649, 2015.
- [32] S. U. Rehman, S. A. Shah, T. Ali, J. I. Chung, and M. O. Kim, “Anthocyanins reversed D-Galactose-induced oxidative stress and neuroinflammation mediated cognitive impairment in adult rats,” *Molecular Neurobiology*, vol. 54, no. 1, pp. 255–271, 2017.
- [33] T. I. Kim, Y. K. Lee, S. G. Park et al., “L-Theanine, an amino acid in green tea, attenuates β -amyloid-induced cognitive dysfunction and neurotoxicity: reduction in oxidative damage and inactivation of ERK/p38 kinase and NF- κ B pathways,” *Free Radical Biology & Medicine*, vol. 47, no. 11, pp. 1601–1610, 2009.
- [34] X. di, J. Yan, Y. Zhao et al., “L-Theanine protects the APP (Swedish mutation) transgenic SH-SY5Y cell against glutamate-induced excitotoxicity via inhibition of the NMDA receptor pathway,” *Neuroscience*, vol. 168, no. 3, pp. 778–786, 2010.
- [35] F. Ahmed, S. Manjunath, and J. N. Narendra Sharath Chandra, “Acetylcholine and memory-enhancing activity of Ficus racemosa bark,” *Pharmacognosy Research*, vol. 3, no. 4, pp. 246–249, 2011.
- [36] T. I. Kim, D. Y. Yuk, S. G. Park et al., “Improvement of memory impairment by the combination of green tea extract and L-theanine through inhibition of acetylcholinesterase activity in mice,” *Laboratory Animal Research*, vol. 24, pp. 87–92, 2008.
- [37] T. Kimura, J. Takamatsu, N. Araki et al., “Are advanced glycation end-products associated with amyloidosis in Alzheimer’s disease?,” *Neuroreport*, vol. 6, no. 6, pp. 866–868, 1995.
- [38] T. Finkel and N. J. Holbrook, “Oxidants, oxidative stress and the biology of ageing,” *Nature*, vol. 408, no. 6809, pp. 239–247, 2000.
- [39] J. Budni, M. L. Garcez, F. Mina et al., “The oral administration of D-galactose induces abnormalities within the mitochondrial respiratory chain in the brain of rats,” *Metabolic Brain Disease*, vol. 32, no. 3, pp. 811–817, 2017.
- [40] J. W. Pak, A. Herbst, E. Bua, N. Gokey, D. McKenzie, and J. M. Aiken, “Mitochondrial DNA mutations as a fundamental mechanism in physiological declines associated with aging,” *Aging Cell*, vol. 2, no. 1, pp. 1–7, 2003.
- [41] R. X. Santos, S. C. Correia, X. Zhu et al., “Mitochondrial DNA oxidative damage and repair in aging and Alzheimer’s disease,” *Antioxidants & Redox Signaling*, vol. 18, no. 18, pp. 2444–2457, 2013.
- [42] T. Wenz, “Mitochondria and PGC-1 α in aging and age-associated diseases,” *Journal of Aging Research*, vol. 2011, no. 4, Article ID 810619, 12 pages, 2011.
- [43] K. Anil, P. Atish, and D. Samrita, “Naringin alleviates cognitive impairment, mitochondrial dysfunction and oxidative stress induced by D-galactose in mice,” *Food and Chemical Toxicology*, vol. 48, no. 2, pp. 626–632, 2010.
- [44] I. Casetta, V. Govoni, and E. Granieri, “Oxidative stress, antioxidants and neurodegenerative diseases,” *Current Pharmaceutical Design*, vol. 11, no. 16, pp. 2033–2052, 2005.
- [45] P. Ben, Z. Zhang, Y. Zhu et al., “L-Theanine attenuates cadmium-induced neurotoxicity through the inhibition of oxidative damage and tau hyperphosphorylation,” *Neurotoxicology*, vol. 57, pp. 95–103, 2016.
- [46] M.-R. Jo, M.-H. Park, D.-Y. Choi et al., “Neuroprotective effect of L-theanine on A β -induced neurotoxicity through anti-oxidative mechanisms in SK-N-SH and SK-N-MC cells,” *Biomolecules & Therapeutics*, vol. 19, no. 3, pp. 288–295, 2011.
- [47] P. L. McGEER and M. Eg, “Inflammation and the degenerative diseases of aging,” *Annals of the New York Academy of Sciences*, vol. 1035, no. 1, pp. 104–116, 2004.
- [48] E. S. Cannizzo, C. C. Clement, R. Sahu, C. Follo, and L. Santambrogio, “Oxidative stress, inflamm-aging and immunosenescence,” *Journal of Proteomics*, vol. 74, no. 11, pp. 2313–2323, 2011.
- [49] S. Vasto, G. Candore, C. R. Balistreri et al., “Inflammatory networks in ageing, age-related diseases and longevity,” *Mechanisms of Ageing and Development*, vol. 128, no. 1, pp. 83–91, 2007.
- [50] M. S. Hayden and S. Ghosh, “Shared principles in NF- κ B signaling,” *Cell*, vol. 132, no. 3, pp. 344–362, 2008.
- [51] V. Bortolotto and M. Grilli, “Every cloud has a silver lining: proneurogenic effects of A β oligomers and HMGB-1 via activation of the RAGE-NF- κ B axis,” *CNS & Neurological Disorders Drug Targets*, vol. 16, no. 10, pp. 1066–1079, 2017.
- [52] S. Jamwal and P. Kumar, “L-theanine, a component of green tea prevents 3-nitropropionic acid (3-NP)-induced striatal toxicity by modulating nitric oxide pathway,” *Molecular Neurobiology*, vol. 54, no. 3, pp. 2327–2337, 2017.
- [53] T. Sumathi, D. Asha, G. Nagarajan, A. Sreenivas, and R. Nivedha, “L-Theanine alleviates the neuropathological changes induced by PCB (Aroclor 1254) via inhibiting

- upregulation of inflammatory cytokines and oxidative stress in rat brain,” *Environmental Toxicology and Pharmacology*, vol. 42, pp. 99–117, 2016.
- [54] S. M. Mooney and M. W. Miller, “Expression of bcl-2, bax, and caspase-3 in the brain of the developing rat,” *Developmental Brain Research*, vol. 123, no. 2, pp. 103–117, 2000.
- [55] H. S. Cho, S. Kim, S. Y. Lee, J. A. Park, S. J. Kim, and H. S. Chun, “Protective effect of the green tea component, L-theanine on environmental toxins-induced neuronal cell death,” *Neurotoxicology*, vol. 29, no. 4, pp. 656–662, 2008.
- [56] M. J. Webster, C. S. Weickert, M. M. Herman, and J. E. Kleinman, “BDNF mRNA expression during postnatal development, maturation and aging of the human prefrontal cortex,” *Developmental Brain Research*, vol. 139, no. 2, pp. 139–150, 2002.
- [57] M. Stepanichev, M. Onufriev, V. Aniol et al., “Effects of cerebrolysin on nerve growth factor system in the aging rat brain,” *Restorative Neurology and Neuroscience*, vol. 35, no. 6, pp. 571–581, 2017.
- [58] D. Silakarma and A. A. R. Sudewi, “The role of brain-derived neurotrophic factor (BDNF) in cognitive functions,” *Bali Medical Journal*, vol. 8, no. 2, pp. 427–434, 2019.
- [59] E. J. Koh, K. J. Kim, J. Choi, D. H. Kang, and B. Y. Lee, “_Spirulina maxima_ extract prevents cell death through BDNF activation against amyloid beta 1-42 ($A\beta_{1-42}$) induced neurotoxicity in PC12 cells,” *Neuroscience letters*, vol. 673, pp. 33–38, 2018.
- [60] M. Bomba, A. Granzotto, V. Castelli et al., “Exenatide reverts the high-fat-diet-induced impairment of BDNF signaling and inflammatory response in an animal model of Alzheimer’s disease,” *Journal of Alzheimer’s Disease*, vol. 70, no. 3, pp. 793–810, 2019.
- [61] D. Y. Xia, X. Huang, C. F. Bi, L. L. Mao, L. J. Peng, and H. R. Qian, “PGC-1 α or FNDC5 is involved in modulating the effects of $A\beta_{1-42}$ oligomers on suppressing the expression of BDNF, a beneficial factor for inhibiting neuronal apoptosis, $A\beta$ deposition and cognitive decline of APP/PS1 Tg Mice,” *Frontiers in Aging Neuroscience*, vol. 9, 2017.
- [62] M. Azimi, R. Gharakhanlou, N. Naghdi, D. Khodadadi, and S. Heysiattalab, “Moderate treadmill exercise ameliorates amyloid- β -induced learning and memory impairment, possibly via increasing AMPK activity and up-regulation of the PGC-1 α /FNDC5/BDNF pathway,” *Peptides*, vol. 102, pp. 78–88, 2018.
- [63] X. X. Kong, R. Wang, X. J. Liu et al., “Function of SIRT1 in physiology,” *Biochemistry*, vol. 74, no. 7, pp. 703–708, 2009.
- [64] D. H. Lee, “Sirt1 as a new therapeutic target in metabolic and age-related diseases,” *Chonnam Medical Journal*, vol. 46, no. 2, pp. 67–73, 2010.
- [65] K. Yaffe, K. Lindquist, A. V. Schwartz et al., “Advanced glycation end product level, diabetes, and accelerated cognitive aging,” *Neurology*, vol. 77, no. 14, pp. 1351–1356, 2011.
- [66] M. W. Poulsen, R. V. Hedegaard, J. M. Andersen et al., “Advanced glycation endproducts in food and their effects on health,” *Food and Chemical Toxicology*, vol. 60, pp. 10–37, 2013.
- [67] F. Yeung, J. E. Hoberg, C. S. Ramsey et al., “Modulation of NF- κ B-dependent transcription and cell survival by the SIRT1 deacetylase,” *The EMBO journal*, vol. 23, no. 12, pp. 2369–2380, 2004.
- [68] A. Salminen and K. Kaarniranta, “AMP-activated protein kinase (AMPK) controls the aging process via an integrated signaling network,” *Ageing Research Reviews*, vol. 11, no. 2, pp. 230–241, 2012.
- [69] C. Cantó, Gerhart-Hines, J. N. Feige et al., “AMPK regulates energy expenditure by modulating NAD⁺ metabolism and SIRT1 activity,” *Nature*, vol. 458, no. 7241, pp. 1056–1060, 2009.

Review Article

Roles of Dietary Bioactive Peptides in Redox Balance and Metabolic Disorders

Qinqin Qiao ¹, Liang Chen,² Xiang Li ³, Xiangyang Lu,² and Qingbiao Xu ³

¹College of Information Engineering, Fuyang Normal University, Fuyang 236041, China

²College of Bioscience and Biotechnology, Hunan Agricultural University, Changsha 410128, China

³College of Animal Sciences and Technology, Huazhong Agricultural University, Wuhan 430070, China

Correspondence should be addressed to Qingbiao Xu; qbxu@mail.hzau.edu.cn

Received 21 January 2021; Revised 30 April 2021; Accepted 21 May 2021; Published 15 June 2021

Academic Editor: Wuquan Deng

Copyright © 2021 Qinqin Qiao et al. This is an open access article distributed under the Creative Commons Attribution License, which permits unrestricted use, distribution, and reproduction in any medium, provided the original work is properly cited.

Bioactive peptides (BPs) are fragments of 2–15 amino acid residues with biological properties. Dietary BPs derived from milk, egg, fish, soybean, corn, rice, quinoa, wheat, oat, potato, common bean, spirulina, and mussel are reported to possess beneficial effects on redox balance and metabolic disorders (obesity, diabetes, hypertension, and inflammatory bowel diseases (IBD)). Peptide length, sequence, and composition significantly affected the bioactive properties of dietary BPs. Numerous studies have demonstrated that various dietary protein-derived BPs exhibited biological activities through the modulation of various molecular mechanisms and signaling pathways, including Kelch-like ECH-associated protein 1/nuclear factor erythroid 2-related factor 2/antioxidant response element *in oxidative stress*; peroxisome proliferator-activated- γ , CCAAT/enhancer-binding protein- α , and sterol regulatory element binding protein 1 in obesity; insulin receptor substrate-1/phosphatidylinositol 3-kinase/protein kinase B and AMP-activated protein kinase in diabetes; angiotensin-converting enzyme inhibition in hypertension; and mitogen-activated protein kinase and nuclear factor-kappa B in IBD. This review focuses on the action of molecular mechanisms of dietary BPs and provides novel insights in the maintenance of redox balance and metabolic diseases of human.

1. Introduction

Dietary food proteins contain short sequences of amino acids (AAs) that possess various biological activities. The short chains of AAs with biological properties are known as bioactive peptides (BPs). BPs usually contain 2–15 AA residues. The BP sequences present in the food proteins are generally hidden in the inner core of the parent proteins [1]. However, bioactive peptides can be released from food proteins with the help of several techniques including proteolysis, microbial fermentation, and gastrointestinal (GI) digestion [2–4]. Among these methods, *in vitro* enzymatic hydrolysis using commercial proteolytic enzymes is the widely employed method in recent times. The proteases cleave the specific sites on the dietary proteins and release the short chains of BPs [5]. Enzymatic hydrolysis of dietary proteins enhances the nutritional value, bioactivity, and functionality and reduces the allergenicity [6]. Several commercial proteases, namely, thermolysin, bromelain, trypsin, alcalase, papain, pepsin,

neutrase, pancreatin, corolase, protamex, and pronase, have been employed to generate biologically active peptides from various dietary proteins. Among the above-mentioned proteases, alcalase, trypsin, pepsin, and pancreatin are the most widely used proteases for the preparation of peptides, with various health benefitting properties, from numerous food sources [7–10]. These enzymes are routinely used due to their broad specificity to produce smaller peptides with various bioactivities and easily availability.

Dietary BPs have been shown to positively affect the various systems of the human body including the immune, cardiovascular, GI, and nervous systems [11]. The BPs must cross the GI barrier and reach the target tissue or organ in order to exhibit health benefits. Dietary peptides exert bioactivities through the modulation (either enhance or decrease) of various molecular mechanisms and pathways. Bioactive properties of dietary peptides are affected by the peptide sequence, length, hydrophobicity, and composition [12–14]. Dietary peptides are easily absorbable across the intestinal

border via peptide transport 1 (PepT1) and possess excellent functional properties (solubility, foaming, and emulsification properties) [15–18]. Additionally, dietary BPs are generally safer than synthetic drugs. Hence, BPs obtained from dietary sources could be used as health foods/nutraceuticals in the management/prevention of various diseases. Numerous BPs derived from whey, casein, milk, soybean, shark, bonita, pacific whiting, porcine, and bovine have been on the market in various countries for human use as functional foods/health foods/nutraceuticals [19].

Redox homeostasis (balance) is an important cellular process that plays a vital role in the maintenance of a normal physiological steady state [20]. Disturbance of balance between oxidants and antioxidants results in the oxidative stress. Recently, many BPs prepared from various food sources such as walnut, egg, fish, quinoa, soybean, millets, corn, wheat, rice, potato, milk, and spirulina have shown to possess beneficial effects in the maintenance of redox homeostasis and prevention/management of metabolic diseases [21–26]. However, reviews describing the role of dietary BPs in the modulation of molecular mechanisms of redox balance and metabolic diseases are scanty in the literature. Hence, the current review focuses on the recent literature related to the effects of dietary BPs on various molecular mechanisms and signaling pathways involved in the redox homeostasis and metabolic diseases (obesity, diabetes, hypertension, and inflammation), as shown in Figure 1.

2. Roles of Dietary Bioactive Peptides in Maintaining Redox Balance

Redox reaction is a chemical reaction that involves the transfer of electrons from the reducing agent to the oxidizing agent [27]. Redox homeostasis (balance) plays a significant role in the maintenance of ordinary physiological functions of the human body. Redox balance is considerably affected by reactive oxygen species (ROS) that are generated during aerobic cellular metabolism [28]. Reactive oxygen species are unstable and highly reactive in the redox reactions due to the presence of unpaired electrons in the outer shells. Under normal physiological conditions, redox balance is maintained through careful regulation of ROS generation and elimination from the body [29]. However, excess production of ROS during oxidative stress conditions could alter the intracellular redox balance and promote the development of numerous diseases such as cancer, diabetes, atherosclerosis, cardiovascular, and neurodegenerative diseases. The body's natural antioxidant defense system, namely, superoxide dismutase (SOD), glutathione peroxidase (GPx), and catalase (CAT), plays a vital role in the maintenance of balance between ROS formation and elimination [30].

Several studies have demonstrated that a number of peptides identified from various dietary sources have shown the ability to suppress oxidative stress and maintain the redox balance through multiple molecular mechanisms such as scavenging free radicals; chelating transition metals; enhancing the production of endogenous antioxidant enzymes SOD, CAT, and GPx; and stimulating the nuclear factor erythroid 2-related factor 2 (Nrf2) antioxidant defense mechanism

[12, 15, 17, 26, 31–34]. The antioxidant mechanisms showed by the dietary peptides mainly depend on the peptide sequence, length, composition, and hydrophobicity [12, 34, 35]. The food-derived antioxidant peptides usually contain 3–15 AA residues [12, 32]. Table 1 shows the AA sequences and molecular mechanisms of antioxidant peptides produced from various dietary proteins.

The Kelch-like ECH-associated protein 1- (*Keap1*-) *Nrf2*-antioxidant response element (ARE) is the main antioxidant signaling pathway that prevents oxidative stress and helps maintain the optimum redox steady state in the body [36]. The *Nrf2* is a vital leucine zipper transcription factor, which controls the expression of several antioxidant proteins in response to ROS stress. Keap1 is a suppressor protein for Nrf2, and under a normal ROS steady state, Keap1 binds with Nrf2 and helps proteasome to degrade the Keap1-Nrf2 complex. However, Nrf2 separates from Keap1 during oxidative stress and migrates to the nucleus where it attaches to ARE and thereby promotes the expression of several antioxidant enzymes/proteins [32, 37, 38]. Endogenous antioxidant enzymes such as SOD, GPx, and CAT scavenge different kinds of ROS and thereby protect the cells from oxidative stress-induced damage. SOD catalyses the transformation of superoxide anion to O₂ and H₂O₂. CAT converts H₂O₂ to H₂O and O₂. GPx helps in the reduction of H₂O₂ to H₂O and O₂ [39]. Hence, it is important to stimulate the Nrf2 antioxidant signaling pathway to suppress/prevent the oxidative stress in the body.

Recently, numerous novel antioxidant peptides that stimulate the *Keap1*-*Nrf2*-ARE antioxidant signaling pathway and antioxidant enzymes have been isolated from different dietary sources such as casein [40], milk protein concentrate [41], corn gluten [31], soybean [42], walnut [43], potato, *Moringa oleifera* seeds [25], watermelon seeds [39], *Crassostrea rivularis* [44], krill [38], turtle [45], *Mytilus coruscus* [46], *Channa argus* [3], and silver carp muscle [12]. Snakehead (*Channa argus*) soup was hydrolyzed using pepsin and pancreatin and identified four antioxidant peptides, IVLPDEGK, PGMLGGSPGLLGGSP, SDGSNIHFPN, and SVSIRADGGEGEVTVFT [3]. The authors performed molecular docking studies for the peptides and indicated that peptides could bind to the active site of Keap1 and thereby activate the cellular antioxidant Keap1-Nrf2 signaling pathway. A peptide RDPEER isolated from alcalase hydrolysate of watermelon seed reduced the oxidative stress by reducing ROS and increasing the antioxidant enzymes, SOD, CAT, and GSH-Px, in HepG2 cells [39]. Four casein-derived peptides, ARHPHPLSFM, AVYPYQR, NPYVPR, and KVLVPVEK, were shown to decrease the oxidative stress in Caco-2 cells by enhancing antioxidant enzymes, namely, SOD1, Trx1, GR, TrxR1, and NQO1, through the activation of the Keap1-Nrf2 signaling mechanism. It was found that the peptides bound to the Nrf2 and prevented the binding between Keap1 and Nrf2 and thereby stimulated the increased expression of antioxidant enzymes [32]. In a study, a peptide, AMVDAIAR, isolated from pepsin hydrolysate of krill enhanced antioxidant enzymes SOD, CAT, and GPx and thereby suppressed the oxidative stress in H₂O₂-induced hepatocytes through increasing the expression of Nrf2 [38].

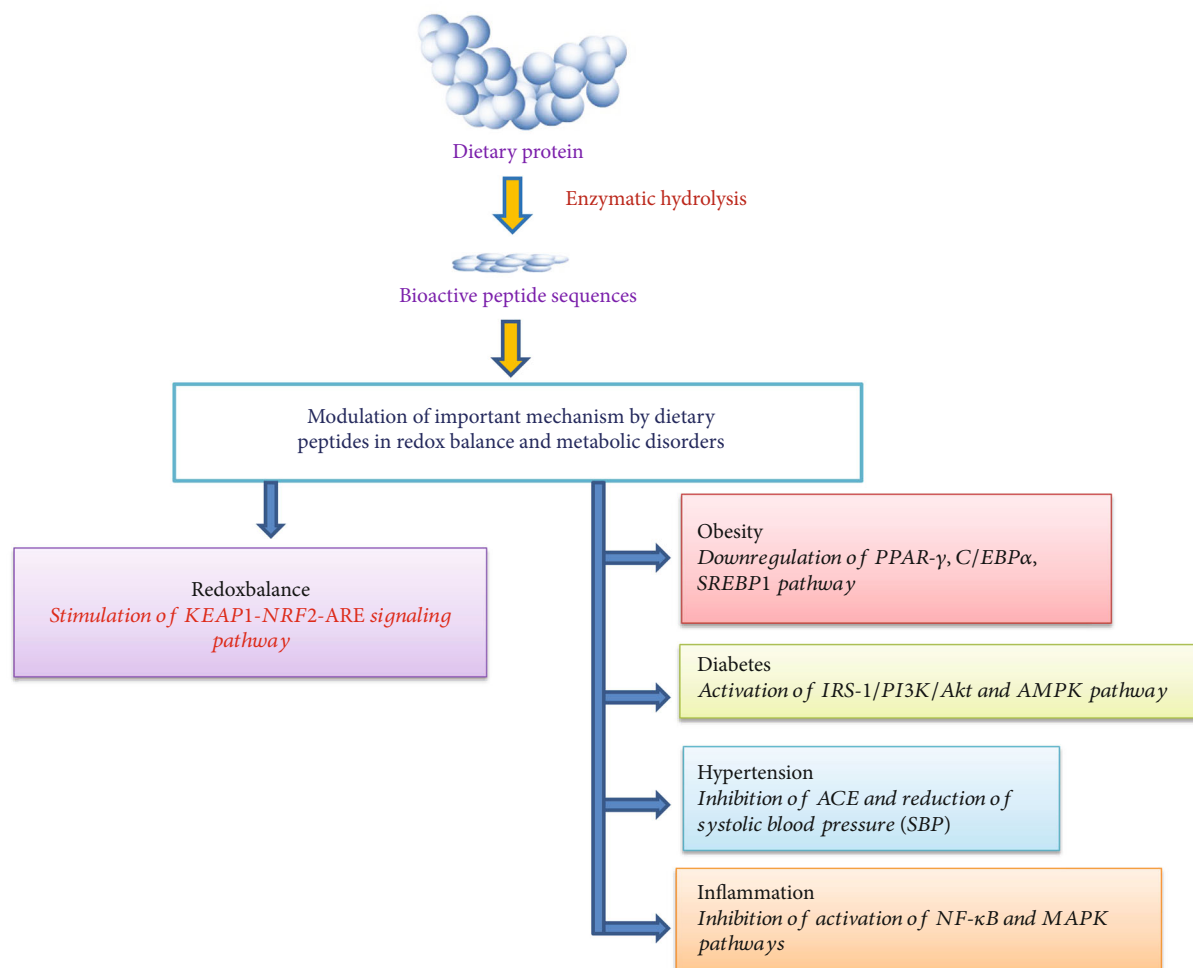


FIGURE 1: Effects of dietary bioactive peptides on molecular mechanisms involved in redox balance and metabolic disorders. ACE: angiotensin-converting enzyme; Akt: protein kinase B; AMPK: AMP-activated protein kinase; ARE: antioxidant response element; C/EBP: CCAAT-enhancer-binding proteins; IRS-1: insulin receptor substrate; PPAR: peroxisome proliferator-activated receptor; Keap1: Kelch-like ECH-associated protein 1; MAPK: mitogen-activated protein kinase; NF- κ B: nuclear factor- κ B; *Nrf2*: nuclear factor erythroid 2-related factor 2; PI3K: phosphatidylinositol 3-kinase; SREBP1: sterol regulatory element-binding protein 1.

Peptide EDYGA derived from soft-shelled turtle enhanced the Nrf2 level through the binding of the glutamate residue of the peptide to Arg 415 of the Kelch receptor pocket [45]. Dipeptide IF identified from potato exhibited antioxidant effects by increasing the antioxidant enzymes GPx 4, SOD1, HO-1, SOD2, and peroxiredoxin 2 in the kidney tissues of the spontaneously hypertensive rats (SHRs) [33]. The authors concluded that the dipeptide showed antioxidative activity through preventing Nrf2 degradation by protein kinase B (Akt) activation and GSK-3 β phosphorylation.

3. Role of Dietary Bioactive Peptides in Obesity

Obesity is a public health issue worldwide and characterized by excessive body fat accumulation due to the difference between energy intake and energy spending, which enhances the risk of metabolic disorders, namely, type 2 diabetes mellitus (T2DM), hypertension, and cardiovascular disorders [47, 48]. It is estimated that globally, 18% men and 21%

women will suffer from obesity by 2025 [49]. Adipocytes are fat cells and the main function of adipocytes is the storage of energy as fat. Preadipocytes differentiate into mature adipocytes through a process known as adipogenesis. Hypertrophy and hyperplasia of adipocytes are two mechanisms that contribute to the obesity and obesity-related metabolic disorders [50, 51].

Several recent studies demonstrated that various dietary peptides from soybean, quinoa, common bean, camel whey, spirulina, blue mussel, skate, tuna, Alaska pollock, sardinella, hazelnut, and kefir exhibited antiobesity effects through modulation of multiple molecular mechanisms including the reduction of adipogenesis through downregulation of the expression of peroxisome proliferator-activated receptor-(PPAR-) γ , CCAAT/enhancer binding protein alpha (C/EBP- α), sterol regulatory element binding protein-(SREBP-) 1, and HMGCR, enhancing lipolysis, reducing body weight (BW) and food intake, inhibiting lipase activity, decreasing the accumulation of triglycerides, and blocking

TABLE 1: Molecular mechanisms of action of dietary peptides in redox balance.

Dietary protein source	Enzyme used to produce peptides	Peptide sequence or molecular weight	Object	IC ₅₀ /EC ₅₀ values	Activity/mechanisms of action	Reference
<i>Ziziphus jujuba</i> fruits	Papain and trypsin	VGQHTR and GWLK	DPPH, ABTS, and metal chelating assays	—	Peptides scavenged ABTS and DPPH and showed strong metal chelating activity	[114]
Corn gluten	Alcalase	<1 kDa and GLLLPH	H ₂ O ₂ -induced HepG2	—	Peptides reduced ROS and increased SOD, CAT activities, and GSH levels and GR activity	[115]
Milk protein concentrate	Trypsin	—	Healthy and diabetic rats	—	Peptides enhanced the activities of CAT, SOD and reduced glutathione, glutathione-S-transferase, and GPx	[41]
<i>Palmaria palmata</i> macroalgal protein	Corolase PP	SDITRPGGNM	ORAC and FRAP assays	—	Peptide showed strong oxygen radical absorbance capacity and ferric-reducing antioxidant power activity	[116]
Rice bran	Trypsin	YSK	DPPH and reducing power assays	DPPH IC ₅₀ 0.15 mg/mL	Peptide exhibited high DPPH free radical scavenging activity and reducing power	[1]
Nile tilapia skin gelatin	Ginger protease	GPA	H ₂ O ₂ -induced IPEC-J2 cell	—	GPA activated the expression of antioxidant response element-driven antioxidant enzyme genes HO-1, NAD(P)H quinone oxidoreductase-1, and glutamyl cysteine ligase modulator and suppressed ROS production	[37]
Manchurian walnut (<i>Juglans mandshurica</i> Maxim.)	Alkaline protease	<3 kDa	Mice	—	Peptides increased the antioxidant capacity by enhancing SOD, GSH-Px, and CAT activities and reducing the MDA content	[43]
Soybean	Alcalase	<3 kDa	H ₂ O ₂ -induced oxidative stress in Caco-2 cell and DPPH assay	DPPH IC ₅₀ 2.56 mg/mL	Peptides displayed DPPH radical scavenging activity and decreased intracellular ROS and stimulated the antioxidant enzymes CAT, GP, and GR	[42]
Oyster (<i>Crassostrea rivularis</i>) meat	Alcalase	<3 kDa	Normal male mice	—	Peptides showed antioxidant capacity by increasing the activities of GSH-Px, SOD, and CAT and reducing MDA levels	[44]
Buffalo casein	—	YFYPQL	H ₂ O ₂ induced Caco-2 cell and ABTS and ORAC assays	—	YFYPQL showed antioxidant and inhibited ROS generation and decreased cellular oxidative products, MDA, and protein carbonyls and increased CAT, SOD, and GPx by stimulating Nrf2	[40]

TABLE 1: Continued.

Dietary protein source	Enzyme used to produce peptides	Peptide sequence or molecular weight	Object	IC ₅₀ /EC ₅₀ values	Activity/mechanisms of action	Reference
Wheat germ protein	Alcalase, pepsin, and proteinase K	TVGGAPAGRIVME, VGGIDEVIK, GNPIPREPGQVPAY, SGGSYAD ELVSTAK, and MDATAALHYENQK	ABTS assay	—	stress signaling and scavenged ABTS and ORAC free radicals Peptides exhibited strong ABTS radical scavenging activity	[117]
Carp (<i>Cyprinus carpio</i>) skin gelatin	Protamex	—	Healthy adult Wistar rats	—	Peptides showed antioxidant activity by increasing the glutathione reductase activity	[118]
Sesame (-icum L.) seed protein	Alcalase and trypsin	RDRHQKIG, TDRHQKLR, MNDRVNQGE, RENIDKPSRA, SYPTECRM, GGVPRSGEQEQQ, and AGEQGFYVTFR	DPPH and ABTS assays	DPPH IC ₅₀ 0.105 and ABTS IC ₅₀ 0.004 mg/mL	SYPTECRM exhibited the highest DPPH and ABTS free radical scavenging antioxidant activity	[34]
Finger millet	Trypsin	STTVGLGISMRSASVR and TSSSLNMAVRGGLTR	DPPH assay	DPPH 75–80%	Peptides exhibited DPPH and ABTS radical scavenging activities by interaction of serine and threonine residues of peptides with free radicals Peptides increased the antioxidant enzymes HO-1, GPx, SOD, and peroxiredoxin 2 through the Akt pathway to regulate Nrf2 activity and prevented Nrf2 degradation by Akt activation and GSK-3 β phosphorylation	[119]
Potato	—	Dipeptide IF	SHR rats	—	Peptides reduced the accumulation of ROS and MDA production and increased the levels of the SOD, CAT, and GSH-Px cellular antioxidant capacities through regulating the Nrf2-driven antioxidant defense mechanisms. Peptides showed strong OH, O ₂ radical scavenging activities and ferric-reducing power	[33]
<i>Mytilus Coruscus</i> mussel	Trypsin	<1 kDa	H ₂ O ₂ -induced HUVEC and OH, O ₂ , and ferric-reducing assays	—	Peptide showed strong DPPH radical scavenging activity with 36% inhibition	[46]
Mackerel (<i>Scomber japonicus</i>) muscle	Protamex	ALSTWTLQLGSTSFSASPM	DPPH assay	DPPH 36.34%	EDYGA modulated the Nrf2/ARE pathway by enhancing the Nrf2 level via Nrf2 stabilization and decreasing the level of	[120]
Soft-shelled turtle	Neutrase, papain, proteinase, pepsin, and trypsin	EDYGA	HepG2 cells	—		[45]

TABLE 1: Continued.

Dietary protein source	Enzyme used to produce peptides	Peptide sequence or molecular weight	Object	IC ₅₀ /EC ₅₀ values	Activity/mechanisms of action	Reference
Foxtail millet (<i>Setaria italica</i>) prolamins	Alcalase	PFLF and IALLIPF	H ₂ O ₂ -induced human keratinocyte HaCaT cells	—	Keap1 and glutamate residues of EDYGA bound to the Arg 415 of Kelch domain receptor pocket. Peptides decreased the production of ROS and MDA and enhanced the GSH level.	[121]
Krill	Pepsin	AMVDAIAR	H ₂ O ₂ -stimulated hepatocytes	DPPH IC ₅₀ 0.87 mM	Peptide reduced oxidative stress by enhancing SOD, CAT, and GPx. Peptide increased Nrf2 and HO-1 expression and activated Nrf2/HO-1 by activating the ERK pathway.	[38]
Watermelon seed protein	Alcalase	RDPEER	H ₂ O ₂ -induced oxidative stress in HepG2 cells	—	RDPEER reduced the oxidative stress by increasing CAT, SOD, and GSH-Px, and reducing MDA production and ROS accumulation.	[39]
Scallop (<i>Patinopecten yessoensis</i>) shellfish	Pepsin, dispase, and alcalase	<3 kDa	DPPH, HO*, and ABTS assays and H ₂ O ₂ -induced PC-12 cells	DPPH EC ₅₀ 1.30–2.40, ABTS EC ₅₀ 0.75–1.98, and OH EC ₅₀ 1.07–1.43 mg/mL	Peptides scavenged the free radicals of DPPH, HO*, ABTS, and inhibited ROS accumulation.	[122]
Milk casein	—	ARHPPHLSFM, AVPYPQR, NPYVPR, and KVLVPVEK	Peroxide-induced oxidative stress Caco-2 cells	—	Peptides enhanced the expression of SOD1, Trx1, TrxR1, GR, and NQO1 by activating the Keap1-Nrf2 pathway. Peptides inhibited the interaction between Keap1 and Nrf2, by binding to Nrf2 in the Keap1 pocket and increased antioxidant enzyme expression.	[32]
Corn gluten meal	Fermentation mice with <i>Bacillus subtilis</i> MTCC5480 (BS5480)	<10 kDa	Aging rats	—	Peptides increased activities of total SOD, CAT, GPx, and total antioxidant capacity and decreased MDA.	[31]
<i>Moringa oleifera</i> seeds	Flavor protease	GY, PFE, YTR, FG, QY, IN, SF, SP, YFE, IY, and LY	H ₂ O ₂ induced oxidative damage in Chang liver cells and DPPH and ABTS assays	DPPH EC ₅₀ 0.75–2.28 mg/mL and ABTS EC ₅₀ 0.32–1.03 mg/mL	Peptides exhibited strong scavenging activities on free radicals DPPH and ABTS*. SF and QY scavenged ROS by increasing SOD and CAT and reducing MDA.	[25]
Ginger	Pepsin and trypsin	VTYM	DPPH and ABTS assays	EC ₅₀ of DPPH 19.9 ± 2.1 and ABTS 24.0 ± 3.7 μmol/L	VTYM showed potent DPPH and ABTS radical scavenging activity.	[9]

[3]

TABLE 1: Continued.

Dietary protein source	Enzyme used to produce peptides	Peptide sequence or molecular weight	Object	IC ₅₀ /EC ₅₀ values	Activity/mechanisms of action	Reference
Snakehead (<i>Channa argus</i>) soup	Pepsin and pancreatin	IVLPDEGK, PGMLGGSPPLLGGSP, SDGSNIHFNP, and SVSIRADGGEGEVTVFT	DPPH and Fe ²⁺ chelating assays and H ₂ O ₂ induced HepG2 cells	DPPH IC ₅₀ 1.39 mM and Fe ²⁺ chelating ability IC ₅₀ 4.60 mM	Peptides exhibited strong DPPH and Fe ²⁺ chelating ability and molecular docking indicated that peptides can bind to the active site of Keap1 and thereby activate the cellular antioxidation Keap1-Nrf2 pathway	
Silver carp muscle	Papain and alcalase	<1 kDa and LVPVAVF	H ₂ O ₂ induced oxidative stress Caco-2 cells and DPPH assay	DPPH EC ₅₀ 0.65 mg/mL	Peptides showed antioxidant activity by enhancing the activity of SOD, CAT, and GSH-Px and reduced ROS and showed strong DPPH scavenging activity	[12]

ARE: antioxidant response element; ATBS: 2,2'-azino-bis (3-ethylbenzothiazoline-6 sulphonic acid) diammonium salt; Akt: protein kinase B; CAT: catalase; DPPH: 2,2-diphenyl-1-picrylhydrazyl; ERK: extracellular signal-regulated kinases; FRAP: ferric reducing antioxidant power; GPx: glutathione peroxidase; GSH: glutathione; GR: glutathione reductase; H₂O₂: hydrogen peroxide; HO-1: heme oxygenase 1; IC₅₀: 50% inhibitory concentration; ROS: reactive oxygen species; SHR: spontaneously hypertensive rats; SOD: superoxide dismutase; MDA: malondialdehyde; NQO1: NAD(P)H quinone dehydrogenase 1; Nrf2: nuclear factor erythroid 2-related factor; HUVEC: human umbilical vein endothelial cells; Keap 1: Kelch-like ECH-associated protein 1; HO: heme oxygenase; Trx1: thioredoxin 1; TrxR1: thioredoxin reductase 1; ORAC: oxygen radical absorbance capacity.

lipogenesis by reducing the fatty acid synthase [2, 10, 52, 53]. Various molecular mechanisms of antiobesity peptides are shown in Table 2.

During maturation of preadipocytes into adipocytes, several transcriptional factors are involved. PPAR and C/EBP are two transcription factors that stimulate adipocyte differentiation [50]. Lipid and carbohydrate metabolism is regulated by the PPARs. SREBP1 is a lipogenic transcription factor upon activation by PPAR- γ which promotes the adipogenesis and lipogenesis. SREBP1 stimulates lipoprotein lipase and fatty acid synthase and thereby enhances the lipid accumulation in the adipocytes [50]. Therefore, inhibition of the PPARs, C/EBP, and SREBP1 transcriptional factors involved the adipogenesis and lipogenesis using dietary-derived BPs is an efficient approach in the prevention or treatment of obesity and related diseases. It has been revealed that numerous dietary peptides from soy bean, quinoa, hazelnut, canola, tuna, ark shell, and blue mussel showed antiobesity activities by inhibiting the expression of PPAR- γ , C/EBP, and SREBP1 transcriptional factors [10, 51, 54].

It was found that the antiobesity effects of dietary BPs are related to the peptide sequence, length, composition, and protein source [13]. Peptides with < 1 kDa from blue mussel by pepsin hydrolysis exhibited antiobesity effects by enhancing lipolysis and downregulating adipogenic transcription factors, such as PPAR- γ , C/EBP- α , and SREBP1 [10]. An antiobesity pentapeptide RLLPH was isolated from alcalase hydrolysate of hazelnut (*Corylus heterophylla* Fisch) and found that the pentapeptide could decrease adipogenesis through reducing the expression of PPAR- γ , C/EBP- α , SREBP-1c, adipocyte protein (aP2), FAS, acetyl-CoA carboxylase 1 (ACC1), and HMGR in 3T3-L1 adipocytes [13].

Additionally, the authors indicated that the hydrophobic AAs, proline, and leucine, of the peptide, might have contributed to the antiobesity effects of the peptides. Peptides with more hydrophobic AAs can easily penetrate the cell membrane and increase lipid solubility. In a study, peptides < 1 kDa from ark shell (*Scapharca subcrenata*) protein inhibited intracellular lipid buildup and enhanced the lipolysis [51]. The authors were also demonstrated that ark shell peptides inhibited adipogenesis by decreasing the expressions of PPAR- γ , C/EBP- α , SREBP-1c, lipoprotein lipase, and FAS in mouse mesenchymal stem cells. Moreover, the expression of PPAR- γ , C/EBP- α , and aP2 was decreased by tuna skin collagen-derived peptides in obese mice, which resulted in the decrease of adipocyte size [55].

In addition to the downregulation of vital transcriptional factors (PPAR- γ , C/EBP- α , and SREBP-1c) of adipogenesis, several *in vivo* studies demonstrated that the antiobesity activity of dietary peptides is due to the decrease of BW and food consumption. Oral administration of peptides (10 mg/mL), produced from smooth hound (*Mustelus mustelus*) muscle by alkaline crude enzyme from *M. mustelus* intestines, for 21 days reduced the BW and food intake in rats [5]. The authors suggested that BW reduction was probably due to the regulation of appetite. The antiobesity effect of Alaska pollack-derived peptides was investigated, and it was found that peptide administration (100 or 300 mg/kg BW) to rats for 3 days decreased the weight of white adipose tissue and reduced the food intake [56]. The authors suggested that the decrease in food intake and white adipose tissue weight of rats after peptide treatment was due to downregulation/suppression of gene expressions of *neuropeptide-Y* and agouti-related peptide in hypothalamus, which may reduce the

TABLE 2: Mechanisms of action of antiobesity peptides derived from various food sources.

Dietary protein source	Enzyme used to produce peptides	Peptide sequence or molecular weight	Object	Dose & duration	Activity/mechanisms of action	Reference
Soy protein	Flavourzyme	<1300 Da	3T3-L1 preadipocytes	100 ppm for 8 d	Peptides reduced GPDH activity and inhibited adipogenesis by affecting the expression of PPAR- γ and CCAAT/enhancer binding protein- α	[123]
Smooth hound (<i>Mustelus mustelus</i>) muscle protein	Alkaline crude enzymes from <i>M. mustelus</i> intestines	200–2500 Da	Rats	0.5 mL (10 mg/mL)/day/kg BW for 21 d	Peptides reduced BW and food intake	[5]
Soy protein	Flavourzyme	ILL, LLL, and VHVV	3T3-L1 adipocytes	4 ppm for 72 h	Peptides exhibited lipolysis-stimulating activity	[52]
Canola protein	Alcalase, chymotrypsin, pepsin trypsin, and pancreatin	<1–10 kDa	C3H10T1/2 murine mesenchymal stem cells	60–100 μ g/mL for 24 h	Peptides showed antiobesity effects by inhibiting PPAR γ expression and pancreatic lipase	[54]
Common bean	Alcalase, bromelain, and pepsin-pancreatin	<1 kDa	Mature adipocytes 3T3-L1	0.1, 1, 10, and 100 μ g/mL for 48 h	Peptides inhibited lipid accumulation (28%)	[53]
Salmon protein	—	—	Placebo-controlled, randomized clinical study	16 g for 42 days	Peptide supplementation for 42 days reduced the body mass index by 5.6% in overweight subjects	[59]
Ark shell (<i>Scapharca subcrenata</i>) protein	Pepsin	<1 kDa	Mouse mesenchymal stem cells	400 μ g/mL for 7 d	Peptides inhibited intracellular lipid accumulation and enhanced lipolysis. Peptides inhibited adipogenesis by downregulating the adipocyte-specific protein expression including PPAR- γ , C/EBP- α , SREBP-1c, downstream lipoprotein lipase, and FAS expression	[51]
Yellow catfish protein	Alcalase	—	HFD fed mice	500, 250 and 125 mg/kg BW for 84 d	Peptides exhibited anti-obesity effects	[124]
Sardinella (<i>Sardinella aurita</i>) protein	<i>Bacillus subtilis</i> A26 and <i>Bacillus amyloliquefaciens</i> An6	150–900 Da	Wistar rats fed high caloric diet	400 mg/kg BW for 10 weeks	Peptides reduced BW gain, food intake, and the relative epididymal adipose tissue and decreased the pancreatic lipase activity	[2]
Alaska pollack protein	Pepsin and pancreatin	—	Rats	0, 100, and 300 mg/kg BW for 3 d	Peptides reduced white adipose tissue weight and food intake	[56]
Tuna skin	Subcritical water hydrolysis	—	3T3-L1 preadipocytes	300 mg/kg/day for 8 weeks		[55]

TABLE 2: Continued.

Dietary protein source	Enzyme used to produce peptides	Peptide sequence or molecular weight	Object	Dose & duration	Activity/mechanisms of action	Reference
Camel whey protein	Pepsin, trypsin, and chymotrypsin	<10 kDa	and obese mice fed HFD In vitro assays	50 μ L for 30 min	Peptides decreased HFD-induced BW gain and inhibited the expression of C/EBP- α , PPAR- γ and adipocyte protein 2 Peptides exhibited antiobesity effects by inhibiting pancreatic lipase and cholesteryl esterase enzymes	[125]
Skate (<i>Raja kenoyei</i>) skin collagen	—	1050 Da	HFD-fed mice	100, 200, or 300 mg/kg BW for 8 weeks	Peptides showed antiobesity effects by reducing BW gain and visceral adipose tissue and improved the dyslipidemia via regulating hepatic lipid metabolism and AMPK	[126]
Camel milk	Alcalase, bromelain, and papain	<10 kDa	In vitro	—	Peptides inhibited the porcine pancreatic lipase	[24]
Kefir	—	>30 kDa, 3–30 kDa, and <3 kDa	HFD-induced obese rats	164 mg/kg BW daily for 8 weeks	Peptides blocked lipogenesis by reducing FAS and increased p-acetyl-CoA carboxylase. Peptides enhanced FA oxidation via increasing the expressions of phosphorylated AMPK, PPAR- α , and hepatic carnitine palmitoyltransferase-1	[127]
<i>Spirulina platensis</i> protein	Trypsin, alcalase, pepsin, papain, and protamex	NALKCCHSCPA, LNNPSVCD CDCMMKAAR, NPVWKRK, and CANPHELPNK	3T3-L1 preadipocytes	1 mg/mL for 48 h	Peptides exhibited antiobesity effects by inhibiting lipase (72%) and 3T3-L1 preadipocytes (72.7–88.1%) and decreased triglyceride accumulation	[8]
Quinoa protein	Papain, pepsin, and pancreatin	FGVSEDIAEKIQAKQDERGNIVL, AEGGLTEVWDTQDQF, YIEQNGISGLMIPG, AVVKQAGEGFEW, and HGSDGNVF	3T3-L1 cells	0–1600 μ g/mL for 48 h	Peptides inhibited lipid accumulation during differentiation and suppressed cell differentiation through PPAR- γ	[128]
<i>Spirulina platensis</i> protein	Pepsin	<10 kDa	HFD-fed mice	2 g/kg BW/d for 4 weeks	Peptides showed antiobesity effects reducing BW, lowering serum glucose, and total cholesterol through modulation of expressions of Acadm, Retn, Fabp4, Ppard, and Slc27a1 in the brain and liver	[57]
Pea (<i>Pisum sativum</i> L.) seed proteins	Pepsin and pancreatin	<6 kDa	3T3-L1 murine preadipocytes	0, 1, 2, 4, and 6 mg/mL for 24 h	Peptides stimulated adipocyte differentiation through upregulation of PPAR- γ expression and ligand activity	[48]
Walleye pollock skin collagen	Flavourzyme and alcalase	500–5000 Da	HFD-fed C57BL/6 mice	800 mg/kg BW for 8 weeks	Peptides inhibited weight gain, adipocyte growth, adipose tissue accumulation, and liver weight and reduced the blood-lipid level	[58]
Blue mussel	Pepsin	<1 kDa	Mouse mesenchymal stem cells	100, 200, and 400 μ g/mL for 7 or 21 d	Peptides enhanced lipolysis and downregulated adipogenic transcription factors including PPAR γ , CCAAT/enhancer-binding protein- α , and SREBP-1	[10]

TABLE 2: Continued.

Dietary protein source	Enzyme used to produce peptides	Peptide sequence or molecular weight	Object	Dose & duration	Activity/mechanisms of action	Reference
Hazelnut (<i>Corylus heterophylla</i> Fisch) protein	Alcalase	Arg-Leu-Leu-Pro-His	3T3-L1 adipocytes	0, 20, 40, and 80 mM for 8 d	Peptides decreased adipogenesis by downregulating the expression of PPAR- γ , C/EBP- α , aP2, SREBP-1c, FAS, ACC1, and 3-hydroxy-3-methylglutaryl-CoA reductase	[13]
Milk β -casein	Trypsin	7 kDa	HepG2 cells and humans	5 mg/mL for 24 h	Casein oligopeptide increased FGF-21	[129]

ACC1: acetyl-CoA carboxylase 1; AMPK: AMP-activated protein kinase; aP2: adipocyte fatty acid-binding protein 2; BW: body weight; C/EBP- α : CCAAT/enhancer binding protein alpha; FAS: fatty acid synthase; FGFs: fibroblast growth factors; HFD: high-fat diet; PPAR- γ : peroxisome proliferator-activated receptor- γ ; SREBP-1: sterol regulatory element-binding protein 1.

appetite. In a study, it was found that antiobesity effects of sardinella- (*Sardinella aurita*-) derived peptides were mediated by reducing the BW gain, food intake, and the relative epididymal adipose tissue weight in Wistar rats after 10 weeks of peptide treatment [2]. It was demonstrated that *Spirulina platensis*-derived peptides exhibited antiobesity effects by reducing BW (39.8%) and lowering serum glucose (23.8%) through altering the gene expressions of Acadm, Retn, Fabp4, Ppard, and Slc27a1 in the brain and liver of mice fed with peptides (2 g/kg BW) for 4 weeks [57]. Recently, it was reported that walleye pollock skin collagen-derived peptides considerably reduced the BW gain in obese mice after 8 weeks of peptide treatment [58]. The authors also pointed that peptides inhibited the growth of adipocytes and the accumulation of adipose tissue in obese mice. Furthermore, in a placebo-controlled, randomized clinical investigation, salmon fish-derived peptide supplementation (16 g/d) for 42 days notably decreased (5.6%) the BMI in obese humans [59].

Pancreatic lipase is an important enzyme that aids in the hydrolysis of dietary fat in the small intestine. Therefore, inhibition of pancreatic lipase is an efficient approach in the management and treatment of being overweight and obesity [2, 24]. Apart from inhibition of adipogenesis and lipogenesis, some dietary peptides exhibited pancreatic lipase inhibitory activity. Peptides produced from camel milk by using alcalase-, bromelin-, and papain-inhibited porcine pancreatic lipase [24]. It was also found that sardinella peptide administration to rats for 10 weeks decreased the pancreatic lipase activity [2].

4. The Role of Dietary Bioactive Peptides in Diabetes Mellitus

Diabetes mellitus (DM) is a complex metabolic disorder with increased blood sugar levels and T2DM accounts for 90% of diabetes patients. T2DM results from insulin resistance (cells less responsive to the insulin actions) and/or insufficient insulin production from pancreatic beta cells. Obesity (BMI ≥ 30 kg/m²) has been reported to greatly increase the risk of developing T2DM [60]. Uncontrolled T2DM can cause severe complications such as high blood pressure, stroke, heart attack, atherosclerosis, retinopathy, nephropathy, neuropathy, and dementia.

Recently, several peptides derived from a variety of dietary protein sources including egg white, whey, casein, egg yolk, rice bran, quinoa, soybean, wheat, corn, black bean, oat globulin, walnut, potato, common bean, millets, spirulina, bovine, porcine, Atlantic cod, Atlantic salmon, halibut skin, *Styela clava*, boarfish, tilapia skin, largemouth bass, zebra blenny, blue whiting, and sea cucumber have shown antidiabetic effects by altering several molecular mechanisms of diabetes such as inhibition of enzymes including α -amylase, dipeptidyl peptidase- (DPP-) IV, and α -glucosidase; reduction of FBG and HbA1C; enhancement of HOMA-IR; stimulation of secretion of glucagon-like polypeptide-1 (GLP-1) and insulin levels; upregulation of phosphatidylinositol 3-kinase (PI3K), p-GSK-3 β , p-Akt, and glucose transporter (GLUT)2/4 signaling pathways; blocking of

glucose transporters GLUT2 and SGLT1; decreasing of the activation of p38 and c-Jun N-terminal kinase (JNK)1/2; enhancement of the stimulation of insulin receptor substrate-1 (IRS-1) tyrosine residue and Akt; and decreasing of gluconeogenesis through activation of IRS-1/PI3K/Akt and AMP-activated protein kinase (AMPK) [6, 21, 61–64]. The isolated peptide sequences and molecular mechanisms of dietary antidiabetic peptides are shown in Table 3.

α -Amylase is an important enzyme in the carbohydrate digestion that breaks down α -1,4 glycosidic linkages of starch and produces oligosaccharides. α -Glucosidase is present in the brush borders of the small intestine and hydrolyzes the disaccharides and starch to glucose by acting upon $\alpha(1 \rightarrow 4)$ glycosidic bonds. Therefore, inhibition of α -amylase and α -glucosidase prevents carbohydrate digestion and thus diminishes the postprandial increase of blood glucose. Several chemical α -glucosidase and α -amylase inhibitors (acarbose, voglibose, and miglitol) have been in use for the management and treatment of T2DM [65]. However, side effects associated with these inhibitors limited their use [63]. Recently, many peptides isolated from several food sources including egg white, corn, oat, egg yolk, spirulina, quinoa, soybean, *Phaseolus vulgaris*, and zebra blenny have exhibited α -amylase and α -glucosidase inhibitory activities [61, 62, 66, 67]. Egg white albumin was hydrolyzed using alcalase, and a pentapeptide KLPGF was isolated with α -glucosidase (50% inhibitory concentration (IC₅₀) 59.5 μ mol/L) and α -amylase (IC₅₀ 120 μ M) inhibitory activities [66]. Three peptides, GVPMPNK, LRSELAAWSR, and RNPVFAPTLLTVAAR, were extracted from spirulina platensis, and it was found that peptide LRSELAAWSR strongly inhibited α -amylase with IC₅₀ of 313.6 μ g/mL and α -glucosidase with IC₅₀ of 134.2 μ g/mL [68]. A α -glucosidase inhibitory peptide, LAPSLPGKPKPD, was identified from egg yolk hydrolysate produced by proteinase from Asian pumpkin with an IC₅₀ value of 1065.6 μ mol/L [67]. Three peptides, LLPLPVL, SWLRL, and WLRL, produced from soy protein showed α -glucosidase inhibitory activity with IC₅₀ 162.2–237.4 μ mol/L [63]. A study reported isolation of α -glucosidase inhibitory peptide, QHPHGLGALCAAPPST, from quinoa with an IC₅₀ of 1.0–1.45 mg/mL [62]. Recently, corn germ protein was hydrolyzed by using alcalase, trypsin, and flavourzyme and it was found that the peptide fraction (2–10 kDa) showed strong α -amylase inhibition (71.3%) and α -glucosidase inhibition (37.1%) activities [61].

Another strategy for the management and treatment of T2DM is to inhibit the DPP-IV that degrades and inactivates incretin hormones, namely, glucose-dependent insulinotropic peptide (GIP) and GLP-1. Therefore, inhibition of DPP-IV by dietary-derived BPs can enhance the half-life of GLP-1 and thereby increase the release of glucose-dependent insulin from pancreatic cells [61]. For inhibition of DPP-IV activity, several synthetic drugs such as saxagliptin, linagliptin, sitagliptin, and vildagliptin are presently used. However, side effects (diarrhea, nausea, stomach pain, headache, and sore throat) associated with these drugs have forced researchers to search for DPP-IV inhibitors from natural dietary sources without any side effects [69]. Many recent studies have reported that dietary protein-derived peptides are an

TABLE 3: Molecular mechanisms of action of antidiabetic peptides isolated from various dietary sources.

Dietary protein source	Enzyme used to produce peptides	Peptide sequence or molecular weight	Object	IC ₅₀ /EC ₅₀ values	Activity/mechanisms of action	Reference
Rice bran	Umamizyme G and bioprase SP	Dipeptides LP and IP	DPP-IV inhibition assay	DPP-IV IC ₅₀ 2.3 ± 0.1 mg/mL	Peptides showed strong DPP-IV inhibition activity	[130]
Egg white albumin	Alcalase	KLPGF	α-Glucosidase and α-amylase inhibitory assays	α-Glucosidase inhibitory IC ₅₀ 59.5 ± 5.7 μM and α-amylase inhibitory IC ₅₀ 120 μM	KLPGF exhibited strong antidiabetic potential by inhibiting α-glucosidase and α-amylase activities	[66]
Casein	Prolyl oligopeptidase	FLQP	DPP-IV inhibition assay	DPP-IV IC ₅₀ 65.3 ± 3.5 μM	FLQP exhibited DPP-IV inhibition activity	[70]
Bovine and porcine meat proteins	Papain and porcine pepsin	PPL	DPP-IV inhibition assay	DPP-IV IC ₅₀ 390.14 μM	Peptides showed DPP-IV inhibition	[131]
Porcine skin	Alcalase and flavourzyme	—	Streptozotocin-induced diabetic rats	—	Peptides improved glucose tolerance and inhibited DPP-IV activity and enhanced GLP-1 and the insulin level	[132]
Egg yolk	Proteinase from Asian pumpkin	LAPSLPGKPKPD	DPP-IV and α-glucosidase assays	DPP-IV IC ₅₀ 361.5 μmol/L and α-glucosidase IC ₅₀ 1065.6 μmol/L	Peptides showed DPP-IV and α-glucosidase inhibitory activities	[67]
Halibut and tilapia skin gelatin	Flavourzyme	SPGSSGPQQFTG, GPVG PANGPANGLN, PPPTGPRGQPNIGF, IPGDPGPPGPPGP, LPGERGRPGAPGP, and GPKGDRGLPGPPGRDGM	Streptozotocin-induced diabetic rats	—	Peptides improved glucose tolerance through DPP-IV inhibition and GLP-1 secretion enhancement	[73]
<i>Styela clava</i>	Protamex	—	Patients with diabetes	—	Peptides exhibited a decreased hemoglobin A1c and plasma insulin levels	[78]
Black bean	Alcalase	AKSPLF, LSKSVL, FEELN, and PHL	Caco-2 cell and rats	—	Peptides showed antidiabetic effects by blocking GLUT2 and SGLT1 and reduced glucose absorption and postprandial glucose and blood glucose	[133]
Wheat	Bacterial protease	770-77740 Da	GLUTag cells and rats	—	Peptides improved hyperglycemia via activating GLP-1 secretion via stimulation of the calmodulin-dependent kinase II pathway mediated by G protein-coupled receptor family C group 6 subtype A	[134]
Atlantic cod (<i>Gadus morhua</i>) meat	Protamex	<2000 Da	41 healthy individuals	—	Peptides decreased the postprandial insulin	[77]

TABLE 3: Continued.

Dietary protein source	Enzyme used to produce peptides	Peptide sequence or molecular weight	Object	IC ₅₀ /EC ₅₀ values	Activity/mechanisms of action	Reference
Oat globulin	Trypsin	OGb, IQAFEPLR, and EFLLAGNNK	Caco-2 cell	DPP-IV IC ₅₀ OGb 188.1 μ g/mL and IQAFEPLR IC ₅₀ 141.7 μ M	Peptides showed potent inhibition on DPP4 and α -glucosidase activity and reduced DPP4 protein expression and upregulated the expressions of α -glucosidase, GLUT2, and GLUT5	[135]
Milk whey protein	Protease	<5000 Da	21 prediabetic humans	—	Peptides (1400 or 2800 mg/kg BW) decreased under glucose curve and showed a minor insulinotropic and reduced HbA1c	[76]
Egg white	Thermolysin and pepsin	IRW	TNF- α -treated L6 rat skeletal muscle cells	—	IRW reduced glucose uptake and enhanced insulin receptor activation and improved insulin sensitivity by inhibiting p38 and JNK1/2 activation	[23]
Boarfish (<i>Capros aper</i>) protein	Alcalase and flavourzyme	<2 kDa	BRIN-BD11 and GLUTag cells and mice	Dpp-IV inhibitory activity IC ₅₀ 1.18 mg/mL	Peptides increased insulin secretion and inhibited DPP-IV activity. Peptides increased insulin levels and reduced glucose concentration	[72]
Blue whiting (<i>Micromesistius poutassou</i>) muscle protein	Alcalase and flavourzyme	<5 kDa	GLUTag cells, BRIN-BD11 cells, 3T3-L1 adipocytes, DPP-IV assay, and mice	DPP-IV inhibitory activity IC ₅₀ 1.28 \pm 0.04 mg/mL	Peptides showed being antidiabetic via DPP-IV inhibitory activity, increasing insulin-stimulated glucose, stimulating insulin secretion and GLP-1, and decreasing glucose	[71]
Potato protein	Alcalase	DIKTNKPVI	Diabetic mice	—	Peptides showed antidiabetic effects via regulation of blood glucose, plasma total glycerol, total cholesterol, insulin, and HbA1c	[6]
Spirulina platensis	—	GYPMPNK, RNPVFAPITLLTVAAR, and LRSELAAWSR	α -Amylase, α -glucosidase, and DPP-IV assay	α -Amylase IC ₅₀ 313.6 μ g/mL, α -glucosidase IC ₅₀ 134.2 μ g/mL, and DPP-IV IC ₅₀ 167.3 μ g/mL	LRSELAAWSR exhibited strong inhibitory activity on α -amylase, α -glucosidase, and DPP-IV	[68]
Beans (<i>Phaseolus vulgaris</i> L.)	Pepsin and pancreaticin	<3 kDa	Wistar rats and mice and in vitro assays	α -Amylase 16.9–89.1% and α -glucosidase inhibition 34.4–89.2%	Fractions inhibited α -amylase and α -glucosidase. Fractions showed both hypoglycemic and antihyperglycemic activities	[136]
Soy protein	Papain, trypsin, and alkaline proteinase	LLPLPVL, SWLRL, and WLRL	α -Glucosidase inhibitory assay	α -Glucosidase IC ₅₀ 162.2–237.4 μ mol/L	Peptides showed strong α -glucosidase inhibitory activity	[63]
Sea cucumber (<i>Holothuria nobilis</i>)	Mixture of papain and protamex	203–1907 Da	Type II diabetic rats induced by streptozotocin	—	Peptides (200 and 400 mg/kg BW) decreased fasting blood glucose. Peptides showed antidiabetic effects by increasing the expressions of PI3K, p-Akt, p-GSK-3 β , and GLUT2/4 signaling pathways and decreasing the expression of p-IRS1	[73]

TABLE 3: Continued.

Dietary protein source	Enzyme used to produce peptides	Peptide sequence or molecular weight	Object	IC ₅₀ /EC ₅₀ values	Activity/mechanisms of action	Reference
Largemouth bass (<i>Micropterus salmoides</i>)	Pepsin, trypsin, and chymotrypsin	ICY	DPP-IV inhibitory assay	DPP-IV IC ₅₀ 0.73 mM	ICY had strong DPP4 inhibitory activities	[137]
Zebra blenny (<i>Salaria basilisca</i>) protein	Crude alkaline protease extract from zebra blenny	>30 kDa	DPP-IV inhibitory assay	DPP-IV IC ₅₀ 71 µg/mL	Fraction showed α-amylase inhibitory activity	[64]
Walnut (<i>Juglans mandshurica</i> Maxim)	Alcalase	LPLLR	Hepatic HepG2 cells and in vitro assays	Inhibiting α-glucosidase 50.12% and α-amylase 39.08% at 2000 µM	LPLLR inhibited α-glucosidase and α-amylase and improved hepatic insulin resistance via enhancing glycogen synthesis and glucose uptake and reduced gluconeogenesis via activating the IRS-1/PI3K/Akt and AMPK pathways	[75]
Quinoa protein	Bromelain, chymotrypsin, and Pronase E	QHPHGLGALCAAPPST	α-Glucosidase and DPP-IV inhibitory assays	DPP-IV IC ₅₀ 0.72–1.12 mg/mL and α-glucosidase IC ₅₀ 1.0–1.45 mg/mL	Peptides showed antidiabetic effects by inhibiting DPP-IV and α-glucosidase	[62]
Corn germ protein	Alcalase, trypsin, and flavourzyme	<2–10 kDa	In vitro assays	Inhibiting α-amylase 71.3%, α-glucosidase 37.1%, and DPP-IV 45.9%	Peptides showed strong α-amylase, α-glucosidase, and DPP-IV inhibition	[61]
Sea cucumber (<i>Stichopus japonicus</i>)	Pepsin, trypsin, and chymotrypsin	<3 kDa	3T3-L1 and Hep G2 cells	DPP-IV IC ₅₀ 0.51–0.52 mg/mL	Peptides improved glucose uptake and DPP-IV inhibitory activity	[7]
α-Lactalbumin-rich whey proteins	Trypsin	LDQWLCEKL	DPP-IV inhibitory activity	DPP-IV inhibition IC ₅₀ 131 µM	LDQWLCEKL exhibited DPP-IV inhibition with a noncompetition	[138]
<i>Palmaria palmata</i>	Alcalase and flavourzyme	<1–5 kDa	Streptozotocin-induced diabetic mice	—	Peptides showed antidiabetic effects by reducing blood glucose and increasing insulin and improved terminal oral glucose tolerance and fasting blood glucose	[139]
Atlantic salmon (<i>Salmo salar</i>) skin	Trypsin	LDKVFR	DPP-IV inhibitory activity assay	DPP-IV inhibition IC ₅₀ 128.7 µM	LDKVFR showed DPP-IV inhibition	[14]
Millet proteins	Papain	NDWHTGPLS and TYPHQQPPILT	DPP-IV inhibition assay	DPP-IV inhibition 75.72%	Peptides inhibited DPP-IV and occupied DPP-IV active center (S1 and S2 subsites) via H-bond and π – π	[21]

Akt: protein kinase B; AMPK: AMP-activated protein kinase; DPP-IV: dipeptidyl peptidase-IV; GLP-1: glucagon-like peptide-1; GLUT: glucose transporter; HbA1c: glycosylated hemoglobin; IC₅₀: 50% inhibitory concentration; STZ: streptozotocin; PI3K: phosphatidylinositol 3-kinase; p-Akt: phosphorylated protein kinase B; p-IRS1: phosphorylated insulin receptor substrate-1; IRS-1: insulin receptor substrate-1; JNK: c-Jun N-terminal kinase.

excellent source of DPP-IV inhibitors. Peptides obtained from millet, corn, quinoa, egg yolk, oat, whey, casein, *Spirulina platensis*, porcine, Atlantic salmon, sea cucumber, largemouth bass, blue whiting, and *Capros aper* inhibited the DPP-IV activity [67, 70–72]. It has been found that dietary peptides inhibit DPP-IV through attaching the peptides to the active sites of DPP-IV via hydrogen bonds and hydrophobic interactions and thereby prevent the enzyme action [14, 21]. Two peptides NDWHTGPLS and TYPHQPPILT derived from papain hydrolysates of millet proteins inhibited DPP-IV activity (75%) [21]. It was demonstrated that both the peptides inhibited DPP-IV activity by occupying the active sites of DPP-IV via hydrogen and pi bonds. In a recent study, Atlantic salmon skin was hydrolyzed by using trypsin and isolated a new DPP-IV inhibitory peptide, LDKVFR, with IC_{50} of 128.7 μ M [14]. Additionally, it was found that 6 H bonds and 8 hydrophobic interactions played a significant role in the inhibition of DPP-IV by LDKVFR. A peptide, LDQWLCEKL, obtained from trypsin hydrolysate of α -lactalbumin-rich whey proteins inhibited DPP-IV (IC_{50} 131 μ M) through a noncompetitive mode of inhibition.

The PI3K/Akt signaling pathway regulates the glucose uptake. When cells are resistant to insulin, glucose uptake is impaired in the liver and skeletal muscles. Insulin activates IRS after binding to IRS and the activated IRS phosphorylates IRS-1. Phosphorylation of IRS-1 results in the activation of PI3K. The activated PI3K phosphorylates Akt, and the activated Akt helps in the migration of intracellular GLUT2/4 to the plasma membrane and therefore increases the glucose absorption into cells. But insulin resistance weakens the PI3K/Akt signaling pathway [73, 74]. Hence, stimulation of the PI3K/Akt molecular pathway is an efficient approach in the management of insulin resistance. In a study, the authors hydrolyzed walnut protein using alcalase and isolated an antidiabetic peptide LPLLR with a molecular weight of 610.4 Da. The authors reported that the identified peptide improved hepatic insulin resistance (IR) through enhancing glycogen synthesis and glucose uptake and reducing gluconeogenesis via activating the IRS-1/PI3K/Akt and AMPK signaling pathways in hepatic HepG2 cells [75]. Two hundred forty-two peptides, with a molecular weight ranging from 203 to 1907 Da, were isolated from the hydrolysate of sea cucumber and found that the peptides showed antidiabetic effects by upregulation of PI3K, p-Akt, p-GSK-3 β , and GLUT2/4 signaling pathways, while decreasing p-IRS1 expression in diabetic rats [73].

In addition to the peptides described above, the antidiabetic activities of dietary peptides have also been investigated in human subjects. In a randomized and crossover clinical trial, whey peptide (<5000 Da) (1400 or 2800 mg/kg BW) administration to 21 prediabetic human subjects decreased under the curve (iAUC) of glucose as well as showed a minor insulinotropic effect and reduced HbA1c [76]. A double-blind crossover clinical trial conducted using peptides (<2000 Da) derived from Atlantic cod showed that a single dose of 20 mg/kg BW considerably decreased the postprandial insulin in 41 healthy individuals [77]. Moreover, peptides derived from *Styela clava* have also been shown to

decrease the hemoglobin A1c and plasma insulin levels after 4 weeks of administration in patients with T2DM [78].

5. The Role of Dietary Bioactive Peptides in Hypertension

Hypertension is an important risk factor that can increase the chance of developing heart attack or stroke. Clinically, systolic blood pressure (SBP) 140 mmHg or above and/or DBP 90 mmHg or above are considered as hypertension [79]. It is estimated that over a billion people (1 in 5 women and 1 in 4 men) are suffering from hypertension.

Food-derived peptides play a significant role in the prevention of hypertension. Recently, numerous antihypertensive peptides are isolated from different food sources such as milk [80], casein [81, 82], egg white ovotransferrin [22], rice bran [1], wheat [83], soybean [84], potato [85], turmeric and ginger [9], quinoa [62], black cumin [86], coix [87], pistachio [88], hazelnut [89], mung bean [90], lentil [91], sea-horse [92], egg white from ostrich [93], chum salmon [94], skate [95], cuttlefish [96], Sipuncula [97], bighead carp [98], shrimp (*Pandalus borealis*) [79], and beef [99]. The isolated dietary protein-derived peptides have been demonstrated to exhibit antihypertensive activities through influencing various molecular mechanisms including inhibition of angiotensin-converting enzyme (ACE), reduction of SBP, decrease of angiotensin II levels and AT1R expression, enhancing vasodilation, improving central blood pressure and arterial stiffness, and inhibition of vasoconstriction via PPAR- γ expression [9, 79, 84, 90]. Table 4 shows the molecular mechanisms of antihypertensive peptides isolated from various dietary sources.

Human blood pressure is regulated by ACE (EC 3.4.15.1). ACE cleaves the dipeptide, HL, from angiotensin I and converts the inactive angiotensin I into angiotensin II and thereby enhances the blood pressure. Angiotensin II is a powerful vasoconstrictor, and ACE inactivates the bradykinin, which is a potent vasodilator. Therefore, inhibition of ACE is an important molecular target in the prevention and management of hypertension. Currently, several peptide drugs, namely, captopril, lisinopril, and enalapril, are used as ACE inhibitors for the management of high blood pressure [80, 97, 100]. Due to the side effects (cough, fatigue, dizziness, headaches, and loss of taste) associated with these synthetic drugs, there is an increasing interest to search for safe ACE inhibitors from natural food sources. Various food sources are an excellent source of ACE inhibitory peptides. Most dietary ACE inhibitory peptides contained 3–15 AA residues. Recently, several peptides have been isolated with ACE inhibitory activity from numerous dietary sources such as milk [80], casein [82], egg white [93], soybean [84], rice bran [1], wheat [83], pistachio [88], potato and rapeseed [85], turmeric and ginger [9], quinoa [62], black cumin [86], hazelnut [89], lentil [91], seahorse [92], chum salmon [94], skate [95], cuttlefish [96], Sipuncula [97], bighead carp [98], and beef [99].

It has been demonstrated that hydrogen bonds play a vital role in the binding of BPs to the ACE catalytic pocket and thereby facilitate ACE inhibition. Three ACE inhibitory peptides, LLSGTQNQPSFLSGF, NSLTLPLRYL, and

TLEPNSVFLPVLLH, were isolated from lentil seeds with IC_{50} of 44–120 μ M, and it was found that the peptides inhibited ACE through interactions by hydrogen bonds with three residues of the ACE catalytic site [91]. A tripeptide YSK with ACE inhibition was identified from trypsin hydrolysate of rice bran, and ACE inhibition of YSK was due to the formation of hydrogen bonds with the binding site of ACE [1]. The molecular interactions between dipeptide, YV, obtained from ostrich egg white and ACE were studied and it demonstrated that YV inhibited ACE (IC_{50} 63.97 μ g/mL) by binding to S1 and S2 pocket sites of ACE through hydrogen bonds [93]. A pentapeptide, ACKEP, purified from pistachio kernel hydrolysates was shown to inhibit ACE (IC_{50} 126 μ M) by binding with seven AAs of the ACE catalytic site (His383, His387, Glu384, Arg522, Asp358, Ala356, and Asn70) and two atoms of ACKEP [88]. In a study, three ACE inhibitory peptides, AVKVL, YLVR, and TLVGR, were identified from alcalase hydrolysate of hazelnut. The authors found that all the three peptides exhibited ACE inhibition (IC_{50} 5.42–249.3 μ M) via a noncompetitive inhibition through the formation of cation– π interactions [89]. In another study, four ACE inhibitory peptides, EDEVSFSP, SRPFNL, RSPFNL, and ENPFNL, were purified from fermented soybean with IC_{50} of 0.131–0.811 mg/mL [84]. It was suggested that the N-terminal sequence and the location of AAs in the peptides play an essential role in ACE inhibition. Recently, a peptide, VTPVGVPK, produced by α -chymotrypsin hydrolysis from black cumin seed was shown to inhibit ACE (IC_{50} 1.8 μ M) through a noncompetitive inhibition [86]. A peptide, QHPHGLGALCAAPPST, identified from chymotrypsin hydrolysate of quinoa inhibited ACE by binding to the number of active hotspots of the ACE enzyme [62]. Moreover, two peptides, SAGGYIW and APATPSFW, were isolated from wheat gluten with ACE inhibition of IC_{50} 0.002–0.036 mg/mL [83]. The authors concluded that two peptides with proline and negatively charged residues inhibited ACE through the modulation of ionic and hydrophobic connections of the ACE active site.

In addition to ACE inhibition, several *in vivo* studies (animal and human) have reported the blood pressure-lowering effects of numerous peptides isolated from various food sources. Peptides, SLVSPSAAAAAPGGS and KKRSKKKSFG, generated from potato and rapeseed were found to reduce (154.7 mmHg) the mean arterial blood pressure of treated rats compared to the control (177 mmHg) group [85]. Two antihypertensive peptides, IQW and LKP, were identified from thermolysin and pepsin hydrolysates prepared from egg white ovotransferrin and demonstrated that tripeptide (IQW and LKP) administration reduced the mean blood pressure by 19 and 30 mmHg, respectively, compared to control SHR [22]. Administration of a peptide, VELYP, produced from *Sepia officinalis* muscle, to SHR exhibited antihypertensive effects by decreasing SBP [96]. In a study, a beef myofibrillar protein-derived peptide LIV-GIIRCV at 400 and 800 mg/kg BW decreased SBP by 28 and 35 mmHg in SHR, respectively [99]. A randomized and double-blind human trial conducted on level 1 hypertensive patients demonstrated that eight-week supplementation of casein-derived tripeptides, VPP and IPP, ameliorated cen-

tral blood pressure and arterial stiffness [81]. In a recent randomized, double-blind clinical trial, the administration of shrimp-derived peptides (1200 mg/d) for eight weeks reduced the BP in mild- or moderate-hypertension patients [79]. Additionally, the authors suggested that the reduction of BP was probably due to the decrease of angiotensin II levels in hypertension patients.

6. The Role of Dietary Bioactive Peptides in Inflammatory Bowel Diseases (IBD)

Inflammation is a complex and natural response of the body in an attempt to resolve harmful stimuli such as pathogens, tissue injuries, infections, or toxins. However, uncontrolled and chronic inflammation has been reported to be linked with several diseases such as T2DM, metabolic syndrome, IBD, cardiovascular disease, cancer, asthma, arthritis, and chronic obstructive lung disease [101]. IBD symptoms such as diarrhea, abdominal pain, fever, vomiting, BW loss, and rectal bleeding affect the quality of life of patients [102]. Crohn's disease (CD) and ulcerative colitis (UC) are two major forms of IBD [103]. UC is the inflammation of colon. Chronic inflammation in the intestine produces excessive and uncontrolled proinflammatory cytokines including tumor necrosis factor- α (TNF- α), interleukin- (IL-) 1 β , IL-6, IL-8, IL-12, interferon- γ (IFN- γ), and IL-17 [102, 103].

The mechanism of anti-inflammation by food protein-derived BPs is that they can inhibit the phosphorylation of signaling pathways including nuclear factor- κ B (NF- κ B), mitogen-activated protein kinase (MAPK), Janus kinase-signal transducer and activator of transcription (JAK-STAT), and peptide transporter PepT1 as shown in Figure 2 [26, 104, 105]. The NF- κ B pathway contains IKKs, I κ Bs, and p65/p50, while the MAPK pathway contains p38, JNK, and extracellular signal-regulated kinases (ERK). BPs can inhibit the NF- κ B receptor, resulting in the inhibition of the activation of inhibitory κ B kinases (IKK $\alpha/\beta/\gamma$), which can lead to phosphorylation of cytoplasmic transcription factor (I κ B $\alpha/\beta/\gamma$) and I κ B α degradation. BPs can inhibit the MAPK receptor and inhibit MAP3K phosphorylation, which can mediate the phosphorylation of the downstream MAP2K and MAPK. The inhibition of phosphorylation of MAPK and JAK2-STATs by BPs can alleviate the release of cytokines. The BP inhibition of translocations of the above transcription factors in nucleus (ATF-2, AP-1, and c-Jun) can cause the gene change, reducing the productions of proinflammatory cytokines, such as IL-1 β , IL-6, IL-8, TNF- α , and IFN- γ , resulting in the inflammation suppression (Figure 2). In addition, the PepT1 can transport small BPs to the bloodstream; therefore, the role of PepT1 is vital to the bioactivity of BPs and needs further investigation [15, 26].

Peptides isolated from a variety of dietary protein sources (e.g., soy bean, common bean, corn, egg white, whey, casein, salmon, and crucian carp) have shown to inhibit intestinal inflammation through multiple molecular mechanisms. These include downregulation of the expression of IL-8, IL-1 β , IL-6, TNF- α , IFN- γ , IL-12, and IL-17; upregulation of IL-10; and inhibition of activation of the NF- κ B and MAPK

TABLE 4: Molecular mechanisms of action of antihypertensive peptides isolated from various food sources.

Dietary protein source	Enzyme used to produce peptides	Peptide sequence or molecular weight	Object	IC ₅₀ /EC ₅₀ values	Activity/mechanisms of action	Reference
Pea protein	Thermolysin	<3 kDa	SHR and clinical trial	—	Peptides (100 and 200 mg/kg BW) reduced SBP	[140]
Casein	—	VPP and IPP	Clinical trial	—	VPP and IPP improved central blood pressure and arterial stiffness	[81]
Pistachio kernel	Pepsin and trypsin	ACKEP	ACE inhibition assay	ACE IC ₅₀ 126 μM	ACKEP inhibited ACE by binding with ACE active site	[88]
Chum salmon (<i>Oncorhynchus keta</i>) skin	Trypsin	GLPLNLP	ACE inhibition assay and SHRs	ACE IC ₅₀ 18.7 μM	GLP exhibited ACE inhibition and antihypertensive effect by decreasing SBP	[94]
Skate (<i>Okamejei kenojei</i>) skin	Alcalase and protease	LGPLGHQ and MVGSAPGVL	ACE inhibition assay and SHRs	ACE IC ₅₀ 3.09–4.22 μM	Peptides inhibited ACE and decreased SBP and inhibited vasoconstriction via PPAR-γ expression, activation, and phosphorylation of eNOS in lungs	[95]
Egg white ovotransferrin	Thermolysin and pepsin	IQW and LKP	SHRs	—	Peptides reduced mean blood pressure	[22]
Cuttlefish (<i>Sepia officinalis</i>) muscle	Crude enzymes from <i>B. mojavensis</i> and cuttle fish hepatopancreas	VELYP, AFVGYVLP, and EKSVELP	ACE inhibition assay and SHRs	ACE IC ₅₀ 5.22 μM	VELYP showed strong ACE inhibition through a noncompetitive inhibition and had antihypertensive effects by decreasing SBP	[96]
Potato and rapeseed	Alcalase and potato autolysis	SLVSPSAAAAAAPGGS and KKRSKKKSFG	Goldblatt rat with hypertension and ACE inhibition	ACE IC ₅₀ 324 μg/mL and 156 μg/mL	Peptides inhibited ACE and exhibited antihypertensive effects by reducing SBP	[85]
Rice bran protein	Trypsin	YSK	ACE inhibition assay	ACE IC ₅₀ 76 mM	YSK showed ACE inhibition through the formation of hydrogen bonds with active pockets of human ACE	[1]
Sipuncula (<i>Phascolosoma esculenta</i>)	Pepsin and trypsin	RYDF, YASGR and GNGSGYVSR	ACE inhibition assay and SHRs	ACE IC ₅₀ 235 μM, 185 μM, and 29 μM	Three peptides inhibited ACE noncompetitively. GNGSGYVSR (5 mg/kg BW) showed antihypertensive effect by decreasing SBP	[97]
Lentil seeds (<i>Lens culinaris</i> var.)	Savinase	LLSGTQNQPSFLSGF, NSLTLPLRYL, and TLEPNSVFLPVLLH	ACE inhibition assay	ACE IC ₅₀ 44–120 μM	Inhibited ACE through interaction by hydrogen bonds with three ACE residues of the catalytic site	[91]
Bighead carp muscle	Pepsin	YNLKERYAAW and YNRLPEL	ACE inhibition assay	ACE IC ₅₀ 1.35–3.42 μM	Peptides inhibited ACE activity	[98]
Bovine casein	Pepsin and trypsin	YQKFPQYLQY	ACE inhibition assay and SHRs	ACE IC ₅₀ 11.1 μM	Peptide inhibited ACE via competitive inhibition and exhibited antihypertension by decreasing SBP	[82]
Hazelnut (<i>Corylus heterophylla</i> Fisch.)	Alcalase	AVKVL, YLVR, and TLVGR	ACE inhibition assay and SHRs	ACE IC ₅₀ 15.42–249.3 μM	Peptides inhibited ACE activity via a noncompetitive mode via the formation of cation-π interactions and YLVR reduced SBP	[89]
		YV				[93]

TABLE 4: Continued.

Dietary protein source	Enzyme used to produce peptides	Peptide sequence or molecular weight	Object	IC ₅₀ /EC ₅₀ values	Activity/mechanisms of action	Reference
Egg white from ostrich	Alkaline hydrolysis		ACE inhibition assay	ACE IC ₅₀ 63.97 μ g/mL	YV showed ACE inhibition by binding to S1 and S2 ACE pocket sites via hydrogen bonds	
Soybean	<i>Pediococcus pentosaceus</i> SDL1409	EDEVSFSP, SRPFNL, RSPFNL, and ENPFNL	ACE inhibition assay	ACE IC ₅₀ 0.131–0.811 mg/mL	Peptides inhibited ACE via essential N-terminal sequence and amino acid position	[84]
Shrimp (<i>Pandalus borealis</i>) protein	—	—	Randomized, double-blind, placebo-controlled, 8-week clinical study	—	Peptides (1200 mg/d) reduced the blood pressure due to a reduction of angiotensin II levels	[79]
Beef (<i>Bos taurus coreanae</i>) myofibrillar proteins	Alkaline-AK and papain	LIVGIIRCV	ACE inhibition assay and SHRs	—	Peptides (400 and 800 mg/kg BW) inhibited ACE by 74.29% and decreased SBP	[99]
Milk	Fermented using <i>L. delbrueckii</i> QS306	LPYPY	ACE inhibition assay	ACE IC ₅₀ 12.87 μ g/mL	LPYPY inhibited ACE with IC ₅₀ 12.87 μ g/mL	[80]
Mung bean protein	Bromelain	LPRL, YADLVE, LRLESF, HLNVVHEN, and PGSGCAGTDL	ACE inhibition assay and SHRs	ACE IC ₅₀ 5.39–1912 μ M	Peptides showed ACE inhibition and reduced SBP	[90]
Seahorse (<i>Hippocampus abdominalis</i>)	Protamex	APTL, CNVPLSP, and PWTPL	ACE inhibition assay and SHRs	ACE IC ₅₀ 0.044 μ M	Peptides exhibited antihypertension by lowering blood pressure via vasodilation and ACE inhibition	[92]
Black cumin seed	α -Chymotrypsin	VTPVGVPK	ACE inhibition assay	ACE IC ₅₀ value 1.8 μ M	VTPVGVPK inhibited ACE via a noncompetitive inhibition	[86]
Quinoa protein	Chymotrypsin	QHPHGLGALCAAPPST	ACE inhibition assay	—	Peptide displayed ACE inhibition by binding to ACE active hotspots	[62]
White turmeric, turmeric, and ginger proteins	Pepsin and trypsin	VTYM, RGPFH, AEPFR, GSGLVP, KM, SPV, CACGGV, DVDP, CGVGAA, HVVV, and RSC	ACE inhibition assay	ACE IC ₅₀ 16.4–36.5 μ M	Peptides showed ACE inhibition	[9]
Coix prolamin	Pepsin	VDMF	ACE inhibition assay	ACE IC ₅₀ 382.28 μ M	VDMF reduced ACE and AT1R expression in AngII-injury HUVECs	[87]
Wheat gluten	Alcalase and PaproA	SAGGYIW and APATPSFW	ACE inhibition assay	ACE IC ₅₀ 0.002–0.036 mg/mL	Peptides and negatively charged amino acids inhibited ACE via modulating ionic and hydrophobic interactions on ACE catalytic sites	[83]

ACE: angiotensin-converting enzyme; BW: body weight; IC₅₀: 50% inhibitory concentration; SBP: systolic blood pressure; SHR: spontaneously hypertensive rat; PPAR- γ : peroxisome proliferator-activated receptor γ .

pathways via suppression of phosphorylation of p65, ERK1/2, p38, JNK1/2, and Syk signaling molecules [102, 103, 106, 107]. The isolated peptides and their molecular mechanisms of anti-intestinal inflammatory effects are presented in Table 5.

Dietary anti-intestinal inflammatory peptides are short chains of AAs that generally contain 2–10 AAs. The common AAs of these peptides are alanine, valine, leucine, serine, methionine, tyrosine, and phenylalanine [102, 103, 108]. Pepsin and pancreatin are the two most commonly employed

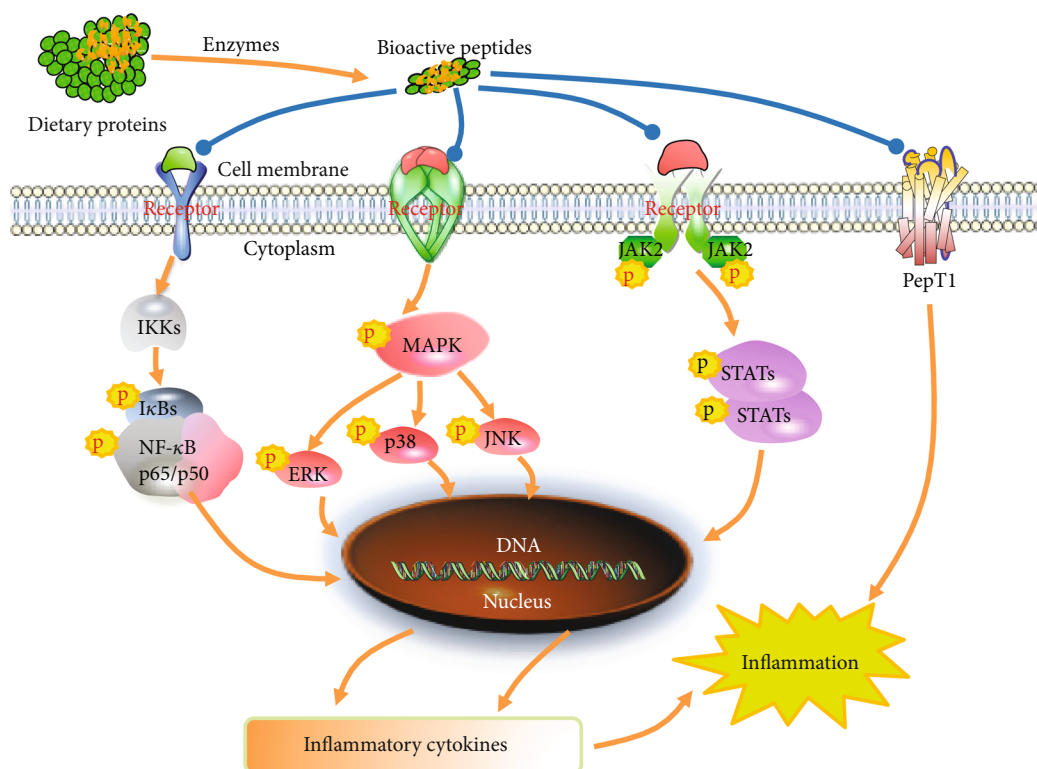


FIGURE 2: The mechanism of anti-inflammation of dietary protein-derived bioactive peptides: NF- κ B, MAPK, JAK2-STAT, and PepT1. ERK: extracellular signal-regulated kinases; MAPK: mitogen-activated protein kinase; NF- κ B: nuclear factor-kappa B; JAK-STAT: Janus kinase-signal transducer and activator of transcription; JNK: c-Jun N-terminal kinase; p: phosphorylation; PepT1: peptide transport 1.

proteolytic enzymes to produce anti-inflammatory peptides from various food proteins [103, 109, 110]. The TNF- α -treated Caco-2 cell is a widely used human intestinal cell model for the investigation of the anti-inflammatory property of dietary peptides. TNF- α activates the both NF- κ B and MAPK signaling pathways in Caco-2 cells and thereby produces large quantities of proinflammatory mediators [110]. Excess and uncontrolled production of proinflammatory cytokines plays a vital role in the progression of intestinal inflammation [103].

Numerous recent studies reported that dietary BPs could inhibit the intestinal inflammation through the reduction of proinflammatory mediators. Four peptides, DEDT-QAMPFR, MLGATSL, SLSFASR, and MSYSAGF, isolated from egg white exerted anti-inflammatory activities in colitis mouse by inhibiting the production of TNF- α and IL-6 as well as reducing the mRNA-expressions TNF- α , IL-6, IL-17, IL-1 β , IFN- γ , and MCP-1 [111]. Tripeptide VPY from soybean inhibited IL-8 secretion in Caco-2 cells [108]. The peptide was also found to decrease the mRNA expressions of inflammatory mediators TNF- α , IL-6, IL-1 β , IFN- γ , and IL-17 in the peptide-treated mice colon. Dipeptides (CR, FL, HC, ILL, and MK) produced from egg white ovotransferrin, by using pepsin and trypsin hydrolysis, decreased the gene expression of TNF- α , IL-8, IL-6, IL-1 β , and IL-12, while enhancing IL-10 expression, in Caco-2 cells [103]. Crucian carp-derived 178 peptides (<1500 Da) at 50, 100, and 150 μ g/mL considerably reduced the secretion of TNF- α , IL-6,

and IL-1 β in IEC-6 small intestine cells as well as in dextran sodium sulfate-induced ulcerative colitis mice [106].

Several recent reports demonstrated the role of NF- κ B in the pathogenesis of IBD [106]. Activation of NF- κ B has been shown to be involved in the IBD patients [112]. The NF- κ B and MAPK pathways are two vital proinflammatory signaling pathways that majorly regulate cellular inflammatory responses by secreting various cytokines after activation by various inflammatory stimuli [113]. Transcription factor NF- κ B regulates the inflammatory responses by stimulating the production of various proinflammatory cytokines and chemokines. Phosphorylation of I κ B by inflammatory stimuli (LPS and TNF- α) releases the NF- κ B that migrates to the nucleus and activates expression of the numerous genes connected with inflammation [110, 112]. The MAPK family contains three components such as p38 MAPK, ERK1/2, and JNK/SAPK. Phosphorylation of MAPK components stimulates the other kinases and migrates to the nucleus where they induce the transcription of several inflammatory genes and thereby enhance the secretion of proinflammatory mediators [110].

Peptides derived from egg, milk, fish, and beans exhibited the anti-intestinal inflammatory activity through the inhibition of MAPK and NF- κ B molecular pathways [102, 103, 110]. A tetrapeptide, IPAV, isolated from whey proteins exhibited anti-inflammatory activity in Caco-2 cells by inhibiting IL-8 expression and by suppression of phosphorylation of p65, ERK1/2, p38, JNK1/2, and Syk signaling

TABLE 5: Mechanisms of action of anti-inflammatory peptides isolated from various food sources.

Dietary protein source	Enzyme used to produce peptides	Peptide sequence or molecular weight	Object	Dose & duration	Activity/mechanisms of action	Reference
Soy bean	—	150–500 Da	Pigs with DSS-induced colitis	250 mg/kg BW for 5 d	Peptides decreased TNF and IL-6 levels and inhibited IFN- γ , IL-1 β , and TNF expression	[141]
Soy bean	—	VPY	Caco-2 cells and mouse of DSS-induced colitis mice	0.1, 1, 2, and 4 mM for 2 h and 10 and 100 mg/kg BW for 14 d	VPY inhibited IL-8 secretion and reduced the expressions of TNF- α , IL-6, IL-1 β , IFN- γ , and IL-17	[108]
Salmon	—	<1000 Da	DSS-induced colitis in rats	3.5% in diet for 29 d	Peptides reduced inflammation by reducing IL-6 and IL-1 β expressions	[142]
Egg shell membrane	Alcalase and protease S	—	TNF- α induced Caco-2 cells and DSS-treated colitis mice	0.001, 0.01, 0.5, and 0.1 mg/mL for 2 h	Peptides inhibited IL-8 secretion and decreased TNF- α and IL-6 levels	[143]
Milk casein	Bacterial food-grade enzyme	<5000 Da	TNF- α -induced Caco-2 cells and ex vivo porcine colonic tissue system	0.01, 0.02, 0.05, 0.1, 0.5, 1, 2.5, and 5 mg/mL for 24 h	Peptides reduced IL-8 by 66–68% and reduced IL-1 α / β , IL-8, TGF- β , and IL-10 expression	[107]
Rat collagen	Pepsin	—	DSS-induced colitis in mice	100 mg/kg BW from days 6 to 15	Peptides reduced IL-1 β and IL-6 expression	[144]
Egg white	Pepsin and pancreatin	—	TNF- α -induced inflammation in Caco-2 cells and DSS-induced colitis mice	0.05, 0.1, 0.5, 1, and 2.5 mg/mL for 2 h	Peptides inhibited IL-8 secretion and decreased expression of TNF- α , IL-6, IL-1 β , IFN- γ , and IL-17 and enhanced IL-10 expression and decreased the expression of TNF- α , IL-6, IL-1 β , IFN- γ , and IL-17	[145]
Egg white ovomucoprotein	Pepsin and trypsin	CR, FL, HC, LL, and MK	TNF- α -induced Caco-2 cells	0.05, 0.1, 0.5, 1, 2.5, and 5 mg/mL for 2 h	Peptides decreased expression of TNF- α , IL-8, IL-6, IL-1 β , and IL-12, and enhanced IL-10 expression. CR and HC attenuated intestinal inflammation by inhibiting NF- κ B and MAPK pathways	[103]
Milk whey	Pronase	IPAV	TNF- α induced Caco-2 cells	2.5 and 5 mg/mL for 1 h	IPAV showed anti-inflammatory effect by inhibiting IL-8 expression and suppressing phosphorylation of p65, ERK1/2, p38, JNK1/2, and Syk signaling	[102]
Egg white	—	DEDTQAMPFR, MLGATSL, SLSFASR, and MSYSAGF	DSS-induced colitis mice	50 or 150 mg/kg/day for 14 d	Peptides inhibited the local production of TNF- α and IL-6 and reduced the expression of TNF- α , IL-6, IL-17, IL-1 β , IFN- γ , and MCP-1	[111]
Common bean (<i>Phaseolus vulgaris</i> L.) milk and yogurts	Pepsin and pancreatin	γ -E-S-(Me)C, γ -EL, and LLV	TNF- α -induced Caco-2 cells	0.5 mg/mL for 2 h	Peptides inhibited TNF- α -induced IL-8 production via inhibiting activation of NF- κ B and MAPK pathways	[113]

TABLE 5: Continued.

Dietary protein source	Enzyme used to produce peptides	Peptide sequence or molecular weight	Object	Dose & duration	Activity/mechanisms of action	Reference
Egg white	Pancreatin	DEDTQAMPFR, DEDTQAMPF, MLGATSL, and MSYSAGF	TNF- α -induced Caco-2 cells	0.1, 0.25, or 0.5 mg/mL for 2 h	Peptides downregulated the expression of IL-8, IL-1 β , IL-6, TNF- α , and IL-12 and upregulated IL-10 expression via inhibiting NF- κ B and MAPK pathways	[110]
Crucian carp	Pancreatin	<1500 Da	IEC-6 cells and DSS-induced colitis mice	0, 50, 100, or 150 μ g/mL for 20 h and 50 mg/kg BW for 15 days	Peptides reduced IL-1 β , IL-6, and TNF- α levels via inhibiting the NF- κ B pathway	[106]
Soy bean	<i>B. subtilis</i> BS12	<3000 Da	Intestinal porcine epithelial cells-J2	50 μ g/mL for 2 h	Soy peptides reduced the expression of IL-6, IL-1 β , and IL-8 and decreased <i>Escherichia coli</i> K88-induced inflammation	[4]
Corn	Alcalase and pancreatin	—	TNF- α -induced Caco-2 cells and colitis mice	500, 1500, and 2500 μ g/mL for 6 h and 100 and 300 mg/kg/d for 14 days	Peptides reduced inflammation via inhibiting IL-8 secretion and iNOS and COX-2 expression and downregulating TNF- α and IL-6 expression	[109]

DSS: dextran sodium sulfate; ERK: extracellular signal-regulated kinases; IL: interleukin; TNF- α : tumor necrosis factor alpha; MAPK: mitogen-activated protein kinase; NF- κ B: nuclear factor- κ B; JNK: c-Jun N-terminal kinase.

molecules [102]. Bean milk- and yogurt-derived LLV, γ -E-S-(Me)C, and γ -EL inhibited TNF- α -induced IL-8 production and gene expression of inflammatory mediators, TNF- α , IL-1 β , IL-8, and IL-6, through the inhibition of phosphorylation of I κ B- α of NF- κ B and JNK of MAPK signaling pathways in Caco-2 cells [113]. Four peptides DEDTQAMPFR, DEDTQAMPF, MLGATSL, and MSYSAGF isolated from egg considerably suppressed the phosphorylation of JNK, p38, and I κ B of NF- κ B and MAPK signaling pathways and thereby reduced the gene expression of IL-8, IL-1 β , IL-6, TNF- α , and IL-12 in TNF- α -stimulated Caco-2 cells [110]. These results indicated that dietary BPs had the potential to treat inflammation or IBD via NF- κ B or MAPK or other signaling pathways.

7. Conclusions and Further Perspectives

Numerous dietary peptides showed beneficial effects on redox balance and metabolic disorders (obesity, T2D, hypertension, and inflammation). Dietary peptides modulated several molecular mechanisms (e.g., *Keap1-Nrf2-ARE signaling pathway in oxidative stress*, PPAR- γ , C/EBP- α , SREBP1 pathway in obesity, IRS-1/PI3K/Akt and AMPK signaling pathways in T2D, ACE inhibition in hypertension, and MAPK in IBD) and thereby exerted positive effects in redox balance and metabolic disorders. Most of the studies are conducted using cell and animal models. Although substantial evidence from cell and animal investigations is available for the BPs as described in this review, scientific evidence from clinical studies is still meager. Hence, more clinical investigations are needed to get in-depth knowledge about the BP's efficacy, absorption, distribution, metabolism, excretion, toxicity, and effect on gut microbiome in the human body in the future. In the future, the benefits and risks of long-term and large-quantity consumption of BPs on human health need to be addressed. The interaction of BPs with other drugs in the human body has to be investigated comprehensively. Additionally, newer technologies are needed to produce BPs cost effectively from dietary sources. The BPs should be produced with consumer-acceptable taste, quality, and stability. Although there are several challenges for future growth, the dietary BPs could be used as health foods in the management/prevention of metabolic disorders (obesity, T2DM, hypertension, and inflammation) and oxidative stress-related diseases (e.g., cancer and IBD). We hope that the BP's industry will have a bright future in the coming years as people are increasingly aware of health benefits of dietary BPs.

Data Availability

No data were used to support this review article.

Conflicts of Interest

The authors declare no conflict of interest.

Authors' Contributions

Qinqin Qiao, Liang Chen, Xiang Li, Xiangyang Lu, and Qingbiao Xu wrote the manuscript. Xiang Li, Xiangyang Lu, and Qingbiao Xu revised the manuscript. All authors reviewed and approved the final manuscript. Qinqin Qiao, Liang Chen, and Xiang Li contributed equally to this work.

Acknowledgments

This work was supported by grants from the Open Project Program of Key Laboratory of Feed Biotechnology, the Fundamental Research Funds for the Central Universities (2662019QD021), the State Key Laboratory of Animal Nutrition (2004DA125184F1906), the National Natural Science Foundation of China (C31802087), and the Key Laboratory of Molecular Animal Nutrition of Zhejiang University.

References

- [1] X. Wang, H. Chen, X. Fu, S. Li, and J. Wei, "A novel antioxidant and ACE inhibitory peptide from rice bran protein: biochemical characterization and molecular docking study," *LWT*, vol. 75, pp. 93–99, 2017.
- [2] I. Jemil, O. Abdelhedi, R. Nasri et al., "Hypolipidemic, anti-obesity and cardioprotective effects of sardinelle meat flour and its hydrolysates in high-fat and fructose diet fed Wistar rats," *Life Sciences*, vol. 176, pp. 54–66, 2017.
- [3] J. Zhang, M. Li, G. Zhang et al., "Identification of novel antioxidant peptides from snakehead (*Channa argus*) soup generated during gastrointestinal digestion and insights into the anti-oxidation mechanisms," *Food Chemistry*, vol. 337, p. 127921, 2021.
- [4] Y. Zhang, S. Chen, X. Zong et al., "Peptides derived from fermented soybean meal suppresses intestinal inflammation and enhances epithelial barrier function in piglets," *Food and Agricultural Immunology*, vol. 31, no. 1, pp. 120–135, 2020.
- [5] A. Bougatef, R. Ravallec, N. Nedjar-Arroume, A. Barkia, D. Guillochon, and M. Nasri, "Evidence of *in vivo* satietogen effect and control of food intake of smooth hound (*Mustelus mustelus*) muscle protein hydrolysate in rats," *Journal of Functional Foods*, vol. 2, no. 1, pp. 10–16, 2010.
- [6] S. Marthandam Asokan, T. Wang, W.-T. Su, and W.-T. Lin, "Antidiabetic effects of a short peptide of potato protein hydrolysate in STZ-induced diabetic mice," *Nutrients*, vol. 11, no. 4, p. 779, 2019.
- [7] P.-X. Gong, B.-K. Wang, Y.-C. Wu, Q.-Y. Li, B.-W. Qin, and H.-J. Li, "Release of antidiabetic peptides from *Stichopus japonicas* by simulated gastrointestinal digestion," *Food Chemistry*, vol. 315, article 126273, 2020.
- [8] X. Fan, Y. Cui, R. Zhang, and X. Zhang, "Purification and identification of anti-obesity peptides derived from *Spirulina platensis*," *Journal of Functional Foods*, vol. 47, pp. 350–360, 2018.
- [9] K. Sompinit, S. Lersiripong, O. Reamtong, W. Pattarayingsakul, N. Patikarnmonthon, and W. Panbangred, "In vitro study on novel bioactive peptides with antioxidant and antihypertensive properties from edible rhizomes," *LWT*, vol. 134, article 110227, 2020.
- [10] Y. Oh, C.-B. Ahn, and J.-Y. Je, "Low molecular weight blue mussel hydrolysates inhibit adipogenesis in mouse

- mesenchymal stem cells through upregulating HO-1/Nrf2 pathway,” *Food Research International*, vol. 136, article 109603, 2020.
- [11] M. Hajfathalian, S. Ghelichi, P. J. García-Moreno, A.-D. Moltke Sørensen, and C. Jacobsen, “Peptides: production, bioactivity, functionality, and applications,” *Critical Reviews in Food Science and Nutrition*, vol. 58, no. 18, pp. 3097–3129, 2018.
- [12] K. Wang, L. Han, H. Hong, J. Pan, H. Liu, and Y. Luo, “Purification and identification of novel antioxidant peptides from silver carp muscle hydrolysate after simulated gastrointestinal digestion and transepithelial transport,” *Food Chemistry*, vol. 342, article 128275, 2021.
- [13] J. Wang, M. Zhou, T. Wu, L. Fang, C. Liu, and W. Min, “Novel anti-obesity peptide (RLLPH) derived from hazelnut (*Corylus heterophylla* Fisch) protein hydrolysates inhibits adipogenesis in 3T3-L1 adipocytes by regulating adipogenic transcription factors and adenosine monophosphate-activated protein kinase (AMPK) activation,” *Journal of Bioscience and Bioengineering*, vol. 129, no. 3, pp. 259–268, 2020.
- [14] R. Jin, X. Teng, J. Shang, D. Wang, and N. Liu, “Identification of novel DPP-IV inhibitory peptides from Atlantic salmon (*Salmo salar*) skin,” *Food Research International*, vol. 133, article 109161, 2020.
- [15] Q. Xu, H. Hong, J. Wu, and X. Yan, “Bioavailability of bioactive peptides derived from food proteins across the intestinal epithelial membrane: a review,” *Trends in Food Science and Technology*, vol. 86, pp. 399–411, 2019.
- [16] Q. Xu, H. Fan, W. Yu, H. Hong, and J. Wu, “Transport study of egg-derived antihypertensive peptides (LKP and IQW) using Caco-2 and HT29 coculture monolayers,” *Journal of Agricultural and Food Chemistry*, vol. 65, no. 34, pp. 7406–7414, 2017.
- [17] Q. Xu, X. Yan, Y. Zhang, and J. Wu, “Current understanding of transport and bioavailability of bioactive peptides derived from dairy proteins: a review,” *International Journal of Food Science and Technology*, vol. 54, no. 6, pp. 1930–1941, 2019.
- [18] Q. Lin, Q. Xu, J. Bai, W. Wu, H. Hong, and J. Wu, “Transport of soybean protein-derived antihypertensive peptide LSW across Caco-2 monolayers,” *Journal of Functional Foods*, vol. 39, pp. 96–102, 2017.
- [19] M. Chalamaiah, S. Keskin Ulug, H. Hong, and J. Wu, “Regulatory requirements of bioactive peptides (protein hydrolysates) from food proteins,” *Journal of Functional Foods*, vol. 58, pp. 123–129, 2019.
- [20] F. Ursini, M. Maiorino, and H. J. Forman, “Redox homeostasis: the Golden mean of healthy living,” *Redox Biology*, vol. 8, pp. 205–215, 2016.
- [21] H. Gu, J. Gao, Q. Shen et al., “Dipeptidyl peptidase-IV inhibitory activity of millet protein peptides and the related mechanisms revealed by molecular docking,” *LWT*, vol. 138, article 110587, 2021.
- [22] K. Majumder, S. Chakrabarti, J. S. Morton et al., “Egg-derived ACE-inhibitory peptides IQW and LKP reduce blood pressure in spontaneously hypertensive rats,” *Journal of Functional Foods*, vol. 13, pp. 50–60, 2015.
- [23] M. Son and J. Wu, “Egg white hydrolysate and peptide reverse insulin resistance associated with tumor necrosis factor- α (TNF- α) stimulated mitogen-activated protein kinase (MAPK) pathway in skeletal muscle cells,” *European Journal of Nutrition*, vol. 58, no. 5, pp. 1961–1969, 2019.
- [24] P. Mudgil, H. Kamal, G. C. Yuen, and S. Maqsood, “Characterization and identification of novel antidiabetic and anti-obesity peptides from camel milk protein hydrolysates,” *Food Chemistry*, vol. 259, pp. 46–54, 2018.
- [25] L. Liang, S. Cai, M. Gao et al., “Purification of antioxidant peptides of *Moringa oleifera* seeds and their protective effects on H₂O₂ oxidative damaged Chang liver cells,” *Journal of Functional Foods*, vol. 64, article 103698, 2020.
- [26] W. Zhu, L. Ren, L. Zhang, Q. Qiao, M. Z. Farooq, and Q. Xu, “The potential of food protein-derived bioactive peptides against chronic intestinal inflammation,” *Mediators of Inflammation*, vol. 2020, Article ID 6817156, 15 pages, 2020.
- [27] E. H. Sarsour, M. G. Kumar, L. Chaudhuri, A. L. Kalen, and P. C. Goswami, “Redox control of the cell cycle in health and disease,” *Antioxidants & Redox Signaling*, vol. 11, no. 12, pp. 2985–3011, 2009.
- [28] A. Ayer, C. W. Gourlay, and I. W. Dawes, “Cellular redox homeostasis, reactive oxygen species and replicative ageing in *Saccharomyces cerevisiae*,” *FEMS Yeast Research*, vol. 14, no. 1, pp. 60–72, 2014.
- [29] R. Basria, S. M. N. Mydin, and S. I. Okekepa, “Reactive Oxygen Species, Cellular Redox Homeostasis and Cancer,” in *Homeostasis - An Integrated Vision*, IntechOpen, 2019.
- [30] B. Marengo, M. Nitti, A. L. Furfaro et al., “Redox homeostasis and cellular antioxidant systems: crucial players in cancer growth and therapy,” *Oxidative Medicine and Cellular Longevity*, vol. 2016, Article ID 6235641, 16 pages, 2016.
- [31] X. Jiang, Z. Cui, L. Wang, H. Xu, and Y. Zhang, “Production of bioactive peptides from corn gluten meal by solid-state fermentation with *Bacillus subtilis* MTCC5480 and evaluation of its antioxidant capacity *in vivo*,” *LWT*, vol. 131, p. 109767, 2020.
- [32] F. Tonolo, A. Folda, L. Cesaro et al., “Milk-derived bioactive peptides exhibit antioxidant activity through the Keap1-Nrf2 signaling pathway,” *Journal of Functional Foods*, vol. 64, article 103696, 2020.
- [33] B. C.-K. Tsai, D. J.-Y. Hsieh, W.-T. Lin et al., “Functional potato bioactive peptide intensifies Nrf2-dependent antioxidant defense against renal damage in hypertensive rats,” *Food Research International*, vol. 129, article 108862, 2020.
- [34] X. Lu, L. Zhang, Q. Sun, G. Song, and J. Huang, “Extraction, identification and structure-activity relationship of antioxidant peptides from sesame (*Sesamum indicum* L.) protein hydrolysate,” *Food Research International*, vol. 116, pp. 707–716, 2019.
- [35] M. Chalamaiah, B. Dinesh kumar, R. Hemalatha, and T. Jyothirmayi, “Fish protein hydrolysates: proximate composition, amino acid composition, antioxidant activities and applications: a review,” *Food Chemistry*, vol. 135, no. 4, pp. 3020–3038, 2012.
- [36] W. Rungratanawanich, M. Memo, and D. Uberti, “Redox homeostasis and natural dietary compounds: focusing on antioxidants of rice (*Oryza sativa* L.),” *Nutrients*, vol. 10, no. 11, p. 1605, 2018.
- [37] L. Zheng, H. Yu, H. Wei et al., “Antioxidative peptides of hydrolysate prepared from fish skin gelatin using ginger protease activate antioxidant response element-mediated gene transcription in IPEC-J2 cells,” *Journal of Functional Foods*, vol. 51, pp. 104–112, 2018.
- [38] I. P. S. Fernando, S. Y. Park, E. J. Han et al., “Isolation of an antioxidant peptide from krill protein hydrolysates as a novel agent with potential hepatoprotective effects,” *Journal of Functional Foods*, vol. 67, article 103889, 2020.

- [39] C. Wen, J. Zhang, Y. Feng, Y. Duan, H. Ma, and H. Zhang, "Purification and identification of novel antioxidant peptides from watermelon seed protein hydrolysates and their cytoprotective effects on H₂O₂-induced oxidative stress," *Food Chemistry*, vol. 327, article 127059, 2020.
- [40] K. Sowmya, M. I. Bhat, R. Bajaj, S. Kapila, and R. Kapila, "Antioxidative and anti-inflammatory potential with trans-epithelial transport of a buffalo casein-derived hexapeptide (YFYPQL)," *Food Bioscience*, vol. 28, pp. 151–163, 2019.
- [41] S. Awad, M. I. El-Sayed, A. Wahba, A. El Attar, M. I. Yousef, and M. Zedan, "Antioxidant activity of milk protein hydrolysate in alloxan-induced diabetic rats," *Journal of Dairy Science*, vol. 99, no. 11, pp. 8499–8510, 2016.
- [42] Q. Zhang, X. Tong, X. Sui et al., "Antioxidant activity and protective effects of alcalase-hydrolyzed soybean hydrolysate in human intestinal epithelial Caco-2 cells," *Food Research International*, vol. 111, pp. 256–264, 2018.
- [43] D. Ren, C. Liu, W. Liu et al., "Antifatigue, antioxidant and immunoregulatory effects of peptides hydrolyzed from Manchurian walnut (*Juglans mandshurica* Maxim.) on mice," *Grain & Oil Science and Technology*, vol. 1, no. 1, pp. 44–52, 2018.
- [44] Z. Zhang, G. Su, F. Zhou, L. Lin, X. Liu, and M. Zhao, "Alcalase-hydrolyzed oyster (*Crassostrea rivularis*) meat enhances antioxidant and aphrodisiac activities in normal male mice," *Food Research International*, vol. 120, pp. 178–187, 2019.
- [45] N. Wang, W. Wang, F. A. Sadiq, S. Wang, L. Caiqin, and J. Jianchang, "Involvement of Nrf2 and Keap1 in the activation of antioxidant responsive element (ARE) by chemopreventive agent peptides from soft-shelled turtle," *Process Biochemistry*, vol. 92, pp. 174–181, 2020.
- [46] Z. Zhang, S. Jiang, Y. Zeng, K. He, Y. Luo, and F. Yu, "Antioxidant peptides from *Mytilus Coruscus* on H₂O₂-induced human umbilical vein endothelial cell stress," *Food Bioscience*, vol. 38, p. 100762, 2020.
- [47] M. Blüher, "Obesity: global epidemiology and pathogenesis," *Nature Reviews Endocrinology*, vol. 15, no. 5, pp. 288–298, 2019.
- [48] R. Ruiz, R. Olías, A. Clemente, and L. A. Rubio, "A pea (*Pisum sativum* L.) seed vicilins hydrolysate exhibits PPAR γ ligand activity and modulates adipocyte differentiation in a 3T3-L1 cell culture model," *Foods*, vol. 9, no. 6, p. 793, 2020.
- [49] I. Kyrou, H. S. Randeve, C. Tsigos, G. Kaltsas, and M. O. Weickert, *Clinical problems caused by obesity*, Endotext, 2000.
- [50] M. Desai, M. Beall, and M. G. Ross, "Developmental origins of obesity: programmed adipogenesis," *Current Diabetes Reports*, vol. 13, no. 1, pp. 27–33, 2013.
- [51] J.-H. Hyung, C.-B. Ahn, and J.-Y. Je, "Ark shell protein hydrolysates inhibit adipogenesis in mouse mesenchymal stem cells through the down-regulation of transcriptional factors," *RSC Advances*, vol. 7, no. 11, pp. 6223–6228, 2017.
- [52] M.-J. Tsou, F.-J. Kao, H.-C. Lu, H.-C. Kao, and W.-D. Chiang, "Purification and identification of lipolysis-stimulating peptides derived from enzymatic hydrolysis of soy protein," *Food Chemistry*, vol. 138, no. 2–3, pp. 1454–1460, 2013.
- [53] M. E. Oseguera Toledo, E. Gonzalez de Mejia, M. Sivaguru, and S. L. Amaya-Llano, "Common bean (*Phaseolus vulgaris* L.) protein-derived peptides increased insulin secretion, inhibited lipid accumulation, increased glucose uptake and reduced the phosphatase and tensin homologue activation *in vitro*," *Journal of Functional Foods*, vol. 27, pp. 160–177, 2016.
- [54] A. M. Alashi, C. L. Blanchard, R. J. Mailer et al., "Effects of canola proteins and hydrolysates on adipogenic differentiation of C3H10T/2 mesenchymal stem cells," *Food Chemistry*, vol. 185, pp. 226–232, 2015.
- [55] E. J. Lee, J. Hur, S. A. Ham et al., "Fish collagen peptide inhibits the adipogenic differentiation of preadipocytes and ameliorates obesity in high fat diet-fed mice," *International Journal of Biological Macromolecules*, vol. 104, Part A, pp. 281–286, 2017.
- [56] T. Mizushige, M. Komiya, M. Onda, K. Uchida, K. Hayamizu, and Y. Kabuyama, "Fish protein hydrolysate exhibits anti-obesity activity and reduces hypothalamic neuropeptide Y and agouti-related protein mRNA expressions in rats," *Biomedical Research*, vol. 38, no. 6, pp. 351–357, 2017.
- [57] B. Zhao, Y. Cui, X. Fan et al., "Anti-obesity effects of Spirulina platensis protein hydrolysate by modulating brain-liver axis in high-fat diet fed mice," *PLoS One*, vol. 14, no. 6, article e0218543, 2019.
- [58] S. Wang, Z. Lv, W. Zhao, L. Wang, and N. He, "Collagen peptide from walleye pollock skin attenuated obesity and modulated gut microbiota in high-fat diet-fed mice," *Journal of Functional Foods*, vol. 74, article 104194, 2020.
- [59] B. Framroze, S. Vekariya, and D. Swaroop, "A placebo-controlled, randomized study on the impact of dietary salmon protein hydrolysate supplementation on body mass index in overweight human subjects," *Journal of Obesity and Weight Loss Therapy*, vol. 6, no. 1, p. 296, 2016.
- [60] T. M. Schnurr, H. Jakupović, G. D. Carrasquilla et al., "Obesity, unfavourable lifestyle and genetic risk of type 2 diabetes: a case-cohort study," *Diabetologia*, vol. 63, no. 7, pp. 1324–1332, 2020.
- [61] A. Karimi, M. H. Azizi, and H. Ahmadi Gavlighi, "Fractionation of hydrolysate from corn germ protein by ultrafiltration: *in vitro* antidiabetic and antioxidant activity," *Food Science & Nutrition*, vol. 8, no. 5, pp. 2395–2405, 2020.
- [62] P. Mudgil, B. P. Kilari, H. Kamal et al., "Multifunctional bioactive peptides derived from quinoa protein hydrolysates: inhibition of α -glucosidase, dipeptidyl peptidase-IV and angiotensin I converting enzymes," *Journal of Cereal Science*, vol. 96, article 103130, 2020.
- [63] R. Wang, H. Zhao, X. Pan, C. Orfila, W. Lu, and Y. Ma, "Preparation of bioactive peptides with antidiabetic, antihypertensive, and antioxidant activities and identification of α -glucosidase inhibitory peptides from soy protein," *Food Science & Nutrition*, vol. 7, no. 5, pp. 1848–1856, 2019.
- [64] N. Ktari, R. Ben Slama-Ben Salem, I. Bkhairia et al., "Functional properties and biological activities of peptides from zebra blenny protein hydrolysates fractionated using ultrafiltration," *Food Bioscience*, vol. 34, article 100539, 2020.
- [65] K. Aoki, H. Sato, and Y. Terauchi, "Usefulness of antidiabetic alpha-glucosidase inhibitors: a review on the timing of administration and effects on gut hormones," *Endocrine Journal*, vol. 66, no. 5, pp. 395–401, 2019.
- [66] Z. Yu, Y. Yin, W. Zhao, J. Liu, and F. Chen, "Anti-diabetic activity peptides from albumin against α -glucosidase and α -amylase," *Food Chemistry*, vol. 135, no. 3, pp. 2078–2085, 2012.
- [67] A. Zambrowicz, E. Eckert, M. Pokora et al., "Antioxidant and antidiabetic activities of peptides isolated from a hydrolysate

- of an egg-yolk protein by-product prepared with a proteinase from Asian pumpkin (*Cucurbita ficifolia*),” *RSC Advances*, vol. 5, no. 14, pp. 10460–10467, 2015.
- [68] S. Hu, X. Fan, P. Qi, and X. Zhang, “Identification of anti-diabetes peptides from *Spirulina platensis*,” *Journal of Functional Foods*, vol. 56, pp. 333–341, 2019.
- [69] P. A. Harnedy-Rothwell, C. M. McLaughlin, M. B. O’Keeffe et al., “Identification and characterisation of peptides from a boarfish (*Capros aper*) protein hydrolysate displaying *in vitro* dipeptidyl peptidase-IV (DPP-IV) inhibitory and insulinotropic activity,” *Food Research International*, vol. 131, article 108989, 2020.
- [70] A. B. Nongonierma and R. J. FitzGerald, “Inhibition of dipeptidyl peptidase IV (DPP-IV) by proline containing casein-derived peptides,” *Journal of Functional Foods*, vol. 5, no. 4, pp. 1909–1917, 2013.
- [71] P. A. Harnedy, V. Parthasarathy, C. M. McLaughlin et al., “Blue whiting (*Micromesistius poutassou*) muscle protein hydrolysate with *in vitro* and *in vivo* antidiabetic properties,” *Journal of Functional Foods*, vol. 40, pp. 137–145, 2018.
- [72] V. Parthasarathy, C. M. McLaughlin, P. A. Harnedy et al., “Boarfish (*Capros aper*) protein hydrolysate has potent insulinotropic and GLP-1 secretory activity *in vitro* and acute glucose lowering effects in mice,” *International Journal of Food Science and Technology*, vol. 54, no. 1, pp. 271–281, 2019.
- [73] T. Wang, L. Zheng, T. Zhao et al., “Anti-diabetic effects of sea cucumber (*Holothuria nobilis*) hydrolysates in streptozotocin and high-fat-diet induced diabetic rats via activating the PI3K/Akt pathway,” *Journal of Functional Foods*, vol. 75, article 104224, 2020.
- [74] Q. Yuan, B. Zhan, M. Du, R. Chang, T. Li, and X. Mao, “Dietary milk fat globule membrane regulates JNK and PI3K/Akt pathway and ameliorates type 2 diabetes in mice induced by a high-fat diet and streptozotocin,” *Journal of Functional Foods*, vol. 60, article 103435, 2019.
- [75] J. Wang, T. Wu, L. Fang et al., “Anti-diabetic effect by walnut (*Juglans mandshurica* Maxim.)-derived peptide LPLLRL through inhibiting α -glucosidase and α -amylase, and alleviating insulin resistance of hepatic HepG2 cells,” *Journal of Functional Foods*, vol. 69, article 103944, 2020.
- [76] T. Sartorius, A. Weidner, T. Dharsono, A. Boulier, M. Wilhelm, and C. Schön, “Postprandial Effects of a Proprietary Milk Protein Hydrolysate Containing Bioactive Peptides in Prediabetic Subjects,” *Nutrients*, vol. 11, no. 7, p. 1700, 2019.
- [77] H. F. Dale, C. Jensen, T. Hausken et al., “Effect of a cod protein hydrolysate on postprandial glucose metabolism in healthy subjects: a double-blind cross-over trial,” *Journal of Nutritional Science*, vol. 7, article e33, 2018.
- [78] S.-C. Ko, W.-K. Jung, S.-H. Lee, D. H. Lee, and Y.-J. Jeon, “Antihypertensive effect of an enzymatic hydrolysate from *Styela clavaflesh* tissue in type 2 diabetic patients with hypertension,” *Nutrition Research and Practice*, vol. 11, no. 5, pp. 396–401, 2017.
- [79] K. Musa-Veloso, L. Paulonis, T. Pelipyagina, and M. Evans, “A randomized, double-blind, placebo-controlled, multicentre trial of the effects of a shrimp protein hydrolysate on blood pressure,” *International Journal of Hypertension*, vol. 2019, Article ID 2345042, 13 pages, 2019.
- [80] N. Wu, W. Xu, K. Liu, Y. Xia, and Shuangquan, “Angiotensin-converting enzyme inhibitory peptides from *Lactobacillus delbrueckii* QS306 fermented milk,” *Journal of Dairy Science*, vol. 102, no. 7, pp. 5913–5921, 2019.
- [81] T. Nakamura, J. Mizutani, K. Ohki et al., “Casein hydrolysate containing Val-Pro-Pro and Ile-Pro-Pro improves central blood pressure and arterial stiffness in hypertensive subjects: a randomized, double-blind, placebo-controlled trial,” *Atherosclerosis*, vol. 219, no. 1, pp. 298–303, 2011.
- [82] L. Xue, X. Wang, Z. Hu et al., “Identification and characterization of an angiotensin-converting enzyme inhibitory peptide derived from bovine casein,” *Peptides*, vol. 99, pp. 161–168, 2018.
- [83] P. Zhang, C. Chang, H. Liu, B. Li, Q. Yan, and Z. Jiang, “Identification of novel angiotensin I-converting enzyme (ACE) inhibitory peptides from wheat gluten hydrolysate by the protease of *Pseudomonas aeruginosa*,” *Journal of Functional Foods*, vol. 65, article 103751, 2020.
- [84] E. B.-M. Daliri, B. H. Lee, M. H. Park, J.-H. Kim, and D.-H. Oh, “Novel angiotensin I-converting enzyme inhibitory peptides from soybean protein isolates fermented by *Pediococcus pentosaceus* SDL1409,” *LWT*, vol. 93, pp. 88–93, 2018.
- [85] S. Mäkinen, T. Streng, L. B. Larsen, A. Laine, and A. Pihlanto, “Angiotensin I-converting enzyme inhibitory and antihypertensive properties of potato and rapeseed protein-derived peptides,” *Journal of Functional Foods*, vol. 25, pp. 160–173, 2016.
- [86] C. C. Y. Sutopo, A. Sutrisno, L.-F. Wang, and J.-L. Hsu, “Identification of a potent angiotensin-I converting enzyme inhibitory peptide from black cumin seed hydrolysate using orthogonal bioassay-guided fractionations coupled with *in silico* screening,” *Process Biochemistry*, vol. 95, pp. 204–213, 2020.
- [87] P. Chen, L. Li, X. Huo et al., “New angiotensin-converting enzyme inhibitory peptide from *Coix* prolamin and its influence on the gene expression of renin-angiotensin system in vein endothelial cells,” *Journal of Cereal Science*, vol. 96, article 103099, 2020.
- [88] P. Li, J. Jia, M. Fang et al., “*In vitro* and *in vivo* ACE inhibitory of pistachio hydrolysates and *in silico* mechanism of identified peptide binding with ACE,” *Process Biochemistry*, vol. 49, no. 5, pp. 898–904, 2014.
- [89] C. Liu, L. Fang, W. Min, J. Liu, and H. Li, “Exploration of the molecular interactions between angiotensin-I-converting enzyme (ACE) and the inhibitory peptides derived from hazelnut (*Corylus heterophylla* Fisch.),” *Food Chemistry*, vol. 245, pp. 471–480, 2018.
- [90] C. Sonklin, M. A. Alashi, N. Laohakunjit, O. Kerdchoechuen, and R. E. Aluko, “Identification of antihypertensive peptides from mung bean protein hydrolysate and their effects in spontaneously hypertensive rats,” *Journal of Functional Foods*, vol. 64, article 103635, 2020.
- [91] P. García-Mora, M. Martín-Martínez, M. Angeles Bonache et al., “Identification, functional gastrointestinal stability and molecular docking studies of lentil peptides with dual antioxidant and angiotensin I converting enzyme inhibitory activities,” *Food Chemistry*, vol. 221, pp. 464–472, 2017.
- [92] J.-G. Je, H. S. Kim, H. G. Lee et al., “Low-molecular weight peptides isolated from seahorse (*Hippocampus abdominalis*) improve vasodilation via inhibition of angiotensin-converting enzyme *in vivo* and *in vitro*,” *Process Biochemistry*, vol. 95, pp. 30–35, 2020.
- [93] S. Khueychai, N. Jangpromma, K. Choowongkamon et al., “A novel ACE inhibitory peptide derived from alkaline

- hydrolysis of ostrich (*Struthio camelus*) egg white ovalbumin," *Process Biochemistry*, vol. 73, pp. 235–245, 2018.
- [94] J. K. Lee, J. K. Jeon, and H. G. Byun, "Antihypertensive effect of novel angiotensin I converting enzyme inhibitory peptide from chum salmon (*Oncorhynchus keta*) skin in spontaneously hypertensive rats," *Journal of Functional Foods*, vol. 7, pp. 381–389, 2014.
- [95] D.-H. Ngo, K. H. Kang, B. M. Ryu et al., "Angiotensin-I converting enzyme inhibitory peptides from antihypertensive skate (*Okamejei kenoei*) skin gelatin hydrolysate in spontaneously hypertensive rats," *Food Chemistry*, vol. 174, pp. 37–43, 2015.
- [96] R. Balti, A. Bougatef, A. Sila, D. Guillochon, P. Dhulster, and N. Nedjar-Arroume, "Nine novel angiotensin I-converting enzyme (ACE) inhibitory peptides from cuttlefish (*Sepia officinalis*) muscle protein hydrolysates and antihypertensive effect of the potent active peptide in spontaneously hypertensive rats," *Food Chemistry*, vol. 170, pp. 519–525, 2015.
- [97] M. Guo, X. Chen, Y. Wu et al., "Angiotensin I-converting enzyme inhibitory peptides from *Sipuncula (Phascolosoma esculenta)*: Purification, identification, molecular docking and antihypertensive effects on spontaneously hypertensive rats," *Process Biochemistry*, vol. 63, pp. 84–95, 2017.
- [98] C. Zhang, Y. Zhang, Z. Wang, S. Chen, and Y. Luo, "Production and identification of antioxidant and angiotensin-converting enzyme inhibition and dipeptidyl peptidase IV inhibitory peptides from bighead carp (*Hypophthalmichthys nobilis*) muscle hydrolysate," *Journal of Functional Foods*, vol. 35, pp. 224–235, 2017.
- [99] S. Y. Lee and S. J. Hur, "Purification of novel angiotensin converting enzyme inhibitory peptides from beef myofibrillar proteins and analysis of their effect in spontaneously hypertensive rat model," *Biomedicine & Pharmacotherapy*, vol. 116, p. 109046, 2019.
- [100] I. Jemil, L. Mora, R. Nasri et al., "A peptidomic approach for the identification of antioxidant and ACE-inhibitory peptides in sardinelle protein hydrolysates fermented by *Bacillus subtilis* A26 and *Bacillus amyloliquefaciens* An6," *Food Research International*, vol. 89, Part 1, pp. 347–358, 2016.
- [101] D. Furman, J. Campisi, E. Verdin et al., "Chronic inflammation in the etiology of disease across the life span," *Nature Medicine*, vol. 25, no. 12, pp. 1822–1832, 2019.
- [102] M. Oyama, T. van Hung, K. Yoda, F. He, and T. Suzuki, "A novel whey tetrapeptide IPAV reduces interleukin-8 production induced by TNF- α in human intestinal Caco-2 cells," *Journal of Functional Foods*, vol. 35, pp. 376–383, 2017.
- [103] X. Wang, Y. Zhao, Y. Yao et al., "Anti-inflammatory activity of di-peptides derived from ovotransferrin by simulated peptide-cut in TNF- α -induced Caco-2 cells," *Journal of Functional Foods*, vol. 37, pp. 424–432, 2017.
- [104] S. Chakrabarti, F. Jahandideh, and J. Wu, "Food-derived bioactive peptides on inflammation and oxidative stress," *BioMed Research International*, vol. 2014, Article ID 608979, 11 pages, 2014.
- [105] S. Li, L. Liu, G. He, and J. Wu, "Molecular targets and mechanisms of bioactive peptides against metabolic syndromes," *Food & Function*, vol. 9, no. 1, pp. 42–52, 2018.
- [106] C. Dai, L. Dai, F. J. Yu et al., "Chemical and biological characteristics of hydrolysate of crucian carp swim bladder: focus on preventing ulcerative colitis," *Journal of Functional Foods*, vol. 75, article 104256, 2020.
- [107] A. Mukhopadhyaya, N. Noronha, B. Bahar et al., "Anti-inflammatory effects of a casein hydrolysate and its peptide-enriched fractions on TNF α -challenged Caco-2 cells and LPS-challenged porcine colonic explants," *Food Science & Nutrition*, vol. 2, no. 6, pp. 712–723, 2014.
- [108] J. Kovacs-Nolan, H. Zhang, M. Ibuki et al., "The PepT1-transportable soy tripeptide VPY reduces intestinal inflammation," *Biochimica et Biophysica Acta (BBA) - General Subjects*, vol. 1820, no. 11, pp. 1753–1763, 2012.
- [109] Q. Liang, X. Ren, M. Chalamaiah, and H. Ma, "Simulated gastrointestinal digests of corn protein hydrolysate alleviate inflammation in caco-2 cells and a mouse model of colitis," *Journal of Food Science and Technology*, vol. 57, no. 6, pp. 2079–2088, 2020.
- [110] M. Zhang, Y. Zhao, Y. Yao et al., "Isolation and identification of peptides from simulated gastrointestinal digestion of preserved egg white and their anti-inflammatory activity in TNF- α -induced Caco-2 cells," *The Journal of Nutritional Biochemistry*, vol. 63, pp. 44–53, 2019.
- [111] M. Zhang, Y. Zhao, N. Wu et al., "The anti-inflammatory activity of peptides from simulated gastrointestinal digestion of preserved egg white in DSS-induced mouse colitis," *Food & Function*, vol. 9, no. 12, pp. 6444–6454, 2018.
- [112] T. Liu, L. Zhang, D. Joo, and S. C. Sun, "NF- κ B signaling in inflammation," *Signal Transduction and Targeted Therapy*, vol. 2, no. 1, article 17023, 2017.
- [113] Y. Chen, H. Zhang, L. Mats et al., "Anti-inflammatory effect and cellular uptake mechanism of peptides from common bean (*Phaseolus vulga* L.) milk and yogurts in Caco-2 mono- and Caco-2/EA.hy926 co-culture models," *Journal of Agricultural and Food Chemistry*, vol. 67, no. 30, pp. 8370–8381, 2019.
- [114] M. Memarpoor-Yazdi, H. Mahaki, and H. Zare-Zardini, "Antioxidant activity of protein hydrolysates and purified peptides from *Zizyphus jujuba* fruits," *Journal of Functional Foods*, vol. 5, no. 1, pp. 62–70, 2013.
- [115] L. Wang, L. Ding, Z. Yu, T. Zhang, S. Ma, and J. Liu, "Intracellular ROS scavenging and antioxidant enzyme regulating capacities of corn gluten meal-derived antioxidant peptides in HepG2 cells," *Food Research International*, vol. 90, pp. 33–41, 2016.
- [116] P. A. Harnedy, M. B. O'Keeffe, and R. J. FitzGerald, "Fractionation and identification of antioxidant peptides from an enzymatically hydrolysed *Palmaria palmata* protein isolate," *Food Research International*, vol. 100, Part 1, pp. 416–422, 2017.
- [117] Z. Karami, S. H. Peighambari, J. Hesari, B. Akbari-Adergani, and D. Andreu, "Antioxidant, anticancer and ACE-inhibitory activities of bioactive peptides from wheat germ protein hydrolysates," *Food Bioscience*, vol. 32, article 100450, 2019.
- [118] J. Tkaczewska, B. Borczak, E. Piątkowska, J. Kapusta-Duch, M. Morawska, and T. Czech, "Effect of protein hydrolysates from carp (*Cyprinus carpio*) skin gelatine on oxidative stress biomarkers and other blood parameters in healthy rats," *Journal of Functional Foods*, vol. 60, article 103411, 2019.
- [119] M. Kumar, T. Ahmad, A. Sharma et al., "Let-7 microRNA-mediated regulation of IL-13 and allergic airway inflammation," *The Journal of Allergy and Clinical Immunology*, vol. 128, no. 5, pp. 1077–1085.e10, 2011.
- [120] K. M. I. Bashir, J. H. Sohn, J. S. Kim, and J. S. Choi, "Identification and characterization of novel antioxidant peptides

- from mackerel (*Scomber japonicus*) muscle protein hydrolysates," *Food Chemistry*, vol. 323, article 126809, 2020.
- [121] Z. Ji, J. Mao, S. Chen, and J. Mao, "Antioxidant and anti-inflammatory activity of peptides from foxtail millet (*Setaria italica*) prolamins in HaCaT cells and RAW264.7 murine macrophages," *Food Bioscience*, vol. 36, article 100636, 2020.
- [122] Z. Wang, X. Liu, H. Xie et al., "Antioxidant activity and functional properties of Alcalase-hydrolyzed scallop protein hydrolysate and its role in the inhibition of cytotoxicity *in vitro*," *Food Chemistry*, vol. 344, p. 128566, 2021.
- [123] M.-J. Tsou, F. J. Kao, C. K. Tseng, and W. D. Chiang, "Enhancing the anti-adipogenic activity of soy protein by limited hydrolysis with flavourzyme and ultrafiltration," *Food Chemistry*, vol. 122, no. 1, pp. 243–248, 2010.
- [124] M.-R. Kim, J. W. Kim, J. B. Park, Y. K. Hong, S. K. Ku, and J. S. Choi, "Anti-obesity effects of yellow catfish protein hydrolysate on mice fed a 45% kcal high-fat diet," *International Journal of Molecular Medicine*, vol. 40, no. 3, pp. 784–800, 2017.
- [125] S. Jafar, H. Kamal, P. Mudgil, H. M. Hassan, and S. Maqsood, "Camel whey protein hydrolysates displayed enhanced cholesterol esterase and lipase inhibitory, anti-hypertensive and anti-haemolytic properties," *LWT*, vol. 98, pp. 212–218, 2018.
- [126] M. Woo, Y. Song, K. H. Kang, and J. Noh, "Anti-obesity effects of collagen peptide derived from skate (*Raja kenoujei*) skin through regulation of lipid metabolism," *Marine Drugs*, vol. 16, no. 9, p. 306, 2018.
- [127] Y.-T. Tung, H. L. Chen, H. S. Wu, M. H. Ho, K. Y. Chong, and C. M. Chen, "Kefir peptides prevent hyperlipidemia and obesity in high-fat-diet-induced obese rats via lipid metabolism modulation," *Molecular Nutrition & Food Research*, vol. 62, no. 3, article 1700505, 2018.
- [128] Z. Shi, Y. Hao, C. Teng, Y. Yao, and G. Ren, "Functional properties and adipogenesis inhibitory activity of protein hydrolysates from quinoa (*Chenopodium quinoa* Willd.)," *Food Science & Nutrition*, vol. 7, no. 6, pp. 2103–2112, 2019.
- [129] D. Fangmann, C. Geisler, K. Schlicht et al., "Differential effects of protein intake versus intake of a defined oligopeptide on FGF-21 in obese human subjects *in vivo*," *Clinical Nutrition*, vol. 40, no. 2, pp. 600–607, 2020.
- [130] T. Hatanaka, Y. Inoue, J. Arima et al., "Production of dipeptidyl peptidase IV inhibitory peptides from defatted rice bran," *Food Chemistry*, vol. 134, no. 2, pp. 797–802, 2012.
- [131] T. Lafarga, P. O'Connor, and M. Hayes, "Identification of novel dipeptidyl peptidase-IV and angiotensin-I-converting enzyme inhibitory peptides from meat proteins using *in silico* analysis," *Peptides*, vol. 59, pp. 53–62, 2014.
- [132] S.-L. Huang, C.-C. Hung, C.-L. Jao, Y.-S. Tung, and K.-C. Hsu, "Porcine skin gelatin hydrolysate as a dipeptidyl peptidase IV inhibitor improves glycemic control in streptozotocin-induced diabetic rats," *Journal of Functional Foods*, vol. 11, pp. 235–242, 2014.
- [133] L. Mojica, E. Gonzalez de Mejia, M. Á. Granados-Silvestre, and M. Menjivar, "Evaluation of the hypoglycemic potential of a black bean hydrolyzed protein isolate and its pure peptides using *in silico*, *in vitro* and *in vivo* approaches," *Journal of Functional Foods*, vol. 31, pp. 274–286, 2017.
- [134] M. Kato, T. Nakanishi, T. Tani, and T. Tsuda, "Low-molecular fraction of wheat protein hydrolysate stimulates glucagon-like peptide-1 secretion in an enteroendocrine L cell line and improves glucose tolerance in rats," *Nutrition Research*, vol. 37, pp. 37–45, 2017.
- [135] F. Wang, Y. Zhang, T. Yu et al., "Oat globulin peptides regulate antidiabetic drug targets and glucose transporters in Caco-2 cells," *Journal of Functional Foods*, vol. 42, pp. 12–20, 2018.
- [136] E. Valencia-Mejía, K. A. Batista, J. J. A. Fernández, and K. F. Fernandes, "Antihyperglycemic and hypoglycemic activity of naturally occurring peptides and protein hydrolysates from easy-to-cook and hard-to-cook beans (*Phaseolus vulgaris* L.)," *Food Research International*, vol. 121, pp. 238–246, 2019.
- [137] K. Wang, X. Yang, W. Lou, and X. Zhang, "Discovery of dipeptidyl peptidase 4 inhibitory peptides from Largemouth bass (*Micropterus salmoides*) by a comprehensive approach," *Bioorganic Chemistry*, vol. 105, article 104432, 2020.
- [138] C. Jia, N. Hussain, O. Joy Ujiroghene et al., "Generation and characterization of dipeptidyl peptidase-IV inhibitory peptides from trypsin-hydrolyzed α -lactalbumin-rich whey proteins," *Food Chemistry*, vol. 318, article 126333, 2020.
- [139] C. M. McLaughlin, S. J. Sharkey, P. Harnedy-Rothwell et al., "Twice daily oral administration of *Palmaria palmata* protein hydrolysate reduces food intake in streptozotocin induced diabetic mice, improving glycaemic control and lipid profiles," *Journal of Functional Foods*, vol. 73, article 104101, 2020.
- [140] H. Li, N. Prairie, C. C. Udenigwe et al., "Blood pressure lowering effect of a pea protein hydrolysate in hypertensive rats and humans," *Journal of Agricultural and Food Chemistry*, vol. 59, no. 18, pp. 9854–9860, 2011.
- [141] D. Young, M. Ibuki, T. Nakamori, M. Fan, and Y. Mine, "Soy-derived Di- and tripeptides alleviate colon and ileum inflammation in pigs with dextran sodium sulfate-induced colitis," *The Journal of Nutrition*, vol. 142, no. 2, pp. 363–368, 2012.
- [142] T. Grimstad, B. Bjørndal, D. Cacabelos et al., "A salmon peptide diet alleviates experimental colitis as compared with fish oil," *Journal of Nutritional Science*, vol. 2, p. e2, 2013.
- [143] Y. Shi, P. Rupa, B. Jiang, and Y. Mine, "Hydrolysate from eggshell membrane ameliorates intestinal inflammation in mice," *International Journal of Molecular Sciences*, vol. 15, no. 12, pp. 22728–22742, 2014.
- [144] S. K. Ramadass, S. L. Jabaris, R. K. Perumal, V. I. HairulIslam, A. Gopinath, and B. Madhan, "Type I collagen and its daughter peptides for targeting mucosal healing in ulcerative colitis: a new treatment strategy," *European Journal of Pharmaceutical Sciences*, vol. 91, pp. 216–224, 2016.
- [145] Y. Zhao, Y. Yao, M. Xu, S. Wang, X. Wang, and Y. Tu, "Simulated gastrointestinal digest from preserved egg white exerts anti-inflammatory effects on Caco-2 cells and a mouse model of DSS-induced colitis," *Journal of Functional Foods*, vol. 35, pp. 655–665, 2017.

Research Article

Dietary Bioactive Peptide Alanyl-Glutamine Attenuates Dextran Sodium Sulfate-Induced Colitis by Modulating Gut Microbiota

Qingbiao Xu ¹, Mingyang Hu,¹ Min Li,¹ Jinxiu Hou ¹, Xianghua Zhang,¹ Ya Gao,¹
Bahram Chachar,² and Xiang Li ¹

¹College of Animal Sciences and Technology, Huazhong Agricultural University, Wuhan 430070, China

²Department of Animal Nutrition, Faculty of Veterinary and Animal Sciences, Lasbela University of Agriculture, Water and Marine Sciences, Uthal, Balochistan 90150, Pakistan

Correspondence should be addressed to Xiang Li; xxiangli@mail.hzau.edu.cn

Received 14 January 2021; Revised 6 April 2021; Accepted 23 April 2021; Published 10 May 2021

Academic Editor: Si Qin

Copyright © 2021 Qingbiao Xu et al. This is an open access article distributed under the Creative Commons Attribution License, which permits unrestricted use, distribution, and reproduction in any medium, provided the original work is properly cited.

Inflammatory bowel disease (IBD) is a chronic intestinal disorder threatening human health. Di-peptide alanyl-glutamine (Ala-Gln) has various beneficial effects on gut health. However, its role and functional mechanism in treating IBD are still not clear. Therefore, the protective effects of Ala-Gln and glutamine (Gln) on dextran sulfate sodium- (DSS-) induced colitic mice were investigated in this study. The results showed that oral supplementation of Ala-Gln or Gln significantly attenuated the colitis symptoms in mice, including body weight loss, colon length, disease activity index, histological scores, and tissue apoptosis. The concentrations of interleukin- (IL-) 1 β , IL-6, tumor necrosis factor- α , and myeloperoxidase were significantly decreased, while the concentrations of immunoglobulins (IgA, IgG, and IgM) and superoxide dismutase were significantly increased by Ala-Gln or Gln supplementation. The expression of occludin and peptide transporter 1 (PepT1) was significantly increased by Ala-Gln or Gln. Interestingly, Ala-Gln had better beneficial effects than Gln in alleviating colitis. In addition, 16S rDNA sequencing showed that the DSS-induced shifts of the microbiome (community diversity, evenness, richness, and composition) in the mouse colon were restored by Gln and Ala-Gln, including *Lactobacillus*, *Bacteroides_acidifaciens*, *Bacteroidales*, *Firmicutes*, *Clostridia*, *Helicobacter*, and *Bacteroides*. Correspondingly, the functions of the microflora metabolism pathways were also rescued by Ala-Gln, including fatty acid metabolism, membrane transporters, infectious diseases, and immune system. In conclusion, the results revealed that Ala-Gln can prevent colitis through PepT1, enhancing the intestinal barrier and modulating gut microbiota and microflora metabolites.

1. Introduction

Inflammatory bowel disease (IBD, including ulcerative colitis) is a chronic gastrointestinal disorder caused by inflammation or oxidative stress in the colon, which has threatened the human health and has various colitis symptoms, such as gut bleeding, bloody diarrhea, body weight (BW) loss, epithelial cell loss, neutrophil infiltration, and the release of proinflammatory mediators (e.g., interleukin- (IL-) 1 β , IL-4, IL-5, IL-6, IL-8, and tumor necrosis factor- (TNF-) α) [1]. However, the use of drugs to treat IBDs often has side effects. The application of bioactive peptides with the

potential to manage chronic intestinal inflammation comes into people's view [1].

Glutamine (Gln) is a well-studied amino acid with immune-modulating effects [2, 3], and it can alleviate intestinal inflammation [4]. The Gln can be utilized to maintain the intestinal structure and function [5], and it also can mediate protein synthesis by intestinal microorganisms [6]. Gln used in human and animal studies is often in the form of alanyl-glutamine (Ala-Gln) [3]. However, the difference of the effects between Ala-Gln and Gln is still not clear. Intriguingly, Ala-Gln has a superior preventive effect on intestinal damage with more mucosal weight, protein content, and

villus height than those in mice with alanine plus Gln mixture [7]. Ala-Gln had a better effect on improving enterocyte proliferation than Gly-Gln or Gln [8]. In other words, Ala-Gln may serve as a bioactive peptide and has better effects than Gln or alanine alone.

It was reported that Ala-Gln can alleviate inflammation via inhibiting cytokine expression and regulating T cells in colitic mice [3, 9, 10] and alleviates the allergic inflammation of the airways and lungs through modulating gut microbiota and their metabolites in mice [11]. The Ala-Gln can attenuate metabolic stress, enhance immunity [12], and inhibit intestinal mucositis in mice [13]. In addition, Ala-Gln can also improve the gastrointestinal epithelial structure and immune status of early-weaned calves [14]. In a number of studies, dextran sulfate sodium- (DSS-) induced mouse colitis is a widely used model to study IBD with the features of ulcerative colitis [1, 15]. The peptide Ala-Gln has attracted an increasing interest of scientists. However, the role and functional mechanism of Ala-Gln on colitis are still unclear, particularly in the gut microbiota. Therefore, the objective of this study is to explore the effects of Ala-Gln on DSS-induced acute colitis in mice.

2. Materials and Methods

2.1. Mouse Treatment. Forty male mice (6-7 weeks old; Institute of Cancer Research; body weight (BW), 28-32 g) were obtained from Liaoning Changsheng Biotechnology Co., Ltd. (Benxi, China). Ala-Gln was obtained from Wuhan Jetide Biotech Co., Ltd. (Wuhan, China). The DSS was purchased from Sangon Biotech Co., Ltd. (A600160-0250, Shanghai, China). Mice were randomly assigned to four groups ($n=10$): control, DSS, DSS+Gln (Gln), and DSS+Ala-Gln (Ala-Gln). Mice in the Gln or Ala-Gln group received Gln (2.5%, w/v , 500 mg Gln/kg BW/d) or Ala-Gln (3.75%, w/v , 750 mg Ala-Gln/kg BW/d, equivalent to 500 mg Gln/kg BW/d) dissolved in sterilized distilled water by daily intragastric gavage from day 1 to 14. From day 8 to 14, the mice in DSS, Gln, and Ala-Gln groups were given 3% DSS (w/v) in water. Mice were kept under the controlled conditions of 12 h light/dark, constant temperature (25°C), and humidity (50 ± 5%). The amount of Gln and Ala-Gln given to mice is a safe dose used in clinical studies [10, 15].

2.2. Disease Activity Index (DAI) and Colon Histologic Analysis. The DAI was assessed with the score sum according to BW loss, stool consistency and bleeding, and mouse condition as previous reports [16, 17]. After sacrificing mice on day 15, the colon length was measured, and the colon tissue (~3.5 cm proximal to the anus) was fixed with 10% buffered formalin and stained with hematoxylin and eosin (HE) to obtain the morphology structure. The tissue damage was evaluated using the degree of inflammatory cell infiltration based on previous descriptions [16, 18]. In addition, the cell apoptotic level was assessed by the terminal deoxynucleotidyl transferase dUTP nick end labeling (TUNEL) assay by using a cell death detection kit with the nuclei stained with DAPI (Roche, Basel, Switzerland). The morphology was observed using fluorescent microscopy (DMIL LED, Leica, Germany).

2.3. Enzyme-Linked Immunosorbent Assay (ELISA). The serum was obtained with blood being centrifuged for 15 min at 1500 g. The concentrations of immunoglobulin (Ig) A, IgG, and IgM in the serum were detected by using ELISA kits (Nanjing Jiancheng Bioengineering Institute, Nanjing, China). The contents of IL-1 β , IL-6, TNF- α , superoxide dismutase (SOD), and myeloperoxidase (MPO) in colon tissues were measured by using ELISA kits according to the manufacturer's instructions [19]. The content of tissue protein was measured using the Bicinchoninic Acid Protein Assay Kit (P0011, Beyotime, Shanghai, China) and analyzed using a microplate reader (Bio-Rad, 680, Hercules, CA, USA).

2.4. Western Blot. Colon tissue was lysed using radioimmuno-precipitation assay lysis buffer (P0013B, Beyotime, Shanghai, China) and PMSF (ST506, Beyotime, Shanghai, China), and the lysate was homogenized and centrifuged to obtain the supernatant. The sample in the supernatant with loading buffer (SibEnzyme, Russia) was kept at 95°C to denature the protein. The sample was condensed and separated via the appropriate concentration of SDS gel electrophoresis and then transferred to a PVDF membrane (Sigma-Aldrich, UK), which was then blocked in 5% BSA. After being washed using TBST buffer, the PVDF membrane was incubated with primary antibodies at 4°C overnight (1:1000), including β -actin (4970S, CST), PepT1 (sc-373742, Santa Cruz, CA, USA), occludin (sc-133255, Santa Cruz, CA, USA), extracellular signal-regulated kinase (ERK; CST 4695S), pERK (CST 4370S), p38 (CST 8690S), pp38 (CST 4511S), c-Jun N-terminal kinase (JNK; CST 3708S), and pJNK (CST 9255S). Subsequently, the membrane was incubated with an HRP-conjugated secondary antibody (1:8000, CST, Danvers, MA, USA). The bands were observed by using Chemiluminescence software (Baygene Biotech, China) with fluorescence excited using HRP-conjugated ECL Western Blotting Substrate (Tanon, Shanghai, China). Band intensity was measured using ImageJ software (NIH, USA) and normalized using β -actin.

2.5. Gut Microbiota. The DNA of mouse colon luminal content was extracted by using the QIAamp DNA Stool Mini Kit (Qiagen, Hilden, Germany). The primers targeting V3 to V4 regions of the 16S rDNA sequence were amplified using polymerase chain reaction (PCR). The PCR products were purified using Agencourt AMPure XP and sequenced using a HiSeq platform. The raw data was filtered, and the Operational Taxonomic Units (OTUs; >97% similarity) were clustered by using USEARCH and the data was analyzed by using an RDP classifier (>80% confidence). The diversity indices of alpha and beta were analyzed using Quantitative Insights into Microbial Ecology (QIIME; <http://qiime.org/>). The distances among samples were computed using principal component analysis (PCA) and partial least squares discriminant analysis (PLS-DA). In addition, linear discriminant analysis (LDA) effect size (LEfSe) was used to determine taxa, which can characterize each population (LDA score > 4) to discover biomarkers. A Venn diagram was drawn by using R software and used to present OTU overlap among samples. Additionally, the cladogram plot was drawn using Figure

Tree software to identify corresponding group biomarkers (<http://tree.bio.ed.ac.uk/software/figtree/>). The taxonomical levels were carried out at the phylum, class, order, genus, and species levels. Moreover, the function of the metagenome was predicted using Phylogenetic Investigation of Communities by Reconstruction of Unobserved States (PICRUSt; <http://picrust.github.com>) and Kyoto Encyclopedia of Genes and Genomes (KEGG) levels 1, 2, and 3.

2.6. Statistical Analysis. Data analysis was performed by Student's *t*-test between two groups and one-way ANOVA followed by Tukey's comparison among multiple groups by using SPSS software (SPSS Inc., Chicago, IL, USA). The results were presented as means \pm standard error of mean (SEM). $p < 0.05$ was considered statistically significant.

3. Results

3.1. Ala-Gln Alleviated DSS-Induced Mouse Colitis. The experiment was carried out according to a timeline as shown in Figure 1(a). Colitis symptoms had appeared in mice after oral treatment with DSS for a week, including low BW (Figure 1(b)), short colon length (Figure 1(c)), and high DAI (Figure 1(d)). However, the BW and colon length were significantly upregulated by Ala-Gln ($p < 0.05$) (Figures 1(b) and 1(c)). The DSS-induced high DAI was significantly decreased by Ala-Gln ($p < 0.05$) (Figure 1(d)). However, the treatment of Gln did not significantly alleviate DSS-induced mouse colitis. These results suggested that the DSS-induced colitis symptom was dramatically alleviated by Ala-Gln.

3.2. Colon Tissue Damage and Apoptosis. The challenge with DSS in mice damaged colon tissue as shown in HE staining morphology, including crypt loss and leukocyte infiltration; however, these damage signs were attenuated by Gln and Ala-Gln. DSS challenge increased the colon histological index. Interestingly, this increase was significantly ameliorated by Gln and Ala-Gln (Figure 2(a)). In addition, DSS treatment enhanced colon apoptosis as shown in TUNEL-positive nuclei; however, this increase was significantly counteracted by Gln and Ala-Gln (Figure 2(b)). These results indicated that Gln and Ala-Gln restored the DSS-induced colon damage.

3.3. Effects of Ala-Gln on Inflammatory Mediators and Immunoglobulins. The contents of inflammatory mediators IL-1 β , IL-6, and TNF- α in colon tissue of DSS-challenged mice were significantly reduced by Gln or Ala-Gln supplementation ($p < 0.05$) (Figures 3(a)–3(c)). The concentrations of immunoglobulins IgA, IgG, and IgM in serum were significantly increased by Ala-Gln ($p < 0.05$) (Figures 3(d)–3(f)). In mouse colon tissues, SOD activity was significantly increased and MPO concentration was significantly decreased by Ala-Gln administration ($p < 0.05$) (Figures 3(g) and 3(h)). These results indicated that Gln and Ala-Gln rescued the immunity status of mice. However, IL-1 β , TNF- α , IgG, SOD, and MPO were not significantly affected by Gln, indicating that Gln is not so effective as Ala-Gln to suppress DSS-induced colitis.

3.4. Western Blot. The expression of the tight junction (TJ) protein occludin was significantly increased by Gln and Ala-Gln ($p < 0.05$) (Figures 4(a) and 4(b)), indicating that the intestinal barrier was enhanced by Gln and Ala-Gln to alleviate the colitis. The expression of the peptide transporter PepT1 (Figures 4(a) and 4(c)) was also significantly upregulated by Gln and Ala-Gln ($p < 0.05$), indicating that PepT1 was involved in colitis alleviation by Ala-Gln. However, no significant difference was detected in the expression of phosphorylation MAPK signaling (p38, JNK, and ERK) (data not shown), suggesting that the MAPK signaling pathway was not involved in alleviating intestinal inflammation of Ala-Gln.

3.5. Gut Microbiota. The colon microbial community of mice was analyzed by the 16S rDNA phylogenetic method with OTU similarity higher than 97%. Alpha diversity of the microbial communities was estimated by using Shannon and Simpson indices. The Shannon index was significantly decreased by DSS treatment ($p < 0.01$), while the Simpson index was significantly increased by DSS ($p < 0.05$), indicating that DSS decreased the diversity of gut microbial community of mice (Figures 5(a) and 5(b)). Moreover, this decrease was drastically rescued by both Gln and Ala-Gln. The microbiota structure was analyzed by PCA, which showed that the gut microbiota was separated by DSS, Gln, and Ala-Gln treatments (Figures 5(c) and 5(d)). Compared with the DSS group, gut microbiota was separated by Gln and Ala-Gln treatments using OTU-based partial least squares discriminant analysis (PLS-DA) (Figure 5(d)). In addition, the Venn diagram illustrated that 261 universal OTUs were detected out of 521 total OTUs in all samples. There were 105, 6, 3, and 11 unique OTUs in control (total 432), DSS (total 346), Gln (total 356), and Ala-Gln (total 381) groups, respectively (Figure 5(e)). The key bacterial alterations in the taxonomic cladogram showed that *Sphingobacteriaceae*, *Sphingobacteriales*, *Sphingobacteria*, *Turicibacteraceae*, and *Turicibacterales* were the unique cluster markers in the Gln group (Figure 5(f)). The LDA score of taxon abundance illustrated that DSS treatment significantly increased the abundances of *Dorea* and *DeFluviitalea*, while Gln significantly increased the abundances of *Ruminococcus* and *Coprococcus* ($p < 0.05$), and Ala-Gln significantly increased *p_75_a5* abundance ($p < 0.05$). Notably, compared with the control group, DSS challenge in all other groups significantly decreased the abundance of probiotics, such as *Prevotellaceae*, *Lactobacillales*, *Lactobacillaceae*, and *Lactobacillus* ($p < 0.05$, Figure 5(g)).

The *Firmicutes* and *Bacteroidetes* were the predominant bacteria at the phylum level, and *Clostridia* and *Bacteroidia* were the predominant bacteria at the class level, while *Clostridia* and *Bacteroidales* were the predominant bacteria at the order level (Figures 6(a)–6(c)). At the phylum level, *Bacteroidetes* abundance and the ratio of *Bacteroidetes*/*Firmicutes* were significantly decreased by Gln and Ala-Gln ($p < 0.05$, Figure 6(a)). At the class level, *Clostridia* abundance was significantly increased by Gln, while the abundances of *Bacteroidia* and *Epsilonproteobacteria* were significantly decreased by Gln or Ala-Gln ($p < 0.05$, Figure 6(b)). At the order level, the abundance of *Clostridiales* was significantly increased by Gln, while the abundances of *Bacteroidales* and

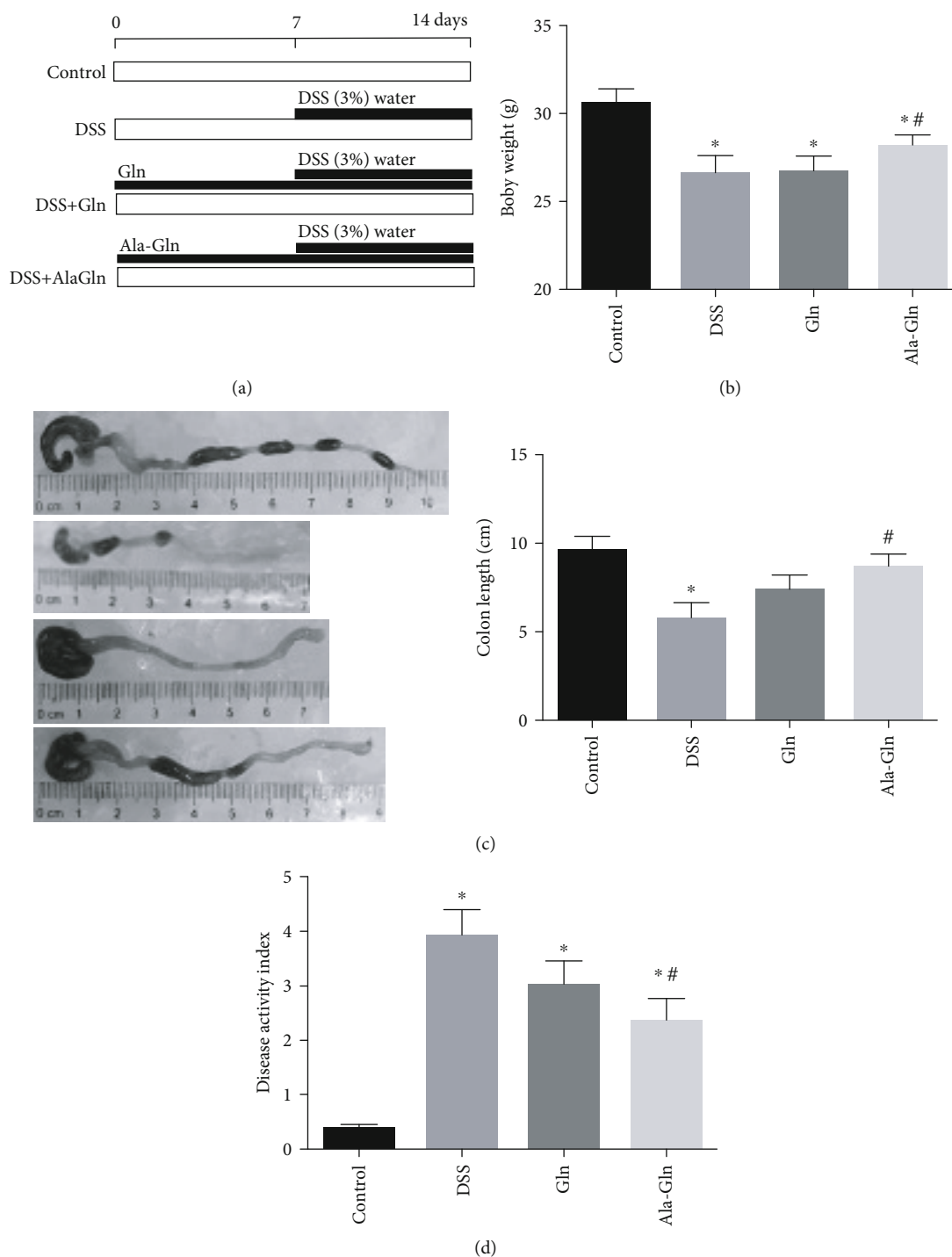


FIGURE 1: Supplementations of Gln and Ala-Gln attenuated the mouse colitis symptoms induced by DSS. (a) Experimental timeline. (b) Body weight. (c) Colon length. (d) Disease activity index. Results were shown as means \pm SEM ($n = 6$). * $p < 0.05$ versus control group; # $p < 0.05$ versus DSS group.

Campylobacterales (gastrointestinal pathogens) were significantly decreased by Gln or Ala-Gln ($p < 0.05$, Figure 6(c)). At the genus level, the abundances of pathogens *Helicobacter* spp. and *Bacteroides* spp. were increased by DSS challenge, while they were significantly decreased by Gln or Ala-Gln to counteract DSS-induced increases ($p < 0.05$, Figure 6(d)). At the species level, the abundance of *Bacteroides_acidifaciens*

was significantly increased by DSS challenge, while it was significantly decreased by Gln ($p < 0.05$, Figure 6(e)). These results indicated that the DSS-induced change of gut microbiota was restored by Gln and Ala-Gln.

3.6. Effects of Ala-Gln on Metabolism Pathways of Gut Microbial Community. The metabolism of microbial

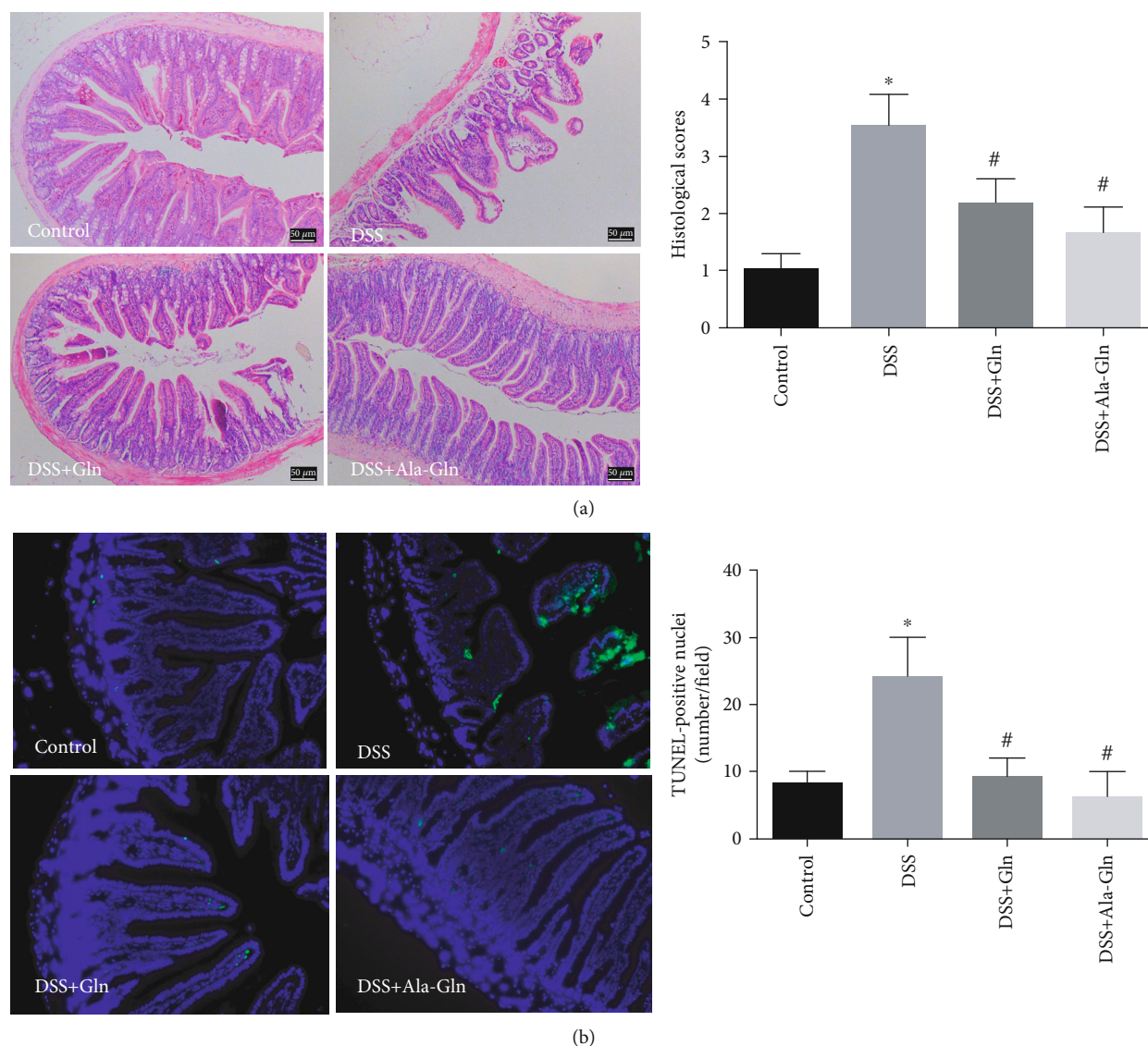


FIGURE 2: Supplementations of Gln and Ala-Gln rescued DSS-induced mouse colon histological damage. (a) The HE staining micrographs and histological scoring of mouse colon morphology. Bar = 50 μm . (b) Fluorescent micrographs and quantitation of TUNEL (green) and DAPI (blue) of colon tissue. Bar = 100 μm . Results were shown as means \pm SEM ($n = 6$). * $p < 0.05$ versus control group; # $p < 0.05$ versus DSS group.

communities was predicted by PICRUSt. At KEGG level 1, the function of environmental information processing was significantly enhanced by Ala-Gln compared with DSS treatment ($p < 0.05$, Figure 7(a)). At KEGG level 2, the functions of membrane transport and enzyme families were significantly enhanced by Ala-Gln ($p < 0.05$, Figure 7(b)). However, the functions of replication and repair, genetic information processing, infectious diseases, immune system, and glycan biosynthesis and metabolism were significantly inhibited by Ala-Gln ($p < 0.05$, Figure 7(b)). At KEGG level 3, compared with the DSS group, the metabolism functions of transporters, ABC transporters, and biosynthesis of ansamycins were significantly enhanced by Ala-Gln treatment. However, the functions of DNA replication proteins, fatty acid biosynthesis, propanoate metabolism, folate biosynthesis, epithelial cell signaling in *Helicobacter pylori* infection, polycyclic aro-

matic hydrocarbon degradation, restriction enzyme, and bacterial toxins were significantly inhibited by Ala-Gln compared with the DSS treatment ($p < 0.05$, Figure 7(c)).

From the above results, the underlying mechanism of Ala-Gln in alleviating colitis of mice can be concluded as follows: (1) the transport of Ala-Gln via PepT1 into intestinal epithelial cells, (2) the decrease in IL-1 β , IL-6, TNF- α , and MPO and the increase in IgA, IgG, IgM, and SOD, and (3) the normalization of microbiota and microbial metabolism (Figure 8).

4. Discussion

The IBD is a complex chronic intestinal inflammation associated with the nutrition and gut microbiome [1]. As we know, the use of drugs to manage IBD has many side effects. It was

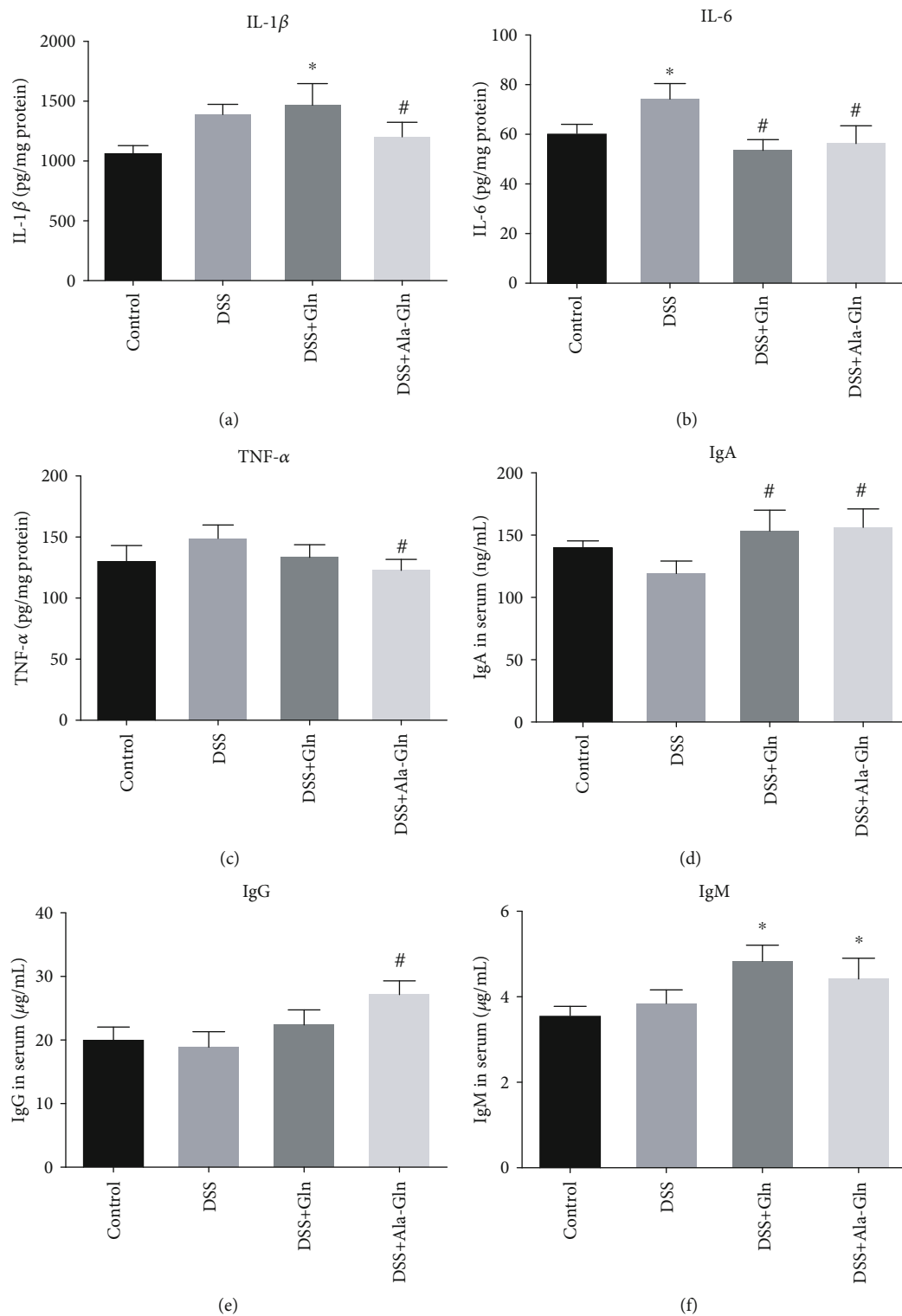


FIGURE 3: Continued.

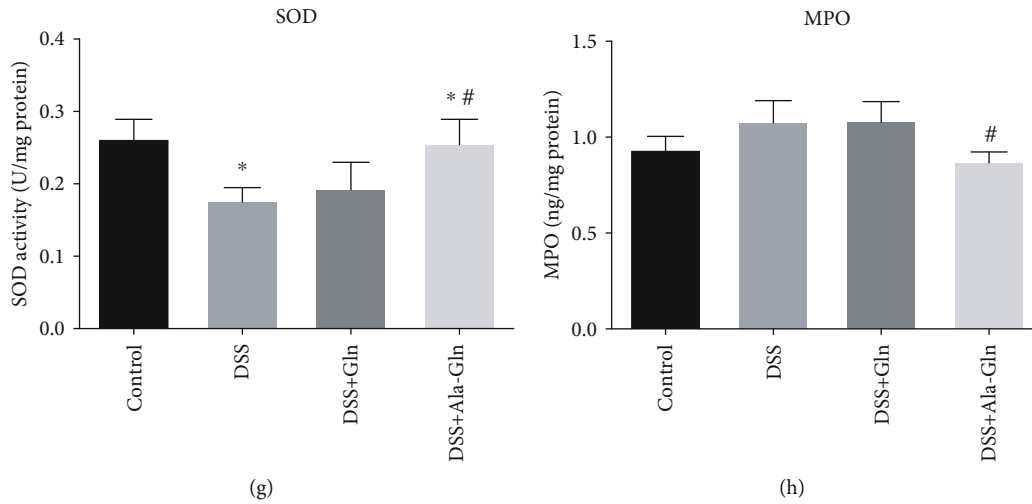


FIGURE 3: Effect of the supplementations of Gln and Ala-Gln on cytokines, immunoglobulins, SOD, and MPO of mice. (a–c) Concentrations of IL-1 β , IL-6, and TNF- α in colon tissue. (d–f) Concentrations of IgA, IgG, and IgM in serum. (g, h) Contents of SOD and MPO in colon tissue. Results were shown as means \pm SEM ($n = 7$). * $p < 0.05$ versus control group; # $p < 0.05$ versus DSS group.

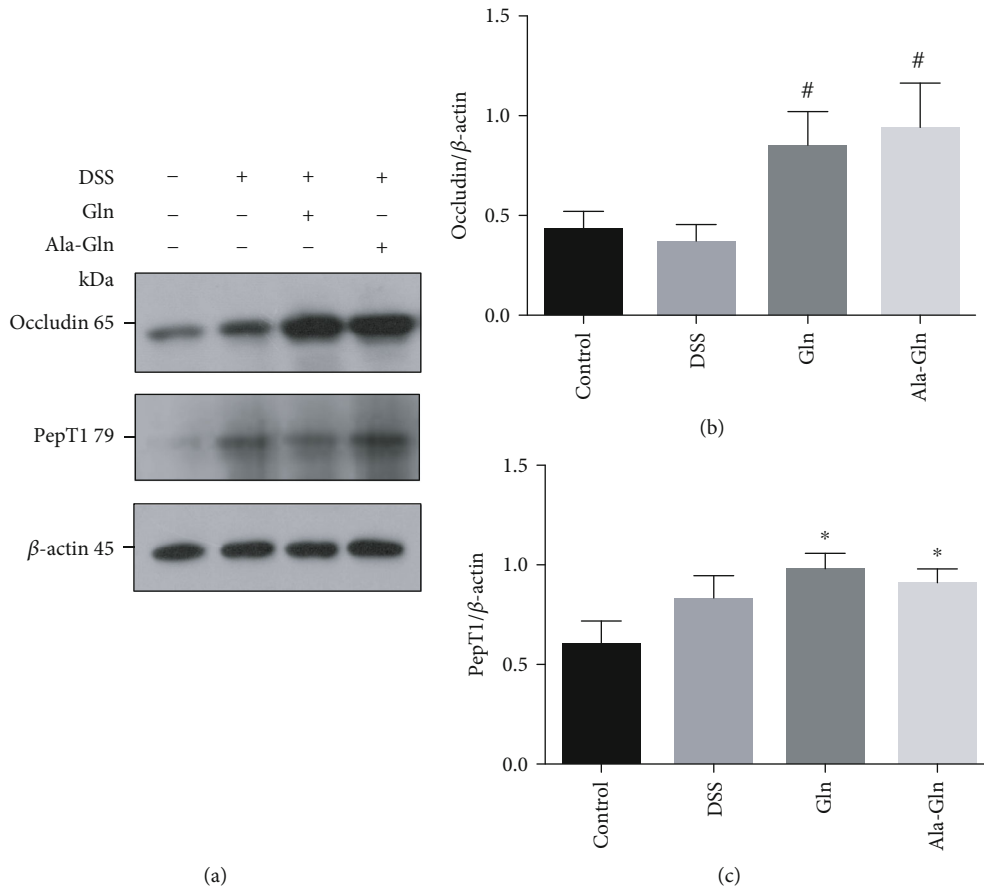


FIGURE 4: Supplementations of Gln and Ala-Gln increased the protein expressions of occludin and peptide transporter 1 (PepT1) in mouse colon tissue. (a) Representative protein bands. (b, c) Statistical analysis of protein bands of occludin and PepT1. Results were shown as means \pm SEM ($n = 7$). * $p < 0.05$ versus control group; # $p < 0.05$ versus DSS group.

reported that bioactive peptides derived from food proteins had anti-inflammatory function with the potential to treat IBD without side effects [1, 20, 21], such as peptides IRW, IQW [22], EWP [23], GLTSK [24], glycomacropeptide [25],

KPV [26], QCQCAVEGGL [27], RILSILRHQNLKELQ-DLAL [28], VPY [29], WH [30], P-317 [31], pyroGlu-Leu [32], γ -EC, and γ -EV [33]. Bioactive peptides can cross the intestinal epithelial wall and enter intact into the bloodstream

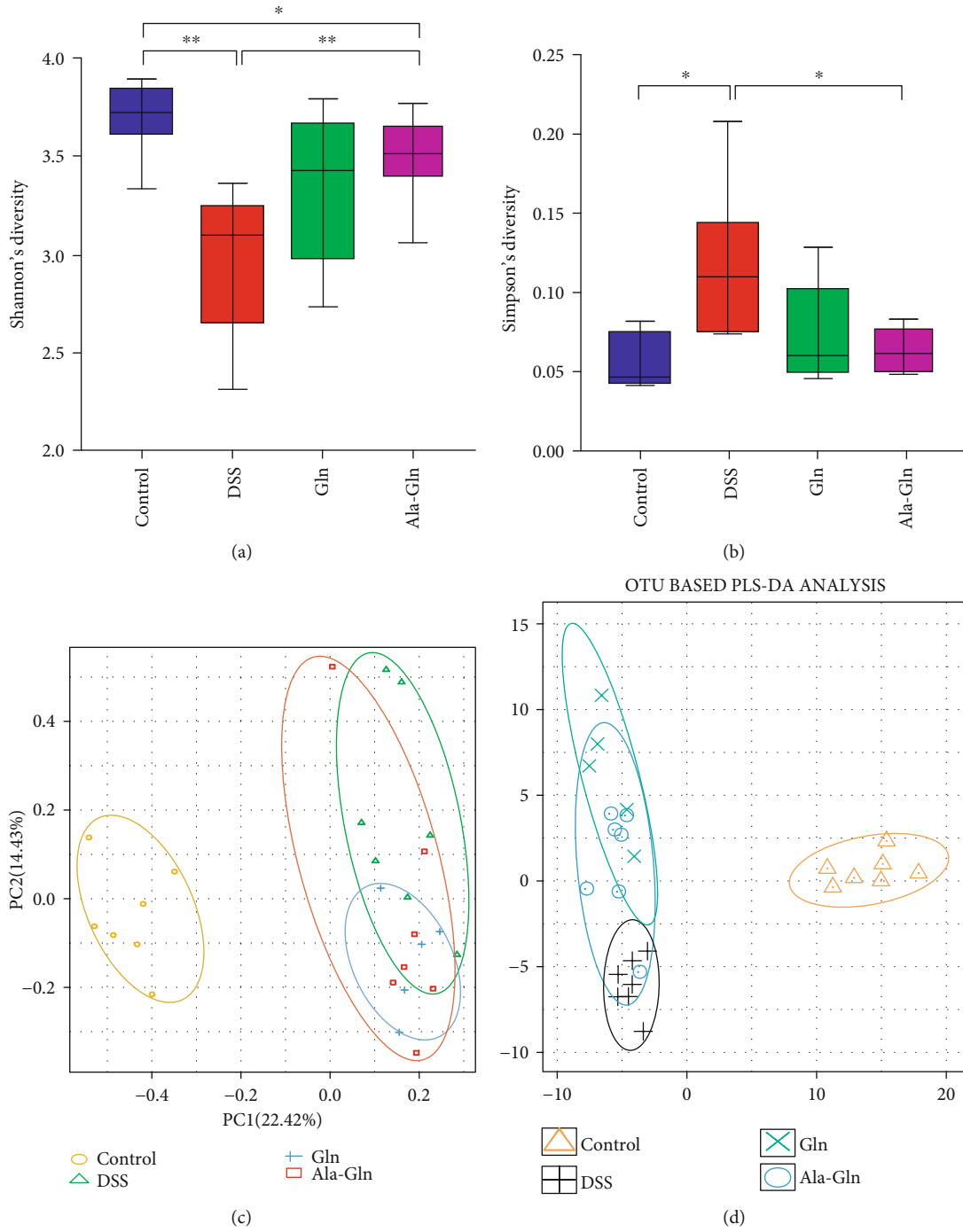


FIGURE 5: Continued.

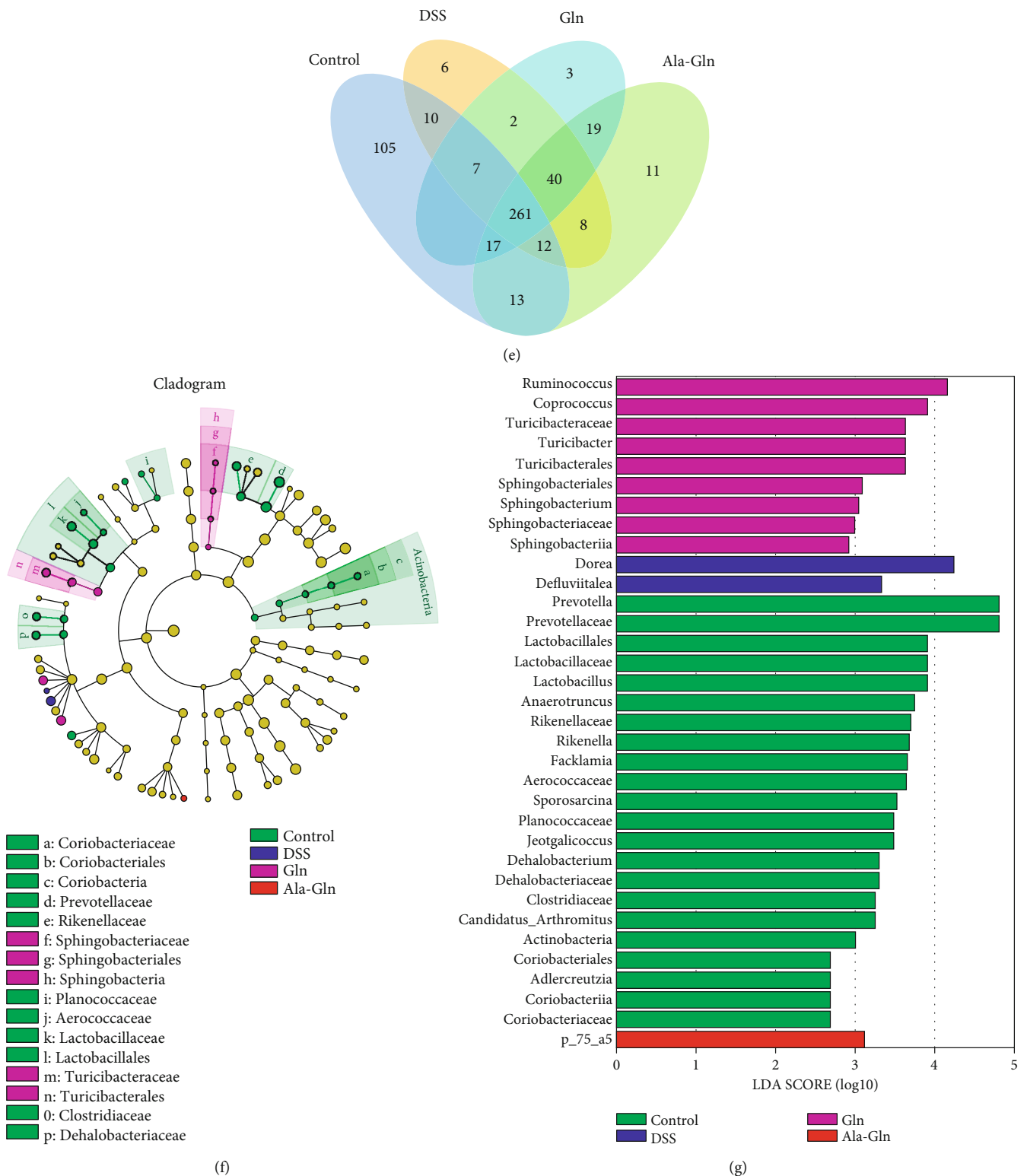
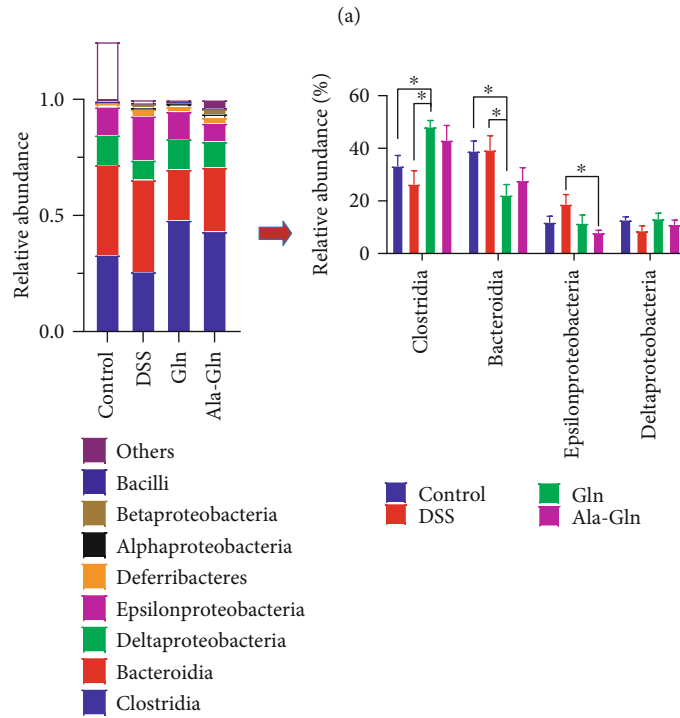
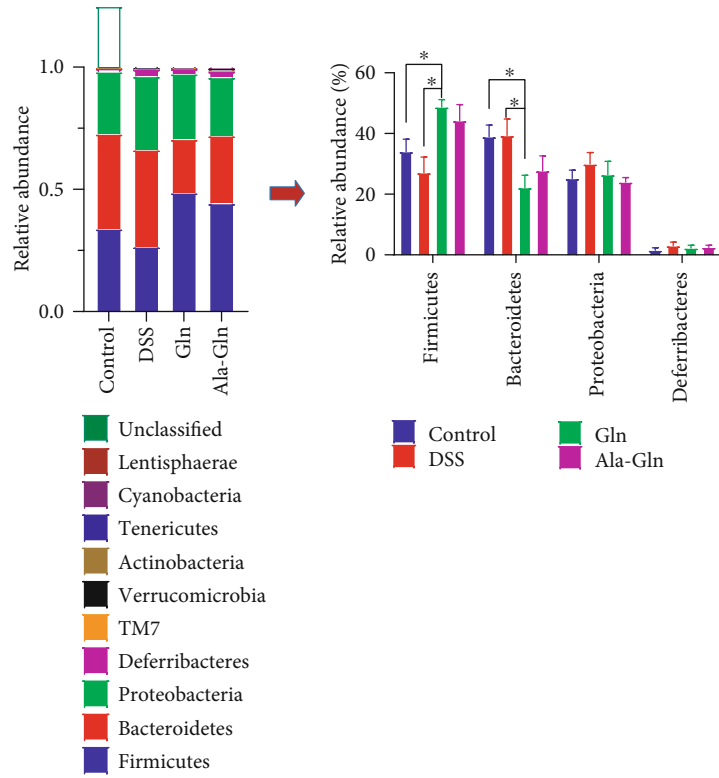
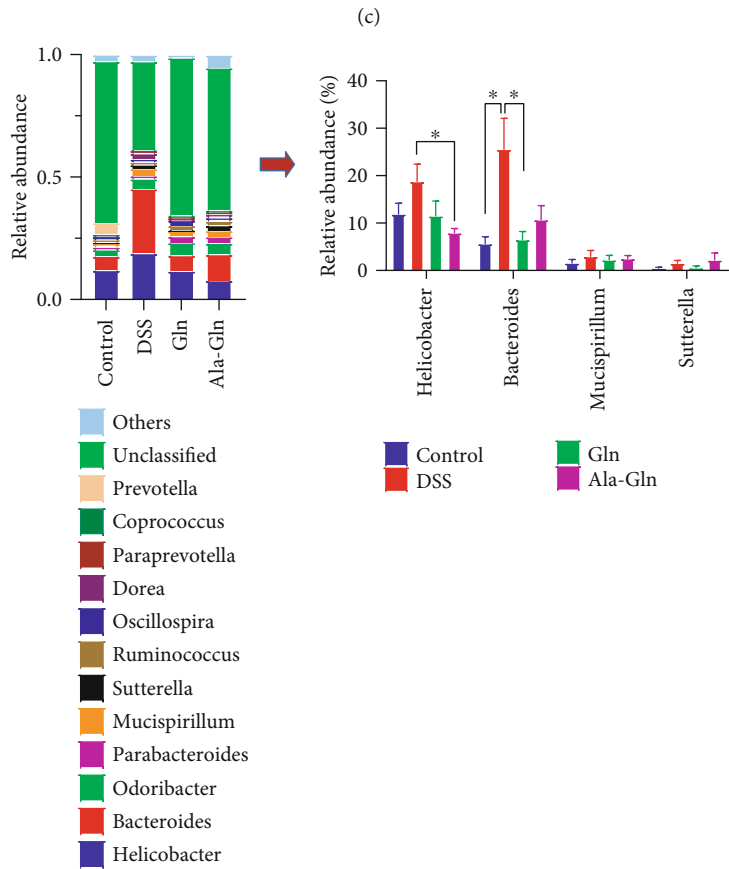
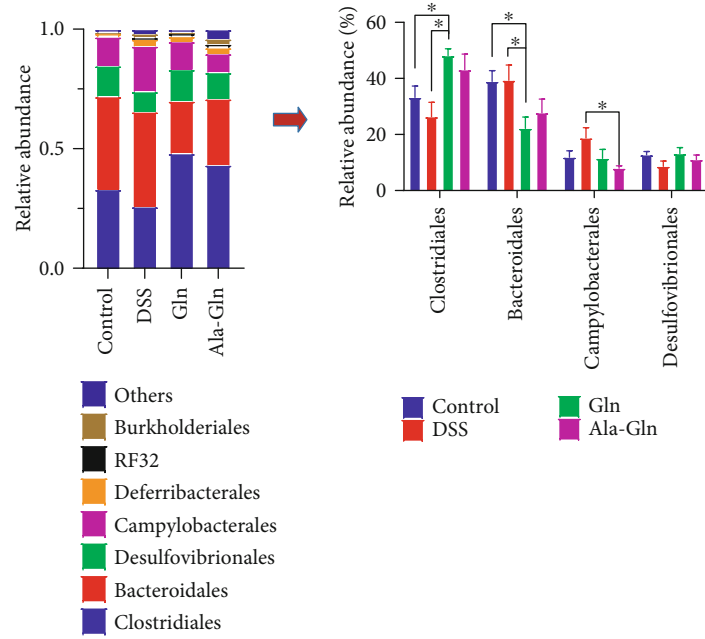


FIGURE 5: Supplementations of Gln and Ala-Gln altered the colon microbiota in colitic mice. (a, b) Alpha diversity was estimated by using Shannon and Simpson indices. (c, d) Principal component analysis (PCA) plot and partial least squares discriminant analysis (PLS-DA) analysis of gut microbiota. (e) Venn graph for OTUs. (f) LEfSe taxonomic cladogram. Different colors represent biomarker taxon enrichment of control (green), DSS (blue), Gln (purple), and Ala-Gln (red) groups. (g) Linear discriminant analysis (LDA) score (log10) of the different bacterial abundances. Results were shown as means \pm SEM ($n = 7$). * $p < 0.05$, ** $p < 0.01$.



(b)

FIGURE 6: Continued.



(d)

FIGURE 6: Continued.

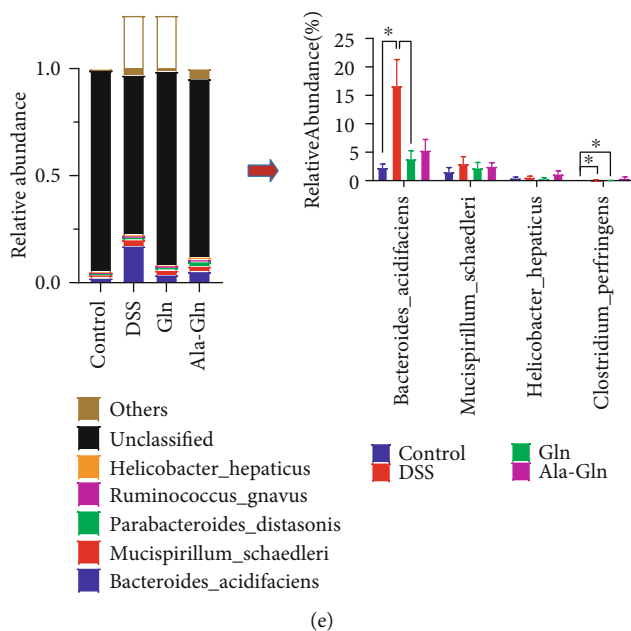


FIGURE 6: The relative abundances of predominant different bacteria after Gln and Ala-Gln treatments were shown at the phylum (a), class (b), order (c), genus (d), and species (e) levels. Results were shown as means \pm SEM ($n = 7$). * $p < 0.05$; ** $p < 0.01$.

having bioactive function; therefore, the efficiency to transport amino acids can be enhanced by peptides [20, 34]. In addition, Gln is a therapeutic candidate for improving intestinal health based on its influence on repairing the intestinal epithelial wall and enhancing immunity [35]. Several studies have been performed to investigate the beneficial effects of Gln and Ala-Gln on colitis and intestinal health [3, 9, 15, 36]. However, little is known about the difference between Gln and Ala-Gln in colitis and gut microbiota in the intestinal inflammation. In addition, a dose of 750 mg Ala-Gln/kg BW/d (equal 500 mg Gln/kg BW/d) was used to manage mice based on previous reports of the safe and effective treated dose [9, 10, 15].

The DSS-induced colitic mice are an intensively used model to study IBD with the evaluation of DAI, BW, colon length, signaling pathways, inflammatory cytokines, and gut microbiome in mice [1, 17, 37]. In this study, high DAI, short colon length, and colon tissue damage were observed in DSS-challenged mice, indicating that the colitis model was established successfully [38]. However, these IBD markers were restored by the oral supplement of Ala-Gln, indicating that the mouse colitis was attenuated by Ala-Gln. As shown in this study, it has been confirmed that Ala-Gln attenuated colon inflammation and increased colon length [9]. The cytokines IL-1 β , IL-6, IL-8, and TNF- α can cause intestinal inflammation [1], and their release can induce intestinal dysfunction [37]. The intestinal inflammatory cytokine disorders always are associated with oxidative stress imbalance [39, 40]. In this study, the decreases in the contents of IL-1 β , IL-6, and TNF- α caused by Ala-Gln were confirmed by a previous study which showed that Gln reduced the expression of these cytokines in mice with *Pasteurella multocida* vaccine [41]. These results can be explained partly by Gln bioactivity, which can inhibit DSS-induced colitis via the decrease in proinflammatory cytokines and SOD [36]. The

Gln has also been found to inhibit inflammatory response by regulating NF- κ B activation, which can cause proinflammatory cytokine release [42], while Gln can inhibit inflammatory cytokines and is beneficial for intestinal mucosa in endotoxemic rats [43]. In the current study, the decrease in inflammatory cytokines by Ala-Gln (not by Gln with IL-1 β and TNF- α) indicated that the extent of colitis was ameliorated by Ala-Gln, which has better beneficial effects than Gln. Additionally, the contents of IgA, IgG, and IgM were increased by Ala-Gln to enhance the immune system. It was reported that Gln can increase IL-6 and SIgA concentrations and protect against *Escherichia coli* infection via intestinal innate immunity in mice [2, 44]. These results indicated that dietary Ala-Gln can ameliorate colitis via enhancing immunoglobulin levels.

The TJ barrier is important to intestinal health by modulating gut permeability and IBD pathogenesis [45], and the impairment of its integrity is a crucial reason to cause colitis. The Gln had defensive effects on the maintenance of intestinal barrier integrity in Caco-2 cells [46]. In the present study, the expression of the TJ protein occludin in the colon was upregulated by Ala-Gln. Another reason for the better suppression effect of Ala-Gln than Gln is that Ala-Gln is the substrate of intestinal PepT1, which can transport Ala-Gln efficiently into the blood circulation [20]. Although PepT1 expression can be upregulated in the IBD colon due to its transport of bacterial peptides into cells, PepT1 can also transport Ala-Gln into intestinal cells and bloodstream to inhibit inflammation [47], such as anti-inflammatory peptides VPY [29], KPV [26], IPAV [48], and β -Ala-His [49]. Therefore, PepT1 is a promising potential target for managing colitis; however, its mechanism underlying the inhibition of colitis by bioactive peptides still needs further investigation. However, in this study, no significant effect of Ala-Gln

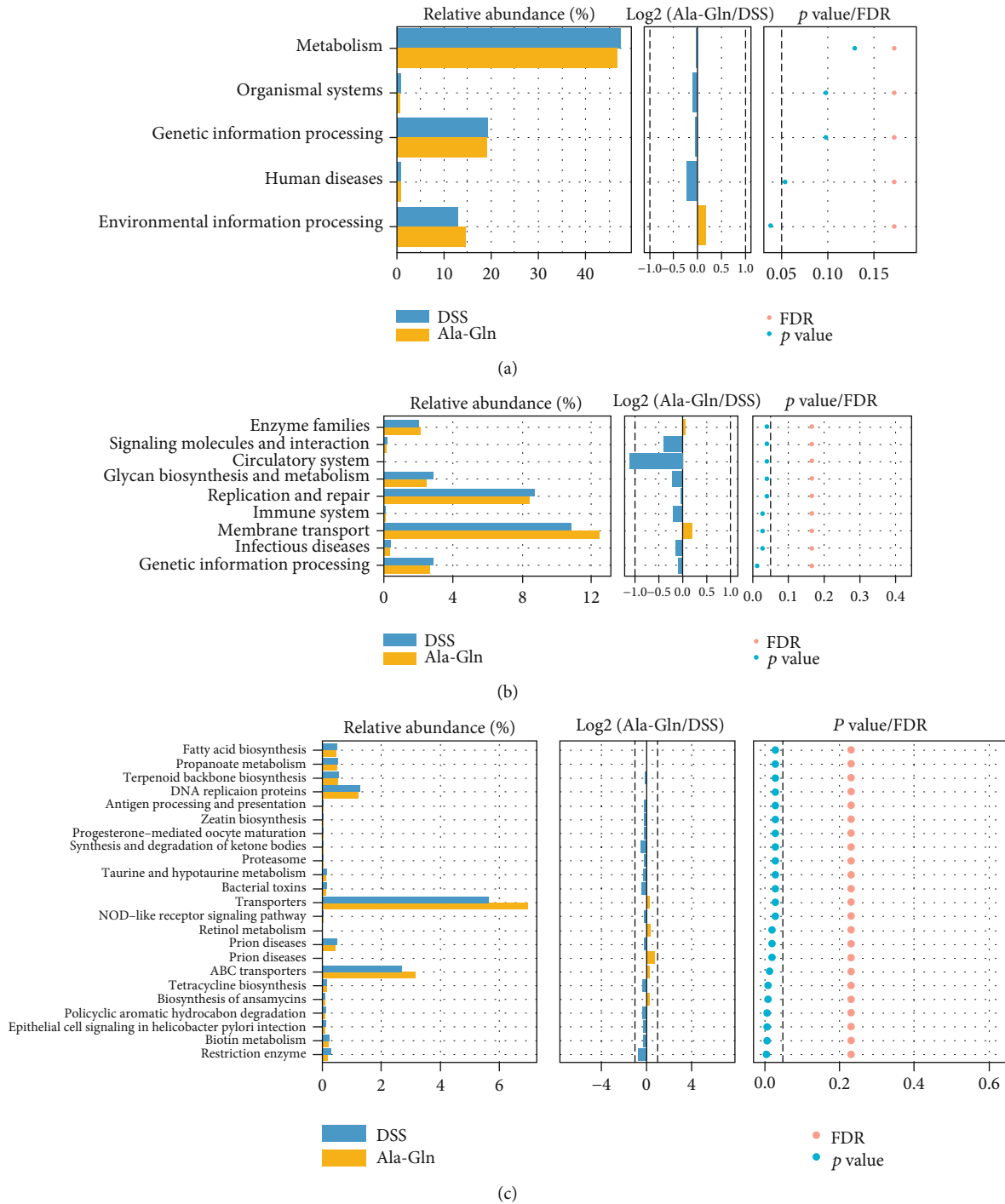


FIGURE 7: The metabolized pathways of the different microflora abundances after Ala-Gln supplementation in DSS-challenged mice at KEGG levels 1 (a), 2 (b), and 3 (c).

was observed on MAPK phosphorylation, indicating that MAPK signaling is not the mechanism for Ala-Gln to ameliorate colitis. In addition, oxidative stress is another mechanism that causes IBD [50], and the SOD activity can be decreased by DSS challenge [16, 22]. As an indicator for colitis extent, MPO can induce tissue damage due to the release of oxyradicals from leukocytes [3]. In this study, Ala-Gln showed defensive effects by increasing SOD, demonstrating

that Ala-Gln could inhibit colitis through mediating oxidation resistance. The MPO concentration was increased by DSS and reversed by Ala-Gln, indicating that Ala-Gln has alleviated colitis inflammation.

The microbiota plays a critical role in maintaining gut oxidative environment and altering chronic inflammation of human and animals [51]. In the current study, intestinal microbial composition was changed and the microbial

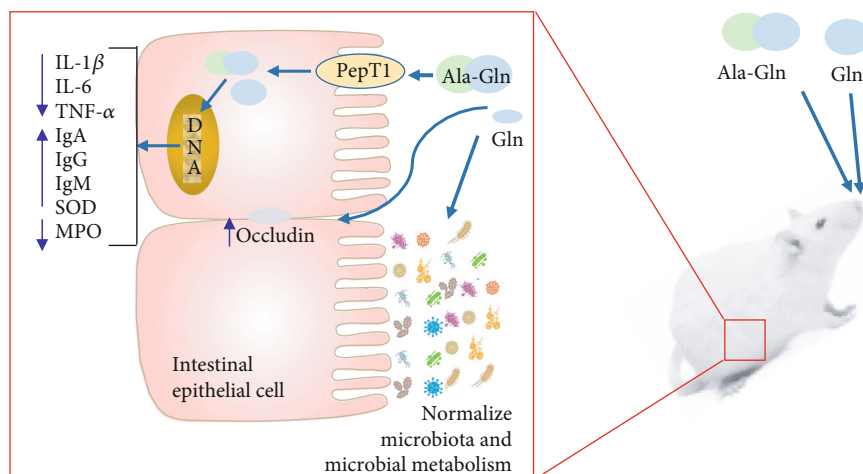


FIGURE 8: A schematic of the underlying mechanism of Ala-Gln and Gln in alleviating the colitis of mice.

diversity was reduced in colitic mice. Gut microbial diversity was decreased by DSS challenge, while it was significantly increased by Gln and Ala-Gln, indicating that Gln and Ala-Gln reversed DSS-induced decrease in microbial diversity. In this study, the DSS challenge decreased the OTU numbers, while Ala-Gln treatment increased OTUs to counteract their shifts, indicating that the richness of the gut microbiome was normalized by Ala-Gln to a certain extent. It was reported that the increase in *Bacteroidetes* and the ratio of *Bacteroidetes/Firmicutes* were the indicators of IBD [17, 37]. In the current study, the microbiota composition was reversed and the ratio of *Bacteroidetes/Firmicutes* was decreased by Ala-Gln treatment. It was also observed that Gln increased the *Firmicutes/Bacteroidetes* ratio, decreased the abundance of *Firmicutes*, and beneficially changed the bacterial community and activated the innate immunity in the intestine [52]. It was reported that the decrease in *Bacteroides* and the increase in *Firmicutes* have a defensive effect on IBD [53]. The abundance of *Firmicutes* in DSS-induced colitic mice was also increased by serine [37]. The decrease in *Bacteroides* abundance linked to intestinal inflammation can explain the colitis amelioration by Ala-Gln [17]. In our study, Gln increased *Clostridiales* abundance, which can promote the development of intestinal IgA-producing cells and benefits the immunological responses [54]. The Ala-Gln or Gln restored DSS-induced change of *Lactobacillus*, *Bacteroidales*, *Firmicutes*, *Bacteroides_acidifaciens*, *Clostridia*, *Helicobacter*, and *Bacteroides*. These results indicated that Ala-Gln alleviated the DSS-induced decrease in microbial diversity, evenness, and composition and rescued gut microbiota dysbiosis, which was confirmed by a previous study that Gly-Gln reduced the inflammatory response in piglets by modulating gut microbial community and metabolism [5]. The reason may be that Gln can regulate amino acid utilization via intestinal microorganisms [6].

The metabolism functions of gut microbiota were also inhibited by Ala-Gln, such as epithelial cell signaling in *Helicobacter pylori* infection, infectious diseases, polycyclic aromatic hydrocarbon degradation, and bacterial toxins. Among them, *Helicobacter pylori* infection is a key factor in

intestinal disease etiology [55]. However, the metabolism of membrane transporters was enhanced by Ala-Gln, indicating that nutritional transporters (e.g., PepT1) may be enhanced to transport more nutrients into epithelial cells and bloodstream to resist inflammation. Furthermore, the role of gut microbiota mediated by Ala-Gln is still lacking; therefore, the modulating mechanism of Ala-Gln on gut microbiota needs to be investigated in the future.

5. Conclusion

This study reveals that the oral administration of Gln and Ala-Gln can protect against DSS-induced colitis through alleviating mucosa damage and inflammatory responses, upregulating the expression of TJ and PepT1 proteins and modulating gut microbiota in mice. The DSS-induced shifts of the microbiome (community diversity, evenness, richness, and composition) in the mouse colon were restored by Gln and Ala-Gln supplementation, including *Lactobacillus*, *Bacteroides_acidifaciens*, *Bacteroidales*, *Firmicutes*, *Clostridia*, *Helicobacter*, and *Bacteroides*. The metabolism functions of gut microflora were also rescued by Ala-Gln, including membrane transporters (PepT1), fatty acid and propanoate metabolism, infectious diseases, immune system, and bacterial toxins. Interestingly, Ala-Gln has a better beneficial effect than Gln in alleviating colitis. In conclusion, Ala-Gln can prevent IBD through PepT1, enhancing the intestinal barrier and modulating gut microbiota and their metabolites. This study provides a new insight into the biological function and protective effect of Ala-Gln in managing IBD. Furthermore, the role and the underlying mechanism of PepT1 and gut microbiota in alleviating colitis need to be investigated in the future.

Abbreviations

Ala-Gln:	Alanyl-glutamine
BW:	Body weight
DAI:	Disease activity index
DSS:	Dextran sulfate sodium

ELISA:	Enzyme-linked immunosorbent assay
ERK:	Extracellular signal-regulated kinase
Gln:	Glutamine
HE:	Hematoxylin and eosin
IBD:	Inflammatory bowel disease
IgA:	Immunoglobulin A
IL-6:	Interleukin-6
JNK:	c-Jun N-terminal kinase
KEGG:	Kyoto Encyclopedia of Genes and Genomes
LDA:	Linear discriminant analysis
LEfSe:	Linear discriminant analysis effect size
MPO:	Myeloperoxidase
PCA:	Principal component analysis
PCR:	Polymerase chain reaction
PepT1:	Peptide transporter 1
PLS-DA:	Partial least squares discriminant analysis
PICRUST:	Phylogenetic Investigation of Communities by Reconstruction of Unobserved States
QIIME:	Quantitative Insights into Microbial Ecology
SEM:	Standard error of the mean
SOD:	Superoxide dismutase
TNF- α :	Tumor necrosis factor- α
TUNEL:	Terminal deoxynucleotidyl transferase dUTP nick end labeling.

Data Availability

All data are available upon request.

Ethical Approval

The animal experiment was performed with a protocol approved by the Laboratory Animal Ethics Committee of Huazhong Agricultural University.

Conflicts of Interest

The authors declare no conflict of interest.

Authors' Contributions

Qingbiao Xu and Xiang Li designed the experiment. Qingbiao Xu, Min Li, Jinxiu Hou, Mingyang Hu, Xianghua Zhang, and Ya Gao performed the animal trials and sample and data analysis. Mingyang Hu and Qingbiao Xu wrote the manuscript. Xiang Li and Bahram Chachar revised the manuscript. All authors reviewed and approved the final manuscript.

Acknowledgments

This research was supported by grants from the State Key Laboratory of Animal Nutrition (2004DA125184F1906), the Open Project Program of Key Laboratory of Feed Biotechnology, the Key Laboratory of Molecular Animal Nutrition of Zhejiang University, and the Fundamental Research Funds for the Central Universities (2662019QD021).

References




- [1] W. Zhu, L. Ren, L. Zhang, Q. Qiao, M. Z. Farooq, and Q. Xu, "The potential of food protein-derived bioactive peptides against chronic intestinal inflammation," *Mediators of Inflammation*, vol. 2020, Article ID 6817156, 15 pages, 2020.
- [2] G. Liu, W. Ren, J. Fang et al., "l-Glutamine and l-arginine protect against enterotoxigenic *Escherichia coli* infection via intestinal innate immunity in mice," *Amino Acids*, vol. 49, no. 12, pp. 1945–1954, 2017.
- [3] C.-C. Chu, Y.-C. Hou, M.-H. Pai, C.-J. Chao, and S.-L. Yeh, "Pretreatment with alanyl-glutamine suppresses T-helper-cell-associated cytokine expression and reduces inflammatory responses in mice with acute DSS-induced colitis," *The Journal of Nutritional Biochemistry*, vol. 23, no. 9, pp. 1092–1099, 2012.
- [4] X. Hu, J. Deng, T. Yu et al., "ATF4 deficiency promotes intestinal inflammation in mice by reducing uptake of glutamine and expression of antimicrobial peptides," *Gastroenterology*, vol. 156, no. 4, pp. 1098–1111, 2019.
- [5] Y. Yan, B. Xu, B. Yin et al., "Modulation of gut microbial community and metabolism by dietary glycyl-glutamine supplementation may favor weaning transition in piglets," *Frontiers in Microbiology*, vol. 10, pp. 1–14, 2020.
- [6] Z.-L. Dai, X.-L. Li, P.-B. Xi, J. Zhang, G. Wu, and W.-Y. Zhu, "l-Glutamine regulates amino acid utilization by intestinal bacteria," *Amino Acids*, vol. 45, no. 3, pp. 501–512, 2013.
- [7] J. Satoh, T. Tsujikawa, Y. Fujiyama, and T. Bamba, "Nutritional benefits of enteral alanyl-glutamine supplementation on rat small intestinal damage induced by cyclophosphamide," *Journal of Gastroenterology and Hepatology*, vol. 18, no. 6, pp. 719–725, 2003.
- [8] B. Tan, H. Liu, G. He et al., "Alanyl-glutamine but not glycyl-glutamine improved the proliferation of enterocytes as glutamine substitution in vitro," *Amino Acids*, vol. 49, no. 12, pp. 2023–2031, 2017.
- [9] Y.-C. Hou, J.-J. Liu, M.-H. Pai, S.-S. Tsou, and S.-L. Yeh, "Alanyl-glutamine administration suppresses Th17 and reduces inflammatory reaction in dextran sulfate sodium-induced acute colitis," *International Immunopharmacology*, vol. 17, no. 1, pp. 1–8, 2013.
- [10] Y.-C. Hou, M.-H. Pai, J.-J. Liu, and S.-L. Yeh, "Alanyl-glutamine resolves lipopolysaccharide-induced lung injury in mice by modulating the polarization of regulatory T cells and T helper 17 cells," *The Journal of Nutritional Biochemistry*, vol. 24, no. 9, pp. 1555–1563, 2013.
- [11] S.-K. Liu, L.-B. Ma, Y. Yuan et al., "Alanylglutamine relieved asthma symptoms by regulating gut microbiota and the derived metabolites in mice," *Oxidative Medicine and Cellular Longevity*, vol. 2020, Article ID 7101407, 18 pages, 2020.
- [12] P. Bunpo, B. Murray, J. Cundiff, E. Brizius, C. J. Aldrich, and T. G. Anthony, "Alanyl-glutamine consumption modifies the suppressive effect of l-asparaginase on lymphocyte populations in mice," *The Journal of Nutrition*, vol. 138, no. 2, pp. 338–343, 2008.
- [13] C. V. Araújo, C. R. Lazzarotto, C. C. Aquino et al., "Alanyl-glutamine attenuates 5-fluorouracil-induced intestinal mucositis in apolipoprotein E-deficient mice," *Brazilian Journal of Medical and Biological Research*, vol. 48, no. 6, pp. 493–501, 2015.
- [14] Y. Zhou, P. Zhang, G. Deng, X. Liu, and D. Lu, "Improvements of immune status, intestinal integrity and gain performance in the early-weaned calves parenterally supplemented with l-

- alanyl-l-glutamine dipeptide," *Veterinary Immunology and Immunopathology*, vol. 145, no. 1–2, pp. 134–142, 2012.
- [15] Y.-C. Hou, C.-C. Chu, T.-L. Ko, C.-L. Yeh, and S.-L. Yeh, "Effects of alanyl-glutamine dipeptide on the expression of colon-inflammatory mediators during the recovery phase of colitis induced by dextran sulfate sodium," *European Journal of Nutrition*, vol. 52, no. 3, pp. 1089–1098, 2013.
 - [16] K. Wang, X. Jin, Q. Li et al., "Propolis from different geographic origins decreases intestinal inflammation and Bacteroides spp. populations in a model of DSS-induced colitis," *Molecular Nutrition & Food Research*, vol. 62, no. 17, p. 1800080, 2018.
 - [17] K. Wang, X. Jin, M. You et al., "Dietary propolis ameliorates dextran sulfate sodium-induced colitis and modulates the gut microbiota in rats fed a western diet," *Nutrients*, vol. 9, no. 8, p. 875, 2017.
 - [18] S. Kitajima, S. Takuma, and M. Morimoto, "Histological analysis of murine colitis induced by dextran sulfate sodium of different molecular weights," *Experimental Animals*, vol. 49, no. 1, pp. 9–15, 2000.
 - [19] A. Zha, D. Yuan, Z. Cui et al., "The evaluation of the antioxidant and intestinal protective effects of baicalin-copper in deoxynivalenol-challenged piglets," *Oxidative Medicine and Cellular Longevity*, vol. 2020, Article ID 5363546, 13 pages, 2020.
 - [20] Q. Xu, H. Hong, J. Wu, and X. Yan, "Bioavailability of bioactive peptides derived from food proteins across the intestinal epithelial membrane: a review," *Trends in Food Science & Technology*, vol. 86, pp. 399–411, 2019.
 - [21] H. Zhang, C. A. A. Hu, J. Kovacs-Nolan, and Y. Mine, "Bioactive dietary peptides and amino acids in inflammatory bowel disease," *Amino Acids*, vol. 47, no. 10, pp. 2127–2141, 2015.
 - [22] G. Liu, W. Yan, S. Ding et al., "Effects of IRW and IQW on oxidative stress and gut microbiota in dextran sodium sulfate-induced colitis," *Cellular Physiology and Biochemistry*, vol. 51, no. 1, pp. 441–451, 2018.
 - [23] M. Lee, J. Kovacs-Nolan, T. Archbold et al., "Therapeutic potential of hen egg white peptides for the treatment of intestinal inflammation," *Journal of Functional Foods*, vol. 1, no. 2, pp. 161–169, 2009.
 - [24] D. A. Luna-Vital, E. González de Mejía, and G. Loarca-Piña, "Dietary peptides from *Phaseolus vulgaris* L. reduced AOM/DSS-induced colitis-associated colon carcinogenesis in Balb/c mice," *Plant Foods for Human Nutrition*, vol. 72, no. 4, pp. 445–447, 2017.
 - [25] M. Ortega-González, F. Capitán-Cañadas, P. Requena et al., "Validation of bovine glycomacropeptide as an intestinal anti-inflammatory nutraceutical in the lymphocyte-transfer model of colitis," *British Journal of Nutrition*, vol. 111, no. 7, pp. 1202–1212, 2014.
 - [26] G. Dalmasso, L. Charrier-Hisamuddin, H. T. T. Nguyen, Y. Yan, S. Sitarman, and D. Merlin, "PepT1-Mediated Tripeptide KPV Uptake Reduces Intestinal Inflammation," *Gastroenterology*, vol. 134, no. 1, pp. 166–178, 2008.
 - [27] J.-W. Hwang, S.-J. Lee, Y.-S. Kim et al., "Purification and characterization of a novel peptide with inhibitory effects on colitis induced mice by dextran sulfate sodium from enzymatic hydrolysates of *Crassostrea gigas*," *Fish & Shellfish Immunology*, vol. 33, no. 4, pp. 993–999, 2012.
 - [28] N. Eissa, H. Hussein, L. Kermarrec et al., "Chromofungin ameliorates the progression of colitis by regulating alternatively activated macrophages," *Frontiers in Immunology*, vol. 8, pp. 1–17, 2017.
 - [29] J. Kovacs-Nolan, H. Zhang, M. Ibuki et al., "The PepT1-transportable soy tripeptide VPY reduces intestinal inflammation," *Biochimica et Biophysica Acta (BBA) - General Subjects*, vol. 1820, no. 11, pp. 1753–1763, 2012.
 - [30] Y. Kobayashi, J. Kovacs-Nolan, T. Matsui, and Y. Mine, "The anti-atherosclerotic dipeptide, Trp-His, reduces intestinal inflammation through the blockade of L-Type Ca²⁺ channels," *Journal of Agricultural and Food Chemistry*, vol. 63, no. 26, pp. 6041–6050, 2015.
 - [31] M. Sobczak, P. K. Zakrzewski, A. I. Cygankiewicz et al., "Anti-inflammatory action of a novel orally available peptide 317 in mouse models of inflammatory bowel diseases," *Pharmacological Reports*, vol. 66, no. 5, pp. 741–750, 2014.
 - [32] S. Wada, K. Sato, R. Ohta et al., "Ingestion of low dose pyroglutamylic leucine improves dextran sulfate sodium-induced colitis and intestinal microbiota in mice," *Journal of Agricultural and Food Chemistry*, vol. 61, no. 37, pp. 8807–8813, 2013.
 - [33] H. Zhang, J. Kovacs-Nolan, T. Koderá, Y. Eto, and Y. Mine, "γ-Glutamyl cysteine and γ-glutamyl valine inhibit TNF-α signaling in intestinal epithelial cells and reduce inflammation in a mouse model of colitis via allosteric activation of the calcium-sensing receptor," *Biochimica et Biophysica Acta (BBA) - Molecular Basis of Disease*, vol. 1852, no. 5, pp. 792–804, 2015.
 - [34] Q. Xu, X. Yan, Y. Zhang, and J. Wu, "Current understanding of transport and bioavailability of bioactive peptides derived from dairy proteins: a review," *International Journal of Food Science & Technology*, vol. 54, no. 6, pp. 1930–1941, 2019.
 - [35] N. A. Kretzmann, H. Fillmann, J. L. Mauriz et al., "Effects of glutamine on proinflammatory gene expression and activation of nuclear factor kappa B and signal transducers and activators of transcription in TNBS-induced colitis," *Inflammatory Bowel Diseases*, vol. 14, no. 11, pp. 1504–1513, 2008.
 - [36] W. Ren, J. Yin, M. Wu et al., "Serum amino acids profile and the beneficial effects of l-arginine or l-glutamine supplementation in dextran sulfate sodium colitis," *PLoS One*, vol. 9, no. 2, p. e88335, 2014.
 - [37] H. Zhang, R. Hua, B. Zhang, X. Zhang, H. Yang, and X. Zhou, "Serine alleviates dextran sulfate sodium-induced colitis and regulates the gut microbiota in mice," *Frontiers in Microbiology*, vol. 9, 2018.
 - [38] L. Hu, C. Wu, Z. Zhang et al., "Pinocembrin protects against dextran sulfate sodium-induced rats colitis by ameliorating inflammation, improving barrier function and modulating gut microbiota," *Frontiers in Physiology*, vol. 10, no. 908, pp. 1–10, 2019.
 - [39] P. Liao, Y. Li, M. Li et al., "Baicalin alleviates deoxynivalenol-induced intestinal inflammation and oxidative stress damage by inhibiting NF-κB and increasing mTOR signaling pathways in piglets," *Food and Chemical Toxicology*, vol. 140, p. 111326, 2020.
 - [40] A. Zha, Z. Cui, M. Qi et al., "Dietary baicalin zinc supplementation alleviates oxidative stress and enhances nutrition absorption in deoxynivalenol challenged pigs," *Current Drug Metabolism*, vol. 21, no. 8, pp. 614–625, 2020.
 - [41] S. Chen, S. Liu, F. Zhang et al., "Effects of dietary l-glutamine supplementation on specific and general defense responses in mice immunized with inactivated *Pasteurella multocida* vaccine," *Amino Acids*, vol. 46, no. 10, pp. 2365–2375, 2014.

- [42] H. Fillmann, N. A. Kretzmann, B. San-Miguel et al., "Glutamine inhibits over-expression of pro-inflammatory genes and down-regulates the nuclear factor kappaB pathway in an experimental model of colitis in the rat," *Toxicology*, vol. 236, no. 3, pp. 217–226, 2007.
- [43] X. Zhou, X. Wu, Y. Yin, C. Zhang, and L. He, "Preventive oral supplementation with glutamine and arginine has beneficial effects on the intestinal mucosa and inflammatory cytokines in endotoxemic rats," *Amino Acids*, vol. 43, no. 2, pp. 813–821, 2012.
- [44] M. Wu, H. Xiao, G. Liu et al., "Glutamine promotes intestinal SIgA secretion through intestinal microbiota and IL-13," *Molecular Nutrition & Food Research*, vol. 60, no. 7, pp. 1637–1648, 2016.
- [45] T. Azuma, M. Shigeshiro, M. Kodama, S. Tanabe, and T. Suzuki, "Supplemental naringenin prevents intestinal barrier defects and inflammation in colitic mice," *The Journal of Nutrition*, vol. 143, no. 6, pp. 827–834, 2013.
- [46] S. Beutheu, I. Ghouzali, L. Galas, P. Déchelotte, and M. Coëffier, "Glutamine and arginine improve permeability and tight junction protein expression in methotrexate-treated Caco-2 cells," *Clinical Nutrition*, vol. 32, no. 5, pp. 863–869, 2013.
- [47] S. A. Ingersoll, S. Ayyadurai, M. A. Charania, H. Laroui, Y. Yan, and D. Merlin, "The role and pathophysiological relevance of membrane transporter PepT1 in intestinal inflammation and inflammatory bowel disease," *American Journal of Physiology-Gastrointestinal and Liver Physiology*, vol. 302, no. 5, pp. G484–G492, 2012.
- [48] M. Oyama, T. Van Hung, K. Yoda, F. He, and T. Suzuki, "A novel whey tetrapeptide IPAV reduces interleukin-8 production induced by TNF- α in human intestinal Caco-2 cells," *Journal of Functional Foods*, vol. 35, pp. 376–383, 2017.
- [49] D. O. Son, H. Satsu, Y. Kiso, M. Totsuka, and M. Shimizu, "Inhibitory effect of carnosine on interleukin-8 production in intestinal epithelial cells through translational regulation," *Cytokine*, vol. 42, no. 2, pp. 265–276, 2008.
- [50] B. Li, R. Alli, P. Vogel, and T. L. Geiger, "IL-10 modulates DSS-induced colitis through a macrophage-ROS-NO axis," *Mucosal Immunology*, vol. 7, no. 4, pp. 869–878, 2014.
- [51] J. Ni, G. D. Wu, L. Albenberg, and V. T. Tomov, "Gut microbiota and IBD: causation or correlation?," *Nature Reviews Gastroenterology & Hepatology*, vol. 14, no. 10, pp. 573–584, 2017.
- [52] W. Ren, J. Duan, J. Yin et al., "Dietary l-glutamine supplementation modulates microbial community and activates innate immunity in the mouse intestine," *Amino Acids*, vol. 46, no. 10, pp. 2403–2413, 2014.
- [53] Y. Zhang, L. Tan, C. Li, H. Wu, D. Ran, and Z. Zhang, "Sulforaphane alter the microbiota and mitigate colitis severity on mice ulcerative colitis induced by DSS," *AMB Express*, vol. 10, no. 1, p. 119, 2020.
- [54] Y. Umesaki, H. Setoyama, S. Matsumoto, A. Imaoka, and K. Itoh, "Differential roles of segmented filamentous bacteria and clostridia in development of the intestinal immune system," *Infection and Immunity*, vol. 67, no. 7, pp. 3504–3511, 1999.
- [55] J. G. Kusters, A. H. M. van Vliet, and E. J. Kuipers, "Pathogenesis of *Helicobacter pylori* infection," *Clinical Microbiology Reviews*, vol. 19, no. 3, pp. 449–490, 2006.

Research Article

Emodin-Induced Oxidative Inhibition of Mitochondrial Function Assists BiP/IRE1 α /CHOP Signaling-Mediated ER-Related Apoptosis

Li-zhen Qiu ^{1,2}, Lan-xin Yue,¹ Yu-hao Ni,¹ Wei Zhou ¹, Cong-shu Huang,^{1,3} Hui-fang Deng,¹ Ning-ning Wang,^{1,2} Hong Liu,^{1,3} Xian Liu,¹ Yong-qiang Zhou,¹ Cheng-rong Xiao,¹ Yu-guang Wang,¹ and Yue Gao ^{1,2}

¹Department of Pharmaceutical Sciences, Beijing Institute of Radiation Medicine, Beijing 100850, China

²Tianjin University of Traditional Chinese Medicine, Tianjin 301617, China

³School of Traditional Chinese Medicine, Guangdong Pharmaceutical University, Guangzhou 510006, China

Correspondence should be addressed to Wei Zhou; zhouweisy1802@163.com and Yue Gao; gaoyue@bmi.ac.cn

Received 30 September 2020; Revised 27 November 2020; Accepted 30 November 2020; Published 22 April 2021

Academic Editor: Si Qin

Copyright © 2021 Li-zhen Qiu et al. This is an open access article distributed under the Creative Commons Attribution License, which permits unrestricted use, distribution, and reproduction in any medium, provided the original work is properly cited.

Cassiae Semen is a widely used herbal medicine and a popular edible variety in many dietary or health beverage. Emerging evidence disclosed that improper administration of Cassiae Semen could induce obvious liver injury, which is possibly attributed to emodin, one of the bioactive anthraquinone compounds in Cassiae Semen, which caused hepatotoxicity, but the underlying mechanisms are not completely understood. Hence, the present study firstly explored the possible role of oxidative stress-mediated mitochondrial dysfunction and ER stress in emodin-cause apoptosis of L02 cells, aiming to elaborate possible toxic mechanisms involved in emodin-induced hepatotoxicity. Our results showed that emodin-induced ROS activated ER stress and the UPR via the BiP/IRE1 α /CHOP signaling pathway, followed by ER Ca²⁺ release and cytoplasmic Ca²⁺ overloading. At the same time, emodin-caused redox imbalance increased mtROS while decreased MMP and mitochondrial function, resulting in the leaks of mitochondrial-related proapoptotic factors. Interestingly, blocking Ca²⁺ release from ER by 2-APB could inhibit emodin-induced apoptosis of L02, but the restored mitochondrial function did not reduce the apoptosis rates of emodin-treated cells. Besides, tunicamycin (TM) and doxorubicin (DOX) were used to activate ER stress and mitochondrial injury at a dosage where obvious apoptosis was not observed, respectively. We found that cotreatment with TM and DOX significantly induced apoptosis of L02 cells. Thus, all the results indicated that emodin-induced excessive ROS generation and redox imbalance promoted apoptosis, which was mainly associated with BiP/IRE1 α /CHOP signaling-mediated ER stress and would be enhanced by oxidative stress-mediated mitochondrial dysfunction. Altogether, this finding has implicated that redox imbalance-mediated ER stress could be an alternative target for the treatment of Cassiae Semen or other medicine-food homologous varieties containing emodin-induced liver injury.

1. Introduction

Cassiae Semen, the dried and ripe seed of *Cassia obtusifolia* L. or *Cassia tora* L., is a well-known Chinese herbal medicine and has been used for more than 2000 years in China and other East Asian countries, thanks to its remarkable efficacy for hepatoprotection, lowering blood pressure, improving eyesight, and antioxidation [1]. Besides, as a popular edible

substance and a common ingredient in many slimming health foods and beverages, Cassiae Semen has displayed excellent performance in the control of blood lipid and body weight [2]. However, this medicine-food homologous variety has been demonstrated to exhibit obvious hepatotoxicity that can eventually result in liver damage and cholestasis [3]. The safety of Cassiae Semen has therefore become a global health concern.

In recent years, there is a growing body of evidence that emodin, an anthraquinone compound extracted from *Cassia Semen*, is not only a major bioactive substance but also the main hepatotoxic substance of this edible herbal medicine [4]. As documented in previous researches, emodin could not only attenuate CCl_4 -, APAP-, and ethanol-induced hepatotoxicity of hepatocytes by inhibiting oxidative stress or lipid peroxidation but also ameliorate LPS-caused fulminant hepatic failure by suppressing immune responses [5]. Given such hepatoprotective activity, emodin was once considered a promising medicine for different liver diseases. But the latest studies showed that emodin (more than $30\ \mu\text{M}$) dose-dependently caused significant disturbance of fatty acid metabolism and apoptosis in human hepatocytes [6, 7]. Pharmacokinetics studies confirmed that emodin was the critical hepatotoxic component of other medicines containing emodin [8]. Nevertheless, the mechanisms by which emodin induces hepatotoxicity are not yet fully understood.

Reactive oxygen species- (ROS-) initiated perturbation of redox homeostasis and the subsequent oxidative stress always participate in xenobiotic-induced hepatotoxicity. Generally speaking, excessive accumulation of intracellular ROS could cause oxidative injuries to biomacromolecules and organelles, mostly resulting in apoptotic cell death [8]. Once ROS causes a decrease in the mitochondrial membrane potential and an increase in mitochondrial membrane permeability, mitochondrial proapoptotic factors will be released to the cytoplasm and trigger the mitochondrial-dependent apoptosis [8]. What is worthy of note is that elevated intracellular ROS generation directly induces the endoplasmic reticulum (ER) stress, which could in turn activate the ER-related apoptotic cell death that is characterized by the calcium release from the ER and the activation of Caspase-12 [9, 10]. More importantly, mitochondrion and the ER coordinate the oxidative stress responses and play an important role in the initiation of apoptosis.

Previous articles have reported that emodin ($50\ \mu\text{M}$) did have an impact on mitochondrial oxidative phosphorylation in hepatocytes and triggered ROS-mediated ER stress in human T cells [11], suggesting that emodin-caused hepatotoxicity would be associated with ROS-induced mitochondrial dysfunction and ER stress. Unfortunately, no report is currently available that emodin induces ROS generation and the consequent ER stress- and/or mitochondrial-related apoptosis in hepatocytes. Instead, emodin ($10\ \mu\text{M}$) could inhibit oxidative stress generated by arachidonic acid plus iron [12]. Thus, the role of ROS-mediated mitochondrial dysfunction, ER stress, and related apoptotic cell death in hepatotoxicity caused by emodin needs to be explored.

In the present study, to determine the toxicity effects of emodin on the liver, the cytotoxicity and redox status of emodin-treated human hepatocytes were examined before the mitochondrial function, ER stress, and toxic mechanisms involved in presenting a possible mode of action of emodin-induced hepatotoxicity were investigated. Furthermore, the role of reduced mitochondrial function in emodin-induced ER-related apoptosis was also discussed.

2. Methods and Materials

2.1. Cell Culture and Reagents. The normal human hepatocyte cell line (L02) was purchased from the Type Culture Collection of the Chinese Academy of Sciences, Shanghai, China. The L02 cells were cultured in complete RPMI-1640 medium (Gibco, Thermo Fisher Scientific, USA) containing 10% fetal bovine serum (FBS, 11011-861, EVERY GREEN) and 1% penicillin-streptomycin (10 kU/mL-10 mg/mL, FG101-01, Transgene, China) and maintained in an incubator with 5% CO_2 at 37°C . The culture medium was renewed every two days, and cells were passaged at 80% confluence using 0.25% trypsin-EDTA. Emodin was purchased from EFEBIO Company (E054323, 98% (HPLC), China). (2-(2,2,6,6-Tetramethylpiperidin-1-oxyl-4-ylamino)-2-oxoethyl) triphenylphosphonium chloride (MitoTEMPO or MT, SML0737, $\geq 98\%$ (HPLC)) and 2-aminoethyl diphenylborinate (2-APB, #9754, 97% (HPLC)) were from Sigma-Aldrich (China). N-Acetyl-L-cysteine was acquired from Beyotime Biotechnology (NAC, S0077, $>99\%$, China). Tunicamycin (TM) and doxorubicin (DOX) were purchased from Solarbio Life Science (T8480 and D8740, China), and their purities were both more than 98%.

2.2. Cell Viability Assay. Cell viability was determined using the Cell Counting Kit-8 assay (CCK-8, Dojindo, Japan) according to the manufacturer's instructions. Cells were seeded in a 96-well plate and treated with emodin (0, 6.25, 12.5, 25, and $50\ \mu\text{M}$) for 24 h. At the end of treatment, cells were washed with PBS buffer and incubated with RPMI-1640 medium containing 10% CCK-8 solution for 2 h in an incubator with 5% CO_2 at 37°C . Sequentially, the absorbance of each well was measured with a microplate reader at 450 nm (Multiskan MK3, Thermo Fisher Scientific, USA). Cell viabilities for treated groups were presented as percentages of that of the control.

2.3. Determination of Cell Apoptosis Rate. An Annexin V-FITC/PI apoptosis detection kit (C1062L, Beyotime, China) was used to detect the apoptosis of L02 cells according to the manufacturer's instructions. The L02 cells (3×10^5) were seeded in 60 mm plates and treated with emodin ($25\ \mu\text{M}$, with or without MT ($5\ \mu\text{M}$), 2-APB ($20\ \mu\text{M}$)), TM ($62.5\ \text{nM}$), and DOX ($125\ \text{nM}$). After treatment, the cells were collected into 15 mL centrifugal tubes and washed with warm PBS. Then, cells in each group were centrifuged for 5 min at 1000 rpm at room temperature (RT). Having the supernatant discarded, $195\ \mu\text{L}$ 1x binding buffer was used to resuspend cells in $1.5\ \text{mL}$ centrifugal tubes, followed by $5\ \mu\text{L}$ Annexin V-FITC and $10\ \mu\text{L}$ PI for double staining. Soon after incubation in the dark at room temperature (RT) for 10 min, the cell suspensions were submitted to a flow cytometer (FACSCalibur, Becton Dickinson, USA) to determine apoptosis rates at an excitation wavelength of 488 nm.

2.4. Measurement of Intracellular ROS. The L02 cells were placed into 35 mm plates at a density of 1×10^5 cells. The next day, the cells were treated with 6.25, 12.5, 25, and $50\ \mu\text{M}$ of emodin with or without 5 mM NAC for 24 h. After being washed with warm PBS, the cells were incubated with

1 mL of serum-free medium containing 10 μM of 2,7-dichlorofluorescein diacetate (DCFH-DA) (C1300-1, Applygen Technologies, China). After 30 min of incubation at 37°C, the cells were washed twice by PBS before the images were captured by one inverted fluorescence microscope (Ti2, Nikon, Japan). Fluorescence images were analyzed using ImageJ software, while fluorescence intensities in treated groups were expressed by normalized values to that of the control.

2.5. Confocal Microscopy. Cells placed into 20 mm glass-bottomed culture dishes were treated with emodin (25 μM) and with or without MitoTEMPO (5 μM) or 2-APB (20 μM) when they grew to 50-70% confluence. After 24 h treatment, the lipophilic cationic fluorescent dye JC-1 (KeyGEN, Nanjing, China) was used to detect the changes in the mitochondrial membrane potential (MMP), and the MitoSOX™ Red mitochondrial superoxide indicator (M36008, Thermo Fisher Scientific, USA) was applied to determine the mitochondrial superoxide anion. All the procedures were performed based on the manufacturer's protocol. For JC-1, fresh staining solution JC-1 (1x) was prepared immediately with a stock solution of JC-1 (200x) diluted in ultrapure water and JC-1 staining buffer (5x) before use. The cells were incubated with 1 mL of JC-1 (1x) for 20 min at 37°C, then washed twice with cold PBS, and examined immediately on a Confocal Laser Scanning Microscope (Leica TCS-SP2 confocal microscope). Fluorescence was excited at 514 nm and measured between 514 and 529 nm (green) and at 585-590 nm (red). For MitoSOX detection, cells were incubated in a warm medium containing 5 μM MitoSOX reagent. After 10 min of incubation at 37°C, these cells were washed with PBS and analyzed by the same confocal microscope but at (Ex/Em) 510/580 nm. All image acquisitions and analyses were performed using Volocity demo software. The intensity of the laser beam and the photodetector sensitivity were kept constant to compare the relative fluorescence intensities between these groups.

2.6. Detection of the Level of Cytoplasmic Calcium (Ca^{2+}). Fluo-4 AM (F312, Dojindo, Japan) was used to detect changes of calcium ions (Ca^{2+}) in the cytoplasm. The cells were seeded in glass culture dishes at a density of 2.5×10^4 /mL. After 24 h treatment with emodin (25 μM) with or without MitoTEMPO (5 μM) or 2-APB (20 μM), cells were stained with the 1 μM Fluo-4 AM for 40 min according to the manufacturer's descriptions. The extra dye was removed by a three-time wash with HBSS. The concentration of cytoplasmic Ca^{2+} was detected with a confocal microscope, the excitation wavelength was 494 nm, and the emission wavelength was 516 nm.

2.7. Western Blotting Analysis. After emodin treatment, the cells were washed and lysed with RIPA buffer (C1053+, Applygen Technologies) and protease inhibitor cocktail (P1265, Applygen Technologies) to collect proteins. A bicinchoninic acid (BCA) protein assay kit (P1511, Applygen Technologies) was used to quantify the concentrations of whole-cell proteins of each group. The proteins were sepa-

rated using a sodium dodecyl sulfate-polyacrylamide gel electrophoresis (SDS-PAGE) and then transferred to PVDF membranes (IPVH00010, Millipore, Germany), subsequently blocked in 5% milk diluted in tris-buffered saline solution with 0.05% Tween 20 (TBST) for 2 h at RT and incubated with primary antibody at 4°C overnight. The membranes were washed with TBST for 3×10 min and incubated with secondary antibodies at RT for 1 h. After another three-time wash, the expressions of proteins were detected by enhanced chemiluminescence (ECL) according to the manufacturer's instructions (WBKLS0500, Millipore). The band intensity of each protein was quantified using ImageJ software. β -Actin was used as a loading control to normalize the protein expression. Information for all indicated antibodies used in our study could be found in supplementary materials (Table S1).

2.8. Seahorse XF Cell Mito Stress Test. Oxygen Consumption Rates (OCRs) and Extracellular Acidification Rates (ECARs) were both detected in real time using the Mito Stress Test Kit (103015-100, Agilent) and carried out with a Seahorse XFe96 Analyzer (Seahorse Bioscience, Agilent, Texas, USA) according to the manufacturer's instructions. Briefly, the cells were seeded in a Seahorse XF 96-well microplate (8000 cells/well, 101085-004, Agilent). After drug treatment, cells were incubated at 37°C with 5% CO_2 for 24 h. Then, the cells were washed and incubated in Seahorse XF assay medium (103575-100, Agilent) supplemented with 2 mM Glutamax (103579-100, Agilent), 1 mM sodium pyruvate (103578-100, Agilent), and 25 mM glucose (103577-100, Agilent) at 37°C for 1 h without CO_2 . Base OCR values were measured, followed by sequential drug injection including oligomycin (2 μM), carbonyl cyanide-p-trifluoromethoxy-phenylhydrazone (FCCP, 0.5 μM), and rotenone/antimycin A (1 μM), respectively, and the detection of OCR values, which would stand for the ATP production (proton leak), maximal respiration, and spare capacity in each group. Finally, cell numbers were counted by DAPI staining after the Mito Stress Test XF metabolic assay using a Scan High-Content System (Thermo Fisher Scientific, Massachusetts, USA). The mitochondrial respiratory capacity of each group was normalized to total cell numbers and presented as pmol/min/10,000 cells.

2.9. Statistical Analysis. All results were presented as mean \pm standard deviation (SD) and generated from at least three independent experiments. One-way ANOVA followed by the LSD post hoc test for multiple comparisons was performed for statistical analysis. Only at $p < 0.05$ was considered significant.

3. Results

3.1. Elevated Intracellular ROS Mediated Emodin-Induced Cytotoxicity on Human Hepatocytes. To determine the cytotoxicity of emodin on human hepatocytes, we exposed L02 cells to various emodin of concentrations (0-100 μM , Figure 1(a)) for 24 h. As shown in Figure 1(b), cell viability was reduced significantly by emodin in a dose-dependent

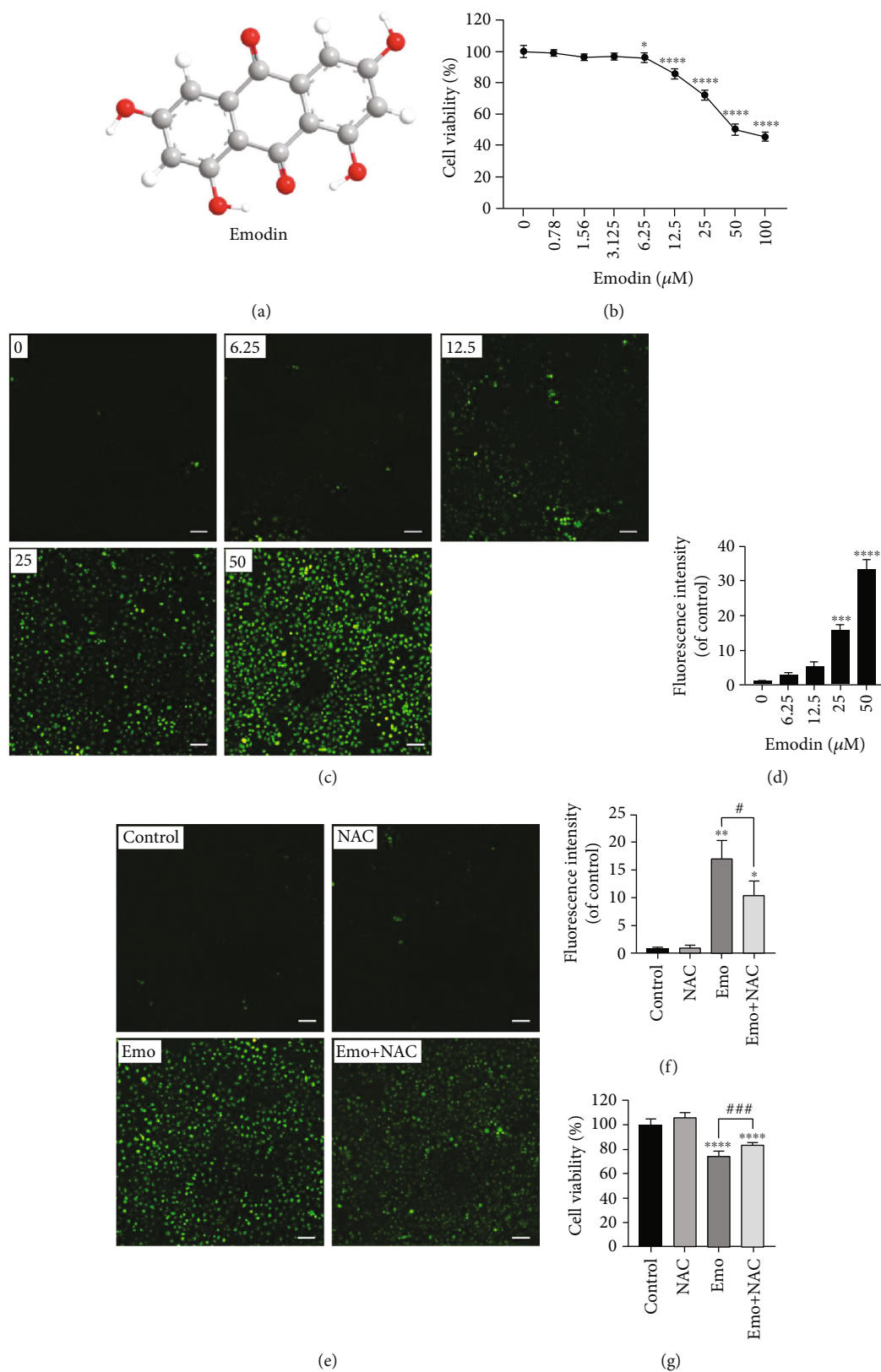


FIGURE 1: Emodin inhibited the viability of L02 cells via enhancing intracellular ROS. (a) Chemical structure of emodin. (b) Cell viability of L02 cells after 24 h emodin treatment was detected using the CCK-8 assay. (c, d) Intracellular ROS levels in L02 induced by emodin ($\times 200$), scale bar: $100 \mu\text{m}$. (e, f) Intracellular ROS levels in L02 treated with NAC, emodin, or NAC+emodin ($\times 200$), scale bar: $100 \mu\text{m}$. (g) Cell viability of L02 cells treated with NAC, emodin, or NAC+emodin. * $p < 0.05$, ** $p < 0.01$, *** $p < 0.001$, and **** $p < 0.0001$ vs. the control groups; # $p < 0.05$, ### $p < 0.001$ vs. the emo groups.

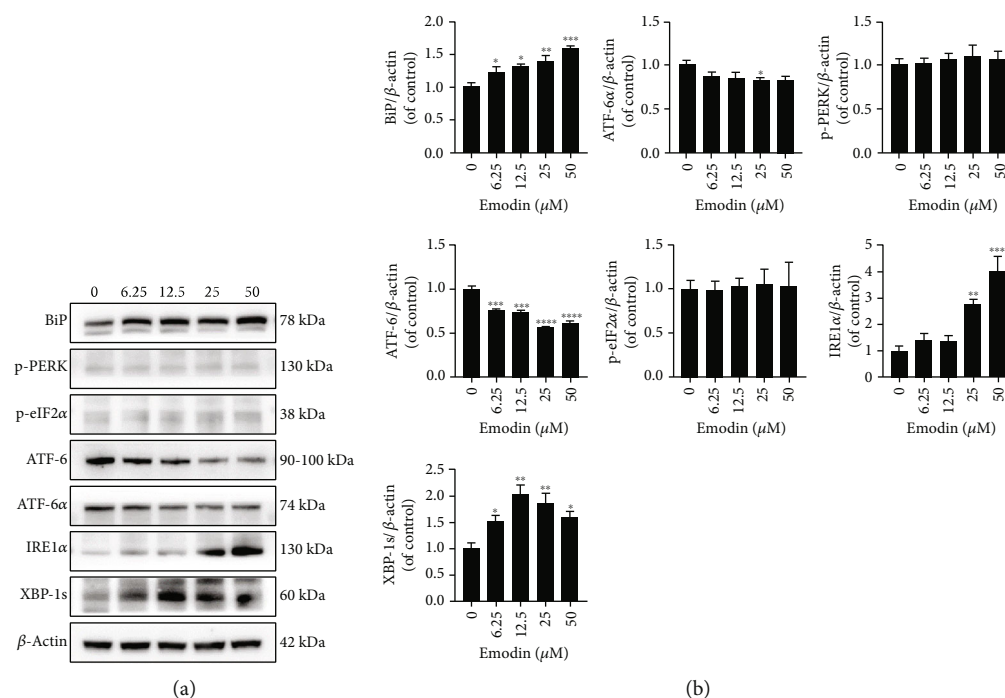


FIGURE 2: Emodin caused the activation of the BiP/IRE1 α /CHOP signaling pathway. (a) The protein levels of BiP, p-RERK, p-eIF2 α , ATF-6, ATF-6 α , IRE1 α , and XBP-1s in L02 were measured by western blotting assay. (b) The quantitative analysis of the indicated proteins. * $p < 0.05$, ** $p < 0.01$, *** $p < 0.001$, and **** $p < 0.0001$ vs. the control groups.

manner. It was found that 25 μ M of emodin decreased L02 cell viability to $72.10 \pm 2.81\%$. Figures 1(c) and 1(d) showed that emodin dose-dependently increased the intracellular levels of ROS. When L02 cells were cotreated with NAC (an inhibitor of ROS) and emodin (25 μ M), intracellular ROS was significantly alleviated (Figures 1(e) and 1(f)). In addition, the cell viability in the NAC and the emodin cotreatment group was evidently increased compared with the emodin group (Figure 1(g)). The results indicated that elevated intracellular ROS promoted emodin-induced cytotoxicity on human hepatocytes.

3.2. Emodin Caused ER Stress and Ca²⁺ Overloading through the BiP/IRE1 α /CHOP Signaling Pathway. To evaluate the effects of emodin on the ER, we detected the levels of ER stress-related proteins in cells treated with emodin using western blotting assay. As shown in Figure 2, compared with the control group, the expressions of BiP, IRE1 α , and XBP-1s were markedly increased, while those of ATF-6 and ATF-6 α were distinctly decreased in the emodin groups in a dose-dependent manner. However, the protein bands of p-RERK and p-eIF2 α were not different between the emodin groups and the control group. Previous studies have demonstrated that the intracellular Ca²⁺ concentration homeostasis is mostly maintained by the ER. Hence, we stained the L02 cells with Fluo-4 AM to explore the intracellular Ca²⁺ flux induced by emodin. As shown in Figures 3(a) and 3(b), enhanced cytoplasmic Ca²⁺ loading was observed in the emodin-treated group, which was suppressed by cotreatment with 2-APB, an antagonist of Ca²⁺ release from the ER. Therefore, these results suggested that emodin could cause

BiP/IRE1 α /XBP-1s signaling pathway-mediated ER stress, which eventually induced Ca²⁺ release from the ER and resulted in cytoplasmic Ca²⁺ loading.

3.3. Emodin-Induced Apoptosis Was Associated with ER Stress-Triggered Ca²⁺ Release. To further elucidate the role of ER stress-induced Ca²⁺ overloading in the apoptosis induced by emodin, the expressions of p-PLC γ and CHOP were detected. As shown in Figures 3(c) and 3(d), the protein levels of both CHOP and Caspase-12 were significantly elevated, especially in the high-dose groups. However, the expression of p-PLC γ remained unchanged in the emodin groups, indicating that ER stress promoted Ca²⁺ release through CHOP rather than PLC γ signaling. Moreover, cotreatment with 2-APB significantly decreased emodin-induced apoptosis of L02 cells, suggesting Ca²⁺ release from the ER participated in emodin-induced apoptosis (Figure 3(e)). Also, the increase in Caspase-12 expression in emodin-treated cells indicated the critical role of the ER in emodin-induced cytotoxicity (Figures 3(c) and 3(d)). Thus, our results demonstrated that emodin-induced apoptosis was mostly ER stress-related.

3.4. Overexpression of Superoxide Anion Decreased MMP and Mitochondrial Function. There is increasing evidence that apoptosis is also closely related to mitochondrial damage or dysfunction. Thence, to detect the production of mitochondrial superoxide anion and its effects on MMP, the MitoSOX red and JC-1 probes were employed, respectively. Our results showed that emodin upregulated the level of mitochondrial superoxide, which could be relieved by a mitochondrial-

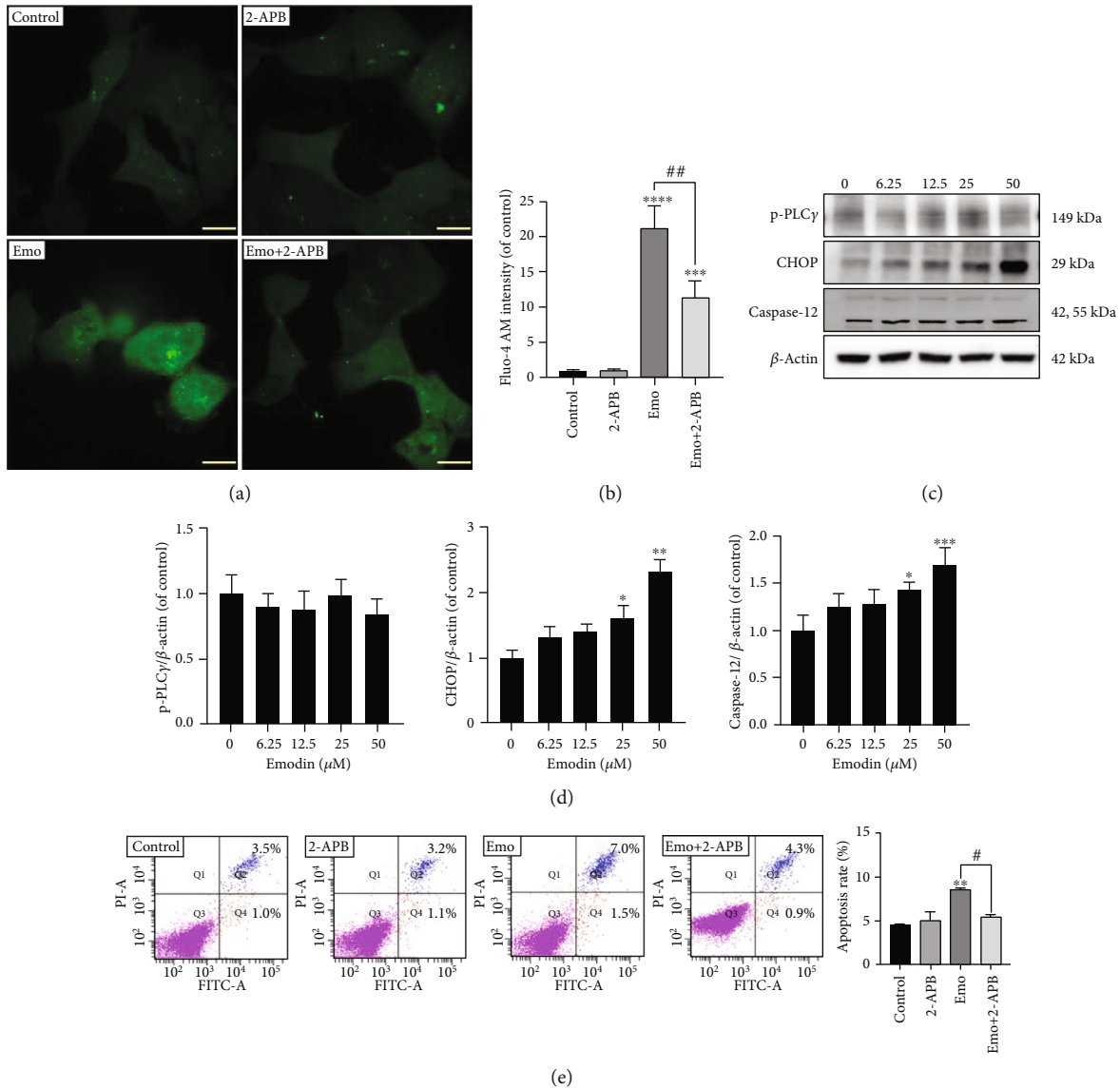


FIGURE 3: Apoptosis induced by emodin was associated with ER stress-triggered Ca^{2+} release. (a, b) The intracellular concentration of Ca^{2+} . Scale bar: $47 \mu\text{m}$. (c, d) The protein levels of p-PLC γ , CHOP, and Caspase-12 in L02 were detected by western blotting assay. (e) Emodin-induced apoptosis of L02 cells cotreated with or without 2-APB was analyzed using FACS analysis. * $p < 0.05$, ** $p < 0.01$, *** $p < 0.001$, and **** $p < 0.0001$ vs. the control groups; # $p < 0.05$, ## $p < 0.01$ vs. the emo groups.

targeted antioxidant MT (Figures 4(a) and 4(c)). As shown in Figures 4(b) and 4(d), an obvious decrease in the ratio of red fluorescence to green fluorescence was observed in emodin-treated cells, and this shift could be reversed by MT cotreatment. Then, the Mito Stress Test was performed to evaluate mitochondrial function in cells after emodin treatment of 24 h, and it was found that L02 cells treated with emodin displayed an evident reduction in basal OCRs, ATP production OCRs, and coupling efficiency OCRs (Figures 4(e) and 4(f)). Emodin enhanced the proton leak OCRs at 25 μM , which also indicated significant damage to mitochondrial function (Figure 4(f)). Besides, mitochondrial-related proapoptosis factors were detected. For example, the ratio of Bax/Bcl-2 and the contents of cytochrome C and Caspase-3 were increased in emodin groups (Figure 4(g)). Furthermore, the proportion of apoptosis of L02 cells displayed a marked

increase in the emodin group, which could be partly reversed by MT cotreatment, but there was no significant difference (Figure 4(h)). Hence, the results suggested that emodin-induced overexpression of mitochondrial superoxide anion could cause mitochondrial dysfunction, but the apoptosis of emodin-treated cells might not be totally mitochondrial-dependent.

3.5. Ca^{2+} Release from ER Participated in Emodin-Induced Mitochondrial Dysfunction. Interestingly, it was found that scavenging of emodin-induced mitochondrial superoxide using MT did not reverse cytoplasmic Ca^{2+} loading compared with the emodin group (Figure 5(a)). However, when Ca^{2+} release from the ER to the cytoplasm was inhibited by 2-APB, emodin (25 μM)-induced mitochondrial superoxide was alleviated (Figure 5(b)). To further elucidate the effects

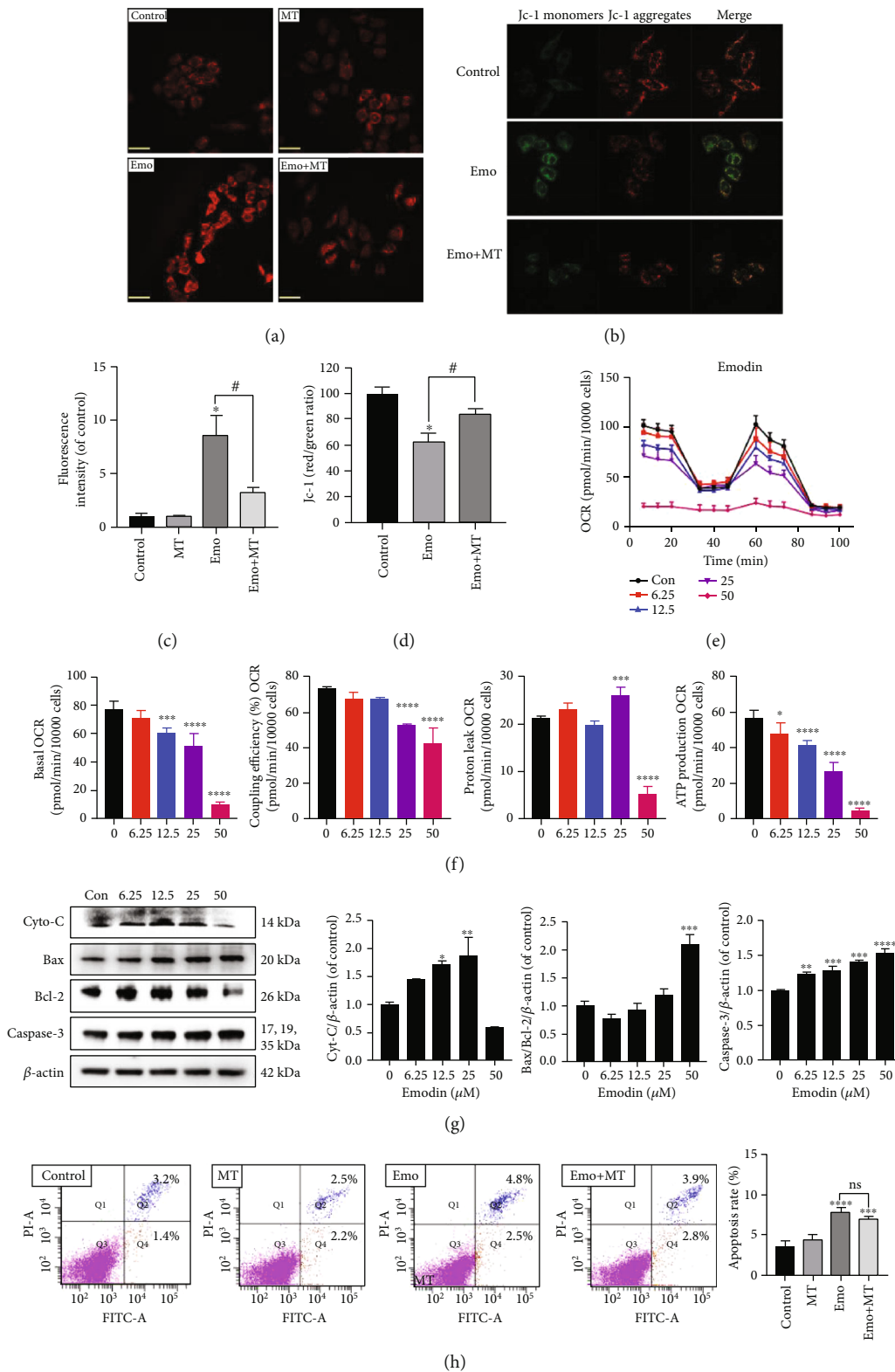


FIGURE 4: Emodin induced oxidative inhibition of MMP and mitochondrial function. (a, c) The intracellular superoxide anion levels in L02 cells were assessed using MitoSOX. Scale bar: 140 μm . (b, d) The MMP levels in L02 cells were detected using the JC-1 probe. Scale bar: 140 μm . (e) Mitochondrial function in L02 cells treated with emodin (0-50 μM) for 24 h was measured via the Mito Stress Test. (f) Effects of emodin on OCRs of basal, ATP production, proton leak, and coupling efficiency. (g) The protein levels of Cyto-C, Bax/Bcl2, and Caspase-3 in emodin-treated L02 cells were detected using western blotting. (h) Emodin-induced apoptosis of L02 cells cotreated with or without MT was analyzed using FACS analysis. * $p < 0.05$, ** $p < 0.01$, *** $p < 0.001$, and **** $p < 0.0001$ vs. the control groups; # $p < 0.05$ vs. the emo groups.

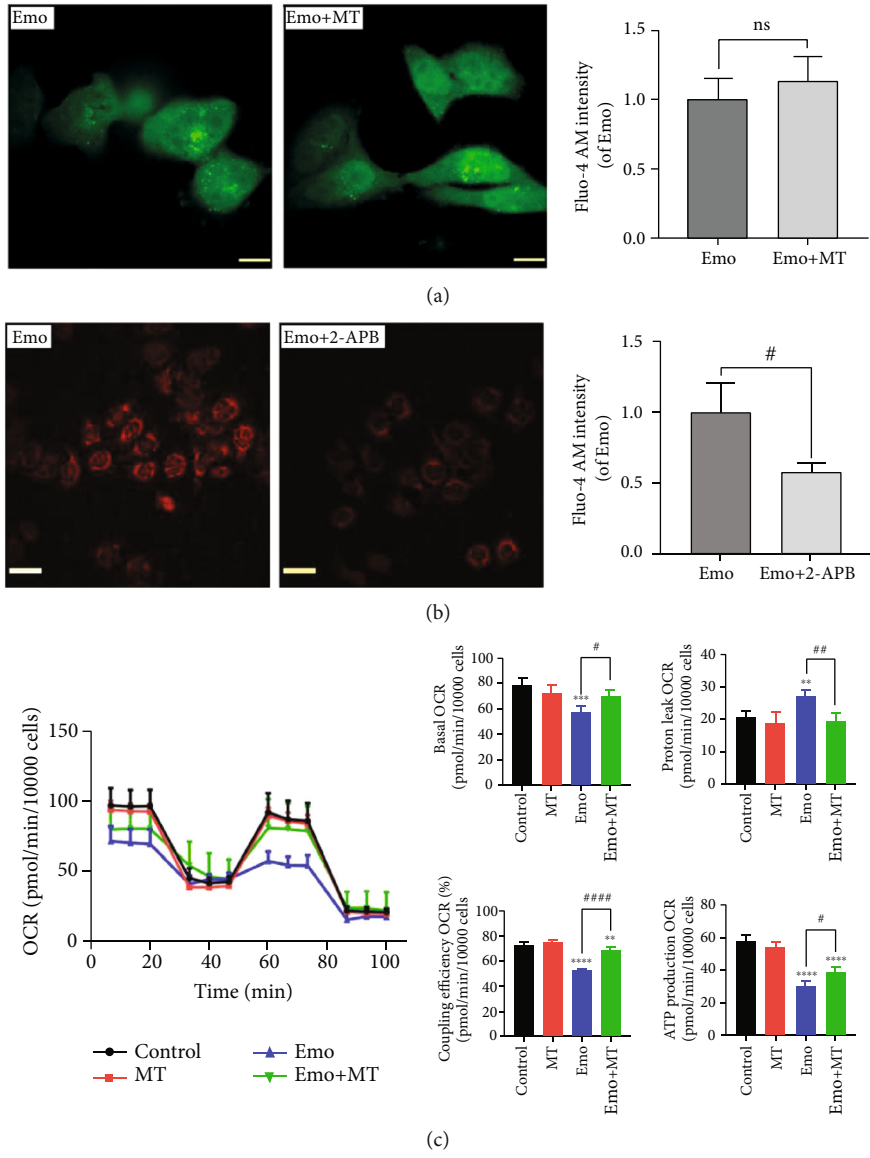


FIGURE 5: Continued.

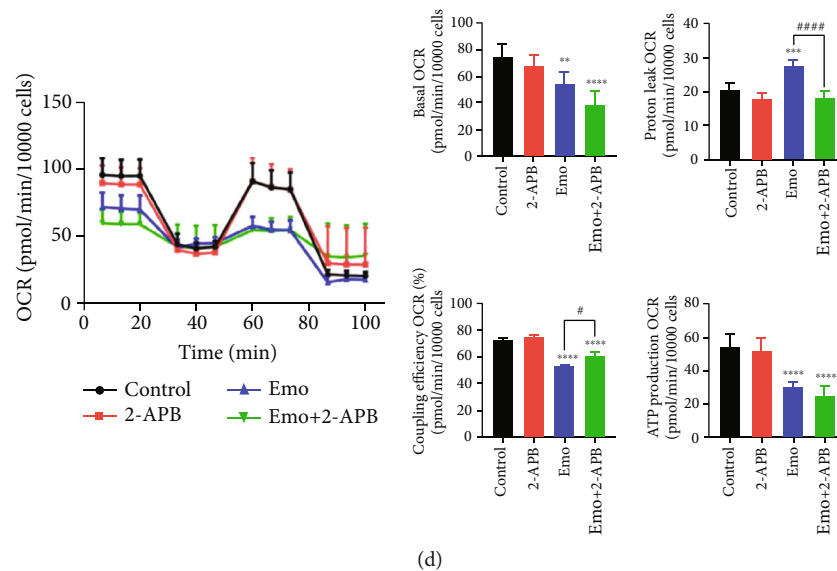


FIGURE 5: Ca^{2+} release produced by ER stress participated in emodin-induced mitochondrial dysfunction. (a) The intracellular Ca^{2+} flux was stained with the Fluo-4 AM dye. (b) The superoxide anion levels were detected with the MitoSOX probe. (c, d) Mitochondrial functions in the L02 cells treated with MT, emodin, or Emodin+MT, 2-APB, and 2-APB+emodin were obtained by the Cell Mito Stress Test Kit, and the quantification analysis of OCR value of basal, ATP production, proton leak, and coupling efficiency. * $p < 0.05$, ** $p < 0.01$, *** $p < 0.001$, and **** $p < 0.0001$ vs. the control groups; # $p < 0.05$, ## $p < 0.01$, ### $p < 0.0001$ vs. the emo groups.

of ER Ca^{2+} release induced by emodin on the mitochondrial function, L02 cells were exposed to emodin with/without MT or 2-APB. As shown in Figure 5(c), MT could restore the reduced function of the mitochondrial respiratory chain induced by emodin. Also, 2-APB cotreatment could markedly reduce emodin-caused proton leak of mitochondria and enhance the coupling efficiency of mitochondrial respiratory chain to some extent in emodin-treated hepatocytes (Figure 5(d)). The results indicated that Ca^{2+} release from the ER participated in emodin-induced mitochondrial dysfunction by disturbing the mitochondrial redox status.

3.6. Oxidative-Related Decrease in Mitochondrial Function Participated in ER-Related Apoptosis. To further explore the relationship between emodin-induced mitochondrial dysfunction and ER stress, DOX and TM were chosen as positive drugs to induce mitochondrion injury and ER stress, respectively. Neither of them caused any significant decrease in cell viability at the indicated concentration (data not shown). Indeed, excessive mitochondrial superoxide anion was detected in L02 cells treated with DOX (125 nM) (Figure 6(a)); TM (62.5 nM) activated the BiP/IRE1 α /CHOP signaling pathway without increasing Caspase-3 content (Figures 6(b) and 6(c)), but DOX did not induce the activation of this signaling pathway (Figures 6(d) and 6(e)). As shown in Figure 6(f), compared with control, DOX or TM administration alone did not induce significant increases in apoptosis of L02 cells, which also provided more evidence that neither DOX at 125 nM nor TM at 62.5 nM had a significant effect on cell viability. However, coexposure to DOX and TM could significantly elevate the apoptosis rate from 6.3% to 14.9%, suggesting that oxidative stress-mediated mitochondrial injury might be involved in ER stress-related apoptosis. Moreover, mitochondrial respiratory function

analysis also demonstrated that TM exacerbated DOX-induced decreases in basal mitochondrial respiratory function and ATP production (Figure 6(g)). Taken together other results described above, it could be concluded that oxidative inhibition of mitochondrial function decreases ATP supply, which might play an important role in ER stress-related cell apoptosis.

4. Discussion

As a popular medicine-food homologous variety, Cassiae Semen has been applied in clinical practice or daily cuisine in China and other East Asia countries for two thousand years, due to the excellent pharmacological effects on vision improvement, kidney and liver protection, and blood lipid control [13]. Recently, there have been many reports on its adverse effects caused by improper administration of traditional Chinese medicines or diet containing Cassiae Semen. Such adverse effects as acute liver injury have raised increasing concerns about the safety of this dietary/medicinal plant seed [3]. Emodin, one of the main bioactive compounds in Cassiae Semen, was considered to be able to alleviate inflammation without toxicity [5]. However, the latest evidence showed that emodin could directly induce cytotoxicity on hepatocytes [6], but the related toxic mechanisms were not entirely understood. Hence, our study was the first to confirm that emodin could promote excessive ROS generation and redox imbalance in human hepatocytes, followed by BiP/IRE1 α /CHOP signaling-mediated ER stress and the unfolded protein response (UPR) and intracellular Ca^{2+} overloading, resulting in ER-related apoptosis but not mitochondrial-dependent apoptosis. Also, oxidative-related mitochondrial dysfunction played an important role in emodin-induced ER-related apoptosis.

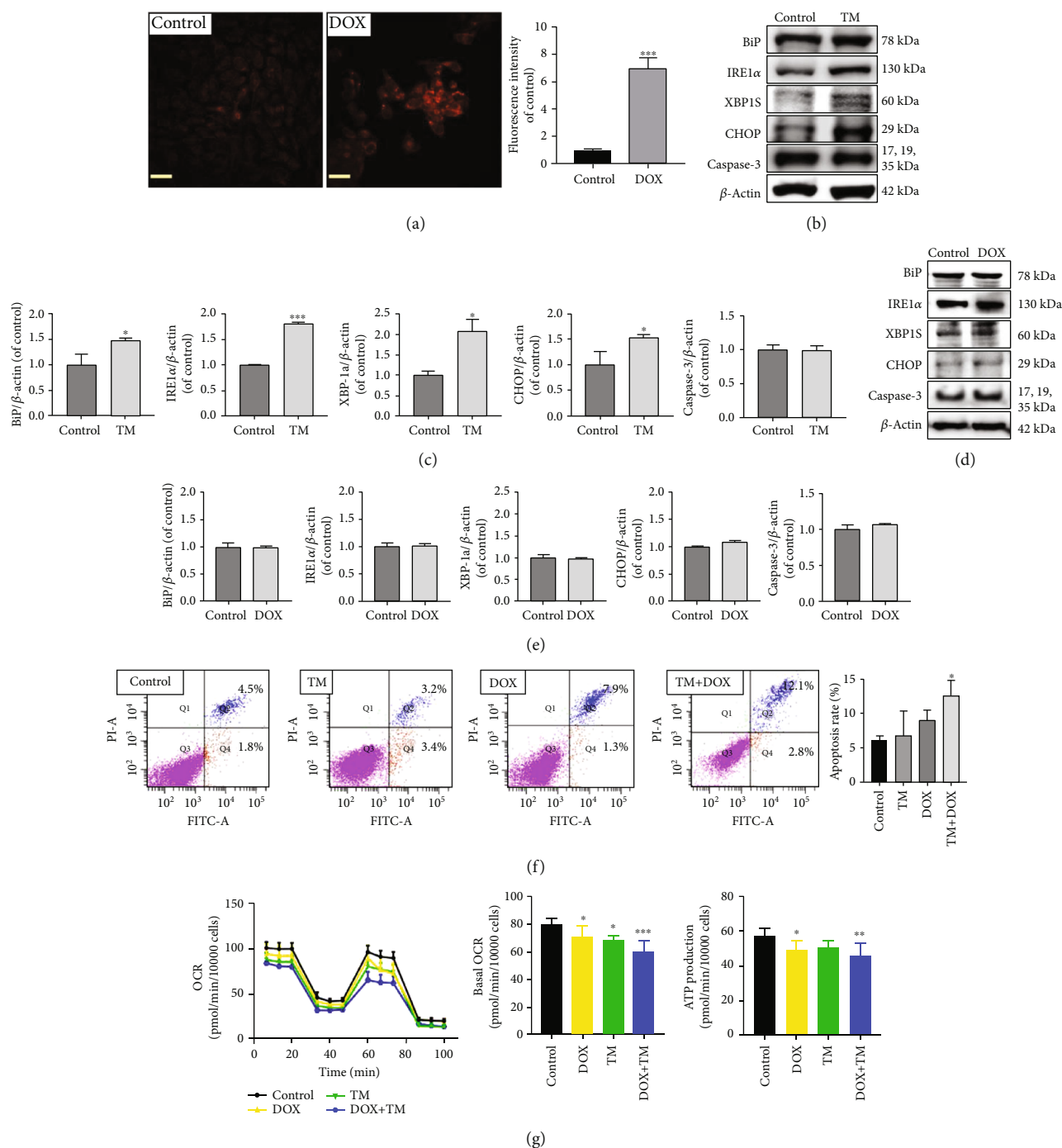


FIGURE 6: Oxidation-related decrease in mitochondrial function participated in ER stress-related apoptosis. (a) The mtROS levels in L02 cells treated with DOX were measured using the MitoSOX probe. (b–e) The expressions and quantification analysis of BiP, IRE1 α , CHOP, and Caspase-3 in cells treated with TM and DOX. (f) The apoptosis rates of L02 cells treated with DOX, TM, or DOX+TM were analyzed using FACS analysis. (g) Mitochondrial functions in the L02 cells treated with TM, DOX, or TM + DOX for 24 h, and the effects of these treatments on OCRs of basal and ATP production. * p < 0.05, ** p < 0.01, and *** p < 0.001 vs. the control groups.

Redox equilibrium is of importance to cell survival and function [14]. Abnormal ROS levels and oxidative stress always participate in the following toxic effects induced by internal toxicants or xenobiotic exposure [15, 16]. A previous study reported that emodin treatment promoted ROS content in the rat liver [17], but several studies found that low doses of emodin could inhibit ROS-mediated oxidative stress

in HeLa cells and rat macrophages [12, 18]. In conformity with earlier findings related to non-hepatocytes, our results demonstrated that emodin-induced ROS generation was associated with emodin-caused hepatic cytotoxicity. Metabolomic profiling identified obvious emodin-cysteine adducts in the cell culture medium, indicating that excessive consumption of cysteine-related antioxidants, such as GSH,

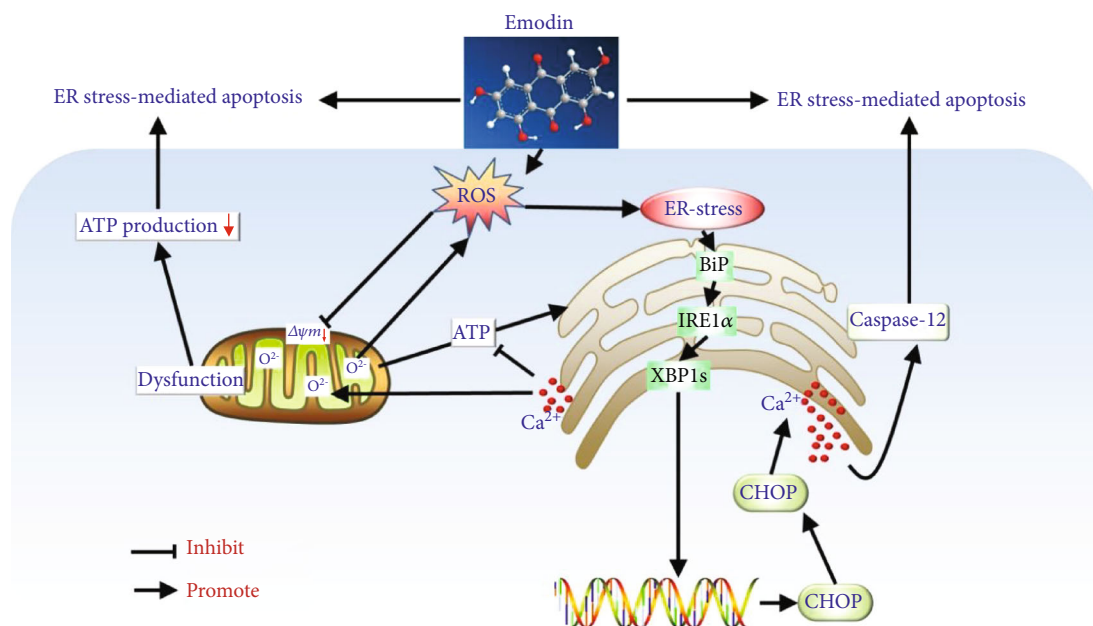


FIGURE 7: Schematic representation of the potential roles of oxidative stress mediated mitochondrial dysfunction and ER stress in emodin-induced hepatotoxicity.

might play a critical role in emodin-induced ROS generation and oxidative stress in hepatocytes [19]. As the main cellular redox hubs, MMP and mitochondrial function in turn were affected by overgenerated superoxide anion free radicals [20]. Obvious reductions in the coupling efficiency of OXHPS and ATP production suggested the depletion of intracellular ATP content. Meanwhile, the increased cytochrome C release, Bax/Bcl-2 ratio, and Caspase-3 expression suggested that emodin-caused hepatocytes' apoptosis would be possibly mitochondrial-dependent [21]. However, we found that MT indeed restored mitochondrial function but did not significantly decrease emodin-induced apoptosis. Therefore, oxidative stress-mediated inhibition of mitochondrial function could not be the core regulatory pathway of emodin-induced apoptosis of human hepatocytes.

Generally, ROS-induced oxidative stress affects the progress of protein folding, maturation, and degradation, all of which are controlled and proceed in the ER [10]. Induced aggregation of misfolded or unfolded proteins in the ER eventually leads to BiP-mediated ER stress, which would induce the UPR to degrade these undesirable proteins [22]. As documented, IRE1 α -, ATF6-, and PERK-mediated signaling transduction mechanisms are the main UPR pathways [23]. Of the three signaling pathways, emodin only induced the activation of IRE1 α , which could increase the folding capacity of the ER by promoting the expression of XBP-1s [24]. At the same time, the entrance of misfolding or misfolding protein would be also repressed by the enhancement of IRE1 α -XBP-1s signaling [25]. Hence, emodin induced the activation of IRE1 α -XBP-1s signaling in order to restore the ER function. But on the other hand, a prolonged increase in IRE1 α -XBP-1s signaling has been reported to trigger apoptosis via activating the downstream apoptotic factors, such as

ASK1, p38 MAPK, and JNK [10]. Besides, CHOP, a multifunctional transcription factor, has been implicated in apoptosis in ER stress. Our study found that CHOP could be induced by IRE1 α -XBP-1s rather than by PERK-ATF4 or PERK-eIF2 α mediated the UPR, which has been reported to be stronger inducer signaling of CHOP [26, 27]. The expressions of downstream apoptotic genes of CHOP, for instance, *DOCs*, *GADD34*, and *TRB3*, and apoptosis ensued [28]. In short, the BiP/IRE1 α /XBP-1s/CHOP signaling pathway might be involved in emodin-induced apoptosis and hepatotoxicity.

Previous studies have reported that CHOP could promote the expression of ER oxidoreduction 1 α (ERO1 α), which would redox regulate the activity of IP3R rather than PLC γ to cause Ca²⁺ release from the ER lumen [29]. Enhanced cytoplasmic Ca²⁺ content was likely to trigger the activation of calcium-dependent protein kinase II (CaMKII), which cleaved Caspase family members and finally activated various apoptotic pathways, including ER-related apoptosis that was mediated by Caspase-12 activation [30, 31]. Interestingly, enhanced CHOP-ERO1 α -CaMKII activation could cause NADPH depletion and ROS generation in the ER lumen [32, 33]. As a result, emodin treatment might create a ROS-CHOP-positive feedback loop, which exacerbated oxidative injury induced by emodin. Also, we found that MT rescued emodin-induced mitochondrial function by inhibiting mitochondrial oxidative stress but could not regain intracellular Ca²⁺ homeostasis and suppress apoptosis, possibly because those ROS productions derived from mitochondria triggered excessive ROS generation in the ER lumen. Also, ROS in ER-caused Ca²⁺ leakage could not be canceled by reducing mitochondrially generated reactive oxygen species (mtROS) levels. Only when the release of

Ca²⁺ from the ER to the cytoplasm was reduced could emodin-induced apoptosis be decreased. Hence, emodin exerted cytotoxic effects on human hepatocytes probably via ER-related apoptosis.

Recent advances have demonstrated the structural or mechanistic connections between the ER and mitochondria, for instance, mitochondrial-associated ER membranes (MAMs) [34]. Importantly, some of IP3Rs are located in MAMs and would provide a pathway to ER-mitochondrial Ca²⁺ transfers [35]. Therefore, emodin-induced ER stress and CHOP expression would enhance the ER Ca²⁺ influx to mitochondria, leading to mtROS in the mitochondrial matrix, both of which have been confirmed in emodin plus 2-APB-treated cells. Moreover, enough energy supply is necessary for protein folding and trafficking, the degradation of misfolded proteins in the ER [36]. Emodin-induced mtROS or Ca²⁺-induced secondary mtROS could both significantly inhibit mitochondrial oxidative phosphorylation. Also, Ca²⁺ overloading in the cytoplasm or mitochondria destroyed the normal Ca²⁺ gradient across the mitochondrial and ER membrane, which plays a key role in the mitochondrial ATP supply of the ER [37]. Altogether, emodin-induced oxidative inhabitation in mitochondrial function would aggravate ER-related apoptosis.

5. Conclusion

In conclusion, as presented in Figure 7, we demonstrated for the first time that emodin caused obvious oxidative stress in human hepatocytes and ER-related apoptosis, which was associated with the activation of the BiP/IRE1 α /CHOP signaling pathway and cytoplasmic Ca²⁺ overloading. During this progress, oxidative stress-mediated mitochondrial dysfunction would enhance emodin-induced-related hepatic apoptosis. Our findings are expected to help gain keen insights into toxic mechanisms underlying emodin-triggered hepatotoxicity and have implications for that oxidative stress-mediated ER stress could be an alternative target for the treatment of Cassiae Semen or other medicine-food homologous varieties containing emodin-induced liver injury.

Abbreviations

2-APB:	2-Aminoethyl diphenylborinate
CCK-8:	Cell Counting Kit-8 assay
DCFH-DA:	2,7-dichlorofluorescein diacetate
DOX:	Doxorubicin
ROS:	Reactive oxygen species
Emo:	Emodin
ER:	Endoplasmic reticulum
MAMs:	Mitochondrial-associated ER membranes
MMP:	Mitochondrial membrane potential
MT:	MitoTEMPO
mtROS:	Mitochondrially generated reactive oxygen species
NAC:	N-Acetyl-L-cysteine
OCRs:	Oxygen Consumption Rates
TM:	Tunicamycin
UPR:	Unfolded protein response.

Data Availability

The data used to support the findings of this study are included within the article.

Conflicts of Interest

There are no conflicts of interest to declare.

Authors' Contributions

Li-zhen Qiu, Lan-xin Yue, and Yu-hao Ni contributed equally to this work.

Acknowledgments

The study was funded by the National Key Research and Development Program (No. 2019YFC1604900) and the National Natural Science Foundation of China (No. 81630102).

Supplementary Materials

Table S1: information for all indicated antibodies used in the WB assay. (*Supplementary Materials*)

References

- [1] Y. Meng, Y. Liu, N. Fang, and Y. Guo, "Hepatoprotective effects of Cassia semen ethanol extract on non-alcoholic fatty liver disease in experimental rat," *Pharmaceutical Biology*, vol. 57, no. 1, pp. 98–104, 2019.
- [2] Q. Wang, J. Zhou, Z. Xiang et al., "Anti-diabetic and renoprotective effects of Cassiae semen extract in the streptozotocin-induced diabetic rats," *Journal of Ethnopharmacology*, vol. 239, p. 111904, 2019.
- [3] J. Yang, A. Zhu, S. Xiao et al., "Anthraquinones in the aqueous extract of Cassiae semen cause liver injury in rats through lipid metabolism disorder," *Phytomedicine*, vol. 64, p. 153059, 2019.
- [4] L. Lin, Y. Liu, S. Fu, C. Qu, H. Li, and J. Ni, "Inhibition of mitochondrial complex function—the hepatotoxicity mechanism of emodin based on quantitative proteomic analyses," *Cell*, vol. 8, no. 3, p. 263, 2019.
- [5] X. Dong, J. Fu, X. Yin et al., "Emodin: a review of its pharmacology, toxicity and pharmacokinetics," *Phytotherapy Research*, vol. 30, no. 8, pp. 1207–1218, 2016.
- [6] C. L. Li, J. Ma, L. Zheng, H. J. Li, and P. Li, "Determination of emodin in L-02 cells and cell culture media with liquid chromatography-mass spectrometry: application to a cellular toxicokinetic study," *Journal of Pharmaceutical and Biomedical Analysis*, vol. 71, pp. 71–78, 2012.
- [7] C. Chen, J. Gao, T. S. Wang et al., "NMR-based metabolomic techniques identify the toxicity of emodin in HepG2 cells," *Scientific Reports*, vol. 8, no. 1, p. 9379, 2018.
- [8] Y. Liu, M. S. Mapa, and R. L. Sprando, "Liver toxicity of anthraquinones: a combined in vitro cytotoxicity and in silico reverse dosimetry evaluation," *Food and Chemical Toxicology*, vol. 140, article 111313, 2020.
- [9] M. W. Stoner, C. F. McTiernan, I. Scott, and J. R. Manning, "Calreticulin expression in human cardiac myocytes induces

- ER stress-associated apoptosis,” *Physiological Reports*, vol. 8, no. 8, article e14400, 2020.
- [10] H. M. Zeeshan, G. H. Lee, H. R. Kim, and H. J. Chae, “Endoplasmic reticulum stress and associated ROS,” *International Journal of Molecular Sciences*, vol. 17, no. 3, p. 327, 2016.
- [11] K. Qu, N. Y. Shen, X. S. Xu et al., “Emodin induces human T cell apoptosis in vitro by ROS-mediated endoplasmic reticulum stress and mitochondrial dysfunction,” *Acta Pharmacologica Sinica*, vol. 34, no. 9, pp. 1217–1228, 2013.
- [12] E. H. Lee, S. Y. Baek, J. Y. Park, and Y. W. Kim, “Emodin in Rheum undulatum inhibits oxidative stress in the liver via AMPK with Hippo/Yap signalling pathway,” *Pharmaceutical Biology*, vol. 58, no. 1, pp. 333–341, 2020.
- [13] M. Guo, W. Jiang, M. Yang, X. Dou, and X. Pang, “Characterizing fungal communities in medicinal and edible *Cassia* semen using high-throughput sequencing,” *International Journal of Food Microbiology*, vol. 319, p. 108496, 2020.
- [14] M. Redza-Dutordoir and D. A. Averill-Bates, “Activation of apoptosis signalling pathways by reactive oxygen species,” *Biochimica et Biophysica Acta (BBA) - Molecular Cell Research*, vol. 1863, no. 12, pp. 2977–2992, 2016.
- [15] M. R. Farag and M. Alagawany, “Erythrocytes as a biological model for screening of xenobiotics toxicity,” *Chemico-Biological Interactions*, vol. 279, pp. 73–83, 2018.
- [16] Z. Lou, X. Li, X. Zhao, K. Du, and B. Wang, “Resveratrol attenuates hydrogen peroxide-induced apoptosis, reactive oxygen species generation, and PSGL1 and VWF activation in human umbilical vein endothelial cells, potentially via MAPK signalling pathways,” *Molecular Medicine Reports*, vol. 17, no. 2, pp. 2479–2487, 2018.
- [17] L. Wu, Y. Chen, H. Liu et al., “Emodin-induced hepatotoxicity was exacerbated by probenecid through inhibiting UGTs and MRP2,” *Toxicology and Applied Pharmacology*, vol. 359, pp. 91–101, 2018.
- [18] S. Zhu, Y. Wang, X. Wang, J. Li, and F. Hu, “Emodin inhibits ATP-induced IL-1 β secretion, ROS production and phagocytosis attenuation in rat peritoneal macrophages via antagonizing P2X7 receptor,” *Pharmaceutical Biology*, vol. 52, no. 1, pp. 51–57, 2014.
- [19] X. Liu, Y. Liu, Y. Qu, M. Cheng, and H. Xiao, “Metabolomic profiling of emodin-induced cytotoxicity in human liver cells and mechanistic study,” *Toxicology Research*, vol. 4, no. 4, pp. 948–955, 2015.
- [20] X. Zhang, C. S. G. G. Gibhardt, T. Will et al., “Redox signals at the ER-mitochondria interface control melanoma progression,” *The EMBO Journal*, vol. 38, no. 15, article e100871, 2019.
- [21] X. Luo, B. Lin, Y. Gao et al., “Genipin attenuates mitochondrial-dependent apoptosis, endoplasmic reticulum stress, and inflammation via the PI3K/AKT pathway in acute lung injury,” *International Immunopharmacology*, vol. 76, article 105842, 2019.
- [22] A. Roy and A. Kumar, “ER stress and unfolded protein response in cancer cachexia,” *Cancers*, vol. 11, no. 12, article 1929, 2019.
- [23] W. Zhou, D. Tian, J. He et al., “Exposure scenario: another important factor determining the toxic effects of PM2.5 and possible mechanisms involved,” *Environmental Pollution*, vol. 226, pp. 412–425, 2017.
- [24] T. A. Riaz, R. P. Junjappa, M. Handigund, J. Ferdous, H. R. Kim, and H. J. Chae, “Role of endoplasmic reticulum stress sensor IRE1 α in cellular physiology, calcium, ROS signaling, and metaflammation,” *Cell*, vol. 9, no. 5, article 1160, 2020.
- [25] S. Huang, Y. Xing, and Y. Liu, “Emerging roles for the ER stress sensor IRE1 α in metabolic regulation and disease,” *The Journal of Biological Chemistry*, vol. 294, no. 49, pp. 18726–18741, 2019.
- [26] D. Uzi, L. Barda, V. Scaiewicz et al., “CHOP is a critical regulator of acetaminophen-induced hepatotoxicity,” *Journal of Hepatology*, vol. 59, no. 3, pp. 495–503, 2013.
- [27] S. Xu, Y. Xu, L. Chen et al., “RCN1 suppresses ER stress-induced apoptosis via calcium homeostasis and PERK-CHOP signaling,” *Oncogene*, vol. 6, no. 3, article e304, 2017.
- [28] Y. Li, Y. Guo, J. Tang, J. Jiang, and Z. Chen, “New insights into the roles of CHOP-induced apoptosis in ER stress,” *Acta Biochimica et Biophysica Sinica*, vol. 46, no. 8, pp. 629–640, 2014.
- [29] G. Li, M. Mongillo, K. T. Chin et al., “Role of ERO1- α -mediated stimulation of inositol 1,4,5-triphosphate receptor activity in endoplasmic reticulum stress-induced apoptosis,” *The Journal of Cell Biology*, vol. 186, no. 6, pp. 783–792, 2009.
- [30] Y. Wang, L. Tu, Y. Li et al., “Notoginsenoside R1 alleviates oxygen-glucose deprivation/reoxygenation injury by suppressing endoplasmic reticulum calcium release via PLC,” *Scientific Reports*, vol. 7, no. 1, p. 16226, 2017.
- [31] M. Kamarehei, S. Kabudanian Ardestani, M. Firouzi, H. Zahednasab, H. Keyvani, and M. H. Harirchian, “Increased expression of endoplasmic reticulum stress-related caspase-12 and CHOP in the hippocampus of EAE mice,” *Brain Research Bulletin*, vol. 147, pp. 174–182, 2019.
- [32] W. Rozpedek, D. Pytel, B. Mucha, H. Leszczynska, J. A. Diehl, and I. Majsterek, “The role of the PERK/eIF2 α /ATF4/CHOP signaling pathway in tumor progression during endoplasmic reticulum stress,” *Current Molecular Medicine*, vol. 16, no. 6, pp. 533–544, 2016.
- [33] I. Tabas and D. Ron, “Integrating the mechanisms of apoptosis induced by endoplasmic reticulum stress,” *Nature Cell Biology*, vol. 13, no. 3, pp. 184–190, 2011.
- [34] Y. Fan and T. Simmen, “Mechanistic connections between endoplasmic reticulum (ER) redox control and mitochondrial metabolism,” *Cell*, vol. 8, no. 9, article 1071, 2019.
- [35] J. Loncke, M. Kerkhofs, A. Kaasik, I. Bezprozvanny, and G. Bultynck, “Recent advances in understanding IP3R function with focus on ER-mitochondrial Ca²⁺ transfers,” *Current Opinion in Physiology*, vol. 17, pp. 80–88, 2020.
- [36] M. R. Depaoli, J. C. Hay, W. F. Graier, and R. Malli, “The enigmatic ATP supply of the endoplasmic reticulum,” *Biological Reviews of the Cambridge Philosophical Society*, vol. 94, no. 2, pp. 610–628, 2019.
- [37] J. Yong, H. Bischof, S. Burgstaller et al., “Mitochondria supply ATP to the ER through a mechanism antagonized by cytosolic Ca²⁺,” *eLife*, vol. 8, 2019.

Research Article

Vinegar/Tetramethylpyrazine Induces Nutritional Preconditioning Protecting the Myocardium Mediated by VDAC1

Huan He,^{1,2} Liang Wang,³ Yang Qiao,² Qing Zhou,² Bin Yang,² Lu Yin,⁴ Dong Yin ,⁵ and Ming He ^{1,2}

¹Institute of Cardiovascular Diseases, Jiangxi Academy of Clinical Medical Sciences, The First Affiliated Hospital of Nanchang University, Nanchang 330006, China

²Jiangxi Provincial Key Laboratory of Basic Pharmacology, Nanchang University School of Pharmaceutical Science, Nanchang 330006, China

³Department of Rehabilitation, The First Affiliated Hospital of Nanchang University, Nanchang 330006, China

⁴Bioprocessing Technology Institute, Agency for Science, Technology and Research, Singapore, Singapore 138668

⁵Jiangxi Provincial Key Laboratory of Molecular Medicine, The Second Affiliated Hospital, Nanchang University, Nanchang 330006, China

Correspondence should be addressed to Dong Yin; dongyin24@126.com and Ming He; jxhm56@hotmail.com

Received 17 December 2020; Revised 10 February 2021; Accepted 1 April 2021; Published 21 April 2021

Academic Editor: Si Qin

Copyright © 2021 Huan He et al. This is an open access article distributed under the Creative Commons Attribution License, which permits unrestricted use, distribution, and reproduction in any medium, provided the original work is properly cited.

Vinegar is good for health. Tetramethylpyrazine (TMP) is the main component of its flavor, quality, and function. We hypothesized that vinegar/TMP pretreatment could induce myocardial protection of “nutritional preconditioning (NPC)” by low-dose, long-term supplementation and alleviate the myocardial injury caused by anoxia/reoxygenation (A/R). To test this hypothesis, TMP content in vinegar was detected by HPLC; A/R injury model was prepared by an isolated mouse heart and rat cardiomyocyte to evaluate the myocardial protection and mechanism of vinegar/TMP pretreatment by many enzymatic or functional, or cellular and molecular biological indexes. Our results showed that vinegar contained TMP, and its content was in direct proportion to storage time. Vinegar/TMP pretreatment could improve hemodynamic parameters, decrease lactate dehydrogenase (LDH) and creatine phosphokinase activities, and reduce infarct size and apoptosis in the isolated hearts of mice with A/R injury. Similarly, vinegar/TMP pretreatment could increase cell viability, decrease LDH activity, and decrease apoptosis against A/R injury of cardiomyocytes. Vinegar/TMP pretreatment could also maintain the mitochondrial function of A/R-injured cardiomyocytes, including improving oxygen consumption rate and extracellular acidification rate, reducing reactive oxygen species generation, mitochondrial membrane potential loss, mitochondrial permeability transition pore openness, and cytochrome c releasing. However, the protective effects of vinegar/TMP pretreatment were accompanied by the downregulation of VDAC1 expression in the myocardium and reversed by pAD/VDAC1, an adenovirus that upregulates VDAC1 expression. In conclusion, this study is the first to demonstrate that vinegar/TMP pretreatment could induce myocardial protection of NPC due to downregulating VDAC1 expression, inhibiting oxidative stress, and preventing mitochondrial dysfunction; that is, VDAC1 is their target, and the mitochondria are their target organelles. TMP is one of the most important myocardial protective substances in vinegar.

1. Introduction

Vinegar, produced via the complex fermentation of grain or fruits, is a worldwide popular condiment [1, 2]. Many works have shown the beneficial effects of vinegar consumption on the health of human [3–7]. Tetramethylpyrazine (TMP, Figure 1(a)), which naturally exists in a variety of fried,

roasted, or fermented foods, is considered to be the main component of vinegar’s flavor, nutrition, and health care function and quality [1, 2, 8]. TMP is also called as ligustrazine, derived from the rhizome of *Ligusticum wallichii*, and has many biological activities [9]. More and more medical scientists believe that TMP is beneficial to human health, especially cardiovascular and cerebrovascular health [10–12].

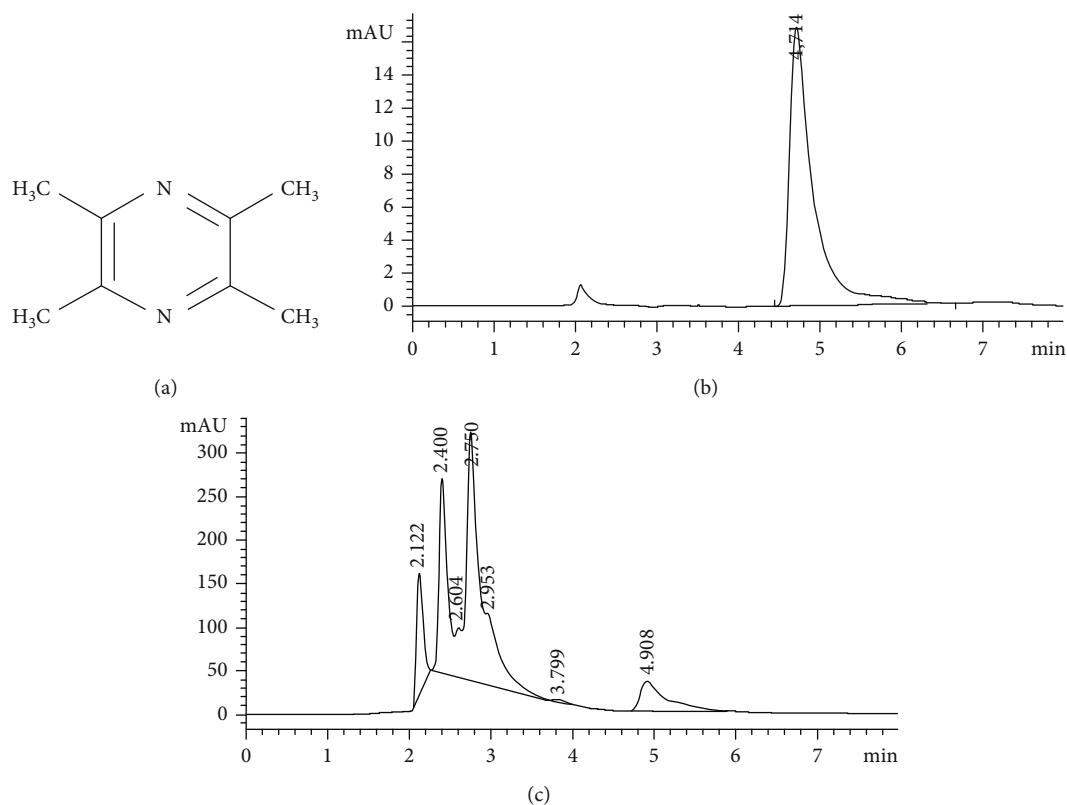


FIGURE 1: TMP concentration test in 6 kinds of commercial food vinegar. (a) Chemical structures of TMP. (b) Standard solution of TMP. (c) A typical vinegar sample of TMP.

Previously, we have found that TMP has an excellent protection on a variety of the myocardium or blood vessel injuries [13–16].

Coronary artery spasm or occlusion may result in myocardial ischemia, or even infarction [17]. In clinical practices, fast coronary flow reconstruction and reperfusion is the first-line treatment. However, reperfusion may lead to more serious tissue injury than the ischemia itself (ischemia/reperfusion, I/R) [18]. Ischemic preconditioning (IPC) and pharmacological preconditioning (PPC) could alleviate myocardial damage [17–19], but the application of these methods is limited by ethical concerns and technical difficulties. We have previously raised the concept of nutritional preconditioning (NPC) and proved it to be as an ideal solution to relieve myocardial damage [20–24]. We have further revealed that NPC inhibits intracellular reactive oxygen species (ROS) generation and mitochondria-mediated apoptosis pathway, which might efficiently alleviate anoxia/reoxygenation (A/R) damage, prevent mitochondrial dysfunction, and improve cardiac function [18, 22–24].

Voltage-dependent anion channel 1 (VDAC1) is a protein on the outer membrane of the mitochondria. VDAC1 is involved in the construction of mitochondrial permeability transition pore (mPTP) and acts as the gatekeeper of mPTP [25]. In responses to A/R, VDAC1 expression is upregulated, mPTP is opened, and myocardial damage is aggravated. We have shown that VDAC1 plays an important role in the

resveratrol's protection against A/R damage; in other words, VDAC1 was the target of resveratrol myocardial protection [20, 26, 27].

Therefore, we intend to explore whether NPC through low-dose, long-term supplementation of vinegar/TMP, representing a healthy dietary habit, could induce myocardial protection, and whether the protection mechanism is mediated by VDAC1 on the mitochondria.

2. Materials and Methods

2.1. Reagents and Vinegar Samples. Vinegars A-F were purchased from supermarket. TMP (purity: 98%) and atractyloside (Atr) were purchased from Sigma-Aldrich (St. Louis, MO, USA). pAD/VDAC1 was purchased from Gene Chem Co., Ltd. (Shanghai, China). Antibodies against VDAC1, cytochrome c (cyt C), and β -actin were purchased from Cell Signaling Technology (Beverly, MA, USA).

2.2. Animals. Adult male Kunming mice (20–22 g) and the neonatal (0–3 days) Sprague-Dawley (SD) rats were purchased through the Animal Center of Nanchang University (Nanchang, China). The animal protocols complied with the NIH *Guide for the Care and Use of Laboratory Animals* (NIH Publication No. 85-23, revised 1996) and were approved by the ethics committee of Nanchang University (No. 2019-0106).

2.3. Determination of TMP in Vinegar Samples. TMP control stock solution, negative control solution, and test solution were weighed and filtered through the 0.22 μm organic membrane. The TMP content in the vinegar samples was measured with HPLC as described previously [28]. A HPLC system (Agilent 1100 HPLC Systems, Santa Clara, CA, USA) with a Chemstation Edition Workstation, aG1313A autosampler, and Hypersil ODS (Thermo, Waltham, MA, USA, 250 mm \times 4.6 mm, 5 μm) was used. The sample injection volume was 20 μl . The mobile phase was comprised of methanol and 40 mM ammonium dihydrogen phosphate (50:50, v/v). The total flow rate was 1 ml/min. The wavelength of detection was 280 nm. The temperature of the column was 35°C.

2.4. In Vivo Experiments. The mice were raised in specific pathogen-free environment at 22°C to 25°C, 50% humidity, and 12 h dark/light cycle. Food (AIN-93G) and water were being fed regularly.

2.4.1. Intramyocardial Gene Delivery. Mice were intraperitoneally injected with 100 mg/kg ketamine and 8 mg/kg xylazine for anesthesia. The endotracheal intubation was performed, and then of the heart was exposed through the left anterior lateral incision of the fourth intercostal space. pAD/VDAC1 (2×10^{11} plaque-forming units/ml) was directly injected into the left ventricular free wall (4-5 sites, 10 μl /site); the residual air was exhausted before closing the chest. Sham-operated mice underwent the same procedures except for the gene delivery [20].

2.4.2. Preparation of Langendorff Isolated Heart Perfusion and A/R Injury Model. 24 h post treatment, mice were anaesthetized by intraperitoneal injection of 100 mg/kg ketamine and 8 mg/kg xylazine. The heart was quickly taken out and kept in precooled Krebs-Henseleit (KH) buffer. Then, the heart was mounted on an improved Langendorff device and perfused with KH buffer saturated with 95% O₂ and 5% CO₂, at 37°C (pH 7.4) under 60-70 mmHg pressure. Carefully inserted a ball filled with water (6-10 mmHg) into the left ventricle. Hemodynamic parameters, including left ventricular developed pressure (LVDP, kPa), maximum positive and negative changes in LVDP ($\pm dp/dt$ max, kPa/s), and coronary flow (CF, ml/min), were measured with PowerLab system (ADInstruments, Sydney, Australia) [20].

Firstly, the hearts were perfused by the above method for 30 min. Then, the normal KH buffer was replaced with modified KH buffer with glucose removed and saturated with 95% N₂ and 5% CO₂ at 37°C and pH 6.8, for 30 min to induce whole heart ischemia. The normal KH buffer was restored for another 30 min to induce A/R injury. The control hearts were only perfused by normal KH buffer [20].

2.4.3. Experimental Design. Mice were randomly divided into 8 groups, namely, (1) control, (2) A/R, (3) vinegar+A/R, (4) TMP+A/R, (5) vinegar+A/R+pAD/VDAC1, (6) TMP+A/R+pAD/VDAC1, (7) vinegar+A/R+Atr, and (8) TMP+A/R+Atr. Mice in groups (3), (5), and (7) were given 0.1 ml/10 g vinegar (Brand vinegar C) by gavage every day for 6 weeks. Mice in groups (4), (6), and (8) were given 6 mg/kg TMP

by gavage every day for 6 weeks. At the beginning of the last two weeks, mice in groups (5) and (6) were injected with pAD/VDAC1 according to the methods described above. Mice in groups (7) and (8) were intraperitoneally injected with 5 mg/kg Atr [23]. Mice in the control and A/R groups were given equal volume of normal saline by gavage for 6 weeks.

2.4.4. Determination of Hemodynamic Parameters and Related Enzyme Activities. Hemodynamic parameters were recorded [20]. Creatine phosphokinase (CPK) and lactate dehydrogenase (LDH) activities were determined with a Bio-Rad 680 microplate reader (Hercules, CA, USA) according to the kit manufacturer's guidelines (Jiancheng, Nanjing, China).

2.4.5. Measurement of Myocardial Infarction or Apoptosis by TTC/TUNEL Staining. After reperfusion, half of the hearts of the mice randomly were selected and cut into 1 mm cross sections. 2,3,5-Triphenyltetrazolium chloride (TTC, Sigma-Aldrich) staining was carried out as described previously [20]. Briefly, the sections incubated with 1% TTC in PBS (pH 7.4) for 30 min at 37°C and stored overnight at room temperature in 10% formaldehyde. Then, the sections were photographed with a digital camera and images were analyzed using planimetry by Image Jo software (National Institutes of Health, Bethesda, MD, USA). The risk area was calculated as the total ventricular area minus the cavity.

At the same time, the risk area of the left ventricular tissue of the remaining half of the mouse hearts was fixed and embedded, and cut into 5 μm sections. The terminal deoxynucleotidyl transferase-mediated nick end labeling (TUNEL, Promega, Madison, WI, USA) staining was performed to evaluate myocardial apoptosis as described previously [20]. TUNEL-positive cells were counted [23].

2.4.6. Caspase-3 Activity Measurement. Caspase-3 activity in the myocardium was measured by caspase-3 activity assay kit (R&D, Minneapolis, Minnesota, USA), according to the instruction of the manufacturer.

2.4.7. Determination of Myocardial Antioxidant Potential and Oxidative Stress Level. For evaluating the antioxidant potential, the ferric reducing antioxidant power (FRAP) of myocardial homogenate pretreated by vinegar/TMP was determined as previously described (Cell Biolabs, Santiago, CA, USA) [23]. Superoxide dismutase (SOD), catalase (CAT), glutathione peroxidase (GSH-Px) activities, and malondialdehyde (MDA) levels were determined according to the instructions (Jiancheng).

2.4.8. Western Blots Assay. Proteins from the myocardial samples and cardiomyocytes were extracted with a protein extraction kit (Applygen Technologies, Beijing, China). Then, the protein content was quantified using the bicinchoninic acid protein assay kit (Thermo). Protein expression was analyzed with western blotting as previously described [29]. From each sample, proteins (30 μg) were separated on a 12% SDS-PAGE gel and transferred onto the polyvinylidene fluoride membranes. After transfer, the membranes were

blocked and incubated overnight at 4°C with the following primary antibodies: VDAC1 (1 : 500), *cyt c* (1 : 500), and β -actin (1 : 2000). Secondary antibody by conjugated horseradish peroxidase (1 : 5000) was used, and β -actin was used as internal control.

2.5. In Vitro Experiments

2.5.1. Primary Cardiomyocyte Culture. Cardiomyocytes from 0-3-day-old SD rats were isolated as previously described [18, 29]. Briefly, the hearts from neonatal rats were removed and placed in precooling D-Hanks' balanced salt solution. The ventricles were digested with 0.1% trypsin and then harvested repeatedly by centrifugation at $600 \times g$ for 5 min. The cells were resuspended in plating medium (80% Dulbecco's minimal essential medium, DMEM), 20% fetal bovine serum, and 100 U/ml of penicillin and streptomycin, and plated in culture dishes that were incubated 37°C for 30 min to remove nonmyocytes. The suspended cells were plated on 60 mm gelatin-coated culture dishes at 1×10^6 cells per dish and incubated at 37°C in a standard humidity incubator with 95% O₂ and 5% CO₂. After 18 h, cardiomyocytes were washed and plated in fresh medium and incubated for additional 3 days at 37°C in a standard humidity incubator with 95% O₂ and 5% CO₂ before the experiment.

2.5.2. Adenovirus Transfection and A/R Damage. pAD/VCAD1 was transfected into cardiomyocytes cultured in fresh DMEM supplemented with 15% FBS. After 48 h, the transfection efficiency was about 85% [18]. The transfected cardiomyocytes were incubated at 37°C, 95% O₂ and 5% CO₂, for 2 h, and then, the subsequent experiments were carried out.

The culture plates with cardiomyocytes were placed in an air-tight anoxic chamber at 37°C, 95% N₂ and 5% CO₂, for 3 h, and then changed to 95% O₂ and 5% CO₂ for 2 h to induce A/R damage [18, 21].

2.5.3. Experimental Design. Firstly, we need to eliminate the possible influence of acidity, confirm the concentration-effect relationship between vinegar/TMP pretreatment, and select the optimal concentration of vinegar/TMP. Cardiomyocytes were divided into the following groups: (1) control: cells were incubated in fresh DMEM for 50 h; (2) A/R: cells were incubated in fresh DMEM for 43 h, and then damaged by A/R with the above methods; (3) vinegar+A/R: cells were pretreated with various concentrations of vinegar (Brand vinegar C 1.25, 5, and 20 μ l/ml) for 43 h and transferred to fresh DMEM, followed by A/R damage; (4) TMP+A/R: cells were pretreated with various concentrations of TMP (5, 20, and 80 μ M) for 43 h and transferred to fresh DMEM, followed by A/R damage; and (5) acetic acid alone/acetic acid+A/R: cells were pretreated by 8% acetic acid 20 μ l/ml for 43 h and transferred to fresh DMEM, followed by A/R damage or normal DMEM. After relevant treatment, cell viability and LDH activity were measured.

Next, we explored whether VDAC1 expression could influence the effects of vinegar/TMP pretreatment against A/R damage. Cardiomyocytes were divided into the following groups: (1) control group; (2) A/R group; (3) vinegar+A/R group; (4) TMP+A/R group; (5) vinegar+A/R+pAD/VCAD1

TABLE 1: Determination of TMP concentration in six different brands of vinegar ($n = 3$).

Sample no.	Peak area	Mean	Concentration (μ g/ml)	Storage time of mark (month)
Brand vinegar A	390.8	394.3	221.73	32
	394.9			32
	397.2			32
Brand vinegar B	451.0	448.4	261.22	40
	450.2			40
	444.1			40
Brand vinegar C	994.2	1006.1	512.59	62
	993.4			62
	1030.8			62
Brand vinegar D	No peak	—	—	
	No peak			
	No peak			
Brand vinegar E	1219.6	1214.7	634.33	70
	1217.3			70
	1207.1			70
Brand vinegar F	824.3	821.4	650.50	76
	813.3			76
	826.7			76

group; (6) TMP+A/R+pAD/VCAD1 group; (7) vinegar+A/R+Atr group; and (8) TMP+A/R+Atr group. The cardiomyocytes of (3), (5), and (7) groups were pretreated with 5 μ l/ml vinegar (brand vinegar C) for 43 h and changed the fresh DMEM and suffered by A/R damage. The cardiomyocytes of (4), (6), and (8) groups were pretreated with 20 μ M TMP for 43 h and changed the medium and suffered by A/R damage. The cardiomyocytes of (5) and (6) groups were pretreated by pAD/VCAD1 for 2 h prior to the pretreatment with vinegar or TMP. The cardiomyocytes of (7) and (8) groups were pretreated by 50 μ M Atr for 2 h prior to A/R damage. After relevant treatment, cell viability, LDH and caspase-3 activities, apoptosis, VCAD1 expression, ROS generation, oxygen consumption rate (OCR), extracellular acidification rate (ECAR), mitochondrial membrane potential (MMP), mPTP openness, and release of *cyt c* to the cytoplasm were determined.

2.5.4. Determination of Cell Viability, LDH and Caspase-3 Activities, Apoptosis, and Intracellular ROS Generation. After relevant treatment, LDH activity of supernatant was measured by LDH kits (Jiancheng). Cardiomyocytes were detected as follows: cell viability was tested by MTS kit (Promega), caspase-3 activity was detected by caspase-3 activity kit (R&D), apoptosis was measured with Annexin V-EGFP/PI apoptotic detection kit (BD Biosciences, San Diego, CA, USA), and intracellular ROS was assessed using a DCFH-DA probe (Invitrogen, Carlsbad, CA, USA), according to their manufacturer's instructions, respectively [15].

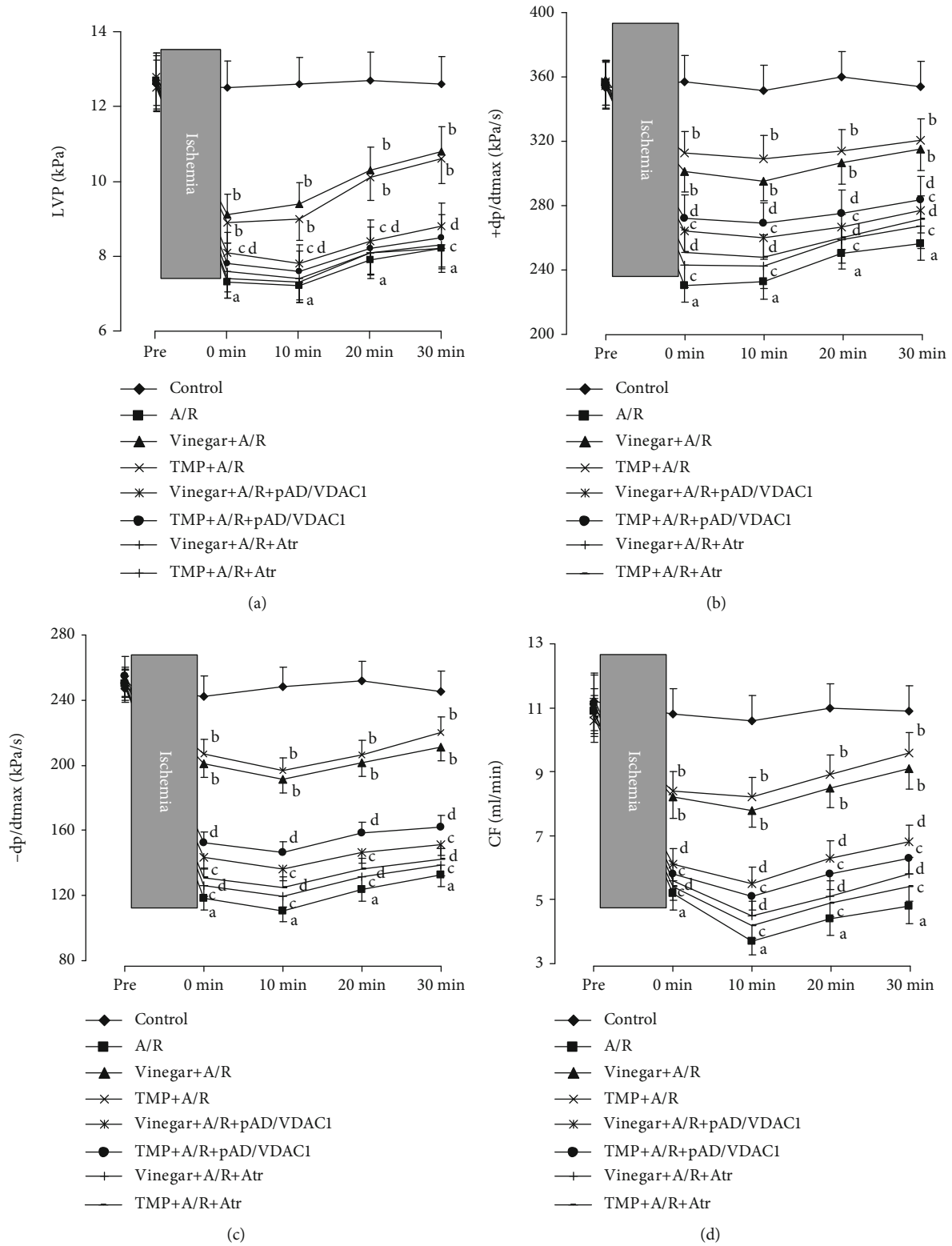


FIGURE 2: Continued.

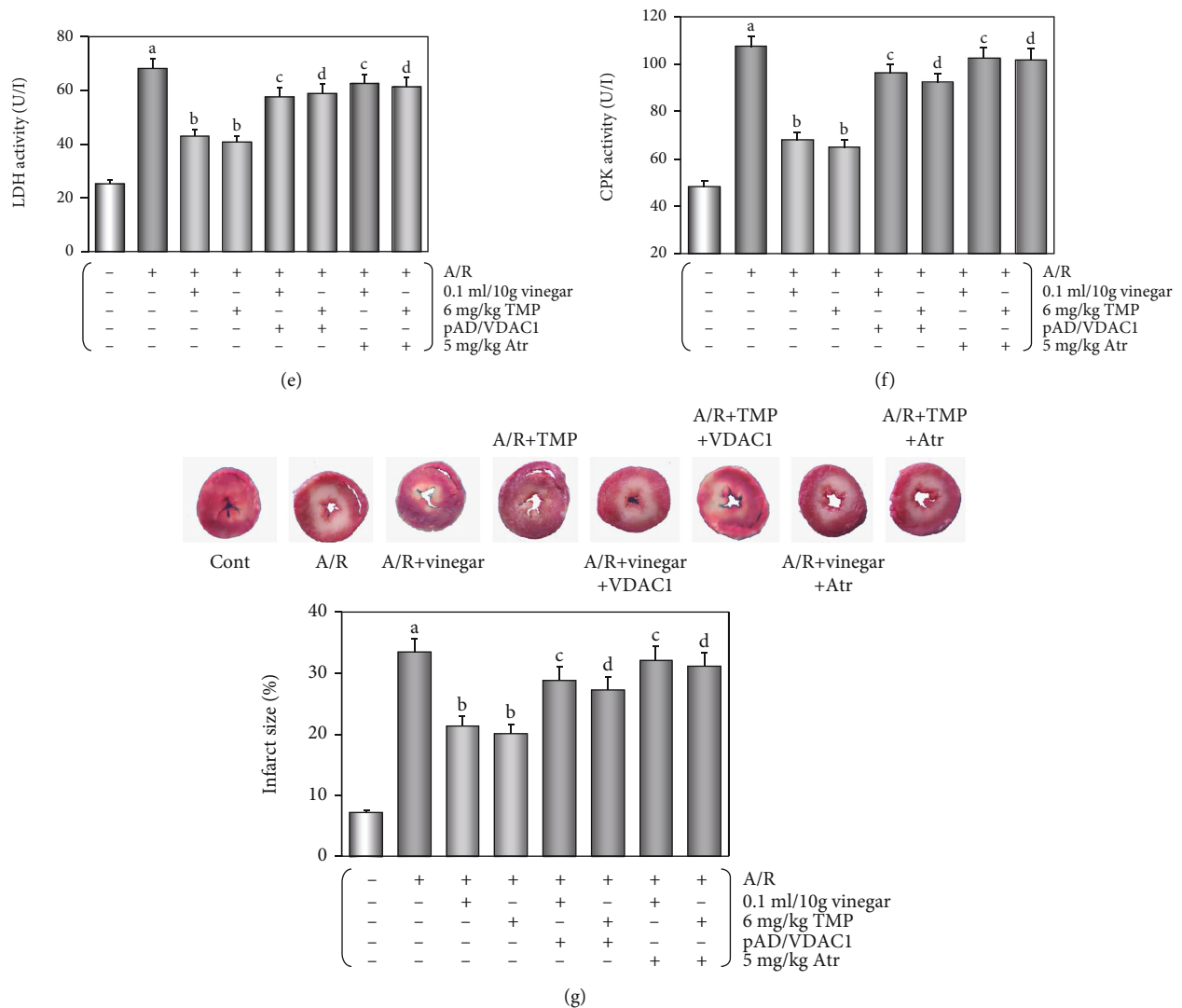


FIGURE 2: Effects of the hemodynamic parameters, LDH and CPK activities, and the myocardial infarct size by vinegar/TMP pretreatment on isolated mouse heart against A/R injury. (a) Histogram of LVDP. (b, c) Histogram of $\pm dp/dt$ max. (d) Histogram of CF. (e, f) Histogram of activities of LDH and CPK. Data were expressed as the mean \pm SEM ($n = 10$). (g) Histogram of myocardial infarct size. Data were expressed as the mean \pm SEM ($n = 5$). (a) $P < 0.01$ vs. the control group. (b) $P < 0.01$ vs. the A/R group. (c) $P < 0.01$ vs. the vinegar+A/R group. (d) $P < 0.01$ vs. the TMP+A/R group.

2.5.5. Measurement of OCR and ECAR. Mitochondrial respiration and glycolysis may reflect bioenergetics and overall cell health. OCR and ECAR detected by XFp Extracellular Flux Analyzer (Seahorse Biosciences, North Billerica, MA, USA) could evaluate the above function in real time as previously described [18].

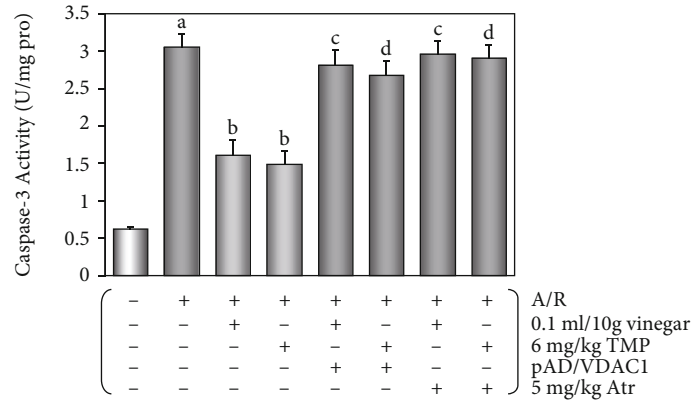
2.5.6. Assessment of MMP and mPTP Opening. MMP loss was measured with the fluorescent probe JC-1 (Invitrogen, Carlsbad, CA, USA) and flow cytometry as previously described [18]. mPTP opening could be measured by the Ca^{2+} -induced mitochondria swelling test as previously reported [23].

2.6. Statistical Analysis. Data were presented as the mean \pm SEM. One-way or two-way analysis of variance with the post

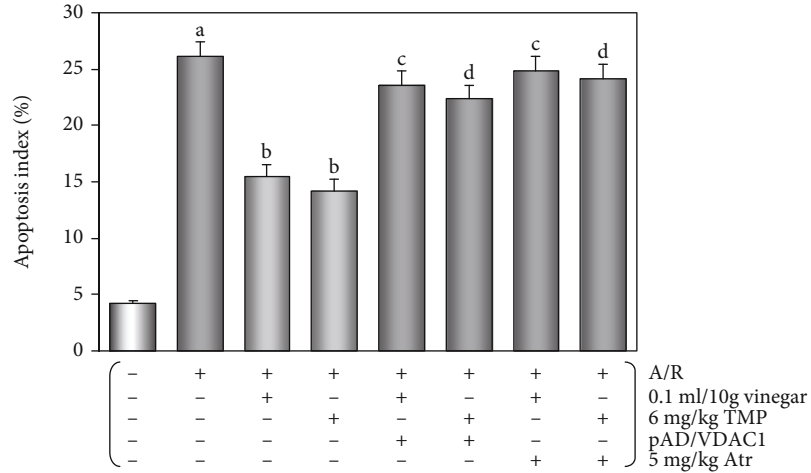
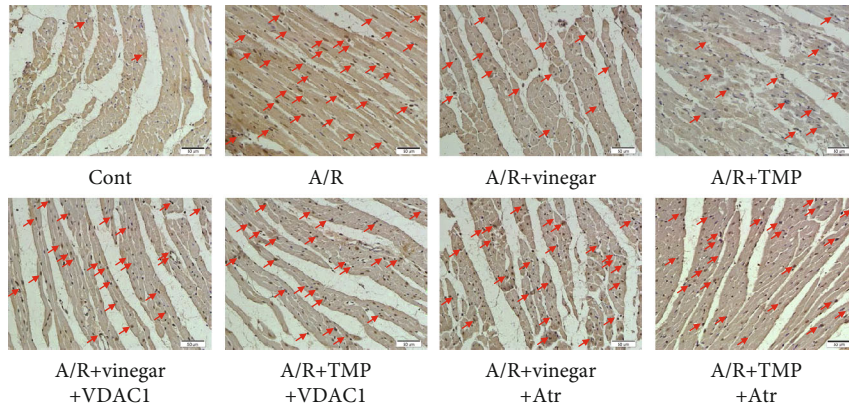
hoc Tukey-Kramer test was used to compare the groups. Statistical analysis was performed by Statistical Package for the Social Sciences (SPSS) software version 22.0 (IBM Corporation, Armonk, NY, USA). $P < 0.05$ was considered as statistically significant.

3. Results

3.1. TMP Concentration in Commercial Food Vinegar. We found that the elution peak of TMP could be detected at 5.0 min of the retention time (Figure 1(b)). TMP peaks of 6 vinegar samples were identified and quantified (Figure 1(c)). As shown in Table 1, brand vinegar A had the lowest TMP concentration at 221.73 $\mu\text{g/ml}$. Brand vinegar F had the highest TMP concentration at 650.50 $\mu\text{g/ml}$. No TMP was detected in brand vinegar D. The average



(a)



(b)

FIGURE 3: Continued.

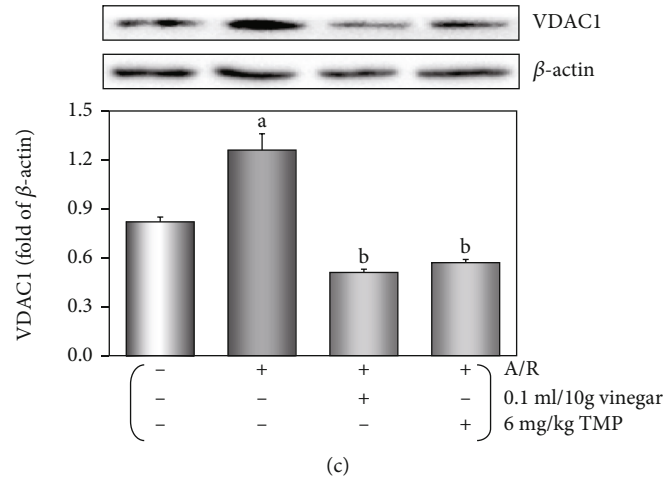


FIGURE 3: Effects of antiapoptotic and the expression of VCAD1 by vinegar/TMP pretreatment on isolated mouse heart against A/R injury. (a) Histogram of caspase-3 activity. (b) Histogram of apoptotic cells (TUNEL staining. Red arrows indicated TUNEL-positive cardiomyocytes). (c) The expression of VCAD1 in the myocardium. Data were expressed as the mean \pm SEM ($n = 5$). (a) $P < 0.01$ vs. the control group. (b) $P < 0.01$ vs. the A/R group. (c) $P < 0.01$ vs. the vinegar+A/R group. (d) $P < 0.01$ vs. the TMP+A/R group.

TABLE 2: Vinegar/TMP preconditioning preserves the myocardial homogenate ferric reducing antioxidant potentiality and the activities of antioxidant enzymes and reduced the levels of lipid peroxidation in the myocardium against A/R injury.

Groups	FRAP (mmol Fe ²⁺ /l)	SOD activity (U/g tissue)	GPx activity (U/g tissue)	CAT activity (U/g tissue)	MDA content (nmol/g tissue)
Control	5.11 \pm 0.20	86.32 \pm 4.22	19.52 \pm 1.46	14.68 \pm 1.25	29.06 \pm 1.83
A/R	1.42 \pm 0.04 ^a	20.82 \pm 1.61 ^a	4.83 \pm 0.51 ^a	6.35 \pm 0.52 ^a	140.28 \pm 7.52 ^a
Vinegar+A/R	4.06 \pm 0.23 ^b	51.61 \pm 2.62 ^b	13.06 \pm 1.35 ^b	10.28 \pm 0.82 ^b	82.31 \pm 5.06 ^b
TMP+A/R	4.35 \pm 0.22 ^b	56.28 \pm 2.81 ^b	15.20 \pm 1.38 ^b	11.06 \pm 0.76 ^b	78.62 \pm 4.91 ^b
Vinegar+A/R+pAD/VDAC1	1.93 \pm 0.06 ^c	25.12 \pm 1.85 ^c	6.62 \pm 0.60 ^c	7.21 \pm 0.54 ^c	135.20 \pm 7.08 ^c
TMP+A/R+pAD/VDAC1	2.15 \pm 0.05 ^d	27.32 \pm 1.66 ^d	6.91 \pm 0.58 ^d	7.02 \pm 0.53 ^d	132.61 \pm 7.63 ^d
Vinegar+A/R+Atr	1.71 \pm 0.05 ^c	22.08 \pm 1.58 ^c	4.51 \pm 0.61 ^c	5.86 \pm 0.55 ^c	146.65 \pm 8.02 ^c
TMP+A/R+Atr	1.86 \pm 0.06 ^d	21.39 \pm 1.62 ^d	4.92 \pm 0.57 ^d	5.98 \pm 0.58 ^d	143.28 \pm 7.31 ^d

Data were presented as the mean \pm SEM for five individual experiments. ^a $P < 0.01$ vs. the control group. ^b $P < 0.01$ vs. the A/R group. ^c $P < 0.01$ vs. the vinegar+A/R group. ^d $P < 0.01$ vs. the TMP+A/R group.

concentration of TMP of the other 5 vinegars is $456.07 \pm 90.85 \mu\text{g/ml}$. In addition, we found that TMP concentration in brand vinegars was proportional to its storage time (calculated from the production date, Table 1), which was consistent with the research results of Xu et al. [30].

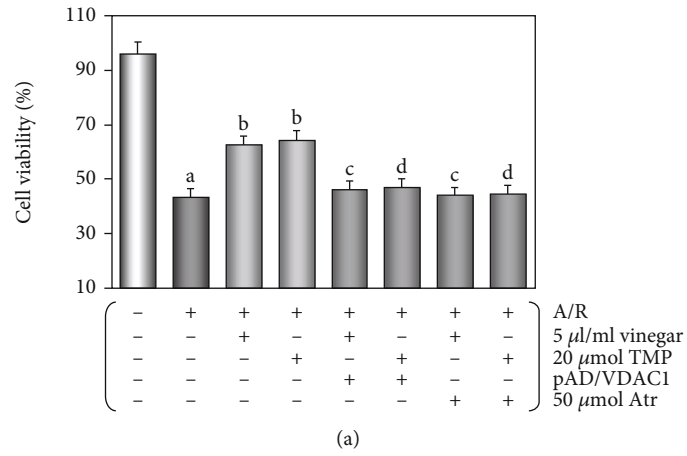
3.2. Protective Effects of Vinegar/TMP Pretreatment on the Isolated Mouse Heart against A/R Damage. Hemodynamic parameters such as LVDP, $\pm dp/dt$ max, and CF are important indicators of cardiac function [20]. After A/R damage, LVDP, $\pm dp/dt$ max, and CF significantly decreased; however, the cardiac function of mice was significantly recovered with vinegar/TMP pretreatment (Figures 2(a)–2(d), $P < 0.01$). Similarly, after A/R injury, the tissue damage-related enzyme LDH and CPK activities and the infarct size, which was the gold index for myocardial damage [23], all significantly increased, and still vinegar/TMP pretreatment could restore the changes ($P < 0.01$, Figures 2(e)–2(g)). Our results also showed a significant increase in caspase-3 activity and TUNEL-positive cells after A/R injury, which was attenuated

by vinegar/TMP pretreatment ($P < 0.01$, Figures 3(a) and 3(b)). Interestingly, the protective effects of vinegar/TMP pretreatment were largely diminished by cotreatment of pAD/VDAC1 or Atr ($P < 0.01$, Figures 2 and 3).

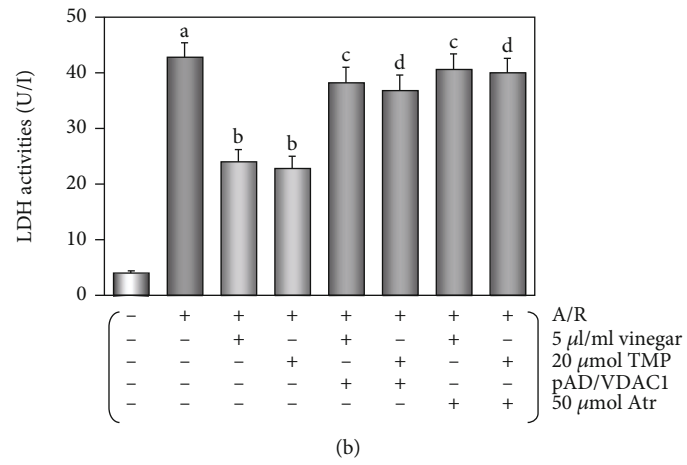
It has been reported that the oxidative stress of the myocardium increases with A/R damage [19, 31]. Our results showed that SOD, CAT, and GSH-Px activities were inhibited, MDA level increased, and the FRAP results showed that myocardial antioxidant capacity decreased after A/R damage. Vinegar/TMP pretreatment could attenuate these adverse responses. However, these effects of vinegar/TMP pretreating were almost canceled by cotreatment of pAD/VDAC1 or Atr ($P < 0.01$, Table 2).

Western blot analysis (Figure 3(c)) indicated that A/R damage resulted in upregulation of VCAD1 ($P < 0.01$), and long-term oral vinegar/TMP intake significantly reduced it ($P < 0.01$).

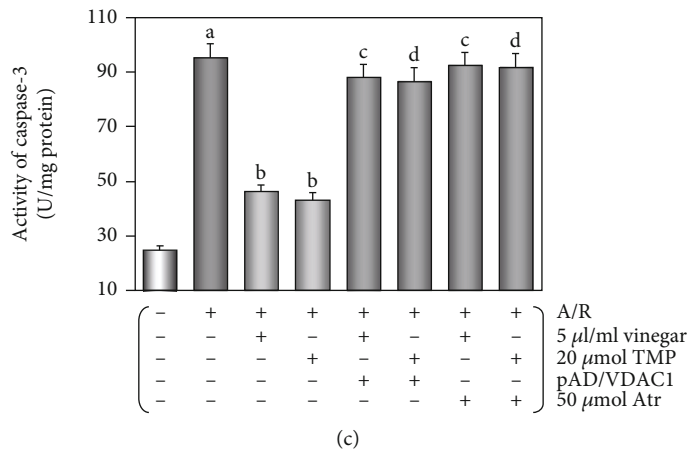
The results showed that low-dose, long-term oral vinegar/TMP intake could induce protection to A/R injury to the isolated mouse heart and this protective effect is



(a)

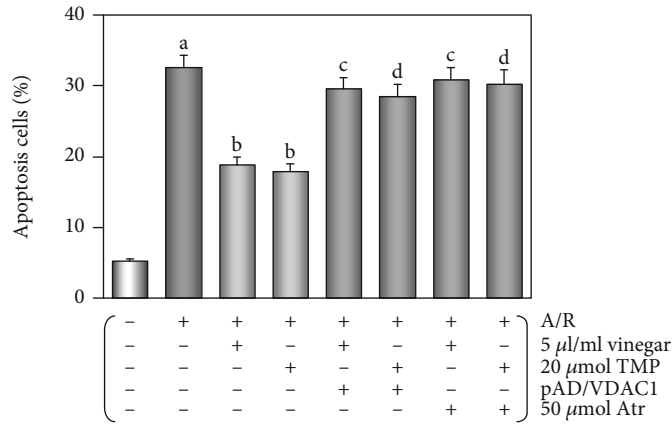
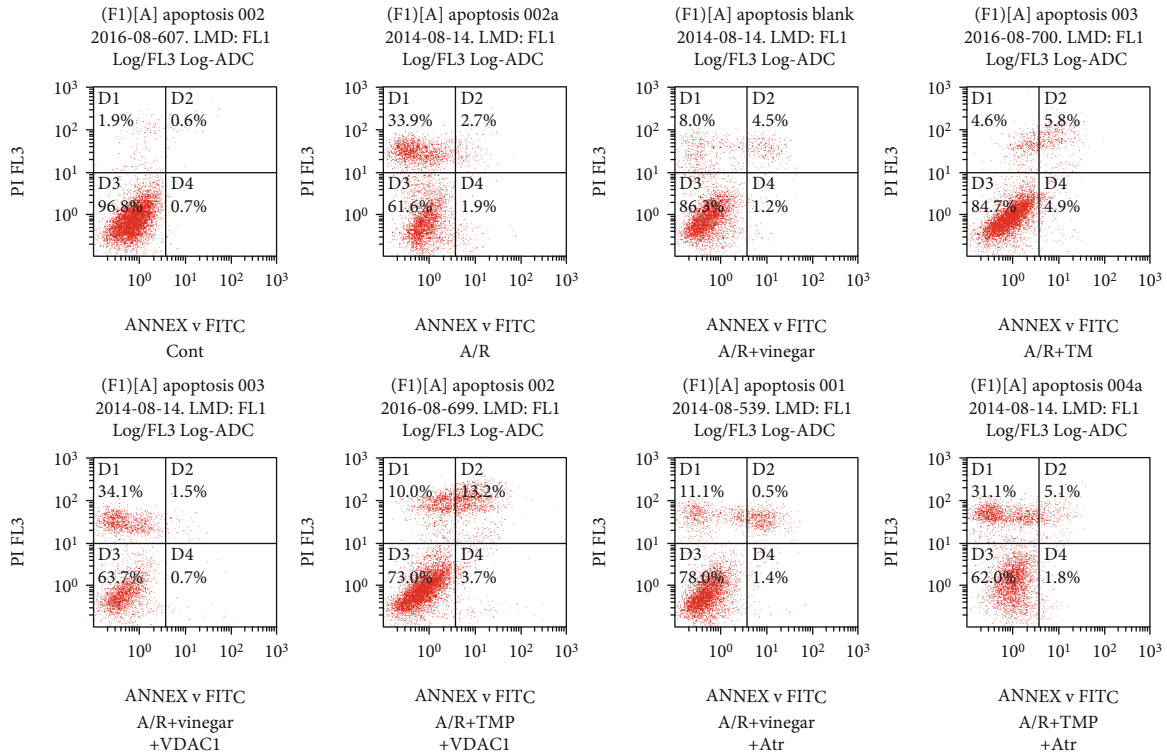


(b)

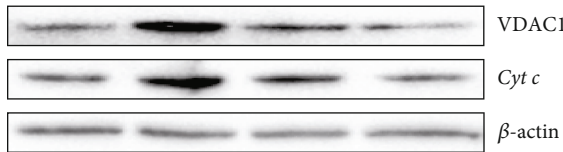


(c)

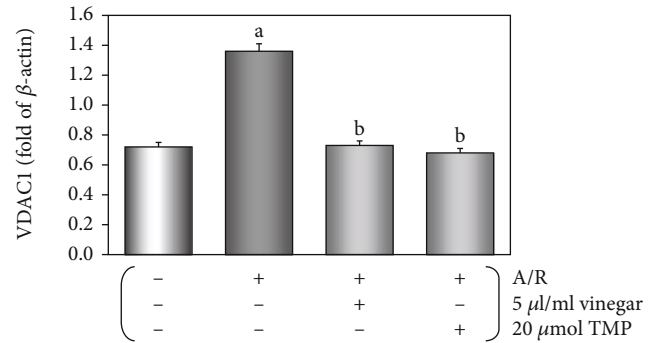
FIGURE 4: Continued.



(d)



(e)



(f)

FIGURE 4: Continued.

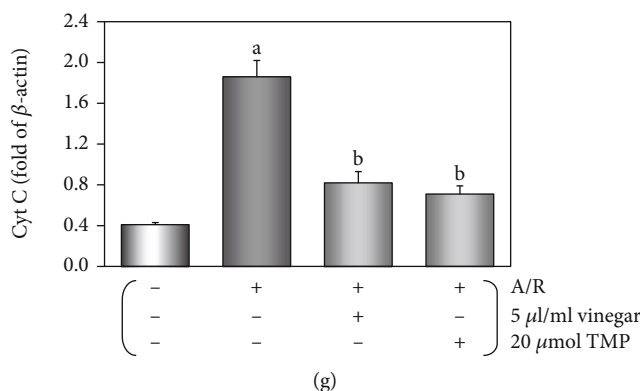


FIGURE 4: Protective effects of vinegar/TMP pretreatment for cardiomyocyte against A/R injury. (a) Histogram of cell viability. (b) Histogram of LDH activity. (c) Histogram of caspase-3 activity. (d) Flow cytometry dot plots and histogram of apoptotic cells. (e) Western blot of VCAD1 and *cyt c* expression in cardiomyocyte. (f) Histogram of VCAD1 expression. (g) Histogram of *cyt c* expression. Data were expressed as the mean \pm SEM ($n = 8$). (a) $P < 0.01$ vs. the control group. (b) $P < 0.01$ vs. the A/R group; (c) $P < 0.01$ vs. the vinegar+A/R group. (d) $P < 0.01$ vs. the TMP+A/R group.

associated with the downregulation of VDAC1 expression in the myocardium and the opening of mPTP [20, 23].

3.3. Protective Effects of Vinegar/TMP Pretreatment on Cardiomyocyte against A/R Damage. As shown in Supplemental Figures S1 and S2, cardiomyocytes subjected to A/R damage displayed decreased cell viability and increased LDH activity, and vinegar/TMP pretreating could reverse the changes in a concentration-dependent manner. In the acetic acid alone/acetic acid+A/R groups, the two indexes did not change, suggesting the observed protective effects from vinegar were independent of its acidity. The concentration of vinegar/TMP pretreating for the subsequent experiment was selected at 5 μ l vinegar/20 μ M TMP (Figures 4(a) and 4(b)).

Compared with the control group, cell viability/LDH activity did not alter in the groups with vinegar alone, TMP alone, pAD/VDAC1 alone, vinegar+pAD/VDAC1, TMP+pAD/VDAC1, vinegar+Atr, and TMP+Atr ($P > 0.05$), but decreased in the group with Atr alone ($P < 0.01$). The same was observed for the pAD/VDAC1+A/R group and Atr+A/R group compared with the A/R group ($P < 0.01$, Supplemental Figures S3 and S4), indicating that the upregulation of VDAC1 expression by pAD/VDAC1 and the opening of mPTP by Atr might aggravate cardiomyocyte damage [20, 23]. As shown in Supplemental Figure S5, in the group of vinegar/TMP alone, VDAC1 expression was significantly downregulated ($P < 0.01$). In the groups of pAD/VDAC1 alone and pAD/VDAC1+A/R, the expression of VDAC1 was upregulated to different degrees ($P < 0.01$, Supplemental Figure S6), indicating that adenovirus pAD/VDAC1 transfection was effective.

After A/R damage, caspase-3 activity and apoptosis rate were increased, whereas vinegar/TMP pretreatment significantly suppressed caspase-3 activity and apoptosis of cardiomyocyte ($P < 0.01$, Figures 4(c) and 4(d)). Similarly, the effects of vinegar/TMP pretreating were almost canceled with cotreatment of pAD/VDAC1 or Atr ($P < 0.01$, Figures 4(a)–4(d)).

Western blot analysis (Figures 4(e) and 4(f)) indicated that the changes of VDAC1 expression in cardiomyocytes were similar to those in the mouse myocardium.

3.4. Effects of Vinegar/TMP on Alleviating Mitochondrial Dysfunction in Cardiomyocyte. The OCR of cardiomyocyte by vinegar/TMP pretreatment was higher than those subjected to A/R. The results showed that the basal respiration, maximal respiration, ATP production, and spare respiratory capacity were significantly higher in cardiomyocytes undergone with vinegar/TMP pretreatment ($P < 0.01$, Figure 5(a)); however, the proton peak was slightly lower. Similarly, the ECAR of vinegar/TMP-pretreated cardiomyocyte was higher than A/R-pretreated cardiomyocyte, indicating significantly increased glycolysis and glycolytic capacity ($P < 0.01$, Figure 5(b)). But nonglycolytic acidification and glycolytic reserve increased slightly.

As shown, A/R damage caused a significant increase in ROS level. Vinegar/TMP pretreatment could significantly reduce ROS ($P < 0.01$, Figure 5(c)). In contrast, A/R damage caused a decline in MMP level, and vinegar/TMP pretreatment could reverse the change ($P < 0.01$, Figure 5(d)).

After A/R treatment, mitochondrial swelling was observed, indicating that mPTP was opened; vinegar/TMP pretreatment with mPTP opening showed a marked mild trend ($P < 0.01$, Figure 5(e)). In addition, A/R injury increased *cyt c* concentration in the cytoplasm ($P < 0.01$), and vinegar/TMP pretreatment significantly reduced it ($P < 0.01$, Figures 4(e) and 4(g)).

Similarly, these effects of vinegar/TMP pretreating were almost canceled with cotreatment of pAD/VCAD1 or Atr ($P < 0.01$, Figures 5(c)–5(e)).

4. Discussion

Vinegar is a worldwide popular food condiment and pickling material due to its taste and flavor [7]. It also has nutrition and health care functions [4, 6] and plays an important role in traditional Chinese medicine (TCM) food therapy [5]

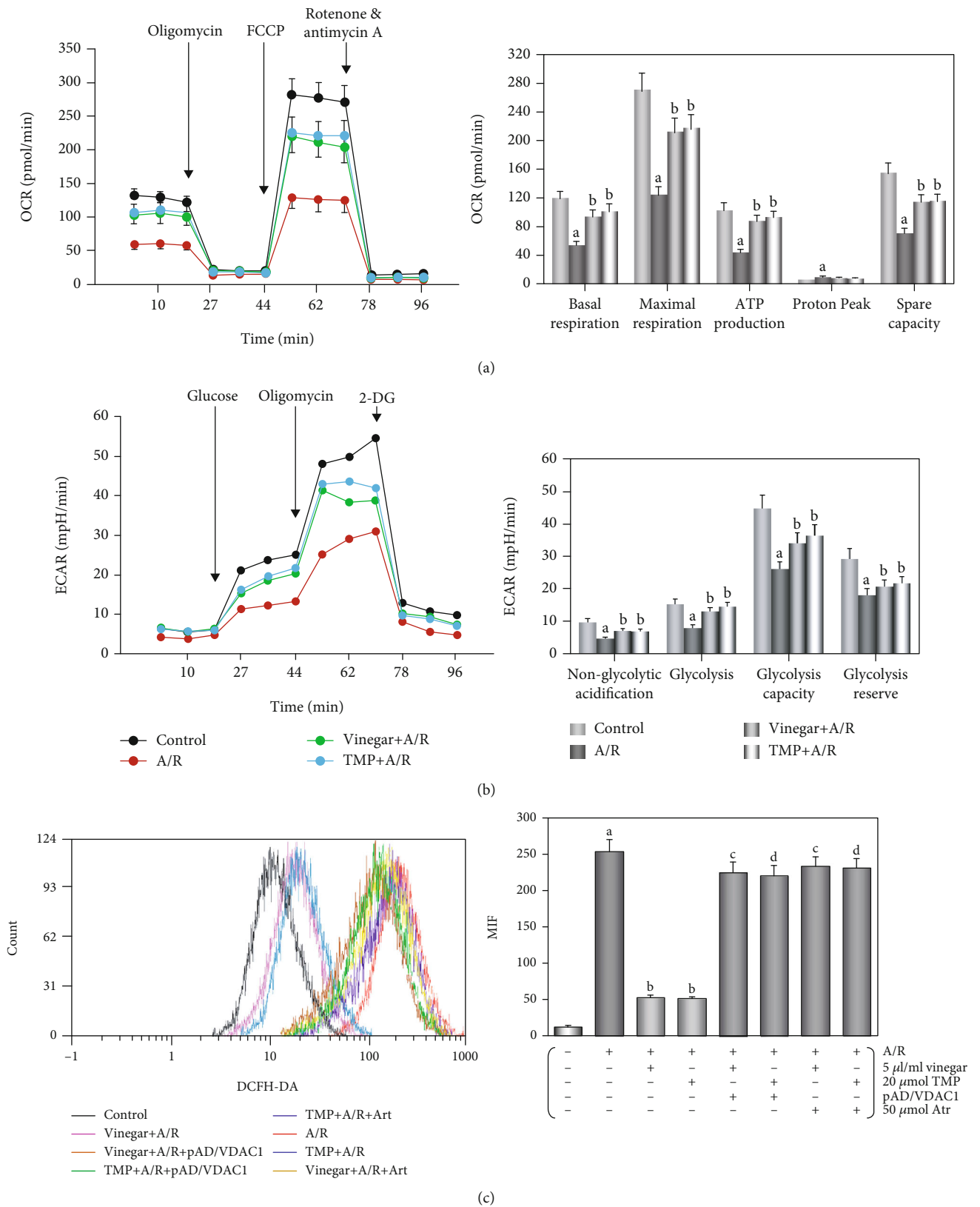


FIGURE 5: Continued.

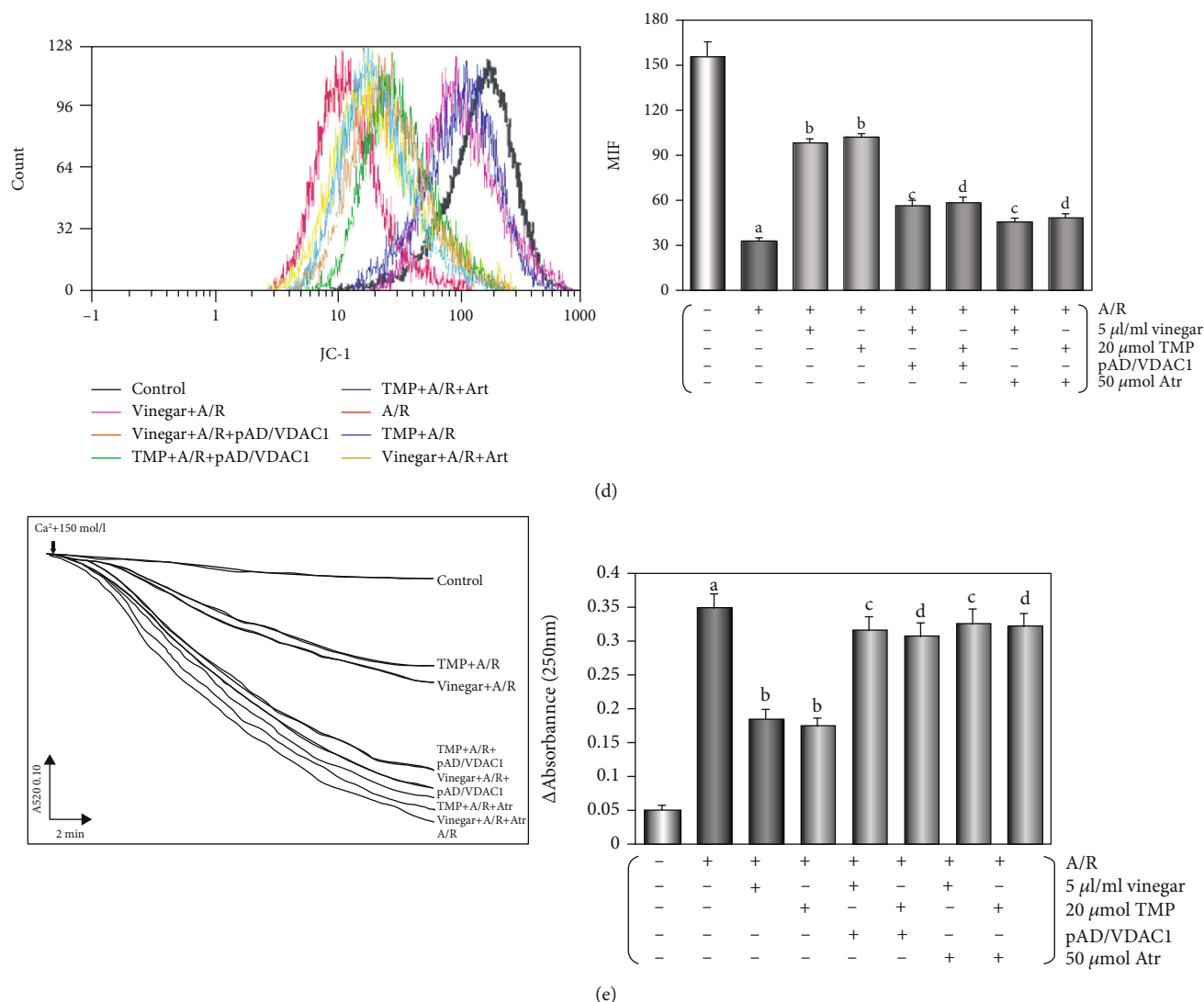


FIGURE 5: Effects of vinegar/TMP on alleviating mitochondrial dysfunction in cardiomyocyte against A/R injury. (a) Mitochondrial OCR curves and histogram of the important parameter. (b) Mitochondrial ECAR curves and histogram of the important parameter. Data were expressed as the mean ± SEM ($n = 3$). (c) Histogram of ROS generation. (d) Histogram of MMP levels. (e) Histogram of mPTP opening. Data were expressed as the mean ± SEM ($n = 8$). (a) $P < 0.01$ vs. the control group. (b) $P < 0.01$ vs. the A/R group. (c) $P < 0.01$ vs. the vinegar+A/R group. (d) $P < 0.01$ vs. the TMP+A/R group.

and Mediterranean diet [3]. Studies have shown that vinegar possesses antioxidant [6, 32], anti-inflammatory, and anti-obesity properties [3, 33], which may affect lipid profile, suppress adipocyte differentiation and fat accumulation, reduce body weight and plasma triglyceride, and prevent HFD-induced obesity and obesity-related cardiovascular complications [3, 6, 32–35]. Many healthy ingredients have been reported in vinegar, such as carbohydrates, organic acids, amino acids, peptides, and some functional factors, including TMP. TMP has pleasant tones of nutty and roasted flavors and is usually used to enhance food special flavor [2]. TMP is considered as one of the most aroma-active compounds [8, 36] and a functional ingredient [2, 37], determining vinegar quality [1, 28]. The formation mechanism of TMP in vinegar is controversial, but its concentration increases significantly with the storage time [30], which was

reconfirmed in this study (Table 1, from 221.73 μg/ml to 650.50 μg/ml).

TMP is an alkaloid with multitarget and multimechanism. It is also extracted from *Ligusticum wallichii*'s rhizome. It has many biological functions, including inhibition of oxidative stress and inducing cytoprotection [9]. TMP is a promising candidate for managing cardiovascular and cerebrovascular diseases [10–12]. Our previous study also articulated that TMP has excellent protective function on a variety of the myocardium and blood vessel injuries [13–16]. In this study, we characterized the effect of vinegar/TMP pretreatment in alleviating A/R-induced myocardial damage by multiple functional, enzymatic, cellular, or molecular biological indicators (Figures 2–5, Table 2). It is worth noting that, firstly, by adopting a high concentration acetic acid as control [30], we ruled out the impact of vinegar on myocardial

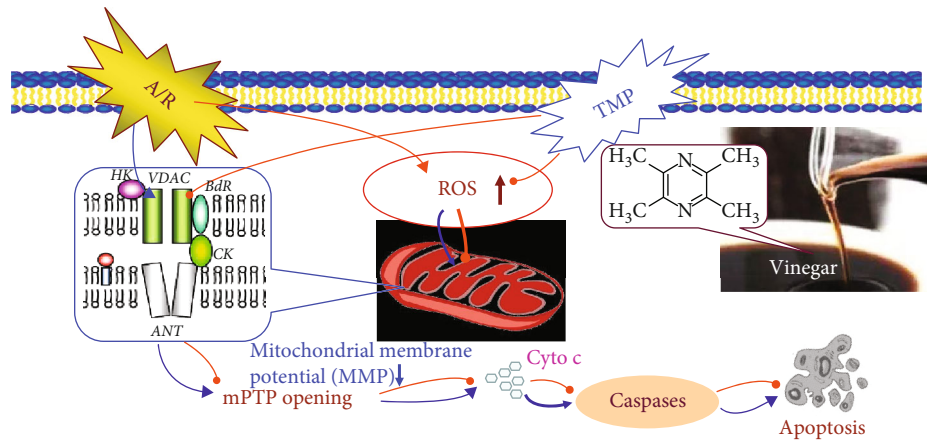


FIGURE 6: The mechanism of myocardial protection induced by vinegar/TMP. Vinegar contains TMP. TMP is one of the most important myocardial protective substances in vinegar. “Nutritional preconditioning” through low-dose long-term consumption of vinegar/TMP is shown to trigger myocardial protection, alleviating A/R-induced myocardial damage *in vivo* and *in vitro*. Vinegar/TMP pretreatment acts through downregulating VDAC1 expression, inhibiting oxidative stress, and preventing mitochondrial dysfunction. VDAC1 is their target, and the mitochondria are their target organelles.

protection due to acidity. Secondly, similar levels of myocardial protection were observed between pretreatment of TMP and pretreatment of vinegar containing equivalent TMP concentration, implying TMP to be the most important myocardial protective factors in vinegar. Thirdly, A/R injury was induced only after complete clearance of the vinegar/TMP in both the *in vitro* (after media change) and *in vivo* (24 h after administration [9]) models. Thus, the observed myocardial protection was likely due to the change of cardiomyocytes’ property during long-term NPC [17], rather than spontaneous response to the vinegar/TMP. Lastly, in this study, physiologically relevant concentration of vinegar was applied in priming to mimic the daily vinegar intake of people [4]. The results suggested that normal dietary consumption of vinegar (15 ml daily) meets the condition of NPC to induce myocardial protection [38].

IPC or PPC may trigger the production of endogenous myocardial protective substances, or change the related bioactive molecules to withstand serious I/R injury [17, 19]. However, the ethical concerns and technical difficulties are the limiting factors of these two methods. NPC is a convenient and feasible substitute, as it provides similar myocardial protection through dietary intake of natural and nontoxic nutrients [20]. In previous studies, we have demonstrated the use of several nutrients (including TMP, ferulic acid, resveratrol, curcumin, astragaloside IV, and apigenin) for NPC to effectively and safely protect the myocardium and blood vessels against various injuries [14, 20–24]. Therefore, it could be concluded that in this study, the effects of vinegar/TMP pretreatment belong to NPC myocardial protection. We further found that A/R injury could significantly upregulate VDAC1 expression, and with the protective effects induced by vinegar/TMP pretreatment, the upregulation of VDAC1 expression was significantly inhibited (Figures 3(c) and 4(e)); however, when combined with the pAD/VDAC1 to reupregulate VDAC1 expression, the protective effects of vinegar/TMP pretreatment were basically

reversed (Figures 2–5). Therefore, it could be concluded that the target of vinegar/TMP pretreatment was VDAC1.

VDAC1 is involved in the formation of an important pore in the mitochondrial membrane, namely, mPTP, which is responsible for the transport of metabolites and signal transduction [25, 39]. VDAC1 is upregulated in A/R-injured cardiomyocytes. It forms complex with Bax, and triggers apoptosis through the release of apoptosis factor such as *cyt c* into the cytoplasm [40]. In the previous studies, we also obtained similar results: VDAC1 was upregulated in cardiomyocytes by A/R injury, which promoted mitochondrial-mediated apoptosis. Resveratrol, another important functional factor, could inhibit the upregulation and modification of VDAC1 and played a role in myocardial protection [20, 26, 27].

After A/R damage, ROS may break out with the increase of free radical and the decrease of scavenging ability [17–19, 31]. Our results found that after A/R injury, the myocardium showed the higher level of oxidative stress, weaker antioxidant potential, and more intracellular ROS generation. Due to TMP possessing stronger antioxidant capacity itself [9], vinegar/TMP pretreatment could partially reverse the above changes (Table 2, Figure 5(c)).

In recent years, it has been found that the mitochondria not only undertake and complete energy metabolism but also actively or passively participate in, or even determine cell function, survival state and death mode [41]. Therefore, to ensure the integrity of its structure and function is the basis of many life activities [23]. mPTP is a multiprotein complex formed between the inner and outer mitochondrial membranes. mPTP opening is regarded as a pivotal event in the irreversible reperfusion injury. Sustained mPTP opening will result in mitochondrial depolarisation, swelling, and rupture of the external membranes, and ultimately lead to mitochondrial dysfunction [42, 43]. As an important protein of mPTP, VDAC1 is located in the outer membrane of the mitochondria, which controls the entry and exit of mitochondrial

metabolites and ions, as well as mPTP opening [25]. Therefore, inhibiting the function of VDAC1 can prevent mPTP opening, which is beneficial to the prevention of myocardial injury [20]. In the previous studies, we found that TMP could target the mitochondria, could prevent mPTP openness, and had an excellent protective effect on a variety of the myocardium or blood vessel injuries [13–15]. In the present study, with the downregulation of VDAC1 expression by vinegar/TMP pretreatment, the mitochondrial function of cardiomyocytes stimulated by A/R injury was significantly improved (Figure 5, including energy metabolism maintenance, acidosis correction, oxidative stress inhibition, and normal membrane function); however, the protection of vinegar/TMP pretreatment could be almost canceled by opening mPTP with Atr [23]. Therefore, the mitochondrion was the ultimate target organelle of vinegar/TMP pretreatment.

In conclusion, the study reconfirmed the existence of TMP in vinegar and a varying concentration associated with storage time. “Nutritional preconditioning” through low-dose long-term consumption of vinegar/TMP was shown to trigger myocardial protection, alleviating A/R-induced myocardial damage *in vivo* and *in vitro* (Figure 6). We also demonstrated that TMP acts through downregulating VDAC1 expression, inhibiting mPTP opening, and preventing mitochondrial dysfunction.

Abbreviations

A/R:	Anoxia/reoxygenation
Atr:	Atractyloside
CAT:	Catalase
CPK:	Creatine phosphokinase
cyt c:	Cytochrome c
ECAR:	Extracellular acidification rate
FRAP:	Ferric reducing antioxidant power
GSH-Px:	Glutathione peroxidase
HPLC:	High-performance liquid chromatography
IPC:	Ischemic preconditioning
I/R:	Ischemia/reperfusion
K-H:	Krebs-Henseleit
LDH:	Lactate dehydrogenase
LVDP:	Left ventricular developed pressure
MDA:	Malondialdehyde
MMP:	Mitochondrial membrane potential
mPTP:	Mitochondrial permeability transition pore
NPC:	Nutrition preconditioning
OCR:	Oxygen consumption rate
PPC:	Pharmacological preconditioning
ROS:	Reactive oxygen species
SOD:	Superoxide dismutase
TMP:	Tetramethylpyrazine
TUNEL:	Terminal deoxynucleotidyl transferase-mediated nick end labeling
VDAC:	Voltage-dependent anion-selective channel.

Data Availability

The data used to support the findings of this study are included within the article.

Conflicts of Interest

The authors declared no conflict of interest.

Authors' Contributions

Huan He and Liang Wang contributed equally to this paper. M.H., D.Y., and L.Y. coordinated and designed the research. H.H., L.W., Y.Q., and Q.Z. conducted the experiments. B.Y. performed the data analysis. H.H., D.Y., and L.Y. took part in the writing and final editing of the manuscript. All authors have approved the final version of the manuscript and are prepared to take public responsibility for the work and share responsibility and accountability for the results.

Acknowledgments

This research was supported by grants from the National Natural Science Foundation of China (Nos. 81660538, 81803534, and 81673431) and the Natural Science Foundation of Jiangxi Province (No. 20171BAB215077).

Supplementary Materials

Figure S1: vinegar/TMP pretreatment protects cardiomyocyte against A/R injury (on the cell viability). Vinegar/TMP pretreatment significantly increased the cell viability ($P < 0.01$) in a concentration-dependent manner. However, in the acetic acid alone/acetic acid+A/R group, the cell viability did not change ($P > 0.05$). Data were presented as the mean \pm SEM for eight individual experiments. (a) $P < 0.01$ vs. the control group. (b) $P < 0.01$ vs. prior dosage. (c) $P > 0.05$ vs. the corresponding vinegar pretreatment. (d) $P > 0.05$ vs. the A/R group. (e) $P > 0.05$ vs. the control group. Figure S2: vinegar/TMP pretreatment protects cardiomyocyte against A/R injury (on the LDH activity). Vinegar/TMP pretreatment significantly increased the LDH activity ($P < 0.01$) in a concentration-dependent manner. However, in the acetic acid alone/acetic acid+A/R group, the LDH activity did not change ($P > 0.05$). Data were presented as the mean \pm SEM for eight individual experiments. (a) $P < 0.01$ vs. the control group. (b) $P < 0.01$ vs. prior dosage. (c) $P > 0.05$ vs. the corresponding vinegar pretreatment. (d) $P > 0.05$ vs. the A/R group. (e) $P > 0.05$ vs. the control group. Figure S3: effects of vinegar/TMP alone, or upregulating VDAC1 expression, or opening mPTP on the cell viability of cardiomyocyte. Cell viability did not change by using vinegar alone, TMP alone, pAD/VDAC1 alone, vinegar+pAD/VDAC1, TMP+pAD/VDAC1, vinegar+Atr, and TMP+Atr when compared with the control group ($P > 0.05$). However, the cell viability with Atr alone was lower compared to that of the control group ($P < 0.01$), which was also the case for the pAD/VDAC1+A/R group and Atr+A/R group compared with the A/R group, indicating that treatment with pAD/VDAC1 upregulated VDAC1 expression, allowing Atr to open the mPTP, thereby aggravating cardiomyocyte injury. Data were presented as the mean \pm SEM for eight individual experiments. (a, b) $P < 0.01$ vs. the control group. (c) $P < 0.01$ vs. the A/R group. Figure S4: effects of vinegar/TMP alone, or upregulating VDAC1

expression, or opening mPTP on the LDH activity of cardiomyocyte. LDH activity did not change by using vinegar alone, TMP alone, pAD/VDAC1 alone, vinegar+pAD/VDAC1, TMP+pAD/VDAC1, vinegar+Atr, and TMP+Atr when compared with the control group ($P > 0.05$). However, the LDH activity with Atr alone was higher compared to that of the control group ($P < 0.01$), which was also the case for the pAD/VDAC1+A/R group and Atr+A/R group compared with the A/R group, indicating that treatment with pAD/VDAC1 upregulated VDAC1 expression, allowing Atr to open the mPTP, thereby aggravating cardiomyocyte injury. Data were presented as the mean \pm SEM for eight individual experiments. (a, b) $P < 0.01$ vs. the control group. (c) $P < 0.01$ vs. the A/R group. Figure S5: effects of vinegar/TMP alone on VDAC1 expression of cardiomyocyte. Vinegar/TMP alone significantly downregulated VDAC1 expression of the normal cardiomyocyte. Data were presented as the mean \pm SEM for three individual experiments. (a) $P < 0.01$ vs. the control group. Figure S6: effects of pAD/VDAC1 alone treatment or pAD/VDAC1+A/R treatment on VDAC1 expression of cardiomyocyte. With pAD/VDAC1 alone treatment and pAD/VDAC1+A/R treatment, the expression of VDAC1 was upregulated in different degrees ($P < 0.01$), indicating that adenovirus pAD/VDAC1 could do good work. Data were presented as the mean \pm SEM for three individual experiments. (a, b) $P < 0.01$ vs. the control group. (c) $P < 0.01$ vs. the A/R group. (Supplementary Materials)

References

- [1] J. Wu, H. Zhao, M. Du, L. Song, and X. Xu, "Dispersive liquid-liquid microextraction for rapid and inexpensive determination of tetramethylpyrazine in vinegar," *Food Chemistry*, vol. 286, pp. 141–145, 2019.
- [2] Z. Xiao, L. Zhao, L. Tian, L. Wang, and J. Zhao, "GC-FID determination of tetramethylpyrazine and acetoin in vinegars and quantifying the dependence of tetramethylpyrazine on acetoin and ammonium," *Food Chemistry*, vol. 239, pp. 726–732, 2018.
- [3] A. Bounihi, A. Bitam, A. Bouazza, L. Yargui, and E. A. Koceir, "Fruit vinegars attenuate cardiac injury via anti-inflammatory and anti-adiposity actions in high-fat diet-induced obese rats," *Pharmaceutical Biology*, vol. 55, no. 1, pp. 43–52, 2017.
- [4] J. Chen, J. Tian, H. Ge, R. Liu, and J. Xiao, "Effects of tetramethylpyrazine from Chinese black vinegar on antioxidant and hypolipidemia activities in HepG2 cells," *Food and Chemical Toxicology*, vol. 109, Part 2, pp. 930–940, 2017.
- [5] P. Zou, "Traditional Chinese medicine, food therapy, and hypertension control: a narrative review of Chinese literature," *The American Journal of Chinese Medicine*, vol. 44, no. 8, pp. 1579–1594, 2016.
- [6] A. Bouazza, A. Bitam, M. Amiali, A. Bounihi, L. Yargui, and E. A. Koceir, "Effect of fruit vinegars on liver damage and oxidative stress in high-fat-fed rats," *Pharmaceutical Biology*, vol. 54, no. 2, pp. 260–265, 2016.
- [7] S. Sakanaka and Y. Ishihara, "Comparison of antioxidant properties of persimmon vinegar and some other commercial vinegars in radical-scavenging assays and on lipid oxidation in tuna homogenates," *Food Chemistry*, vol. 107, no. 2, pp. 739–744, 2008.
- [8] J. Liang, J. Xie, L. Hou et al., "Aroma constituents in Shanxi aged vinegar before and after aging," *Journal of Agricultural and Food Chemistry*, vol. 64, no. 40, pp. 7597–7605, 2016.
- [9] P. Donkor, Y. Chen, L. Ding, and F. Qiu, "Locally and traditionally used *Ligusticum* species - A review of their phytochemistry, pharmacology and pharmacokinetics," *Journal of Ethnopharmacology*, vol. 194, pp. 530–548, 2016.
- [10] Y. Zhao, Y. Liu, and K. Chen, "Mechanisms and clinical application of tetramethylpyrazine (an interesting natural compound isolated from *Ligusticum wallichii*): current status and perspective," *Oxidative Medicine and Cellular Longevity*, vol. 2016, Article ID 2124638, 2016.
- [11] H. J. Gao, P. F. Liu, P. W. Li et al., "Ligustrazine monomer against cerebral ischemia/reperfusion injury," *Neural Regeneration Research*, vol. 10, no. 5, pp. 832–840, 2015.
- [12] J. Z. Hu, J. H. Huang, Z. M. Xiao, J. H. Li, X. M. Li, and H. B. Lu, "Tetramethylpyrazine accelerates the function recovery of traumatic spinal cord in rat model by attenuating inflammation," *Journal of the Neurological Sciences*, vol. 324, no. 1–2, pp. 94–99, 2013.
- [13] Q. Zhou, S. Chen, H. Li et al., "Tetramethylpyrazine alleviates iron overload damage in vascular endothelium via upregulating DDAHII expression," *Toxicology In Vitro*, vol. 65, p. 104817, 2020.
- [14] B. Yang, H. Li, Y. Qiao et al., "Tetramethylpyrazine attenuates the endotheliotoxicity and the mitochondrial dysfunction by doxorubicin via 14-3-3 γ /Bcl-2," *Oxidative Medicine and Cellular Longevity*, vol. 2019, Article ID 5820415, 2019.
- [15] B. Huang, J. You, Y. Qiao et al., "Tetramethylpyrazine attenuates lipopolysaccharide-induced cardiomyocyte injury via improving mitochondrial function mediated by 14-3-3 γ ," *European Journal of Pharmacology*, vol. 832, pp. 67–74, 2018.
- [16] H. Chen, M. He, Q. Huang, G. Zeng, and D. Liu, "Delayed protection of tetramethylpyrazine on neonatal rat cardiomyocytes subjected to anoxia-reoxygenation injury," *Basic & Clinical Pharmacology & Toxicology*, vol. 100, no. 6, pp. 366–371, 2007.
- [17] D. J. Hausenloy and D. M. Yellon, "Ischaemic conditioning and reperfusion injury," *Nature Reviews Cardiology*, vol. 13, no. 4, pp. 193–209, 2016.
- [18] Y. Qiao, T. Hu, B. Yang et al., "Capsaicin alleviates the deteriorative mitochondrial function by upregulating 14-3-3 η in anoxic or anoxic/reoxygenated cardiomyocytes," *Oxidative Medicine and Cellular Longevity*, vol. 2020, Article ID 1750289, 16 pages, 2020.
- [19] D. J. Hausenloy and D. M. Yellon, "The therapeutic potential of ischemic conditioning: an update," *Nature Reviews Cardiology*, vol. 8, no. 11, pp. 619–629, 2011.
- [20] Z. Liao, D. Liu, L. Tang et al., "Long-term oral resveratrol intake provides nutritional preconditioning against myocardial ischemia/reperfusion injury: involvement of VDAC1 downregulation," *Molecular Nutrition & Food Research*, vol. 59, no. 3, pp. 454–464, 2015.
- [21] Z. Liao, H. He, G. Zeng et al., "Delayed protection of ferulic acid in isolated hearts and cardiomyocytes: upregulation of heat-shock protein 70 via NO-ERK1/2 pathway," *Journal of Functional Foods*, vol. 34, pp. 18–27, 2017.
- [22] H. He, Y. Luo, Y. Qiao et al., "Curcumin attenuates doxorubicin-induced cardiotoxicity via suppressing oxidative stress and preventing mitochondrial dysfunction mediated by 14-3-3 γ ," *Food & Function*, vol. 9, no. 8, pp. 4404–4418, 2018.

- [23] Y. Luo, Q. Wan, M. Xu et al., "Nutritional preconditioning induced by astragaloside IV on isolated hearts and cardiomyocytes against myocardial ischemia injury via improving Bcl-2-mediated mitochondrial function," *Chemico-Biological Interactions*, vol. 309, p. 108723, 2019.
- [24] H. Huang, S. Lai, Y. Luo et al., "Nutritional preconditioning of apigenin alleviates myocardial anoxia/reoxygenation injury via mitochondrial pathway mediated by Notch1/Hes1," *Oxidative Medicine and Cellular Longevity*, vol. 2019, Article ID 7973098, 2019.
- [25] A. K. S. Camara, Y. Zhou, P. C. Wen, E. Tajkhorshid, and W. M. Kwok, "Mitochondrial VDAC1: a key gatekeeper as potential therapeutic target," *Frontiers in Physiology*, vol. 8, p. 4, 2017.
- [26] M. Tian, Y. Xie, Y. Meng et al., "Resveratrol protects cardiomyocytes against anoxia/reoxygenation via dephosphorylation of VDAC1 by Akt-GSK3 β pathway," *European Journal of Pharmacology*, vol. 843, pp. 80–87, 2019.
- [27] Z. Tong, Y. Xie, M. He et al., "VDAC1 deacetylation is involved in the protective effects of resveratrol against mitochondria-mediated apoptosis in cardiomyocytes subjected to anoxia/reoxygenation injury," *Biomedicine & Pharmacotherapy*, vol. 95, pp. 77–83, 2017.
- [28] C. Chen, Q. Chen, Q. Guo et al., "Simultaneous determination of acetoin and tetramethylpyrazine in traditional vinegars by HPLC method," *Food Chemistry*, vol. 122, no. 4, pp. 1247–1252, 2010.
- [29] H. He, Y. Zhou, J. Y. Huang et al., "Capsaicin protects cardiomyocytes against anoxia/reoxygenation injury via preventing mitochondrial dysfunction mediated by SIRT1," *Oxidative Medicine and Cellular Longevity*, vol. 2017, Article ID 1035702, 2017.
- [30] W. Xu, Q. Xu, J. Chen et al., "Ligustrazine formation in Zhenjiang aromatic vinegar: changes during fermentation and storing process," *Journal of the Science of Food and Agriculture*, vol. 91, no. 9, pp. 1612–1617, 2011.
- [31] S. Cadenas, "ROS and redox signaling in myocardial ischemia-reperfusion injury and cardioprotection," *Free Radical Biology and Medicine*, vol. 117, pp. 76–89, 2018.
- [32] R. Huang, Q. Huang, G. Wu, C. Chen, and Z. Li, "Evaluation of the antioxidant property and effects in *Caenorhabditis elegans* of Xiangxi flavor vinegar, a Hunan local traditional vinegar," *Journal of Zhejiang University SCIENCE B*, vol. 18, no. 4, pp. 324–333, 2017.
- [33] J. Qui, C. Ren, J. Fan, and Z. Li, "Antioxidant activities of aged oat vinegar in vitro and in mouse serum and liver," *Journal of the Science of Food and Agriculture*, vol. 90, no. 11, pp. 1951–1958, 2010.
- [34] J. H. O'Keefe, N. M. Gheewala, and J. O. O'Keefe, "Dietary strategies for improving post-prandial glucose, lipids, inflammation, and cardiovascular health," *Journal of the American College of Cardiology*, vol. 51, no. 3, pp. 249–255, 2008.
- [35] E. Ostman, Y. Granfeldt, L. Persson, and I. Björck, "Vinegar supplementation lowers glucose and insulin responses and increases satiety after a bread meal in healthy subjects," *European Journal of Clinical Nutrition*, vol. 59, no. 9, pp. 983–988, 2005.
- [36] K. Takuo, Z. Hiroshi, T. Kunio, Y. Takeshi, and N. Hiroko, "Studies on flavor components of foodstuffs-part I. Distribution of tetramethylpyrazine in fermented foodstuffs," *Agricultural and Biological Chemistry*, vol. 35, pp. 693–696, 1971.
- [37] A. Wang, H. Song, C. Ren, and Z. Li, "Key aroma compounds in Shanxi aged Tartary buckwheat vinegar and changes during its thermal processing," *Flavour and Fragrance Journal*, vol. 27, pp. 47–53, 2012.
- [38] G. G. Abdukeyum, A. J. Owen, and P. L. McLennan, "Dietary (n-3) long-chain polyunsaturated fatty acids inhibit ischemia and reperfusion arrhythmias and infarction in rat heart not enhanced by ischemic preconditioning," *The Journal of Nutrition*, vol. 138, no. 10, pp. 1902–1909, 2008.
- [39] Y. C. Hseu, V. Thiyagarajan, T. T. Ou, and H. L. Yang, "CoQ0-induced mitochondrial PTP opening triggers apoptosis via ROS-mediated VDAC1 upregulation in HL-60 leukemia cells and suppresses tumor growth in athymic nude mice/xenografted nude mice," *Archives of Toxicology*, vol. 92, no. 1, pp. 301–322, 2018.
- [40] D. B. Huckabee and M. B. Jekabsons, "Identification of Bax-voltage-dependent anion channel 1 complexes in digitonin-solubilized cerebellar granule neurons," *Journal of Neurochemistry*, vol. 119, no. 5, pp. 1137–1150, 2011.
- [41] J. S. Bhatti, G. K. Bhatti, and P. H. Reddy, "Mitochondrial dysfunction and oxidative stress in metabolic disorders – A step towards mitochondria based therapeutic strategies," *Biochimica et Biophysica Acta (BBA)-Molecular Cell Research*, vol. 1863, no. 5, pp. 1066–1077, 2017.
- [42] K. Boengler, G. Lochnit, and R. Schulz, "Mitochondria "THE" target of myocardial conditioning," *American Journal of Physiology-Heart and Circulatory Physiology*, vol. 315, no. 5, pp. H1215–H1231, 2018.
- [43] D. J. Hausenloy, S. B. Ong, and D. M. Yellon, "The mitochondrial permeability transition pore as a target for preconditioning and postconditioning," *Basic Research in Cardiology*, vol. 104, no. 2, pp. 189–202, 2009.

Review Article

Bacteriocins: Potential for Human Health

Fuqing Huang ^{1,2}, Kunling Teng ¹, Yayong Liu ^{1,2}, Yanhong Cao,³ Tianwei Wang ¹,
Cui Ma ¹, Jie Zhang ¹, and Jin Zhong ^{1,2}

¹State Key Laboratory of Microbial Resources, Institute of Microbiology, Chinese Academy of Sciences, Beijing 100101, China

²University of Chinese Academy of Sciences, Beijing 100008, China

³The Animal Husbandry Research Institute of Guangxi Zhuang Autonomous Region, Nanning 530000, China

Correspondence should be addressed to Jin Zhong; zhongj@im.ac.cn

Received 13 January 2021; Revised 25 March 2021; Accepted 30 March 2021; Published 12 April 2021

Academic Editor: Si Qin

Copyright © 2021 Fuqing Huang et al. This is an open access article distributed under the Creative Commons Attribution License, which permits unrestricted use, distribution, and reproduction in any medium, provided the original work is properly cited.

Due to the challenges of antibiotic resistance to global health, bacteriocins as antimicrobial compounds have received more and more attention. Bacteriocins are biosynthesized by various microbes and are predominantly used as food preservatives to control foodborne pathogens. Now, increasing researches have focused on bacteriocins as potential clinical antimicrobials or immune-modulating agents to fight against the global threat to human health. Given the broad- or narrow-spectrum antimicrobial activity, bacteriocins have been reported to inhibit a wide range of clinically pathogenic and multidrug-resistant bacteria, thus preventing the infections caused by these bacteria in the human body. Otherwise, some bacteriocins also show anticancer, anti-inflammatory, and immune-modulatory activities. Because of the safety and being not easy to cause drug resistance, some bacteriocins appear to have better efficacy and application prospects than existing therapeutic agents do. In this review, we highlight the potential therapeutic activities of bacteriocins and suggest opportunities for their application.

1. Introduction

Many human diseases are associated with bacterial infections. While antibiotics have played an instrumental role in the fight against them, the widespread misuse of antibiotics has led to the emergence of a serious worldwide drug resistance problem; the discovery of new antimicrobial drugs is therefore urgent [1]. Bacteriocins are peptides with antibacterial activity synthesized by bacterial ribosomes, and they are usually inhibitory to proximate bacteria. [2] Bacteriocins are typically classified into Class I (heat-stable posttranslationally modified peptides below 10 kDa) including lanthipeptide, lasso peptide, head-to-tail cyclized peptides, thiopeptide, glycosylated bacteriocin, and sactipeptide; Class II (heat-stable unmodified small peptides below 10 kDa) including IIa/b/c/d; and Class III (thermally unstable peptides larger than 10 kDa) [3]. Due to its unique mechanism of action, such as modification of the pyrophosphate moiety of lipid-II, bacteriocins have a relatively narrower spectrum of inhibition against bacteria and are less likely to develop widespread drug resistance than antibiotics [4, 5].

Bacteriocins can inhibit many disease-causing bacteria, including some antibiotic-resistant strains, suggesting the potential application of bacteriocins in antagonizing pathogenic infections. The human body (e.g., in gastrointestinal tract, respiratory tract, and skin and reproductive tract) has a large number of microorganisms, and the host microbiota is constantly interacting with the host cells. Many human microorganisms can produce bacteriocins which are reported to be closely related to human health, such as promoting the balance of the gut microbiota and inhibiting the invasion of foreign pathogenic bacteria [6]. In addition to inhibiting pathogenic bacteria, bacteriocins have shown inhibitory effects on a wide range of cancer cells as well as modulating effects on inflammation and immunity, suggesting that they also show anticancer and anti-inflammatory activities. Therefore, bacteriocins have a great potential for application in human health.

In recent years, there have been some reports on bacteriocins and human health, but there is still a lack of systematic reviews in this field of research. Therefore, it is necessary to summarize the bacteriocins produced by different bacteria

and their beneficial effects on human health, so as to provide a theoretical basis for the research and development of bacteriocins. In this review, we summarized the antibacterial, anti-cancer, anti-inflammatory, and immune-modulatory activities of bacteriocins and concluded their mechanisms of action.

2. Functional Properties and Mechanisms of Bacteriocins

Pathogenic microorganisms pose a major threat to human health and may even endanger human lives. It is predicted that millions of people will die from bacterial infections in the coming decades, because of the emergence of multidrug-resistant (MDR) bacteria [7, 8]. Despite the important contribution of antibiotics in the fight against pathogenic infections, the widespread use and misuse of antibiotics have led to some serious adverse consequences, such as the emergence of superbugs. [9] New compounds for inhibiting the multiresistant pathogens and limiting the spread of antibiotic resistance are urgently needed. Bacteriocins are ribosomally synthesized antimicrobial peptides. Some bacteriocins need to be modified by a posttranslational modified enzyme system and transported by a special transport system to outside of the cell to exert their biological activities (e.g., lantibiotics) [10]. In contrast to antibiotics, the unique mechanism of action (binds the pyrophosphate moiety of Lipid-II [11]) prevents bacteriocins from developing resistance, and treating pathogenic infections with bacteriocins or bacteriocins in combination with antibiotics instead of antibiotics can reduce the overuse of antibiotics, thereby reducing the spread of antibiotic resistance. [5, 12] Moreover, some strains that are resistant to antibiotics appear to have a higher susceptibility to antimicrobial peptides. [13] Leon et al. points out that the mechanism of antimicrobial activities of bacteriocins is completely different from that of antibiotics, which indicated that bacteriocins will be possible as “new age infection fighters” [14]. Some bacteriocins show inhibitory activities against pathogenic microorganisms and can effectively inhibit infections of the human body by pathogenic microorganisms. This suggests that bacteriocin is an effective alternative for the treatment of pathogenic microbial infections. The anti-infection effects of bacteriocins and mechanisms are summarized in Table 1 and Figure 1. Many bacteriocins (e.g., lanthipeptides) demonstrate inhibitory activity against the pathogens. In addition, some bacteriocins have demonstrated inhibitory effects on viruses and parasites.

2.1. Inhibiting Bacterial Infections. Many bacteriocins typically exhibit antibacterial activity against the critical pathogenic bacteria, including some antibiotic-resistant Gram-positive (G^+) bacteria including *Mycobacterium tuberculosis*, methicillin-resistant *Staphylococcus aureus* (MRSA), *Listeria monocytogenes*, vancomycin-resistant enterococci (VRE), *Clostridium difficile*, and Gram-negative (G^-) bacteria including *Escherichia coli* and *Salmonella enterica*. Bacteriocins exert their antimicrobial action through inhibiting the bacteria cell wall biosynthesis by complexing the lipid II and forming the pore in cell membrane, disrupting bacterial

population sensing as a signaling molecule, or targeting the ATP-dependent protease, or binding to a site on 23S rRNA and inhibits elongation factor-dependent reactions (Table 1).

Nisin, produced by *Lactococcus lactis*, is the most researched and developed bacteriocin. Since nisin was found in 1928, it has been used for decades as a safe, natural food biopreservative that significantly inhibits the growth of a wide range of pathogenic microorganisms [15]. For example, nisin can inhibit the growth of *Streptococcus pneumoniae* [16] which could cause the disease of pneumonia, meningitis, and sepsis. In addition, nisin has an inhibitory effect on many pathogenic bacteria and ameliorates infections caused by these pathogens, such as respiratory tract infections caused by *S. aureus* [17] and gastrointestinal infections by VRE in mice [18].

In addition, many diseases associated with pathogenic bacterial infections can be treated by bacteriocin interventions. *M. tuberculosis* is the pathogen that causes tuberculosis, which affects a quarter of the world's population. Some bacteriocins have been reported to inhibit *M. tuberculosis in vitro*. For example, griselimycin, a cyclic bacteriocin, is effective in curing mice infected with tuberculosis *in vivo*. [19] *S. aureus* infections can lead to diseases such as mastitis and bacteraemia. Laterosporulin10, microbisporicin, NVB333, and mersacidin can inhibit *S. aureus in vitro* and/or *in vivo*, thereby treating respiratory tract, foot, abdominal cavity, and nasal cavity of *S. aureus* infection. [20–22] *L. monocytogenes* is the pathogen of listeriosis. It mainly uses food as a vector and is one of the deadliest foodborne pathogens, causing 20 to 30% of the infected deaths [23]. Moreover, it also has the ability to cross the intestinal barrier to reach the blood and extraintestinal organs. Some studies have reported that certain bacteriocins, such as pediocin PA-1, lactocin AL705, and enterocin CRL35, inhibit the growth of *L. monocytogenes* and also reduce the number of their passage through the intestinal barrier [24, 25]. *E. coli* and *Salmonella* infections usually cause diarrhea and intestinal inflammation and lead to the disorder of the intestinal flora and the destruction of the intestinal barrier. They cross the intestinal barrier into the blood and reach other extraintestinal organs and cause the aggravation of the symptoms of the infection. Some studies have shown that bacteriocins (e.g., microcin and colicin) have an inhibitory effect on *E. coli* and *Salmonella in vitro* and can effectively reduce the numbers of *E. coli* (e.g., O157:H7) and *Salmonella* in the infected mice, improving the adverse effects caused by these pathogens [26–28]. In addition, some bacteriocins (e.g., subtilisin and gasserin E) have a significant inhibitory effect on the pathogens (e.g., *Gardnerella vaginalis*) which can cause the bacterial vaginal diseases [29, 30].

Interestingly, some studies have shown that bacteriocin alone or in combination with antibiotics can not only broaden the antibacterial spectrum (even effective against antibiotic-resistant bacteria) but also significantly reduce the MIC value [20, 31–34]. For example, Singh et al. reported that the combinations of nisin-ceftioxone and nisin-cefotaxime were found to be highly synergistic against *S. enterica* serovar typhimurium than in those treated with drugs alone, specifically manifested in lower MIC value and

TABLE 1: Antimicrobial effects of bacteriocins.

Bacteriocins -classification	Producing bacteria	Target organism	Mode of action	Model	Security
Nisin lanthipeptide [17, 103–105]	<i>L. lactis</i>	<i>S. aureus</i> , <i>C. difficile</i>	Lipid II binding and pore formation	<i>In vitro</i> , mice and rats (intraperitoneal injection and nasal administration)	FDA approved and generally regarded as safe
NAI-107 lanthipeptide [106, 107]	<i>Microbispora</i> sp.	<i>S. aureus</i>	Inhibits the synthesis of peptidoglycan	<i>In vitro</i> and mice (intravenous and subcutaneous administration)	Low acute toxicity
Mutacin B-Ny266 lanthipeptide [108, 109]	<i>S. mutans</i>	<i>S. aureus</i> , <i>Neisseria Helicobacter</i>	Unknown	<i>In vitro</i> and mice (intraperitoneal injection)	Not evaluated
OG716 lanthipeptide [110]	<i>S. mutans</i> JH1140	<i>C. difficile</i>	Binding the pyrophosphate moiety of lipid-II	<i>In vitro</i> and hamster	Low toxicity
Mersacidin lanthipeptide [22, 111–113]	<i>Bacillus</i> sp. HIL-Y85/54728	MRSA	Inhibits bacterial cell wall biosynthesis by complexing lipid II	<i>In vitro</i> and mice (nasal administration and subcutaneously administered)	Not evaluated
Actagardine A lanthipeptide [114]	<i>A. garbadinensis</i> ATCC 31049	<i>C. difficile</i> , VRE MRSA	Inhibits cell wall biosynthesis by binding to lipid II and blocking transglycosylation	<i>In vitro</i>	Not evaluated
NVB302 lanthipeptide [115, 116]	Derivative of deoxyactagardine B from <i>A. liguriae</i>	<i>C. difficile</i>	Binding to lipid II	<i>In vitro</i> and hamsters (oral gavage) and <i>ex vivo</i> gut model	Nontoxic
NVB333 lanthipeptide [117]	<i>L. lactis</i> DPC3147	<i>S. aureus</i>	Binding to lipid II	<i>In vitro</i> and mice (i.v. injection)	No signs of any drug-related adverse effects
Lactacin 3147 lanthipeptide [118]	<i>Lentzea kentuckyensis</i>	<i>C. difficile</i> , <i>L. monocytogenes</i>	Binding to lipid II and lytic	<i>In vitro</i>	Not evaluated
Lassomycin class I-lasso peptide [119]	<i>E. coli</i>	<i>M. tuberculosis</i>	Target the ATP-dependent protease	<i>In vitro</i>	Not evaluated
Microcin J25 lasso peptide [26, 80, 120, 121]	<i>E. faecalis</i>	<i>Salmonella</i> , <i>E. coli</i>	Inhibiting RNA polymerase and increasing superoxide production	<i>In vitro</i> and mice	No cytotoxicity
Enterocin AS-48 head-to-tail cyclized peptides [122–125]	<i>Streptomyces</i> sp.	<i>M. tuberculosis</i>	Accumulating a positive charge on the membrane surface and disrupts the membrane potential	<i>In vitro</i> and macrophages	No cytotoxicity
Thiostrepton thiopeptide [126, 127]	<i>E. durans</i> 61A	<i>M. abscessus</i>	Binding to a site on 23S rRNA and inhibits elongation factor-dependent reactions	<i>In vitro</i> , zebrafish and macrophages	US FDA-approved drug
Durancin 61A glycosylated bacteriocin [128, 129]	<i>B. thuringiensis</i> DPC 6431	<i>C. difficile</i> , VRE, MRSA, <i>L. innocua</i>	Targeting the bacterial membrane	<i>In vitro</i>	Not hemolytic
Thuricin CD sactipeptide [87, 130, 131]	<i>R. gnavus</i> E1	<i>C. difficile</i> , <i>L. monocytogenes</i>	Permeabilize and depolarize the membrane	<i>In vitro</i> and mice	Not evaluated
Ruminococcin C sactipeptide [132, 133]	<i>L. gasseri</i> EV1461	Pathogenic clostridia and MDR strains	Inhibiting nucleic acid synthesis in a metronidazole-like manner	<i>In vitro</i>	Not toxic to eukaryotic cells
Gassericin E head-to-tail cyclized peptides [30]	<i>E. coli</i> Nissle 1917	Multiple pathogens associated with bacterial vaginosis	Unknown	<i>In vitro</i>	Not evaluated
Microcin H47 [134]	<i>K. pneumoniae</i> RYC492	<i>E. coli</i>	Targeting the F ₀ proton channel of ATP synthase	<i>In vitro</i>	Not evaluated
Microcin E492 [135]	<i>K. Enterobacter</i> <i>E. coli</i> <i>Salmonella</i> sp.	<i>K. Enterobacter</i> <i>E. coli</i> <i>Salmonella</i> sp.	Permeabilize the inner membrane with the mannose permease	<i>In vitro</i>	Induces apoptosis in some human cell lines

TABLE 1: Continued.

Bacteriocins -classification	Producing bacteria	Target organism	Mode of action	Model	Security
Microcin M [136]	<i>E. coli</i> Nissle 1917	<i>E. coli</i> <i>Salmonella</i> sp.	Compete against other enterobacteria that utilize catecholate siderophores	<i>In vitro</i>	Not evaluated
Lactocin 160 [137, 138]	<i>L. Rhammosus</i>	<i>G. vaginalis</i> <i>Bacillus pertussis</i>	Causing the efflux of ATP molecules and dissipative the proton motive force	In epivaginal	Minimal irritation
Enterocin CRL35 class IIa [25, 139]	<i>E. mundtii</i>	<i>L. monocytogenes</i>	Forming holes in the cell wall and cell membrane	<i>In vitro</i> and mice (orally administrated)	Not evaluated
Lactocin AL705 class IIa [140, 141]	<i>L. curvatus</i>	<i>L. monocytogenes</i>	Disrupting quorum sensing through a signal molecule inactivation	<i>In vitro</i>	Not evaluated
Pediocin PA-1 class IIa [24, 142, 143]	<i>P. acidilactici</i>	<i>L. monocytogenes</i>	Forms hydrophilic pores in the cytoplasmic membrane	In intra-gastric administration	Commercial applications with no adverse effect
Laterosporulin10 class IId [21]	<i>B. laterosporus</i> SKDU10	<i>S. aureus</i> , <i>M. smegmatis</i>	Membrane permeabilization	<i>In vitro</i> and macrophages	No hemolytic activity
Subtilosin class II [29, 144, 145]	<i>B. subtilis</i>	<i>G. vaginalis</i> , <i>L. monocytogenes</i> , <i>S. agalactiae</i>	Binding to lipid bilayers, results in membrane permeabilization	In epivaginal	Human cells remained viable after prolonged exposures to subtilosin
Colicin Z class III [27]	<i>E. coli</i> B1356	<i>E. coli</i> <i>Shigella</i>	Via cjrc receptor recognition and cjrb- and exbb- and exbd-mediated colicin translocation	<i>In vitro</i>	Not evaluated
Colicin F Y class III [28, 146]	<i>E. coli</i>	<i>Y. enterocolitica</i>	Yiur-mediated reception, tonb import, and cell membrane pore formation	In mice	Not evaluated
Diffocin class III [102, 147]	<i>C. difficile</i> CD4	<i>C. difficile</i>	Dissipating the membrane potential	In vitro and mice	Not evaluated
ESL5 [148]	<i>E. faecalis</i> SL-5	<i>P. acnes</i>	Unknown	<i>In vitro</i> and human	Not evaluated
Bacteriocin OR-7 [149]	<i>L. salivarius</i> NRR1 B-30514	<i>C. jejuni</i>	Unknown	In chicken	Not evaluated
Bacteriocin E-50-52 class IIa [150]	<i>E. faecium</i> NRR1 B-30746	<i>S. enteritidis</i>	Unknown	In chicken	Not evaluated
Subtilosin class II [37]	<i>B. subtilis</i>	HSV-1 and HSV-2	Inhibiting virus multiplication	<i>In vitro</i>	Human cells remained viable after prolonged exposures to subtilosin
Labyrinthopeptin A1 lantipeptide [40, 41, 151]	<i>A. nambiensis</i> DSM 6313	HSV, HIV, zika virus, and dengue virus	Acting as an entry inhibitor possibly by targeting the HSV glycoproteins	<i>In vitro</i>	Does not harm the vaginal epithelium or the normal vaginal lactic acid flora
Enterocin CRL35 class IIa [38, 39]	<i>E. mundtii</i>	HSV-1 and HSV-2	Affecting a late step of virus multiplication	<i>In vitro</i>	Low cytotoxicity for eukaryotic cells
Mundticin ST4SA class IIa [42]	<i>E. mundtii</i> ST4V	HSV-1, HSV-2, poliovirus and measles virus	Unknown	<i>In vitro</i>	Not evaluated
Enterocin AS-48 class I-head-to-tail cyclized peptides [48, 125, 152]	<i>E. faecalis</i>	<i>Trypanosoma cruzi</i>	Mitochondrial membrane depolarization and reactive oxygen species production	<i>In vitro</i> and mice	No cytotoxicity
Addip class II [49]	<i>A. dehalogenans</i>	<i>Plasmodium falciparum</i>	Unknown	<i>In vitro</i>	Nontoxic to mammalian cells

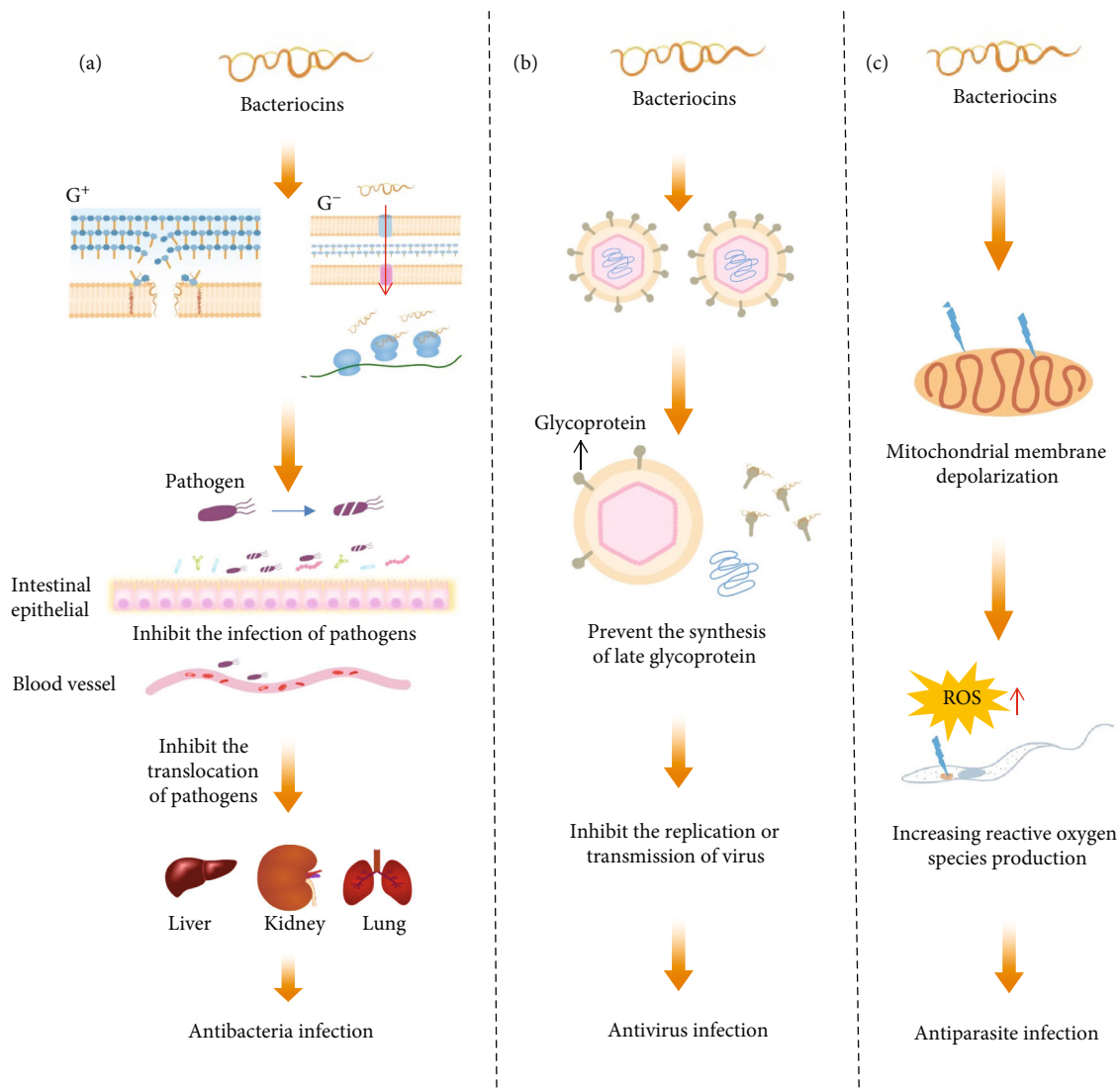


FIGURE 1: Bacteriocins protect the human body from infection by inhibiting a wide variety of pathogenic microorganisms via different mechanisms. (a) For bacteria, bacteriocins can directly kill pathogenic bacteria by inhibiting the bacteria cell wall biosynthesis by complexing the lipid II and forming the pore in cell membrane, disrupting bacterial population sensing as a signaling molecule, or enters the cell via a transporter and interacts with critical enzymes (e.g., ATP-dependent protease). This eliminates the presence of pathogenic bacteria in the organism and reduces their migration to various extraintestinal organs, i.e., the lung, kidney, and liver. (b) For viruses, bacteriocins can inhibit the proliferation or transfer of viruses by blocking the synthesis of glycoproteins in the late stage of virus replication. (c) For parasites, bacteriocins can inhibit the parasites through mitochondrial membrane depolarization and reactive oxygen species production.

less organ cell load [31]. This suggests that bacteriocins could be considered an effective way to reduce the spread of antibiotic resistance.

2.2. Inhibiting Virus Infections. Viral infections can attack and destroy the immune system, leading to the formation of malignant tumors. Current treatments for viral infections are mainly chemical drugs, such as inhibitors of DNA polymerase activity that inhibit the replication of the virus [35]. However, the virus is prone to mutate and easily leads to be resistant to these drugs. Therefore, the search for new antiviral drugs is imminent. It has been reported that certain bacteriocins are demonstrated to show antiviral activities to a

variety of viruses. Herpes simplex virus types 1 and 2 (HSV-1 and HSV-2) are human viral pathogens that can cause serious clinical conditions including genital ulcerations, corneal blindness, and encephalitis, and over 530 million people worldwide are infected with HSV-2 [36]. Studies reported that several bacteriocins show inhibitory effects against HSV. For example, subtilosin targets intracellular transport of viral glycoproteins in the late stages of the viral replication cycle to exert antiviral or virucidal effects [37]. Similarly, enterocin CRL35 affects the late steps of virus multiplication [38, 39] and labyrinthopeptin A1 targets the glycoproteins, exerting an antiviral effect [40, 41]. In addition, bacteriocins have been reported to have antiviral or

TABLE 2: Anticancer effects of bacteriocins.

Bacteriocins	Classification	Source	Target cancer cells (mechanism) or effects <i>in vivo</i>
Nisin	Lanthipeptide	<i>L. lactis</i>	SW1088 [57]; HNSCC (arresting the cell cycles) [53]; SW480 (increasing the apoptosis index of bax/bcl-2) [54]; LS180, HT29, and Caco2 (decreasing the expression of genes related to proliferation and migration) [55]. IMR-32 (enhancing cell membrane fluidity) [59]. Combining with doxorubicin can reduce the tumor volume of skin cancer in mice [60]. Decreasing the IC50 of 5-FU on A431 cells and promote the elimination of tumors in mice [61, 153]
Nisin Z	Lanthipeptide	<i>L. lactis</i>	A375 (inducing cell membrane damage, increasing ROS accumulation, inhibiting mitochondrial respiration and glycolytic metabolism) [58]; HNSCC (induces apoptosis and reduces proliferation and clone formation). Reduces the occurrence of tumors in mice and prolongs survival [154]
Bovicin HC5	Lanthipeptide	<i>S. bovis</i> HC5	MCF-7 and HepG2 [155]
Duramycin	Lanthipeptide	<i>S. griseovorticillatum</i>	MCA-RH 7777 (enhancing the sensitization) [67]
Chaxapeptin	Lasso peptide	<i>S. leeuwenhoekii</i> C58	A549 [66]
Thiostrepton	Thiopeptide	<i>S. aureus</i>	MCF-7 (inhibiting FOXM1 expression) [68, 69]. Inhibiting endometriosis lesions and reducing the levels of MMP9 and bcl-2 in rats [70]
Microcin E492	Microcin	<i>K. pneumoniae</i>	HeLa, Jurkat, and Ramos (forming ion channels) [63]. Tumor inhibition in SW480 and SW620 zebrafish xenograft models [156]
Pediocin CP2	Class IIa	<i>P. acidilactis</i> CP2	MCF-7, HepG2, Sp2/0-Ag14 and HeLa (affecting cell division and DNA synthesis) [64]
Pediocin PA-1	Class IIa	<i>P. acidilactis</i> K2a2-3	HT29 and HeLa [24]
Plantaricin A	Class IIc	<i>L. Plantarum</i>	Jurka (disrupting cell membrane structure) [65]
Laterosporulin 10	Class IIc	<i>B. laterosporus</i> SKDU10	MCF-7, HEK293T, HT1080, HeLa and H1299 (disrupting cell membrane structure) [62]

virucidal effects against a variety of other viruses, such as human immunodeficiency virus (HIV), zika virus, and dengue virus [37, 42]. Compared to be antibacterial agents, bacteriocins have been much less studies as antiviral agents, and the mechanisms of bacteriocins involved are less well understood and need further research.

2.3. Inhibiting Parasite Infection. There are 342 species of helminth parasites and 70 species of protozoan parasites in humans [43]. The relationship between the parasite and the host is complex, as it may either promote host health or cause diseases [44, 45]. Protozoa such as *Plasmodium*, *Trypanosoma*, and *Entamoeba* can cause serious diseases (e.g., malaria, sleeping sickness, and amoebic dysentery) in humans [46, 47]. Several bacteriocins have been reported to have an inhibitory effect on some parasites and can ameliorate diseases caused by parasites. For example, AS-48 is a head-to-tail cyclized peptide, synthesized by *Enterococcus faecalis*. It not only has bactericidal effect on many G^+ bacteria and several G^- bacteria but also effectively reduces the number of *Trypanosoma cruzi* by mitochondrial membrane depolarization and reactive oxygen species production, improving the symptoms of Chagas' disease [48]. AdDLP is the first bacterial defensin-like peptide identified in the G^- bacterium *Anaeromyxobacter dehalogenans*. 10 μ M AdDLP can kill 100% of *Plasmodium falciparum* without harming mammalian red blood cells [49]. Although the research about bacteriocins inhibiting parasites are still limiting, bacteriocins are potential to be an effective drug to fight against parasite infection.

3. Anticancer Activities

Cancer is a major public health problem worldwide and is the leading cause of death in the global [50]. Although there have been new breakthroughs in cancer research in recent years, there are still many challenges that need to be addressed, and the prevention and treatment of cancer need to be further explored continuously. Cancer occurs when the cells that line the tissue become abnormal and grow out of control. With the enhancement of migration ability, some cancers might even be present without any signs or symptoms [51, 52]. Inhibiting the proliferation and migration of cancer cells is an effective measure to prevent and treat cancer.

In recent years, researches on the anticancer effect of peptide have gradually become the focus of attention. Bacteriocins have shown anticancer activities such as killing and inhibiting invasion of some cancer cells. Table 2 and Figure 2 summarize the anticancer effects of bacteriocins and the mechanisms reported so far, including induction of cell apoptosis, blocking of cell cycle, inhibition of cell migration, and destruction of cell membrane structure.

Nisin can induce the apoptosis of a wide range of cancer cells (e.g., HNSCC, SW480, LS180, HT29, Caco2, SW1088, A375, and IMR-32) [53–59] through multiple mechanisms. After treatment with different concentrations of nisin, the apoptosis index (i.e., bax/bcl-2) of cancer cells was increased, the cell cycle was arrested, and the expression of genes related to proliferation and migration (e.g., *cea*, *ceam6*, and *mmp2f*) were suppressed. In addition, nisin also induces the cell membrane damage, promotes the release of lactate dehydrogenase (LDH), increases the accumulation of reactive oxygen

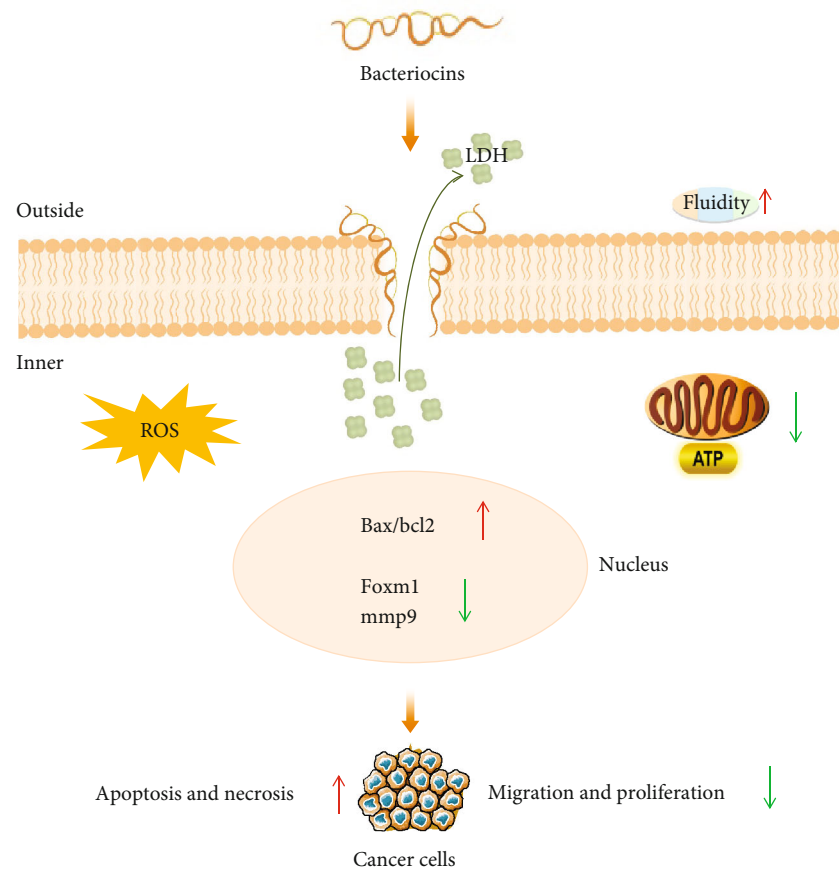


FIGURE 2: Bacteriocins inhibit the development of cancer by inhibiting the growth of cancer cells through various mechanisms. Bacteriocins increase the fluidity of cell membranes and form ion channels on cancer cell membranes, increasing the release of LDH. Bacteriocins promote the accumulation of intracellular ROS, increase the apoptotic index (bax/bcl2), reduce the expression of FOXM1 and MMP9, inhibit mitochondrial energy metabolism and glycolysis, reduce its energy supply leading to apoptosis and necrosis, or inhibit its migration and proliferation, which ultimately promotes the apoptosis and necrosis, inhibiting the migration and proliferation of cancers.

species (ROS), and inhibits the mitochondrial respiration and glycolytic metabolism (lead to cancer cells running out of energy). Interestingly, nisin can also be used in combination with anticancer drugs to significantly enhance their anticancer effects *in vivo*. Preet et al. [60] reported that nisin as an adjunct can promote the effects of doxorubicin against DMBA-induced skin carcinogenesis by improving histopathological features, promote cell apoptosis of tumor, and increase superoxide dismutase (SOD) levels, thereby reducing the average load and volume of the tumor. Similarly, Rana et al. [61] demonstrated that nisin and 5-FU combination be synergistic against DMBA-induced skin cancer and could promote the rapid removal of tumors *in vivo*. These results point towards the possible use of bacteriocins as an adjunct to anticancer drug to prevent local tumor invasion, metastasis, and recurrence and develop alternate strategies to combat currently and developing drug resistance in cancer cells.

Apart from nisin, laterosporulin10 (LS10), a class IId bacteriocin produced by *Brevibacillus laterosporus* SKDU10, not only effectively inhibits pathogens [21] (i.e., *M. tuberculosis* and *S. aureus*) but also kills a variety of cancer cells (e.g., MCF-7, HEK293T, HT1080, HeLa, and H1299 cell lines) at

10 μM by destroying the membrane structure. Interestingly, it shows low toxicity towards normal prostate epithelium cells (RWPE-1) [62]. Microcin E492 produced by *K. pneumoniae* can trigger cancer cells to form ion channels, resulting in cell shrinkage, DNA fragmentation, extracellular exposure of phosphatidylserine, caspase activation, and loss of mitochondrial membrane potential, inhibiting the growth of HeLa, Jurkat RJ 2.25, and Ramos cell lines at the concentration more than 5 $\mu\text{g}/\text{mL}$. Like LS10, microcin E492 also had no effect on normal cells (KG-1 and a primary culture of human tonsil endothelial cell) [63]. Pediocin CP2, a class IIa bacteriocin from *Pediococcus acidilactici* MTCC 5101, can affect cell division and DNA synthesis and induce programmed cell death of multiple cancer cells (MCF-7, HepG2, and HeLa) at 25 $\mu\text{g}/\text{mL}$ without selective cytotoxicity. [56, 64] In addition, plantaricin A [65] from *Lactobacillus plantarum*, pediocin PA-1 [56] from *P. acidilactici* K2a2-3, chaxapeptin [66] from *Streptomyces leeuwenhoekii* C58, and duramycin [67] from *Streptoverticillium griseoverticillatum* have been reported to inhibit Jurkat, HeLa, A549, and MCA-RH 7777 cell lines, respectively. Thiostrepton, produced by *Streptomyces*, is an exciting bacteriocin that was reported to have *in vivo* anticancer properties as of nisin.

TABLE 3: Anti-inflammation and immunomodulation effects of bacteriocins.

Bacteriocins	Classification	Resource	Highlights
Nisin A	Lanthipeptide	<i>L. lactis</i>	Decreasing the levels of IL-6, IL-8, and TNF- α and reduce the growth of bacteria in the wound [73]
Nisin Z	Lanthipeptide	<i>L. lactis</i>	Inhibiting <i>S. agalactiae</i> and <i>S. aureus</i> , alleviating mastitis in cows [74]
Nisin	Lanthipeptide	<i>L. lactis</i>	Increasing the level of IL-12 in macrophages [82], adjust the levels of inflammatory factors in both directions and promote immune balance [83]. Decrease the levels of TNF- α , TNF- β , NF- κ B, IL-1, and ROS in mice [153]
Nisin P	Lanthipeptide	<i>S. lactis</i> SMN003	Regulating cytokine concentration to reduce uterine inflammation in rats [75]
Thiostrepton	Thiopeptide	<i>Streptomyces</i> sp.	Inhibiting psoriasis-like inflammation induced by TLR7, TLR8, and TLR9 [86]
Microcin M	Microcin	<i>E. coli</i> MC4100	Inhibiting intestinal pathogenic bacteria and reducing intestinal inflammation [77]
Microcin J25	Lasso peptide	<i>E. coli</i>	Improving intestinal inflammation of broiler and mouse caused by <i>Salmonella</i> and ETEC [78, 79]
Sublancin	Glycocin	<i>B. subtilis</i> 800	Enhancing macrophage function, increase CD 4 ⁺ and CD 8 ⁺ cells, thereby enhancing immune response [84, 85]. Inhibiting NF- κ B, relieving intestinal inflammation [157]
Gassericin A	Circular bacteriocins	<i>L. gasseri</i> LA39	Binding to KRT19 thus promote fluid absorption and decrease secretion early-weaned piglets [158]
Salivaricin LHM	Class II	<i>L. salivarius</i>	Inhibiting inflammation caused by <i>P. aeruginosa</i> , with immune regulation in mice [81]
Plantaricin EF	Class IIb	<i>L. plantarum</i>	Reducing obesity and fat inflammation [76]
Lmo2776	Class IId	<i>L. monocytogenes</i>	Targeting the commensal <i>P. copri</i> and modulate intestinal infection in mice [159]

Thiostrepton not only forms a tight complex with the fork-head box M1 (FOX M1, a key regulator of the cell cycle) binding domain and inhibits FOX M1 expression, inhibiting MCF7 cell *in vitro* at 10 μ M, but also decreases FOX M1 expression and acts as a proapoptotic agent, thereby inhibiting endometriosis and reducing MMP9 and bcl-2 levels *in vivo* at 150 mg/kg [68–70]. Therefore, many bacteriocins have the potential to be used as antitumor agents by interfering with some aspect of cancer progress. They have a significant potential for developing as antitumor drugs.

4. Anti-Inflammation and Immunomodulation Activities

The immune system is a complex network of cells, tissues, and organs that work together to protect the body from harmful substances and defend against disease, which plays an important role in maintaining the health of human [71]. Many diseases are linked to disturbances in the immune system, such as inflammation and immune deficiency [72]. Bacteriocins also have anti-inflammatory and immunomodulatory effects as detailed in Table 3 and Figure 3. Bacteriocins can inhibit the inflammatory effects caused by pathogen-associated molecular patterns (PAMPs) or other irritants by modulating cytokine levels. This is characterized by an increase in anti-inflammatory cytokines and a decrease in proinflammatory cytokines by regulating the activation of certain pathways, such as Toll-like receptor (TLR), nuclear factor kappa-B (NF- κ B), and mitogen-activated protein kinase (MAPK) signaling pathways. Bacteriocins also promote the secretion of antimicrobial substances from epithelial cells to kill proinflammatory bacteria. And they inhibit the infection-induced inflammation and migration of pathogens by increasing the expression of tight junction proteins (TJP), strengthening the intestinal barrier, and reducing the

invasion of proinflammatory pathogens into the bloodstream and extraintestinal organs.

Nisin has been reported to have a significant anti-inflammatory effect *in vitro* and *in vivo*. Nisin A can increase the activity of human keratinocytes HaCaT, inhibit LPS-induced proinflammatory cytokine levels (TNF- α), and reduce bacterial growth, promoting wound healing [73]. Nisin Z inhibits *S. agalactiae* and *S. aureus* and leads to a significantly decreased milk somatic cell count in cows with mastitis, thus effectively relieving the symptoms of mastitis [74]. Nisin P from *Streptococcus lactis* SMN003 reduces uterine inflammation in rats by regulating the concentration of proinflammatory and anti-inflammatory cytokines (regulate the levels of B7-2, IFN- γ , IL-2, and IL-8) and normalized uterine neutrophils thus restoring endometrial architecture [75].

Plantaricin EF, class IIb bacteriocins which are produced by *L. plantarum*, can promote the expression of TJP in obese mice, increase the integrity of intestinal barrier, reduce the weight of obese mice, and reduce the inflammation of fat [76]. Microcin M produced by *E. coli* MC4100 mediates the competition of *Enterobacter* in inflammatory bowel, reduces the colonization of intestinal pathogenic bacteria, and reduces intestinal inflammation [77]. A lasso peptide of microcin J25 from *E. coli* can reduce the levels of IL-6, IL-8, and TNF- α to prevent intestinal damage and inflammation caused by ETEC K88. Microcin J25 also can effectively improve the production performance of *salmonella*-infected broilers, systemic inflammation, and the composition of fecal microflora [32, 78–80]. This is inconsistent with the commonly held view that bacteriocins have little effect on the structure of intestinal flora. It might be due to the special structure of microcin J25 (a lasso peptide), which makes it insensitive to proteases and thus affects intestinal microorganisms. Besides, microcin J25 also improves the fecal microbiota of weaned piglets, thereby promoting piglet growth,

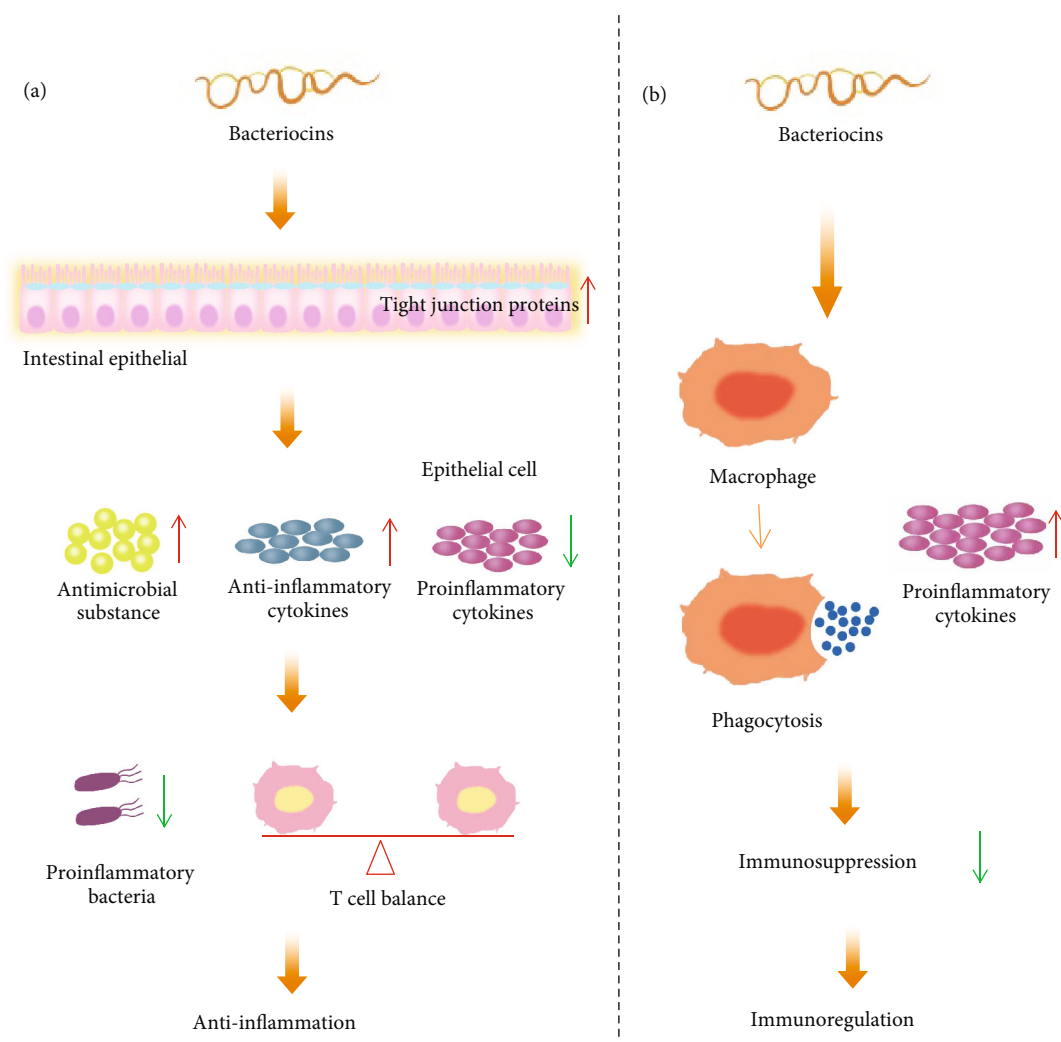


FIGURE 3: Anti-inflammation and immunomodulation effect of bacteriocins. (a) For the anti-inflammatory effect, some bacteriocins can increase anti-inflammatory cytokine levels, decrease proinflammatory cytokine levels, and maintain the balance between immune cells by inhibiting the activation of inflammatory signaling pathways in a state of inflammation. Some bacteriocins can act directly on pathogenic bacteria or reduce colonization of pathogenic bacteria by stimulating the production of antimicrobial substances. Some bacteriocins can promote the expression of intestinal tight junction proteins and strengthen the intestinal barrier. (b) For immune regulation, some bacteriocins can promote the body to produce inflammatory cytokines and promote the phagocytosis of macrophages, thus boosting the immunity and achieving immune regulation in the immunosuppressive state.

apparent total digestibility, and intestinal barrier function [32]. Salivaricin LHM from *Lactobacillus salivarius* inhibits the growth and biofilm formation of *Pseudomonas aeruginosa* (often cause nosocomial infection) and can also reduce the inflammation and prevent injury caused by *P. aeruginosa* infection. So, the salivaricin LHM has anti-inflammation effect *in vivo* and *in vitro* [81].

In fact, whether it is an anti-infective, antitumor, or anti-inflammatory effect, this is inseparable from immune regulation. Nisin can not only reduce the level of proinflammatory factors to play an anti-inflammatory function but also promote the secretion of proinflammatory factors under certain conditions. For example, nanoparticles synthesized by nisin and Ag (nisin-Ag) increased the level of the proinflammatory cytokine IL-12 in macrophages [82]. Interestingly, nisin promotes the proliferation of peripheral blood mononuclear cells (PBMC), stimulate the production of IL-1 and IL-6,

and increase the proportion of CD4⁺ CD8⁺ T cells. Contrary, when PBMC is stimulated by LPS, nisin reduces the production of LPS-induced proinflammatory cytokine IL-6 [83]. It indicates that nisin has strong immune-modulatory activity. Sublancin (1.0 mg/kg) can enhance macrophage function, increase CD 4⁺ and CD 8⁺ cells, and protect mice from MRSA infection [84]. It also prevents cyclophosphamide-induced immunosuppression in mice and inhibits NF- κ B activation to balance the immune response during infection, alleviating intestinal inflammation [85]. Thioestrepton is a kind of thiopeptide, which can inhibit the psoriatic inflammation, which induced by TLR7, TLR8, and TLR9 *in vivo* [86].

As mentioned above, bacteriocins have a wide range of biological activities, suggesting that they may be used as anti-infective compounds and effective therapeutic agents in the treatment of a number of immune-related diseases,

and they may even have promising applications in cancer therapy.

5. Opportunities of the Application of Bacteriocins in Human Health

5.1. Delivery Systems for Bacteriocins. Bacteriocins are an essential class of polypeptide substance. They are reported to be involved in improving gut health, such as reducing pathogenic bacteria colonization, improving the intestinal barrier, and alleviating intestinal inflammation. Besides, bacteriocins are not easy to cause drug resistance and have little influence on commensal flora. For example, thuricin CD, a posttranslationally modified bacteriocin produced by *B. thuringiensis* DPC 6431 with an activity against *C. difficile*, has potential as a targeted therapy in the treatment of *C. difficile*-associated infection while also reducing collateral impact on the commensal flora [87]. Some bacteriocins, such as lasso peptide microcin J25, have stable structures to avoid degradation by proteases in digestive tract [80]; however, most bacteriocins are susceptible to be degraded by proteases when administered orally, leading to the loss of antimicrobial activity. As a result, only a small fraction of bacteriocins has been tested *in vivo* by intraperitoneal injection, nasal feeding, or applying to skin. Therefore, effective delivery methods are necessary to ensure that they are not degraded when they reach the intestine.

Nanoparticles (i.e., metal nanoparticles, organic nanoparticles, nanospheres, and nanofibers), probiotics, and gels may be used as bacteriocin delivery systems [88]. For example, nisin nanoparticles have sustained release effect compared with nisin alone, prolonging the action time for the recurrent vaginal candidiasis treatment [89], and slow release contributes to prolonging the duration of the effect. In addition, some delivery modes enhance the activity of bacteriocins. For example, compared with enterocin alone, enterocin-capped silver nanoparticles (En-SNPs) synthesized by enterocin and nanosilver have stronger antibacterial activity against multiple foodborne pathogens (i.e., *E. coli* ATCC 25922, *B. cereus*, *K. pneumoniae*, *L. monocytogenes*, *M. luteus*, *P. acidilactici* LB42, *S. flexneri*, and *S. aureus*) [90]. Mohid et al. described five bacteriocins which are effective against *M. tuberculosis*. After being embedded in liposomes (phosphatidylcholine: cardiolipin=3:1), four of them are better than rifampicin (traditionally used to treat *M. tuberculosis* infection) *in vivo* [91]. However, as the best of our knowledge, those delivery systems has only little effect to solve the protease degradation problem.

Many probiotics have been reported to tolerate the gastrointestinal environment and successfully colonize the intestine. Consequently, bacteriocin-producing probiotics act as vehicles to transport the bacteriocins to the intestinal tract for their beneficial effects. Malvisi et al. found that nisin-producing strains show stronger antimicrobial activity against mastitis-causing bacteria than nonnisin-producing strains [92]. Similarly, Yin et al. demonstrated greater anti-inflammatory activity in mice fed *L. plantarum* compared to the mutant strain lacking the bacteriocin plantaricin [93]. In turn, the production of bacteriocins promotes the colonization of probiotic

bacteria, facilitating their occupation of ecological niches and reducing the colonization of pathogenic bacteria [94]. Thus, bacteriocin-producing strains can be used as vehicles to help bacteriocins colonize and function in gastrointestinal research.

5.2. Increasing Bacteriocins Production and Activity by Genetic Engineering. The production of bacteriocins in the original strains is usually low, and some bacteriocins are encoded by plasmids and are not produced in stable yields. Increasing the yield of bacteriocins is of great importance for the research and application of bacteriocins. In addition, the activity of some bacteriocins has to be improved in practice, which can also reduce the amount of bacteriocins used and thus indirectly solve the problem of insufficient bacteriocin production. Genetic engineering is a good solution to both of these problems. For the increase of bacteriocin production, Ni et al. used the shuttle expression vector pMG36e with the strong constitutive promoter p32 to further enhance the production of nisin by overexpressing the genes *nisA*, *nisRK* and *nisFEG* in *L. lactis* LS01 [95]. Kong et al. obtained the 14.5 kb complete gene cluster of nisin from *L. lactis* K29 nisin-producing bacteria, transferred it into *L. lactis* MG1363 with pCCAM β 1 plasmid, and overexpressed the core peptide gene *nisA*, thereby increasing the yield of nisin [96]. For the enhancement of the bacteriocins activity, Zhou et al. attached the tail (PRPPHPRL) of apidaecin 1b to nisin, and the activity of nisin against *E. coli* CECT101 was increased by more than twofold [97]. Recently, Steven et al. have improved the activity of antimicrobial peptides against pathogenic bacteria and broadened the spectrum of inhibition by combinatorically shuffling the peptide modules of 12 lanthipeptides. [98] Overall, genetic engineering is an effective approach to increase bacteriocin production and enhance bacteriocin activity.

5.3. Bacteriocins as Narrow-Spectrum Antimicrobials to Be Needed for Healthy Human Microbiota. The human microbiota is composed of a diverse community of bacteria, and the microbial composition and abundance changes are related to a range of human diseases. Broad-spectrum antibiotic administration could dramatically reduce gut microbiota diversity and cause many side effects. For example, antibiotic-associated diarrhea occurs when the balance of “good and bad bacteria” in the gastrointestinal is disrupted after taking antibiotics.

Many bacteriocins have a relatively narrower spectrum and targeted against a little specific bacteria compared to antibiotics which have a broad-spectrum activity. As bacteriocins usually inhibit closely related bacteria, some bacteriocins produced by pathogens showed specific antimicrobial activity to the related pathogenic bacteria. For example, lantibiotic suicin from *S. suis* has an inhibitory effect against *S. gordonii* which can cause human sepsis [99]. Klebocin from clinical isolates of *K. pneumoniae* show antimicrobial activity to pathogenic species from enterobacteriaceae [100]. Aureocins produced by *S. aureus* has a strong inhibitory effect on *S. aureus* and *S. agalactiae* [101]. In addition, bacteriocins have no impact on normal microbial flora due to their narrow spectrum. For instance, diffocin is produced by *C. difficile*

CD4 and can specifically kill other *C. difficile* strains. The modified diffocins completely prevented the intestinal settlement of *C. difficile* without infecting gut flora by oral administration in mice [102]. Similarity, thuricin CD produced by *B. thuringiensis* DPC 6431 showed elimination of *C. difficile* and has little impact on normal genera in gut [87]. Microcin J25 intervention in a diarrhea model reduces pathogenic *E. coli* colonization while improving intestinal microbiology [32]. Therefore, bacteriocins have a great potential to be used as a narrow-spectrum bacterial inhibitor for the treatment of infection-related diseases in human.

In practice, the safety of some bacteriocins is of concern as their producing bacteria are pathogenic. Therefore, for these bacteriocins, using purified bacteriocins or heterogeneous probiotic bacteria expressing the bacteriocin rather than the producing strains is applicable. It is worth mentioning that a rigorous safety assessment of bacteriocins *in vitro* and *in vivo* is necessary before practical application, regardless of whether the source is probiotic or pathogenic.

6. Conclusion and Prospect

This review highlights the potential of bacteriocins as novel therapeutic treatments in microbe infection, cancer, and immune system in human body. There is an abundance of knowledge on the bacteriocins applied in food industry, agriculture, and veterinary fields. However, there is limiting available *in vitro* and *in vivo* data regarding human health. Due to the sensitivity of some bacteriocins to protease, many studies on the activity of bacteriocins are confined to *in vitro* experiments and have not been deeply studied in the model of animals. Some posttranslationally modified bacteriocins show higher stabilities in the digestive tract, while less is known about their impact in an *in vivo* environment. The bacteriocin delivery system might be an important path to solve the degradation of bacteriocin in the digestive tract. Besides, more and more bacteriocin biosynthesis clusters are predicted using bioinformatic approaches; however, the bacteriocin-producing strain is not easy to obtain. The combination of high-throughput sequencing and culture omics may provide ideas for the discovery of new bacteriocins and their producing strains. More research related to the cytotoxicity, hemolytic activity, distribution, and metabolism of bacteriocins is needed to explore their contribution to human health. The unique antibacterial mechanism of bacteriocins compared to conventional antibiotics makes them a potential alternative to antibiotics. Further studies on the function and mechanism of action of bacteriocins will help advance their practical application in anti-infection, anticancer, and anti-inflammation or immunomodulation.

Conflicts of Interest

The authors declare that they have no conflicts of interest.

Authors' Contributions

Fuqing Huang provided the ideas and wrote this manuscript. Kunling Teng wrote and revised this manuscript. Yayong

Liu, Yanhong Cao, Tianwei Wang, Cui Ma, and Jie Zhang have performed the literature search. Jin Zhong gave guidance and revised this manuscript. All authors read and approved the final manuscript. Fuqing Huang and Kunling Teng have contributed equally to this work and should be considered co-first authors.

Acknowledgments

This work was supported by the National Natural Science Foundation of China (31972049, U20A2066, and 31900025), Strategic Priority Research Program of the Chinese Academy of Sciences (XDA26040201), grants from the Guangxi Major Science and Technology Project (AA18118041), and Jilin Province and the Chinese Academy of Sciences cooperation in science and technology high-tech industrialization special funds project (2019SYHZ0033).

References

- [1] C. L. Ventola, "The antibiotic resistance crisis: part 1: causes and threats," *Pharmacy & Therapeutics*, vol. 40, no. 4, pp. 277–283, 2015.
- [2] Y. Qin, Y. Wang, Y. He et al., "Characterization of subtilin L-Q11, a novel class I bacteriocin synthesized by *Bacillus subtilis* L-Q11 isolated from orchard soil," *Frontiers in Microbiology*, vol. 10, p. 484, 2019.
- [3] P. Alvarez-Sieiro, M. Montalbán-López, D. Mu, and O. P. Kuipers, "Bacteriocins of lactic acid bacteria: extending the family," *Applied Microbiology and Biotechnology*, vol. 100, no. 7, pp. 2939–2951, 2016.
- [4] J. Stangier, "Clinical pharmacokinetics and pharmacodynamics of the oral direct thrombin inhibitor dabigatran etexilate," *Clinical Pharmacokinetics*, vol. 47, no. 5, pp. 285–295, 2008.
- [5] J. A. Kers, R. E. Sharp, A. W. Defusco et al., "Mutacin 1140 lantibiotic variants are efficacious against *Clostridium difficile* infection," *Frontiers in Microbiology*, vol. 9, p. 415, 2018.
- [6] S. Altveş, H. K. Yildiz, and H. C. Vural, "Interaction of the microbiota with the human body in health and diseases," *Bio-science of Microbiota, Food and Health*, vol. 39, no. 2, pp. 23–32, 2020.
- [7] P. R. Shankar, "Book review: tackling drug-resistant infections globally," *Archives of Pharmacy Practice*, vol. 7, no. 3, pp. 110–111, 2016.
- [8] A. J. O'Neill, "New antibacterial agents for treating infections caused by multi-drug resistant gram-negative bacteria," *Expert Opinion on Investigational Drugs*, vol. 17, no. 3, pp. 297–302, 2008.
- [9] S. F. Nadeem, U. F. Gohar, S. F. Tahir et al., "Antimicrobial resistance: more than 70 years of war between humans and bacteria," *Critical Reviews in Microbiology*, vol. 46, no. 5, pp. 578–599, 2020.
- [10] O. McAuliffe, R. P. Ross, and C. Hill, "Lantibiotics: structure, biosynthesis and mode of action," *FEMS Microbiology Reviews*, vol. 25, no. 3, pp. 285–308, 2001.
- [11] S. T. Hsu, E. Breukink, E. Tischenko et al., "The nisin-lipid II complex reveals a pyrophosphate cage that provides a blueprint for novel antibiotics," *Nature Structural & Molecular Biology*, vol. 11, no. 10, pp. 963–967, 2004.
- [12] T. J. Krieger, R. Taylor, D. Erfle, J. R. Fraser, M. H. P. West, and P. J. McNichol, "Compositions and methods for treating

- infections using cationic peptides alone or in combination with antibiotics: U.S. Patent 6,503,881," 2003.
- [13] V. Lázár, A. Martins, R. Spohn et al., "Antibiotic-resistant bacteria show widespread collateral sensitivity to antimicrobial peptides," *Nature Microbiology*, vol. 3, no. 6, pp. 718–731, 2018.
 - [14] L. M. T. Dicks, L. Dreyer, C. Smith, and A. D. van Staden, "A review: the fate of bacteriocins in the human gastro-intestinal tract: do they cross the gut-blood barrier?," *Frontiers in Microbiology*, vol. 9, 2018.
 - [15] E. Severina, A. Severin, and A. Tomasz, "Antibacterial efficacy of nisin against multidrug-resistant Gram-positive pathogens," *The Journal of Antimicrobial Chemotherapy*, vol. 41, no. 3, pp. 341–347, 1998.
 - [16] B. P. Goldstein, J. Wei, K. Greenberg, and R. Novick, "Activity of nisin against *Streptococcus pneumoniae*, *in vitro*, and in a mouse infection model," *The Journal of Antimicrobial Chemotherapy*, vol. 42, no. 2, pp. 277–278, 1998.
 - [17] M. De Kwaadsteniet, K. T. Doeschate, and L. M. T. Dicks, "Nisin F in the treatment of respiratory tract infections caused by *Staphylococcus aureus*," *Letters in Applied Microbiology*, vol. 48, no. 1, pp. 65–70, 2009.
 - [18] M. Millette, G. Cornut, C. Dupont, F. Shareck, D. Archambault, and M. Lacroix, "Capacity of human Nisin and pediocin-producing lactic acid bacteria to reduce intestinal colonization by vancomycin-resistant enterococci," *Applied and Environmental Microbiology*, vol. 74, no. 7, pp. 1997–2003, 2008.
 - [19] A. Kling, P. Lukat, D. V. Almeida et al., "Targeting DnaN for tuberculosis therapy using novel griselimycins," *Science*, vol. 348, no. 6239, pp. 1106–1112, 2015.
 - [20] L. Fernández, S. Delgado, H. Herrero, A. Maldonado, and J. M. Rodríguez, "The bacteriocin nisin, an effective agent for the treatment of staphylococcal mastitis during lactation," *Journal of Human Lactation*, vol. 24, no. 3, pp. 311–316, 2008.
 - [21] P. Baindara, N. Singh, M. Ranjan et al., "Laterosporulin10: a novel defensin like class IId bacteriocin from *Brevibacillus* sp. strain SKDU10 with inhibitory activity against microbial pathogens," *Microbiology*, vol. 162, no. 8, pp. 1286–1299, 2016.
 - [22] D. Kruszezwska, H. G. Sahl, G. Bierbaum, U. Pag, S. O. Hynes, and Å. Ljungh, "Mersacidin eradicates methicillin-resistant *Staphylococcus aureus* (MRSA) in a mouse rhinitis model," *Journal of Antimicrobial Chemotherapy*, vol. 54, no. 3, pp. 648–653, 2004.
 - [23] V. Ramaswamy, V. M. Cresence, J. S. Rejitha et al., "Listeria-review of epidemiology and pathogenesis," *Journal of Microbiology Immunology and Infection*, vol. 40, no. 1, pp. 4–13, 2007.
 - [24] N. Dabour, A. Zihler, E. Kheadr, C. Lacroix, and I. Fliss, "In vivo study on the effectiveness of pediocin PA-1 and *Pediococcus acidilactici* UL5 at inhibiting *Listeria monocytogenes*," *International Journal of Food Microbiology*, vol. 133, no. 3, pp. 225–233, 2009.
 - [25] E. Salvucci, L. Saavedra, E. M. Hebert, C. Haro, and F. Sesma, "Enterocin CRL35 inhibits *Listeria monocytogenes* in a murine model," *Foodborne Pathogens and Disease*, vol. 9, no. 1, pp. 68–74, 2012.
 - [26] F. E. Lopez, P. A. Vincent, A. M. Zenoff, R. A. Salomón, and R. N. Farias, "Efficacy of microcin J25 in biomatrices and in a mouse model of *Salmonella* infection," *Journal of Antimicrobial Chemotherapy*, vol. 59, no. 4, pp. 676–680, 2007.
 - [27] L. Micenková, J. Bosák, J. Kucera et al., "Colicin Z, a structurally and functionally novel colicin type that selectively kills enteroinvasive *Escherichia coli* and *Shigella* strains," *Scientific Reports*, vol. 9, no. 1, article 11127, 2019.
 - [28] J. Bosák, L. Micenková, M. Hrala et al., "Colicin F_Y inhibits pathogenic *Yersinia enterocolitica* in mice," *Scientific Reports*, vol. 8, no. 1, article 12242, 2018.
 - [29] K. E. Sutyak, R. A. Anderson, S. E. Dover et al., "Spermicidal activity of the safe natural antimicrobial peptide subtilosin," *Infectious Diseases in Obstetrics and Gynecology*, vol. 2008, Article ID 540758, 6 pages, 2008.
 - [30] A. Maldonado-Barragán, B. Caballero-Guerrero, V. Martín, J. L. Ruiz-Barba, and J. M. Rodríguez, "Purification and genetic characterization of gassericin E, a novel co-culture inducible bacteriocin from *Lactobacillus gasseri* EV1461 isolated from the vagina of a healthy woman," *BMC Microbiology*, vol. 16, no. 1, p. 37, 2016.
 - [31] A. P. Singh, V. Prabha, and P. Rishi, "Value addition in the efficacy of conventional antibiotics by nisin against *Salmonella*," *PLoS One*, vol. 8, no. 10, article e76844, 2013.
 - [32] H. T. Yu, X. L. Ding, N. Li et al., "Dietary supplemented antimicrobial peptide microcin J25 improves the growth performance, apparent total tract digestibility, fecal microbiota, and intestinal barrier function of weaned pigs," *Journal of Animal Science*, vol. 95, no. 11, pp. 5064–5076, 2017.
 - [33] C. J. Minahk, F. Dupuy, and R. D. Morero, "Enhancement of antibiotic activity by sub-lethal concentrations of enterocin CRL35," *Journal of Antimicrobial Chemotherapy*, vol. 53, no. 2, pp. 240–246, 2004.
 - [34] J. C. Ellis, R. P. Ross, and C. Hill, "Nisin Z and lactacin 3147 improve efficacy of antibiotics against clinically significant bacteria," *Future Microbiology*, vol. 14, no. 18, pp. 1573–1587, 2019.
 - [35] R. R. Razonable, "Antiviral drugs for viruses other than human immunodeficiency virus," *Mayo Clinic Proceedings*, vol. 86, no. 10, pp. 1009–1026, 2011.
 - [36] A. A. Chentoufi and L. BenMohamed, "Mucosal herpes immunity and immunopathology to ocular and genital herpes simplex virus infections," *Clinical and Developmental Immunology*, vol. 2012, Article ID 149135, 22 pages, 2012.
 - [37] V. M. Quintana, N. I. Torres, M. B. Wachsmann, P. J. Sinko, V. Castilla, and M. Chikindas, "Antiherpes simplex virus type 2 activity of the antimicrobial peptide subtilosin," *Journal of Applied Microbiology*, vol. 117, no. 5, pp. 1253–1259, 2014.
 - [38] M. B. Wachsmann, M. E. Farias, E. Takeda et al., "Antiviral activity of enterocin CRL35 against herpesviruses," *International Journal of Antimicrobial Agents*, vol. 12, no. 4, pp. 293–299, 1999.
 - [39] M. B. Wachsmann, V. Castilla, A. P.d. R. Holgado, R. A.d. Torres, F. Sesma, and C. E. Coto, "Enterocin CRL35 inhibits late stages of HSV-1 and HSV-2 replication *in vitro*," *Antiviral Research*, vol. 58, no. 1, pp. 17–24, 2003.
 - [40] G. Férir, M. I. Petrova, G. Andrei et al., "Dual anti-HSV and anti-HIV activity of the lantibiotic labyrintheptin A1," *BMC Infectious Diseases*, vol. 14, article P79, Supplement 2, 2014.
 - [41] S. Gordts, G. Férir, C. Sandra, R. Süßmuth, and M. Brönstrup, "Labyrintheptins, a novel class of lantibiotics, exhibit broad and potent anti-dengue virus activity," in

- International Scientific Conference on Probiotics and Prebiotics*, Budapest, Hungary, 2015.
- [42] S. D. Todorov, M. B. Wachsmann, H. Knoetze, M. Meincken, and L. M. T. Dicks, "An antibacterial and antiviral peptide produced by *Enterococcus mundtii* ST4V isolated from soya beans," *International Journal of Antimicrobial Agents*, vol. 25, no. 6, pp. 508–513, 2005.
- [43] M. V. K. Sukhdeo, "Where are the parasites in food webs?," *Parasites & Vectors*, vol. 5, no. 1, p. 239, 2012.
- [44] G. A. W. Rook, "The hygiene hypothesis and the increasing prevalence of chronic inflammatory disorders," *Transactions of the Royal Society of Tropical Medicine and Hygiene*, vol. 101, no. 11, pp. 1072–1074, 2007.
- [45] R. C. Massey, A. Buckling, and R. French-Constant, "Interference competition and parasite virulence," *Proceedings of the Royal Society of London. Series B: Biological Sciences*, vol. 271, no. 1541, pp. 785–788, 2004.
- [46] K. J. Esch and C. A. Petersen, "Transmission and epidemiology of zoonotic protozoal diseases of companion animals," *Clinical Microbiology Reviews*, vol. 26, no. 1, pp. 58–85, 2013.
- [47] L. C. Pollitt, P. MacGregor, K. Matthews, and S. E. Reece, "Malaria and trypanosome transmission: different parasites, same rules?," *Trends in Parasitology*, vol. 27, no. 5, pp. 197–203, 2011.
- [48] R. Martín-Escolano, R. Cebrián, M. Maqueda et al., "Assessing the effectiveness of AS-48 in experimental mice models of Chagas' disease," *Journal of Antimicrobial Chemotherapy*, vol. 75, no. 6, pp. 1537–1545, 2020.
- [49] B. Gao, M. d. C. Rodriguez, H. Lanz-Mendoza, and S. Zhu, "AdDLP, a bacterial defensin-like peptide, exhibits anti-*Plasmodium* activity," *Biochemical and Biophysical Research Communications*, vol. 387, no. 2, pp. 393–398, 2009.
- [50] Z. H. Ren, C. Y. Hu, H. R. He, Y. J. Li, and J. Lyu, "Global and regional burdens of oral cancer from 1990 to 2017: results from the global burden of disease study," *Cancer Communications*, vol. 40, no. 2-3, pp. 81–92, 2020.
- [51] T. N. Seyfried and L. C. Huysentruyt, "On the origin of cancer metastasis," *Critical Reviews in Oncogenesis*, vol. 18, no. 1-2, pp. 43–73, 2013.
- [52] W. G. Jiang, A. J. Sanders, M. Katoh et al., "Tissue invasion and metastasis: molecular, biological and clinical perspectives," *Seminars in Cancer Biology*, vol. 35, Supplement, pp. S244–S275, 2015.
- [53] N. E. Joo, K. Ritchie, P. Kamarajan, D. Miao, and Y. L. Kapila, "Nisin, an apoptogenic bacteriocin and food preservative, attenuates HNSCC tumorigenesis via CHAC 1," *Cancer Medicine*, vol. 1, no. 3, pp. 295–305, 2012.
- [54] S. Ahmadi, M. Ghollasi, and H. M. Hosseini, "The apoptotic impact of nisin as a potent bacteriocin on the colon cancer cells," *Microbial Pathogenesis*, vol. 111, pp. 193–197, 2017.
- [55] Z. Norouzi, A. Salimi, R. Halabian, and H. Fahimi, "Nisin, a potent bacteriocin and anti-bacterial peptide, attenuates expression of metastatic genes in colorectal cancer cell lines," *Microbial Pathogenesis*, vol. 123, pp. 183–189, 2018.
- [56] K. I. Villarante, F. B. Elegado, S. Iwatani, T. Zendo, K. Sonomoto, and E. E. de Guzman, "Purification, characterization and *in vitro* cytotoxicity of the bacteriocin from *Pediococcus acidilactici* K2a2-3 against human colon adenocarcinoma (HT29) and human cervical carcinoma (HeLa) cells," *World Journal of Microbiology and Biotechnology*, vol. 27, no. 4, pp. 975–980, 2011.
- [57] N. Zainodini, G. Hassanshahi, M. Hajizadeh, S. Khanamani Falahati-Pour, M. Mahmoodi, and M. R. Mirzaei, "Nisin induces cytotoxicity and apoptosis in human astrocytoma cell line (SW1088)," *Asian Pacific Journal of Cancer Prevention: APJCP*, vol. 19, no. 8, pp. 2217–2222, 2018.
- [58] A. Lewies, J. F. Wentzel, H. C. Miller, and L. H. du Plessis, "The antimicrobial peptide nisin Z induces selective toxicity and apoptotic cell death in cultured melanoma cells," *Biochimie*, vol. 144, pp. 28–40, 2018.
- [59] A. Prince, A. Tiwari, P. Ror et al., "Attenuation of neuroblastoma cell growth by nisin is mediated by modulation of phase behavior and enhanced cell membrane fluidity," *Physical Chemistry Chemical Physics*, vol. 21, no. 4, pp. 1980–1987, 2019.
- [60] S. Preet, S. Bharati, A. Panjeta, R. Tewari, and P. Rishi, "Effect of nisin and doxorubicin on DMBA-induced skin carcinogenesis—a possible adjunct therapy," *Tumor Biology*, vol. 36, no. 11, pp. 8301–8308, 2015.
- [61] K. Rana, R. Sharma, and S. Preet, "Augmented therapeutic efficacy of 5-fluorouracil in conjunction with lantibiotic nisin against skin cancer," *Biochemical and Biophysical Research Communications*, vol. 520, no. 3, pp. 551–559, 2019.
- [62] P. Baidara, A. Gautam, G. P. S. Raghava, and S. Korpole, "Anticancer properties of a defensin like class IId bacteriocin Laterosporulin10," *Scientific Reports*, vol. 7, no. 1, article 46541, 2017.
- [63] C. Hetz, M. R. Bono, L. F. Barros, and R. Lagos, "Microcin E492, a channel-forming bacteriocin from *Klebsiella pneumoniae*, induces apoptosis in some human cell lines," *Proceedings of the National Academy of Sciences*, vol. 99, no. 5, pp. 2696–2701, 2002.
- [64] B. Kumar, P. P. Balgir, B. Kaur, B. Mittu, and A. Chauhan, "*In vitro* cytotoxicity of native and recombinant CP2 against cancer cell lines: a comparative study," *Pharmaceutica Analytica Acta*, vol. 3, no. 8, article 1000183, 2012.
- [65] H. Zhao, R. Sood, A. Jutila et al., "Interaction of the antimicrobial peptide pheromone Plantaricin A with model membranes: implications for a novel mechanism of action," *Biochimica et biophysica acta (BBA)-biomembranes*, vol. 1758, no. 9, pp. 1461–1474, 2006.
- [66] S. S. Elsayed, F. Trusch, H. Deng et al., "Chaxapeptin, a lasso peptide from extremotolerant *Streptomyces leeuwenhoekii* strain C58 from the hyperarid Atacama desert," *The Journal of Organic Chemistry*, vol. 80, no. 20, pp. 10252–10260, 2015.
- [67] B. Yang, X. Huang, W. Li, S. Mouli, R. J. Lewandowski, and A. C. Larson, "Duramycin radiosensitization of MCA-RH 7777 hepatoma cells through the elevation of reactive oxygen species," *Journal of Cancer Research and Therapeutics*, 2019.
- [68] J. M. M. Kwok, S. S. Myatt, C. M. Marson, R. C. Coombes, D. Constantinidou, and E. W. F. Lam, "Thiostrepton selectively targets breast cancer cells through inhibition of forkhead box M1 expression," *Molecular Cancer Therapeutics*, vol. 7, no. 7, pp. 2022–2032, 2008.
- [69] M. Kongsema, S. Wongkhieo, M. Khongkew et al., "Molecular mechanism of forkhead box M1 inhibition by thiostrepton in breast cancer cells," *Oncology Reports*, vol. 42, no. 3, pp. 953–962, 2019.
- [70] P. Jin, X. Chen, G. Yu, Z. Li, Q. Zhang, and J. V. Zhang, "The clinical and experimental research on the treatment of endometriosis with thiostrepton," *Anti-Cancer Agents in Medicinal Chemistry*, vol. 19, no. 3, pp. 323–329, 2019.

- [71] L. V. Hooper, D. R. Littman, and A. J. Macpherson, "Interactions between the microbiota and the immune system.," *Science*, vol. 336, no. 6086, pp. 1268–1273, 2012.
- [72] J. Varadé, S. Magadán, and Á. González-Fernández, "Human immunology and immunotherapy: main achievements and challenges," *Cellular & Molecular Immunology*, vol. 18, no. 4, pp. 805–828, 2021.
- [73] M. V. Mouritzen, A. Andrea, K. Qvist, S. S. Poulsen, and H. Jenssen, "Immunomodulatory potential of Nisin A with application in wound healing," *Wound Repair and Regeneration*, vol. 27, no. 6, pp. 650–660, 2019.
- [74] J. Wu, S. Hu, and L. Cao, "Therapeutic effect of nisin Z on subclinical mastitis in lactating cows," *Antimicrobial Agents and Chemotherapy*, vol. 51, no. 9, pp. 3131–3135, 2007.
- [75] Z. Jia, M. He, C. Wang et al., "Nisin reduces uterine inflammation in rats by modulating concentrations of pro- and anti-inflammatory cytokines," *American Journal of Reproductive Immunology*, vol. 81, no. 5, article e13096, 2019.
- [76] D. D. Heeney, Z. Zhai, Z. Bendiks et al., "Lactobacillus plantarumbacteriocin is associated with intestinal and systemic improvements in diet-induced obese mice and maintains epithelial barrier integrity in vitro," *Gut Microbes*, vol. 10, no. 3, pp. 382–397, 2019.
- [77] M. Sassone-Corsi, S. P. Nuccio, H. Liu et al., "Microcins mediate competition among *Enterobacteriaceae* in the inflamed gut," *Nature*, vol. 540, no. 7632, pp. 280–283, 2016.
- [78] H. Yu, X. Ding, L. Shang et al., "Protective ability of biogenic antimicrobial peptide microcin J25 against enterotoxigenic *Escherichia Coli*-induced intestinal epithelial dysfunction and inflammatory responses IPEC-J2 cells," *Frontiers in Cellular and Infection Microbiology*, vol. 8, p. 242, 2018.
- [79] G. Wang, Q. Song, S. Huang et al., "Effect of antimicrobial peptide microcin J25 on growth performance, immune regulation, and intestinal microbiota in broiler chickens challenged with *Escherichia coli* and *Salmonella*," *Animals*, vol. 10, no. 2, p. 345, 2020.
- [80] H. Yu, Y. Wang, X. Zeng et al., "Therapeutic administration of the recombinant antimicrobial peptide microcin J25 effectively enhances host defenses against gut inflammation and epithelial barrier injury induced by enterotoxigenic *Escherichia coli* infection," *The FASEB Journal*, vol. 34, no. 1, pp. 1018–1037, 2020.
- [81] L. H. Mahdi, H. S. Jabbar, and I. G. Auda, "Antibacterial immunomodulatory and antibiofilm triple effect of Salivarin LHM against *Pseudomonas aeruginosa* urinary tract infection model," *International Journal of Biological Macromolecules*, vol. 134, pp. 1132–1144, 2019.
- [82] M. Moein, A. A. Imani Fooladi, and H. Mahmoodzadeh Hosseini, "Determining the effects of green chemistry synthesized Ag-nisin nanoparticle on macrophage cells," *Microbial Pathogenesis*, vol. 114, pp. 414–419, 2018.
- [83] J. Małaczewska, E. Kaczorek-Lukowska, R. Wójcik, W. Rękawek, and A. K. Siwicki, "In vitro immunomodulatory effect of nisin on porcine leucocytes," *Journal of Animal Physiology and Animal Nutrition*, vol. 103, no. 3, pp. 882–893, 2019.
- [84] S. Wang, Q. Ye, K. Wang et al., "Enhancement of macrophage function by the antimicrobial peptide sublancin protects mice from methicillin-resistant *Staphylococcus aureus*," *Journal of Immunology Research*, vol. 2019, Article ID 3979352, 13 pages, 2019.
- [85] S. Wang, S. Huang, Q. Ye et al., "Prevention of cyclophosphamide-induced immunosuppression in mice with the antimicrobial peptide sublancin," *Journal of Immunology Research*, vol. 2018, Article ID 4353580, 11 pages, 2018.
- [86] C. Y. Lai, D. W. Yeh, C. H. Lu et al., "Thiostrepton inhibits psoriasis-like inflammation induced by TLR7, TLR8, and TLR9," *The Journal of Immunology*, vol. 196, 1 Supplement, p. 124.41, 2016.
- [87] M. C. Rea, C. S. Sit, E. Clayton et al., "Thuricin CD, a post-translationally modified bacteriocin with a narrow spectrum of activity against *Clostridium difficile*," *Proceedings of the National Academy of Sciences*, vol. 107, no. 20, pp. 9352–9357, 2010.
- [88] T. D. Arthur, V. L. Cavera, and M. L. Chikindas, "On bacteriocin delivery systems and potential applications," *Future Microbiology*, vol. 9, no. 2, pp. 235–248, 2014.
- [89] L. C. L. de Abreu, V. Todaro, P. C. Sathler et al., "Development and characterization of nisin nanoparticles as potential alternative for the recurrent vaginal candidiasis treatment," *AAPS PharmSciTech*, vol. 17, no. 6, pp. 1421–1427, 2016.
- [90] T. K. Sharma, M. Sapra, A. Chopra et al., "Interaction of bacteriocin-capped silver nanoparticles with food pathogens and their antibacterial effect," *International Journal of Green Nanotechnology*, vol. 4, no. 2, pp. 93–110, 2012.
- [91] S. A. Mohid and A. Bhunia, "Combining antimicrobial peptides with nanotechnology: an emerging field in theranostics," *Current Protein and Peptide Science*, vol. 21, no. 4, pp. 413–428, 2020.
- [92] M. Malvisi, M. Stuknyté, G. Magro et al., "Antibacterial activity and immunomodulatory effects on a bovine mammary epithelial cell line exerted by nisin A-producing *Lactococcus lactis* strains," *Journal of Dairy Science*, vol. 99, no. 3, pp. 2288–2296, 2016.
- [93] X. Yin, D. Heeney, Y. Srisengfa, B. Golomb, S. Griffey, and M. Marco, "Bacteriocin biosynthesis contributes to the anti-inflammatory capacities of probiotic *Lactobacillus plantarum*," *Beneficial Microbes*, vol. 9, no. 2, pp. 333–344, 2018.
- [94] S. Kommineni, D. J. Bretl, V. Lam et al., "Bacteriocin production augments niche competition by *enterococci* in the mammalian gastrointestinal tract," *Nature*, vol. 526, no. 7575, pp. 719–722, 2015.
- [95] Z. J. Ni, X. Zhang, F. Liu et al., "Effect of co-overexpression of nisin key genes on nisin production improvement in *Lactococcus lactis* LS01," *Probiotics and Antimicrobial Proteins*, vol. 9, no. 2, pp. 204–212, 2017.
- [96] W. Kong and T. Lu, "Cloning and optimization of a nisin biosynthesis pathway for bacteriocin harvest," *ACS Synthetic Biology*, vol. 3, no. 7, pp. 439–445, 2014.
- [97] L. Zhou, A. J. van Heel, M. Montalban-Lopez, and O. P. Kuipers, "Potentiating the activity of nisin against *Escherichia coli*," *Frontiers in Cell and Developmental Biology*, vol. 4, p. 7, 2016.
- [98] S. Schmitt, M. Montalbán-López, D. Peterhoff et al., "Analysis of modular bioengineered antimicrobial lanthipeptides at nanoliter scale," *Nature Chemical Biology*, vol. 15, no. 5, pp. 437–443, 2019.
- [99] J. Wang, Y. Gao, K. Teng, J. Zhang, S. Sun, and J. Zhong, "Restoration of bioactive lantibiotic suicin from a remnant lan locus of pathogenic *Streptococcus suis* serotype 2," *Applied*

- and *Environmental Microbiology*, vol. 80, no. 3, pp. 1062–1071, 2014.
- [100] Z. Z. Khalaf and A. R. Hussein, “Antibiofilm activity of klebocin crude extract against some species of *Enterobacteriaceae*,” *Iraqi Journal of Science*, vol. 59, no. 4A, pp. 1826–1835, 2018.
- [101] M. L. Varella Coelho, J. d. Santos Nascimento, P. C. Fagundes et al., “Activity of staphylococcal bacteriocins against *Staphylococcus aureus* and *Streptococcus agalactiae* involved in bovine mastitis,” *Research in Microbiology*, vol. 158, no. 7, pp. 625–630, 2007.
- [102] D. Gebhart, S. Lok, S. Clare et al., “A modified R-type bacteriocin specifically targeting *Clostridium difficile* prevents colonization of mice without affecting gut microbiota diversity,” *MBio*, vol. 6, no. 2, p. e02368, 2015.
- [103] A. M. Brand, M. De Kwaadsteniet, and L. M. T. Dicks, “The ability of nisin F to control *Staphylococcus aureus* infection in the peritoneal cavity, as studied in mice,” *Letters in Applied Microbiology*, vol. 51, no. 6, pp. 645–649, 2010.
- [104] R. Santos, D. Ruza, E. Cunha, L. Tavares, and M. Oliveira, “Diabetic foot infections: application of a nisin-biogel to complement the activity of conventional antibiotics and antiseptics against *Staphylococcus aureus* biofilms,” *PLoS One*, vol. 14, no. 7, article e0220000, 2019.
- [105] C. Le Lay, L. Dridi, M. G. Bergeron, M. Ouellette, and I. Fliss, “Nisin is an effective inhibitor of *Clostridium difficile* vegetative cells and spore germination,” *Journal of Medical Microbiology*, vol. 65, no. 2, pp. 169–175, 2016.
- [106] A. J. Lepak, K. Marchillo, W. A. Craig, and D. R. Andes, “*In vivo* pharmacokinetics and pharmacodynamics of the lantibiotic NAI-107 in a neutropenic murine thigh infection model,” *Antimicrobial Agents and Chemotherapy*, vol. 59, no. 2, pp. 1258–1264, 2015.
- [107] F. Castiglione, A. Lazzarini, L. Carrano et al., “Determining the structure and mode of action of microbisporicin, a potent lantibiotic active against multiresistant pathogens,” *Chemistry & Biology*, vol. 15, no. 1, pp. 22–31, 2008.
- [108] M. Mota-Meira, H. Morency, and M. C. Lavoie, “*In vivo* activity of mutacin B-Ny266,” *Journal of Antimicrobial Chemotherapy*, vol. 56, no. 5, pp. 869–871, 2005.
- [109] M. Mota-Meira, G. Lapointe, C. Lacroix, and M. C. Lavoie, “MICs of mutacin B-Ny266, nisin A, vancomycin, and oxacillin against bacterial pathogens,” *Antimicrobial Agents and Chemotherapy*, vol. 44, no. 1, pp. 24–29, 2000.
- [110] J. A. Kers, A. W. DeFusco, J. H. Park et al., “OG716: designing a fit-for-purpose lantibiotic for the treatment of *Clostridium difficile* infections,” *PLoS One*, vol. 13, no. 6, article e0197467, 2018.
- [111] W. W. Niu and H. C. Neu, “Activity of mersacidin, a novel peptide, compared with that of vancomycin, teicoplanin, and daptomycin,” *Antimicrobial Agents and Chemotherapy*, vol. 35, no. 5, pp. 998–1000, 1991.
- [112] H. Brötz, G. Bierbaum, K. Leopold, P. E. Reynolds, and H. G. Sahl, “The lantibiotic mersacidin inhibits peptidoglycan synthesis by targeting lipid II,” *Antimicrobial Agents and Chemotherapy*, vol. 42, no. 1, pp. 154–160, 1998.
- [113] H. Brotz, G. Bierbaum, A. Markus, E. Molitor, and H. G. Sahl, “Mode of action of the lantibiotic mersacidin: inhibition of peptidoglycan biosynthesis via a novel mechanism?,” *Antimicrobial Agents and Chemotherapy*, vol. 39, no. 3, pp. 714–719, 1995.
- [114] S. Boakes, T. Ayala, M. Herman, A. N. Appleyard, M. J. Dawson, and J. Cortés, “Generation of an actagardine A variant library through saturation mutagenesis,” *Applied Microbiology and Biotechnology*, vol. 95, no. 6, pp. 1509–1517, 2012.
- [115] G. S. Crowther, S. D. Baines, S. L. Todhunter, J. Freeman, C. H. Chilton, and M. H. Wilcox, “Evaluation of NVB302 versus vancomycin activity in an *in vitro* human gut model of *Clostridium difficile* infection,” *Journal of Antimicrobial Chemotherapy*, vol. 68, no. 1, pp. 168–176, 2013.
- [116] S. Boakes, A. N. Appleyard, J. Cortés, and M. J. Dawson, “Organization of the biosynthetic genes encoding deoxyactagardine B (DAB), a new lantibiotic produced by *Actinoplanes liguriae* NCIMB41362,” *The Journal of Antibiotics*, vol. 63, no. 7, pp. 351–358, 2010.
- [117] S. Boakes, W. J. Weiss, M. Vinson, S. Wadman, and M. J. Dawson, “Antibacterial activity of the novel semisynthetic lantibiotic NVB333 *in vitro* and in experimental infection models,” *The Journal of Antibiotics*, vol. 69, no. 12, pp. 850–857, 2016.
- [118] M. C. Rea, E. Clayton, P. M. O’Connor et al., “Antimicrobial activity of lacticin 3147 against clinical *Clostridium difficile* strains,” *Journal of Medical Microbiology*, vol. 56, no. 7, pp. 940–946, 2007.
- [119] E. Gavrish, C. S. Sit, S. Cao et al., “Lassomycin, a ribosomally synthesized cyclic peptide, kills *Mycobacterium tuberculosis* by targeting the ATP-dependent protease ClpC1P1P2,” *Chemistry & Biology*, vol. 21, no. 4, pp. 509–518, 2014.
- [120] S. Sable, A. M. Pons, S. Gendron-Gaillard, and G. Cottenceau, “Antibacterial activity evaluation of microcin J25 against diarrheagenic *Escherichia coli*,” *Applied and Environmental Microbiology*, vol. 66, no. 10, pp. 4595–4597, 2000.
- [121] A. Bellomio, P. A. Vincent, B. F. de Arcuri, R. N. Farias, and R. D. Morero, “Microcin J25 has dual and independent mechanisms of action in *Escherichia coli*: RNA polymerase inhibition and increased superoxide production,” *Journal of Bacteriology*, vol. 189, no. 11, pp. 4180–4186, 2007.
- [122] C. Aguilar-Pérez, B. Gracia, L. Rodrigues et al., “Synergy between circular bacteriocin AS-48 and ethambutol against *Mycobacterium tuberculosis*,” *Antimicrobial Agents and Chemotherapy*, vol. 62, no. 9, article e00359, 2018.
- [123] M. Sánchez-Hidalgo, M. Montalbán-López, R. Cebrián, E. Valdivia, M. Martínez-Bueno, and M. Maqueda, “AS-48 bacteriocin: close to perfection,” *Cellular and Molecular Life Sciences*, vol. 68, no. 17, pp. 2845–2857, 2011.
- [124] M. J. Sánchez-Barrena, M. Martínez-Ripoll, A. Gálvez et al., “Structure of bacteriocin AS-48: from soluble state to membrane bound state,” *Journal of Molecular Biology*, vol. 334, no. 3, pp. 541–549, 2003.
- [125] R. Cebrián, M. E. Rodríguez-Cabezas, R. Martín-Escolano et al., “Preclinical studies of toxicity and safety of the AS-48 bacteriocin,” *Journal of Advanced Research*, vol. 20, pp. 129–139, 2019.
- [126] T. H. Kim, B. T. B. Hanh, G. Kim et al., “Thiostrepton: a novel therapeutic drug candidate for *Mycobacterium abscessus* infection,” *Molecules*, vol. 24, no. 24, p. 4511, 2019.
- [127] M. V. Rodnina, A. Savelsbergh, N. B. Matassova, V. I. Katunin, Y. P. Semenov, and W. Wintermeyer, “Thiostrepton inhibits the turnover but not the GTPase of elongation factor G on the ribosome,” *Proceedings of the National Academy of Sciences*, vol. 96, no. 17, pp. 9586–9590, 1999.
- [128] H. Hanchi, R. Hammami, B. Fernandez, R. Kourda, J. Ben Hamida, and I. Fliss, “Simultaneous production of

- formylated and nonformylated enterocins L50A and L50B as well as 61A, a new glycosylated durancin, by *Enterococcus durans* 61A, a strain isolated from artisanal fermented milk in Tunisia,” *Journal of Agricultural and Food Chemistry*, vol. 64, no. 18, pp. 3584–3590, 2016.
- [129] H. Hanchi, R. Hammami, H. Gingras et al., “Inhibition of MRSA and of *Clostridium difficile* by durancin 61A: synergy with bacteriocins and antibiotics,” *Future Microbiology*, vol. 12, no. 3, pp. 205–212, 2017.
- [130] H. Mathur, V. Fallico, P. M. O’Connor et al., “Insights into the mode of action of the sactibiotic thuricin CD,” *Frontiers in Microbiology*, vol. 8, p. 696, 2017.
- [131] M. C. Rea, D. Alemayehu, P. G. Casey et al., “Bioavailability of the anti-clostridial bacteriocin thuricin CD in gastrointestinal tract,” *Microbiology*, vol. 160, no. 2, pp. 439–445, 2014.
- [132] S. Chiumento, C. Roblin, S. Kieffer-Jaquinod et al., “Ruminococcin C, a promising antibiotic produced by a human gut symbiont,” *Science Advances*, vol. 5, no. 9, article eaaw9969, 2019.
- [133] C. Balty, A. Guillot, L. Fradale et al., “Ruminococcin C, an anti-clostridial sactipeptide produced by a prominent member of the human microbiota *Ruminococcus gnavus*,” *Journal of Biological Chemistry*, vol. 294, no. 40, pp. 14512–14525, 2019.
- [134] J. D. Palmer, B. M. Mortzfeld, E. Piattelli, M. W. Silby, B. A. McCormick, and V. Bucci, “Microcin H47: a class IIb microcin with potent activity against multidrug Resistant Enterobacteriaceae,” *ACS Infectious Diseases*, vol. 6, no. 4, pp. 672–679, 2020.
- [135] S. Bieler, F. Silva, C. Soto, and D. Belin, “Bactericidal activity of both secreted and nonsecreted microcin E492 requires the mannose permease,” *Journal of Bacteriology*, vol. 188, no. 20, pp. 7049–7061, 2006.
- [136] G. Vassiliadis, D. Destoumieux-Garzón, C. Lombard, S. Rebuffat, and J. Peduzzi, “Isolation and characterization of two members of the siderophore-microcin family, microcins M and H47,” *Antimicrobial Agents and Chemotherapy*, vol. 54, no. 1, pp. 288–297, 2010.
- [137] Y. Turovskiy, R. D. Ludescher, A. A. Aroutcheva, S. Faro, and M. L. Chikindas, “Lactocin 160, a bacteriocin produced by vaginal *Lactobacillus rhamnosus*, targets cytoplasmic membranes of the vaginal pathogen, *Gardnerella vaginalis*,” *Probiotics and Antimicrobial Proteins*, vol. 1, no. 1, pp. 67–74, 2009.
- [138] S. E. Dover, A. A. Aroutcheva, S. Faro, and M. L. Chikindas, “Safety study of an antimicrobial peptide lactocin 160, produced by the vaginal *Lactobacillus rhamnosus*,” *Infectious Diseases in Obstetrics and Gynecology*, vol. 2007, Article ID 78248, 6 pages, 2007.
- [139] C. J. Minahk, M. Á.-E. FarÁ-as, F. Sesma, and R. D. Morero, “Effect of enterocin CRL35 on *Listeria monocytogenes* cell membrane,” *FEMS Microbiology Letters*, vol. 192, no. 1, pp. 79–83, 2000.
- [140] M. C. Verdi, C. Melian, P. Castellano, G. Vignolo, and M. Blanco Massani, “Synergistic antimicrobial effect of lactocin AL705 and nisin combined with organic acid salts against *Listeria innocua* 7 in broth and a hard cheese,” *International Journal of Food Science & Technology*, vol. 55, no. 1, pp. 267–275, 2020.
- [141] C. Melian, F. Segli, R. Gonzalez, G. Vignolo, and P. Castellano, “Lactocin AL705 as quorum sensing inhibitor to control *Listeria monocytogenes* biofilm formation,” *Journal of Applied Microbiology*, vol. 127, no. 3, pp. 911–920, 2019.
- [142] M. L. Chikindas, M. J. García-Garcerá, A. J. Driessen et al., “Pediocin PA-1, a bacteriocin from *Pediococcus acidilactici* PAC1. 0, forms hydrophilic pores in the cytoplasmic membrane of target cells,” *Applied and Environmental Microbiology*, vol. 59, no. 11, pp. 3577–3584, 1993.
- [143] M. Kaur and V. Kumar, “Microorganisms improving food quality and safety,” *Microbial diversity, interventions and scope*, pp. 75–83, 2020.
- [144] S. Thennarasu, D. K. Lee, A. Poon, K. E. Kawulka, J. C. Vederas, and A. Ramamoorthy, “Membrane permeabilization, orientation, and antimicrobial mechanism of subtilisin A,” *Chemistry and Physics of Lipids*, vol. 137, no. 1-2, pp. 38–51, 2005.
- [145] K. E. Sutyak, R. E. Wirawan, A. A. Aroutcheva, and M. L. Chikindas, “Isolation of the *Bacillus subtilis* antimicrobial peptide subtilisin from the dairy product-derived *Bacillus amyloliquefaciens*,” *Journal of Applied Microbiology*, vol. 104, no. 4, pp. 1067–1074, 2008.
- [146] J. Bosak, P. Laiblova, J. Smarda, D. Dedicova, and D. Smajs, “Novel colicin FY of *Yersinia frederiksenii* inhibits pathogenic *Yersinia* strains via YiuR-mediated reception, TonB import, and cell membrane pore formation,” *Journal of Bacteriology*, vol. 194, no. 8, pp. 1950–1959, 2012.
- [147] C. T. Kährström, “Targeting of *C. difficile* made easy,” *Nature Reviews Microbiology*, vol. 13, no. 5, p. 251, 2015.
- [148] B. S. Kang, J. G. Seo, G. S. Lee et al., “Antimicrobial activity of enterocins from *Enterococcus faecalis* SL-5 against *Propionibacterium acnes*, the causative agent in acne vulgaris, and its therapeutic effect,” *The Journal of Microbiology*, vol. 47, no. 1, pp. 101–109, 2009.
- [149] N. J. Stern, E. A. Svetoch, B. V. Eruslanov et al., “Isolation of a *Lactobacillus salivarius* strain and purification of its bacteriocin, which is inhibitory to *Campylobacter jejuni* in the chicken gastrointestinal system,” *Antimicrobial Agents and Chemotherapy*, vol. 50, no. 9, pp. 3111–3116, 2006.
- [150] E. A. Svetoch, B. V. Eruslanov, V. V. Perelygin et al., “Diverse antimicrobial killing by *Enterococcus faecium* E 50-52 Bacteriocin,” *Journal of Agricultural and Food Chemistry*, vol. 56, no. 6, pp. 1942–1948, 2008.
- [151] M. Brönstrup, H. P. Prochnow, N. V. S. Birudukota, N. V. S. Birudukota, T. Schulz et al., “Labyrinthopeptins as anti-viral agents: U.S. Patent application,” 2019.
- [152] R. Martín-Escolano, R. Cebrián, J. Martín-Escolano et al., “Insights into Chagas treatment based on the potential of bacteriocin AS-48,” *International Journal for Parasitology: Drugs and Drug Resistance*, vol. 10, pp. 1–8, 2019.
- [153] S. Preet, S. K. Pandey, K. Kaur, S. Chauhan, and A. Saini, “Gold nanoparticles assisted co-delivery of nisin and doxorubicin against murine skin cancer,” *Journal of Drug Delivery Science and Technology*, vol. 53, article 101147, 2019.
- [154] P. Kamarajan, T. Hayami, B. Matte et al., “Nisin ZP, a bacteriocin and food preservative, inhibits head and neck cancer tumorigenesis and prolongs survival,” *PLoS One*, vol. 10, no. 7, article e0131008, 2015.
- [155] A. D. Paiva, M. D. de Oliveira, S. O. de Paula, M. C. Baracat-Pereira, E. Breukink, and H. C. Mantovani, “Toxicity of bovicin HC5 against mammalian cell lines and the role of cholesterol in bacteriocin activity,” *Microbiology*, vol. 158, no. 11, pp. 2851–2858, 2012.

- [156] M. A. Varas, C. Muñoz-Montecinos, V. Kallens et al., “Exploiting zebrafish xenografts for testing the in vivo antitumorogenic activity of microcin E492 against human colorectal cancer cells,” *Frontiers in Microbiology*, vol. 11, p. 405, 2020.
- [157] S. Wang, Q. Wang, X. Zeng et al., “Use of the antimicrobial peptide sublancin with combined antibacterial and immunomodulatory activities to protect against methicillin-resistant *Staphylococcus aureus* infection in mice,” *Journal of Agricultural and Food Chemistry*, vol. 65, no. 39, pp. 8595–8605, 2017.
- [158] J. Hu, L. Ma, Y. Nie et al., “A microbiota-derived bacteriocin targets the host to confer diarrhea resistance in early-weaned piglets,” *Cell Host & Microbe*, vol. 24, no. 6, pp. 817–832.e8, 2018.
- [159] N. Rolhion, B. Chassaing, M. A. Nahori et al., “A *Listeria monocytogenes* Bacteriocin Can Target the Commensal *Prevotella copri* and Modulate Intestinal Infection,” *Cell Host & Microbe*, vol. 26, no. 5, pp. 691–701.e5, 2019.

Review Article

Dietary Fiber: An Opportunity for a Global Control of Hyperlipidemia

Ying Nie ^{1,2} and Feijun Luo ²

¹School of Food Technology and Biological Science, Hanshan Normal University, Chaozhou 521041, China

²Laboratory of Molecular Nutrition, College of Food science and Engineering, National Engineering Laboratory for Deep Processing of Rice and Byproducts, Central South University of Forestry and Technology, Changsha 410004, China

Correspondence should be addressed to Feijun Luo; luofeijun@hotmail.com

Received 16 January 2021; Revised 6 March 2021; Accepted 17 March 2021; Published 9 April 2021

Academic Editor: Wuquan Deng

Copyright © 2021 Ying Nie and Feijun Luo. This is an open access article distributed under the Creative Commons Attribution License, which permits unrestricted use, distribution, and reproduction in any medium, provided the original work is properly cited.

Dietary fiber has a long history in the intervention study of hyperlipidemia. In this review, current understandings of structures, sources, and natures of various kinds of dietary fibers (DFs) were analyzed first. Available evidences for the use of different varieties of DFs in the lipid-lowering action both *in vitro* and *in vivo* were subsequently classified, including both soluble ones, such as glucans, pectins, and gums, and insoluble ones, including arabinooxylans and chitosans, in order to draw a primary conclusion of their dose and molecular weight relationship with lipid-lowering effect. Their potential mechanisms, especially the related molecular mechanism of protective action in the treatment and prevention of hyperlipidemia, were summarized at last. Five major mechanisms are believed to be responsible for the antihyperlipidemic benefits of DFs, including low levels of energy, bulking effect, viscosity, binding capacity, and fermentation thus ameliorating the symptoms of hyperlipidemia. From the molecular level, DFs could possibly affect the activities of HMG-CoA reductase, LDL receptors, CYP7A1, and MAPK signaling pathway as well as other lipid metabolism-related target genes. In summary, dietary fibers could be used as alternative supplements to exert certain lipid-lowering effects on humans. However, more clinical evidence is needed to strengthen this proposal and its fully underlying mechanism still requires more investigation.

1. Introduction

Cardiovascular disease (CVD), including atherosclerosis, stroke, and myocardial infarction, is a leading factor to cause death in modern industrialized societies, which indicates that to reduce the risk factors for CVD plays a critical role in the management of public health, including decreased concentrations of plasma total cholesterol (TC), low-density lipoprotein cholesterol (LDL-C), and triacylglycerols (TG). It has been estimated that a reduction in LDL-C for 10 mmol/L correlated with a 22% reduction in the risk of CVD mortality and morbidity and greater than 10 mmol/L TG concentrations is associated with significantly increased risk of acute pancreatitis and CVD [1, 2]. Besides these factors, high levels of plasma high-density lipoprotein cholesterol (HDL-C) are also found to be inversely related to the risk of CVD, although the application of state-of-the-art medical interven-

tions targeting on HDL-C to reduce the CVD burden failed to show the anticipated beneficial effect.

Cholesterol, a subtype of lipids, originates from two sources in the human body; one is synthesized in the liver (about 700-900 mg/d), and another is taken in by diet (about 300-500 mg/d). In spite of small amounts of cholesterol that are used for the synthesis of steroid hormones and cell membranes, most of them are used by the liver to synthesize bile acids, such as cholic acid, which is essential to increase the absorption of hydrophobic nutrients. Bile acids are stored in the gall bladder and released into the duodenum and proximal jejunum after the stimulation of cholecystokinin. About 95% of excreted bile acids are reabsorbed and recycled by reuptake through enterohepatic circulation, and the lost fraction is compensated by synthesis and diet uptake. Cholesterol is critical in the lipid metabolism for it participates in the transportation of lipids as the form of lipoproteins, which

are small spheres containing phospholipids, apolipoproteins, and cholesterol. These lipoproteins can be divided into subgroups: LDL-C, HDL-C, and VLDL-C. LDL-C delivers fat molecules to the cells and can drive the progression of atherosclerosis if they become oxidized and form plaque within the walls of arteries. Conversely, HDL-C is considered “good” cholesterol that protects against cardiovascular diseases and helps scavenge LDL-C from the arteries and carries it back to the liver, where it is broken down [3, 4]. Given the central role of cholesterol in the lipid metabolism, a reduction of cholesterol is closely related with a lowering action of other lipids. Understanding the process of lipid metabolism will help to reveal the underlying mechanisms of lipid-lowering action and its molecular mechanism.

Hyperlipidemia, referring to a metabolism disorder, is a common disease in modern society along with an unhealthy diet and less physical activity and has been regarded as the most crucial risk factor leading to CVD [5]. Its diagnosis is often based on the abnormal deviation of one or several plasma lipids, which composed of increased TG, TC, and LDL-C and decreased HDL-C. Measures to adjust the dysfunction of lipid metabolism is commonly agreed to prevent the outbreak of CVD, including restricted diet of less carbohydrates and fats and more exercise plus medicine intervention. However, hyperlipidemic patients regularly taking drugs, such as statins and fibrates, have various complaints about their adverse effects or contraindications [6, 7]. Meanwhile, a number of functional foods or nutraceuticals, such as plant stanols and sterols, soya protein, garlic, β -glucans, and other dietary fibers, have also been identified with antihyperlipidemic function [8, 9]. Dietary fiber, “the seventh nutrient” of the body, is particular and nonreplaceable to maintain the health and composed of two types: hydrosoluble and insoluble ones, and they are classically believed to exert their influence on lipid metabolism in different patterns: hydrosoluble fiber forms an unstirred water layer on the intestinal wall and delays the absorption of sugar and fat, while the insoluble ones increase the volume of the stool. However, this categorization is criticized for its inaccuracy to represent the effects of all fibers in the lipid-lowering action [10].

The impactions of dietary fiber on reducing serum lipids stem from a study carried out in the 1970s. At that time, the same dose between 2 and 10 g/d of oats, pectins, or guar gum was regarded as equal in the action of reducing TC and LDL-C [11]. Recent analyses have focused on specific fiber type, especially the molecular weight, indicating that different kinds of dietary fibers may not be equal, and there is a dose-response relationship that existed between fiber intake and the effects of lipid reduction. In the present paper, we summarized the relationship of different structures, molecular weights, and doses of each kind of dietary fiber and their antihyperlipidemic effect and their underlying mechanisms.

2. Structures, Compositions, and Sources of Different DFs

Dietary fiber has a long history of multiple health beneficial effects, preventing or withstanding a series of common diseases, including cancer, diabetes, hyperlipemia, CVD, series

of intestinal diseases, and obesity [12, 13]. The major subtypes of DFs consist of cellulose, hemicellulose, chitosan, pectin, β -glucan, gum, and pectin, which all refuse to be hydrolyzed by any digestive enzymes secreted by nonruminant animals. Therefore, the majority of DFs cannot be absorbed by the small intestine and is thus utilized by the intestinal microorganisms for fermentation in the caecum and colon. Though plants usually harbor both hydrosoluble and insoluble DFs, their ratio differs according to the species and maturity degree of the plant.

Cellulose, hemicellulose, lignin, and chitosan compose the whole part of insoluble DFs. Binding as many as 10,000 D-glucose residues with β -1,4-glycosidic and β -1,6-glycosidic bonds forms a tree-like molecule, defined as cellulose, which is the base of the microfibril structure and the reason why it absolutely cannot be dissolved in water. Hemicelluloses are assembled with a series of heterogenic monosaccharides, and most of them are also insoluble in water but in alkali solutions. Various cereals contain hemicellulose, which consists of mainly arabinoxylans and arabinogalactans with mainly xylans or galactans as backbone and arabinose or pentosans as side chains. The water solubility of hemicellulose is strongly affected by the branching and substitution: the more branched the molecule is and the more hydrophilic the substitutions are, the more soluble the hemicellulose will be [14]. Lignin constitutes with amorphous molecules of phenyl propyl alcohol or its derivatives and exists widely in plant xylem, which is seldom considered edible. This paper abandons the discussion of lignin for this reason. Chitosan is derived from chitin with alkaline deacetylation, which composes of β -1-4-linked D-glucosamine and N-acetyl-D-glucosamine, and participates in the forming of the exoskeleton of crustaceans and the cell walls of fungi. Chitosan can exist either in a primary and unorganized structure or in a microcrystalline form, which normally can be hardly resolved in water.

Most other DFs are water soluble, including β -glucan, alginates, carrageenans, agar, pectin, gum, and some prebiotics. The endospermic cell wall polysaccharides of wheat, oat, and rye are mainly water soluble, whose major constituents are β -1,3- and β -1,4-linked glucose and the β -1,3-linkages usually appear after several β -1,4-linkages [15]. Glucan is also commonly stored in various kinds of fungus, such as *Ganoderma* and *Lentinula edodes*, and thus attaching them with biological activity. The fungi glucans are characteristic of β -1,3- and β -1,6-linkages while β -1,3- and β -1,4-linkages appear in cereal glucans. The backbones of these glucans are composed of mixed α - and β -D-glucan or pure β -D-glucan while their side chains are heterogeneous of xylose, mannose, galactose, or uronic acid. Based on the different components and structures, these glucans can be both water soluble or insoluble [16]. The insoluble parts of fungi glucans, holding about 50–80% of the total glucan, form the structural components of the cell wall and are usually cross-linked to other molecules like chitin or to proteins [17]. Seaweed includes red, brown, green, and blue ones, and their polysaccharide extracts vary from one another, which can be further divided into glucans, alginates, carrageenans, agar, and fucoidan for their different compositions. The structure of

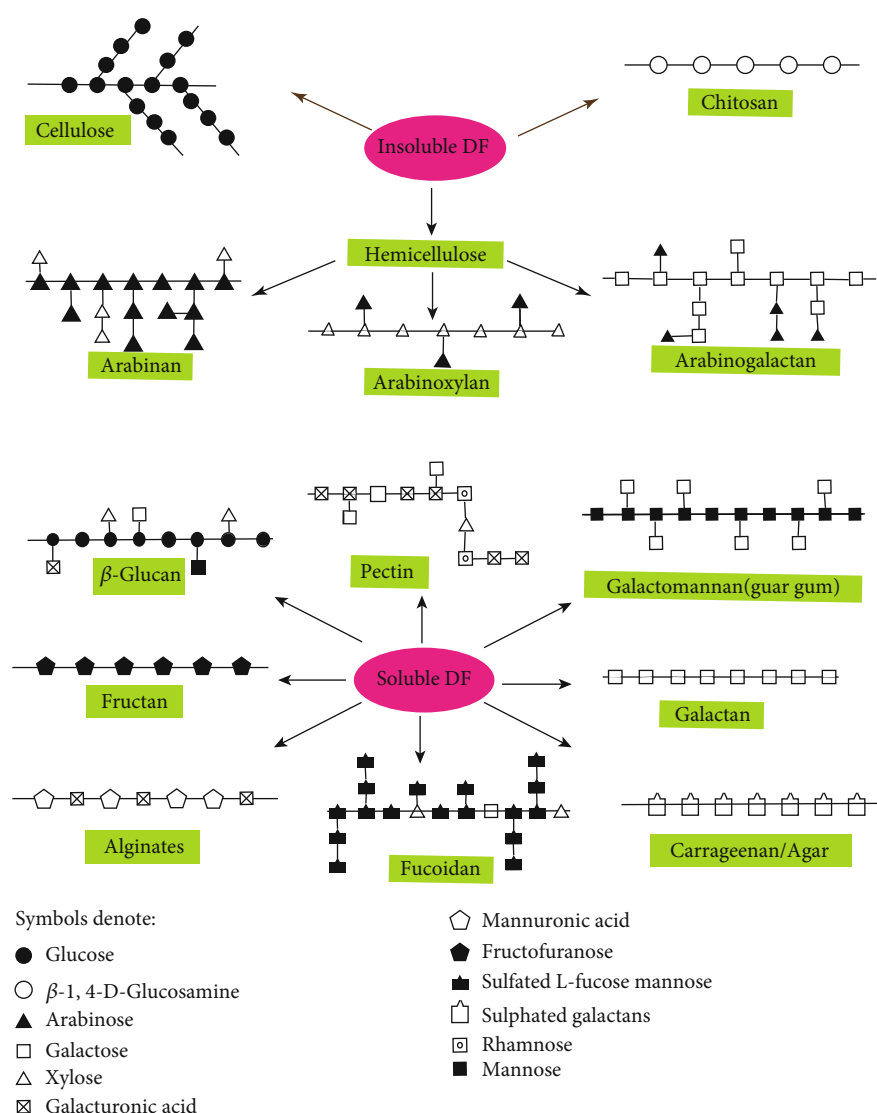


FIGURE 1: Structures and classifications of typical dietary fibers.

seaweed glucans showed by NMR spectroscopy is composed of two parts: β -1,3-glucan as backbone and about another one-fifth of β -1,6-glucan as sidechains [18]. Alginates are typically bonded with hundreds of D-mannuronic acid and L-guluronic acid residues. Carrageenan and agar are sulphated galactans with basic linear structure of galactose residues, but they differ from each other in whether the 1,4-linked anhydrogalactose is D or L form [19, 20]. Fucooidans are acidic and sulfated macromolecules composed of L-fucose along with several other oligosaccharides such as mannose, galactose, and xylose, which are usually extracted from brown algae like *Fucus vesiculosus* and sporophyll of *Undaria pinnatifida*. Pectin can dissolve in hot water and form a gel when it cools down, which owns an extremely diverse structure, but the main monomeric residue remains almost unchanged, mainly D-galacturonic acid with interruptions of rhamnose or galactose. Three major kinds of pectin molecules are recognized: homogalacturonan, rhamnogalacturonan-I, and rhamnogalacturonan-II [21], and

they exist not separately but to form covalently linked domains. Plant-secreted gums usually possess highly branched structures and thus are highly water soluble. The molecules of endosperm cell walls of leguminous seeds are galactomannans, which are usually referred to as guar gum or locust bean gum. Fructooligosaccharides (FOS) and fructans are widely stored in various plants like garlic, onion, leek, chicory, and green algae. They vary in both molecular structure and weight: FOS are a common name for only lower polymers, referring to less than 10 fructooligomers, while fructans are molecules with a high degree of polymerization. Fructans may be classified into three main types: inulin, levan, and the branched ones. The inulin consists of fructose that connected mostly or exclusively with 1,2-linkages while levan fructose residues are joint mostly or exclusively with 2,6-linkages, and the branched ones contains both [22]. FOS and inulin are often served as prebiotics in modern functional food industries. The structures of the most typical DFs are illustrated in Figure 1.

3. Lipid-Lowering Effect of Different DFs

Based on current knowledge, certain kinds of nutraceuticals could exert significant lipid-lowering activity, although not effective enough to compare with statins, such as plant sterols and stanols, red yeast rice extract, garlic, bergamot, green tea extracts, and multiple kinds of soluble dietary fiber [23].

3.1. Oat or Oat β -Glucans. β -Glucan is an important dietary fiber with a biological function, which existed mainly in yeast, bacteria, oats, and barley as well as medicinal mushrooms. There are hundreds of studies involved in the effect of oat β -glucan on metabolism diseases. A meta-analysis that included 17 RCTs (916 hypercholesterolemic patients) showed that β -glucan consumption significantly reduced LDL-C (-0.21 mmol/L (8.1 mg/dL); 95% CI, -0.27 to -0.14; $p < 0.00001$), [24]. In a randomized, single-blind, wheat bran-controlled study, it suggested that consumption of 11 g oat bran β -glucan nearly doubled the plasma secretion of bile acids within 8 h and thus decreases serum cholesterol by measuring the metabolite 7-hydroxy-4-cholesten-3-one in the plasma [25]. Similarly, the supplementation of oat β -glucan (5 g/meal, twice a day) muesli diet significantly increased the synthesis of bile acid and lowered cholesterol absorption when compared to the control diet. It further suggested that the combination 5 g oat β -glucan plus 1.5 g plant stanols per meal enhances the lipid-lowering effect by reducing the absorption of cholesterol ($p < 0.001$) while the synthesis of bile acid remains unchanged [26]. Another study found that young adults consumed 6 g β -glucan containing oat bran diet daily for 2 weeks and had significantly lowered their TC, TG, LDL-C, VLDL-C, plasminogen activator inhibitor-1 (PAI-1), and factor VII (fVII), as well as fecal volumes and dry matter of the experiment group than the control group, while both groups had no significant differences in body weight [27]. Multiple studies verified that high level of PAI-1 is correlated with increased risk of CVD while both PAI-1 and fVII could influence postprandial TG levels [28, 29]. Another meta-analysis that included 28 randomized controlled trials declared that oat β -glucan in doses of 3 g/d reduced LDL-C and TC relative to control by 0.25 mmol/L and 0.30 mmol/L, respectively, without changing HDL-C or TG [30]. A recent 6-week randomized controlled trial was designed to assign 87 mildly hypercholesterolemia patients to one of the three groups: control or low dose of oat β -glucan (1.5 g/d, OL) or high dose (3.0 g/d, OH), whose plasma TC levels are situated between 5 and 7.5 mmol/L. Results showed that while TC reduced significantly in all groups, only OL and OH reduced significantly the plasma LDL-C and the intake of 1.5 g/d was proved to be as effective as the dose of 3 g/d irrelevant with different food formats [31]. However, another clinical trial aiming to test the effects of physicochemical properties of β -glucan on its ability to lower serum LDL-C found that the β -glucan must be served with sufficient quantity (3 g/d) and the efficacy of oat β -glucan in lowering blood TC was decreased by 50% when its molecular weight (MW) was reduced from 2,210,000 g/mol to 210,000 g/mol, suggesting that molecular weight plays an important role in the lipid-lowering action of oat β -glucan. Given that the viscosity of

β -glucan is determined by its solubility and MW [32], this indicates further that mechanism of the lipid-lowering action of soluble β -glucan may be modulated by its physicochemical properties in the intestine. Similar results were found by another randomized clinical trial, in which 345 patients of both Caucasians and non-Caucasians were randomly assigned to consume cereal containing wheat fiber (control, $n = 74$: 13 Caucasian:non-Caucasian) or 4 different oat β -glucan groups: 3 g/d of high-MW 2,250,000 g/mol ($n = 67$:19), 4 g/d medium-MW 850,000 g/mol ($n = 50$:17), 3 g/d medium-MW 530,000 g/mol ($n = 54$:9), or 4 g/d low-MW 210,000 g/mol ($n = 51$:12) for 4 weeks. Individuals that consumed medium to high MW β -glucan all had significantly reduced LDL-C by 4.8 to 6.5% in both race, but low-MW had no effect compared to control [33]. Moreover, a latest systematic review that included 58 trials also claimed that a median dose of 3.5 g/d of oat β -glucan significantly lowered LDL-C by 0.14-0.23 mmol/L ($p < 0.00001$), non-HDL-C by 0.15-0.26 mmol/L ($p < 0.00001$), and apoB by 0.02-0.05 g/L ($p < 0.0001$) compared with control [34]. However, there is also controversial result. 66 overweight females were randomized into one of three 2 MJ energy-deficit diets: a control and two interventions including 5-6 g or 8-9 g β -glucan. After 3 months, all groups lost weight ($p < 0.001$) and significant reductions in TC, LDL-C, HDL-C, and leptin while no significant differences were noted between the groups, suggesting that oat β -glucan cannot enhance the antihyperlipidemic effect in energy-restricted diets [35]. From the above evidences, it is commonly agreed that oat and its enriched β -glucans are effective lipid-lowering agents, 3 g/d may be the effective dosage, and low molecular weight β -glucans (less than 200 kDa) have minor hypolipidemic effect. However, what is the ideal MW of the β -glucans for hyperlipidemic patients needs further investigation.

3.2. Barley or Barley β -Glucan. Many studies pointed out that barley β -glucan also possesses lipid-lowering properties. Eight eligible trials lasted 4 to 12 weeks involving 391 subjects, which are aimed at evaluating the lipid-reducing effect of barley, were identified in a meta-analysis. It found that the intake of 3-10 g barley β -glucan lowered TC by about 14 mg/dL, LDL-C by about 10 mg/dL, and TG by about 12 mg/dL but did not significantly alter the HDL-C level [36]. A later meta-analysis conducted with 11 studies reached similar conclusions; supplementation of comparable barley glucan could lower TC and LDL-C concentrations by 0.30 mmol/L and 0.27 mmol/L, respectively; and this lipid-lowering action had no dose-dependent relationship [37]. Hamsters were fed with high-fat diets plus different kinds of grain including whole grain wheat, barley, barley supplemented with HPMC (2%-3%), debranned oat, and oat supplemented with HPMC, which were all compared to a diet containing cellulose as control. Results showed that all supplementations significantly lowered plasma LDL-C concentrations compared to the control and HPMC further strengthened the lipid-lowering effect both in the plasma and liver. It appears that whole grain barley especially when HPMC is applied could reduce the cholesterol mainly

through modulation of the synthesis and excretion of hepatic cholesterol and bile acid [38]. Another study also supports the idea that consumption of 3 g/d high MW β -glucan from barley lowered TC effectively by circa 0.12 mol/L, while low MW β -glucan did not alter serum TC levels and even raise the dose to 5 g/d. This effect was further found to be correlated with gene-diet interaction, whereby individuals with G allele carriers of the CYP7A1 gene, namely, GG homozygotes or GT heterozygotes, exhibited more pronounced cholesterol-lowering effects than TT carriers ($p = 0.0006$) [39].

3.3. Mushroom Polysaccharides. Mushroom polysaccharides existed in varied forms including β -glucan. A great variety of active polysaccharide molecules, including heteroglucans, heterogalactans, and heteromannans have been obtained from various kinds of mushrooms such as fungi, basidiomycetes, and ascomycetes, whose biological function has been explored by abundant studies over the past decades [40]. In a study, *Pleurotus ostreatus* DF fraction (PDF) led to a reduction of hepatic TG because Dgat1 was downregulated in HFD mouse models. It could also reduce hepatic TG accumulation by modulating cholesterol-related gene expression in a manner similar to that of typical antihypercholesterolemic drugs including simvastatin and ezetimibe, although no significant change in plasma and liver biochemical data were noticed [41]. They further prepared 4 different mushroom extracts including β -glucans, water-soluble polysaccharides, ergosterol, and their mixture to examine the underlying molecular mechanisms involved in cholesterol-lowering action, in which the mRNA levels of 17 cholesterol-related genes from the jejunum, caecum, and liver of high cholesterol-fed mice were evaluated. The 4 tested supplements decreased plasma TC by 22–42% and LDL-C by 27–51%, and two of them increased mRNA levels of jejunal Npc1l1 and Abcg5 and hepatic Npc1l1, which indicates that the mushroom extracts could decrease dietary cholesterol absorption and increase bile acid excretion [42]. Zou et al. [43] developed a two-stage pH control strategy to enhance the production of polysaccharide in mushroom fermentation. Results showed that this mycelia zinc polysaccharide of 3.64×10^4 Da improves both the blood and the liver lipid levels and the antioxidant status and attenuates the liver cell injury in hyperlipidemic mice [44]. These findings suggested that mushroom extracts including β -glucan and other water-soluble heteropolysaccharides may have potential to serve as the novel cholesterol-lowering functional foods.

Besides, β -glucan (source unknown) appeared to be more effective in lowering plasma LDL-C, TC, apoA-I, and glucose levels, compared with rice bran-enriched food in a 14-week trial [45]. Another meta-analysis that included 17 randomized controlled trials with 916 subjects showed that 3–10.3 g/d β -glucan consumption in hypercholesterolemic population significantly lowered TC by average 0.26 mmol/L and LDL-C concentration by average 0.21 mmol/L, with no significant differences in HDL-C, TG, and glucose, and no reports of adverse effects were received [24], which suggested the feasibility of β -glucan as adjuvant agents of antihyperlipidemia. According to the scientific opinion of EFSA, 3 g/d β -glucans from cereals including oats and barley or from

mixtures of nonprocessed or minimally processed whole grain should be equal and served in one or more times to achieve the experimental hypolipidemic effect. However, some study criticized that a typical serving of cereals containing this amount of β -glucans requires more than 100 g/d [46]. In practice, this is quite difficult to realize unless this amount is separated into more than two portions per day. Maybe developing purified β -glucan products could help to solve this difficulty of application.

3.4. Konjac Glucomannan. 12 male baboons were included in a 9 wk crossover, randomized trial, in which they were fed a typical western human diet with or without supplements of 5% konjac glucomannan (KGM). Serum TC levels were observed to be about 25% higher than baseline when baboons consumed the western diet without supplements while KGM could reverse this increase. KGM supplementation also led to significant reduction of TG from baseline values and circulating FFAs. Liver cholesterol concentration was 31–34% lower with KGM than with the western diet [47]. The effectiveness of 3.9 g/d KGM on a reduced serum cholesterol (10%, $p < 0.0001$), LDL-C (7.2%, $p < 0.007$), and TG (23%, $p < 0.03$) in men was also observed in a double-blind crossover, placebo-controlled 4 wk study back in 1995. Besides, this hypolipidemic effect of KGM is observed without adverse effects, showing that KGM is an effective cholesterol-lowering dietary adjunct [48]. A meta-analysis that involved 12 studies ($n = 370$), 8 in adults and 4 in children, declared that the intake of 3 g/d KGM significantly lowered LDL-C for 10% (MD: 20.35 mmol/L; 95% CI: 20.46, 20.25 mmol/L) and non-HDL-C for 7% (MD: 20.32 mmol/L; 95% CI: 20.46, 20.19 mmol/L) and 6 of them suggested no impact of KGM on apolipoprotein B [49]. Another meta-analysis included 14 RCTs with 531 patients concluded that the use of glucomannan (dose ranging between 1.24 and 15.1 g/d) significantly reduces TC (WMD: -19.28 mg/dL; 95% CI: -24.30, -14.26), LDL cholesterol (WMD: -15.99 mg/dL; 95% CI: -21.31, -10.67), and triglycerides (WMD: -11.08 mg/dL; 95% CI: -22.07, -0.09) [50].

3.5. Pectins. Another viscous DF called pectin, distributed widely in cell walls of fruits and vegetables, consists of linear chains of α -1-4-galacturonic acid units with side chains including galacturonic and glucuronic acids and also shows a prominent blood cholesterol-lowering effect. By reference to an early meta-analysis, 7 relevant studies ($n = 277$ subjects) around the 1990s showed that the intake of pectins at 4.7 g/d caused a significant lowering effect on TC and LDL-C and there existed a significant dose-dependent relationship between the intake and the lowering effect, but no significant dose-response exhibited for HDL-C and TG [11]. A later study found that when hamsters were fed with high-cholesterol (0.1% w/w) diets plus 3% of lemon pectin or the same dose of the polygalacturonic acid region fraction of the lemon pectin for 8 weeks, both groups showed significant lower blood TC levels than the cellulose group. However, only the polygalacturonic acid region fraction group reached statistical significance in the lowering experiment of liver cholesterol which may suggest that the polygalacturonic acid

regions of the pectin are responsible for the cholesterol-lowering action of the pectins [51]. The team studied further to find out whether the cholesterol-lowering effect of the peels of lemon contributed mainly from the pectin component using the same experiment model. Results suggested that lemon peel is as effective as the pectin extracted from the peels in lowering blood and liver cholesterol in hamsters [52]. Another study found the cooperation of pea proteins and apple pectin is extremely effective to reduce plasma cholesterol in rats by upregulating CYP7A1 and NTCP genes, which are involved in hepatic cholesterol turnover [53]. A 12-week, placebo-controlled, randomized, parallel double-blinded study enrolled 66 middle-aged patients with abnormal glucose metabolism to examine the effects of sugar beet pectin (SBP) or polydextrose (PDX) on fasting glucose and lipid levels. Both the SBP and PDX had an increase in fasting serum HDL-C concentration compared to the control [54]. Another study compared serum cholesterol-lowering effect of different nutritional supplements, including 30 g/d of pectin, 20 g/d of polyphenols, 6 g/d of phytosterols, and all possible combinations compared to 3 mg/kg of lovastatin using familial hypercholesterolemic (FH) swine. Although the effect of pectin is not the best during the 4-week experiment, however, both phytosterol and polyphenol enhanced the reduction in LDL-C of pectin. All supplementation group showed about a half of the efficiency of lovastatin to reduce TC in FH swine, which suggested the possibility of these diets alone or in combination with drugs to reduce LDL-C [55]. From the above evidences, it is not hard to recognize that pectin and other functional foods may serve as an adjuvant therapy agent for hyperlipidemia and it was suggested by the EFSA that in order to achieve the cholesterol-lowering effect on adults, it should provide more than 6 g pectins/d in one or more servings [56].

3.6. Brown Alga Polysaccharides. Alginates and fucoidan are usually extracted from brown algae like *Fucus vesiculosus* and sporophyll of *Undaria pinnatifida*. Multiple studies found that brown alga extracts also possess the hypolipidemic activity. An extract of brown algae, *Padina arborescens* (PAE; 0.5%, w/w), was proved to reduce the blood glucose, glycosylated hemoglobin, and plasma insulin levels, as well as plasma TC, LDL-C, TG, and FFA levels, and improve glucose tolerance in a 6-week mouse experiment. These may be modulated through the PAE-caused significantly lowered hepatic activities of glucose-6-phosphatase and phosphoenolpyruvate carboxykinase and increased glucokinase activity [57]. As an alginate modifier, 2% calcium alginate (Ca-Alg) was found can significantly reduce the plasma TC in rats fed a high-cholesterol diet for 2 weeks, and this was induced by increased fecal excretion of bile acid and reduced intestinal reabsorption, evidenced by a notably lowered portal concentration of bile acid, which in turn stimulates bile acid synthesis and leads to a decrease in plasma cholesterol [58]. Polysaccharide from the sporophyll of a brown alga *Undaria pinnatifida* (AP) could reach a yield of 38.7% from its dry matter, which was composed of about 80% alginate and 20% fucoidan. The 1.7% AP supplementation obviously reduced total weight gain and fat accumulation and

improved the serum lipid profile in HFD-rats, including TG, TC, and VLDL-C, which were all closely linked with increased fecal weight and reduced gastrointestinal transit time. Moreover, the hepatic lipid peroxidation was reduced, suggesting a protective action of the liver against HFD [59]. Alginate at 20 g/kg notably reduced hepatic cholesterol to 13.1 $\mu\text{mol/g}$ but did not influence serum lipids. However, the amidated alginate at 20 g/kg significantly decreased serum TC from 2.93 to 2.00 mol/L, TG from 1.66 to 0.92 mol/L, hepatic cholesterol from 17.5 to 5.9 $\mu\text{mol/g}$, and total hepatic lipids from 67.4 to 51.7 mg/g in female HFD rats through significantly increased fecal concentrations of neutral sterols from 98.7 to 122.4 $\mu\text{mol/g}$ dry matter [60]. Apolipoprotein E-deficient mice fed a HFD plus either 1% or 5% fucoidan for 12 weeks showed a significant reduction of liver and adipose tissue weight, blood lipid, TC, TG, non-HDL-C, and glucose levels but increased plasma lipoprotein lipase (LPL) activity and HDL-C levels. Fucoidan also improved hepatic steatosis and lipid profile [61]. Fucoidan treatment also significantly improved the serum lipid profile 2 h after administration of poloxamer-407, which induces acute hyperlipidemia in mice [62]. From above evidences, polysaccharide extracts from brown algae could exert obvious hypolipidemic action; however, the effective dosage may have not yet been systematically studied.

3.7. Some Types of Prebiotics. Prebiotics are resistant to be hydrolyzed in the small intestine but are fermentable by commensal intestinal microorganism and, therefore, gives growth-promoting effects on beneficial microbes such as *Bifidobacterium* sp. and *Lactobacillus* sp. The major type of prebiotics includes inulin, fructooligosaccharides (FOSs), galactooligosaccharides (GOSs), xylooligosaccharides (XOSs), maltooligosaccharides (MOSs), lactulose, lactulosucrose, fructans, resistant starch, etc. [63]. Soluble prebiotics are able to increase the viscosity of the digestive tract and the thickness of the unstirred layer in the small intestine and thus inhibit the uptake of cholesterol [64]. The hypotriglyceridemic effect of prebiotics is also believed to be due to a reduction in hepatic reesterification of fatty acids in addition to modulation of the expression of liver lipogenesis-related genes, resulting in lower hepatic secretion rate of TG [65]. In addition, the beneficial modulation of microorganism-induced metabolite variation including SCFAs may also contribute to the hypolipidemic effect of prebiotics. Inulin, FOS, and GOS are the most popular prebiotics used in food industries, including infant food.

3.7.1. Fructooligosaccharides (FOS). FOS are naturally bioactive compounds, stored in many common foods, such as banana, garlic, asparagus, onion, wheat, and rye, and consisted of glucose and fructose residues joined by β -1,2-glycosidic linkages. An early study found that FOS prevents serum lipid disorders and lowered the activity of fatty acid synthase in the liver of rats [66]. A later study found that when rats received 2.5 g/kg lipid emulsion supplemented with FOS, their plasma TG was significantly suppressed compared with ones without FOS, and this may be caused by enhanced fecal excretion of lipids [67]. A reduced hepatic lipogenesis and steatosis caused by FOS is regulated by a reduction of the

activity of lipogenic enzymes, leading to the reduction of VLDL-C and TG secretion [68]. Either 340 or 6800 mg FOS/kg body weight/day yacon root FOS supplementation for 90 days was observed with a significant decrease in fasting plasma TG and VLDL levels in a diabetic rat model [69]. The results of a human study indicate that the FOS supplementation enhanced obviously the reduction of LDL-C and steatosis of patients, who had more exercise and a balanced diet [70]. A systematic review also supported this idea, and the most obvious reduction is plasma TC levels [71]. Another study found that 2 g/d FOS plus probiotic increased significantly serum HDL-C levels, but no significant reduction of TC and TG in elderly people with type 2 diabetes mellitus was observed [72]. However, another team evaluated the supplementation with short-chain FOS 10.6 g/d in mild hypercholesterolemic patients and reported no significant reduction in plasma TC concentrations [73]. From the above evidences, most studies approve the beneficial effects of FOS on hyperlipidemia; however, the inconsistent results suggested more efforts are required.

3.7.2. Inulin. When male hamsters were fed HFD plus 8, 12, or 16% inulin for 5 wks, their serum TC concentrations were significantly reduced by 15%-29%, TG were significantly lowered by 40%-63%, and only 16% inulin specifically decreased VLDL-C, while LDL-C and HDL-C were not significantly altered. Further notable changes in the bile acid and hepatic lipid profile demonstrate that the lipid-lowering action of inulin is possibly due to an altered hepatic triacylglycerol synthesis and VLDL secretion and reduced reabsorption of bile acids [74]. Hypercholesterolemic rats had a significant decline in plasma LDL-C and a significant rise of HDL-C levels compared to the control after 4 weeks of inulin intake, and this is associated with more excretions of fecal lipid and cholesterol [75]. Although enough positive data of lipid-lowering effects have been observed in animals, a relatively high dose of inulin had to be applied. There are also some human studies evolving. Unbalanced serum lipid levels accompanied by diabetes mellitus were found to be alleviated by inulin supplementation, including a significant reduction in TC by 12.90%, TG by 23.60%, and LDL-C by 35.30% and a rise of HDL-C by 19.90% [76]. In another 4-week trial, subjects consumed 50 g cereal, which includes 18% of inulin, showed significantly decreased plasma TC, TG, and total facultative anaerobes and increased bifidobacteria, while the weight, fecal bile acid excretion, SCFAs, and fecal pH were not notably altered. Besides, there is a remarkable finding that the modulation of serum lipids was negatively correlated with bifidobacteria number and positively related to the output of secondary bile acid [77]. A review that included 9 inulin or oligofructose supplementation in human volunteer studies found 3 of them exhibited significant reductions in TG, 4 of them showed modest reductions in TC and LDL-C, while only 2 of them reported with no effects [78]. Considering these studies have been conducted in both normal and moderately hyperlipidemic subjects and the dose and experimental duration were all varied, it is thus reasonable that their results are inconsistent. Besides several important animal studies that have supported the idea that the lipid-

lowering effects of inulin and oligofructose originate mainly from the inhibition of fatty acid synthesis in the liver, however, this pathway is relatively inactive in man for human seldom consumes a high-carbohydrate diet. There are also other controversial results. Pedersen et al. [79] investigated the effect of 14 g/d of inulin consumption on blood lipids in young healthy women having a limited fat intake for 2 months and did not find any significant differences between the two groups. Similarly, 17 healthy subjects after 6 months of daily administration of inulin and oligofructose without modifying their way of life exhibited no effect on serum TG levels and hepatic lipogenesis and only a slight decrease in TC and LDL-C levels [80]. These two results may be explained by a recent study, in which the hypolipidemic effect of inulin differed depending on dietary fat content (5% versus 20%). This study also suggested that lipid-lowering action of inulin mainly comes from the increased excretion of total lipid and neutral sterol [81].

3.7.3. Resistant Starch (RS). Resistance for digestion of RS originates from its compact structure and partial crystalline structure, which has been regarded as a kind of prebiotics to be beneficial for health, including lose weight, reduce lipids, and prevent intestine diseases. Compared with the wheat starch group, 20% RS significantly induced the cecal hypertrophy by 2.4 times and accumulation of SCFAs, while the cholesterol absorption was reduced from 47% to 14%. RS also effectively reduced the plasma TC by about 30% and TG by about 25%. Moreover, there were apparent lower concentrations of TC and TG (-50%) in the livers of RS-fed rats, too [82]. Similarly, the plasma TC, VLDL-C, and LDL-C concentrations were all significantly reduced and fecal total bile acid concentration, total SCFAs, and acetic acid were all significantly higher when rats received 0.5% cholesterol plus 15% bean RS. This also suggested that the hypolipidemic effect of RS may be attributed by its action against absorption and fermentation effect in the intestine [83]. RS has been well characterized for its glycemic control properties, which may also have impact on lipid metabolism. Besides the doubled HDL-C concentration, the results of 2 g/d RS administration in type 2 diabetic rats showed that blood glucose level and TC and TG concentrations were all significantly reduced ($p < 0.01$) [84]. On the contrary, another experiment using 12 8-week-old male pigs consumed a synthetic western diet with (10 g/RS/day) or without potato starch reached different lipid profiles. Although the serum lipids including TC, LDL-C, VLDL-C, and TG were similar, HDL-C particles were obviously higher by 28% and fasting serum glucose was lowered by 20% in the RS group [85]. Healthy overweight patients were given either 24 g/d of RS or regular corn starch for 21 d in addition to their regular meals. Although RS resulted in no significant changes in their weight or other physical parameters, there were significant lowering effects of plasma TC, LDL-C, and the mean fasting serum glucose levels in subjects supplemented RS [86]. These studies all suggested that the consumption of RS may be beneficial in lipid management strategies in addition to lowering blood glucose, but the connection with SCFA production and glycemic effect still needs further study. In order to prove RS

as a novel therapeutic agent of hyperlipidemia especially in diabetic patients, controlled trials with larger sample sizes and longer duration both in animal and human are required.

3.8. Gum. A study found that guar gum significantly lowered the fecal lipid digestibility and the intestinal conjugated bile salts ($p=0.0001$) for both control chicken and sterilized one [87]. One milligram partially hydrolyzed guar gum (PHGG) significantly decreased the TC, LDL-C, TG, and VLDL-C and delayed the formation of arterial thrombus in rat fed HFD. In addition, the increased Bax and decreased Bcl-2 and HSP-70 protein expression were found to be balanced by PHGG in the arteries of HFD hamsters [88]. Diet containing either 5%, 10%, or 20% guar gum was fed to diabetic rats for a month. Although diabetes elevated serum lipids in all rats within 2 weeks, the guar gum diet significantly reduced the plasma TC, TG, and LDL-C levels as well as the atherogenic index, suggesting that guar gum was effective in the treatment of hyperlipidemia in diabetes rats [89]. Guar gum treatment also decreased markers of the metabolic syndrome, including body weight, adipose weight, TG, glucose, and insulin levels in a dose-dependent manner in HFD mice [90]. Guar gum of 3 different viscosities was assessed in male rats fed HFD for 3 weeks indicating while all guar gum can reduce TC, liver steatosis, and blood glucose levels, only the medium one was most effective in preventing the diet-induced hyperlipidemia and liver steatosis [91]. The effect of 6 g PHGG in yogurt on postprandial plasma lipid concentrations was tested in 11 healthy male adults. Results indicated that the supplementation significantly suppressed the incremental peaks and areas of postprandial plasma TC and TG [92]. After 10 wks of HFD plus 5% guar gum in rats, the fat mass percentage, epididymal fat pad weight, and the liver lipid concentrations were all significantly lower than the controls [93]. However, there is also controversial result. A study reported that supplementation of dietary fiber at the 5% level for 3 weeks, including cellulose, guar gum, PHGG, glucomannan, highly methoxylated pectin, and guar gum, on normal rats induced no significant effect on the serum lipid levels [94]. Considering this study is referred to only normal subjects, most other animal study showed that guar gum and PHGG are effective lipid-lowering agents; however, the effect on human still needs more experimental data.

3.9. Hydroxypropylmethylcellulose (HPMC). HPMC is also a food gum, which shares many common characteristics with soluble fibers, such as high viscosity, and has been widely adopted in the food and medicine industries as emulsifier, diaphragm, suspender, thickener, dispersant, and stabilizer. It is a nonfermentable dietary fiber and has also been also demonstrated with modulation effect of lipid metabolism. In a trial, after a baseline period, 51 mild-to-moderate hypercholesterolemic men were randomly divided into two groups to consume 5.0 g/d HPMC with or between meals for 2 weeks. In the between-meal group, TC was reduced by 5.1%, LDL-C by 7.7% (both $p < 0.01$), while in the with-meal group, reductions were 8.3% for TC and 12.8% for LDL-C (both $p < 0.01$), which suggested that HPMC has a better lipid-lowering effect when taken with meals [95]. In

another trial, HPMC were given differently in dose 3, 5, or 10 g/d of low, moderate, moderately high, or high viscosity to hypercholesterolemic patients. Results showed that all HPMC could reduce LDL-C ranging from 6.1% to 13.3%, and the reduction of TC and non-HDL-C was associated with that for LDL-C, but HDL-C, TG, and apolipoprotein B were not significantly altered [96]. This team also conducted another experiment to examine the lipid profile of 2.5 g \times 2/d HPMC consumed subjects with hypercholesterolemia after at least 4 weeks of statin therapy. Results showed that HPMC consumption resulted in significantly larger reductions in TC (10.9 vs. 3.5%), non-HDL-C (12.8 vs. 2.9%), LDL-C (15.7 vs. 5.1%), and Apo B (8.7 vs. 3.9%), which support the view that HPMC is an effective adjunct to statin therapy in patients with primary hypercholesterolemia [97]. Another study found that rats with a HFD plus 5% HPMC had obviously reduced epididymal fat pad weight and liver lipid concentrations. The HPMC group also had an obvious higher *ex vivo* palmitate oxidation in muscle compared with the same dose of a fermentable fiber, guar gum, implying a higher oxidation capacity to FAs, which demonstrate that HPMC can reduce the adiposity and hepatic steatosis induced by HFD, and this ability does not correlate with fermentability [93]. Another study found that 6% HPMC could significantly reduce 55% of body weight gain, 13% of liver weight, and 45% of plasma LDL-C concentration of mice compared to the same dosage of microcrystalline cellulose- (MCC-) fed mice through upregulating genes related to fatty acid oxidation and synthesis of cholesterol and bile acids and downregulating genes related to oxidative stress, triglyceride synthesis, and polyunsaturated fatty acid elongation in the liver [98]. The above evidences suggest that 5 g/d in human diet or 5-6% of HPMC in animal feeding could both exert relative strong lipid-lowering effect; more research will be required to define the roles of viscosity on the lipid-modulating effects of HPMC and the dosage relationship between human and animals.

3.10. Whole Grain or Arabinoxylan. Whole grain, referring to grain with unpeeled bran, which includes wheat, rye, and oat, owns high content of both soluble and insoluble DFs, which comprises mainly of arabinoxylans and glucans. A multi-compartmental metabolomics study comparing whole grain rye with added rye bran with refined wheat in pig found that rye bran induces lower levels of linoleic acid-derived oxylipins and TC in the plasma [99]. Compared to 0% wheat bran (WB), 10 or 20% of WB induced obvious decrease in TC and HDL-C, while 5, 10, or 20% WB induced similar reduction in PL and TL in a dose-dependent manner [100]. In another study, hamster feeding experiment found that 5 g/kg of wheat bran arabinoxylans (Axs) lowered plasma TC and LDL-C concentrations and increased the output of TL, TC, and bile acids through reducing the activity of HMG-CoA reductase and increasing the activity of CYP7A1 in the liver as well as concentrations of SCFAs in the gut [101]. These results indicated the AXs lower the plasma lipids through promoting the excretion of fecal lipids, regulating the lipid metabolism related genes, and producing more colonic SCFAs. Besides a significant reduction in TG, LDL-C, and an increase in HDL-C, a wheat fermented powder also caused a significant

variation of important antioxidant biomarkers in a rabbit feeding experiment [102].

3.11. Chitosans. There are multiple studies reporting the hypolipidemic effect of chitosan in animal models. It was suggested that subacute toxicity of chitosan was small and the observed adverse effect level was considered to be over 2,000 mg/kg in rats [103]. Supplementation of 5% chitosan for 12 wks in rats could significantly decrease serum concentrations of TC, LDL-C, and hepatic levels TC, TG and increase the output of fecal bile acids, but the plasma levels of TG and HDL-C were considered unaltered. In addition, the result of RT-PCR showed that chitosan could reverse the reduction of LDL receptor mRNA levels, which led by the intake of saturated fat and cholesterol [104]. 250–1000 mg/kg chitosan oligosaccharide (COS) administration of mice caused a significant reduction of serum TC and LDL-C and a significant increase in peritoneal macrophage-derived ^3H -cholesterol in liver and bile as well as in feces, which suggested a positive role for COS in reversion of the cholesterol transport. In addition, the observed lipid-lowering action was in a dose-related relationship of the modulation of hepatic protein expressions of CYP7A1, SR-BI, and LDL receptor (LDL-R) by COS [105]. Six weeks of 5% chitosan supplement was found to significantly decrease the body weight gain and the lipids level both in the plasma and liver, while it was found to increase the output of fecal fat and cholesterol and hepatic lipoprotein lipase activities of HFD rats compared with rats only fed a HFD, which suggested that chitosan improves obviously the hypercholesterolemia in rats through reducing the absorption of fat and cholesterol [106]. Lower plasma TC, LDL-C, VLDL-C, and apolipoprotein B (Apo B) concentrations as well as higher HDL-C and no significant difference in TG or glucose levels were observed in rats fed a diet containing chitosan for 2 wks. In addition, rats fed the chitosan diet had a changed composition in VLDL particles as evidenced by increased TG percentages and core lipid proportions and decreased free cholesterol, cholesteryl ester, phospholipid, and the surface lipid proportions, suggesting that chitosan has a great influence on the VLDL particle formation and regulation of lipoprotein metabolism in rats [107]. Three studies are involved in the evaluation of different MW of chitosan. Among 21, 46, and 130 kDa, the medium one was the most effective one to inhibit pancreatic lipase activity *in vitro* and to reduce the serum TG and thus, it was fed to mice together with a HFD for 20 weeks. It prevented the increase of body weight, mainly the accumulation of white adipose tissue and liver lipids including TC and TG, and further increased the fecal bile acid and fat. The results suggested that the hypolipidemic action of this chitosan may be through increasing the excretion of fecal fat and bile acid caused by its binding activity and through inhibition of pancreatic lipase activity and subsequently decrease the absorption of dietary lipids from the small intestine [108]. Similarly, another study compared the lipid-lowering activities of high (712.6 kDa) and low (39.8 kDa) MW chitosan in rats fed HFD for 8 weeks. The low one was more effective in decreasing the body weight gain, serum TC, and LDL-C, as well as decreased liver TG.

The activities of liver and serum lipoprotein lipase and fecal fat level were also higher than the high MW group [109]. However, the result is quite opposite in streptozotocin-(STZ-) induced diabetic rats, which reported that rats fed with both high MW (100 kDa) and low MW (14 kDa) chitosan had increased HDL-C, whereas significantly decreased plasma glucose and TC and increased fecal cholesterol excretion were observed only in diabetic rats fed with high MW chitosan [110]. From these results, we could draw a primary conclusion that the MW of chitosan strongly affect its hypolipidemic effect and the ideal MW is between 21 and 100 kDa. Moreover, compared with untreated chitosan, the reducing effects of medium-milled chitosan on serum TG, TC, and LDL-C and liver TG and TC were all increased by about 10% [111].

There are just a few reports about chitosan's lipid-lowering effect in humans. A meta-analysis of 6 RCTs with 416 hypercholesterolemia patients concluded that it has a significant effect on TC (-0.3 mmol/L (11.6 mg/dL); $p = 0.002$) but not on LDL-C, HDL-C, or TGs [112]. However, several other studies showed that it could exert an effect on LDL-C. One of them declared that the dietary chitosan could reduce serum TC levels by 5.8–42.6% and LDL-C levels by 15.1–35.1% [113]. A 12-week trial found an overall treatment effect of a 40 kDa chitosan from the placebo group. The 2.4 g once-daily group reducing LDL-C by 16.9% showed the best, even better than the same dosage but separately administered group, which reduce the LDL-C only by 9.7%. But there were 29 mild adverse events reported by 23% patients related to the chitosan treatment, including constipation and diarrhea [114]. The EFSA suggested that evidences from chitosan indicated a small, but statistically significant effect on the reduction of both TC and LDL-C levels, with no effect observed on HDL-C. The panel suggested further that in order to achieve this effect on blood lipids, 3 g/d chitosan should be applied [115]. Taken together, chitosan possesses the ability to lower lipids but may cause some side effects; therefore, more controlled clinical trials of a longer duration are essential to assess the dose-hypolipidemic effects besides the evaluation of its adverse effects.

3.12. Other Insoluble DFs. Different insoluble dietary fibers cholestyramine, chitosan, and cellulose have been assumed with high, intermediate, and low ability to bind with bile acids, respectively. Especially, the cholestyramine has long been clinically applied as a cholesterol-lowering, bile acid-binding drug. A study reported that the consumption of 7.5% of either one of the three dietary fibers showed similar hypolipidemic activity in mice fed a diet containing high levels of fat and cholesterol; however, cholestyramine showed the best ability to deplete the hepatic cholesterol and this may be induced by a decrease of cholesterol absorption efficiency and an increase of fecal bile acid and cholesterol excretion, which is caused by its high capacity to bind with bile acids. However, chitosan or cellulose reduced only the food intake including cholesterol, but the impact is neither on intestinal cholesterol absorption nor on the output of fecal bile [116]. Lignin extracted from olive stones was found to be able to bind significantly more bile acids than any other fraction,

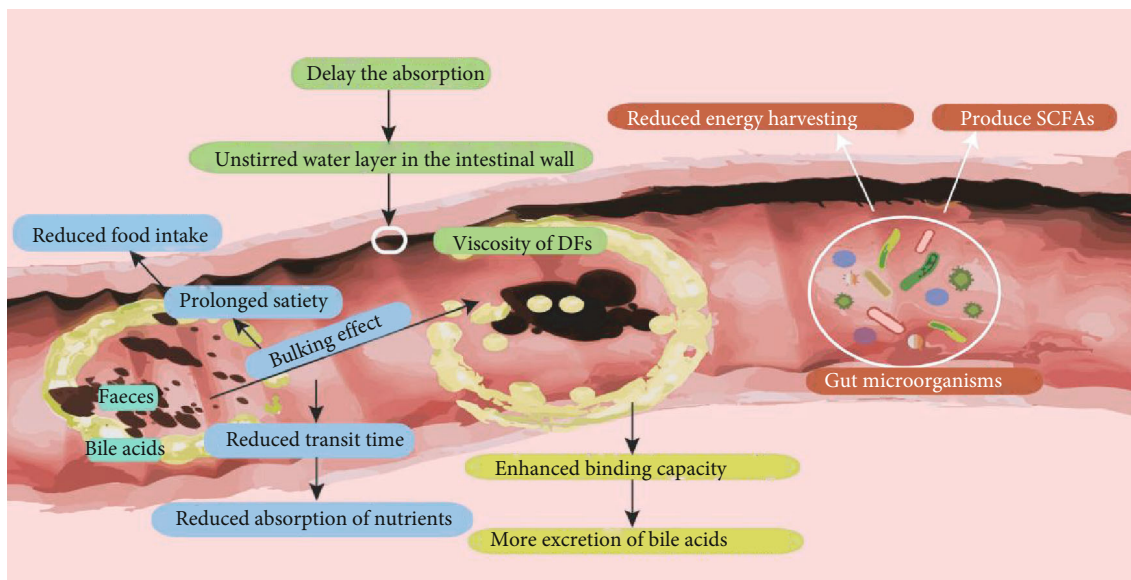


FIGURE 2: Possible positive effects of typical dietary fibers on hypolipidemic process.

and the capacity is similar to that of cholestyramine, especially when cholic acid was applied *ex vivo* [117]. From these evidences, the hydroinsoluble DF may contribute more to affect the absorption of cholesterol.

3.13. Combination of Soluble and Insoluble DFs. Okara owns a high dietary fiber content of 54–55%, mainly IDF but also SDF content. High-cholesterol-fed rats supplemented with enzymatically treated okara showed a significant reduced TG levels both in serum and in the liver but a higher TL, TG, and bile acid ($p < 0.001$) in the feces. The improved intestinal transit by increasing fecal bulk, the decreased pH, and increased SCFA production indicated that this okara exerts a potential prebiotic effect [118]. Another study compared the effects of cellulose and pectin on the metabolism of lipid and carbohydrate in rats for 6 wks. The TC level in plasma was significantly lower while plasma HDL-C was significantly higher in 5% of the pectin group while rats fed the same dosage of cellulose had lower contents of TC and TG in the liver. However, a significantly lower plasma glucose was observed in 2.5% of cellulose plus 2.5% of the pectin group [119]. These results suggested that a diet containing fiber may be a possible adjuvant treatment for correcting some disturbances of metabolism, but IDF and SDF should be considered separately for their different mechanism to exert the balancing effect. However, in some occasions, they need to be applied in a combination to maximize this effect.

3.14. Modifiers of DFs. It has long been predicted that chemical modifications may increase the cholesterol-lowering effect of polysaccharides. Hydrophobic derivatives of highly alkyl or acyl group-substituted pectin, chitosan, and cellulose, all confirmed this prediction, which have high binding capacity to cholesterol and thus left fewer cholesterol for enterohepatic circulation [120]. A study also found that hydrophobic amidated pectins significantly altered cholesterol homeostasis in rats and amidation of pectin decreased

its fermentability to produce lower cecal SCFAs in rats [121]. The administration of *Cymodocea nodosa* sulphated polysaccharide (CNSP) exhibited a better serum lipid level by decreasing lipase activity of obese rats compared with untreated polysaccharides. Additionally, CNSP administration to HFD rats induces further antioxidant activity [122]. A modifier was further prepared by this team using highly methoxylated citrus pectin with a degree of 60% substitution of N-octadecylamine, which significantly decreased the concentrations of cholesterol in hepatic tissue and triacylglycerols in serum. The feeding experiment showed its potential to substitute typical antilipidemic drugs at a low dose and used for a period shorter than 3 months [123]. In another study, the interaction of chitosan and its two derivatives with plasma leptin, glucose, insulin, and total cholesterol and further interaction with mRNA expression of adipocytokines were investigated in a diet-induced insulin-resistant rat model. The results proved that all the three substances not only lowered the level of plasma leptin, glucose, insulin, and TC *in vivo* but also downregulated the mRNA expression of leptin and resistin and up-regulated the mRNA expression of adiponectin and PPAR- γ *in vitro*. In addition, the two chitosan derivatives exhibited better regulating effect [124].

4. Mechanisms of DFs to Affect Lipid Metabolism

Five major mechanisms are believed to be responsible for the antihyperlipidemic benefits of DFs, including low levels of energy, bulking effect, viscosity, binding capacity, and fermentation, which are summarized in Figure 2. Foods rich in DFs include whole grain products, legumes, and fruits classified as low GI foods, which refer to a relatively low glycemic effect compared to an equal amount of available carbohydrate (usually from white bread or glucose). Fully fermentable RS, for instance, has been estimated to contribute about 8.8 kJ/g, whereas glucose contributes 17 kJ/g

[125]. Some fibers, generally referred to as IDF, provide bulking effect, hence increasing stool mass, alleviating constipation, and improving regularity. Meanwhile, most of the SDF is associated with a great water-holding capacity. Lactulose, for example, has long been considered a laxative and proved to be effective in multiple constipation intervention studies. The increased stool weight is due to the physical presence of DF as well as the water held inside the fiber matrix, such as cellulose and lignin; although are mostly not fermentable in the colon, they can effectively increase fecal bulk by their particle formation and water-holding capacity. Due to the increased bulk and water content, the nutrients in the intestine are diluted, including sugar and lipids, and their migration to the intestinal walls also slows down. The IDFs are also associated with decrease in intestinal transit time that helps reduce the absorption time of these sugars and lipids. As a result, they can reduce the absorption of macronutrients, especially carbohydrates and cholesterol either by delaying gastric emptying or by shortening small intestinal transit time, in addition to a reduced glycemic response, which could further assist the reduction in insulin stimulation of hepatic cholesterol synthesis [126]. These intrinsic properties of DFs that relate to bulking and viscosity effects also promote prolonged satiety and reductions in food intake, which accounts for another important mechanism of lipid lowering [20]. In addition to the fiber's viscosity, the ability of DFs to bind to bile to disturb the reabsorption of bile salt from the small intestine is another factor that leads to synthesis of new bile acids from cholesterol and hence reducing blood cholesterol levels and lipid-lowering effect [127]. Since the production and excretion of bile acids represent the major pathway of cholesterol removal from the body and the biosynthesis of bile acids in the liver is modulated through a series of positive and negative feedback mechanisms, the increased fecal removal of bile acids reduces the amount of bile acids present in the plasma. 5% guar gum, for an example, significantly lower lymph flow and lymphatic lipid transport and thereby diminishes lipid transport by means of its physicochemical properties related to water behavior in the intestine [128]. DFs undergo a fermentation process to produce short-chain fatty acids (SCFAs), including propionate, acetate, and butyrate. The concentration of both acetate and propionate is reported to be increased more than 2-fold in the rats' portal plasma after the oligofructose intake. However, the involvement of SCFAs is, as for lipid-lowering effect, makes it difficult to draw a conclusion with complete identity, as they have an antagonistic effect: propionate has been reported to inhibit fatty acid synthesis [129], whereas acetate is a lipogenic substrate. Despite a large part of SCFAs absorbed by the host, which accounts for about 10% of daily energy supply [130], gut microorganisms rely fast entirely on the energy from fermentation process. This fermentation process reduces the total energy supply of the body, thus balancing the lipid metabolism in hyperlipidemic patients. From this perspective, this fermentable property of DFs exerts beneficial effect on balancing lipid metabolism compared to other nutrients being directly digested in the small intestine. Studies also revealed that SCFAs could cause satiety and inhibit cholesterol synthesis [131, 132]. We will

discuss the relationship between lipid metabolism and SCFAs more specifically below for its complexity, focusing on the molecular mechanism. Each kind of DF distinguishes from one another in these five properties for sure. For instance, the different molecular weights of β -glucan were found to have no impact on its total fermentation products but affect its viscosity, which has further impact on its binding capacity to bile acid, absorptive layer in the small intestine, and transit time [133]. However, more or less of these five major properties of DFs indicates that DFs play a positive role in the hypolipidemic process.

5. Molecular Mechanism of the Hypolipidemic Effect of DFs

5.1. 3-Hydroxy-3-methylglutaryl Coenzyme A (HMG-CoA) Reductase. HMG-CoA reductase, officially abbreviated as HMGCR, is the rate-controlling enzyme of the mevalonate pathway, which is the metabolic pathway producing cholesterol and other isoprenoids. In mammalian cells, this enzyme is suppressed by cholesterol and degradation of LDL via the LDL receptor as well as oxidized species of cholesterol. Meanwhile, its competitive inhibitors will induce the hepatic expression of LDL receptors, which in turn increases the catabolism of plasma LDL-C and lowers the plasma concentration of lipids. This enzyme is thus the target of the widely used cholesterol-lowering drugs, such as the statins. An early study found that the addition of 5% chitosan to sterol diet suppressed the increase of plasma and liver cholesterol by 54% and 64%, respectively, and this is correlated with the chitosan-modulated reduction of HMG-CoA reductase activity by four times, compared to high-sterol diet-alone rats [134]. Most of the later studies referring to the hypolipidemic mechanism of dietary fiber come to a similar finding that HMG-CoA reductase activity was downregulated [38, 53, 62, 83, 101, 135], which indicates the possibility of DFs as adjunct to traditional lipid-lowering drug or adjuvant therapy for hyperlipidemic patients.

5.2. LDL Receptors. As discussed above, the upregulated expression of LDL receptors will increase the decomposition of LDL-C, which means a balance of lipid metabolism in hyperlipidemic patients. A study found that hepatic protein expressions of LDL receptor were improved in a dosage-dependent manner in chitosan oligosaccharide- (COS-) administered mice. In addition, the expression of scavenger receptor BI (SR-BI), which plays a critical role in cholesterol uptake from plasma to the liver, was also upregulated in a dose-dependent manner of COS supplementation mice, while the main transporters for transferring cholesterol to plasma HDL, the level of ABCA1 and ABCG1 remains unchanged, which also correlates with the unchanged HDL-C level [105]. However, barley bread enriched with HPMC was found to downregulate the expression of the ABCG5 gene [38]. Fucoidan was found to attenuate the hepatic expression of mature SREBP-2 protein with a subsequent decrease in hepatic HMG-CoA reductase mRNA expression and an increase in hepatic LDL receptor mRNA expression, indicating that fucoidan improves serum lipid

levels by regulating the expression of key enzymes of TC and LDL-C metabolism in the liver through modulation of SREBP-2 [62].

5.3. Cytochrome P450 7A1 (CYP7A1). Cytochrome P4507A1 (CYP7A1) also known as cholesterol 7- α -monooxygenase or cholesterol 7 α -hydroxylase, an important member belonging to the cytochrome family, has an important role in cholesterol metabolism because it catalyzes the conversion process from cholesterol to 7- α -hydroxycholesterol, the first and rate-limiting step in bile acid synthesis. The activation of CYP7A1 leads to an increase of bile acid biosynthesis thus decreasing the concentration of cholesterol. Bile acids provide feedback inhibition of CYP7A1 by at least two different pathways, one involving the farnesoid X receptor (FXR) and small heterodimer (SHP) as well as liver receptor homolog (LRH-1) and another involving inflammatory cytokines, including TNF- α and IL-1 β [136]. CYP7A1 is upregulated by the nuclear receptor liver X receptor (LXR) when cholesterol levels are high and downregulated by sterol regulatory element-binding proteins (SREBP) when plasma cholesterol levels are low [137]. The activity of CYP7A1 in the liver was significantly increased by β -glucan from both barley and oats compared with the control [135]. The extreme lipid-lowering action of pea proteins plus apple pectin was also found to be regulated by CYP7A1 and sodium/bile acid cotransporter (also known as the Na⁺-taurocholate cotransporting polypeptide (NTCP) or liver bile acid transporter (LBAT)) [53]. The lowered TC and LDL-c concentrations and increased excretions of TL, TC, and bile acids caused by wheat bran arabinoxylans were also found to be modulated by increased activity of CYP7A1 in the liver [101]. Similarly, the mRNA level of CYP7A1 of the HMPC group was found upregulated by 1.9-fold and the expression levels of SREBP-1c and stearoyl-CoA desaturase (SCD-1) were downregulated by 2- and 5-fold, respectively, relative to the control group [98]. Hepatic gene expression profiles demonstrated that polysaccharide from *Lycium barbarum* (LBP), a well-known Chinese traditional herbal medicine, can activate the phosphorylation of AMPK, suppress nuclear expression of SREBP-1c, and decrease protein and mRNA expression of lipogenic genes *in vivo* and *in vitro*. Moreover, LBP significantly elevated uncoupling protein-1 (UCP1) and peroxisome proliferator-activated receptor coactivator-1 (PGC-1) expression of brown adipose tissue [138]. The fecal effect of glucan also could activate CYP7A1, which catalyzes the rate-limiting step in the biosynthesis of bile acids from cholesterol, leading to an upregulation of bile acid synthesis from plasma cholesterol and thus lowering the circulating LDL-c levels [139]. Most of the other studies also found that CYP7A1 is an important target of DF's lipid-lowering action [38, 105].

5.4. MAPK Signaling Pathway. The MAPK signaling pathway was found to regulate the expression of CCAAT-enhancer-binding proteins α (C/EBP α) and peroxisome proliferator-activated receptors γ (PPAR γ) mRNA during adipogenesis process in 3T3-L1 cells and thus play an important role in the process of lipid metabolism. A water-soluble extract of *P. binghamiae thalli* (PBEE) including water-soluble polysac-

charides is able to inhibit preadipocyte differentiation and adipogenesis in a dose-dependent manner, which is caused by the decreased the expression of PPAR γ and fatty acid-binding protein aP2 [140]. Similarly, mice fed a high-fat diet supplemented with 10% guar gum for 12 weeks also induced correction of metabolic abnormalities caused by PPAR γ repression, subsequently increasing mitochondrial uncoupling protein 2 (UCP2) expression and AMP/ATP ratio, leading to the activation of AMPK [141]. Fucoidan could decrease the lipid accumulation through inhibiting the expression of both early C/EBP α and PPAR γ and late aP2 adipogenic transcription factors, which play a crucial role for adipocyte development. Moreover, fucoidan also inhibited the early activation of p38 MAPKs, extracellular signal-regulated kinases p-ERK1/2, and Jun N-terminal kinase p-JNK activity in a dose-dependent manner [142].

5.5. Other Lipid Metabolism-Related Genes. A study found that fucoidan decreases the expression of FAS and ACC mRNA with only moderate inhibitory effect on SREBP-1c mRNA expression in both HepG2 hepatocytes and the mouse liver [62]. Our latest work also focused on the molecular mechanism of the antihyperlipidemic effect of rice bran polysaccharides (RBP) in high-fat diet mice. Besides significantly reduced weight and liver and fat pad weight, improved lipid profile in the plasma and recovered fat liver lesion were observed under the protection of RBP. Microarray analysis revealed that RBP could result in a regulation of over 150 genes, including multiple genes involved in the hepatic lipid metabolism like Sult3a1, Sult3a2, several CYPs, Acnat2, Acot6, SERPINA3, SERPINA6, RORA, and several APOs. IPA database suggested further that NF- κ B may play a vital role in the lipid-lowering effect of RBP. Real-time quantitative PCR and western blot confirmed that RBP affect several lipid metabolism target genes including PPAR- α , PPAR- γ , PPAR- δ , SREBP-1C, FASN, ACC, SIRT, and CD36 [143]. Another microarray test compared the hepatic expression level of gene between HPMC supplementation and only HFD-fed rats, and the results overlapped with our results to a large extent: Serpina6, Aqp8, Hsd17b7, Nsdhl, Tm7sf2, and Cyp51. There are also some genes involved in fatty acid β -oxidation, such as Ehhadh and Acacb, and the elongation of very long-chain fatty acid-like 2 (Elovl2), sterol-C4-methyl oxidase-like (Sc4 mol), and patatin-like phospholipase domain-containing 2 (Pnpla2), which is involved in triglyceride breakdown by regulating adipose triglyceride lipase, was all upregulated [98]. DNA microarray analysis and q-PCR also demonstrated that fucoidan induces differential expression of genes encoding proteins involved in lipid metabolism, energy homeostasis, and insulin sensitivity, by activating PPAR α , inactivating Srebf1, and affecting LPL activity in HFD-fed ApoEshl mice [61]. Another study evaluated gene expression profiles in the small intestinal mucosa of db/db mice fed with PHGG. DNA microarray and real-time PCR analyses reported that PHGG upregulated the expression of 9 genes, including Oas3, Oas1g, Duo2, and Nlrc5, potentially related to host defense functions, and downregulated the expression of 8 genes, including sterol O-acyltransferase (Soat1), which is involved in cholesterol

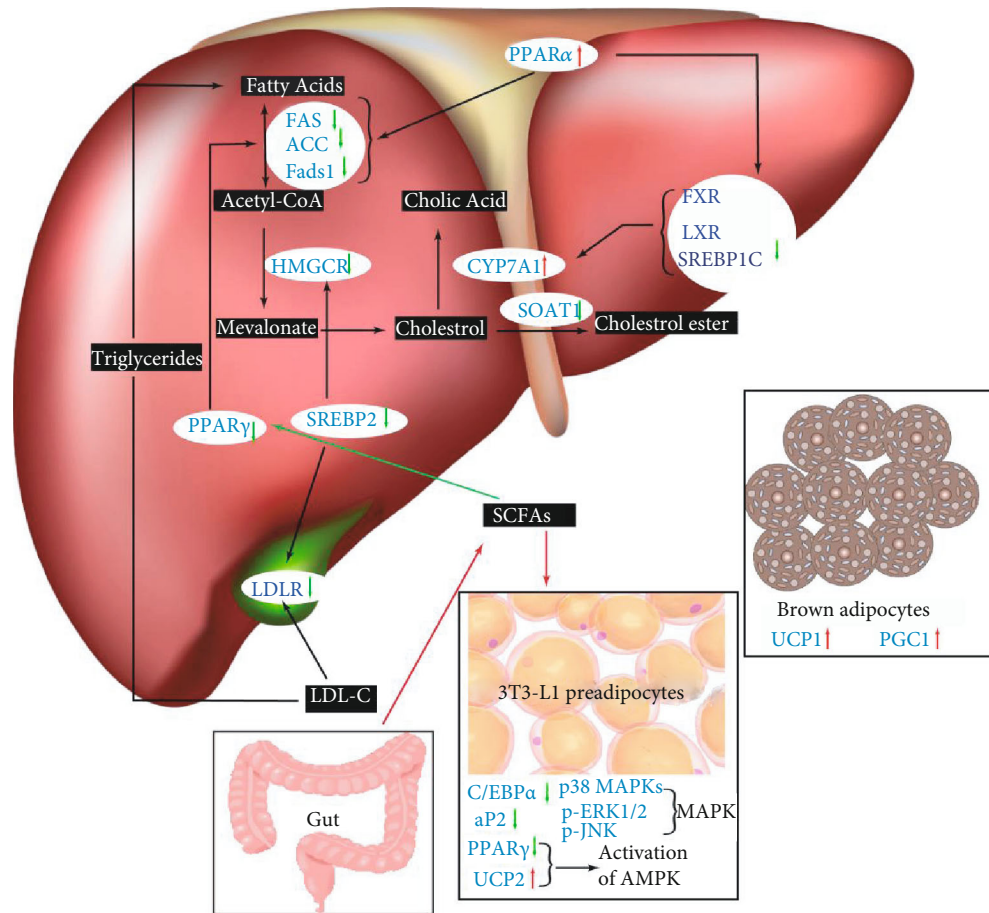


FIGURE 3: Possible molecular mechanism of dietary fibers on lipid lowering.

esterification and absorption, in the small intestine [144]. The expression levels of lipid oxidation gene *Acox1*, glycogen synthesis genes, *GS2* and *GYG1*, and insulin-induced genes, *Insig-1* and *Insig-2*, were significantly upregulated while fatty acids and triglyceride synthesis and metabolism-related gene *SREBP-1*, fatty acid synthesis gene (*Fads1*), and gluconeogenesis gene *G6PC1* were greatly downregulated in RS-administrated diabetic rats [84].

5.6. SCFAs. Given that SCFAs also count for a part of lipids and energy, food rich in DFs seemed to stimulate hyperlipidemia through harvesting the metabolites. But epidemiological study results suggest that they prevent it rather than promote it. Propionate, for instance, at the concentration of 0.6 mmol/L, could decrease the expression level of fatty acid synthase mRNA in cultured hepatocytes and thus considered a mediator having an antilipogenic property [68]. In addition, a 2-fold concentration of propionate at the portal vein of rats supplemented with fructan compared to controls selectively decreased the transition of acetate into total lipids [145]. A study found that the fluxes of SCFAs rather than concentrations reversely correlate with biomarkers of the metabolic syndrome in an animal experiment, including body weight, adipose weight, and TG [90]. The same team suggest further that SCFAs induce a PPAR γ -mediated switch

from lipid synthesis to consumption. Oral sodium acetate, sodium propionate, and sodium butyrate supplementation prevented and reversed HFD-induced metabolic abnormalities in mice by decreasing PPAR γ expression and activity. This increased the expression of mitochondrial uncoupling protein 2 and increased the ratio of AMP to ATP, leading to an acceleration of the hepatic and adipose oxidative metabolism via AMPK. The mediator function of PPAR γ could also be proved by PPAR γ -absent mice, who exhibited no protective effect of the same supplementation. These results demonstrated that adipose and hepatic PPAR γ are critical mediators of the beneficial effects of SCFAs on the metabolic syndrome, indicating that SCFAs may be used therapeutically as cheap and selective PPAR γ modulators [146]. Studies also revealed that SCFAs could cause satiety via increased production of GLP-1 and PYY by stimulating FFARs and inhibit the rate-limiting enzyme of cholesterol HMGCoA reductase to inhibit cholesterol synthesis [131, 132]. Guar gum-induced obvious increase of peripheral glucose clearance also may be mediated by the SCFAs, for they are responsible for the change of colonic hormone glucagon-like peptide-1 (GLP-1), which also has impaction on the lipid metabolism [141]. We summarized these possible molecular mechanisms of typical dietary fibers affecting the lipid metabolism in Figure 3.

6. Future Perspectives

Other than the direct effect of DFs on hyperlipidemia, the site of action-targeted drug delivery system using polysaccharides as package, such as pectin, dextran, gum, alginate, inulin, and konjac glucomannan, has attracted increased attention because this method could increase the bioavailability of the drug at the target site and meanwhile reduce the side effects. A study suggested that the employment of ultrafine redispersible spray dried emulsion with pectin as a carrier to form a delivery method for atorvastatin calcium holds a promising approach for an enhanced antihyperlipidemic effect for the widely used drug [147]. Another test that found an optimized formulation using glycyrrhetic acid-modified chitosan as a liver-targeted carrier of atorvastatin showed increased plasma concentration, and the accumulation in the liver was nearly 2.59 times more than the plain drug nanoparticles [148]. Pharmaceutical and pharmacological indicators suggested that the proposed strategy can be successfully utilized for liver targeting of therapeutics.

There has been increasing interest in the effect of dietary fiber, on lowering the blood lipid concentration. There are various mechanisms by which serum and hepatic lipids are reduced by dietary fiber: binding to bile, viscosity, and bucking in the small intestine caused the suppression of glucose and lipid absorption, increased production of SCFAs, and modulation of lipid metabolism-related genes. In addition, dietary fibers, classified as the seventh nutrients, are generally considered safe, but overconsumption could cause intestinal discomfort. From the above evidences, dietary fibers could be used as alternative supplements to exert health benefits, including lipid-lowering effects on humans. However, more clinical evidence is needed to strengthen this proposal and its fully underlying mechanism still requires more investigation. Only if we fully understand the mechanism and dose relationship of each kind of DFs we are able to apply them in the intervention of hyperlipidemic patients.

Abbreviations

SCFA:	Short-chain fatty acids
CVD:	Cardiovascular diseases
PL:	Phospholipid
TL:	Total lipid
TC:	Total cholesterol
TG:	Triacylglycerols
LDL-C:	Low-density lipoprotein cholesterol
HDL-C:	High-density lipoprotein cholesterol
VLDL:	Very low-density lipoprotein
FOS:	Fructooligosaccharides
PAI-1:	Plasminogen activator inhibitor-1
fVII:	Factor VII
HPMC:	Hydroxypropyl methyl cellulose
EFSA:	European Food Safety Authority
KGM:	Konjac glucomannan
FFAs:	Free fatty acids
GOS:	Galactooligosaccharides
XOS:	Xylooligosaccharides
MO:	Maltooligosaccharides

SDF:	Soluble dietary fiber
IDF:	Insoluble dietary fiber
RS:	Resistant starch
GG:	Guar gum
PHGG:	Partially hydrolyzed guar gum
AX:	Arabia xylan
APO:	Apolipoprotein
ACC:	Acetyl-CoA carboxylase
LDLR:	Low-density lipoprotein receptor
Dgat1:	Diacylglycerol acyltransferase1
SR-BI:	Scavenger receptor-BI
ABCA:	ATP binding cassette subfamily A
ABCG:	ATP binding cassette subfamily G
P450:	Cytochrome P450
P4507A1:	Cytochrome P450 7A1
AMPK:	Adenosine 5'-monophosphate- (AMP-) activated protein kinase
HMG-CoA:	3-Hydroxy-3-methylglutaryl-coenzyme A
SREBP:	Sterol regulatory element-binding protein
SHP:	Small heterodimer partner
MCC:	Microcrystalline cellulose
WB:	Wheat bran
MAPK:	Mitogen-activated protein kinase
C/EBP α :	CCAAT/enhancer binding protein α
aP2:	Adipocyte fatty acid-binding protein
ERK:	Extracellular signal-related kinase
JNK:	JUN N-terminal kinase
Soat:	Sterol O-acyltransferase
ACOX:	Accyl-CoA oxidase
FAS:	Fatty acid synthase
FFARs:	Free fatty acid receptors
GLP-1:	Glucagon like peptide 1
MW:	Molecular weight
PPARs:	Peroxisome proliferator-activated receptors
SERPINA:	Serpin family A member
FXR:	Farnesol X receptor
LXR:	Liver X receptor
RXR:	Retinoid X receptor.

Conflicts of Interest

The authors declare that there is no conflict of interest regarding the publication of this paper.

Acknowledgments

This work was supported by the “2011 Collaborative Innovation Center of Hunan province” (2013, No. 448), the “start-up project for Ph.D. of Hanshan Normal University” (XJ2020001703), and the Key Project of the Education Department of Guangdong province (2019KTSCX098).

References

- [1] J. I. Harland, “Food combinations for cholesterol lowering,” *Nutrition Research Reviews*, vol. 25, no. 2, pp. 249–266, 2012.
- [2] B. G. Nordestgaard and A. Varbo, “Triglycerides and cardiovascular disease,” *The Lancet*, vol. 384, no. 9943, pp. 626–635, 2014.

- [3] P. Gunness and M. J. Gidley, "Mechanisms underlying the cholesterol-lowering properties of soluble dietary fibre polysaccharides," *Food & Function*, vol. 1, no. 2, pp. 149–155, 2010.
- [4] T. van der Gronde, A. Hartog, C. van Hees, H. Pellikaan, and T. Pieters, "Systematic review of the mechanisms and evidence behind the hypocholesterolaemic effects of HPMC, pectin and chitosan in animal trials," *Food Chemistry*, vol. 199, pp. 746–759, 2016.
- [5] Y. Ma, W. Wang, J. Zhang et al., "Hyperlipidemia and atherosclerotic lesion development in Ldlr-deficient mice on a long-term high-fat diet," *PLoS One*, vol. 7, no. 4, article e35835, 2012.
- [6] J. Pedro-Botet, J. Millán Núñez-Cortés, J. J. Chillarón, J. A. Flores-le Roux, and J. Rius, "Severity of statin-induced adverse effects on muscle and associated conditions: data from the DAMA study," *Expert Opinion on Drug Safety*, vol. 15, no. 12, pp. 1583–1587, 2016.
- [7] S. Cham, H. J. Koslik, and B. A. Golomb, "Mood, personality, and behavior changes during treatment with statins: a case series," *Drug Safety - Case Reports*, vol. 3, no. 1, p. 1, 2016.
- [8] D. Kerckhoffs, F. Brouns, G. Hornstra, and R. P. Mensink, "Effects on the human serum lipoprotein profile of β -glucan, soy protein and isoflavones, plant sterols and stanols, garlic and tocotrienols," *The Journal of Nutrition*, vol. 132, no. 9, pp. 2494–2505, 2002.
- [9] R. Deng, "Food and food supplements with hypocholesterolemic effects," *Recent Patents on Food, Nutrition & Agriculture*, vol. 1, no. 1, pp. 15–24, 2009.
- [10] S. Y. Kim, H. J. Song, Y. Y. Lee, K.-H. Cho, and Y. K. Roh, "Biomedical issues of dietary fiber β -glucan," *Journal of Korean Medical Science*, vol. 21, no. 5, pp. 781–789, 2006.
- [11] L. Brown, B. Rosner, W. W. Willett, and F. M. Sacks, "Cholesterol-lowering effects of dietary fiber: a meta-analysis," *The American Journal of Clinical Nutrition*, vol. 69, no. 1, pp. 30–42, 1999.
- [12] J. M. Lattimer and M. D. Haub, "Effects of dietary fiber and its components on metabolic health," *Nutrients*, vol. 2, no. 12, pp. 1266–1289, 2010.
- [13] Y. Nie, Q. Lin, and F. Luo, "Effects of non-starch polysaccharides on inflammatory bowel disease," *International Journal of Molecular Sciences*, vol. 18, no. 7, p. 1372, 2017.
- [14] M. S. Izydorczyk and C. G. Biliaderis, "Cereal arabinoxylans: advances in structure and physicochemical properties," *Carbohydrate Polymers*, vol. 28, no. 1, pp. 33–48, 1995.
- [15] M. Mendis, E. Leclerc, and S. Simsek, "Arabinoxylans, gut microbiota and immunity," *Carbohydrate Polymers*, vol. 139, pp. 159–166, 2016.
- [16] X. Huang and S. Nie, "The structure of mushroom polysaccharides and their beneficial role in health," *Food & Function*, vol. 6, no. 10, pp. 3205–3217, 2015.
- [17] B. Schwartz and Y. Hadar, "Possible mechanisms of action of mushroom-derived glucans on inflammatory bowel disease and associated cancer," *Annals of Translational Medicine*, vol. 2, no. 2, p. 19, 2014.
- [18] F. Bobadilla, C. Rodriguez-Tirado, M. Imarai, M. J. Galotto, and R. Andersson, "Soluble β -1,3/1,6-glucan in seaweed from the southern hemisphere and its immunomodulatory effect," *Carbohydrate Polymers*, vol. 92, no. 1, pp. 241–248, 2013.
- [19] N.-G. Asp, "Dietary fibre-definition, chemistry and analytical determination," *Molecular Aspects of Medicine*, vol. 9, no. 1, pp. 17–29, 1987.
- [20] A. Lovegrove, C. H. Edwards, I. De Noni et al., "Role of polysaccharides in food, digestion, and health," *Critical Reviews in Food Science and Nutrition*, vol. 57, no. 2, pp. 237–253, 2015.
- [21] W. G. T. Willats, J. P. Knox, and J. D. Mikkelsen, "Pectin: new insights into an old polymer are starting to gel," *Trends in Food Science & Technology*, vol. 17, no. 3, pp. 97–104, 2006.
- [22] N. Benkeblia, "Fructooligosaccharides and fructans analysis in plants and food crops," *Journal of Chromatography A*, vol. 1313, pp. 54–61, 2013.
- [23] A. F. G. Cicero, A. Colletti, G. Bajraktari et al., "Lipid-lowering nutraceuticals in clinical practice: position paper from an International Lipid Expert Panel," *Nutrition Reviews*, vol. 75, no. 9, pp. 731–767, 2017.
- [24] X. Zhu, X. Sun, M. Wang et al., "Quantitative assessment of the effects of beta-glucan consumption on serum lipid profile and glucose level in hypercholesterolemic subjects," *Nutrition, metabolism, and cardiovascular diseases : NMCD*, vol. 25, no. 8, pp. 714–723, 2015.
- [25] M. Andersson, L. Ellegård, and H. Andersson, "Oat bran stimulates bile acid synthesis within 8 h as measured by 7α -hydroxy-4-cholesten-3-one," *The American Journal of Clinical Nutrition*, vol. 76, no. 5, pp. 1111–1116, 2002.
- [26] E. Theuwissen and R. P. Mensink, "Simultaneous intake of β -glucan and plant stanol esters affects lipid metabolism in slightly hypercholesterolemic subjects," *The Journal of Nutrition*, vol. 137, no. 3, pp. 583–588, 2007.
- [27] M. Kristensen and S. Bugel, "A diet rich in oat bran improves blood lipids and hemostatic factors, and reduces apparent energy digestibility in young healthy volunteers," *European Journal of Clinical Nutrition*, vol. 65, no. 9, pp. 1053–1058, 2011.
- [28] H. Peng, F. Yeh, G. de Simone et al., "Relationship between plasma plasminogen activator inhibitor-1 and hypertension in American Indians: findings from the Strong Heart Study," *Journal of Hypertension*, vol. 35, no. 9, pp. 1787–1793, 2017.
- [29] H. Mieszcanska, N. K. Kaba, C. W. Francis et al., "Effects of pioglitazone on fasting and postprandial levels of lipid and hemostatic variables in overweight non-diabetic patients with coronary artery disease," *Journal of Thrombosis and Haemostasis*, vol. 5, no. 5, pp. 942–949, 2007.
- [30] A. Whitehead, E. J. Beck, S. Tosh, and T. M. S. Wolever, "Cholesterol-lowering effects of oat β -glucan: a meta-analysis of randomized controlled trials," *The American Journal of Clinical Nutrition*, vol. 100, no. 6, pp. 1413–1421, 2014.
- [31] K. E. Charlton, L. C. Tapsell, M. J. Batterham et al., "Effect of 6 weeks' consumption of β -glucan-rich oat products on cholesterol levels in mildly hypercholesterolaemic overweight adults," *The British Journal of Nutrition*, vol. 107, no. 7, pp. 1037–1047, 2012.
- [32] T. M. Wolever, S. M. Tosh, A. L. Gibbs et al., "Physicochemical properties of oat β -glucan influence its ability to reduce serum LDL cholesterol in humans: a randomized clinical trial," *The American Journal of Clinical Nutrition*, vol. 92, no. 4, pp. 723–732, 2010.
- [33] T. M. S. Wolever, A. L. Gibbs, J. Brand-Miller et al., "Bioactive oat β -glucan reduces LDL cholesterol in Caucasians and non-Caucasians," *Nutrition Journal*, vol. 10, no. 1, p. 130, 2011.

- [34] H. V. T. Ho, J. L. Sievenpiper, A. Zurbau et al., "The effect of oat β -glucan on LDL-cholesterol, non-HDL-cholesterol and apoB for CVD risk reduction: a systematic review and meta-analysis of randomised-controlled trials," *The British Journal of Nutrition*, vol. 116, no. 8, pp. 1369–1382, 2016.
- [35] E. J. Beck, L. C. Tapsell, M. J. Batterham, S. M. Tosh, and X. F. Huang, "Oat β -glucan supplementation does not enhance the effectiveness of an energy-restricted diet in overweight women," *The British Journal of Nutrition*, vol. 103, no. 8, pp. 1212–1222, 2010.
- [36] R. Talati, W. L. Baker, M. S. Pablonia, C. M. White, and C. I. Coleman, "The effects of barley-derived soluble fiber on serum lipids," *Annals of Family Medicine*, vol. 7, no. 2, pp. 157–163, 2009.
- [37] S. S. AbuMweis, S. Jew, and N. P. Ames, " β -Glucan from barley and its lipid-lowering capacity: a meta-analysis of randomized, controlled trials," *European Journal of Clinical Nutrition*, vol. 64, no. 12, pp. 1472–1480, 2010.
- [38] H. Kim, M. Turowski, W. H. Anderson, S. A. Young, Y. Kim, and W. Yokoyama, "Supplementation of hydroxypropyl methylcellulose into yeast leavened all-whole grain barley bread potentiates cholesterol-lowering effect," *Journal of Agricultural and Food Chemistry*, vol. 59, no. 14, pp. 7672–7678, 2011.
- [39] Y. Wang, S. V. Harding, P. Eck et al., "High-molecular-weight β -glucan decreases serum cholesterol differentially based on the CYP7A1 rs3808607 polymorphism in mildly hypercholesterolemic adults," *The Journal of Nutrition*, vol. 146, no. 4, pp. 720–727, 2016.
- [40] A. C. Ruthes, F. R. Smiderle, and M. Iacomini, "Mushroom heteropolysaccharides: a review on their sources, structure and biological effects," *Carbohydrate Polymers*, vol. 136, pp. 358–375, 2016.
- [41] V. Caz, A. Gil-Ramírez, C. Largo et al., "Modulation of cholesterol-related gene expression by dietary fiber fractions from edible mushrooms," *Journal of Agricultural and Food Chemistry*, vol. 63, no. 33, pp. 7371–7380, 2015.
- [42] V. Caz, A. Gil-Ramírez, M. Santamaría et al., "Plasma cholesterol-lowering activity of lard functionalized with mushroom extracts is independent of Niemann-Pick C1-like 1 protein and ABC sterol transporter gene expression in hypercholesterolemic mice," *Journal of Agricultural and Food Chemistry*, vol. 64, no. 8, pp. 1686–1694, 2016.
- [43] X. Zou, X. Guo, and M. Sun, "pH control strategy in a shaken mini-bioreactor for polysaccharide production by medicinal mushroom *Phellinus linteus* and its anti-hyperlipemia activity," *Bioprocess and Biosystems Engineering*, vol. 32, no. 2, pp. 277–281, 2009.
- [44] L. Zheng, G. Zhai, J. Zhang et al., "Antihyperlipidemic and hepatoprotective activities of mycelia zinc polysaccharide from *Pholiota nameko*_ SW-02," *International Journal of Biological Macromolecules*, vol. 70, pp. 523–529, 2014.
- [45] M. Rondanelli, A. Opizzi, F. Monteferrario, C. Klersy, R. Cazzola, and B. Cestaro, "Beta-glucan- or rice bran-enriched foods: a comparative crossover clinical trial on lipidic pattern in mildly hypercholesterolemic men," *European Journal of Clinical Nutrition*, vol. 65, no. 7, pp. 864–871, 2011.
- [46] EFSA, "Scientific opinion on the substantiation of a health claim related to barley beta-glucans and lowering of blood cholesterol and reduced risk of (coronary) heart disease pursuant to Article 14 of Regulation (EC) No 1924/2006," *EFSA Journal*, vol. 9, no. 12, p. 2470, 2011.
- [47] C. S. Venter, H. H. Vorster, and D. G. van der Nest, "Comparison between physiological effects of konjac glucomannan and propionate in baboons fed "Western", diets," *The Journal of Nutrition*, vol. 120, no. 9, pp. 1046–1053, 1990.
- [48] A. Arvill and L. Bodin, "Effect of short-term ingestion of konjac glucomannan on serum cholesterol in healthy men," *The American Journal of Clinical Nutrition*, vol. 61, no. 3, pp. 585–589, 1995.
- [49] H. V. T. Ho, E. Jovanovski, A. Zurbau et al., "A systematic review and meta-analysis of randomized controlled trials of the effect of konjac glucomannan, a viscous soluble fiber, on LDL cholesterol and the new lipid targets non-HDL cholesterol and apolipoprotein B," *The American Journal of Clinical Nutrition*, vol. 105, no. 5, pp. 1239–1247, 2017.
- [50] N. Sood, W. L. Baker, and C. I. Coleman, "Effect of glucomannan on plasma lipid and glucose concentrations, body weight, and blood pressure: systematic review and meta-analysis," *The American Journal of Clinical Nutrition*, vol. 88, no. 4, pp. 1167–1175, 2008.
- [51] A. H. M. Terpstra, J. A. Lapré, H. T. de Vries, and A. C. Beynen, "Intact pectin and its polygalacturonic acid regions have similar hypocholesterolemic properties in hybrid F1B hamsters," *Nahrung*, vol. 46, no. 2, pp. 83–86, 2002.
- [52] A. H. M. Terpstra, J. A. Lapré, H. T. de Vries, and A. C. Beynen, "The hypocholesterolemic effect of lemon peels, lemon pectin, and the waste stream material of lemon peels in hybrid F1B hamsters," *European Journal of Nutrition*, vol. 41, no. 1, pp. 19–26, 2002.
- [53] C. Parolini, S. Manzini, M. Busnelli et al., "Effect of the combinations between pea proteins and soluble fibres on cholesterolaemia and cholesterol metabolism in rats," *The British Journal of Nutrition*, vol. 110, no. 8, pp. 1394–1401, 2013.
- [54] U. Schwab, A. Louheranta, A. Törrönen, and M. Uusitupa, "Impact of sugar beet pectin and polydextrose on fasting and postprandial glycemia and fasting concentrations of serum total and lipoprotein lipids in middle-aged subjects with abnormal glucose metabolism," *European Journal of Clinical Nutrition*, vol. 60, no. 9, pp. 1073–1080, 2006.
- [55] B. T. Metzger, D. M. Barnes, and J. D. Reed, "A comparison of pectin, polyphenols, and phytosterols, alone or in combination, to lovastatin for reduction of serum lipids in familial hypercholesterolemic swine," *Journal of Medicinal Food*, vol. 12, no. 4, pp. 854–860, 2009.
- [56] EFSA, "Scientific opinion on the substantiation of health claims related to pectins and reduction of post-prandial glycaemic responses (ID 786), maintenance of normal blood cholesterol concentrations (ID 818) and increase in satiety leading to a reduction in ene," *EFSA Journal*, vol. 8, no. 10, p. 1747, 2010.
- [57] M. H. Park and J. S. Han, "Padina arborescens ameliorates hyperglycemia and dyslipidemia in C57BL/KsJ-db/db mice, a model of type 2 diabetes mellitus," *Journal of Medicinal Food*, vol. 18, no. 10, pp. 1088–1094, 2015.
- [58] Y. Idota, Y. Kogure, T. Kato et al., "Cholesterol-lowering effect of calcium alginate in rats," *Biological & Pharmaceutical Bulletin*, vol. 39, no. 1, pp. 62–67, 2016.
- [59] B. M. Kim, J. H. Park, D. S. Kim et al., "Effects of the polysaccharide from the sporophyll of brown alga *Undaria pinnatifida* on serum lipid profile and fat tissue accumulation in rats fed a high-fat diet," *Journal of Food Science*, vol. 81, no. 7, pp. H1840–H1845, 2016.

- [60] M. Marounek, Z. Volek, E. Skřivanová, T. Taubner, A. Pebriansyah, and D. Dušková, "Comparative study of the hypocholesterolemic and hypolipidemic activity of alginate and amidated alginate in rats," *International Journal of Biological Macromolecules*, vol. 105, Part 1, pp. 620–624, 2017.
- [61] T. Yokota, K. Nomura, M. Nagashima, and N. Kamimura, "Fucoidan alleviates high-fat diet-induced dyslipidemia and atherosclerosis in ApoE^{shl} mice deficient in apolipoprotein E expression," *The Journal of Nutritional Biochemistry*, vol. 32, pp. 46–54, 2016.
- [62] J. Park, M. Yeom, and D. H. Hahm, "Fucoidan improves serum lipid levels and atherosclerosis through hepatic SREBP-2-mediated regulation," *Journal of Pharmacological Sciences*, vol. 131, no. 2, pp. 84–92, 2016.
- [63] S. P. Singh, J. S. Jadaun, L. K. Narnoliya, and A. Pandey, "Prebiotic oligosaccharides: special focus on fructooligosaccharides, its biosynthesis and bioactivity," *Applied Biochemistry and Biotechnology*, vol. 183, no. 2, pp. 613–635, 2017.
- [64] C. L. Dikeman, M. R. Murphy, and G. C. Fahey Jr., "Dietary fibers affect viscosity of solutions and simulated human gastric and small intestinal digesta," *The Journal of Nutrition*, vol. 136, no. 4, pp. 913–919, 2006.
- [65] M. Beylot, "Effects of inulin-type fructans on lipid metabolism in man and in animal models," *British Journal of Nutrition*, vol. 93, Supplement 1, p. S163, 2007.
- [66] N. Agheli, M. Kabir, S. Berni-Canani et al., "Plasma lipids and fatty acid synthase activity are regulated by short-chain fructo-oligosaccharides in sucrose-fed insulin-resistant rats," *The Journal of Nutrition*, vol. 128, no. 8, pp. 1283–1288, 1998.
- [67] Y. Nakamura, M. Natsume, A. Yasuda, M. Ishizaka, K. Kawahata, and J. Koga, "Fructooligosaccharides suppress high-fat diet-induced fat accumulation in C57BL/6J mice," *BioFactors*, vol. 43, no. 2, pp. 145–151, 2017.
- [68] N. M. Delzenne, C. Daubioul, A. Neyrinck, M. Lasa, and H. S. Taper, "Inulin and oligofructose modulate lipid metabolism in animals: review of biochemical events and future prospects," *British Journal of Nutrition*, vol. 87, Supplement 2, pp. S255–S259, 2002.
- [69] N. C. Habib, S. M. Honoré, S. B. Genta, and S. S. Sánchez, "Hypolipidemic effect of *Smallanthus sonchifolius* (yacon) roots on diabetic rats: Biochemical approach," *Chemico-Biological Interactions*, vol. 194, no. 1, pp. 31–39, 2011.
- [70] M. Malaguarnera, M. Vacante, T. Antic et al., "Bifidobacterium longum with fructo-oligosaccharides in patients with non alcoholic steatohepatitis," *Digestive Diseases and Sciences*, vol. 57, no. 2, pp. 545–553, 2012.
- [71] G. T. Costa, G. C. Abreu, A. B. B. Guimarães, P. R. L. Vasconcelos, and S. B. Guimarães, "Fructo-oligosaccharide effects on serum cholesterol levels. An overview," *Acta Cirurgica Brasileira*, vol. 30, no. 5, pp. 366–370, 2015.
- [72] C. Moroti, L. Souza Magri, M. de Rezende Costa, D. C. U. Cavallini, and K. Sivieri, "Effect of the consumption of a new symbiotic shake on glycemia and cholesterol levels in elderly people with type 2 diabetes mellitus," *Lipids in Health and Disease*, vol. 11, no. 1, p. 29, 2012.
- [73] R. Giacco, G. Clemente, D. Luongo et al., "Effects of short-chain fructo-oligosaccharides on glucose and lipid metabolism in mild hypercholesterolaemic individuals," *Clinical Nutrition*, vol. 23, no. 3, pp. 331–340, 2004.
- [74] E. A. Trautwein, D. Rieckhoff, and H. F. Erbersdobler, "Dietary inulin lowers plasma cholesterol and triacylglycerol and alters biliary bile acid profile in hamsters," *The Journal of Nutrition*, vol. 128, no. 11, pp. 1937–1943, 1998.
- [75] M. Kim and H. K. Shin, "The water-soluble extract of chicory influences serum and liver lipid concentrations, cecal short-chain fatty acid concentrations and fecal lipid excretion in rats," *The Journal of Nutrition*, vol. 128, no. 10, pp. 1731–1736, 1998.
- [76] P. Dehghan, B. Pourghassem Gargari, and M. Asgharijafarabadi, "Effects of high performance inulin supplementation on glycemic status and lipid profile in women with type 2 diabetes: a randomized, placebo-controlled clinical trial," *Health promotion perspectives*, vol. 3, no. 1, pp. 55–63, 2013.
- [77] F. Brighenti, M. Casiraghi, E. Canzi, and A. Ferrari, "Effect of consumption of a ready-to-eat breakfast cereal containing inulin on the intestinal milieu and blood lipids in healthy male volunteers," *European Journal of Clinical Nutrition*, vol. 53, no. 9, pp. 726–733, 1999.
- [78] C. M. Williams and K. G. Jackson, "Inulin and oligofructose: effects on lipid metabolism from human studies," *British Journal of Nutrition*, vol. 87, Supplement 2, pp. S261–S264, 2002.
- [79] A. Pedersen, B. Sandström, and J. M. M. Van Amelsvoort, "The effect of ingestion of inulin on blood lipids and gastrointestinal symptoms in healthy females," *British Journal of Nutrition*, vol. 78, no. 2, pp. 215–222, 2007.
- [80] F. Forcheron and M. Beylot, "Long-term administration of inulin-type fructans has no significant lipid-lowering effect in normolipidemic humans," *Metabolism: clinical and experimental*, vol. 56, no. 8, pp. 1093–1098, 2007.
- [81] K. H. Han, A. Yamamoto, K. I. Shimada, H. Kikuchi, and M. Fukushima, "Dietary fat content modulates the hypolipidemic effect of dietary inulin in rats," *Molecular Nutrition & Food Research*, vol. 61, no. 8, 2017.
- [82] H. W. Lopez, M. A. Levrat-Verny, C. Coudray et al., "Class 2 resistant starches lower plasma and liver lipids and improve mineral retention in rats," *The Journal of Nutrition*, vol. 131, no. 4, pp. 1283–1289, 2001.
- [83] Z. Zhou, F. Wang, X. Ren, Y. Wang, and C. Blanchard, "Resistant starch manipulated hyperglycemia/hyperlipidemia and related genes expression in diabetic rats," *The British Journal of Nutrition*, vol. 94, no. 6, pp. 902–908, 2005.
- [84] Z. Zhou, F. Wang, X. Ren, Y. Wang, and C. Blanchard, "Resistant starch manipulated hyperglycemia/hyperlipidemia and related genes expression in diabetic rats," *International Journal of Biological Macromolecules*, vol. 75, pp. 316–321, 2015.
- [85] T. C. Rideout, S. V. Harding, A. Raslawsky, and C. B. Rempel, "Dietary resistant starch supplementation increases high-density lipoprotein particle number in pigs fed a western diet," *Journal of Dietary Supplements*, vol. 14, no. 3, pp. 334–345, 2016.
- [86] O. J. Park, N. Kang, M. J. Chang, and W. K. Kim, "Resistant starch supplementation influences blood lipid concentrations and glucose control in overweight subjects," *The Journal of Nutritional Biochemistry*, vol. 14, no. 3, pp. 166–172, 2003.
- [87] S. Maisonnier, J. Gomez, A. Bree, C. Berri, E. Baeza, and B. Carre, "Effects of microflora status, dietary bile salts and guar gum on lipid digestibility, intestinal bile salts, and histomorphology in broiler chickens," *Poultry Science*, vol. 82, no. 5, pp. 805–814, 2003.

- [88] D. C. Kuo, S. P. Hsu, and C. T. Chien, "Partially hydrolyzed guar gum supplement reduces high-fat diet increased blood lipids and oxidative stress and ameliorates FeCl₃-induced acute arterial injury in hamsters," *Journal of Biomedical Science*, vol. 16, no. 1, p. 15, 2009.
- [89] S. Samarghandian, M. A. Hadjzadeh, F. Amin Nya, and S. Davoodi, "Antihyperglycemic and antihyperlipidemic effects of guar gum on streptozotocin-induced diabetes in male rats," *Pharmacognosy Magazine*, vol. 8, no. 29, pp. 65–72, 2012.
- [90] G. den Besten, R. Havinga, A. Bleeker et al., "The short-chain fatty acid uptake fluxes by mice on a guar gum supplemented diet associate with amelioration of major biomarkers of the metabolic syndrome," *PLoS One*, vol. 9, no. 9, article e107392, 2014.
- [91] F. Fåk, G. Jakobsdottir, E. Kulcinskaja et al., "The physico-chemical properties of dietary fibre determine metabolic responses, short-chain fatty acid profiles and gut microbiota composition in rats fed low- and high-fat diets," *PLoS One*, vol. 10, no. 5, article e0127252, 2015.
- [92] S. Kondo, J. Z. Xiao, N. Takahashi, K. Miyaji, K. Iwatsuki, and S. Kokubo, "Suppressive effects of dietary fiber in yogurt on the postprandial serum lipid levels in healthy adult male volunteers," *Bioscience, Biotechnology, and Biochemistry*, vol. 68, no. 5, pp. 1135–1138, 2004.
- [93] D. A. Brockman, X. Chen, and D. D. Gallaher, "High-viscosity dietary fibers reduce adiposity and decrease hepatic steatosis in rats fed a high-fat diet," *The Journal of Nutrition*, vol. 144, no. 9, pp. 1415–1422, 2014.
- [94] K. Yamada, Y. Tokunaga, A. Ikeda et al., "Effect of dietary fiber on the lipid metabolism and immune function of aged Sprague-Dawley rats," *Bioscience, Biotechnology, and Biochemistry*, vol. 67, no. 2, pp. 429–433, 2003.
- [95] K. C. Maki, M. H. Davidson, S. Torri et al., "High-molecular-weight hydroxypropylmethylcellulose taken with or between meals is hypocholesterolemic in adult men," *The Journal of Nutrition*, vol. 130, no. 7, pp. 1705–1710, 2000.
- [96] K. C. Maki, M. L. Carson, W. H. Kerr Anderson et al., "Lipid-altering effects of different formulations of hydroxypropylmethylcellulose," *Journal of Clinical Lipidology*, vol. 3, no. 3, pp. 159–166, 2009.
- [97] K. C. Maki, M. L. Carson, M. P. Miller et al., "Hydroxypropylmethylcellulose lowers cholesterol in statin-treated men and women with primary hypercholesterolemia," *European Journal of Clinical Nutrition*, vol. 63, no. 8, pp. 1001–1007, 2009.
- [98] H. Kim, G. E. Bartley, S. A. Young, K. H. Seo, and W. Yokoyama, "Altered hepatic gene expression profiles associated with improved fatty liver, insulin resistance, and intestinal permeability after hydroxypropyl methylcellulose (HPMC) supplementation in diet-induced obese mice," *Journal of Agricultural and Food Chemistry*, vol. 61, no. 26, pp. 6404–6411, 2013.
- [99] N. P. Nørskov, M. S. Hedemann, H. N. Lærke, and K. E. B. Knudsen, "Multicompartmental nontargeted LC-MS metabolomics: explorative study on the metabolic responses of rye fiber versus refined wheat fiber intake in plasma and urine of hypercholesterolemic pigs," *Journal of Proteome Research*, vol. 12, no. 6, pp. 2818–2832, 2013.
- [100] M. Numan Ahmad and H. Rabah Takruri, "The effect of dietary wheat bran on sucrose-induced changes of serum glucose and lipids in rats," *Nutricion Hospitalaria*, vol. 32, no. 4, pp. 1636–1644, 2015.
- [101] L. T. Tong, K. Zhong, L. Liu et al., "Effects of dietary wheat bran arabinoxylans on cholesterol metabolism of hypercholesterolemic hamsters," *Carbohydrate Polymers*, vol. 112, pp. 1–5, 2014.
- [102] L. Pozzo, F. Vizzarri, M. Ciardi et al., "The effects of fermented wheat powder (Lisosan G) on the blood lipids and oxidative status of healthy rabbits," *Food and Chemical Toxicology*, vol. 84, pp. 1–7, 2015.
- [103] S. K. Kim, P. J. Park, H. P. Yang, and S. S. Han, "Subacute toxicity of chitosan oligosaccharide in Sprague-Dawley rats," *Arzneimittelforschung*, vol. 51, no. 9, pp. 769–774, 2001.
- [104] G. Xu, X. Huang, L. Qiu, J. Wu, and Y. Hu, "Mechanism study of chitosan on lipid metabolism in hyperlipidemic rats," *Asia Pacific Journal of Clinical Nutrition*, vol. 16, Supplement 1, pp. 313–317, 2007.
- [105] C. Zong, Y. Yu, G. Song et al., "Chitosan oligosaccharides promote reverse cholesterol transport and expression of scavenger receptor BI and CYP7A1 in mice," *Experimental Biology and Medicine*, vol. 237, no. 2, pp. 194–200, 2012.
- [106] J. Zhang, J. Liu, L. Li, and W. Xia, "Dietary chitosan improves hypercholesterolemia in rats fed high-fat diets," *Nutrition Research*, vol. 28, no. 6, pp. 383–390, 2008.
- [107] H. T. Yao and M. T. Chiang, "Plasma lipoprotein cholesterol in rats fed a diet enriched in chitosan and cholesterol," *Journal of Nutritional Science and Vitaminology (Tokyo)*, vol. 48, no. 5, pp. 379–383, 2002.
- [108] M. Sumiyoshi and Y. Kimura, "Low molecular weight chitosan inhibits obesity induced by feeding a high-fat diet long-term in mice," *The Journal of Pharmacy and Pharmacology*, vol. 58, no. 2, pp. 201–207, 2006.
- [109] J. Zhang, W. Zhang, B. Mamadouba, and W. Xia, "A comparative study on hypolipidemic activities of high and low molecular weight chitosan in rats," *International Journal of Biological Macromolecules*, vol. 51, no. 4, pp. 504–508, 2012.
- [110] H. T. Yao, S. Y. Huang, and M. T. Chiang, "A comparative study on hypoglycemic and hypocholesterolemic effects of high and low molecular weight chitosan in streptozotocin-induced diabetic rats," *Food and Chemical Toxicology: An International Journal Published for the British Industrial Biological Research Association*, vol. 46, no. 5, pp. 1525–1534, 2008.
- [111] W. Zhang and W. Xia, "Effect of media milling on lipid-lowering and antioxidant activities of chitosan," *International Journal of Biological Macromolecules*, vol. 72, pp. 1402–1405, 2015.
- [112] W. L. Baker, A. Tercius, M. Anglade, C. M. White, and C. I. Coleman, "A meta-analysis evaluating the impact of chitosan on serum lipids in hypercholesterolemic patients," *Annals of Nutrition & Metabolism*, vol. 55, no. 4, pp. 368–374, 2009.
- [113] R. Ylitalo, S. Lehtinen, E. Wuolijoki, P. Ylitalo, and T. Lehtimäki, "Cholesterol-lowering properties and safety of chitosan," *Arzneimittelforschung*, vol. 52, no. 1, pp. 1–7, 2002.
- [114] S. Jaffer and J. S. Sampalis, "Efficacy and safety of chitosan HEP-40 in the management of hypercholesterolemia: a randomized, multicenter, placebo-controlled trial," *Alternative Medicine Review*, vol. 12, no. 3, pp. 265–273, 2007.
- [115] EFSA, "Scientific opinion on the substantiation of health claims related to chitosan and reduction in body weight (ID 679, 1499), maintenance of normal blood LDL-cholesterol concentrations (ID 4663), reduction of intestinal transit time

- (ID 4664) and reduction o,” *EFSA Journal*, vol. 9, no. 6, p. 2214, 2011.
- [116] A. M. van Bennekum, D. V. Nguyen, G. Schulthess, H. Hauser, and M. C. Phillips, “Mechanisms of cholesterol-lowering effects of dietary insoluble fibres: relationships with intestinal and hepatic cholesterol parameters,” *British Journal of Nutrition*, vol. 94, no. 3, pp. 331–337, 2005.
- [117] G. Rodríguez-Gutiérrez, F. Rubio-Senent, A. Lama-Muñoz, A. García, and J. Fernández-Bolaños, “Properties of lignin, cellulose, and hemicelluloses isolated from olive cake and olive stones: binding of water, oil, bile acids, and glucose,” *Journal of Agricultural and Food Chemistry*, vol. 62, no. 36, pp. 8973–8981, 2014.
- [118] M. J. Villanueva-Suárez, M. L. Pérez-Cózar, I. Mateos-Aparicio, and A. Redondo-Cuenca, “Potential fat-lowering and prebiotic effects of enzymatically treated okara in high-cholesterol-fed Wistar rats,” *International Journal of Food Sciences and Nutrition*, vol. 67, no. 7, pp. 828–833, 2016.
- [119] M. Krzysik, H. Grajeta, A. Prescha, and R. Weber, “Effect of cellulose, pectin and chromium(III) on lipid and carbohydrate metabolism in rats,” *Journal of Trace Elements in Medicine and Biology*, vol. 25, no. 2, pp. 97–102, 2011.
- [120] J. Čopíková, T. Taubner, J. Tůma, A. Synytsya, D. Dušková, and M. Marounek, “Cholesterol and fat lowering with hydrophobic polysaccharide derivatives,” *Carbohydrate Polymers*, vol. 116, pp. 207–214, 2015.
- [121] M. Marounek, Z. Volek, A. Synytsya, and J. Čopíková, “Effect of pectin and amidated pectin on cholesterol homeostasis and cecal metabolism in rats fed a high-cholesterol diet,” *Physiological Research*, vol. 56, no. 4, pp. 433–442, 2007.
- [122] R. Ben Abdallah Kolsi, A. Ben Gara, R. Chaaben et al., “Anti-obesity and lipid lowering effects of *Cymodocea nodosa* sulphated polysaccharide on high cholesterol-fed-rats,” *Archives of Physiology and Biochemistry*, vol. 121, no. 5, pp. 210–217, 2015.
- [123] M. Marounek, Z. Volek, D. Dušková, J. Tůma, and T. Taubner, “Dose-response efficacy and long-term effect of the hypocholesterolemic effect of octadecylpectinamide in rats,” *Carbohydrate Polymers*, vol. 97, no. 2, pp. 772–775, 2013.
- [124] X. Liu, F. Yang, T. Song et al., “Therapeutic effect of carboxymethylated and quantized chitosan on insulin resistance in high-fat-diet-induced rats and 3T3-L1 adipocytes,” *Journal of Biomaterials Science Polymer Edition*, vol. 23, no. 10, pp. 1271–1284, 2012.
- [125] C. J. Rebello, A. G. Liu, F. L. Greenway, and N. V. Dhurandhar, “Dietary strategies to increase satiety,” *Advances in Food and Nutrition Research*, vol. 69, pp. 105–182, 2013.
- [126] F. J. Dai and C. F. Chau, “Classification and regulatory perspectives of dietary fiber,” *Journal of Food and Drug Analysis*, vol. 25, no. 1, pp. 37–42, 2017.
- [127] E. Theuwissen and R. P. Mensink, “Water-soluble dietary fibers and cardiovascular disease,” *Physiology & Behavior*, vol. 94, no. 2, pp. 285–292, 2008.
- [128] B. Shirouchi, S. Kawamura, R. Matsuoka et al., “Dietary guar gum reduces lymph flow and diminishes lipid transport in thoracic duct-cannulated rats,” *Lipids*, vol. 46, no. 8, pp. 789–793, 2011.
- [129] R. S. Wright, J. W. Anderson, and S. R. Bridges, “Propionate inhibits hepatocyte lipid synthesis,” *Proceedings of the Society for Experimental Biology and Medicine*, vol. 195, no. 1, pp. 26–29, 1990.
- [130] E. N. Bergman, “Energy contributions of volatile fatty acids from the gastrointestinal tract in various species,” *Physiological Reviews*, vol. 70, no. 2, pp. 567–590, 1990.
- [131] B. S. Samuel, A. Shaito, T. Motoike et al., “Effects of the gut microbiota on host adiposity are modulated by the short-chain fatty-acid binding G protein-coupled receptor, Gpr 41,” *Proceedings of the National Academy of Sciences of the United States of America*, vol. 105, no. 43, pp. 16767–16772, 2008.
- [132] C. K. Chakraborti, “New-found link between microbiota and obesity,” *World journal of gastrointestinal pathophysiology*, vol. 6, no. 4, pp. 110–119, 2015.
- [133] T. Immerstrand, K. E. Andersson, C. Wange et al., “Effects of oat bran, processed to different molecular weights of β -glucan, on plasma lipids and caecal formation of SCFA in mice,” *The British Journal of Nutrition*, vol. 104, no. 3, pp. 364–373, 2010.
- [134] J. G. LeHoux and F. Grondin, “Some effects of chitosan on liver function in the rat,” *Endocrinology*, vol. 132, no. 3, pp. 1078–1084, 1993.
- [135] L. T. Tong, K. Zhong, L. Liu, X. Zhou, J. Qiu, and S. Zhou, “Effects of dietary hull-less barley β -glucan on the cholesterol metabolism of hypercholesterolemic hamsters,” *Food Chemistry*, vol. 169, pp. 344–349, 2015.
- [136] J. Y. L. Chiang, “Bile acids: regulation of synthesis: thematic review series: bile acids,” *Journal of Lipid Research*, vol. 50, no. 10, pp. 1955–1966, 2009.
- [137] A. Chawla, E. Saez, and R. M. Evans, “Don't know much bileology,” *Cell*, vol. 103, no. 1, pp. 1–4, 2000.
- [138] W. Li, Y. Li, Q. Wang, and Y. Yang, “Crude extracts from *Lycium barbarum* suppress SREBP-1c expression and prevent diet-induced fatty liver through AMPK activation,” *BioMed Research International*, vol. 2014, Article ID 196198, 10 pages, 2014.
- [139] J. C. Cohen, “Contribution of cholesterol 7 α -hydroxylase to the regulation of lipoprotein metabolism,” *Current Opinion in Lipidology*, vol. 10, no. 4, pp. 303–308, 1999.
- [140] S. I. Kang, M. H. Kim, H. S. Shin et al., “A water-soluble extract of *Petalonia binghamiae* inhibits the expression of adipogenic regulators in 3T3-L1 preadipocytes and reduces adiposity and weight gain in rats fed a high-fat diet,” *The Journal of Nutritional Biochemistry*, vol. 21, no. 12, pp. 1251–1257, 2010.
- [141] G. den Besten, A. Gerding, T. H. van Dijk et al., “Protection against the metabolic syndrome by guar gum-derived short-chain fatty acids depends on peroxisome proliferator-activated Receptor γ and glucagon-like peptide-1,” *PLoS One*, vol. 10, no. 8, article e0136364, 2015.
- [142] K. J. Kim, O. H. Lee, and B. Y. Lee, “Fucoxanthin, a sulfated polysaccharide, inhibits adipogenesis through the mitogen-activated protein kinase pathway in 3T3-L1 preadipocytes,” *Life Sciences*, vol. 86, no. 21–22, pp. 791–797, 2010.
- [143] Y. Nie, F. Luo, L. Wang et al., “Anti-hyperlipidemic effect of rice bran polysaccharide and its potential mechanism in high-fat diet mice,” *Food & Function*, vol. 8, no. 11, pp. 4028–4041, 2017.
- [144] Z. Yasukawa, Y. Naito, T. Takagi et al., “Partially hydrolyzed guar gum affects the expression of genes involved in host defense functions and cholesterol absorption in colonic mucosa of db/db male mice,” *Journal of Clinical Biochemistry and Nutrition*, vol. 51, no. 1, pp. 33–38, 2012.

- [145] C. Daubioul, N. Rousseau, R. Demeure et al., "Dietary fructans, but not cellulose, decrease triglyceride accumulation in the liver of obese Zucker fa/fa rats," *The Journal of Nutrition*, vol. 132, no. 5, pp. 967–973, 2002.
- [146] G. den Besten, A. Bleeker, A. Gerding et al., "Short-chain fatty acids protect against high-fat diet-induced obesity via a PPAR γ -dependent switch from lipogenesis to fat oxidation," *Diabetes*, vol. 64, no. 7, pp. 2398–2408, 2015.
- [147] M. Basha, A. H. Salama, and S. El Awdan, "Reconstitutable spray dried ultra-fine dispersion as a robust platform for effective oral delivery of an antihyperlipidemic drug," *International Journal of Pharmaceutics*, vol. 532, no. 1, pp. 478–490, 2017.
- [148] R. Rohilla, T. Garg, J. Bariwal, A. K. Goyal, and G. Rath, "Development, optimization and characterization of glycyrrhetic acid-chitosan nanoparticles of atorvastatin for liver targeting," *Drug Delivery*, vol. 23, no. 7, pp. 2290–2297, 2016.

Research Article

Dietary Beta-Hydroxy Beta-Methyl Butyrate Supplementation Alleviates Liver Injury in Lipopolysaccharide-Challenged Piglets

Yehui Duan ¹, Bo Song ^{1,2}, Changbing Zheng ¹, Yinzhao Zhong¹, Qiuping Guo¹, Jie Zheng^{1,2}, Yulong Yin^{1,3}, Jianjun Li ¹ and Fengna Li ¹

¹CAS Key Laboratory of Agro-ecological Processes in Subtropical Region, Hunan Provincial Key Laboratory of Animal Nutritional Physiology and Metabolic Process, National Engineering Laboratory for Pollution Control and Waste Utilization in Livestock and Poultry Production, Institute of Subtropical Agriculture, Chinese Academy of Sciences, Changsha 410125, China

²University of Chinese Academy of Sciences, Beijing 100039, China

³Animal Nutritional Genome and Germplasm Innovation Research Center, College of Animal Science and Technology, Hunan Agricultural University, Changsha, Hunan 410128, China

Correspondence should be addressed to Jianjun Li; jianjunli@isa.ac.cn and Fengna Li; lifengna@isa.ac.cn

Received 13 January 2021; Revised 6 March 2021; Accepted 22 March 2021; Published 2 April 2021

Academic Editor: Janusz Gebicki

Copyright © 2021 Yehui Duan et al. This is an open access article distributed under the Creative Commons Attribution License, which permits unrestricted use, distribution, and reproduction in any medium, provided the original work is properly cited.

The current study was performed to investigate whether dietary β -hydroxy- β -methylbutyrate (HMB) could regulate liver injury in a lipopolysaccharide- (LPS-) challenged piglet model and to determine the mechanisms involved. Thirty piglets (21 ± 2 days old, 5.86 ± 0.18 kg body weight) were randomly divided into the control (a basal diet, saline injection), LPS (a basal diet), or LPS +HMB (a basal diet + 0.60% HMB-Ca) group. After 15 d of treatment with LPS and/or HMB, blood and liver samples were obtained. The results showed that in LPS-injected piglets, HMB supplementation ameliorated liver histomorphological abnormalities induced by LPS challenge. Compared to the control group, the activities of serum aspartate aminotransferase and alkaline phosphatase were increased in the LPS-injected piglets ($P < 0.05$). The LPS challenge also downregulated the mRNA expression of L-PFK, ACO, L-CPT-1, ICDH β , and AMPK α 1/2 and upregulated the mRNA expression of PCNA, caspase 3, TNF- α , TLR4, MyD88, NOD1, and NF- κ B p65 ($P < 0.05$). However, these adverse effects of the LPS challenge were reversed by HMB supplementation ($P < 0.05$). These results indicate that HMB may exert protective effects against LPS-induced liver injury, and the underlying mechanisms might involve the improvement of hepatic energy metabolism via regulating AMPK signaling pathway and the reduction of liver inflammation via modulating TLR4 and NOD signaling pathways.

1. Introduction

As a key metabolic organ and a major site for detoxification in the body, the liver contributes importantly to protect body from bacteria and their toxic products, such as lipopolysaccharide (LPS) [1, 2]. Consequently, it is of major health and scientific significance for animals and humans to maintain the liver health. LPS is a component of the outer membrane of Gram-negative bacteria. Through the recognition by Toll-like receptor 4 (TLR4), LPS can excessively activate immune cells such as Kupffer cells (macrophages) and neutrophils [3]. The TLR4/myeloid differentiation factor 88- (MyD88-) mediated pathway can activate nuclear factor- κ B (NF- κ B) and induce productions of proinflammatory cyto-

kines, such as tumor necrosis factor- α [4]. Subsequently, excessive liver inflammatory response leads to severe liver injury, such as cytoplasm vacuolization, hepatocyte karyolysis, disruption of hepatic cell cords, and inflammatory cell infiltration [5]. Moreover, inflammatory liver injury is often accompanied by insufficient energy supply in the liver [6, 7]. Therefore, modulating hepatic inflammatory response plays an essential role in attenuating LPS-induced liver injury. With the joint efforts of many researchers, several nutritional supplements (such as aspartate, N-acetylcysteine, chondroitin sulfate-rich extract of skate cartilage, and α -ketoglutarate) have been demonstrated to have the potential to alleviate LPS challenge-induced liver damage [6–9]. In spite of these interesting observations, it is still urgent to find

low-cost drugs that doctors and animal producers are more preferable for.

β -Hydroxy- β -methylbutyrate (HMB) is a derivative of leucine and metabolized in the liver from the keto acid of leucine by α -ketoisocaproate dioxygenase [10]. Studies have shown that HMB is used as a nutritional supplement to exert positive roles in animals and humans under stressful or inflammatory conditions [11–13]. We recently reported that dietary supplementation with 0.60% HMB prevents muscle protein degradation and alleviates intestinal injury in LPS-challenged piglets [12, 13]. Given its beneficial roles under inflammatory condition, we hypothesized that HMB may also exert positive roles in the liver of LPS-challenged piglets. Intriguingly, recent evidence points to a strong relationship between HMB supplementation and liver health. First, HMB supplementation in patients after liver transplant has been reported to be safe and well tolerated [14]. Further evidence comes from the finding that HMB exerts beneficial effects in ameliorating insulin resistance via inhibiting glucose transporter type 2 in rat liver [15]. These metabolic enhancements that have been related to HMB make it a prime substrate to be used in subjects suffering from liver injury. Surprisingly, although most of the endogenous HMB is generated in the liver, there are few reports concerning the effects of HMB supplementation in subjects with liver disease. Therefore, further investigation is certainly necessary.

Therefore, we here seek to determine whether HMB could attenuate liver injury in LPS-challenged weanling piglets and, if so, to elucidate the underlying mechanisms. Pigs are similar to human in physiology and anatomy, and the swine model is hence considered to be a good animal model for investigating human nutrition and physiology [16, 17]. The present results will offer insight into the mechanisms of HMB's actions in the liver of piglets and also provide useful information for nutritionally ameliorating liver injury in inflammatory condition in humans.

2. Materials and Methods

2.1. Animals and Experimental Diets. The animal use protocol for this study was approved by the Committee on Animal Care of the Institute of Subtropical Agriculture, Chinese Academy of Sciences. Thirty healthy pigs (Landrace, 21 ± 2 d, barrow, 5.86 ± 0.18 kg) were chosen and randomly assigned to three groups ($n = 10$): (1) nonchallenged control (CON); (2) LPS-challenged control (LPS, *E. coli* serotype 055:B5; Sigma Chemical, St. Louis, MO, USA); (3) LPS +0.60% HMB-Ca treatment (LPS+HMB; HMB-Ca, purity = 99.2%, Ca = 13.6%, Sipu Biochemical Co. LTD, Zhangjia-gang, China). The HMB-Ca and LPS doses were used in accordance with our previous studies [12]. On days 1, 3, 5, 7, 9, 11, 13, and 15 of the trial, overnight fasted piglets of the LPS and LPS+HMB groups were intraperitoneally administered LPS, whereas piglets in the CON group were injected with the same volume of sterile saline as previously described [12]. Piglets were raised individually in cages (1.80×1.10 m pen) and had *ad libitum* access to diets and clean drinking water. Diets were formulated to meet the

nutritional needs for piglets according to the National Research Council (NRC, Supplementary Table 1) [18]. The experiment lasted for 15 days.

2.2. Sample Collection. All pigs were slaughtered by electrically stunning (250 V, 0.5 A, for 5–6 s) and exsanguinating at 3 h after LPS or saline injection on day 15 of the trial. Before slaughter, blood samples were obtained from the jugular vein and centrifuged at $3,000 \times g$ at 4°C for 15 min to recover the serum, which was stored at -80°C until further analysis. After slaughter, liver samples were immediately and rapidly obtained and fixed in 4% formaldehyde or stored at -80°C until further analysis.

2.3. Serum Biochemical Parameters. The concentrations of serum aspartate aminotransferase (ASAT), alanine aminotransferase (ALAT), alkaline phosphatase (AKP), and glutamyl transpeptidase (GGT) were analyzed using the Biochemical Analytical Instrument (Beckman CX4) and commercial kits (Sino-German Beijing Leadman Biotech Ltd., Beijing, China).

2.4. Liver Morphology. After a 24 h fixation, liver morphology was examined as previously described [19].

2.5. Reverse Transcription and Real-Time Quantitative PCR. The quantitative RT-PCR analysis was conducted according to our previous studies [20, 21]. Briefly, total RNA of the liver tissue was extracted using Trizol reagent (Invitrogen, Carlsbad, CA, USA). The primer sequences for the selected genes were shown in Table 1. The expression of the target genes relative to housekeeping gene (β -actin) was determined by the $2^{-\Delta\Delta\text{Ct}}$ method [20].

2.6. Western Blot Analysis. Relative protein levels for claudin-1 (Invitrogen Technology, Danvers, MA, USA) and p-AMPK α (Thr172, Cell Signaling Technology Inc., Danvers, MA, USA) obtained from the liver tissue were determined by the Western blotting technique according to our previous studies [22–24]. The bands of the protein were visualized using a chemiluminescent reagent (Pierce, Rockford, USA) with a ChemiDoc XRS system (Bio-Rad, Philadelphia, PA, USA). We quantified the resultant signals using Alpha Imager 2200 software (Alpha Innotech Corporation, CA, USA) and normalized the data with the value of the inner control β -actin or the corresponding total protein.

2.7. Statistical Analyses. All data in this study was analyzed by the one-way ANOVA of SAS software version 9.2 (SAS Institute Inc., Cary, NC, United States), followed by a Duncan's multiple-range test to determine treatment effects. Results are presented as means with standard errors. Differences between significant means were considered as statistically different at $P < 0.05$.

3. Results

3.1. Liver Morphology. Compared to the CON, the pigs treated with LPS exhibited liver injury, as evidenced by hepatocyte caryolysis, karyopycnosis, hypatocyte vacuolization, and hepatic cell cords arrangement in disorder,

TABLE 1: Primers used for real-time quantitative PCR.

Genes	Forward (5' -3')	Reverse (5' -3')
HexoK 2	CTCATCACAACCGTTACCA	TGTCATTAGTGTCTCATCC
L-PFK	CTGCACCGCATCATGGA	CCCCATCACCTCCAGAACA
PK	TCACTCCACAGACCTCAT	TACCTAGCCACCTGATGT
PDH	GCAGACTTACCGTTACCAT	GATAGCCGAGTTCTTCCAA
ACO	CTCGCAGACCCAGATGAAAT	TCCAAGCCTCGAAGATGAGT
L-CPT-1	GGACCGCCACCTGTTCTGCCTCTA	GCCCCCTCCGCTCGACACATAC
CS	TCTCAGCTCAGTGCAGCCATTACA	CTGCAACACAAGGTAGCTTTGCGA
ICDH β	TGTGGTTCTCTGGTGAGAG	CGAGATTGAGATGCCGTAG
ICDH γ	GGTGGAGAGCCTCAAGAT	TGGTGGTGTGTCTACGA
AMPK α 1	AAATCGGCCACTACATCCTG	GGATGCCTGAAAAGCTTGAG
AMPK α 2	AACATGGACGGGTTGAAGAG	CGCAGAACTCACCATCTGA
Sirt1	CTGGAACAGGTTGCAGGAAT	CCTAGGACATCGAGGAACCA
PGC-1 α	GATGTGTCGCCCTTCTTGTTT	CATCCTTTGGGGTCTTTGAG
PCNA	TACGCTAAGGGCAGAAGATAATG	CTGAGATCTCGGCATATACGTG
Caspase-3	ACCCAAACTTTTCATAATTCA	ACCAGGTGCTGTAGAATATGC
TNF- α	TCCAATGGCAGAGTGGGTATG	AGCTGGTTGTCTTTCAGCTTCAC
COX2	ATGATCTACCCGCTCACAC	AAAAGCAGCTCTGGGTCAA
HSP70	GCCCTGAATCCGCAGAATA	TCCCCACGGTAGGAAACG
TLR4	TCAGTTCTCACCTTCCTCCTG	GTTCATTCTCACCAGTCTTC
MyD88	GATGGTAGCGGTTGTCTCTGAT	GATGCTGGGGAACTCTTCTTC
IRAK1	CAAGGCAGGTCAGGTTTCGT	TTCGTGGGGCGTGTAGTGT
TRAF6	CAAGAGAATACCCAGTCGCACA	ATCCGAGACAAAGGGGAAGAA
NOD1	CTGTCGTCAACACCGATCCA	CCAGTTGGTGACGCAGCTT
NOD2	GAGCGCATCCTCTTAACTTTCG	ACGCTCGTGATCCGTGAAC
RIPK2	CAGTGTCCAGTAAATCGCAGTTG	CAGGCTTCCGTCATCTGGTT
NF- κ B p65	AGTACCCTGAGGCTATAACTCGC	TCCGCAATGGAGGAGAAGTC
β -Actin	TGCGGGACATCAAGGAGAAG	AGTTGAAGGTGGTCTCGTGG

ACO: acyl-coenzyme A oxidase; AMPK α : AMP-activated protein kinase α ; CS: citrate synthase; Hexok 2: hexokinase2; HSP70: heat shock protein 70; ICDH β : isocitrate dehydrogenase β ; ICDH γ : isocitrate dehydrogenase γ ; IRAK1: IL-1 receptor-associated kinase 1; L-CPT-1: liver carnitine palmitoyltransferase I; L-PFK: 6-phosphofructokinase (liver type-like); MyD88: myeloid differentiation factor 88; NODs: nucleotide-binding oligomerization domain protein; PCNA: proliferation cell nuclear antigen; PDH: pyruvate dehydrogenase; PGC-1 α : peroxisome proliferator-activated receptor- γ coactivator-1 α ; PK: pyruvate kinase; RIPK2: receptor-interacting serine/threonine-protein kinase 2; SIRT1: silent information regulator transcript 1; TLR4: toll-like receptor 4; TNF- α : tumor necrosis factor- α ; TRAF6: TNF- α receptor-associated factor 6.

inflammatory cell infiltration, fibroblast proliferation, and hyperaemia in hepatic sinusoids (Figures 1(a) and 1(b)). Furthermore, the impairment of liver induced by LPS was largely recovered by HMB supplementation (Figure 1(c)).

3.2. Serum Biochemical Parameters. As presented in Figure 2, the activities of serum ASAT and AKP were increased by LPS challenge, and the elevation of these parameters was nearly reversed to the level of control diet-fed pigs by HMB supplementation ($P < 0.05$). Serum activities of ALAT and GGT were not significantly different among groups ($P > 0.05$).

3.3. Liver mRNA Expression of Genes Related to the Energy Metabolism. The mRNA expression of genes involved in carbohydrate metabolism (hexokinase 2, Hexok2; phosphofructokinase, L-PFK; pyruvate kinase, PK; pyruvate dehydrogenase, PDH), fatty acid oxidation (acyl-coenzyme A

oxidase, ACO; liver carnitine palmitoyltransferase I, L-CPT-1), and tricarboxylic acid cycle (citrate synthase, CS; isocitrate dehydrogenase β ; isocitrate dehydrogenase γ , ICDH γ) in the liver of pigs was shown in Figure 3. Compared to the CON, LPS challenge significantly downregulated the mRNA expression of ACO and L-CPT-1 ($P < 0.05$) and had a tendency to downregulate the mRNA expression of L-PFK and ICDH β ($P < 0.01$). Among the LPS-challenged pigs, HMB supplementation upregulated the mRNA expression of L-PFK, L-CPT-1, and ICDH β ($P < 0.05$) and had a tendency to increase the ACO mRNA expression ($P < 0.01$).

3.4. Liver mRNA Expression of Genes Related to the Energy Sensing Network. The mRNA expression of AMP-activated protein kinase α (AMPK α) 1/2, peroxisome proliferator-activated receptor γ coactivator 1 α (PGC-1 α), and silent information regulator 1 (SIRT1) in the liver of pigs was

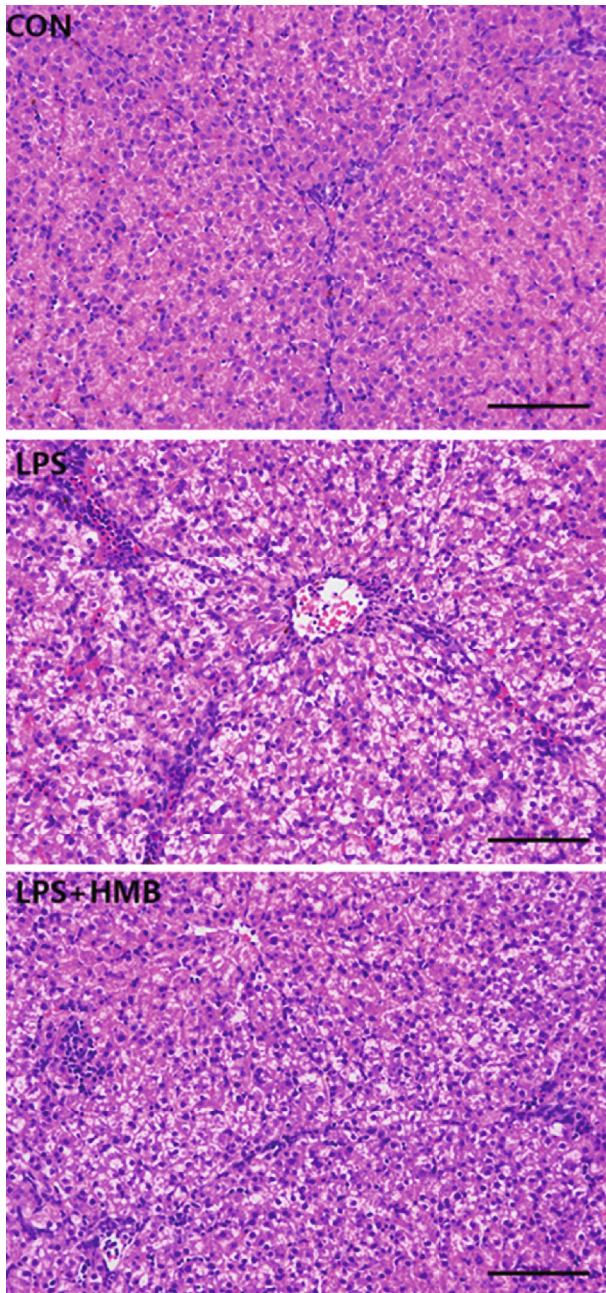


FIGURE 1: Histological examination of the liver samples of piglets injected with lipopolysaccharide (LPS) or saline. Sections were obtained with haematoxylin and eosin ($\times 200$). CON: control; HMB: β -hydroxy- β -methylbutyrate.

shown in Figure 4. Compared to the CON, significant decreases in the expression of AMPK α 1 and AMPK α 2 were shown in the liver of pigs after treatment with LPS ($P < 0.05$). Among the LPS-challenged pigs, HMB supplementation tended to increase the mRNA expression of AMPK α 1 and AMPK α 2 by 15.85% and 22.37%, respectively, but these decreases did not reach statistical difference ($P > 0.05$). Dietary treatments had no significant effects on the mRNA expression of Sirt1 and PGC-1 α ($P > 0.05$).

3.5. Liver mRNA Expression of Proliferation Cell Nuclear Antigen (PCNA), Caspase-3, Tumor Necrosis Factor- α (TNF- α), and Heat Shock Protein 70 (HSP70). As shown in Figure 5, compared to the CON, LPS challenge significantly upregulated the mRNA expression of liver PCNA, caspase 3, and TNF- α ($P < 0.05$). Compared to pigs treated with LPS, HMB supplementation significantly decreased the caspase 3 mRNA expression ($P < 0.05$) and downregulated the mRNA expression of PCNA and TNF- α by 14.07% and 11.02%, respectively, but this decrease did not reach statistical difference ($P > 0.05$). Dietary treatments did not significantly affect the mRNA expression of Sirt1 and PGC-1 α ($P > 0.05$).

3.6. Liver mRNA Expression of TLR4 and Nucleotide-Binding Oligomerization Domain Protein (NODs) and Their Downstream Signals. As shown in Figure 6, LPS challenge significantly upregulated the mRNA expression of liver TLR4, MyD88, NOD1, and NF- κ B p65 relative to the CON ($P < 0.05$). Dietary HMB supplementation to the LPS-challenged pigs significantly downregulated the mRNA expression of MyD88 and NF- κ B p65 ($P < 0.05$) and decreased the mRNA expression of TLR4 and NOD1 by 16.30% and 8.27%, respectively, but this decrease did not reach statistical difference ($P > 0.05$).

3.7. Liver Protein Expression of P-AMPK α and Claudin-1. As shown in Figure 7, no significant effect was observed for liver claudin-1 protein expression in response to dietary treatments ($P > 0.05$). The phosphorylation of AMPK α was downregulated by LPS challenge relative to the saline-injected pigs ($P < 0.05$). Compared to the LPS pigs, HMB supplementation significantly increased the protein expression of p-AMPK α ($P < 0.05$).

4. Discussion

The awareness of the roles of HMB in many biological and physiological processes including liver physiology is increasing [14, 15]. Our previous studies have revealed that dietary supplementation with 0.6% HMB mitigated growth suppression and intestinal injury of LPS-challenged weanling piglets [12, 13]. In the present study, we extended it into the liver to investigate the effects of 0.6% HMB supplementation on liver injury. We found that in response to LPS challenge, serum activities of ASAT and AKP (useful biochemical indicator of liver injury [8, 25]) were increased. These findings indicated that LPS could cause liver injury. Further evidence for a relationship between LPS challenge and liver injury comes from the findings of liver histopathological alterations, including infiltration of inflammatory leucocytes and karyolysis, karyopyknosis, vacuolation, and haemorrhage of hepatocytes. These results were consistent with other studies [2, 8]. Interestingly, HMB decreased serum activities of ASAT and AKP and ameliorated LPS-induced hepatocyte karyolysis, karyopyknosis, and fibroblast proliferation. These findings suggest that HMB offered a beneficial effect on the inhibition of liver injury.

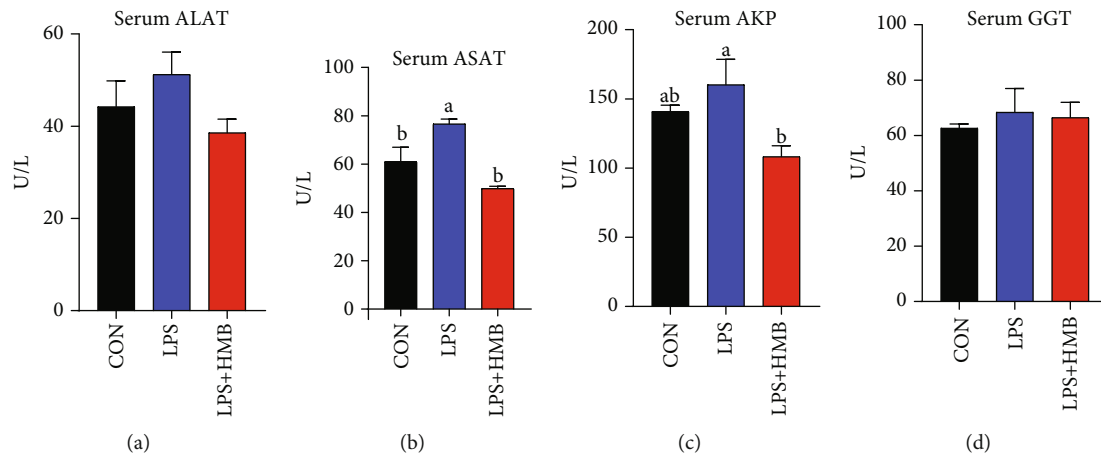


FIGURE 2: Effects of dietary supplementation of HMB on serum biochemical parameters of piglets injected with LPS or saline. (a) Aspartate aminotransferase (ASAT); (b) alanine aminotransferase (ALAT); (c) alkaline phosphatase (AKP); (d) glutamyl transpeptidase (GGT). Values are means, with their standard errors represented by vertical bars ($n = 10$). ^{a,b}Mean values with different letters were considered to be significantly different ($P < 0.05$). CON: control; HMB: β -hydroxy- β -methylbutyrate; LPS: lipopolysaccharide.

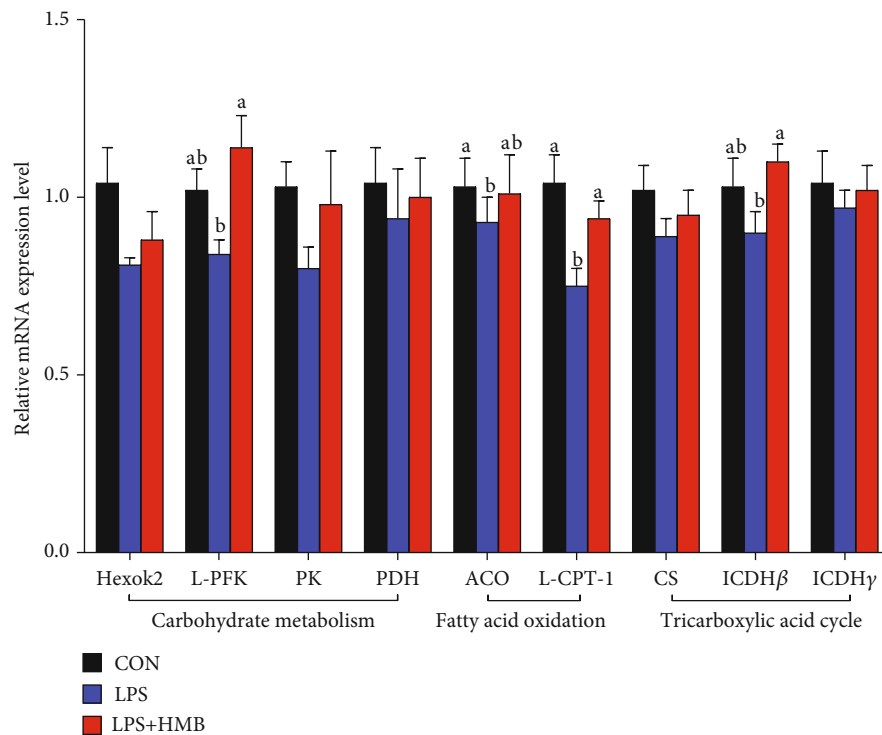


FIGURE 3: The mRNA expression of energy metabolism-related genes in the liver of piglets injected with LPS or saline. Carbohydrate metabolism-related genes: Hexok2: hexokinase 2; L-PFK: phosphofructokinase; PK: pyruvate kinase; PDH: pyruvate dehydrogenase. Fatty acid oxidation-related genes: ACO: acyl-coenzyme A oxidase; L-CPT-1: liver carnitine palmitoyltransferase I. Tricarboxylic acid cycle-related genes: CS: citrate synthase; isocitrate dehydrogenase β ; ICDH γ : isocitrate dehydrogenase γ . Values are means, with their standard errors represented by vertical bars ($n = 10$). ^{a,b}Mean values with different letters were considered to be significantly different ($P < 0.05$). CON: control; HMB: β -hydroxy- β -methylbutyrate; LPS: lipopolysaccharide.

To evaluate the mechanisms of HMB's mode of action, we initiated studies to analyze the mRNA expression of genes related to the energy metabolism. First, we found that HMB supplementation upregulated the mRNA expression of PFK, ACO, L-CPT-1, and ICDH β in the liver of LPS-challenged piglets. PFK is involved in catalyzing the first step

of glycolysis, that is, the phosphorylation of glucose to glucose 6-phosphate to produce ATP and pyruvate [26]. ICDH β , a key enzyme in TCA cycle, transports metabolic intermediates from the cytosol into mitochondria to support the TCA cycle [27]. ACO and L-CPT-1 are implicated in the process of fatty acid oxidation, which is an important source of

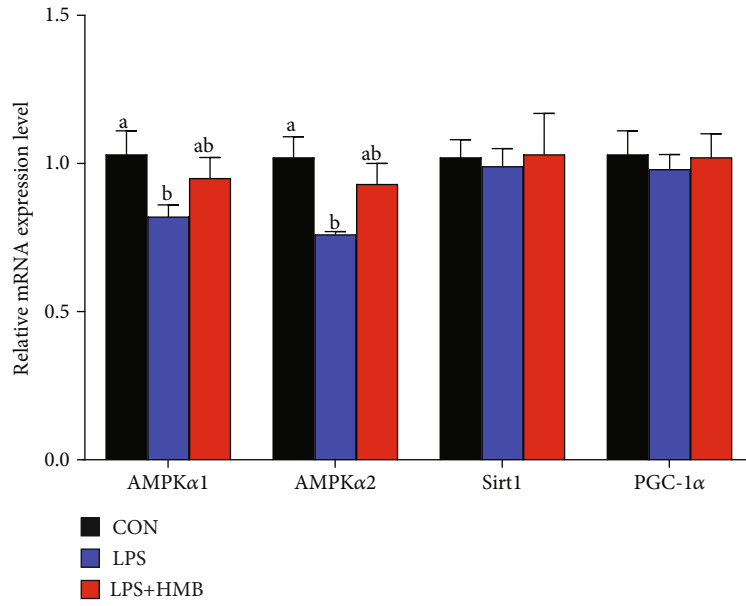


FIGURE 4: The mRNA expression of AMPK α 1/2, Sirt1, and PGC-1 α in the liver of piglets injected with LPS or saline. Values are means, with their standard errors represented by vertical bars ($n = 10$). ^{a,b}Mean values with different letters were considered to be significantly different ($P < 0.05$). AMPK α 1/2: AMP-activated protein kinase α 1/2; CON: control; HMB: β -hydroxy- β -methylbutyrate; LPS: lipopolysaccharide; PGC-1 α : peroxisome proliferator-activated receptor-g coactivator-1 α ; SIRT1: silent information regulator transcript 1.

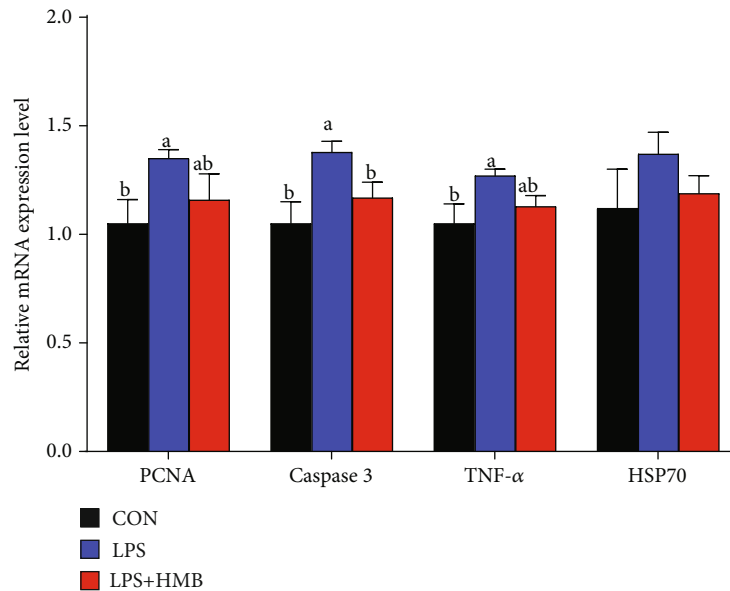


FIGURE 5: The mRNA expression of proliferation cell nuclear antigen (PCNA), caspase-3, tumor necrosis factor- α (TNF- α), and heat shock protein 70 (HSP70) in the liver of piglets injected with LPS or saline. Values are means, with their standard errors represented by vertical bars ($n = 10$). ^{a,b}Mean values with different letters were considered to be significantly different ($P < 0.05$). CON: control; HMB: β -hydroxy- β -methylbutyrate; LPS: lipopolysaccharide.

energy [7]. Therefore, the findings of the current study suggested that HMB, to some extent, could stimulate glycolysis, fatty acid oxidation, and TCA cycle to produce more ATP to mitigate LPS-induced energy stress in the liver of piglets. Such improved liver energy status prompted us to investigate whether HMB supplementation could activate AMPK signaling pathway in the liver of LPS-challenged piglets. AMPK is a cellular sensor of energy status; it functions to restore cellular

ATP by switching off anabolic processes (further ATP consumption) in favor of catabolic processes (ATP generation). Enhanced AMPK activation has been reported to attenuate LPS-induced injury severity of tissues such as the liver, intestinal, and lung in animals [7, 13, 28]. In the present study, HMB supplementation upregulated the mRNA expression of AMPK α 1/2 in the liver of LPS-injected piglets, accompanied by elevated AMPK α phosphorylation. Overall, these

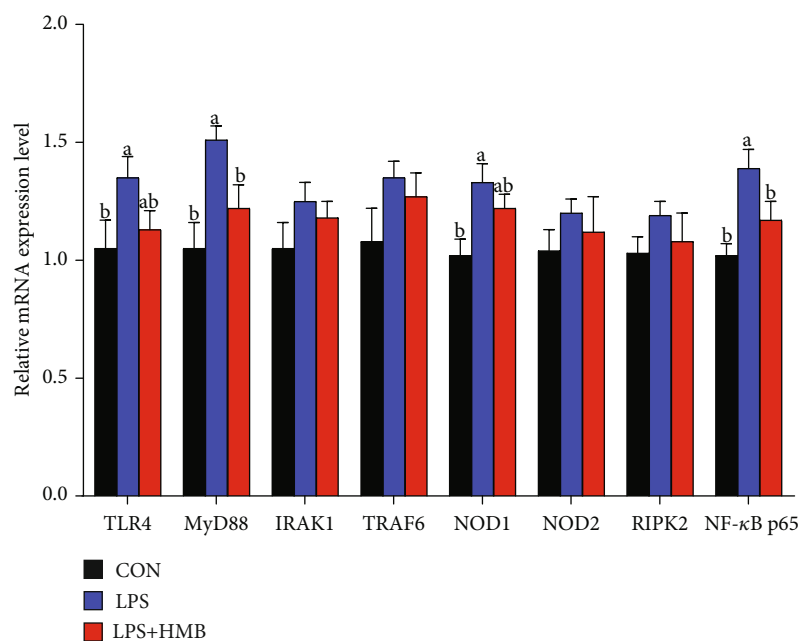


FIGURE 6: The mRNA expression of toll-like receptor 4 (TLR4) and nucleotide-binding oligomerization domain protein (NODs) and their downstream signaling molecules in the liver of piglets injected with LPS or saline. Values are means, with their standard errors represented by vertical bars ($n = 10$). ^{a,b}Mean values with different letters were considered to be significantly different ($P < 0.05$). CON: control; HMB: β -hydroxy- β -methylbutyrate; IRAK1: IL-1 receptor-associated kinase 1; LPS: lipopolysaccharide; MyD88: myeloid differentiation factor 88; RIPK2: receptor-interacting serine/threonine-protein kinase 2; TRAF6: TNF- α receptor-associated factor 6.

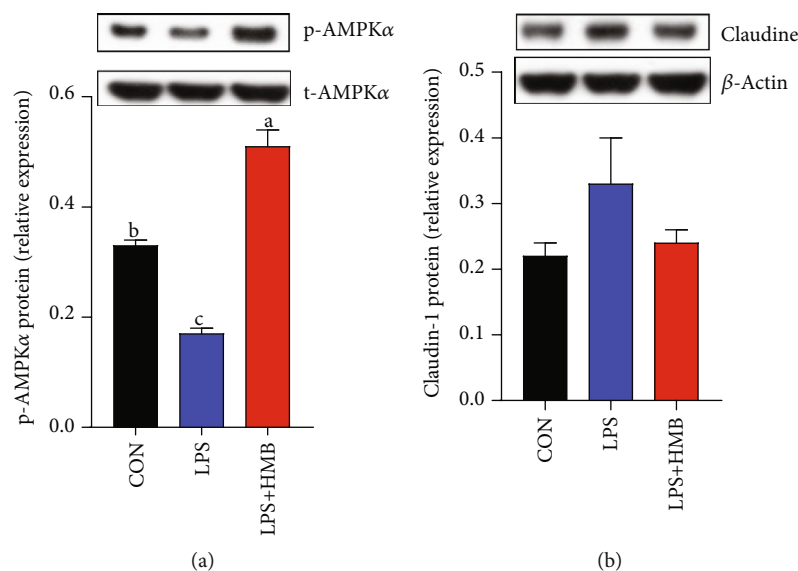


FIGURE 7: Western blot analysis of AMPK α phosphorylation (a) and claudin (b) expression in the liver of piglets injected with LPS or saline. Values are means, with their standard errors represented by vertical bars ($n = 10$). ^{a,b,c}Mean values with different letters were considered to be significantly different ($P < 0.05$). CON: control; HMB: β -hydroxy- β -methylbutyrate; LPS: lipopolysaccharide.

data suggested that HMB supplementation led to an improved energy status in the injured liver of LPS-injected piglets via activating AMPK signaling pathway.

Apart from energy, cell turnover including cell proliferation and apoptosis also affects tissue integrity and homeostasis [29, 30]. In particular, premature apoptosis occurs in response to errors in the signaling cascade of tissues under pathological condition. On the other hand, injured cells

may proliferate uncontrolled and become a cancerous cell mass when they were unable to enter the apoptotic pathway [31]. In this study, we found that LPS challenge gave rise to hepatocyte proliferation and apoptosis, as evidenced by upregulated mRNA expression levels of PCNA and caspase-3. Other studies corroborate these results [32]. In agreement with expectations, the mRNA expression levels of PCNA and caspase-3 in the liver of LPS-challenged piglets

were upregulated in response to HMB supplementation. These results revealed that inhibition of hepatocyte proliferation and apoptosis might be a contributing mechanism for the improved liver health in the LPS-injected piglets upon HMB supplementation.

Intrigued by decreased levels of serum proinflammatory cytokines upon HMB supplementation [12], we wondered whether HMB could ameliorate liver inflammatory response to improve liver integrity. Consistent with our serum TNF- α data, we found that hepatic TNF- α mRNA expression was upregulated following LPS challenge, and this elevation was reversed to the level of LPS-challenged piglets by HMB treatment. Emerging evidence has revealed that overproduction of proinflammatory cytokines leads to liver damage [33, 34]. Therefore, these data suggested that HMB might exert a role in reducing liver LPS-induced inflammation, which prompted us to perform in-depth studies to investigate the underlying mechanisms. TLR4 and NOD1/2 are the most popular signaling among others to respond primarily to LPS and to trigger the activation of inflammatory response [35, 36]. In this study, in good accordance with the alterations in serum TNF- α level and liver TNF- α mRNA expression, we observed that mRNA expressions of TLR4 and MyD88 (TLR4 signaling related genes), NOD1 (NOD signaling related genes), and NF- κ B p65 were increased in the liver of LPS-injected piglets, and then reversed by HMB. Therefore, inhibition of hepatic TLR4 and NOD signaling pathways in the LPS-injected piglets could be one possible mechanism to explain the ability of HMB to counter liver injury. Similar results were obtained in resistance-trained men (22.3 ± 2.4 years), in which HMB decreased circulating TNF- α and TNF- α receptor 1 expression during recovery [37]. Taken together, we expanded our scope from muscle and intestine to liver and demonstrated that HMB could also protect liver tissue from LPS-induced injury via inhibiting TLR4 and NOD signaling pathways.

In conclusion, our data demonstrate that dietary HMB supplementation could ameliorate liver injury in the LPS-challenged piglets. These beneficial effects of HMB might be associated with improved hepatic energy metabolism via regulating AMPK signaling pathway and reduced liver inflammation via modulating TLR4 and NOD signaling pathways. These findings contribute to developing new interventions to ameliorate liver injury and dysfunction in animals and humans with exposure to endotoxin.

Data Availability

The data used to support the findings of this study are available from the corresponding author upon request.

Conflicts of Interest

The authors declare that they have no conflict of interest.

Authors' Contributions

Yehui Duan and Bo Song contributed equally to this study.

Acknowledgments

This study was jointly supported by the National Natural Science Foundation of China (31802077, U19A2037, and 31972582); the Training Program for Excellent Young Innovators of Changsha (kq2009020); the Natural Science Foundation of Guangxi Province (2020JJA130102 and 2018JJB130239); Special Funds for the Construction of Innovative Provinces in Hunan Project (2019NK2193 and 2019RS3022); the Earmarked Fund for China Agriculture Research System (CARS-35); the "Strategic Priority Research Program" of the Chinese Academy of Sciences (XDA24030204); Fuyang Normal University Undertakes Fuyang Science and Technology Project (SXHZ202007); and Open Fund of Key Laboratory of Agro-ecological Processes in Subtropical Region, Chinese Academy of Sciences (ISA2020203 and ISA2020204).

Supplementary Materials

Supplementary Table 1: composition and nutrient levels of the diets (air-dried basis, %). (*Supplementary Materials*)

References

- [1] D. Zhao, T. Wu, D. Yi et al., "Dietary supplementation with *Lactobacillus casei* alleviates lipopolysaccharide-induced liver injury in a porcine model," *International Journal of Molecular Sciences*, vol. 18, no. 12, p. 2535, 2017.
- [2] P. Kang, Y. Liu, H. Zhu et al., "The effect of dietary asparagine supplementation on energy metabolism in liver of weaning pigs when challenged with lipopolysaccharide," *Asian-Australian Journal of Animal Sciences*, vol. 31, no. 4, pp. 548–555, 2018.
- [3] J.-H. Chen, G.-F. Yu, S.-Y. Jin et al., "Activation of $\alpha 2$ adrenoceptor attenuates lipopolysaccharide-induced hepatic injury," *International Journal of Clinical and Experimental Pathology*, vol. 8, no. 9, pp. 10752–10759, 2015.
- [4] J. L. Lai, Y. H. Liu, C. Liu et al., "Indirubin inhibits LPS-induced inflammation via TLR4 abrogation mediated by the NF- κ B and MAPK signaling pathways," *Inflammation*, vol. 40, no. 1, pp. 1–12, 2017.
- [5] J. Zhang, X. Xu, H. Zhu, Y. Wang, Y. Hou, and Y. Liu, "Dietary fish oil supplementation alters liver gene expressions to protect against LPS-induced liver injury in weanling piglets," *Innate Immunity*, vol. 25, no. 1, pp. 60–72, 2019.
- [6] L. Wang, Y. Q. Hou, D. Yi et al., "Dietary supplementation with glutamate precursor α -ketoglutarate attenuates lipopolysaccharide-induced liver injury in young pigs," *Amino Acids*, vol. 47, no. 7, pp. 1309–1318, 2015.
- [7] P. Kang, Y. Liu, H. Zhu et al., "The effect of aspartate on the energy metabolism in the liver of weanling pigs challenged with lipopolysaccharide," *European Journal of Nutrition*, vol. 54, no. 4, pp. 581–588, 2015.
- [8] D. Yi, Y. Hou, L. Wang et al., "Dietary N-acetylcysteine supplementation alleviates liver injury in lipopolysaccharide-challenged piglets," *The British Journal of Nutrition*, vol. 111, no. 1, pp. 46–54, 2014.
- [9] Y. O. Song, M. Kim, M. Woo et al., "Chondroitin sulfate-rich extract of skate cartilage attenuates lipopolysaccharide-

- induced liver damage in mice,” *Marine Drugs*, vol. 15, no. 6, p. 178, 2017.
- [10] Y. Duan, F. Li, Y. Li et al., “The role of leucine and its metabolites in protein and energy metabolism,” *Amino Acids*, vol. 48, no. 1, pp. 41–51, 2016.
- [11] M. Holecek, “Beta-hydroxy-beta-methylbutyrate supplementation and skeletal muscle in healthy and muscle-wasting conditions,” *Journal of Cachexia, Sarcopenia and Muscle*, vol. 8, no. 4, pp. 529–541, 2017.
- [12] Y. Duan, C. Zheng, Y. Zhong et al., “Beta-hydroxy beta-methyl butyrate decreases muscle protein degradation via increased Akt/FoxO3a signaling and mitochondrial biogenesis in weanling piglets after lipopolysaccharide challenge,” *Food & Function*, vol. 10, no. 8, pp. 5152–5165, 2019.
- [13] C. Zheng, B. Song, Y. Duan et al., “Dietary β -hydroxy- β -methylbutyrate improves intestinal function in weaned piglets after lipopolysaccharide challenge,” *Nutrition*, vol. 78, p. 110839, 2020.
- [14] B. Lattanzi, M. Giusto, C. Albanese et al., “The effect of 12 weeks of β -hydroxy- β -methyl-butyrate supplementation after liver transplantation: a pilot randomized controlled study,” *Nutrients*, vol. 11, no. 9, p. 2259, 2019.
- [15] M. H. Sharawy, M. S. El-Awady, N. Megahed, and N. M. Gameil, “The ergogenic supplement β -hydroxy- β -methylbutyrate (HMB) attenuates insulin resistance through suppressing GLUT-2 in rat liver,” *Canadian Journal of Physiology and Pharmacology*, vol. 94, no. 5, pp. 488–497, 2016.
- [16] P. Puiman and B. Stoll, “Animal models to study neonatal nutrition in humans,” *Current Opinion in Clinical Nutrition and Metabolic Care*, vol. 11, no. 5, pp. 601–606, 2008.
- [17] C. A. Merrifield, M. Lewis, S. P. Claus et al., “A metabolic system-wide characterisation of the pig: a model for human physiology,” *Molecular BioSystems*, vol. 7, no. 9, pp. 2577–2588, 2011.
- [18] NRC, *Nutrient Requirements of Swine (eleventh revised edition)*, National Academic Press, Washington, DC, 2012.
- [19] Q. Li, Y. Liu, Z. Che et al., “Dietary L-arginine supplementation alleviates liver injury caused by *Escherichia coli* LPS in weaned pigs,” *Innate Immunity*, vol. 18, no. 6, pp. 804–814, 2012.
- [20] Y. Duan, Y. Duan, F. Li et al., “Effects of supplementation with branched-chain amino acids to low-protein diets on expression of genes related to lipid metabolism in skeletal muscle of growing pigs,” *Amino Acids*, vol. 48, no. 9, pp. 2131–2144, 2016.
- [21] Y. H. Duan, F. N. Li, B. E. Tan et al., “Myokine interleukin-15 expression profile is different in suckling and weaning piglets,” *Animal Nutrition*, vol. 1, no. 1, pp. 30–35, 2015.
- [22] Y. Li, F. Li, L. Wu et al., “Effects of dietary protein restriction on muscle fiber characteristics and mTORC1 pathway in the skeletal muscle of growing-finishing pigs,” *Journal of Animal Science and Biotechnology*, vol. 7, no. 1, p. 47, 2016.
- [23] Y. Duan, F. Li, L. Li, J. Fan, X. Sun, and Y. Yin, “n-6:n-3 PUFA ratio is involved in regulating lipid metabolism and inflammation in pigs,” *The British Journal of Nutrition*, vol. 111, no. 3, pp. 445–451, 2014.
- [24] F. Li, Y. Li, Y. Tang et al., “Protective effect of myokine IL-15 against H₂O₂-mediated oxidative stress in skeletal muscle cells,” *Molecular Biology Reports*, vol. 41, no. 11, pp. 7715–7722, 2014.
- [25] N. J. Fernandez and B. A. Kidney, “Alkaline phosphatase: beyond the liver,” *Veterinary Clinical Pathology*, vol. 36, no. 3, pp. 223–233, 2007.
- [26] P. D. Currie and D. T. Sullivan, “Structure and expression of the gene encoding phosphofructokinase (PFK) in *Drosophila melanogaster*,” *The Journal of Biological Chemistry*, vol. 269, no. 40, pp. 24679–24687, 1994.
- [27] M. J. MacDonald, L. J. Brown, M. J. Longacre, S. W. Stoker, M. A. Kendrick, and N. M. Hasan, “Knockdown of both mitochondrial isocitrate dehydrogenase enzymes in pancreatic beta cells inhibits insulin secretion,” *Biochimica et Biophysica Acta (BBA) - General Subjects*, vol. 1830, no. 11, pp. 5104–5111, 2013.
- [28] X. Zhao, J. W. Zmijewski, E. Lorne et al., “Activation of AMPK attenuates neutrophil proinflammatory activity and decreases the severity of acute lung injury,” *American Journal of Physiology. Lung Cellular and Molecular Physiology*, vol. 295, no. 3, pp. L497–L504, 2008.
- [29] X. Zhang, G. Barile, S. Chang et al., “Apoptosis and cell proliferation in proliferative retinal disorders: PCNA, Ki-67, caspase-3, and PARP expression,” *Current Eye Research*, vol. 30, no. 5, pp. 395–403, 2009.
- [30] S. Sakao, L. Taraseviciene-Stewart, J. D. Lee, K. Wood, C. D. Cool, and N. F. Voelkel, “Initial apoptosis is followed by increased proliferation of apoptosis-resistant endothelial cells,” *The FASEB Journal*, vol. 19, no. 9, pp. 1178–1180, 2005.
- [31] R. Schulte-Hermann, W. Bursch, B. Kraupp-Grasl, F. Oberhammer, A. Wagner, and R. Jirtle, “Cell proliferation and apoptosis in normal liver and preneoplastic foci,” *Environmental Health Perspectives*, vol. 101, Suppl 5, pp. 87–90, 1993.
- [32] W. Leng, Y. Liu, H. Shi et al., “Aspartate alleviates liver injury and regulates mRNA expressions of TLR4 and NOD signaling-related genes in weaned pigs after lipopolysaccharide challenge,” *The Journal of Nutritional Biochemistry*, vol. 25, no. 6, pp. 592–599, 2014.
- [33] F. Chen, Y. Liu, H. Zhu et al., “Fish oil attenuates liver injury caused by LPS in weaned pigs associated with inhibition of TLR4 and nucleotide-binding oligomerization domain protein signaling pathways,” *Innate Immunity*, vol. 19, no. 5, pp. 504–515, 2013.
- [34] G. Kanuri, A. Spruss, S. Wagnerberger, S. C. Bischoff, and I. Bergheim, “Role of tumor necrosis factor α (TNF α) in the onset of fructose-induced nonalcoholic fatty liver disease in mice,” *The Journal of Nutritional Biochemistry*, vol. 22, no. 6, pp. 527–534, 2011.
- [35] O. Takeuchi and S. Akira, “Pattern recognition receptors and inflammation,” *Cell*, vol. 140, no. 6, pp. 805–820, 2010.
- [36] L. O. Moreira and D. S. Zamboni, “NOD1 and NOD2 signaling in infection and inflammation,” *Frontiers in Immunology*, vol. 3, p. 328, 2012.
- [37] J. R. Townsend, M. S. Fragala, A. R. Jajtner et al., “ β -Hydroxy- β -methylbutyrate (HMB)-free acid attenuates circulating TNF- α and TNFR1 expression postresistance exercise,” *Journal of Applied Physiology*, vol. 115, no. 8, pp. 1173–1182, 2013.

Research Article

Gut Immunity and Microbiota Dysbiosis Are Associated with Altered Bile Acid Metabolism in LPS-Challenged Piglets

Xiao Xiao ^{1,2}, Yuanzhi Cheng,^{1,2} Jie Fu,^{1,2} Zeqing Lu,^{1,2} Fengqin Wang,^{1,2} Mingliang Jin,^{1,2} Xin Zong ^{1,2} and Yizhen Wang ^{1,2}

¹National Engineering Laboratory of Biological Feed Safety and Pollution Prevention and Control, Zhejiang University, Hangzhou 310058, China

²Key Laboratory of Animal Nutrition and Feed Science in Eastern China, Ministry of Agriculture, Zhejiang University, Hangzhou 310058, China

Correspondence should be addressed to Xin Zong; zongxin@zju.edu.cn and Yizhen Wang; yzwang321@zju.edu.cn

Received 19 December 2020; Revised 8 March 2021; Accepted 12 March 2021; Published 26 March 2021

Academic Editor: Si Qin

Copyright © 2021 Xiao Xiao et al. This is an open access article distributed under the Creative Commons Attribution License, which permits unrestricted use, distribution, and reproduction in any medium, provided the original work is properly cited.

Bacterial infections are among the major factors that cause stress and intestinal diseases in piglets. Lipopolysaccharide (LPS), a major component of the Gram-negative bacteria outer membrane, is commonly employed for inducing an immune response in normal organisms for convenience. The association between LPS stimulation and gut immunity has been reported. However, the effects of gut immunity on microbial homeostasis and metabolism of host, especially bile acid and lipid metabolism in piglets, remain unclear. Hence, in the current study, we elucidated the effect of gut immunity on microbial balance and host metabolism. Twenty-one-day-old healthy piglets (male) were randomly assigned into the CON and LPS groups. After 4 hours of treatment, related tissues and cecal contents were obtained for further analysis. The obtained results showed that stimulated LPS considerably damaged the morphology of intestinal villi and enhanced the relative expression of proinflammatory cytokines. Besides, LPS partially changed the microbial structure as indicated by β -diversity and increased operational taxonomic units (OTUs) related to *Oxalobacter* and *Ileibacterium*. Furthermore, bile acid, a large class of gut microbiota metabolites, was also assessed by many proteins related to the enterohepatic circulation of bile acids. It was also revealed that LPS markedly inhibited the mRNA and protein expression of TGR5 and FXR (bile acid receptors) in the ileum, which expressed negative feedback on bile acid de novo synthesis. Additionally, results indicated upregulated mRNA of genes associated with the production of bile acid in the liver tissues. Moreover, LPS reduced the expression of bile acid transporters in the ileum and liver tissues and further disturbed the normal enterohepatic circulation. Taken together, gut immunity and microbial dysbiosis are associated with altered bile acid metabolism in LPS-challenged piglets, which provided theoretical basis for revealing the potential mechanism of intestinal inflammation in swine and seeking nutrients to resist intestinal damage.

1. Introduction

The gastrointestinal tract of neonatal piglets is vulnerable to external stimuli, such as weaning, diarrhea, pathogens infection, and hostile environmental condition during the early life period [1–3]. Gut microbiota in the enteric cavity is important for the protection of the host intestine against damage [4]. The host intestine and gut microbiota remain in a steady-state condition under normal physiological conditions. During dysbiosis and intestinal injury, inflammatory bowel disease (IBD) results in a detrimental change of micro-

bial community structure, the rapid proliferation of pathogenic bacteria, and invasion of epithelial and lamina propria cells by pathogens [5, 6]. Conversely, dysregulation or imbalance of gut microbiota also leads to metabolic syndrome and many other diseases, thus affecting the host health negatively for the long term [7, 8]. The gut microbiota and metabolites considerably contribute to the crosstalk between microbiota and host homeostasis, which leads to their participation in the occurrence and development of cardiovascular diseases, host metabolism, immune responses, and energy expenditure [9–13].

Recently, microbiota-derived metabolites, including the endotoxin LPS, bile acids (BAs), trimethylamine N-oxide (TMAO), indolepropionic acid (IPA), and short-chain fatty acids (SCFAs), have attracted wider scientific attentions [11, 14–16], though SCFAs are the most common and abundant metabolites [17]. However, BAs, important endogenous molecules, have gradually been paid more attention in the field of liver diseases and intestinal inflammation [18–20]. Compared with SCFAs, BAs have been identified to be more relevant with gut microbiota in mice feeding on a high-fat diet (HFD) [21]. Studies have revealed that primary BAs synthesized in the liver can be transformed into secondary BAs by the metabolic activities of enteric anaerobic bacteria [22]. At the terminal ileum, the majority of BAs are reabsorbed by multiple protein complexes, such as ileal bile acid-binding protein (Ibapb) and apical sodium-dependent bile acid transporter (ASBT) into enterocytes [23]. This is followed by their secretion into the portal circulation via the basolateral BA transporters organic solute transporter subunit- α (OST- α), OST- β , and multidrug resistance-associated protein 2 (MRP2). BAs are then taken up by transporters into hepatocytes. The underlined procedures consist of the whole enterohepatic circulation of BA [18, 24]. BA de novo synthesis in the liver depends on the regulatory factors such as FXR and its downstream targets in the ileum and liver [23, 25]. The whole circulation of BAs effectively emulsifies and drives the fat-soluble vitamins or lipid absorption in the intestine [26, 27]. Furthermore, BAs have been reported for their participation in the development of metabolic diseases and maintenance of intestinal homeostasis [28]. However, under microbial dysbiosis, whether bile acid metabolism (biosynthesis, transport, and circulation) participates in the process of gut microbiota in regulating host immune and metabolism is not clear.

Thus, this study is aimed at systematically evaluating the role of intestinal injury in changing the gut microbial composition, disturbing the bile acid metabolism, and disturbing lipid metabolism in a piglet model. The intestinal injury model was conducted by intraperitoneal injection of LPS, and then gut immunity, microbial balance, bile acid, and lipid metabolism were measured. Our results showed that LPS stimulation in piglets resulted in the occurrence of inflammation both in the ileum and liver, and further disturbed microbial homeostasis with alteration of bile acid and lipid metabolism.

2. Materials and Methods

2.1. Animals and Experimental Treatments. The approval for each animal experiment was provided by the Animal Care and Use Committee of Zhejiang University (Hangzhou, China) and was in accordance with the institutional guidelines. A total of twenty healthy male 21-day-old piglets (Duroc \times Landrace \times Yorkshire, body weight of 7.05 ± 0.13 kg) were purchased and then randomly assigned into two groups ($n = 10$ per treatment). Piglets were injected intraperitoneally with phosphate-buffered solution (PBS, the equivalent volume to LPS) or LPS (10 mg/kg body weight). Then

after 4 h, the piglets were slaughtered, followed by the collection of samples for further evaluation.

2.2. Sample Collection and Processing. After 4 h treatment with LPS, piglets were sacrificed. The distal ileum was fixed in 4% paraformaldehyde, while the freezing of the remaining ileum, whole colon, and liver tissues was carried out in liquid nitrogen, followed by their storage at -80°C until analysis. Fresh cecal contents from each individual were collected into sterile plastic tubes and then frozen in liquid nitrogen, followed by storage at -80°C until DNA extraction.

2.3. Intestinal Morphology. For distal ileum histological analyses, formalin-fixed and paraffin-embedded tissues were cut into thick ($4\ \mu\text{m}$) sections, followed by slicing as well as staining with haematoxylin and eosin (H&E). Leica DM3000 Microsystem was used for obtaining the images of the slices. Next, the height of the villi and the depth of the crypt were evaluated by Image-Pro Plus software (IPP; produced by Media Cybernetics Corporation, USA).

2.4. RNA Extraction and Real-Time Quantitative PCR (q-PCR) Analysis. TRIzol reagent (Invitrogen, USA) was used for the extraction of total RNA, as suggested by our earlier protocol [29, 30]. NanoDrop 2000 (Thermo Fisher Scientific, Waltham, USA) was employed for evaluating the purity as well as the concentration of the RNA. Next, cDNA was synthesized from RNA ($2\ \mu\text{g}$) by RevertAid RT Reverse Transcription Kit (Thermo Fisher Scientific, Waltham). q-PCR was conducted with FastStart Universal SYBR Green master mix (Roche, Mannheim, Germany) via StepOnePlus Real-Time PCR system (Applied Biosystems, Foster City, USA). Table 1 shows gene-specific primers for q-PCR. The reference gene β -actin was used as an internal control. Each sample was run in triplicate, and the $2^{-\Delta\Delta\text{Ct}}$ method was employed for evaluating relative mRNA expression of the target gene.

2.5. Western Blot Analysis. Total Protein Extraction Kit was used for the extraction of total proteins of the ileum and colon, followed by determining the concentration of proteins by Standard BCA Protein Assay Kit. The underlined kits were procured from Keygen Biotech (Nanjing, China). Western blotting was used for evaluating the expression level of proteins [29, 30]. Briefly, the separation of proteins (in equal amounts) was carried out by an SDS-PAGE, followed by transferring into a PVDF membrane (Millipore, USA). Then, skimmed milk (5%) was used for membrane blockage for 60 min at $\sim 25^{\circ}\text{C}$ and then overnight incubated with appropriate primary antibodies for iNOS (1:1000, Proteintech, China), FXR (1:4000, Abcam, USA), TGR5 (1:4000, Abcam, USA), and β -actin (1:5000, Abcam, USA) at 4°C . After washing with TBST, membranes were incubated with secondary antibodies (1:5000, EarthOx, USA) for 1 h at room temperature. Chemiluminescence detection was performed using an ECL luminescence reagent (Biosharp, Hangzhou, China) according to the manufacturer's instructions. Specific bands were detected, analyzed, and quantified by ImageJ software (NIH, Bethesda, MD, USA).

TABLE 1: Primer sequences for q-PCR.

Gene	Primer sequence (5' → 3')	GenBank number
ACACA	Forward: TGGACAGGGCTCTTACCTGT Reverse: GAGACCAGTGAAGGCTGCTT	XM_021066229.1
Acs11	Forward: GTCCTTCCTCCGATGATACTCTG Reverse: GGACCACAGGGAAGATGGTG	NM_001167629.2
ASBT	Forward: CCAGAGTGCCTGGATCATCG Reverse: GGAGTAACCGGCCAAAGGAA	NM_001244463.1
β -Actin	Forward: GAAGCTGTGATGGACGCAGG Reverse: CCTGGAGAGGTTACCCGGAA	XM_021086047.1
BSEP	Forward: CGCAGCGTGAAGAAATGTGG Reverse: AACCGAAACAGTTGAAAGAGGC	XM_003133457.5
CD36	Forward: TAGGAATCCCCTGCCTCAC Reverse: GCTTCAAGTGCTGGGTCAAA	NM_001044622.1
CPT1A	Forward: TGGTGTCCAAATACCTCGCC Reverse: GATAATCGCCACGGCTCAGA	NM_001129805.1
CYP27A1	Forward: GAGGGCAAGTACCCAGTACG Reverse: TGA CTCTCCTTCCGTGGTGA	NM_001243304.1
CYP7A1	Forward: CCGCTTCTGATACCTGTGGA Reverse: GGTTTGCTCGGAGGAACTCA	NM_001005352.3
CYP8B1	Forward: CAAGTTCGACCGCATGTTCC Reverse: TTATGCCGTGCCTCTCCAAG	NM_214426.1
Dbi	Forward: GCCACTACAAACAAGCGACC Reverse: TTGGAAGTCCCTTTAGCCC	NM_214119.1
FABP5	Forward: AGGCACCAGTCCGCTTATTC Reverse: TTTTCGTAGGGCCATTCCCAC	NM_001039746.2
FASN	Forward: CGTTGGGTCGACTCACTGAA Reverse: GAGACAGTTCACCATGCCCA	NM_001099930.1
FATP4	Forward: CAGAGTGGCTGTGCTTCCG Reverse: GGTTACCAACCTCCCAGCAAG	XM_021069619.1
FGF19	Forward: TGAGTACCGTGGCGATCAAG Reverse: GCGGATCTCCTCCTCGAAAG	XM_003122420.3
FGFR4	Forward: CCAGGAGTTCCTTGCTTCTC Reverse: GCGACTACCTCCTTGTAAC	XM_013987555.2
FXR	Forward: TGAGCTTTGTGTCGTTTCCG Reverse: ACATTCAGCCAACATTCCCATC	NM_001287412.1
IBABP	Forward: GCGACATAGAGACCATCGGG Reverse: GTAGTTGGGGCTGTTACCA	NM_214215.2
IL-10	Forward: GGGTGTGCCCTATGGTGTTT Reverse: GGGTGGGTAGGCTTGGAATG	NM_214041.1
IL-1 β	Forward: CCAGCCAGTCTTCATTGTTCA Reverse: GCTGGATGCTCCCATTTCTC	NM_214055.1
IL-6	Forward: ACAAAGCCACCACCCCTAAC Reverse: CGTGGACGGCATCAATCTCA	NM_214399.1
KLB	Forward: ATCGACGACCAGTCTCTGGA Reverse: TGACTTTATCAAGCAGGTGTGC	XM_003482367.4
L-FABP	Forward: CATCACTACCGGGTCCAAGG Reverse: TTCTCCCCAGTCAGGGTCTC	NM_001004046.2
LPL	Forward: CAGCCCTGGCTTTGCTATTGA Reverse: GACTCCACGTGCTGTTCCCTC	NM_214286.1
LRH-1	Forward: CGAAGAGCTCTGTCCCTTACTGTC Reverse: GTCCATTGGCTCGGATGAGG	NM_001267893.1
MDR3	Forward: AAACCGGGTGTCTCAGACT Reverse: TCGGGGAGATCGACCAGATT	XM_021063468.1
MRP2		XM_021073710.1

TABLE 1: Continued.

Gene	Primer sequence (5' → 3')	GenBank number
MRP3	Forward: GGCTACTCCTGCGTGTCTT Reverse: TCCTCAGCAACATCCCACAC	XM_003131575.6
	Forward: GGTTGGAAGGCCACCGTTTT Reverse: GTGTGCAAGGACAGGTTGGA	
NOS2	Forward: TTGAATCTGGGTGAAGAGCCC Reverse: GCGGTGAAAGTGTGTCTTGGA	NM_001143690.1
	Forward: TTCCTGCACCATAGGCATC Reverse: CGAGCATTGAGGCGGAAAAG	
NTCP	Forward: CAGAAGATCCATCAGAGTGTGTGA Reverse: GTGTTACCCGATCCAGTGTCA	XM_001927695.5
	Forward: GACGGAGCCAGAAGGAAAGAC Reverse: CAGACGGAGGGGATGCTGTA	
OST- α	Forward: GCGTGTGCTAAATGCAGAG Reverse: GTTTTCCACACGGCTGTCAC	NM_001244266.1
	Forward: GAAGTACGGCGTCTACGAGG Reverse: CGCACCAAATGATAGCAGCC	
OST- β	Forward: TGCTGCCTGGAGTCCTTATG Reverse: ACAGGGCGAAAGAAGAGGTC	XM_003127720.4
	Forward: GAGCCGCCCTTCACAGAG Reverse: GTCTTCGATGTCGGTCAGCA	
PPAR- α	Forward: GAGAGCCTCAACTTCCCTCC Reverse: CCATGTCGATGGTCTTGCAG	NM_214015.2
	Forward: AGATTAGCTGAGCGGTAGCAGG Reverse: CCATGGCTTGCCATCAAGGT	
SHP	Forward: CGACTCAGTGCCGAGATCAA Reverse: CTCACAGGGCAATGATCCCA	NM_214022.1
	Forward: GAGAGCCTCAACTTCCCTCC Reverse: CCATGTCGATGGTCTTGCAG	
SREBF1	Forward: GAGAGCCTCAACTTCCCTCC Reverse: CCATGTCGATGGTCTTGCAG	XM_013984487.2
	Forward: AGATTAGCTGAGCGGTAGCAGG Reverse: CCATGGCTTGCCATCAAGGT	
TGF- β	Forward: CGACTCAGTGCCGAGATCAA Reverse: CTCACAGGGCAATGATCCCA	XM_013984487.2
	Forward: GAGAGCCTCAACTTCCCTCC Reverse: CCATGTCGATGGTCTTGCAG	
TGR5	Forward: CGACTCAGTGCCGAGATCAA Reverse: CTCACAGGGCAATGATCCCA	NM_214022.1
	Forward: GAGAGCCTCAACTTCCCTCC Reverse: CCATGTCGATGGTCTTGCAG	
TNF- α	Forward: GAGAGCCTCAACTTCCCTCC Reverse: CCATGTCGATGGTCTTGCAG	XM_013984487.2
	Forward: AGATTAGCTGAGCGGTAGCAGG Reverse: CCATGGCTTGCCATCAAGGT	

2.6. *Microbiota Analysis Based on 16S rRNA High-Throughput Sequencing.* Genomic DNA of cecal contents was extracted using a DNA kit (TIANGEN Biotech Co. Ltd., Beijing, China) according to the manufacturer's instructions. The NanoDrop 2000 was used for evaluating the concentration as well as purity of the extracted genomic DNA. The integrity of genomic DNA was determined by electrophoresis on 1% (*w/v*) agarose gels. Then, the DNA samples were sent to Majorbio Bio-pharm Technology (Shanghai, China) to perform amplicon pyrosequencing on the Illumina MiSeq platform. The distinct V3-V4 regions of the 16S rRNA genes were amplified by PCR with specific primers 338F (5'-ACTCCTACGGGAGGCA GCAG-3') and 806R (5'-GGACTACHVGGGTWTCTA AT-3'). The clean sequences were assigned to the same operational taxonomic units (OTUs) with $\geq 97\%$ similarity. The data was analyzed on the free online platform of Majorbio Cloud Platform (<https://cloud.majorbio.com/>). Alpha diversity, including Shannon, Simpson, Sobs, Ace, Chao1, and Coverage, was calculated to reflect the bacterial diversity and richness. Beta diversity on unweighted UniFrac was calculated based on OTU level. UniFrac-based principal component analysis (PCA) and principal coordinate analysis (PCoA) were performed to get principal coordinates and visualized from complex data. Dissimilarity in community structure between samples was calculated by nonmetric

dimensional scaling (NMDS). The relative abundance of microbiota was examined at different taxonomic levels. The relative abundance of significant differences in family, genus, species, and OTU levels was calculated by the Wilcoxon rank sum test.

2.7. *Statistical Analysis.* The obtained results were represented as the mean \pm SEM. GraphPad Prism version 8.0 (San Diego, USA) was used for statistical analysis. Statistical significance was assessed by a two-tailed Student's *t*-test or Wilcoxon rank sum test. $P < 0.05$ was considered statistically considerable.

3. Results

3.1. *Intestinal Inflammation in Piglets after LPS Stimulation.* LPS is the endotoxin portion of the Gram-negative bacterial cell wall [31] and is the most abundant proinflammatory stimulus in the gastrointestinal tract. In the current study, LPS was used to induce immune responses in piglets. As shown in Figures 1(a) and 1(b), LPS stimulation considerably decreased villi height and the ratio of villi height : crypt depth (VCR) of the ileum, which showed elevated histological destruction of the ileum (caused by LPS). For further analysis, mRNA expressions of proinflammatory cytokines in the ileum and colon were also measured. The obtained results

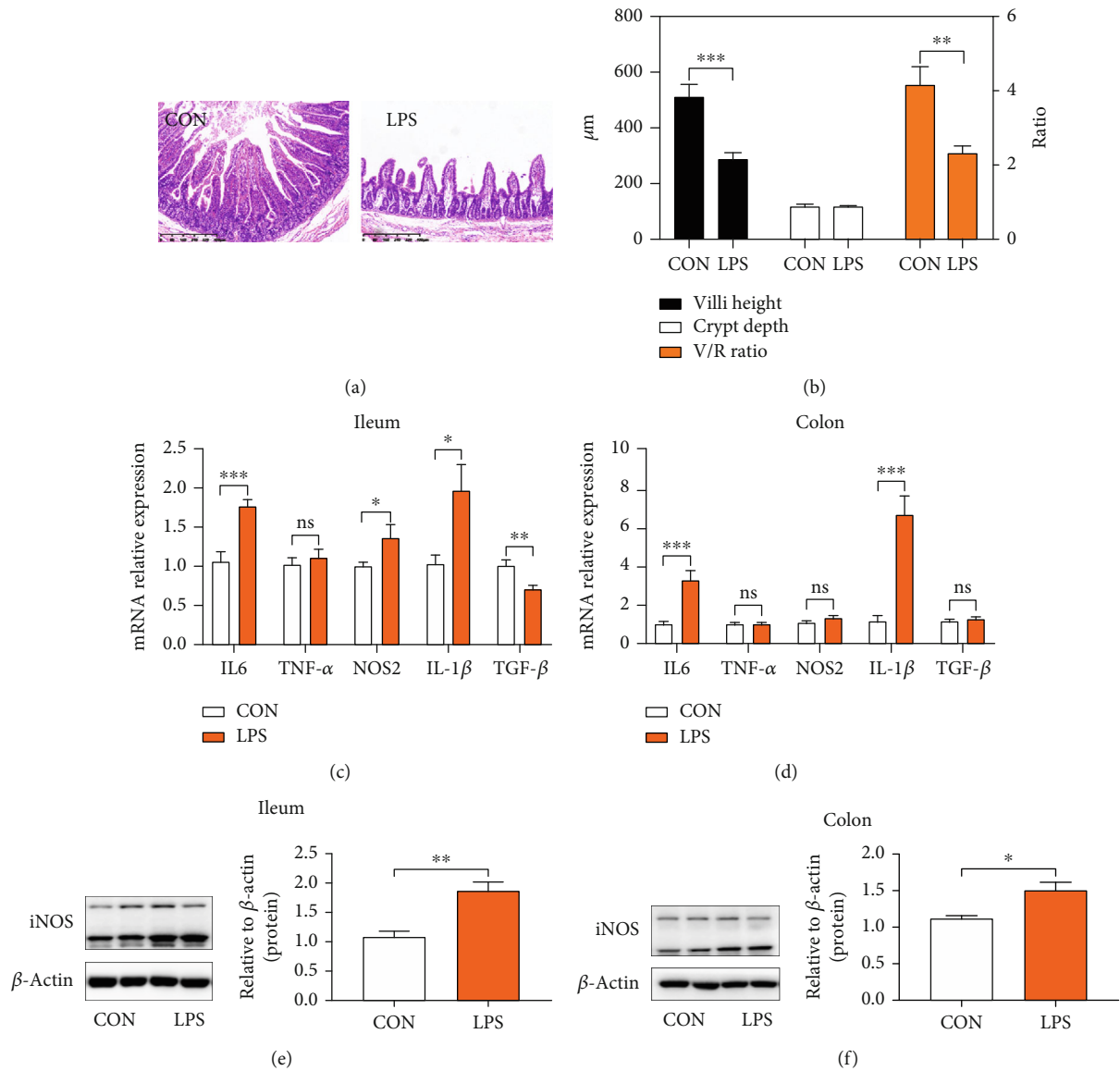


FIGURE 1: Intestinal inflammation occurred in piglets after LPS stimulation. (a) Representative H&E staining images of the distal ileum. (b) Villi height; crypt depth; the ratio of villi height : crypt depth (VCR). (c) q-PCR results of cytokine expression in the ileum. Expression was normalized to β -actin. (d) q-PCR results of cytokine expression in the colon. Expression was normalized to β -actin. (e) Immunoblot analysis of total protein extracts from piglets' ileum tissue samples. (f) Immunoblot analysis of total protein extracts from piglets' colon tissue samples. iNOS: inducible nitric oxide synthase. * $P < 0.05$, ** $P < 0.01$, *** $P < 0.001$, and **** $P < 0.0001$ were regarded as statistically significant.

revealed that the LPS challenge considerably elevated the expression of IL-6, NOS2, and IL-1 β , and lowered the expression level of anti-inflammatory cytokines such as TGF- β in the ileum, as depicted in Figure 1(c). Furthermore, LPS enhanced the expression of IL-1 β and IL-6 in the colon, as shown in Figure 1(d). To verify the occurrence of intestinal inflammation, the protein level of proinflammatory inducible nitric oxide synthase (iNOS), the enzyme responsible for nitric oxide (NO) production, was also detected and the obtained results revealed that the expression of iNOS in the LPS group was considerably elevated in the ileum and colon, as shown in Figures 1(e) and 1(f). Taken together, LPS stim-

ulation successfully induced intestinal inflammation and harmed the gut immunity of piglets.

3.2. The Variations of Gut Microbiota between Noninflammatory and Inflammatory Piglets. It has been reported in the literature that intestinal inflammation is usually accompanied by microbiota dysbiosis [32–34]. The above results showed that LPS resulted in severe inflammatory responses in the gastrointestinal tract. Whether it damages the balance of gut microbiota is unclear. Therefore, it is important to identify the differences that exist in the gut microbial richness and populations between different subject

TABLE 2: The microbial alpha diversity based on whole OTU table in the cecal contents of piglets challenged with LPS.

Items	CON	LPS	P value
Shannon	3.2765 ± 0.3300	3.1117 ± 0.6580	>0.9999
Simpson	0.0949 ± 0.0284	0.1418 ± 0.1081	>0.9999
Sobs	250.2000 ± 29.9370	244.8000 ± 27.7070	0.9975
Ace	303.3700 ± 34.3760	296.9600 ± 15.9010	0.9937
Chao1	304.3800 ± 34.2980	304.2200 ± 16.3850	>0.9999
Coverage	0.9980 ± 0.0002	0.9980 ± 0.0002	>0.9999

Data is presented as the mean ± SEM ($n = 6$). All numbers were unified as 0.0000. P values are from the Wilcoxon rank sum test.

groups. 16S sequencing of cecal contents was profiled to evaluate the dynamic changes in gut microbiota. Alpha diversity index is an important indicator of species diversity and richness. Among which the coverage index, a marker of sequencing depth, indicated that the data met the requirements of subsequent analysis (Table 2). Moreover, results in Table 2 demonstrated that the species diversity and richness were not affected as assessed by Shannon, Simpson, Sobs, Ace, and Chao1 index between the CON and LPS groups. Furthermore, the structure of microbial composition was analyzed. Among various methods, the principal component analysis (PCA) and the principal coordinate analysis (PCoA) are predominant. PCA and PCoA based on unweighted UniFrac metrics showed partially distinct clustering of intestinal microbe communities of each group (Figure 2(a)). In addition, nonmetric multidimensional scaling (NMDS) ordination performed on the Bray-Curtis dissimilarity also showed that the bacterial community profiles from LPS-treated piglets were partly separated from those of samples in the CON group (Figure 2(a)). The underlined results indicated that LPS treatment leads to the change of gut microbiota structure.

The relative abundance of bacteria was further evaluated at various levels; a detailed phylogenetic analysis of the taxonomic composition of the microbiome based on OTU was conducted. At the phylum level, a total of 14 phyla were shared by piglets from all groups, and six bacteria had relative abundance exceeding 1% in at least one sample: *Firmicutes*, *Bacteroidetes*, *Synergistota*, *Proteobacteria*, *Actinobacteriota*, and *Desulfobacterota*. As shown in Figure 2(b), the major phyla in all piglets were *Firmicutes* and *Bacteroidetes*; these findings are in good agreement with other reported studies [35]. In detail, the relative abundance of *Firmicutes* (86.31%) in the CON group was slightly decreased to *Firmicutes* (82.06%) in the LPS group, while the relative abundance of *Bacteroidetes* (8.24%) in the CON group was slightly increased to *Bacteroidetes* (13.14%) in the LPS group, resulting in a lower *Firmicutes*-*Bacteroidetes* ratio. Surprisingly, there were no significant differences in the top 10 at family and genus levels between the CON group and the LPS group (Figures 2(c) and 2(d)).

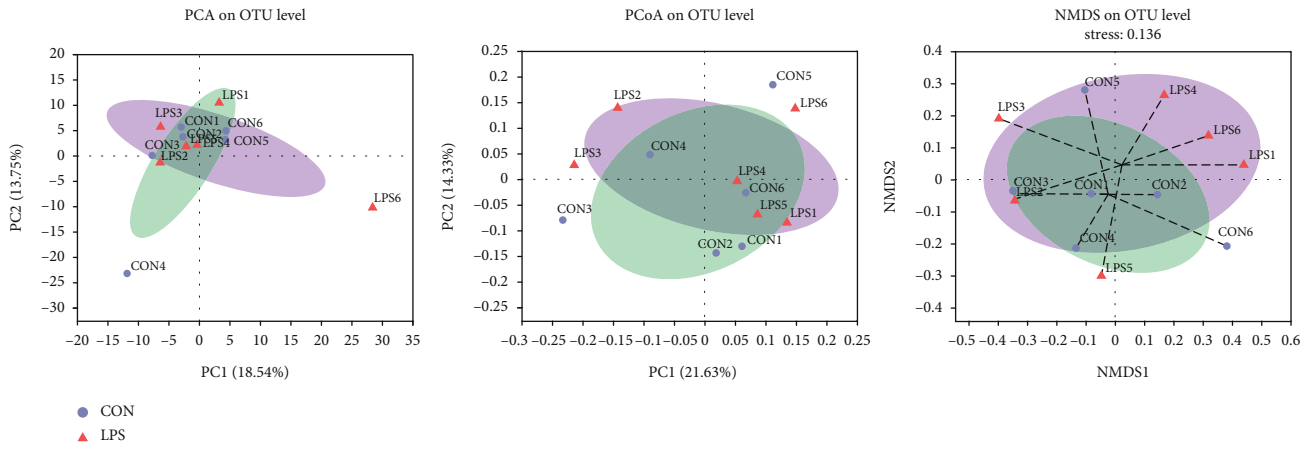
Nonetheless, variations in the microbial composition of both groups were further explored. Statistical figures revealed

the relative abundance of significant differences on family, genus, species, and OTU levels. As shown in Figure 3(a), only *Oxalobacteraceae*, a family in the subclass of *Betaproteobacteria*, was upregulated by the LPS challenge. Among all genera, *Oxalobacter* and *Ileibacterium* were significantly expanded in LPS-treated piglets (Figure 3(b)). Concretely, the relative abundance of *Oxalobacter formigenes* and *Ileibacterium valens* at the species level was upregulated in the LPS group (Figure 3(c)). The Wilcoxon rank sum test based on OTU level revealed that OTU131 (*Rikenellaceae RC9 gut group*) was dramatically downregulated, while OTU225 (*Oxalobacter formigenes*) and OTU332 (*Ileibacterium valens*) were increased by LPS stimulation (Figure 3(d)). The above results indicated that LPS treatment resulted in a reshuffling of the microbiota communities.

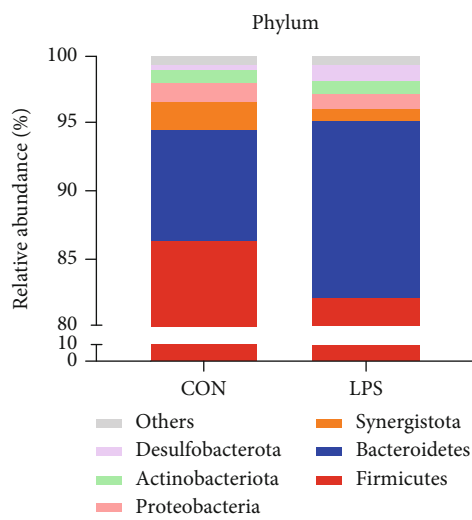
3.3. Microbiota Dysbiosis Results in the Disturbance of Bile Acid Enterohepatic Circulation. The gut microbiota regulates host immunity and metabolism through abundant microbial metabolites [4, 9, 11, 36], among which SCFAs and bile acids are the most common metabolites [17]. To the best of our knowledge, bile acids have been synthesized from cholesterol in the liver [21, 25, 37], then further metabolized by the gut microbiota, and moved through enterohepatic circulation [24, 38]. Thus, proteins associated with enterohepatic circulation were evaluated for the measurement of the underlined process. As depicted in Figure 4(a), LPS stimulation considerably attenuated the protein expression of two important BA receptors, as farnesoid X receptor (FXR) and G protein-coupled bile acid receptor 1 (GPBAR1, also called TGR5). Meanwhile, mRNA expression of the underlined receptors further validated the harmful effect of LPS on the metabolism of bile acid, as depicted in Figure 4(a).

In addition, bile acids activate FXR in enterocytes to induce the expression level of its downstream targets, *i.e.*, small heterodimer partner (SHP) and fibroblast growth factor 19 (FGF19, swine FGF19, and mouse FGF15 are homologous). The obtained results revealed a low expression level of TGR, FXR, and FGF19 in the piglets exposed to LPS, as shown in Figure 4(b). However, the expression of SHP was not affected. The underlined results suggested that LPS stimulation reduced the concentration of BAs in the ileum. Furthermore, BA-binding proteins and transporters in the ileum, such as ASBT, OST- α , OST- β , and Ibabp, were significantly inhibited by LPS, while the obvious variations were not observed in MRP2, as depicted in Figure 4(c), which results in decreasing of BAs transferring across the enterocyte for entering into the portal vein, thus disrupting enterohepatic circulation and further inducing BA de novo synthesis.

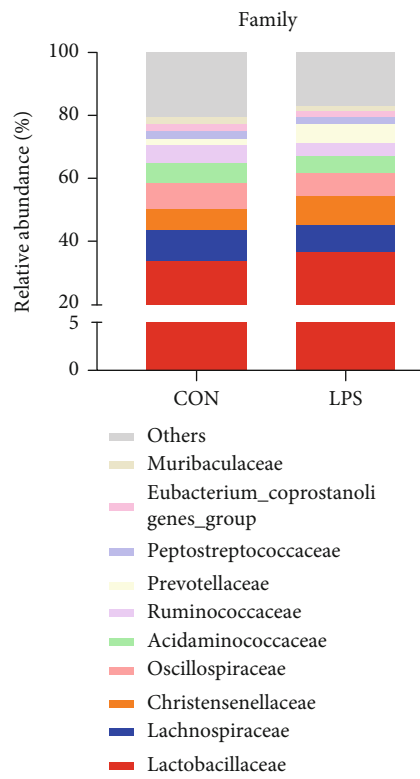
To check the variation of bile acids in the liver, genes associated with the synthesis and transportation of BA were also evaluated. The obtained results revealed that LPS administration considerably decreased the mRNA expression of FXR and its downstream targets, *i.e.*, SHP and liver receptor homolog-1 (LRH-1), as shown in Figure 5(a). Decreased ileal FGF19 indeed led to a lower level of FGF receptor 4 (FGFR4)/ β -Klotho (KLB) heterodimer complex (Figure 5(a)). FXR in the ileum and liver cooperated to



(a)



(b)



(c)

FIGURE 2: Continued.

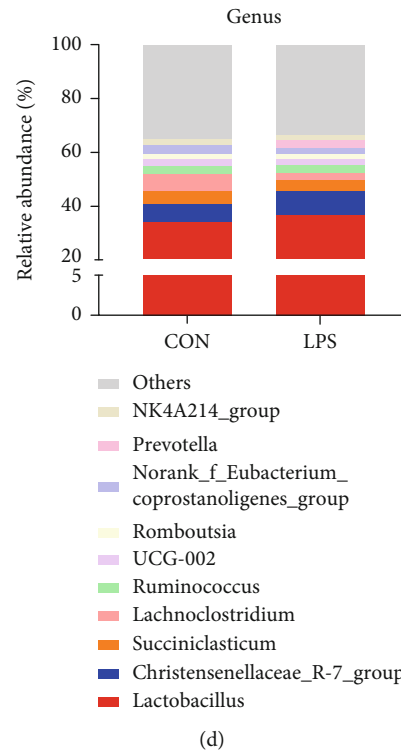


FIGURE 2: LPS changed the composition and structure of piglet's gut microbiota in the cecal contents. (a) The microbial beta diversity was accessed by principal component analysis (PCA), principal coordinate analysis (PCoA), and nonmetric multidimensional scaling (NMDS) analysis based on the OTU table. (b) Relative abundance > 1% of bacterial phyla. (c) Relative abundance of the top 10 families. (d) Relative abundance of the top 10 genera.

regulate BA de novo synthesis. CYP7A1 and CYP8B1 are the hepatic genes required for primary BA synthesis, and the obtained results revealed that CYP7A1 was upregulated by LPS while CYP8B1 was not affected, as shown in Figure 5(b), which agreed with the theoretical analysis. Additionally, BA transporters were also measured in the liver. Proteins encoded by Na⁺-taurocholate cotransporting polypeptide (NTCP) and organic anion-transporting polypeptide (OATP) are transporters responsible for BA uptake at the basolateral side of the hepatocytes. Results indicated that the expression level of NTCP was suppressed by LPS, while OATP was not affected by LPS, as depicted in Figure 5(c), which further induced BA de novo synthesis. Transporters encoded by bile salt export protein (BSEP), MRP2, and ATP binding cassette subfamily B member 4 (MDR3) pump BAs into the gallbladder. Results showed that LPS notably repressed the mRNA expression of BSEP, MRP2, and MDR3 (Figure 5(c)), which leads to a reduction in the level of bile acid in the intestine. The other transporters encoded by OST- α , OST- β , and multidrug resistance-associated protein 3 (MRP3) are responsible for the export of BAs from the liver into the systemic circulation. Figure 5(c) reveals that LPS considerably elevated the mRNA expression of OST- α , thus driving the excretion of bile acids into the systemic circulation. Collectively, LPS-induced microbial dysbiosis damaged the enterohepatic circulation of BAs and increased the expenditure of BA synthesis.

3.4. Disturbance of BA Enterohepatic Circulation Is Harmful to the Normal Lipid Metabolism. The signaling of BA in the liver and intestine contributes to the regulation of lipid metabolism [39]. For example, when stimulated, bile acids were pumped from the gallbladder into the small intestine for emulsifying and solubilizing fats for absorption [40]. The above results showed that LPS stimulation broke down the BA enterohepatic circulation. Thus, whether the disturbance of BA enterohepatic circulation had negatively affected the lipid metabolism needs further investigation. Firstly, genes related to lipolysis were measured in mRNA level. As shown in Figure 6(a), piglets challenged with LPS expressed lower lipoprotein lipase (LPL) and fatty acid-binding protein 5 (Fabp5), with no effect on diazepam binding inhibitor (Dbi) in the ileum. Then, fatty acid transporters in the ileum showed seemingly controversial results, and an upregulated expression of CD36 and reduced expression of liver fatty acid-binding proteins (L-FABP) were observed (Figure 6(b)). The above results indicated that LPS inhibited lipolysis and transportation in the intestine. In addition, we also measured genes related to fatty acid synthesis and oxidation in the liver. Fatty acid synthase (FASN) and acetyl-CoA carboxylase alpha (ACACA) are the rate-limiting enzymes in the process of fatty acid synthesis, while sterol regulatory element-binding transcription factor 1 (SREBF1) is an important transcription factor involved in lipid metabolism [41]. Results in Figure 6(c) showed that the expression of SREBF1 was significantly

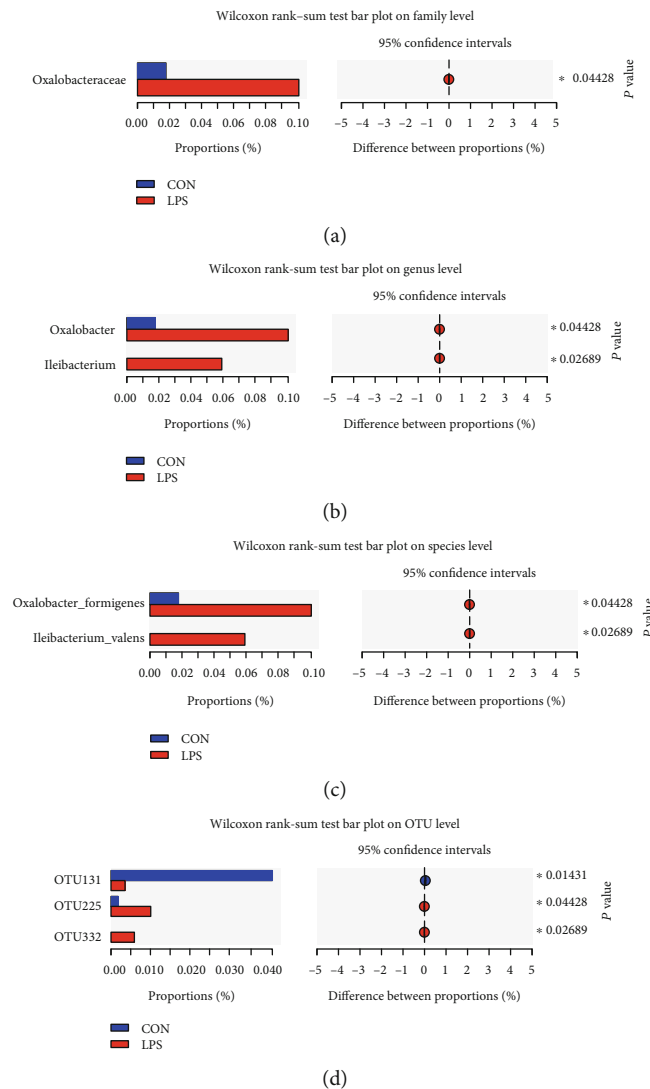


FIGURE 3: Effects of LPS challenge on the relative abundance of significant differential bacteria on (a) family, (b) genus, (c) species, and (d) OTU levels. Statistical differences between two groups were calculated by the Wilcoxon rank sum test. * $P < 0.05$ was regarded as statistically significant.

upregulated by LPS, whereas no change was observed in FASN and ACACA. Moreover, the expression of acyl-CoA synthetase long-chain family member 1 (*Acs11*) and carnitine palmitoyltransferase 1A (*Cpt1a*), two essential rate-limiting enzymes of fatty acid β -oxidation, was suppressed by LPS (Figure 6(d)). Peroxisome proliferator-activated receptor alpha (*PPAR- α*) is a key nuclear transcription factor that affects the target genes involved in lipid metabolism, cell proliferation, cell differentiation, and immune responses, and the obtained results revealed the downregulation of the underlined transcription factor, as depicted in Figure 6(d). The fatty acid transporter, such as *CD36*, was considerably induced by LPS stimulation (Figure 6(e)). Above results elucidated that LPS challenge disturbed the enterohepatic circulation of bile acids and further destroyed the normal lipid metabolism.

3.5. Intestinal Inflammation Further Caused Liver Inflammation. The reported studies have been revealed that

intestinal inflammation can influence the liver through the gut-liver axis [42, 43]. Our results indicated that the LPS challenge contributed to severe intestinal inflammation. However, whether it can be transferred to the liver in our model is not clear. The mRNA expression of cytokines was measured. The obtained results revealed an elevated expression level of proinflammatory cytokines, *i.e.*, IL6, IL-1 β , and TNF- α ; however, LPS stimulation did not affect the two key anti-inflammatory cytokines, *i.e.*, IL-10 and TGF- β , as depicted in Figure 7. Taken together, inflammation in the gut can be transferred to the liver and may further influence host metabolism.

4. Discussion

Gross lesion score and histopathological examinations are commonly used for evaluating the severity of necrotic enteritis [22, 44]. The villi height, crypt depth, and VCR are important indicators for assessing intestinal function and

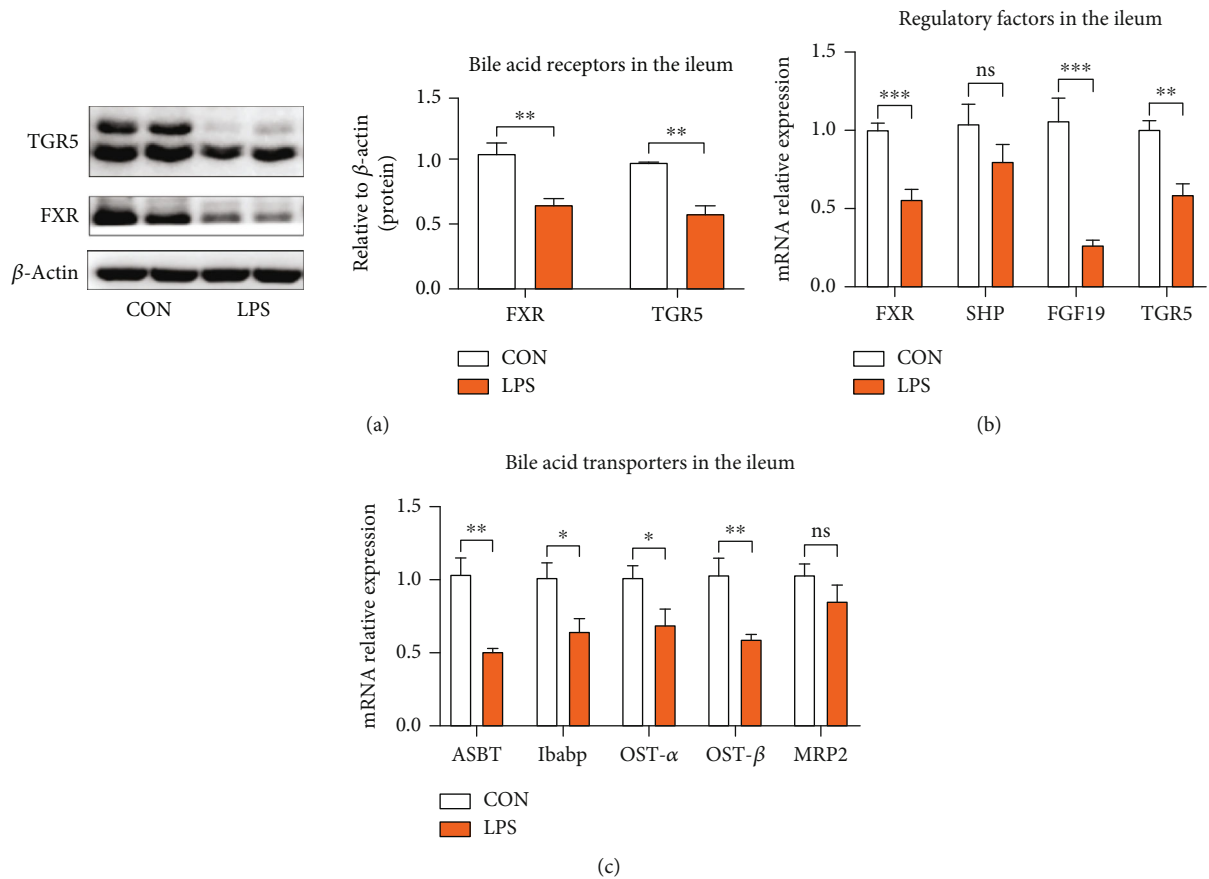


FIGURE 4: LPS damaged the ileal genes and protein expression related to enterohepatic circulation of bile acids. (a) Protein expression of bile acid receptors FXR and TGR5. FXR: farnesoid X receptor; TGR5: G protein-coupled bile acid receptor 1. (b) Expression of genes that regulate bile acid metabolism. SHP: small heterodimer partner; FGF19: fibroblast growth factor 19. (c) Expression of genes required for bile acid transportation. ASBT: apical sodium-dependent BA transporter; Ibabp: ileal bile acid-binding protein; OST- α : organic solute transporter subunit α ; OST- β : organic solute transporter subunit β ; MRP2: multidrug resistance-associated protein 2. * $P < 0.05$, ** $P < 0.01$, and *** $P < 0.001$ were regarded as statistically significant.

health [45]. In this study, LPS-induced piglets showed reduced villi height and VCR in the ileum, implying the decreased surface area for nutrient absorption and harmful effect on gut health. Meanwhile, homeostasis of cytokines in the intestine also plays a pivotal role in maintaining gut immunity, including proinflammatory cytokines, *i.e.*, iNOS, IL6, IL-1 β , and TNF- α , and anti-inflammatory cytokines, *i.e.*, IL-10 and TGF- β [46]. The reported studies revealed an elevated expression level of proinflammatory cytokines in patients affected with IBD, which implied that targeting the balance between proinflammatory and anti-inflammatory cytokines could be a potential treatment for gut inflammation [47]. In the current study, the obtained results indicated that LPS stimulation not only enhanced the mRNA expression of IL-6 and IL-1 β but also enhanced the transcriptional and translational level of iNOS, and further induced intestinal inflammation, which showed consistency with the other reported studies [48, 49].

Some studies revealed that gut immunity has been considerably associated with gut microbiota [4, 5], and a wide range of gastrointestinal diseases, such as recurrent *C. difficile* infection (CDI), inflammatory bowel diseases (IBD),

including Crohn's disease (CD) and ulcerative colitis (UC), colorectal cancer (CRC), and metabolic disorders, are affected by the variations observed in the composition and functions of gut microbiota [6, 50]. Researchers implied that the variations in gut microbiota between Jinhua and Landrace pigs may contribute to the disease resistance disparity [51, 52]. Given the strict interdependence between gut immunity and the host microbiota, 16S rRNA gene sequencing of the piglets' cecum contents was conducted. Our results confirmed that LPS had no effect on microbial diversity and richness, but partially changed the structure and composition of gut microbiota, especially the upregulated abundance of *Oxalobacter formigenes* and *Ileibacterium valens*. *Oxalobacter formigenes* were first reported in 1985, which is a group of anaerobic bacteria that degrade oxalic acid and it is believed that the underlined bacteria may considerably affect the host [53]. Up to now, *Oxalobacter formigenes* has been used in a phase II study in subjects with primary hyperoxaluria type 1 and end-stage renal disease [54]. *Ileibacterium valens*, a novel member of the family *Erysipelotrichaceae*, was first reported in 2017 [55]. In light of late discovery, only one paper postulated that this bacterium might do with

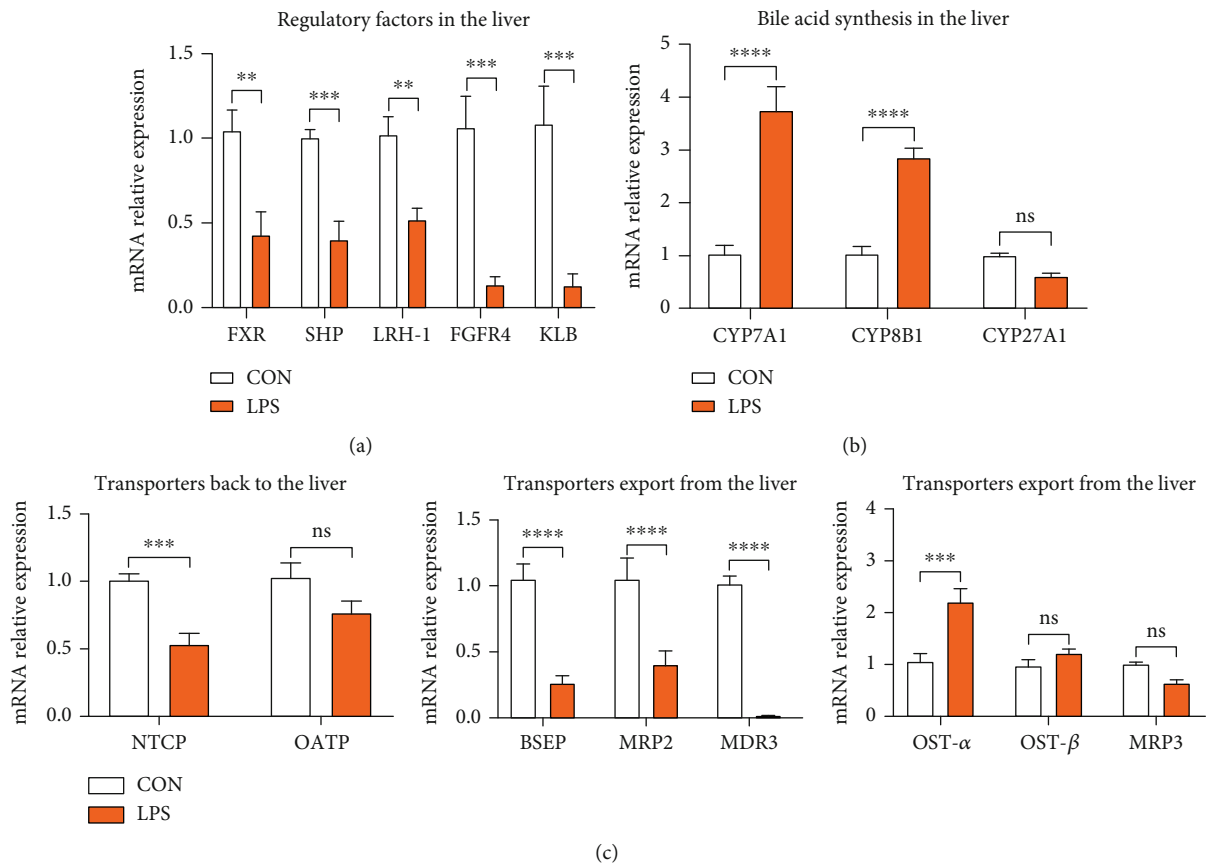


FIGURE 5: Hepatic gene expression related to enterohepatic circulation of bile acids by q-PCR. (a) Hepatic expression of genes that regulate bile acid metabolism. LRH-1: liver receptor homologue 1; FGFR4: fibroblast growth factor receptor 4; KLB: Klotho beta. (b) Hepatic expression of genes required for primary bile acid synthesis. CYP7A1: 7 α -hydroxylase; CYP8B1: 12 α -hydroxylase; CYP27A1: sterol 27-hydroxylase. (c) Expression of genes required for bile acid transportation. NTCP: Na⁺-taurocholate cotransporting polypeptide; OATP: organic anion transporting polypeptide; BSEP: bile salt export protein; MDR3: ATP binding cassette subfamily B member 4; MRP3: multidrug resistance-associated protein 3. * $P < 0.05$, ** $P < 0.01$, *** $P < 0.001$, and **** $P < 0.0001$ were regarded as statistically significant.

energy expenditure [56]. Further studies are warranted to experimentally verify the relative contribution of each enriched bacterial species and their effect on host metabolism and health.

Microbial dysbiosis results in IBD, obesity, and metabolic diseases [5, 7]. Metabolites produced by gut microbiota are considered essential intermediates between the microbiota and its host [57]. The metabolites of gut microbiota can cause modulation in the immune reactions of the host, thereby influencing their immune system and plays a considerable role in the inflammations and diseases [13]. Among them, SCFAs were the most abundant and extensively investigated metabolites [58]. In HFD mice and DSS mice, BA was evaluated as an effective metabolic factor correlated with the gut microbiota which affects the health of the host relative to SCFAs [19–21]. Our results also showed that microbial change induced by LPS stimulation is deleterious to BA enterohepatic circulation. Reduced BA regulatory factors in the ileum and liver had negative feedback on BA synthesis. As a result, increased synthesis of BA in the liver and impairment of BA uptake were also observed. The above results indicated that LPS stimulation reduced the content of BA

in the gut. It has also been indicated that increased BA biosynthesis from cholesterol might prevent hepatic cholesterol accumulation, thus improving host metabolism; however, the underlined process is not clearly understood and needs further investigation.

The reported studies and accumulating evidence indicated that BA is a metabolic regulator in the intestine, which considerably affects the emulsification and absorption of fats [27, 39, 59, 60]. In this study, it has been revealed that disturbance in BA enterohepatic circulation influenced lipid metabolism. Lipolysis is the process of the breakdown of fatty acids or lipids by a chemical reaction [61]. Our results showed that reduction of BAs in the intestine prevented the expression of genes related to lipolysis and fatty acid transporters, and thus damaged lipid metabolism in the gastrointestinal tract. Furthermore, the variations were also observed in the *de novo* synthesis and oxidation of fatty acid in the liver, which leads to further deposition of fat in the liver. The underlined process can trigger lipid metabolic reprogramming. The above results indicated that BA enterohepatic circulation is closely related to host lipid metabolism. Other reported studies also have confirmed that various types

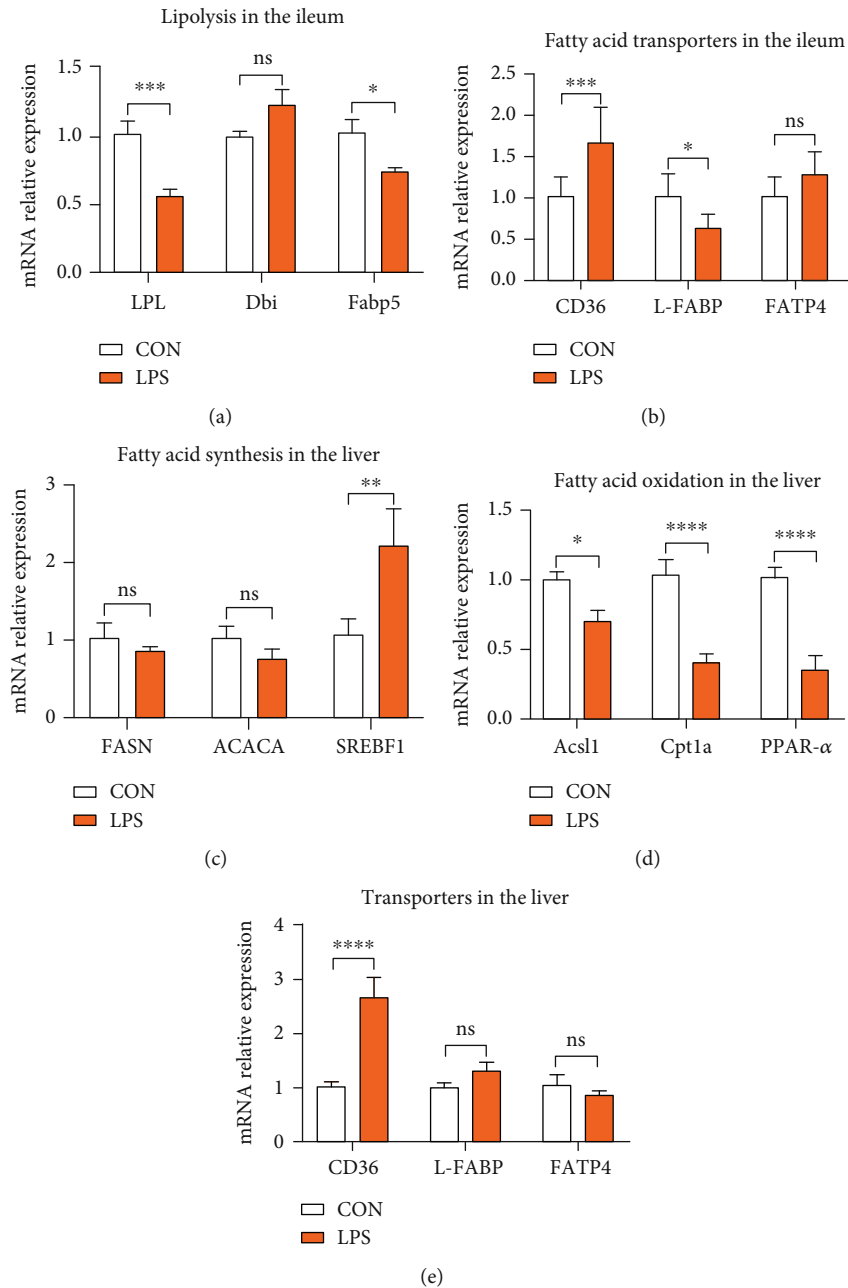


FIGURE 6: The obstruction of bile acid enterohepatic circulation made against the normal lipid metabolism. (a) Ileal expression of genes that regulate lipolysis. LPL: lipoprotein lipase; Dbi: diazepam binding inhibitor; Fabp5: fatty acid-binding protein 5. (b) Ileal gene expression of fatty acid transporters. (c) Hepatic expression of genes related to fatty acid synthesis. FASN: fatty acid synthase; ACACA: acetyl-CoA carboxylase alpha; SREBF1: sterol regulatory element binding transcription factor 1. (d) Hepatic expression of genes required for fatty acid β -oxidation. Acsl1: acyl-CoA synthetase long-chain family member 1; Cpt1a: carnitine palmitoyltransferase 1a; PPAR- α : peroxisome proliferator-activated receptor alpha. (e) Hepatic gene expression of fatty acid transporters. * $P < 0.05$, ** $P < 0.01$, *** $P < 0.001$, and **** $P < 0.0001$ were regarded as statistically significant.

of BAs exert different effects on lipid metabolism in mice and humans [37, 62, 63]. However, there is still a lack of clarity regarding the association between the metabolism of bile acids and lipid which needs further exploration.

Intestinal inflammation can be transferred to the liver through the gut-liver axis [42] and further impacts host

metabolism in the liver [59]. Our results revealed an elevation in the level of proinflammatory cytokines in the liver (upon LPS stimulation), which indicated hepatic inflammation. Our observations contrasted with published data together suggested that intestinal damage induced by various stimulators enhanced hepatic inflammation [44]. Whether

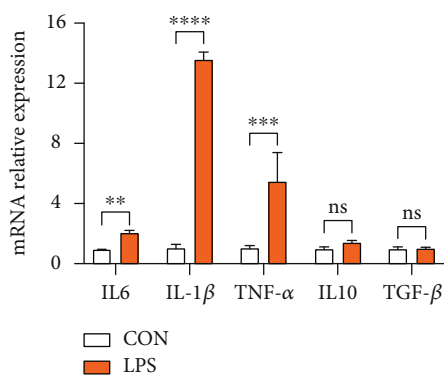


FIGURE 7: LPS stimulation triggered the gene expression of proinflammatory cytokines and further damaged liver. * $P < 0.05$, ** $P < 0.01$, *** $P < 0.001$, and **** $P < 0.0001$ were regarded as statistically significant.

liver injury dampened host metabolism is vague and limited in our study.

In the current study, we evaluated the effects of gut immunity and microbial dysbiosis on bile acids and lipid metabolism in the piglets exposed to LPS. However, some areas are poorly explored and need further investigation, *i.e.*, the bacteria that regulate the metabolism of bile acids, the association of microbiome with host metabolism, and the relationship between host immunity and gut microbiota. Besides, their potential mechanism also needs to be further explored.

5. Conclusion

In conclusion, the obtained results revealed that LPS stimulation results in intestinal erosion and the release of proinflammatory cytokines further lead to profound changes in the gut microbial composition and structure, especially the relative abundance of *Oxalobacter formigenes* and *Ileibacterium valens*. The underlined variations led to a disturbance in the enterohepatic circulation of BAs, which further damages lipid metabolism. However, there is still a lack of clarity regarding the relationship of gut immunity and intestinal microbiota with host metabolism and their potential mechanism which needs further investigation.

Data Availability

The datasets used and/or analyzed during the current study are available from the corresponding author on reasonable request.

Conflicts of Interest

The authors declare that there is no conflict of interest regarding the publication of this paper.

Authors' Contributions

XX, YW, and XZ designed the experiment. XX, YC, JF, and XZ performed the experiment. XX, JF, ZL, and FW analyzed

the experimental data. MJ analyzed the 16S rRNA sequence data. XX, YC, and XZ wrote this paper. ZL, FW, and MJ revised the manuscript. All authors critically reviewed the manuscript for intellectual content and gave final approval for the version to be published.

Acknowledgments

We would like to thank the staff at our laboratory for their ongoing assistance. This study was supported by the Modern Agroindustry Technology Research System (No. CARS-35) and the Key Projects of Science and Technology Plan of Zhejiang Province and Shandong Province (2019C02051, 2019JZZY020602, and CTZB-2020080127).

References

- [1] J.-P. Lallès, P. Bosi, H. Smidt, and C. R. Stokes, "Nutritional management of gut health in pigs around weaning," *The Proceedings of the Nutrition Society*, vol. 66, no. 2, pp. 260–268, 2007.
- [2] J. Hu, L. Ma, Y. Nie et al., "A microbiota-derived bacteriocin targets the host to confer diarrhea resistance in early-weaned piglets," *Cell Host & Microbe*, vol. 24, no. 6, 2018.
- [3] G. Chan, A. Farzan, G. Soltes et al., "The epidemiology of *Clostridium perfringens* type A on Ontario swine farms, with special reference to cpb2-positive isolates," *BMC Veterinary Research*, vol. 8, no. 1, p. 156, 2012.
- [4] L. Lin and J. Zhang, "Role of intestinal microbiota and metabolites on gut homeostasis and human diseases," *BMC Immunology*, vol. 18, no. 1, p. 2, 2017.
- [5] Y. Belkaid and T. W. Hand, "Role of the microbiota in immunity and inflammation," *Cell*, vol. 157, no. 1, pp. 121–141, 2014.
- [6] J. C. Clemente, J. Manasson, and J. U. Scher, "The role of the gut microbiome in systemic inflammatory disease," *BMJ*, vol. 360, 2018.
- [7] C. L. Boulangé, A. L. Neves, J. Chilloux, J. K. Nicholson, and M.-E. Dumas, "Impact of the gut microbiota on inflammation, obesity, and metabolic disease," *Genome Medicine*, vol. 8, no. 1, p. 42, 2016.
- [8] T. M. Loo, F. Kamachi, Y. Watanabe et al., "Gut microbiota promotes obesity-associated liver cancer through PGE2-mediated suppression of antitumor immunity," *Cancer Discovery*, vol. 7, no. 5, pp. 522–538, 2017.
- [9] Z. Wang and Y. Zhao, "Gut microbiota derived metabolites in cardiovascular health and disease," *Protein & Cell*, vol. 9, no. 5, pp. 416–431, 2018.
- [10] M. Beaumont, C. Paës, E. Mussard et al., "Gut microbiota derived metabolites contribute to intestinal barrier maturation at the suckling-to-weaning transition," *Gut Microbes*, vol. 11, no. 5, pp. 1268–1286, 2020.
- [11] A. Lavelle and H. Sokol, "Gut microbiota-derived metabolites as key actors in inflammatory bowel disease," *Nature Reviews. Gastroenterology & Hepatology*, vol. 17, no. 4, pp. 223–237, 2020.
- [12] E. E. Canfora, R. C. R. Meex, K. Venema, and E. E. Blaak, "Gut microbial metabolites in obesity, NAFLD and T2DM," *Nature Reviews. Endocrinology*, vol. 15, no. 5, pp. 261–273, 2019.

- [13] G. R. Nicolas and P. V. Chang, "Deciphering the chemical lexicon of host-gut microbiota interactions," *Trends in Pharmacological Sciences*, vol. 40, no. 6, pp. 430–445, 2019.
- [14] D. Dodd, M. H. Spitzer, W. Van Treuren et al., "A gut bacterial pathway metabolizes aromatic amino acids into nine circulating metabolites," *Nature*, vol. 551, no. 7682, pp. 648–652, 2017.
- [15] A. B. Roberts, X. Gu, J. A. Buffa et al., "Development of a gut microbe-targeted nonlethal therapeutic to inhibit thrombosis potential," *Nature Medicine*, vol. 24, no. 9, pp. 1407–1417, 2018.
- [16] B. J. H. Verhaar, D. Collard, A. Prodan et al., "Associations between gut microbiota, faecal short-chain fatty acids, and blood pressure across ethnic groups: the HELIUS study," *European Heart Journal*, vol. 41, no. 44, pp. 4259–4267, 2020.
- [17] M. van de Wouw, M. Boehme, J. M. Lyte et al., "Short-chain fatty acids: microbial metabolites that alleviate stress-induced brain-gut axis alterations," *The Journal of Physiology*, vol. 596, no. 20, pp. 4923–4944, 2018.
- [18] A. Rao, A. Kusters, J. E. Mells et al., "Inhibition of ileal bile acid uptake protects against nonalcoholic fatty liver disease in high-fat diet-fed mice," *Science Translational Medicine*, vol. 8, no. 357, 2016.
- [19] L. Wang, Z. Gong, X. Zhang et al., "Gut microbial bile acid metabolite skews macrophage polarization and contributes to high-fat diet-induced colonic inflammation," *Gut Microbes*, vol. 12, no. 1, 2020.
- [20] R. Y. Gao, C. T. Shearn, D. J. Orlicky et al., "Bile acids modulate colonic MAdCAM-1 expression in a murine model of combined cholestasis and colitis," *Mucosal Immunology*, vol. 14, 2020.
- [21] X. J. Zheng, F. J. Huang, A. H. Zhao et al., "Bile acid is a significant host factor shaping the gut microbiome of diet-induced obese mice," *BMC Biology*, vol. 15, no. 1, p. 120, 2017.
- [22] S. R. Sinha, Y. Haileselassie, L. P. Nguyen et al., "Dysbiosis-induced secondary bile acid deficiency promotes intestinal inflammation," *Cell Host & Microbe*, vol. 27, no. 4, 2020.
- [23] Y. Wang, S. Gunewardena, F. Li et al., "An FGF15/19-TFEB regulatory loop controls hepatic cholesterol and bile acid homeostasis," *Nature Communications*, vol. 11, no. 1, p. 3612, 2020.
- [24] W. Jia, G. Xie, and W. Jia, "Bile acid-microbiota crosstalk in gastrointestinal inflammation and carcinogenesis," *Nature Reviews. Gastroenterology & Hepatology*, vol. 15, no. 2, pp. 111–128, 2018.
- [25] N. Jiao, S. S. Baker, A. Chapa-Rodriguez et al., "Suppressed hepatic bile acid signalling despite elevated production of primary and secondary bile acids in NAFLD," *Gut*, vol. 67, no. 10, pp. 1881–1891, 2018.
- [26] J. M. Ridlon, D.-J. Kang, and P. B. Hylemon, "Bile salt biotransformations by human intestinal bacteria," *Journal of Lipid Research*, vol. 47, no. 2, pp. 241–259, 2006.
- [27] N. I. Hanafi, A. S. Mohamed, S. H. S. A. Kadir, and M. H. D. Othman, "Overview of bile acids signaling and perspective on the signal of ursodeoxycholic acid, the most hydrophilic bile acid, in the heart," *Biomolecules*, vol. 8, no. 4, 2018.
- [28] H.-X. Liu, R. Keane, L. Sheng, and Y.-J. Y. Wan, "Implications of microbiota and bile acid in liver injury and regeneration," *Journal of Hepatology*, vol. 63, no. 6, pp. 1502–1510, 2015.
- [29] X. Zong, J. Zhao, H. Wang et al., "Mettl3 deficiency sustains long-chain fatty acid absorption through suppressing Traf6-dependent inflammation response," *Journal of Immunology*, vol. 202, no. 2, pp. 567–578, 2019.
- [30] X. Zong, X. Cao, H. Wang, X. Xiao, Y. Wang, and Z. Lu, "Cathelicidin-WA facilitated intestinal fatty acid absorption through enhancing PPAR- γ dependent barrier function," *Frontiers in Immunology*, vol. 10, p. 1674, 2019.
- [31] J. M. Bates, J. Akerlund, E. Mittge, and K. Guillemin, "Intestinal alkaline phosphatase detoxifies lipopolysaccharide and prevents inflammation in zebrafish in response to the gut microbiota," *Cell Host & Microbe*, vol. 2, no. 6, pp. 371–382, 2007.
- [32] H. Tilg, N. Zmora, T. E. Adolph, and E. Elinav, "The intestinal microbiota fuelling metabolic inflammation," *Nature Reviews Immunology*, vol. 20, no. 1, pp. 40–54, 2020.
- [33] M. Saleh and C. O. Elson, "Experimental inflammatory bowel disease: insights into the host-microbiota dialog," *Immunity*, vol. 34, no. 3, pp. 293–302, 2011.
- [34] W. Zhu, M. G. Winter, M. X. Byndloss et al., "Precision editing of the gut microbiota ameliorates colitis," *Nature*, vol. 553, no. 7687, pp. 208–211, 2018.
- [35] M. Tschurtschenthaler, J. Wang, C. Fricke et al., "Type I interferon signalling in the intestinal epithelium affects Paneth cells, microbial ecology and epithelial regeneration," *Gut*, vol. 63, no. 12, pp. 1921–1931, 2014.
- [36] M. Levy, E. Blacher, and E. Elinav, "Microbiome, metabolites and host immunity," *Current Opinion in Microbiology*, vol. 35, pp. 8–15, 2017.
- [37] M. Mueller, A. Thorell, T. Claudel et al., "Ursodeoxycholic acid exerts farnesoid X receptor-antagonistic effects on bile acid and lipid metabolism in morbid obesity," *Journal of Hepatology*, vol. 62, no. 6, pp. 1398–1404, 2015.
- [38] W. Jia, M. Wei, C. Rajani, and X. Zheng, "Targeting the alternative bile acid synthetic pathway for metabolic diseases," *Protein Cell*, 2020.
- [39] A. Macierzanka, A. Torcello-Gómez, C. Jungnickel, and J. Maldonado-Valderrama, "Bile salts in digestion and transport of lipids," *Advances in Colloid and Interface Science*, vol. 274, p. 102045, 2019.
- [40] M. O. Reynier, J. C. Montet, A. Gerolami et al., "Comparative effects of cholic, chenodeoxycholic, and ursodeoxycholic acids on micellar solubilization and intestinal absorption of cholesterol," *Journal of Lipid Research*, vol. 22, no. 3, pp. 467–473, 1981.
- [41] L. Hodson and P. J. Gunn, "The regulation of hepatic fatty acid synthesis and partitioning: the effect of nutritional state," *Nature Reviews. Endocrinology*, vol. 15, no. 12, pp. 689–700, 2019.
- [42] T. Shao, C. Zhao, F. Li et al., "Intestinal HIF-1 α deletion exacerbates alcoholic liver disease by inducing intestinal dysbiosis and barrier dysfunction," *Journal of Hepatology*, vol. 69, no. 4, pp. 886–895, 2018.
- [43] C. Acharya, S. E. Sahingur, and J. S. Bajaj, "Microbiota, cirrhosis, and the emerging oral-gut-liver axis," *JCI Insight*, vol. 2, no. 19, 2017.
- [44] E. Gäbele, K. Dostert, C. Hofmann et al., "DSS induced colitis increases portal LPS levels and enhances hepatic inflammation and fibrogenesis in experimental NASH," *Journal of Hepatology*, vol. 55, no. 6, pp. 1391–1399, 2011.
- [45] V. Snoeck, B. Goddeeris, and E. Cox, "The role of enterocytes in the intestinal barrier function and antigen uptake," *Microbes and Infection*, vol. 7, no. 7-8, pp. 997–1004, 2005.

- [46] D. Yao, M. Dong, C. Dai, and S. Wu, "Inflammation and inflammatory cytokine contribute to the initiation and development of ulcerative colitis and its associated cancer," *Inflammatory Bowel Diseases*, vol. 25, no. 10, pp. 1595–1602, 2019.
- [47] M. F. Neurath, "Targeting immune cell circuits and trafficking in inflammatory bowel disease," *Nature Immunology*, vol. 20, no. 8, pp. 970–979, 2019.
- [48] B. Huang, D. Xiao, B. Tan et al., "Chitosan oligosaccharide reduces intestinal inflammation that involves calcium-sensing receptor (CaSR) activation in lipopolysaccharide (LPS)-challenged piglets," *Journal of Agricultural and Food Chemistry*, vol. 64, no. 1, pp. 245–252, 2015.
- [49] R. Hu, Z. He, M. Liu et al., "Dietary protocatechuic acid ameliorates inflammation and up-regulates intestinal tight junction proteins by modulating gut microbiota in LPS-challenged piglets," *Journal of Animal Science and Biotechnology*, vol. 11, no. 1, p. 92, 2020.
- [50] X. Zong, J. Fu, B. Xu, Y. Wang, and M. Jin, "Interplay between gut microbiota and antimicrobial peptides," *Animal Nutrition*, vol. 6, no. 4, pp. 389–396, 2020.
- [51] Y. Xiao, F. Kong, Y. Xiang et al., "Comparative biogeography of the gut microbiome between Jinhua and Landrace pigs," *Scientific Reports*, vol. 8, no. 1, p. 5985, 2018.
- [52] H. Diao, H. L. Yan, Y. Xiao et al., "Intestinal microbiota could transfer host gut characteristics from pigs to mice," *BMC Microbiology*, vol. 16, no. 1, p. 238, 2016.
- [53] M. J. Allison, K. A. Dawson, W. R. Mayberry, and J. G. Foss, "Oxalobacter formigenes gen. nov., sp. nov.: oxalate-degrading anaerobes that inhabit the gastrointestinal tract," *Archives of Microbiology*, vol. 141, no. 1, pp. 1–7, 1985.
- [54] B. Hoppe, P. A. Pellikka, B. Dehmel, A. Banos, E. Lindner, and U. Herberg, "Effects of Oxalobacter formigenes in subjects with primary hyperoxaluria type 1 and end-stage renal disease: a phase II study," *Nephrology, Dialysis, Transplantation*, 2020.
- [55] L. M. Cox, J. Sohn, K. L. Tyrrell et al., "Description of two novel members of the family Erysipelotrichaceae: *Ileibacterium valens* gen. nov., sp. nov. and *Dubosiella newyorkensis*, gen. nov., sp. nov., from the murine intestine, and emendation to the description of *Faecalibaculum rodentium*," *International Journal of Systematic and Evolutionary Microbiology*, vol. 67, no. 5, pp. 1247–1254, 2017.
- [56] L. J. den Hartigh, Z. Gao, L. Goodspeed et al., "Obese mice losing weight due to trans-10,cis-12 conjugated linoleic acid supplementation or food restriction harbor distinct gut microbiota," *The Journal of Nutrition*, vol. 148, no. 4, pp. 562–572, 2018.
- [57] K. A. Krautkramer, J. Fan, and F. Bäckhed, "Gut microbial metabolites as multi-kingdom intermediates," *Nature Reviews Microbiology*, vol. 19, 2021.
- [58] A. Koh, F. De Vadder, P. Kovatcheva-Datchary, and F. Bäckhed, "From dietary fiber to host physiology: short-chain fatty acids as key bacterial metabolites," *Cell*, vol. 165, no. 6, pp. 1332–1345, 2016.
- [59] J. Y. L. Chiang and J. M. Ferrell, "Bile acids as metabolic regulators and nutrient sensors," *Annual Review of Nutrition*, vol. 39, no. 1, pp. 175–200, 2019.
- [60] T. Li and J. Y. L. Chiang, "Bile acid signaling in liver metabolism and diseases," *Journal of Lipids*, vol. 2012, Article ID 754067, 9 pages, 2012.
- [61] R. Zechner, F. Madeo, and D. Kratky, "Cytosolic lipolysis and lipophagy: two sides of the same coin," *Nature Reviews Molecular Cell Biology*, vol. 18, no. 11, pp. 671–684, 2017.
- [62] A. Schmid, J. Schlegel, M. Thomalla, T. Karrasch, and A. Schäffler, "Evidence of functional bile acid signaling pathways in adipocytes," *Molecular and Cellular Endocrinology*, vol. 483, pp. 1–10, 2019.
- [63] P. Hartmann, K. Hochrath, A. Horvath et al., "Modulation of the intestinal bile acid/farnesoid X receptor/fibroblast growth factor 15 axis improves alcoholic liver disease in mice," *Hepatology*, vol. 67, no. 6, pp. 2150–2166, 2018.

Research Article

The Role of lncRNA AF117829.1 in the Immunological Pathogenesis of Severe Aplastic Anaemia

Yang Li , Ling Deng , Xiaofeng Pan, Chunyan Liu, and Rong Fu 

Department of Haematology, Tianjin Medical University General Hospital, Tianjin 300052, China

Correspondence should be addressed to Rong Fu; furong8369@tmu.edu.cn

Received 16 January 2021; Revised 20 February 2021; Accepted 3 March 2021; Published 16 March 2021

Academic Editor: Si Qin

Copyright © 2021 Yang Li et al. This is an open access article distributed under the Creative Commons Attribution License, which permits unrestricted use, distribution, and reproduction in any medium, provided the original work is properly cited.

Objective. Severe aplastic anaemia (SAA) is an autoimmune disease with immune tolerance dysfunction mediated by hyperactivated T lymphocytes that target the haematopoietic system. Numerous studies suggest that long noncoding RNAs (lncRNAs) play a significant role in almost every level of gene function/regulation. However, their specific mechanisms in SAA remain undetermined. This study is aimed at determining the role of key lncRNAs in CD8+ T lymphocytes in the mechanisms of SAA. **Methods.** RNA-seq was performed to detect all lncRNAs and mRNAs in peripheral CD8+ T lymphocytes from SAA patients and healthy controls. The lncRNA targets were predicted by bioinformatics, Gene Ontology (GO) analysis, and Kyoto Encyclopedia of Genes and Genomes (KEGG) analysis. RT-qPCR was used to verify the expression of key lncRNAs and their predicted targets. We screened lncRNA AF117829.1, which was correlated with autoimmune diseases and downregulated in CD8+ T lymphocytes, and further validated its effects on CD8+ T lymphocytes from SAA patients. **Results.** We systematically described the lncRNA/mRNA expression changes in CD8+ T lymphocytes in SAA patients and assessed their possible biological functions and signalling pathways. A total of 194 lncRNAs and 2099 mRNAs were changed in SAA patients versus healthy controls. These differentially expressed lncRNAs/mRNAs were associated with organelle components, catalytic activity, the response to stimulation, signal transduction, the immune system and metabolic processes. The downregulated expression of one altered factor, lncRNA AF117829.1, in CD8+ T lymphocytes from SAA patients increased CD8+ T lymphocyte immune function by promoting RIP2 expression. lncRNA AF117829.1 overexpression in CD8+ T lymphocytes reduced perforin and granzyme B expression. The same effect was achieved with GSK583, a RIP2 kinase inhibitor. **Conclusions.** The proliferation and overactivation of CD8+ T lymphocytes, also known as cytotoxic T cells (CTLs), directly induce bone marrow (BM) failure in SAA patients, but the specific mechanism remains unclear. We found that lncRNA AF117829.1 and its target genes were associated with T cell proliferation, differentiation, and immune dysregulation and that lncRNA AF117829.1 regulated CD8+ T lymphocyte function in SAA patients by promoting RIP2 expression. These findings improve our understanding of the molecular mechanism of immune pathogenesis and provide potential targets for SAA diagnosis and treatment.

1. Introduction

Severe aplastic anaemia (SAA) refers to a haematological disease represented by pancytopenia in association with bone marrow (BM) hypoplasia/aplasia. The typical clinical symptoms of SAA comprise severe anaemia, infection, and bleeding/bruising; SAA is an acute condition that progresses rapidly [1]. If effective treatment is not given in time, patients often die from severe bleeding or infection. At present, immunosuppressive therapy (IST) and haematopoietic therapy based on antithymocyte globulin, antilymphocyte globu-

lin (ATG/ALG), and cyclosporine A (CsA) have been widely used in the treatment of this disease with an effective rate of up to more than 70%, but these approaches are ineffective in nearly 30% of SAA patients, some of which die from the disease [2]. Even after treatment, 10% of patients in remission may relapse [2]. Therefore, further exploration of the immune pathogenesis of SAA is of great significance for determining new treatment directions and establishing effective diagnostic and prognostic indicators.

Current research has revealed that environmental factors (cytotoxic chemicals, drugs, viral infection, or ionizing

radiation) facilitate SAA development by inducing autoimmune damage (mainly mediated by CD8+ T lymphocytes) to haematopoietic stem cells or by inducing other immune responses; the features of these immune cells have aroused great attention from scholars [3]. CD8+ T lymphocytes exert their cytotoxic function on target cells mainly through perforin and granzyme B and the Fas-FasL interaction [4]. We found that the number of activated inhibitory T lymphocytes (mostly CD8+ T lymphocytes) increased and that the cells were in a hyperactive state in SAA patients [5–7]. CD8+ T lymphocytes isolated from SAA patients can cause meaningful damage to BM cells *in vitro* [8]. Therefore, CD8+ T lymphocytes play a critical role in the pathogenic mechanism of SAA.

Long noncoding RNAs (lncRNAs) were first proposed by Brannan et al. in the 1990s [9]. Studies on lncRNAs are increasing due to state-of-the-art high-throughput sequencing techniques. lncRNAs are greater than 200 nt in length and do not have obvious protein-coding functions [10–12]. In recent decades, increasing evidence has shown that lncRNAs have crucial regulatory effects on mammalian biology [13]. The regulatory role of lncRNAs in autoimmune diseases has attracted widespread attention. The persistent expression of lncRNA-NEAT1 might be a potential cause of the increased production of multiple cytokines in patients with systemic lupus erythematosus (SLE) [14]. The lipopolysaccharide- (LPS-) induced expression of chemokines and cytokines, including IL-6 and CXCL10, was significantly attenuated as a result of NEAT1 silencing, and lncRNA-NEAT1 might be a target in SLE treatment. Li et al. analysed the lncRNA and mRNA expression profiles of peripheral blood mononuclear cells from immune thrombocytopenia (ITP) patients by gene chip technology [15]. They found that 1177 lncRNAs and 632 mRNAs were significantly downregulated in newly diagnosed ITP patients compared to healthy controls. Furthermore, CD4+ T lymphocytes from ITP patients exhibited increased expression of lncRNA maternally expressed gene 3 (MEG3) [16]. Overexpression of lncRNA MEG3 inhibited miR-125A-5P transcription in CD4+ T lymphocytes under the action of dexamethasone. *In vitro* experiments showed that downregulation of MEG3 or overexpression of miR-125A-5P could facilitate Foxp3 transcription, inhibit ROR γ t expression, and lead to Treg/Th17 imbalance, which provided new ideas for elucidating the molecular mechanism of ITP. There are thousands of lncRNAs in the mammalian genome that regulate gene expression in immunocytes, such as T lymphocytes and dendritic cells (DC), during various immune processes [17, 18]. lncRNA CD244 mediates the methylation of H3K27 at the IFN- γ /TNF- α gene site and then inhibits IFN- γ /TNF- α secretion from CD8+ T lymphocytes [19]. Mao et al. found that IL-36 β enhances the activity of CD8+ T lymphocytes in killing tumour cells by regulating lncRNA-GM16343 [20].

In summary, lncRNAs play an essential role in the development and activation of immune cells. Nevertheless, the expression of lncRNAs in CD8+ T lymphocytes and the mechanism by which they influence the biological activity of CD8+ T lymphocytes from SAA patients are still unknown. To further address these gaps in knowledge, we

assessed lncRNA expression and the function of CD8+ T lymphocytes in SAA to provide new insights for the effective diagnosis and management of SAA.

2. Materials and Methods

2.1. Study Populations. The study enrolled patients and control subjects, each with a signed informed consent form, and was approved by the Ethical Committee of Tianjin Medical University General Hospital. From September 2017 to January 2020, we enrolled 48 newly diagnosed SAA patients who had never received IST; the median age was 44.5 (24–59) years old. We also enrolled 33 patients in remission after IST (R-SAA) and 38 healthy volunteers to serve as controls. The diagnosis of SAA was made according to standard criteria [21].

2.2. CD8+ T Lymphocyte Isolation, Enrichment Analysis, and Functional Test. We isolated CD8+ T lymphocytes from the peripheral blood of newly diagnosed SAA patients and healthy controls using CD8 MicroBeads (Miltenyi Biotec, Germany) in accordance with the manufacturer's protocol. To assess CD8+ T lymphocyte enrichment, the cells were stained with antibodies against CD3-APC and CD8-FITC and analysed with the Beckman Coulter CytoFLEX™ Flow Cytometer (CytoFLEX) according to a standard procedure. Perforin and granzyme B expression and cell apoptosis were also analysed with CytoFLEX according to standard procedures.

2.3. RNA-seq. RNA-seq was performed as described by Springer Nature Experiments (http://experiments.springernature.com/articles/10.1007/978-1-4939-6539-7_10) [22–24]. After that, Gene Ontology (GO) analysis and Kyoto Encyclopedia of Genes and Genomes (KEGG) enrichment analysis were applied to predict the function of lncRNAs and perform gene annotation [25, 26]. Bedtools (v2.17.0) and Blast (v2.2.28+) software were used to predict whether specific lncRNAs regulate gene expression *in cis* or *in trans*, respectively.

2.4. RNA Extraction and RT-qPCR. After total RNA was extracted from CD8+ T lymphocytes with TRIzol, the samples were subjected to subsequent reverse transcription to synthesize complementary DNA using the FastQuant RT Kit (with gDNase) according to the manufacturer's instructions. Then, we performed RT-qPCR on a Bio-Rad iQ5 Real-Time System to detect the relative expression of lncRNA AF117829.1, TCONS_00043638, TCONS_00329529, TCONS_00002554, RIP2, ADAM8, DUOX2, and BCR with the primers shown in Table 1 (normalized to the expression of β -actin). The data were analysed by using a modification of the 2- $\Delta\Delta$ Ct method.

2.5. Western Blotting. Western blotting was carried out as described by Abcam (<http://www.abcam.com/ps/pdf/protocols/WB-beginner.pdf>). We incubated the blots overnight at 4°C with rabbit anti-GAPDH, rabbit anti-RIP2, rabbit anti-MAPK, and rabbit NF- κ B primary antibodies from Cell Signalling Technology to probe the target proteins.

TABLE 1: Primer sequences.

Primer	Sequence (5' to 3')
β -Actin forward	TGGACATCCGCAAAGACCTGT
β -Actin reverse	CACACGGAGTACTTGCGCTCA
lncRNA AF117829.1 forward	GGAGTCAGTGTGACAGTTGGAGTG
lncRNA AF117829.1 reverse	ACCTGTATTGCTTGGCTCATGGC
TCONS_00043638 forward	GAGGACAGAAGGTGGAAGTCAAGC
TCONS_00043638 reverse	AAGACCGCAGAGGAGAGTGAGAC
TCONS_00329529 forward	TCCGAACGCCTCGTGGACTG
TCONS_00329529 reverse	ACAACGCAGAATGAAGGAGGTGAC
TCONS_00002554 forward	AGCAGTGGCTCATGCCTATAATCC
TCONS_00002554 reverse	GAGTTGGAGACCAGCCTGGATAAC
mRNA RIP2 forward	ATTCTGTGATCACAAGACCACT
mRNA RIP2 reverse	CCTTGTAGGCTTGGTACTAACA
mRNA ADAM8 forward	TGAATCACGTGGACAAGCTATA
mRNA ADAM8 reverse	GAACCTGTCTGACTATTCCAA
mRNA DUOX2 forward	TTGCTCAGGTGCTGGACATCAAC
mRNA DUOX2 reverse	GAAGGACAGGTAGCCATTGCCATC
mRNA BCR forward	CAGCCTATCACCATGACTGACAGC
mRNA BCR reverse	GACTTCGGTGGAGAACAGGATGC

Band density was quantified by ImageJ and normalized to that of GAPDH.

2.6. Lentivirus Transduction. Lentiviruses expressing lncRNA AF117829.1 were constructed by GeneChem (Shanghai, China). Empty vectors were also purchased from GeneChem. After CD8+ T lymphocyte activation with the T Cell Activation/Expansion Kit (Miltenyi Biotec, Germany), cell transfections of lentivirus expressing lncRNA AF117829.1 or negative control lentivirus were performed in strict accordance with the manufacturer's instructions at a multiplicity of infection (MOI) = 100. Puromycin dihydrochloride (Thermo Fisher) was used as the antibiotic selection agent. The infection rate and subsequent perforin and granzyme B expression were analysed by flow cytometry (FCM) as described above.

2.7. Treatment of CD8+ T Lymphocytes with a RIP2 Kinase Inhibitor (GSK583). After cell magnetic separation and purification, peripheral blood CD8+ T lymphocytes from SAA patients and healthy controls were treated with GSK583 (80 nM) or an equivalent volume of DMSO for 24 h [27]. Apoptosis and perforin and granzyme B expression were detected by FCM as previously described.

2.8. Enzyme-Linked Immunosorbent Assay (ELISA). After culturing the cells for 24h, the cell supernatants were obtained by centrifugation, and the changes in IL-6 and IL-1 β were detected by using IL-6 and IL-1 β ELISA kits (Nanjing SenBeiJia Biological Technology Co., Ltd.).

2.9. Statistical Analysis. Normally distributed data were presented as the mean \pm standard error, and nonnormally distributed data were presented as the median (25%, 75%). Student's *t*-test (two-tailed), chi-squared *t*-test, one-way ANOVA, and Mann-Whitney *U* test were used to analyse the experimental data. Data analysis was performed with

GraphPad Prism (version 7.0) and SPSS 24.0. $p < 0.05$ was deemed to indicate significance.

3. Results

3.1. Analysis of the Expression Profiles of lncRNAs and mRNAs in Peripheral CD8+ T Lymphocytes from Patients with SAA. The expression profiles of lncRNAs and mRNAs in CD8+ T lymphocytes were analysed by RNA-seq technology in 4 newly diagnosed SAA patients and 4 healthy controls. The basic characteristics of the populations are shown in Table 2. A total of 2099 altered mRNAs (1104 upregulated mRNAs and 995 downregulated mRNAs) were observed (Figure 1) (Supplementary file S1). GO analysis indicated that the differentially expressed mRNAs were enriched in catalysis, transduction activity, molecular function regulation, cell metabolism, immune system, and other functions. KEGG analysis showed that the differentially expressed mRNAs were mainly enriched in the c-Jun N-terminal kinase (JNK), RAS, nucleotide-binding oligomerization domain 2/ receptor-interacting protein 2 (NOD2/RIP2), and mitogen-activated protein kinase (MAPK) signalling pathways. A total of 194 lncRNAs, including 107 upregulated and 87 downregulated lncRNAs, were altered in SAA patients versus healthy controls (Figure 1) (Supplementary file S2). GO analysis showed that the differentially expressed lncRNAs were associated with organelle components, catalytic activity, the response to stimulation, signal transduction inside and outside of cells, biological regulation, and metabolic processes. KEGG analysis revealed that the differentially expressed lncRNAs were involved in ubiquitin-mediated proteomics, antigen processing and presentation, NOD, and other signalling pathways (Figure 2).

According to the microarray data, the lncRNAs related to immune regulation included TCONS_00379951 (lncRNA AF117829.1), TCONS_00043638, TCONS_00329529, and TCONS_00002554. The predicted target gene transcripts related to the above lncRNAs included ENST00000540020, ENST00000415217, ENST00000606851, and ENST00000487968 (Table 3).

4. The Expression of lncRNA AF117829.1 in the CD8+ T Lymphocytes of SAA Patients

4.1. lncRNA and mRNA Expression in CD8+ T Lymphocytes. We enrolled 48 newly diagnosed SAA patients, 33 R-SAA patients, and 38 healthy volunteers. The baseline characteristics are shown in Table 4. Among all subjects, differential lncRNA and mRNA expression was considered to be meaningful if the following conditions (gene expression change > 2 -fold and $FDR \leq 0.05$) were met. As shown in Table 5, we found that lncRNA AF117829.1 expression was notably decreased in the SAA and R-SAA groups compared with the healthy control group ($p = 0.0109$; $p = 0.00005$). The mRNA expression of its target gene, RIP2, was increased in the SAA and R-SAA groups compared with the healthy control group ($p = 0.9897$; $p = 0.0003$) (Figure 3(a), A and B). lncRNA TCONS_00043638 ($p = 0.00006$; $p = 0.0174$) and its target gene mRNA ADAM8 ($p = 0.9532$; $p = 0.0362$)

TABLE 2: Clinical data and laboratory values for 4 newly diagnosed SAA patients and 4 healthy controls.

No.	Sex	Age	WBC ($\times 10^9/L$)	RBC ($\times 10^{12}/L$)	Hb (g/L)	RET ($\times 10^9/L$)	PLT ($\times 10^9/L$)	NEU ($\times 10^9/L$)
SAA1	F	59	1.59	2.61	85	15.3	24	0.47
SAA2	M	24	1.55	1.84	53	4.7	15	0.45
SAA3	F	57	0.36	2.21	68	3.1	17	0.22
SAA4	M	32	2.35	1.65	61	3.6	15	0.37
HC1	F	61	6.86	3.29	84	88.2	166	2.77
HC2	M	33	4.09	4.22	109	54.1	161	4.11
HC3	F	56	5.76	3.16	65	64.8	275	3.31
HC4	M	30	5.53	3.63	104	52.9	319	4.62

had the same expression tendency as lncRNA AF117829.1 (Figure 3(a), C and D). The expression of lncRNA TCONS_00329529 ($p = 0.1423$; $p = 0.0048$) and its target gene mRNA DUOX2 was increased in both the SAA and R-SAA groups compared with the healthy control group ($p = 0.0256$; $p = 0.0008$) (Figure 3(a), E and F). The expression of lncRNA TCONS_00002554 and its target gene mRNA BCR was not significantly different between the groups (Figure 3(a), G and H). The above results were basically consistent with the sequencing results.

4.2. Perforin and Granzyme B Expression Was Increased in CD8+ T Lymphocytes from SAA Patients. The expression of both perforin and granzyme B was upregulated in the CD8+ T lymphocytes of newly diagnosed SAA patients (33.34% (23.7%, 41.95%); 21.68% (14.45%, 38.9%)) compared with those of R-SAA patients (21.55% (12.57%, 31.85%); 9.8% (0.9%, 19%)) and healthy controls (14.6% (9.91%, 20.33%); 2.75% (0.517%, 10.25%)) ($p < 0.05$) (Figure 3(b)).

4.3. The Correlation between the Expression of the Previously Mentioned lncRNAs and the Expression of Perforin and Granzyme B in CD8+ T Lymphocytes. lncRNA AF117829.1 expression had a negative correlation with perforin and granzyme B expression. lncRNA TCONS_00043638 expression was also negatively correlated with perforin and granzyme B expression. The expression of both lncRNA TCONS_00329529 and lncRNA TCONS_00002554 was positively correlated with the perforin expression but not the granzyme B expression (Figure 4(a)).

4.4. The Correlation between lncRNA AF117829.1 Expression in CD8+ T Lymphocytes and Clinical Indexes. The results showed that lncRNA AF117829.1 expression was positively correlated with the clinical indexes of SAA patients, including the white blood cell count (WBC), red blood cell count (RBC), haemoglobin (Hb), percentage of reticulocytes (RET%), platelet count (PLT), and absolute neutrophil count (NEU). All p values were less than 0.05 (Figure 4(b)).

4.5. RIP2 Signalling Pathway-Related Protein Levels Were Significantly Increased in SAA Patients. Considering the above RT-qPCR results for lncRNAs and mRNAs, we further verified the signalling pathways that might be regulated by lncRNAs. According to the sequencing results, the mRNA expression of RIP2, the predicted target gene of lncRNA

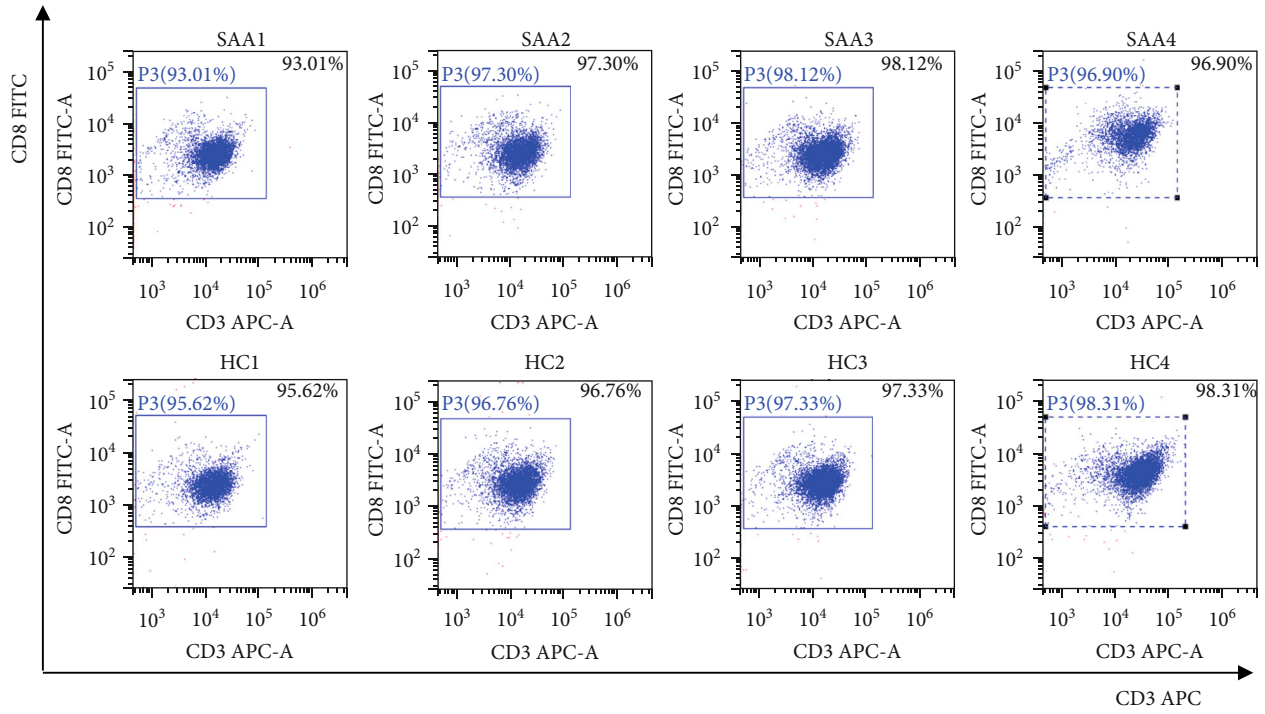
AF117829.1, satisfied the differential expression conditions of high-throughput omics (difference > 2 -fold, p value < 0.05). The downstream targets of RIP2 could regulate the NF- κ B and MAPK pathways, which are closely related to T cell proliferation. Therefore, we used western blotting to detect the levels of key proteins, including RIP2, NF- κ B, and MAPK. The results showed that the RIP2, NF- κ B, and MAPK protein levels were significantly increased in the CD8+ T lymphocytes of SAA patients compared to those of R-SAA patients and healthy controls (Figure 3(c)).

5. lncRNA AF117829.1 Mediated the Effect of CD8+ T Lymphocytes in SAA Patients

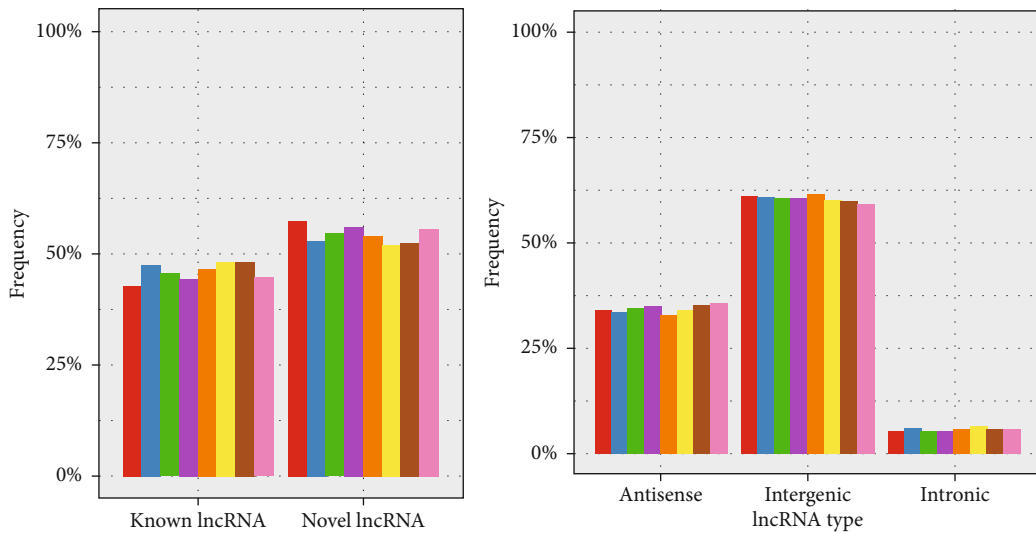
5.1. The Expression of lncRNA AF117829.1 and mRNA RIP2 in lncRNA AF117829.1-Overexpressing CD8+ T Lymphocytes. We used FCM to detect the transfection rate of lncRNA AF117829.1 in the CD8+ T lymphocytes of newly diagnosed SAA patients, R-SAA patients, and healthy controls. The transfection rate reached more than 40% (Figure 5(a)). lncRNA AF117829.1 expression was increased in CD8+ T lymphocytes of the lncRNA AF117829.1 lentivirus group (27.36 ± 4.026) compared with those of the blank group (2.375 ± 1.016) ($p < 0.001$). RIP2 mRNA expression was significantly decreased (0.06786 ± 0.0148 ; 0.1353 ± 0.02897) ($p < 0.05$) (Figure 5(d)).

5.2. lncRNA AF117829.1 Overexpression Suppressed the Apoptosis of CD8+ T Lymphocyte. We assessed the changes in the apoptosis rate of CD8+ T lymphocytes transfected with lncRNA AF117829.1 by FCM. The results showed that lncRNA AF117829.1-overexpressing CD8+ T cells had lower apoptosis rates ($22.85 \pm 3.767\%$) than blank control cells ($38.48 \pm 1.566\%$) ($p = 0.0086$) (Figure 5(b)).

5.3. Perforin and Granzyme B Expression in lncRNA AF117829.1-Overexpressing CD8+ T Lymphocytes. Next, we detected perforin and granzyme B expression in CD8+ T lymphocytes transfected with lncRNA AF117829.1 lentivirus by FCM. Perforin and granzyme B expression was significantly downregulated in lncRNA AF117829.1-overexpressing CD8+ T cells ($2.549 \pm 0.5219\%$; $0.6118 \pm 0.2415\%$) compared with blank control cells ($5.012 \pm 0.8285\%$; $2.549 \pm 0.5219\%$) ($p = 0.022$; $p = 0.003$) (Figure 5(e)).



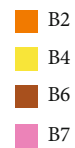
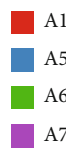
(a)



(A)

(B)

Sample name



(b)

FIGURE 1: Continued.

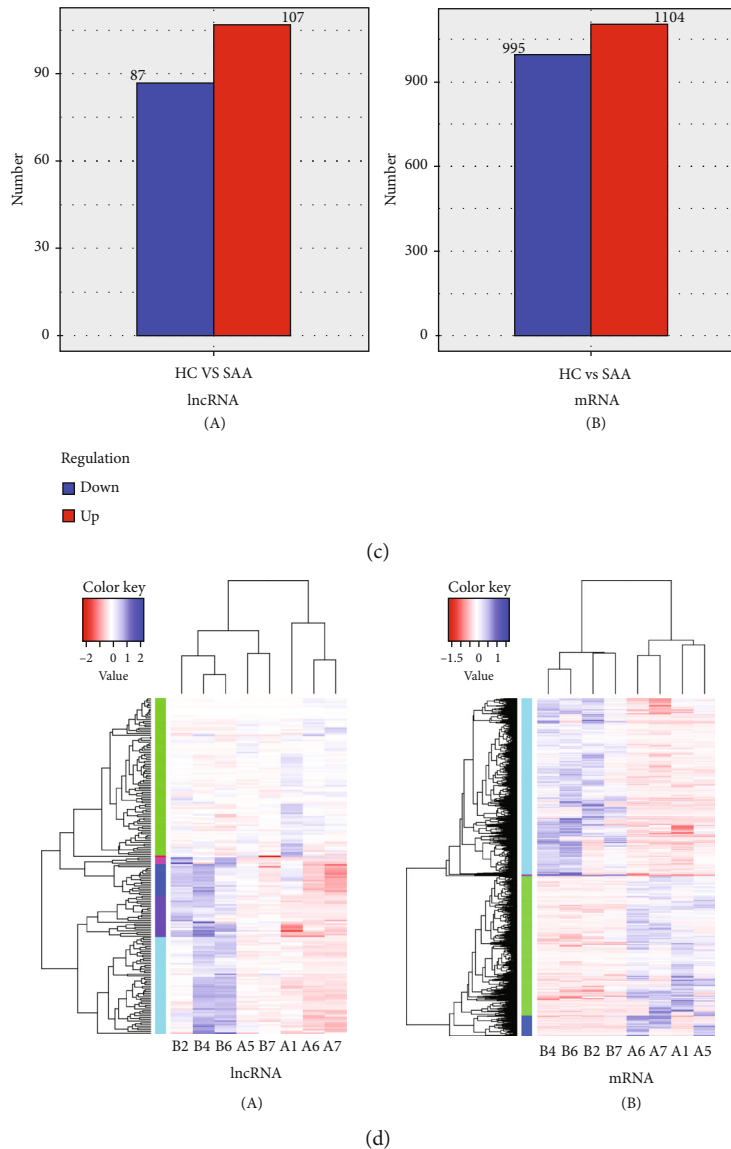
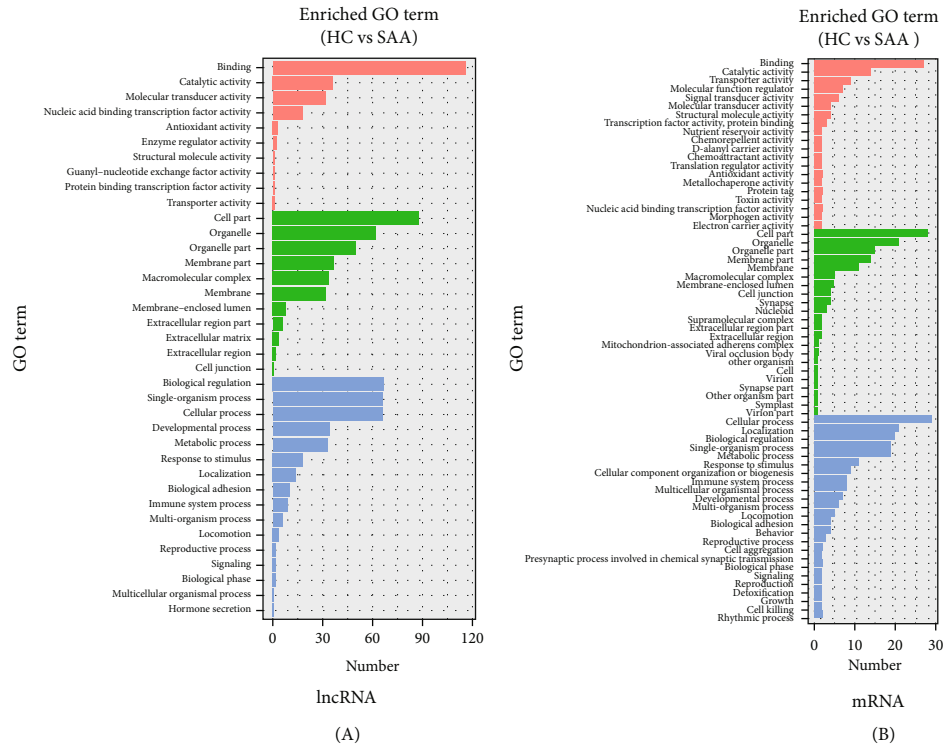
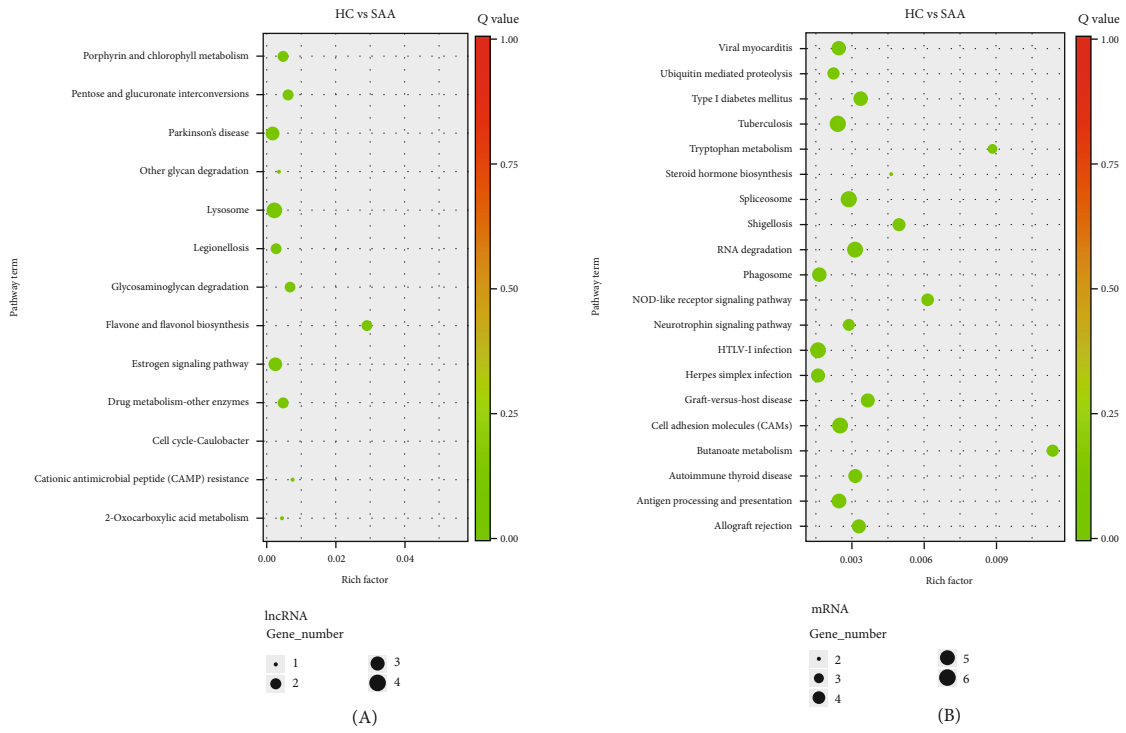


FIGURE 1: Analysis of the lncRNA and mRNA expression profiles of CD8+ T lymphocytes from patients with SAA. (a) Magnetic-activated cell sorting (MACS) was used to sort CD8+ T lymphocytes from the peripheral mononuclear cells of 4 newly diagnosed SAA patients and 4 healthy controls, and the enrichment of CD8+ T lymphocytes (>90%) was detected by FCM. (b) Description of lncRNAs and related statistics. When annotating known lncRNAs, we first integrated the lncRNA information of the Ensembl database, GENCODE database, University of California, Santa Cruz (UCSC) database, and other authoritative databases. We also used CuffCompare software for annotation (A). Based on the information regarding the position of lncRNAs on the reference genome, the obtained lncRNAs were divided into the following three categories: intergenic lncRNAs, antisense lncRNAs, and intronic lncRNAs, and the number of each type of lncRNA was statistically analysed (B). (c) Screening of differentially expressed target genes of lncRNAs and mRNAs. The test results were screened according to the significance criteria for differences (gene expression change > 2-fold and $FDR \leq 0.05$), and we assessed whether the significant differentially expressed target genes of lncRNAs (A) and mRNAs (B) were up- or downregulated. Blue represents downregulation of the target gene, whereas red represents upregulation of the target gene. There were 194 lncRNAs (107 upregulated and 87 downregulated) and 2099 mRNAs (1104 upregulated and 995 downregulated) with significant expression changes. (d) Hierarchical clustering analysis based on the lncRNA (A) and mRNA (B) expression profiles. Cluster analysis is used to determine the similarity of the data and classify the data according to the similarity. This method was used to cluster closely related genes or genes with the same function into groups, to identify the function of unknown genes or the unknown function of known genes, and to infer whether the genes are involved in the same metabolic process or cell pathway. Different coloured regions represent different clusters and groupings, and the gene expression patterns within each group are similar, indicating that genes within each group may have similar functions or participate in the same biological processes. B2, B4, B6, and B7 represented 4 SAA patients. A1, A5, A6, and A7 represented 4 healthy controls. The blue column indicates highly expressed genes, and the red column indicates genes with lower expression; the \log_{10} (fragments per kilobase of transcript per million mapped reads (FPKM) + 1) value was used for clustering. The colour sequence from red to blue represents an increase in gene expression.

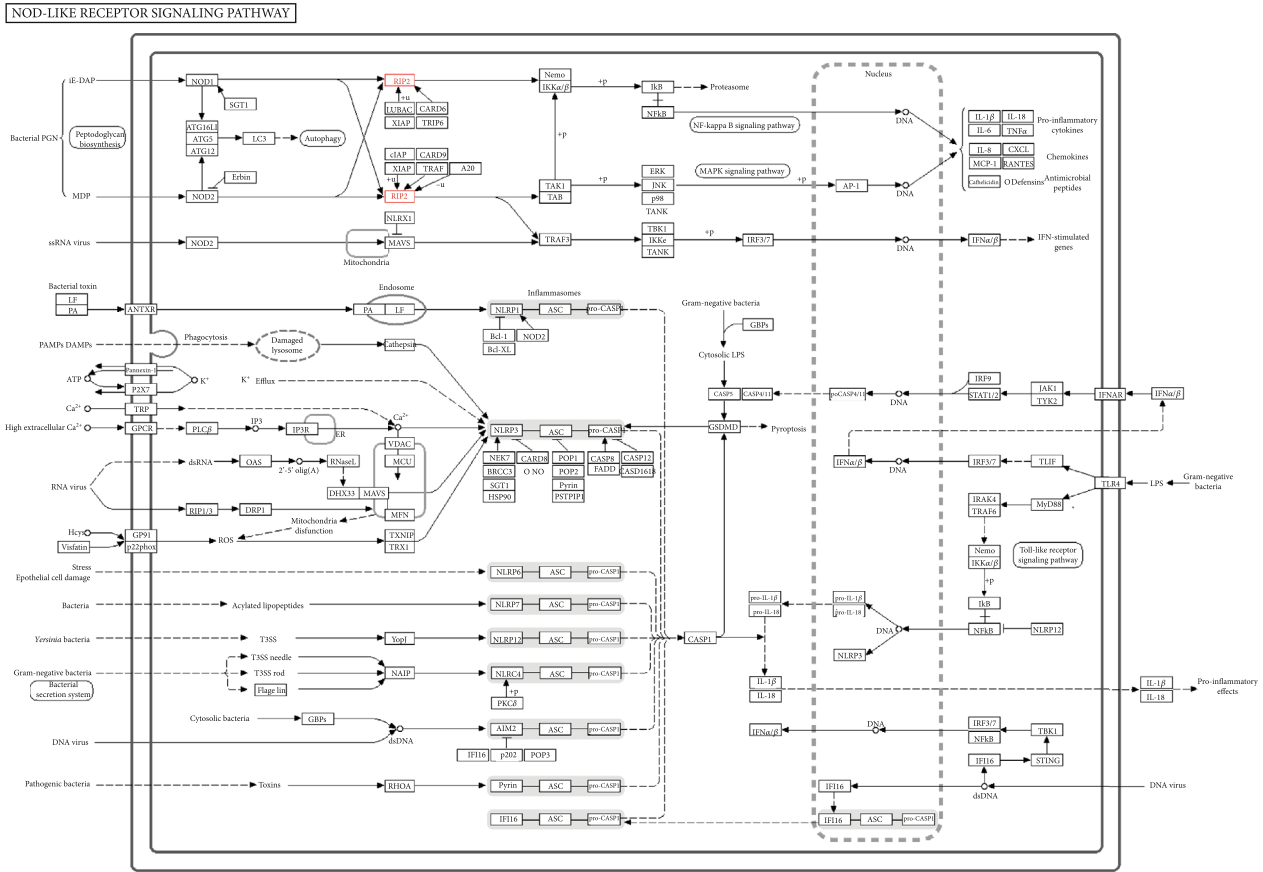


(a)



(b)

FIGURE 2: Continued.



(c)

FIGURE 2: GO and KEGG analysis of the lncRNA and mRNA expression profiles of CD8+ T lymphocytes from patients with SAA. (a) GO analysis of differentially expressed lncRNAs (A) and mRNAs (B). (b) KEGG enrichment bubble plot for differentially expressed lncRNAs (A) and mRNAs (B). (c) The pathway related to our study from KEGG analysis. In this pathway map, RIP2 was upregulated, which is represented in red. The MAPK signalling pathway is closely related to various biological functions, such as T cell differentiation and proliferation. After activation of the NOD1/NOD2 signalling pathway by the NOD-like receptor (NLR) family, the NOD-RIP2 interaction leads to the activation of nuclear factor- κ B (NF- κ B) and the MAPK pathway and promotes the transcription of proinflammatory cytokines (IL-6, IL-1 β).

TABLE 3: Predicted lncRNA target genes and correlated transcripts.

lncRNA	Acting	Transcript ID	Effect	Gene ID	Regulation
TCONS_00379951	Cis*	ENST00000540020	Promote	ENSG00000104312	Down
TCONS_00043638	Cis*	ENST00000415217	Promote	ENSG00000151651	Down
TCONS_00329529	Cis*	ENST00000606851	Promote	ENSG00000272168	Up
TCONS_00002554	Trans [#]	ENST00000487968	Inhibit	ENSG00000186716	Down
TCONS_00026350	Cis*	ENST00000261465	Promote	ENSG00000117594	Down
TCONS_00380395	Cis*	ENST00000521559	Inhibit	ENSG00000132549	Down
TCONS_00117395	Trans [#]	ENST00000481617	Inhibit	ENSG00000133138	Down

*Cis refers to cis-acting regulation. Cis-acting regulation usually refers to the way in which DNA sequences on the same chromosome directly regulate the expression of other adjacent genes. [#]Trans refers to trans-acting regulation. Trans-acting regulation is another mechanism by which lncRNAs can regulate target genes. In this mode, lncRNAs and target genes directly recognize each other through base pairing independent of chromosome position.

5.4. RIP2, NF- κ B, and MAPK Protein Levels in lncRNA AF117829.1-Overexpressing CD8+ T Lymphocytes. The protein levels of RIP2, NF- κ B, and MAPK showed a tendency

to decrease in the overexpression group compared with the blank group. The RIP2 and NF- κ B protein levels were significantly reduced (Figure 5(c)).

TABLE 4: Baseline characteristics of SAA and R-SAA patients and healthy controls.

	Sex (M/F)	Median age (range)	WBC ($\times 10^9/L$)	RBC ($\times 10^{12}/L$)	Hb (g/L)	RET ($\times 10^9/L$)	PLT ($\times 10^9/L$)	NEU ($\times 10^9/L$)
SAA	23/25	44.5 (15-79)	1.53 \pm 0.17	1.73 \pm 1.13	67.4 \pm 2.59	8.93 \pm 1.45	40.40 \pm 6.13	0.37 \pm 0.13
R-SAA	19/14	30 (11-64)	5.01 \pm 0.64	4.16 \pm 0.56	121 \pm 8.13	73.13 \pm 9.77	98.67 \pm 17.89	2.77 \pm 0.54
HC	15/23	38 (20-52)	5.2 \pm 0.34	4.39 \pm 1.02	117 \pm 6.23	77.88 \pm 3.55	263 \pm 10.57	3.83 \pm 1.09

TABLE 5: lncRNA and mRNA expression in CD8+ T lymphocytes as detected by RT-qPCR. The data were represented as the median (25%, 75%).

	SAA	R-SAA	HC
AF117829.1	0.74 (0.431, 1.205)	2.215 (0.8442, 5.136)	6.688 (3.342, 10.32)
RIP2	5.494 (2.144, 30.95)	4.274 (2.398, 9.056)	1.991 (0.4553, 4.655)
TCONS_00043638	0.3 (0.15, 0.5)	0.6373 (0.4093, 1.15)	1.6 (0.6, 2.4)
ADAM8	3.327 (1.678, 4.467)	2.454 (1.624, 4.226)	2.328 (0.5487, 2.98)
TCONS_00329529	4.691 (1.873, 10.79)	3.9 (0.2907, 6.495)	1.739 (0.152, 5.036)
DUOX2	6.923 (3.937, 9.961)	3.443 (1, 8.3)	2.17 (1.075, 4.175)

5.5. Perforin and Granzyme B Expression Decreased in CD8+ T Lymphocytes Treated with GSK583. GSK583, a RIP2 kinase inhibitor, was used to treat CD8+ T lymphocytes collected from the peripheral blood of SAA patients in vitro. MACS was used to sort CD8+ T lymphocytes, and the purity was greater than 90%, as detected by FCM (Figure 5(f)). Perforin expression in GSK583-treated CD8+ T lymphocytes was decreased compared with that in DMSO-treated cells ($22.23 \pm 2.517\%$; $35.2 \pm 4.237\%$; $p = 0.025$). The expression of granzyme B tended to decrease but was not significantly different between the two groups ($38.63 \pm 3.392\%$; $46.35 \pm 6.345\%$; $p = 0.33$) (Figure 5(g)).

5.6. RIP2 and MAPK Protein Levels Were Also Decreased in CD8+ T Lymphocytes Treated with GSK583. Protein was extracted from CD8+ T lymphocytes after GSK583 intervention, and western blotting was used to detect the RIP2 and MAPK protein levels. The results suggested that RIP2 and MAPK were significantly downregulated in CD8+ T lymphocytes treated with GSK583 (Figure 5(h)).

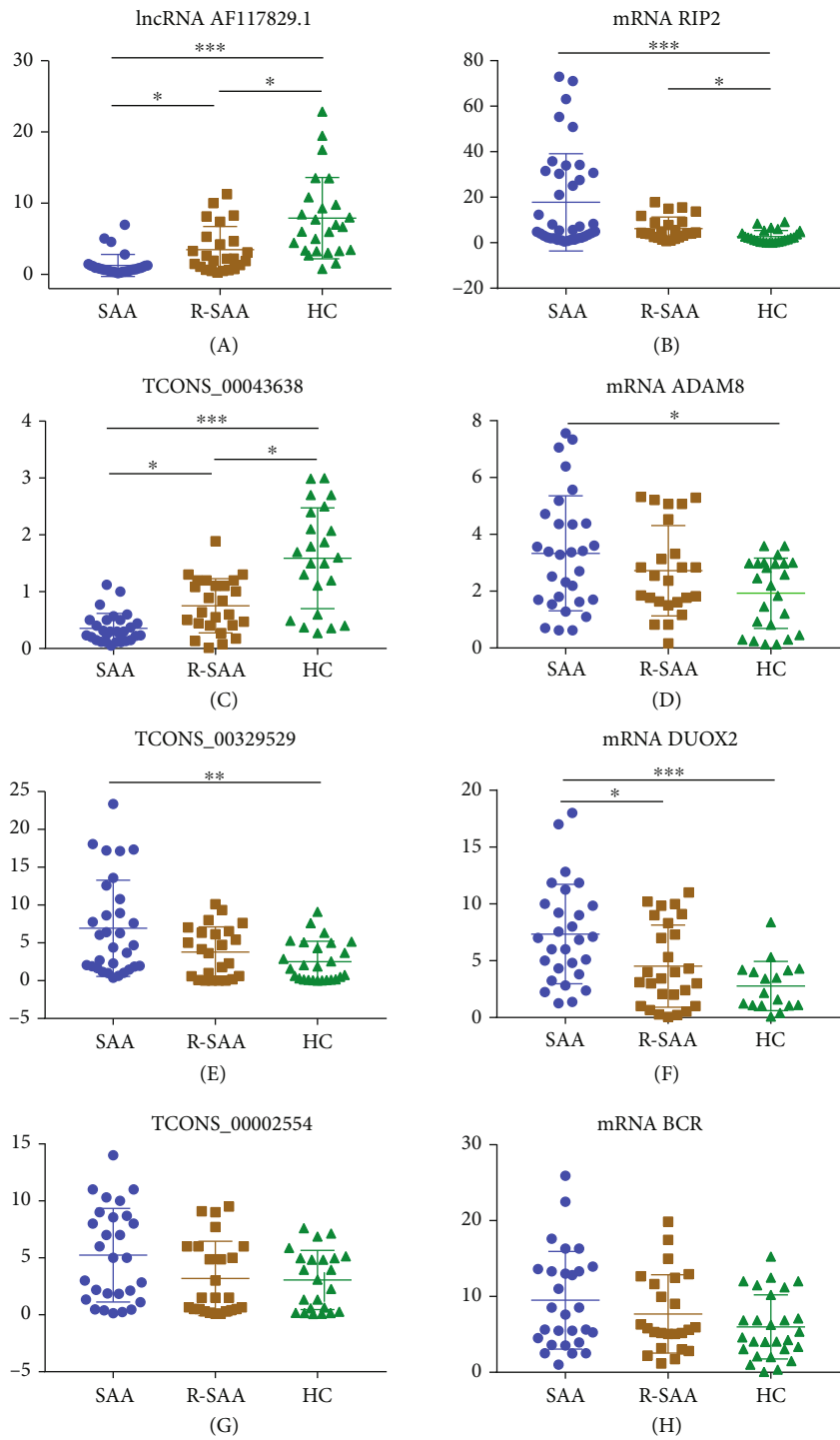
5.7. Changes in IL-6 and IL-1 β in the Culture Supernatants after GSK583 Intervention. Changes in IL-6 and IL-1 β were detected in the culture supernatants after GSK583 intervention by ELISA. The results showed that the IL-6 levels decreased with GSK583 treatment compared with DMSO treatment (2.95 ± 0.337 ; 4.538 ± 0.579 ; $p = 0.036$). The IL-1 β levels exhibited a decreasing trend but did not show a significant difference (5.793 ± 0.275 ; 6.575 ± 0.2527 ; $p = 0.828$) (Figure 5(i)).

6. Discussion

SAA is an autoimmune disease, and its immune tolerance mechanism is dysregulated by hyperfunctional T lymphocytes targeting the haematopoietic system [28]. The abnormal immune regulation mechanism is the main pathogenesis

mode. First, myeloid dendritic cell (mDC) dysfunction leads to an insufficient number of T regulatory cells (Tregs), which causes Th1/Th2 imbalance. Then, haematopoietic stem/progenitor cells are attacked by activated CD8+ T lymphocytes through the Fas/FasL pathway, perforin, granzyme B, and TNF- β , causing serious pancytopenia [29, 30]. CD8+ T lymphocytes play very important roles in the pathogenesis of SAA, which is characterized by an increase in the number and activity of CD8+ T lymphocytes [31, 32]. Moreover, oligoclonal T cell expansion exists in autoimmune diseases such as SLE [33, 34]. Our group detected the expression of tumour necrosis factor-related apoptosis-inducing ligand (TRAIL) in the CD8+ T lymphocytes of SAA patients and found that TRAIL expression was negatively correlated with the expression of perforin and granzyme B in CD8+ T lymphocytes and apoptosis. The TRAIL pathway may activate CD8+ T lymphocytes abnormally and induce the pathogenesis of SAA [35]. The frequency of mutations/polymorphisms of the T cell receptor (TCR)/CD3 signalling complex seems to be decreased in autoimmune disease, chronic inflammation, and malignant tumour states compared to healthy states, which might be caused by T lymphocyte immunodeficiency [36, 37]. The above findings indicate that abnormal immune responses to haematopoietic stem cells/progenitor cells are due to dysregulation of the T cell activation pathway [8].

Based on our previous high-throughput sequencing results and further studies, we found that lncRNA AF117829.1 expression was notably decreased in CD8+ T lymphocytes from patients with SAA, whose function was associated with T lymphocyte proliferation and activation. lncRNAs regulate gene expression independent of protein coding and interact with protein-coding genes in various cell types through multiple processes, such as epigenetic regulation of transcription, mRNA stability, and protein localization [38]. lncRNAs have been shown to be closely related to various immune diseases [39–41]. Downregulation of lncRNA ITS1-2 is associated with rheumatoid arthritis (RA). lncRNA ITS1-2 may reduce



(a)

FIGURE 3: Continued.

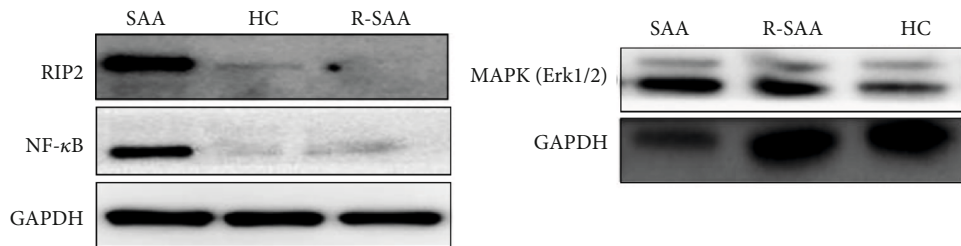
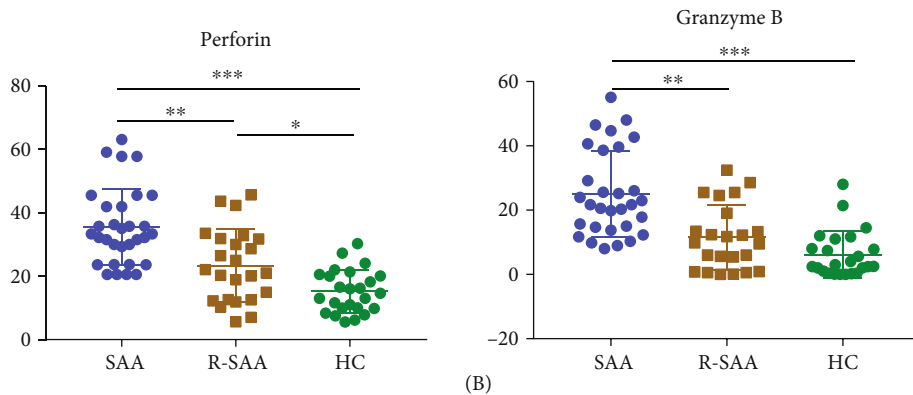
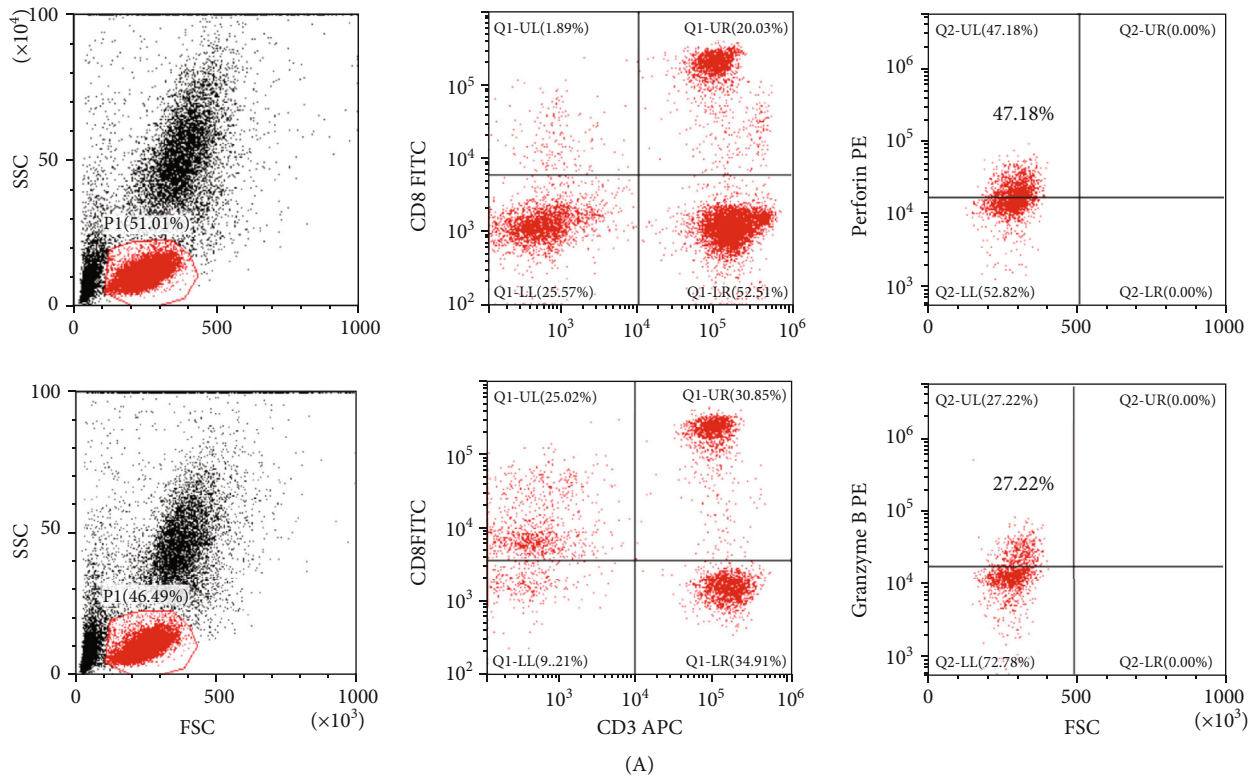
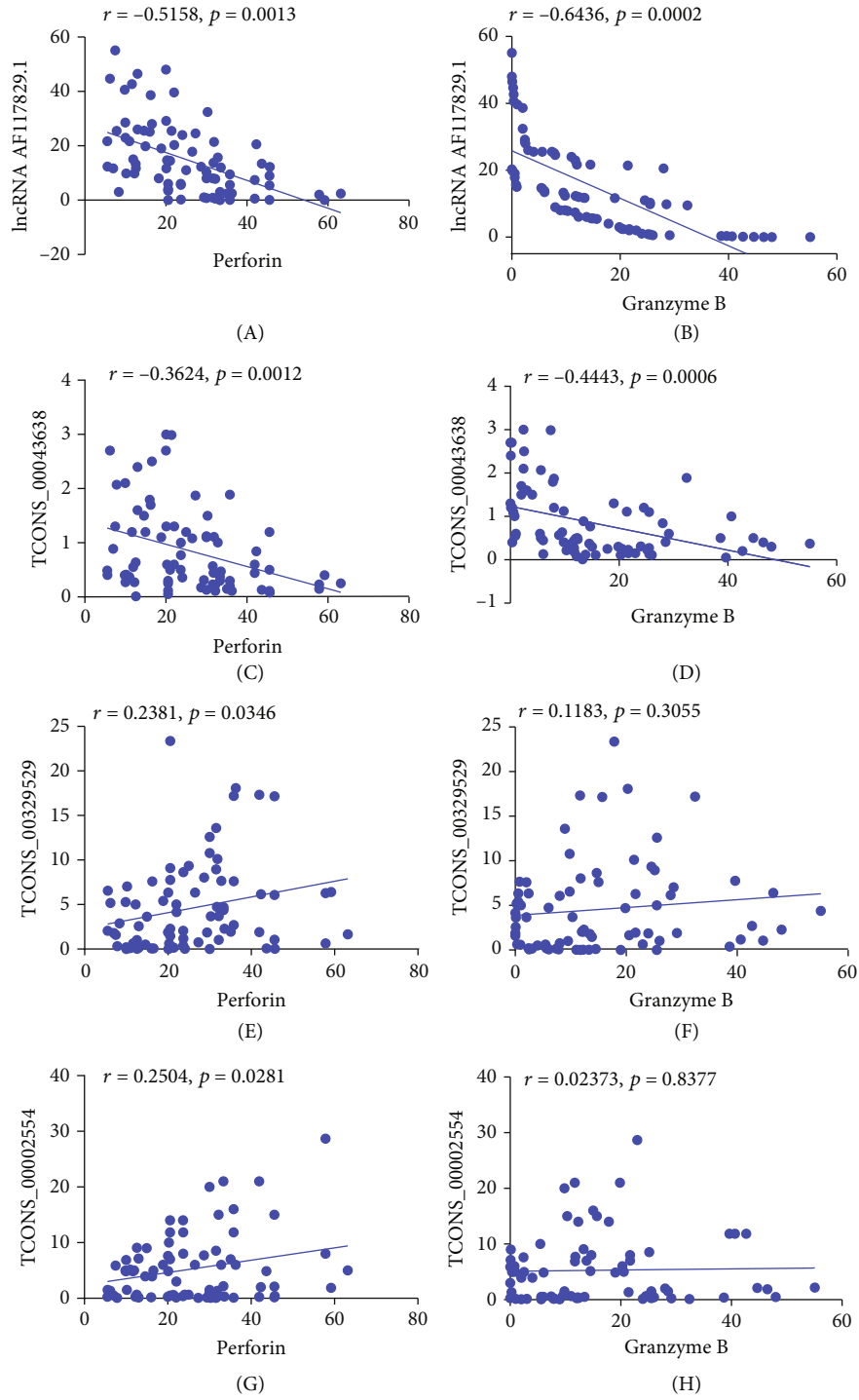


FIGURE 3: The expression of lncRNA AF117829.1 in the CD8+ T lymphocytes of patients with SAA. (a) lncRNA and mRNA expression in CD8+ T lymphocytes. (b) Perforin and granzyme B expression in CD8+ T lymphocytes detected by FCM (A), and those expressions were upregulated in the CD8+ T lymphocytes of newly diagnosed SAA patients (B). (c) Expression of relevant proteins involved in the RIP2 signalling pathway.

the proliferation and immunoreaction of fibroblast-like synovocytes by inhibiting the NOD2/RIP2 signalling pathway in RA patients [42]. Qiu et al. found that lncRNA MEG3 in

peripheral blood CD4+ T lymphocytes could affect the balance of Treg/Th17 cells by regulating microRNA-17 in asthma patients [43].



(a)

FIGURE 4: Continued.

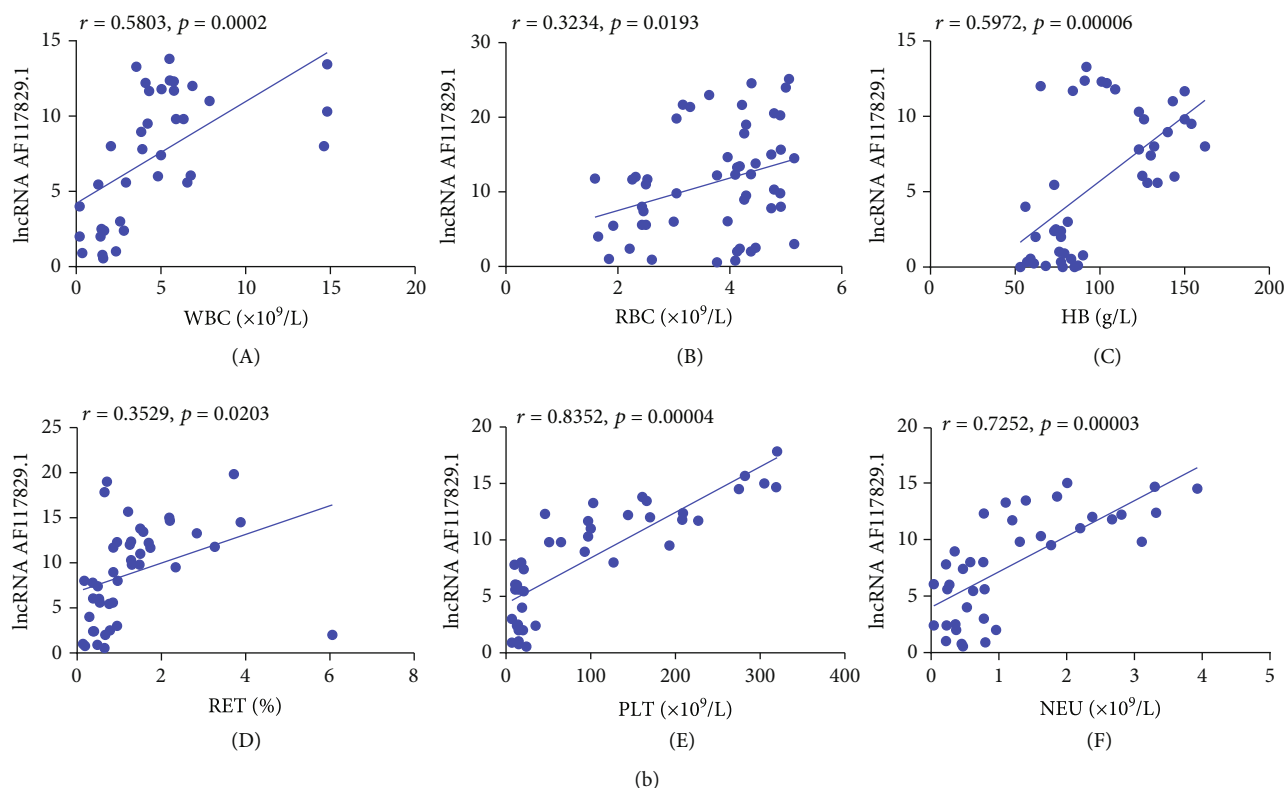


FIGURE 4: The correlation between the expression of screened lncRNAs, the expression of molecules related to CD8+ T lymphocyte function, and SAA patient clinical characteristics. (a) The correlation between lncRNA expression and perforin and granzyme B expression in the CD8+ T lymphocytes of SAA patients, including lncRNA AF117829.1 (A, B), lncRNA TCONS_00043638 (C, D), lncRNA TCONS_00329529 (E, F), and lncRNA TCONS_00002554 (G, H). (b) The correlation between lncRNA AF117829.1 expression in CD8+ T lymphocytes and the clinical indexes of SAA patients, including WBC (A), RBC (B), Hb (C), RET% (D), PLT (E), and NEU (F).

At present, there are few studies on lncRNAs in SAA. In our study, we performed high-throughput sequencing and predicted the target genes of differentially expressed lncRNAs in CD8+ T lymphocytes from patients with SAA. The GO analysis showed that the predicted target genes of lncRNAs were mainly related to signal transduction activity, metabolic process, the response to stimuli, and organelle components. The KEGG analysis showed that the predicted target genes of lncRNAs were related to antigen processing and presentation and the NOD, MAPK, and PKC signalling pathways. The MAPK signalling pathway plays an extremely crucial role in various biological functions, such as T lymphocyte differentiation and proliferation [44]. After activation of the NOD1/NOD2 signalling pathway, the interaction between NOD and RIP2 activates the NF- κ B and MAPK pathways, which promotes the activation of proinflammatory cytokine transcription [45]. Our results are consistent with the sequencing results. lncRNA AF117829.1 expression in CD8+ T lymphocytes was significantly decreased in SAA patients compared with healthy controls and was significantly negatively correlated with perforin and granzyme B expression. lncRNA TCONS_00043638 expression was negatively correlated with perforin and granzyme B expression. lncRNA TCONS_00329529 and lncRNA TCONS_00002554 expression was positively correlated with perforin expression. This suggests that these lncRNAs could

regulate CD8+ T lymphocyte function in the pathogenesis of SAA.

Among these lncRNAs, lncRNA AF117829.1 expression had a significantly negative correlation with perforin and granzyme B expression and a significant positive correlation with the blood cell counts of SAA patients. RIP2, the predicted target gene of lncRNA AF117829.1, is closely related to immunity. The downstream signalling pathway of RIP2 can regulate the NF- κ B and MAPK pathways. RIP2 participates in the TCR signalling pathway, activates NF- κ B and MAPK signalling, and induces the transcription of inflammatory factors by recruiting TNFR1 and CD14 receptor signalling complexes [46]. However, there are no relevant reports on the mechanism of RIP2 in CD8+ T lymphocytes in SAA. We found that the protein levels of RIP2, NF- κ B, and MAPK were significantly increased in CD8+ T lymphocytes in SAA patients. Overexpression of lncRNA AF117829.1 in CD8+ T lymphocytes from SAA patients decreased the expression of mRNA RIP2 and related proteins (RIP2, NF- κ B, and MAPK) in the RIP2 signalling pathway. Similarly, perforin and granzyme B expression decreased, and the apoptosis of CD8+ T lymphocytes decreased. Our results suggest that the overexpression of lncRNA AF117829.1 may affect the RIP2 signalling pathway and regulate the apoptosis and inflammation of CD8+ T lymphocytes in SAA. RIP2 kinase is a multidomain, dual-specific

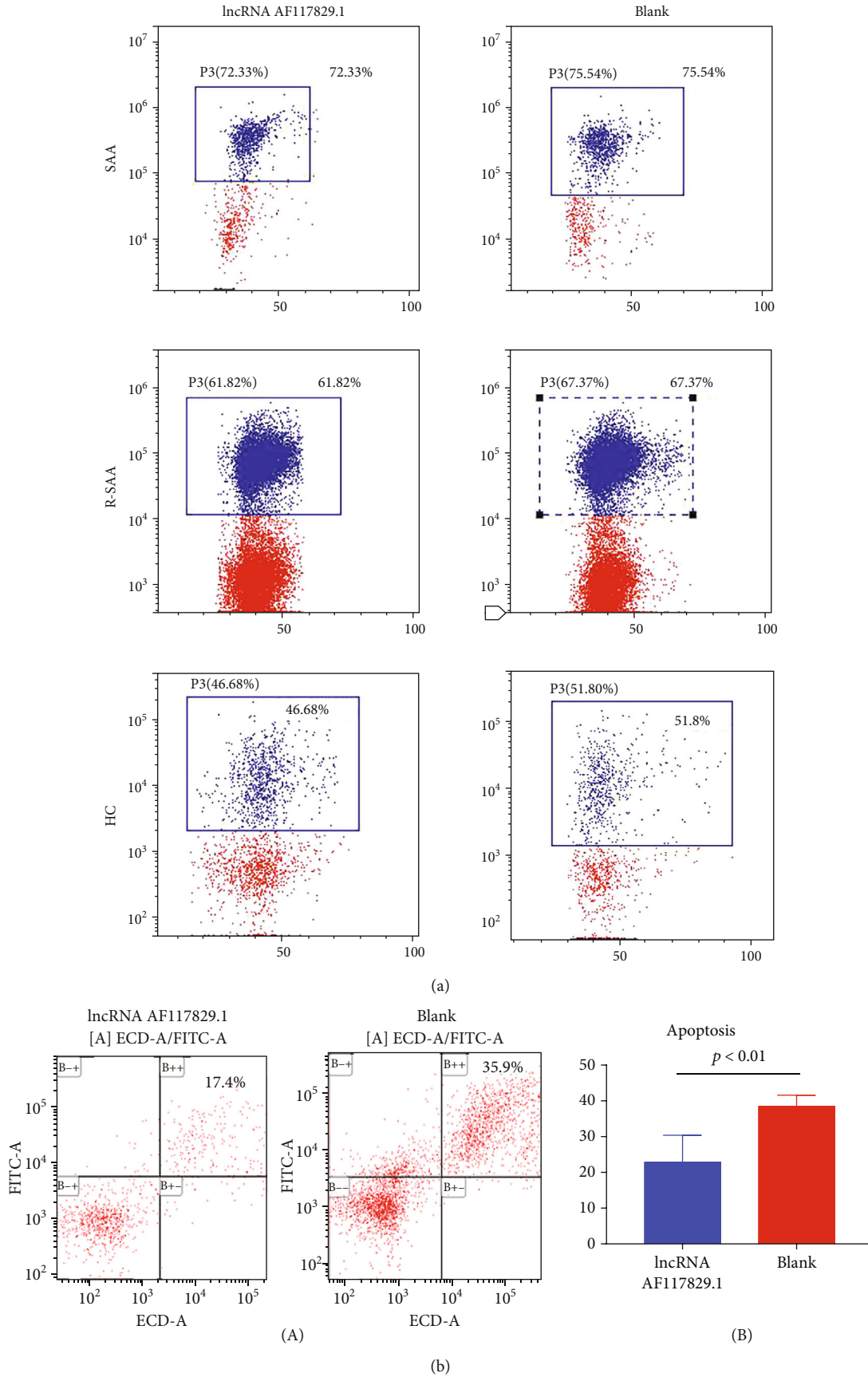
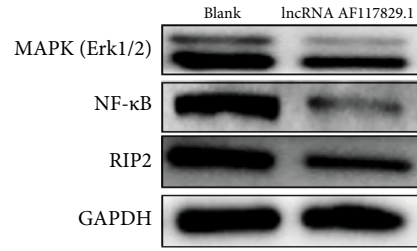
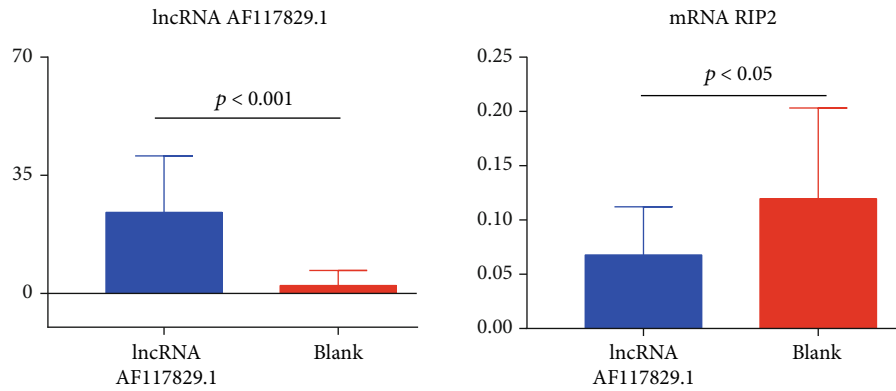


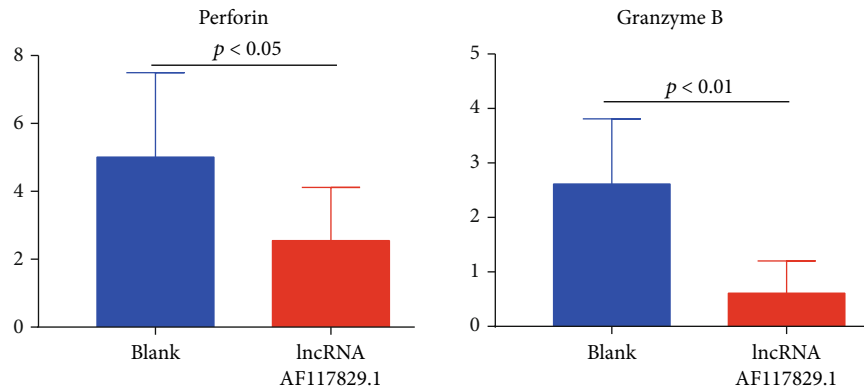
FIGURE 5: Continued.



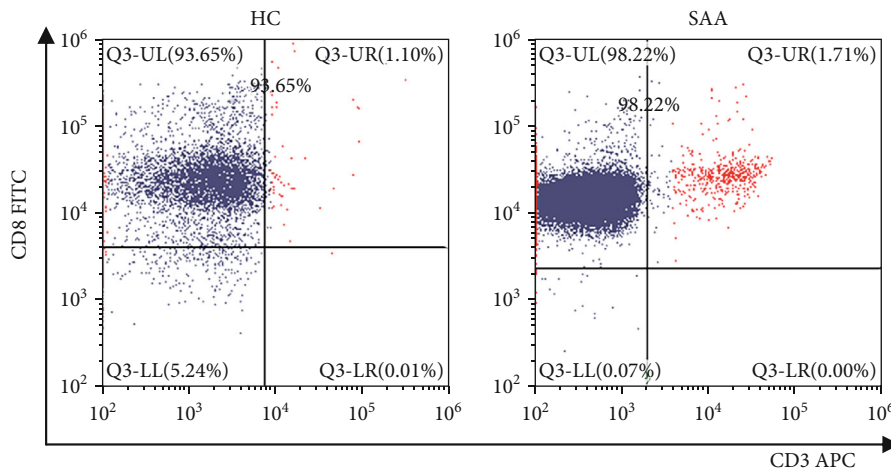
(c)



(d)



(e)



(f)

FIGURE 5: Continued.

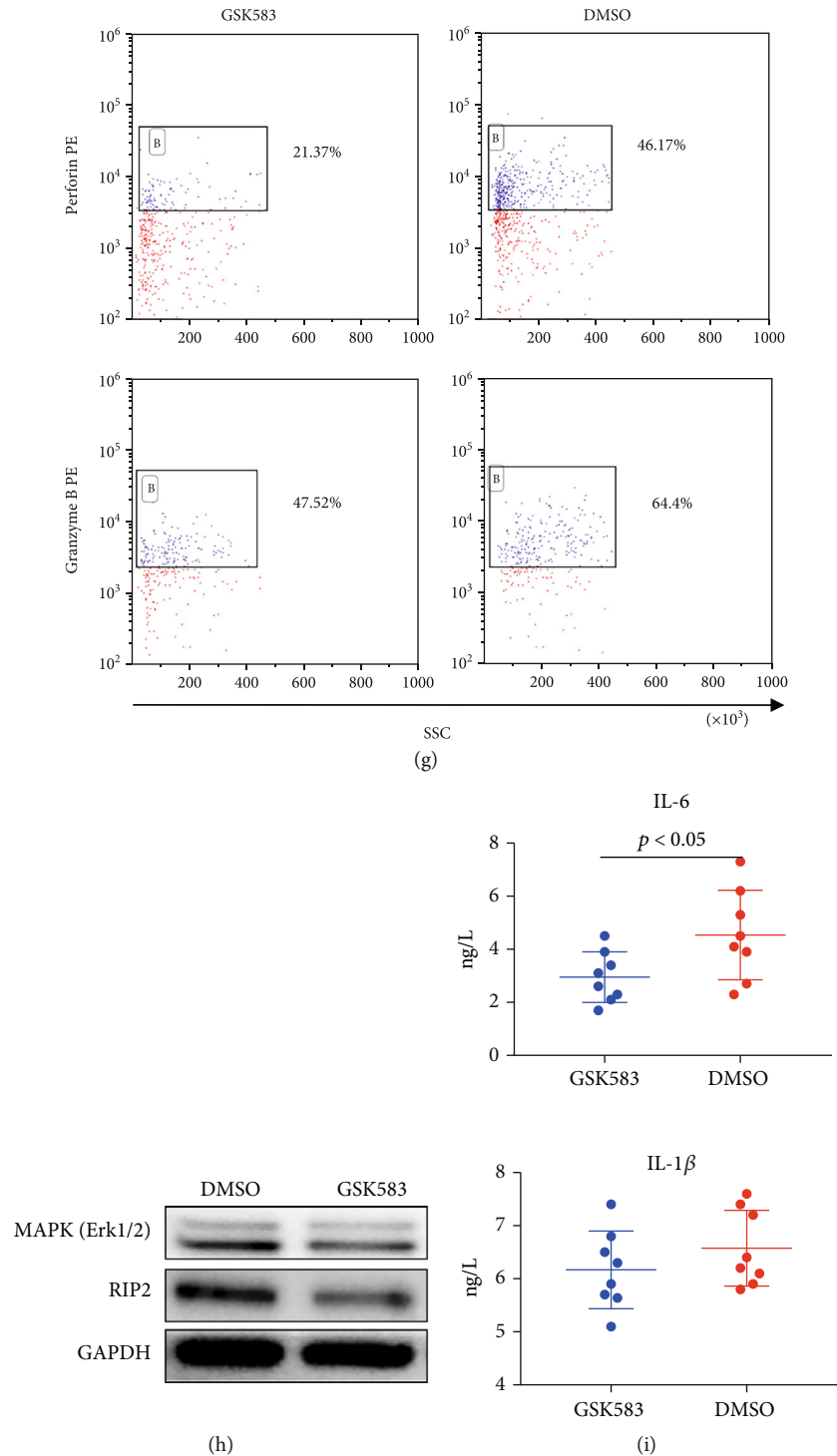


FIGURE 5: lncRNA AF117829.1 mediated the effect of CD8+ T lymphocytes in SAA patients. (a) FCM to detect the transfection rate of lncRNA AF117829.1 in the CD8+ T lymphocytes of newly diagnosed SAA patients, R-SAA patients, and healthy controls. (b) FCM to detect the apoptosis rate of CD8+ T lymphocytes overexpressing lncRNA AF117829.1 (A), and lncRNA AF117829.1 overexpression suppressed the apoptosis of CD8+ T lymphocytes (B). (c) Western blotting to detect RIP2, NF- κ B, and MAPK protein levels in lncRNA AF117829.1-overexpressing CD8+ T lymphocytes. (d) lncRNA AF117829.1 and mRNA RIP2 expression detected by RT-qPCR in the lncRNA AF117829.1-overexpressing CD8+ T lymphocytes. (e) Perforin and granzyme B expression in the lncRNA AF117829.1-overexpressing CD8+ T lymphocytes. (f) The purity of CD8+ T lymphocytes isolated from newly diagnosed SAA patients as detected by FCM. (g) Perforin and granzyme B expression decreased in CD8+ T lymphocytes treated with GSK583, as determined by FCM. (h) RIP2 and MAPK protein levels detected by western blotting in CD8+ T lymphocytes treated with GSK583. (i) The changes in IL-6 and IL-1 β levels tested by ELISA in the culture supernatants of cells treated with GSK583.

kinase [47]. After phosphorylation and ubiquitination, RIP2 kinase can activate NF- κ B and MAPK to achieve downstream signal transduction and the transcription of inflammatory cytokines [48, 49]. RIP2 kinase is considered to be a therapeutic target to treat several autoimmune diseases. GSK583 is a highly effective and selective RIP2 kinase inhibitor. Haile et al. demonstrated the effectiveness of GSK583 in blocking downstream NOD2/RIP2 signals in cell models, in vivo animal models, and isolated human disease models [50]. In animal models of experimental colitis, RIP2 kinase inhibitors can effectively reduce inflammation [51]. In our experiments, we found that perforin and granzyme B expression significantly decreased in CD8+ T lymphocytes with GSK583 intervention. In addition, IL-1 β and IL-6 secretion also decreased.

In summary, lncRNAs are mostly involved in the pathogenesis of diseases through indirect regulation of immune pathogenesis via pathways such as the cytokine-cytokine receptor interaction pathway and the RIP2, NF- κ B, and MAPK signalling pathways. In this study, we verified that, at low levels, lncRNA AF117829.1 mediates the RIP2 signalling pathway to activate CD8+ T lymphocyte function and participate in the pathogenesis of SAA immune abnormalities.

7. Conclusions

SAA is recognized as an autoimmune disease with immune tolerance dysfunction mediated by hyperactivated T lymphocytes that target the haematopoietic system. Previous studies have shown that the proliferation and overactivation of CD8+ T lymphocytes, also known as CTLs, is a direct factor causing bone marrow failure in SAA patients, but the specific mechanism remains unclear. Our present research displayed the RNA-seq results, possible biological functions, and signalling pathways of CD8+ T lymphocytes from patients with SAA. A total of 194 lncRNAs and 2099 mRNAs exhibited expression changes in the CD8+ T lymphocytes of SAA patients versus R-SAA patients and healthy controls. The predicted target genes of differentially expressed lncRNAs are related to biological processes such as catalytic activity, the response to stimuli, and intra- and extracellular signal transduction. The decreased expression of lncRNA AF117829.1 is closely related to the overactivation of CD8+ T lymphocytes in SAA patients. lncRNA AF117829.1 can regulate the function of CD8+ T lymphocytes by promoting the expression of its target gene RIP2, and the function of CD8+ T lymphocytes is inhibited by treatment with GSK583, a RIP2 kinase inhibitor. Our findings reveal a possible mechanism of lncRNA AF117829.1 in the CD8+ T lymphocytes of patients with SAA, which is helpful for understanding the molecular mechanism of immune pathogenesis and provides potential targets for the diagnosis and treatment of SAA.

Data Availability

The RNA-seq data used to support the findings of this study are included within the article and the supplementary information files. And the RNA-seq data used to support the findings of this study are available from the corresponding author upon request.

Ethical Approval

The study complied with the Declaration of Helsinki and was approved by the Ethics Committee of Tianjin Medical University General Hospital.

Consent

Informed written consent was obtained.

Disclosure

A version of the abstract was published at the 62nd ASH Annual Meeting and Exposition (<https://ash.confex.com/ash/2020/webprogram/Paper139567.html>), and a poster was published at the European Haematology Association Annual meeting (https://library.ehaweb.org/eha/2020/eha25th/294767/rong.fu.the.role.of.lncrna-af117829.1.in.the.immunopathogenesis.of.cd82b.t.html?f=menu%3D6%2Abrowseby%3D8%2Asortby%3D2%2Amedia%3D3%2Ace_id%3D1766%2Aot_id%3D23228%2Amarker%3D757).

Conflicts of Interest

The authors declare no conflicts of interest.

Authors' Contributions

Yang Li and Ling Deng contributed equally to this manuscript. CL conceived and designed the study. YL and LD performed the experiments and were major contributors in writing the manuscript. XP analysed and interpreted the data. RF conceived the study, participated in its design and coordination, and helped to draft the manuscript. All authors read and approved the final manuscript.

Acknowledgments

We thank the staffs of the Department of Haematology, Tianjin Medical University General Hospital, for their supports. We also give special thanks to Dr. Zonghong Shao, Dr. Zhaoyun Liu, and Dr. Hui Liu for their kind help and suggestions during conducting the experiments and preparing the manuscript. This work was supported by the Scientific research projects of Tianjin Municipal Education Commission (2019KJ199), the Tianjin Natural Science Foundation (17JCQNJC11500, 18JCYBJC91700, and 18ZXDBSY00140), and the National Natural Science Foundation of China (NSFC) (81770110, 81970115, 81800120, 81870101, 81800119, 81770118, 81700118, 81700117, 81900125, and 81970116).

Supplementary Materials

Supplementary 1. Supplementary file S1: the RNA-seq results of 2099 differentially expressed mRNAs (1104 upregulated and 995 downregulated mRNAs) in CD8+ T lymphocytes from SAA patients, including transcript ID, its length, log₂ fold change, *p* values, adjusted *p* values, expression (up- or downregulation), and gene ID and the corresponding gene symbol.

Supplementary 2. Supplementary file S2: the RNA-seq results of 194 differentially expressed lncRNAs (107 upregulated and 87 downregulated lncRNAs) in CD8+ T lymphocytes from SAA patients, including lncRNA ID, its length, log₂ fold change, *p* values, adjusted *p* values, and expression (up- or downregulation).

References

- [1] N. S. Young, "Aplastic anemia," *The New England Journal of Medicine*, vol. 379, no. 17, pp. 1643–1656, 2018.
- [2] N. Frickhofen, H. Heimpel, J. P. Kaltwasser, and H. Schrezenmeier, "Antithymocyte globulin with or without cyclosporin a: 11-year follow-up of a randomized trial comparing treatments of aplastic anemia," *Blood*, vol. 101, no. 4, pp. 1236–1242, 2003.
- [3] N. Stanley, T. S. Olson, and D. V. Babushok, "Recent advances in understanding clonal haematopoiesis in aplastic anaemia," *British Journal of Haematology*, vol. 177, no. 4, pp. 509–525, 2017.
- [4] H. Schrezenmeier, S. Körper, and B. Höchsmann, "Aplastic anemia," *Deutsche Medizinische Wochenschrift*, vol. 139, no. 49, pp. 2503–2506, 2014.
- [5] W. Sheng, C. Liu, R. Fu et al., "Abnormalities of quantities and functions of linker for activations of T cells in severe aplastic anemia," *European Journal of Haematology*, vol. 93, no. 3, pp. 214–223, 2014.
- [6] W. Qi, L. Yan, C. Liu, R. Fu, H. Wang, and Z. Shao, "Abnormal histone acetylation of CD8+ T cells in patients with severe aplastic anemia," *International Journal of Hematology*, vol. 104, no. 5, pp. 540–547, 2016.
- [7] L. Xing, C. Liu, R. Fu et al., "CD8+HLA-DR+ T cells are increased in patients with severe aplastic anemia," *Molecular Medicine Reports*, vol. 10, no. 3, pp. 1252–1258, 2014.
- [8] N. S. Young, R. T. Calado, and P. Scheinberg, "Current concepts in the pathophysiology and treatment of aplastic anemia," *Blood*, vol. 108, no. 8, pp. 2509–2519, 2006.
- [9] C. I. Brannan, E. C. Dees, R. S. Ingram, and S. M. Tilghman, "The product of the H19 gene may function as an RNA," *Molecular and Cellular Biology*, vol. 10, no. 1, pp. 28–36, 1990.
- [10] L. W. Harries, "Long non-coding RNAs and human disease," *Biochemical Society Transactions*, vol. 40, no. 4, pp. 902–906, 2012.
- [11] T. Derrien, R. Johnson, G. Bussotti et al., "The GENCODE v7 catalog of human long noncoding RNAs: analysis of their gene structure, evolution, and expression," *Genome Research*, vol. 22, no. 9, pp. 1775–1789, 2012.
- [12] J. J. Quinn and H. Y. Chang, "Unique features of long non-coding RNA biogenesis and function," *Nature Reviews. Genetics*, vol. 17, no. 1, pp. 47–62, 2016.
- [13] T. R. Mercer, M. E. Dinger, and J. S. Mattic, "Long non-coding RNAs: insights into functions," *Nature Reviews. Genetics*, vol. 10, no. 3, pp. 155–159, 2009.
- [14] F. Zhang, L. Wu, J. Qian et al., "Identification of the long non-coding RNA NEAT1 as a novel inflammatory regulator acting through MAPK pathway in human lupus," *Journal of Autoimmunity*, vol. 75, pp. 96–104, 2016.
- [15] T. Li, M. Gu, P. Liu et al., "Abnormal expression of long non-coding RNAs in primary immune thrombocytopenia: a microarray related study," *Cellular Physiology and Biochemistry*, vol. 48, no. 2, pp. 618–632, 2018.
- [16] J.-Q. Li, S.-Y. Hu, Z.-Y. Wang et al., "Long non-coding RNA MEG3 inhibits microRNA-125a-5p expression and induces immune imbalance of Treg/Th17 in immune thrombocytopenic purpura," *Biomedicine & Pharmacotherapy*, vol. 83, pp. 905–911, 2016.
- [17] J. S. Mattick and M. J. Gagen, "The evolution of controlled multitasked gene networks: the role of introns and other non-coding RNAs in the development of complex organisms," *Molecular Biology and Evolution*, vol. 18, no. 9, pp. 1611–1630, 2001.
- [18] T. R. Mercer and J. S. Mattick, "Structure and function of long noncoding RNAs in epigenetic regulation," *Nature Structural & Molecular Biology*, vol. 20, no. 3, pp. 300–307, 2013.
- [19] Y. Wang, H. Zhong, X. Xie et al., "Long noncoding RNA derived from CD244 signaling epigenetically controls CD8+ T cell immune responses in tuberculosis infection," *Proceedings of the National Academy of Sciences of the United States of America*, vol. 112, no. 29, pp. E3883–E3892, 2015.
- [20] D. Mao, C. Hu, J. Zhang et al., "Long noncoding RNA GM16343 promotes IL-36 β to regulate tumor microenvironment by CD8+T cells," *Technology in Cancer Research & Treatment*, vol. 18, p. 153303381988363, 2019.
- [21] S. B. Killick, N. Bown, J. Cavenagh et al., "Guidelines for the diagnosis and management of adult aplastic anaemia," *British Journal of Haematology*, vol. 172, no. 2, pp. 187–207, 2016.
- [22] D. F. B. Miller, P. Yan, F. Fang et al., "Complete transcriptome RNA-Seq," *Methods in Molecular Biology*, vol. 1513, pp. 141–162, 2017.
- [23] Y. Erlich, P. P. Mitra, M. dela Bastide, W. R. McCombie, and G. J. Hannon, "Alta-Cyclic: a self-optimizing base caller for next-generation sequencing," *Nature Methods*, vol. 5, no. 8, pp. 679–682, 2008.
- [24] A. Mortazavi, B. A. Williams, K. McCue, L. Schaeffer, and B. Wold, "Mapping and quantifying mammalian transcriptomes by RNA-Seq," *Nature Methods*, vol. 5, no. 7, pp. 621–628, 2008.
- [25] The Gene Ontology Consortium, "The Gene Ontology resource: 20 years and still GOing strong," *Nucleic Acids Research*, vol. 47, no. D1, pp. D330–D338, 2019.
- [26] M. Kanehisa, M. Furumichi, M. Tanabe, Y. Sato, and K. Morishima, "KEGG: new perspectives on genomes, pathways, diseases and drugs," *Nucleic Acids Research*, vol. 45, no. D1, pp. D353–D361, 2017.
- [27] P. A. Haile, B. J. Votta, R. W. Marquis et al., "The identification and pharmacological characterization of 6-(tert-butylsulfonyl)-N-(5-fluoro-1H-indazol-3-yl)quinolin-4-amine (GSK583), a highly potent and selective inhibitor of RIP2 kinase," *Journal of Medicinal Chemistry*, vol. 59, no. 10, pp. 4867–4880, 2016.
- [28] A. Bacigalupo, "How I treat acquired aplastic anemia," *Blood*, vol. 129, no. 11, pp. 1428–1436, 2017.
- [29] L. Yan, R. Fu, H. Liu et al., "Abnormal quantity and function of regulatory T cells in peripheral blood of patients with severe aplastic anemia," *Cellular Immunology*, vol. 296, no. 2, pp. 95–105, 2015.
- [30] H. He, Z. Shao, G. He et al., "Role of Th1 cell in the pathogenesis of aplastic anemia," *Zhonghua Xue Ye Xue Za Zhi*, vol. 23, no. 11, pp. 574–577, 2002.
- [31] K. Kaito, H. Otsubo, N. Usui, and M. Kobayashi, "Th1/Th2 lymphocyte balance in patients with aplastic anemia," *Rinsho Byori*, vol. 52, no. 7, pp. 569–573, 2004.

- [32] P. C. Boddu and T. M. Kadia, "Updates on the pathophysiology and treatment of aplastic anemia: a comprehensive review," *Expert Review of Hematology*, vol. 10, no. 5, pp. 433–448, 2017.
- [33] H. Murata, R. Matsumura, A. Koyama et al., "T cell receptor repertoire of T cells in the kidneys of patients with lupus nephritis," *Arthritis and Rheumatism*, vol. 46, no. 8, pp. 2141–2147, 2002.
- [34] T. Kato, M. Kurokawa, H. Sasakawa et al., "Analysis of accumulated T cell clonotypes in patients with systemic lupus erythematosus," *Arthritis and Rheumatism*, vol. 43, no. 12, pp. 2712–2721, 2000.
- [35] C. Liu, M. Zheng, T. Zhang et al., "TRAIL in CD8+ T cells from patients with severe aplastic anemia," *International Journal of Hematology*, vol. 106, no. 4, pp. 490–499, 2017.
- [36] L. Ciszak, E. Pawlak, A. Kosmaczewska, S. Potoczek, and I. Frydecka, "Alterations in the expression of signal-transducing CD3 ζ chain in T cells from patients with chronic inflammatory/autoimmune diseases," *Archivum Immunologiae et Therapiae Experimentalis (Warsz)*, vol. 55, no. 6, pp. 373–386, 2007.
- [37] Y. Li, "Alterations in the expression pattern of TCR ζ chain in T cells from patients with hematological diseases," *Hematology*, vol. 13, no. 5, pp. 267–275, 2013.
- [38] V. R. Paralkar and M. J. Weiss, "Long noncoding RNAs in biology and hematopoiesis," *Blood*, vol. 121, no. 24, pp. 4842–4846, 2013.
- [39] S. ROY and A. AWASTHI, "Emerging roles of noncoding RNAs in T cell differentiation and functions in autoimmune diseases," *International Reviews of Immunology*, vol. 38, no. 5, pp. 232–245, 2019.
- [40] Y. Gao, S. Li, Z. Zhang, X. Yu, and J. Zheng, "The role of long non-coding RNAs in the pathogenesis of RA, SLE, and SS," *Frontiers in Medicine*, vol. 5, p. 193, 2018.
- [41] M. J. Pearson and S. W. Jones, "Review: long noncoding RNAs in the regulation of inflammatory pathways in rheumatoid arthritis and osteoarthritis," *Arthritis & Rheumatology*, vol. 68, no. 11, pp. 2575–2583, 2016.
- [42] T. Yue, X. Fan, Z. Zhang et al., "Downregulation of lncRNA ITS1-2 correlates with decreased disease risk and activity of rheumatoid arthritis (RA), and reduces RA fibroblast-like synoviocytes proliferation and inflammation via inhibiting NOD2/RIP2 signaling pathway," *American Journal of Translational Research*, vol. 11, no. 8, pp. 4650–4666, 2019.
- [43] Y.-y. Qiu, Y. Wu, M.-j. Lin, T. Bian, Y.-l. Xiao, and C. Qin, "LncRNA-MEG3 functions as a competing endogenous RNA to regulate Treg/Th17 balance in patients with asthma by targeting microRNA-17/ ROR γ t," *Biomedicine & Pharmacotherapy*, vol. 111, pp. 386–394, 2019.
- [44] M. Rincón, D. Conze, L. Weiss et al., "Do T cells care about the mitogen-activated protein kinase signalling pathways?," *Immunology and Cell Biology*, vol. 78, no. 2, pp. 166–175, 2000.
- [45] R. Caruso, N. Warner, N. Inohara, and G. Núñez, "NOD1 and NOD2: signaling, host defense, and inflammatory disease," *Immunity*, vol. 41, no. 6, pp. 898–908, 2014.
- [46] A. A. Ruefli-Brasse, W. P. Lee, S. Hurst, and V. M. Dixit, "Rip2 participates in Bcl10 signaling and T-cell receptor-mediated NF- κ B activation," *The Journal of Biological Chemistry*, vol. 279, no. 2, pp. 1570–1574, 2004.
- [47] C. Nembrini, J. Kisielow, A. T. Shamshiev et al., "The kinase activity of Rip2 determines its stability and consequently Nod1- and Nod2-mediated immune responses," *The Journal of Biological Chemistry*, vol. 284, no. 29, pp. 19183–19188, 2009.
- [48] J. T. Tigno-Aranjuez, J. M. Asara, and D. W. Abbott, "Inhibition of RIP2's tyrosine kinase activity limits NOD2-driven cytokine responses," *Genes & Development*, vol. 24, no. 23, pp. 2666–2677, 2010.
- [49] F. Humphries, S. Yang, B. Wang, and P. N. Moynagh, "RIP kinases: key decision makers in cell death and innate immunity," *Cell Death and Differentiation*, vol. 22, no. 2, pp. 225–236, 2015.
- [50] P. A. Haile, L. N. Casillas, M. J. Bury et al., "Identification of quinoline-based RIP2 kinase inhibitors with an improved therapeutic index to the hERG ion channel," *ACS Medicinal Chemistry Letters*, vol. 9, no. 10, pp. 1039–1044, 2018.
- [51] J. T. Tigno-Aranjuez, P. Benderitter, F. Rombouts et al., "In vivo inhibition of RIPK2 kinase alleviates inflammatory disease," *The Journal of Biological Chemistry*, vol. 289, no. 43, pp. 29651–29664, 2014.

Research Article

***Eurotium cristatum* Fermented Loose Dark Tea Ameliorates Cigarette Smoke-Induced Lung Injury by MAPK Pathway and Enhances Hepatic Metabolic Detoxification by PXR/AhR Pathway in Mice**

Xiang-Xiang Huang ¹, Shuai Xu ¹, Li-Jun Yu ¹, Yu-Fei Zhou ¹, Ying Zhou ¹,
and Zhong-Hua Liu ^{1,2}

¹Key Laboratory of Tea Science of Ministry of Education, National Research Center of Engineering Technology for Utilization of Functional Ingredients from Botanicals, College of Horticulture, Hunan Agricultural University, Changsha 410128, China

²Hunan Provincial Key Laboratory for Germplasm Innovation and Utilization of Crop, Hunan Agricultural University, Changsha 410128, China

Correspondence should be addressed to Li-Jun Yu; yulijun_tea@qq.com and Zhong-Hua Liu; larkin-liu@163.com

Received 7 October 2020; Revised 5 January 2021; Accepted 26 February 2021; Published 11 March 2021

Academic Editor: Silvana Hrelia

Copyright © 2021 Xiang-Xiang Huang et al. This is an open access article distributed under the Creative Commons Attribution License, which permits unrestricted use, distribution, and reproduction in any medium, provided the original work is properly cited.

Cigarette smoke- (CS-) induced oxidative stress and inflammation in the lung are serious health problems. Primary and reprocessed tea products contain multiple antioxidants that have been reported to protect the lung against CS-induced injury. However, the beneficial effects of *Eurotium cristatum* fermented loose dark tea (ECT) and *Eurotium cristatum* particle metabolites (ECP) on CS-induced lung injury and its potential hepatic metabolic detoxification are still unclear. Therefore, sixty mice were randomly divided into six equal groups. CS-exposed mice were prevented or treated with ECP or ECT infusions for 12 or 8 weeks to determine the antioxidative stress, anti-inflammatory and potential metabolic detoxification of ECT and ECP. Thirty-six mice were randomly divided into six equal groups to observe the effects on hepatic metabolic detoxification by replacing daily drinking water with ECT. Results showed that CS significantly decreased the activities of glutathione peroxidase (GSH-Px) and superoxide dismutase (SOD) and upregulated the expressions of malondialdehyde (MDA), tumor necrosis factor alpha (TNF- α), interleukin-6 (IL-6), IL-8, and IL-1 β in serum. These adverse effects were modulated by ECP and ECT. In addition, ECT upregulated the mRNA expression of pregnane X receptor (PXR) and cytochrome P450 (CYP450) in the liver on daily free drinking ECT mice group. Western blot analysis further revealed that in CS-exposed mice, ECP and ECT significantly decreased the phosphorylation of mitogen-activated protein kinase (MAPK) in the lung but upregulated the protein expressions of PXR and aryl hydrocarbon receptor (AhR) in the liver. Overall, our findings demonstrated that ECT and ECP protected against lung injury induced by CS via MAPK pathway and enhanced hepatic metabolic detoxification via PXR and AhR pathways. Therefore, daily intake of ECT and ECP can potentially protect against CS-induced oxidative and inflammatory injuries.

1. Introduction

Cigarette smoke (CS) contains more than 6,000 chemicals, and 40 of which are carcinogenic [1]. Exposure to CS triggers an increase in colossal free radicals and production of reactive oxygen species (ROS). Combined, they induce oxi-

dative stress damages and lipid peroxidation and disrupt the oxidation/antioxidation system [2, 3]. In humans, the antioxidant system regulates accumulation of free radicals, which modulates oxidative damages. CS exposure disrupts antioxidative processes catalyzed by superoxide dismutase (SOD) and glutathione peroxidase (GSH-Px). At the same

time, CS increases the expression of malondialdehyde (MDA), which is a product of lipid peroxidation that damages the lung [4]. In addition, oxidative stress promotes inflammation in the lung [5]. Moreover, the inflammatory responses from the initial occult exogenous oxidative stress are secondary sources of endogenous ROS. Overall ROS induces a vicious cycle of lung damage [6]. Smoking induces damages beyond the organs directly in contact with CS such as the liver. CS contains toxic chemical substances that increases oxidative stress, necroinflammation, and liver fibrosis [7]. In addition, smoking also disrupts the expression of important xenobiotic pregnane X receptor (*PXR*) and ligand-activated transcription factor aryl hydrocarbon receptor (*AhR*) in the liver. This in turn represses the expression of cytochrome P450 (*CYP450*), which adversely affects drug metabolism and detoxification in the liver [8, 9]. These studies underline the integral antioxidants play roles in preventing and reversing CS-induced lung and liver injury. Meanwhile, tea has been extensively demonstrated to be an excellent natural antioxidant [10]. *Eurotium cristatum* fermented loose dark tea (ECT) is a potential excellent antioxidant, attributed to the interaction between the tea and the fungi.

ECT is a type of primary dark tea (PDT) that fermented with *Eurotium cristatum* strains and covered with “golden flora.” Similar to Fu brick tea (FBT, a brick-shaped *Eurotium cristatum*-fermented dark tea), ECT is a daily beverage and nutritional supplement frequently consumed at the border and southern regions of China. Previous studies have shown that dark tea lowers lipid levels in the body [11] and participates in antiobesity [12], antioxidative [4], anti-inflammatory [13], and detoxification [14] processes. Further, FBT aqueous extract inhibits the mitogen-activated protein kinase (MAPK) and nuclear factor-erythroid 2-related factor-2 (*Nrf2*) signaling pathways in cells, thereby reducing oxidative stress levels [4]. ECT contains catechins, alkaloids, gallic acid (GA), and covers with lots of *Eurotium cristatum* particle metabolites (ECP). Research shows that catechins inhibit oxidative stress, lipid peroxidation, and the expression of proinflammatory mediators [15]. Caffeine (CAF) is the most abundant alkaloid in tea. It possesses antioxidative properties and protects against lung damages by modulation pulmonary inflammation [16]. Notably, GA inhibits oxidative stress and inflammation [17]. Several researches report that nonfungi-fermented teas including green and black tea modulate oxidative stress and undesirable inflammatory response caused by CS exposure [18, 19]. Yet, how the tea performs these functions, alone or in combination with ECP, remains to be validated.

This study therefore investigated the ameliorative effects of ECT and ECP on CS-induced oxidative stress and inflammation via MAPK pathway and hepatic metabolic detoxification via *PXR/AhR* pathway in mice. These findings provide a theoretical basis for the antioxidation, anti-inflammatory, and metabolic detoxification capabilities of ECT and ECP.

2. Materials and Methods

2.1. Animals. Ninety-six (experiment 1, $n = 36$; experiment 2, $n = 60$, respectively), 4-week-old SPF female C57BL/6 exper-

imental mice were purchased from Changsha Slack Jingda Experimental Animal Co., Ltd. (Changsha, Hunan, China). They were reared under 12/12 hours of light and dark alternating cycles. The room temperature was maintained at $25 \pm 1^\circ\text{C}$, under 40-70% relative humidity. Adequate food and water were provided throughout the experimental period. The protocol for the experiments was approved by the Animal Testing Committee of Hunan Agricultural University. Before the experiments, there was one-week adaptation period to the feeds.

2.2. Chemicals and Reagents. Raw PDT leaves, FBT, and Hua Juan Tea (HJT) were purchased from the Baishaxi Tea Factory Co., Ltd. (Yiyang, Hunan, China). The *Eurotium cristatum* strains were isolated from Baishaxi brick tea using the direct separation technique. Tea-lyophilized powder was prepared at the Hunan Agricultural University. Cigarettes were purchased from the Hunan China Tobacco Industry Co., Ltd. (Changsha, Hunan, China). Vacuum diaphragm pumps were purchased from Kamoer, KVP15-KL-1 (Shanghai, China). Analytical kits for GSH-Px, SOD, and MDA were purchased from Nanjing Jiancheng Bioengineering Institute (Nanjing, Jiangsu, China). ELISA kits for the analysis of tumor necrosis factor alpha (TNF- α), interleukin-6 (IL-6), IL-8, and IL-1 β were purchased from Wuhan Hualianke Biotechnology Co. Ltd. (Wuhan, Hubei, China). Antibodies against p-p38 (4511S), p38 (8690S), p-Jun N-terminal kinase (p-JNK, (9251S)), JNK (9252S), p-extracellular-regulated kinase (p-ERK, (4370S)), and ERK (4695S) were purchased from Cell Signaling Technology, Inc. (Danvers, MA, USA). Monoclonal antibodies against *PXR* (ab192579), *AhR* (ab84833), and GAPDH (ab181602) were purchased from Abcam (Cambridge, UK). All other chemicals and reagents were at analytical grade.

2.3. Experiment 1. ECT Enhances Potential Metabolic Detoxification by Modulating *PXR* and *CYP450* in Mice Liver. To evaluate the potential hepatic metabolic detoxification property of dark tea, 36 healthy mice were randomly divided into 6 groups ($n = 6$, per group): (1) control, (2) epigallocatechin gallate (EGCG), (3) PDT, (4) FBT, (5) HJT, and (6) ECT group. Notably, EGCG solution (80 mg/kg) and dark tea infusions (800 mg/kg) were used to instead of daily drinking water during the 8 weeks feeding period. Dark tea infusions were prepared using freeze-dried powder of PDT, FBT, HJT, ECT, and sterilized water. The relative mRNA expressions of *PXR*- and *CYP450*-related genes (*CYP1A2*, *CYP2B1*, *CYP2C6*, *CYP3A1*, *CYP3A9*, and *CYP3A18*) in mice liver tissues were assessed using real-time fluorescent quantitative PCR.

2.4. Experiment 2. ECT and ECP Ameliorate CS-Induced Lung Injury via MAPK and Enhance Hepatic Metabolic Detoxification via *PXR* and *AhR* in CS-Exposed Mice. To determine the antioxidative stress, anti-inflammatory, and potential metabolic detoxification properties of ECP and ECT on CS-induced damages, 60 mice were randomly divided into 6 groups ($n = 10$): (1) control, (2) CS model group, (3) CS exposure and ECP preventive group, (4) CS

exposure and ECT preventive group, (5) CS exposure and ECP cure group and (6) CS exposure and ECT cure group. Preventive group, which received ECP/ECT for 12 weeks, was also exposed to air/CS for the entire experimental period. The interval between smoke exposure and feeding was about 5 hours per day. Cure group, which was exposed to air/CS for 8 weeks, received ECP/ECT from weeks 9 to 12. CS-exposed groups were exposed to 4% (vol/vol, CS/air) CS for 1 hour per day (12 cigarettes) for 12/8 weeks using a modified ventilated CS exposure chambers connected to 2 vacuum diaphragm pumps. One pump was connected to a burning cigarette to deliver fresh smoke (40 mL/min), whereas the other pump simultaneously delivered fresh air (960 mL/min) from outside the chamber. Control group were exposed to fresh air in a separate ventilated chamber using a similar procedure. Biochemical analyses were then performed to detect the effects of GSH-Px and SOD, as well as the expression of MDA, TNF- α , IL-6, IL-8, and IL-1 β in mice serum. Western blot analysis was performed to detect the expression of phosphorylated p38/JNK/ERK MAPK and expression of *PXR/AhR* proteins.

2.5. Expression of *PXR*, *CYP1A2*, *CYP2B1*, *CYP2C6*, *CYP3A1*, *CYP3A9*, and *CYP3A18* mRNA in the Liver. Total RNA of liver was extracted using cold TRIzol reagent (Tiangen, Beijing, China). The quality and concentration of total RNA at 260/280 nm was detected by spectrophotometry. cDNA was synthesized based on the FastQuant RT Kit (Tiangen, Beijing, China). The primers were synthesized at Sangon Biotech Co., Ltd. (Shanghai, China) and listed in Table 1. Amplification of the cDNA was performed using the SuperReal PreMix Plus kit (Tiangen, Beijing, China) following the manufacturer's instruction. The relative expression of *PXR*, *CYP1A2*, *CYP2B1*, *CYP2C6*, *CYP3A1*, *CYP3A9*, and *CYP3A18* mRNA in the liver was then evaluated. The reaction was performed using the real-time PCR system (Roter-Gene Q), under the following parameters: predenaturation at 95°C for 10 minutes, subsequent denaturation at 95°C for 10 seconds, annealing at 55°C for 20 seconds, and elongation at 72°C for 30 seconds. The amplification was performed through 40 cycles, with the mRNA expression of the target gene analyzed based on the $2^{-\Delta\Delta Ct}$ equation normalized to the mean values of internal reference GAPDH gene.

2.6. Preparation of ECT. PDT leaves were sterilized at 121°C for 20 min, cooled, and thereafter inoculated with fungal suspension. The fermentation was conducted in an incubator at 28–30°C under 80% humidity. After drying at 90–120°C for 60 min, the ECT leaves were stored at -20°C refrigerator for further use.

2.7. Preparation of ECP and ECT Infusion. The gold ECP were first passed through a 100-mesh screen from ECT, and the ECP were extracted with boiling ultrapure water for 30 min in a boiling water bath. The ECP infusion was then filtered under reduced pressure. ECT were extracted using ultrapure boiling water for 30 min in a boiling water bath. The ECT infusion was then filtered under reduced pressure.

ECP and ECT dosages depended on the weight of the mice (600 mg/kg). All samples were divided into small portions and stored under -20°C. The procedures were repeated weekly to keep the samples fresh.

2.8. HPLC Analysis. The concentration of catechins, alkaloids, and GA on PDT, ECT, and ECP infusions was analyzed using an Agilent LC-1260 high-performance liquid chromatography (HPLC) (Santa Clara, USA). The HPLC was equipped with a Welchrom C₁₈ column (250 mm \times 4.6 mm \times 5 μ m). The mobile phase was ultrapure water (A) and N, N-dimethylformamide:methanol:glacial acetic acid = 39.5:2:1.5 (B) with a gradient elution of 9–14% B at 0–10 min, 14–23% B at 10–15 min, 23–36% B at 15–27 min, 36%–36% B at 27–31 min, 36%–9% B at 31–32 min, and 9% B at 32–37 min. The temperature of the chromatographic column was maintained at 30°C throughout all experiments. The injection volume was 10 μ L. The HPLC chromatogram was monitored at UV 278 nm.

2.9. Collection of Mice Serum, Lung Tissue, and Liver Tissue. Before sample collection, the mice were starved of food for 12 h. The mice were sacrificed following intraperitoneal anesthetization using pentobarbital sodium. Blood was drawn from the eyelids for serum collection. Briefly, after 1 h incubation at room temperature, the blood was centrifuged for 10 min 2500 r/min for 10 min under at 4°C. The upper serum was collected and stored at -80°C for future use. The lung and liver tissues were removed, washed 3 times with precooled saline, and dried. The right lung tissues were placed in formalin for preparation of pathological tissue sections. Some of the lung not in formalin and liver tissues were stored at -80°C.

2.10. Histological Evaluation. The right lung tissues were fixed in formalin for 3 days, embedded in paraffin, and thereafter stained using hematoxylin and eosin solution (H&E). The sections were observed under an optical microscope at 200x magnification to assess any morphological changes in lung tissue.

2.11. Biochemical Analysis. The oxidative stress index in mice serum was assessed by measuring the catalytic activities of GSH-Px and SOD, as well as the expression of MDA using ELISA kits (Nanjing Jiancheng, Nanjing, Jiangsu, China). On the other hand, the inflammatory responses were assessed by measuring the concentrations of TNF- α , IL-6, IL-8, and IL-1 β using ELISA kits (Hualianke, Wuhan, Hubei, China). All ELISA kits were strictly used based on the manufacturer's instructions.

2.12. Western Blot Analysis. The MAPK proteins in the lung and *PXR/AhR* proteins in the liver were extracted using total protein extraction kit (Solarbio, Beijing, China), and quantified based on the BCA protein assay kit (Solarbio, Beijing, China). Thereafter, 20 μ g of denatured proteins were separated in 10% polyacrylamide gel using electrophoresis and then transferred to PVDF membrane (80 V, 30 min, 120 V, 60 min). The membranes were blocked for 1 h at room temperature using 5% nonfat milk in TBS-Tween (TBST),

TABLE 1: Primers used in the quantitative real-time polymerase chain reactions.

Gene	Gene accession number	Primer sequence 5'-3'	Product size (bp)
<i>PXR</i>	—	F: GACGGCAGCATCTGGAACACTAC R: TGATGACGCCCTTGAACATG	112
<i>CYP1A2</i>	NM_012541	F: AAGCGCCGGTGCATTG R: GCAGGAGGATGGCTAAGAAGAG	1,882
<i>CYP2B1</i>	J00719	F: CCCCATGTGCGAGAGAAAAGT R: GCGGTCATCAAGGGTTGGTA	1,567
<i>CYP2C6</i>	BC100092	F: CTCTGTTGCTCCTGCTGAAGTG R: TGCCAACCACACGATCAATC	1,268
<i>CYP3A1</i>	L24207	F: TTATGCTCTTCACCGTGATCCA R: GATCAATGCTGCCCTTGTCTC	2,015
<i>CYP3A9</i>	NM_147206	F: GGCCTACAGCATGGATGTGA R: CTGTGGGTTGTTAAGGGAATCAA	1,976
<i>CYP3A18</i>	NM_145782	F: AAGCACCTCCATTTCTTCATAAT R: TCTCATTCTGGAGTTTCTTTTGCA	2,005
<i>GAPDH</i>	AF106860	F: CCTTCCGTGTTCTACCC R: CCCAAGATGCCCTTCAGT	2,039

F: forward; R: reverse.

washed 3 times using TBST, and then incubated overnight at 4°C with several primary antibodies (p-p38 and p38, p-JNK and JNK, p-ERK and ERK, *PXR* and *GAPDH*, *AhR* and *GAPDH* (1:10000)). After three washes with TBST, the membranes were re-incubated for 1.5 h at room temperature with horseradish peroxidase-conjugated secondary antibodies in TBST supplemented with 5% BSA. After 3 washes with TBST, the immunoblots were visualized after chemiluminescence. Protein concentrations were quantified by using Image J software.

2.13. Statistical Analysis. Data was analyzed using Prism version 7 (GraphPad Software, La Jolla, CA, USA). Difference between groups was analyzed using one-way ANOVA and Student's *t*-tests, based on Fisher's LSD. Continuous variables were expressed as mean \pm SD. Statistical significance was set at $P < 0.05$ or $P < 0.01$.

3. Result

3.1. HPLC Analysis. Catechins, alkaloids, and GA were the major metabolites detected in PDT (Figure 1(a)), ECT (Figure 1(b)), and ECP (Figure 1(c)). As shown in Figure 1(d), after fermentation, total content of catechins in ECT was 34.37 ± 0.79 mg/g, decreasing by 63.54% in PDT ($P < 0.01$). However, the concentration of GA was 11.86 ± 0.49 mg/g with an increase percentage of 85.85 ($P < 0.01$). Three alkaloids (theobromine, theophy, CAF) all increased in ECT. Notably, CAF was the most abundant alkaloid at 38.99 ± 0.99 mg/g in ECT. All catechins, alkaloids, and GA were only slightly detected in ECP, perhaps due to the fact the detection method for ECP is different from the others. The decrease in ECT polyphenols was due to fermentation, in which the polyphenols were converted to bioactive theabrownins [20]. These findings suggest that *Eurotium cristatum*

fermentation changes the composition of metabolites on ECT compared to PDT, with the fungi retaining several bioactive and potential antioxidation substances.

3.2. Effects of EGCG, PDT, FBT, HJT, and ECT on the Expression Level of *PXR*- and *CYP450*-Related Genes (*CYP1A2*, *CYP2B1*, *CYP2C6*, *CYP3A1*, *CYP3A9*, and *CYP3A18*) in Liver Tissues. As shown in Figure 2, compared with the control group, PDT and ECT significantly increased the expression of *PXR* mRNA. FBT and ECT induced a significant increase in the expression of *CYP1A2* mRNA. ECT significantly increased the mRNA expression of *CYP2B1*. PDT, FBT, HJT, and ECT all significantly increased the mRNA expression of *CYP2C6*. EGCG and ECT significantly increased the mRNA expression of *CYP3A1*. PDT, HJT, and ECT significantly increased the expression of *CYP3A9* mRNA. The expression of *CYP3A18* mRNA decreased in all groups. These findings demonstrate that ECT plays a significant role in upregulating the expressions of *PXR*- and *CYP450*-related genes (*CYP1A2*, *CYP2B1*, *CYP2C6*, *CYP3A1*, *CYP3A9*, and *CYP3A18*). Also, the effect of ECT was superior to that of EGCG, PDT, FBT, and HJT. Statistical significance was set at $P < 0.01$ for all the analyses.

3.3. Histological Status of Mice Lung Tissues. Mice exposed to CS gradually but slowly gained weight with exposure frequency. Their fur turned yellow, and compared to controls, were rough and dull. Some mice shed their hair, lost appetite, and moved relatively slowly. After CS exposure, it took about 30 min for the mice to recover from the depressive symptoms.

As shown in Figure 3(a), the bronchi and alveolar of mice in the control group were intact with normal alveolar spaces. In contrast, those of CS group displayed dilated alveolar spaces, infiltration of inflammatory cells, shedding of

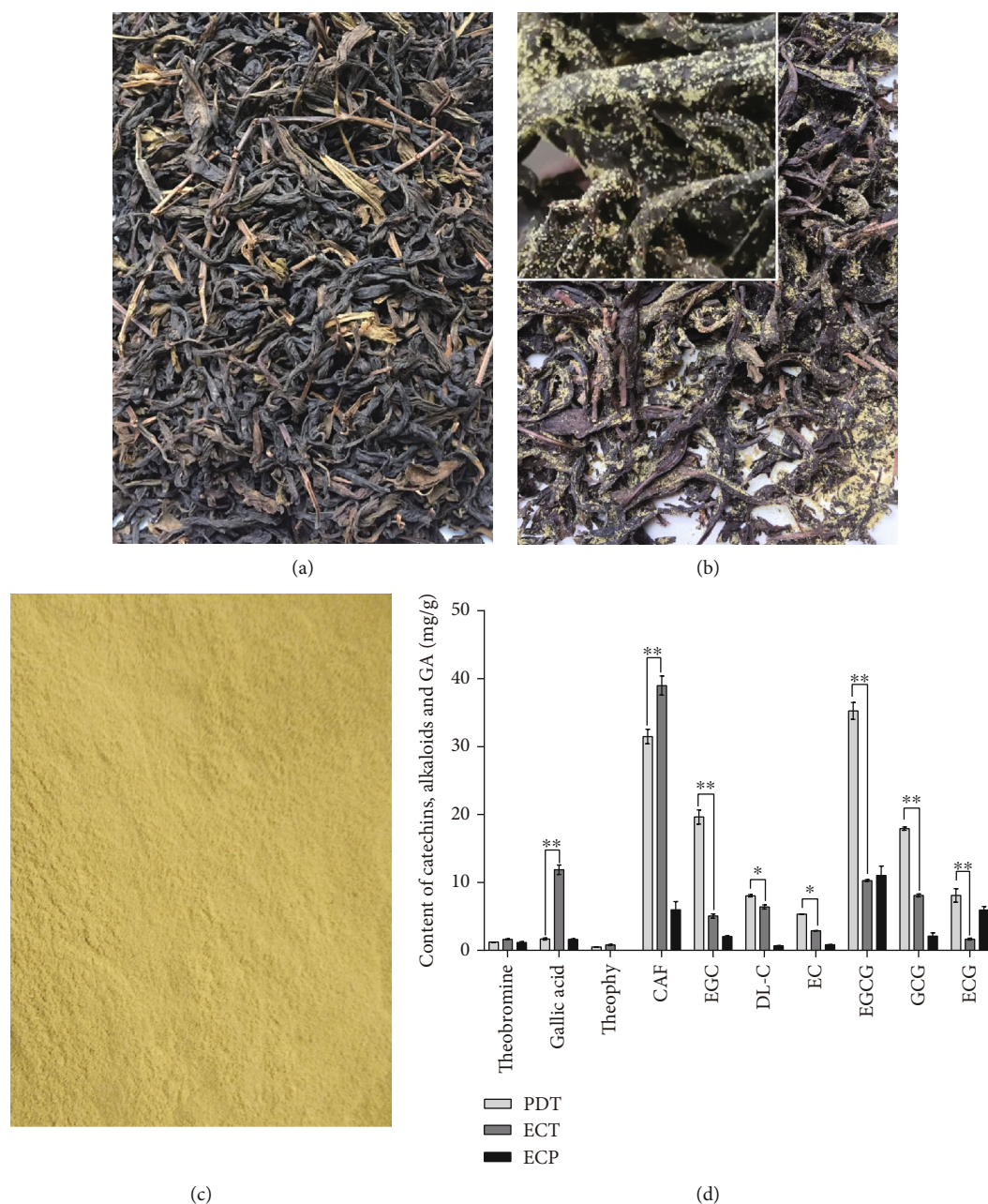


FIGURE 1: Photos of (a) PDT, (b) ECT, and (c) ECP. (d) The concentration of catechins, alkaloids, and GA in PDT, ECT, and ECP by HPLC method. * and ** represent significant difference at $P < 0.05$ and $P < 0.01$ level, respectively.

epithelial cells in the tracheal cavity, and congestion in the pulmonary interstitial space (Figure 3(b)). Intriguingly, ECP and ECT treatment prevented or reversed the development of these pathological changes (Figures 3(c)–3(f)).

3.4. Effects of ECP and ECT on the Activities of Serum Antioxidant Enzymes. The effect of ECP and ECT on the activity of antioxidant enzymes of mice was shown in Figures 4(a)–4(c). Compared with the control, CS exposure significantly decreased the activity of SOD and GSH-Px as well as upregulated the expression of MDA. In contrast, compared with control, ECP and ECT treatment significantly enhanced the activity of SOD and GSH-Px and significantly

decreased the expression of MDA. The statistical significance was set at $P < 0.01$ for all the analyses.

3.5. Expressions of Inflammatory Cytokines in Serum. Compared with CS exposure significantly upregulated the expression levels of TNF- α , IL-6, IL-8, and IL-1 β (Figures 5(a)–5(d)). However, ECP and ECT treatment conferred reduced expression levels of TNF- α , IL-6, IL-8, and IL-1 β ($P < 0.01$) in CS-exposed mice.

3.6. Western Blot Analysis. Phosphorylations of p38, JNK, and ERK protein were measured to uncover the molecular mechanism underlying modulation of CS-induced inflammatory

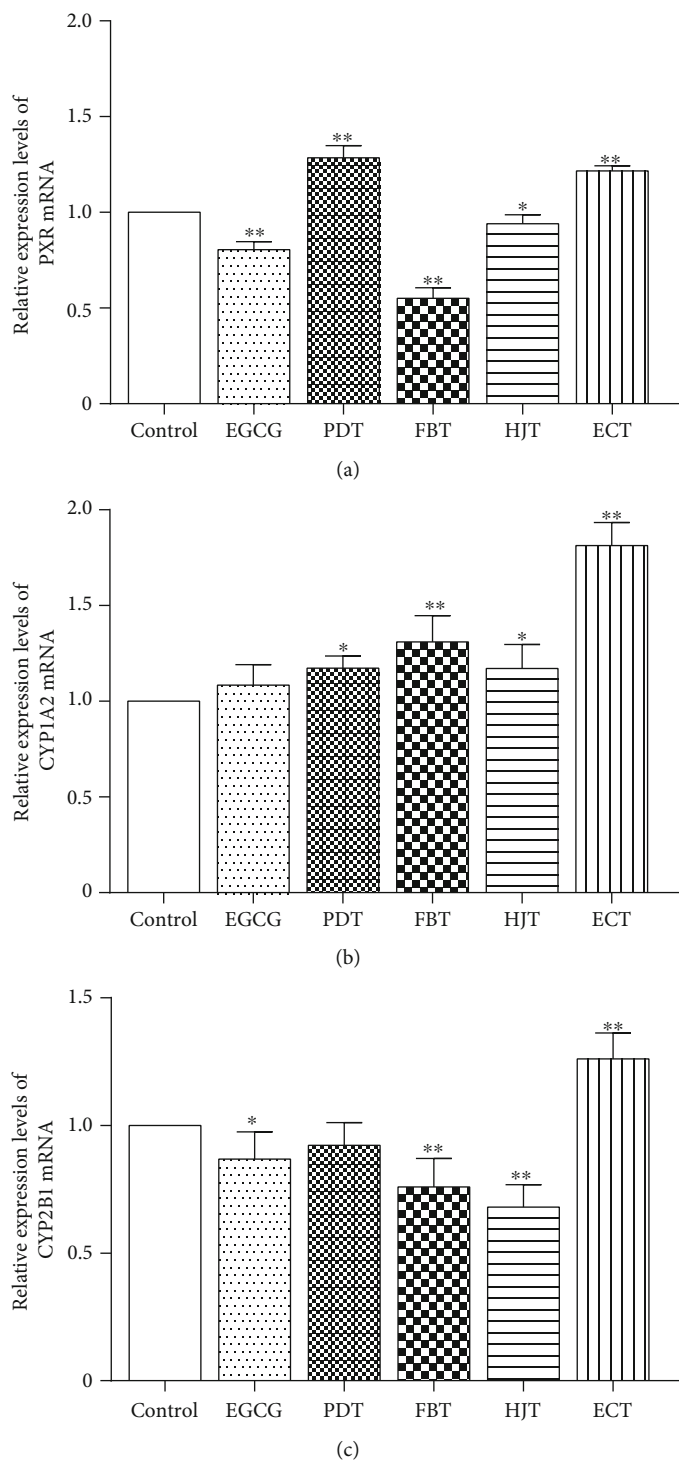


FIGURE 2: Continued.

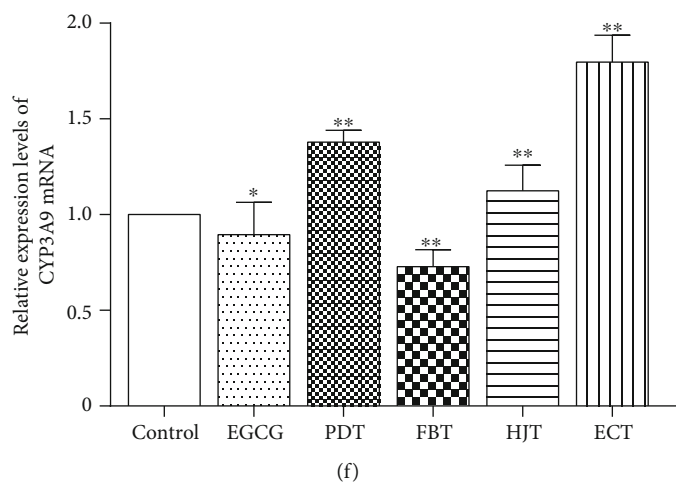
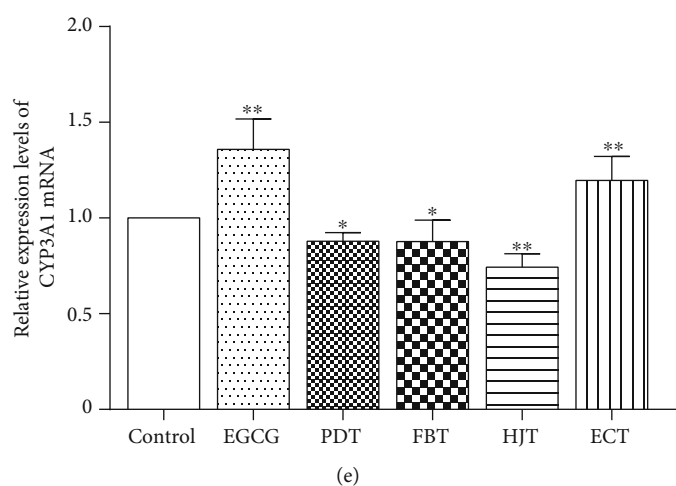
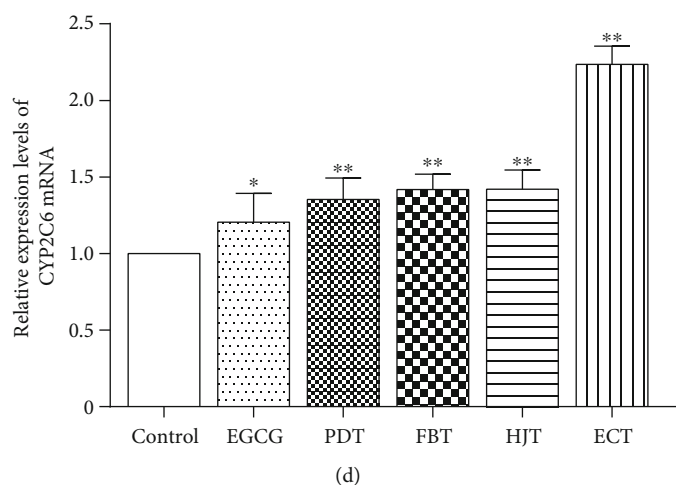


FIGURE 2: Continued.

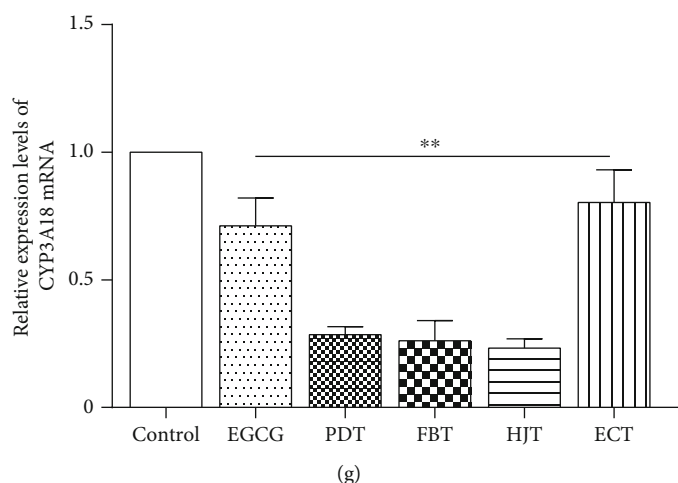


FIGURE 2: Effects of EGCG, PDT, FBT, HJT, and ECT on the expression of *PXR* and *CYP450* mRNA in mice liver. (a–g) Represent changes in *PXR*, *CYP1A2*, *CYP2B1*, *CYP2C6*, *CYP3A1*, *CYP3A9*, and *CYP3A18*, respectively. Values represents mean \pm SD. *Statistical significance at $P < 0.05$; **statistical significance at $P < 0.01$.

response by ECP and ECT. Meanwhile, the expressions of *PXR* and *AhR* protein were evaluated to investigate the molecular mechanism underlying hepatic metabolic detoxification of ECP and ECT in CS-exposed mice. Compared with the control group, the phosphorylations of p38, JNK, and ERK protein were significantly ($P < 0.01$) upregulated in the lung of the CS mice (Figures 6(a)–6(c)). However, ECP and ECT intake, either as preventive or treatment intervention, regulated abnormal phosphorylations of p38, JNK, and ERK. In addition, compared with controls, CS exposure significantly ($P < 0.01$) repressed the expression levels of *PXR* and *AhR* protein (Figures 6(d) and 6(e)). However, preventive ECT or cure treatment with ECP and ECT significantly ($P < 0.01$) upregulated the expression of *PXR* protein (Figure 6(d)). Furthermore, cure treatment with ECP and ECT restored normal expression of *AhR* protein (Figure 6(e)).

4. Discussion

CS causes several health issues worldwide. Persistent CS exposure causes numerous chronic respiratory complications in the lung such as chronic obstructive pulmonary disease (COPD), emphysema, and in severe cases, lung cancer [21–23]. Also, smoking causes direct and indirect toxic effects on the liver, including oxidative stress, necroinflammation, and metabolic disorder [7]. The metabolic detoxification of the liver is related to the systemic antioxidant and anti-inflammatory effects. Studies have showed that several natural antioxidants including tea can modulate the oxidative stress, inflammation, and liver toxicity caused by CS [24–27]. Even though mechanism with which tea inhibits oxidative stress and inflammation has been described, how it mediates metabolic detoxification remains to be validated. Therefore, we first simulated daily tea intake, and in C57BL/6 mice, daily water intake was replaced with aqueous EGCG, PDT, FBT, HJT, and ECT infusions to evaluate the effect of different dark teas on the hepatic metabolic detoxifi-

cation. We found ECT significantly increased the mRNA expression levels of *PXR* and *CYP450*. Yao et al. reported similar findings, in which tea was found to increase the expression of *CYP450*-related genes [28]. Subsequently, we established a lung injury mice model by CS to investigate the mechanism of ECT and ECP to ameliorate CS-induced lung injury and as well how it mediates hepatic metabolic detoxification.

ECT is an antioxidant with lower levels of total catechin but high alkaloid, GA, and theabrownins compared to PDT [29]. In this study, HPLC revealed that after fermentation, the concentration of alkaloids and GA in ECT increased, whereas that of total catechins decreased. However, only low levels of the metabolites were detected in ECP. Given that ECP is an *Eurotium cristatum* metabolite, the HPLC method for tea might not be suitable for measuring ECP. Elsewhere, Zou et al. showed that in addition to the 4 commonly known metabolites (echinulin, dehydroechinulin, neo-echinulin A, and varicolorin O), cristatumin F, a novel metabolite, was also detected in *Eurotium cristatum* crude extracts isolated from Fu brick tea. Among them, cristatumin F exhibited scavenging effects on free radicals [30]. These findings demonstrated that ECT and ECP have high level of active antioxidant and anti-inflammatory substances. Based on these findings, we hypothesized that ECT and ECP could alleviate CS-induced lung injury by inhibiting oxidative damages and inflammatory responses and may also has the ability to enhance the hepatic metabolic detoxification.

CS exposure greatly impacts on the survival of mice. Compared with controls, mice in the ECP and ECT cure groups showed consistent unhealthy status during the first 2 months. These adverse events were significantly reversed after the cessation of smoking and the beginning of gavage during the final month. Also, ECP and ECT preventive groups significantly improved the adverse status of the mice. Pathological examination of the tissue sections revealed that the lung tissues of mice in the control group displayed normal structure with no inflammatory cell infiltration. In

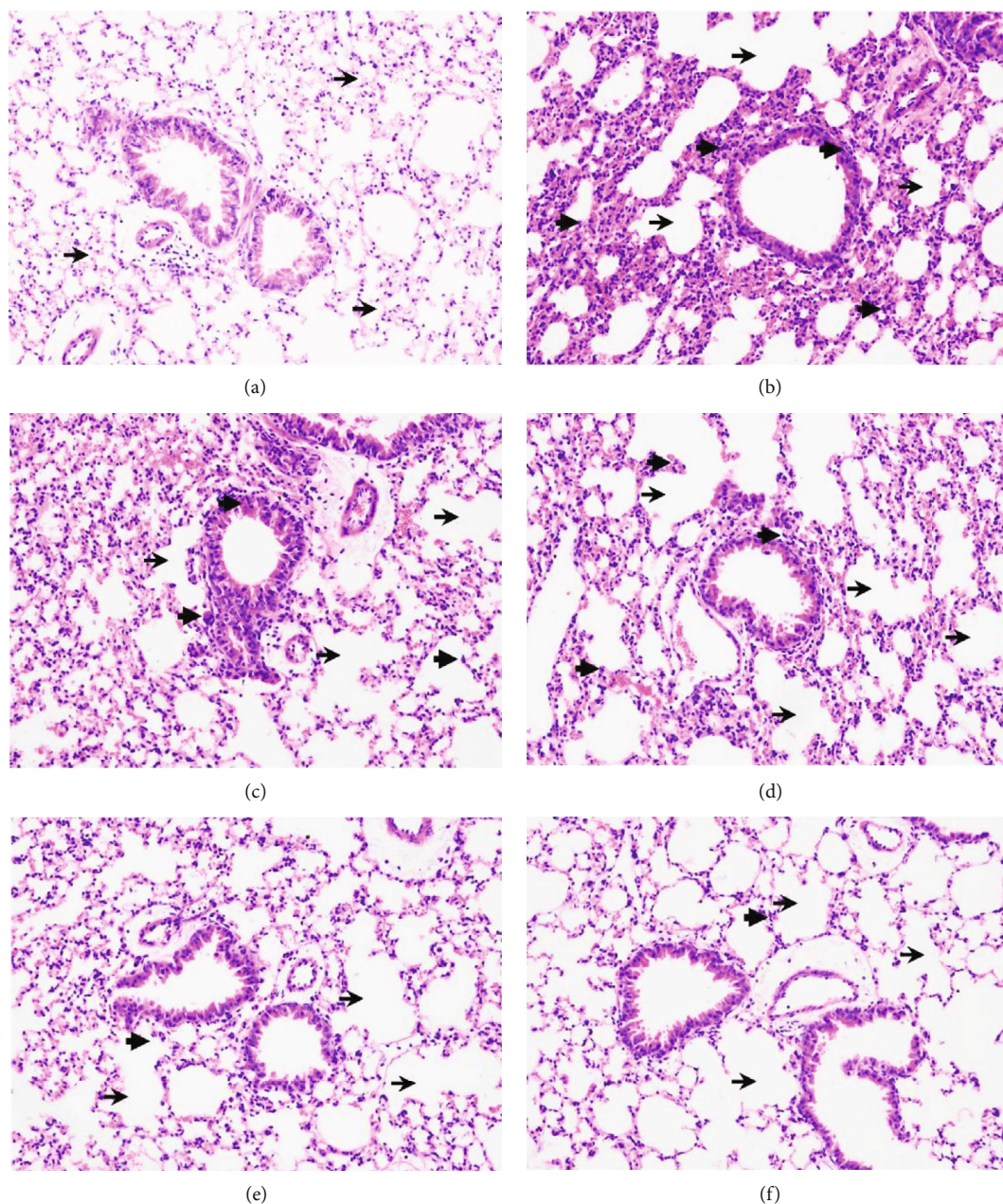


FIGURE 3: The effects of ECP and ECT on pathological appearance in the lung tissues exposed to CS (200x). (a) Control group shows normal lung tissue with uniform alveolar spaces (thin arrow). (b) CS model group shows dilated alveolar spaces (thin arrow), inflammatory cell infiltration (thick arrow), epithelial cells in the tracheal cavity are shed, and pulmonary interstitial congestion. (c) CS with ECP preventive group shows dilated alveolar spaces (thin arrow) and inflammatory cell infiltration (thick arrow). (d) CS with ECT preventive group shows dilated alveolar spaces (thin arrow) and inflammatory cell infiltration (thick arrow). (e) CS with ECP cure group shows dilated alveolar spaces (thin arrow), but less inflammatory cell infiltration (thick arrow). (f) CS with ECT cure group shows dilated alveolar spaces (thin arrow), but less inflammatory cell infiltration (thick arrow). Thin arrows show dilated alveolar spaces, whereas the thick one shows infiltration of inflammatory cells. Preventive group, included ECP/ECT intake from weeks 1 to 12 of mice exposed to CS through the same period. The interval between smoke exposure and feeding was about 5 hours per day. Cure group, mice were exposed to CS commenced from weeks 1 to 8, after which the mice received ECP/ECT from weeks 9 to 12.

contrast, there were abnormal alterations in alveolar and epithelial cells and infiltration of inflammatory cells in CS model group. However, cure and preventive treatment of ECP and ECT significantly reversed these changes. The protective effects of ECP and ECT are associated with its antioxidative and anti-inflammatory effects.

Oxidative stress disrupts the antioxidant system and increases lipid peroxidation. Therefore, functions of SOD and GSH-Px antioxidant enzymes and MDA peroxidation are key indicators of oxidative stress in the body [4]. In this study, we found CS exposure significantly suppressed SOD and GSH-Px activities. Nevertheless, ECP and ECT

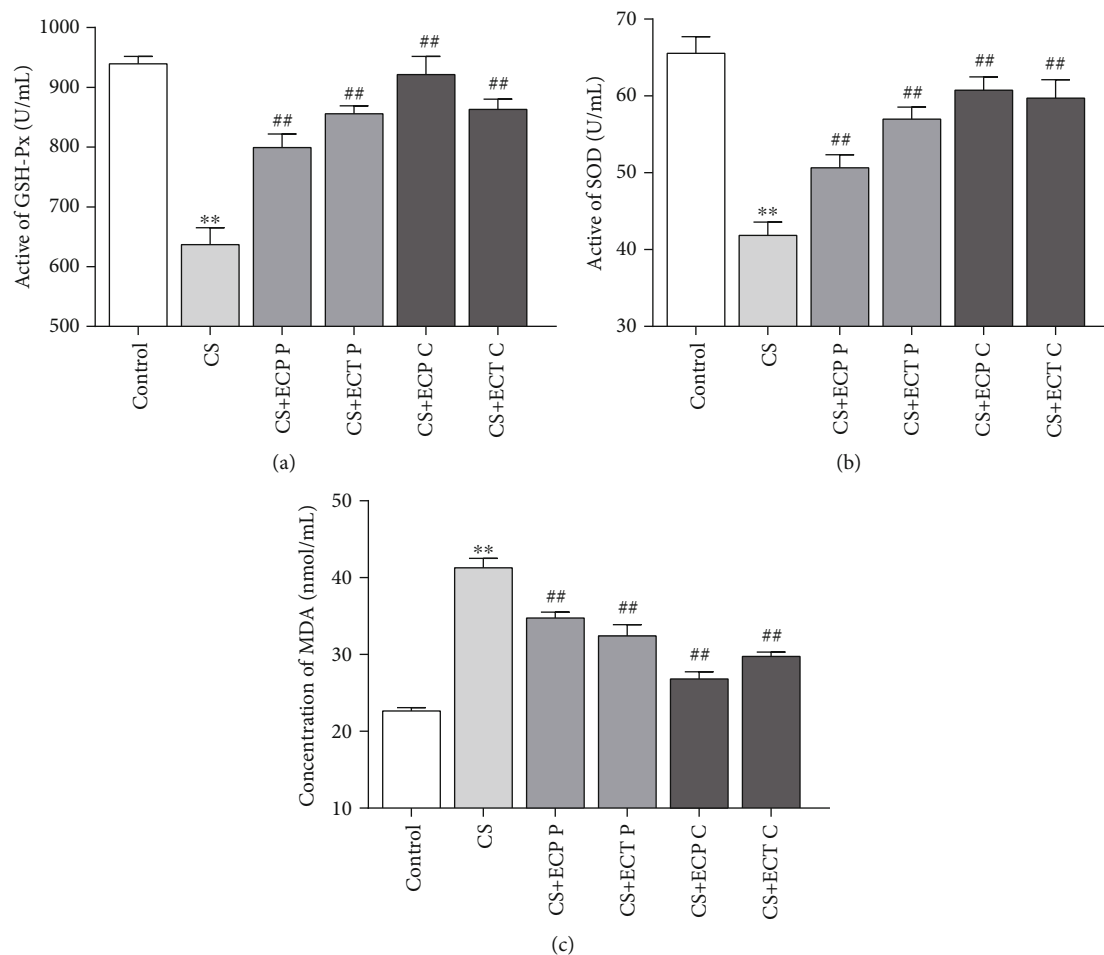


FIGURE 4: The effects of ECP and ECT on GSH-Px and SOD activities and the expression of MDA levels in serum of mice exposed to CS. Preventive group (P), included ECP/ECT intake from week s1 to 12 of mice exposed to CS through the same period. The interval between smoke exposure and feeding was about 5 hours per day. Cure group (C), mice were exposed to CS commenced from weeks 1 to 8, after which the mice received ECP/ECT from weeks 9 to 12. (a) Active unit of GSH-Px. (b) Activity of SOD. (c) Concentration of MDA. The values represent mean \pm SD of each measure. ** $P < 0.01$, compared with the normal control group; ## $P < 0.01$, compared with the CS model group.

treatment restored these changes. Notably, the effect was superior in cure groups than preventive groups. These findings underline the protective effect of ECP and ECT against CS-induced oxidative damages. Previous studies showed that CS-induced lung injury is associated with excess free radicals and lipid peroxidation [31]. Herein, the CS group exhibited higher MDA levels compared to the control group significantly. However, both preventive and cure groups with ECP and ECT significantly decreased CS-induced damages and expression of MDA. These findings suggest that ECP and ECT inhibit CS-induced oxidative stress.

To further clarify the pathophysiological effects of ECP and ECT on CS-exposed mice, we measured the concentration of 4 inflammatory markers including TNF- α , IL-6, IL-8, and IL-1 β . In a separate study, it was found that TNF- α and IL-1 β in human endothelial cells exposed to CS for longer periods were significantly higher than in nonsmokers [32]. Significant IL-1 β increases in lung tissue of COPD patients and induces sputum production [33]. On the other hand, CS exposure significantly increased secretion of IL-8

in human bronchial epithelial cells [34]. IL-6 is a robust cytokine that activates proliferation of T and B cells and regulates inflammatory response. CS exposure increases infiltration of inflammatory cells and expression of IL-6 and TNF- α in bronchial alveolar lavage fluid (BALF) [35, 36]. In this study, compared to control group, CS exposure significantly upregulated the expression of TNF- α , IL-6, IL-8, and IL-1 β . However, ECP and ECT treatment significantly downregulated the expression of the above pro-inflammatory cytokines. Notably, the effect of ECP and ECT was superior in cure groups than the preventive groups. This is probably because CS exposure in the cure groups was stopped after 8 weeks, whereas that of preventive groups continued for 4 more weeks, thus, the extended smoke exposure severely hindered recovery from the oxidative damages. Interestingly, ECP conferred better effects than ECT in the cure groups. In contrast, the effect of ECT in the preventive groups was superior to that of ECP. This tendency may be due to the fact that the mice in the cure groups were already injured before receiving ECP and ECT and that acute

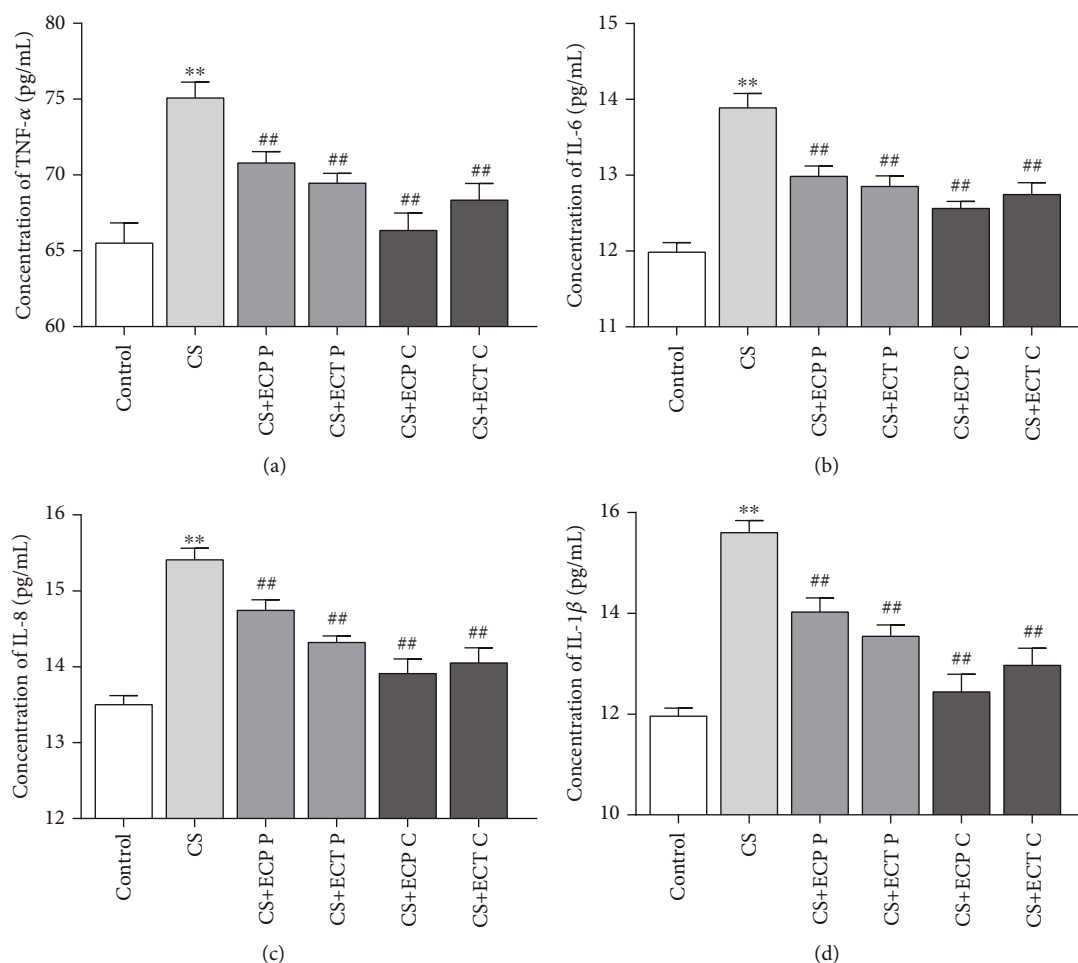


FIGURE 5: The effects of ECP and ECT on TNF- α , IL-6, IL-8, and IL-1 β levels in serum of mice exposed to CS. (a–d) Concentration of TNF- α , IL-6, IL-8, and IL-1 β , respectively. The measures represent mean \pm SD. ** $P < 0.01$, compared with the normal control group; ## $P < 0.01$, compared with the CS model group.

ingestion of CAF may exacerbate lung injury after ECT feeding [37]. Yet in the preventive groups, after long-term treatment with smoking and feeding, mice showed increased tolerance to the CAF in ECT. Therefore, in the preventive groups, ECT was more effective than ECP in ameliorating lung injury in mice as a result of its higher content of tea polyphenols and GA. Hence, we hypothesized that the use of mild antioxidants such as ECP in the early stages would be more effective in improving the oxidative stress and inflammatory response after cessation of long-term CS exposure. However, ECT consumption was more effective in improving oxidative stress and inflammatory responses during prolonged CS exposure.

MAPK signaling pathway regulates extracellular signaling in cells. The tertiary MAPK kinase pathway regulates important physiological and pathological processes including cell growth, differentiation, apoptosis, and inflammation. It further regulates expression of p38, JNK, and ERK proteins. ERK mediates cellular inflammatory and transcriptional activities. During COPD development, activated ERK promotes the release of proinflammatory cytokines such as TNF- α , IL-6, and IL-1 β . This exacerbates inflammation in

the airways and increases oxidative DNA and alveolar cell damages [38, 39]. p38 and JNK pathways are regulated by stress-induced signals and lung proinflammatory cytokines [40, 41]. Moreover, recent findings show that TNF- α activates the p38 MAPK signaling pathway, which induces asthma and the development of COPD [42]. CS metabolites induce phosphorylation of cellular H3S10 histones via the JNK and phosphatidylinositol 3-kinase/protein kinase B pathways, which directly promotes tumorigenesis [43]. In both COPD and non-COPD patients, CSE treatment upregulated the expression of IL-6 and IL-8 in lung bronchial cells and activated the p38 and JNK signaling pathways. Therefore, in general, CS induces proinflammatory responses that exacerbate COPD [44]. This study showed that CS exposure significantly upregulated the expression of phosphorylated p38, JNK, and ERK proteins and activated the MAPK signaling pathway. However, both preventive as well as ECP and ECT treatments reversed the above effects. Notably, the ECP and ECT protective effects were superior in cure than in preventive groups. This was in agreement with recent studies that showed that FBT reduces the level of UVB-induced oxidative stress in human keratinocytes by

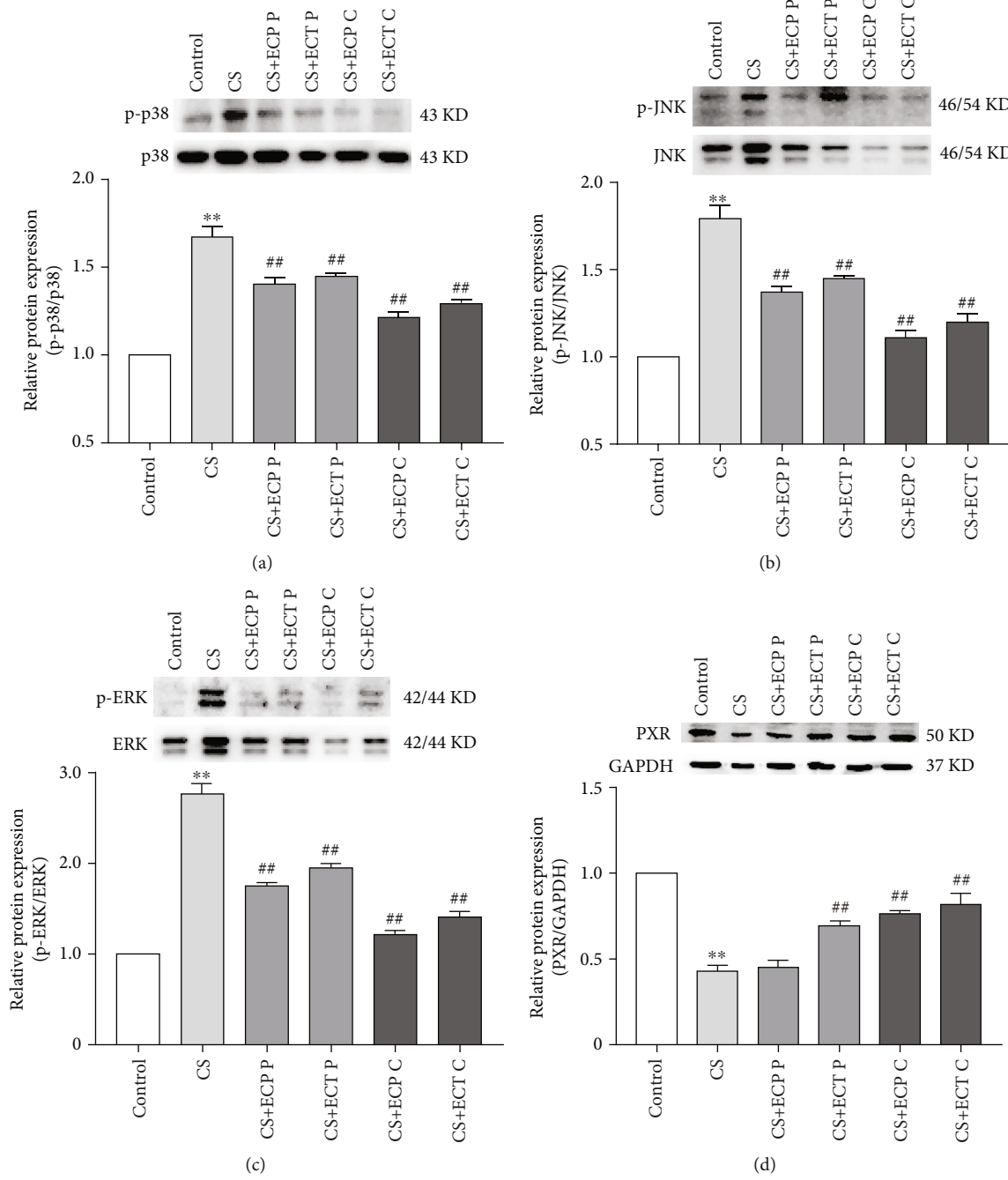


FIGURE 6: Continued.

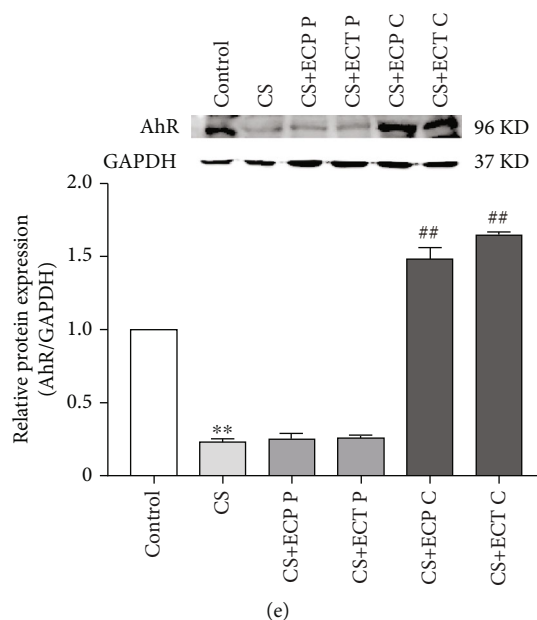


FIGURE 6: The effects of ECP and ECT on the expression of p38 and p-p38, JNK and p-JNK, and ERK and pERK proteins in the lung and *PXR* and *AhR* protein in the liver of mice exposed to CS. Western blot analysis for the expression of (a) phosphorylated p-p38 and total p38, (b) p-JNK and total JNK, (c) p-ERK and total ERK in lung tissues of mice exposed to CS. Expression of (d) *PXR* and (e) *AhR* proteins in the liver tissues of mice exposed to CS. Measurements represents mean \pm SD. ** $P < 0.01$, compared with the normal control group; ## $P < 0.01$, compared with the CS model group.

modulating the MAPKs/Nrf2 signaling pathway [45]. Also, it has been demonstrated that metabolites with antioxidant and anti-inflammatory properties such as GA, catechins, and *Eurotium cristatum* metabolites modulate the MAPK signaling pathway [4, 46, 47]. Therefore, our findings demonstrated that ECT and ECP inhibit CS-induced activation of lung MAPK signaling pathway, phosphorylation of p38, JNK, and ERK proteins, oxidative stress, and inflammation in mice.

PXR, a member of nuclear receptor superfamily NR1I2, plays a critical role in the metabolic detoxification system by detecting biological xenobiotics and triggering detoxification reactions, primarily expressed in the liver and intestine [48]. As already mentioned, *PXR* is a xenosensor that modulates the expression of xenobiotic-metabolizing enzymes and transporters. Therefore, this mediates the elimination of xenobiotics and endogenous toxic chemicals such as bile acids [49]. A recent study showed that exposing *PXR* knockout mice to 2,2',4,4',5,5'-hexachlorobiphenyl (PCB-153) markedly reduced the expression of GSH-Px and increased oxidative stress levels *in vivo*. On the other hand, PCB metabolites were significantly upregulated in mice liver, indicative of oxidative stress and DNA damage in the mice liver [50]. Naspinski et al. reported that *PXR* enhances cellular detoxification by upregulating expression of metabolizing enzyme, effectively protecting cells from benzopyrene- (BaP-) induced DNA damage [51]. These findings suggest that *PXR* protective against oxidative liver damage modulates expression of metabolic enzyme and enhances metabolic detoxification [49]. *AhR* is a xenobiotic receptor strongly expressed in the liver cells. It detects environmental toxins

and regulates metabolism of xenobiotic [52]. Also, *AhR* participates in liver development, regulates liver regeneration, and inhibits tumor development. Moreover, mice models showed that *AhR* prevents activation of hepatic stellate cells and liver fibrogenesis [53, 54]. Numerous studies have also demonstrated that *AhR* alleviates oxidative stress, inflammation, and apoptosis induced by CS [55–57]. In this study, we found CS exposure significantly decreased the expression of *PXR* and *AhR*. However, both preventive and cure ECP as well as ECT increased the expression of *PXR* and *AhR* proteins after CS exposure. Therefore, findings of this study suggest ECP and ECT are potential antioxidants that could enhance hepatic metabolic detoxification.

Meanwhile, increasing evidence suggests of a potential cross talk between MAPK, *PXR*, *AhR*, and other inflammatory signaling pathways. In particular, CS exposure activates the MAPK pathway in the lung [58], consistent with our findings. CS exposure also induces the overexpression of other inflammatory signaling pathways such as nuclear factor kappa B (NF- κ B) and TNF- α [59]. It also reduces the expression of *AhR* protein in lung, decreasing the protective capacity of *AhR* against inflammatory and oxidative damages in lung [60]. The effect of CS exposure on *PXR* in lung has not been reported, probably because *PXR* is mainly expressed in liver and intestine. Our findings demonstrated that ECT and associated ECP represses the MAPK signaling pathway and proinflammatory cytokine. Therefore, we speculate ECT and the fungi protects against CS-induced lung injury may be related to the *AhR*, MAPK, and NF- κ B pathways (Figure 7(a)). The effect of CS exposure on *PXR* and *AhR* signaling pathways in the liver is scarcely reported. However,

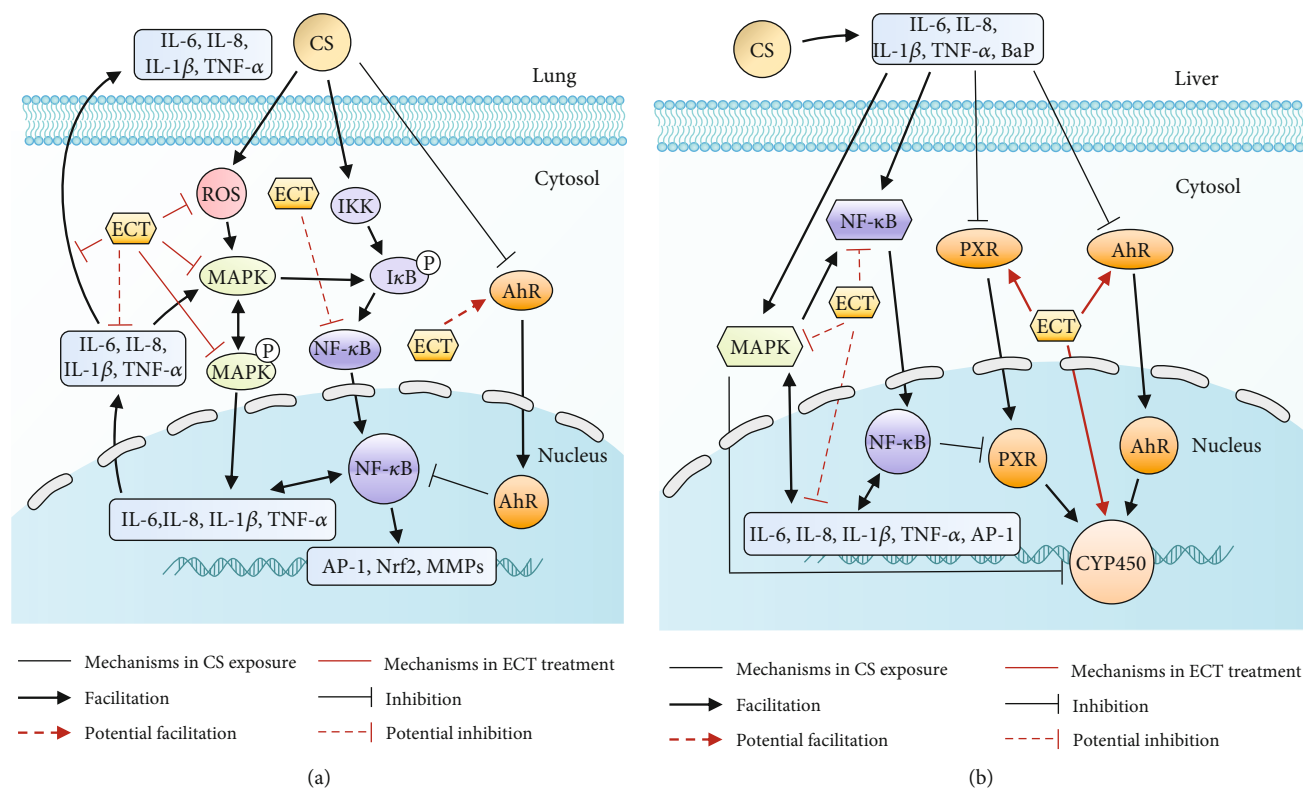


FIGURE 7: (a) Effect of ECT on MAPK, *AhR*, and NF- κ B signaling pathways in CS-induced lung injury in mice. CS upregulates the expression of MAPK and NF- κ B proteins but inhibits expression of *AhR* protein in the lung. It also induces secretion of proinflammatory cytokines. CS also induces oxidative stress and inflammation, causing lung injury. However, ECT ameliorated the lung injury. (b) Effect of ECT on MAPK, *PXR*, *AhR*, and NF- κ B signaling pathways in CS-induced liver injury in mice. CS activated the MAPK and NF- κ B signaling pathways, inhibited the expression of *PXR* and *AhR* proteins and the expression of *CYP450*-related genes, released proinflammatory cytokines, and disrupted metabolic detoxification processes in the liver. However, ECT may enhance the hepatic metabolic detoxification.

mice models show that chronic CS exposure activates the MAPK and NF- κ B signaling pathways and induces the release of proinflammatory cytokines in the liver [59, 61]. Activated MAPK pathway inhibits expression of *CYP450*-related genes affecting drug metabolism and detoxification in the hepatocytes [62]. NF- κ B inhibits expression of *PXR* mRNA and disrupts the *PXR-CYP450* gene responses [48]. In this study, ECT and associated ECP enhanced the expression of *PXR/AhR* proteins in the liver induced by CS exposure. Hence, it is reasonable to hypothesize that CS exposure disrupts the *PXR*, *AhR*, MAPK, and NF- κ B signaling pathways and inhibit hepatic drug metabolism and detoxification. Moreover, ECT and associated ECP are antioxidant that can reverse these events (Figure 7(b)). However, we did not assess genes and proteins expression of MAPK and NF- κ B in the liver as well as NF- κ B, *PXR*, and *AhR* in the lung of the experimental mice. In addition, expression of key tissue molecular indicators for inflammation such as NF- κ B and activator protein-1 was not evaluated. Nevertheless, these researches will continue to be investigated in the future.

5. Conclusion

This study demonstrated that ECT and ECP significantly improved the health and restored normal pathophysiology

in the lung induced by CS. Moreover, they remarkably enhanced the SOD and GSH-Px functions and downregulated the expression of MDA, IL-6, IL-8, IL-1β, and TNF-α in the serum. In addition, ECT and ECP downregulated phosphorylation of lung p38, JNK, and ERK proteins in mice. Furthermore, ECT remarkably upregulated the expression of mRNA for *PXR*- and *CYP450*-related genes. It also upregulated the protein expression of *PXR* and *AhR* in the liver. Overall, this study demonstrated that ECT and ECP protects against CS-induced oxidative stress and inflammatory damages in mice lung, via the MAPK signaling pathway. Meanwhile, ECT and ECP also protects against modulation of metabolic detoxification in the liver via the *PXR/AhR* signaling pathway. Accordingly, daily intake of ECT and ECP can potentially protect against CS-induced oxidative and inflammatory injury.

Data Availability

The data used to support the findings of this study are available from the corresponding author upon request.

Conflicts of Interest

The authors declare no conflict of interest.

Acknowledgments

This work was supported by National Key R&D Program of China (Grant no. 2018YFC1604403) and Department of Science and Technology of Hunan Province (Grant no. 2017NK2180). Thanks to Mr. ChunLin Shi, 2019 student of School of Economics and Management, The Chinese University of Hong Kong (Shenzhen), for the helpful discussion on this paper.

References

- [1] J. Fowles and E. Dybing, "Application of toxicological risk assessment principles to the chemical constituents of cigarette smoke," *Tobacco Control*, vol. 12, no. 4, pp. 424–430, 2003.
- [2] E. Pace, M. Ferraro, S. di Vincenzo et al., "Oxidative stress and innate immunity responses in cigarette smoke stimulated nasal epithelial cells," *Toxicology In Vitro*, vol. 28, no. 2, pp. 292–299, 2014.
- [3] S. Aboulmaouahib, A. Madkour, I. Kaarouch et al., "Impact of alcohol and cigarette smoking consumption in male fertility potential: looks at lipid peroxidation, enzymatic antioxidant activities and sperm DNA damage," *Andrologia*, vol. 50, no. 3, article e12926, 2018.
- [4] X. Xu, H. Huang, X. Yin, H. Fang, and X. Shen, "Effect of lentivirus-mediated CFTR overexpression on oxidative stress injury and inflammatory response in the lung tissue of COPD mouse model," *Bioscience Reports*, vol. 40, no. 1, 2020.
- [5] Y.-L. Wu, A.-H. Lin, C.-H. Chen et al., "Glucosamine attenuates cigarette smoke-induced lung inflammation by inhibiting ROS-sensitive inflammatory signaling," *Free Radical Biology and Medicine*, vol. 69, pp. 208–218, 2014.
- [6] R. Pandey, M. Singh, U. Singhal, K. B. Gupta, and S. K. Aggarwal, "Oxidative/nitrosative stress and the pathobiology of chronic obstructive pulmonary disease," *Journal of Clinical and Diagnostic Research*, vol. 7, no. 3, pp. 580–588, 2013.
- [7] A. R. El-Zayadi, "Heavy smoking and liver," *World Journal of Gastroenterology*, vol. 12, no. 38, pp. 6098–6101, 2006.
- [8] S. Zevin and N. L. Benowitz, "Drug interactions with tobacco smoking. An update," *Clinical Pharmacokinetics*, vol. 36, no. 6, pp. 425–438, 1999.
- [9] T. Kumagai, H. Suzuki, T. Sasaki et al., "Polycyclic aromatic hydrocarbons activate CYP3A4 gene transcription through human pregnane X receptor," *Drug Metabolism and Pharmacokinetics*, vol. 27, no. 2, pp. 200–206, 2012.
- [10] C. N. Zhao, G. Y. Tang, S. Y. Cao et al., "Phenolic profiles and antioxidant activities of 30 tea infusions from green, black, oolong, white, yellow and dark teas," *Antioxidants*, vol. 8, no. 7, p. 215, 2019.
- [11] G. Chen, M. Wang, M. Xie et al., "Evaluation of chemical property, cytotoxicity and antioxidant activity in vitro and in vivo of polysaccharides from Fuzhuan brick teas," *International Journal of Biological Macromolecules*, vol. 116, pp. 120–127, 2018.
- [12] G. Chen, M. Xie, Z. Dai et al., "Kudingcha and Fuzhuan brick tea prevent obesity and modulate gut microbiota in high-fat diet fed mice," *Molecular Nutrition & Food Research*, vol. 62, no. 6, article e1700485, 2018.
- [13] Y. Wang, A. Xu, P. Liu, and Z. Li, "Effects of Fuzhuan brick-tea water extract on mice infected with *E. coli* O157:H7," *Nutrients*, vol. 7, no. 7, pp. 5309–5326, 2015.
- [14] Q. Zheng, W. Li, H. Zhang, X. Gao, and S. Tan, "Optimizing synchronous extraction and antioxidant activity evaluation of polyphenols and polysaccharides from Ya'an Tibetan tea (*Camellia sinensis*)," *Food Science & Nutrition*, vol. 8, no. 1, pp. 489–499, 2019.
- [15] S. P. Lakshmi, A. T. Reddy, L. D. Kodihela, and N. C. Varadacharyulu, "Epigallocatechin gallate diminishes cigarette smoke-induced oxidative stress, lipid peroxidation, and inflammation in human bronchial epithelial cells," *Life Sciences*, vol. 259, no. 15, article 118260, 2020.
- [16] U. Weichelt, R. Cay, T. Schmitz et al., "Prevention of hyperoxia-mediated pulmonary inflammation in neonatal rats by caffeine," *European Respiratory Journal*, vol. 41, no. 4, pp. 966–973, 2013.
- [17] E. Singla, V. Dharwal, and A. S. Naura, "Gallic acid protects against the COPD-linked lung inflammation and emphysema in mice," *Inflammation Research*, vol. 69, no. 4, pp. 423–434, 2020.
- [18] K. H. Chan, S. C. Chan, S. C. Yeung, R. Y. K. Man, M. S. M. Ip, and J. C. W. Mak, "Inhibitory effect of Chinese green tea on cigarette smoke-induced up-regulation of airway neutrophil elastase and matrix metalloproteinase-12 via antioxidant activity," *Free Radical Research*, vol. 46, no. 9, pp. 1123–1129, 2012.
- [19] S. Banerjee, P. Maity, S. Mukherjee et al., "Black tea prevents cigarette smoke-induced apoptosis and lung damage," *Journal of Inflammation*, vol. 4, no. 1, p. 3, 2007.
- [20] Q. Wang, J. Gong, Y. Chisti, and S. Sirisansaneeyakul, "Fungal isolates from a Pu-erh type tea fermentation and their ability to convert tea polyphenols to theabrownins," *Journal of Food Science*, vol. 80, no. 4, pp. M809–M817, 2015.
- [21] M. Bodas, D. Silverberg, K. Walworth, K. Brucia, and N. Vij, "Augmentation of S-nitrosoglutathione controls cigarette smoke-induced inflammatory-oxidative stress and chronic obstructive pulmonary disease-emphysema pathogenesis by restoring cystic fibrosis transmembrane conductance regulator function," *Antioxidants & Redox Signaling*, vol. 27, no. 7, pp. 433–451, 2017.
- [22] P. J. Barnes, "Inflammatory mechanisms in patients with chronic obstructive pulmonary disease," *Journal of Allergy and Clinical Immunology*, vol. 138, no. 1, pp. 16–27, 2016.
- [23] S. S. Hecht, "Cigarette smoking and lung cancer: chemical mechanisms and approaches to prevention," *Lancet Oncology*, vol. 3, no. 8, pp. 461–469, 2002.
- [24] M. A. Kaiser, S. Prasad, and L. Cucullo, "Protecting the BBB endothelium against cigarette smoke-induced oxidative stress using popular antioxidants: are they really beneficial?," *Brain Research*, vol. 1627, no. 19, pp. 90–100, 2015.
- [25] B. Fischer, J. Voynow, and A. Ghio, "COPD: balancing oxidants and antioxidants," *International Journal of Chronic Obstructive Pulmonary Disease*, vol. 10, no. 1, pp. 261–276, 2015.
- [26] S. Li, H.-Y. Tan, N. Wang et al., "The role of oxidative stress and antioxidants in liver diseases," *International Journal of Molecular Sciences*, vol. 16, no. 11, pp. 26087–26124, 2015.
- [27] L. Chen, H. Mo, L. Zhao et al., "Therapeutic properties of green tea against environmental insults," *The Journal of Nutritional Biochemistry*, vol. 40, pp. 1–13, 2017.
- [28] H. T. Yao, Y. R. Hsu, C. K. Lii, A. H. Lin, K. H. Chang, and H. T. Yang, "Effect of commercially available green and black tea beverages on drug-metabolizing enzymes and oxidative

- stress in Wistar rats,” *Food and Chemical Toxicology*, vol. 70, pp. 120–127, 2014.
- [29] Y. Xiao, K. Zhong, J.-R. Bai, Y.-P. Wu, J.-Q. Zhang, and H. Gao, “The biochemical characteristics of a novel fermented loose tea by *Eurotium cristatum* (MF800948) and its hypolipidemic activity in a zebrafish model,” *Food Science and Technology*, vol. 117, 2020.
- [30] X. Zou, Y. Li, X. Zhang et al., “A new prenylated indole diketopiperazine alkaloid from *Eurotium cristatum*,” *Molecules*, vol. 19, no. 11, pp. 17839–17847, 2014.
- [31] T. Jian, J. Chen, X. Ding et al., “Flavonoids isolated from loquat (*Eriobotrya japonica*) leaves inhibit oxidative stress and inflammation induced by cigarette smoke in COPD mice: the role of TRPV1 signaling pathways,” *Food Function*, vol. 11, no. 4, pp. 3516–3526, 2020.
- [32] S. S. Barbieri, E. Zacchi, P. Amadio et al., “Cytokines present in smokers' serum interact with smoke components to enhance endothelial dysfunction,” *Cardiovascular Research*, vol. 90, no. 3, pp. 475–483, 2011.
- [33] N. S. Pauwels, K. R. Bracke, L. L. Dupont et al., “Role of IL-1 and the Nlrp3/caspase-1/IL-1 axis in cigarette smoke-induced pulmonary inflammation and COPD,” *European Respiratory Journal*, vol. 38, no. 5, pp. 1019–1028, 2011.
- [34] J. Nadigel, S. Audusseau, C. J. Baglole, D. H. Eidelman, and Q. Hamid, “IL-8 production in response to cigarette smoke is decreased in epithelial cells from COPD patients,” *Pulmonary Pharmacology Therapeutics*, vol. 26, no. 5, pp. 596–602, 2013.
- [35] H. Liu, J. Ren, H. Chen et al., “Resveratrol protects against cigarette smoke-induced oxidative damage and pulmonary inflammation,” *Journal of Biochemical and Molecular Toxicology*, vol. 28, no. 10, pp. 465–471, 2014.
- [36] J.-W. Lee, N.-R. Shin, J.-W. Park et al., “*Callicarpa japonica* Thunb. attenuates cigarette smoke-induced neutrophil inflammation and mucus secretion,” *Journal of Ethnopharmacology*, vol. 175, pp. 1–8, 2015.
- [37] J. Li, G. Li, J.-L. Hu et al., “Chronic or high dose acute caffeine treatment protects mice against oleic acid-induced acute lung injury via an adenosine A2A receptor-independent mechanism,” *European Journal of Pharmacology*, vol. 654, no. 3, pp. 295–303, 2011.
- [38] C. Li, Y. Yan, Q. Shi et al., “Recuperating lung decoction attenuates inflammation and oxidation in cigarette smoke-induced COPD in rats via activation of ERK and Nrf2 pathways,” *Cell Biochemistry and Function*, vol. 35, no. 5, pp. 278–286, 2017.
- [39] L. E. Tebay, H. Robertson, S. T. Durant et al., “Mechanisms of activation of the transcription factor Nrf2 by redox stressors, nutrient cues, and energy status and the pathways through which it attenuates degenerative disease,” *Free Radical Biology and Medicine*, vol. 88, Part B, pp. 108–146, 2015.
- [40] M. Jin, C. J. Xue, Y. Wang et al., “Protective effect of hydroxy-safflor yellow a on inflammatory injury in chronic obstructive pulmonary disease rats,” *Chinese Journal of Integrative Medicine*, vol. 25, no. 10, pp. 750–756, 2019.
- [41] W. H. Kuo, J. H. Chen, H. H. Lin, B. C. Chen, J. D. Hsu, and C. J. Wang, “Induction of apoptosis in the lung tissue from rats exposed to cigarette smoke involves p38/JNK MAPK pathway,” *Chemico-Biological Interactions*, vol. 155, no. 1-2, pp. 31–42, 2005.
- [42] K. de Jong, J. M. Vonk, M. Imboden et al., “Genes and pathways underlying susceptibility to impaired lung function in the context of environmental tobacco smoke exposure,” *Respiratory Research*, vol. 18, no. 1, p. 142, 2017.
- [43] Y. Ibuki, T. Toyooka, X. Zhao, and I. Yoshida, “Cigarette side-stream smoke induces histone H3 phosphorylation via JNK and PI3K/Akt pathways, leading to the expression of proto-oncogenes,” *Carcinogenesis*, vol. 35, no. 6, pp. 1228–1237, 2014.
- [44] A. Hulina-Tomašković, I. H. Heijink, M. R. Jonker, A. Somborac-Baćura, M. G. Rajković, and L. Rumora, “Pro-inflammatory effects of extracellular Hsp70 and cigarette smoke in primary airway epithelial cells from COPD patients,” *Biochimie*, vol. 156, pp. 47–58, 2019.
- [45] P. Zhao, M. Alam, and S.-H. Lee, “Protection of UVB-induced photoaging by Fuzhuan-brick tea aqueous extract via MAPKs/Nrf2-mediated down-regulation of MMP-1,” *Nutrients*, vol. 11, no. 1, p. 60, 2019.
- [46] M. Tanaka, Y. Kishimoto, M. Sasaki et al., “*Terminalia bellirica* (Gaertn.) Roxb. Extract and Gallic Acid Attenuate LPS-Induced Inflammation and Oxidative Stress via MAPK/NF- κ B and Akt/AMPK/Nrf2 Pathways,” *Oxidative Medicine and Cellular Longevity*, vol. 2018, Article ID 9364364, 15 pages, 2018.
- [47] Y. Liang, M. S. M. Ip, and J. C. W. Mak, “(-)-Epigallocatechin-3-gallate suppresses cigarette smoke-induced inflammation in human cardiomyocytes via ROS-mediated MAPK and NF- κ B pathways,” *Phytomedicine*, vol. 58, article 152768, 2019.
- [48] P. Pavek, “Pregnane X receptor (PXR)-mediated gene repression and cross-talk of PXR with other nuclear receptors via coactivator interactions,” *Frontiers in Pharmacology*, vol. 7, p. 456, 2016.
- [49] P. O. Oladimeji and T. Chen, “PXR: more than just a master xenobiotic receptor,” *Molecular Pharmacology*, vol. 93, no. 2, pp. 119–127, 2017.
- [50] R. J. Egusquiza, M. E. Ambrosio, S. G. Wang et al., “Evaluating the role of the steroid and xenobiotic receptor (SXR/PXR) in PCB-153 metabolism and protection against associated adverse effects during perinatal and chronic exposure in mice,” *Environmental Health Perspectives*, vol. 128, no. 4, pp. 047011–47011, 2020.
- [51] C. Naspinski, X. Gu, G. D. Zhou, S. U. Mertens-Talcott, K. C. Donnelly, and Y. Tian, “Pregnane X receptor protects HepG2 cells from BaP-induced DNA damage,” *Toxicological Sciences*, vol. 104, no. 1, pp. 67–73, 2008.
- [52] V. Rothhammer and F. J. Quintana, “The aryl hydrocarbon receptor: an environmental sensor integrating immune responses in health and disease,” *Nature Reviews Immunology*, vol. 19, no. 3, pp. 184–197, 2019.
- [53] J. Yan, H. C. Tung, S. Li et al., “Aryl hydrocarbon receptor signaling prevents activation of hepatic stellate cells and liver fibrogenesis in mice,” *Gastroenterology*, vol. 157, no. 3, pp. 793–806.e14, 2019.
- [54] N. Moreno-Marín, J. M. Merino, A. Alvarez-Barrientos et al., “Aryl hydrocarbon receptor promotes liver polyploidization and inhibits PI3K, ERK, and Wnt/ β -catenin signaling,” *iScience*, vol. 4, pp. 44–63, 2018.
- [55] C. J. Baglole, S. B. Maggirwar, T. A. Gasiewicz, T. H. Thatcher, R. P. Phipps, and P. J. Sime, “The aryl hydrocarbon receptor attenuates tobacco smoke-induced cyclooxygenase-2 and prostaglandin production in lung fibroblasts through regulation of the NF- κ B family member RelB,” *The Journal of Biological Chemistry*, vol. 283, no. 43, pp. 28944–28957, 2008.

- [56] T. H. Thatcher, S. B. Maggirwar, C. J. Baglole et al., "Aryl hydrocarbon receptor-deficient mice develop heightened inflammatory responses to cigarette smoke and endotoxin associated with rapid loss of the nuclear factor-kappaB component RelB," *American Journal of Pathology*, vol. 170, no. 3, pp. 855–864, 2007.
- [57] A. Rico de Souza, M. Zago, S. J. Pollock, P. J. Sime, R. P. Phipps, and C. J. Baglole, "Genetic ablation of the aryl hydrocarbon receptor causes cigarette smoke-induced mitochondrial dysfunction and apoptosis," *The Journal of Biological Chemistry*, vol. 286, no. 50, pp. 43214–43228, 2011.
- [58] R. Foronjy and J. D'Armiento, "The effect of cigarette smoke-derived oxidants on the inflammatory response of the lung," *Clinical and Applied Immunology Reviews*, vol. 6, no. 1, pp. 53–72, 2006.
- [59] F. Savari, M. Badavi, A. Rezaie, M. K. Gharib-Naseri, and S. A. Mard, "Evaluation of the therapeutic potential effect of Fas receptor gene knockdown in experimental model of non-alcoholic steatohepatitis," *Free Radical Research*, vol. 53, no. 5, pp. 486–496, 2019.
- [60] A. R. de Souza, M. Zago, D. H. Eidelman, Q. Hamid, and C. J. Baglole, "Aryl hydrocarbon receptor (AhR) attenuation of sub-chronic cigarette smoke-induced pulmonary neutrophilia is associated with retention of nuclear RelB and suppression of intercellular adhesion molecule-1 (ICAM-1)," *Toxicological Sciences*, vol. 140, no. 1, pp. 204–223, 2014.
- [61] C. Xie, J. Zhu, X. Wang et al., "Tobacco smoke induced hepatic cancer stem cell-like properties through IL-33/p38 pathway," *Journal of Experimental & Clinical Cancer Research*, vol. 38, no. 1, p. 39, 2019.
- [62] H. Tang, M. Xu, F. Shi et al., "Effects and mechanism of nano-copper exposure on hepatic cytochrome P450 enzymes in rats," *International Journal of Molecular Sciences*, vol. 19, no. 7, p. 2140, 2018.

Research Article

Ca²⁺-Dependent Glucose Transport in Skeletal Muscle by Diphloretohydroxycarmalol, an Alga Phlorotannin: *In Vitro* and *In Vivo* Study

Hye-Won Yang,¹ Yun-Fei Jiang,¹ Hyo-Geun Lee,¹ You-Jin Jeon ^{1,2} and BoMi Ryu ¹

¹Department of Marine Life Science, Jeju National University, Jeju 63243, Republic of Korea

²Marine Science Institute, Jeju National University, Jeju 63333, Republic of Korea

Correspondence should be addressed to You-Jin Jeon; youjinj@jejunu.ac.kr and BoMi Ryu; ryu.bomi@gmail.com

Received 1 September 2020; Revised 21 December 2020; Accepted 13 January 2021; Published 10 February 2021

Academic Editor: Si Qin

Copyright © 2021 Hye-Won Yang et al. This is an open access article distributed under the Creative Commons Attribution License, which permits unrestricted use, distribution, and reproduction in any medium, provided the original work is properly cited.

Diphloretohydroxycarmalol (DPHC), a type of phlorotannin isolated from the marine alga *Ishige okamurae*, reportedly alleviates impaired glucose tolerance. However, the molecular mechanisms of DPHC regulatory activity and by which it exerts potential beneficial effects on glucose transport into skeletal myotubes to control glucose homeostasis remain largely unexplored. The aim of this study was to evaluate the effect of DPHC on cytosolic Ca²⁺ levels and its correlation with blood glucose transport in skeletal myotubes *in vitro* and *in vivo*. Cytosolic Ca²⁺ levels upon DPHC treatment were evaluated in skeletal myotubes and zebrafish larvae by Ca²⁺ imaging using Fluo-4. We investigated the effect of DPHC on the blood glucose level and glucose transport pathway in a hyperglycemic zebrafish. DPHC was shown to control blood glucose levels by accelerating glucose transport; this effect was associated with elevated cytosolic Ca²⁺ levels in skeletal myotubes. Moreover, the increased cytosolic Ca²⁺ level caused by DPHC can facilitate the Glut4/AMPK pathways of the skeletal muscle in activating glucose metabolism, thereby regulating muscle contraction through the regulation of expression of troponin I/C, CaMKII, and ATP. Our findings provide insights into the mechanism of DPHC activity in skeletal myotubes, suggesting that increased cytosolic Ca²⁺ levels caused by DPHC can promote glucose transport into skeletal myotubes to modulate blood glucose levels, thus indicating the potential use of DPHC in the prevention of diabetes.

1. Introduction

Glucose is stored as glycogen in the skeletal muscle, a major site of glucose uptake that is critical to whole-body glucose metabolism in humans. Previous studies have shown that genetic activation of glycolytic metabolism in the skeletal muscle leads to an improvement in whole-body glucose homeostasis in mice [1]. Indeed, elevation in blood glucose levels results in increased glycolytic metabolism, which may represent an important aspect of the adaptive response in skeletal muscle [1].

Glucose uptake to control the blood glucose homeostasis can be induced through the activation of muscle contraction [2]. Some of the signaling mechanisms that mediate an increase in the expression of glucose transporter 4 (Glut4) in response to exercise have been identified to be driven by

a rise in cytosolic Ca²⁺ levels due to increased release of Ca²⁺ from the sarcoplasmic reticulum (SR) [3, 4]. These studies showed that an increase in glucose uptake during muscle contractions does not require membrane depolarization but only a release of Ca²⁺ to the cytoplasm [5]. Cytosolic Ca²⁺ in the skeletal muscle regulates several signaling pathways and metabolic events related to contraction and relaxation [6].

Increased cytosolic Ca²⁺ levels in the skeletal muscle leads to the initiation of contraction, generating signals for the activation of Glut4 translocation [7, 8]. In addition, contractile activity results in an increase in the phosphorylation of Ca²⁺/calmodulin-dependent protein kinase II (CaMKII) in skeletal muscle, leading to the upregulation of Glut4 [4]. Glucose uptake in the skeletal muscle tissue is achieved by at least two major mechanisms: (1) insulin-dependent

activation of PI3-K/Akt and (2) activation of AMPK by muscle contraction due to exercise, in order to maintain energy balance [9]. Activation of AMPK plays a key role in maintaining cellular energy levels and stimulation of glucose uptake.

Furthermore, muscle contraction can stimulate Glut4 and 5' AMP-activated protein kinase (AMPK) expression to increase adenosine triphosphate (ATP) production [10, 11]. ATP hydrolysis, via the interaction between actin and myosin molecules, generates the force for muscle contraction [12]. The actomyosin ATPase activity is regulated by troponin-tropomyosin interaction, which is a crucial part of the protein interaction [13]. In addition, the binding of Ca^{2+} to troponin results in the contraction of muscle fibers [14]. In particular, the Ca^{2+} regulation mechanisms include the release upon Ca^{2+} binding to troponin C and the inhibition of contractile interaction through troponin I.

Previous studies have shown that diabetes mellitus is commonly linked to a decreased efficiency in utilizing ATP as energy in the skeletal muscles [15]. Increasing glucose uptake is derived from muscle contractile activity, resulting in the prevention of diabetes [16]. Alterations in Ca^{2+} homeostasis in skeletal muscles are strongly associated with metabolic stress and diabetes, as Ca^{2+} is indispensable for glucose uptake during muscle contraction in response to fluctuations in blood glucose [17, 18]. Therefore, in this study, we hypothesized that glucose transport can be regulated by the Ca^{2+} -dependent cytosolic signaling pathways in muscle cells; this helps in regulating blood glucose levels.

In our previous studies, we demonstrated that the marine alga *Ishige okamurae* shows antidiabetic associated responses through the modulation of blood glucose levels as well as inhibition of carbohydrate-digestive enzymes [19]. In addition, diphlorethohydroxycarmalol (DPHC), a phlorotannin isolated from *Ishige okamurae*, was revealed to have potential antidiabetic activity via prominent inhibitory effects against the α -glucosidase and α -amylase enzymes [20]. However, regulating glucose homeostasis and the underlying mechanisms of glucose uptake in skeletal muscle by DPHC treatment to control blood glucose levels have not yet been examined.

In the present study, we found that during impaired glucose tolerance, DPHC can induce glucose uptake in the skeletal muscle to improve blood glucose homeostasis. In addition, we explored the effects of DPHC on cytosolic Ca^{2+} levels in the skeletal muscle and the underlying signaling mechanisms in *in vitro* and *in vivo* models. Further, the effect of DPHC on muscle contraction was evaluated in a zebrafish model with alloxan-induced hyperglycemia. Data from this study demonstrate that glucose transport is an important part of the mechanism underlying the effect of DPHC and further provide insights into strategies aimed at improving glucose homeostasis to help ameliorate metabolic disorders in patients with diabetes in the future.

2. Materials and Methods

2.1. Materials. Diphlorethohydroxycarmalol (DPHC) was isolated as previously described by Heo et al. [19]. Fluo-4

Direct™ Calcium Assay kit was purchased from Invitrogen by Thermo Fisher Scientific (Waltham, MA, USA). 3-(4,5-Dimethylthiazol-2-yl)-2,5-diphenyltetrazolium bromide (MTT); 2-deoxy-2-[(7-nitro-2,1,3-benzoxadiazol-4-yl)amino]-D-glucose (2-NBDG); 1,2-bis(2-aminophenoxy)ethane-N,N,N',N'-tetraacetic acid tetrakis(acetoxymethyl ester) (BAPTA-AM); D-(+)-glucose (glucose); 2,4,5,6(1H,3H)-pyrimidinotetron (alloxan monohydrate); and 1,1-dimethylbiguanide hydrochloride (metformin) were purchased from Sigma-Aldrich (St. Louis, MO, USA). Antibodies against phospho-AMP-activated protein kinase (Thr172), AMPK and p-Akt (Ser473), Akt, Glut4, and GAPDH were obtained from Cell Signaling Technology (Bedford, MA, USA), and anti-rabbit secondary antibodies were purchased from Santa Cruz Biotechnology (Santa Cruz, CA, USA). ATP Assay Kit (colorimetric/fluorometric) was purchased from Abcam (Abcam Inc., Cambridge, USA).

2.2. C2C12 Cell Culture, Differentiation, and Cell Viability Assay. Previous studies have shown that C2C12 cells represent a model to study insulin resistance in diabetes and improvement in muscle function [21, 22]. C2C12 skeletal muscle cells (American Type Culture Collection) were maintained in DMEM with 10% FBS and antibiotics, at 37°C in a humidified incubator of 5% CO_2 . When the cells reached 80% confluence, C2C12 cells were differentiated into skeletal myotubes in DMEM-low glucose with 2% horse serum for 5 days. Viability levels of C2C12 cells were determined by the ability of mitochondria to convert MTT to an insoluble formazan product. Cells were maintained in 96-well plates at a density of 3×10^4 cells/well and subsequently subjected to different concentrations of DPHC (0.1, 2, 10, and 30 μM) for 24 h. Cells were pretreated with MTT solution (2 mg/mL) for 3 h. Subsequently, cell density was determined by measuring optical density (OD) at 540 nm using a microplate reader (Gen5 version 2.05, BioTek, Winooski, Vermont, USA).

2.3. Glucose Uptake Assay. Differentiated cells and skeletal myotubes were maintained in serum-free and low-glucose DMEM for 6 h before treatment with DPHC. After incubation, cells were treated with DPHC in glucose-free media. Subsequently, 2-NBDG at 50 μM final concentration was added for 24 h at 37°C. Then, cells were washed twice with PBS, serum-free medium was added, and the fluorescence intensity was immediately measured in a microplate reader at an excitation wavelength of 485 nm and an emission wavelength of 530 nm. After being taken up by the cells, 2-NBDG was converted into a nonfluorescent derivative (2-NBDG metabolite). The overall glucose uptake was obtained by quantifying the diminution in the fluorescence. The assay was performed as described by Blodgett et al. [23].

2.4. Cytosolic Ca^{2+} Level by Fluo-4 in Skeletal Myotubes. Cytosolic Ca^{2+} level was detected using the Ca^{2+} -sensitive probe Fluo-4 in 1x PBS (phosphate-buffered saline, comprised of 140 mM NaCl, 5.9 mM KCl, 1.8 mM MgCl_2 , 10 mM HEPES, 11.5 mM glucose, 1.2 mM NaH_2PO_4 , and 5 mM NaHCO_3). Skeletal myotubes were incubated in 1x Fluo-4 for 30 minutes at 37°C, washed with PBS and added

1x PSS with 0.1% BSA. After recording basal fluorescence for 10 sec at interval time of 1 sec, cells were directly added 1x PSS or DPHC (3, 10, and 30 μ M) in 0.1% BSA. After recording fluorescence for 55 sec with interval time of 1 sec, reflecting cytosolic Ca^{2+} levels were obtained to the microscope (Gen 5 version 3.03, BioTek, Winooski, Vermont, USA). A box plot was used to visualize descriptive statistics of the different groups [24].

2.5. Experimental Animals

2.5.1. Maintenance of Parental Zebrafish and Collection of Embryos. Adult zebrafish was obtained from a commercial dealer (Jeju aquarium, Jeju, Korea). Fifteen fishes were kept in 3.5 L acrylic tank according to the conditions: $28.5 \pm 1^\circ\text{C}$, fed two times a day (Tetra GmgH D-49304, Melle, Germany) with a 14/10 light/dark cycle [25]. Embryos were mated, and spawning was stimulated by setting of light, after breeding 1 female and 2 males. Embryos were collected within 30 min and transferred to Petri dishes containing embryo media. The zebrafish experiment received approval from the Animal Care and Use Committee of the Jeju National University (Approval No. 2017-0001).

2.5.2. Toxicity of DPHC in Zebrafish Embryos. From approximately 4 hours postfertilization (hpf), embryos ($n = 15$) were transferred to individual wells of 12-well plates containing 950 μ L embryo media with 50 μ L of DPHC (0.1, 2, 10, and 30 μ M). Percent survival of zebrafish embryos exposed to DPHC up to 168 hpf was measured.

2.5.3. Cytosolic Ca^{2+} Level Measurement in Zebrafish Larvae. In accordance with a previous study [26], the cytosolic Ca^{2+} level of zebrafish larvae was detected using the Ca^{2+} -sensitive probe, Fluo-4. Zebrafish larvae were incubated in the 2x Fluo-4 for 30 minutes at $28.5 \pm 1^\circ\text{C}$ and subsequently treated with DPHC (0.1, 2, and 10 μ M). As a control, to ensure if the Ca^{2+} signal was completely blocked by chelation of cytosolic Ca^{2+} with BAPTA-AM, we preincubated fish with 0.1 mM BAPTA-AM for 1 h before loading the Fluo-4.

2.5.4. Blood Glucose Level. Wild-type zebrafish were exposed to 2 mg/mL alloxan for 1 h and transferred to 1% glucose for another 1 h. The media was then changed to water for 1 h, and zebrafish were injected with saline, or DPHC, or metformin, with or without BAPTA-AM for 90 min. Adult zebrafish were divided into six groups: normal, alloxan-treated group, DPHC (0.3 μ g/g body weight), metformin (5 μ g/g body weight; a positive control with known blood glucose level-controlling activity) [27], BAPTA-AM (3 μ g/g body weight), and BAPTA-AM (3 μ g/g body weight) with DPHC (0.3 μ g/g body weight). Blood glucose level was measured using the protocol described by Zang et al. [28].

2.5.5. Plasma Membrane Protein Extraction of Zebrafish Muscle Tissue. In accordance with a previous study [29], membrane protein of zebrafish muscle tissue was extracted using a membrane protein extraction kit (Catalog number 89842, Thermo Scientific, Waltham, Massachusetts, USA) according to the manufacturer's protocols. For the zebrafish

muscle tissue collection, the fish's head, tail, fins, skin, and internal organs were removed using a scalpel and forceps. Zebrafish muscle tissue (20-40 mg) was washed in 4 mL of cell wash solution and homogenized in 1 mL of permeabilization buffer. And then, tissue was incubated for 10 min at 4°C . The homogenates were centrifuged at $16,000 \times g$ for 15 min at 4°C to pellet permeabilized cells, and then the supernatant containing cytosolic proteins was removed. The membrane proteins pellet was resuspended in 1 mL of solubilization buffer, then pipetted up and down, incubated 30 min at 4°C , and centrifuged at $16,000 \times g$ for 15 min at 4°C . The supernatant containing solubilized membrane and membrane-associated proteins was stored for western blot analysis.

2.6. Western Blot Analysis. Western blot analysis was carried out using the protocol described by Ko et al. [30]. The phospho-AMPK (Thr172), total-AMPK (Ser473), phospho-Akt, total-Akt, and Glut4 were used at 1 : 1000 dilution, and secondary antibodies were used at 1 : 3000 dilution.

2.7. ATP Assay. Using 0.1 mM ATP standard dilution, a standard curve was generated following the ATP assay kit protocol (ab83355, Abcam, America). 10 mg of muscle tissue was harvested for each assay and washed in cold PBS. Tissue was homogenized in ice-cold 2N PCA with 10-15 passes. Following maintaining on ice for 30-45 min, samples were centrifuged at $13,000 g$ for 3 min at 4°C , and supernatants were collected. Samples were adjusted to pH between 6.5 and 8 to neutralize the samples and precipitate the excess PCA. Samples were centrifuged at $13,000 g$ for 15 min at 4°C , and supernatants were collected. The supernatants were transferred to individual wells of 96-well plates mixed with the same volume of ATP reaction mix and incubated at $21 \pm 1^\circ\text{C}$ for 30 min, protected from light. ATP levels in each sample were determined by measuring optical density (OD) at 570 nm using a microplate reader (Gen5 version 2.05, Bio-Tek, Winooski, Vermont, USA). The amount of ATP in the samples was calculated according to the standard curve.

2.8. Immunofluorescence (IF). To conduct histological analysis, the muscle tissue of zebrafish was fixed in Bouin's solution for 24h and subsequently transferred to 70% ethanol for storage. Following this, the tissue was dehydrated in a graded ethanol series and embedded in paraffin. The muscle tissue was sectioned into 7 μ m sections using a microtome (Leica, Nussloch, Germany) and mounted onto glass slides. The tissue slides were deparaffinized and treated with animal serum to block antibody binding and then incubated with anti-GLUT4 antibodies (1 : 400), troponin I (1 : 400), and troponin C (1 : 400) overnight at 4°C . In addition, the tissue slides were rinsed with PBS and incubated with fluorescent-dye conjugated secondary antibodies (1 : 200) for 1 h at $21 \pm 1^\circ\text{C}$. Rinsed tissue slides were mounted with slide mounting medium (SIGMA). The fluorescence from tissue slides was observed and imaged under the microscope (Gen5 version 3.03, BioTek, Winooski, Vermont, USA).

2.9. Statistical Analysis. All of the data were presented as means \pm standard error (SE). The mean values were calculated

based on data from at least three independent experiments which were conducted on separate days using freshly prepared reagents. All the experiments were statistically analyzed using one-way analysis of variance (one-way ANOVA) and Fisher's LSD test (in GraphPad Prism Version 7.03). A p value of less than 0.05 ($^{\#}p < 0.05$, $^{\#\#}p < 0.01$, $^{\#\#\#}p < 0.001$, and $^{\#\#\#\#}p < 0.0001$) was considered statistically significant and compared with the nontreated group. A p value of less than 0.05 ($*p < 0.05$, $**p < 0.01$, $***p < 0.001$, and $****p < 0.0001$) was considered statistically significant and compared with the no sample-treated group.

3. Results

3.1. Regulation of Blood Glucose Levels in Adult Zebrafish. To assess whether blood glucose levels are influenced by DPHC, we used an alloxan-induced hyperglycemic zebrafish model [25]. Initially, to evaluate the toxicity of DPHC, zebrafish embryos were exposed to 0.1, 2, 10, and 30 μM of DPHC in the embryo media for 168 hpf. As shown in Figure 1(a), 90%, 90%, and 80% of the zebrafish survived after treatment with 1.2, 6, and 12 μM DPHC, respectively, whereas 30 μM DPHC treatment showed a significant decrease in survival to $70 \pm 4.71\%$ compared to that observed in the control group. Therefore, the subsequent zebrafish experiments were conducted with concentrations that permitted $\geq 80\%$ survival (Figure 1(a)).

Zebrafish treated with 2 mg/mL alloxan showed pancreatic islet damage, leading to reduced glucose-mediated insulin secretion, resulting in a diabetic condition (Figure 1(b)). Blood glucose levels of zebrafish in the 0.6% glucose group increased 3.28-fold compared to those in the normal group (Figure 1(c)), which were comparable to the blood glucose levels in a hyperglycemic mouse model. Injection with increasing concentrations of DPHC (0.03, 0.1, and 0.3 $\mu\text{g/g}$) in 0.6% glucose to zebrafish decreased blood glucose levels by 269, 223, and 206 mg/dL, respectively, whereas metformin (3 $\mu\text{g/g}$) led to a 176 mg/dL decrease in the blood glucose level. These data suggest that DPHC can reduce blood glucose levels in a hyperglycemic zebrafish model.

3.2. Measurement of Cell Viability and Glucose Uptake in Skeletal Myotubes. As glucose uptake by skeletal muscles is the key step in glucose homeostasis [31], we examined the effect of DPHC on glucose uptake in differentiated myocytes. Initially, the cells were treated with DPHC (0.1, 2, 10, and 30 μM) for 24 h, and cell viability was assessed using an MTT assay. As shown in Figure 2(a), cells treated with DPHC did not show a significant difference in cell viability compared to those of the control group. It was therefore confirmed that these concentrations of DPHC were nontoxic and were used for further *in vitro* experiments.

Glucose uptake following DPHC treatment in skeletal myotubes was evaluated without insulin stimulation (Figure 2(b)). Treatment of the skeletal myotubes with DPHC led to an increase in glucose uptake in a concentration-dependent manner, and 30 μM of DPHC led to a significant increase in glucose uptake of 154% compared to that in the

control group. These data suggested that DPHC treatment can induce glucose uptake in the absence of insulin in skeletal myotubes.

3.3. Increasing the Cytosolic Ca^{2+} Level in Skeletal Myotubes. To investigate the change of cytosolic Ca^{2+} levels by DPHC treatment, we performed Ca^{2+} imaging using Fluo-4-AM, a cell permeable and sensitive calcium indicator. Exposure of skeletal myotubes to DPHC in the presence of extracellular Ca^{2+} in this PSS buffer with the addition of CaCl_2 resulted in a rapid and robust increase in cytosolic calcium levels (Figure 2(c)). Similarly, in the absence of external Ca^{2+} , elevation in cytosolic Ca^{2+} levels upon DPHC treatment in the skeletal myotubes was also observed, indicating that no difference was observed by the presence or absence of extracellular Ca^{2+} (Figure 2(d)). In Figure 2(e), the box plot of the Ca^{2+} response for 60 sec from Figures 2(c) and 2(d) in the presence or absence of extracellular Ca^{2+} shows that cytosolic Ca^{2+} levels following 30 μM DPHC treatment were not significantly altered by extracellular Ca^{2+} . Additionally, the skeletal myotubes pretreated with BAPTA-AM, a cytosolic Ca^{2+} chelator, elicited no change in cytosolic Ca^{2+} upon DPHC treatment in both the presence or absence of extracellular Ca^{2+} . Elevation of cytosolic Ca^{2+} in skeletal myotubes treated with DPHC regardless of the existence of extracellular Ca^{2+} suggests that the Ca^{2+} increase by DPHC is likely to be related to the release of Ca^{2+} to the cytosol from the SR and not to Ca^{2+} influx by plasma membrane Ca^{2+} channels.

Next, the level of cytosolic Ca^{2+} with different concentrations of DPHC (3, 10, and 30 μM) was analyzed by measuring fluorescence changes in skeletal myotubes in the absence of extracellular Ca^{2+} . Cytosolic Ca^{2+} was instantly observed to increase upon DPHC treatment, while in the presence of BAPTA-AM, this calcium response was abolished (Figures 3(a) and 3(b)). The Ca^{2+} response in total skeletal myotubes upon DPHC treatment was quantified as shown in Figure 3(c), indicating that cytosolic Ca^{2+} significantly increased with 3, 10, and 30 μM DPHC compared to that with PSS treatment. This response was also observed in single skeletal myotubes (Figure 3(d)). These data showed that the Ca^{2+} release from the SR is induced in response to DPHC treatment of the skeletal myotubes.

3.4. DPHC Engages Cytosolic Ca^{2+} Signaling to Regulate Blood Glucose. Given that cytosolic Ca^{2+} release is indispensable for glucose uptake in myocytes [32], we postulated that DPHC might engage Ca^{2+} signaling to regulate skeletal muscle glucose homeostasis. To test this, we performed Ca^{2+} imaging studies in 3 hdf zebrafish embryos using Fluo-4 dye in the absence of external Ca^{2+} following exposure to DPHC. Initially, we confirmed that no significant fluorescence was induced by treatment with different concentrations of DPHC alone (without Fluo-4) compared to that in the controls (N, no Fluo-4 and no drugs exposed, and F, only Fluo-4 exposed) (Figure 4(a)). Moreover, fluorescence in the zebrafish in the Fluo-4 alone (F) sample increased 1.62-folds compared to that in the normal (N) control. These data showed that the intracellular Ca^{2+} in zebrafish embryos were detected by Fluo-4. Next, the effect of DPHC in Fluo-4-exposed embryos

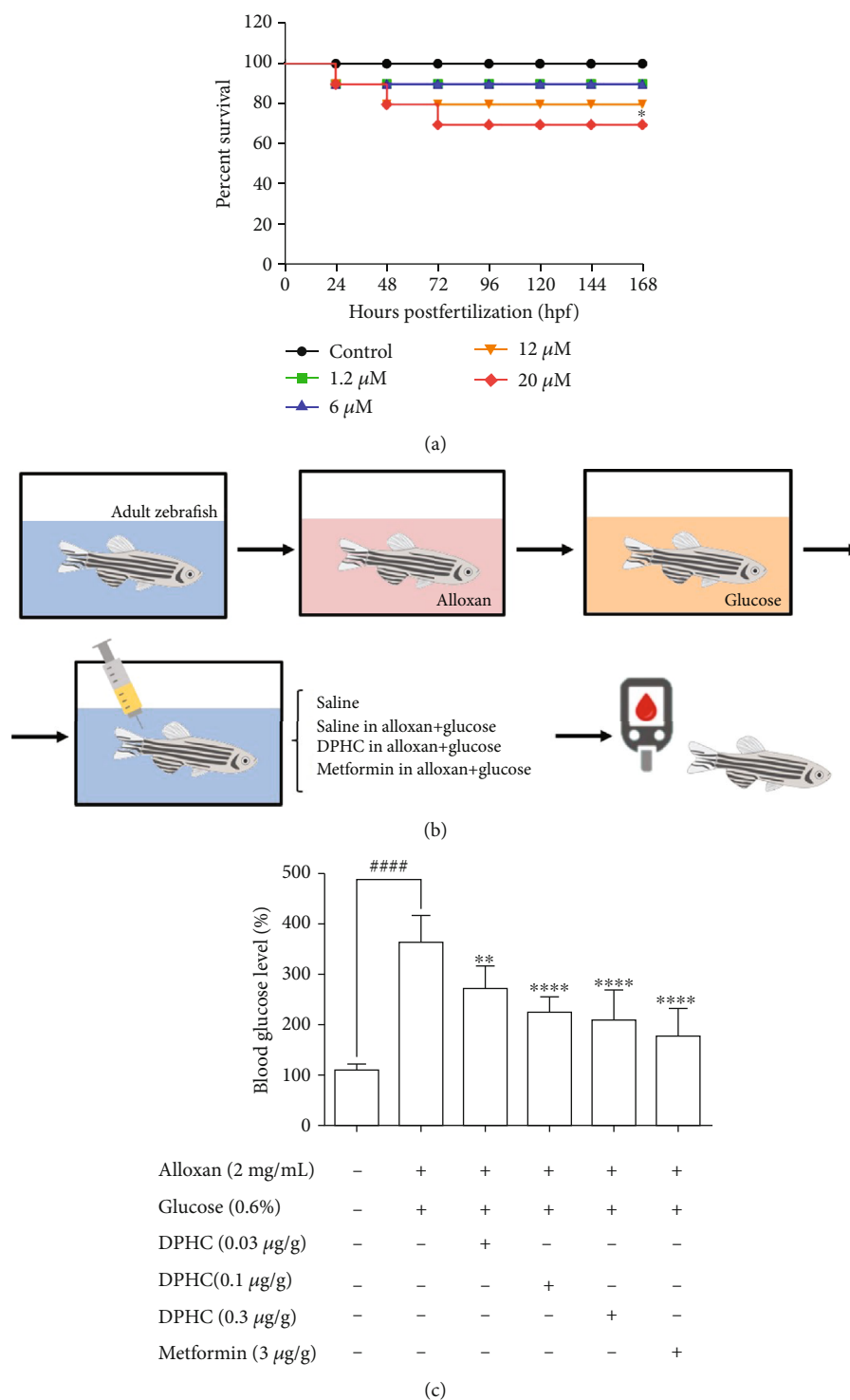


FIGURE 1: Evaluation of toxicity of DPHC by assessment of survival rate and measurement of blood glucose level in zebrafish. The zebrafish were treated with various concentrations of DPHC from *Ishige okamurae*. (a) Survival curves of zebrafish embryos after exposure to DPHC ($n = 15$ for each group). (b) Diagram and (c) result for blood glucose level of zebrafish injected with DPHC and metformin for 90 min. Data are expressed as the mean \pm SE ($n = 3$ for each group). *# Values having different superscripts are significantly different at * $p < 0.05$, ** $p < 0.01$, and **** $p < 0.0001$ compared with the no sample-treated group; #### $p < 0.0001$ compared with the nontreated group.

was assessed. Zebrafish embryos exposed to DPHC and Fluo-4 had a rapid rise in cytosolic Ca^{2+} ; however, this increase was abolished with preincubation of the 10 μM DPHC-treated zebrafish embryos with 0.1 mM BAPTA-AM for 1 h

(Figure 4(b)). This finding suggests that DPHC can induce cytosolic Ca^{2+} elevation in zebrafish embryos.

To examine whether Ca^{2+} is required for the blood glucose-lowering effect of DPHC, we treated alloxan-

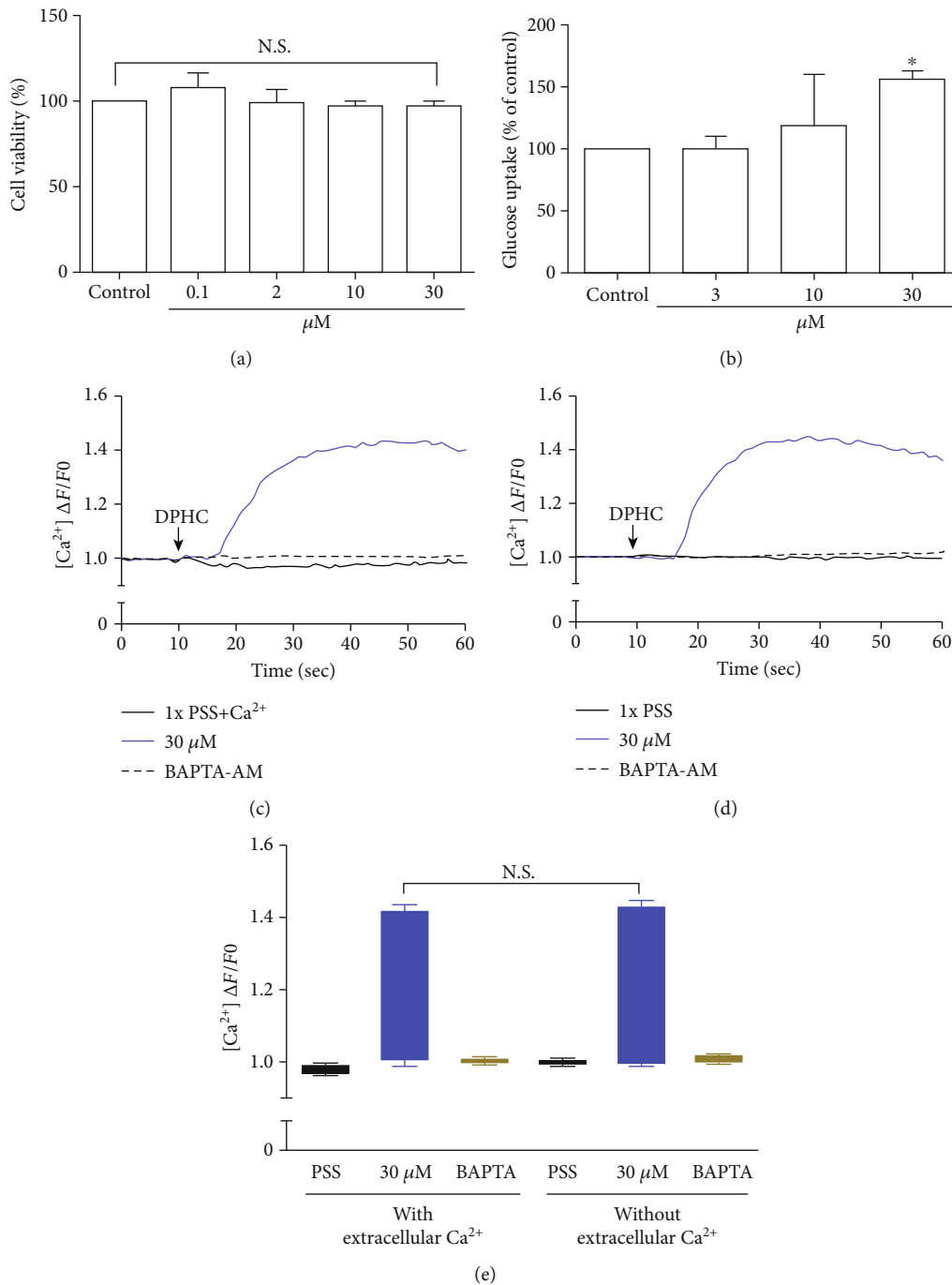


FIGURE 2: Determination of cell viability by the MTT assay in the myotubes. (a) Myotubes were incubated with the indicated concentrations of DPHC for 24 h. (b) Myotubes were starved in serum-free media and incubated for 24 h with DPHC (3, 10, and 30 μM) and 2-NBDG (50 μM). Detection of cytosolic Ca^{2+} levels using the Fluo-4 calcium indicator in the myotubes. Myotubes were loaded with Fluo-4 in PSS in the (c) presence or (d) absence of Ca^{2+} and treated with control (PSS only), 30 μM of DPHC, or BAPTA-AM. Box plots representation of (e) the cytosolic Ca^{2+} levels in myotube responses after 30 μM of DPHC or BAPTA-AM treatment as presented in (c) and (d). Data are expressed as the mean \pm SE, $n = 3$ per group, * $p < 0.05$ compared with the nontreated group. N.S.: no significance compared with the DPHC in the presence or absence of extracellular Ca^{2+} .

induced hyperglycemic zebrafish with DPHC and measured blood glucose and ATP levels. As shown in Figure 4(c), the alloxan-treated group had blood glucose levels of up to 278 mg/dL, while they were significantly lower in the DPHC (0.3 $\mu\text{g/g}$) and metformin (3 $\mu\text{g/g}$) (149 mg/dL and

151 mg/dL, respectively) treatment groups and the blank group (first column, saline only injected group). Importantly, this blood glucose-lowering effect of DPHC was significantly attenuated with BAPTA-AM treatment, resulting in blood glucose being at the same level as in the non-

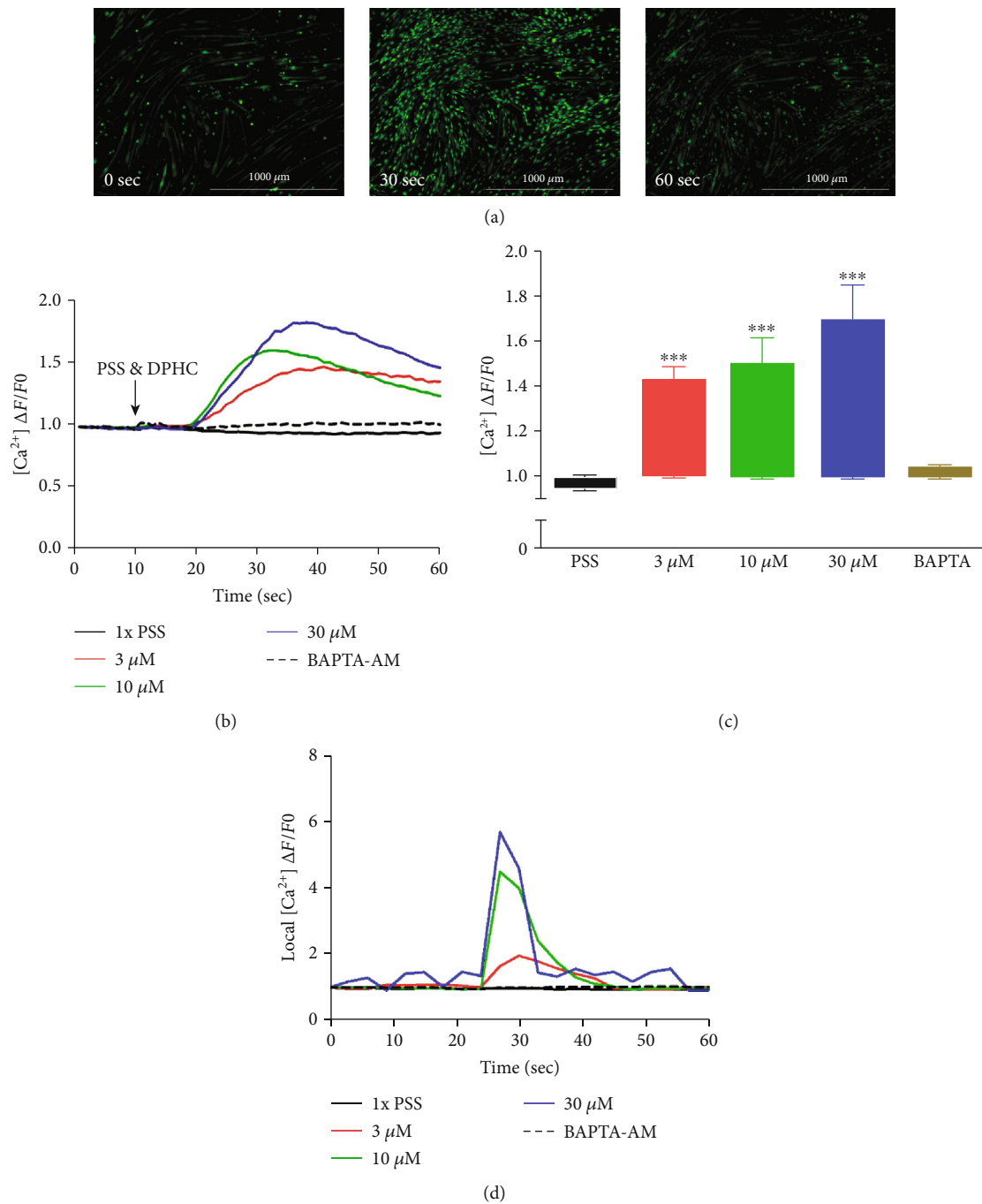


FIGURE 3: Detection of cytosolic Ca^{2+} levels in the absence of extracellular Ca^{2+} using the Fluo-4 indicator in the myotubes. (a) Representative images of myotubes at time zero (0 sec) and after stimulation with 30 μM of DPHC at time 30 sec and 60 sec. (b) Traces and (c) box plot representation of Ca^{2+} levels in response to addition of DPHC or BAPTA-AM in myotubes. The fluorescence levels of single myotubes after addition of DPHC or BAPTA-AM was also monitored (d). * $p < 0.05$ and *** $p < 0.001$ compared with the PSS group.

DPHC-treated zebrafish. Furthermore, STZ/saline groups in the diabetic mouse model showed a lower glucose tolerance, with higher glucose level after 90 min, compared with the normal/saline group in Figure S1a. We calculated the area under the curve (AUC) of IGTT in each group. In Figure S1b, the AUC of IGTT in the STZ/saline group was significantly increased compared with that in the normal/saline group.

However, the increased AUC of IGTT were significantly decreased by STZ/DPHC and STZ/metformin. In particular, the STZ/BAPTA+DPHC group showed no significant change in AUC of IGTT.

These results showed that the cytosolic Ca^{2+} release from the SR by DPHC is indispensable for its effect on blood glucose homeostasis in hyperglycemic zebrafish with suppressed

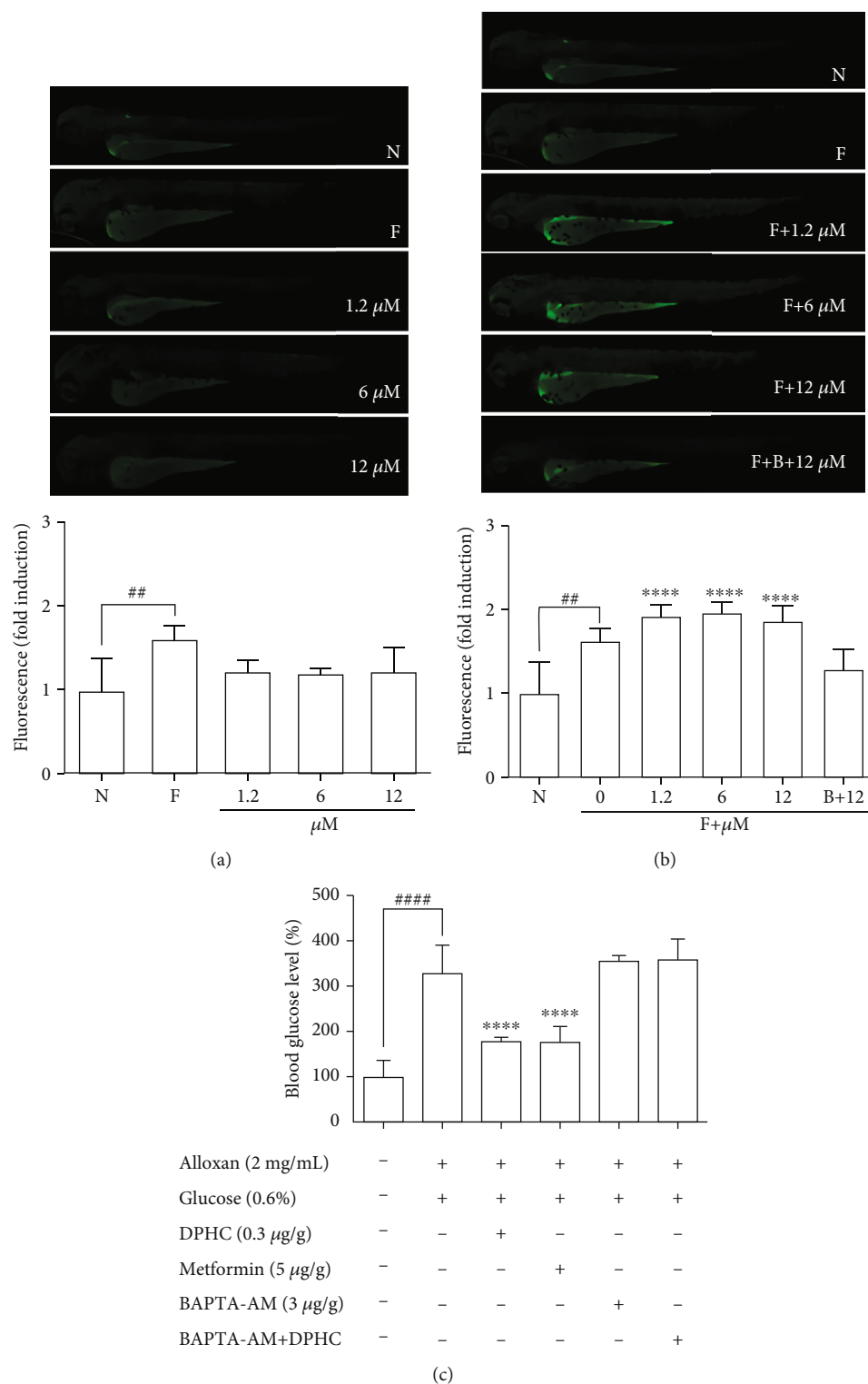


FIGURE 4: Detection of cytosolic Ca^{2+} changes using the Fluo-4 in zebrafish larvae. (a) Zebrafish larvae were stimulated with only DPHC (1.2, 6, and 12 μM). (b) Zebrafish larvae were stimulated with DPHC in Fluo-4 and compared with/without Fluo-4 groups. Changes in cytosolic Ca^{2+} levels were measured by changes in fluorescence intensity of Fluo-4 using ImageJ. (c) Measurement of blood glucose level in zebrafish. Zebrafish were injected with BAPTA-AM (3 $\mu\text{g/g}$ body weight) for 1 h, after which the zebrafish were injected with DPHC (0.3 $\mu\text{g/g}$ body weight) for 90 min. Experiments were performed in triplicate, and the data are expressed as the mean \pm SE, $n = 4$ per group. **Values having different superscripts are significantly different at **** $p < 0.0001$ compared with the no sample-treated group; ## $p < 0.01$ and #### $p < 0.0001$ compared with the nontreated group.

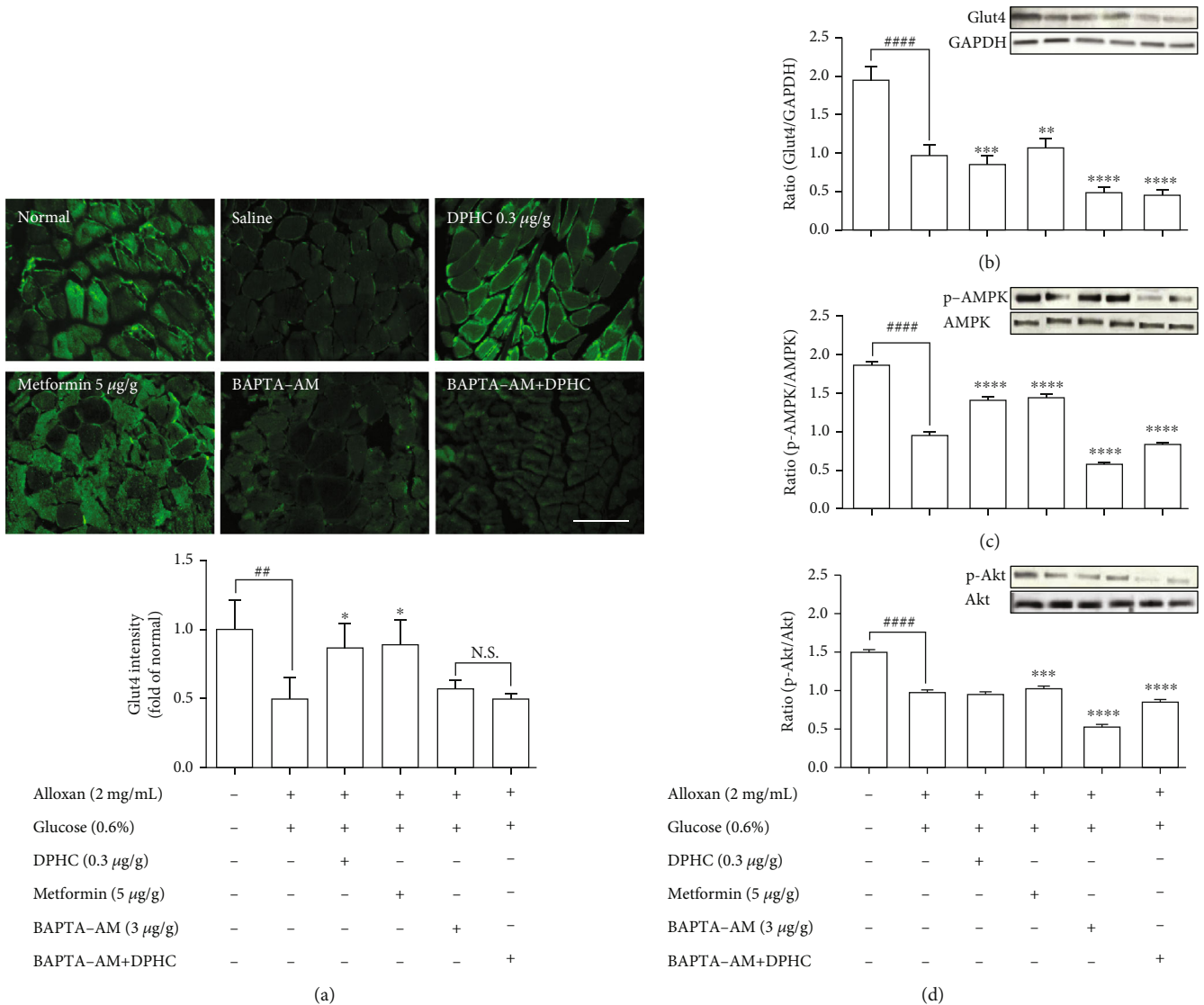


FIGURE 5: Expression of (a) Glut4 in zebrafish muscle tissues by immunofluorescence. Analysis of (b) Glut4, (c) AMPK, and (d) Akt signaling pathway in zebrafish muscle tissues by western blotting. The muscle extract was analyzed by western bottling, and the signal intensities were examined by the Fusion FX7 acquisition system (Vilber Lourmat, Eberhardzell, Germany). Experiments were performed in triplicate, and the data are expressed as mean \pm SE, $n = 4$ per group. * $p < 0.05$, ** $p < 0.01$, *** $p < 0.001$, and **** $p < 0.0001$ compared with the no sample-treated group; # $p < 0.01$ and #### $p < 0.0001$ compared with the nontreated group. N.S.: no significance compared with the BAPTA-AM group.

insulin secretion, suggesting that DPHC-induced blood glucose homeostasis requires activation of cytosolic Ca^{2+} release and the downstream signaling pathway.

3.5. Assessment of the Expression of Glucose Transport Pathway Components in Zebrafish Muscle Tissue. We examined the effect of DPHC on Glut4 translocation in the muscle membranes of hyperglycemic zebrafish by immunofluorescence. As shown in Figure 5(a), Glut4 intensity significantly decreased 0.5-fold relative to those in the nontreated group. When injected with DPHC or metformin, the Glut4 intensity increased to 0.87- or 0.90-fold relative to that in the alloxan-treated group. In particular, BAPTA-AM-injected groups with/without DPHC showed no significant change in inten-

sity. This finding suggests that DPHC can induce Glut4 translocation by increasing the cytosolic Ca^{2+} level in hyperglycemic zebrafish muscle.

To evaluate the molecular components that are involved in the regulation of glucose uptake by DPHC, the protein levels of membrane-associated Glut4 and phosphorylation of AMPK and Akt in the muscle of alloxan-induced hyperglycemic zebrafish were analyzed by western blotting. As shown in Figures 5(b)–5(d), the membrane localization of Glut4 and phosphorylation levels of AMPK and Akt significantly decreased in the muscle of alloxan-induced hyperglycemic zebrafish compared to those in the blank-treated animals. However, DPHC and metformin promoted Glut4 translocation to the membrane and phosphorylation of

AMPK, indicating that DPHC can stimulate the glucose transport pathway in hyperglycemic zebrafish. However, DPHC did not affect the expression of Akt compared to that in the alloxan-induced hyperglycemic zebrafish. As shown in Figure S2, membrane Glut4 level of the STZ/saline group in the diabetic mouse model was significantly decreased compared with that in the normal/saline group. However, the decreased membrane Glut4 levels were significantly increased by STZ/DPHC and STZ/metformin. In particular, the STZ/BAPTA+DPHC group showed no significant change in membrane Glut4 level.

In contrast, Ca^{2+} depletion by BAPTA-AM failed to activate phosphorylation of these proteins, and protein levels remained unchanged even with DPHC treatment compared to those in the alloxan-induced hyperglycemic zebrafish, suggesting that DPHC can induce Ca^{2+} -dependent activation of the Glut4/AMPK pathway in the muscles of hyperglycemic zebrafish to control glucose homeostasis.

3.6. Determination of Muscle Contraction in Zebrafish Muscle. To assess whether skeletal muscle contraction in hyperglycemic zebrafish is affected by DPHC, we examined troponin C and I intensity in hyperglycemic zebrafish using immunofluorescence. As shown in Figure 6(a), troponin C intensity in skeletal muscles of hyperglycemic zebrafish significantly decreased by 0.33-fold of that in the nontreated group ($p < 0.001$). However, DPHC significantly increased troponin C intensity ($p < 0.01$). In addition, troponin I intensity in the skeletal muscle of hyperglycemic zebrafish significantly increased to 3.3-fold of that in the nontreated group (Figure 6(b)). However, DPHC treatment significantly decreased troponin I intensity. These results indicated that DPHC can stimulate muscle contraction in hyperglycemic zebrafish.

We examined the CaMKIIs that are involved in the improvement of glucose homeostasis by DPHC in skeletal muscles of hyperglycemic zebrafish. As shown in Figure 6(c), DPHC treatment significantly reduced the CaMKII level in the alloxan-induced hyperglycemic zebrafish. However, BAPTA-AM-injected groups with/without DPHC did not significantly change the CaMKII expression level. This finding suggests that DPHC can induce muscle contraction by CaMKII expression, the latter being induced in turn by increased cytosolic Ca^{2+} level in the hyperglycemic zebrafish muscle. Furthermore, DPHC treatment modestly increased the alloxan-induced reduction in ATP levels in the skeletal muscle in hyperglycemic zebrafish, whilst this increase was reversed with BAPTA-AM treatment (Figure 6(d)). The data suggest that DPHC can improve glucose homeostasis by inducing muscle contraction in hyperglycemic zebrafish.

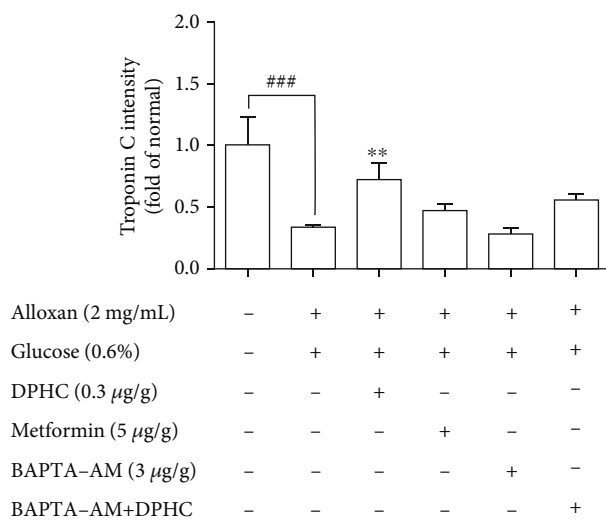
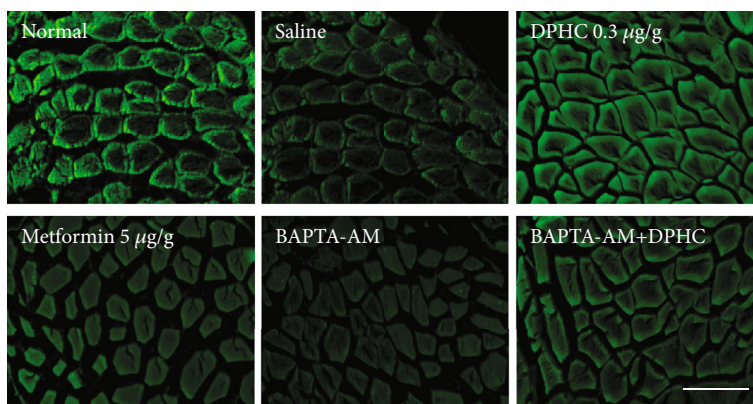
4. Discussion

Abnormal metabolism of glucose in diabetes reduces insulin sensitivity and induces postprandial hyperglycemia contractile activity in the skeletal muscle. Previous studies have reported the antidiabetic effects of *Ishige okamurae* extract on blood glucose level and insulin resistance in C57BL/KsJ-*db/db* mice [20]. We showed that DPHC isolated from *Ishige*

okamurae significantly reduced the blood glucose level in the hyperglycemic zebrafish model with impaired glucose tolerance. In addition, DPHC can induce glucose uptake in the absence of insulin in C2C12 cells (Figure 2(b)). Our data suggest that DPHC can induce glucose transport in the skeletal muscle through contractile activity, resulting in the regulation of blood glucose level in a hyperglycemic model.

Glucose uptake by the skeletal muscle is regulated by glucose delivery to the skeletal muscle cells, surface membrane permeability to glucose, and flux through intracellular metabolism. In addition, the skeletal muscle possesses contractile activity that can effectively restore glucose regulation in an insulin-independent manner [2, 33]. Previous studies using different methods and models show that muscle contractions enhance glucose uptake similar to that by insulin action [33, 34]. Zebrafish models have been established to study a wide range of human pathologies, including genetic disorders and acquired diseases [35, 36]. Previous studies used alloxan or streptozotocin or only glucose water to generate an acute hyperglycemic zebrafish model [37, 38]. Shin et al. [38] suggested that a hyperglycemic zebrafish model is appropriate for experiments that call for a short-term model.

Skeletal muscle contraction is initiated by depolarization of the plasma membrane and T tubules, which not only triggers Ca^{2+} release from the SR but also leads to the interaction of actin and myosin filaments and development of tension in the fibers. The contraction and relaxation cycle produced by muscle fibers is called twitch [39]. In previous studies, the time course of Ca^{2+} in skeletal muscle fibers was studied by Ca^{2+} indicators [40], and Garcia and Schneider [41] also suggested that the kinetic properties that were characterized in the fast-twitch skeletal muscle fiber were controlled by Ca^{2+} release from the SR. The transient increase in calcium levels is important for intermediate signaling between the excitation and contraction phase in skeletal myotubes [42]. In this study, we present data supporting an association between the cytosolic Ca^{2+} release by DPHC in skeletal myotubes and its antidiabetic activity [20] that can improve impaired glucose uptake in diabetes to enable the maintenance of glucose homeostasis. Glucose uptake through the cell membrane is the rate-limiting step in glucose homeostasis in the skeletal muscle under physiological conditions [43] and is independently stimulated by Ca^{2+} /contraction-dependent processes [44, 45]. The period between muscle stimulation and contraction is called latent period [46], which is a period of 10 seconds after DPHC treatment. After 10 seconds, the skeletal myotubes undergo a contracting period followed by a relaxation period. The basic unit of activity in the muscle fiber is the twitch that can induce short contractions [42]. DPHC significantly increased cytosolic Ca^{2+} levels in the skeletal myotubes, independent of extracellular Ca^{2+} , ruling out the involvement of Ca^{2+} influx pathways and suggesting induction of Ca^{2+} release from the SR by DPHC [3, 5]. Although Ca^{2+} release from the SR of myotube cells can facilitate attachment/detachment of myosin to actin and the energy supply to ensure the excitation-contraction-relaxation cycle of muscle cells [47], the role of Ca^{2+} in glucose uptake, as well as its pathogenic contribution to diabetes, remains elusive.



Alloxan (2 mg/mL)	-	+	+	+	+	+
Glucose (0.6%)	-	+	+	+	+	+
DPHC (0.3 μg/g)	-	-	+	-	-	-
Metformin (5 μg/g)	-	-	-	+	-	-
BAPTA-AM (3 μg/g)	-	-	-	-	+	-
BAPTA-AM+DPHC	-	-	-	-	-	+

(a)

FIGURE 6: Continued.

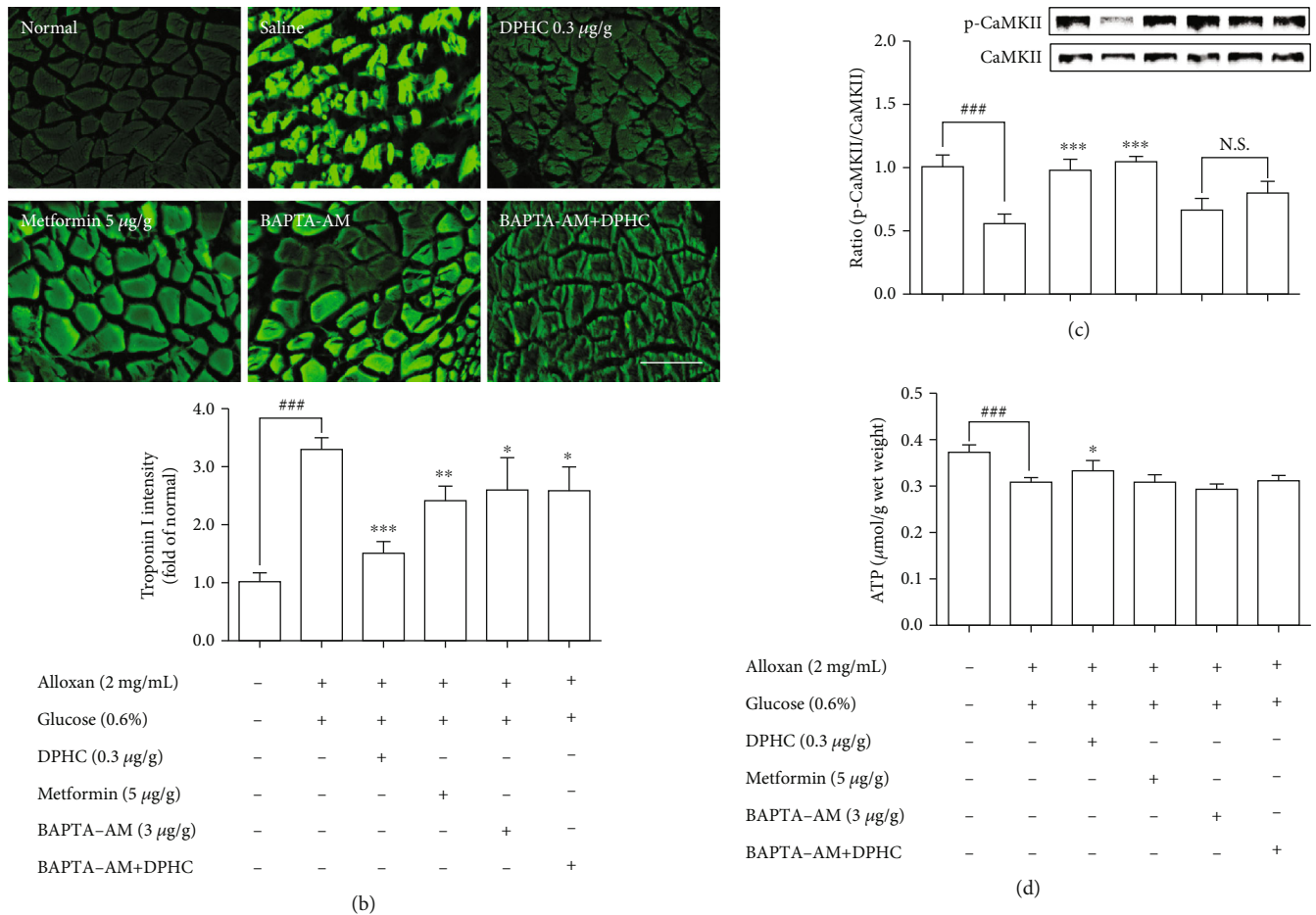


FIGURE 6: Measurement of (a) troponin C, (b) troponin I, (c) CaMKII, and (d) ATP levels in zebrafish muscle tissues. Zebrafish were injected with BAPTA-AM (3 µg/g body weight) for 1 h, after which the zebrafish were injected with DPHC (0.3 µg/g body weight) for 90 min. Experiments were performed in triplicate, and the data are expressed as mean ± SE, $n = 3$ per group. * $p < 0.05$, ** $p < 0.01$, and *** $p < 0.001$ compared with the no sample-treated group; ### $p < 0.001$ compared with the nontreated group.

The remarkable observation in our study is that cytosolic Ca^{2+} release by DPHC treatment can induce glucose uptake resulting in the modulation of blood glucose levels in the hyperglycemic zebrafish model, suggesting that cytosolic Ca^{2+} in skeletal myotubes can improve glucose homeostasis. Increased intracellular Ca^{2+} levels, even at low concentrations to induce contractions, provide the signal to activate Glut4 translocation to the cell surface in skeletal muscle independently of insulin [48]. Depending on the coordination and integration of several physiological systems, blood glucose homeostasis is maintained. Moreover, during exercise, an increased need for glucose by contracting muscle results in glucose uptake from blood into the working skeletal muscles [48, 49]. This study suggests that glucose homeostasis in muscles can be suggested as an important strategy for diabetes therapy [50] and can improve insulin sensitivity and reduce postprandial hyperglycemia [23, 30, 51].

Overexpression of key signaling proteins regulating energy metabolism in the skeletal muscle can improve metabolic disturbances associated with hyperglycemia. The diabetic mouse model generated using alloxan has been

reported to affect expression of Glut4, resulting in a decreased uptake of glucose and increased blood glucose levels [52]. In addition, AMPK activation promotes Glut4 translocation and increases glucose uptake directly in the skeletal muscle [25]. Muscle contraction stimulates glucose transport by AMPK activation, increasing cytosolic Ca^{2+} level and Glut4 activation. Furthermore, previous studies have shown that increasing the cytosolic Ca^{2+} level induces glucose uptake in isolated rat muscle without increasing AMPK phosphorylation [34, 53, 54], suggesting that cytosolic Ca^{2+} levels increase glucose uptake during contractile activity. Our results showed that DPHC can stimulate Glut4 translocation and phosphorylation of AMPK, which was dependent on cytosolic Ca^{2+} in skeletal myotubes, while there was no effect on Akt activation. The cytosolic Ca^{2+} regulation by DPHC treatment in skeletal myotubes can reinforce the Glut4/AMPK pathways for a profound effect on glucose uptake metabolism. Our data further indicated that DPHC can normalize metabolic disturbances in diabetes and improve glucose homeostasis in skeletal muscles.

Skeletal muscle contraction is regulated by Ca^{2+} by controlling the action of specific regulatory proteins such as tropomyosin and troponin [55]. Troponin C is a Ca^{2+} -binding component in muscle contraction. Troponin I is an inhibitory component of contractile interaction between myosin and actin in the presence of tropomyosin [56]. Our results showed that alloxan-induced hyperglycemic zebrafish can stimulate dysfunction of muscle contraction. We confirmed that the DPHC can promote muscle contraction by increasing cytosolic Ca^{2+} levels in the hyperglycemic zebrafish muscle. In addition, CaMKII activation promotes Glut4 translocation to increase glucose uptake directly in the skeletal muscle [4]. Previous studies have shown that caffeine treatment induces the activation of CaMKII by muscle contraction via Ca^{2+} release from the SR in rat muscle [53]. We confirmed that DPHC can stimulate CaMKII production in skeletal muscle tissues of hyperglycemic zebrafish. Our results showed that DPHC can enhance CaMKII expression levels; this is influenced by cytosolic Ca^{2+} in skeletal muscles of hyperglycemic zebrafish.

Muscle contraction initiates Ca^{2+} release into the myofibril and, as a result, increases ATP demand through the activity of myosin and Ca^{2+} ATPases. Since the SR (source of Ca^{2+}) and mitochondria (source of ATP) are both necessary for the flawless execution of the contractile cycle [49], we confirmed that the ATP level in hyperglycemic zebrafish, the model where we observed the blood glucose-lowering effect of DPHC, was increased by DPHC treatment.

5. Conclusions

In this study, we uncovered the molecular mechanisms underlying the euglycemic effects of DPHC in the skeletal muscle of a hyperglycemic zebrafish model. DPHC can increase cytosolic Ca^{2+} level to activate Glut4/AMPK pathways of the skeletal muscle, which promotes glucose transport in hyperglycemic zebrafish. Also, increased Ca^{2+} by DPHC is linked with the regulation of troponin I/C, CaMKII, and ATP levels that enable muscle contraction. Therefore, the findings from this study provide a mechanistic and integrative approach demonstrating the upregulation of cytosolic Ca^{2+} by DPHC in the skeletal muscle as a potential therapeutic mechanism for improving glucose metabolism during diabetes.

Abbreviations

DPHC:	Diphloretrohydroxycarmalol
SR:	Sarcoplasmic reticulum
MTT:	3-(4,5-Dimethylthiazol-2-yl)-2,5-diphenyltetrazolium bromide
2-NBDG:	2-Deoxy-2-[(7-nitro-2,1,3-benzoxadiazol-4-yl)amino]-D-glucose
BAPTA-AM:	1,2-Bis(2-aminophenoxy)ethane-N,N,N',N'-tetraacetic acid tetrakis(acetoxymethyl ester)
Glucose:	D-(+)-Glucose
Alloxan:	2,4,5,6(1H,3H)-Pyrimidinetetrone
Metformin:	1,1-Dimethylbiguanide hydrochloride
AMPK:	Phospho-AMP-activated protein kinase
PSS:	Phosphate-buffered saline
HpF:	Hours postfertilization.

Data Availability

The data used to support the findings of this study are available from the corresponding authors upon request.

Ethical Approval

Ethical approval was obtained from the Animal Care and Use Committee of the Jeju National University, Korea (Approval No. 2017-0001).

Conflicts of Interest

The authors declare no competing interests.

Authors' Contributions

H.Y. performed the experiments and data analysis. Y.J. isolated and provided diphloretrohydroxycarmalol. H.L. performed additional *in vivo* experiments. H.Y. wrote the article and prepared the Figures. B.R. and Y.J. supervised the study and take responsibility for the entire study. Yun-Fei Jiang and Hye-Won Yang contributed equally to this work.

Acknowledgments

This research was a part of the project titled "Development of Functional Food Products with Natural Materials derived from Marine Resources (no. 20170285)," funded by the Ministry of Oceans and Fisheries, Korea.

Supplementary Materials

Figure S1: evaluation of IGTT in streptozotocin-induced diabetic mice. (a) Measurement of blood glucose level after glucose intake in mice fed with 30 mg/kg DPHC or 100 mg/kg metformin. Mice were injected with 2.5 mg/kg BAPTA-AM for 30 min, before glucose intake. (b) Quantitative analysis of the area under the curve (AUC) from IGTT. Data are expressed as the mean \pm SE, $n = 4$ per group. ^{*}[#]Values having different superscripts are significantly different at $*p < 0.05$ compared with the no sample-treated group; ^{##} $p < 0.01$ compared with the nontreated group. Figure S2: expression of membrane and cytosolic Glut4 level in mice muscle tissues by western blotting. The muscle extract was analyzed by western blotting, and the signal intensities were examined by the Fusion FX7 acquisition system (Vilber Lourmat, Eberhardzell, Germany). Membrane Glut4 was normalized by cytosolic Glut4. Data are expressed as the mean \pm SE, $n = 4$ per group. ^{*}[#]Values having different superscripts are significantly different at $*p < 0.05$ and $***p < 0.001$ compared with the no sample-treated group; ^{###} $p < 0.001$ compared with the nontreated group. (*Supplementary Materials*)

References

- [1] Z.-X. Meng, S. Li, L. Wang et al., "Baf60c drives glycolytic metabolism in the muscle and improves systemic glucose homeostasis through Deptor-mediated Akt activation," *Nature Medicine*, vol. 19, no. 5, pp. 640–645, 2013.

- [2] A. J. G. Castro, M. J. S. Frederico, L. H. Cazarolli et al., "The mechanism of action of ursolic acid as insulin secretagogue and insulinomimetic is mediated by cross-talk between calcium and kinases to regulate glucose balance," *Biochimica et Biophysica Acta (BBA)-General Subjects*, vol. 1850, no. 1, pp. 51–61, 2015.
- [3] E. R. Chin, "Role of Ca²⁺/calmodulin-dependent kinases in skeletal muscle plasticity," *Journal of Applied Physiology*, vol. 99, no. 2, pp. 414–423, 2005.
- [4] E. O. Ojuka, V. Goyaram, and J. A. H. Smith, "The role of CaMKII in regulating GLUT4 expression in skeletal muscle," *American Journal of Physiology-Endocrinology and Metabolism*, vol. 303, no. 3, pp. E322–E331, 2012.
- [5] J. O. Holloszy and H. T. Narahara, "Nitrate ions: potentiation of increased permeability to sugar associated with muscle contraction," *Science*, vol. 155, no. 3762, pp. 573–575, 1967.
- [6] M. W. Berchtold, H. Brinkmeier, and M. Muntener, "Calcium ion in skeletal muscle: its crucial role for muscle function, plasticity, and disease," *Physiological Reviews*, vol. 80, no. 3, pp. 1215–1265, 2000.
- [7] N. Jessen and L. J. Goodyear, "Contraction signaling to glucose transport in skeletal muscle," *Journal of Applied Physiology*, vol. 99, no. 1, pp. 330–337, 2005.
- [8] A. P. Waller, A. Kalyanasundaram, S. Hayes, M. Periasamy, and V. A. Lacombe, "Sarcoplasmic reticulum Ca²⁺ ATPase pump is a major regulator of glucose transport in the healthy and diabetic heart," *Biochimica et Biophysica Acta (BBA)-Molecular Basis of Disease*, vol. 1852, no. 5, pp. 873–881, 2015.
- [9] Y. Tsuchiya, H. Hatakeyama, N. Emoto, F. Wagatsuma, S. Matsushita, and M. Kanzaki, "Palmitate-induced down-regulation of sortilin and impaired GLUT4 trafficking in C2C12 myotubes," *Journal of Biological Chemistry*, vol. 285, no. 45, pp. 34371–34381, 2010.
- [10] J. Ihlemann, T. Ploug, Y. Hellsten, and H. Galbo, "Effect of tension on contraction-induced glucose transport in rat skeletal muscle," *American Journal of Physiology-Endocrinology and Metabolism*, vol. 277, no. 2, pp. E208–E214, 1999.
- [11] W. Liu and J. Zhao, "Insights into the molecular mechanism of glucose metabolism regulation under stress in chicken skeletal muscle tissues," *Saudi Journal of Biological Sciences*, vol. 21, no. 3, pp. 197–203, 2014.
- [12] L. A. Stein, P. B. Chock, and E. Eisenberg, "Mechanism of the actomyosin ATPase: effect of actin on the ATP hydrolysis step," *Proceedings of the National Academy of Sciences of the United States of America*, vol. 78, no. 3, pp. 1346–1350, 1981.
- [13] E. P. Morris and S. S. Lehrer, "Troponin-tropomyosin interactions. Fluorescence studies of the binding of troponin, troponin T and chymotryptic troponin T fragments to specifically labeled tropomyosin," *Biochemistry*, vol. 23, no. 10, pp. 2214–2220, 2002.
- [14] A. Galińska-Rakoczy, P. Engel, C. Xu et al., "Structural basis for the regulation of muscle contraction by troponin and tropomyosin," *Journal of Molecular Biology*, vol. 379, no. 5, pp. 929–935, 2008.
- [15] S. L. Hebert and K. S. Nair, "Protein and energy metabolism in type 1 diabetes," *Clinical Nutrition*, vol. 29, no. 1, pp. 13–17, 2010.
- [16] J. He, S. Watkins, and D. E. Kelley, "Skeletal muscle lipid content and oxidative enzyme activity in relation to muscle fiber type in type 2 diabetes and obesity," *Diabetes*, vol. 50, no. 4, pp. 817–823, 2001.
- [17] H. Eshima, D. C. Poole, and Y. Kano, "In vivo calcium regulation in diabetic skeletal muscle," *Cell Calcium*, vol. 56, no. 5, pp. 381–389, 2014.
- [18] M. Fernández-Velasco, G. Ruiz-Hurtado, A. M. Gómez, and A. Rueda, "Ca²⁺ handling alterations and vascular dysfunction in diabetes," *Cell Calcium*, vol. 56, no. 5, pp. 397–407, 2014.
- [19] S.-J. Heo, J.-Y. Hwang, J.-I. Choi, J.-S. Han, H.-J. Kim, and Y.-J. Jeon, "Diphlorethohydroxycarmalol isolated from *Ishige okamurae*, a brown algae, a potent α -glucosidase and α -amylase inhibitor, alleviates postprandial hyperglycemia in diabetic mice," *European Journal of Pharmacology*, vol. 615, no. 1–3, pp. 252–256, 2009.
- [20] K.-H. Min, H.-J. Kim, Y.-J. Jeon, and J.-S. Han, "Ishige okamurae ameliorates hyperglycemia and insulin resistance in C57BL/KsJ-db/db mice," *Diabetes Research and Clinical Practice*, vol. 93, no. 1, pp. 70–76, 2011.
- [21] H. F. Dugdale, D. C. Hughes, R. Allan et al., "The role of resveratrol on skeletal muscle cell differentiation and myotube hypertrophy during glucose restriction," *Molecular and Cellular Biochemistry*, vol. 444, no. 1–2, pp. 109–123, 2018.
- [22] C. Y. Wong, H. Al-Salami, and C. R. Dass, "C2C12 cell model: its role in understanding of insulin resistance at the molecular level and pharmaceutical development at the preclinical stage," *Journal of Pharmacy and Pharmacology*, vol. 72, no. 12, pp. 1667–1693, 2020.
- [23] A. B. Blodgett, R. K. Kothinti, I. Kamyshko, D. H. Petering, S. Kumar, and N. M. Tabatabai, "A fluorescence method for measurement of glucose transport in kidney cells," *Diabetes Technology and Therapeutics*, vol. 13, no. 7, pp. 743–751, 2011.
- [24] Z. Bozoky, S. Ahmadi, T. Milman et al., "Synergy of cAMP and calcium signaling pathways in CFTR regulation," *Proceedings of the National Academy of Sciences of the United States of America*, vol. 114, no. 11, pp. E2086–E2095, 2017.
- [25] E.-A. Kim, S. H. Lee, J. H. Lee et al., "A marine algal polyphenol, dieckol, attenuates blood glucose levels by Akt pathway in alloxan induced hyperglycemia zebrafish model," *RSC Advances*, vol. 6, no. 82, pp. 78570–78575, 2016.
- [26] B. S. Muntean, C. M. Horvat, J. H. Behler et al., "A comparative study of embedded and anesthetized zebrafish in vivo on myocardial calcium oscillation and heart muscle contraction," *Frontiers in Pharmacology*, vol. 1, p. 139, 2010.
- [27] H. K. R. Karlsson, K. Hallsten, M. Bjornholm et al., "Effects of metformin and rosiglitazone treatment on insulin signaling and glucose uptake in patients with newly diagnosed type 2 diabetes: a randomized controlled study," *Diabetes*, vol. 54, no. 5, pp. 1459–1467, 2005.
- [28] L. Zang, Y. Shimada, Y. Nishimura, T. Tanaka, and N. Nishimura, "A novel, reliable method for repeated blood collection from aquarium fish," *Zebrafish*, vol. 10, no. 3, pp. 425–432, 2013.
- [29] X. Zhang, L. Wang, K. Qiu, D. Xu, and J. Yin, "Dynamic membrane proteome of adipogenic and myogenic precursors in skeletal muscle highlights EPHA2 may promote myogenic differentiation through ERK signaling," *The FASEB Journal*, vol. 33, no. 4, pp. 5495–5509, 2019.
- [30] S.-C. Ko, M. Lee, J.-H. Lee, S.-H. Lee, Y. Lim, and Y.-J. Jeon, "Dieckol, a phlorotannin isolated from a brown seaweed, *Ecklonia cava*, inhibits adipogenesis through AMP-activated protein kinase (AMPK) activation in 3T3-L1 preadipocytes," *Environmental Toxicology and Pharmacology*, vol. 36, no. 3, pp. 1253–1260, 2013.

- [31] R. Balasubramanian, B. Robaye, J.-M. Boeynaems, and K. A. Jacobson, "Enhancement of glucose uptake in mouse skeletal muscle cells and adipocytes by P2Y6 receptor agonists," *PLoS One*, vol. 9, no. 12, article e116203, 2014.
- [32] J. H. Youn, E. A. Gulve, and J. O. Holloszy, "Calcium stimulates glucose transport in skeletal muscle by a pathway independent of contraction," *American Journal of Physiology-Cell Physiology*, vol. 260, no. 3, pp. C555–C561, 1991.
- [33] A. J. Rose and E. A. Richter, "Skeletal muscle glucose uptake during exercise: how is it regulated?," *Physiology*, vol. 20, no. 4, pp. 260–270, 2005.
- [34] C. Cantó, A. V. Chibalin, B. R. Barnes et al., "Neuregulins mediate calcium-induced glucose transport during muscle contraction," *Journal of Biological Chemistry*, vol. 281, no. 31, pp. 21690–21697, 2006.
- [35] S. Berghmans, C. Jette, D. Langenau et al., "Making waves in cancer research: new models in the zebrafish," *BioTechniques*, vol. 39, no. 2, pp. 227–237, 2005.
- [36] G. J. Lieschke and P. D. Currie, "Animal models of human disease: zebrafish swim into view," *Nature Reviews Genetics*, vol. 8, no. 5, pp. 353–367, 2007.
- [37] A. S. Olsen, M. P. Sarras Jr., and R. V. Intine, "Limb regeneration is impaired in an adult zebrafish model of diabetes mellitus," *Wound Repair and Regeneration*, vol. 18, no. 5, pp. 532–542, 2010.
- [38] E. Shin, B. N. Hong, and T. H. Kang, "An optimal establishment of an acute hyperglycemia zebrafish model," *African Journal of Pharmacy and Pharmacology*, vol. 6, no. 42, pp. 2922–2928, 2012.
- [39] J. J. Feher, T. D. Waybright, and M. L. Fine, "Comparison of sarcoplasmic reticulum capabilities in toadfish (*Opsanus tau*) sonic muscle and rat fast twitch muscle," *Journal of Muscle Research & Cell Motility*, vol. 19, no. 6, pp. 661–674, 1998.
- [40] F. Eusebi, R. Miledi, and T. Takahashi, "Aequorin-calcium transients in mammalian fast and slow muscle fibers," *Biomedical Research*, vol. 6, no. 3, pp. 129–138, 1985.
- [41] J. Garcia and M. F. Schneider, "Calcium transients and calcium release in rat fast-twitch skeletal muscle fibres," *Journal of Physiology*, vol. 463, no. 1, pp. 709–728, 1993.
- [42] S. M. Baylor and S. Hollingworth, "Intracellular calcium movements during excitation-contraction coupling in mammalian slow-twitch and fast-twitch muscle fibers," *Journal of General Physiology*, vol. 139, no. 4, pp. 261–272, 2012.
- [43] C. J. Tanner, T. R. Koves, R. L. Cortright et al., "Effect of short-term exercise training on insulin-stimulated PI 3-kinase activity in middle-aged men," *American Journal of Physiology-Endocrinology and Metabolism*, vol. 282, no. 1, pp. E147–E153, 2002.
- [44] I. Y. Kuo and B. E. Ehrlich, "Signaling in muscle contraction," *Cold Spring Harbor Perspectives in Biology*, vol. 7, no. 2, p. a006023, 2015.
- [45] K. S. C. Röckl, C. A. Witczak, and L. J. Goodyear, "Signaling mechanisms in skeletal muscle: acute responses and chronic adaptations to exercise," *IUBMB Life*, vol. 60, no. 3, pp. 145–153, 2008.
- [46] A. V. Hill, "The development of the active state of muscle during the latent period," *Proceedings of the Royal Society of London. Series B. Biological Sciences*, vol. 137, no. 888, pp. 320–329, 1950.
- [47] I. M. P. Gommans, M. H. M. Vlak, A. de Haan, and B. G. M. van Engelen, "Calcium regulation and muscle disease," *Journal of Muscle Research & Cell Motility*, vol. 23, no. 1, pp. 59–63, 2002.
- [48] E. A. Richter and M. Hargreaves, "Exercise, GLUT4, and skeletal muscle glucose uptake," *Physiological Reviews*, vol. 93, no. 3, pp. 993–1017, 2013.
- [49] M. Casas, S. Buvinic, and E. Jaimovich, "ATP signaling in skeletal muscle," *Exercise and Sport Sciences Reviews*, vol. 42, no. 3, pp. 110–116, 2014.
- [50] U. Özcan, E. Yilmaz, L. Ozcan et al., "Chemical chaperones reduce ER stress and restore glucose homeostasis in a mouse model of type 2 diabetes," *Science*, vol. 313, no. 5790, pp. 1137–1140, 2006.
- [51] B. Braun, M. B. Zimmermann, and N. Kretschmer, "Effects of exercise intensity on insulin sensitivity in women with non-insulin-dependent diabetes mellitus," *Journal of Applied Physiology*, vol. 78, no. 1, pp. 300–306, 1995.
- [52] M. R. Siddiqui, K. Moorthy, A. Taha, M. E. Hussain, and N. Z. Baquer, "Low doses of vanadate and *Trigonella* synergistically regulate Na⁺/K⁺-ATPase activity and GLUT4 translocation in alloxan-diabetic rats," *Molecular and Cellular Biochemistry*, vol. 285, no. 1-2, pp. 17–27, 2006.
- [53] D. C. Wright, P. C. Geiger, J. O. Holloszy, and D.-H. Han, "Contraction- and hypoxia-stimulated glucose transport is mediated by a Ca²⁺-dependent mechanism in slow-twitch rat soleus muscle," *American Journal of Physiology-Endocrinology and Metabolism*, vol. 288, no. 6, pp. E1062–E1066, 2005.
- [54] D. C. Wright, K. A. Hucker, J. O. Holloszy, and D. H. Han, "Ca²⁺ and AMPK both mediate stimulation of glucose transport by muscle contractions," *Diabetes*, vol. 53, no. 2, pp. 330–335, 2004.
- [55] S. Ebashi, M. Endo, and I. Ohtsuki, "Control of muscle contraction," *Quarterly Reviews of Biophysics*, vol. 2, no. 4, pp. 351–384, 1969.
- [56] M. Hatakenaka and I. Ohtsuki, "Effect of removal and reconstitution of troponins C and I on the Ca²⁺-activated tension development of single glycerinated rabbit skeletal muscle fibers," *European Journal of Biochemistry*, vol. 205, no. 3, pp. 985–993, 1992.

Research Article

Chlorogenic Acid Alleviates Colon Mucosal Damage Induced by a High-Fat Diet via Gut Microflora Adjustment to Increase Short-Chain Fatty Acid Accumulation in Rats

M. Gui Xie ¹, Y. Quan Fei ¹, Y. Wang ^{1,2}, W. Yan Wang ¹, and Z. Wang ¹

¹College of Bioscience and Biotechnology, Hunan Agricultural University, Changsha, Hunan 410128, China

²College of Agriculture and Biotechnology, Hunan University of Humanities, Science and Technology, Loudi 417000, China

Correspondence should be addressed to Z. Wang; wz8918@163.com

Received 23 July 2020; Revised 16 October 2020; Accepted 18 January 2021; Published 10 February 2021

Academic Editor: Daniele Vergara

Copyright © 2021 M. Gui Xie et al. This is an open access article distributed under the Creative Commons Attribution License, which permits unrestricted use, distribution, and reproduction in any medium, provided the original work is properly cited.

A high-fat diet (HFD) has been previously associated with the development of diseases such as chronic colitis. While chlorogenic acid (CGA) is known to exhibit potent antioxidant, antibacterial, and anti-inflammatory properties, little is known about its effects on intestinal inflammation. In this study, we investigated the effects of CGA on intestinal inflammation in an HFD-induced obesity rat model and assessed whether these effects were related to changes in gut microbiota composition. This was achieved by examining physiological and biochemical indicators, the liver transcriptome, and the structure of the fecal microflora. CGA treatment significantly reduced HFD-induced internal organ weight gain, promoted colon tissue repair, downregulated the expression of inflammatory cytokines, and promoted the accumulation of the tight junction protein. KEGG enrichment analysis of differentially expressed genes, applied to data from the RNA-seq of rat liver tissue, revealed that CGA treatment significantly affected amino acid and lipid metabolism in the liver. Furthermore, CGA decreased the abundance of bacteria belonging to the genera *Blautia*, *Sutterella*, and *Akkermansia* and increased butyric acid levels, which were positively correlated with the abundance of *Ruminococcus* (butyric acid producer). Moreover, the beneficial changes observed in the HFD group were not as pronounced as those in the CGA treatment group. In summary, CGA can alleviate colitis in HFD-induced obesity through its anti-inflammatory effects associated with changes in gut microbiota composition and an increase in the production of short-chain fatty acids and thus can be used as a potential drug for the treatment of this pathology.

1. Introduction

Obesity has become a global epidemic, increasing in prevalence in both developed and developing countries. Moreover, the current trend shows that obesity develops at an earlier age in humans [1]. Approximately 937 million obese and 396 million overweight adults were reported globally in 2005, and these numbers are predicted to increase to 1.35 billion and 573 million, respectively, by 2030 [2]. A long-term high-fat diet (HFD) can lead to obesity [1], metabolic disorders, and an increased risk of developing a series of chronic diseases, such as type II diabetes or cardiovascular disease [3]. Structural and functional changes in the intestinal microbiota occur as a result of HFD intake, leading to an increase in the accumulation of inflammation-promoting metabolites,

which in turn contribute to an increased risk of developing colorectal cancer [4].

Several studies have shown that food polyphenols influence the community structure and morphology of the intestinal microflora [5, 6]. For example, resveratrol regulates intestinal microflora composition as well as lipogenesis by suppressing lipoprotein lipase expression and the expression of genes involved in fatty acid biosynthesis [5]. Tea polyphenols improve dysbiotic intestinal flora by upregulating antioxidant enzyme activity and tight junction protein levels in the ileum [7].

Chlorogenic acid (CGA) is a well-known phenolic acid derived from caffeic acid and quinic acid [8] and is widely found in plants, fruits, and vegetables [9]. It has antibacterial, antiviral, antitumor, and antioxidant properties. Furthermore,

it has been reported to lower blood pressure and blood lipid levels, increase white blood cell counts, protect the liver and gallbladder, and scavenge free radicals [10, 11]. Our previous studies have shown that CGA supplementation in HFD-fed rats can decrease body weight and improve lipid metabolism disorders and obesity-related hormone levels. Furthermore, CGA supplementation reduces macrophage infiltration and suppresses inflammatory signaling [12]. Additionally, CGA can attenuate colon barrier damage by decreasing myosin light chain kinase expression and promoting the dynamic distribution of tight junction proteins in a colitis rat model [13]. CGA supplementation also ameliorates 2.5% dextran sulfate sodium-induced colitis by suppressing signaling pathways involved in the inflammatory response and apoptosis [14]. Long-term CGA supplementation increases gut microbiota diversity, thereby potentially improving overall metabolism. Furthermore, chronic dietary CGA attenuates diet-induced inflammation as well as cardiovascular, liver, and metabolic changes [15].

The HFD-induced obesity rat model has been widely used to study insulin resistance, blood glucose homeostasis, dyslipidemia, and genetic fatty liver disease [16–19]. However, few studies have investigated the effects of CGA on intestinal inflammation induced by HFD. Therefore, we aimed to investigate the ability of CGA to slow down or inhibit intestinal inflammation in rats after 7 weeks of HFD feeding. For this purpose, rats were divided into three groups (HFD, HFD+SPR (high-fat recovery group), and HFD+CGA). Furthermore, we compared the effects of natural recovery and CGA treatment on HFD-induced colon inflammation by analyzing physiological and biochemical indices, the liver transcriptome, and the intestinal flora of rats. Finally, we aimed to explain the underlying mechanisms of action of CGA.

2. Materials and Methods

2.1. Animal Experiments. All animal experiments were in accordance with the Guide for the Care and Use of Laboratory Animals of Hunan Agricultural University and performed in compliance with the Guide for the Protection and Use of Laboratory Animals of Hunan Agricultural University. The protocol was approved by the Animal Protection and Utilization Committee of Hunan Agricultural University. Forty male Sprague-Dawley (SD) rats (Hunan Silaike Jingda Co., Changsha, China; certificate number, HNASLKJ2016-0002) were reared in the animal room of the Institute of Subtropical Agricultural Research, Chinese Academy of Sciences, with two rats housed in each cage. All rats were provided free access to food and water throughout the experiment. The room was maintained at $22 \pm 1^\circ\text{C}$ and approximately 60% humidity. After one week of adaptive feeding under a 12-hour light/dark cycle, the rats were randomly divided into the following two groups: normal control group (NC; $n = 10$) and high-fat diet group (HFD; $n = 30$). After 7 weeks, the rat obesity model was established (the average body weight of rats in the HFD group was $>20\%$ higher than the average body weight of the NC group [20]). The body weight of rats in the NC group was unaltered. Next, the HFD group was equally divided into the following three

subgroups: the HFD group ($n = 10$, fed a high-fat diet, with distilled water administered by gavage), the high-fat recovery group (HFD+SPR; $n = 10$, switched to normal feed, with distilled water administered by gavage), and the CGA group (HFD+CGA; $n = 10$, fed a high-fat diet, with 100 mg/kg CGA (CAS: 327-97-9) administered by gavage). The NC group was fed a diet of 3.6 kcal/g, containing 72.3% carbohydrates, 19.7% protein, and 10% fat. The HFD group received a diet of 4.6 kcal/g, containing 46.4% carbohydrates, 19.6% protein, and 34.6% fat. Chow was ordered from Botai Hongda Biotechnology Co. (Beijing, China). Figure 1 provides a schematic diagram of the treatment schedule. Gastric perfusion was performed after 8 weeks of experimentation. In the later stage of treatment, rat feces were collected after fasting for 12 h before administering the gavage. The collected fecal samples were placed in a sterile enzyme-free Eppendorf tube and stored at -80°C . Blood samples were collected from the heart, incubated at room temperature for 30 min, and centrifuged at 3,500 rpm at 4°C for 15 min. The isolated serum was stored at -80°C . At the end of the experimental period, the rats were sacrificed using pentobarbital sodium. Then, the rats were dissected, and tissues and organs of interest were removed, weighed, washed with normal saline, and preserved in liquid nitrogen. Parts of the colon and liver tissues were removed and fixed in 10% formalin for subsequent histopathological analysis.

2.2. Histomorphological Examination. The colon and liver tissues from each group ($n = 6$) were fixed in 10% formalin. Tissue samples were slowly flushed with water, dehydrated in different concentrations of ethanol at $37\text{--}45^\circ\text{C}$ for 2–4 h, and embedded in wax (SVA, Uppsala, Sweden). Tissue was cut and sectioned into $5\ \mu\text{m}$ sample slices, dewaxed, stained, and sealed. Cross-sections of colon and liver tissues were photographed under a 10x and 40x objective lens using a biomicroscope (ML31; MSHOT, Guangzhou, China), and gross pathological changes in the tissue were observed and recorded.

2.3. Enzyme-Linked Immunosorbent Assays. For the four groups, plasma levels of tumor necrosis factor- α (TNF- α), monocyte chemoattractant protein-1 (MCP-1), interleukin 6 (IL-6), and lipopolysaccharide (LPS) were measured using commercially available kits (CSB-E14247r/E04640r/E04595r/E11987r/E07429r; CUSABIO, Wuhan, China) and a microplate reader (BioTek, Winooski, VT, USA).

2.4. Quantitative PCR Analysis. Total RNA was extracted from colon tissues using TriQuick Reagent (Solarbio, Beijing, China), and the obtained precipitate was washed and dissolved. RNA quality was assessed using an ultra-micro UV-visible spectrophotometer (NanoDrop 2000; Thermo Fisher Scientific, Waltham, MA, USA). RNA was reverse-transcribed into cDNA, and quantitative PCR was performed. For all samples, the RNA concentration was adjusted to $1,000\ \text{ng}/\mu\text{L}$. Reverse-transcription was performed using a FastKing RT Kit with gDNase (TaKaRa, Kusatsu, Japan) to remove genomic DNA, in accordance with the manufacturer's instructions. A SuperReal PreMixPlus SYBR Green kit (TIANGEN, Beijing, China) was used for quantitative

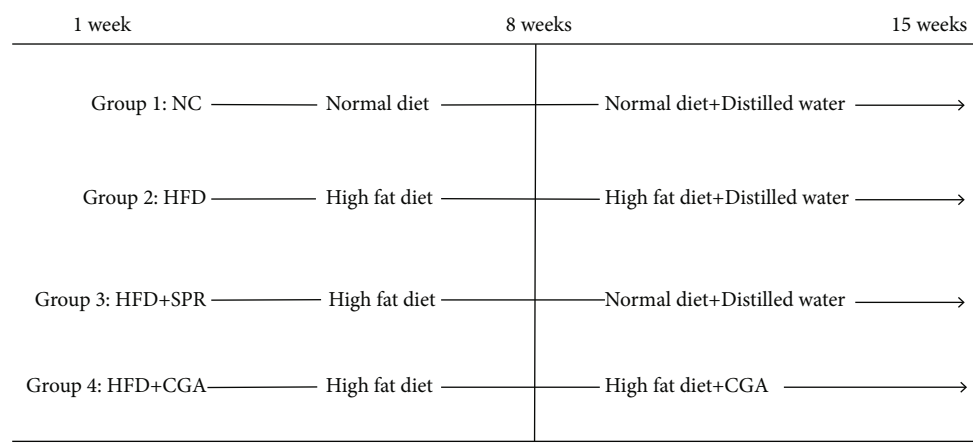


FIGURE 1: Time chart of the experimental treatment plan.

RT-PCR. Ct values were generated for *TNF- α* , *MCP-1*, *IL-6*, and β -*actin* from rat colon tissue using an ABI 7300 Real-Time PCR Instrument (Applied Biosystems, Foster City, CA, USA). Relative expression was determined using the $2^{-\Delta\Delta C_t}$ method.

2.5. Determination of Protein Expression Levels by Western Blotting. After thoroughly grinding the protein samples with a liquid, RIPA buffer solution was added (a piece of protease inhibitor was added per 10 mL of RIPA buffer solution), followed by lysis on ice for approximately 30 min. The lysed sample was centrifuged at 12,000 rpm at 4°C for 5 min, and the supernatant was collected into a new EP tube. The protein concentration was determined using a BCA protein concentration determination kit (Beyotime Biotechnology, Shanghai, China). The concentration of all samples was adjusted to 1000 ng/ μ L, and samples were transferred into new EP tubes. Next, the samples were denatured in a water bath at 99°C for 10 min, immediately cooled to 4°C in ice (liquid water vapor was removed from the tube wall), shaken and mixed thoroughly, and finally aliquoted and stored at -80°C until western blotting. Based on the molecular weight of the selected antibody, the concentration of the resolving (lower) gel was 12% and that of the stacking (upper) gel was 5%. Electrophoresis was performed at 80 V for approximately 20 min, with the sample separating in the separation gel. The voltage was increased to 120 V, and electrophoresis was continued for approximately 1 h. The proteins were transferred from the gel onto blotting membranes at 180 mA for 75 min and blocked with skimmed milk powder for 2 h. The membrane was washed once with TBST (Beyotime Biotechnology, Shanghai, China), and the corresponding primary antibody (Proteintech, Chicago, USA) was applied overnight (the dilution ratio of TNF- α (17590-1-AP), IL-10 (60269-1-Ig), Ocln (13409-1-AP), IL-6 (66146-1-Ig), and β -actin (66009-1-Ig) was 1:1000). Then, the primary antibody was washed off, and the secondary antibody was applied for 2 h (the dilution ratio of Goat anti-rabbit IgG (H+L) (SA00002-2) and Goat anti-rat IgG (H+L) (SA00002-9) was 1:5000). Before chemiluminescent detection, the membrane was washed and the color was developed with a luminous chromogenic solution.

Results were analyzed using ImageJ (NIH, Bethesda, MD, USA), converting the destination strip image to grayscale image, compared the intensity of destination strips with β -actin strip as the control.

2.6. Liver Transcriptome Analysis by RNA-seq. Total RNA was extracted from the liver tissue using TriQuick Reagent (Solarbio, Beijing, China). RNA quality was then assessed using the ultra-micro UV-visible spectrophotometer Agilent 2100 Bioanalyzer (Agilent RNA 6000 Nano Kit), and RNA integrity was determined by gel electrophoresis. Next, quality control analysis of raw reads was performed to determine whether the sequenced data were suitable for the follow-up analysis (<https://github.com/BGI-flexlab/SOAPnuke>). Hierarchical Indexing for Spliced Alignment of Transcripts was used to align reads with the reference genome in directional mode (<http://www.ccb.jhu.edu/software/hisat>). Clean reads were mapped to the reference genome using Bowtie 2 (<http://bowtie-bio.sourceforge.net/Bowtie2/index.shtml>), and then, gene expression levels were calculated with RSEM (<http://deweylab.biostat.wisc.edu/RSEM>). We detected DEGs with DESeq2, which is based on the negative binomial distribution (<https://bioconductor.org/packages/release/bioc/html/DESeq2.html>). Based on KEGG annotation results, we classified DEGs according to the official classification and performed KEGG pathway functional enrichment using phyper, a function of R.

2.7. Determination of Short-Chain Fatty Acid Levels in Feces by GC-MS. In brief, rat feces were added to 1 mL of ddH₂O, mixed thoroughly on a vortex mixer, and shaken on an oscillator for 30 min. Then, the samples were incubated overnight at 4°C, after centrifugation at 15,000 rpm for 20 min, and the supernatant was transferred to a new EP tube. The supernatant was mixed with 25% metaphosphoric acid at a volume ratio of 9:1 and then reacted at room temperature for 4 h. The samples were centrifuged at 12,000 rpm for 15 min, and the resulting supernatant was filtered through a 0.45 μ m disposable water membrane and added to an N10149 automatic liquid sampler (Agilent, Santa Clara, CA, USA) for evaluation by gas chromatography-mass spectrometry (GC-MS)

to create a standard curve for analyzing various known short-chain fatty acids (SCFAs). Each stock solution of different SCFAs (Sigma, St. Louis, MO, United States) was prepared, and gradient of 10 μL , 20 μL , 50 μL , 100 μL , 300 μL , and 500 μL of stock solutions were, respectively, mixed with 100 μL of 25% metaphosphoric acid, then diluted to 1000 μL with ddH₂O. The stock solution and diluted solution were stored at 4°C away from light. Chromatographic analysis was determined using DB-FFAP column of 30 m (length) \times 0.25 μm (inner diameter) \times 0.25 μm (film thickness) with a flame ionization detector (FID), and high purity nitrogen (99.999%) was used as the carrier gas at a flow rate of 0.8 mL/min, and high purity hydrogen (99.999%) was used as the auxiliary gas. The initial temperature was 60°C, and the temperature increased to 220°C at a rate of 20°C/min and maintained for 1 min.

2.8. Determination of Intestinal Microorganisms. DNA was extracted from rat feces using a DNA Stool Mini Kit (Qiagen, Hilden, Germany). DNA sample integrity was assessed by 1% agarose gel electrophoresis, with a NanoDrop 2000 spectrophotometer used to determine DNA concentration and purity. The V3 and V4 hypervariable regions of 16S rRNA were selected for DNA amplification. The NEB Next Ultra DNA Library Prep Kit for Illumina (New England Biolabs, Ipswich, MA, USA) was used to construct the library, and libraries were sequenced on a MiSeq instrument (Illumina, San Diego, CA, USA) after passing Qubit quantification and the library test specifications. Raw sequencing data were spliced and filtered to obtain clean reads. Paired-end sequencing fragments were spliced using Adobe Flash Professional, with a threshold of 97% similarity. Operational taxonomic unit (OTU) clustering and species analysis were performed. The diversity of the sequence data was analyzed using QIIME software, and sample richness and evenness information were obtained. Additionally, the samples were analyzed by weighted principal coordinate analysis (PCoA) and clustered based on UniFrac distance. The community structure among different samples and groups was analyzed. All offline data were analyzed by the Beijing Genomics Institute.

2.9. Statistical Analysis. Statistical analysis was performed using SPSS 25.0 software (IBM, Armonk, NY, USA), and single-factor analysis of variance was used to analyze data from the same group and different groups. Data are expressed as mean \pm SEM. Data from multiple groups were analyzed by analysis of variance. The results were analyzed and plotted using Prism 7 (GraphPad, San Diego, CA, USA).

3. Results and Discussion

3.1. Effects of High-Fat Diet on Body Weight and Body Fat Content of SD Rats. In terms of the initial body weight, no significant difference was observed between groups (the average initial weight was 338.45 \pm 14.8 g). After 2 weeks of feeding the HFD, body weights were significantly different between the NC and HFD groups ($P < 0.05$). As shown in Figure 2(a), after 8 weeks of HFD feeding, the average body weight of rats in the HFD group was more than 20% higher

than the average body weight of the NC group, indicating that the obesity model was successfully established. The weight change in rats receiving CGA treatment is shown in Figure 2(b). No significant difference was observed between the four treatment groups; however, compared with the HFD group, the weight of rats in the HFD+SPR and HFD+CGA groups increased at a slower rate. The effects of CGA on BMI and Lee index values are presented in Figures 2(c) and 2(d). CGA treatment significantly reduced the BMI ($P < 0.05$) and Lee index ($P < 0.05$) values of HFD rats. Furthermore, the HFD+SPR group presented significantly reduced BMI values ($P < 0.05$) and Lee index values, to a certain extent. The various physical indicators of SD rats in each group are shown in Table 1. Compared with the NC group, the weight of all important organs, except the testicular tissue in the HFD group, increased significantly; compared with the HFD group, the weight of all important organs, except testicular tissue, decreased significantly after CGA treatment. The increased weight of all internal organs demonstrated that the obesity model was successful. Aspartate aminotransferase (AST) and alanine aminotransferase (ALT) values assess the extent of liver damage, whereas immunoglobulin G (IgG) and IgM determine the presence of inflammation as their expression is elevated during inflammatory conditions. Typically, low-density lipoprotein cholesterol (LDL-C) and high-density lipoprotein cholesterol (HDL-C) are used to assess high-fat obesity models and, hence, were accordingly selected to model obesity. Additionally, cholesterol values are assessed to examine cholesterol metabolism in rats. Compared with the NC group, the plasma levels of LDL-C, HDL-C, IgG, IgM, AST, and ALT decreased significantly in the HFD group. Moreover, the declining LDL-C/HDL-C ratio, often considered to attenuate the risk of metabolic disorders associated with obesity [21], indicated that the HFD disrupted the blood lipid metabolism in rats to a certain extent; however, following CGA treatment, the above indices were significantly improved. These results showed that CGA can alleviate obesity caused by the HFD, demonstrating efficacy consistent with the effects of dietary correction (HFD+SPR).

3.2. Histopathological Analysis Showed That Chlorogenic Acid Reduces Colonic and Liver Tissue Inflammation Caused by a High-Fat Diet. Figure 3 presents the hematoxylin and eosin (HE) staining of rat colon and liver tissue sections of each group. In the NC group (Figure 3(a)), the colon epithelium was intact and the crypt structure appeared normal. In the HFD group (Figure 3(b)), the colon epithelial mucosa was slightly swollen, with damaged and irregular crypts. In the HFD+SPR group (Figure 3(c)), the colon crypts presented a relatively compact structure, without significant damage, which was significantly improved when compared with the HFD group. In contrast, in the HFD+CGA group (Figure 3(d)), the colon epithelial mucosa was slightly ulcerated, the colon epithelial tissue was damaged, the crypt structure was normal, and no inflammation-associated infiltrations were observed. Figures 3(e)–3(h) present the HE-stained micrographs of rat liver tissues. A normal phenotype was observed in the liver tissues of normal rats (Figure 3(e)).

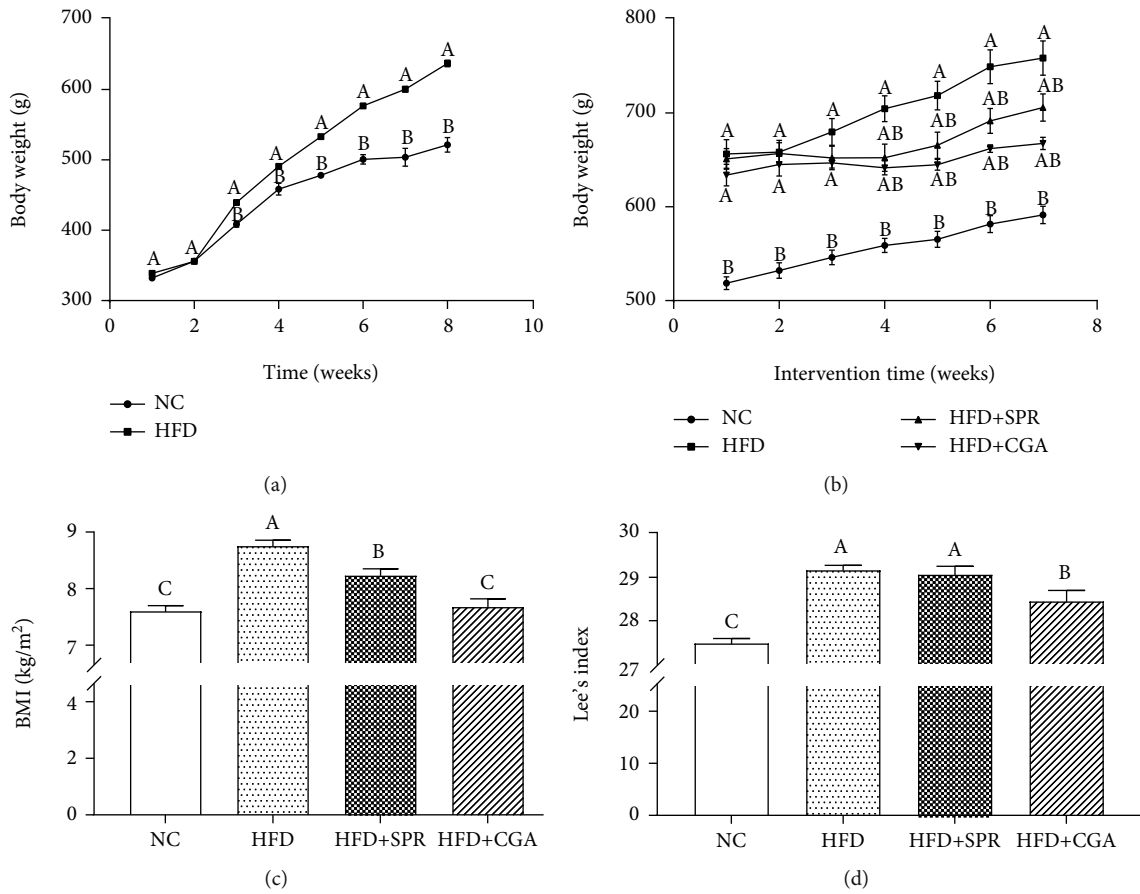


FIGURE 2: Effect of chlorogenic acid on body index values: (a) weight changes during the establishment of the model; (b) weight changes during chlorogenic acid (CGA) treatment; (c) BMI; (d) Lee's index. NC: natural control group; HFD: high-fat diet group; HFD+SPR: high-fat recovery group; HFD+CGA: CGA treatment group. All data are expressed as mean \pm SEM. The values in the same row with different letters are significantly different ($*P < 0.05$), and the values of each group with the same letters are not significantly different ($P > 0.05$).

TABLE 1: Physical indicators of rats fed the experimental diet.

Parameter	NC	HFD	HFD+SPR	HFD+CGA
Liver (g)	14.93 \pm 1.59 ^c	26.80 \pm 2.47 ^a	18.76 \pm 2.93 ^b	17.83 \pm 2.14 ^b
Kidney (g)	3.37 \pm 0.39 ^b	4.04 \pm 0.22 ^a	3.96 \pm 0.42 ^a	3.29 \pm 0.49 ^b
Thymus (g)	0.08 \pm 0.04 ^b	0.15 \pm 0.04 ^a	0.10 \pm 0.03 ^b	0.12 \pm 0.05 ^{ab}
Spleen (g)	0.77 \pm 0.14 ^b	0.99 \pm 0.14 ^a	0.97 \pm 0.17 ^a	0.83 \pm 0.09 ^{ab}
Heart (g)	1.49 \pm 0.08 ^c	1.69 \pm 0.13 ^a	1.61 \pm 0.14 ^{ab}	1.52 \pm 0.11 ^{bc}
Lung (g)	2.19 \pm 0.10 ^c	3.05 \pm 0.45 ^a	2.74 \pm 0.41 ^b	2.31 \pm 0.29 ^b
Testicular (g)	4.30 \pm 0.26 ^a	3.85 \pm 0.23 ^b	4.37 \pm 0.25 ^a	4.26 \pm 0.52 ^a
Perirenal fat (g)	9.57 \pm 2.33 ^c	25.68 \pm 5.32 ^a	14.19 \pm 2.27 ^b	16.92 \pm 3.14 ^b
Testicular fat (g)	8.61 \pm 2.53 ^d	21.60 \pm 3.2 ^a	17.29 \pm 2.36 ^b	12.73 \pm 4.38 ^c
IgG (g/L)	1.65 \pm 0.24 ^a	1.26 \pm 0.24 ^b	1.51 \pm 0.29 ^{ab}	1.74 \pm 0.26 ^a
IgM (g/L)	0.12 \pm 0.04 ^a	0.07 \pm 0.02 ^b	0.10 \pm 0.02 ^a	0.11 \pm 0.02 ^a
ALT (U/L)	60.00 \pm 8.72 ^a	99.67 \pm 20 ^b	56.70 \pm 7.13 ^a	48.99 \pm 14.48 ^a
AST (U/L)	97.92 \pm 14.28 ^a	193.50 \pm 48.17 ^b	119.76 \pm 33.87 ^a	84.50 \pm 10.24 ^a
LDL-C (mmol/L)	1.39 \pm 0.27 ^a	1.08 \pm 0.11 ^b	1.37 \pm 0.26 ^a	1.11 \pm 0.17 ^b
HDL-C (mmol/L)	1.38 \pm 0.28 ^a	0.83 \pm 0.10 ^b	1.29 \pm 0.26 ^a	1.21 \pm 0.15 ^a
LDL-C/HDL-C	1.01 \pm 0.10 ^b	1.31 \pm 0.29 ^a	1.07 \pm 0.17 ^b	0.96 \pm 0.15 ^b

All data are expressed as the mean \pm SD. The values in the same row with different letters are significantly different ($*P < 0.05$), and the values of each group with the same letters are not significantly different ($P > 0.05$).

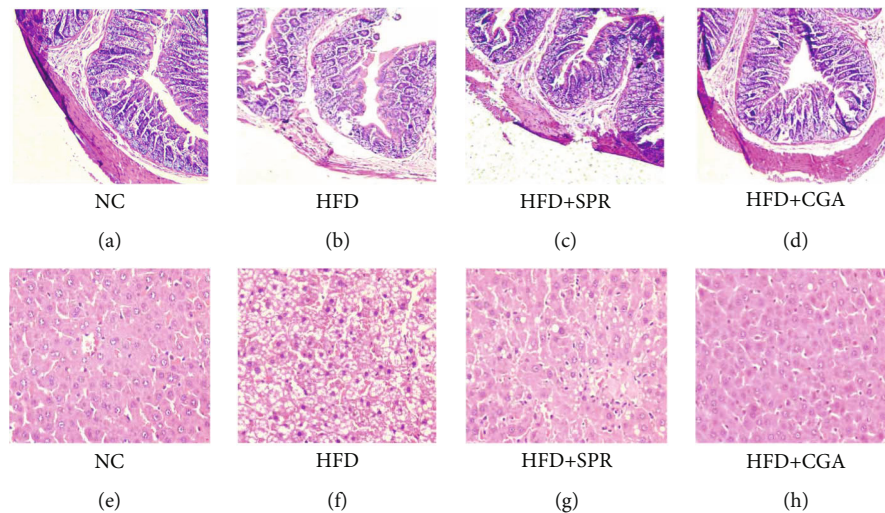


FIGURE 3: Hematoxylin-eosin staining of rat colonic and liver tissue from each group. Hematoxylin-eosin staining of colonic and liver tissue of rats from the natural control (NC, (a, e)), high-fat diet (HFD, (b, f)), high-fat recovery (HFD+SPR, (c, g)), and chlorogenic acid treatment (HFD+CGA, (d, h)) groups. Stained colonic and liver tissue sections were photographed using a Mingmei ML31 biomicroscope under 10x and 40x objective lens.

However, liver tissue sections from HFD-fed rats (Figure 3(f)) showed enlarged hepatocytes, disorganized vacuolar degeneration, and deposits of fatty granules. The HFD-specific vacuolar phenotypes were significantly alleviated in the HFD+SPR group (Figure 3(g)), while the hepatocyte size was normal in the HFD+CGA group (Figure 3(h)). Therefore, CGA treatment can significantly reduce HFD-induced colon inflammation in SD rats.

3.3. Effect of Chlorogenic Acid on Serum LPS Levels and the Expression of Related Inflammatory Cytokines. Serum inflammatory cytokine levels for each animal group are shown in Figure 4. Compared with the NC group, the levels of the proinflammatory factors, $TNF-\alpha$, MCP-1, IL-6, and LPS, increased by 69.63%, 94.99%, 59.39%, and 207.33%, respectively, in the HFD group. The levels of $TNF-\alpha$, MCP-1, IL-6, and LPS in the HFD+SPR and HFD+CGA groups were significantly lower than those observed in the HFD group ($P < 0.05$); in the HFD+SPR group, the levels of these factors decreased by 12.37%, 225.95%, 53.52%, and 302.93%, respectively, and in the HFD+CGA group, the levels were decreased by 135.23%, 308.16%, 66.78%, and 265.34%, respectively. These results revealed that CGA can relieve inflammation caused by an HFD, and its effect was superior to that demonstrated by dietary correction.

3.4. Effect of Chlorogenic Acid on Cytokine Gene Expression in Colonic Tissue. The relative mRNA expression levels of related genes in rat colonic tissues for each group are shown in Figure 5. The relative mRNA expression levels of $TNF-\alpha$ and MCP-1 were significantly higher in the HFD group than in the NC group, with lower expression levels observed in the HFD+CGA group than in the HFD+SPR group. Compared with the NC group, the relative mRNA expression levels of $TNF-\alpha$ increased by 52.64% in the HFD group, and the relative mRNA expression levels of MCP-1 increased by 488.48%. Compared with the HFD group, the relative mRNA

expression levels of $TNF-\alpha$, MCP-1, and IL-6 decreased by 2365.92%, 673.30%, and 73.58%, respectively, in the HFD+CGA group, which significantly differed from expression levels in the HFD group. In summary, CGA treatment inhibited colonic tissue inflammation in rats fed an HFD.

3.5. Effect of Chlorogenic Acid on Cytokine Protein Expression in Colonic Tissue. The expression levels of relevant proteins in rat colonic tissues from each group are shown in Figure 6. No significant differences in $TNF-\alpha$ protein expression levels were observed among the NC, HFD+SPR, and HFD+CGA groups; however, $TNF-\alpha$ protein expression levels were significantly lower in the HFD+CGA and HFD+SPR groups than in the HFD group. The protein expression of IL-6 was significantly higher in the HFD group than in the NC group and the HFD+CGA group ($P < 0.05$). CGA may have inhibited the expression of IL-6 protein and alleviated colonic inflammation to a certain extent. Compared with the NC group, the expression of Occludin, an intestinal epithelial tight junction protein, was significantly higher in the HFD+SPR and HFD+CGA groups ($P < 0.05$). IL-10 expression levels were higher in the HFD+CGA group than in the NC group; however, inflammation induced by hyperlipidemia was not significantly alleviated following CGA treatment.

3.6. KEGG Pathway Analysis of Differentially Expressed Genes in Liver Tissue. Based on the classification and enrichment analysis of KEGG biological pathways, the classification of biological pathways of differential genes between the HFD and HFD+CGA groups was enriched (Figure 7). The pathways were divided into six categories including human diseases, metabolism, organismal systems, cellular processes, and environmental and genetic information processing. A total of 422 differentially expressed genes were involved in 208 pathways between the HFD group and the HFD+CGA group, of which 41 pathways were significantly enriched, including 11 significant signaling pathways related to amino

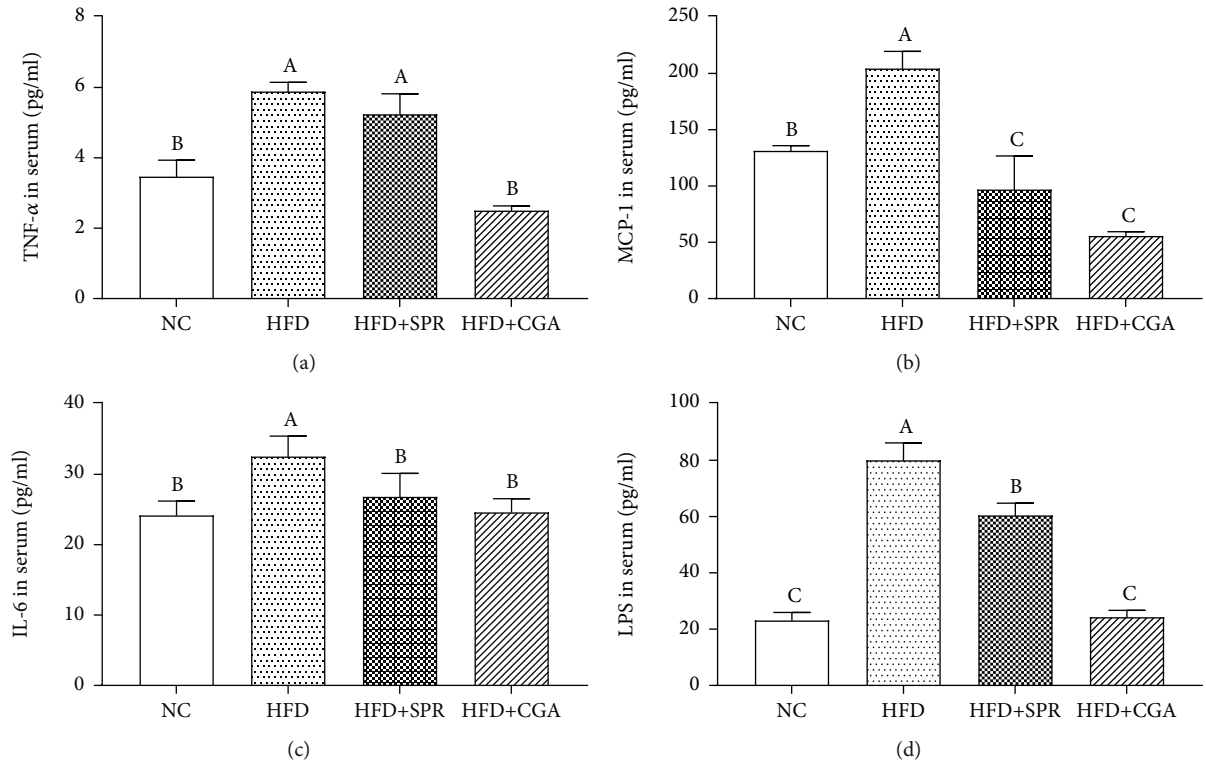


FIGURE 4: Effects of chlorogenic acid on the expression of inflammatory cytokines and LPS. Serum levels of TNF- α (a), MCP-1 (b), IL-6 (c), and LPS (d). NC: natural control group; HFD: high-fat diet group; HFD+SPR: high-fat recovery group; HFD+CGA: chlorogenic acid treatment group.

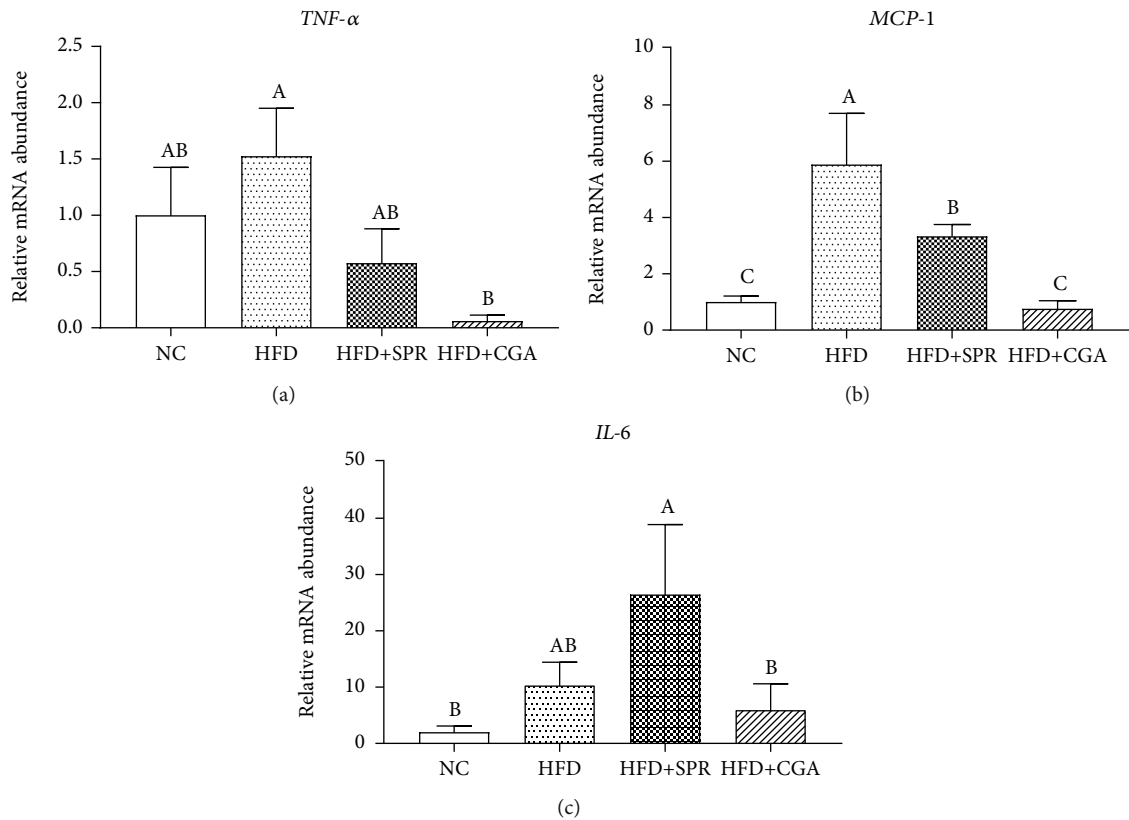


FIGURE 5: Expression levels of related genes in colonic tissue of rats in each group. Relative mRNA expression of TNF- α (a), MCP-1 (b), and IL-6 (c) in colonic tissue of rats.

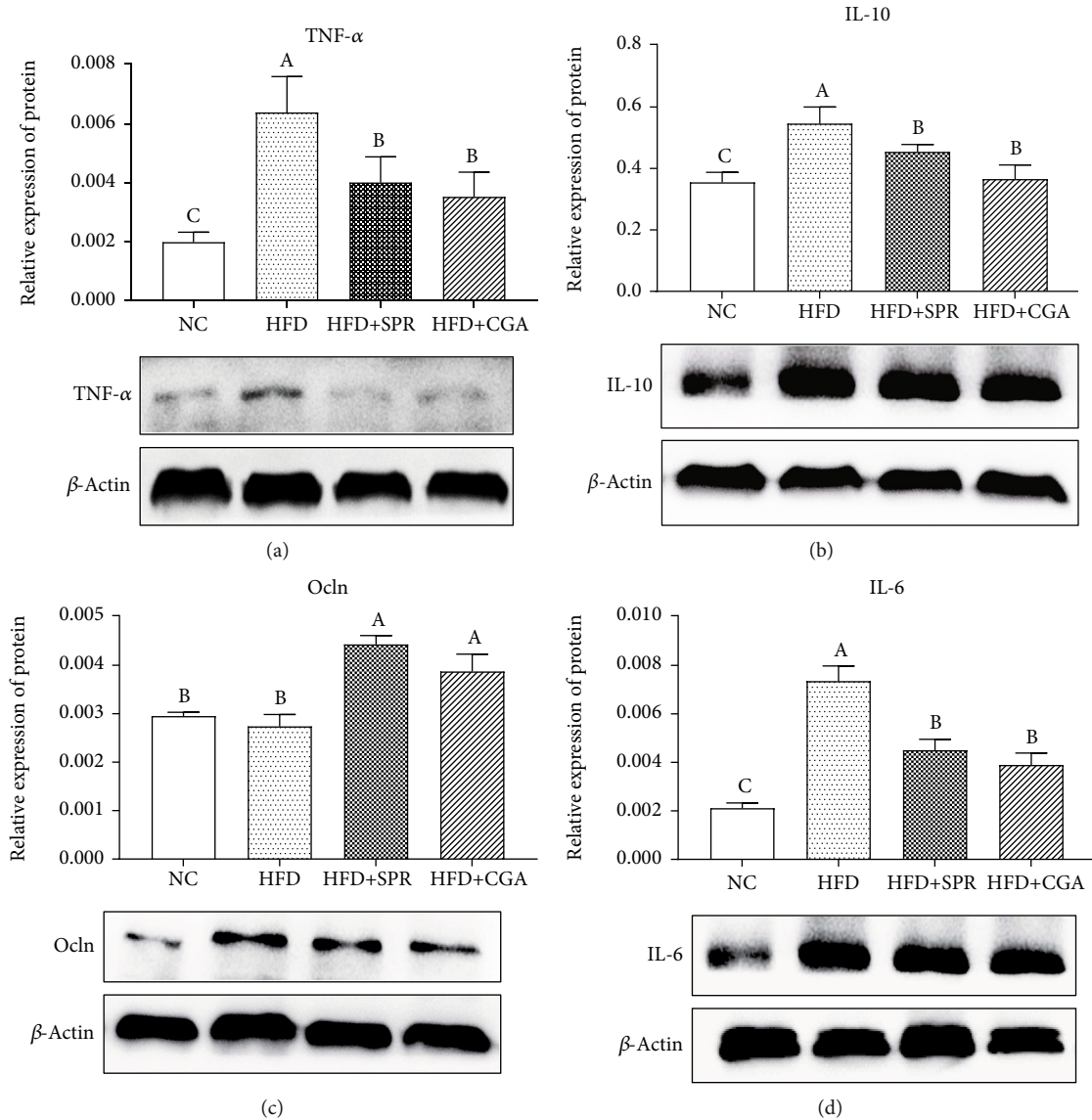


FIGURE 6: Protein expression levels in colonic tissue of rats in each group. Protein expression levels of TNF- α (a), IL-6 (b), Ocln (c), and IL-10 (d) in rat colonic tissue.

acid and lipid metabolism, listed top place (Table 2). Additionally, the bile acid excretion pathway was also included.

3.7. Effect of Chlorogenic Acid on Intestinal Microbial Diversity. The analysis of β -diversity and α -diversity of rat intestinal microbiota for each group is shown in Figure 8. A principal component analysis (PCA) diagram (Figure 8(a)) and a heat map of the genus-based β -diversity matrix (Figure 9(f)) are presented to highlight significant differences among the four groups; however, no significant differences were observed among the four groups, indicating that the experimental groups were homogeneous. Unique and overlapping OTUs, for a total of 1,618 OTUs, are represented in a Venn diagram (Figure 8(b)). Some OTUs were common among all four groups, while others were unique to a specific group. The NC, HFD, HFD+SPR, and HFD+CGA groups had 53, 95, 97, and 45 unique OTUs, respectively. As shown

in the box chart (Figures 8(c)–8(e)), compared with the NC group, the Sobs, Chao index, and ACE index values of the HFD group decreased significantly, by 41.66%, 35.29%, and 37.00%, respectively. These results revealed that long-term HFD can reduce the abundance and diversity of intestinal microorganisms. Conversely, in the HFD+CGA group, the Sobs, Chao index, and ACE index values significantly increased by 34.50%, 27.89%, and 31.08%, respectively, compared with the HFD group, indicating that after CGA treatment, the richness of intestinal microorganisms returned to a level similar to that observed in the NC group.

3.8. Effect of Chlorogenic Acid on Intestinal Microflora. The composition of the intestinal microflora of rats in each group was analyzed and is shown in Figure 9. At the phylum level (Figure 9(a)), *Bacteroidetes*, *Firmicutes*, *Spirochaetes*, *Proteobacteria*, *Cyanobacteria*, *Verrucomicrobia*, *Tenericutes*,

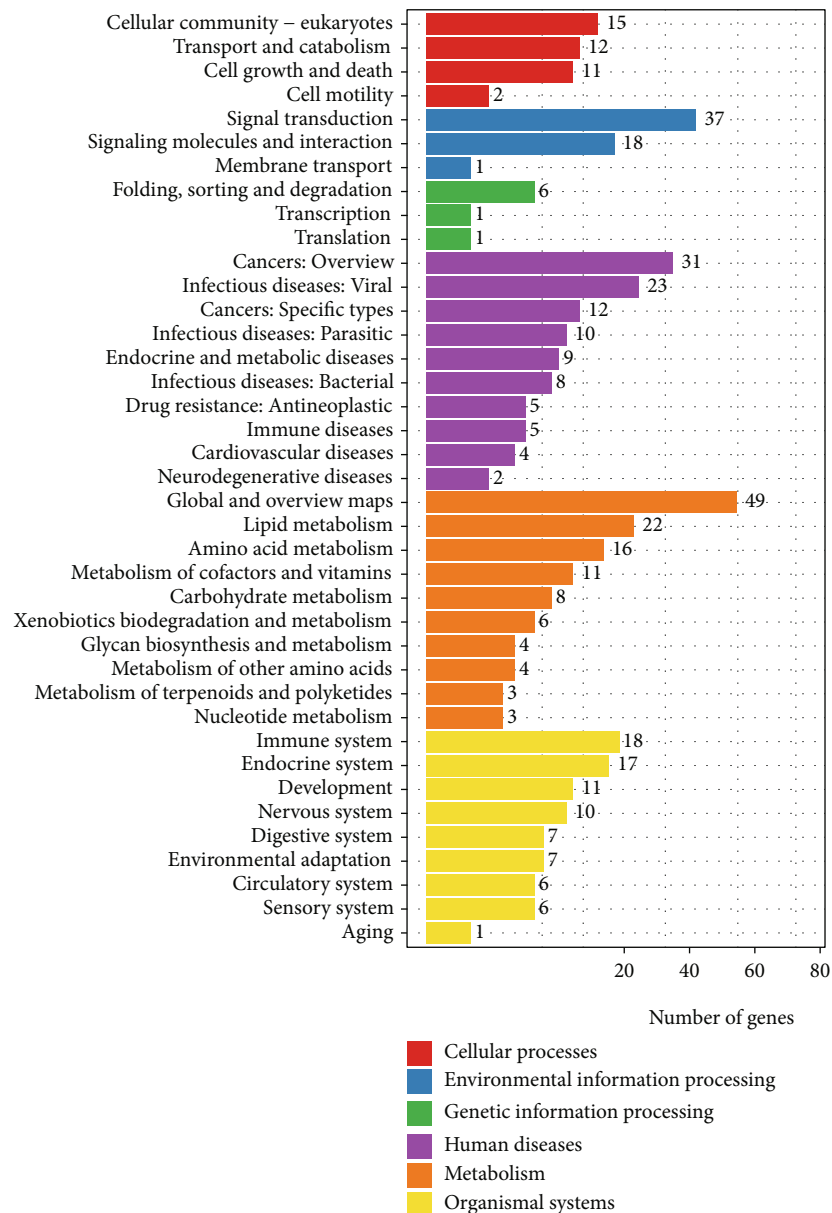


FIGURE 7: The classification of biological pathways of differential genes between the HFD and HFD+CGA groups.

Actinobacteria, and *Elusimicrobia* were the most abundant in all four groups. Compared with the NC group, the HFD group presented a lower relative abundance of *Tenericutes* and a higher relative abundance of *Proteobacteria*. After CGA treatment, the relative abundance of *Chlorophyta* significantly increased ($P < 0.05$). Simultaneously, the abundance of *Tenericutes* increased by 65.93% and the abundance of *Elusimicrobia* decreased by 80.52%. Based on the horizontal heat map of genus (Figure 9(e)), the relative abundance of bacteria in the HFD group significantly differed from that in the NC, HFD+SPR, and HFD+CGA groups, but the relative abundance in the NC, HFD+SPR, and HFD+CGA groups tended to be consistent. Compared with the NC group, the HFD group presented a significantly higher relative abundance of *Blautia*, *Sutterella*, and *Akker-*

mansia ($P < 0.05$), and a lower relative abundance of *Blautia* and *Sutterella* CGA treatment.

3.9. Effect of Chlorogenic Acid on Short-Chain Fatty Acid Levels in Feces. The analysis of SCFA levels in rat feces of each group is shown in Figure 10. Butyric acid and acetic acid levels were significantly lower in the HFD group than in the NC group ($P < 0.05$). Compared with the HFD group, a significant increase in butyric acid levels was observed in the CGA-treated group ($P < 0.05$). No significant difference was noted in propionic acid levels among the four groups; however, propionic acid levels were 22.57% lower in the HFD group than in the NC group. As HFD demonstrated the greatest effect on butyric acid levels, we analyzed the relative abundance of related intestinal microflora at the

TABLE 2: KEGG pathway enrichment of the differential expressed genes involved in amino acid and lipid metabolism between the HFD and HFD+CGA groups.

Serial	Pathway	DEGs	<i>P</i> value	<i>Q</i> value	Pathway ID
4	Glycine, serine, and threonine metabolism	6/42	0.00004	0.00228	ko00260
6	Steroid biosynthesis	4/26	0.00065	0.02269	ko00100
7	Cysteine and methionine metabolism	5/58	0.00205	0.06087	ko00270
8	Valine, leucine, and isoleucine biosynthesis	2/5	0.00234	0.06087	ko00290
9	Linoleic acid metabolism	4/41	0.00370	0.08540	ko00591
11	Glycerophospholipid metabolism	6/106	0.00626	0.11017	ko00564
12	Phenylalanine, tyrosine, and tryptophan biosynthesis	2/8	0.00636	0.11017	ko00400
18	Arachidonic acid metabolism	6/119	0.01079	0.12472	ko00590
25	Alanine, aspartate, and glutamate metabolism	3/41	0.02574	0.21416	ko00250
30	Arginine biosynthesis	2/23	0.04930	0.33080	ko00220
31	Phenylalanine metabolism	2/23	0.04930	0.33080	ko00360
37	Bile secretion	4/95	0.06103	0.34306	ko04976

KEGG pathway enrichment of the differential expressed genes involved in amino acid and lipid metabolism between the HFD and HFD+CGA groups. Notice: we just showed the *P* value is equal or smaller than 0.05 about the pathway of amino acid and lipid metabolism, and bile secretion.

genus level. Furthermore, we analyzed the correlation between the abundance of intestinal microorganisms at the genus level and butyric acid levels. As shown in Figures 10(b)–10(f), butyric acid levels negatively correlated with the abundance of *Allobaculum*, *Blautia*, *Coprobacillus*, and *Sutterella* and positively correlated with the abundance of *Ruminococcus*. Therefore, we speculate that, to a certain extent, changes in the abundance and diversity of intestinal flora resulted in changes in the SCFA content.

4. Discussion

CGA supplementation has shown promising results for the regulation of lipid metabolism [22] and glucose homeostasis [23] via multiple mechanisms, including the promotion of lipid β -oxidation via PPAR- α [24], its antioxidant effects [25], and its capacity to improve insulin sensitivity in peripheral tissues [26]. In addition, CGA exhibits antibacterial and anti-inflammatory properties [27]. Our results indicate that a long-term HFD significantly increases body weight and induces colon inflammation in rats, compared to the NC group. Additionally, HFD-fed rats exhibited fat deposition in the liver and lipid metabolism disorders. CGA intervention improved the negative effects of HFD in rats, which is in line with the results of previous studies [12, 28, 29].

Accumulating evidence suggests that HFD has a strong effect on the gut microbiota, converting healthy gut microbiota into a dysbiotic disease-associated entity [30]. Numerous studies have shown that HFD-induced obesity leads to the development of chronic diseases, damaged intestinal mucosa, and chronic intestinal inflammation by compromising the intestinal flora of animals [30–32]. A previous study reported that approximately 30% of CGA can be absorbed into the bloodstream through the stomach and small intestine, while the remaining 70% reaches the large intestine. CGA is metabolized in the liver, and its metabolites might interact with the gut microbiota [33]. Thus, we propose two mechanisms through which CGA may exert its effects on the microbiota.

One mechanism is represented by the direct entry of CGA into the large intestine, which may change the microbial structure and reduce the abundance of certain pathogenic bacterial species. For instance, the relative abundance of *Blautia* and *Sutterella* was significantly reduced ($P < 0.05$) in the intestine of CGA-treated mice compared to controls. However, our experiment found that the relative abundance of *Akkermansia* in the HFD group was significantly higher than that in the control group, which was inconsistent with the results of previous studies [34, 35]. *Akkermansia* species have been identified as mucin-degrading bacteria that reside in the mucus layer [36]. Furthermore, *Akkermansia* can help maintain the health of the digestive tract and reduce the risk of obesity, diabetes, and inflammation [37]. Interestingly, several studies have reported that resveratrol administration alters the composition and function of the gut microbiome of obese mice, and these have been characterized by a decreased abundance of *Akkermansia* [38]. Moreover, omeprazole-induced dysbiosis of the intestinal flora promotes the growth of *Akkermansia* and inhibits bifidobacterial growth, thus leading to thinning of the mucus layer through a reduced number of goblet cells in the small intestine [39]. Therefore, *Akkermansia* species may play diverse roles in the regulation of intestinal functioning, and exploring their relationship with other microorganisms in the gut environment might elucidate these roles. Additionally, we noted that, at the genus level, the abundance of *Staphylococcus* and *Escherichia* in the HFD group was higher than that in the other three groups, thereby indicating that CGA administration and the cessation of HFD could reduce the abundance of these two genera. This is consistent with previous *in vitro* CGA antibacterial test results [27, 40]. These observations describe a possible mechanism by which CGA administration may alleviate colon inflammation.

There is a second mechanism that might explain the effects of CGA. KEGG enrichment analysis revealed 11 significantly enriched signaling pathways related to amino acid and lipid metabolism in the liver, suggesting that CGA is

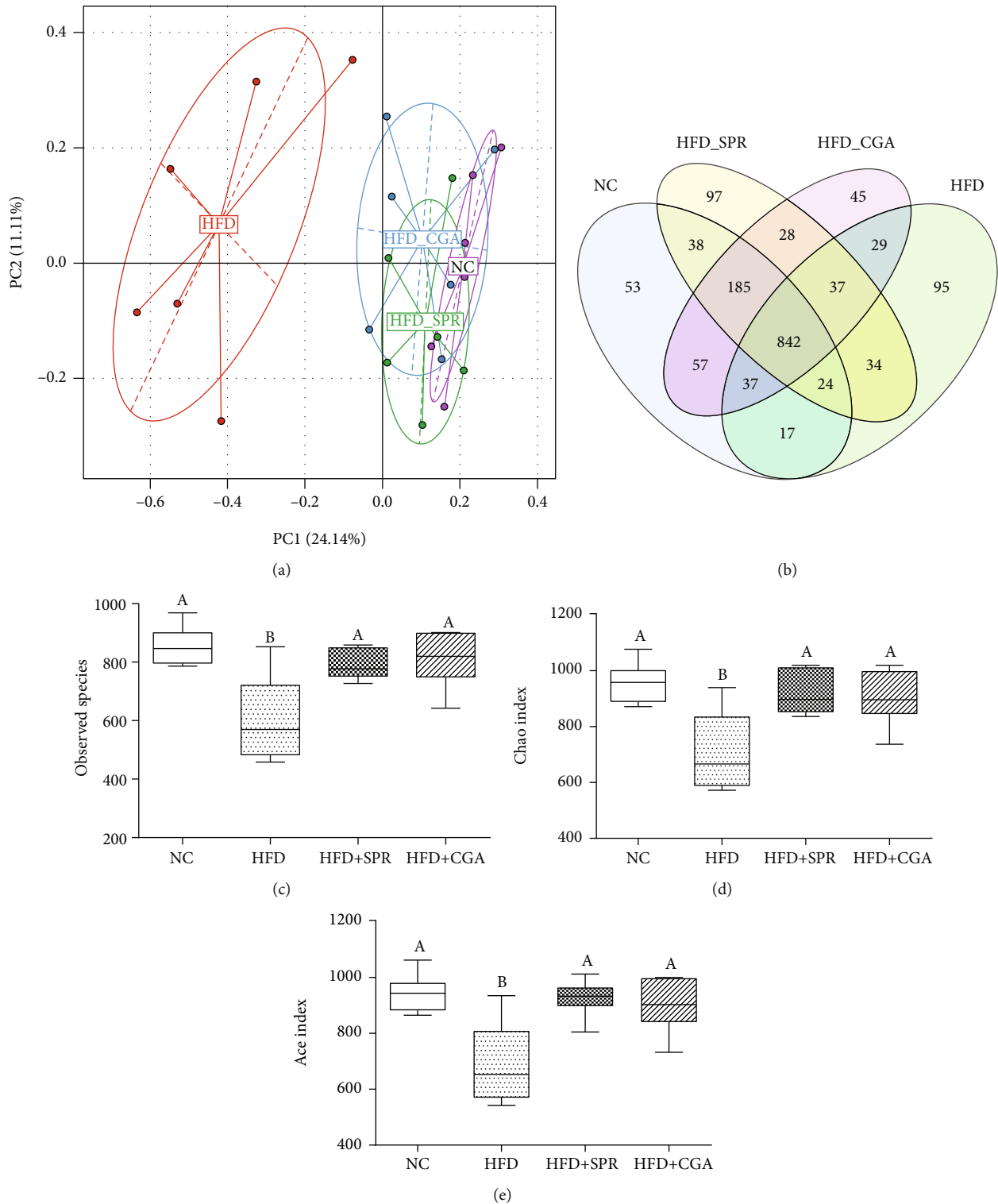


FIGURE 8: Analysis of β -diversity and α -diversity of the intestinal microflora of rats in each group. Principal component analysis (PCA) diagram (a); OTU Venn diagram (b) of rats in each group; box diagrams of Sobs (c), Chao (d), and ACE (e) of rats in each group.

absorbed in the stomach and small intestine and ultimately enters the liver through the bloodstream. In particular, CGA administration may significantly affect amino acid metabolism in the liver of HFD-fed obese rats, although this has not been suggested in previous studies. In our study, CGA administration downregulated the expression of phosphoserine

aminotransferase (EC2.6.1.52) and D-3-phosphoglycerate dehydrogenase, which indicates lower serine biosynthesis. Conversely, the expression of L-serine/L-threonine ammonia lyase (EC:4.3.1.17,4.3.1.19) was upregulated (Fig. S1). Therefore, the synthesis of branched-chain amino acids (BCAAs) includes leucine (Leu), isoleucine (Ile), and valine (Val).

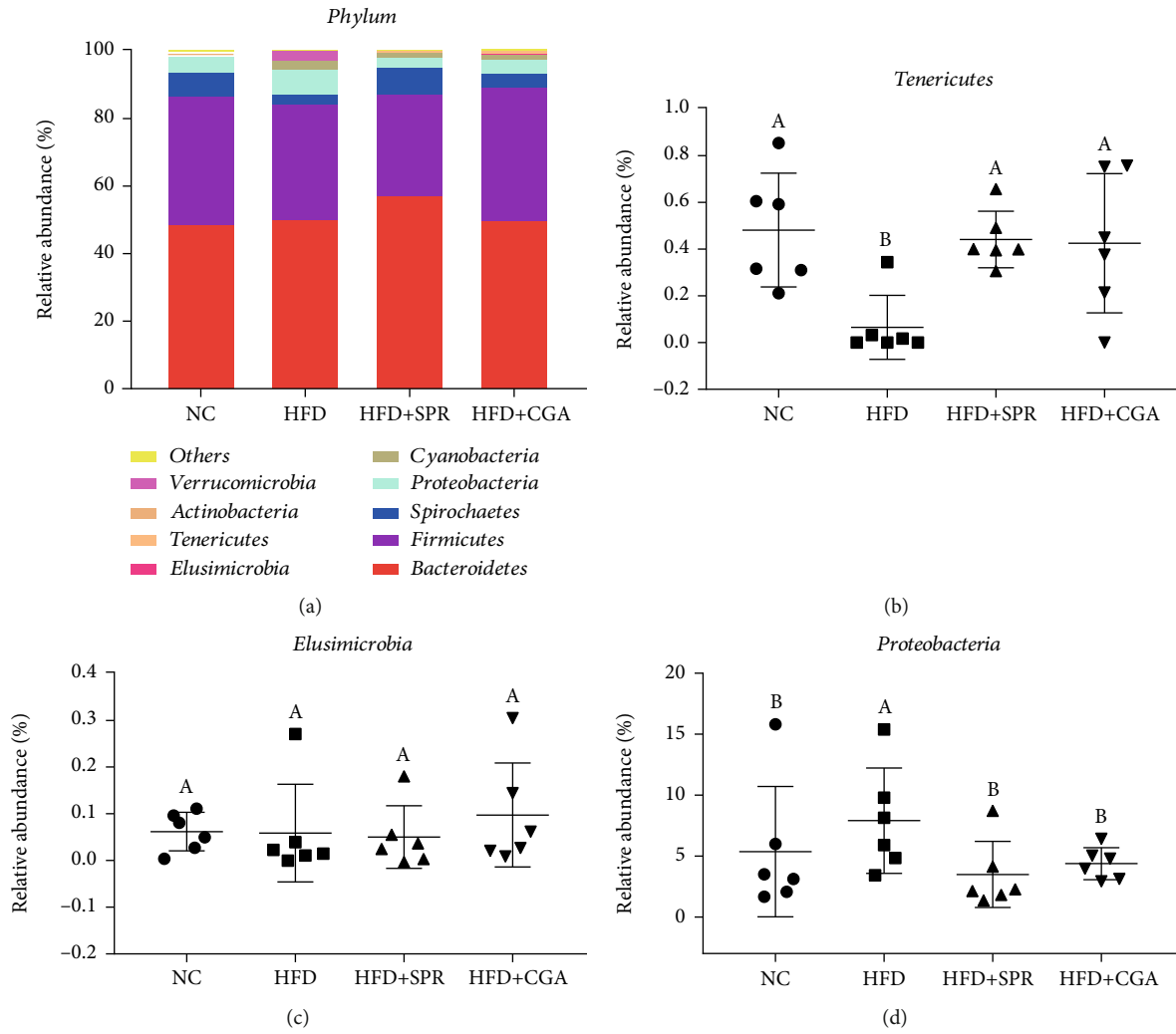
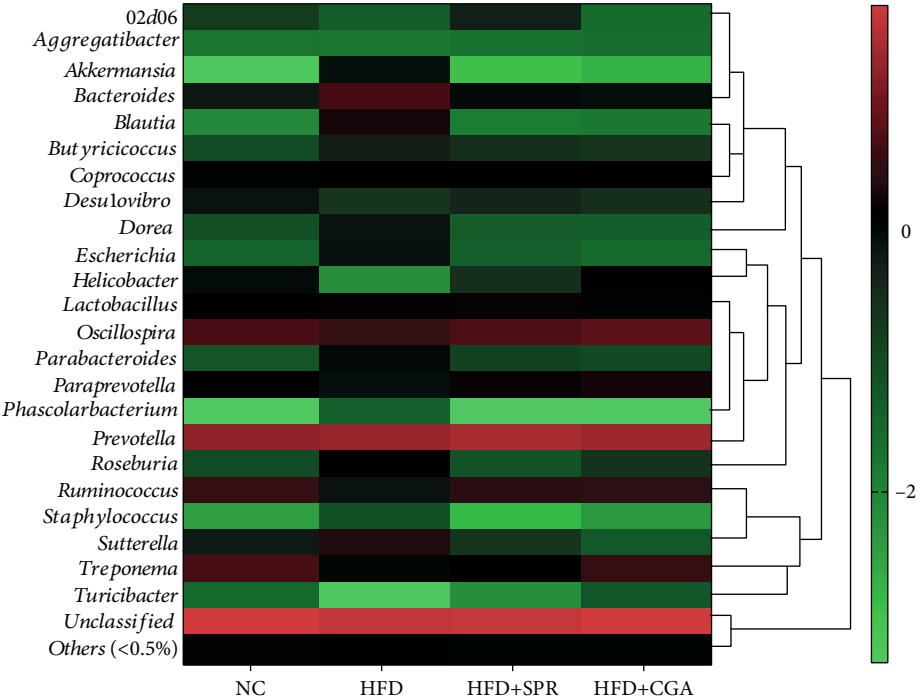
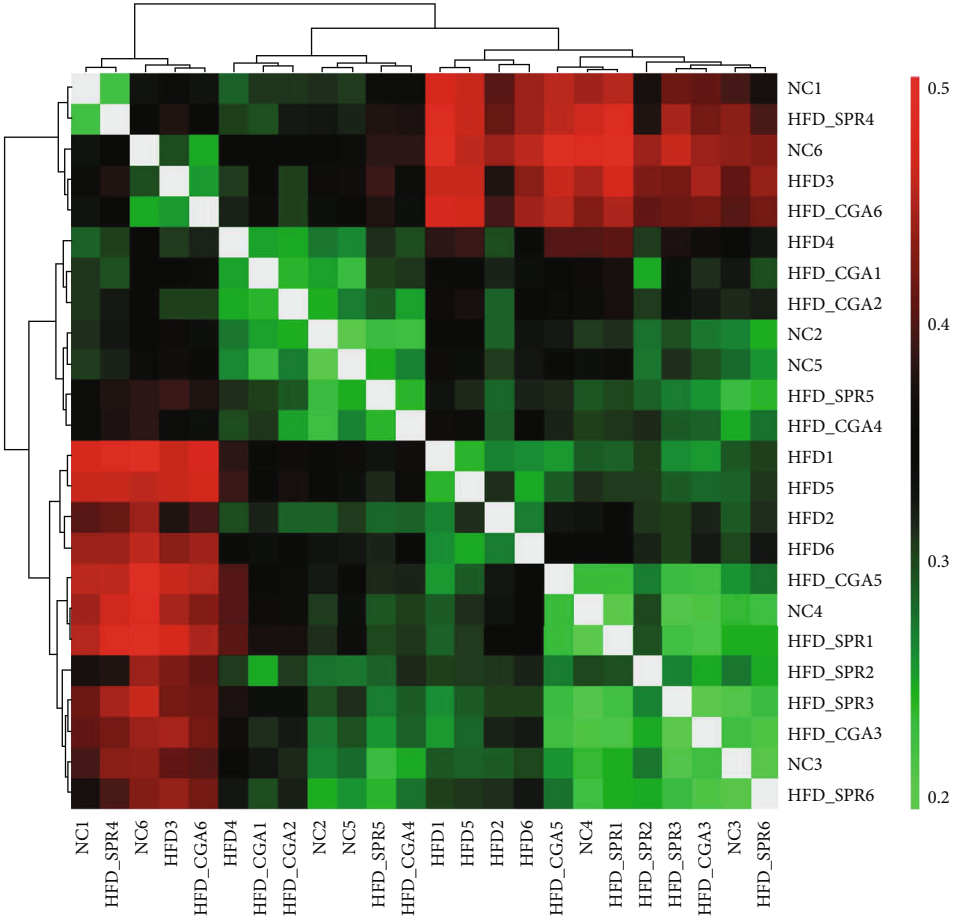


FIGURE 9: Continued.



(e)



(f)

FIGURE 9: Continued.

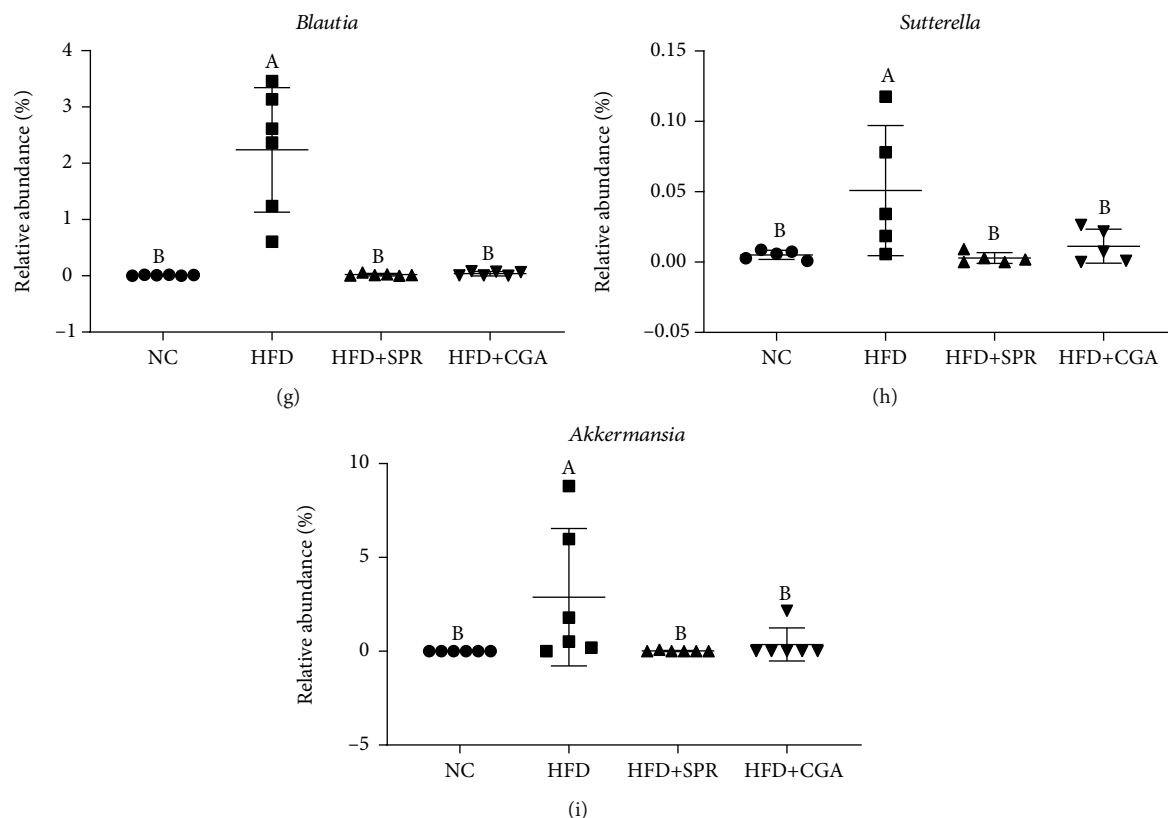


FIGURE 9: Analysis of intestinal microbial composition of rats in each group ($n = 6$). Changes in the flora composition at the level of phylum (a), changes in the horizontal heat map of genus (e), and changes in the β -diversity matrix heat map of genus (f). Changes in the abundance of *Tenericutes* (b), *Elusimicrobia* (c), *Proteobacteria* (d), *Blautia* (g), *Sutterella* (h), and *Akkermansia* (i) in each group.

Furthermore, the synthesis of glutamic acid (Glu), arginine (Arg), tyrosine (Tyr), and phenylalanine (Phe) was also affected (Fig. S2), indicating that CGA might be involved in modulating the synthesis of these BCAAs. BCAAs also act as nitrogen donors for amino acids (AAs) such as Ala, Glu, and Gln. Through signaling pathways, especially the PI3K-AKT-mTOR pathway, BCAAs are involved in the regulation of energy balance, nutrient metabolism, gut health, and immunity and thus play a key role in the etiology of diseases, such as insulin resistance or type 2 diabetes mellitus [41, 42]. In fact, metabolic imbalances in BCAAs can lead to various health problems, including diabetes and cancer [42]. Furthermore, BCAAs act as regulators, promoting intestinal development, nutrient transport, and immune-related functions, resulting in improved gut health [43–45]. Thus, a dynamic balance of BCAAs is essential for physiological and immunological health. Further, we speculate that CGA might affect bile acid excretion by modulating AA and lipid metabolism. CGA affects the composition and species abundance of the intestinal microbiota through the liver-intestine axis and alleviates HFD-induced colon mucosal injuries. Indeed, the microbial abundance of the HFD+CGA and HFD+SPR groups was similar to that of the NC group, but higher than that of the HFD group. This might be explained by the similar lipid metabolism between the HFD+CGA and HFD+SPR groups. Moreover, bile acid metabolism was also similar between the two treatment groups.

In this study, a long-term HFD led to an increase in the abundance of gram-negative *Escherichia* bacteria, which was decreased by CGA treatment. Thus, CGA treatment might be the reason for the significant decrease in serum LPS levels in the HFD+CGA group. LPS is a component of the outer wall of gram-negative bacteria, which increases intestinal tight junction permeability. Furthermore, it triggers TLR4 signal transduction, which activates the NF- κ B (p50/p65) pathway [46], resulting in the upregulation of inflammatory cytokines. The serum and colon levels of inflammatory cytokines observed in this study support this hypothesis. Nevertheless, our results showed that the expression level of certain proteins in the colon is not fully consistent with the expression level of the related genes in terms of mRNA accumulation. However, since mRNA molecules and proteins are the products of gene expression at different levels, this discrepancy is not surprising. In fact, efficient translation of an mRNA molecule to a protein requires editing, posttranslational processing, etc. Therefore, possibly owing to the different efficiency of transcription and translation, we did not detect perfectly corresponding mRNA and protein levels, although we measured similar trends [47]. However, we found that ELISA and western blotting yielded almost identical protein levels. At the mRNA level, the expression of the proinflammatory factor-coding genes *MCP-1* and *IL-6* in the HFD+CGA group was significantly lower than that in the HFD+SPR group. Moreover, the body

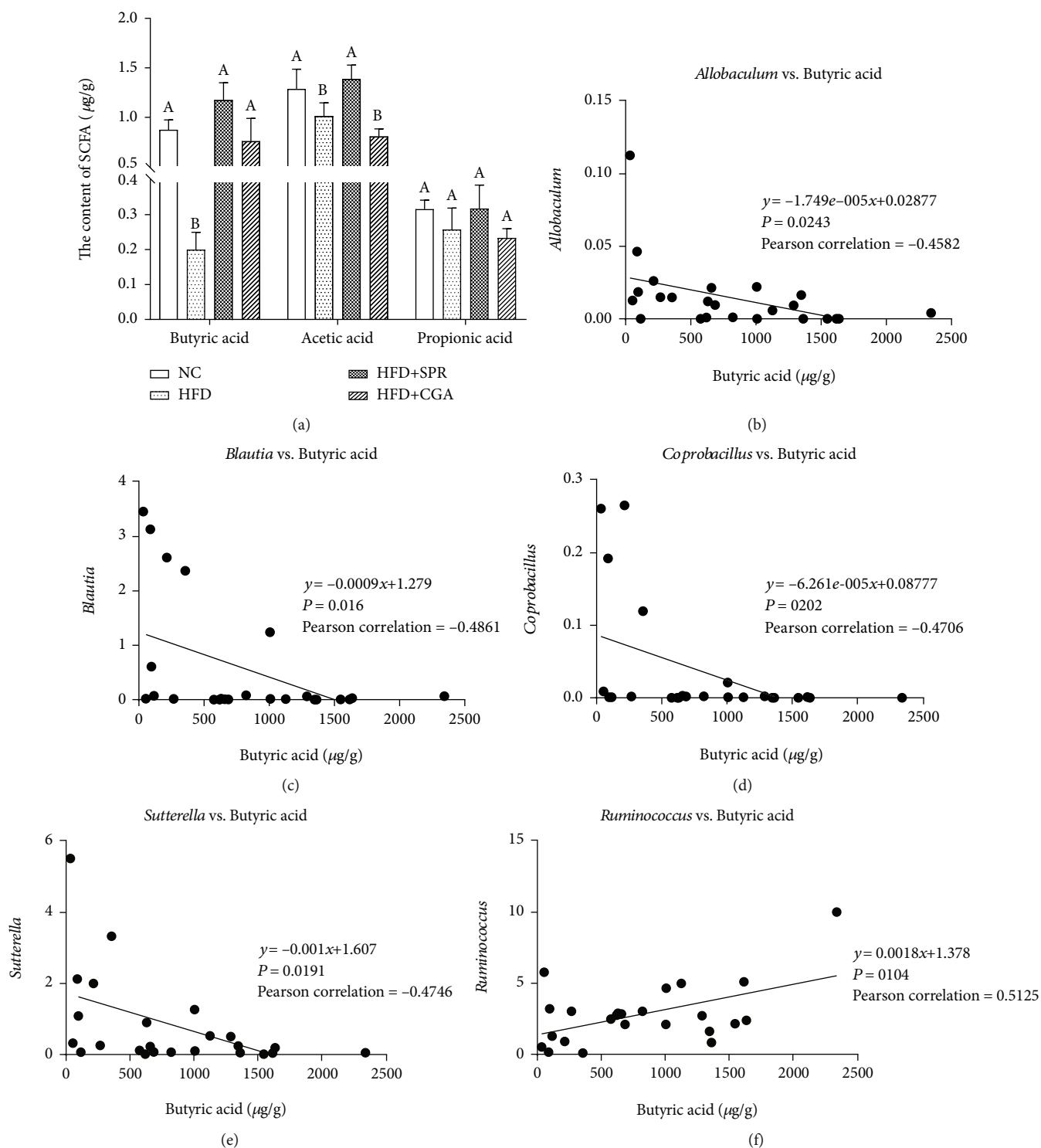


FIGURE 10: Analysis of short-chain fatty acids in the fecal of each group. (a) Butyric acid, acetic acid, and propionic acid levels in feces ($\mu\text{g/g}$); correlation between butyric acid levels and the abundance of *Allobaculum* (b), *Blautia* (c), *Coprobacillus* (d), *Sutterella* (e), and *Ruminococcus* (f).

weight, BMI, and Lee's index of the HFD+CGA group were significantly lower than those of the HFD+SPR group. We conclude that the partial effect of CGA administration to the HFD+CGA group led to a better outcome than that of the HFD+SPR group.

Recently, a large number of studies have shown that short-chain fatty acids (SCFAs) are effective in protecting rodents and humans from inflammation-related damage [47] and reduce the occurrence of intestinal inflammation by regulating host intestinal immunity [48]. Butyric acid,

one of the fundamental SCFAs, can regulate the expression of various genes and is used as an energy source, either directly or indirectly. As an important signal transduction molecule, butyric acid can regulate gene expression by inhibiting histone deacetylases or activating G protein-coupled receptors 41 and 43 to alter the metabolic activity [49]. There are various bacterial species that produce butyric acid, including representatives of *Actinomycetes*, *Bacteroides*, *Clostridium*, *Proteus*, *Spirochetes*, and *Thermophiles* [50]. Our results reveal that the diversity of intestinal microorganisms changed after CGA treatment. The abundance of SCFA-producing bacteria increased, resulting in increased SCFA production. Compared to the NC group, the microbial diversity of the HFD+CGA group decreased, while the percentage of butyric acid-producing strains, such as *Ruminococcus*, increased significantly and showed a positive correlation with butyric acid levels. These results are in agreement with the studies discussed above.

5. Conclusions

To summarize, our study reveals that CGA alleviates obesity-induced colon mucosal damage. We hypothesized that chlorogenic acid changes the composition of the intestinal microbiota by regulating amino acid and lipid metabolism in SD rats or by directly acting on the microflora, thereby reducing serum LPS levels and enhancing the production of short-chain fatty acids to inhibit the development of colitis. The results provide a meaningful reference for how to adjust food composition to promote gut health.

Data Availability

The datasets for this research can be found in NCBI SRA, <https://www.ncbi.nlm.nih.gov/Traces/study/?acc=PRJNA658840>.

Conflicts of Interest

The authors declare that there are no conflicts of interest regarding the publication of this paper.

Acknowledgments

The financial supports for this research from the Hunan Provincial Natural Science Foundation (2019JJ40134), the Scientific Research Fund of Hunan Provincial Education Department (18A098), and the Hunan Provincial Graduate Research and Innovation Project (CX2018B404) are gratefully acknowledged. The authors would like to express their thanks to the Institute of Subtropical Agriculture, Chinese Academy of Sciences in Changsha for providing experimental facilities. We would like to thank Editage (<http://www.editage.cn>) for English language editing.

Supplementary Materials

Supplementary Description: Figure S1: KEGG pathway enrichment of the differential expressed genes of biosynthesis of amino acids. Upregulated steps are marked with red lines and downregulated steps with green lines. Figure

S2: KEGG pathway enrichment of the differential expressed genes of glycine, serine, and threonine metabolism. (*Supplementary Materials*)

References

- [1] L. Qu, Q. Liu, Q. Zhang et al., "Kiwifruit seed oil prevents obesity by regulating inflammation, thermogenesis, and gut microbiota in high-fat diet-induced obese C57bl/6 mice," *Food and Chemical Toxicology*, vol. 125, pp. 85–94, 2019.
- [2] T. Kelly, W. Yang, C. S. Chen, K. Reynolds, and J. He, "Global burden of obesity in 2005 and projections to 2030," *International Journal of Obesity*, vol. 32, no. 9, pp. 1431–1437, 2008.
- [3] C. Hein and E. L. Batista Jr., "Obesity and cumulative inflammatory burden: a valuable risk assessment parameter in caring for dental patients," *The Journal of Evidence-Based Dental Practice*, vol. 14, pp. 17–26.e1, 2014.
- [4] J. Yang and J. Yu, "The association of diet, gut microbiota and colorectal cancer: what we eat may imply what we get," *Protein & Cell*, vol. 9, no. 5, pp. 474–487, 2018.
- [5] Y. Qiao, J. Sun, S. Xia, X. Tang, Y. Shi, and G. le, "Effects of resveratrol on gut microbiota and fat storage in a mouse model with high-fat-induced obesity," *Food & Function*, vol. 5, no. 6, pp. 1241–1249, 2014.
- [6] R. Rastmanesh, "High polyphenol, low probiotic diet for weight loss because of intestinal microbiota interaction," *Chemo-Biological Interactions*, vol. 189, no. 1-2, pp. 1–8, 2011.
- [7] L. Zhang, S. Gui, J. Wang et al., "Oral administration of green tea polyphenols (TP) improves ileal injury and intestinal flora disorder in mice with *Salmonella typhimurium* infection via resisting inflammation, enhancing antioxidant action and preserving tight junction," *Journal of Functional Foods*, vol. 64, article 103654, 2020.
- [8] M. Naveed, V. Hejazi, M. Abbas et al., "Chlorogenic acid (Cga): a pharmacological review and call for further research," *Biomedicine & Pharmacotherapy*, vol. 97, pp. 67–74, 2018.
- [9] I. Nallamuthu, A. Devi, and F. Khanum, "Chlorogenic acid loaded chitosan nanoparticles with sustained release property, retained antioxidant activity and enhanced bioavailability," *Asian Journal of Pharmaceutical Sciences*, vol. 10, no. 3, pp. 203–211, 2015.
- [10] D. S. Sinasac, J. D. Riordan, S. H. Spiezio, B. S. Yandell, C. M. Croniger, and J. H. Nadeau, "Genetic control of obesity, glucose homeostasis, dyslipidemia and fatty liver in a mouse model of diet-induced metabolic syndrome," *International Journal of Obesity*, vol. 40, no. 2, pp. 346–355, 2016.
- [11] L. G. Naso, M. Valcarcel, M. Roura-Ferrer et al., "Promising antioxidant and anticancer (human breast cancer) oxidovanadium(IV) complex of chlorogenic acid. Synthesis, characterization and spectroscopic examination on the transport mechanism with bovine serum albumin," *Journal of Inorganic Biochemistry*, vol. 135, pp. 86–99, 2014.
- [12] S. L. Liu, B. J. Peng, Y. L. Zhong, Y. L. Liu, Z. Song, and Z. Wang, "Effect of 5-caffeoylquinic acid on the NF- κ B signaling pathway, peroxisome proliferator-activated receptor gamma 2, and macrophage infiltration in high-fat diet-fed Sprague-Dawley rat adipose tissue," *Food & Function*, vol. 6, no. 8, pp. 2779–2786, 2015.
- [13] Z. Ruan, S. Mi, L. Zhou et al., "Chlorogenic acid enhances intestinal barrier by decreasing Mlck expression and promoting dynamic distribution of tight junction proteins in

- colitic rats,” *Journal of Functional Foods*, vol. 26, pp. 698–708, 2016.
- [14] I. Vukelić, D. Detel, L. B. Pučar, I. Potočnjak, S. Buljević, and R. Domitrović, “Chlorogenic acid ameliorates experimental colitis in mice by suppressing signaling pathways involved in inflammatory response and apoptosis,” *Food and Chemical Toxicology*, vol. 121, pp. 140–150, 2018.
- [15] N. S. Bhandarkar, L. Brown, and S. K. Panchal, “Chlorogenic acid attenuates high-carbohydrate, high-fat diet-induced cardiovascular, liver, and metabolic changes in rats,” *Nutrition Research*, vol. 62, pp. 78–88, 2019.
- [16] C. Marques, M. Meireles, S. Norberto et al., “High-fat diet-induced obesity rat model: a comparison between Wistar and Sprague-Dawley rat,” *Adipocytes*, vol. 5, no. 1, pp. 11–21, 2016.
- [17] M. Zhang, X. Y. Lv, J. Li, Z. G. Xu, and L. Chen, “The characterization of high-fat diet and multiple low-dose streptozotocin induced type 2 diabetes rat model,” *Experimental Diabetes Research*, vol. 2008, Article ID 704045, 9 pages, 2008.
- [18] M. R. Bomhof, D. C. Saha, D. T. Reid, H. A. Paul, and R. A. Reimer, “Combined effects of oligofructose and Bifidobacterium animalis gut microbiota and glycemia in obese rats,” *Obesity*, vol. 22, no. 3, pp. 763–771, 2014.
- [19] X. Q. Deng, L. L. Chen, and N. X. Li, “The expression of Sirt 1 in nonalcoholic fatty liver disease induced by high-fat diet in rats,” *Liver International*, vol. 27, no. 5, pp. 708–715, 2007.
- [20] P. Chandler, J. Viana, K. Oswald, P. Wauford, and M. Boggiano, “Feeding response to melanocortin agonist predicts preference for and obesity from a high-fat diet,” *Physiology & Behavior*, vol. 85, no. 2, pp. 221–230, 2005.
- [21] F. K. Welty, “How do elevated triglycerides and low Hdl-cholesterol affect inflammation and atherothrombosis?,” *Current Cardiology Reports*, vol. 15, no. 9, 2013.
- [22] S. Meng, J. Cao, Q. Feng, J. Peng, and Y. Hu, “Roles of chlorogenic acid on regulating glucose and lipids metabolism: a review,” *Evidence-Based Complementary and Alternative Medicine*, vol. 2013, Article ID 801457, 11 pages, 2013.
- [23] B. J. Peng, Q. Zhu, Y. L. Zhong, S. H. Xu, and Z. Wang, “Chlorogenic acid maintains glucose homeostasis through modulating the expression of Sglt-1, Glut-2, and Plg in different intestinal segments of Sprague-Dawley rats fed a high-fat diet,” *Biomedical and Environmental Sciences*, vol. 28, no. 12, pp. 894–903, 2015.
- [24] M. B. Sanchez, E. Miranda-Perez, J. C. G. Verjan, M. de Los Angeles Fortis Barrera, J. Perez-Ramos, and F. J. Alarcon-Aguilar, “Potential of the chlorogenic acid as multitarget agent: Insulin-secretagogue and PPAR α/γ dual agonist,” *Biomedicine & Pharmacotherapy*, vol. 94, pp. 169–175, 2017.
- [25] P. Akila and L. Vennila, “Chlorogenic acid a dietary polyphenol attenuates isoproterenol induced myocardial oxidative stress in rat myocardium: an in vivo study,” *Biomedicine & Pharmacotherapy*, vol. 84, pp. 208–214, 2016.
- [26] H. E. Ghadieh, Z. N. Smiley, M. W. Kopfman, M. G. Najjar, M. J. Hake, and S. M. Najjar, “Chlorogenic acid/chromium supplement rescues diet-induced insulin resistance and obesity in mice,” *Nutrition & Metabolism*, vol. 12, 2015.
- [27] Z. Lou, H. Wang, S. Zhu, C. Ma, and Z. Wang, “Antibacterial activity and mechanism of action of chlorogenic acid,” *Journal of Food Science*, vol. 76, no. 6, pp. M398–M403, 2011.
- [28] Z. Wang, K. L. Lam, J. Hu et al., “Chlorogenic acid alleviates obesity and modulates gut microbiota in high-fat-fed mice,” *Food Science & Nutrition*, vol. 7, no. 2, pp. 579–588, 2019.
- [29] Y. Xue, F. Huang, R. Tang et al., “Chlorogenic acid attenuates cadmium-induced intestinal injury in Sprague-Dawley rats,” *Food and Chemical Toxicology*, vol. 133, 2019.
- [30] H. N. Choi, M. J. Kang, S. J. Lee, and J. I. Kim, “Ameliorative effect of myricetin on insulin resistance in mice fed a high-fat, high-sucrose diet,” *Nutrition Research and Practice*, vol. 8, no. 5, pp. 544–549, 2014.
- [31] K. Brown, D. DeCoffe, E. Molcan, and D. L. Gibson, “Diet-induced dysbiosis of the intestinal microbiota and the effects on immunity and disease,” *Nutrients*, vol. 4, no. 8, pp. 1095–1119, 2012.
- [32] M. S. Riaz Rajoka, J. Shi, H. M. Mehwish et al., “Interaction between diet composition and gut microbiota and its impact on gastrointestinal tract health,” *Food Science and Human Wellness*, vol. 6, no. 3, pp. 121–130, 2017.
- [33] A. Stalmach, H. Steiling, G. Williamson, and A. Crozier, “Bio-availability of chlorogenic acids following acute ingestion of coffee by humans with an ileostomy,” *Archives of Biochemistry and Biophysics*, vol. 501, no. 1, pp. 98–105, 2010.
- [34] Q. Shang, G. Song, M. Zhang et al., “Dietary fucoidan improves metabolic syndrome in association with increased *Akkermansia* population in the gut microbiota of high-fat diet-fed mice,” *Journal of Functional Foods*, vol. 28, pp. 138–146, 2017.
- [35] L. Zhu, D. Zhang, H. Zhu et al., “Berberine treatment increases *Akkermansia* in the gut and improves high-fat diet-induced atherosclerosis in *ApoE*^{-/-} mice,” *Atherosclerosis*, vol. 268, pp. 117–126, 2018.
- [36] M. Derrien, E. E. Vaughan, C. M. Plugge, and W. M. de Vos, “*Akkermansia muciniphila* gen. nov., sp. nov., a human intestinal mucin-degrading bacterium,” *International Journal of Systematic and Evolutionary Microbiology*, vol. 54, no. 5, pp. 1469–1476, 2004.
- [37] A. Everard, C. Belzer, L. Geurts et al., “Cross-talk between *Akkermansia muciniphila* and intestinal epithelium controls diet-induced obesity,” *Proceedings of the National Academy of Sciences of the United States of America*, vol. 110, no. 22, pp. 9066–9071, 2013.
- [38] M. M. Sung, T. T. Kim, E. Denou et al., “Improved glucose homeostasis in obese mice treated with resveratrol is associated with alterations in the gut microbiome,” *Diabetes*, vol. 66, no. 2, pp. 418–425, 2017.
- [39] T. Yoshihara, Y. Oikawa, T. Kato et al., “The protective effect of *Bifidobacterium bifidum* G9-1 against mucus degradation by *Akkermansia muciniphila* following small intestine injury caused by a proton pump inhibitor and aspirin,” *Gut Microbes*, vol. 11, no. 5, pp. 1385–1404, 2020.
- [40] G. Li, X. Wang, Y. Xu, B. Zhang, and X. Xia, “Antimicrobial effect and mode of action of chlorogenic acid on *Staphylococcus aureus*,” *European Food Research and Technology*, vol. 238, no. 4, pp. 589–596, 2013.
- [41] C. J. Lynch and S. H. Adams, “Branched-chain amino acids in metabolic signalling and insulin resistance,” *Nature Reviews Endocrinology*, vol. 10, no. 12, pp. 723–736, 2014.
- [42] C. Nie, T. He, W. Zhang, G. Zhang, and X. Ma, “Branched chain amino acids: beyond nutrition metabolism,” *International Journal of Molecular Sciences*, vol. 19, no. 4, p. 954, 2018.
- [43] M. Ren, S. H. Zhang, X. F. Zeng, H. Liu, and S. Y. Qiao, “Branched-chain amino acids are beneficial to maintain growth performance and intestinal immune-related function in weaned piglets fed protein restricted diet,” *Asian-*

- Australasian Journal of Animal Sciences*, vol. 28, no. 12, pp. 1742–1750, 2015.
- [44] M. Ren, S. Zhang, X. Liu et al., “Different lipopolysaccharide branched-chain amino acids modulate porcine intestinal endogenous β -defensin expression through the Sirt1/ERK/90RSK pathway,” *Journal of Agricultural and Food Chemistry*, vol. 64, no. 17, pp. 3371–3379, 2016.
- [45] R. de Simone, F. Vissicchio, C. Mingarelli et al., “Branched-chain amino acids influence the immune properties of microglial cells and their responsiveness to pro-inflammatory signals,” *Biochimica et Biophysica Acta*, vol. 1832, no. 5, pp. 650–659, 2013.
- [46] M. Nighot, M. Rawat, R. al-Sadi, E. F. Castillo, P. Nighot, and T. Y. Ma, “Lipopolysaccharide-induced increase in intestinal permeability is mediated by TAK-1 activation of IKK and MLCK/ *_MYLK_* gene,” *The American Journal of Pathology*, vol. 189, no. 4, pp. 797–812, 2019.
- [47] X. Wu, W. Zhao, Q. Cui, and Y. Zhou, “Computational screening of potential regulators for Mrna-protein expression level discrepancy,” *Biochemical and Biophysical Research Communications*, vol. 523, no. 1, pp. 196–201, 2020.
- [48] J. Sun, F. Wang, H. Li et al., “Neuroprotective effect of sodium butyrate against cerebral ischemia/reperfusion injury in mice,” *Bio Med Research International*, vol. 2015, article 395895, pp. 1–8, 2015.
- [49] J. Chen and L. Vitetta, “Inflammation-modulating effect of butyrate in the prevention of colon cancer by dietary fiber,” *Clinical Colorectal Cancer*, vol. 17, no. 3, pp. e541–e544, 2018.
- [50] M. Vital, A. C. Howe, and J. M. Tiedje, “Revealing the bacterial butyrate synthesis pathways by analyzing (meta) genomic data,” *mBio*, vol. 5, no. 2, article e00889, 2014.

Review Article

The Role of Oxidative Stress and Antioxidants in Diabetic Wound Healing

Liling Deng ¹, Chenzhen Du ¹, Peiyang Song ¹, Tianyi Chen ¹, Shunli Rui ¹,
David G. Armstrong ² and Wuquan Deng ¹

¹Department of Endocrinology, Multidisciplinary Diabetic Foot Medical Center, Chongqing Emergency Medical Center, Chongqing University Central Hospital, Chongqing 400014, China

²Department of Surgery, Keck School of Medicine of the University of Southern California, CA, USA

Correspondence should be addressed to Wuquan Deng; wuquandeng@cqu.edu.cn

Received 12 October 2020; Accepted 29 December 2020; Published 8 February 2021

Academic Editor: Alin Ciobica

Copyright © 2021 Liling Deng et al. This is an open access article distributed under the Creative Commons Attribution License, which permits unrestricted use, distribution, and reproduction in any medium, provided the original work is properly cited.

Foot ulcers are one of the most common and severe complication of diabetes mellitus with significant resultant morbidity and mortality. Multiple factors impair wound healing include skin injury, diabetic neuropathy, ischemia, infection, inadequate glycemic control, poor nutritional status, and severe morbidity. It is currently believed that oxidative stress plays a vital role in diabetic wound healing. An imbalance of free radicals and antioxidants in the body results in overproduction of reactive oxygen species which lead to cell, tissue damage, and delayed wound healing. Therefore, decreasing ROS levels through antioxidant systems may reduce oxidative stress-induced damage to improve healing. In this context, we provide an update on the role of oxidative stress and antioxidants in diabetic wound healing through following four perspectives. We then discuss several therapeutic strategies especially dietary bioactive compounds by targeting oxidative stress to improve wounds healing.

1. Introduction

Diabetes mellitus (DM) and its complications are increasingly prevalent worldwide with a serious burden on patients and health care systems [1]. Diabetic foot ulcers have a substantial impact on disability, morbidity, and mortality. The mechanism of diabetic wound chronicity has not been well understood. It is currently believed that oxidative stress plays a vital role in the occurrence and development of diabetic wound [2, 3]. Oxidative stress is caused by overproduction of reactive oxygen species and insufficient antioxidant systems. However, the process of oxidative stress in wound development and healing remains unclear. This review will further develop the discussion on how oxidative stress may affect diabetic wound healing in terms of skin injury, neuropathy, arterial disease, and infection. Furthermore, the plausible role of antioxidants including plant bioactive compounds on promoting wound healing will be addressed in order to explore novel approaches and strategies for promotion of diabetic wound healing.

2. Oxidative Stress State in the Development and Healing of Diabetic Wound

Reactive oxygen species (ROS) are crucial regulators of several phases of wound healing. Indeed, low levels of ROS are required for the fight against external damage [4]. However, excessive oxidative stress on tissues and the decrease of antioxidant ability results in redox imbalance, which is a major cause of nonhealing diabetic wounds [5]. Clinical studies investigated that nonhealing diabetic wounds are infiltrated by the highly oxidizing environment, which is associated with hyperglycemia and tissue hypoxia, that leads to delayed wound repair. People with long-term type 2 diabetes have significant reductions in the antioxidant enzyme activity [6]. Oxidative stress may influence diabetic wound healing through skin injury, neuropathy, ischemic lesion, and topical infection (Figure 1).

2.1. Diabetic Skin Injury. The repair process of diabetic skin injury includes the temporally overlapping stages of coagulation, inflammation, migration-proliferation, and

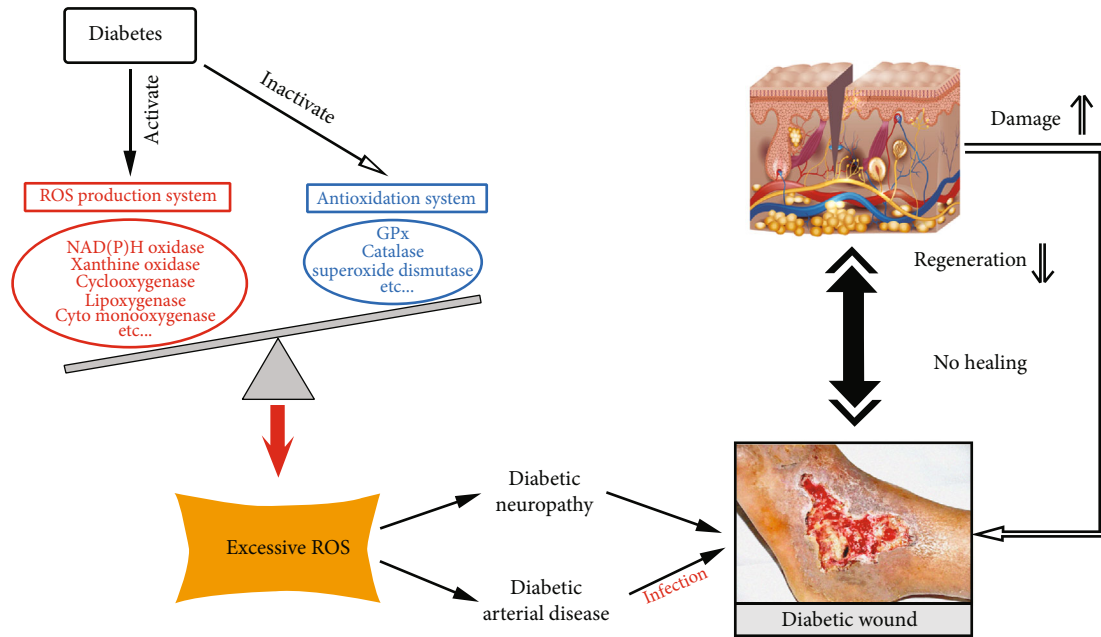


FIGURE 1: The role of oxidative stress in development and chronicity of diabetic wound.

remodeling [7]. While the molecular mechanisms underlying such defects have not yet been clarified, some have reported that a hyperglycemic state directly affects the keratinocyte and fibroblast activity inducing changes in protein synthesis, proliferation, and migration, reduced antimicrobial peptide expression, and increased oxidative stress. These myriad changes may result in the injury of the skin barrier function making the skin susceptible to damage and infection [8–11]. A balanced redox state is likely critical for prompt healing. Diabetic skin appears to be infiltrated with more inflammatory cells, edema, and less granulation tissue formation than the normal skin, suggesting a deterioration in diabetic ulcer healing reserve [2, 7]. Additionally, the periwound and central wound tissue in people with diabetes appears to also be more likely to be prone to excessive oxidative stress and damage, which results in poor healing [12, 13]. Kim et al. suggested that both high oxidative stress levels and bacteria set the wound up for chronic wound development [14].

Experiments that have evaluated hypoxia and oxidative stress suggest that they may lead to the downregulation of miRNA biogenesis genes in cultured fibroblasts [15]. Recent efforts have indicated the levels of serum advanced glycation end product (AGE), and its epidermal receptors were elevated in diabetes [9, 16]. AGEs bind to receptors on the endothelial cell surface inducing the overproduction of ROS [17]. AGE in the diabetic wound microenvironment appears to impair wound contraction and prolongs the inflammatory response and appears to deleteriously damage extracellular matrix (ECM) proliferation [18]. Nrf2 is a key transcription factor involved in wound healing by regulating angiogenesis and antioxidant gene expression, which is impaired in diabetes [19, 20]. A recent study indicates that activation of Nrf2 signaling significantly increased TGF- β 1 and reduced MMP9 in keratinocytes in diabetic wound healing [12]. Another study reported that SIRT1 (silent mating informa-

tion regulation 2 homolog) activation could protect vascular endothelial cells from oxidative stress damage to improve angiogenesis in wounds to accelerate wound healing in diabetic mice, and this effect may be through the AKT-Nrf2 pathway [21]. Sirtuins are class III histone deacetylase enzymes which are evolutionarily conserved and possess NAD⁺ dependent deacetylase activity. Sirtuin 3 (SIRT3) is a protein deacetylase located in the mitochondria. It serves to regulate the mitochondrial function, which is involved in regulating cellular redox status, mitochondrial energetics, biogenesis, dynamics, and apoptosis. Recent work has demonstrated that the lack of SIRT3 reduced blood supply, inhibited vascular endothelial growth factor (VEGF) expression, promoted superoxide production, impaired total antioxidant capacity, and consequently resulted in delayed skin wound healing in diabetic mice [22]. Therefore, sirtuins may be a new therapeutic target to improve diabetic wound healing.

2.2. Diabetic Neuropathy. At least half of the people with diabetes will develop clinically significant peripheral neuropathy [23–25]. Sensory nerve dysfunction leads to the loss or weakening of skin protection. Motor neuropathy, which increases plantar pressure that directly destroys the tissue, causes plantar capillary occlusion, local tissue ischemia, and destruction [26]. The autonomic neuropathy of sweat glands in people with diabetes leads to reduced skin sweating, abnormal temperature regulation, and dry and chapped skin, which in turn damages the integrity of the skin, leading to a reduced barrier to infection. It also leads to perturbations in the skin blood flow and microcirculatory disorders such as loss of peripheral sympathetic nerve innervation and tension, leading to vasomotor dysfunction and abnormal arteriovenous shunting. As a result, the abnormal blood flow distribution and nutritional capillary ischemia could occur.

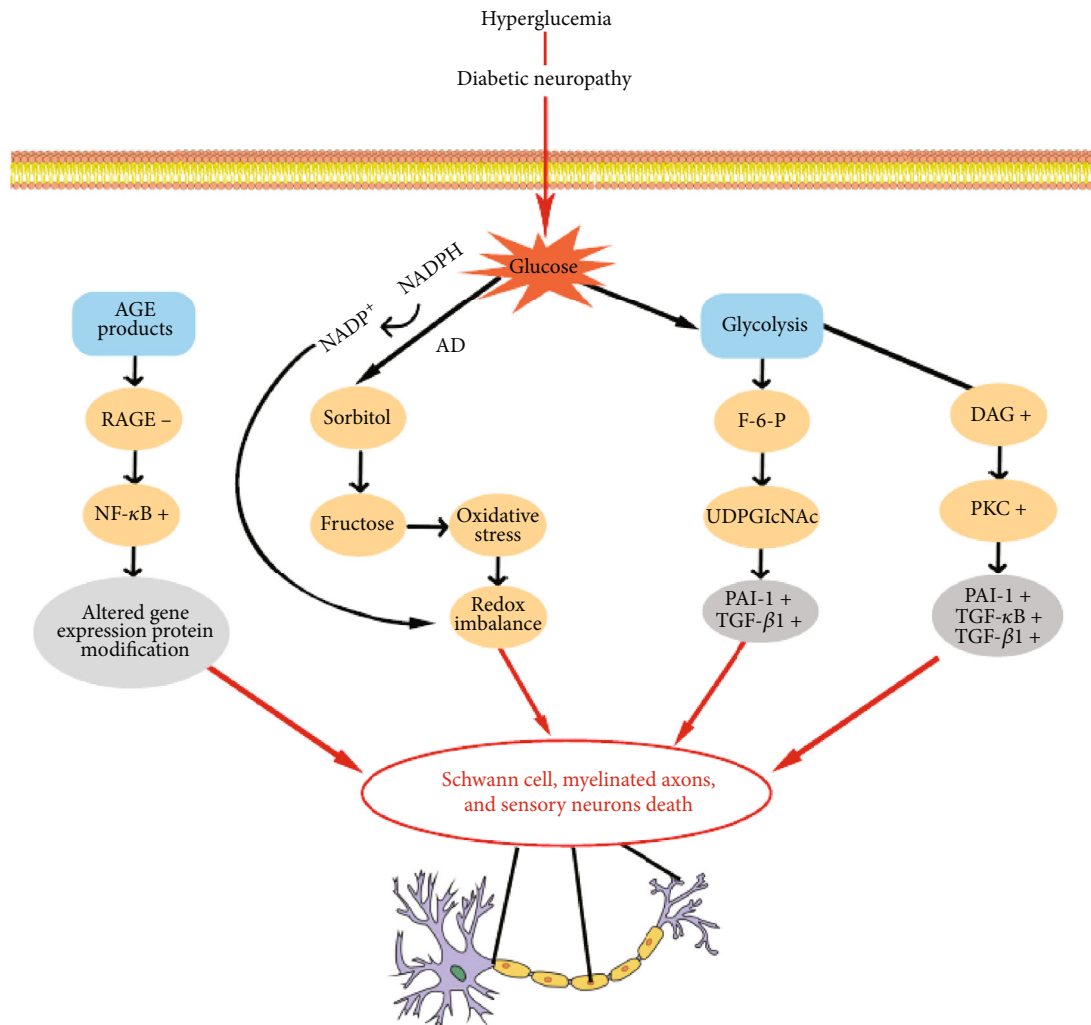


FIGURE 2: The main pathways with oxidative stress in diabetic neuropathy.

It has been well demonstrated that hyperglycemia is a critical mechanism in the induction of oxidative stress. Increased oxidative stress appears to deleteriously affect blood supply, structure, and metabolism of the peripheral nerve [26] that leads to extensive deterioration to the all aspects of the peripheral nervous system including Schwann cells, myelinated axons, and sensory neurons located in the dorsal root ganglia [27]. Meanwhile, insufficient ATP supplies could lose the ability to transport axons, as axons were rich in mitochondria, providing direct nerve energy supply, thereby further promoting axonal injury, causing diabetic neuropathy. The loss of ability of detoxify the excess oxidative stress with insufficient ATP supplies led the axons oxidative stress damage in hyperglycemia, which precipitated axonal degeneration or apoptosis [28]. Studies have suggested that multiple biochemical pathways are deleteriously affected by oxidative stress (Figure 2).

2.2.1. Activated Polyol Pathway. The polyol pathway mainly includes the conversion of glucose to sorbitol by aldose reductase (AR) and the conversion of sorbitol to fructose by

sorbitol dehydrogenase. In patients with diabetes, elevated intracellular levels of glucose cause the affinity of AR for glucose to also increase. This then leads to the increased production of sorbitol. Subsequent accumulation of sorbitol reduces the activity of $\text{Na}^+\text{K}^+-\text{ATPase}$ which reduces the physiological reserve of nerve cells and commensurate reduction of nerve conduction velocity. It is also understood that the hyperglycemia-induced polyol pathway leads to increased oxidative stress because of depletion of NADPH, which is derived from the pentose phosphate pathway that generates GSH from glutathione. Meanwhile, excess fructose, as a product in metabolism, accelerates glycation and further consumption of NADPH to aggravate intracellular oxidative stress [29]. It has been confirmed in diabetic mice with high expression of aldose reductase. Diabetic mouse models indicate that sorbitol accumulates significantly in the sciatic nerve of diabetic AR $+/+$ mice. Traces of oxidative stress and DNA damage in the sciatic nerve were additionally observed [30]. Until now, aldose reductase inhibitors have been used to inhibit oxidative stress through the polyol pathway [31]. This may be beneficial for improving diabetic ulcer with concomitant neuropathy.

2.2.2. Activated Hexosamine Pathway. In an environment characterized by hyperglycemia, fructose-6 phosphate, a metabolic intermediate of glycolysis, is shifted from the glycolytic pathway to the hexosamine pathway and then converted to uridine diphosphate N-acetylglucosamine (UDPGlcNAc). Subsequently, UDPGlcNAc attaches to the serine and threonine residues of transcription factors [32].

Studies have reported activation of the hexosamine pathway leading to the impaired nerve function. In addition, the hexosamine pathway can promote the expression of cytokines such as TGF- α and TGF- β 1 [33, 34].

Hyperglycemia activates the hexosamine pathway that eventually results in increasing of transcription factor Sp1, which is promoting the overexpression of TGF- β 1 and plasminogen activator inhibitor-1 (PAI-1) in arterial endothelial cells [35, 36]. In addition, hyperglycemia induces the hexosamine pathway, and NF- κ B signaling increases the expression of thrombospondin 2 (TSP2). TSP2 is a critical extracellular matrix protein in injury responses. This appears to delay diabetic wound healing [37].

2.2.3. Activated AGE Pathway. In DM, nonenzymatic glycosylation of glucose can chemically interact with amino acids, lipids, and nucleic acids, which lead to the formation of reversible early glycosylation products. After chemical reconstitution irreversible AGEs subsequently form, AGE receptors exist in a variety of cell types such as vascular endothelial, vascular smooth cells, and others. As AGEs combine with their receptors, ultimately, extracellular and intracellular structure and function are altered [38].

The formation of AGEs on ECM molecules can increase ECM production and tissue stiffness directly or indirectly through activation of TGF- β receptors to stimulate cell growth. A signaling cascade triggered by the binding of AGEs to its receptor on the endothelial cell surface leads to activation of NADPH oxidase and overproduction of ROS, p21, RAS, and MAPKs. NF- κ B is a key target of AGE-RAGE signaling. Excess oxidative stress derived from the AGE-RAGE axis activates NF- κ B and affects transcriptional activation of numerous cytokines and adhesion molecules including endothelin-1, ICAM-1, E-selectin, and tissue factor, many of which are closely linked to inflammation and diabetic angiopathy [17].

AGEs also reduce the bioavailability of endothelium NO and cause the overproduction of ROS [39, 40]. It has been suggested that the AGEs-RAGE axis contributes to microvascular and macrovascular complications of diabetes [41]. Thus, the process of the AGE pathway might induce neuropathy via impairing vasodilation, thickening capillary basement membrane, and endothelial hyperplasia.

In addition to the aforementioned effects, AGEs negatively impact diabetic ulcer healing by increasing apoptosis, decreasing the proliferation of fibroblasts, and reducing the activity of growth factors such as fibroblast growth factor [42]. Moreover, AGE-induced autophagy is associated with delayed cutaneous ulcer healing through stimulation of M1 polarized macrophage [43, 44].

2.2.4. Activated PKC Pathway. PKC is comprised of a group of serine/threonine protein kinases with important physio-

logical functions affecting many cellular signaling transduction pathways [45]. There are several isoforms of PKC, which play a critical role in multiple biological systems. PKC α , β I, β II, and δ are main components of the peripheral nerve [46]. In the environment of hyperglycemia, overproduction of oxygen free radicals inhibits the activity of glyceraldehyde phosphate dehydrogenase (GAPD). This leads to increased conversion of dihydroxyacetone phosphate (DHAP) to diacylglycerol (DAG), which in turn activates the PKC pathway [47]. Activated PKC can mediate the production of oxygen free radicals, inhibiting the activity of NO, thus leading to damage of the endothelial function.

A diabetic mouse study paradoxically reported decreased PKC activity. The difference from the previously stated results was likely due to the reduced expression of membrane PKC- α translocated to the cytoplasm, while the expression of membrane PKC β II increased [48]. Recent studies have reported improved neural function of diabetic rats with the administration of nonselective PKC isoform inhibitors or selective PKC β inhibitors. In addition, the sustained increasing PKC δ of human fibroblasts of DM hindered wound healing and insulin signaling was observed, thereby PKC δ inhibition may be a novel approach for treating diabetic wounds [49]. In summary, the mechanism of the PKC pathway in diabetic complications remains unclear.

Recent experiments have suggested that benfotiamine, a lipid-soluble analogue of vitamin B1, might improve diabetic wound healing via preventing the activation of the hexosamine pathway and the AGE and PKC pathway [50]. Preclinical studies showed that stimulating Nrf2-mediated antioxidant in the local regenerative environment of diabetic wounds significantly improved the molecular and cellular composition of wound beds [51].

The process of OS is irreversible and exerts a memory effect on metabolism with the correction of hyperglycemia [52, 53]. It was well demonstrated that the duration and severity of hyperglycemia were associated with the occurrence and progression of diabetic neuropathy, and enhanced glucose control delayed the process of developing clinical neuropathy in type 1 diabetes mellitus [3, 54]. However, conclusions in type 2 diabetes mellitus remain elusive [3, 55]. Indeed, strict glucose control does appear to impair nerve conduction velocity and vibration threshold in type 2 diabetes mellitus. This might be because neurons are more prone to severe hypoglycemic episodes. With acute glucose fluctuations, the PKC pathway is activated while inflammatory factors and adhesion molecules were secreted [56, 57], which further results in endothelial dysfunction and oxidative stress of the peripheral nerve.

2.3. Diabetic Peripheral Artery Disease. The role of diabetic angiopathy is well described in diabetic wounds. Diabetic microangiopathy and macroangiopathy are the combined result of irreversible complex nonenzymatic glycation, elevated oxidative stress and inflammation, and endothelial dysfunction and hypercoagulability state [58].

Oxidative stress caused by activated biochemical pathways, such as the AGE/RAGE pathway, the polyol pathway, PKC activation, and the hexosamine pathway, results in

production of inflammatory mediators, pericyte degeneration, thickening basement membrane, endothelial hyperplasia, NO reduction, impaired vasodilation, and increasing procoagulant biomarkers, such as IL-6, TNF- α , D-dimer, and PAI-1. All of these are in one way or another involved in the development of diabetic microangiopathy [59–62]. The alteration of the capillary or arteriolar vessel structure prevented the delivery of nutrients and activated white blood cells to specific tissues, increases the susceptibility and severity of infections, and accelerates the occurrence and progression of diabetic ulcer. In addition, microthromboembolism might be more prone to occur in terminal vessels of smaller diameter, which aggravates ischemia and hypoxia of the local tissue in diabetic wounds. SKQ1 as a mitochondria-targeted antioxidant increased the number of myofibroblasts, lowered the levels of neutrophils, and elevated macrophage infiltration; moreover, SKQ1 decreased lipid peroxidation levels without alteration of circulatory IL-6 and TNF levels. SKQ1 treatment also improved cell migration, thereby improving dermal wound healing of genetically diabetic mice [63].

The biochemical pathways participated in the development of diabetic macroangiopathy were as follows: AGEs-RAGE axis, polyol pathway, hexosamine pathway, PKC activation, overproduction of ROS, and chronic inflammation [64, 65]. In turn, atherosclerosis induced endothelial dysfunction and inflammation, and these processes are worsened in diabetes [59]. Moreover, recent evidences investigated that hypoglycemia may also play a vital role in vascular complications of diabetes [66]. Hyperglycemia or short-term glucose fluctuations induced OS and proatherogenic gene expression alteration which will be long-lasting later even in normal glycemic conditions [67]. As a result, the lumen of large vessels in diabetes narrow or abstract, and tissue ischemia deteriorated, which lead to a delay in diabetic wound closure.

2.4. Topical Infection. Patients with uncontrolled DM are more prone to skin infections such as fungal and bacterial infections. In turn, infections make the wound difficult to heal. The microbiome in diabetic wounds is closely related to the skin microbiome showing complex time-dependent features as well as individual differences. Diabetic wounds display disease-related changes. Staphylococcal species dominate [68–71].

3. Antioxidants in Diabetic Wound Healing

3.1. Antioxidant Effects of Antimetabolism Imbalance Drugs on Wound Healing. Metformin is a classic therapy for DM. Recent literatures have reported that metformin improved angiogenic functions of endothelial and endothelial progenitor cells by activating the NOS pathway, and it is effective in the treatment of skin wounds in diabetic mice [72, 73].

SGLT2 inhibitors, as a novel glucose-lowering approach, grow evidence suggesting that it can lower the mRNA expression of TNF- α , IL-6 and MCP-1, and infiltration of inflammatory cells in the plaque and adipose tissue to improve inflammation and endothelial function, which seem to be

involved in the alleviation of atherosclerosis by empagliflozin [74, 75]. Furthermore, with SGLT2 inhibitor therapy, the proinflammatory phenotype and glucotoxicity in experimental diabetic animals were reversed [75]. In addition, hyperglycemia-induced mitochondrial dysfunction was relieved by SGLT2i in hyperglycemic mouse aorta vascular cultures [76]. Therefore, SGLT2i may be beneficial to diabetic wounds for healing.

Dipeptidyl peptidase-4 (DPP-4) inhibitors can lower blood glucose and reduce cardiovascular risk in patients with type 2 diabetes mellitus. Previous studies indicated that DPP-4 exerts a preventive effect on oxidative stress via Nrf2 or other pathways. Therefore, DPP-4 may be a treatment option for patients with diabetic chronic wounds [77, 78].

Fenofibrates, along with a proper diet to fight against high cholesterol and triglyceride levels, has been indicated to simulate keratinocyte differentiation and improve the skin barrier in vivo [79]. It also ameliorated oxidative stress and blockade of Wnt/ β -catenin signaling [80]. These findings provide insights into treatment for diabetic ulcers. Systemically, use of statins exerts a reduction on cholesterol and can stimulate angiogenesis. Recent researches have revealed that statins can improve wound healing process in diabetic mice [81–83]. These may be a considerable therapy for patients with diabetic chronic wounds in clinic.

3.2. Antioxidant Effects of Drugs for Diabetic Neuropathy on Wound Healing. α -Lipoic acids (ALA) have been demonstrated to inhibit the progression of diabetic neuropathy by scavenging ROS, regeneration of endogenous and exogenous antioxidants, renovation of oxidized proteins, inhibition of NF- κ B, and regulation of gene transcription. Nowadays, it is widely used in the clinic for diabetic microangiopathy [64, 84, 85].

Coenzyme Q10, an endogenous synthesized lipid and a vitamin-like substance primarily present in the mitochondria, ameliorates oxidant stress and apoptosis [86]. CoQ10 is an electron transport in the mitochondrial respiratory chain, consequently increasing energy generation of ATP and enhancing the mitochondrial antioxidant activity [87]. Aldose reductase inhibitors are used to inhibit oxidative stress by the polyol pathway [31], and it may be beneficial for improving diabetic ulcer with neuropathy.

3.3. Antioxidant Effects of Drugs for Diabetic Angiopathies on Wound Healing. Cilostazol, a phosphodiesterase type 3 inhibitor, has been suggested to be involved in the procedure of antiatherosclerosis with antiplatelet and vasodilatory effects. A study on diabetic mice indicated that cilostazol significantly reduced RAGE, ROS, NF- κ B signaling, downstream gene expressions, and cell functions induced by hyperglycemia in VSMCs [88]. Low molecular-weight heparin ameliorates chronic diabetic wound healing, possibly by increasing microcirculation of wound margin [89, 90], but it is still controversy [91]. Iloprost improved limb perfusion and may be an important therapy for diabetic ulcerative lesions with severe ischemia [92]. However, there are only sparse data and lack of high-quality randomized controlled studies to show efficacy in any of these three agents [93].

TABLE 1: Antioxidants and their potential benefit in diabetic wound healing.

	Drugs	Observation	Mechanism	Reference
Antimetabolism imbalance	Metformin	Improved angiogenic functions of ECs and EPCs	NO, AMPK/mTOR pathway	[72, 73]
	SGLT2i	Improve inflammation and endothelial function	Lower mRNA expression of TNF- α , IL-6, and MCP-1	[74–76]
	DDP-4i	Antioxidative stress	Nrf2 pathway	[77, 78]
	Fenofibrates	Improve skin barrier	Wnt/ β -catenin pathway	[79, 80]
	Statins	Promote angiogenesis and lymphangiogenesis	PI3-kinase/Akt pathway	[81–83]
Therapy for diabetic neuropathy	ALA	Antioxidative stress	Inhibition of NF- κ B	[64, 84, 85]
	Aldose reductase inhibitors	Antioxidative stress	Polyol pathway	[31]
	Coenzyme Q10	Ameliorates oxidant stress and apoptosis	Increasing energy generation of ATP	[86, 87]
Therapy for diabetic angiopathies	Cilostazol	Antiatherosclerosis		[88]
	Low molecular-weight heparin	Increase microcirculation	Anticoagulation	[89–91]
	Iloprost	Improve limb perfusion	/	[92]
Therapy for the diabetic skin	EGF	Antioxidative stress	/	[94]
	Biogenic AgNPs	Accelerate wound healing	Inhibit overexpression of MMP-2 and MMP-9, antimicrobial	[95]
	NaB	Accelerate wound healing	Antimicrobial activity and improve proliferation	[96]
Therapy for infection	Antibiotics	Fight against for infection	/	[97, 98]
Plant ingredients for OS	Ferulic acid	Antioxidative stress	Reduce MMP (2, 8, 9) and increase TIMP-1 and 2	[99, 100]
	Chlorogenic acid	Antioxidative stress	Elevate the level of reduced glutathione	[102]
Potential antioxidants	The drug-loaded ROS-scavenging hydrogel	Accelerate wound healing	Decrease ROS level and upregulate M2 phenotype macrophages	[103]
	Deferoxamine	Promote neovascularization and regeneration	Suppress OS and activate hypoxia-inducible factor-1 alpha ion	[104]
	Propolis	/	Increase GSH/GSSG) ratio	[108]
	N-Acetyl cysteine (NAC)	Accelerate wound healing	Accelerate wound healing	[109, 110]

3.4. Antioxidant Effects of Drugs for Diabetic Skin on Wound Healing. The epidermal growth factor (EGF) administration was beneficial for the alleviation of oxidative stress to improve wound repair [94]. Biogenic AgNPs synthesized from *Brevibacillus brevis* KN8 could inhibit the overexpression of MMP-2 and MMP-9 in granulation tissues and accelerated wound healing in diabetic mice beyond the antimicrobial activity [95]. Sodium pentaborate pentahydrate (NaB) displayed great antimicrobial properties and improved proliferation, migration, and the expression of growth factor and gene expression in dermis, and studies on diabetic rats proved that NaB improve diabetic wound healing rate [96].

3.5. Antioxidant Effects of Drugs for Diabetic Infection on Wound Healing. Strict antimicrobial dressing should be performed in diabetic ulcers with infection [97]. The micro-

biome in wound is associated to the skin microbiome showing complex and time-dependent features, as well as individual differences [68]. The microbial culture can be used to guide antimicrobial therapy.

Efficient antimicrobial treatment with daptomycin [98] exerted positive effects on wound healing at the molecular level, such as reducing the level of local IL-6 and MMP-9 and increasing TIMP-1 in the MRSA-infected diabetic wound.

3.6. Antioxidant Effects of Plant Ingredients on Wound Healing. Ferulic acid (FA) is a natural antioxidant derived from fruits and vegetables that inhibited lipid peroxidation and increased the expression of catalase, superoxide dismutase, glutathione, nitric oxide, and serum zinc and copper, probably improving the healing process in diabetic ulcer [99]. Besides, syringic acid treatment also promotes migration and proliferation to improve wound healing [100].

The fusion protein decreased serum proinflammatory cytokines such as IL-6, TNF- α , expression of cyclooxygenase-2, and increased activities of antioxidant enzyme including superoxide dismutase, glutathione peroxidase, and catalase, and it also increased proangiogenic cytokines levels including VEGF, intercellular adhesion molecule, and expression of VEGF, FGF-2, p-ERK, and p-Akt protein in granulation in diabetic rats, which significantly accelerated the diabetic wound healing [101].

Animal study has indicated chlorogenic acid, a dietary antioxidant, that could accelerate wound healing, enhance hydroxyproline content, decrease malondialdehyde/nitric oxide, and elevate the level of reduced glutathione in wound bed [102]. However, a number of researches are needed to furtherly confirm these data.

3.7. Antioxidant Effects of Potential Antioxidants on Wound Healing. The drug-loaded ROS-scavenging hydrogel promotes wound closure by decreasing the ROS level and upregulating M2 phenotype macrophages around the wound. Moreover, such hydrogels formed in wound also increased the release of granulocyte macrophage colony-stimulating factor to fight against external bacteria and improve the wound closure [103].

The experiment has indicated that deferoxamine (DFO) could reduce oxidative stress and promote hypoxia-inducible factor-1 α activation to facilitate neovascularization and regeneration in chronic diabetic wounds. Dominik Duscher has demonstrated the treatment of DFO and the enhanced concept drug delivery system treatment eTDDS that markedly increased wound vascularity, dermal thickness, collagen deposition, and tensile strength, thereby accelerating wound healing. Therefore, DFO eTDDS may have the potential in treatment of diabetic wounds [104].

In addition, vitamins A, C, and E are antioxidants [105]; however, some literature has reported that high doses of vitamins possibly increase the mortality of cardiovascular events and risk of tumors such as lung and skin tumors [106, 107]. Propolis could increase the glutathione (GSH) and GSH/glutathione disulfide (GSSG) ratio, deplete TNF, and increased interleukin10 levels to reduce the wound area [108]. Antioxidant with *N*-acetyl cysteine (NAC) is known to improve endothelial cell function and angiogenesis, and Mohamed et.al reported that daily NAC use improved postamputation stump healing, perfusion, neovascularization, and reduced muscle fiber damage [109, 110] (Table 1).

Further research is needed to confirm or refute whether these therapies are beneficial to diabetic wound healing. In addition, melatonin, taurine, and acetyl L-carnitine have been reported to improve oxidative stress in diabetic wounds in the recent literatures. However, a number of randomized controlled studies are needed to confirm.

4. Conclusion

Wound healing is a complex, dynamic process. However, most diabetic wounds are difficult to heal. Multiple factors such as hyperglycemia, neuropathy, blood supply, matrix turnover, wound contraction, and the microbiome play a role

in the complex symphony of diabetic wound healing. Oxidative stress regulates wound healing through several related signal pathways. It therefore stands to reason that active control of ROS levels through antioxidants and antioxidative enzyme systems may reduce oxidative stress-induced damage to improve wound healing. Traditional systemic and topical medications could be beneficial for wound healing. Clinicians and scientists would do well to focus on development and testing of antioxidants to facilitate diabetic wound healing, thereby reducing the unnecessary burden of amputation, morbidity, and mortality in this population.

Conflicts of Interest

The authors declare no conflicts of interest.

Authors' Contributions

WD conceived of and designed the study and revised the manuscript for important intellectual content. LD, PS, and TC performed the literature search. CD generated the figures and tables. WD and LD performed the background research. WD and DGA edited the manuscript. LD and WD drafted the manuscript. All authors have read and approved the content of the manuscript.

Acknowledgments

This research was funded by the Natural Science Foundation of Chongqing Municipal Science and Technology Bureau (cstc2018jcyjAX0335; cstc2020jcyj-msxmX0298), the Fundamental Research Funds of Central Universities at Chongqing University (2019CDYGYB020) awarded to Dr. Wuquan Deng, and also partially supported by the National Institutes of Health, National Institute of Diabetes and Digestive and Kidney Diseases (1R01124789-01A1) awarded to Dr. Armstrong DG.

References

- [1] D. G. Armstrong, M. A. Swerdlow, A. A. Armstrong, M. S. Conte, W. V. Padula, and S. A. Bus, "Five year mortality and direct costs of care for people with diabetic foot complications are comparable to cancer," *Journal of Foot and Ankle Research*, vol. 13, no. 1, p. 16, 2020.
- [2] A. J. M. Boulton, D. G. Armstrong, M. J. Hardman et al., *Diagnosis and management of diabetic foot infections*, American Diabetes Association, Arlington, (VA), 2020.
- [3] B. C. Callaghan, A. A. Little, E. L. Feldman, and R. A. C. Hughes, "Enhanced glucose control for preventing and treating diabetic neuropathy," *Cochrane Database of Systematic Reviews*, vol. 6, article Cd007543, 2012.
- [4] C. Dunnill, T. Patton, J. Brennan et al., "Reactive oxygen species (ROS) and wound healing: the functional role of ROS and emerging ROS-modulating technologies for augmentation of the healing process," *International Wound Journal*, vol. 14, no. 1, pp. 89–96, 2017.
- [5] M. C. Sanchez, S. Lancel, E. Boulanger, and R. Neviere, "Targeting oxidative stress and mitochondrial dysfunction in the

- treatment of impaired wound healing: a systematic review,” *Antioxidants*, vol. 7, no. 8, p. 98, 2018.
- [6] J. Dworzanski, M. Strycharz-Dudziak, E. Kliszczewska et al., “Glutathione peroxidase (GPx) and superoxide dismutase (SOD) activity in patients with diabetes mellitus type 2 infected with Epstein-Barr virus,” *PLoS One*, vol. 15, no. 3, article e0230374, 2020.
- [7] D. G. Armstrong and G. C. Gurtner, “A histologically hostile environment made more hospitable?,” *Nature Reviews Endocrinology*, vol. 14, no. 9, pp. 511–512, 2018.
- [8] A. L. Lima, T. Illing, S. Schliemann, and P. Elsner, “Cutaneous manifestations of diabetes mellitus: a review,” *American Journal of Clinical Dermatology*, vol. 18, no. 4, pp. 541–553, 2017.
- [9] J. H. Kim, N. Y. Yoon, D. H. Kim et al., “Impaired permeability and antimicrobial barriers in type 2 diabetes skin are linked to increased serum levels of advanced glycation end-product,” *Experimental Dermatology*, vol. 27, no. 8, pp. 815–823, 2018.
- [10] H.-Y. Park, J.-H. Kim, M. Jung et al., “A long-standing hyperglycaemic condition impairs skin barrier by accelerating skin ageing process,” *Experimental Dermatology*, vol. 20, no. 12, pp. 969–974, 2011.
- [11] T. A. M. Andrade, D. S. Masson-Meyers, G. F. Caetano et al., “Skin changes in streptozotocin-induced diabetic rats,” *Biochemical and Biophysical Research Communications*, vol. 490, no. 4, pp. 1154–1161, 2017.
- [12] M. Long, M. R. de la Vega, Q. Wen et al., “An essential role of NRF2 in diabetic wound healing,” *Diabetes*, vol. 65, no. 3, pp. 780–793, 2016.
- [13] C.-C. E. Lan, C.-S. Wu, S.-M. Huang, I.-H. Wu, and G.-S. Chen, “High-glucose environment enhanced oxidative stress and increased interleukin-8 secretion from keratinocytes: new insights into impaired diabetic wound healing,” *Diabetes*, vol. 62, no. 7, pp. 2530–2538, 2013.
- [14] J. H. Kim, B. Yang, A. Tedesco et al., “High levels of oxidative stress and skin microbiome are critical for initiation and development of chronic wounds in diabetic mice,” *Scientific Reports*, vol. 9, no. 1, p. 19318, 2019.
- [15] E. Baldini, E. Testa, C. Voellenkle et al., “Dysregulation of microRNA expression in diabetic skin,” *Journal of Dermatological Science*, vol. 98, no. 3, pp. 186–194, 2020.
- [16] Y. W. Niu, M. Y. Miao, W. Dong, J. Y. Dong, X. Z. Cao, and S. L. Lu, “Effects of advanced glycation end products and its receptor on oxidative stress in diabetic wounds,” *Zhonghua Shao Shang Za Zhi*, vol. 28, pp. 32–35, 2012.
- [17] A. Goldin, J. A. Beckman, A. M. Schmidt, and M. A. Creager, “Advanced glycation end products: sparking the development of diabetic vascular injury,” *Circulation*, vol. 114, no. 6, pp. 597–605, 2006.
- [18] J. A. David, W. J. Rifkin, P. S. Rabbani, and D. J. Ceradini, “The Nrf2/Keap1/ARE pathway and oxidative stress as a therapeutic target in type II diabetes mellitus,” *Journal Diabetes Research*, vol. 2017, article 4826724, 15 pages, 2017.
- [19] M. A. Soares, O. D. Cohen, Y. C. Low et al., “Restoration of Nrf2 signaling normalizes the regenerative niche,” *Diabetes*, vol. 65, no. 3, pp. 633–646, 2016.
- [20] R. Teena, U. Dhamodharan, D. Ali, K. Rajesh, and K. M. Ramkumar, “Genetic polymorphism of the Nrf2 promoter region (rs35652124) is associated with the risk of diabetic foot ulcers,” *Oxidative Medicine and Cellular Longevity*, vol. 2020, Article ID 9825028, 9 pages, 2020.
- [21] X. Li, G. Wu, F. Han et al., “SIRT1 activation promotes angiogenesis in diabetic wounds by protecting endothelial cells against oxidative stress,” *Archives of biochemistry and biophysics*, vol. 661, pp. 117–124, 2019.
- [22] S. Yang, M. Xu, G. Meng, and Y. Lu, “SIRT3 deficiency delays diabetic skin wound healing via oxidative stress and necroptosis enhancement,” *Journal of Cellular and Molecular Medicine*, vol. 24, no. 8, pp. 4415–4427, 2020.
- [23] D. G. Armstrong, A. J. M. Boulton, and S. A. Bus, “Diabetic foot ulcers and their recurrence,” *The New England Journal of Medicine*, vol. 376, no. 24, pp. 2367–2375, 2017.
- [24] D. G. Armstrong, “The 10-g monofilament: the diagnostic divining rod for the diabetic foot?,” *Diabetes Care*, vol. 23, no. 7, p. 887, 2000.
- [25] D. G. Armstrong, L. A. Lavery, and L. B. Harkless, “Who is at risk for diabetic foot ulceration?,” *Clinics in Podiatric Medicine and Surgery*, vol. 15, no. 1, pp. 11–19, 1998.
- [26] I. G. Obrosova, “Update on the pathogenesis of diabetic neuropathy,” *Current Diabetes Reports*, vol. 3, no. 6, pp. 439–445, 2003.
- [27] D. C. Rosenberger, V. Blechschmidt, H. Timmerman, A. Wolff, and R.-D. Treede, “Challenges of neuropathic pain: focus on diabetic neuropathy,” *Journal of Neural Transmission*, vol. 127, pp. 589–624, 2020.
- [28] P. Fernyhough and J. McGavock, “Mechanisms of disease,” *Handbook of clinical neurology*, vol. 126, pp. 353–377, 2014.
- [29] L. Pang, X. Lian, H. Liu et al., “Understanding diabetic neuropathy: focus on oxidative stress,” *Oxidative Medicine and Cellular Longevity*, vol. 2020, Article ID 9524635, 13 pages, 2020.
- [30] E. C. M. Ho, K. S. L. Lam, Y. S. Chen et al., “Aldose reductase-deficient mice are protected from delayed motor nerve conduction velocity, increased c-Jun NH2-terminal kinase activation, depletion of reduced glutathione, increased superoxide accumulation, and DNA damage,” *Diabetes*, vol. 55, no. 7, pp. 1946–1953, 2006.
- [31] S. K. Srivastava, U. C. S. Yadav, A. B. M. Reddy et al., “Aldose reductase inhibition suppresses oxidative stress-induced inflammatory disorders,” *Chemico-Biological Interactions*, vol. 191, pp. 330–338, 2011.
- [32] A. Hosseini and M. Abdollahi, “Diabetic neuropathy and oxidative stress: therapeutic perspectives,” *Oxidative Medicine and Cellular Longevity*, vol. 2013, Article ID 168039, 15 pages, 2013.
- [33] P. P. Sayeski and J. E. Kudlow, “Glucose metabolism to glucosamine is necessary for glucose stimulation of transforming growth factor- α gene transcription,” *The Journal of Biological Chemistry*, vol. 271, no. 25, pp. 15237–15243, 1996.
- [34] V. Kolm-Litty, U. Sauer, A. Nerlich, R. Lehmann, and E. D. Schleicher, “High glucose-induced transforming growth factor beta1 production is mediated by the hexosamine pathway in porcine glomerular mesangial cells,” *The Journal of Clinical Investigation*, vol. 101, no. 1, pp. 160–169, 1998.
- [35] X. L. Du, D. Edelstein, L. Rossetti et al., “Hyperglycemia-induced mitochondrial superoxide overproduction activates the hexosamine pathway and induces plasminogen activator inhibitor-1 expression by increasing Sp1 glycosylation,” *Proceedings of the National Academy of Sciences of the United States of America*, vol. 97, no. 22, pp. 12222–12226, 2000.

- [36] Y.-Q. Chen, M. Su, R. R. Walia, Q. Hao, J. W. Covington, and D. E. Vaughan, "Sp1 sites mediate activation of the plasminogen activator inhibitor-1 promoter by glucose in vascular smooth muscle cells," *Journal of Biological Chemistry*, vol. 273, pp. 8225–8231, 1998.
- [37] B. Kunkemoeller, T. Bancroft, H. Xing et al., "Elevated thrombospondin 2 contributes to delayed wound healing in diabetes," *Diabetes*, vol. 68, no. 10, pp. 2016–2023, 2019.
- [38] C. Y. Chen, A. M. Abell, Y. S. Moon, and K. H. Kim, "An advanced glycation end product (AGE)-receptor for AGEs (RAGE) axis restores adipogenic potential of senescent preadipocytes through modulation of p53 protein function," *The Journal of biological chemistry*, vol. 287, no. 53, pp. 44498–44507, 2012.
- [39] G. D. Frank, S. Eguchi, and E. D. Motley, "The role of reactive oxygen species in insulin signaling in the vasculature," *Antioxidants & redox signaling*, vol. 7, no. 7-8, pp. 1053–1061, 2005.
- [40] R. Bucala, K. J. Tracey, and A. Cerami, "Advanced glycosylation products quench nitric oxide and mediate defective endothelium-dependent vasodilatation in experimental diabetes," *The Journal of clinical investigation*, vol. 87, no. 2, pp. 432–438, 1991.
- [41] M. Brownlee, H. Vlassara, and A. Cerami, "Nonenzymatic glycosylation and the pathogenesis of diabetic complications," *Annals of internal medicine*, vol. 101, no. 4, pp. 527–537, 1984.
- [42] Y. Duraisamy, M. Slevin, N. Smith et al., "Effect of glycation on basic fibroblast growth factor induced angiogenesis and activation of associated signal transduction pathways in vascular endothelial cells: possible relevance to wound healing in diabetes," *Angiogenesis*, vol. 4, no. 4, pp. 277–288, 2001.
- [43] R. Kang, D. Tang, M. T. Lotze, and H. J. Zeh 3rd., "RAGE regulates autophagy and apoptosis following oxidative injury," *Autophagy*, vol. 7, pp. 442–444, 2014.
- [44] Y. Guo, C. Lin, P. Xu et al., "AGEs induced autophagy impairs cutaneous wound healing via stimulating macrophage polarization to M1 in diabetes," *Scientific Reports*, vol. 6, no. 1, article 36416, 2016.
- [45] M. Freeley, D. Kelleher, and A. Long, "Regulation of protein kinase C function by phosphorylation on conserved and non-conserved sites," *Cellular signalling*, vol. 23, no. 5, pp. 753–762, 2011.
- [46] C. P. Tseng and A. K. Verma, "Functional expression and characterization of the mouse epitope tag-protein kinase C isoforms, alpha, beta I, beta II, gamma, delta and epsilon," *Gene*, vol. 169, no. 2, pp. 287–288, 1996.
- [47] M. Brownlee, "Biochemistry and molecular cell biology of diabetic complications," *Nature*, vol. 414, no. 6865, pp. 813–820, 2001.
- [48] K. Uehara, S.-I. Yamagishi, S. Otsuki, S. Chin, and S. Yagihashi, "Effects of polyol pathway hyperactivity on protein kinase C activity, nociceptive peptide expression, and neuronal structure in dorsal root ganglia in diabetic mice," *Diabetes*, vol. 53, no. 12, pp. 3239–3247, 2004.
- [49] M. Khamaisi, S. Katagiri, H. Keenan et al., "PKC δ inhibition normalizes the wound-healing capacity of diabetic human fibroblasts," *The Journal of clinical investigation*, vol. 126, no. 3, pp. 837–853, 2016.
- [50] A. Stirban, M. Negrean, B. Stratmann et al., "Benfotiamine prevents macro- and microvascular endothelial dysfunction and oxidative stress following a meal rich in advanced glycation end products in individuals with type 2 diabetes," *Diabetes Care*, vol. 29, no. 9, pp. 2064–2071, 2006.
- [51] P. S. Rabbani, T. Ellison, B. Waqas et al., "Targeted Nrf2 activation therapy with RTA 408 enhances regenerative capacity of diabetic wounds," *Diabetes Research and Clinical Practice*, vol. 139, pp. 11–23, 2018.
- [52] A. Ceriello, S. Kumar, L. Piconi, K. Esposito, and D. Giugliano, "Simultaneous control of hyperglycemia and oxidative stress normalizes endothelial function in type 1 diabetes," *Diabetes Care*, vol. 30, no. 3, pp. 649–654, 2007.
- [53] A. Ceriello, M. A. Ihnat, and J. E. Thorpe, "Clinical review 2: the "metabolic memory": is more than just tight glucose control necessary to prevent diabetic complications?," *The Journal of Clinical Endocrinology and Metabolism*, vol. 94, no. 2, pp. 410–415, 2009.
- [54] B. Fullerton, K. Jeitler, M. Seitz, K. Horvath, A. Berghold, and A. Siebenhofer, "Intensive glucose control versus conventional glucose control for type 1 diabetes mellitus," *Cochrane Database of Systematic Reviews*, vol. 2014, article Cd009122, 2014.
- [55] K. M. Pantalone, A. D. Misra-Hebert, T. M. Hobbs et al., "Effect of glycemic control on the diabetes complications severity index score and development of complications in people with newly diagnosed type 2 diabetes," *Journal of Diabetes*, vol. 10, no. 3, pp. 192–199, 2018.
- [56] L. Monnier, E. Mas, C. Ginet et al., "Activation of oxidative stress by acute glucose fluctuations compared with sustained chronic hyperglycemia in patients with type 2 diabetes," *Journal of the American Medical Association*, vol. 295, no. 14, pp. 1681–1687, 2006.
- [57] A. Ceriello, K. Esposito, L. Piconi et al., "Oscillating glucose is more deleterious to endothelial function and oxidative stress than mean glucose in normal and type 2 diabetic patients," *Diabetes*, vol. 57, no. 5, pp. 1349–1354, 2008.
- [58] R. B. Goldberg, "Cytokine and cytokine-like inflammation markers, endothelial dysfunction, and imbalanced coagulation in development of diabetes and its complications," *The Journal of Clinical Endocrinology and Metabolism*, vol. 94, no. 9, pp. 3171–3182, 2009.
- [59] G. Balasubramanian, P. Vas, N. Chockalingam, and R. Naemi, "A Synoptic Overview of Neurovascular Interactions in the Foot," *Frontiers in Endocrinology*, vol. 11, 2020.
- [60] B. T. Ngo, K. D. Hayes, D. J. DiMiao, S. K. Srinivasan, C. J. Huerter, and M. S. Rendell, "Manifestations of cutaneous diabetic microangiopathy," *American Journal of Clinical Dermatology*, vol. 6, no. 4, pp. 225–237, 2005.
- [61] C. P. Domingueti, L. M. Sant'Ana Dusse, M. das Graças Carvalho, L. P. de Sousa, K. B. Gomes, and A. P. Fernandes, "Diabetes mellitus: the linkage between oxidative stress, inflammation, hypercoagulability and vascular complications," *Journal of Diabetes and its Complications*, vol. 30, no. 4, pp. 738–745, 2016.
- [62] F. Semeraro, F. Morescalchi, A. Cancarini, A. Russo, S. Rezzola, and C. Costagliola, "Diabetic retinopathy, a vascular and inflammatory disease: therapeutic implications," *Diabetes & Metabolism*, vol. 45, no. 6, pp. 517–527, 2019.
- [63] I. A. Demyanenko, V. V. Zakharova, O. P. Ilyinskaya et al., "Mitochondria-targeted antioxidant SkQ1 improves dermal wound healing in genetically diabetic mice," *Oxidative Medicine and Cellular Longevity*, vol. 2017, Article ID 6408278, 10 pages, 2017.

- [64] K. G. Park, M. J. Kim, H. S. Kim, S. J. Lee, D. K. Song, and I. K. Lee, "Prevention and treatment of macroangiopathy: focusing on oxidative stress," *Diabetes Research and Clinical Practice*, vol. 66, Suppl 1, pp. S57–S62, 2004.
- [65] N. Katakami, "Mechanism of development of atherosclerosis and cardiovascular disease in diabetes mellitus," *Journal of Atherosclerosis and Thrombosis*, vol. 25, no. 1, pp. 27–39, 2018.
- [66] M. Hanefeld, E. Duetting, and P. Bramlage, "Cardiac implications of hypoglycaemia in patients with diabetes - a systematic review," *Cardiovascular Diabetology*, vol. 12, no. 1, p. 135, 2013.
- [67] A. El-Osta, D. Brasacchio, D. Yao et al., "Transient high glucose causes persistent epigenetic changes and altered gene expression during subsequent normoglycemia," *The Journal of Experimental Medicine*, vol. 205, no. 10, pp. 2409–2417, 2008.
- [68] G. Daeschlein, P. Hinz, T. Kiefer, and M. Jünger, "Role of the microbiome in chronic wounds," *Der Hautarzt*, vol. 70, pp. 422–431, 2019.
- [69] A. Spichler, B. L. Hurwitz, D. G. Armstrong, and B. A. Lipsky, "Microbiology of diabetic foot infections: from Louis Pasteur to 'crime scene investigation,'" *BMC Medicine*, vol. 13, no. 1, p. 2, 2015.
- [70] A. S. Moffarah, M. Al Mohajer, B. L. Hurwitz, and D. G. Armstrong, "Skin and soft tissue infections," in *Diagnostic Microbiology of the Immunocompromised Host*, pp. 51–68, Wiley, 2016.
- [71] G. S. Watts, J. E. Thornton, K. Youens-Clark et al., "Identification and quantitation of clinically relevant microbes in patient samples: comparison of three k-mer based classifiers for speed, accuracy, and sensitivity," *PLoS Computational Biology*, vol. 15, no. 11, article e1006863, 2019.
- [72] L. M. Shawky, E. A. El Bana, and A. A. Morsi, "Stem cells and metformin synergistically promote healing in experimentally induced cutaneous wound injury in diabetic rats," *Folia Histochemica et Cytobiologica*, vol. 57, no. 3, pp. 127–138, 2019.
- [73] X. Han, Y. Tao, Y. Deng, J. Yu, Y. Sun, and G. Jiang, "Metformin accelerates wound healing in type 2 diabetic db/db mice," *Molecular Medicine Reports*, vol. 16, no. 6, pp. 8691–8698, 2017.
- [74] J. H. Han, T. J. Oh, G. Lee et al., "The beneficial effects of empagliflozin, an SGLT2 inhibitor, on atherosclerosis in ApoE (-/-) mice fed a western diet," *Diabetologia*, vol. 60, no. 2, pp. 364–376, 2017.
- [75] M. Oelze, S. Kröller-Schön, P. Welschhof et al., "The sodium-glucose co-transporter 2 inhibitor empagliflozin improves diabetes-induced vascular dysfunction in the streptozotocin diabetes rat model by interfering with oxidative stress and glucotoxicity," *PLoS One*, vol. 9, article e112394, 2014.
- [76] V. K. Pulakazhi Venu, M. El-Daly, M. Saifeddine et al., "Minimizing hyperglycemia-induced vascular endothelial dysfunction by inhibiting endothelial sodium-glucose cotransporter 2 and attenuating oxidative stress: implications for treating individuals with type 2 diabetes," *Canadian Journal of Diabetes*, vol. 43, no. 7, pp. 510–514, 2019.
- [77] S. H. Choi, S. Park, C. J. Oh, J. Leem, K. G. Park, and I. K. Lee, "Dipeptidyl peptidase-4 inhibition by gemigliptin prevents abnormal vascular remodeling via NF-E2-related factor 2 activation," *Vascular Pharmacology*, vol. 73, pp. 11–19, 2015.
- [78] A. Avogaro and G. P. Fadini, "The effects of dipeptidyl peptidase-4 inhibition on microvascular diabetes complications," *Diabetes Care*, vol. 37, pp. 2884–2894, 2014.
- [79] L. G. Kömüves, K. Hanley, A. M. Lefebvre et al., "Stimulation of PPAR α promotes epidermal keratinocyte differentiation in vivo," *The Journal of Investigative Dermatology*, vol. 115, no. 3, pp. 353–360, 2000.
- [80] Q. Liu, X. Zhang, R. Cheng, J. X. Ma, J. Yi, and J. Li, "Salutary effect of fenofibrate on type 1 diabetic retinopathy via inhibiting oxidative stress-mediated Wnt/ β -catenin pathway activation," *Cell and Tissue Research*, vol. 376, no. 2, pp. 165–177, 2019.
- [81] J. Asai, H. Takenaka, S. Hirakawa et al., "Topical simvastatin accelerates wound healing in diabetes by enhancing angiogenesis and lymphangiogenesis," *The American journal of pathology*, vol. 181, no. 6, pp. 2217–2224, 2012.
- [82] A. P. Sawaya, I. Jozic, R. C. Stone et al., "Mevastatin promotes healing by targeting caveolin-1 to restore EGFR signaling," *JCI insight*, vol. 4, no. 23, 2019.
- [83] A. Bitto, L. Minutoli, D. Altavilla et al., "Simvastatin enhances VEGF production and ameliorates impaired wound healing in experimental diabetes," *Pharmacological Research*, vol. 57, no. 2, pp. 159–169, 2008.
- [84] G.-D. Xiang, H.-L. Sun, L.-S. Zhao, J. Hou, L. Yue, and L. Xu, "The antioxidant alpha-lipoic acid improves endothelial dysfunction induced by acute hyperglycaemia during OGTT in impaired glucose tolerance," *Clinical Endocrinology*, vol. 68, pp. 716–723, 2008.
- [85] A. S. Ametov, A. Barinov, P. J. Dyck et al., "The sensory symptoms of diabetic polyneuropathy are improved with alpha-lipoic acid: the SYDNEY trial," *Diabetes Care*, vol. 26, no. 3, pp. 770–776, 2003.
- [86] N. Sadeghiyan Galeshkalami, M. Abdollahi, R. Najafi et al., "Alpha-lipoic acid and coenzyme Q10 combination ameliorates experimental diabetic neuropathy by modulating oxidative stress and apoptosis," *Life Sciences*, vol. 216, pp. 101–110, 2019.
- [87] N. Bhadri, T. Sanji, H. M. Guggilla, and R. Razdan, "Amelioration of behavioural, biochemical, and neurophysiological deficits by combination of monosodium glutamate with resveratrol/alpha-lipoic acid/coenzyme Q10 in rat model of cisplatin-induced peripheral neuropathy," *ScientificWorld-Journal*, vol. 2013, article 565813, 8 pages, 2013.
- [88] S.-C. Su, Y.-J. Hung, C.-L. Huang et al., "Cilostazol inhibits hyperglucose-induced vascular smooth muscle cell dysfunction by modulating the RAGE/ERK/NF- κ B signaling pathways," *Journal of Biomedical Science*, vol. 26, p. 68, 2019.
- [89] G. Jörneskog, K. Brismar, and B. Fagrell, "Low molecular weight heparin seems to improve local capillary circulation and healing of chronic foot ulcers in diabetic patients," *VASA Zeitschrift für Gefasskrankheiten*, vol. 22, pp. 137–142, 1993.
- [90] M. Kalani, J. Apelqvist, M. Blombäck et al., "Effect of dalteparin on healing of chronic foot ulcers in diabetic patients with peripheral arterial occlusive disease: a prospective, randomized, double-blind, placebo-controlled study," *Diabetes Care*, vol. 26, no. 9, pp. 2575–2580, 2003.
- [91] J. Aragón-Sánchez and J. L. Lázaro-Martínez, "Comments on the use of bemiparin in diabetic foot ulcers," *Diabetic Medicine*, vol. 26, no. 1, p. 110, 2009.
- [92] F. Mirenda, M. La Spada, D. Baccellieri, F. Stilo, F. Benedetto, and F. Spinelli, "Iloprost infusion in diabetic patients with

- peripheral arterial occlusive disease and foot ulcers,” *Chirurgia italiana*, vol. 57, pp. 731–735, 2005.
- [93] T. Elraiyah, A. Tsapas, G. Prutsky et al., “A systematic review and meta-analysis of adjunctive therapies in diabetic foot ulcers,” *Journal of Vascular Surgery*, vol. 63, 2016.
- [94] A. G. Ojalvo, J. B. Acosta, Y. M. Mari et al., “Healing enhancement of diabetic wounds by locally infiltrated epidermal growth factor is associated with systemic oxidative stress reduction,” *International Wound Journal*, vol. 14, no. 1, pp. 214–225, 2017.
- [95] N. Krishnan, B. Velramar, B. Ramachandirin et al., “Effect of biogenic silver nanocubes on matrix metalloproteinases 2 and 9 expressions in hyperglycemic skin injury and its impact in early wound healing in streptozotocin-induced diabetic mice,” *Materials Science and Engineering: C*, vol. 91, pp. 146–152, 2018.
- [96] S. Demirci, A. Doğan, S. Aydın, E. Ç. Dülger, and F. Şahin, “Boron promotes streptozotocin-induced diabetic wound healing: roles in cell proliferation and migration, growth factor expression, and inflammation,” *Molecular and Cellular Biochemistry*, vol. 417, no. 1–2, pp. 119–133, 2016.
- [97] J. C. Dumville, B. A. Lipsky, C. Hoey, M. Cruciani, M. Fiscon, and J. Xia, “Topical antimicrobial agents for treating foot ulcers in people with diabetes,” *Cochrane Database of Systematic Review*, vol. 6, article Cd011038, 2017.
- [98] A. Ambrosch, D. Halevy, B. Fwity, T. Brin, and R. Lobmann, “Effect of daptomycin on local interleukin-6, matrix metalloproteinase-9, and metalloproteinase inhibitor 1 in patients with MRSA-infected diabetic foot,” *The international journal of lower extremity wounds*, vol. 13, no. 1, pp. 12–16, 2014.
- [99] M. M. Ghaisas, S. B. Kshirsagar, and R. S. Sahane, “Evaluation of wound healing activity of ferulic acid in diabetic rats,” *International Wound Journal*, vol. 11, no. 5, pp. 523–532, 2014.
- [100] J. Ren, M. Yang, F. Xu, J. Chen, and S. Ma, “Acceleration of wound healing activity with syringic acid in streptozotocin induced diabetic rats,” *Life Sciences*, vol. 233, p. 116728, 2019.
- [101] Q. Chen, W. Li, J. Wang, X. Qu, and G. Wang, “Lysozyme-antimicrobial peptide fusion protein promotes the diabetic wound size reduction in streptozotocin (STZ)-induced diabetic rats,” *Medical science monitor : international medical journal of experimental and clinical research*, vol. 24, pp. 8449–8458, 2018.
- [102] D. Bagdas, B. C. Etoz, Z. Gul et al., “In vivo systemic chlorogenic acid therapy under diabetic conditions: wound healing effects and cytotoxicity/genotoxicity profile,” *Food and chemical toxicology : an international journal published for the British Industrial Biological Research Association*, vol. 81, pp. 54–61, 2015.
- [103] H. Zhao, J. Huang, Y. Li et al., “ROS-scavenging hydrogel to promote healing of bacteria infected diabetic wounds,” *Bio-materials*, vol. 258, p. 120286, 2020.
- [104] D. Duscher, A. A. Trotsyuk, Z. N. Maan et al., “Optimization of transdermal deferoxamine leads to enhanced efficacy in healing skin wounds,” *Journal of Controlled Release*, vol. 308, pp. 232–239, 2019.
- [105] A. F. M. Pessoa, J. C. Florim, H. G. Rodrigues et al., “Oral administration of antioxidants improves skin wound healing in diabetic mice,” *Wound Repair and Regeneration*, vol. 24, pp. 981–993, 2016.
- [106] G. S. Omenn, G. E. Goodman, M. D. Thornquist et al., “Risk factors for lung cancer and for intervention effects in CARET, the Beta-carotene and retinol efficacy trial,” *JNCI: Journal of the National Cancer Institute*, vol. 88, no. 21, pp. 1550–1559, 1996.
- [107] J. J. Challem, “Re: risk factors for lung cancer and for intervention effects in CARET, the Beta-carotene and retinol efficacy trial,” *Journal of the National Cancer Institute*, vol. 89, no. 4, pp. 325–326, 1997.
- [108] V. Mujica, R. Orrego, R. Fuentealba, E. Leiva, and J. Zúñiga-Hernández, “Propolis as an adjuvant in the healing of human diabetic foot wounds receiving care in the diagnostic and treatment centre from the regional hospital of Talca,” *Journal Diabetes Research*, vol. 2019, article 2507578, 10 pages, 2019.
- [109] M. A. Babizhayev, I. A. Stokov, V. V. Nosikov et al., “The role of oxidative stress in diabetic neuropathy: generation of free radical species in the glycation reaction and gene polymorphisms encoding antioxidant enzymes to genetic susceptibility to diabetic neuropathy in population of type I diabetic patients,” *Cell Biochemistry and Biophysics*, vol. 71, no. 3, pp. 1425–1443, 2015.
- [110] M. A. Zayed, X. Wei, K. M. Park et al., “N-Acetylcysteine accelerates amputation stump healing in the setting of diabetes,” *FASEB Journal*, vol. 31, no. 6, pp. 2686–2695, 2017.

Research Article

Bixin Attenuates High-Fat Diet-Caused Liver Steatosis and Inflammatory Injury through Nrf2/PPAR α Signals

Shasha Tao ^{1,2}, Youjing Yang ², Jianzhong Li ³, Hongyan Wang ¹ and Yu Ma ¹

¹Chongqing University Central Hospital & Chongqing Emergency Medical Center, No. 1 Jiankang Road, Yuzhong District, Chongqing 400014, China

²School of Public Health, Medical College of Soochow University, 199 Ren'ai Road, Suzhou 215123, China

³Department of Nephrology, The First Affiliated Hospital of Soochow University, Suzhou, Jiangsu 215006, China

Correspondence should be addressed to Shasha Tao; taoqishu619@126.com

Received 14 October 2020; Revised 29 December 2020; Accepted 21 January 2021; Published 2 February 2021

Academic Editor: Si Qin

Copyright © 2021 Shasha Tao et al. This is an open access article distributed under the Creative Commons Attribution License, which permits unrestricted use, distribution, and reproduction in any medium, provided the original work is properly cited.

Nonalcoholic fatty liver disease is the most common liver disease worldwide. Hepatic steatosis and oxidative stress are the main characteristics of NAFLD (nonalcoholic fatty liver disease), which also affect its prognosis. Bixin acts as novel Nrf2 (NF-E2 p45-related factor 2) activator with the cytoprotection against oxidative stress and inflammation; this study mainly focused on the mechanism of Nrf2 activation by bixin and explored its potential feasibilities in long-term high-fat diet- (HFD-) caused hepatic steatosis and inflammatory response *in vitro* and *in vivo*. Bixin was found to activate Nrf2 signals by the modification of critical Keap1 (Kelch-like ECH-associated protein 1) cystine and competitive interaction with Keap1 with upregulating P62 mRNA and protein expression. In human liver cells exposed to FFA (free fatty acid), bixin displayed a pronounced cytoprotective activity with upregulation of Nrf2-mediated gene expression, such as PPAR α and its targets related with fatty acid oxidation. In HFD-fed mice, systemic administration of bixin attenuated lipid accumulation, decreased oxidant inflammatory damage in the liver, and reduced circulating lipid levels through Nrf2. Different from most of other established inducers, bixin activated Nrf2 signals through two different mechanisms with safe administration for protection of oxidant inflammatory damage and attenuation of lipid accumulation in the *in vivo* long-term HFD-fed mice. Bixin represents a prototype Nrf2 activator that displays cytoprotective activity upon system administration targeting hepatic steatosis and oxidant inflammation originating from long-term HFD-fed mice. And bixin-based Nrf2-directed systemic intervention may also provide therapeutic benefit in protecting other organs in the process of metabolic syndrome.

1. Introduction

Nonalcoholic fatty liver disease (NAFLD) affects approximately 30% of adult population and has become one of the most common liver diseases around the world [1–3]. Characterized by steatosis, inflammation, cell ballooning, tissue necrosis, or apoptosis, NAFLD is regarded as the hepatic manifestation of metabolic syndrome, ranging from simple hepatic steatosis to severe stages of nonalcoholic steatohepatitis (NASH), which could be further developed into cirrhosis and hepatocellular carcinoma [4–6]. Therefore, development of novel therapeutic strategies to limit and prevent the initiation and development of NAFLD is urgently needed.

Lipid accumulation and oxidative stress are considered as the major factors that affect the procedure of NAFLD [7, 8]. Hepatic accumulative lipid induces the tissue oxidative stress, which subsequently causes the lipid peroxidation [9, 10]. These series of events lead to hepatic damage, such as inflammatory response, cell apoptosis, or necrosis, which exacerbate the NAFLD. Studies have reported that levels of reactive oxygen species (ROS) in NAFLD patients are markedly increased compared with those in healthy subjects [11, 12]. Thus, attenuation of lipid accumulation and suppression of oxidative stress would be an efficient method to treat the NAFLD. Cumulative studies reported that the NF-E2 p45-related factor 2 (Nrf2) signals serve as a critical cellular defense

system that prevents tissue damage in the process of several diseases by regulating a range of genes [13–15]. We and others have also demonstrated the feasibilities of diet-derived Nrf2 activators including sulforaphane (SF), cinnamaldehyde (CA), and tanshinone I (T-I) for the prevention of tissue damage in various diseases (including inflammation, fibrosis, diabetic nephropathy, and tumor) through modulation of the Nrf2-dependent cellular defense mechanism [16–18]. Besides that, Nrf2 signals are also involved in negatively controlling the lipid accumulation not only by suppressing the FFA uptake factors such as cluster of differentiation 36 (CD36) and fatty acid transport proteins (FATPs) but also through regulating fatty acid metabolism and transport by activating peroxisome proliferator-activated receptor α (PPAR α) signals [19, 20]. For example, depletion of n-3 long polyunsaturated fatty acids decreased PPAR α signals, contributing liver steatosis by inhibiting FFA oxidation [21].

Apocarotenoid bixin is a Food and Drug Administration (FDA-) approved natural food colorant and additive, which is extracted from the seeds of the *achiote* tree and proven to be safe for human administration [22]. Derived from lycopene through oxidative cleavage, bixin has traditionally been used in Mexico and South America to treat infectious and inflammatory diseases like skin, prostate, and chest pain [23, 24]. Previous *in vitro* biochemical measurement indicated bixin could quench the environmental reactive oxygen species (ROS). Similarly, animal studies also showed that bixin protects against oxidative DNA damage and suppresses lipid peroxidation [25]. Furthermore, our previous study has identified that bixin is a novel Nrf2 inducer, which could quench the ROS and inhibit the lung tissue inflammation and fibrosis [26, 27]. In addition, we also found that bixin could protect against UV exposure-caused skin tissue damage in an Nrf2-dependent manner as well [28].

Nrf2 is primarily regulated by Keap1, a substrate adaptor for a Cul3-containing E3 ubiquitin ligase [29]. Under basal conditions, the Keap1-Cul3-E3 ubiquitin ligase complex constantly ubiquitinates Nrf2 protein and promotes it for degradation by 26s proteasome to maintain it at a low level [30]. Nrf2 is primarily localized in a complex with Keap1 via direct protein-protein interactions between the Keap1 Kelch domain and the ETGE (strong binding) and DLG (weak binding) motifs of Nrf2 Neh2 domain [31]. So far, there are two potential mechanisms reported to activate Nrf2 signals via regulation of Keap1: canonical mechanism, which confers the activation by cellular exposure to oxidative or electrophilic stress that modified the critical cysteine residues in Keap1, leading to a conformational change of Keap1-Cul3-E3 complex that releases the bind with DLG motif and subsequently stabilized Nrf2 [32], while the noncanonical mechanism does not modify Keap1 cysteines. P62 (also termed as sequestosome 1, SQSTM1) is an important mediator that involved in the noncanonical mechanism, which binds with the Kelch domain of Keap1 with its pSTGE motif [33]. By this competition, Nrf2 was released and translocated to the nucleus to activate its target genes.

In this study, we explored the mechanism of bixin in the activation of Nrf2 signals and demonstrated that activation of Nrf2 by bixin suppressed the NF- κ B pathway and upregu-

lated the PPAR α with its targets, which plays a pivotal role in hepatic steatosis and inflammation by using a high-fat diet- (HFD-) fed mice model. These results suggest that pharmacological activation of Nrf2 by bixin may provide therapeutic benefit against metabolic syndrome-related organs' abnormal and oxidant inflammatory damage.

2. Materials and Methods

2.1. Chemicals, Antibodies, and Cell Culture. Bixin was purchased from Spectrum (New Brunswick, NJ). Oleic acid, palmitic acid, DAPI, cycloheximide, rapamycin, and bafilomycin A1 were purchased from Sigma (St. Louis, MO). MG132 was purchased from Amquar (Colorado, USA). Primary antibodies against Nrf2 (sc-13032), Keap1 (sc-15246), HO-1 (sc-136960), P65 (sc-8008), p-P65 (sc-136548), P62 (sc-28359), ubiquitin (Ub) (sc-8017), PPAR α (sc-398394), Acox1 (sc-517306), CPTII (sc-37294), and GAPDH (sc-32233) were purchased from Santa Cruz (Santa Cruz, CA). Antibody against 8-oxo-dG was purchased from Trevigen (Gaithersburg, MD; #3154-MC-050). Horseradish peroxidase- (HRP-) conjugated secondary antibodies were all purchased from ImmunoWay (Plano, TX; #RS001, #RS002). Alexa Fluor 488 anti-mouse and Alexa Fluor 594 anti-rabbit were purchased from Santa Cruz. Human hepatic cell line LO2 was purchased from Cell Bank of the Chinese Academy of Sciences in Shanghai, China. Cells were cultured in Dulbecco's modified Eagle's medium (DMEM) containing 10% FBS, 100 units/ml penicillin, and 100 μ g/ml streptomycin. All cells were kept in a humidified incubator at 37°C with 5% CO₂.

2.2. Transfections of siRNA and Plasmids, and Luciferase Reporter Gene Assay. Plasmid transfection was performed with Lipofectamine 2000 (Invitrogen), and HiPerfect transfection reagent (Qiagen, Hilden, Germany) was used for transfection with small interfering RNA (siRNA) according to the manufacturer's instructions. Nontargeted siRNA (Ctrl-siRNA, #1027281), Nrf2-targeted siRNA (Nrf2-siRNA, #SI00657937), and P62-targeted siRNA (P62-siRNA, #SI00057596) were purchased from Qiagen. Activation of Nrf2 transcriptional activity was performed as previously described [34]. LO2 cells were cotransfected with expression vectors for either Keap1 wild-type (Keap1 WT) or a mutant Keap1 (Keap1 C151S), along with mGst-ARE firefly and Renilla luciferase reporters. At 24 h posttransfection, cells were treated with SF (5 μ M), tBHQ (50 μ M), As (5 μ M), or bixin (40 μ M) for 16 h, and then lysed for analysis of the reporter gene activity using the Beyotime Biotechnology dual-luciferase reporter gene assay system.

2.3. Cell Viability Assay. Potential cytotoxicity of bixin in LO2 cells was assessed by the functional impairment of the mitochondria with 3-(4,5-dimethylthiazol-2-yl)-2,5-diphenyltetrazolium bromide (MTT, Sigma). About 1×10^4 cells per well were plated in a 96-well plate. After overnight incubation, the cells were treated with different doses of bixin for 48 h. Then, 40 μ g MTT was added into the cells. After 2 h incubation, the medium was removed by aspiration. 100 μ l

isopropanol/HCl was added into each well to dissolve the crystals. Absorbance at 570 nm was measured by a synergy 2 multimode microplate reader (BioTek, Seattle, USA).

2.4. ROS and Cell Apoptosis Detection. Followed by Ctrl-siRNA or Nrf2-siRNA transfection, cells were treated with bixin 40 μ M for 24 h prior to FFA exposure 1 mM (oleic acid/palmitic acid = 2 : 1 dissolved in 20% BSA). In the detection of ROS, the cells were incubated with fresh medium containing 10 μ g/ml 2',7'-dichlorodihydrofluorescein diacetate (H₂DCFDA, Sigma) for 1 h. And cell apoptosis detection was performed with Annexin V-FITC Apoptosis Detection Kit purchased from Beyotime (China). Finally, the cells were resuspended to 10⁶/ml in PBS. Fluorescence was measured by flow cytometry (Becton Dickinson and Company, USA) with the excitation at 488 nm and emission at 515 nm (ROS detection). The entire process was performed in the dark.

2.5. Preparation of Nuclear and Cytoplasmic Fractions. Nuclear and cytoplasmic fractions were prepared according to manufacturer's instructions (CWBiotech, China, CW0199S). Briefly, cells were scraped into ice-cold PBS, centrifuged at 3000g, and resuspended in ice-cold buffer A with protease inhibitor cocktail. After added buffer B, the mixture was centrifuged at 13400g for 15 min for collecting the cytoplasmic fraction. Then, the buffer C was used to solve the nuclear fraction from the cell pellet. To ensure the subcellular fractions were separated properly, subcellular lysates were verified by the antibodies against the corresponding fractions.

2.6. Immunoblot Analysis, Immunoprecipitation, Ubiquitination Assay, Protein Half-Life, Indirect Immunofluorescence, and Oil Red O Staining. The immunoblot analysis was employed to detect protein expression. Cell and tissue lysates were prepared the same as previously reported [35]. Lysates were run in the SDS-polyacrylamide gel and subjected to immunoblot analysis with the indicated antibodies. For immunoprecipitation and ubiquitination assay, cells were harvested in RIPA buffer (Thermo) and incubated with the indicated antibodies (1 μ g) together with protein A agarose beads (Invitrogen) at 4°C for 16 h. Immunoprecipitated proteins were analyzed by immunoblot with antibodies against Ub, Keap1, Nrf2, and P62 (Santa Cruz). To clarify Nrf2 stability, cell lysates at different time points from control- or bixin-treated cells were subjected to immunoblot analyses with the anti-Nrf2 and anti-GAPDH antibodies. The intensity of Nrf2 and GAPDH bands was quantified with ImageJ and plotted against the time after addition of cycloheximide (CHX). For indirect immunofluorescence, cells were seeded on round glass coverslips (Fisher Scientific). After fixed with chilled methanol, coverslips were incubated with the primary antibodies and the respective secondary antibodies for 50 min each. Coverslips were mounted with antifade mounting solution (Invitrogen). For Oil Red O staining, the cells' coverslips and frozen liver sections (10 μ m) were fixed and stained with freshly made Oil Red O solution. Images were captured with a fluorescence microscope (Leica DM2500).

2.7. RNA Extraction and Quantitative Real-Time PCR (qRT-PCR). Total RNA was extracted from both cells and liver tissues with TRIzol reagent purchased from CWBio (Beijing, China). cDNA was generated with equal amounts of mRNA with HiFiScript cDNA synthesis kit according to the manufacturer's instructions (CWBio, Beijing, China). Primer sequences of human Nrf2, HO-1, NQO1, P62, and GAPDH and mouse P62, Nrf2, HO-1, NQO1, IL-6, TNF- α , and GAPDH were described previously [26, 28]. The ABI 7500 (Applied Biosystems) was used to evaluate mRNA expression. Procedures of qRT-PCR were as follows: initial denaturation (95°C, 10 min), 40 cycles of amplification (95°C, 15 s; 60°C, 1 min), and melting curve (95°C, 15 s; 60°C, 1 min; 95°C, 15 s; 60°C, 15 s) with 96-well PCR plates (nest, 402101). Mean crossing point (Cp) values and standard deviations (SD) were determined. Cp values were normalized to the respective Cp values of human GAPDH or mouse β -actin reference gene. Data are presented as a fold change in gene expression compared to the control group.

2.8. Animals and Treatments. Nrf2 wild-type (WT) and knockout (KO) mice were obtained by breeding Nrf2 heterozygote mice. All mice maintained in a 12 h light/dark cycle, pathogen-free condition. Eight-week-old Nrf2 WT and Nrf2 KO mice were randomly divided into 4 groups ($n = 10$ per group): control (Ctrl; corn oil), bixin (dissolved in corn oil), HFD-fed group (HFD), and bixin+HFD. HFD mice were generated by a high-fat diet (60 kcal% high-fat diets, D12492, Research Diets, USA) for 25 weeks. The respective control mice were fed with normal standard permitted food (D12450J) and water consumption *ad libitum*. The mice received bixin (200 mg/kg) or corn oil once every three days from the 12th week after HFD feeding. The study protocols were approved by the Soochow University Institutional Animal Care and Use Committee. Animal handling here is according to the *Guide for the Care and Use of Laboratory Animals*.

2.9. Hematoxylin and Eosin (H&E) and Immunohistochemistry (IHC) Staining. The tissues were embedded in the paraffin followed by fixing with 4% paraformaldehyde for 24 h. After dehydration, the slides (4 μ M) were cut. H&E staining was used to assess the morphologies of live tissues with the indicated treatments. The procedures of IHC and DNA damage of 8-oxo-dG were performed the same as our previous study [26]. Positive proteins' staining was performed by EnVision+System-HRP kit (Dako) based on the manufacturer's instructions. The sections were analyzed with a fluorescence microscope (Leica DM2500).

2.10. Biochemical Measurements. The levels of aspartate transaminase (AST), alanine aminotransferase (ALT), low-density lipoprotein (LDL) cholesterol, high-density lipoprotein (HDL) cholesterol, total cholesterol (TC), and triglyceride (TG) were measured by the respective kit according to the manufacturer's instructions. Kits of AST (C0010-2), ALT (C009-2), LDL (A113-1-1), HDL (A112-1-1), TC (A111-1), and TG (A110-1) were purchased from Nanjing Jiancheng Institute of Biotechnology (Nanjing, China).

2.11. Statistical Analyses. The results are expressed as the means \pm SD. SPSS 19.0 was used to perform the statistical tests. Student's *t*-test (unpaired) was employed to compare multiple groups, while one-way ANOVA with Bonferroni adjustment was used to control type 1 error for multiple comparisons. A $p < 0.05$ was considered statistically significant.

3. Results

3.1. Bixin Activated the Nrf2 Signals in Liver Cells without Detectable Toxicity. According to bixin's chemical structure (Figure 1(a)) and our previous study, the cytotoxicity of bixin was first needed to be determined before investigating its effects on Nrf2 signals in LO2 cells [26]. The MTT assay showed that there was no cytotoxicity observed at the doses below 200 μ M (Figure 1(b)). The dose range of 0–40 μ M without toxicity was chosen for the subsequent studies. Immunoblot analyses indicated that bixin increased the protein expression of Nrf2, HO-1, and NQO1 in a dose-dependent manner (Figure 1(c)). And bixin (40 μ M) increased Nrf2 expression as early as 8 h and persisted up to 24 h. The expression of its targets (HO-1 and NQO1) was upregulated as early as 8 h and peaked at 24 h, which could persist to 48 h. Keap1, the adaptor protein of Nrf2, was a little decrease along with the upregulation of Nrf2 expression as determined in Figures 1(c) and 1(d). To verify the data, indirect immunofluorescence of Nrf2 was performed. Bixin increased the expression of Nrf2 especially in the nucleus of LO2 cells (Figure 1(e)). Then, the separation of the cytoplasm and nucleus was performed. The results showed that bixin increased the expression of Nrf2 in the nucleus (Figure 1(f)). Taken together, these data indicated that bixin could activate Nrf2 signals with no toxicity.

3.2. Bixin Upregulates Nrf2 Signals by Decreasing Nrf2 Ubiquitination and Increasing Its Protein Stability in a Keap1 C151-Dependent Manner. Next, the mRNA expression of Nrf2 and its targets (HO-1 and NQO1) was investigated. As shown in Figure 2(a), bixin increased the expression of HO-1 and NQO1 at 24 h without the upregulation of Nrf2, which indicated that bixin activated Nrf2 signals on the posttranscriptional level. To further explore the mechanism of Nrf2 activation by bixin, an *in vivo* ubiquitination assay was performed in LO2 cells. Bixin decreased the ubiquitination of Nrf2 compared with untreated cells (Figure 2(b)). Besides that, Nrf2 protein stability also affects the activation of Nrf2 signals. Thus, the half-life of endogenous Nrf2 protein was determined in LO2 cells with bixin treatment. Bixin elongated Nrf2 half-life from 19.2 min to 47.8 min (Figure 2(c)). To further investigate whether bixin activated Nrf2 in a canonical manner, endogenous expression of Keap1 was silenced by siRNA in LO2 cells. The cells were then cotransfected with Keap1-WT or Keap1-C151S plasmids as well as ARE firefly luciferase and Renilla luciferase reporters to evaluate Nrf2 transcriptional activity. Nrf2 transcriptional activity by SF or tBHQ was inhibited with Keap1-C151S transfection (Figure 2(d)). In contrast, arsenic treatment was still able to induce Nrf2 transcriptional activity in the Keap1-C151S cells consistent with our previous finding that arsenic is a nonca-

nonical Nrf2 inducer that works through a Keap1 C151-independent mechanism [18]. And bixin partially inhibited the induction of Nrf2 transcription activity in Keap1 C151S cells. Taken together, these results indicated that bixin upregulates Nrf2 signals by decreasing Nrf2 ubiquitination and increasing its protein stability, which is partially related with the critical C151 sensor residue in Keap1.

3.3. Bixin Activates Nrf2 by the Upregulation of P62. With the evidence showing that bixin activates Nrf2 signals which is partially Keap1-C151-dependent, the further mechanism of bixin on the regulation of Nrf2 was then investigated. Since Figures 3(a) and 3(b) have shown that bixin could time-dependently increase the P62 expression in mRNA and protein levels, we next silenced the expression of P62 with siRNA; the upregulation of Nrf2 by bixin was dramatically inhibited as shown in Figure 3(c). Consistent with our previous study, P62 containing a "pSTGE" domain could competitively bind with "Kelch" domain of Keap1 to activate Nrf2, and bixin could increase the expression of P62 (Figures 3(a)–3(c)). An immunoprecipitation assay was performed in LO2 cells to explore the interaction of P62 and Keap1. Bixin treatment could increase the binding of P62 and Keap1 (Figure 3(d)). Additionally, the cells were fixed and immunostained with Keap1 (green) and P62 (red). The images showed that bixin increased the colocalization of Keap1 and P62 (Figure 3(e)). Taken together, these results indicated that bixin increased Nrf2 protein expression through the increased P62 competitively binding with Keap1.

3.4. Bixin Protects LO2 Cells from FFA-Induced Lipid Accumulation and Cytotoxicity through Nrf2. As reported previously, Nrf2 improved the lipid accumulation caused by FFA exposure [36]. The fatty acid oxidation and lipogenesis-related proteins' expression were next evaluated with bixin treatment in our study. After cells were exposed to bixin, fatty acid oxidation-related proteins (PPAR α and its targets Acox1, CPTII) increased in a dose-dependent manner, but did not affect the protein expression related with lipogenesis (Figure 4(a)). In Nrf2 knockdown cells, the expression of PPAR α and its targets (Acox1, CPTII) was mostly inhibited as shown in Figure 4(b), which indicated that bixin upregulated the fatty acid oxidation-related proteins in the Nrf2-dependent manner. Next, the prevention of lipid accumulation was investigated in the cells exposed with FFA. The results from Oil Red O staining showed that the lipid accumulation was dramatically decreased in bixin-treated cells, while siNrf2 could attenuate this prevention (Figure 4(c)). Then, the feasibility of bixin for cytoprotection against FFA-induced toxicity was investigated. Oxidative stress and cell apoptosis were measured after LO2 cells were challenged by FFA with or without bixin pretreatment. Bixin pretreatment decreased the levels of ROS and cell apoptosis induced by FFA exposure. Bixin alone has no effects, which indicated that bixin itself could not trigger the oxidative stress and has less toxicity. However, bixin-mediated suppression was not detected in Nrf2 knockdown cells, indicating that the cytoprotection of bixin was through Nrf2 signals (Figures 4(d) and 4(e)). These data indicated

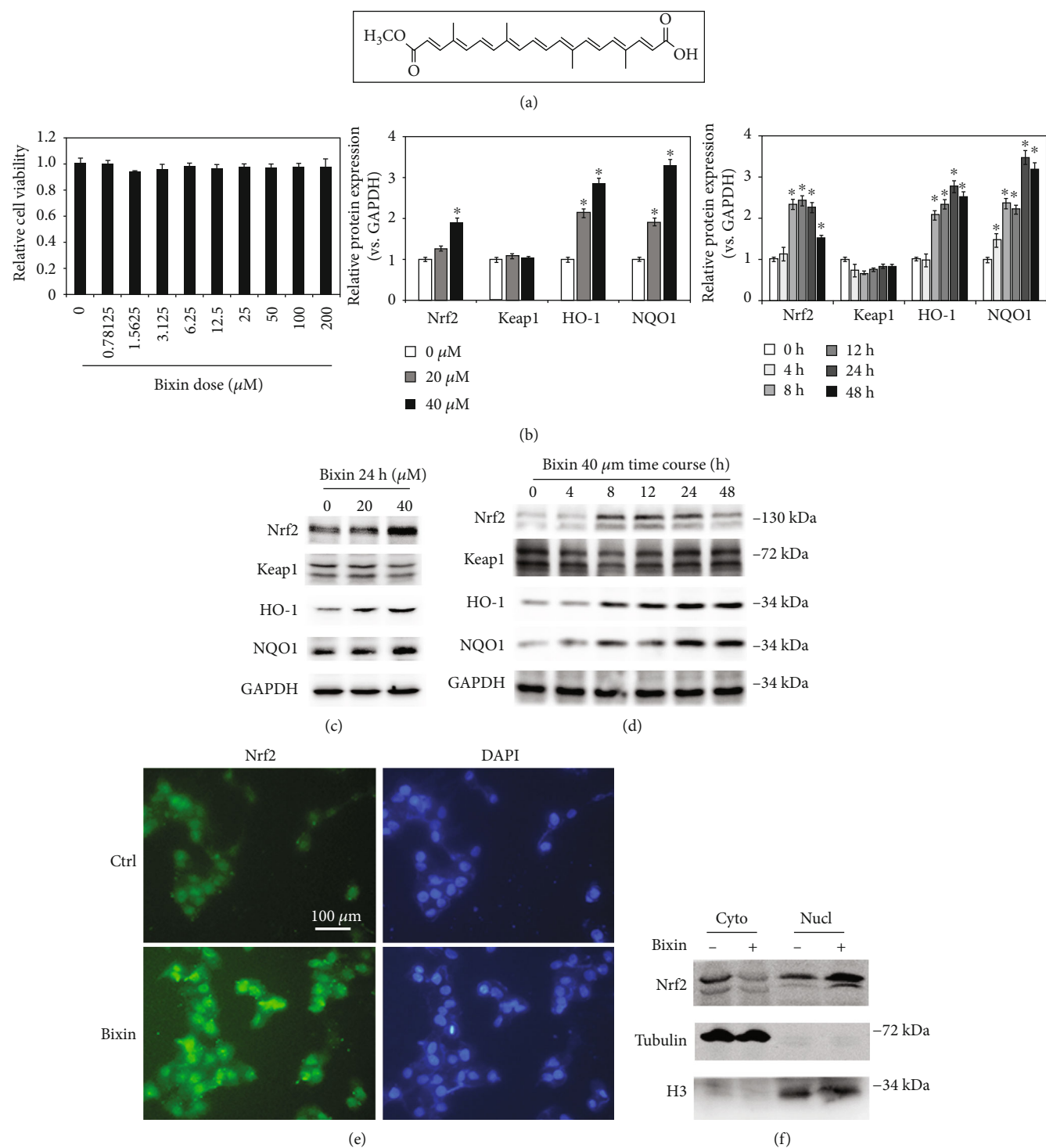


FIGURE 1: Bixin activated the Nrf2 signals in liver cells without detectable toxicity. (a) Bixin's chemical structure. (b) Cell viability was measured in LO2 cells administrated with the indicated doses of bixin for 48 h. (c) LO2 cells were administrated with bixin (0-40 μM) for 24 h or treated with bixin 40 μM for the indicated time (d). Cell lysates were subjected to immunoblot analyses with the indicated antibodies. Quantification of relative protein expression was determined; results are expressed as the means \pm SD (* $p < 0.05$, Ctrl vs. bixin treatments). (e) After treated with bixin (40 μM) for 24 h, LO2 cells were fixed and subjected to indirect immunofluorescence staining of Nrf2 (green); nucleus was stained with DAPI (the representative images were shown, scale bar = 100 μm). (f) Immunoblot analysis of Nrf2 in nuclear and cytoplasmic fractions of LO2 cells with or without bixin treatment with the indicated antibodies. Cyto: cytoplasmic fraction of LO2 cells; Nucl: nuclear fraction of LO2 cell.

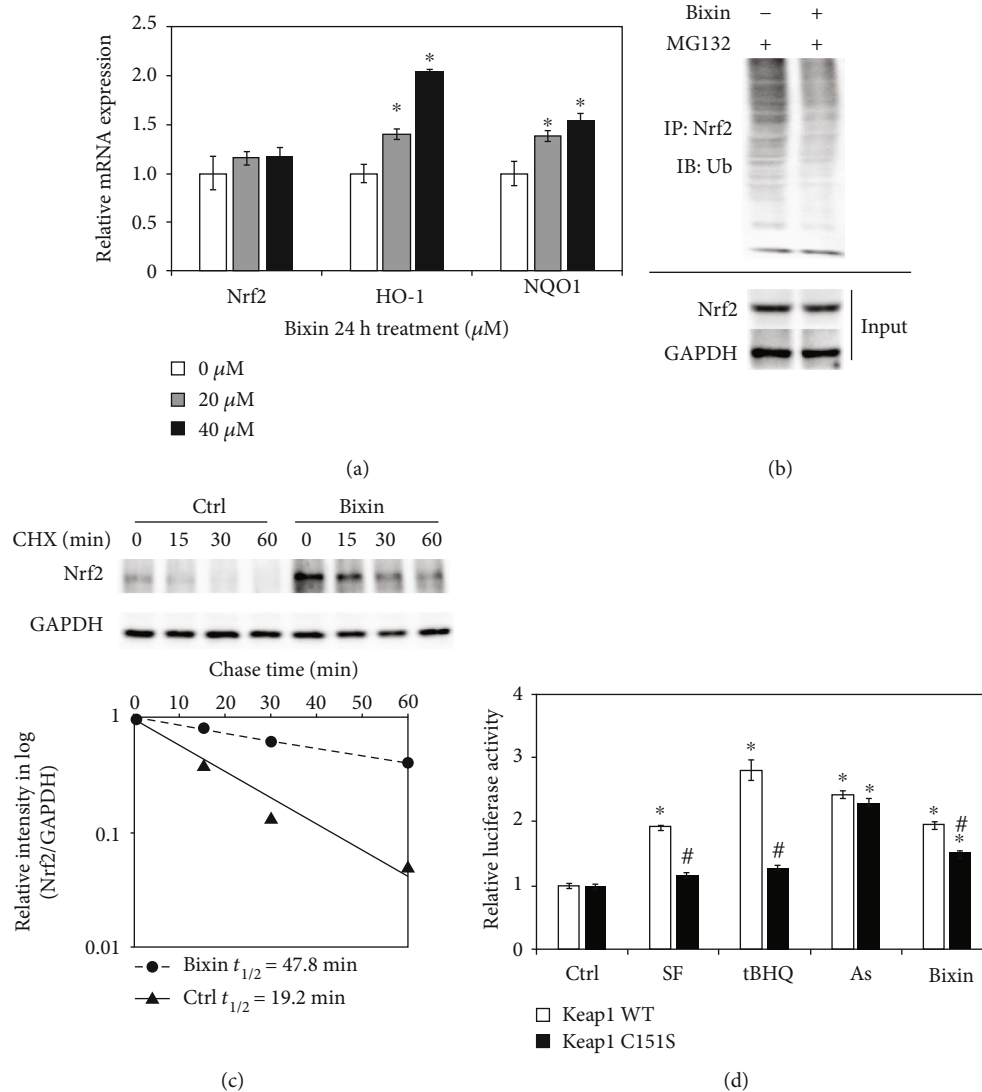


FIGURE 2: Bixin upregulates Nrf2 signals by decreasing Nrf2 ubiquitination and increasing its protein stability in a Keap1 C151-dependent manner. (a) LO2 cells were treated with the indicated doses of bixin for 24 h; the mRNA expression of Nrf2 and its targets (HO-1 and NQO1) was investigated by qRT-PCR ($*p < 0.05$, Ctrl vs. bixin treatments). (b) LO2 cells were treated with bixin (40 μM) for 24 h along with MG132 (10 μM) for 4 h. Anti-Nrf2 immunoprecipitates were analyzed by immunoblot analyses with anti-Ub antibody for the detection of ubiquitin-conjugated Nrf2. (c) LO2 cells were either left untreated or treated with bixin (40 μM) for 24 h. CHX (100 μM) was added for the indicated time points, and cell lysates were subjected to immunoblot analyses with anti-Nrf2 and anti-GAPDH antibodies. The intensity of Nrf2 and GAPDH bands was quantified and plotted against the time after addition of CHX, and the half-life of Nrf2 was calculated. (d) LO2 cells cotransfected with the plasmids expressing either wild-type Keap1 (Keap1 WT) or C151-mutated Keap1 (Keap1 C151S) along with mGst-ARE firefly luciferase and Renilla luciferase reporters were left untreated or treated with the indicated compounds for 16 h. Dual luciferase activities were measured, and the data are expressed as the means \pm SD ($*p < 0.05$, Ctrl vs. compound-treated groups; $\#p < 0.05$, Keap1 WT vs. Keap1 C151S group).

that bixin could attenuate the lipid accumulation, maintain the redox balance upon FFA exposure, and protect cells from FFA-caused cell apoptosis through Nrf2 signals.

3.5. Bixin Blunts Hepatosteatosis and Reduces Circulating Lipid Levels in HFD-Fed Mice through Nrf2 Signals. To explore the impacts of bixin on the regulation of Nrf2 signals in the process of hepatic lipid metabolism, Nrf2 WT and KO mice with a long-term HFD were employed in this study. The duration of HFD feeding and bixin administration is shown

in Figure 5(a). There is no significant difference of food and water consumption among the indicated group of mice (Figures 5(b) and 5(c)). After 25 weeks on the HFD, body weight (BW), the ratio of liver weight to BW (LW/BW), liver TG contents, and liver TC contents were significantly increased, which was inhibited by bixin in Nrf2 WT mice (Figures 5(d)–5(g)). And Nrf2 KO mice exhibited aggravated hepatic steatosis in comparison with HFD-fed mice, showing increased levels of BW, LW/BW, and liver TG contents, which could not be decreased by bixin administration. In

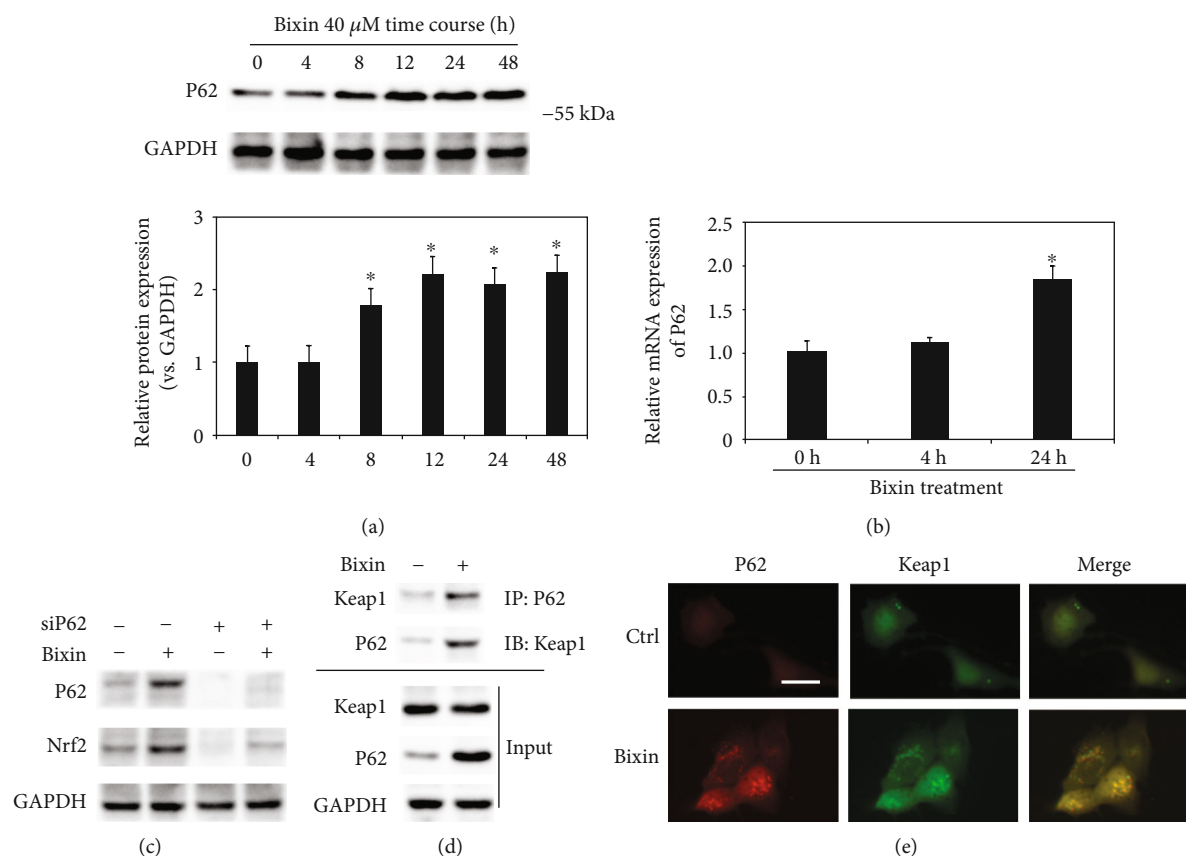


FIGURE 3: Bixin activates Nrf2 by the upregulation of P62. (a) LO2 cells were treated with bixin 40 μ M for the indicated time. Cell lysates were subjected to immunoblot analyses with the indicated antibodies. Quantification of relative protein expression was determined; results are expressed as the means \pm SD ($*p < 0.05$, Ctrl vs. bixin treatments). (b) LO2 cells were treated with bixin 40 μ M for 4 h and 24 h. mRNA was extracted, and P62 mRNA expression was detected by qRT-PCR assay; results are expressed as the means \pm SD ($*p < 0.05$, Ctrl vs. bixin treatments). (c) LO2 cells were transfected with nontargeted siRNA or P62-targeted siRNA for 24 h, and then treated with bixin 40 μ M for another 24 h. The indicated protein expression was investigated by immunoblot analysis. (d) LO2 cells were treated with bixin (40 μ M) for 24 h. Cell lysates were immunoprecipitated with the anti-P62 antibody and analyzed by immunoblot analyses with the anti-Keap1 antibody. The total protein expression was analyzed by immunoblot assay with the anti-P62, anti-Keap1, and anti-GAPDH antibodies (input). (e) LO2 cells were treated with bixin (40 μ M) for 24 h. The cells were fixed and subjected to indirect immunofluorescence staining of P62 (red) and Keap1 (green).

addition, the circulating lipid levels were also investigated. After 25 weeks on the HFD, both Nrf2 WT and KO mice developed marker hypercholesterolemia. Serum total cholesterol (TC), serum low-density lipoprotein (LDL), and serum high-density lipoprotein (HDL) cholesterol levels showed a little increase in Nrf2 KO mice without significant difference (Figures 5(f)–5(k)). Bixin could reduce the levels of serum TC, serum LDL, and serum HDL only in Nrf2 WT mice as well. In addition, the hepatic functional changes were measured accordingly; serum aminotransferase (ALT) and aspartate aminotransferase (AST) were determined. HFD feeding increased the levels of ALT and AST, which were blunted by bixin administration (Figures 5(l) and 5(m)). Oil Red O staining exhibited widespread lipid vacuoles deposited in the liver sections of both Nrf2 WT and KO mice with HFD. And bixin administration could only decrease the lipid accumulation in the livers of Nrf2 WT mice (Figure 5(n)). Taken together, these results demonstrated that bixin could reduce the lipid accumulation and improve liver dysfunction in the Nrf2-dependent manner.

3.6. Bixin Upregulates Nrf2 Signals and PPAR α Involved in HFD-Induced Hepatic Steatosis. To further explore the feasibility of Nrf2 signals regulated by bixin in prevention against HFD-induced hepatic steatosis, H&E staining was then performed to investigate the tissue pathology. Consistent with the Oil Red O staining, H&E staining revealed cell ballooning in the liver of HFD-fed mice in both Nrf2 WT and KO mice. In addition, Nrf2 deficiency aggravated the lipid accumulation in the liver tissue section, which is consistent with Figures 5(e) and 5(f). Bixin injection did not cause any pathological changes of the tissue. Importantly, in Nrf2 WT mice fed with HFD and cotreated with bixin, hepatic pathological changes were ameliorated (Figure 6(a)). Then, the related protein expression was next detected (Figure 6(b)). HFD induced the expression of fatty acid synthase (FASN), an indicator of liver steatosis in both Nrf2 WT and KO mice. And the expression of FASN is higher in the liver of Nrf2 KO mice as well. Besides that, the expression of P62 was increased with bixin treatment in both Nrf2 WT and KO mice. The protein expression of Nrf2 and its targets

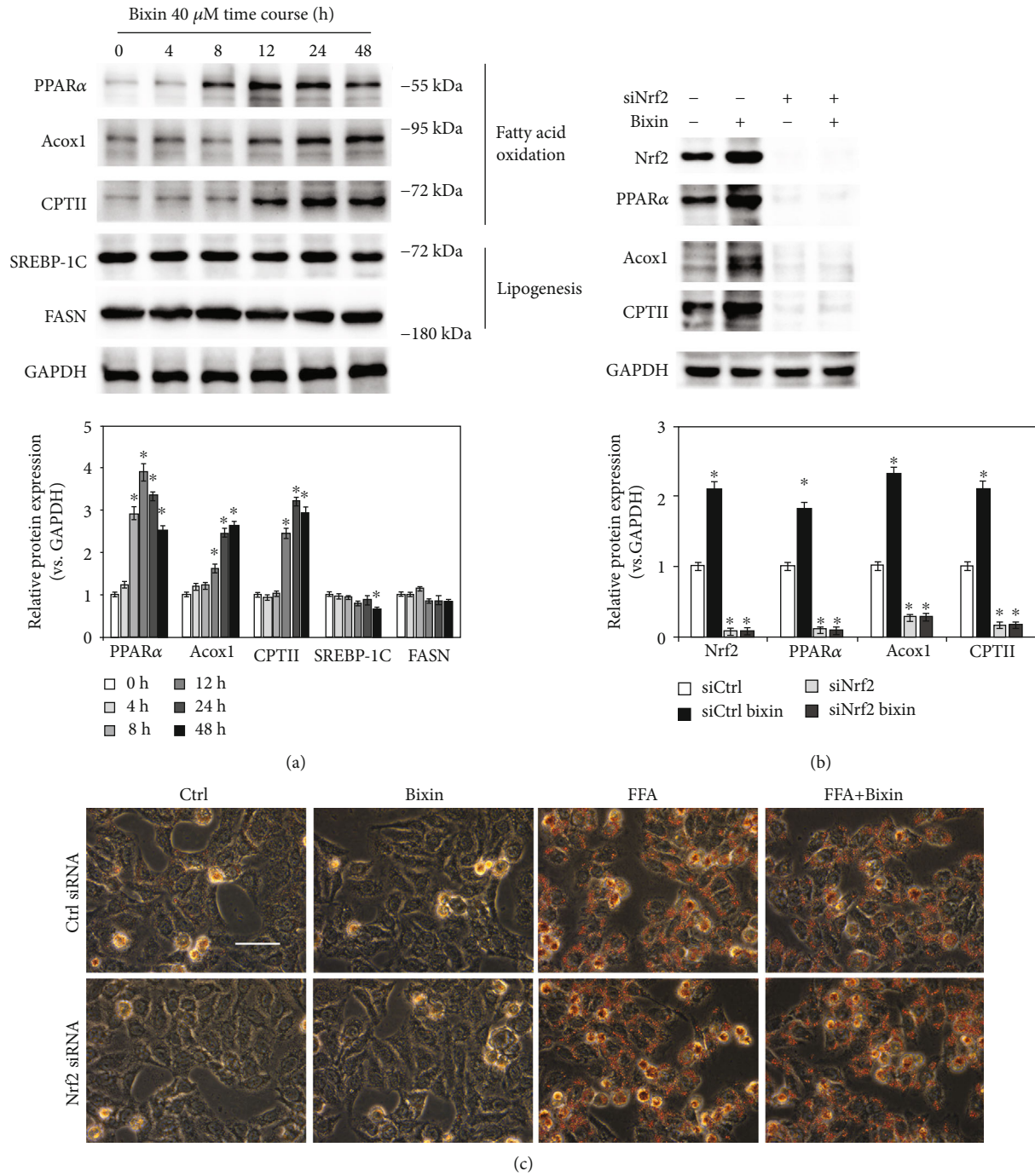


FIGURE 4: Continued.

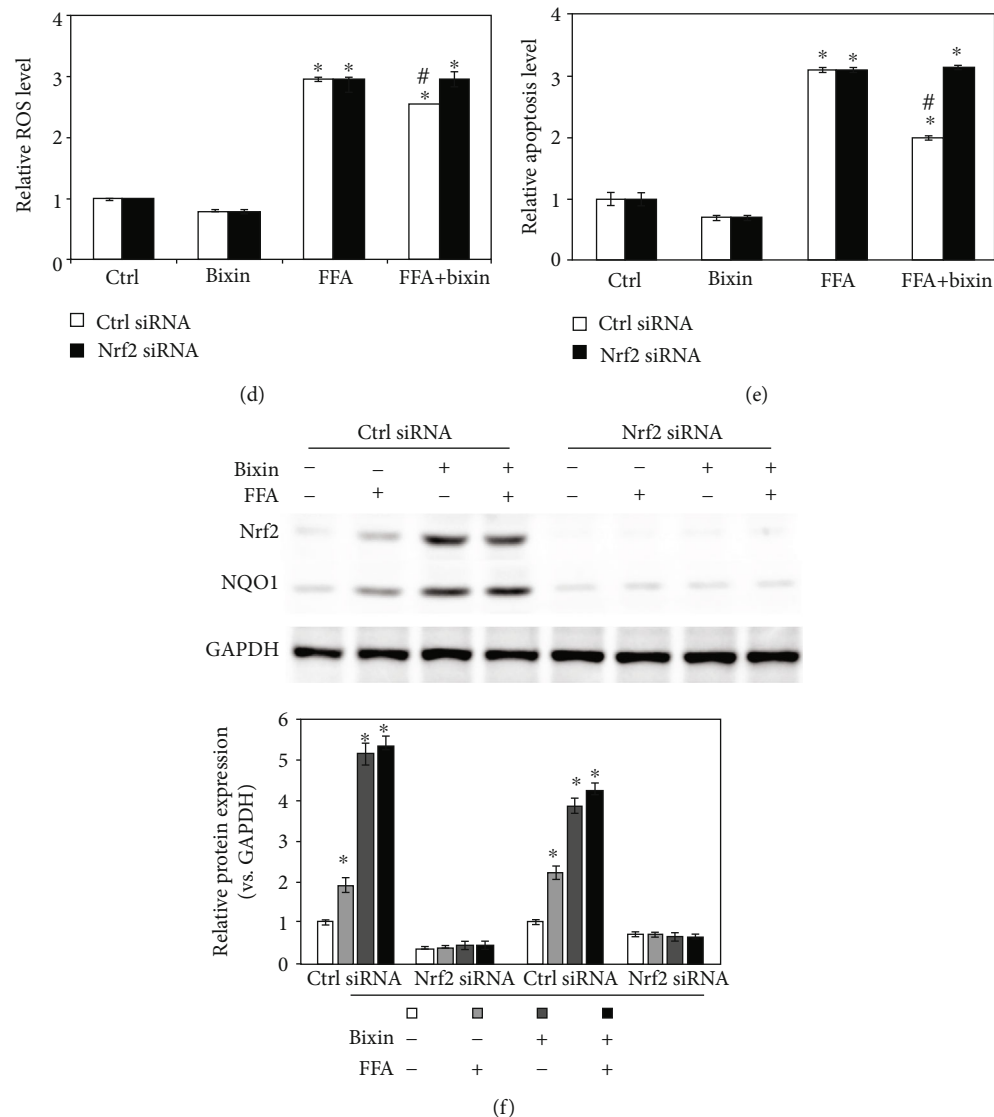


FIGURE 4: Bixin protects LO2 cells from FFA-induced lipid accumulation and cytotoxicity in an Nrf2-dependent manner. (a) LO2 cells were treated with the indicated time points of bixin (40 μ M). The cell lysates were subjected to the immunoblot analyses with the indicated antibodies. (b) LO2 cells were transfected with Ctrl or Nrf2 siRNA for 24 h. After pretreatment of bixin (40 μ M) for 24 h, the indicated protein expression was detected by immunoblot analysis. Quantification of relative protein expression was determined; results are expressed as the means \pm SD ($*p < 0.05$, Ctrl vs. treatment). (c) After transfected with siRNAs, the cells were exposed with FFA 1 mM for another 24 h cells. Cells were fixed and subjected to Oil Red O staining. The representative images from each treatment are shown (scale bar: 50 μ m). (d) Cells were harvested for the detection of oxidative stress caused by FFA. Harvested cells were stained with H₂DCFDA; then, the levels of ROS were detected. (e) The levels of cell apoptosis were determined. Results are expressed as the means \pm SD ($*p < 0.05$, Ctrl vs. treatment groups; $#p < 0.05$, FFA group vs. FFA+bixin group). (f) The cell lysates were subjected to immunoblot analyses with the indicated antibodies to investigate the efficiency of Nrf2 siRNA transfection. Quantification of relative protein expression was determined; results are expressed as the means \pm SD ($*p < 0.05$, Ctrl vs. treatments).

(NQO1, HO-1) increased in the liver tissue of Nrf2 WT mice with bixin injection, HFD feeding, or combination compared with the control group. Then, the expression of PPAR α and its targets (Acox1, CPTII) was explored in the liver sections of both Nrf2 WT and KO mice. Consistent with the in vitro study, bixin could increase the expression of PPAR α and its targets via Nrf2. In Nrf2 WT mice, the expression of PPAR α and its targets (Acox1, CPTII) increased in the bixin, HFD, and combination groups of mice. And there is no significant induction of lipid metabolism-related protein (PPAR α and

its targets) in the liver with Nrf2 deficiency. Interestingly, it was also reported that using combined supplementations such as DHA and HT is warranted to prevent liver steatosis through regulating PPAR α and Nrf2 signals. Given this, these results indicated that bixin upregulates Nrf2 signals and PPAR α involved in HFD-induced hepatic steatosis.

3.7. Bixin Attenuates the Hepatic Inflammation and Blunts the Liver Abnormality through Nrf2. H&E staining exhibited the HFD-caused liver steatosis combined with the infiltration

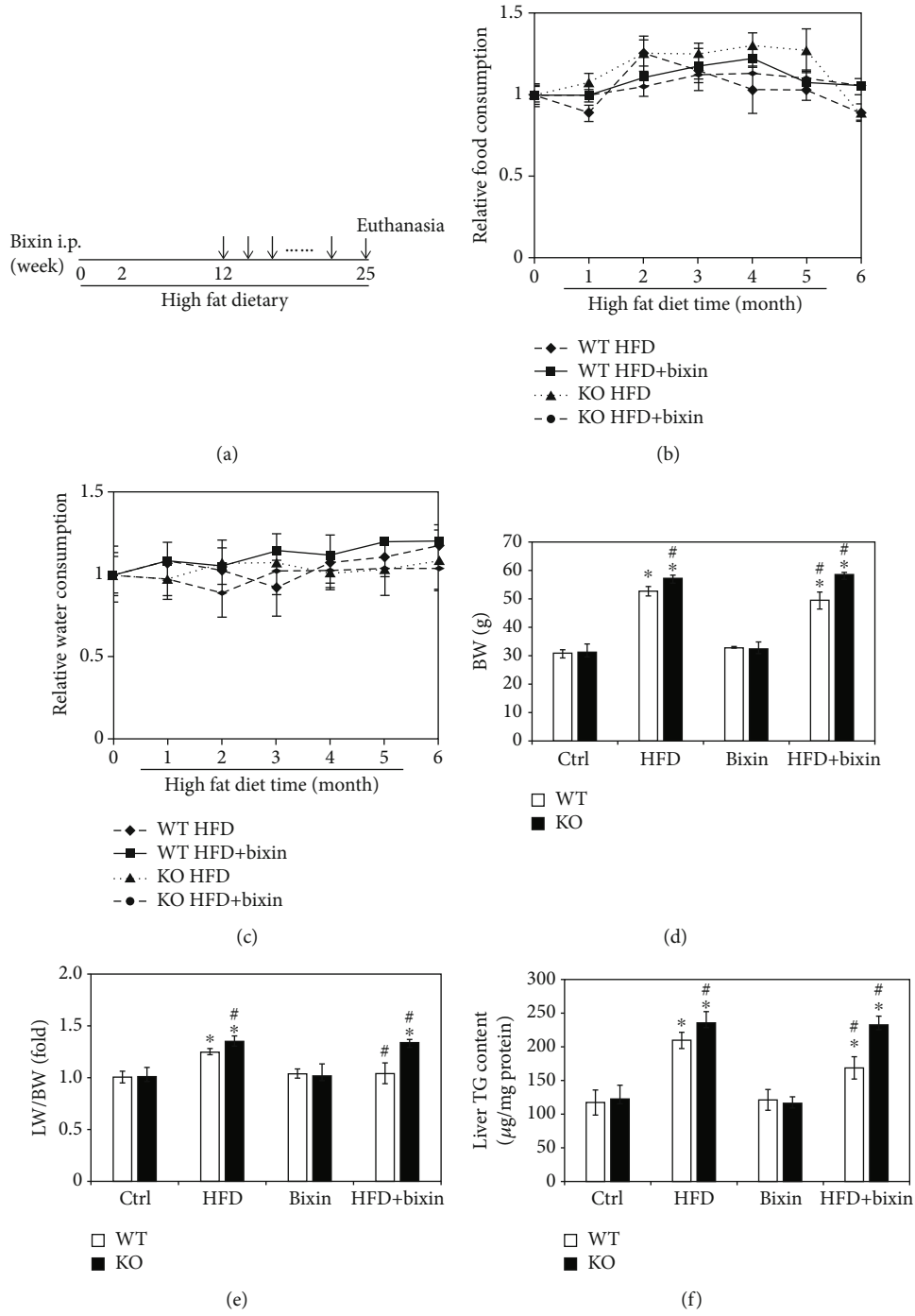


FIGURE 5: Continued.

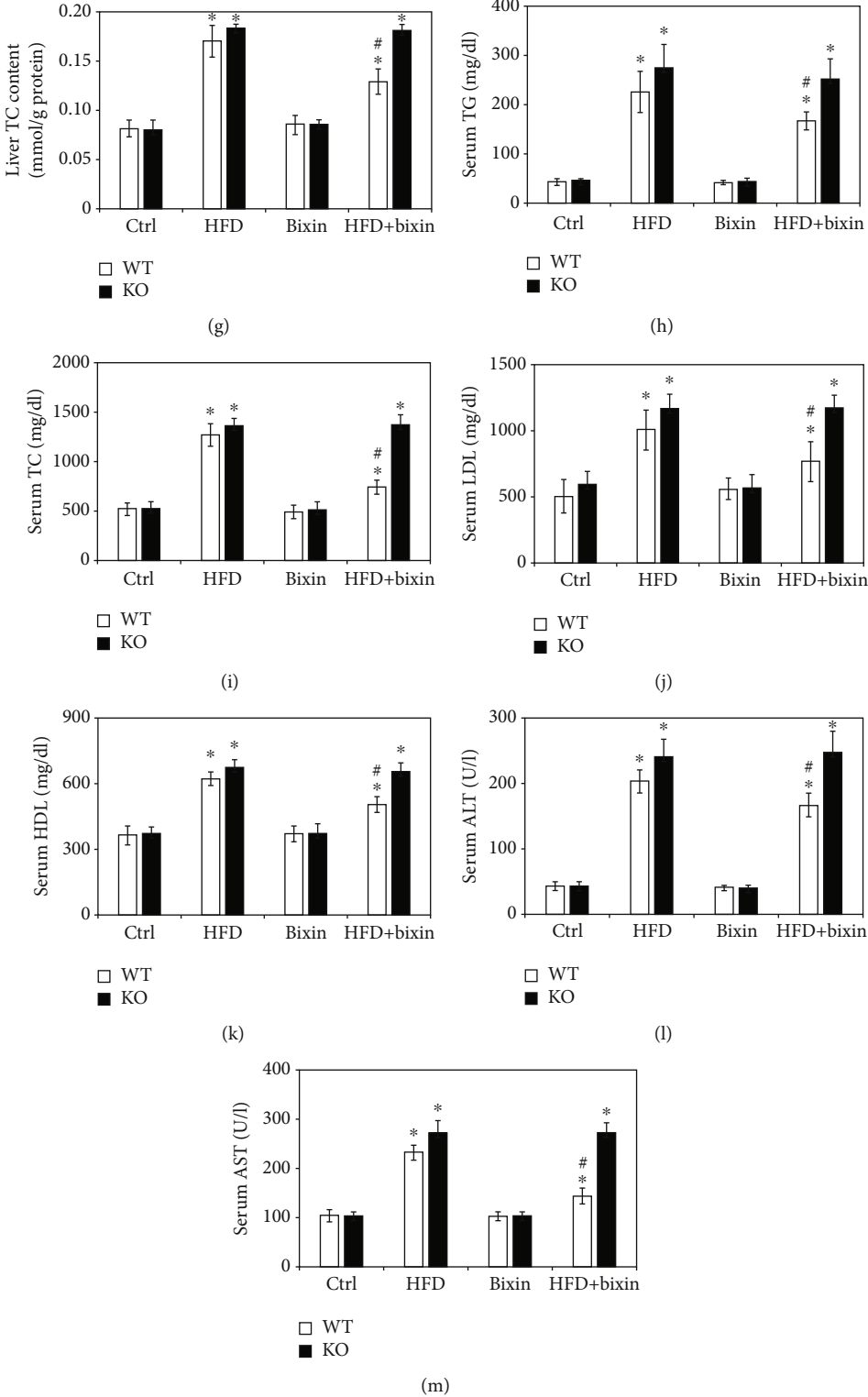


FIGURE 5: Continued.

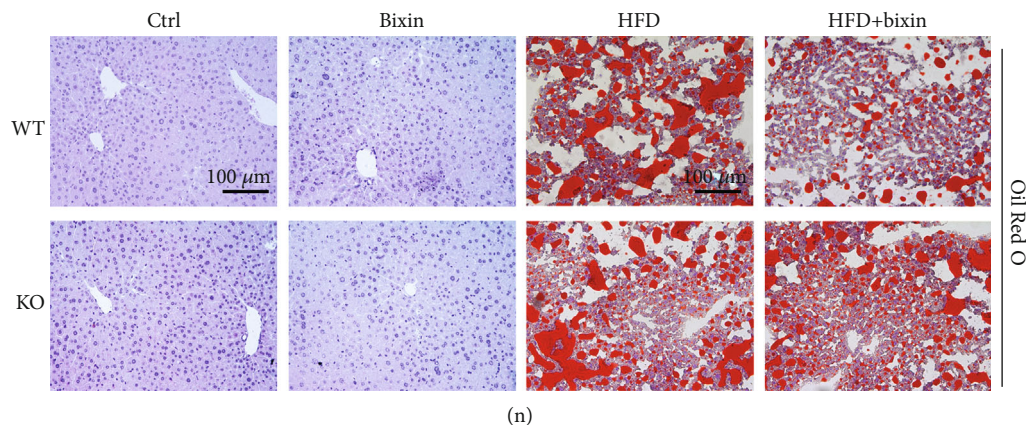


FIGURE 5: Bixin blunts hepatosteatosis and reduces circulating lipid levels in HFD-fed mice through Nrf2 signals. (a) Schematic representation of HFD feeding and bixin administration duration in Nrf2 WT and KO mice. (b) Food consumption, (c) water consumption, (d) BW, (e) LW/BW, (f) liver TG content, (g) liver TC content, (h) serum TG, (i) serum TC, (j) serum LDL, (k) serum HDL, (l) serum ALT, and (m) serum AST of mice with the indicated treatments are provided. Results are expressed as the means \pm SD ($n = 10$; * $p < 0.05$, Ctrl vs. treatment groups; # $p < 0.05$, HFD group vs. HFD+bixin group). (n) Liver tissue sections from different groups of Nrf2 WT and Nrf2 KO mice were subjected to Oil Red O staining ($n = 10$; scale bar = $100 \mu\text{m}$. Representative images from each group are shown).

of inflammation cells. NF- κ B is the most common signal regulating inflammatory response, and the protein levels of p-P65 were employed to assess the activation of NF- κ B. A significant increase of p-P65 protein was observed with long-term HFD in both Nrf2 WT and KO mice. Bixin alone did not affect either p-P65 or P65 expression. In the HFD-fed Nrf2 WT mice injected with bixin, p-P65 protein levels were significantly decreased compared to those in HFD-fed mice (Figure 7(a)). And the qRT-PCR analysis of interleukin-(IL-) 6 and TNF- α confirmed that HFD-fed activated NF- κ B in both types of mice and bixin attenuated this activation only in Nrf2 WT mice (Figure 7(b)). Next, IHC analysis for 8-hydroxy-2'-deoxyguanosine (8-oxo-dG) was performed to detect HFD-caused oxidative DNA damage. HFD dramatically enhanced 8-oxo-dG staining in both types of mice, indicating the serious oxidative stress in the tissue, which could adoptively induce Nrf2 signals. Bixin itself did not have any effect, but could suppress 8-oxo-dG staining caused by HFD in Nrf2 WT mice (Figure 7(c) and S1). To further confirm that, the cell apoptosis was investigated by TUNEL assay. HFD-fed-caused cell apoptosis could be repressed in only Nrf2 WT mice as showed in Figure 7(d) and S1. Taken together, these results indicated that bixin attenuates the hepatic inflammation and blunts the liver abnormality in the Nrf2-dependent manner.

4. Discussion

NAFLD is a common liver disease worldwide. Hepatic steatosis and inflammation are the main characteristics of NAFLD, which also affect the prognosis as well [7, 37]. An urgent need exists for the exploration of efficient strategies that prevent and limit lipid accumulation and inflammatory response in the duration of NAFLD. Bixin, extracted from the seeds of *Bixa orellana*, has emerged as defined antioxidant and anti-inflammatory properties, which could prevent oxidative DNA damage and lipid peroxidation. And in our pre-

vious study, we identified bixin is a novel Nrf2 activator, which could suppress the NF- κ B regulated inflammatory response and improve the lung fibrosis through inhibition of TGF β 1 signals in an Nrf2-dependent manner [22, 26]. Nrf2 serves as an important role against inflammation and has been confirmed to suppress HFD-induced oxidative stress with hydroxytyrosol administration. And according to the previous studies, AR-EVOO supplementation reversed IRD-induced oxidative stress, lipid peroxidation, and protein oxidation through NF- κ B inactivation. Based on this, here we mainly focused on the mechanism of Nrf2 signals' activation by bixin and explored its potential feasibilities in HFD-caused hepatic steatosis and inflammatory response.

In this study, we demonstrated that bixin activates Nrf2 signals at the posttranscriptional level by decreasing the Nrf2 ubiquitination and stabilizing its protein expression (Figure 1). We found that the induction of Nrf2 signals was partially related with the critical C151 sensor residue in Keap1 (Figure 2). In addition, bixin could also enhance the protein and mRNA expression of P62, which could interact with Keap1 "Kleeh" domain through its "STGE" motif (Figure 3). Thus, bixin administration could activate Nrf2 signals through two different mechanisms: (i) canonical mechanism, which modifies the critical cysteine residues in Keap1, leading to a conformational change of Keap1-Cul3-E3 complex that releases the bind with DLG motif of Nrf2 and subsequently stabilized Nrf2 [32] and (ii) noncanonical mechanism that P62 binds with the Kelch domain of Keap1 with its pSTGE motif to stabilize Nrf2 [33].

The induction of Nrf2 signals inhibited the NF- κ B signaling pathway and decreased the oxidative DNA damage, which attenuated inflammatory response, cell apoptosis, and tissue functional disorder and histological damage (Figures 4–7). In addition, according to the previous reports, Nrf2 signals activated PPAR α signals, which can restrain lipid peroxidation and attenuate FFA accumulation in the tissues [36]. Together with the report that bixin protects

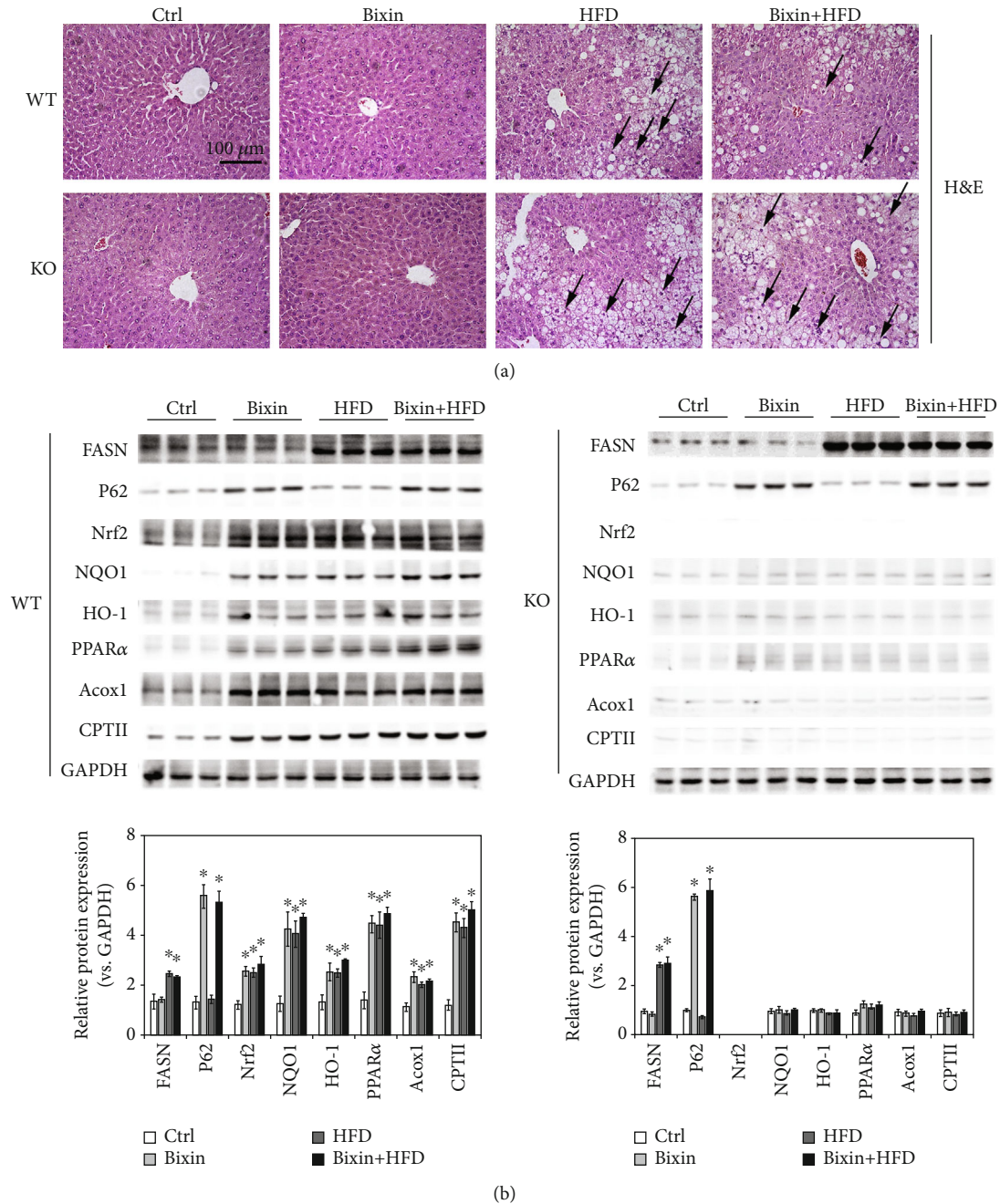


FIGURE 6: Bixin upregulates Nrf2 signals and PPAR α involved in HFD-induced hepatic steatosis. (a) Liver tissue sections from different groups of Nrf2 WT and Nrf2 KO mice were subjected to Oil Red O staining; black arrow indicates the infiltration of inflammatory cells. ($n = 10$; scale bar = $100 \mu\text{m}$. Representative images from each group are shown). (b) Liver tissue lysates from each group were subjected to immunoblot analyses with the indicated antibodies. Representative blots of three independent samples from each group were shown; quantification of relative protein expression was determined; results are expressed as the means \pm SD ($n = 10$; $*p < 0.05$, Ctrl vs. treatment groups; $\#p < 0.05$, HFD group vs. HFD+bixin group).

against lipid peroxidation, the expression of PPAR α and its targets (Acox1 and CPTII) was investigated (Figures 4(a) and 4(b)) [38]. We found that PPAR α and its targets were upregulated by bixin in a dose- and time-dependent manner (Figure 4(a)). As a result, bixin decreased the accumulation of lipid in the cells and liver tissues as well, while bixin could not improve the situation in the cells with Nrf2-siRNA transfection, which indicated that bixin regulated the PPAR α signals

and suppressed the lipid accumulation via Nrf2 (Figures 4(c) and 6(b)). Our next step of study will directly focus on the regulation of Nrf2 and PPAR α signals by bixin and its role in the lipid metabolism.

Then, in this work, we also unveiled the mechanism of P62 induced by bixin on the induction of Nrf2 signals. We found that bixin treatment increased the level of P62 (Figures 3(a) and 3(b)). According to the previous studies,

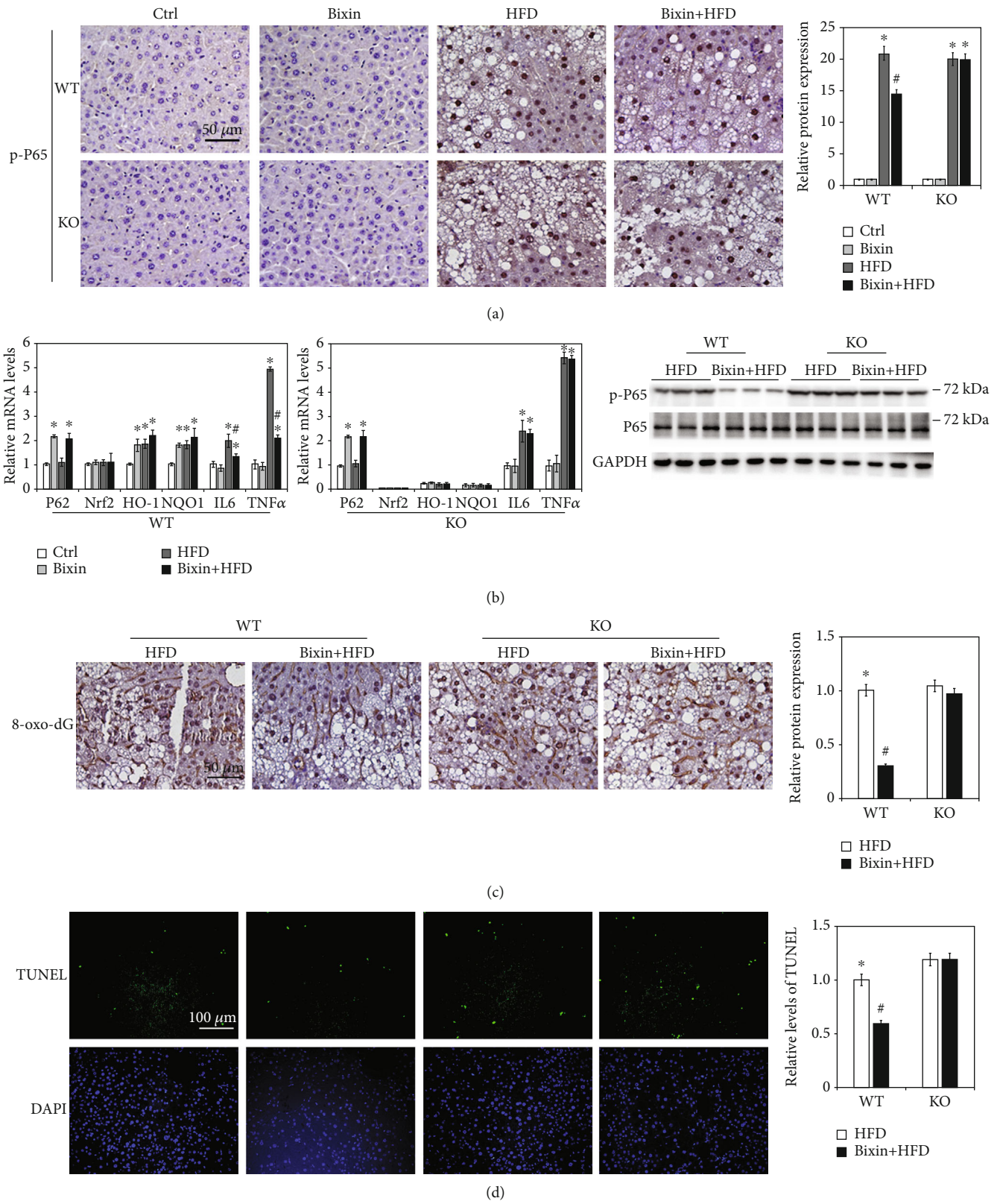


FIGURE 7: Continued.

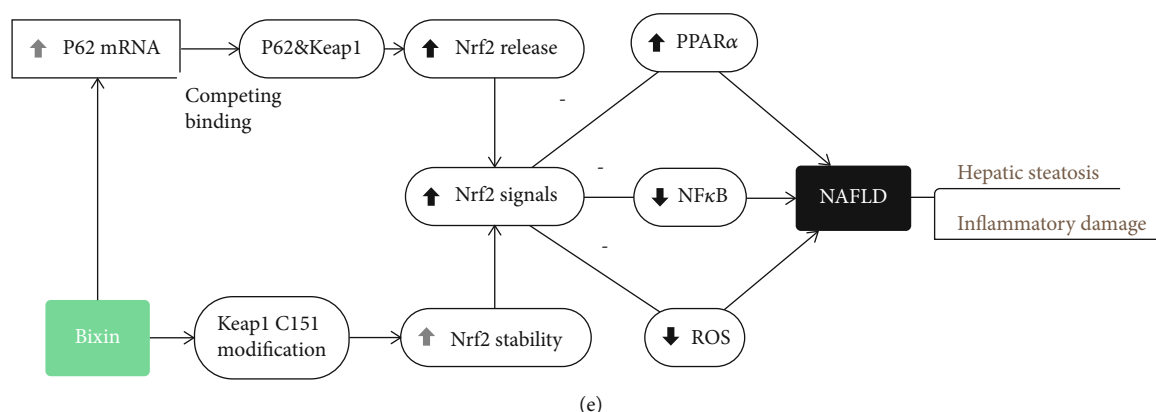


FIGURE 7: Bixin attenuates the hepatic inflammation and blunts the liver abnormality through Nrf2. (a) Liver tissue sections from each group of mice were subjected to IHC staining of p-P65. (b) The total RNA from different group was extracted. mRNA levels of P62, Nrf2, HO-1, NQO1, IL-6, and TNF- α were measured by qRT-PCR assay; results are expressed as the means \pm SD (* $p < 0.05$, Ctrl vs. treatment groups; # $p < 0.05$, FFA group vs. FFA+bixin group). (c) The IHC staining of 8-oxo-dG in the liver tissue from the HFD and bixin+HFD groups of Nrf2 WT and KO mice was performed. (d) TUNEL staining of liver tissue from the HFD and bixin+HFD groups of Nrf2 WT and KO mice (DAPI indicates the nucleus in liver tissues). Representative images from each group are shown ($n = 6$; scale bar = 50 or 100 μm ; * $p < 0.05$, Ctrl vs. treatment groups; # $p < 0.05$, HFD group vs. HFD+bixin group). (e) Proposed model for the therapeutic action of bixin against NAFLD: bixin administration could activate Nrf2 signals through two different mechanisms: (i) canonical mechanism, which modifies the critical cysteine residues in Keap1, leading to a conformational change of Keap1-Cul3-E3 complex that releases the bind with DLG motif of Nrf2 and subsequently stabilized Nrf2 and (ii) noncanonical mechanism that P62 binds with the Kelch domain of Keap1 with its pSTGE motif to stabilize Nrf2. The upregulation of Nrf2 improves the hepatic steatosis and inflammatory damage.

there is a “STGE” domain in the protein of P62, which could interact with the Kelch domain of Keap1, leading to the release of Nrf2 [39–41]. Therefore, we analyzed the interaction of P62 and Keap1 by immunoprecipitation and immunofluorescence (Figures 3(d) and 3(e)). After bixin treatment, the binding of P62 and Keap1 was increased as data shown in Figure 4(d), which indicated that bixin activated Nrf2 by increasing P62 to connect with Keap1. And silencing the P62 expression, which reduced this interaction, could affect the increase of Nrf2 caused by bixin (Figure 4(c)). In addition, as demonstrated previously, there are two different mechanisms of Nrf2 induction [32, 34, 42]. ROS and most of classical Nrf2 inducers activate Nrf2 by modification of critical cysteine residues in Keap1, which usually causes the obvious cytotoxicity even though Nrf2 expression can be dramatically increased accordingly, such as the upregulation of Nrf2 caused by HFD in Figure 6(b) [43]. Here except for the canonical mechanism, bixin activated Nrf2 via the induction of P62, which may be contributed to its low toxicity characteristic. In addition, compared with single treatment, the Nrf2 signaling pathway did not show further increase in the liver of mice from the combination group. The reason for this may be because bixin pretreatment could activate Nrf2 signals, which upregulate the antioxidant capability in the tissue and directly polish the accumulative lipid-caused ROS and protect the tissue cells from the oxidative stress damage.

Cumulative studies have reported that NAFLD is the hepatic manifestation of metabolic syndrome [5, 44]. For example, the hepatic steatosis and inflammation could be caused by the abnormal lipid metabolism and chronic inflammation in the adipose tissue in the metabolic diseases, which means that the hepatic disorder would be solved by

etiological correction [45, 46]. But as we have known, these kinds of diseases are usually complicated with multiple factors for their initiation and development, which are difficult to target and treat with. Bixin here was conferred with the cytoprotection to the liver tissue against lipid accumulation and inflammation induced by HFD-fed mice, which is important for the tissues that have already been injured. Bixin i.p. injection could also increase the antioxidant and inflammatory capability of other tissues in HFD-caused metabolic syndrome, which may cooperatively improve these hepatic abnormalities as well. Bixin-based Nrf2-directed systemic intervention may also provide therapeutic benefit in protecting other organs in the process of metabolic syndrome.

5. Conclusion

Bixin activated the Nrf2 signals through both canonical and noncanonical mechanisms and represents a prototype Nrf2 activator that displays cytoprotective activity upon system administration targeting hepatic steatosis and oxidant inflammation originating from long-term HFD-fed mice.

Abbreviations

ALT:	Alanine aminotransferase
AST:	Aspartate transaminase
BW:	Body weight
CA:	Cinnamaldehyde
CHX:	Cycloheximide
Cp:	Crossing point
DMEM:	Dulbecco's modified Eagle's medium
FATPs:	Fatty acid transport proteins
FDA:	Food and Drug Administration

HDL:	High-density lipoprotein
H&E:	Hematoxylin and eosin
HFD:	High-fat diet
HRP:	Horseradish peroxidase
IHC:	Immunohistochemistry
Keap1:	Kelch-like ECH-associated protein 1
KO:	Knockout
LDL:	Low-density lipoprotein
IL-6:	Interleukin-6
NAFLD:	Nonalcoholic fatty liver disease
NASH:	Nonalcoholic steatohepatitis
Nrf2:	NF-E2 p45-related factor 2
PPAR α :	Peroxisome proliferator-activated receptor α
ROS:	Reactive oxygen species
SD:	Standard deviations
SF:	Sulforaphane
T-I:	Tanshinone I
TC:	Total cholesterol
TG:	Triglyceride
WT:	Wild-type
8-oxo-dG:	8-Hydroxy-2'-deoxyguanosine.

Data Availability

The data used to support the findings of this study are available from the corresponding author upon request.

Conflicts of Interest

The authors have declared that no competing interest exists.

Acknowledgments

The grants that supported our study are as follows: the National Natural Science Foundation of China (81703205), the Foundation from Chongqing Yuzhong District Science and Technology Bureau (201930), a project funded by the Priority Academic Program Development of Jiangsu Higher Education Institutions (PAPD), and the Natural Science Foundation of Chongqing (cstc2020jcyj-msxm3187).

Supplementary Materials

Supplementary Figure 1: the IHC staining of 8-oxo-dG and TUNEL staining of liver tissue from the Ctrl and bixin groups of Nrf2 WT and KO mice (DAPI indicates the nuclear in the liver tissues; $n = 6$; scale bar = 100 μm). (*Supplementary Materials*)

References

- [1] G. Musso, M. Cassader, and R. Gambino, "Non-alcoholic steatohepatitis: emerging molecular targets and therapeutic strategies," *Nature reviews Drug discovery*, vol. 15, no. 4, pp. 249–274, 2016.
- [2] N. Katsiki, D. P. Mikhailidis, and C. S. Mantzoros, "Non-alcoholic fatty liver disease and dyslipidemia: an update," *Metabolism*, vol. 65, no. 8, pp. 1109–1123, 2016.
- [3] M. E. Rinella and A. J. Sanyal, "Management of NAFLD: a stage-based approach," *Nature Reviews. Gastroenterology & Hepatology*, vol. 13, no. 4, pp. 196–205, 2016.
- [4] M. Eslam, L. Valenti, and S. Romeo, "Genetics and epigenetics of NAFLD and NASH: clinical impact," *Journal of Hepatology*, vol. 68, no. 2, pp. 268–279, 2018.
- [5] X. Zhang, X. Ji, Q. Wang, and J. Z. Li, "New insight into inter-organ crosstalk contributing to the pathogenesis of non-alcoholic fatty liver disease (NAFLD)," *Protein & Cell*, vol. 9, no. 2, pp. 164–177, 2018.
- [6] E. Vilar-Gomez and N. Chalasani, "Non-invasive assessment of non-alcoholic fatty liver disease: clinical prediction rules and blood-based biomarkers," *Journal of Hepatology*, vol. 68, no. 2, pp. 305–315, 2018.
- [7] S. L. Friedman, B. A. Neuschwander-Tetri, M. Rinella, and A. J. Sanyal, "Mechanisms of NAFLD development and therapeutic strategies," *Nature Medicine*, vol. 24, no. 7, pp. 908–922, 2018.
- [8] J. Mun, S. Kim, H. G. Yoon et al., "Water extract of *Curcuma longa* L. ameliorates non-alcoholic fatty liver disease," *Nutrients*, vol. 11, no. 10, 2019.
- [9] Z. Gong, E. Tas, S. Yakar, and R. Muzumdar, "Hepatic lipid metabolism and non-alcoholic fatty liver disease in aging," *Molecular and Cellular Endocrinology*, vol. 455, pp. 115–130, 2017.
- [10] L. Zhang, H. X. Li, W. S. Pan et al., "Administration of methyl palmitate prevents non-alcoholic steatohepatitis (NASH) by induction of PPAR- α ," *Biomedicine & Pharmacotherapy*, vol. 111, pp. 99–108, 2019.
- [11] L. A. Videla, R. Rodrigo, M. Orellana et al., "Oxidative stress-related parameters in the liver of non-alcoholic fatty liver disease patients," *Clinical science*, vol. 106, no. 3, pp. 261–268, 2004.
- [12] L. Malaguarnera, R. Madeddu, E. Palio, N. Arena, and M. Malaguarnera, "Heme oxygenase-1 levels and oxidative stress-related parameters in non-alcoholic fatty liver disease patients," *Journal of Hepatology*, vol. 42, no. 4, pp. 585–591, 2005.
- [13] I. M. Copple, A. T. Dinkova-Kostova, T. W. Kensler, K. T. Liby, and W. C. Wigley, "NRF2 as an emerging therapeutic target," *Oxidative Medicine and Cellular Longevity*, vol. 2017, Article ID 8165458, 2 pages, 2017.
- [14] A. P. Gureev, E. A. Shaforostova, and V. N. Popov, "Regulation of mitochondrial biogenesis as a way for active longevity: interaction between the Nrf2 and PGC-1 α signaling pathways," *Frontiers in Genetics*, vol. 10, 2019.
- [15] L. Yang, X. Fan, T. Cui, E. Dang, and G. Wang, "Nrf2 promotes keratinocyte proliferation in psoriasis through up-regulation of keratin 6, keratin 16, and keratin 17," *The Journal of Investigative Dermatology*, vol. 137, no. 10, pp. 2168–2176, 2017.
- [16] Y. Zheng, S. Tao, F. Lian et al., "Sulforaphane prevents pulmonary damage in response to inhaled arsenic by activating the Nrf2-defense response," *Toxicology and Applied Pharmacology*, vol. 265, no. 3, pp. 292–299, 2012.
- [17] R. Zhu, H. Liu, C. Liu et al., "Cinnamaldehyde in diabetes: a review of pharmacology, pharmacokinetics and safety," *Pharmacological Research*, vol. 122, pp. 78–89, 2017.
- [18] S. Tao, Y. Zheng, A. Lau et al., "Tanshinone I activates the Nrf2-dependent antioxidant response and protects against As(III)-induced lung inflammation *in vitro* and *in vivo*,"

- Antioxidants & Redox Signaling*, vol. 19, no. 14, pp. 1647–1661, 2013.
- [19] S. F. Xia, J. Shao, S. Y. Zhao et al., “Niga-ichigoside F1 ameliorates high-fat diet-induced hepatic steatosis in male mice by Nrf2 activation,” *Food & Function*, vol. 9, no. 2, pp. 906–916, 2018.
 - [20] Z. Zhang, J. Chen, S. Zhou et al., “Magnolia bioactive constituent 4-O-methylhonokiol prevents the impairment of cardiac insulin signaling and the cardiac pathogenesis in high-fat diet-induced obese mice,” *International Journal of Biological Sciences*, vol. 11, no. 8, pp. 879–891, 2015.
 - [21] J. Araya, R. Rodrigo, L. A. Videla et al., “Increase in long-chain polyunsaturated fatty acid n-6/n-3 ratio in relation to hepatic steatosis in patients with non-alcoholic fatty liver disease,” *Clinical science*, vol. 106, no. 6, pp. 635–643, 2004.
 - [22] L. Xue, H. Zhang, J. Zhang, B. Li, Z. Zhang, and S. Tao, “Bixin protects against particle-induced long-term lung injury in an NRF2-dependent manner,” *Toxicology research*, vol. 7, no. 2, pp. 258–270, 2018.
 - [23] X. Cai, J. Sheng, C. Tang et al., “Frequent mutations in EGFR, KRAS and TP53 genes in human lung cancer tumors detected by ion torrent DNA sequencing,” *PLoS One*, vol. 9, no. 4, article e95228, 2014.
 - [24] O. Gjyshi, S. Flaherty, M. V. Veettil, K. E. Johnson, B. Chandran, and V. Bottero, “Kaposi’s sarcoma-associated herpesvirus induces Nrf2 activation in latently infected endothelial cells through SQSTM1 phosphorylation and interaction with polyubiquitinated Keap1,” *Journal of Virology*, vol. 89, no. 4, pp. 2268–2286, 2015.
 - [25] Z. Xu and X. Q. Kong, “Bixin ameliorates high fat diet-induced cardiac injury in mice through inflammation and oxidative stress suppression,” *Biomedicine & Pharmacotherapy*, vol. 89, pp. 991–1004, 2017.
 - [26] S. Tao, M. Rojo de la Vega, H. Quijada et al., “Bixin protects mice against ventilation-induced lung injury in an NRF2-dependent manner,” *Scientific Reports*, vol. 6, no. 1, article 18760, 2016.
 - [27] J. Li, Y. Yang, S. Wei et al., “Bixin confers prevention against ureteral obstruction-caused renal interstitial fibrosis through activation of the nuclear factor erythroid-2-related factor2 pathway in mice,” *Journal of Agricultural and Food Chemistry*, vol. 68, no. 31, pp. 8321–8329, 2020.
 - [28] S. Tao, S. L. Park, M. R. de la Vega, D. D. Zhang, and G. T. Wondrak, “Systemic administration of the apocarotenoid bixin protects skin against solar UV-induced damage through activation of NRF2,” *Free Radical Biology & Medicine*, vol. 89, pp. 690–700, 2015.
 - [29] M. C. Jaramillo and D. D. Zhang, “The emerging role of the Nrf2-Keap1 signaling pathway in cancer,” *Genes & Development*, vol. 27, no. 20, pp. 2179–2191, 2013.
 - [30] L. Fão, S. I. Mota, and A. C. Rego, “Shaping the Nrf2-ARE-related pathways in Alzheimer’s and Parkinson’s diseases,” *Ageing Research Reviews*, vol. 54, article 100942, 2019.
 - [31] M. Rojo de la Vega, E. Chapman, and D. D. Zhang, “NRF2 and the hallmarks of cancer,” *Cancer Cell*, vol. 34, no. 1, pp. 21–43, 2018.
 - [32] L. Baird, D. Llères, S. Swift, and A. T. Dinkova-Kostova, “Regulatory flexibility in the Nrf2-mediated stress response is conferred by conformational cycling of the Keap1-Nrf2 protein complex,” *Proceedings of the National Academy of Sciences of the United States of America*, vol. 110, no. 38, pp. 15259–15264, 2013.
 - [33] I. M. Copple, A. Lister, A. D. Obeng et al., “Physical and functional interaction of sequestosome 1 with Keap1 regulates the Keap1-Nrf2 cell defense pathway,” *The Journal of Biological Chemistry*, vol. 285, no. 22, pp. 16782–16788, 2010.
 - [34] X. J. Wang, Z. Sun, W. Chen, Y. Li, N. F. Villeneuve, and D. D. Zhang, “Activation of Nrf2 by arsenite and monomethylarsonous acid is independent of Keap1-C151: enhanced Keap1-Cul3 interaction,” *Toxicology and Applied Pharmacology*, vol. 230, no. 3, pp. 383–389, 2008.
 - [35] S. Tao, S. Wang, S. J. Moghaddam et al., “Oncogenic KRAS confers chemoresistance by upregulating NRF2,” *Cancer Research*, vol. 74, no. 24, pp. 7430–7441, 2014.
 - [36] X. J. Zhao, H. W. Yu, Y. Z. Yang et al., “Polydatin prevents fructose-induced liver inflammation and lipid deposition through increasing miR-200a to regulate Keap1/Nrf2 pathway,” *Redox Biology*, vol. 18, pp. 124–137, 2018.
 - [37] Y. Sumida and M. Yoneda, “Current and future pharmacological therapies for NAFLD/NASH,” *Journal of Gastroenterology*, vol. 53, no. 3, pp. 362–376, 2018.
 - [38] T. Goto, N. Takahashi, S. Kato et al., “Bixin activates PPAR α and improves obesity-induced abnormalities of carbohydrate and lipid metabolism in mice,” *Journal of Agricultural and Food Chemistry*, vol. 60, no. 48, pp. 11952–11958, 2012.
 - [39] A. Lau, Y. Zheng, S. Tao et al., “Arsenic inhibits autophagic flux, activating the Nrf2-Keap1 pathway in a p62-dependent manner,” *Molecular and Cellular Biology*, vol. 33, no. 12, pp. 2436–2446, 2013.
 - [40] Y. Ichimura and M. Komatsu, “Activation of p62/SQSTM1-Keap1-nuclear factor erythroid 2-related factor 2 pathway in cancer,” *Frontiers in Oncology*, vol. 8, 2018.
 - [41] X. Sun, Z. Ou, R. Chen et al., “Activation of the p62-Keap1-NRF2 pathway protects against ferroptosis in hepatocellular carcinoma cells,” *Hepatology*, vol. 63, no. 1, pp. 173–184, 2016.
 - [42] M. Komatsu, H. Kurokawa, S. Waguri et al., “The selective autophagy substrate p62 activates the stress responsive transcription factor Nrf2 through inactivation of Keap1,” *Nature Cell Biology*, vol. 12, no. 3, pp. 213–223, 2010.
 - [43] R. Abeti, A. Baccaro, N. Esteras, and P. Giunti, “Novel Nrf2-inducer prevents mitochondrial defects and oxidative stress in Friedreich’s ataxia models,” *Frontiers in Cellular Neuroscience*, vol. 12, p. 188, 2018.
 - [44] C. D. Byrne and G. Targher, “NAFLD: a multisystem disease,” *Journal of Hepatology*, vol. 62, no. 1, pp. S47–S64, 2015.
 - [45] M. Nikolova-Karakashian, “Sphingolipids at the crossroads of NAFLD and senescence,” *Advances in Cancer Research*, vol. 140, pp. 155–190, 2018.
 - [46] N. L. Gluchowski, M. Becuwe, T. C. Walther, and R. V. Farese Jr., “Lipid droplets and liver disease: from basic biology to clinical implications,” *Nature Reviews. Gastroenterology & Hepatology*, vol. 14, no. 6, pp. 343–355, 2017.

Review Article

The Landscape of Interactions between Hypoxia-Inducible Factors and Reactive Oxygen Species in the Gastrointestinal Tract

Yirui Shao ^{1,2}, Kexing Wang,³ Xia Xiong ¹, Hongnan Liu,¹ Jian Zhou,^{1,2} Lijun Zou,⁴ Ming Qi,^{1,2} Gang Liu ⁵, Ruilin Huang,¹ Zhiliang Tan,¹ and Yulong Yin^{1,2}

¹Hunan Province Key Laboratory of Animal Nutritional Physiology and Metabolic Process, Key Laboratory of Agro-ecological Processes in Subtropical Region, National Engineering Laboratory for Pollution Control and Waste Utilization in Livestock and Poultry Production, Institute of Subtropical Agriculture, Chinese Academy of Sciences, Changsha, 410125 Hunan, China

²University of Chinese Academy of Sciences, Beijing 100008, China

³Laboratory of Animal Nutrition and Human Health, College of Life Sciences, Hunan Normal University, Changsha 410081, China

⁴Laboratory of Basic Biology, Hunan First Normal University, Changsha 410205, China

⁵College of Bioscience and Biotechnology, Hunan Agricultural University, Changsha 410128, China

Correspondence should be addressed to Xia Xiong; xx@isa.ac.cn

Received 29 September 2020; Revised 29 October 2020; Accepted 26 December 2020; Published 21 January 2021

Academic Editor: Si Qin

Copyright © 2021 Yirui Shao et al. This is an open access article distributed under the Creative Commons Attribution License, which permits unrestricted use, distribution, and reproduction in any medium, provided the original work is properly cited.

The gastrointestinal tract (GT) is the major organ involved in digestion, absorption, and immunity, which is prone to oxidative destruction by high levels of reactive oxygen species (ROS) from luminal oxidants, such as food, drugs, and pathogens. Excessive ROS will lead to oxidative stresses and disrupt essential biomolecules, which also act as cellular signaling molecules in response to growth factors, hormones, and oxygen tension changes. Hypoxia-inducible factors (HIFs) are critical regulators mediating responses to cellular oxygen tension changes, which are also involved in energy metabolism, immunity, renewal, and microbial homeostasis in the GT. This review discusses interactions between HIF (mainly HIF-1 α) and ROS and relevant diseases in the GT combined with our lab's work. It might help to develop new therapies for gastrointestinal diseases associated with ROS and HIF-1 α .

1. Introduction

The gastrointestinal tract (GT) is the major place of nutrient digestion and absorption, and it is prone to oxidative destruction by highly reactive oxygen species (ROS) [1, 2]. Reactive oxygen species are byproducts of normal cellular metabolism. They usually contain an unstable number of electrons, and they make them extraordinarily reactive. Excessive ROS do harm to essential biomolecules, including nucleic acids, proteins, and lipids. Accumulated ROS will lead to oxidative stresses, which contribute to various diseases in the GT [3]. However, ROS also act as important signaling molecules in response to growth factors, hormones, and oxygen tension changes [4, 5]. Hypoxia-inducible factors (HIFs) are indispensable transcription factors in response to low oxygen [6]. HIFs have drawn lots of attention from researchers for

their role involved in gastrointestinal energy metabolism, immunity, renewal, and microbial homeostasis. Intriguingly, there are close relationships between ROS and HIFs. This review is aimed at summarizing interactions between HIFs and ROS in the GT to help develop new treatments for gastrointestinal diseases induced by ROS and HIFs.

2. The Role of ROS in the GT

ROS include superoxide ($O_2^{\cdot-}$), hydroxyl radicals (OH \cdot), hydrogen peroxide (H_2O_2), singlet oxygen (1O_2), hypochlorous acid (HOCl), chloramines (RNHCl), and ozone (O_3) [7]. Gastrointestinal ROS are usually classified as endogenous and exogenous ROS. As has been reviewed by Bhattacharyya et al., endogenous ROS mainly comes from mitochondrial electron transport chain (mETC), NADPH oxidase (NOX),

cyclooxygenase (COX), myeloperoxidase (MPO), lipoxygenases (LOXs), xanthine oxidase (XO), and transition metals; correspondingly, food, drink, xenobiotics, cigarettes, and radiation lead to exogenous ROS in the GT [8].

In addition, toxins and environmental stresses can also contribute to exogenous ROS in the GT. Reportedly, aflatoxin B₁ and aflatoxin M₁ treatment inhibited cell viability, enhanced LDH release, and led to DNA damage in Caco-2 cells, which was related to elevated ROS [9]. Patulin also induced endoplasmic reticulum stress and mitochondrial apoptosis in human intestinal cells in the ROS-dependent way [10]. Our lab's work also showed that deoxynivalenol treatment significantly upregulated the MDA levels and downregulated the total antioxidant capacity, which further led to reduced villus height and increased lymphocytes in the piglet ileum and jejunum [11]. The environment is a major source of ROS in the GT. For instance, heat stress led to elevated ROS and MDA levels and reduced antioxidant activity, accounting for increased apoptosis and intestinal permeability in the rat small intestine [12]. In addition, noise also contributes to oxidative stress. Noise-treated rats suffered mast cell degranulation, damages to the endothelial cell membrane, and increased eosinophils in the lamina propria of villi in the intestine, which might be caused by excessive ROS [13]. Additionally, transport stress contributed to oxidative stresses in the intestine, including increased MDA, endotoxin, NOX1, and lactic dehydrogenase (LDH) levels and decreased expression of SOD and tight junction proteins [14]. Our lab's work also showed that weaning stress decreased antioxidant enzyme levels and affected the expression of genes involved in ROS generation in piglets [15]. As mentioned above, multiple variables can affect the generation of ROS and, eventually, lead to oxidative stress-induced diseases in the GT.

Excessive ROS can do harm to DNA, proteins, and lipids. Further, we found that ROS significantly inhibited the proliferation rate, mitochondrial respiration, and antioxidative capacity and contributed to cell apoptosis in IPEC-J2 cells [16]. However, ROS also act as signaling molecules and contribute to defense systems in the body. ROS act as the activator of Ca²⁺ permeable cationic channels formed by transient receptor potential melastatin 2 protein in immune cells [17]. Tyrosine-protein kinase Lyn is a member of the Src family of protein tyrosine kinase, which is involved in multiple cellular signaling transduction [18]. ROS are critical for intestinal epithelial cell activities. NOX-derived O₂^{•-} has been reported to augment host defense in colon epithelial cells [19]. Additionally, NOX-derived ROS plays a key role in modulations of the actin cytoskeleton, monolayer permeability, cell migration, cell proliferation, and focal adhesion kinase phosphorylation [20]. Further, ROS participate in the regulation of bacteria to the host. VvpE is an elastase encoded by an opportunistic gram-negative pathogen *Vibrio vulnificus* [21]. And lipid raft-mediated ROS signaling is essential for the inhibition of mucin 2 expression by VvpE in the intestinal epithelial cells [22]. Further, our work also showed that the low dosage of H₂O₂ might play a feedback regulatory role against oxidative injury via upregulating the expression of UCP2 and mitochondrial proton leak in IPEC-J2 cells [23]. ROS act as signaling molecules in the modulation of various signaling

pathways, leading us to investigate whether ROS participate in the regulation of HIF-1 α .

3. The Role of HIFs in the GT

HIF-1 was first discovered by Semenza and Wang when they studied the transcription of the hypoxia-inducible human erythropoietin gene [24]. HIFs are heterodimers consisting of hypoxia-inducible α -subunit (HIF-1 α , HIF-2 α , and HIF-3 α) and β -subunit (aryl hydrocarbon receptor nuclear translocator (ARNT)/HIF-1 β and ARNT2) [25]. Among them, HIF-1 α is the most ubiquitously expressed [26].

The degradation of HIF- α is mainly regulated on the posttranslational level [27]. HIF- α is continuously synthesized, and it is rapidly degraded by proteasomal pathways under normoxia. However, under hypoxia, the degradation of HIF- α is hindered. As reviewed by Strowitzki et al., the degradation is mainly regulated by HIF prolyl 4-hydroxylases (PHDs): PHD1, PHD2, and PHD3; two prolyl residues in the oxygen-dependent degradation domain of HIF- α -subunits are hydroxylated by PHDs, contributing to the ubiquitination mediated by von Hippel-Lindau (VHL) ubiquitin ligase; factor-inhibiting HIF (FIH) can hydroxylate an asparagine residue in the C-terminal transactivation domain of HIF-1 α ; under hypoxic conditions, the hydroxylation of HIF- α by PHD and FIH is retarded; accumulated HIF- α forms complexes with HIF- β and translocates to the nucleus to initiate transcription of target genes [28].

The physiological gastrointestinal mucosa has a uniquely steep oxygen gradient that the vascularized subepithelial mucosa is rich in oxygen while the luminal epithelium is hypoxic [29]. Moreover, under pathological states such as inflammation, the GT often has reduced oxygen levels [30, 31]. As the central sensor of hypoxia, HIF-1 α governs the transcription of numerous genes, which also act as a double-edged sword in energy metabolism, immunity, renewal, and microbial homeostasis of the GT (Figure 1).

HIF-1 α takes part in gastrointestinal energy metabolism, including glycolysis and nutrient absorption (glucose, lipid, and glutamine) [32, 33]. It was also an essential regulator in gastrointestinal immunity. The knockout of HIF-1 α led to a significant decrease of CD8 $\alpha\alpha^+$ and TCR $\gamma\delta^+$ population in intestinal epithelial cells of mice [34]. Further, activation of HIF-1 α attenuated *C. difficile*-induced colitis in mice [35]. In line with this, suppression of the HIF-1 α /COX-2 pathway contributed to the releases of inflammatory cytokines induced by NF- κ B p65 in the porcine ileum [36]. However, there were also studies that suggest that HIF-1 α contributes to pathological progress in gastrointestinal diseases. As has been reported, Jian-Pi Qing-Chang treatment attenuated the intestinal epithelial permeability and inflammation by inhibiting NF- κ B/HIF-1 α pathways in colitis mice [37]. Further, the interferon-gamma (IFN- γ) induced intestinal epithelial permeability and disruption of the intestinal tight junction by activating HIF-1 α [38]. Similarly, berberine treatment can suppress the activation of HIF-1 α , thus alleviating IFN- γ - and TNF- α -induced intestinal epithelial barrier dysfunction [39].

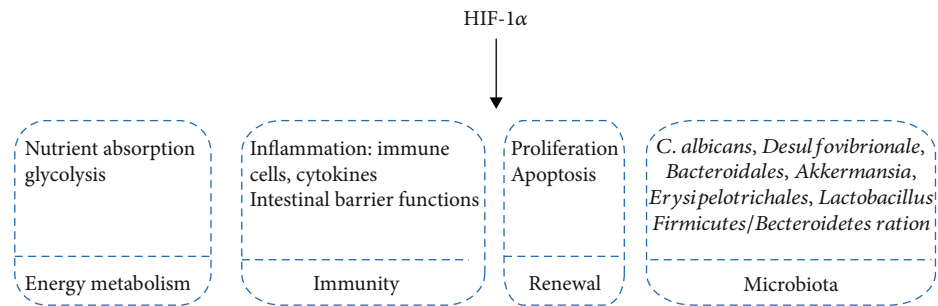


FIGURE 1: The role of HIF-1 α in the gastrointestinal tract. HIF-1 α is involved in gastrointestinal energy metabolism, immunity, renewal, and microbiota.

Further, HIF-1 α played a key role in the renewal of the GT. A recent study reported that downregulated HIF-1 α inhibited the proliferation of gastric cancer cells [40, 41]. Moreover, the transcription factor Krüppel-like factor 2 overexpression inhibited proliferation and promoted apoptosis by suppressing the expression of Notch-1 via inhibition of HIF-1 α in colorectal cancer cells [42]. In line with this, the 4-(2-phenylpyridin-4-yl)pyrazoles exerted antiproliferation and apoptosis-inducing effect by inhibiting the activation of HIF-1 α in HCT116 cells [43]. However, the evodiamine treatment suppressed proliferation and induced apoptosis by upregulating bone morphogenetic protein 9 (BMP9), which could activate p53 via the upregulation of the HIF-1 α in HCT116 cells [44].

There is a strong correlation between HIF-1 α and intestinal microbiota. The activation of HIF-1 α significantly suppressed the colonization of *C. albicans* and mortality from invasive disease by enhancing the expression of CRAMP in the mouse colon [45]. Further, there was a significant decrease in the *Firmicutes/Bacteroidetes* ratio and *Lactobacillus* abundance, as well as an increased abundance of *Akkermansia* in intestinal epithelial-specific HIF-1 α knockout mice [46]. In line with this, it was reported that the abundance of *Erysipelotrichales* and *Lactobacillales* increased while the abundance of *Bacteroidales* and *Desulfovibrionales* decreased in intestinal epithelial-specific HIF-1 α knockout mice [34].

HIF-1 has been reported to be regulated by other stimuli in addition to oxygen, including hormones such as insulin, growth factors such as platelet-derived growth factor, transforming growth factor-beta, and insulin-like growth factor, and vasoactive peptides such as angiotensin-2 [47]. Apart from these nonhypoxic stimuli, a few studies suggest that ROS also participate in the regulation of HIF-1 α in the GT.

4. Mechanism of HIF-1 α Regulation by ROS in the GT

4.1. ROS Regulate the Expression of HIF-1 α . As important cellular signal molecules, ROS are implicated in numerous signal MAPK, PI3K/Akt/mTOR, and NF- κ B pathways, which further regulate the expression of HIF-1 α . Under hypoxia, ROS activated ERK1/2 and further enhanced the HIF-1 α transcriptional activity, leading to the photodynamic

therapy-resistant phenotype in colorectal spheroids [48]. Further, both endogenous and exogenous H₂O₂ could upregulate the expression of HIF-1 α via activating PI3K/Akt/mTOR pathways in human colorectal carcinoma cells [49, 50]. Accordingly, H₂O₂ treatment activated Akt and ERK and subsequently increased the expression of HIF-1 α as well as its target genes in gastric mucosal epithelial cells, which could be reversed by ROS scavengers [51]. In line with this, the expression of HIF-1 α was mediated in an ERK-dependent way under hypoxia in H₂O₂-treated gastric cancer cells [52].

Moreover, ROS can activate I κ B kinase (IKK), which contributes to the degradation of I κ B and the release of NF- κ B proteins [53, 54]. Activated NF- κ B played a key role in the transcription of HIF-1 α . As p50 and p65 directly bounded to the promoter of HIF-1 α , overexpression of p50 and p65 enhanced expression of HIF-1 α mRNA while elevated expression of I κ B had a reverse effect under hypoxia [55]. Consistently, treating human intestinal epithelial cells with the IKK2 inhibitor led to diminished expression of HIF-1 α protein, suggesting NF- κ B acted as upstream of HIF-1 α [56]. In line with this, it is reported that ROS upregulated the expression of HIF-1 α via activating the NF- κ B pathway in gastric cancer cells, which could be attenuated by antioxidants [57].

4.2. ROS Regulate the Stability and Activity of HIF-1 α . Under normoxia, HIF-1 α is rapidly degraded via hydroxylation by PHDs, binding to VHL, ubiquitylation, and proteasomal degradation. During hypoxia, there are intracellular generations of ROS and NO [58], and NO can react with ROS to form RNS [59], which can modulate the posttranslation of proteins by S-nitrosation [60]. As has been reported, RNS, formed by endogenous ROS and NO, induced the S-nitrosation of PHD2, contributing to the elevated stabilization of HIF-1 α in HCT116 cells [58]. Besides, an earlier study reported that brusatol treatment diminished the production of mitochondrial ROS, leading to the activation of PHDs and subsequent degradation of HIF-1 α in colorectal cancer cells [61].

VHL is the major component of E3 ubiquitin ligases, which regulates the ubiquitylation and consequent proteasomal degradation of HIF- α . An earlier study reported that indomethacin treatment led to elevated expression of VHL through oxidative stress in IEC6 cells [62]. Further, increased

VHL contributed to the degradation of HIF-1 α , which can be reversed by the MnSOD mimetic [62].

The bHLH- (basic helix-loop-helix-) PAS (Per/ARNT/Sim) domains of HIF mediate the generation of the heterodimer and DNA binding [63]. The activity of HIF-1 α will be suppressed when its association with ARNT is retarded [64]. An early study reported that curcumin treatment degraded ARNT via the ubiquitin-proteasome system in the ROS-dependent way, leading to the inhibition of HIF-1 in MKN28 cells [65].

5. HIF-1 α Regulated by ROS Plays a Role in Gastrointestinal Diseases

Different sources of ROS participate in the modulation of HIF-1 α and further play a role in the pathologic progress of various gastrointestinal diseases (Figure 2). There is evidence that cigarette smoke exposure led to increased ROS, contributing to the disruption of intestinal tight junctions by upregulating HIF-1 α expression in the rat small intestine [66]. Further, elevated ROS mediated by NOX2 upregulated the expression of HIF-1 α in the small intestine and rectal cancer cells, contributing to rectal cancer cell proliferation [67]. ROS derived from *Helicobacter pylori*-infected gastric epithelial cells mediated the expression of HIF-1 α and its target gene vascular endothelial growth factor (VEGF), which contributed to gastric carcinogenesis [68]. Further, HIF-1 α may lead to high-altitude polycythemia- (HAPC-) induced gastric mucosal lesions (increased apoptosis, microvessel density, and swollen mitochondria) in a ROS-mediated signaling pathway [69]. Moreover, limb ischemia reperfusion-induced ROS contribute to the proliferation of gastric epithelial cells and vascular endothelial cells of gastric tissue by upregulating HIF-1 α expression [70]. However, *Clostridium difficile* toxin-mediated ROS play a key role in the stabilization of HIF-1 α , leading to the innate protection of colon epithelial barrier function, which suggested that HIF-1 α played a dual role in gastrointestinal diseases [71].

Mitochondria are the major source of intracellular ROS. However, there is a debate about whether mitochondrial ROS can regulate the expression of HIF-1 α . It is reported that brusatol treatment downregulated mitochondrial ROS levels, leading to diminished HIF-1 α protein levels and cell death in colorectal cancer under hypoxia [61]. In contrast, treating SNU-638 cells with the mitochondrial electron transport system inhibitor (rotenone, amobarbital, antimycin A, and KCN) did not affect the expression of HIF-1 α protein [72]. The difference may be due to different cell types.

Moreover, the glutathione system is critical for the regulation of nonhypoxic HIF-1 α in gastrointestinal diseases. *N*-Acetylcysteine, a thiol-containing antioxidant, is a precursor of reduced glutathione and a direct ROS scavenger [73]. Under hypoxia, *N*-acetylcysteine treatment can significantly decrease the expression of HIF-1 α by diminishing ROS, suppressing the survival and invasion ability of gastric cancer cells under hypoxia [74]. Cysteamine, the reduced form of cystamine, contributes to the generation of glutathione, one of the most important antioxidants [75]. However, cysteamine treatment has been shown to decrease the activities

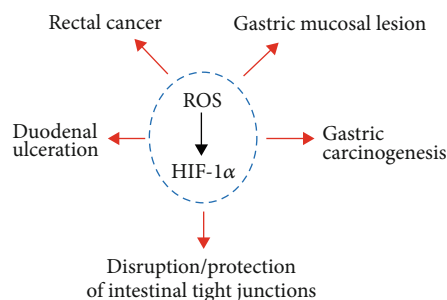


FIGURE 2: HIF-1 α regulated by ROS plays a role in gastrointestinal diseases. HIF-1 α regulated by ROS contributes to rectal cancer, gastric carcinogenesis, gastric mucosal lesions, duodenal ulceration, and disruption/protection of intestinal tight junctions.

of SOD and GSH-PX, leading to increased ROS in the rat duodenum [76], and augmented the HIF-1 α expression in the early stage of duodenal ulceration [77].

Further, a variety of antioxidants can modulate HIF-1 α expression via affecting ROS levels in the GT. For example, vitamin E supplementation diminished HIF-1 α protein expression, protecting from intestinal injury induced by hypoxia in the rat ileum [78]. Quercetin and its metabolite isorhamnetin possess antioxidation effects in different tissues [79]. Under hypoxia, quercetin treatment reduced the activity of HIF-1 α and enhanced apoptosis in colon cancer cells [80]. Further, isorhamnetin and melatonin treatment could reduce HIF-1 α expression via suppressing the ROS level, contributing to the inhibition of invasion and migration of human colon cancer cells [81]. L-Carnosine, an endogenously synthesized histidine dipeptide with antioxidant activity [82, 83], can mediate the generation of ATP and ROS in HCT116 cells [84]. It is reported that L-carnosine treatment decreased the HIF-1 α protein levels and suppressed the proliferation of colon cancer cells [85]. Resveratrol, a natural phenol with antioxidant properties, reduced the expression of HIF-1 α by scavenging ROS, leading to suppressed glucose uptake and glycolytic metabolism in colon cancer cells [86]. Overall, HIF-1 α regulated by ROS plays a key role in gastrointestinal diseases.

6. HIF-1 α Regulates ROS Levels in the GT

As an important transcriptional regulator, HIF-1 α regulates the transcription of numerous genes involved in different cell progress [87]. HIF-1 α can also modulate ROS generation in the GT. As has been reported, HIF-1 α knockdown leads to increased ROS production in gastric cancer cells [74]. Consistently, there is a significant increase in ROS levels in Caco-2 treated with CoCl₂, one of the hypoxic mimetic agents [88].

Mitochondria are the main source of intracellular ROS that oxidative phosphorylation (OXPHOS) consumes 90% to 95% of cellular oxygen, 3% of which can be transformed into superoxide [89]. Moreover, the mTOR pathway plays a key role in the regulation of HIF-1 α . Leucine treatment can activate mTOR and subsequently activates HIF-1 α in intestinal epithelial cells of weaned piglets; elevated HIF-1 α inhibits

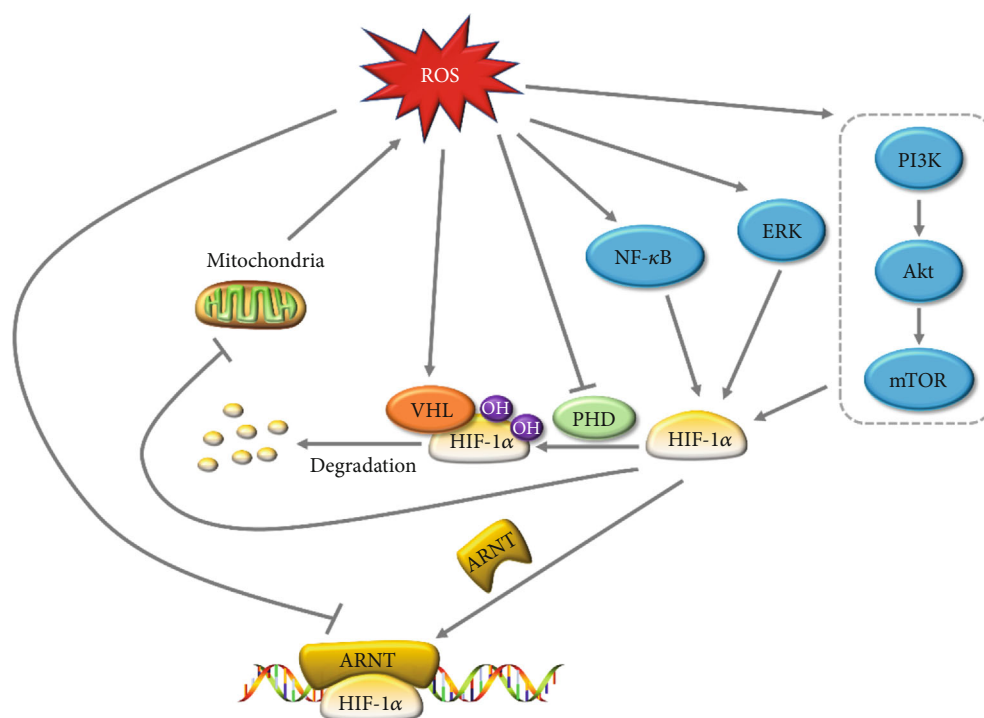


FIGURE 3: Interactions between HIF-1 α and ROS in the gastrointestinal tract. ROS induce the expression of HIF-1 α by activating ERK, NF- κ B, and PI3K/Akt/mTOR signaling pathways. Further, ROS regulate the stability and activity of HIF-1 α by targeting VHL, PHD, and ARNT. In return, HIF-1 α suppresses ROS generation by inhibiting mitochondrial OXPHOS. HIF-1 α : hypoxia-inducible transcription factor-1 α ; ROS: reactive oxygen species; PI3K: phosphoinositide 3-kinase; mTOR: mammalian target of rapamycin; NF- κ B: nuclear factor kappa-light-chain-enhancer of activated B cells; VHL: von Hippel-Lindau; PHD: prolyl 4-hydroxylase; ARNT: aryl hydrocarbon receptor nuclear translocator.

OXPHOS and induces glycolysis, leading to total ROS reduction [90]. Further, HIF-1 α knockdown increased ROS production in different gastric cancer cell lines under hypoxia [74]. In line with this, the treatment of *N*-oxalyl-D-phenylalanine, an FIH inhibitor, can ameliorate ionizing radiation-induced DNA damage and apoptosis by suppressing ROS levels [91], which indicated the effect of HIF on regulating ROS generation. However, few studies reported the underlying mechanism behind regulations of ROS by HIF-1 α in the GT. Thus, further studies are required, which may help to develop new therapies for gastrointestinal diseases induced by ROS.

7. Conclusion

As a double-edged sword, ROS act as indispensable signaling molecules while excessive content causes oxidative tissue damage in the GT. Moreover, HIF-1 α is also a key regulator in gastrointestinal health involved in energy metabolism, immunity, renewal, and microbial homeostasis. There are strong correlations between ROS and HIF-1 α in the GT, which are as yet ill-defined. It is now evident that ROS regulate HIF-1 α in different ways (Figure 3). However, the mechanism of ROS levels modulated by HIF-1 α is vague and controversial. As the crosstalk between HIF-1 α and ROS plays a key role in gastrointestinal diseases, it might be a promising target for disease treatment. Thus, broader and deeper studies are needed to understand the underlying

mechanism of their interactions in the gastrointestinal pathologic processes.

Conflicts of Interest

The authors declare no conflict of interest.

Authors' Contributions

The contributions of the authors involved in this study are as follows: conceptualization, X.X. and Y.R.S.; writing—original draft preparation, Y.R.S.; and writing—review and editing, K.X.W., X.X., H.N.L., J.Z., L.J.Z., M.Q., G.L., R.L.H., Z.L.T., and Y.L.Y. All authors have read and agreed to the published version of the manuscript.

Acknowledgments

This work was funded by the Natural Science Foundation of Hunan Province (2018JJ1028), the Innovation Team of Key areas of the Ministry of Science and Technology, the National Key Research and Development Program of China (2018YFD0501101), the Science and Technology Program of Changsha (kq1907074), the Science and Technology Leadership Program of Hunan Province (2019RS3021), and the Research Foundation of Education Bureau of Hunan Province, China (18B476).

References

- [1] H. Li, X. Hou, R. Lin et al., "Advanced endoscopic methods in gastrointestinal diseases: a systematic review," *Quantitative Imaging in Medicine and Surgery*, vol. 9, no. 5, pp. 905–920, 2019.
- [2] L. F. N. Nuñez, S. H. S. Parra, D. De la Torre et al., "Isolation of avian nephritis virus from chickens showing enteric disorders," *Poultry Science*, vol. 97, no. 10, pp. 3478–3488, 2018.
- [3] G. Aviello and U. G. Knaus, "ROS in gastrointestinal inflammation: rescue or sabotage?," *British Journal of Pharmacology*, vol. 174, no. 12, pp. 1704–1718, 2017.
- [4] R. Aljehni, F. Ibrahim, Y. C. Guillaume, and C. Andre, "Reactive oxygen species and nitric oxide effect on the steroid hormone binding with serum albumin," *Journal of Pharmaceutical and Biomedical Analysis*, vol. 62, pp. 129–134, 2012.
- [5] J. S. Choi, A. R. Paek, S. Y. Kim, and H. J. You, "GIPC mediates the generation of reactive oxygen species and the regulation of cancer cell proliferation by insulin-like growth factor-1/IGF-1R signaling," *Cancer Letters*, vol. 294, no. 2, pp. 254–263, 2010.
- [6] W. G. Kaelin and P. J. Ratcliffe, "Oxygen sensing by metazoans: the central role of the HIF hydroxylase pathway," *Molecular Cell*, vol. 30, no. 4, pp. 393–402, 2008.
- [7] K. Bedard and K. H. Krause, "The NOX family of ROS-generating NADPH oxidases: physiology and pathophysiology," *Physiological Reviews*, vol. 87, no. 1, pp. 245–313, 2007.
- [8] A. Bhattacharyya, R. Chattopadhyay, S. Mitra, and S. E. Crowe, "Oxidative stress: an essential factor in the pathogenesis of gastrointestinal mucosal diseases," *Physiological Reviews*, vol. 94, no. 2, pp. 329–354, 2014.
- [9] J. Zhang, N. Zheng, J. Liu, F. D. Li, S. L. Li, and J. Q. Wang, "Aflatoxin B1 and aflatoxin M1 induced cytotoxicity and DNA damage in differentiated and undifferentiated Caco-2 cells," *Food and Chemical Toxicology*, vol. 83, pp. 54–60, 2015.
- [10] M. Boussabbeh, I. Ben Salem, A. Prola et al., "Patulin induces apoptosis through ROS-mediated endoplasmic reticulum stress pathway," *Toxicological Sciences*, vol. 144, no. 2, pp. 328–337, 2015.
- [11] M. Wu, H. Xiao, W. Ren et al., "Therapeutic effects of glutamic acid in piglets challenged with deoxynivalenol," *PLoS One*, vol. 9, no. 7, article e100591, 2014.
- [12] J. Yu, F. Liu, P. Yin et al., "Involvement of oxidative stress and mitogen-activated protein kinase signaling pathways in heat stress-induced injury in the rat small intestine," *Stress*, vol. 16, no. 1, pp. 99–113, 2012.
- [13] A. L. Baldwin, R. L. Primeau, and W. E. Johnson, "Effect of noise on the morphology of the intestinal mucosa in laboratory rats," *Journal of the American Association for Laboratory Animal Science*, vol. 45, no. 1, pp. 74–82, 2006.
- [14] Y. He, Z. Sang, Y. Zhuo et al., "Transport stress induces pig jejunum tissue oxidative damage and results in autophagy/mitophagy activation," *Journal of Animal Physiology and Animal Nutrition*, vol. 103, no. 5, pp. 1521–1529, 2019.
- [15] J. Yin, M. M. Wu, H. Xiao et al., "Development of an antioxidant system after early weaning in piglets," *Journal of Animal Science*, vol. 92, no. 2, pp. 612–619, 2014.
- [16] H. Xiao, M. Wu, F. Shao et al., "N-Acetyl-L-cysteine protects the enterocyte against oxidative damage by modulation of mitochondrial function," *Mediators of Inflammation*, vol. 2016, Article ID 8364279, 9 pages, 2016.
- [17] S. Mortadza, S. Alawieyah, L. Wang, D. Li, and L.-H. Jiang, "TRPM2 channel-mediated ROS-sensitive Ca²⁺ signaling mechanisms in immune cells," *Frontiers in Immunology*, vol. 6, 2015.
- [18] J. B. Bolen, R. Rowley, C. Spana, and A. Tsygankov, "The Src family of tyrosine protein kinases in hemopoietic signal transduction," *The FASEB Journal*, vol. 6, no. 15, pp. 3403–3409, 1992.
- [19] M. Geiszt, K. Lekstrom, S. Brenner et al., "NAD(P)H oxidase 1, a product of differentiated colon epithelial cells, can partially replace glycoprotein 91phox in the regulated production of superoxide by phagocytes," *The Journal of Immunology*, vol. 171, no. 1, pp. 299–306, 2003.
- [20] P. Barcellos-de-Souza, J. A. Moraes, J. C. M. De-Freitas-Junior, J. A. Morgado-Díaz, C. Barja-Fidalgo, and M. A. Arruda, "Heme modulates intestinal epithelial cell activation: involvement of NADPHox-derived ROS signaling," *American Journal of Physiology-Cell Physiology*, vol. 304, pp. C170–C179, 2013.
- [21] K. C. Jeong, H. S. Jeong, J. H. Rhee et al., "Construction and phenotypic evaluation of a *Vibrio vulnificus* vvpE mutant for elastolytic protease," *Infection and Immunity*, vol. 68, no. 9, pp. 5096–5106, 2000.
- [22] S. Lee, Y. Jung, S. Oh et al., "Vibrio vulnificus VvpE inhibits mucin 2 expression by hypermethylation via lipid raft-mediated ROS signaling in intestinal epithelial cells," *Cell Death & Disease*, vol. 6, no. 6, pp. e1787–e1787, 2015.
- [23] J. Yin, M. Wu, Y. Li et al., "Toxicity assessment of hydrogen peroxide on Toll-like receptor system, apoptosis, and mitochondrial respiration in piglets and IPEC-J2 cells," *Oncotarget*, vol. 8, no. 2, pp. 3124–3131, 2017.
- [24] G. L. Semenza and G. L. Wang, "A nuclear factor induced by hypoxia via de novo protein synthesis binds to the human erythropoietin gene enhancer at a site required for transcriptional activation," *Molecular and Cellular Biology*, vol. 12, no. 12, pp. 5447–5454, 1992.
- [25] L. Schito and G. L. Semenza, "Hypoxia-inducible factors: master regulators of cancer progression," *Trends Cancer*, vol. 2, no. 12, pp. 758–770, 2016.
- [26] B. Chiavarina, U. E. Martinez-Outschoorn, D. Whitaker-Menezes et al., "Metabolic reprogramming and two-compartment tumor metabolism: opposing role (s) of HIF1 α and HIF2 α in tumor-associated fibroblasts and human breast cancer cells," *Cell Cycle*, vol. 11, pp. 3280–3289, 2014.
- [27] G. N. Masoud and W. Li, "HIF-1 α pathway: role, regulation and intervention for cancer therapy," *Acta Pharmaceutica Sinica B*, vol. 5, no. 5, pp. 378–389, 2015.
- [28] M. Strowitzki, E. Cummins, and C. Taylor, "Protein hydroxylation by hypoxia-inducible factor (HIF) hydroxylases: unique or ubiquitous?," *Cells*, vol. 8, 2019.
- [29] C. T. Taylor and S. P. Colgan, "Hypoxia and gastrointestinal disease," *Journal of Molecular Medicine*, vol. 85, no. 12, pp. 1295–1300, 2007.
- [30] M. C. Manresa and C. T. Taylor, "Hypoxia inducible factor (HIF) hydroxylases as regulators of intestinal epithelial barrier function," *Cellular and Molecular Gastroenterology and Hepatology*, vol. 3, no. 3, pp. 303–315, 2017.
- [31] N. E. Zeitouni, S. Chotikatam, M. von Köckritz-Blickwede, and H. Y. Naim, "The impact of hypoxia on intestinal epithelial cell functions: consequences for invasion by bacterial pathogens," *Molecular and cellular pediatrics*, vol. 3, no. 1, p. 14, 2016.

- [32] R. Archid, W. Solass, C. Tempfer et al., “Cachexia anorexia syndrome and associated metabolic dysfunction in peritoneal metastasis,” *International Journal of Molecular Sciences*, vol. 20, no. 21, p. 5444, 2019.
- [33] F. Dengler and G. Gabel, “The fast lane of hypoxic adaptation: glucose transport is modulated via a HIF-hydroxylase-AMPK-axis in jejunum epithelium,” *International Journal of Molecular Sciences*, vol. 20, no. 20, p. 4993, 2019.
- [34] L. Sun, T. Li, H. Tang et al., “Intestinal epithelial cells-derived hypoxia-inducible factor-1 α is essential for the homeostasis of intestinal intraepithelial lymphocytes,” *Frontiers in Immunology*, vol. 10, 2019.
- [35] J. L. Fachi, J. de Souza Felipe, L. P. Pral et al., “Butyrate protects mice from *Clostridium difficile*-induced colitis through an HIF-1-dependent mechanism,” *Cell Reports*, vol. 27, no. 3, pp. 750–761.e7, 2019.
- [36] C. Y. Fan, J. Han, X. J. Liu, F. Zhang, Y. S. Long, and Q. T. Xie, “Modulation of hypoxia-inducible factor-1 α /cyclo-oxygenase-2 pathway associated with attenuation of intestinal mucosa inflammatory damage by *Acanthopanax senticosus* polysaccharides in lipopolysaccharide-challenged piglets,” *British Journal of Nutrition*, vol. 122, no. 6, pp. 666–675, 2019.
- [37] Y. L. Chen, Y. Y. Zheng, Y. C. Dai, Y. L. Zhang, and Z. P. Tang, “Systems pharmacology approach reveals protective mechanisms of Jian-Pi Qing-Chang decoction on ulcerative colitis,” *World Journal of Gastroenterology*, vol. 25, no. 21, pp. 2603–2622, 2019.
- [38] S. Yang, M. Yu, L. Sun et al., “Interferon- γ -induced intestinal epithelial barrier dysfunction by NF- κ B/HIF-1 α pathway,” *Journal of Interferon & Cytokine Research*, vol. 34, no. 3, pp. 195–203, 2014.
- [39] M. Cao, P. Wang, C. Sun, W. He, and F. Wang, “Amelioration of IFN- γ and TNF- α -induced intestinal epithelial barrier dysfunction by berberine via suppression of MLCK-MLC phosphorylation signaling pathway,” *PLoS One*, vol. 8, 2013.
- [40] L. Hong, J. Wang, H. Wang et al., “Linc-pint overexpression inhibits the growth of gastric tumors by downregulating HIF-1 α ,” *Molecular Medicine Reports*, vol. 20, pp. 2875–2881, 2019.
- [41] R. Huang, X. Jin, Y. Y. Gao, H. M. Yuan, F. Wang, and X. M. Cao, “DZNep inhibits Hif-1 α and Wnt signalling molecules to attenuate the proliferation and invasion of BGC-823 gastric cancer cells,” *Oncology Letters*, vol. 18, pp. 4308–4316, 2019.
- [42] H. G. Wang, B. Cao, L. X. Zhang et al., “KLF2 inhibits cell growth via regulating HIF-1 α /Notch-1 signal pathway in human colorectal cancer HCT116 cells,” *Oncology Reports*, vol. 38, no. 1, pp. 584–590, 2017.
- [43] Y. W. Li, X. Y. Li, S. Li et al., “Synthesis and evaluation of the HIF-1 α inhibitory activity of 3(5)-substituted-4-(quinolin-4-yl)- and 4-(2-phenylpyridin-4-yl)pyrazoles as inhibitors of ALK5,” *Bioorganic & Medicinal Chemistry Letters*, vol. 30, no. 2, p. 126822, 2020.
- [44] F. S. Li, J. Huang, M. Z. Cui et al., “BMP9 mediates the anticancer activity of evodiamine through HIF-1 alpha/p53 in human colon cancer cells,” *Oncology Reports*, vol. 43, pp. 415–426, 2019.
- [45] D. Fan, L. A. Coughlin, M. M. Neubauer et al., “Activation of HIF-1 α and LL-37 by commensal bacteria inhibits *Candida albicans* colonization,” *Nature Medicine*, vol. 21, no. 7, pp. 808–814, 2015.
- [46] T. Shao, C. Zhao, F. Li et al., “Intestinal HIF-1 α deletion exacerbates alcoholic liver disease by inducing intestinal dysbiosis and barrier dysfunction,” *Journal of Hepatology*, vol. 69, no. 4, pp. 886–895, 2018.
- [47] T. Kietzmann and A. Gorch, “Reactive oxygen species in the control of hypoxia-inducible factor-mediated gene expression,” *Seminars in Cell & Developmental Biology*, vol. 16, no. 4-5, pp. 474–486, 2005.
- [48] M. J. Lamberti, M. F. Pansa, R. E. Vera, M. E. Fernandez-Zapico, N. B. R. Vittar, and V. A. Rivarola, “Transcriptional activation of HIF-1 by a ROS-ERK axis underlies the resistance to photodynamic therapy,” *PLoS One*, vol. 12, no. 5, p. e0177801, 2017.
- [49] F. Pez, F. Dayan, J. Durivault et al., “The HIF-1-inducible lysyl oxidase activates HIF-1 via the Akt pathway in a positive regulation loop and synergizes with HIF-1 in promoting tumor cell growth,” *Cancer Research*, vol. 2011, p. 71, 2011.
- [50] L. Quintos, I. A. Lee, H. J. Kim et al., “Significance of p27kip1 as potential biomarker for intracellular oxidative status,” *Nutrition Research and Practice*, vol. 4, no. 5, pp. 351–355, 2010.
- [51] L. Liu, X. Ning, S. Han et al., “Hypoxia induced HIF-1 accumulation and VEGF expression in gastric epithelial mucosa cells: involvement of ERK1/2 and PI3K/Akt,” *Molecular Biology*, vol. 42, no. 3, pp. 403–412, 2008.
- [52] L. Liu, H. Zhang, L. Sun et al., “ERK/MAPK activation involves hypoxia-induced MGr1-Ag/37LRP expression and contributes to apoptosis resistance in gastric cancer,” *International Journal of Cancer*, vol. 127, 2010.
- [53] I. O. Minatel, F. Francisqueti, C. Correa, and G. Lima, “Antioxidant activity of γ -oryzanol: a complex network of interactions,” *International Journal of Molecular Sciences*, vol. 17, no. 8, p. 1107, 2016.
- [54] Z. Wang, S. Li, Y. Cao et al., “Oxidative stress and carbonyl lesions in ulcerative colitis and associated colorectal cancer,” *Oxidative Medicine and Cellular Longevity*, vol. 2016, 15 pages, 2016.
- [55] R. S. BelAiba, S. Bonello, C. Zähringer et al., “Hypoxia up-regulates hypoxia-inducible factor-1 α transcription by involving phosphatidylinositol 3-kinase and nuclear factor κ B in pulmonary artery smooth muscle cells,” *Molecular Biology of the Cell*, vol. 18, no. 12, pp. 4691–4697, 2007.
- [56] S. Mimouna, D. Gonçalves, N. Barnich, A. Darfeuille-Michaud, P. Hofman, and V. Vouret-Craviari, “Crohn disease-associated *Escherichia coli* promote gastrointestinal inflammatory disorders by activation of HIF-dependent responses,” *Gut Microbes*, vol. 2, pp. 335–346, 2014.
- [57] W. Qin, C. Li, W. Zheng et al., “Inhibition of autophagy promotes metastasis and glycolysis by inducing ROS in gastric cancer cells,” *Oncotarget*, vol. 6, pp. 39839–39854, 2015.
- [58] R. Chowdhury, L. C. Godoy, A. Thiantanawat, L. J. Trudel, W. M. Deen, and G. N. Wogan, “Nitric oxide produced endogenously is responsible for hypoxia-induced HIF-1 α stabilization in colon carcinoma cells,” *Chemical Research in Toxicology*, vol. 25, no. 10, pp. 2194–2202, 2012.
- [59] C. W. Ward, B. L. Prosser, and W. J. Lederer, “Mechanical stretch-induced activation of ROS/RNS signaling in striated muscle,” *Antioxidants & Redox Signaling*, vol. 20, no. 6, pp. 929–936, 2014.
- [60] F. J. Corpas, J. C. Begara-Morales, B. Sánchez-Calvo, M. Chaki, and J. B. Barroso, “Nitration and S-nitrosylation: two post-translational modifications (PTMs) mediated by reactive nitrogen species (RNS) and their role in signalling processes of plant cells,” in *In Reactive Oxygen and Nitrogen Species*

- Signaling and Communication in Plants*, pp. 267–281, Springer, 2015.
- [61] E. T. Oh, C. W. Kim, H. G. Kim, J. S. Lee, and H. J. Park, “Brsatol-mediated inhibition of c-Myc increases HIF-1 α degradation and causes cell death in colorectal cancer under hypoxia,” *Theranostics*, vol. 7, no. 14, pp. 3415–3431, 2017.
- [62] S. Yokoe, T. Nakagawa, Y. Kojima, K. Higuchi, and M. Asahi, “Indomethacin-induced intestinal epithelial cell damage is mediated by pVHL activation through the degradation of collagen I and HIF-1 α ,” *Biochemical and Biophysical Research Communications*, vol. 468, no. 4, pp. 671–676, 2015.
- [63] D. Wu, N. Potluri, J. Lu, Y. Kim, and F. Rastinejad, “Structural integration in hypoxia-inducible factors,” *Nature*, vol. 524, no. 7565, pp. 303–308, 2015.
- [64] A. Kalousi, I. Mylonis, A. S. Politou, G. Chachami, E. Paraskeva, and G. Simos, “Casein kinase 1 regulates human hypoxia-inducible factor HIF-1,” *Journal of Cell Science*, vol. 123, no. 17, pp. 2976–2986, 2010.
- [65] H. Choi, Y.-S. Chun, S.-W. Kim, M.-S. Kim, and J.-W. Park, “Curcumin inhibits hypoxia-inducible factor-1 by degrading aryl hydrocarbon receptor nuclear translocator: a mechanism of tumor growth inhibition,” *Molecular Pharmacology*, vol. 70, no. 5, pp. 1664–1671, 2006.
- [66] H. W. Li, Q. Wu, L. Xu et al., “Increased oxidative stress and disrupted small intestinal tight junctions in cigarette smoke-exposed rats,” *Molecular Medicine Reports*, vol. 11, no. 6, pp. 4639–4644, 2015.
- [67] Y. F. Guo, B. Han, K. L. Luo, Z. J. Ren, L. Cai, and L. Sun, “NOX2-ROS-HIF-1 α signaling is critical for the inhibitory effect of oleanolic acid on rectal cancer cell proliferation,” *Bio-medicine & Pharmacotherapy*, vol. 85, pp. 733–739, 2017.
- [68] M. J. Kang, E. J. Song, B. Y. Kim, D. J. Kim, and J. H. Park, “Helicobacter pylori induces vascular endothelial growth factor production in gastric epithelial cells through hypoxia-inducible factor-1 α -dependent pathway,” *Helicobacter*, vol. 19, no. 6, pp. 476–483, 2014.
- [69] K. Li and C. He, “Gastric mucosal lesions in Tibetans with high-altitude polycythemia show increased HIF-1A expression and ROS production,” *BioMed Research International*, vol. 2019, 2019.
- [70] T. Wang, Y.-F. Leng, Y. Zhang, X. Xue, Y.-Q. Kang, and Y. Zhang, “Oxidative stress and hypoxia-induced factor 1 α expression in gastric ischemia,” *World journal of gastroenterology: WJG*, vol. 17, no. 14, pp. 1915–1922, 2011.
- [71] J. Y. Lee, S. A. Hirota, L. E. Glover, G. D. Armstrong, P. L. Beck, and J. A. MacDonald, “Effects of nitric oxide and reactive oxygen species on HIF-1 α stabilization following Clostridium difficile toxin exposure of the Caco-2 epithelial cell line,” *Cellular Physiology and Biochemistry*, vol. 32, no. 2, pp. 417–430, 2013.
- [72] J.-H. Park, T.-Y. Kim, H.-S. Jong et al., “Gastric epithelial reactive oxygen species prevent normoxic degradation of hypoxia-inducible factor-1 α in gastric cancer cells,” *Clinical Cancer Research*, vol. 9, pp. 433–440, 2003.
- [73] A. M. Sadowska, B. Manuel-y-Keenoy, and W. A. De Backer, “Antioxidant and anti-inflammatory efficacy of NAC in the treatment of COPD: discordant in vitro and in vivo dose-effects: a review,” *Pulmonary Pharmacology & Therapeutics*, vol. 20, pp. 9–22, 2007.
- [74] M. Shida, Y. Kitajima, J. Nakamura et al., “Impaired mitophagy activates mtROS/HIF-1 α interplay and increases cancer aggressiveness in gastric cancer cells under hypoxia,” *International Journal of Oncology*, vol. 48, no. 4, pp. 1379–1390, 2016.
- [75] M. Besouw, R. Masereeuw, L. van den Heuvel, and E. Levchenko, “Cysteamine: an old drug with new potential,” *Drug Discovery Today*, vol. 18, no. 15–16, pp. 785–792, 2013.
- [76] F. Saghaei, I. Karimi, A. Jouyban, and M. Samini, “Effects of captopril on the cysteamine-induced duodenal ulcer in the rat,” *Experimental and Toxicologic Pathology*, vol. 64, no. 4, pp. 373–377, 2012.
- [77] T. Khomenko, X. Deng, Z. Sandor, A. S. Tarnawski, and S. Szabo, “Cysteamine alters redox state, HIF-1 α transcriptional interactions and reduces duodenal mucosal oxygenation: novel insight into the mechanisms of duodenal ulceration,” *Biochemical and Biophysical Research Communications*, vol. 317, no. 1, pp. 121–127, 2004.
- [78] C. L. Xu, R. Sun, X. J. Qiao et al., “Effect of vitamin E supplementation on intestinal barrier function in rats exposed to high altitude hypoxia environment,” *The Korean Journal of Physiology & Pharmacology*, vol. 18, no. 4, pp. 313–320, 2014.
- [79] T. Bakir, İ. Sönmezoğlu, F. İmer, and R. Apak, “Antioxidant/prooxidant effects of α -tocopherol, quercetin and isorhamnetin on linoleic acid peroxidation induced by Cu (II) and H₂O₂,” *International Journal of Food Sciences and Nutrition*, vol. 65, pp. 226–234, 2013.
- [80] H.-S. Kim, T. Wannatung, S. Lee et al., “Quercetin enhances hypoxia-mediated apoptosis via direct inhibition of AMPK activity in HCT116 colon cancer,” *Apoptosis*, vol. 17, no. 9, pp. 938–949, 2012.
- [81] S. Seo, K. Seo, S. H. Ki, and S. M. Shin, “Isorhamnetin inhibits reactive oxygen species-dependent hypoxia inducible factor (HIF)-1 α accumulation,” *Biological & Pharmaceutical Bulletin*, vol. 39, no. 11, pp. 1830–1838, 2016.
- [82] R. Di Paola, D. Impellizzeri, A. T. Salinaro et al., “Administration of carnosine in the treatment of acute spinal cord injury,” *Biochemical Pharmacology*, vol. 82, no. 10, pp. 1478–1489, 2011.
- [83] V. Calabrese, C. Cornelius, A. M. G. Stella, and E. J. Calabrese, “Cellular stress responses, mitostress and carnitine insufficiencies as critical determinants in aging and neurodegenerative disorders: role of hormesis and vitagenes,” *Neurochemical Research*, vol. 35, no. 12, pp. 1880–1915, 2010.
- [84] B. Iovine, M. L. Iannella, F. Nocella, M. R. Pricolo, and M. A. Bevilacqua, “Carnosine inhibits KRAS-mediated HCT116 proliferation by affecting ATP and ROS production,” *Cancer Letters*, vol. 315, no. 2, pp. 122–128, 2012.
- [85] B. Iovine, G. Oliviero, M. Garofalo et al., “The anti-proliferative effect of L-carnosine correlates with a decreased expression of hypoxia inducible factor 1 alpha in human colon cancer cells,” *PLoS One*, vol. 9, no. 5, article e96755, 2014.
- [86] K. H. Jung, J. H. Lee, C. H. T. Quach et al., “Resveratrol suppresses cancer cell glucose uptake by targeting reactive oxygen species-mediated hypoxia-inducible factor-1 Activation,” *Journal of Nuclear Medicine*, vol. 54, no. 12, pp. 2161–2167, 2013.
- [87] K. Lisy and D. Peet, “Turn me on: regulating HIF transcriptional activity,” *Cell Death & Differentiation*, vol. 15, no. 4, pp. 642–649, 2008.
- [88] Y. L. Liu, C. H. Wang, Y. H. Wang et al., “Cobalt chloride decreases fibroblast growth factor-21 expression dependent on oxidative stress but not hypoxia-inducible factor in Caco-2 cells,” *Toxicology and Applied Pharmacology*, vol. 264, no. 2, pp. 212–221, 2012.

- [89] S. Marchi, C. Giorgi, J. M. Suski et al., “Mitochondria-ROS crosstalk in the control of cell death and aging,” *Journal of Signal Transduction*, vol. 2012, 329617 pages, 2012.
- [90] J. Hu, Y. Nie, S. Chen et al., “Leucine reduces reactive oxygen species levels via an energy metabolism switch by activation of the mTOR-HIF-1 α pathway in porcine intestinal epithelial cells,” *The International Journal of Biochemistry & Cell Biology*, vol. 89, pp. 42–56, 2017.
- [91] Y. Y. Meng, F. J. Yang, W. Long, and W. Q. Xu, “Radioprotective activity and preliminary mechanisms of N-oxalyl-d-phenylalanine (NOFD) in vitro,” *International Journal of Molecular Sciences*, vol. 20, no. 1, p. 37, 2019.

Research Article

Ophiopogonin D Increases SERCA2a Interaction with Phospholamban by Promoting CYP2J3 Upregulation

Jia Wang,^{1,2} Wenting You,^{1,3} Ningning Wang,^{1,2} Wei Zhou,¹ Yunxuan Ge,¹ Zengchun Ma,¹ Hongling Tan,¹ Yuguang Wang^{ID},¹ and Yue Gao^{ID}¹

¹Department of Pharmaceutical Sciences, Beijing Institute of Radiation Medicine, Beijing 100850, China

²Guangdong Pharmaceutical University, Guangzhou 510006, China

³Department of Pharmacology, Anhui Medical University, Hefei 230032, China

Correspondence should be addressed to Yuguang Wang; wangyg@bmi.ac.cn and Yue Gao; gaoyue@bmi.ac.cn

Received 30 September 2020; Revised 12 November 2020; Accepted 8 December 2020; Published 31 December 2020

Academic Editor: Wuquan Deng

Copyright © 2020 Jia Wang et al. This is an open access article distributed under the Creative Commons Attribution License, which permits unrestricted use, distribution, and reproduction in any medium, provided the original work is properly cited.

Ophiopogonin D (OPD), a compound from the Chinese herb *Radix Ophiopogonis*, reportedly induces increased levels of cytochrome P450 2J3 (CYP2J3)/epoxyeicosatrienoic acids (EETs) and Ca^{2+} in rat cardiomyocytes. Little is known regarding the specific mechanism between CYP2J3 and Ca^{2+} homeostasis. Here, we investigated whether CYP2J3 is involved in the protective action of OPD on the myocardium by activating the Ca^{2+} homeostasis-related protein complex (SERCA2a and PLB) in H9c2 rat cardiomyoblast cells. The interaction between SERCA2a and PLB was measured using fluorescence resonance energy transfer. OPD attenuated heart failure and catalyzed the active transport of Ca^{2+} into the sarcoplasmic reticulum by inducing the phosphorylation of PLB and promoting the SERCA2a activity. These beneficial effects of OPD on heart failure were abolished after knockdown of CYP2J3 in a model of heart failure. Together, our results identify CYP2J3 as a critical intracellular target for OPD and unravel a mechanism of CYP2J3-dependent regulation of intracellular Ca^{2+} .

1. Introduction

Cytochrome P450 2J3 (CYP2J3) is a member of the cytochrome P450 superfamily of enzymes and catalyzes many reactions involved in the metabolism of drugs and other xenobiotics. They are highly expressed in the myocardium and are involved in the metabolism of arachidonic acid (AA). The metabolites of AA are epoxyeicosatrienoic acids (EETs), which reportedly have anti arrhythmic [1], anti-inflammatory [2], antiapoptotic [3], and antioxidant [4] effects, as well as a role in cardiovascular protection [5]. Specifically, EETs can maintain Ca^{2+} homeostasis in myocardial cells and alleviate the symptoms of heart failure in rats by upregulating the expression of sarcoplasmic reticulum Ca^{2+} -ATPase (SERCA) and phospholamban (PLB). Additionally, the CYP2J3 overexpression and increased levels of EETs reportedly decrease endoplasmic reticulum (ER) stress signaling and ER stress-mediated apoptosis in rats with heart failure (HF) by maintaining the sarcoplasmic reticulum

Ca^{2+} -ATPase (SERCA2a) activity and intracellular Ca^{2+} homeostasis [6].

Research has indicated that the decreased SERCA2a activity and expression are hallmarks of HF in both experimental animal models and patients [7, 8]. SERCA2a regulates Ca^{2+} reuptake into the sarcoplasmic reticulum (SR), and dysregulated Ca^{2+} homeostasis is an initiating event in HF [9]. Furthermore, the SERCA2a activity can be regulated by a small intrinsic protein located in the SR named phospholamban (PLB). In the dephosphorylated state, PLB inhibits the SERCA2a activity and SR Ca^{2+} transport. Phosphorylation of PLB by either cAMP-dependent protein kinase (PKA) at Ser¹⁶ residue or Ca^{2+} -calmodulin-dependent protein kinase (CaMKII) at Thr¹⁷ residue relieves the inhibition of the SERCA2a activity, thus increasing the rate of SR Ca^{2+} uptake [10]. As a result, the SERCA2a-PLB Ca^{2+} -regulatory system has been implicated in cardiovascular disease [11, 12]. Industry and academic researchers have extensively searched for the affinity of the regulatory interaction between SERCA2a

and PLB. For instance, fluorescence resonance energy transfer (FRET) has been used to directly detect the interaction of donor-labeled SERCA2a with acceptor-labeled PLB or acceptor-labeled SERCA2a with donor-labeled PLB in membranes [12–14]. We previously showed that ophiopogonin D (OPD), a steroidal glycoside isolated from *Radix Ophiopogonis* (a tuber of *Ophiopogon japonicus* KerGawl), can induce the SERCA2a expression by upregulating the CYP2J3/EET system [12]. However, the relative contribution of CYP2J3 to OPD's effects on Ca^{2+} homeostasis and interaction between SERCA and PLB has not been investigated. Whether CYP2J3 participates in modulating the interaction between SERCA2a with PLB remains unknown.

Here, we report a compound extracted from the root of *Radix Ophiopogonis* as a potent CYP2J3 agonist. Our results demonstrate that OPD confers its anti-HF effects by inducing the CYP2J3 expression and subsequently promoting the interaction between SERCA2a and PLB, which is helpful for maintaining Ca^{2+} homeostasis.

2. Material and Methods

2.1. Antibodies and Reagents. OPD (purity: 98% by high-performance liquid chromatography) and isoproterenol-HCl (ISO) were purchased from the National Institutes for Control of Pharmaceutical and Biological Products (Beijing, China) and Sigma-Aldrich (St Louis, MO, USA), respectively. The TransScript™ First-Step RT-PCR SuperMixFast and SYBR® Green Master Mix were purchased from TransGen Biotech Co., Ltd. (Beijing, China). Antibodies against GAPDH and phosphorylated PLB (p-PLB) (Ser¹⁶/Thr¹⁷) were from Cell Signaling Technology Inc. (CST, Danvers, MA, USA). Antibodies against CaMKII, p-CaMKII, p-T197-PKA, PKA, p-PLB (p-Ser¹⁶), and SERCA2-ATPase were from Abcam (Cambridge, UK). The antibody against p-PLB (p-Thr¹⁷) was from Zen BioScience (Chengdu, China) [15], and the antibody against CYP2J3 was from Bioss (Boston, MA, USA). The Universal Magnetic Co-IP Kit was obtained from Active Motif, Inc. (Carlsbad, CA, USA). Normal Rabbit IgG was from Cell Signaling Technology. Oregon Green 488 BAPTA was purchased from Invitrogen (Carlsbad, CA, USA). p-CMV-N-CFP-PLB, p-CMV-N-YFP-SERCA2a, and pLVX-IRES-ZsGreen-1-CYP2J3 were from Biomed (Beijing, China). The specific inhibitors of CaMKII (KN-93) and PKA (H-89) were purchased from Selleck Chemicals (Houston, TX, USA). Helicid was from TargetMol (Shanghai, China). All other reagents were purchased from commercial suppliers unless otherwise indicated.

2.2. Cell Culture and Treatment. H9c2 cells, a subclone of the original clonal cell line derived from embryonic BD1X rat heart tissue, were obtained from the American Type Culture Collection (Manassas, VA, USA). Cells were cultured in Dulbecco's Modified Eagle's Medium (DMEM) supplemented with 10% fetal bovine serum (FBS) and penicillin-streptomycin (100 IU/mL) in a humidified atmosphere of 95% air and 5% CO_2 at 37°C. The cells were seeded in 96- or 6-cell culture plates for each experiment and grown in a humidified incubator containing 5% CO_2 . ISO was dissolved

in distilled water. OPD, Helicid, H-89, and KN-93 were dissolved in dimethyl sulfoxide and diluted with DMEM.

2.3. Cell Viability Assay. Cell viability was determined with the Cell Counting Kit-8 (CCK-8) assay. Briefly, cells were seeded in 96-well plates at a density of 4×10^3 per well in 100 mL complete medium. After being treated with different concentrations of OPD (1–80 $\mu\text{mol/L}$), the cells were further incubated in a medium containing 0.5% CCK-8 for 0.5–4 h. The absorbance of 450 nm was measured with a microplate reader.

2.4. Measurement of ER-Free Ca^{2+} . H9c2 cells were treated with different concentrations of OPD (0.25, 0.5, 1 $\mu\text{mol/L}$) and ISO (1 $\mu\text{mol/L}$). After 24 h, the ER Ca^{2+} concentration was measured using the Mag-Fluo-4/AM Kit from GENMED Scientific Inc. (Arlington, VA, USA), according to the supplier's instructions, as previously described [16, 17]. The cultured cells were incubated with 1 mL of 5 $\mu\text{mol/L}$ Mag-Fluo-4/AM for 30 min at 37°C to optimize loading into the ER. Cells were washed three times with D-Hank's solution to remove the probes. Relative ER Ca^{2+} was expressed as a percentage of the control.

2.5. Measurement of Ca^{2+} -ATPase Activity. H9c2 cells were treated with OPD and ISO as previously mentioned. The enzyme activity of SERCA2a in SR was detected with a microplate system. SERCA2a vesicles were obtained as previously described for the measurement of its activity [18], which was detected using an inorganic phosphorus colorimetric method with the Ultramicro-ATPase Assay Kit (Jiancheng, China). Briefly, this test includes an enzymatic and phosphorus reaction based on the theory that ATP is decomposed into ADP and inorganic phosphate (Pi) by ATPase. The activity of ATPase was measured by the quantity of Pi, and the amount of Pi decomposed by ATPase per mg tissue or cell protein per h ($\mu\text{mol Pi/mg prot/h}$) was regarded as one unit of the ATPase activity. The values for the maximal SERCA2a activity were taken directly from the experimental data and normalized for total protein concentration (mmol/g protein/min). These data were analyzed by nonlinear regression with computer software (GraphPad Software, San Diego, CA, USA).

2.6. RNA Isolation and Quantitative PCR. After being treated with the corresponding drugs as described above, total RNA was extracted. The expression of specific mRNAs was quantified with quantitative PCR (qPCR) as previously described. Briefly, total RNA was prepared from H9c2 cells using Trizol reagent. The RNA integrity and concentration were measured using the DU-600 ultraviolet spectrophotometer (Beckman Coulter, Brea, CA, USA). All RNA samples with an OD260/OD280 between 1.8 and 2.0 were used for qPCR. Total RNA was reverse transcribed with the Transcriptor First-strand cDNA Synthesis Kit to obtain the cDNAs. qPCR was performed using the ABI Prism 7500 Real-Time PCR System (Applied Biosystems, Waltham, MA, USA) using the Trans Script™ SYBR® Green Master Mix Kit, according to the instructions provided. Each target gene was quantified, with GAPDH serving as the internal control. The primer sequences are listed in Table 1.

TABLE 1: Primer sequences used for qPCR.

Gene	Forward primer (5'-3')	Reverse primer (5'-3')
CYP2J3	CATTGAGCTCACAAGTGGCTTT	CAATTCCTAGGCTGTGATGTCG
r-PXR	AAAGCAGTGGCCACCTAACA	CCCCACATACACGGCAGATT
GAPDH	CAAGGTCATCCATGACAACCTTTG	GGGCCATCCACAGTCTTCTG
PKA	GCTGGCTTTGATTTACGG	GATGTTTTCGCTTGAGGATA
CaMKII	CCTGAACCCTCACATCCACC	CCAGGTACTGAGTGATGCGG
SERCA2a	TCTGACTTTCGTTGGCTGTG	GCCTTTGTTATCCCCAGTGA
PLB	TACCTTACTCGCTCGGCTATC	GAGAAGCATCACAAATGATGACC

2.7. Western Blot Analysis. Protein concentrations were determined using a BCA protein assay kit. Proteins were analyzed by sodium dodecyl sulfate-polyacrylamide gel electrophoresis (SDS-PAGE) and blotted using standard protocols [19]. The expression was quantified by densitometry and normalized to the GAPDH expression. Then, all groups were normalized to their respective controls.

2.8. Coimmunoprecipitation Assay. A coimmunoprecipitation (co-IP) assay was conducted to examine the physical association between SERCA2a and p-PLB/PLB. A co-IP assay was performed using the Universal Magnetic Co-IP Kit (Active Motif) according to the manufacturers' protocol. Briefly, H9c2 cells were treated with phosphate-buffered saline (PBS)/inhibitor solution and collected by brief centrifugation and lysed in lysis buffer. Protein complexes were immunoprecipitated using SERCA2a antibody (CST) or IgG as a control. The immunoprecipitation was performed overnight at 4°C. The complexes were incubated with Protein G Magnetic Beads for 1 h at 4°C on a rotator. The resin was washed four times with 500 μ L complete co-IP/wash buffer. The eluted protein complexes were resolved by SDS-PAGE (10% gel) and detected with PLB/p-PLB antibody.

2.9. Immunofluorescence Colocalization. The colocalization of SERCA2a and PLB/p-PLB proteins in ISO-induced HF was detected. H9c2 cells were cultured in DMEM supplemented with 10% FBS and penicillin-streptomycin (100 IU/mL) in a humidified atmosphere of 95% air and 5% CO₂ at 37°C. The cells were seeded on laser confocal small dish for each experiment and grown in a 37°C humidified incubator containing 5% CO₂. After 24 h drug treatment, the cell culture media was removed, and cells were washed with 1 \times PBS. The cells were fixed in 100% ice-cold methanol for 10–15 min at room temperature and allowed to dry for 15 min. Next, the cells were washed twice with 1 \times PBS/IFA for 5 min and permeabilized with 0.3% Triton-X 100 in 1 \times PBS/IFA for 10 min followed by washing twice with 0.03% Triton-X 100 for 5 min. The cells were blocked in 5% BSA in 1 \times PBS/IFA for 1 h. Then, the cells were incubated with the appropriate primary antibody (rabbit-SERCA2a, mouse-PLB, rabbit-p-PLB; both diluted 1:1000) at 4°C for overnight. After washing, the cells were incubated with the corresponding secondary antibody (goat anti-mouse IgG, FITC-conjugated and goat anti-rabbit IgG, RBITC-conjugated), diluted 1:500 for another 1 h. 4',6-diamidino-2-phenylindole (DAPI) was added to cells at a dilution of 1:2000 for 1 h in the dark. Then, the cells were

washed six times with 0.03% Triton-X 100 for 5 min and sealed with the Prolong[®] Gold antifade reagent. Sections were examined using the LSM800 confocal laser scanning microscope. The immersion-oil Plan Neofluar 60/0.75 objective was used. Double fluorescence for green and red channels was imaged using excitation of an argon-krypton laser at wavelengths of 488 and 543 nm. Images were acquired and processed for colocalization analysis in the TIFF format. Quantitative analysis was performed employing ImageJ Pro Plus Software.

2.10. H9c2 Cell Culture and Small Interfering RNA Transfection. H9c2 cells were seeded at a density of 1.2×10^6 /well in a 6-well dish. At 12 h after plating, the cells were incubated with 80 nmol/L CYP2J3 small interfering RNA (siRNA) and control siRNA in 1 mL Opti-MEM medium for 6 h as previously described. After 6 h, new serum-free DMEM with OPD and ISO was added. Cells were incubated for another 24 or 48 h for different experiments.

2.11. Small-Molecule Inhibition of Kinase and Metabolic Targets. H-89 and KN-93 (1 μ mol/L; Selleck), specific inhibitors for PKA and CaMKII, respectively, were used to investigate PKA/Ser¹⁶-PLB, and CaMKII/Thr¹⁷-PLB signaling pathways mediated the effect of OPD. Cells were treated with the abovementioned medium containing H-89 and KN-93 for 6 h, finally cultured in a medium containing ISO (1 μ mol/L) and the highest concentration of OPD (1 μ mol/L).

2.12. Molecular Biology and HEK293T Cell Culture. Rat PLB fused to the C-terminus of the cyan fluorescent protein (CFP), and rat SERCA2a fused to the C-terminus of the enhanced yellow fluorescent protein (YFP). Extraction of fluorescent protein plasmid was performed with Qiagen Company's Plasmid Extraction Kit (Plasmid DNA Maxiprep Kit; Germantown, MD, USA). HEK293T cells were cultured on dishes coated with polylysine. The dishes were filled with complete DMEM growth medium containing 10% heat-inactivated FBS. The cells were transfected according to the manufacturer's instructions after the cell density reached 10%. MEM growth medium was used instead of complete DMEM growth medium during the 6 h incubation of HEK293T with plasmid. For the FRET experiments, HEK293T cells were cotransfected with CFP-PLB plasmid and YFP-SERCA2a plasmid at a concentration of 500 ng/ μ L.

2.13. Plasmid Detection and Time-Resolved FRET Imaging. Plasmids were transfected into HEK293T cells according to

the abovementioned procedures. The DNA sequencing results of the two recombinant plasmids were correct and can be used in downstream experiments. To verify the transfection efficacy of CFP-PLB plasmid and YFP-SERCA2a PLB into HEK293T cells, after a 24 h transfection, cells were lysed, and proteins from the cell lysates were resolved by electrophoresis followed by western blot analysis (see Section 2.7). The mixture was incubated with horseradish peroxidase-conjugated goat-anti-mouse or goat-anti-rabbit IgG secondary antibodies (1:2000) for 1 h at room temperature and visualized using the ImageQuant LAS 500 (Healthcare Biosciences AB, Uppsala, Sweden). Fluorescence imaging was performed with an inverted microscope equipped with the Plan-Apochromat 100 \times /1.40 Oil DIC M27 objective. For epifluorescence imaging, illumination was introduced through an excitation filter wheel equipped with 427/10 nm (for CFP) and 504/12 nm (for YFP) narrowband filters and a multiple band dichroic mirror. Emission was detected with a back-thinned electron-multiplying charged couple device camera (LSM 880; AxioObserver, Zeiss, Oberkochen, Germany) through the emission filter wheel, 472/30 nm (for CFP) and 542/27 nm (for YFP). "Prismless" total internal reflection fluorescence (TIRF) used the 458-nm Ar laser line, directed through the objective with a multiple band dichroic mirror. TIRF emission was selected with filters described above. For spatially resolved, acceptor-selective photobleaching, the Ar laser 514-nm line was selected by a laser line filter and directed to the sample with a10/90 beam splitter. The bleach beam was focused to a spot on the specimen using a Keplerian telescope composed of two planoconvex lenses. Laser photobleaching exposure time was controlled by a Uni-blitz shutter and was typically for 54.55 s with 20 frames. The above activity was measured using software (ZEN). Image records from multiple experiments were averaged together to reduce error. Analysis of the evolution of the line-out profiles was performed by fitting image data with a custom analysis program written in Graphpad Software.

2.14. Statistical Analyses. All data were expressed as the mean \pm standard deviation (SD). Comparisons between groups were performed by a one-way analysis of variance. $P < 0.05$ was considered statistically significant.

3. Results

3.1. Effects of OPD on the Viability of H9c2 Cells. Cells were treated with different concentrations of OPD (1–80 μ mol/L), and the viability of H9c2 cells was detected by the CCK-8 assay. The cell viability was apparently decreased after the incubation with OPD. The results suggested that the responses stimulated by OPD on cell viability were concentration-dependent. High concentrations of OPD had obvious inhibitory effects on cell vitality. To investigate the effects of OPD on cardiomyocytes, OPD concentrations of 0.25, 0.5, and 1 μ mol/L were used in subsequent experiments (Figure 1).

3.2. Activation of the CYP2J3 Expression in H9c2 Cells and HEK293T Cells by OPD. To determine the effect of OPD on the CYP2J3 protein expression in cardiomyocytes, we per-

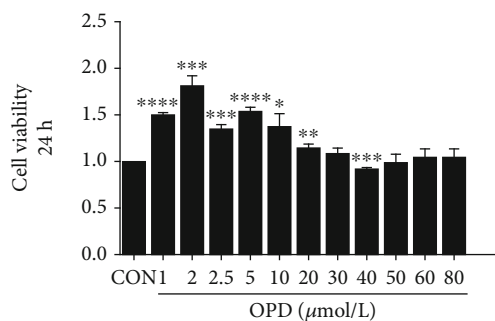


FIGURE 1: Effect of OPD on the viability of H9c2 cells. H9c2s were treated with different concentrations of OPD (1–80 μ mol/L) for 24 h, and the cell viability was detected by the CCK-8 assay, * $P < 0.05$, ** $P < 0.01$, and *** $P < 0.005$ versus the control group, $n = 4$ per group.

formed immunoblot analyses and qPCR. OPD qualitatively induced the CYP2J3 mRNA and protein expression as expected (Figure 2(a)), in accordance with previous results [16, 20]. Next, we determined the effects of OPD on CYP2J3 using an ISO-induced cell model, which represents a state of heart failure. H9c2 cell lysates were prepared for the estimation of the CYP2J3 immunoreactive protein; GAPDH was used to indicate protein loading. From Figure 2(b), the CYP2J3 mRNA and protein expression was increased at each concentration by OPD and ISO cotreatment. ISO is a β -adrenergic receptor agonist, which induces HF both in vitro and in vivo [21]. The expression of CYP2J3 was decreased in the ISO-induced HF group. The role of OPD was illustrated by data showing that transfection of CYP2J3 siRNA into H9c2 cells, which inhibited the CYP2J3 expression, abrogated the inhibitory of ISO on CYP2J3 degradation (Figures 2(c) and 2(d)). pLVX-IRES-ZsGreen-1-CYP2J3 plasmid was transfected into HEK293T cells for 24 h, and cells were treated with OPD for another 24 h. The fluorescence intensity of CYP2J3 was detected by laser confocal focusing (Figure 2(e)). Compared with the CYP2J3 group, the fluorescence intensity in the OPD-treatment group was significantly increased.

3.3. OPD Induces Colocalization of SERCA2a and p-PLB through CYP2J3 at the ER. To determine whether SERCA2a colocalized with PLB/p-PLB, colocalization of three proteins in H9c2 cells was examined by immunofluorescence using a confocal microscope. The results showed some colocalization between SERCA2a and PLB/p-PLB to different degrees. OPD induced colocalization between SERCA2a and p-PLB (Figure 3(b)), while SERCA2a and PLB protein showed decreased colocalization in H9c2 cells after OPD treatment (Figure 3(a)). Transfection of CYP2J3 siRNA was performed to test the CYP2J3 function in the colocalization of SERCA2a/PLB and SERCA2a/p-PLB. After the transfection of CYP2J3 siRNA, H9c2 cells were treated with OPD and ISO as mentioned above to determine the induction of OPD in HF cells (Figures 4(a) and 4(b)). Images show immunofluorescence of SERCA2a (green) and p-PLB (red) proteins in H9c2 cells and changes of their colocalization pattern following the OPD (1 μ mol/L) and ISO (1 μ mol/L) administration

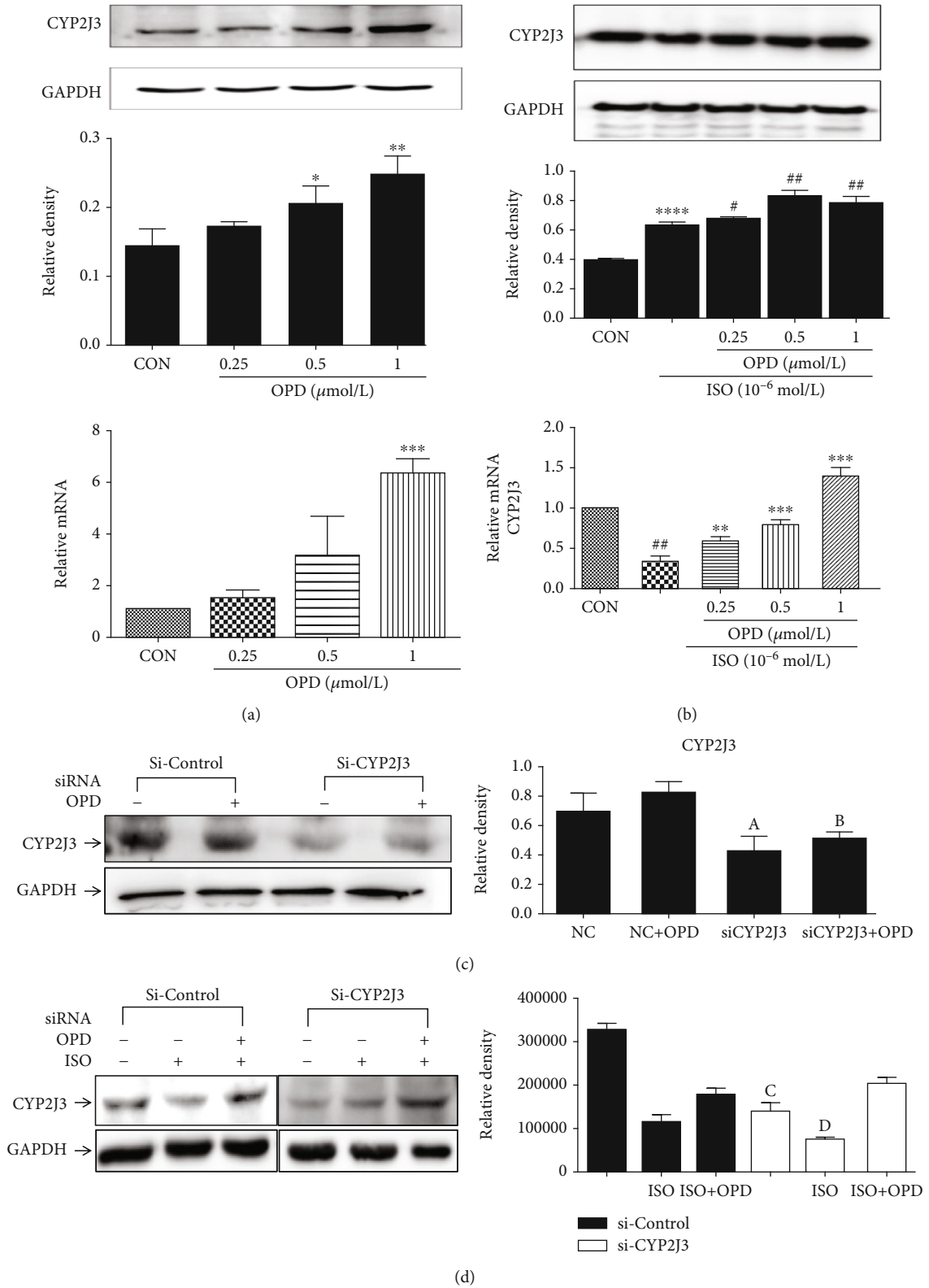


FIGURE 2: Continued.

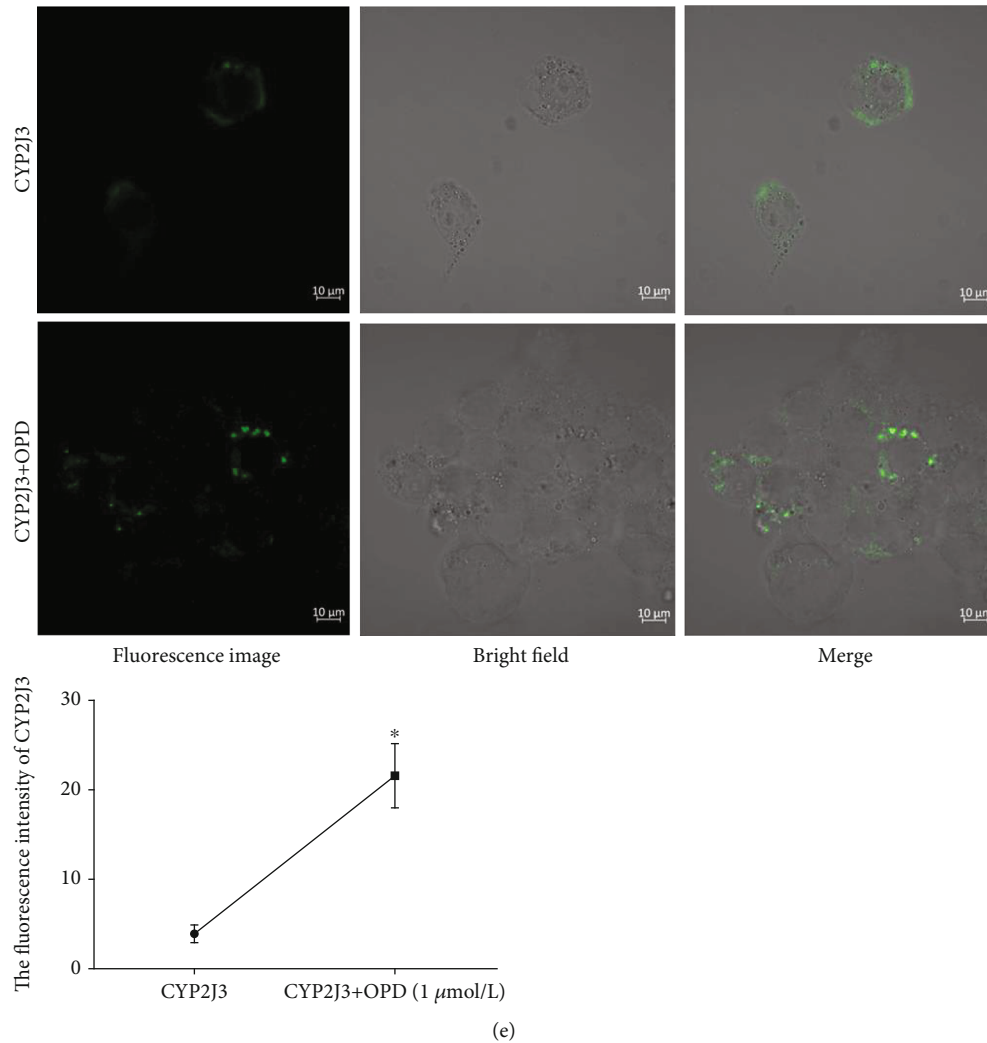


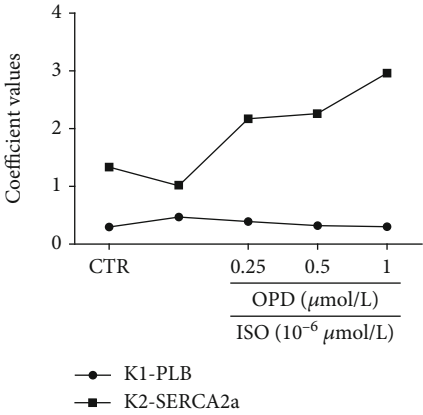
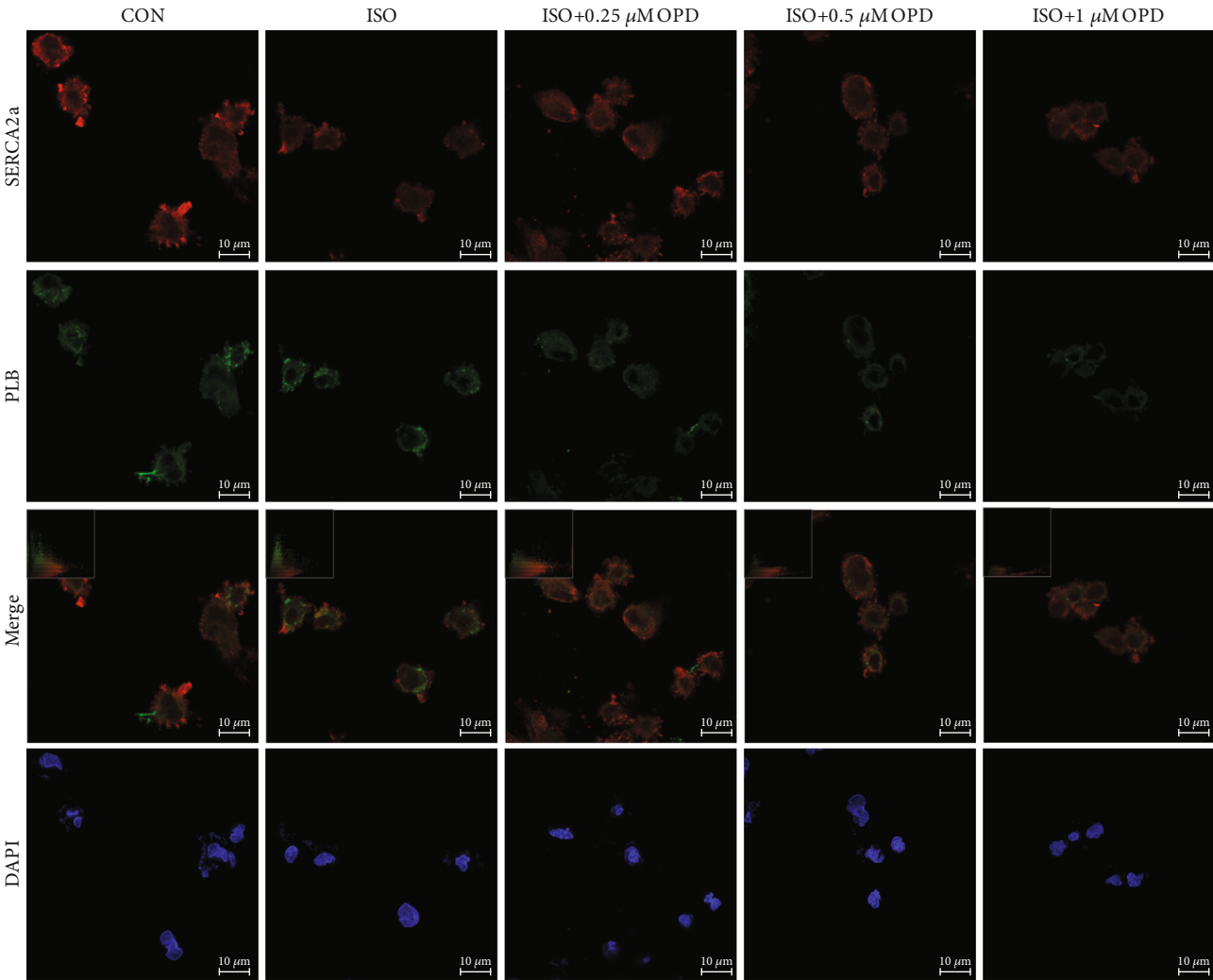
FIGURE 2: Effect of OPD on the expression of CYP2J3 in H9c2 cells and 293 T cells. (a) H9c2s were treated with different concentrations of OPD (0.25, 0.5, 1 μmol/L) for 24 h. CYP2J3 mRNA and protein expression were increased in OPD-treatment groups $^*P < 0.05$, $^{**}P < 0.01$ versus the control group; $^{***}P < 0.005$ versus the ISO-treatment group (1 μmol/L). (b) H9c2s were cotreated with ISO (1 μmol/L) and different concentrations of OPD (0.25, 0.5, 1 μmol/L) for 24 h. CYP2J3 mRNA and protein expression were decreased in the ISO-treatment group $^{***}P < 0.005$ versus the control group; $^*P < 0.05$, $^{**}P < 0.01$, and $^{***}P < 0.005$ versus the ISO-treatment group. (c) CYP2J3-siRNA and negative control- (NC-) siRNA were transfected into H9c2s. Cells were treated with OPD (1 μmol/L) and ISO (1 μmol/L) as mentioned above. CYP2J3 mRNA and protein expression were decreased in the Si-CYP2J3 group, $^aP < 0.05$ versus the si-control group; the CYP2J3 protein and mRNA level were increased in the OPD-treated group, $^bP < 0.01$ versus the OPD-treated NC group. (d) CYP2J3-siRNA and NC-siRNA were transfected with H9c2s. Cells were cotreated with OPD (1 μmol/L) and ISO (1 μmol/L) as mentioned above. CYP2J3 mRNA and protein expression were decreased in the si-CYP2J3 group, $^cP < 0.05$ versus the si-control group; CYP2J3 mRNA and the protein expression were decreased in the ISO-treated si-CYP2J3 group, $^dP < 0.01$ versus the ISO-treated NC group. (e) 293 T cells were transfected with pLVX-IRES-ZsGreen-1-CYP2J3 plasmid for 24 h. Cells were treated with OPD (1 μmol/L) for 24 h. The CYP2J3 expression was increased in the OPD-treated+CYP2J3 transfected group versus the CYP2J3 transfected group, $n = 3$ per group.

as mentioned above. An embedded scattergram estimated the amount of each detected antigen based on colocalization. Colocalized pixels of yellow color are located along the diagonal of the scattergram. Compared with the NC group, the red (p-PLB) intensity decreased in the si-CYP2J3 group. The OPD-treated si-CYP2J3 group showed increased p-PLB intensity compared with the OPD-treated NC group.

3.4. OPD Increases the Physical Association between SERCA2a and p-PLB through CYP2J3.

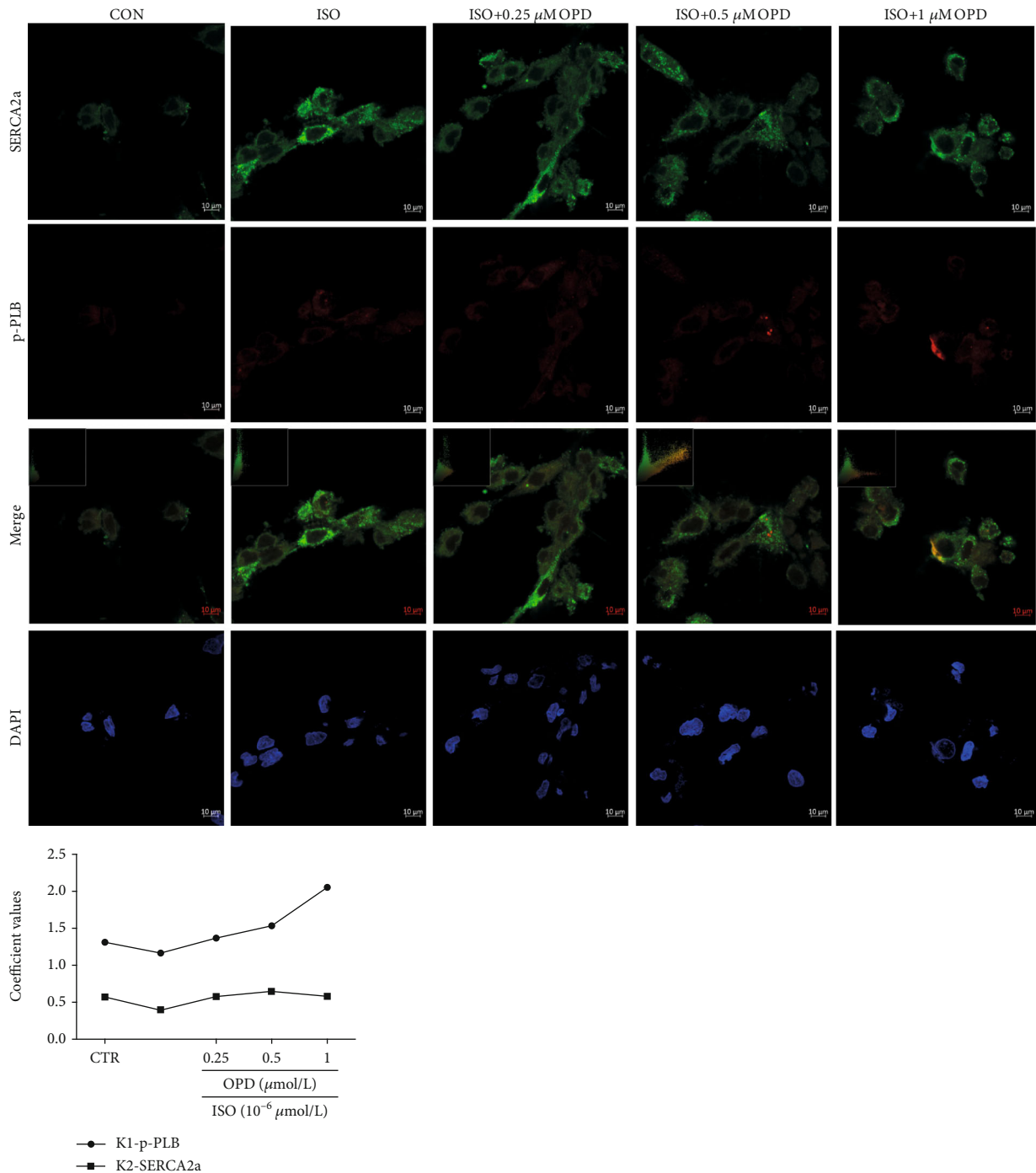
To evaluate the influ-

ence of OPD in the interaction of p-PLB with SERCA2a, H9c2 cells were treated with OPD and ISO as mentioned above. Total cellular proteins were extracted. After preclearing with protein G sepharose beads, the cell lysates were incubated with or without an anti-SERCA2a antibody followed by incubation with protein G sepharose beads. The co-IP'd protein complexes were eluted and analyzed by western blotting using antibodies against p-PLB and PLB. Co-IP'd bands were seen for p-PLB and PLB (Figure 5(a)), while the antibody used could detect the capsid protein in western blot



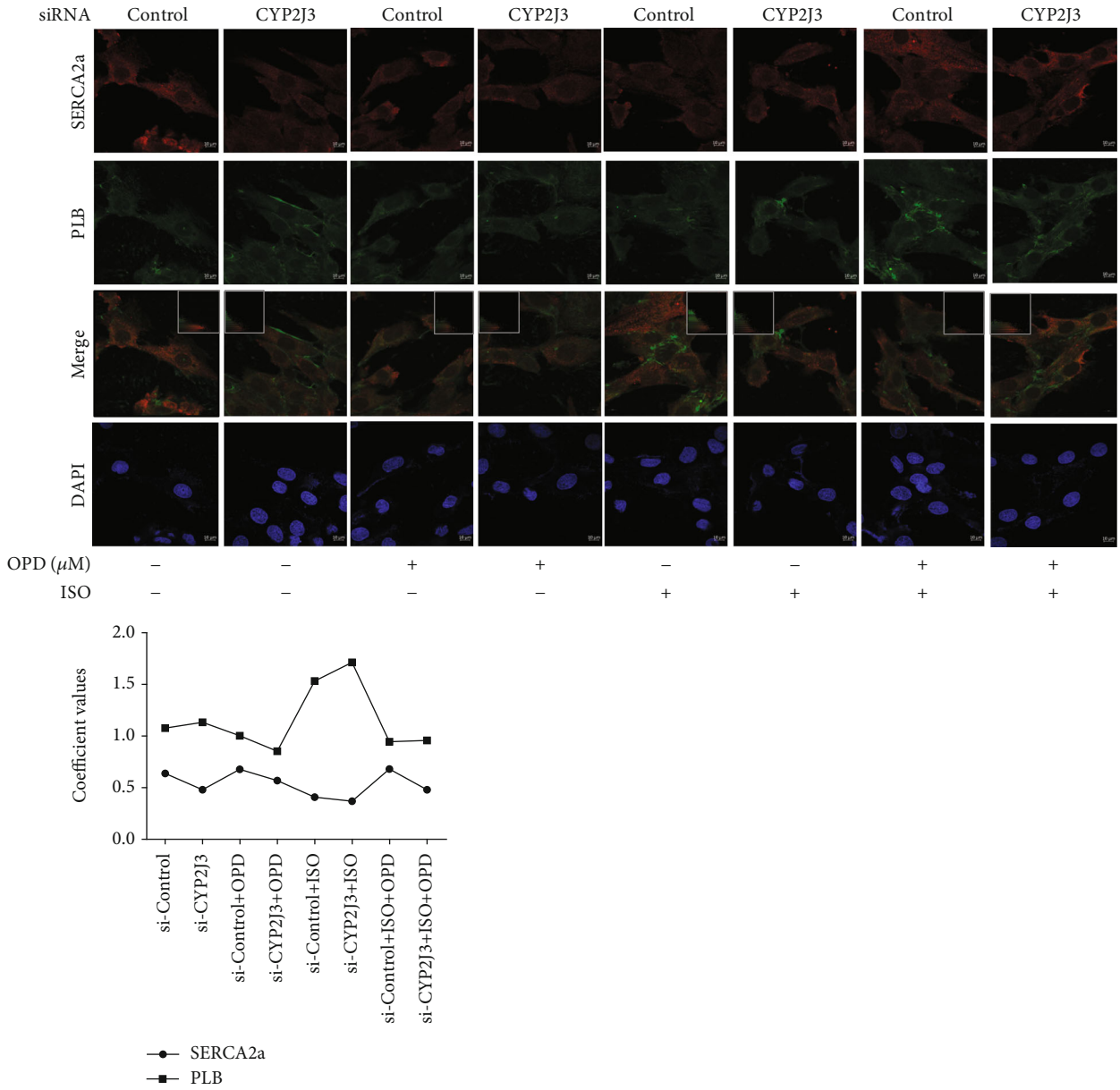
(a)

FIGURE 3: Continued.



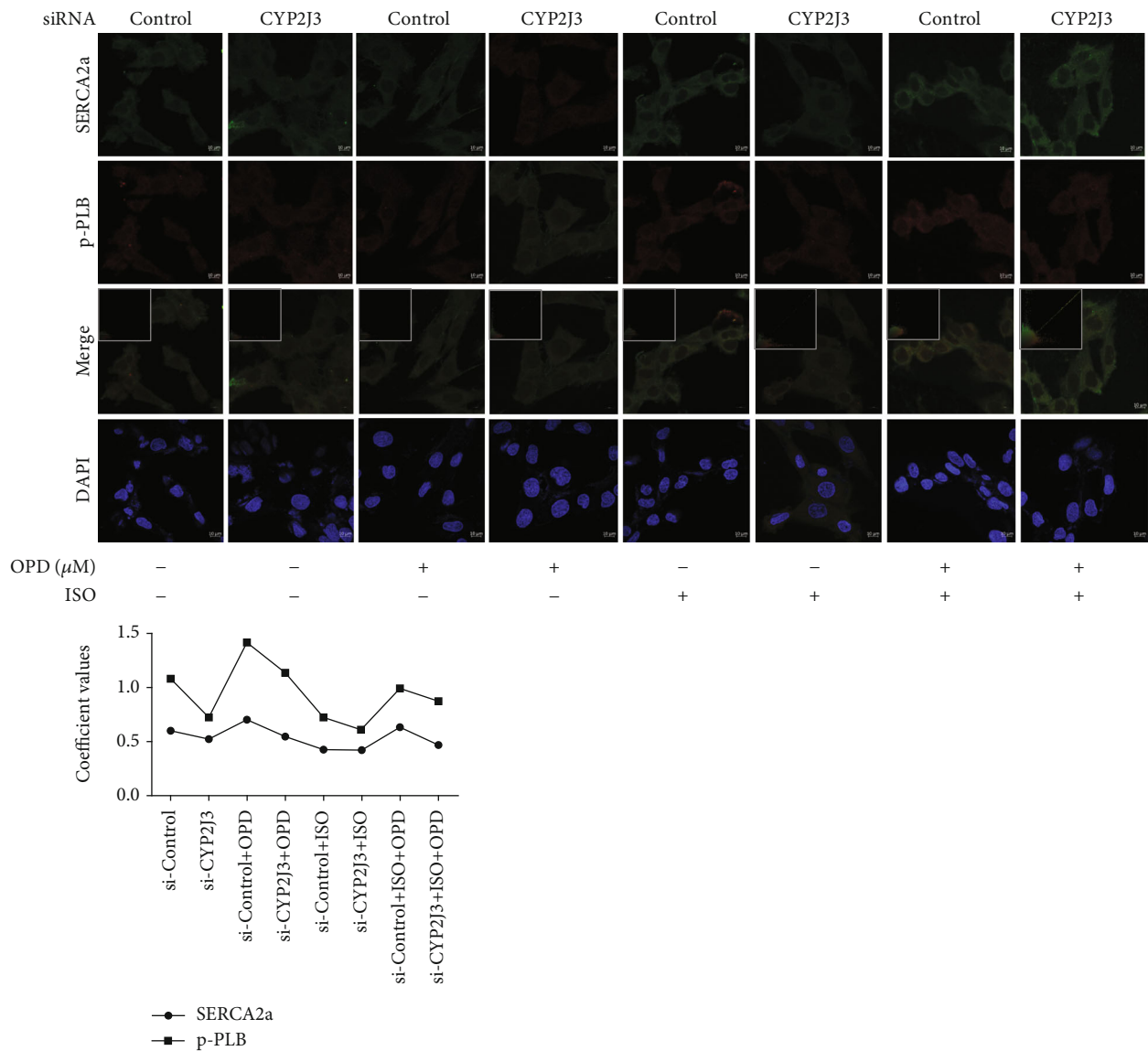
(b)

FIGURE 3: OPD induces SERCA2a colocalization of SERCA2a and p-PLB in HF cells. Images were collected on the LSM880 confocal microscope with Plan-Apochromat $\times 63$. (a) Images showing immunofluorescence of SERCA2a (red) and PLB (green) proteins in H9c2 cells and changes of their colocalization pattern following OPD (1 $\mu\text{mol/L}$) and ISO (1 $\mu\text{mol/L}$) administration. An embedded scattergram estimated the amount of each detected antigen based on colocalization. Colocalized pixels of yellow color are located along the diagonal of the scattergram. Compared with the control group, the green (PLB) intensity increased in the ISO-treated group while the red (SERCA2a) intensity decreased. The OPD-treated group showed decreased PLB intensity compared with the ISO-treated group. (b) Images showing immunofluorescence of SERCA2a (green) and p-PLB (red) proteins in H9c2 cells and changes of their colocalization pattern following OPD (1 $\mu\text{mol/L}$) and ISO (1 $\mu\text{mol/L}$) administration. An embedded scattergram estimated the amount of each detected antigen based on colocalization. Colocalized pixels of yellow color are located along the diagonal of the scattergram. Compared with the control group, the red (p-PLB) intensity decreased in the ISO-treated group. The OPD-treated group showed increased p-PLB intensity compared with the ISO-treated group.



(a)

FIGURE 4: Continued.



(b)

FIGURE 4: OPD induced SERCA2a colocalization of SERCA2a and p-PLB through CYP2J3 in H9c2 cells. Cells were transfected with CYP2J3 siRNA for 24 h. ISO and OPD were administrated as mentioned above. (a) Images showing immunofluorescence of SERCA2a (red) and PLB (green) proteins in H9c2 cells and changes of their colocalization. An embedded scattergram estimated the amount of each detected antigen based on colocalization. Colocalized pixels of yellow color are located along the diagonal of the scattergram. Compared with the NC group, the green (PLB) intensity increased in the Si-CYP2J3 group while the red (SERCA2a) intensity decreased. The OPD-treated si-CYP2J3 group showed decreased PLB intensity compared with the OPD-treated NC group. (b) Images showing immunofluorescence of SERCA2a (green) and p-PLB (red) proteins in H9c2 cells and changes of their colocalization pattern following OPD ($1 \mu\text{mol/L}$) and ISO ($1 \mu\text{mol/L}$) administration as mentioned above. An embedded scattergram estimated the amount of each detected antigen based on colocalization. Colocalized pixels of yellow color are located along the diagonal of scattergram. Compared with the NC group, the red (p-PLB) intensity decreased in the si-CYP2J3 group. The OPD-treated si-CYP2J3 group showed increased p-PLB intensity compared with the OPD-treated NC group.

analysis. The co-IP assay demonstrated that the endogenous SERCA2a protein was specifically co-IP'd with p-PLB in an OPD-dependent manner (Figure 5(a)). To confirm the regulatory function of CYP2J3 in the interaction between SERCA2a and p-PLB/PLB proteins, H9c2 cells were transfected with CYP2J3 si-RNA for 24 h, and the immunoprecipitations were repeated. Membranes were initially probed with an antibody against SERCA2a and subsequently with antibodies

against the immunoprecipitating protein. The results suggest that the suppression of CYP2J3 alleviates the physical binding between SERCA2a and p-PLB (Figure 5(b)). Furthermore, OPD may induce the expression of CYP2J3 to promote the interaction of SERCA2a and p-PLB.

3.5. OPD Increases the Ca^{2+} -ATPase Activity and Ca^{2+} Uptake in the ER after 24H of ISO Supplementation. ISO

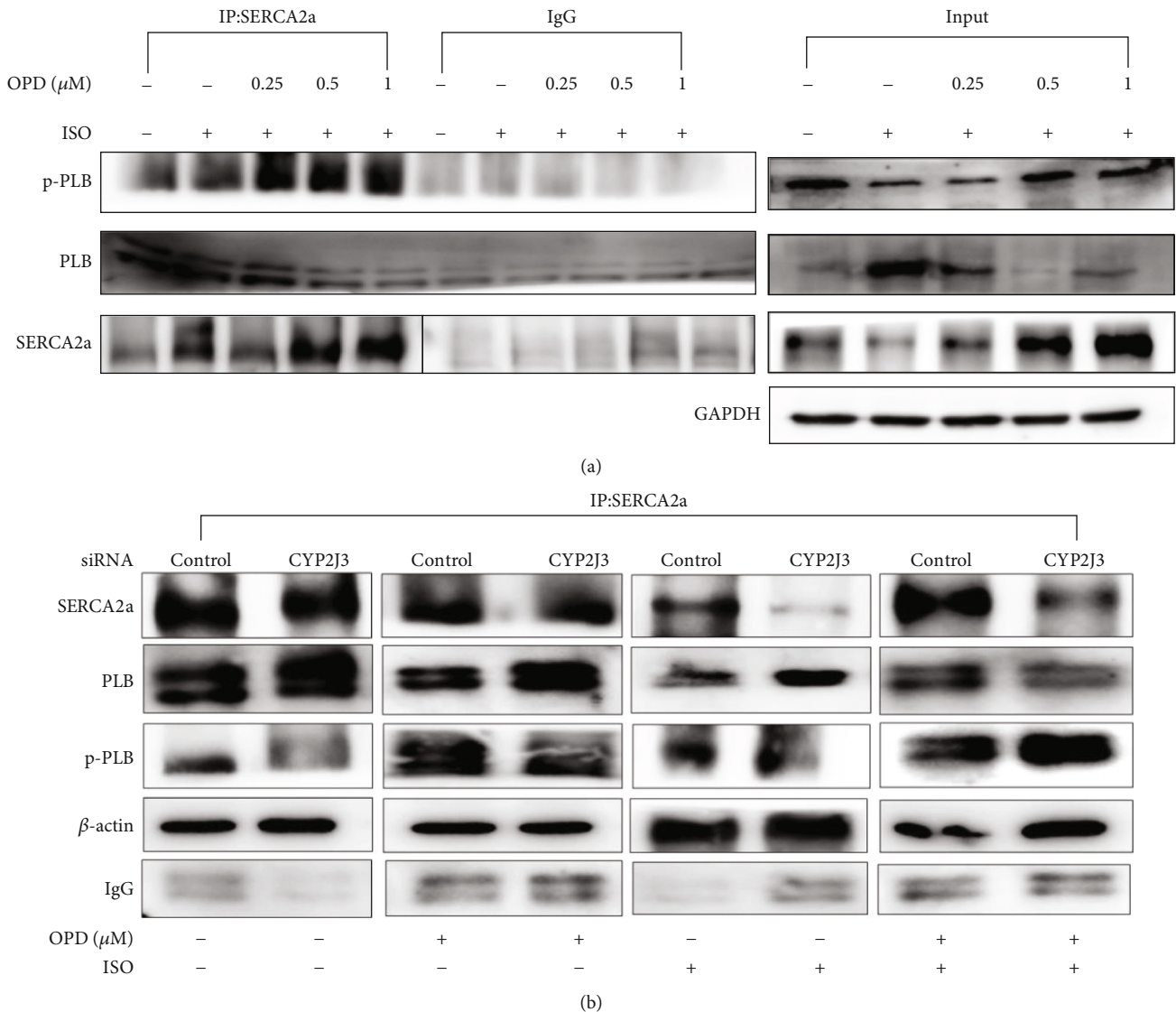


FIGURE 5: SERCA2a co-IP analysis of p-PLB and PLB proteins. (a) H9c2 cells were pretreated with ISO (1 μmol/L) and OPD (0.25, 0.5, 1 μmol/L) at the indicated concentrations mentioned above. The physical association between SERCA2a and PLB/p-PLB was examined by a co-IP assay. Compared with the ISO-treated group, OPD induced the interaction between SERCA2a and p-PLB in a dose-dependent manner. (b) CYP2J3-siRNA and NC-siRNA were transfected into H9c2s. Cells were cotreated with OPD (1 μmol/L) and ISO (1 μmol/L) as mentioned above. Western blot analysis of the interaction between SERCA2a and p-PLB/PLB proteins by co-IP. CYP2J3 depletion weakened the physical binding of SERCA2a and p-PLB in H9c2 cells, and OPD treatment improved the faint binding caused by CYP2J3.

supported Ca²⁺ uptake in the ER was significantly lower than the control. In addition, compared with the ISO-treated group, OPD supported Ca²⁺ uptake was much higher (Figures 6(b) and 6(c)). Next, we explored the possible action of OPD on the Ca²⁺-ATPase. The activity of Ca²⁺-ATPase was weaker in ISO-treated HF cells than in nontreated control cardiomyocytes. Importantly, treatment with OPD markedly improved the activity of Ca²⁺-ATPase in a dose-dependent manner (Figure 6(a)).

3.6. OPD Activates PLB Phosphorylation in HF Cells. To verify whether OPD transcriptionally modulates the expression of proteins involved in Ca²⁺ transportation, we performed qPCR to measure the steady-state levels of mRNA encoding the subunits of SERCA2a and PLB. As already observed at

the protein level, the expression of SERCA2a and PLB mRNA was increased in the OPD-treated group compared with the controls (Figure 7). The phosphorylation status of PLB was able to remove the inhibitory effect of PLB on SERCA2a, resulting in increased SR-Ca²⁺ uptake and enhanced myocyte contractility and relaxation (Ca²⁺ and excitation-contraction coupling in the heart). We actually measured a marked decrease in total PLB associated with a more evident increase in the phosphorylated form of the protein, resulting in a significant increase in the p-PLB/PLB ratio. Consistent with this finding, a more efficient intracellular Ca²⁺ dynamic was observed in H9c2 cells. It is worth noting that OPD-treated cells exhibited a significantly higher p-PLB/PLB ratio compared with ISO-induced (Figure 8(a)) and AngII-induced (Figure 8(b)) HF cardiomyocytes.

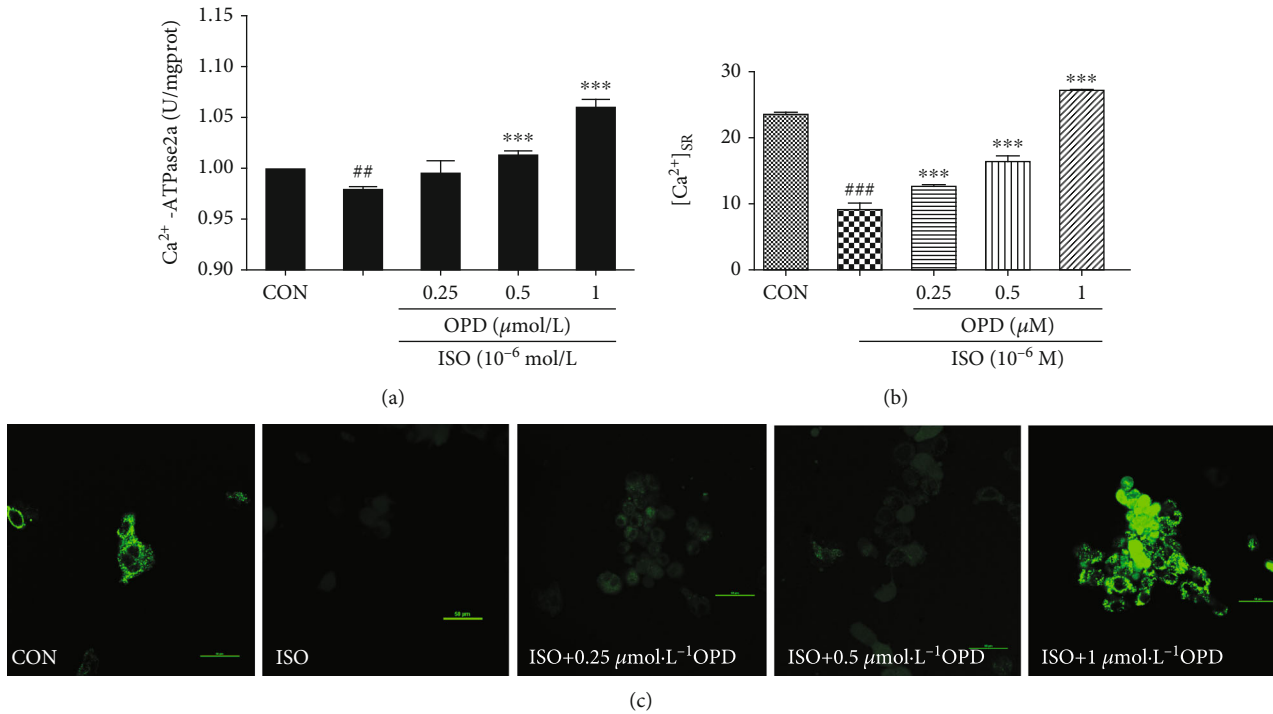


FIGURE 6: Effects of OPD on ER Ca^{2+} uptake and Ca^{2+} -ATPase activity in HF cells. (a) Effects of OPD on the Ca^{2+} -ATPase activity measured by the quantity of Pi. The activity of SERCA2a was decreased in the ISO-treatment group, $^{##}P < 0.01$ versus the control group; OPD ($1 \mu\text{mol/L}$) induced the Ca^{2+} -ATPase activity, $^{***}P < 0.005$ versus the ISO-treatment group. (b, c) Effects of OPD followed ISO ($1 \mu\text{M}$) on $[\text{Ca}^{2+}]_{\text{SR}}$. Application of $1 \mu\text{M}$ ISO indicated complete depletion of $[\text{Ca}^{2+}]_{\text{SR}}$ compared with the control group, $^{###}P < 0.005$. Twenty-four hour application of OPD increased the Ca^{2+} uptake in ER, $^{***}P < 0.005$ versus the ISO-treated group, $n = 3$ per group.

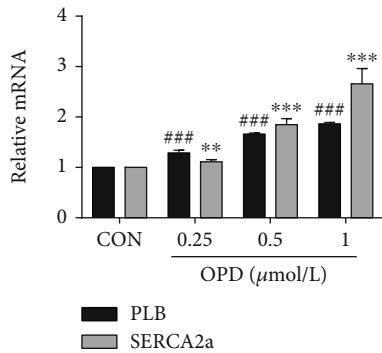


FIGURE 7: Effects of OPD on the expression of SERCA2a and PLB mRNA. The PLB and SERCA2a mRNA expression increased compared with the control group, $^{**}P < 0.01$, $^{***}P < 0.005$, $^{###}P < 0.005$, $n = 3$ per group.

3.7. Inhibition of the PKA and CaMKII Cascade Does Not Abolish the Effect of OPD on Phosphorylation of PLB. It is already known that PLB is phosphorylated by either PKA at the Ser¹⁶ residue or CaMKII at the Thr¹⁷ residue [22]. To examine whether activation of the two kinase pathways by OPD results in the phosphorylation of PLB-mediated regulation of the SERCA2a, we performed a series of experiments with chemical modulators of the PKA and CaMKII pathway, such as the H-89 (PKA inhibitor) and KN-93(CaMKII inhibitor). The results showed a clear dissociation between the phosphorylation of Ser¹⁶

and Thr¹⁷ residues of PLB after AngII and ISO treatment, respectively. The H-89 (PKA inhibitor) selectively induced a decrease in Ser¹⁶ phosphorylation during AngII and OPD cotreatment (Figure 9(a)). In other words, OPD played a role in the phosphorylation of PLB-Ser¹⁶ through the AngII-induced PKA cascade. As a result, we examined the expression of PKA and p-PKA after AngII and OPD cotreatment. We found that OPD induced the activation of PKA cascade in AngII-treated HF cells (Figure 9(c)). Interestingly, CaMKII seems not to be activated in the AngII-induced HF cell model (Figure 9(c)). During ISO treatment, KN-93 (CaMKII) selectively induced a decrease in Thr¹⁷ phosphorylation after OPD application (Figure 9(b)). OPD selectively induced phosphorylation of PLB-Thr¹⁷ through the CaMKII pathway with ISO treatment in H9c2 cells. OPD induced the expression of phosphorylated CaMKII in ISO-treated HF cells (Figure 9(d)), indicating that selective underlying mechanisms are involved in the phosphorylation of two sites. This point was further explored in subsequent experiments.

3.8. The FRET Assay of HEK293T Cells Expressing SERCA2a and PLB. To optimize the conditions of transient transfection in HEK293T cells, cells were infected with YFP-SERCA2a and CFP-PLB (Figure 10(a)) for 24 h. Total cellular proteins were extracted, resolved by electrophoresis, and transferred to nitrocellulose membranes before being subjected to western blot analysis to determine the expression of PLB and SERCA2a with GAPDH used as a loading control. The results showed the expected band sizes of SERCA2a

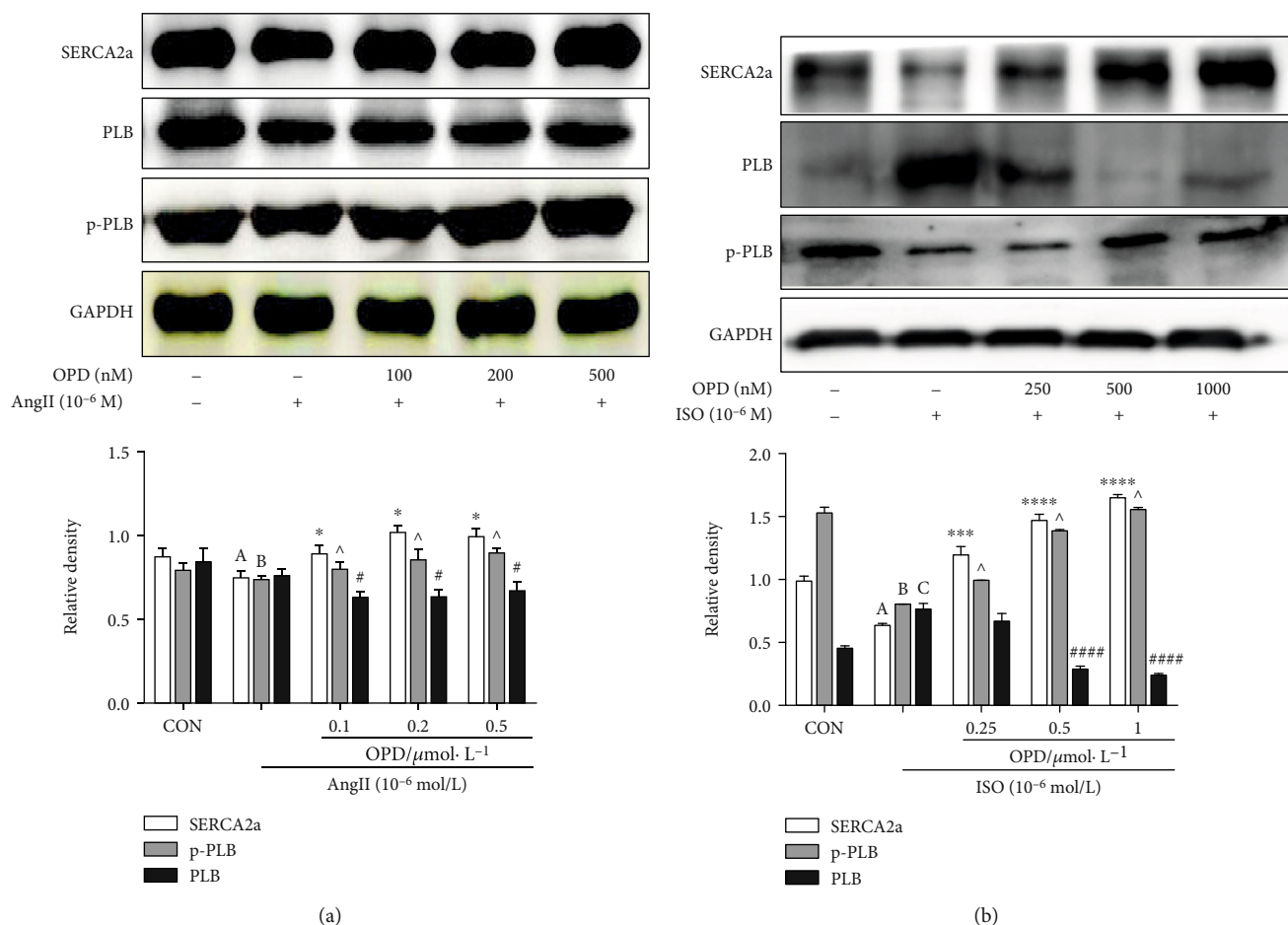


FIGURE 8: Effects of OPD on the phosphorylated status of PLB in different HF cardiomyocytes. (a) SERCA2a and p-PLB protein levels were decreased in AngII-induced HF cells, ^{a,b} $P < 0.005$ versus the control group. The PLB expression increased compared with the control group, ^c $P < 0.005$. Different concentrations of OPD (0.1, 0.2, 0.5 $\mu\text{mol/L}$) reversed the change compared with the AngII-treated group, ^{*} $P < 0.05$, [^] $P < 0.05$, [#] $P < 0.05$. **(b)** SERCA2a and p-PLB protein levels were decreased in ISO-induced HF cells, ^{a,b} $P < 0.005$ versus the control group. The PLB expression increased compared with the control group, ^c $P < 0.005$. Different concentrations of OPD (0.25, 0.5, 1 $\mu\text{mol/L}$) reversed the change compared with the ISO-treated group, ^{*} $P < 0.05$, [^] $P < 0.05$, [#] $P < 0.05$, $n = 3$ per group.

(170 kDa), PLB (35 kDa), and GAPDH (25 kDa), which indicated the suitable transfection conditions (Figure 10(b)). When two fluorescent probes are brought into close proximity ($< 100 \text{ \AA}$), they can undergo FRET [23, 24]. FRET between YFP-SERCA2a and CFP-PLB was detected by selective photobleaching of YFP. CFP fluorescence increased locally after brief YFP exposure to a focused spot of 514 nm laser illumination (Figure 10(c), arrow). CFP-SERCA intensity (postbleach/prebleach) indicated that about 18% increase in CFP-SERCA fluorescence was restricted to the target site (Figure 10(c)). Donor enhancement after acceptor photobleaching is diagnostic of FRET [25]. After OPD pretreatment for 6 h, FRET between YFP-SERCA2a and CFP-PLB was observed as mentioned above (Figure 10(d), arrow). The intensity of CFP did not significantly change after YFP photobleaching (Figure 10(d)). This may be attributed to OPD blocking the unphosphorylated status of PLB.

3.9. OPD Induces Pregnane X Receptor Nuclear Translocation.

It is known that pregnane X receptor (PXR) is a “master regulator” or “xenosensor” for the metabolism and clearance of

diverse endogenous and exogenous compounds [26]. When a ligand (prescription drugs, herbal supplements, vitamins, and other endobiotics) binds to PXR [22], target genes are upregulated through transcriptional induction. CYP3A4 is the most important and well-studied target gene of PXR, which is the crucial drug/xenobiotic enzyme and metabolizes about 50% of all drugs and xenobiotics [27]. In addition, PXR regulates the expression of several other important drug/xenobiotic-metabolizing enzymes such as CYP2C9, CYP2B6, CYP2C19, and CYP3A5 [22]. The regulation of CYP2J is relatively deficient when compared with other isoforms belonging to the CYP2 subfamily, such as CYP2C, 2D, and 2E. Furthermore, the transcriptional regulator of CYP2J3 still remains ambiguous. Our previous study demonstrated that OPD promoted the translocation of PXR from the cytoplasm to the nucleus in a concentration-dependent manner (Figure 11(a)). To identify the regulatory effect of PXR on CYP2J3, the expression of CYP2J3 decreased after the transfection of PXR-siRNA into H9c2 cells (Figure 11(b)). In addition, OPD reversed the decline in the PXR expression after Helicid (specific inhibitor of

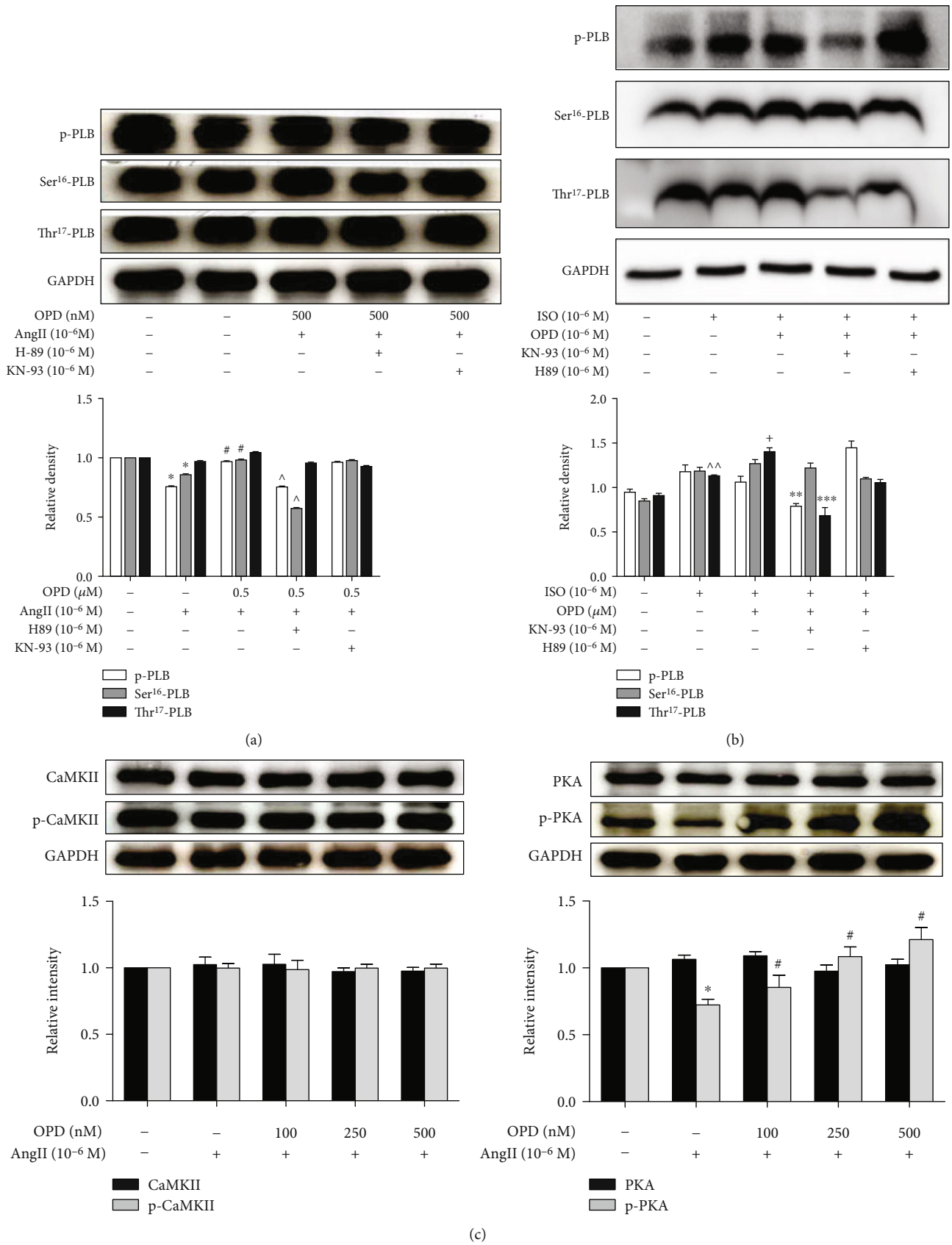


FIGURE 9: Continued.

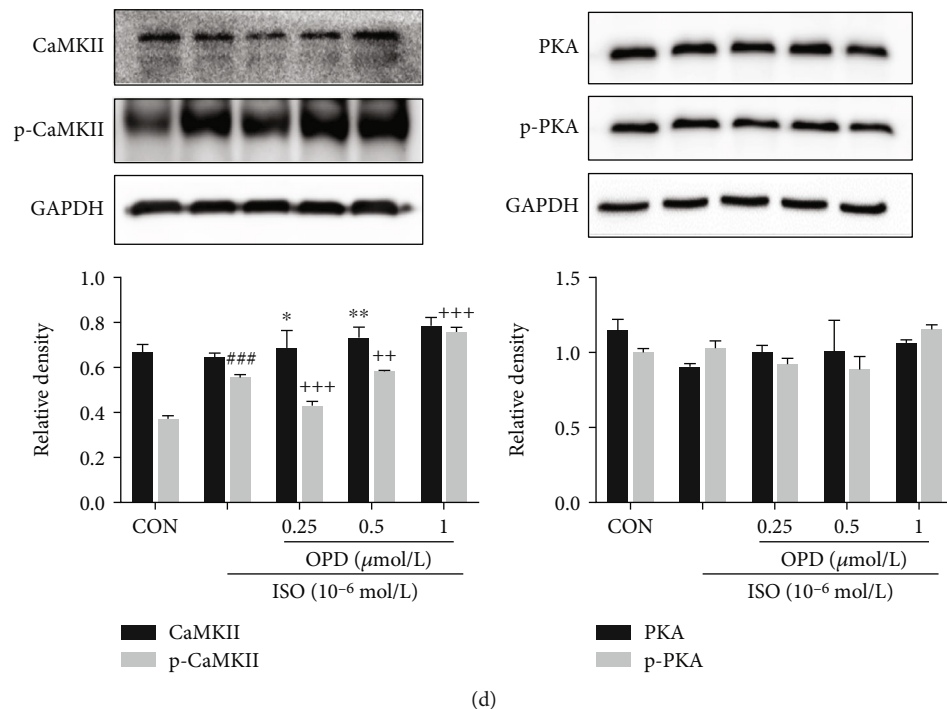


FIGURE 9: Effects of OPD on the phosphorylated status of PLB in ISO or Ang-II induced HF cells. (a) H-89 selectively inhibited Ser¹⁶ phosphorylation of PLB during AngII and OPD cotreatment. (b) KN-93 selectively inhibited Thr¹⁷ phosphorylation of PLB during ISO (1 μmol/L) and OPD (1 μmol/L) cotreatment. (c) PKA was phosphorylated in Ang-II induced HF cells, **P* < 0.05 versus the control group. OPD promoted the expression of p-PKA (the activation state of PKA), **P* < 0.05 versus the Ang-II-treated group. Furthermore, there was no significance in the expression of CaMKII and p-CaMKII. (d) CaMKII was phosphorylated in ISO-induced HF cells, ****P* < 0.005 versus the control group. OPD promoted the expression of p-CaMKII (activation state of CaMKII), ++*P* < 0.05, +++*P* < 0.05 versus the ISO-treated group, *n* = 3 per group. Furthermore, there was no significance in the expression of PKA and p-PKA.

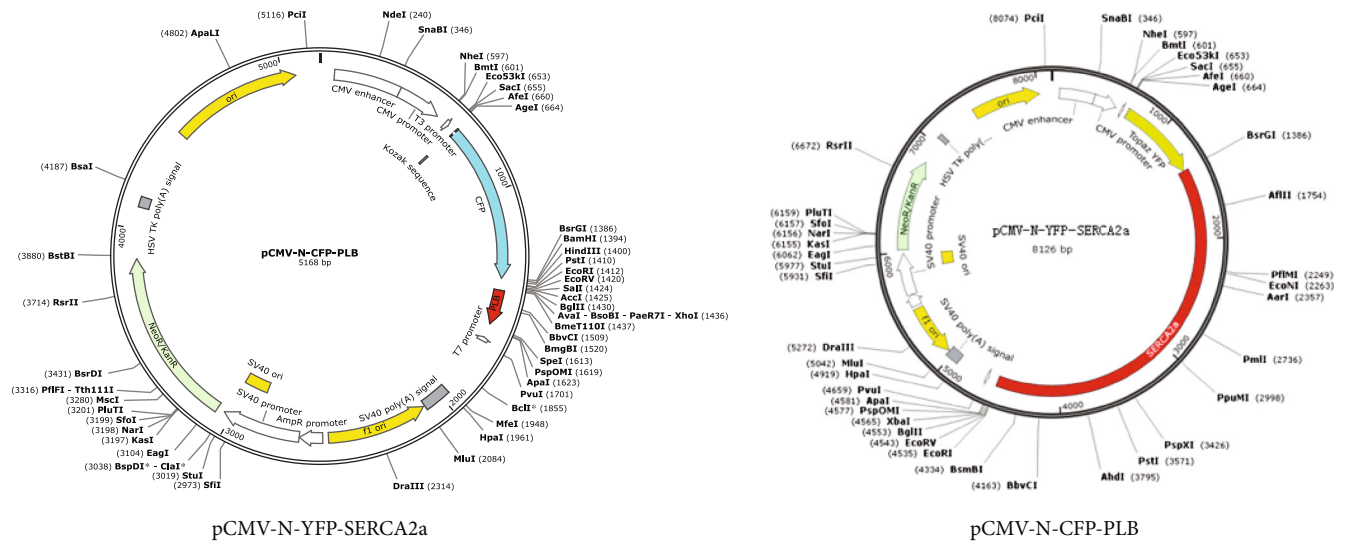
PXR) treatment (Figure 11(c)). After the transfection of si-PXR in ISO-induced HF H9c2 cells, the expression of CYP2J3 decreased, and OPD could reverse this decrease (Figure 11(d)).

4. Discussion and Conclusions

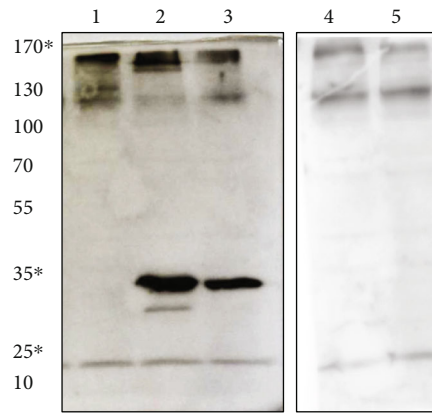
OPD is a steroidal glycoside isolated from *Radix ophiopogonis*, which has recently garnered increasing interest for its anti-inflammatory and antioxidative activities in different cardiovascular diseases [28–30]. Our previous studies first reported that OPD can induce both the CYP2J3 and CYP2J2 expression. Specifically, OPD significantly reduced intracellular Ca²⁺ overload by upregulating the levels of CYP2J3/EETs in rat myocardial cells. Moreover, OPD promoted Ca²⁺ homeostasis by regulating Ca²⁺ handling proteins, which included SERCA2a and PLB [29]. The above studies in our laboratory reported for the first time that OPD can effectively induce CYP2J and affect the expression of calmodulin. However, there is no in-depth study on whether OPD can directly affect the interaction between SERCA2a and PLB, or whether CYP2J3 participates in modulating the interaction between SERCA2a with PLB remains unknown. The current study is a further study of the above work. It is first confirmed that OPD can directly enhance the interaction between SERCA and phosphorylated PLB. Our previous two in vivo studies verified the cardiovascular protective effect of

OPD through the ischemia-reperfusion model and myocardial hypertrophy animal model [20]. In the current study, we reported that in vitro OPD can exert its anti-HF effects by inducing the interaction between SERCA2a and PLB through CYP2J3, identifying CYP2J3 as a direct intracellular target of OPD and providing important insight into the mechanism of OPD actions. The primary myocardial cells, as the cells derived from the myocardial tissue, are closest to the myocardial tissue. In the further study, we will verify the effect of OPD on HF in mice such as the TCA heart failure model or primary myocardial cells. The previous experiment results in our lab demonstrated that OPD (0.1 μmol/L~80 μmol/L) had no obvious toxic effect on cells (cell viability > 84%). Besides, cells were treated with different times and concentrations of OP-D (0.1~200 μmol/L), the viability of HUVECs was detected by MTT assay, and the results suggested that high concentrations (80 μmol/L) of OPD had obvious inhibitory effect on cell vitality (>85%) [20]. Similarly, in the current experiment, OPD had no obvious toxic effect on H9c2 cells.

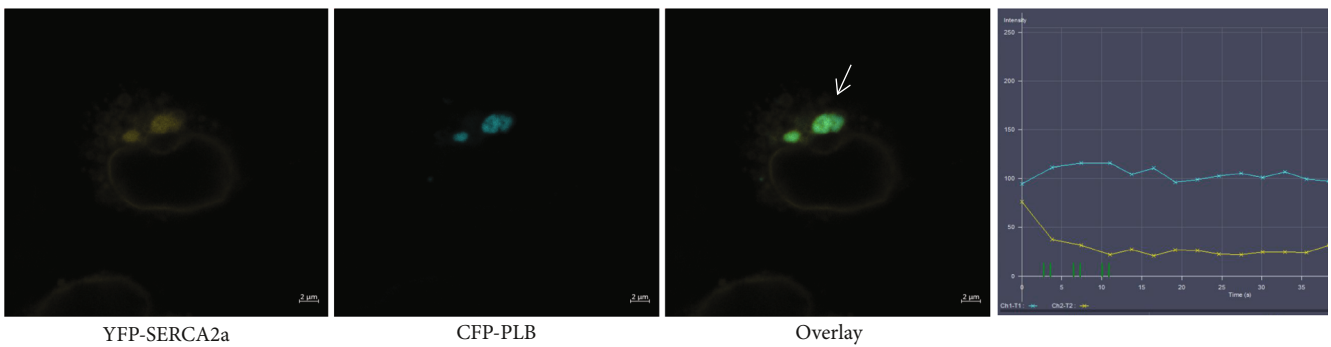
In addition, it can be concluded that OPD targets Ca²⁺ homeostasis in the ER. The results of this study revealed that the reduction PLB can restore the frequency response in failing cardiomyocytes [31, 32]. The intracellular Ca²⁺ handling system of the SR plays a critical role in the maintenance of the normal cardiac pumping activity [31, 32]. PLB is recognized as an important regulator for the normal cardiac function



(a)



(b)



(c)

FIGURE 10: Continued.

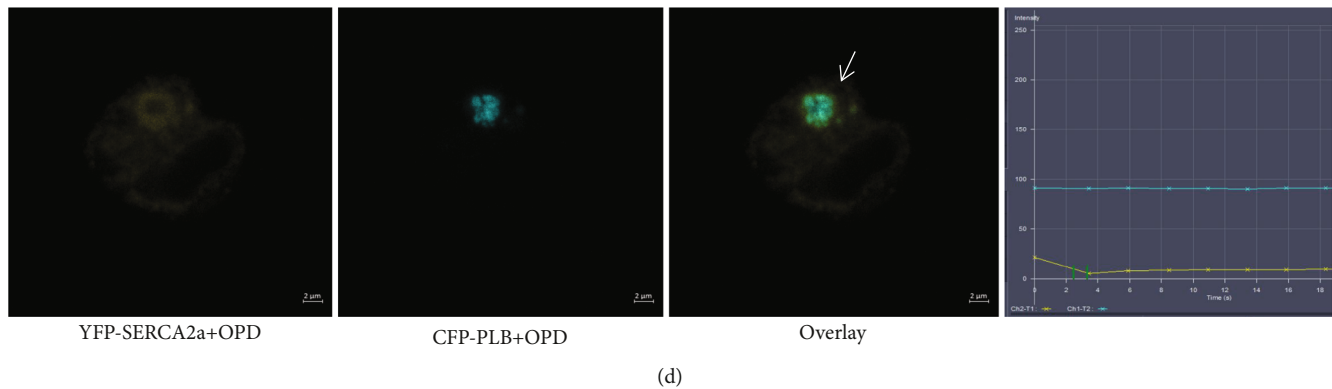
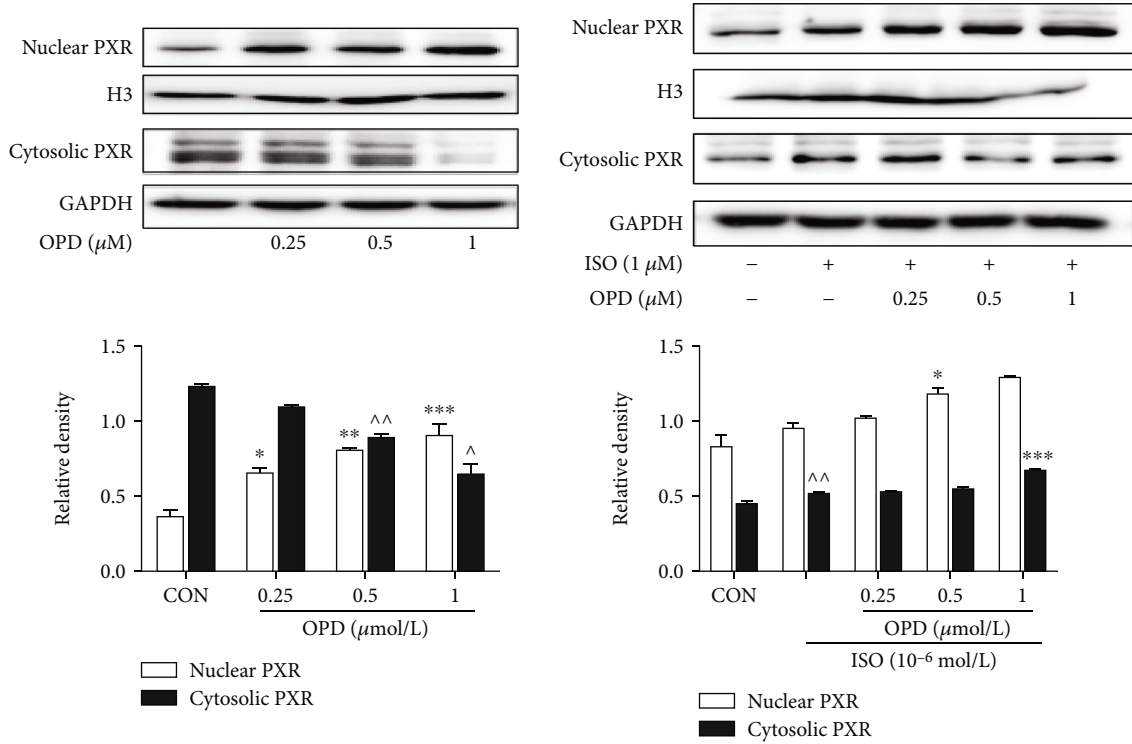


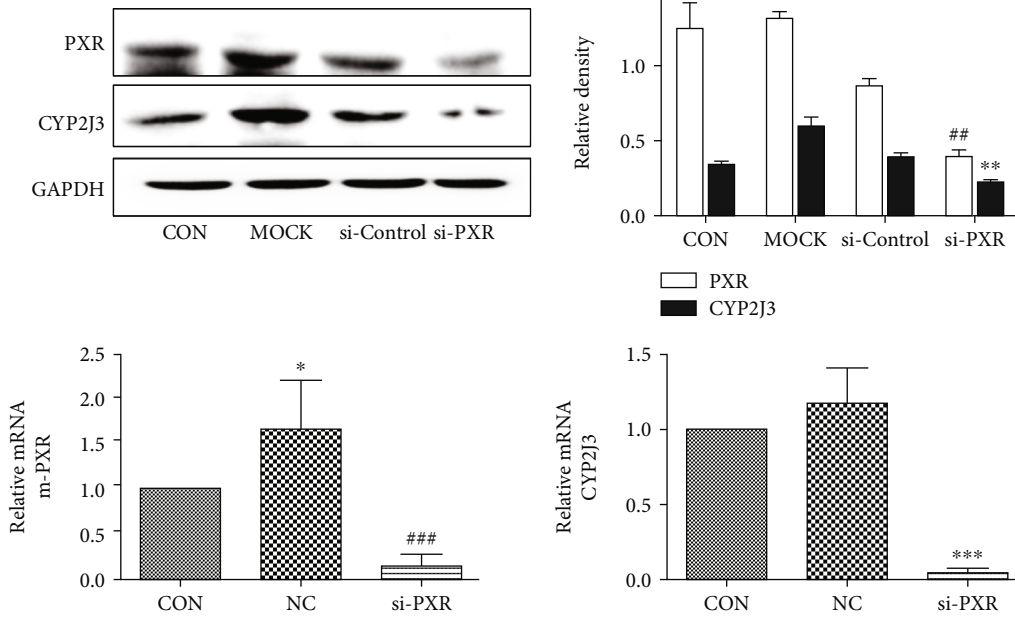
FIGURE 10: The FRET assay of HEK293T cells expressing SERCA2a and PLB. (a) The plasmid profiles of pCMV-N-YFP-SERCA2a and pCMV-N-CFP-PLB. (b) Immunoblot of CFP-PLB, YFP-SERCA2a, and CFP/YFP with anti-PLB monoclonal antibody, anti-SERCA2a antibody, and anti-GFP antibody, respectively. Lanes from the left are (1) pCMV-N-YFP-SERCA2a (predicted band size: 170 kDa), (2) pCMV-N-CFP-PLB (predicted band size: 35 kDa), (3) pCMV-N-CFP-PLB+pCMV-N-YFP-SERCA2a, (4) untransfected HEK293T cell homogenate control, and (5) pCMV-N-YFP + pCMV-N-CFP (predicted band size: 27 kDa). (c) Profiles of YFP-SERCA2a (yellow points) and CFP-PLB (blue points) fluorescence at 10 s after YFP-selective laser spot photobleaching. The data are described in the line chart, and the arrow shows the relationship between YFP-SERCA2a and CFP-PLB fluorescence across the target region. The intensity indicates 18% energy transfer. (d) Profiles of YFP-SERCA2a (yellow points) and CFP-PLB (blue points) fluorescence after OPD treatment. There is no obvious change in the CFP intensity after YFP-selective laser spot photobleaching.

[34]. In this study, we demonstrate that OPD associates with downregulation of PLB and upregulation of p-PLB and SERCA2a in two HF cell models (Figures 8(a) and 8(b)). The expression of PLB and SERCA2a is likely related to the size of Ca^{2+} stores in the SR and ultimately influences intracellular Ca^{2+} release and cardiac contractility. Upregulation of PLB may be harmful to cardiac performance by elevating diastolic Ca^{2+} attributable to suppression of SERCA2a. Central regulators of cardiac excitation-contraction coupling are PKA and CaMKII. An interesting phenomenon showed that OPD promoted the phosphorylation of PLB at Ser16 not Thr17 by increasing the PKA activity and no effects on CaMKII in the AngII-induced HF cell model, while in the ISO-induced HF cell model, OPD promoted the phosphorylation of PLB at Thr17 not Ser16 by increasing the CaMKII activity and no effects on PKA. Meanwhile, a series of inhibitors were used to confirm this phenomenon (Figure 9). The study reveals that CaMKII can be activated by oxidation at Met281/282 and phosphorylation at Thr287 [34]. Our results showed that OPD activated the phosphorylation of CaMKII in an ISO-induced HF cell model. CaMKII was phosphorylated by ISO, while OPD influenced the phosphorylation status. By contrast, ox-CaMKII was altered very little. Oxidative CaMKII was activated by AngII, while OPD released the oxidation (Figure 12). Interestingly, there was no obvious change in phosphorylated CaMKII (Figure 9). Previous research has revealed that OPD can clean the ROS to protect endothelial cells from H_2O_2 -induced oxidative stress [29]. OPD may ease the AngII-mediated oxidative burden to reduce the ox-CaMKII expression. In the heart, autophosphorylation of CaMKII is particularly prevalent during β -adrenergic signaling [32, 33]. HF and many of the conditions are associated with significant oxidative stress. ROS have been reported to lead to a dynamic PTM at methionine residues in vitro, which reveals that AngII and endothelin-1 (ET-1) activate CaMKII by a primarily oxidation-dependent

pathway [34]. The underlying mechanism may be related to the ISO-induced β -adrenergic signaling and AngII-induced primarily oxidation-dependent pathway [35]. We had checked the oxidized and phosphorylated expression of CaMKII in two HF cell models (Figure 11). It is the first time to discover and confirm that OPD has selectivity for PLB phosphorylation sites in heart failure models induced by different factors. Above results indicated that OPD can protect cardiomyocytes by directly promoting the phosphorylation of PKA or CaMKII or by reducing the oxidation level of CaMKII. All data showed that OPD-induced SERCA2a interaction and colocalization with PLB are mediated by CYP2J3 (Figures 3–5). Furthermore, our results support that OPD promotes PXR translocation from cytoplasm to the nucleus (Figures 3–5). PXR siRNA significantly attenuated the expression of CYP2J3 (Figures 10(b) and 10(c)). The PXR was originally discovered as a nuclear receptor for transcription regulation [36]. In our previous study, knocking down PXR might diminished the induced effect of OPD on CYP2J3 [16]. However, since this phenomenon was only initially discovered at that time, the data was not very sufficient at that time. Therefore, in the current study, we continued to verify and further confirmed that PXR was involved in OPD's transcriptional regulation of CYP2J with detailed results. The results further indicated that PXR might participate in the regulation of CYP2J3. Nuclear receptors, including PXR, CAR, and AHR, have regulatory effects on CYP enzyme. It is the first time that has been found and confirmed that PXR participates in the transcription induction of CYP2J. Whether other nuclear receptors or transcription factors participate in the transcription regulation of CYP2J needs further studies. Taken together, our finding that CYP2J3 mediates the interaction between SERCA2a and PLB suggesting that the appropriate expression and function of CYP2J3 is critical in maintaining Ca^{2+} homeostasis. Indeed, alterations in the CYP2J3 expression and translational modification are

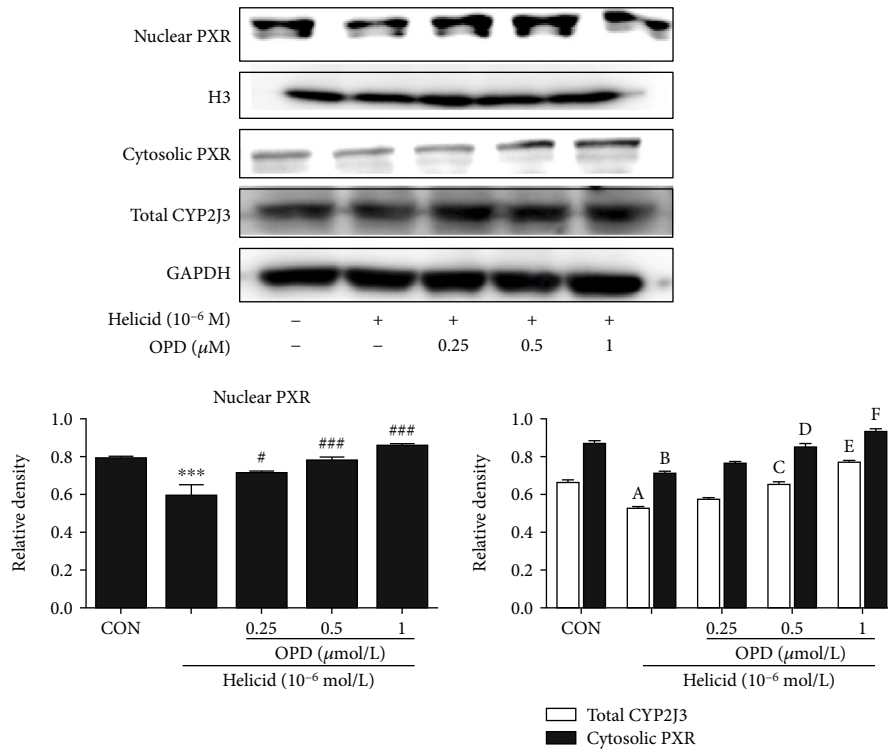


(a)

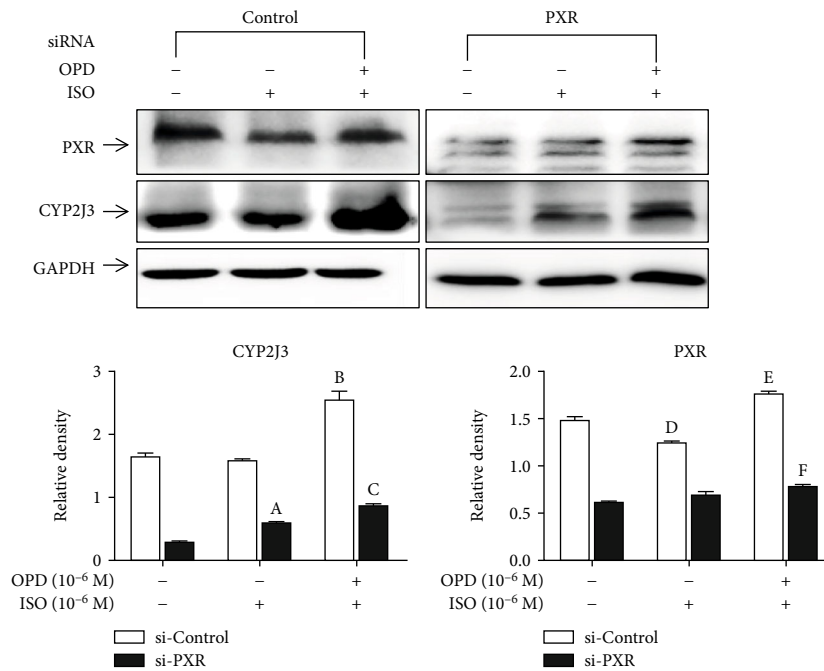


(b)

FIGURE 11: Continued.



(c)



(d)

FIGURE 11: The expression of CYP2J3 decreased after the PXR was knocked down. (a) OPD induces PXR nuclear translocation in H9c2 cells. **P* < 0.05, ***P* < 0.01 compared with the control group. (b) The expression of CYP2J3 decreased after the PXR was knocked down, ****P* < 0.001, ###*P* < 0.001 versus the NC group. The effect of OPD on the transcription of the genes encoding CYP2J3 in HF H9c2 cells transfected with siPXR. ^a*P* < 0.01, ^d*P* < 0.01 versus the si-control group. ^b*P* < 0.05, ^c*P* < 0.05 versus the si-control group. ^e*P* < 0.001, ^f*P* < 0.001 versus the si-control group. (c) The expression of CYP2J3 decreased after the PXR was knocked down. ****P* < 0.001 versus the control group, ^a*P* < 0.05, ^b*P* < 0.001 versus the Helicid group. ^c*P* < 0.05, ^d*P* < 0.05, ^e*P* < 0.05, ^f*P* < 0.05 compared with the Helicid group. (d) The effect of OPD on the expression of CYP2J3 and PXR after PXR was knocked down in HF H9c2 cells. ^a*P* < 0.01, ^d*P* < 0.01 versus the si-control group. ^b*P* < 0.05, ^c*P* < 0.05 versus the si-control group. ^e*P* < 0.001, ^f*P* < 0.001 versus the si-control group, *n* = 3 per group.

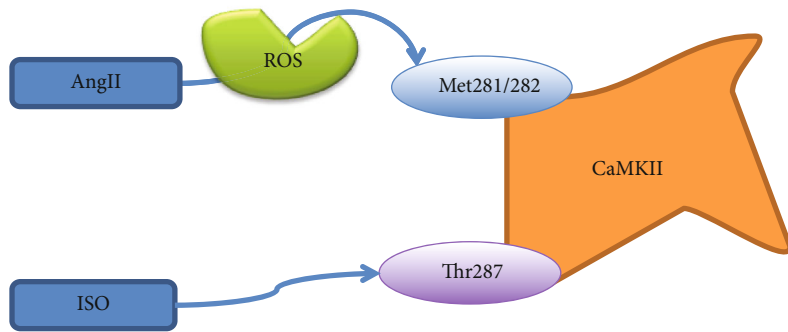
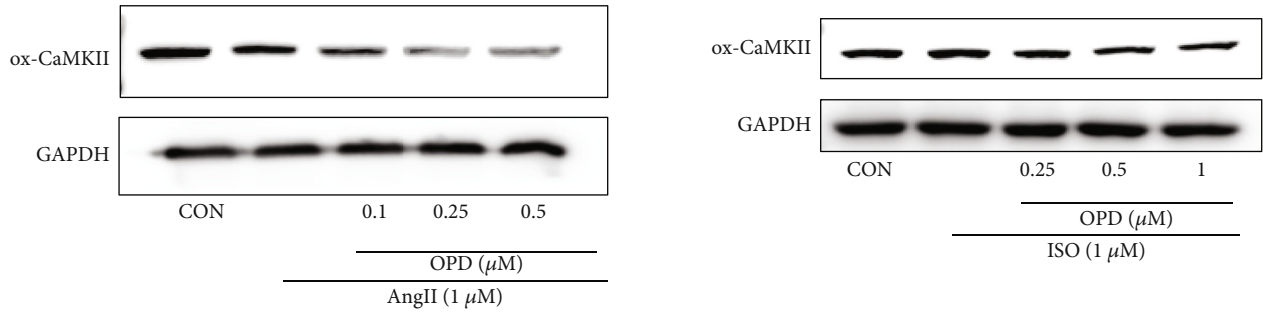


FIGURE 12: Effect of OPD on CaMKII. OPD activated the phosphorylation of CaMKII in this ISO-induced HF cell model. By contrast, ox-CaMKII was altered very little. Oxidative CaMKII was activated by AngII, whereas OPD released the oxidation.

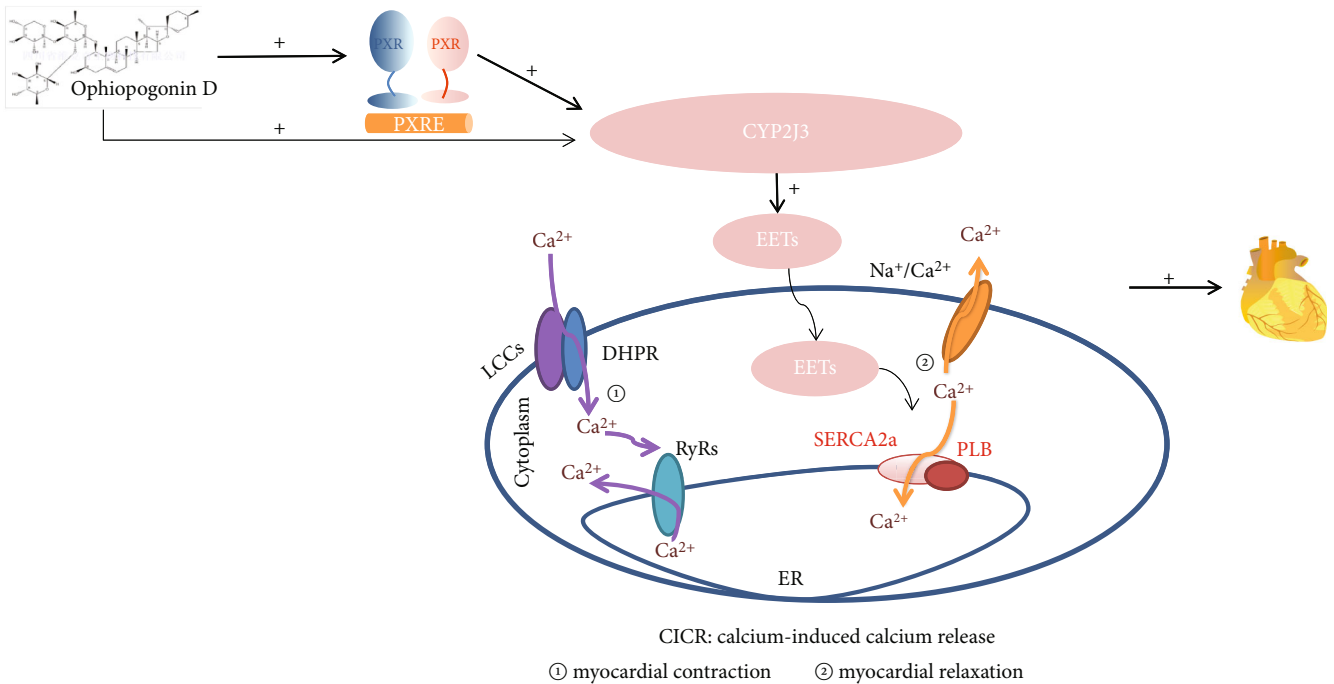


FIGURE 13: Ophiopogonin D increases SERCA2a interaction with phospholamban by promoting CYP2J3 upregulation (abbreviation: LCCs: L-type calcium channel; EETs: epoxyeicosatrienoic acids; DHPR: dihydropyridine receptor; RyRs: ryanodine receptor; SERCA2a: Ca²⁺-ATPase2a; PLB: phospholamban; ER: endoplasmic) reticulum.

implicated in the onset and progression of cardiac hypertrophy, myocardial I/R injury, and other disordered Ca²⁺ regulation diseases [37–40]. Our laboratory has carried out systematic research around OPD, which has proved that

OPD has a very good pharmacological effect on heart failure, mainly by inducing CYP2J to promote the SERCA2a activity, maintaining intracellular calcium homeostasis, and then protecting myocardial cells. It showed that OPD has a good

prospect and development value to become a drug for the treatment of cardiovascular disease. Whether it can become a drug for the treatment of heart failure needs to be carried out according to the guiding principle of new drug development, but OPD as the leading compound for the treatment of heart failure is beyond doubt. To this end, our results identify CYP2J3 as an attractive target and OPD as a promising lead for HF therapy (Figure 13).

Abbreviations

FRET:	Fluorescence resonance energy transfer
PXR:	Pregnane X receptor
OPD:	Ophiopogonin D
SERCA2a:	Ca ²⁺ -ATPase2a
PLB:	Phospholamban.

Data Availability

The [cell viability, measurement of ER Ca²⁺ and Ca²⁺-ATPase activity, qPCR, western blot analysis, coimmunoprecipitation assay, immunofluorescence colocalization, small interfering RNA transfection, time-resolved FRET imaging] data used to support the findings of this study are included within the article.

Disclosure

This Declaration acknowledges that this paper adheres to the principles for transparent reporting and scientific rigour of preclinical research recommended by funding agencies, publishers, and other organizations engaged with supporting research.

Conflicts of Interest

The authors declared that they have no conflicts of interest to this work. We declare that we do not have any commercial or associative interest that represents a conflict of interest in connection with the work submitted.

Authors' Contributions

Yuguang Wang designed this study. Jia Wang performed the experiments, analyzed the data, and drafted the manuscript. Wenting You, Ningning Wang, Wei Zhou, Yunxuan Ge, Zengchun Ma, and Hongling Tan assisted with in the experiments. Jia Wang and Yuguang Wang wrote the manuscript. Yuguang Wang and Yue Gao reviewed the manuscript.

Acknowledgments

We are grateful to Dr Huang who give us useful suggestions and to Dr Yang who provided cells. For listed authors, Yuguang Wang, Jia Wang, and Yue Gao designed this study. Jia Wang performed the experiments, analyzed the data, and drafted the manuscript; Wenting You, Ningning Wang, Wei Zhou, Yunxuan Ge, Zengchun Ma, and Hongling Tan assisted with in the experiments. Jia Wang and Yuguang Wang wrote the manuscript. Yuguang Wang and Yue Gao

reviewed the manuscript. We sincerely appreciate all those who have helped us. This work was supported by the National Science Foundation [81873032]. This research was supported by the National Key Research and Development Program [No. 2018YFC1704500].



References

- [1] C. Westphal, B. Spallek, A. Konkel et al., "CYP2J2 overexpression protects against arrhythmia susceptibility in cardiac hypertrophy," *PLoS One*, vol. 8, no. 8, article e73490, 2013.
- [2] W. B. Campbell, "New role for epoxyeicosatrienoic acids as anti-inflammatory mediators," *Trends in Pharmacological Sciences*, vol. 21, no. 4, pp. 125–127, 2000.
- [3] H.-X. Wang, D.-M. Zhang, X.-J. Zeng et al., "Upregulation of cytochrome P450 2J3/11,12-epoxyeicosatrienoic acid inhibits apoptosis in neonatal rat cardiomyocytes by a caspase-dependent pathway," *Cytokine*, vol. 60, no. 2, pp. 360–368, 2012.
- [4] L. Liu, C. Chen, W. Gong et al., "Epoxyeicosatrienoic acids attenuate reactive oxygen species level, mitochondrial dysfunction, caspase activation, and apoptosis in carcinoma cells treated with arsenic trioxide," *The Journal of Pharmacology and Experimental Therapeutics*, vol. 339, no. 2, pp. 451–463, 2011.
- [5] X. Xu, R. Li, G. Chen, S. L. Hoopes, D. C. Zeldin, and D. W. Wang, "The role of cytochrome P 450 epoxygenases, soluble epoxide hydrolase, and epoxyeicosatrienoic acids in metabolic diseases," *Advances in Nutrition*, vol. 7, no. 6, pp. 1122–1128, 2016.
- [6] X. Wang, L. Ni, L. Yang et al., "CYP2J2-derived epoxyeicosatrienoic acids suppress endoplasmic reticulum stress in heart failure," *Molecular Pharmacology*, vol. 85, no. 1, pp. 105–115, 2014.
- [7] M. B. Sikkil, C. Hayward, K. T. MacLeod, S. E. Harding, and A. R. Lyon, "SERCA2a gene therapy in heart failure: an anti-arrhythmic positive inotrope," *British Journal of Pharmacology*, vol. 171, no. 1, pp. 38–54, 2014.
- [8] D. C. White, J. A. Hata, A. S. Shah, D. D. Glower, R. J. Lefkowitz, and W. J. Koch, "Preservation of myocardial beta-adrenergic receptor signaling delays the development of heart failure after myocardial infarction," *Proceedings of the National Academy of Sciences*, vol. 97, no. 10, pp. 5428–5433, 2000.
- [9] E. G. Kranias and R. J. Hajjar, "Modulation of cardiac contractility by the phospholamban/SERCA2a regulatome," *Circulation Research*, vol. 110, no. 12, pp. 1646–1660, 2012.
- [10] M. A. Movsesian, M. Nishikawa, and R. S. Adelstein, "Phosphorylation of phospholamban by calcium-activated, phospholipid-dependent protein kinase," *Journal of Biological Chemistry*, vol. 259, pp. 8029–8032, 1984.
- [11] N. DHALLA, "Alterations in heart membrane calcium transport during the development of ischemia-reperfusion injury," *Journal of Molecular & Cellular Cardiology*, vol. 20, pp. 3–13, 1988.
- [12] S. Minamisawa, M. Hoshijima, G. Chu et al., "Chronic phospholamban-sarcoplasmic reticulum calcium ATPase interaction is the critical calcium cycling defect in dilated cardiomyopathy," *Cell*, vol. 99, no. 3, pp. 313–322, 1999.
- [13] B. Mueller, C. B. Karim, I. V. Negrashov, H. Kutchai, and D. D. Thomas, "Direct Detection of Phospholamban and

- Sarcoplasmic Reticulum Ca-ATPase Interaction in Membranes Using Fluorescence Resonance Energy Transfer†,” *Biochemistry*, vol. 43, no. 27, pp. 8754–8765, 2004.
- [14] H. Wallrabe and A. Periasamy, “Imaging protein molecules using FRET and FLIM microscopy,” *Current Opinion in Biotechnology*, vol. 16, no. 1, pp. 19–27, 2005.
- [15] E. L. Lockamy, R. L. Cornea, C. B. Karim, and D. D. Thomas, “Functional and physical competition between phospholamban and its mutants provides insight into the molecular mechanism of gene therapy for heart failure,” *Biochemical and Biophysical Research Communications*, vol. 408, no. 3, pp. 388–392, 2011.
- [16] W. T. You, T. Zhou, Z. C. Ma et al., “Ophiopogonin D maintains Ca²⁺ homeostasis in rat cardiomyocytes *in vitro* by upregulating CYP2J3/EETs and suppressing ER stress,” *Acta Pharmacologica Sinica*, vol. 37, no. 3, pp. 368–381, 2016.
- [17] G. Fan, F. Zhou, C. Feng et al., “Lead-induced ER calcium release and inhibitory effects of methionine choline in cultured rat hippocampal neurons,” *Toxicology In Vitro*, vol. 27, no. 1, pp. 387–395, 2013.
- [18] J.-M. Pei, G. M. Kravtsov, S. Wu, R. Das, M. L. Fung, and T. M. Wong, “Calcium homeostasis in rat cardiomyocytes during chronic hypoxia: a time course study,” *American Journal of Physiology. Cell Physiology*, vol. 285, no. 6, pp. C1420–C1428, 2003.
- [19] Q. Duan, X. Wang, W. Gong et al., “ER stress negatively modulates the expression of the miR-199a/214 cluster to regulates tumor survival and progression in human hepatocellular cancer,” *PLoS One*, vol. 7, no. 2, article e31518, 2012.
- [20] X. Huang, Y. Wang, Z. Zhang et al., “Ophiopogonin D and EETs ameliorate Ang II-induced inflammatory responses via activating PPAR α in HUVECs,” *Biochemical and Biophysical Research Communications*, vol. 490, no. 2, pp. 123–133, 2017.
- [21] W. Feng and W. Li, “The study of ISO induced heart failure rat model,” *Experimental & Molecular Pathology*, vol. 88, no. 2, pp. 299–304, 2010.
- [22] R. G. Tirona and R. B. Kim, “Nuclear receptors and drug disposition gene regulation,” *Journal of Pharmaceutical Sciences*, vol. 94, no. 6, pp. 1169–1186, 2005.
- [23] P. T. T. Wong, I. S. Girons, Y. Guillou, G. N. Cohen, O. Barzu, and H. H. Mantsch, “Pressure-induced changes in the secondary structure of the *Escherichia coli* methionine repressor protein,” *Biochimica et Biophysica Acta*, vol. 996, no. 3, pp. 260–262, 1989.
- [24] A. K. Kenworthy, “Imaging protein-protein interactions using fluorescence resonance energy transfer microscopy,” *Methods*, vol. 24, no. 3, pp. 289–296, 2001.
- [25] E. Li and K. Hristova, “Imaging forster resonance energy transfer measurements of transmembrane helix interactions in lipid bilayers on a solid support†,” *Langmuir*, vol. 20, no. 21, pp. 9053–9060, 2004.
- [26] P. Pavék and Z. Dvorák, “Xenobiotic-induced transcriptional regulation of xenobiotic metabolizing enzymes of the cytochrome p 450 superfamily in human extrahepatic tissues,” *Current Drug Metabolism*, vol. 9, no. 2, pp. 129–143, 2008.
- [27] C. Martínez-Jiménez, R. Jover, M. T. Donato, J. Castell, and M. J. Gómez-Lechón, “Transcriptional regulation and expression of cyp3a4 in hepatocytes,” *Current Drug Metabolism*, vol. 8, no. 2, pp. 185–194, 2007.
- [28] L. K. A. M. Leal, M. Nechio, E. R. Silveira et al., “Anti-inflammatory and smooth muscle relaxant activities of the hydroalcoholic extract and chemical constituents from *Amburana cearensis* A. C. Smith,” *Phytotherapy Research*, vol. 17, no. 4, pp. 335–340, 2003.
- [29] J. Qian, F. Jiang, B. Wang et al., “Ophiopogonin D prevents H₂O₂-induced injury in primary human umbilical vein endothelial cells,” *Journal of Ethnopharmacology*, vol. 128, no. 2, pp. 438–445, 2010.
- [30] S. J. Ann, J. H. Chung, B. H. Park et al., “PPAR α agonists inhibit inflammatory activation of macrophages through upregulation of β -defensin 1,” *Atherosclerosis*, vol. 240, no. 2, pp. 389–397, 2015.
- [31] F. del Monte, S. E. Harding, G. W. Dec, J. K. Gwathmey, and R. J. Hajjar, “Targeting phospholamban by gene transfer in human heart failure,” *Circulation*, vol. 105, no. 8, pp. 904–907, 2002.
- [32] E. N. Olson, “A decade of discoveries in cardiac biology,” *Nature Medicine*, vol. 10, no. 5, pp. 467–474, 2004.
- [33] D. H. MacLennan and E. G. Kranias, “Phospholamban: a crucial regulator of cardiac contractility,” *Nature Reviews Molecular Cell Biology*, vol. 4, no. 7, pp. 566–577, 2003.
- [34] M. Y. Mollova, H. A. Katus, and J. Backs, “Regulation of CaMKII signaling in cardiovascular disease,” *Frontiers in Pharmacology*, vol. 6, 2015.
- [35] D. M. Zhang, Y. Chai, J. R. Erickson, J. H. Brown, D. M. Bers, and Y. F. Lin, “Intracellular signalling mechanism responsible for modulation of sarcolemmal ATP-sensitive potassium channels by nitric oxide in ventricular cardiomyocytes,” *The Journal of Physiology*, vol. 592, no. 5, pp. 971–990, 2014.
- [36] J. R. Erickson, R. Patel, A. Ferguson, J. Bossuyt, and D. M. Bers, “Fluorescence resonance energy transfer-based sensor camui provides new insight into mechanisms of calcium/calmodulin-dependent protein kinase ii activation in intact cardiomyocytes,” *Circulation Research*, vol. 109, no. 7, pp. 729–738, 2011.
- [37] M. Dewenter, S. Neef, C. Vettel et al., “Calcium/calmodulin-dependent protein kinase ii activity persists during chronic β -Adrenoceptor blockade in experimental and human heart failure,” *Circulation Heart Failure*, vol. 10, no. 5, article e003840, 2017.
- [38] F. P. Guengerich, “Cytochrome P-450 3A4: regulation and role in drug metabolism,” *Annual Review of Pharmacology and Toxicology*, vol. 39, no. 1, pp. 1–17, 1999.
- [39] X. Xu, L. Tu, W. Feng et al., “Cyp2j3 gene delivery up-regulated adiponectin expression via reduced endoplasmic reticulum stress in adipocytes,” *Endocrinology*, vol. 154, no. 5, pp. 1743–1753, 2013.
- [40] A. A. El-Sherbeni and A. O. S. El-Kadi, “Alterations in cytochrome P450-derived arachidonic acid metabolism during pressure overload-induced cardiac hypertrophy,” *Biochemical Pharmacology*, vol. 87, no. 3, pp. 456–466, 2014.

Research Article

Alanylglutamine Relieved Asthma Symptoms by Regulating Gut Microbiota and the Derived Metabolites in Mice

Shao-Kun Liu ^{1,2,3}, Li-Bing Ma,^{4,5} Yu Yuan,^{1,2,3} Xiao-Ying Ji,⁶ Wen-Jin Sun,^{1,2,3} Jia-Xi Duan,^{1,2,3} Qing-Ping Zeng,^{1,2,3} Binaya Wasti,^{1,2,3} Bing Xiao,^{1,2,3} Jian-Fei Zheng,^{1,2,3} Ping Chen,^{1,2,3} and Xu-Dong Xiang ^{1,2,3}

¹Pulmonary and Critical Care Medicine, The Second Xiangya Hospital, Central South University, Changsha, Hunan 410011, China

²Research Unit of Respiratory Disease, Central South University, Changsha, Hunan 410011, China

³Diagnosis and Treatment Center of Respiratory Disease, Central South University, Changsha, Hunan 410011, China

⁴Department of Respiratory Medicine, The Affiliated Hospital of Guilin Medical University, Guilin 541001, China

⁵Institute of Respiratory Diseases, Guilin Medical University, Guilin 541001, China

⁶Department of Respiratory Medicine, The Seventh Affiliated Hospital, Sun Yat-sen University, Shenzhen 518106, China

Correspondence should be addressed to Xu-Dong Xiang; xudongxiang@csu.edu.cn

Received 16 July 2020; Revised 26 November 2020; Accepted 4 December 2020; Published 29 December 2020

Academic Editor: Si Qin

Copyright © 2020 Shao-Kun Liu et al. This is an open access article distributed under the Creative Commons Attribution License, which permits unrestricted use, distribution, and reproduction in any medium, provided the original work is properly cited.

Objective. Allergic asthma is a chronic inflammatory disease, which seriously affects the life quality of patients, especially children. Alanylglutamine is a nutritional supplement with potential protective and anti-inflammatory effects, but its function in allergic asthma remains elusive. In this study, we focused on the investigations of the roles and functional mechanism of Alanylglutamine in asthma. **Methods.** Ovalbumin (OVA) induction was utilized to establish a mouse asthma model. 16S rDNA sequencing was performed to compare the diversity of intestinal microorganisms under different treatments. Gas chromatography was utilized to screen the intestinal microbe-short-chain fatty acids in the stool. The lung tissue was extracted to determine signaling pathways, including AMPK, NF- κ B, mTOR, STAT3, IKK β , TGF- β , and IL-1 β through Western blot or RT-qPCR. **Results.** It was observed that Alanylglutamine reduced the cytokine in OVA-induced allergic asthma mice. H&E staining showed obvious pneumonia symptoms in the asthma group, while Alanylglutamine alleviated the inflammatory infiltration. Alanylglutamine reversed gut microbiota compositions in OVA-induced allergic asthma mice and enhanced the butyric acid level. The protective role of Alanylglutamine may be associated with the gut microbiota-butyric acid-GPR43 pathway in asthma mice. In contrast to the OVA group, Alanylglutamine activated the protein expression of P-AMPK/AMPK and inhibited the protein expression of P-mTOR/mTOR, P-P65/P65, P-STAT3/STAT3, P-IKK β /IKK β , TGF- β , and IL-1 β , with similar effects from butyric acid. **Conclusion.** The results indicated that Alanylglutamine might be beneficial for asthma, and its effect was achieved through the regulation on microbiota and the derived metabolites. The therapeutic effects might be associated with AMPK, NF- κ B, mTOR, and STAT3 signaling pathways. These findings will help identify effective therapeutic direction to alleviate allergic inflammation of the lungs and airways.

1. Introduction

Asthma, also known as bronchial asthma, is a respiratory disease with complex etiology, involving a variety of cells and different molecular mechanisms in the lungs and airways [1]. It is a chronic inflammatory disease, which seriously affects the life quality of patients, especially children [2]. According to the latest scientific statistics, more than 300

million people suffer from asthma worldwide [3, 4]. The total incidence of asthma for children under 5 years old is 23/1,000 per year, and 4.4/1,000 for adolescents aged from 12 to 17 [3, 5]. Corticosteroids inhibit inflammation in asthmatic airways, which can be used in asthma therapy currently [6]. Although it is effective in alleviating acute symptoms, its adverse reactions, such as cardiotoxicity, are causing increasing concern during long time therapy. Besides, there are

growing numbers of patients who are recognized as corticosteroid-resistant [7]. Therefore, it is urgent to develop effective and safe drugs to relieve asthma symptoms.

Alanylglutamine is a nutritional supplement consisting of the amino acids of L-glutamine and L-alanine. It is a stable water-soluble dipeptide with potential protection and absorption promoting activity. According to previous studies, Alanylglutamine plays an important role in the inflammatory injury of lung tissue. For example, Alanylglutamine can improve acute lung injury induced by endotoxin (LPS) through regulating Th17/Treg [8]. It also relieved intestinal epithelial cells with LPS-induced inflammation and barrier function damage [9]. It was confirmed that oral administration of both free amino acid (alanyl and glutamine) and dipeptide form (Alanylglutamine) can significantly alleviate LPS-induced inflammation [10]. As allergic asthma is an inflammation-related disease, we are interested in whether Alanylglutamine could exert a protection role in the asthma symptoms.

In recent years, accumulative evidence suggested that the intestinal functions are closely related with lung mucosal immune organs. Intestinal-pulmonary axis regulation plays an important role in respiratory diseases. Intestinal microorganisms may affect lung and respiratory diseases, such as lung infection, asthma, and chronic obstructive pulmonary disease [11]. Studies have reported that flora transplantation into the intestinal tract could change the microecology of the intestine, thereby affecting the immune and metabolic functions with therapeutic effects [12]. In the preliminary experiment, we transplanted the flora of Alanylglutamine on ordinary mice into sterile mice and established an ovalbumin (OVA) model to observe the phenotype. It was found that Alanylglutamine relieved asthma symptoms through intestinal flora. Further researches are necessary to identify their inner associations regarding the combined therapeutic effects for the asthma.

In this study, we intend to verify the relationship among Alanylglutamine dipeptide, gut microbiota, and derived metabolites in the OVA asthma model. We will examine the allergic inflammation of the lungs and airways under different treatments from the perspective of improving intestinal microorganisms by Alanylglutamine. In addition, we will investigate the expressions of related molecules, and discuss the possibility of enhancing the treatment of asthma with related drugs.

2. Material and Methods

2.1. Animal and Asthmatic Model. The experiment animals utilized in this research were maintained following the protocol approved by the Institutional Animal Care and Use Committee of Second Xiangya Hospital. Adult male BALB/c mice of 8 weeks old, weighing about 20 grams, were all purchased from Well-bio (Changsha, China) and categorized into three groups: the control group, the OVA model, and the Alanylglutamine treatment+OVA model (Alanylglutamine) ($n = 10$). All mice were placed in specific pathogen conditions and maintained at a 12 h light-dark cycle, with diet freedom. In the OVA model group, 20 μ g OVA (Sigma-Aldrich, USA)

injection was performed on days 1 and 8. According to previous research [13, 14], aerosol (with 1% OVA in PBS) stimulated for 20 minutes on day 24, day 25, and day 26 using an ultrasonic nebulizer (Omron, Vernon) to induce allergic asthmatic mice model. Mice in the Alanylglutamine group received OVA with a diet containing 0.15% Alanylglutamine. Samples were collected after 48 hours following the last treatment.

2.2. Antibiotic Treatment. 30 adult male BALB/c mice were treated with antibiotics in drinking water for two weeks. The antibiotics contain 1 mg/mL streptomycin sulfate, 1 mg/mL gentamicin, 1 mg/mL penicillin, and 0.5 mg/mL vancomycin. Then, water was replaced and mice were further sorted into three groups: the control group, the OVA model, and the Alanylglutamine treatment+OVA model (Alanylglutamine) ($n = 10$). OVA induction and Alanylglutamine supplementation were the same with the above treatments.

2.3. Sodium Butyrate (NaB) Treatment. 40 adult male BALB/c mice were assigned into 4 groups: the OVA model, the OVA+NaB, the OVA+antibiotics, and the OVA+antibiotics+NaB ($n = 10$). OVA induction and antibiotic treatment were the same with the above treatments. NaB was ingested through gavage, with a dosage of 200 mg/kg/day.

2.4. Leukocyte Count in Bronchoalveolar Lavage Fluid (BALF). After separating the lungs from the mice, who were sacrificed by intraperitoneal injection of pentobarbital sodium (150 mg/kg), 0.9 mL cold PBS with 2 mM EDTA and 2% fetal bovine serum (FBS) were instilled into them. Then, the BAL fluid was collected through a procedure according to the previous study [15]. BALF was acquired after lavage and centrifuged at 2000 g at 4°C for 5 minutes. The sediment was resuspended in 50 μ L PBS, and the number of cells was calculated using a hemocytometer. The collected BALF was centrifuged at 800 g, and its supernatant was utilized for analysis of the cytokine level.

2.5. ELISA Measurement of Cytokines. Concentrations of total leukocyte count, IFN- γ , IL-1 β , IL-6, TNF- α , and TGF- β 1 in BALF were measured by murine cytokine-specific Quantikine ELISA kits (eBioscience), in accordance with the manufacturers' instructions.

2.6. Western Blot. Tissue lysates were made in a radioimmunoprecipitation assay (RIPA) buffer containing 25 mM Tris-HCl (pH 7.2), 0.15 M NaCl, 0.1% SDS, 1% Triton X-100, 1% sodium deoxycholate, and 1 mM EDTA. Determination of protein concentration was carried out by bicinchoninic acid protein assay kit (Pierce). After being subjected to sodium dodecyl sulfate polyacrylamide gel electrophoresis, the protein was transferred to a nitrocellulose membrane. Total protein or phosphorylation was detected using a goat polyclonal antibody against rabbit or mouse after blocking. The protein bands were quantified using a digital imaging system (UVtec).

2.7. RT-qPCR. TRIzol[®] reagents (Invitrogen Life Technologies; Thermo Fisher Scientific, Waltham, MA, USA) were

employed to extract total RNA. Subsequently, a PrimeScript™ RT reagent kit (Thermo Fisher Scientific) was utilized for reverse transcription. We conducted real-time RNA quantification on an ABI StepOne Plus Detection System (Applied Biosystems) using a Power SYBR Green PCR Master Mix (Applied Biosystems). The primer sequences were designed in the laboratory and synthesized by Sangon Biotech Co., Ltd. (Shanghai, China). The primers were designed as follows: AMPK forward, 5'-CGGGGTCATTC TCTATGCTT-3', and reverse, 5'-TTTAAACCACTCGT GTTCCCT-3'; mTOR forward, 5'-ACCAACTATACCCG CTCCC-3', and reverse, 5'-TAGTTGCCATCCAGACCCG TA-3'; P65 forward, 5'-TAGCCAGCGAATCCAGACCAA CA-3', and reverse, 5'-TGGTCCCGCACTGTCACCT-3'; STAT3 forward, 5'-CAATACCATTGACCTGCCGAT-3', and reverse, 5'-GAGCGACTCAAAGTCCCT-3'; and β -actin forward, 5'-ACATCCGTAAGACCTCTATGCC-3', and reverse, 5'-TACTCCTGCTTGCTGATCCAC-3'.

2.8. 16S rDNA Sequencing. The bacterial 16S rDNA gene of the stool was analyzed via a TIANamp Stool DNA Extraction Kit (TIANGEN Biotechnology, China) with Ribonuclease A (QIAGEN, Germany). We measured the purity and concentrations of the DNA through NanoDrop 1000 (Thermo Fisher Scientific). The primer sequences were used as follows: 341F primer: 5'-CCTAYGGGRBGCASCAG-3', and 806R primer: 5'-GGACTACHVGGGTWCTAAT-3'. Then, we constructed an amplicon sequencing library and performed sequencing using Illumina HiSeq 2500 (Illumina, San Diego, CA, USA). The data filtering, detection, and detachment of chimeric sequences were fulfilled by the Quantitative Insights Into Microbial Ecology (QIIME) pipeline (2019.07) and UCHIME algorithm, respectively. Sequences with similarities greater than 97% were defined as the same operational taxonomic unit (OTU) through UPARSE. Mothur and SSU data sets of the SILVA rRNA Database were applied for species annotation with a confidence threshold of 0.8. The analysis of sequencing data on the alpha and beta diversities was fulfilled by QIIME and R. According to the Kyoto Encyclopedia of Genes and Genomes (KEGG) gene function spectrum data, the overall metabolic function of the flora was converted and calculated, which was presented as a differentiated KEGG pathway analysis.

2.9. Determination of Short-Chain Fatty Acids (SCFAs) in Stool. The SCFAs in stool samples of the mice, including acetic acid, propionic acid, butyric acid, and its isomer isobutyric acid, were detected using Gas Chromatograph Mass Spectrometer-QP2010 (GC-MS) (Shimadzu, Tokyo, Japan). Every stool sample was homogenized with 50 mg/mL methanol by vortex for 10 seconds and treated by ultrasound for 10 minutes. Next, the mixed samples in each group were centrifuged at room temperature at 14,000 rpm for 5 minutes. The supernatant was diluted with methanol 10 times. Upon injection, 1 μ L of sample was evaporated at 230°C. The compounds were separated via an Agilent J&W fused silica capillary column DB-FFAP (Agilent, Santa Clara, CA, USA). After being ionized by electron impact at -70 eV at 200°C,

the samples were analyzed via a quadrupole mass spectrometer. Each SCFA was identified using GCMSsolution software (Shimadzu, Japan). The concentrations of SCFAs were quantified according to the peak areas of the total ion current.

2.10. Immunofluorescence Analysis. To determine the expression of GPR43 in eosinophils of lung tissue, we performed immunofluorescence staining on slides of paraffin-embedded lung tissue. The slides were incubated with primary GPR43 antibody overnight. Subsequently, the slides were cultured by Alexa Fluor 488 and Alexa Fluor 594 secondary antibodies (Invitrogen, Carlsbad, CA, USA) for 1 hour. Then, the slides were mounted by Vectashield (Vector Laboratories, USA) with DAPI. LSM 510 confocal microscope (Zeiss, Germany) was used for cell photography and counting.

2.11. H&E Staining of Lung. After being fixed with 4% paraformaldehyde and embedded in paraffin, 4 μ m sections of mouse lung tissues were stained with Hematoxylin and Eosin (H&E) (Beyotime, China) for standard histopathological examination. Each pathological section was observed under an optical microscope. The representative images for pathological analysis were utilized to evaluate the infiltration of inflammatory cells in the mouse airway and perivascular and alveolar cells.

2.12. Statistical Analysis. The data from the experiments were expressed as mean values \pm standard deviation (SD). Statistical significance from different groups of mice was calculated by one-way ANOVA (>2 groups). *P* value less than 0.05 was considered to be statistically significant.

3. Results

3.1. Alanylglutamine Reduced the Cytokine Productions and Alleviated Inflammatory Infiltration in OVA-Induced Allergic Asthma Mice. In the allergic asthma model, the leukocyte count in BALF was significantly reduced (Figure 1(a)), while Alanylglutamine treatment reversed the BALF leukocyte concentration. It indicates the protective effect of Alanylglutamine in OVA-induced allergic asthma mice. As inflammation is widely associated with asthma symptoms, we measured the inflammatory indicators in BALF, including IL-1 β (Figure 1(b)), IL-6 (Figure 1(c)), TNF- α (Figure 1(d)), TGF- β (Figure 1(e)), and IFN- γ (Figure 1(f)). In the OVA-treated mice, a significant inflammatory response was observed by the increased IL-1 β , IL-6, TNF- α , TGF- β , and IFN- γ concentrations (*P* < 0.01). Alanylglutamine showed an anti-inflammatory effect by significantly reducing IL-1 β , IL-6, and TGF- β level in BALF. Meanwhile, H&E staining showed obvious pneumonia symptoms in the OVA group, while Alanylglutamine alleviated the inflammatory infiltration (Figure 1(g)).

3.2. Alanylglutamine Reversed Gut Microbiota Compositions in OVA-Induced Allergic Asthma Mice. Fecal microbiota diversity and compositions were further tested by 16S rDNA sequencing. To evaluate the microbiota α -diversity, observed OTUs and Simpson, Shannon, Chao, and PD indexes were analyzed. The results showed that OVA treatment markedly reduced bacterial α -diversity, with the decreased levels of

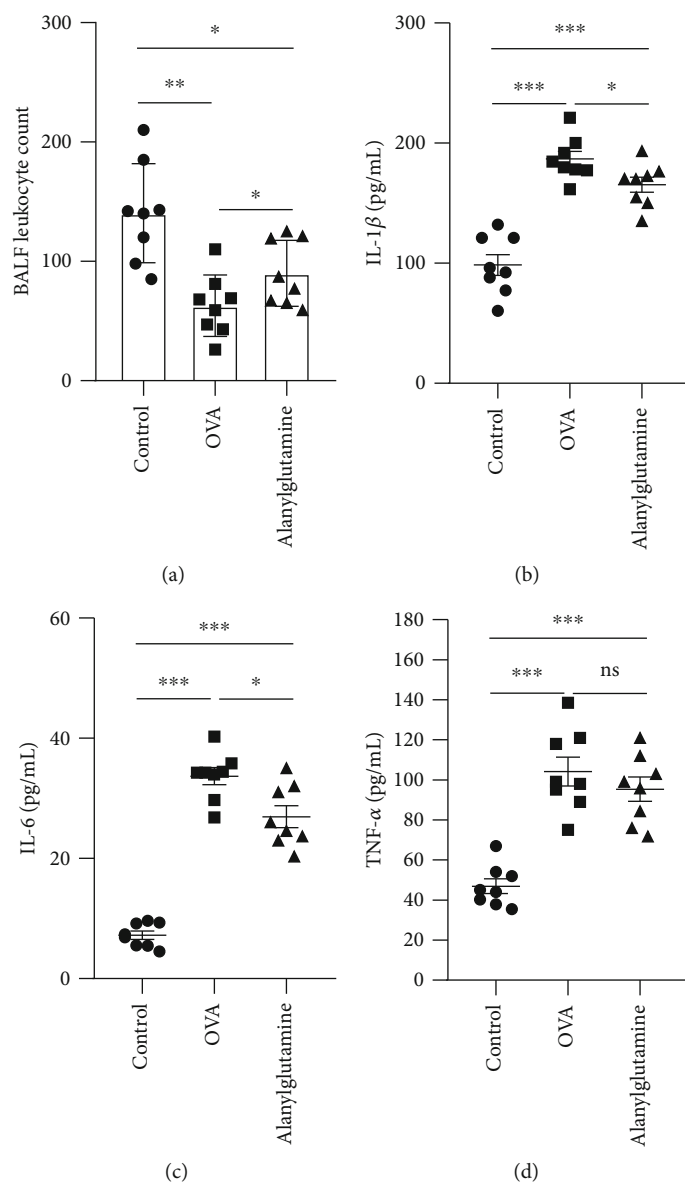


FIGURE 1: Continued.

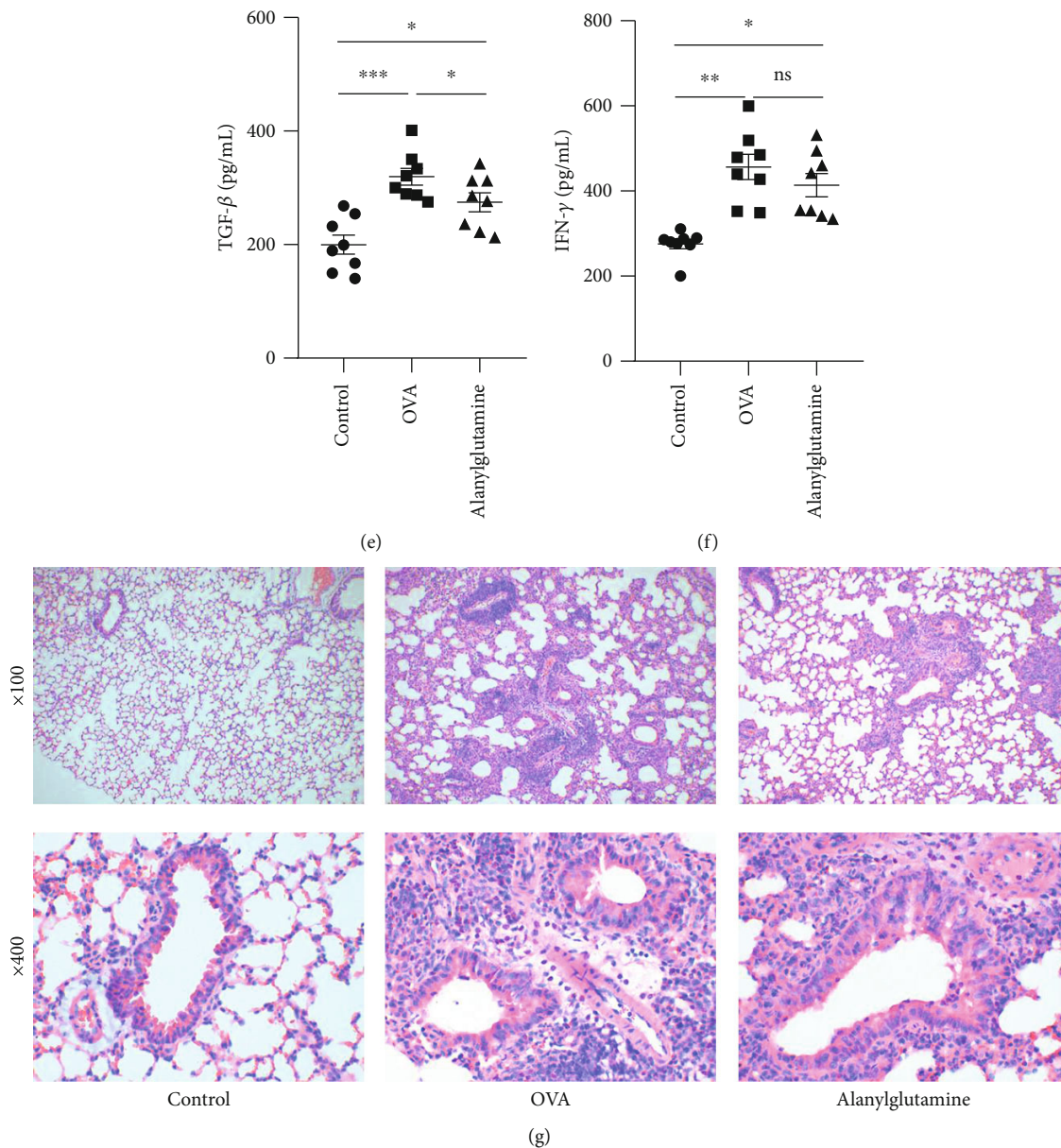


FIGURE 1: Alanylglutamine reduced the cytokine productions and alleviated inflammatory infiltration in OVA-induced allergic asthma mice: (a) BALF leukocyte count; (b) IL-1 β ; (c) IL-6; (d) TNF- α ; (e) TGF- β ; (f) IFN- γ level in BALF; (g) lung tissue morphology depicted by H&E staining. $n = 8$. * $P < 0.05$; ** $P < 0.01$; *** $P < 0.001$; ns: not significant.

observed OTUs, Shannon index, and PD, while Alanylglutamine treatment reversed the observed OTUs and Shannon index. Meanwhile, Chao1 index was increased in the Alanylglutamine group compared with the control and OVA groups (Figures 2(a)–2(e)). Fecal dysbiosis was observed in OVA-induced allergic asthma mice, which was reversed in the Alanylglutamine group.

Microbiota at the phylum was further analyzed (Figure 2(f)). It revealed that the major phyla were Bacteroidetes and Firmicutes, accounting for 95%. We found that three phyla were markedly changed in this study (Figures 2(g)–2(i)). Although OVA treatment failed to affect Bacteroidetes and Firmicutes abundance, Alanylglutamine markedly reduced Bacteroidetes and increased Firmicutes abundance, compared

with the OVA group ($P < 0.05$). Meanwhile, the relative abundance of Tenericutes was significantly enhanced in OVA-challenged mice, which was reversed by dietary Alanylglutamine ($P < 0.05$). Microbiota at the genus level (top 20) was also analyzed. 11 genera were markedly altered in response to OVA or Alanylglutamine treatment (Supplementary Figure 1). *Corynebacterium*, *Odoribacter*, *Staphylococcus*, and *Turicibacter* were markedly enhanced and *Parabacteroides*, *Streptococcus*, *Coprococcus*, *Bacteroidetes*, *Allobaculum*, and *Sutterella* were decreased in OVA-challenged mice, in contrast to the control mice ($P < 0.05$). However, the relative abundance of *Corynebacterium*, *Parabacteroides*, *Odoribacter*, *Coprococcus*, *Bacteroidetes*, and *Allobaculum* was significantly reversed in Alanylglutamine-fed mice ($P < 0.05$). It showed

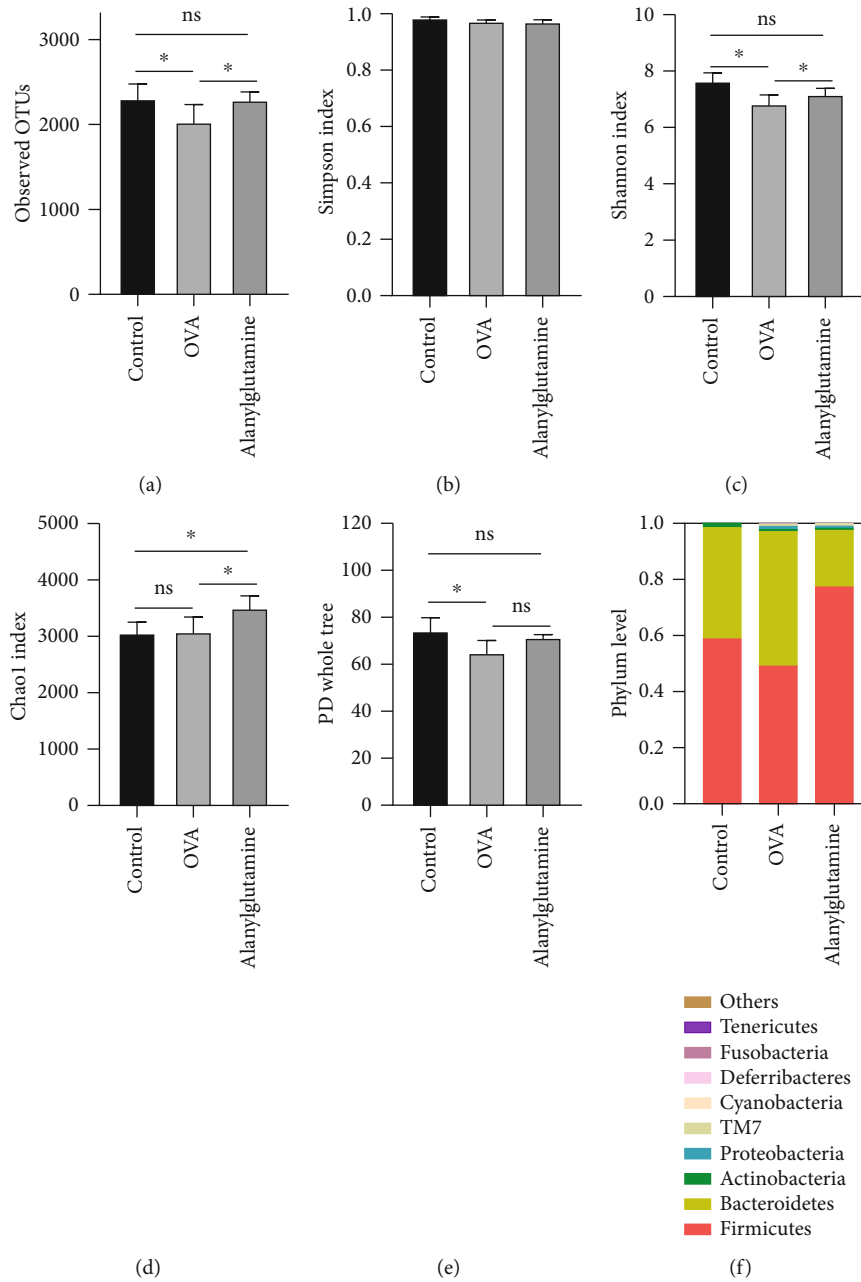


FIGURE 2: Continued.

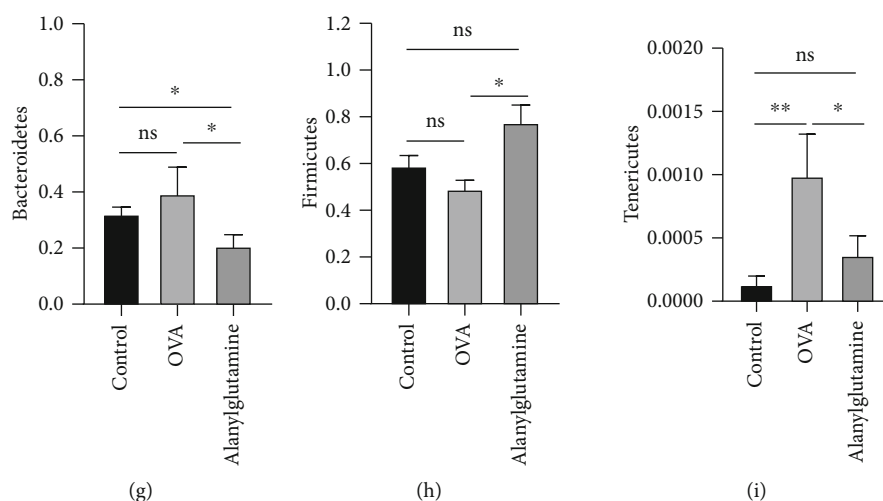


FIGURE 2: Differences of α -diversity index and species composition of the phylum level: (a) observed OTUs; (b) Simpson index; (c) Shannon index; (d) Chao1 index; (e) PD whole tree; (f) phylum level; (g) Bacteroidetes; (h) Firmicutes; (i) Tenericutes. OTUs: operational taxonomic units. * $P < 0.05$; ns: not significant.

that Alanylglutamine might improve asthma by regulating Tenericutes, Corynebacterium, Parabacteroides, etc.

PICRUSt was used to analyze functional profiling of microbial communities, including amino acid metabolism, carbohydrate metabolism, cell motility, cellular processes and signaling, energy metabolism, enzyme families, folding, sorting and degradation, genetic information processing, glycan biosynthesis and metabolism, lipid metabolism, membrane transport, metabolism, metabolism of cofactors and vitamins, nucleotide metabolism, poorly characterized, replication and repair, and transcription and translation.

Based on the function prediction and analysis results of the KEGG pathway database, the total number of genes annotated to the pathway database in all samples was counted, and a bar chart was drawn. As shown in Figure 3(a), the gene quantity distribution of the KEGG pathway of level 1 or 2 was visually displayed. The abscissa showed the number of genes enriched in the signal pathway of three groups of samples. The ordinate showed the significantly enriched signal pathways. According to Figures 3(b)–3(f), OVA treatment markedly reduced cell motility, genetic information processing, nucleotide metabolism, and replication and repair ($P < 0.05$), while Alanylglutamine significantly increased cell motility ($P < 0.05$). Meanwhile, it also revealed that Alanylglutamine enhanced folding, sorting, and degradation.

3.3. Effects of Alanylglutamine on Bacterial Metabolites in the Stool in OVA-Induced Allergic Asthma Mice. Bacterial metabolites such as acetic acid (Figure 4(a)), propanoic acid (Figure 4(b)), butyric acid (Figure 4(c)), isobutyric acid (Figure 4(d)), valeric acid (Figure 4(e)), and isovaleric acid (Figure 4(f)) in the stool were further analyzed. OVA treatment markedly reduced fecal butyric acid, isobutyric acid, and valeric acid concentrations ($P < 0.05$). However, dietary supplementation with Alanylglutamine enhanced the butyric acid level ($P < 0.05$), indicating that butyric acid may involve

in alleviating the role of Alanylglutamine in OVA-induced allergic asthma mice.

3.4. Alanylglutamine Treatment Failed to Alleviate OVA-Induced Allergic Asthma in Antibiotic-Challenged Mice. To further investigate the association of Alanylglutamine with gut microbiota in asthma, antibiotics were employed to eliminate the microbiota. Similarly, the leukocyte in BALF was markedly reduced (Figure 5(a)). The concentrations of IL-1 β , IL-6, TNF- α , and TGF- β were elevated in OVA and antibiotic-cotreated mice (Figures 5(b)–5(f)). However, Alanylglutamine failed to affect leukocyte, IL-1 β , IL-6, and TNF- α level in BALF, but it alleviated TGF- β concentration in antibiotic-challenged mice. H&E staining also showed no obvious alleviating effect on the inflammatory infiltration in Alanylglutamine and antibiotic cotreatment (Figure 5(g)). In summary, these results indicated gut microbiota might involve in the role of Alanylglutamine in the OVA-induced allergic asthma.

SCFA content analysis in the stool was further conducted to investigate the effects of Alanylglutamine treatment in asthma mice with antibiotics (Figures 6(a)–6(f)). The levels of butyric acid and isovaleric acid in asthma mice were significantly downregulated (Figures 6(c) and 6(f)). It was verified that butyric acid may have important effects on the regulation procedure of Alanylglutamine or intestinal microorganism. Therefore, in the following experiments, butyric acid was directly added to the mice to examine its exact functional mechanism.

3.5. Effects of Butyric Acid in OVA-Induced Allergic Asthma Mice. Microbial and metabolite analyses indicated that gut microbiota and butyric acid might involve in the role of Alanylglutamine in OVA-induced allergic asthma mice. Thus, NaB was further administrated to identify the potential mechanism. An OVA-induced allergic asthma model was induced with or without antibiotics. BALF leukocyte and

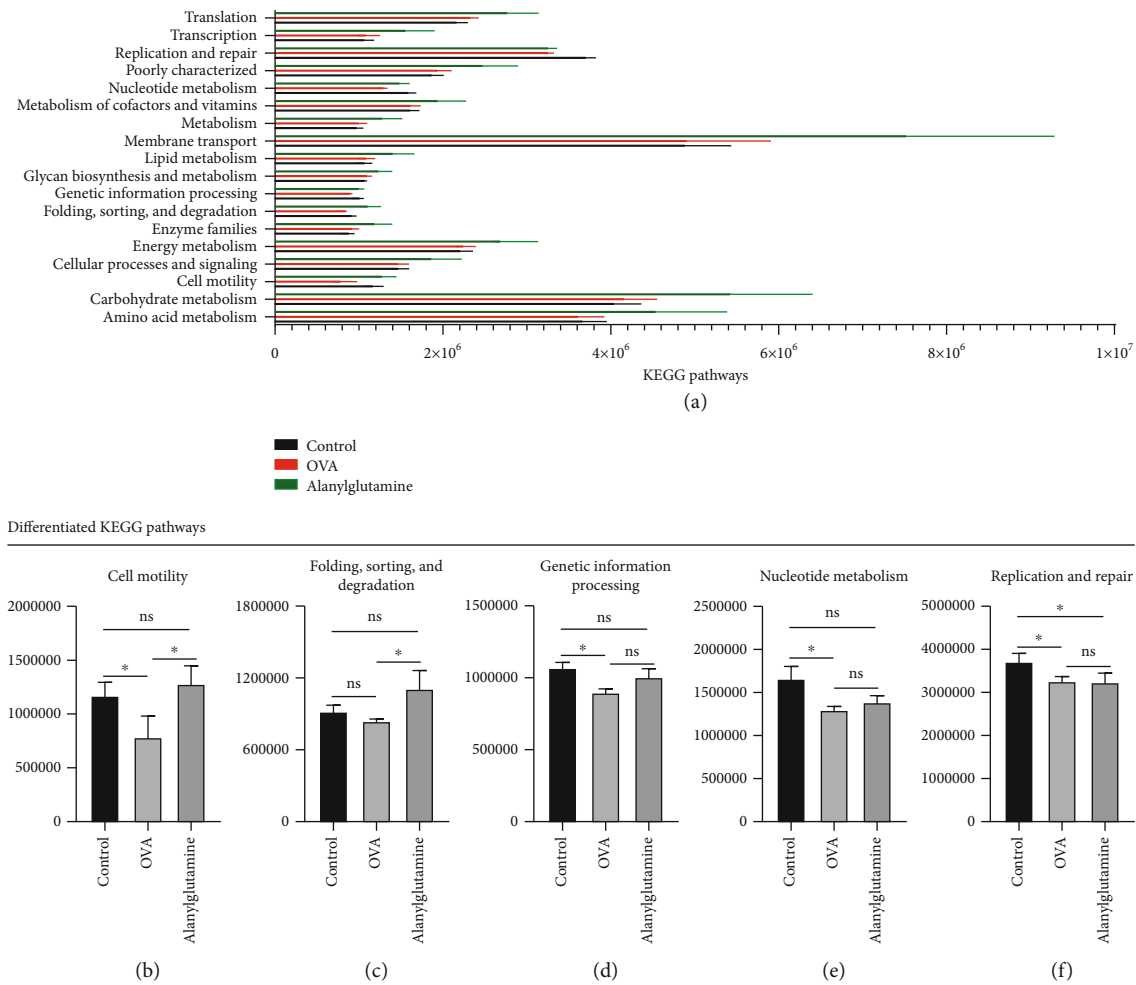


FIGURE 3: Difference analysis among samples from control, OVA, and Alanylglutamine mice: (a) KEGG pathway; (b–f) differentiated KEGG pathways for the analysis in cell mobility, folding, sorting and degradation, genetic information processing, nucleotide metabolism, and replication and repair. The vertical axis is absolute abundance of microbiota, and there was no unit for this. * $P < 0.05$; ns: not significant.

cytokines were further tested (Figures 7(a)–7(f)). The results showed that NaB treatment significantly enhanced BALF leukocyte contents. The OVA+antibiotic+NaB group also enhanced BALF leukocyte content. It reduced the IL-1 β , IL-6, TNF- α , and TGF- β level in OVA-induced allergic asthma both in antibiotic-free and antibiotic-treated mice notably, indicating an anti-inflammatory effect in the OVA-induced allergic asthma model. Compared with the model group, NaB treatment showed reduced inflammatory infiltration on the H&E-stained sections of lung tissue (Figure 7(g)), supporting the effect of butyric acid on leukocyte count. The above results indicated that both NaB and antibiotics had a certain anti-inflammatory effect. The anti-inflammatory treatment of NaB was more effective than that of antibiotics, and their combination had the most effective treatment.

Considering that GPR43 served as the specific receptor of butyric acid, lung tissues were collected for analysis of GPR43 expression using the immunofluorescence (Figure 8). In the asthma model (OVA), the GPR43 expression was reduced compared with the control group, while the treatment of OVA+Alanylglutamine and OVA+NaB markedly enhanced the expression of GPR43 (Figure 8). The immunofluores-

cence staining results further confirmed the protective role of Alanylglutamine in asthma mice, which might be associated with the gut microbiota-butyric acid-GPR43 pathway.

3.6. Alanylglutamine Inhibited the NF- κ B Pathway and STAT3 Pathway. To clarify the molecular mechanisms of Alanylglutamine in OVA-induced allergic asthma, we further collected the lung samples from control, OVA, Alanylglutamine-treated asthma mouse (OVA+Alanylglutamine), and NaB treatment groups (OVA+NaB). We analyzed the protein and mRNA expressions of several relative signaling pathways through Western blot (Figures 9(a) and 9(b)) and RT-qPCR (Figure 9(c)). It was shown that both Alanylglutamine and butyric acid could affect AMPK, NF- κ B, mTOR, and STAT3 signaling pathways. In contrast to the OVA group, Alanylglutamine activated the protein expressions of P-AMPK/AMPK. It inhibited the protein expressions of P-mTOR/mTOR, P-P65/P65, and P-STAT3/STAT3, with similar effects from butyric acid (Figure 9(a)). Abnormal activation of NF- κ B is usually closely related to IKK β phosphorylation. Therefore, the upstream and downstream pathway proteins of NF- κ B were tested by Western blot. Compared

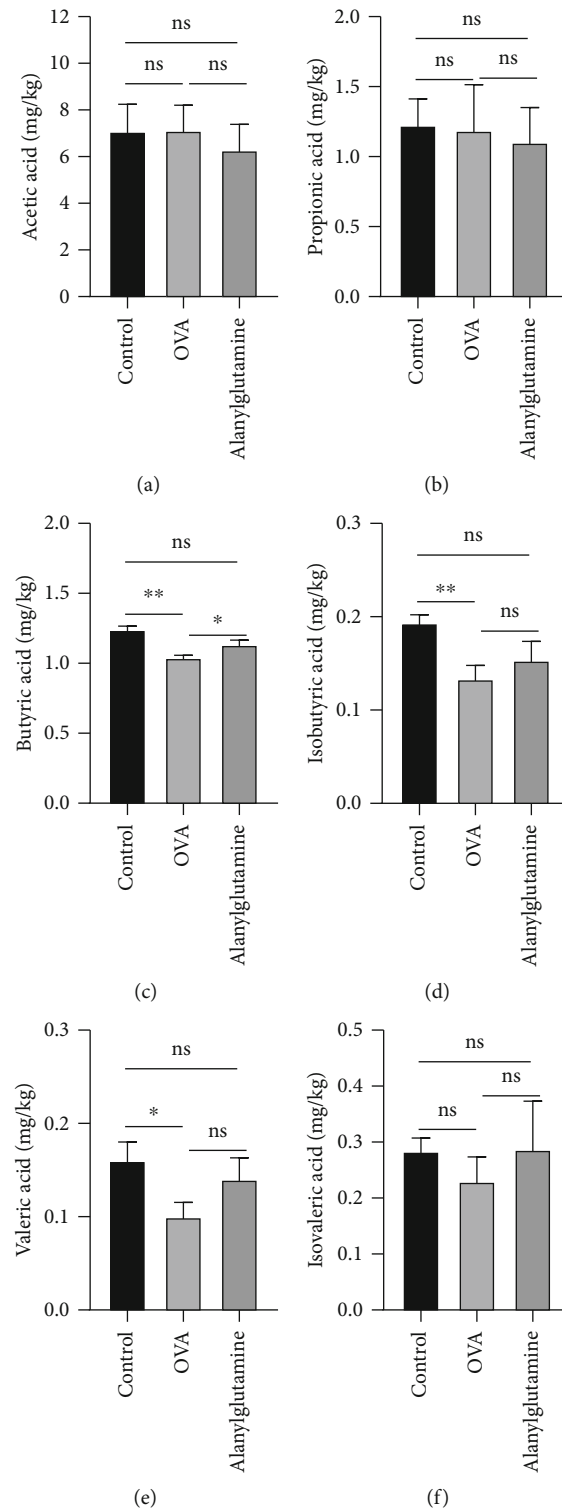


FIGURE 4: Effects of Alanylglutamine on bacterial metabolites in the stool in OVA-induced allergic asthma mice: (a) acetic acid; (b) propionic acid; (c) butyric acid; (d) isobutyric acid; (e) valeric acid; (f) isovaleric acid. * $P < 0.05$; ** $P < 0.01$; ns: not significant.

with the OVA group, Alanylglutamine suppressed the protein expressions of P-IKK β /IKK β , TGF- β , and IL-1 β (Figure 9(b)). The results of RT-qPCR indicated that Alanylglutamine failed to affect the mRNA expression of

AMPK, mTOR, P65, and STAT3 (Figure 9(c)). In summary, the results demonstrated that Alanylglutamine activated the AMPK pathway and inactivated the mTOR, P65, and STAT3 pathway.

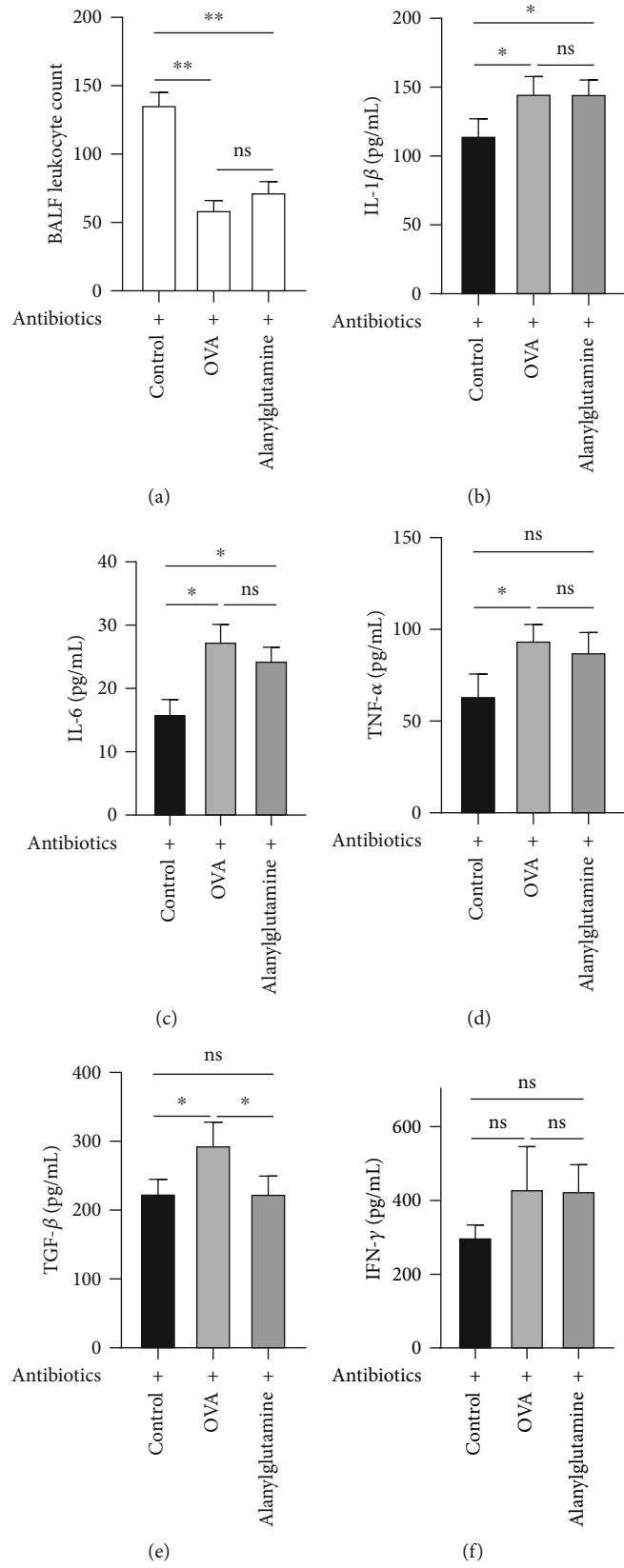


FIGURE 5: Continued.

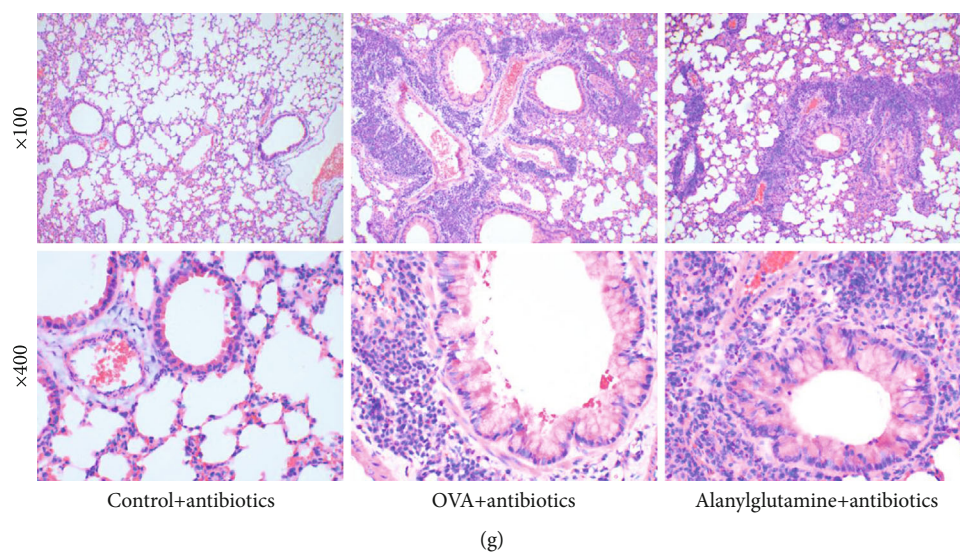


FIGURE 5: Alanylglutamine treatment failed to alleviate OVA-induced allergic asthma in antibiotic-challenged mice. The expression of inflammatory cytokines by ELISA in the groups of control+antibiotic, OVA+antibiotic, and Alanylglutamine+antibiotic mice: (a) BALF leukocyte count; (b) IL-1 β ; (c) IL-6; (d) TNF- α ; (e) TGF- β ; (f) IFN- γ levels from BALF; (g) lung tissue morphology study measured by H&E staining. $n = 8$. * $P < 0.05$; ** $P < 0.01$; ns: not significant.

4. Discussion

Colonized gut microbiota is presently recognized as potential mediators of host immune responses in different diseases. The remodeling of microbiota contributed to different effects on inflammation in the lung. For instance, it was confirmed that gut microbiota was overtly changed. Susceptibility to the TH2 model of allergic asthma was also increased, with perinatal exposure to vancomycin, but not streptomycin [16]. The importance of immune regulation by commensal microbiota in the respiratory mucosa via inflammasome activation was also revealed. Alanylglutamine was reported to reduce muscle wastage of alanine and glutamine in anesthetized dogs after operation [17]. In oxidatively stressed Caco-2 cells, the dipeptide could hold PepT1-mediated transport [18]. Based on the relationship between gut microbiota and immunity, we analyzed the roles of the dipeptide Alanylglutamine in OVA-induced asthma with allergic lung inflammation. Administrations of Alanylglutamine with different feeding routes by parenteral or enteral led to an enhanced plasma glutamine response compared to baseline [19]. Herein, we discovered that the uptake of Alanylglutamine changed the gut microbiota, especially in the OVA-induced asthma model.

Probiotics are used to modify the intestinal flora, which is beneficial for improving the nonalcoholic fatty liver disease (NAFLD) in ob/ob mice [20]. NAFLD is characterized by intestinal bacterial overgrowth. Thus, we postulated that Alanylglutamine-mediated changes of probiotics might improve the inflammation condition through intestinal flora modification. Indeed reshaping of the gut microbiota as well as increased levels of short-chain fatty acids by high-fiber feeding exhibited beneficial roles in food allergy with increased Treg differentiation [21]. SCFA are microbial

metabolites derived from bacterial fermentation serving as a sign of gut health, which are also considered to modulate chronic inflammation illnesses. SCFA-producing bacteria are the connection between microbiota functions and epigenetic regulation of inflammatory mechanisms [22]. SCFAs, such as acetate, propionate, and butyrate, are produced when dietary fiber is fermented by gut microbiota. As for butyrate, it was reported that sodium butyrate is capable of inducing apoptosis in tumor cell lines [23]. Recent studies have unveiled that sodium butyrate and other short-chain fatty acids can guard against inflammation in colon diseases. Butyrate in CNS is anti-inflammatory in brain-derived microglial cells. However, it shows proinflammation in the microglial cell line, which may be related to the anticancer properties of butyrate observed in tumor cells [24]. In this study, we also found that Alanylglutamine mediated SCFA during remodeling of gut microbiota and protected against airway allergy such as asthma.

In the respiratory tract, there was synergistic antitumor activity against lung cancer cells with a combination therapy of lovastatin and butyrate in vitro [25]. LPS-induced acute lung injury was also ameliorated by sodium butyrate with reduced HMGB1 release [26–28]. In this study, we found that the butyrate displayed protective effects on asthma. After the intervention of the chemicals, the signaling pathways including AMPK, mTOR, P65, and STAT3 were also affected. It was noticed that Alanylglutamine had almost the same effects on asthma, compared with butyrate. The AMPK phosphorylation was upregulated markedly, while NF- κ B, STAT3, and Akt/mTOR signals were downregulated significantly after the Alanylglutamine treatment. Alanylglutamine also inhibited the phosphorylation of IKK β and the protein expression of TGF- β and IL-1 β . The effects on molecular signaling pathways of AMPK, mTOR, P65, and STAT3 are also consistent

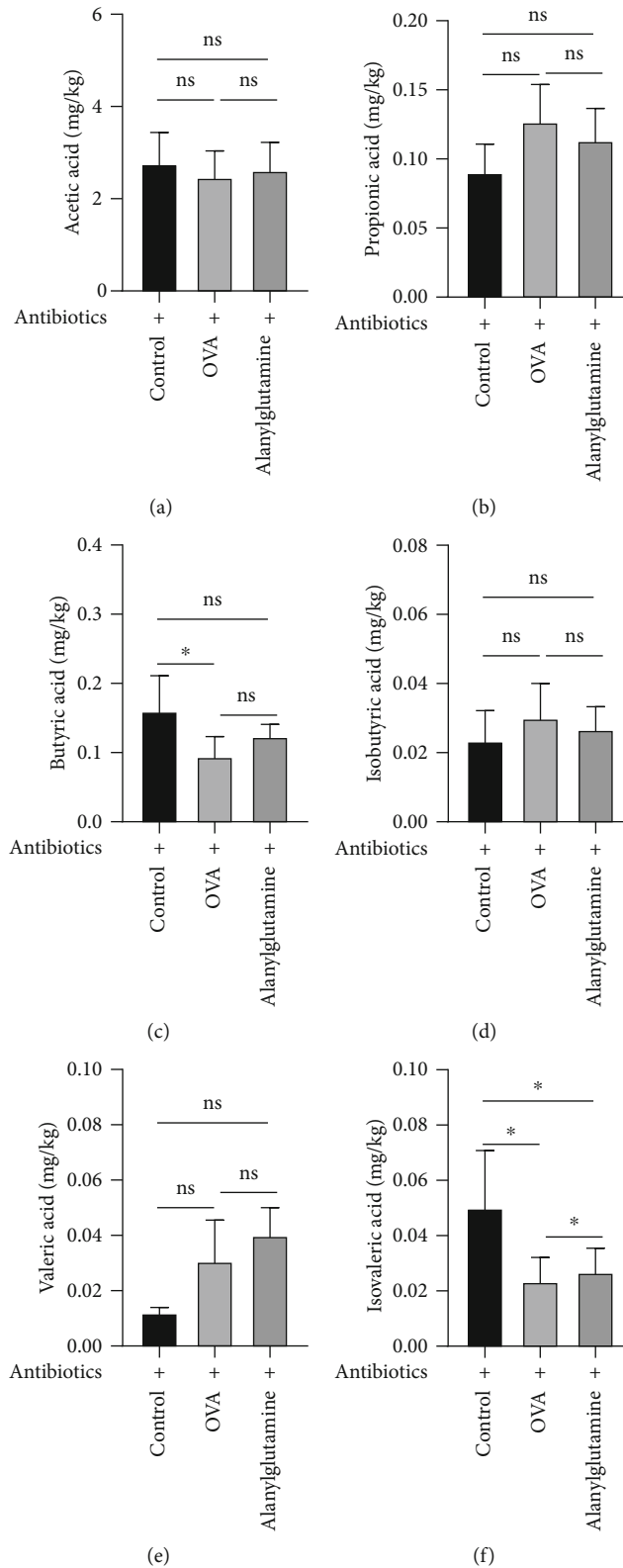


FIGURE 6: Amino acid content (mg/kg) in the groups of control+antibiotic, OVA+antibiotic, and Alanylglutamine+antibiotic mice: (a) acetic acid; (b) propionic acid; (c) butyric acid; (d) isobutyric acid; (e) valeric acid; (f) isovaleric acid. * $P < 0.05$; ns: not significant.

with the previous researches, in which Plumbagin protects liver against fulminant hepatic failure and chronic liver fibrosis in LX-2 cells [29].

Although we performed analysis in several signaling pathways, the exact molecular pathways involved in the pathogenesis and treatment of various diseases are quite complex

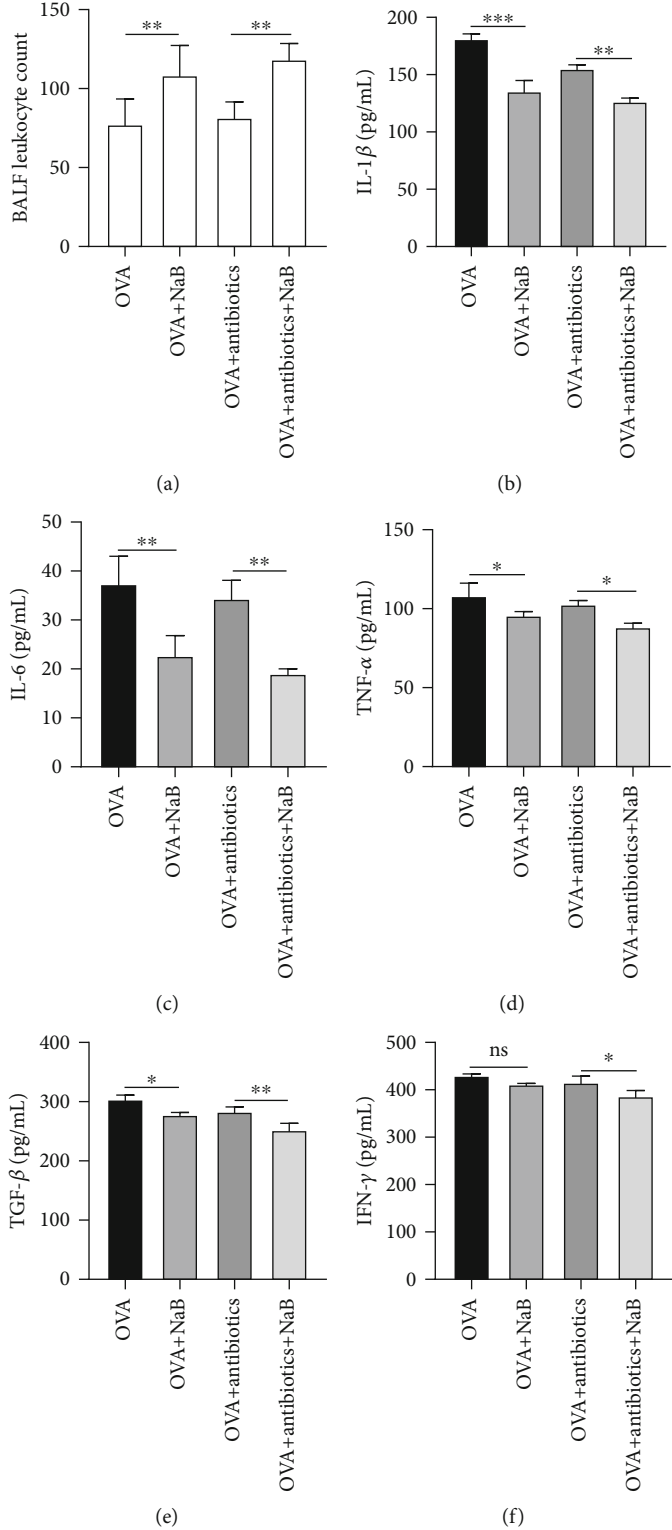


FIGURE 7: Continued.

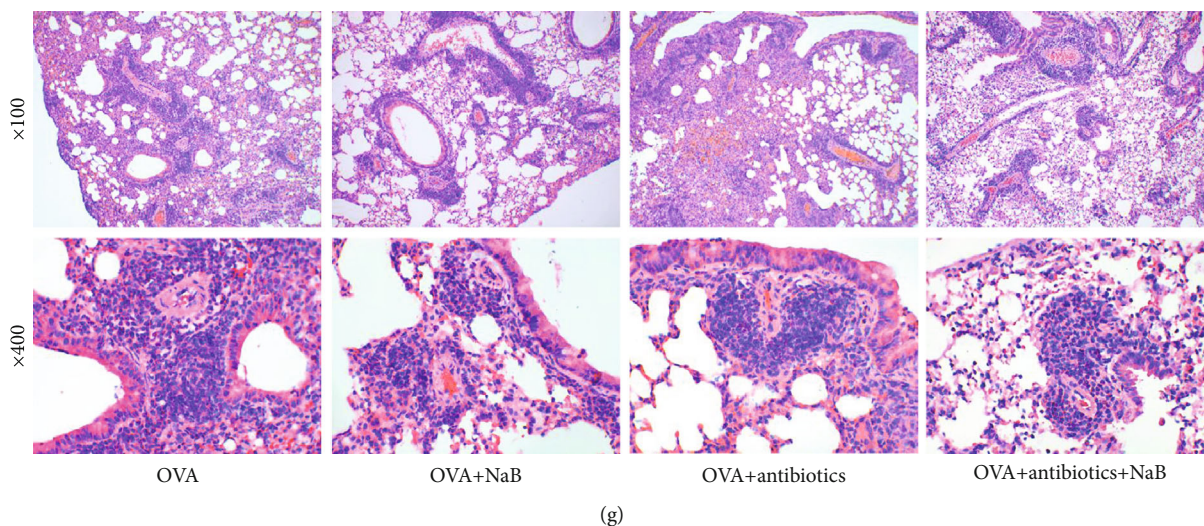


FIGURE 7: Effects of butyric acid on OVA-induced allergic asthma through cytokine productions in BALF and inflammatory infiltration in the lung tissue. The expression of inflammatory cytokines by ELISA in the groups of OVA, OVA+NaB, OVA+antibiotic, and OVA+antibiotic+NaB mice: (a) BALF leukocyte count; (b) IL-1 β ; (c) IL-6; (d) TNF- α ; (e) TGF- β ; (f) IFN- γ level from BALF; (g) lung tissue morphology study measured by H&E staining. $n = 8$. * $P < 0.05$; ** $P < 0.01$; ns: not significant.

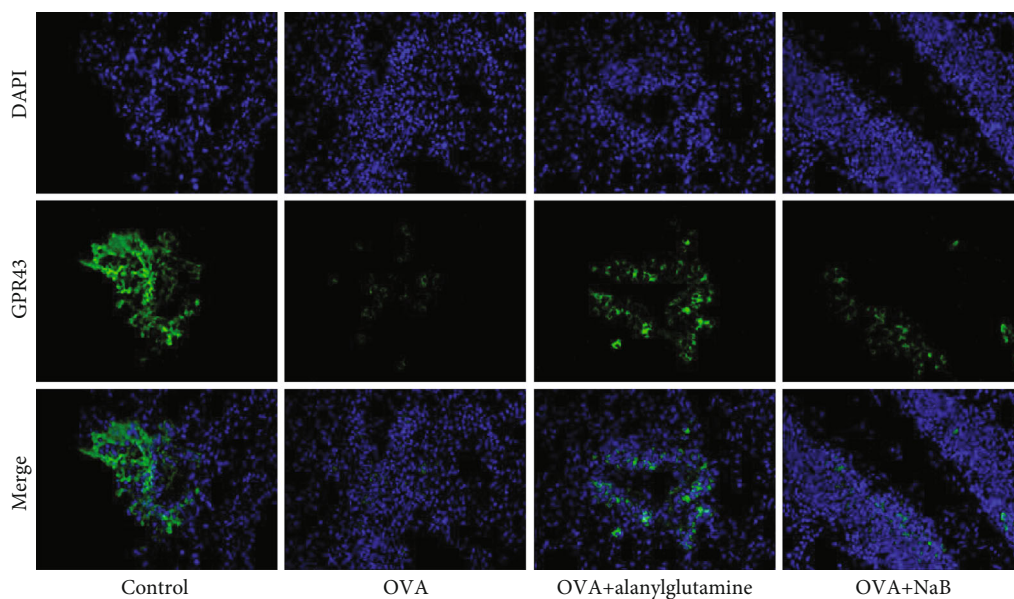
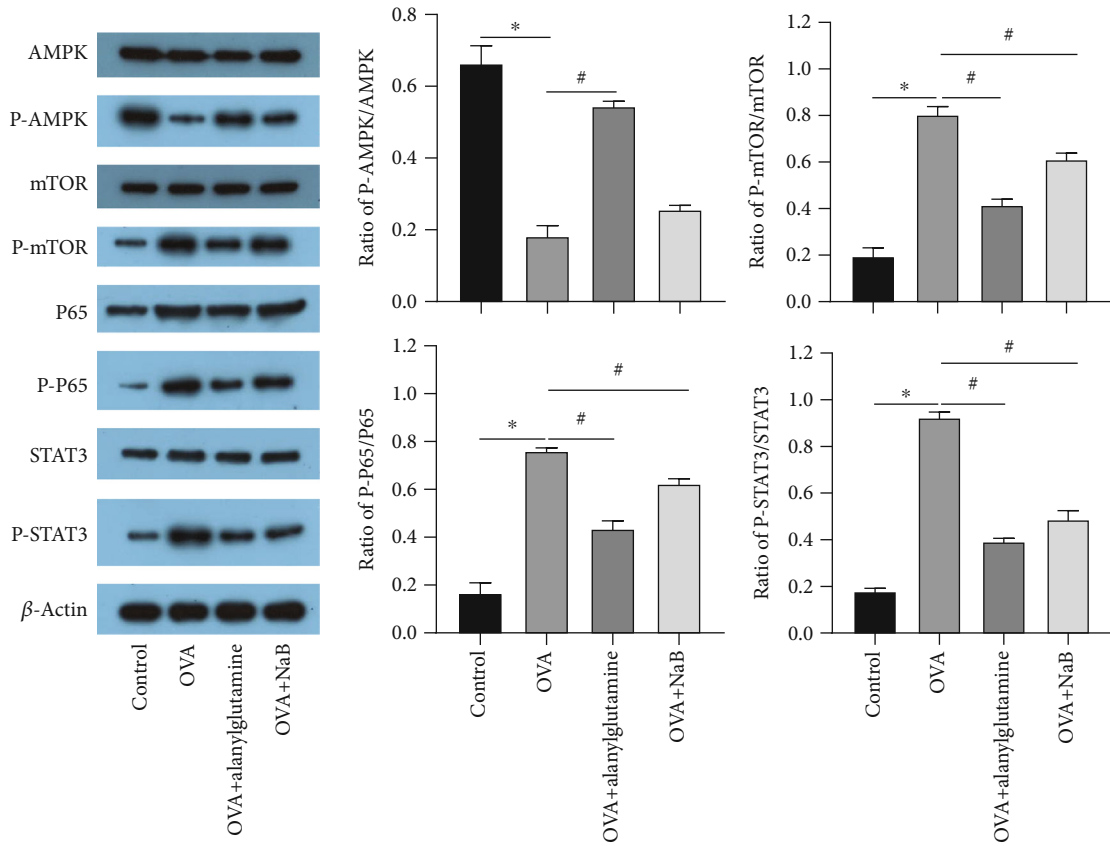


FIGURE 8: Immunofluorescence staining for the expressions of GPR43, DAPI, and their merge results in the groups of control, OVA, OVA+Alanylglutamine, and OVA+NaB mice. $n = 8$.

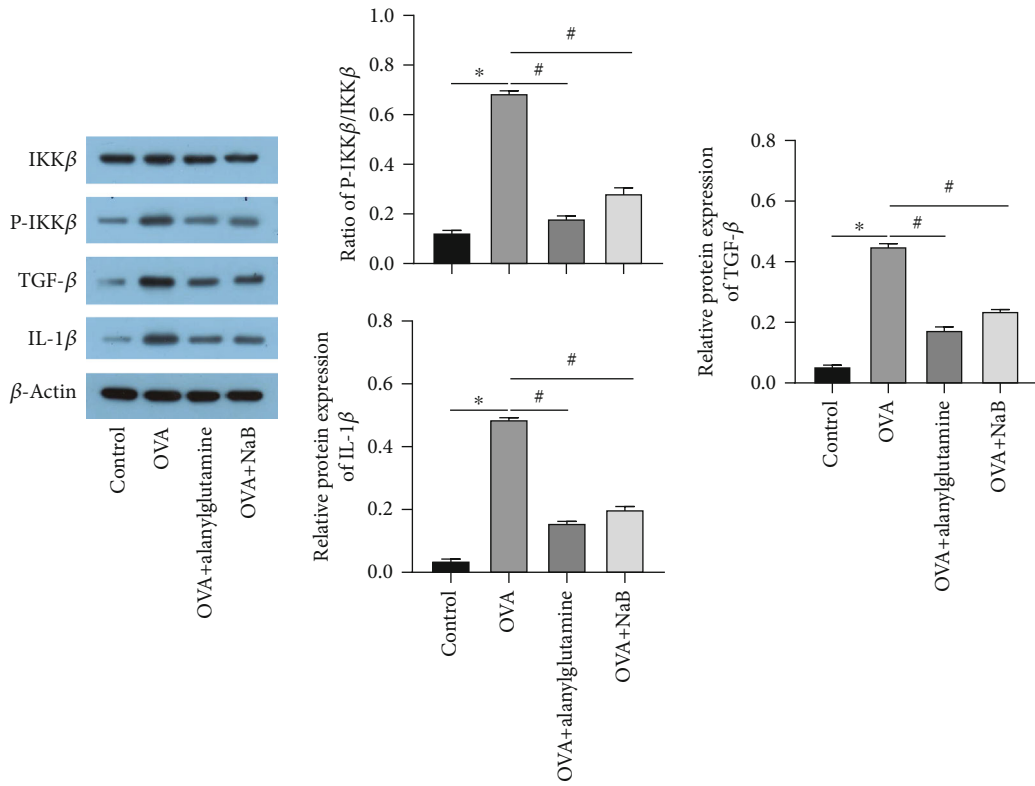
and complicated. In a previous study, the scientist demonstrated that diet supplemented with baicalin could alleviate oxidative stress and enhance nutrition absorption in deoxynivalenol-challenged pigs. The effects of baicalin might be related to the inhibition of NF- κ B and activation of the mTOR pathway, which are different from our results [30–33]. Another study showed that anti-inflammatory and antioxidative stress effects of baicalin about atherosclerosis might be in connection with inhibiting the NF- κ B and p38 MAPK signaling pathways [33]. Considering the complexities in the signaling pathways involved in the functional procedures from Alanylglutamine, we plan to further study the relevant

molecular mechanisms in its therapy to asthma in the future research.

It is established that intestinal flora closely involves in the development of asthma [34], which is often accompanied by inflammatory reaction. In the peripheral blood of children with asthma, the possibility of intestinal flora disorders and gastrointestinal discomfort symptoms increases, with the elevation in the levels of inflammatory factors such as TNF- α and IL-6 [35]. In a previous study, Stephanie et al. showed that TNF- α , IL-33, and IL-13 had a crucial role in treatment of asthma in obese mice, of which the gut microbiome was altered in contrast to the control mice [36]. In this study,



(a)



(b)

FIGURE 9: Continued.

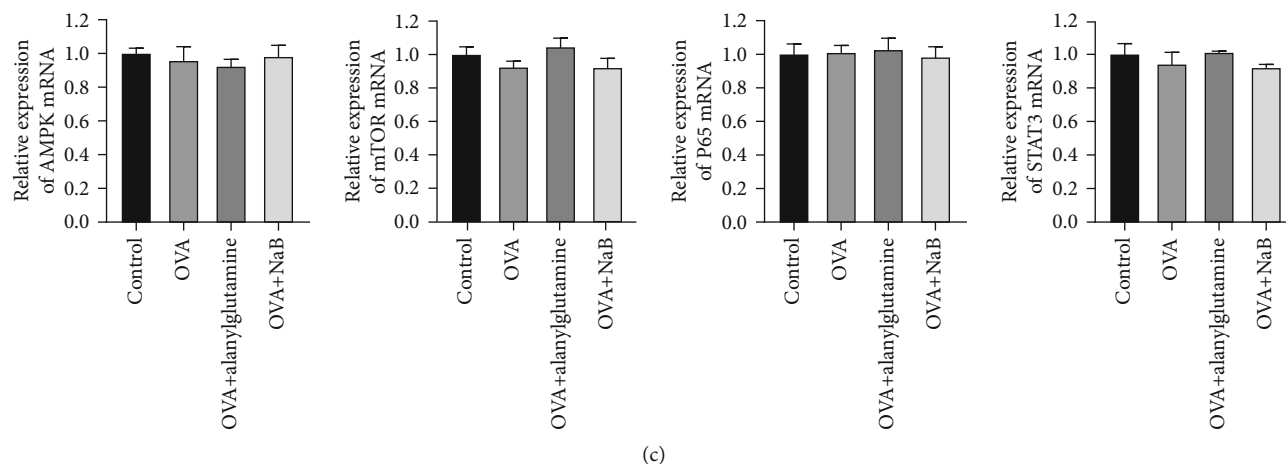


FIGURE 9: Alanylglutamine inhibited the NF- κ B pathway and STAT3 pathway. (a) The expressions of AMPK, P-AMPK, mTOR, P-mTOR, P65, P-P65, STAT3, P-STAT3, and β -Actin and quantitative ratio statistics of P-AMPK/AMPK, P-mTOR/mTOR, P-P65/P65, and P-STAT3/STAT3. (b) The expressions of IKK β , P-IKK β , TGF- β , and IL-1 β and their corresponding quantitative statistics. (c) Related mRNA expressions of AMPK, mTOR, P65, and STAT3 by RT-qPCR in the groups. $n = 3$. * $P < 0.05$ vs. the control; # $P < 0.05$ vs. the OVA group.

we found that Alanylglutamine could reverse the changes of intestinal flora and inflammatory factors, inducing by OVE. Due to funding and time limitations, we did not provide the molecular evidence for the direct correlation between gut microbiota and the symptom. In the future work, we will perform in-depth analysis on this aspect and hope to further enhance the treatment effects of asthma with related drugs.

5. Conclusions

We established the relationship among Alanylglutamine dipeptide, SCFA, and antibiotics in the asthma model through a series of experimental verifications. Our results implicated that Alanylglutamine might be beneficial for asthma, and its effect was achieved through regulation on microbiota and the derived metabolites of butyric acid. Moreover, the therapeutic effects might involve in the regulation of AMPK, NF- κ B, mTOR, and STAT3 signaling pathways. These findings will help identify the effective therapeutic direction to alleviate allergic inflammation of the lungs and airways.

Data Availability

The authors confirm that all data underlying the findings are available. All relevant data are within the paper or its supplementary materials.

Ethical Approval

All experimental animals used in this study were maintained under a protocol approved by the Institutional Animal Care and Use Committee of Second Xiangya Hospital.

Conflicts of Interest

The authors declare that the research was conducted in the absence of any commercial or financial relationships that could be construed as a potential conflict of interest.

Authors' Contributions

SL performed the experiment and analyzed the data; LM, YY, XJ, WS, JD, QZ, BW, BX, JZ, and PC handled data collection and analysis and edited the manuscript; and XX supervised the whole study, data analysis, and manuscript preparation.

Acknowledgments

This work was supported by the General Program of the Hunan Provincial Natural Science Foundation of China (2019JJ40453).

Supplementary Materials

Supplementary Figure 1: microbiota at the genus level (top 20) was analyzed, including *Corynebacterium*, *Adlercreutzia*, *Bacteroides*, *Parabacteroides*, *Prevotella*, *Odoribacter*, *Prevotella*, *Sporosarcina*, *Staphylococcus*, *Lactobacillus*, *Streptococcus*, *Turicibacter*, *Dehalobacterium*, *Coprococcus*, *Dorea*, *Ruminococcus*, *Oscillospira*, *Butyricimonas*, *Allobaculum*, and *Sutterella*. 11 genera were markedly altered in response to OVA or Alanylglutamine treatment. ** $P < 0.01$; *** $P < 0.001$; ns: not significant. (*Supplementary Materials*)

References

- [1] S. Kleinert and R. Horton, "After asthma: airways diseases need a new name and a revolution," *The Lancet*, vol. 391, no. 10118, pp. 292–294, 2018.
- [2] B. N. Lambrecht, H. Hammad, and J. V. Fahy, "The cytokines of asthma," *Immunity*, vol. 50, no. 4, pp. 975–991, 2019.
- [3] C. Nunes, A. M. Pereira, and M. Morais-Almeida, "Asthma costs and social impact," *Asthma Research and Practice*, vol. 3, no. 1, p. 1, 2017.
- [4] J. L. Brożek, J. Bousquet, I. Agache et al., "Allergic rhinitis and its impact on asthma (ARIA) guidelines—2016 revision," *Journal of Allergy and Clinical Immunology*, vol. 140, no. 4, pp. 950–958, 2017.

- [5] A. H. Liu, J. D. Spahn, and D. Y. M. Leung, "Childhood asthma," in *Nelson Textbook of Pediatrics*, R. E. Behrman, R. M. Kliegman, and H. B. Jenson, Eds., pp. 760–774, PA: Saunders, Philadelphia, 17th edition, 2004.
- [6] P. Barnes, "Efficacy of inhaled corticosteroids in asthma," *Journal of Allergy and Clinical Immunology*, vol. 102, no. 4, pp. 531–538, 1998.
- [7] J. Carmichael, I. C. Paterson, P. Diaz, G. K. Crompton, A. B. Kay, and I. W. Grant, "Corticosteroid resistance in chronic asthma," *BMJ*, vol. 282, no. 6274, pp. 1419–1422, 1981.
- [8] V. F. Cruzat, A. Bittencourt, S. P. Scomazzon, J. S. M. Leite, P. I. H. de Bittencourt, and J. Tirapegui, "Oral free and dipeptide forms of glutamine supplementation attenuate oxidative stress and inflammation induced by endotoxemia," *Nutrition*, vol. 30, no. 5, pp. 602–611, 2014.
- [9] X. Zhang, X. Tan, Y. Liu et al., "Alanyl-glutamine ameliorates lipopolysaccharide-induced inflammation and barrier function injury in bovine jejunum epithelial cells," *Biochemistry and Cell Biology*, vol. 97, no. 6, pp. 670–680, 2019.
- [10] Y.-C. Hou, C.-C. Chu, T.-L. Ko, C.-L. Yeh, and S.-L. Yeh, "Effects of alanyl-glutamine dipeptide on the expression of colon-inflammatory mediators during the recovery phase of colitis induced by dextran sulfate sodium," *European Journal of Nutrition*, vol. 52, no. 3, pp. 1089–1098, 2013.
- [11] Y.-C. Hou, M.-H. Pai, J.-J. Liu, and S.-L. Yeh, "Alanyl-glutamine resolves lipopolysaccharide-induced lung injury in mice by modulating the polarization of regulatory T cells and T helper 17 cells," *The Journal of Nutritional Biochemistry*, vol. 24, no. 9, pp. 1555–1563, 2013.
- [12] D. M. Pinn, O. C. Aroniadis, and L. J. Brandt, "Is fecal microbiota transplantation (FMT) an effective treatment for patients with functional gastrointestinal disorders (FGID)?," *Neurogastroenterology and Motility*, vol. 27, no. 1, pp. 19–29, 2015.
- [13] J. Liu, H. Xiong, Y. Cheng et al., "Effects of taraxasterol on ovalbumin-induced allergic asthma in mice," *Journal of Ethnopharmacology*, vol. 148, no. 3, pp. 787–793, 2013.
- [14] C. Wu, G. Yang, L. G. Bermúdez-Humarán et al., "Immunomodulatory effects of IL-12 secreted by *Lactococcus lactis* on Th1/Th2 balance in ovalbumin (OVA)-induced asthma model mice," *International Immunopharmacology*, vol. 6, no. 4, pp. 610–615, 2006.
- [15] M. Tsang, S.-W. Cheng, J. Zhu et al., "Anti-inflammatory activities of pentaherbs formula and its influence on gut microbiota in allergic asthma," *Molecules*, vol. 23, no. 11, p. 2776, 2018.
- [16] S. L. Russell, M. J. Gold, L. A. Reynolds et al., "Perinatal antibiotic-induced shifts in gut microbiota have differential effects on inflammatory lung diseases," *Journal of Allergy and Clinical Immunology*, vol. 135, no. 1, pp. 100–109.e5, 2015.
- [17] E. Roth, J. Karner, G. Ollenschläger et al., "Alanylglutamine reduces muscle loss of alanine and glutamine in post-operative anaesthetized dogs," *Clinical Science*, vol. 75, no. 6, pp. 641–648, 1988.
- [18] B. Alteheld, M. E. Evans, L. H. Gu et al., "Alanylglutamine dipeptide and growth hormone maintain PepT1-mediated transport in oxidatively stressed Caco-2 cells," *The Journal of Nutrition*, vol. 135, no. 1, pp. 19–26, 2005.
- [19] G. C. Melis, P. G. Boelens, J. R. M. van der Sijp et al., "The feeding route (enteral or parenteral) affects the plasma response of the dipeptide Ala-Gln and the amino acids glutamine, citrulline and arginine, with the administration of Ala-Gln in preoperative patients," *British Journal of Nutrition*, vol. 94, no. 1, pp. 19–26, 2005.
- [20] Z. Li, S. Yang, H. Lin et al., "Probiotics and antibodies to TNF inhibit inflammatory activity and improve nonalcoholic fatty liver disease," *Hepatology*, vol. 37, no. 2, pp. 343–350, 2003.
- [21] J. Tan, C. McKenzie, P. J. Vuillermier et al., "Dietary fiber and bacterial SCFA enhance oral tolerance and protect against food allergy through diverse cellular pathways," *Cell Reports*, vol. 15, no. 12, pp. 2809–2824, 2016.
- [22] B. Hippe, M. Remely, E. Aumueller, A. Pointner, and A. G. Haslberger, "SCFA producing gut microbiota and its effects on the epigenetic regulation of inflammation," in *Beneficial Microorganisms in Medical and Health Applications*, pp. 181–197, Springer, 2015.
- [23] M. A. Rank, T. Kabayashi, K. R. Bartemes, and H. Kita, "Activation of dendritic cells by IL-33 initiates a Th2 response," *Journal of Allergy and Clinical Immunology*, vol. 123, no. 2, p. S53, 2009.
- [24] H. Yin, X. Y. Li, T. Liu et al., "Adenovirus-mediated delivery of soluble ST2 attenuates ovalbumin-induced allergic asthma in mice," *Clinical & Experimental Immunology*, vol. 170, no. 1, pp. 1–9, 2012.
- [25] A. Hague, D. J. E. Elder, D. J. Hicks, and C. Paraskeva, "Apoptosis in colorectal tumour cells: induction by the short chain fatty acids butyrate, propionate and acetate and by the bile salt deoxycholate," *International Journal of Cancer*, vol. 60, no. 3, pp. 400–406, 1995.
- [26] J. Huuskonen, T. Suuronen, T. Nuutinen, S. Kyrylenko, and A. Salminen, "Regulation of microglial inflammatory response by sodium butyrate and short-chain fatty acids," *British Journal of Pharmacology*, vol. 141, no. 5, pp. 874–880, 2004.
- [27] A. Giermasz, M. Makowski, E. Kozłowska et al., "Potentiating antitumor effects of a combination therapy with lovastatin and butyrate in the Lewis lung carcinoma model in mice," *International Journal of Cancer*, vol. 97, no. 6, pp. 746–750, 2002.
- [28] N. Li, X.-x. Liu, M. Hong et al., "Sodium butyrate alleviates LPS-induced acute lung injury in mice via inhibiting HMGB1 release," *International Immunopharmacology*, vol. 56, pp. 242–248, 2018.
- [29] H. Wang, H. Zhang, Y. Zhang et al., "Plumbagin protects liver against fulminant hepatic failure and chronic liver fibrosis via inhibiting inflammation and collagen production," *Oncotarget*, vol. 7, no. 50, pp. 82864–82875, 2016.
- [30] P. Liao, Y. Li, M. Li et al., "Baicalin alleviates deoxynivalenol-induced intestinal inflammation and oxidative stress damage by inhibiting NF- κ B and increasing mTOR signaling pathways in piglets," *Food and Chemical Toxicology*, vol. 140, article 111326, 2020.
- [31] A. Zha, Z. Cui, M. Qi et al., "Dietary baicalin zinc supplementation alleviates oxidative stress and enhances nutrition absorption in deoxynivalenol challenged pigs," *Current Drug Metabolism*, vol. 21, no. 8, pp. 614–625, 2020.
- [32] A. Zha, D. Yuan, Z. Cui et al., "The evaluation of the antioxidant and intestinal protective effects of baicalin-copper in deoxynivalenol-challenged piglets," *Oxidative Medicine and Cellular Longevity*, vol. 2020, Article ID 5363546, 13 pages, 2020.
- [33] Y. Wu, F. Wang, L. Fan et al., "Baicalin alleviates atherosclerosis by relieving oxidative stress and inflammatory responses via inactivating the NF- κ B and p38 MAPK signaling pathways," *Biomedicine & Pharmacotherapy*, vol. 97, pp. 1673–1679, 2018.

- [34] Y. B. Kang, Y. Cai, and H. Zhang, "Gut microbiota and allergy/asthma: from pathogenesis to new therapeutic strategies," *Allergologia et Immunopathologia*, vol. 45, no. 3, pp. 305–309, 2017.
- [35] Y. Zhang, T. Li, H. Yuan, W. Pan, and Q. Dai, "Correlations of inflammatory factors with intestinal flora and gastrointestinal incommensurate symptoms in children with asthma," *Medical Science Monitor*, vol. 24, pp. 7975–7979, 2018.
- [36] S. A. Shore, "Mechanistic basis for obesity-related increases in ozone-induced airway hyperresponsiveness in mice," *Annals of the American Thoracic Society*, vol. 14, Supplement 5, pp. S357–S362, 2017.

Research Article

Inhibitory Effect of *Lactobacillus plantarum* CCFM8724 towards *Streptococcus mutans*- and *Candida albicans*-Induced Caries in Rats

Qiuxiang Zhang ^{1,2,3}, Sujia Qin ^{1,3}, Xianyin Xu ⁴, Jianxin Zhao ^{1,3}, Hao Zhang ^{1,3,5,6},
Zhenmin Liu ² and Wei Chen ^{1,3,5,7}

¹State Key Laboratory of Food Science and Technology, Jiangnan University, Wuxi, Jiangsu 214122, China

²State Key Laboratory of Dairy Biotechnology, Shanghai Engineering Research Center of Dairy Biotechnology, Dairy Research Institute, Bright Dairy & Food Co., Ltd., Shanghai 200436, China

³School of Food Science and Technology, Jiangnan University, Wuxi, Jiangsu 214122, China

⁴Department of Stomatology, Wuxi Children's Hospital, Wuxi, Jiangsu 214023, China

⁵National Engineering Research Center for Functional Food, Jiangnan University, Wuxi, Jiangsu 214122, China

⁶Wuxi Translational Medicine Research Center and Jiangsu Translational Medicine Research Institute Wuxi Branch, China

⁷Beijing Innovation Centre of Food Nutrition and Human Health, Beijing Technology and Business University (BTBU), Beijing 100048, China

Correspondence should be addressed to Zhenmin Liu; liuzhenmin@brightdairy.com and Wei Chen; chenwei66@jiangnan.edu.cn

Received 23 July 2020; Revised 26 November 2020; Accepted 6 December 2020; Published 21 December 2020

Academic Editor: Wuquan Deng

Copyright © 2020 Qiuxiang Zhang et al. This is an open access article distributed under the Creative Commons Attribution License, which permits unrestricted use, distribution, and reproduction in any medium, provided the original work is properly cited.

Streptococcus mutans is a recognized cariogenic bacterium and a major producer of biofilm matrix. The presence of *Candida albicans* in dental plaque with *S. mutans* enhances the virulence leading to the onset of rampant caries which is similar to early childhood caries (ECC). The purpose of this study was to explore the effect of *Lactobacillus plantarum* CCFM8724 (CCFM8724) on the treatment and prevention of dental caries induced by *S. mutans* and *C. albicans* *in vivo*. Rats were divided into 6 groups: the control group and model group, 2 treatment groups, and 2 prevention groups (0.02% chlorhexidine or CCFM8724). The fluctuation of microbial colonization and the change of bacteria flora in rat oral cavity after sowing of *L. plantarum* CCFM8724 were investigated by colony-forming units (CFU) and microflora analysis. The caries of rats were assessed by microcomputed tomography (micro-CT) and Keyes scoring method. The results showed that *L. plantarum* CCFM8724 in both the treatment and prevention groups could significantly decrease the population of *S. mutans* and *C. albicans* in the rats' oral cavity ($p < 0.001$), the mineral loss of enamel ($p < 0.05$), and the scores of caries ($p < 0.05$). Besides, *L. plantarum* CCFM8724 exhibited better effects than chlorhexidine. Hence, *L. plantarum* CCFM8724 was proved to be a potential oral probiotic on caries treatment and prevention *in vivo* and it may have the prospect of application in dental caries (especially ECC) prevention products.

1. Introduction

Dental caries is one of the most prevalent oral bacterial infectious diseases that afflict children and adults worldwide. It can lead to the irreversible tooth demineralization, which is mainly associated with acidic biofilm formation and sugar intake [1]. Early childhood caries (ECC) is a unique form of rampant caries developed in babies and toddlers, especially preschool children. ECC can result in rapid and aggressive

destruction of primary teeth which not only causes painful pulpal but also impacts on the development of permanent dentition and systemic health [2, 3]. Traditional treatment for deciduous caries is extremely costly and time consuming. Hence, ECC has been a major challenge in public health until today.

Streptococcus mutans has been recognized as the main cariogenic bacteria for its strong acidogenic and aciduric capacities [4]. And it is also the major producer of biofilm

matrix, providing acid milieu within which caries-associated organisms thrive [5]. Intriguingly, recent studies have found that, in addition to *S. mutans*, fungus such as *Candida albicans* was detected frequently in high numbers in plaque biofilms from toddlers with caries [6, 7]. Moreover, the presence of *C. albicans* in mixed-species biofilms induces *S. mutans* glucosyltransferase (GTF) expression, which converts dietary sucrose into extracellular polysaccharides (EPS) and build more cariogenic biofilms [8]. Rather, the synergistic alliance of them amplifies the biofilm virulence which led to rampant caries similar to ECC in an animal model [9].

Common mechanical measures for dental caries control, although effective, have been limited by the preference of children and the elderly. It is known that chlorhexidine (CHX) has a bactericidal effect on *S. mutans* and fungicidal effect on *C. albicans* [10]. While the limitation of antimicrobial drugs is that once the intervention with CHX stops, the same pathogens will repopulate in oral niches and result in recurrence of tooth decay. To avoid this, lower dental plaque virulence with ecological methods are being increasingly preferred over broad-spectrum antimicrobials for long-term caries control [11]. In this regard, it is essential to develop an alternative product which can disrupt the cariogenic virulence and promote oral microecological balance with no adverse effects.

The FAO/WHO (Food and Agriculture Organization of the United Nations, World Health Organization) define probiotics as live microorganisms that play a beneficial role in the health of the host by taking appropriate amounts. In the past 10 years, probiotics have achieved a lot in preventing or treating gastrointestinal infections and diseases such as acute diarrhea, ulcerative colitis, Crohn's disease, and pouchitis [12, 13]. Currently, with the increasing acceptance of probiotics, more and more attention has been paid to probiotic usage in other areas such as dental caries prevention, periodontitis relieving, and regulation of oral microecological balance [14]. And several clinical trials have demonstrated that the administration of *Lactobacillus* genus including *L. rhamnosus*, *L. reuteri*, and *L. paracasei* decreased the lesion of caries in children [15–17]. However, the number of studies on the interaction of *Lactobacillus* with cariogenic bacteria and fungi and the effects of the probiotic *L. plantarum* on ECC caries model *in vivo* is limited, which prompted us to address these knowledge gaps.

In our previous study, *L. plantarum* CCFM8724 isolated from healthy human feces exhibited a considerable effect on inhibiting *S. mutans* and *C. albicans* dual biofilm formation *in vitro* [18]. In this study, we examined the changes of *S. mutans* and *C. albicans* colonization and caries development in the rat oral cavity by plate culture counting, 16S rDNA sequencing, micro-CT, and caries scoring to evaluate the effect of *L. plantarum* CCFM8724 on the prevention or treatment of caries *in vivo*. These results will provide enlightenment and proof on probiotics preventing and treating rampant caries induced by *S. mutans* and *C. albicans*.

2. Methods

2.1. Ethics Statement. This research methodology was conducted in accordance with institutional ethical standards.

The study on animals was approved by “Jiangsu Institute of Parasitic Diseases, Animal Care and Use Committee” (IACUC-JIPD-2019030). All experiments were in accordance with the guidelines of the China Ministry of Science and Technology Guide for the Care and Use of Laboratory Animals.

2.2. Strains and Inoculum Preparation. *L. plantarum* CCFM8724 was isolated from healthy human feces and inoculated in MRS broth (Difco™, Detroit, MI, USA) under anaerobic conditions at 37°C. *S. mutans* ATCC 25175 was purchased from the China Common Microbial Species Preservation and Management Center (CGMCC, Beijing, China) and cultured in Tryptic Soy Broth (TSB, Difco™, Detroit, MI, USA) under anaerobic conditions at 37°C. *C. albicans* SJ was isolated from human carious dentin, which was grown in Yeast Extract Peptone Dextrose Medium (YPD, Difco™, Detroit, MI, USA) under aerobic conditions at 37°C. All strains were frozen in 30% (*v/v*) glycerol broth at -80°C and routinely streaked on corresponding agar plates. The plates were cultured at 37°C for 48 h and at least three times consecutively using 2% (*v/v*) inoculum in corresponding broth at 37°C for 18 h before use.

Prior to use in animal experiments, the microbial cultures were centrifuged at 3000 g for 10 min and washed twice with sterile saline solution. The bacteria and yeast were then centrifuged and resuspended in saline solution and diluted to a suspension of 1×10^9 living cells (CCFM8724 and *S. mutans*) or 10^6 (*C. albicans*) by colony counting.

2.3. Animals and General Procedures. Animal experimental design is shown in Figure 1. Female SPF Wistar rats (21 days old) were purchased from Charles River Laboratories (Beijing, China). All of the rats were divided randomly into 6 groups, comprising of 2 treatment groups (T1-CHX and T2-CCFM8724), 2 prevention groups (P1-CHX and P2-CCFM8724), and the caries-free and caries model groups. The rats in the caries-free group were given normal diet and distilled water during the whole experiment. Other groups were offered a cariogenic diet 2000 (obtained from Nantong Trophy Feed Technology Co., Ltd.) and water containing 5% sucrose *ad libitum*. The oral flora of rats was suppressed by ampicillin (0.5 µg/mL) and streptomycin (200 µg/mL) for 3 days before the experiment.

The caries model group was infected with *S. mutans* and *C. albicans* for 5 consecutive days from the first day of the experiment. The specific manipulation was to saturate the sterile cotton sticks with suspension of the two cariogenic microorganisms separately and then coat the suspension onto the rat oral cavity for 15 s per quadrant, as described by Beiraghi et al. [19]. Diet and water were forbidden for half an hour after tooth coating to ensure the colonization of microorganisms [20]. The establishment of tested strains was verified on day 6 and 7. The treatment groups were then applied with 0.02% CHX or CCFM8724 from day 8 to 12 and day 15 to 56. After verifying the successful colonization of lactobacilli, CHX or *Lactobacillus* was given three times a week until the end of the experiment (from day 15 to 56).

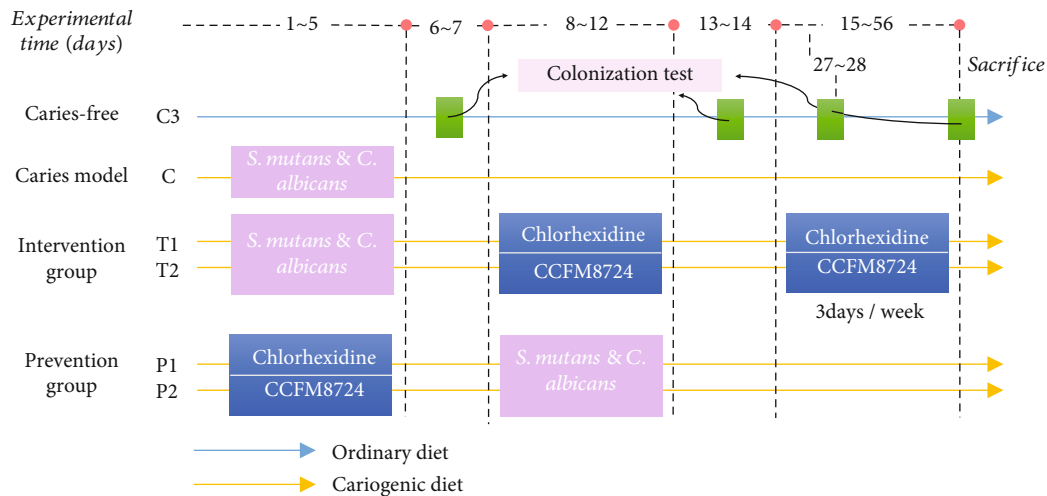


FIGURE 1: Animal experimental design.

To test the prevention effect of *Lactobacillus* on caries, CHX or CCFM8724 was firstly applied to coat the teeth on day 1-5. After the establishment of lactobacilli, *S. mutans* and *C. albicans* were used for another 5 consecutive days. No treatment was done in the prevention groups for the next 6 weeks to the end of the experiment. The whole experiment period was 8 weeks. The rats were weighed daily, and their weight gains were calculated.

2.4. Oral Microbial Count. Four samples (day 6, 13, 27, and 56) were taken during the whole experiment. Specific sampling method was scraping the surface of rat dentin with sterile cotton stick back and forth three to four times. *S. mutans* was counted on Mitis Salivarius Agar (Difco, No. 229810, BD Diagnostic Systems) with 200 IU/L bacitracin (MSB) [21], and *C. albicans* was plated on BIGGY Agar (BBL, No. 211027, BD Diagnostic Systems) [22], while MRS supplemented with 12 $\mu\text{g}/\text{mL}$ vancomycin was used to enumerate lactobacilli [23].

2.5. DNA Extraction, PCR, and 16S rDNA Sequencing. Cotton swabs sampled from the rat oral cavity on day 56 before sacrificed were stored at -80°C before examination. According to the instructions, FastDNA Spin Kit for feces (MP Biomedical, United States) was used to extract microbial genome DNA. The V3-V4 region of the 16S rDNA gene was amplified by PCR. After cutting from the 1.5% agarose gel, the product was purified by a QIAquick Gel Extraction Kit (Qiagen, Germany) and quantified by a Quant-iT PicoGreen dsDNA Assay Kit (Life Technologies, United States). Libraries were established by a TruSeq DNA LT Sample Preparation Kit (Illumina, United States) and were sequenced for 500 + 7 cycles on Illumina MiSeq using a MiSeq Reagent Kit. At last, the sequence data of 16S rDNA were analyzed by QIIME pipeline as described previously [24].

2.6. Caries Scoring. On day 56, the rats were anesthetized and decapitated. The soft tissues on the teeth and jaws were peeled off with a scalpel, and the residual debris in the sutures was washed by ultrasonic cleaning for 20 minutes. The max-

illary and mandibular molars were soaked in 10% polyformaldehyde for 24 hours [25, 26], then washed and dried. All the specimens were immersed in a 0.4% ammonium purpurate staining solution for 12 h and hemisectioned in the mesiodistal direction with an ultrathin carborundum disk (0.2 mm in thickness). The caries of rat molars were observed under a stereomicroscope (Leica CLS 100X, Wetzlar, Germany) and scored according to the method reported by Keyes [27].

2.7. Micro-CT Analysis. All mandibles were imaged using a microcomputed tomography (micro-CT) system (Quantum GX2; PerkinElmer, Hopkinton, MA, USA). An acquisition setting was used for scanning all the samples: 90 KV, 88 μA ; field of view: 18 μm ; acquisition time: 4 min; camera mode: high resolution. Each sample was rotated 360° , and all images were imported into Analyze 12.0 software (AnalyzeDirect, Overland Park, KS, USA) to reconstruct three-dimensional images of the mandibles, respectively. And a fixed threshold of 5,200 Hounsfield units was used to separate enamel from the whole mandible [28]. Mineral density (MD) of the enamel was calculated after calibration with hydroxyapatite standards of appropriate density.

2.8. Statistical Analysis. SPSS Statistics 25.0 (SPSS, Inc., Chicago, IL, USA) was used for the analysis. Graphpad Prism 8.0 and Origin 8.5 were used to map and analyze the data. The differences between the mean values of the groups were analyzed by one-way analysis of variance using Duncan's multiple range tests. Data expressed as mean \pm standard error of the mean (s.d, $n = 8$).

3. Results

3.1. Microorganism Colonization of the Rat Oral Cavity. During the animal experiment, all animals appeared to be in good physical condition and no significant differences in weight gain were observed among the groups ($p > 0.05$). The colonization of *S. mutans* and *C. albicans* were 5.6 and 4.1 log (CFU/mL) in the first sampling, respectively (Figures 2(a)

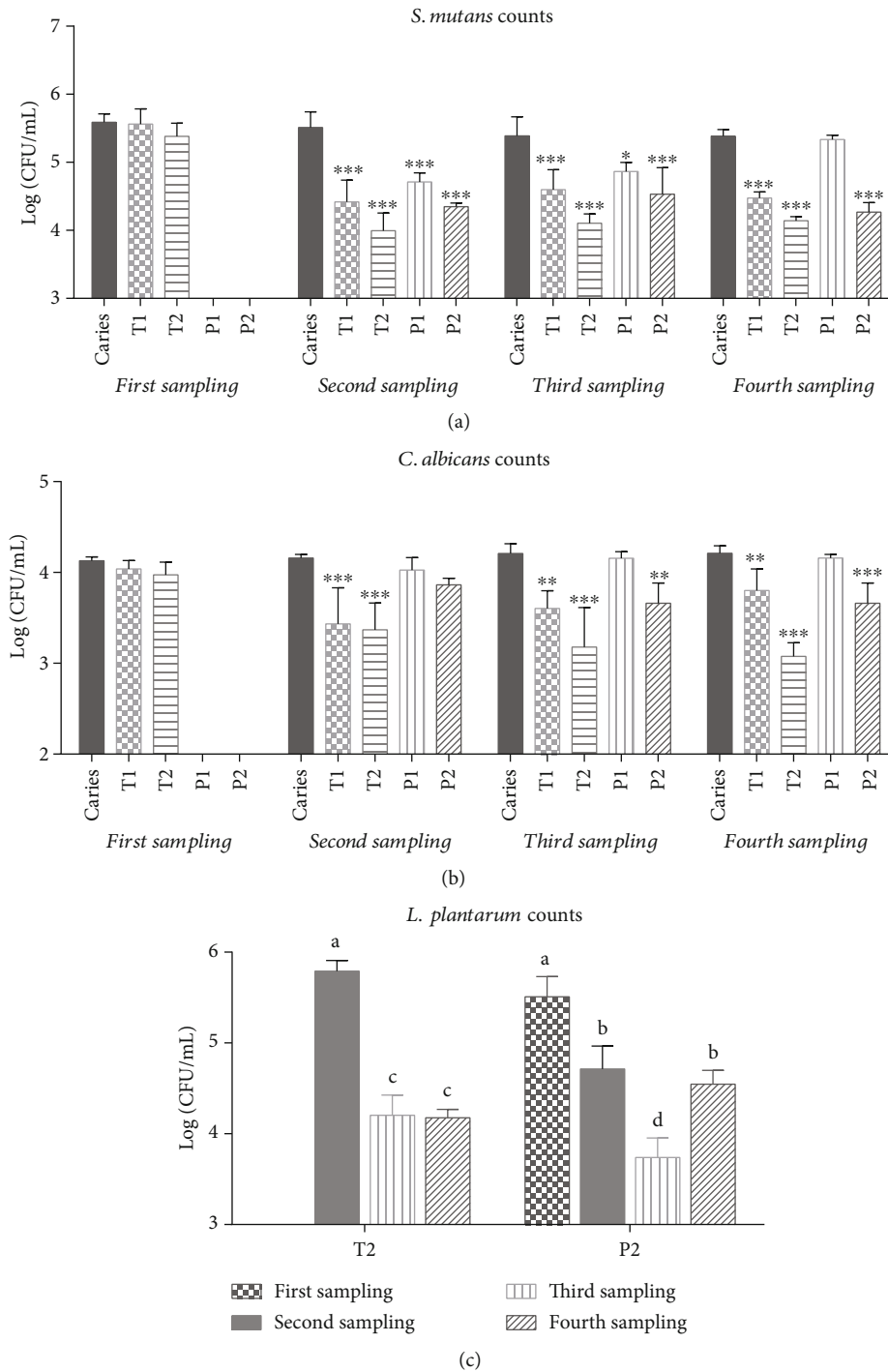


FIGURE 2: Microorganism count (log CFU/mL) recovered from rat oral swabs for 4 times. (a) Counting results of *S. mutans*. (b) Counting results of *C. albicans*. Values are significantly different from the caries model group in each sampling at * $p < 0.05$, ** $p < 0.01$, or *** $p < 0.001$ (a, b). (c) Counting results of *L. plantarum*. Groups with dissimilar letters differ, $p < 0.05$.

and 2(b)). After 5 consecutive days of *Lactobacillus* intervention, the population of *S. mutans* in T2 groups decreased from 5.4 to 4.0 log (CFU/mL) ($p < 0.001$) and remained at 4.1 log (CFU/mL) until the end of the experiment. CHX (T1) also inhibited the growth of *S. mutans* throughout the experiment, which reduced the population of *S. mutans* to 4.5 log (CFU/mL) ($p < 0.001$) and stabilized at this level.

After administered 0.02% CHX or CCFM8724 on day 1-5, the colonization of *S. mutans* in the prevention groups (P1 and P2) was significantly lower than that in the caries model group ($p < 0.001$). However, once CHX was stopped, the number of *S. mutans* continued rising, from 4.7 log (CFU/mL) (second sampling) to 5.3 log (CFU/mL) (fourth sampling), which was close to the number observed in the

caries model group ($p > 0.05$), while the population of *S. mutans* in the oral cavity (P2) remained at a low level (4.3 log (CFU/mL), $p < 0.001$) until the end of the experiment after CCFM8724 administration was stopped.

A similar phenomenon was observed on the change of *C. albicans* (Figure 2(b)). The effect of CHX treatment (T1) on *C. albicans* tended to decrease with time. Moreover, CHX cannot prevent the colonization and growth of *C. albicans* (P1, $p > 0.05$), while CCFM8724 intervention exhibited a significant inhibitory effect on *C. albicans* ($p < 0.001$) during the experiment. Interestingly, the CCFM8724 prevention group (P2) did not immediately affect *C. albicans* after the colonization of *Lactobacillus* but reduced the number of *C. albicans* in the third ($p < 0.05$) and fourth ($p < 0.001$) sampling.

According to the counts of *L. plantarum* (Figure 2(c)), cariogenic bacterial and fungi did not affect the colonization of *Lactobacillus* (P2 and T2, $p > 0.05$), which ranged from 5.5 to 5.8 log (CFU/mL) in both two groups. The population of *L. plantarum* in the CCFM8724 prevention group (P2) experienced significant fluctuations in the second, third, and fourth sampling, from 4.7 (CFU/mL) to 3.7 log (CFU/mL), and back to 4.5 log (CFU/mL) ($p < 0.05$), while that in the CCFM8724 treatment group decreased from 5.8 log (CFU/mL) (second sampling) to 4.2 log (CFU/mL) (third sampling) and then stabilized to 4.2 log (CFU/mL) (fourth sampling).

3.2. Microflora Analysis. Since the counts of *S. mutans*, *C. albicans*, and *Lactobacillus* shifted in different groups during the experiment, we also revealed the alterations of bacterial abundance and proportion among different groups by Illumina 16S rDNA gene sequencing. Compared with the caries-free group, the application of 0.02% CHX or CCFM8724 revealed major changes in relative abundance in the oral microbiome of rats (Figure 3(a)). The notable difference in *Streptococcus* was found between the caries-free group (CF, 3.65%) and the caries model group (C, 22.5%) ($p < 0.05$). Treatment with CCFM8724 significantly decreased the abundance of *Streptococcus* when compared with the caries model group ($p < 0.05$), although there was no difference observed between the T1 (7.24%) and T2 (6.01%) groups (Figure 3(b)). The same degree of decrease was obtained in the two prevention groups (P1, 17.24%, P2, 9.43%, $p < 0.05$). Relative abundance of *Lactobacillus* remained lowest in the caries-free group (CF, 0.22%), caries model group (C, 0.43%), and CHX treatment group (T1, 0.22%). No significant difference was observed among these three groups. Treatment with CCFM8724 can significantly increase the relative abundance of *Lactobacillus*, as shown in Figure 3(b), while the *Lactobacillus* abundance in the CCFM8724 prevention group (P2) was more than 1%, which is the highest in all groups (1.5%, $p < 0.05$).

3.3. Micro-CT Analysis. To enhance the visibility of caries site on rat molars, 3D reconstructions of mandible molars were performed by micro-CT. Enamel and dentin were stripped according to the density threshold (Hounsfield units). Meanwhile, the corresponding sagittal slice of the same molar was taken for comparative observation (Figure 4). Compared with the sagittal slice image between the caries model group

and caries-free group, it is obvious that the enamel (green) of sulcal or adjacent areas were not continuous if caries occurred.

To evaluate the results of micro-CT, the mean enamel volume (Figure 5(a)) and density (Figure 5(b)) of molars were analyzed in each group. Morphometric volume analysis revealed that the enamel volume in the CCFM8724 prevention group (P2) was closest to that of the caries-free group, followed by the CCFM8724 intervention group (T2). There was no significant difference in enamel volume between the CHX prevention group (P1) and intervention group (T1), but the enamel volume in both two groups was significantly larger than that of the caries model group ($p < 0.05$). The enamel density showed a similar result to those of enamel volume, but there was no difference in enamel density between the CHX prophylaxis group (P1) and dental caries model group ($p > 0.05$).

3.4. Caries Scoring. Under stereoscopic microscopy, various caries lesions were observed in all of the dyed molars except the caries-free group. The caries scores (Table 1) indicated that the lesion level E (enamel caries) of smooth surface or sulcal surface was considerably decreased in all the four groups, except that the CHX prevention group did not exhibit a significant effect on sulcal caries. According to the scores of different severity, the CCFM8724 prevention group showed the best effect, in which smooth surface and fissures did not appear with extensive caries (Dm, 3/4 of the dentin affected). And the total score (E) of this group was the lowest. The order of anticaries effect is as follows: the *Lactobacillus* treatment group, CHX treatment group, and lastly, CHX prevention group.

4. Discussion

In view of the increasing incidence and prevalence of dental cavity and its detrimental effects on oral health, novel strategies are required for its prevention and control. In recent years, the application of probiotics to prevent dental caries has become more and more common. Krzyściak et al. proved that *L. salivarius* HM6 could inhibit *S. mutans* and *C. albicans* dual biofilm formation and reduce the pathogenic species *in vitro* [29]. Although lactobacilli themselves could produce organic acid, it can be concluded that the overall effect of lactobacilli on caries prevention seems favorable when probiotics candidates are carefully selected [30]. And other studies have shown that *Lactobacillus* could attenuate the growth of *S. mutans* [31] or *C. albicans* [32] in human mouth. However, little is known whether *Lactobacillus* could exhibit effect on the mutually reinforcing alliances of *S. mutans* and *C. albicans* that coexist in the mouth.

In our study, CCFM8724 showed a considerable inhibitory effect on *S. mutans* and *C. albicans* during the intervention which lasted less than 2 months, three times a week (Figures 2(a), 2(b), and 3(b)). The prevention group in which CCFM8724 colonized firstly succeeded in controlling the proliferation of *S. mutans* but did not affect the colonization of *C. albicans* at first (Figures 2(a) and 2(b)). Although *C. albicans* decreased significantly and stabilized at a certain

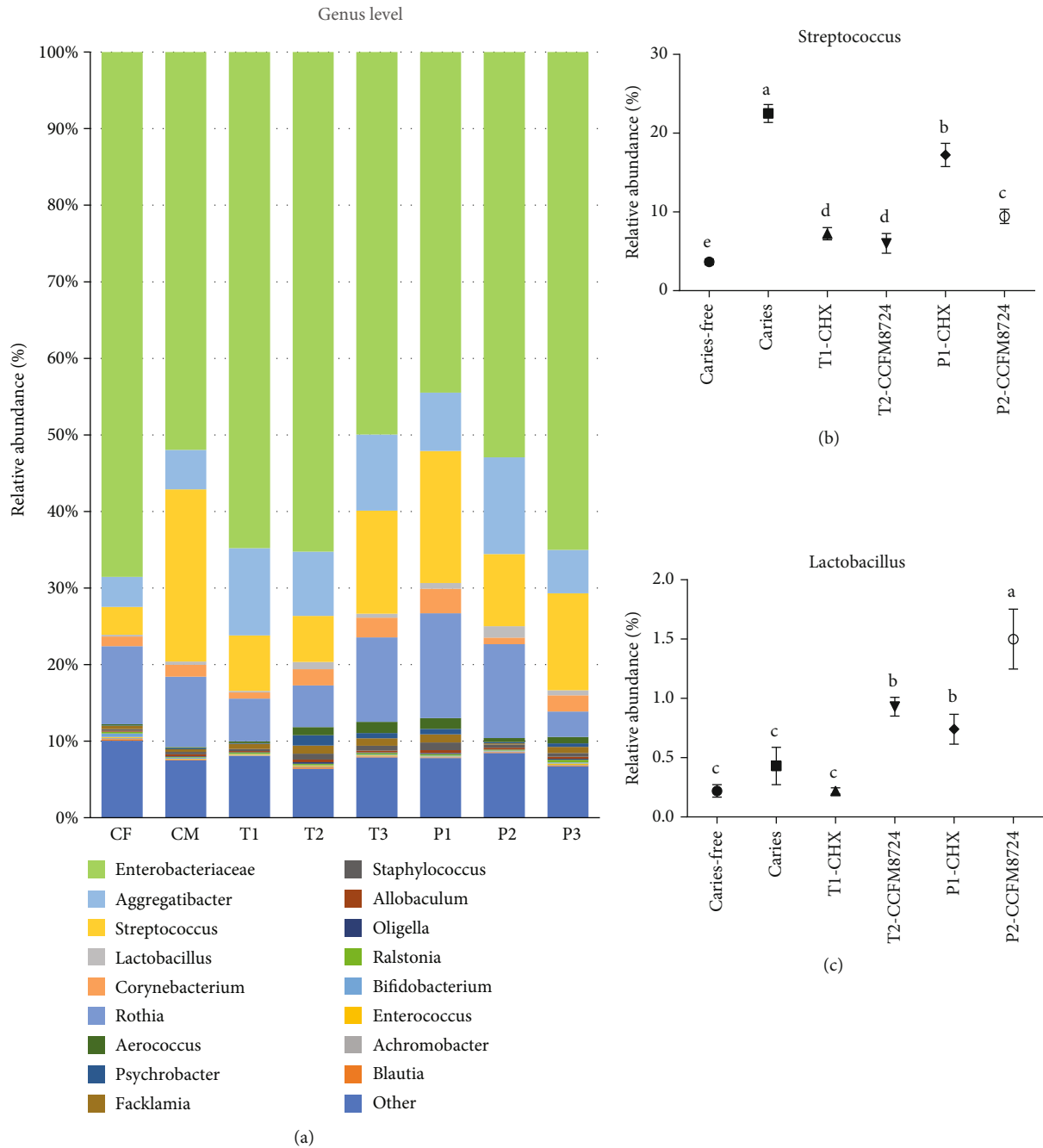


FIGURE 3: Changes in the level of genus in the oral cavity of rats in different groups. (a) Relative abundance of main genus > 0.1% in different groups. (b) Changes of the abundance of *Streptococcus* genus in different groups. Groups with dissimilar letters differ, $p < 0.05$. (c) Changes of the abundance of *Lactobacillus* genus in different groups. Groups with dissimilar letters differ, $p < 0.05$.

level in the later stage, this may be related to the protective effect of *S. mutans* on *C. albicans* [33, 34]. The colonization of *Lactobacillus* is also the key to its function. From Figure 2(c), it can be seen that the colonization of CCFM8724 was a fluctuating process, which may be the result of competitive adherence with pathogenic bacteria in the mouth [35]. Meanwhile, *Lactobacillus* could maintain a healthy oral environment by producing antimicrobial substances including organic acids, hydrogen peroxide, bacteriolytic enzymes, bacteriocins, and biosurfactants to inhibit the growth of patho-

genic bacteria [36, 37]. However, the oral cavity is a nutrient fluctuating environment, whether CCFM8724 could maintain the balance of the oral environment for a longer time should be investigated further.

The oral microbiome analysis of the rats in different tested groups was a novel aspect to supplementarily certificate the CFU counting results. The genus level composition of all groups seemed no notable differences, and the major genus detected throughout the study were *Enterobacteriaceae*, *Aggregatibacter*, *Streptococcus*, and *Lactobacillus* as

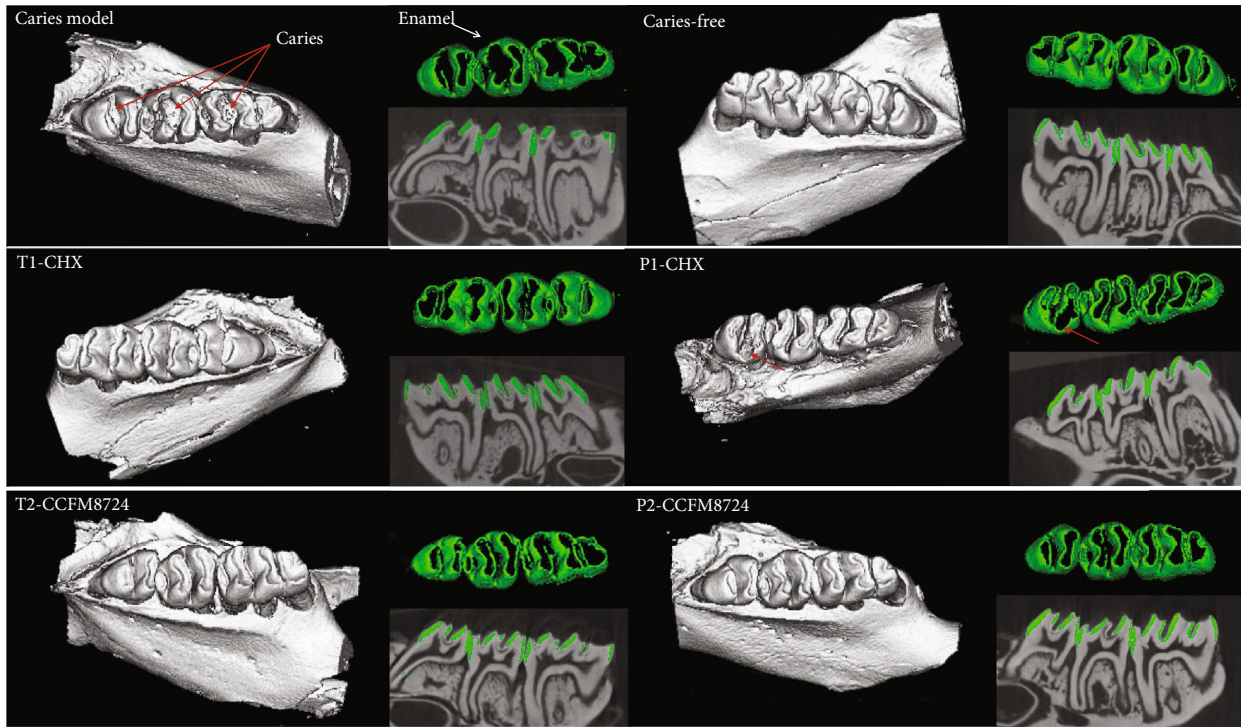


FIGURE 4: 3D micro-CT image of mandibular molars, separated enamel (green), and corresponding 2D scale sagittal slice of the same molar (enamel is green) in each group. Red arrows: caries lesion site.

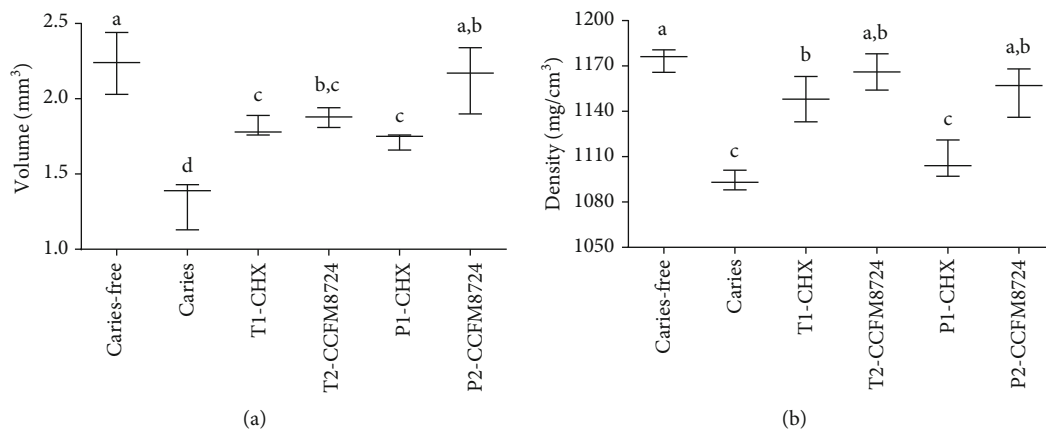


FIGURE 5: (a) Volume of enamel of mandibular molars. (b) MD of enamel of mandibular molars. Groups with dissimilar letters differ, $p < 0.05$.

TABLE 1: Effect of different groups on caries development (incidence and severity) in rats.

Group	Total E	Smooth surface Severity		Total E	Sulcal surface Severity	
		Ds	Dm		Ds	Dm
Caries model	13.2 ± 5.2	8.3 ± 0.8	5.7 ± 0.5	23.7 ± 5.2	18.8 ± 4.1	9.3 ± 2.4
T1-CHX	8.6 ± 2.6*	5.0 ± 1.1*	2.1 ± 0.6*	21.3 ± 6.8*	12.9 ± 3.5*	7.1 ± 1.4
T2-CCFM8724	6.6 ± 3.8*	4.7 ± 1.1*	2.0 ± 1.4*	19.6 ± 4.0*	6.6 ± 2.7*	2.4 ± 0.8*
P1-CHX	7.9 ± 5.6*	6.5 ± 2.8	4.5 ± 2.1	21.8 ± 6.2	16.3 ± 4.9	6.9 ± 1.9
P2-CCFM8724	6.5 ± 2.4*	1.9 ± 0.1*	—	15.4 ± 7.3*	3.1 ± 3.0*	—

Data are expressed as mean ± standard error of the mean ($n = 8$). E: enamel caries; Ds: dentin exposed; Dm: 3/4 of the dentin affected. * $p < 0.05$ when compared with the caries model group.

displayed in Figure 3(a). Meanwhile, the relative abundance of *S. mutans* in the caries model (22.5%) is in agreement to a recent report by Garcia et al. [38], in which the caries model was established by *S. mutans* alone. The diversity of oral microbiota in the caries model seemed to decrease, which may be attributed to the colonization of *Candida*. Haukioja et al. also found that increased *Candida* was related to reduced diversity of salivary microbiota [39]. Furthermore, the relative abundance of the *Lactobacillus* and *Streptococcus* in T2 and P2 (Figure 3(b)) groups was negatively correlated, which was consistent with the counting results in Figure 2. Intriguingly, *Aggregatibacter actinomycetemcomitans* has been reported to produce a signaling molecule called autoinducer-2 (AI-2) which could regulate the *C. albicans* biofilm formation [40]. Combined with the relative abundance changes of *Aggregatibacter* in the model group and other test groups, there may be a negative correlation between *Aggregatibacter* and *C. albicans*. More explorations should be taken to demonstrate this in further study. After all, *C. albicans* can affect the composition of bacteria in the oral cavity and its status in the oral ecosystem is no longer neglectable [41]. However, the microbiome of oral fungi in caries model needs to be further explored by gene sequencing.

Microtomography (micro-CT) is a modified version of medical computed tomography, which can capture images from multiple angles and produce nondestructive visualization of dental structures in three dimensions [42]. As a tool to provide high-resolution images as well as both qualitative and quantitative analyses of the tooth, microtomography is the gold standard for caries detection and evaluation in vitro, which gained increasing popularity in use for dental research [43]. Hence, micro-CT has been recommended as a reliable method to evaluate the volume and MD of dental hard tissue, especially to focus on the density of the hard tissues [42, 44]. It is well known that caries occur with demineralization of hard tissues, and enamel is the initial site of dental caries. Therefore, the enamel which separated from the dentin is often used to analyze the caries severity in most studies [45–47]. In this study, the enamel volume and MD of one side of the mandible were calculated. The larger the volume of the residual enamel indicated the stronger the anticaries effect of the tested group. And the higher MD value proved the less loss of minerals or the stronger remineralization effect. And the result showed that the enamel caries severity increased in the order of P2, T2, T1, and P1, which provided evidence of the notable effect of *Lactobacillus*, while little effect of CHX prevention.

Despite these considerable advantages of micro-CT, the high cost and long scanning time are the disadvantages. Therefore, the Keyes scoring method is still widely used for analyzing the primary caries in animal models along with the supplementary testimony of micro-CT. Klinka et al. [22] revealed that the combination of *S. mutans* and *C. albicans* could lead to more serious pit and fissure caries than smooth caries, which is similar to the results of the model group (Table 1). No significant difference of smooth surface caries was observed in caries scores or images among four tested groups. What really widened the score gap was the

relief of pit and fissure caries. Except that the CHX intervention group had no significant effect on occlusal caries, other groups showed a notable effect on smooth and fissure caries. The lowest total score (level E) was the CCFM8724 prevention group, which indicated that *Lactobacillus* exhibited better anticaries effect when colonized firstly in the oral cavity than later treatment. Probiotics can be promising candidates for novel anticariogenic substances owing to their essential ability of oral colonization and competition with oral pathogens for adhesion sites [35, 48].

In this study, both CCFM8724 treatment and prevention significantly attenuated the growth of *S. mutans* and *C. albicans* in the rat oral cavity, while CCFM8724 showed potential ability to colonize the oral cavity which is also the key to its function. In addition, the significant difference of caries lesions between the model group and lactobacillus-associated groups were verified via micro-CT and Keyes scoring method, demonstrating the anticaries properties of CCFM8724 *in vivo*. Further confirmation by clinical studies, would confirm the oral probiotic nature of CCFM8724 in alleviating dually infected caries.

Data Availability

Data used to support the findings of this study are available from the corresponding author upon request.

Conflicts of Interest

The authors declare no conflict of interests.

Authors' Contributions

Qiuxiang Zhang contributed to the conception, design, and data analysis of the study and critically revised the manuscript. Sujia Qin contributed to the conception, design, data acquisition, analysis, and interpretation of the study and drafted and critically revised the manuscript. Xianyin Xu contributed to the study conception and critically revised the manuscript. Jianxin Zhao contributed to the study conception and critically revised the manuscript. Hao Zhang contributed to the study conception and critically revised the manuscript. Zhenmin Liu contributed to the study conception and critically revised the manuscript. Wei Chen contributed to the study conception and critically revised the manuscript. All authors gave their final approval and agree to be accountable for all aspects of the work.

Acknowledgments

This work was supported by the National Key R&D Program of China (2017YFD0400600), the National Natural Science Foundation of China (Nos. 31820103010, 31530056), National First-class Discipline Program of Food Science and Technology (JUFSTR20180102), and Collaborative innovation center of food safety and quality control in Jiangsu Province.

References

- [1] N. B. Pitts, D. T. Zero, P. D. Marsh et al., “Dental caries,” *Nature Reviews Disease Primers*, vol. 3, no. 1, article 17030, 2017.
- [2] S. Anil and P. S. Anand, “Early childhood caries: prevalence, risk factors, and prevention,” *Frontiers in Pediatrics*, vol. 5, p. 157, 2017.
- [3] K. Chen, S. Gao, D. Duangthip, E. Lo, and C. Chu, “Managing early childhood caries for young children in China,” *Healthcare*, vol. 6, no. 1, p. 11, 2018.
- [4] A. Simón-Soro and A. Mira, “Solving the etiology of dental caries,” *Trends in Microbiology*, vol. 23, no. 2, pp. 76–82, 2015.
- [5] M. I. Klein, M. L. Falsetta, J. Xiao, W. H. Bowen, and H. Koo, *The Role of Extracellular Polysaccharides Matrix in Virulent Oral Biofilms*, Caister Academic Press, Norfolk, UK, 2013.
- [6] M. Raja, A. Hannan, and K. Ali, “Association of oral candidal carriage with dental caries in children,” *Caries Research*, vol. 44, p. 272, 2010.
- [7] X. Q. Yang, Q. Zhang, L. Y. Lu, R. Yang, Y. Liu, and J. Zou, “Genotypic distribution of *Candida albicans* in dental biofilm of Chinese children associated with severe early childhood caries,” *Archives of Oral Biology*, vol. 57, pp. 1048–1053, 2012.
- [8] S. Gregoire, J. Xiao, B. Silva et al., “Role of glucosyltransferase B in interactions of *Candida albicans* with *Streptococcus mutans* and with an experimental pellicle on hydroxyapatite surfaces,” *Applied and Environmental Microbiology*, vol. 77, pp. 6357–6367, 2011.
- [9] M. L. Falsetta, M. I. Klein, P. M. Colonne et al., “Symbiotic relationship between *Streptococcus mutans* and *Candida albicans* synergizes virulence of plaque biofilms in vivo,” *Infection and Immunity*, vol. 82, pp. 1968–1981, 2014.
- [10] B. Shino, F. C. Peedikayil, S. R. Jaiprakash, G. Ahmed Bijapur, S. Kottayi, and D. Jose, “Comparison of antimicrobial activity of chlorhexidine, coconut oil, probiotics, and ketoconazole on *Candida albicans* isolated in children with early childhood caries: an in vitro study,” *Scientifica*, vol. 2016, 5 pages, 2016.
- [11] N. Philip, B. Suneja, and L. J. Walsh, “Ecological approaches to dental caries prevention: paradigm shift or shibboleth?,” *Caries Research*, vol. 52, pp. 153–165, 2018.
- [12] S. Jun, Z. Zhi-Xiang, and M. Ai-Ping, “Effect of probiotics on inducing remission and maintaining therapy in ulcerative colitis, Crohn’s disease, and pouchitis: meta-analysis of randomized controlled trials,” *Inflammatory Bowel Diseases*, vol. 20, pp. 21–35, 2014.
- [13] S. Pooneh, N. Shekoufeh, and A. Mohammad, “A meta-analysis and systematic review on the effect of probiotics in acute diarrhea,” *Inflammation & Allergy - Drug Targets*, vol. 11, no. 1, pp. 3–14, 2012.
- [14] D. Gruner, S. Paris, and F. Schwendicke, “Probiotics for managing caries and periodontitis: systematic review and meta-analysis,” *Journal of Dentistry*, vol. 48, pp. 16–25, 2016.
- [15] A. Marigo, C. Marega, R. Zannetti, G. Morini, and G. Ferrara, “Oral administration of *Lactobacillus reuteri* during the first year of life reduces caries prevalence in the primary dentition at 9 years of age,” *Caries Research*, vol. 48, pp. 111–117, 2014.
- [16] L. Näse, K. Hatakka, E. Savilahti et al., “Effect of long-term consumption of a probiotic bacterium, *Lactobacillus rhamnosus* GG, in milk on dental caries and caries risk in children,” *Caries Research*, vol. 35, pp. 412–420, 2001.
- [17] N. Pahumunto, S. Piwat, O. Chankanka, N. Akkarachaneeyakorn, K. Rangitsathian, and R. Teanpaisan, “Reducing mutans streptococci and caries development by *Lactobacillus paracasei* SD1 in preschool children: a randomized placebo-controlled trial,” *Acta Odontologica Scandinavica*, vol. 1, 2018.
- [18] Q. Sujia, X. Wanqing, Z. Qiuxiang, Z. Jianxin, Z. Hao, and C. Wei, “Inhibitory effect of *Lactobacillus plantarum* CCFM8724 on caries-causing dual biofilms,” *Food and Fermentation Industries*, vol. 46, pp. 127–132, 2020.
- [19] S. Beiraghi, S. Rosen, and F. Beck, “The effect of stannous and sodium fluoride on coronal caries, root caries and bone loss in rice rats,” *Archives of Oral Biology*, vol. 35, pp. 79–80, 1990.
- [20] R. Wang, P. Zhao, B. Zhu, and J. Li, “Inhibitive effect of extracts of *Galla chinensis* on caries development in rats,” *Sichuan da xue xue bao Yi xue ban= Journal of Sichuan University Medical Science Edition*, vol. 39, pp. 474–477, 2008.
- [21] C. C. C. Quishida, E. G. D. O. Mima, J. H. Jorge, C. E. Vergani, V. S. Bagnato, and A. C. Pavarina, “Photodynamic inactivation of a multispecies biofilm using curcumin and LED light,” *Lasers in Medical Science*, vol. 31, pp. 997–1009, 2016.
- [22] T. Klinke, B. Guggenheim, W. Klimm, and T. Thurnheer, “Dental caries in rats associated with *Candida albicans*,” *Caries Research*, vol. 45, pp. 100–106, 2011.
- [23] R. Montella, P. Malfa, A. Giuliano, G. Brustia, J. D. Coisson, and M. Arlorio, “Vaginal adhesion of *Lactobacillus plantarum* P17630 after probiotic food supplement oral administration: a preliminary in vivo study,” *Nutrafoods*, vol. 12, pp. 35–42, 2013.
- [24] L. Wang, M. Pan, D. Li et al., “Metagenomic insights into the effects of oligosaccharides on the microbial composition of cecal contents in constipated mice,” *Journal of Functional Foods*, vol. 38, pp. 486–496, 2017.
- [25] W. H. Bowen, “Rodent model in caries research,” *Odontology*, vol. 101, pp. 9–14, 2013.
- [26] G. Stookey, J. Warrick, L. Miller, and A. Greene, “Animal caries models for evaluating fluoride dentifrices,” *Advances in Dental Research*, vol. 9, pp. 198–207, 1995.
- [27] H. P. Keyes, “Dental caries in the molar teeth of rats: II. A method for diagnosing and scoring several types of lesions simultaneously,” *Journal of Dental Research*, vol. 37, p. 1088, 1958.
- [28] K. C. S. Gasque, B. L. Foster, P. Kuss et al., “Improvement of the skeletal and dental hypophosphatasia phenotype in *Alpl*? mice by administration of soluble (non-targeted) chimeric alkaline phosphatase,” *Bone*, vol. 72, pp. 137–147, 2015.
- [29] W. Krzyściak, D. Kościelniak, M. Papież et al., “Effect of a *Lactobacillus salivarius* probiotic on a double-species *Streptococcus mutans* and *Candida albicans* caries biofilm,” *Nutrients*, vol. 9, p. 1242, 2017.
- [30] I. Stamatova and J. H. Meurman, “Probiotics: health benefits in the mouth,” *American Journal of Dentistry*, vol. 22, pp. 329–338, 2009.
- [31] N. Pahumunto, B. Sophatha, S. Piwat, and R. Teanpaisan, “Increasing salivary IgA and reducing *Streptococcus mutans* by probiotic *Lactobacillus paracasei* SD1: a double-blind, randomized, controlled study,” *Journal of Dental Sciences*, vol. 14, 2019.
- [32] K. H. Ishikawa, M. P. Mayer, T. Y. Miyazima et al., “A multispecies probiotic reduces oral *Candida* colonization in denture wearers,” *Journal of Prosthodontics*, vol. 24, pp. 194–199, 2015.

- [33] D. S. A. V. Barbieri, V. A. Vicente, F. C. Fraiz, O. J. Lavoranti, T. I. E. Svidzinski, and R. L. Pinheiro, "Analysis of the in vitro adherence of *Streptococcus mutans* and *Candida albicans*," *Brazilian Journal of Microbiology*, vol. 38, pp. 624–631, 2007.
- [34] D. K. Morales and D. A. Hogan, "Candida albicans interactions with bacteria in the context of human health and disease," *PLoS Pathogens*, vol. 6, article e1000886, 2010.
- [35] T.-H. Lin, C.-H. Lin, and T.-M. Pan, "The implication of probiotics in the prevention of dental caries," *Applied Microbiology and Biotechnology*, vol. 102, pp. 577–586, 2018.
- [36] T. A. Oelschlaeger, "Mechanisms of probiotic actions—a review," *International Journal of Medical Microbiology*, vol. 300, pp. 57–62, 2010.
- [37] P. Wannun, S. Piwat, and R. Teanpaisan, "Purification, characterization, and optimum conditions of fermencin SD11, a bacteriocin produced by human orally *Lactobacillus fermentum* SD11," *Applied Biochemistry and Biotechnology*, vol. 179, pp. 572–582, 2016.
- [38] S. S. Garcia, M. S. Blackledge, S. Michalek et al., "Targeting of *Streptococcus mutans* biofilms by a novel small molecule prevents dental caries and preserves the oral microbiome," *Journal of Dental Research*, vol. 96, pp. 807–814, 2017.
- [39] A. Haukioja, V. Loimaranta, and J. Tenovuo, "Probiotic bacteria affect the composition of salivary pellicle and streptococcal adhesion in vitro," *Oral Microbiology and Immunology*, vol. 23, pp. 336–343, 2008.
- [40] E. W. Bachtiar, B. M. Bachtiar, L. M. Jarosz et al., "AI-2 of *Aggregatibacter actinomycetemcomitans* inhibits *Candida albicans* biofilm formation," *Frontiers in Cellular and Infection Microbiology*, vol. 4, p. 94, 2014.
- [41] M. Janus, W. Crielaard, C. Volgenant, M. Van der Veen, B. Brandt, and B. Krom, "Candida albicans alters the bacterial microbiome of early in vitro oral biofilms," *Journal of Oral Microbiology*, vol. 9, article 1270613, 2017.
- [42] M. V. Swain and X. Jing, "State of the art of micro-CT applications in dental research," *International Journal of Oral Science*, vol. 1, pp. 177–188, 2009.
- [43] E. C. M. Lo, Q. H. Zhi, and A. Itthagarun, "Comparing two quantitative methods for studying remineralization of artificial caries," *Journal of Dentistry*, vol. 38, pp. 352–359, 2010.
- [44] G. Dong, Q. Dong, Y. Liu et al., "High-resolution micro-CT scanning as an innovative tool for evaluating dental hard tissue development," *Journal of Applied Clinical Medical Physics*, vol. 15, pp. 335–344, 2014.
- [45] Y. Chih-Ko, S. E. Harris, M. Sumathy et al., "Hyperglycemia and xerostomia are key determinants of tooth decay in type 1 diabetic mice," *Laboratory Investigation*, vol. 92, p. 868, 2012.
- [46] D. G. Gantt, J. Kappleman, R. A. Ketcham, M. E. Alder, and T. H. Deahl, "Three-dimensional reconstruction of enamel thickness and volume in humans and hominoids," *European Journal of Oral Sciences*, vol. 114, pp. 360–364, 2006.
- [47] T. T. Zhang, H. J. Guo, X. J. Liu, J. P. Chu, and X. D. Zhou, "Galla chinensis compounds remineralize enamel caries lesions in a rat model," *Caries Research*, vol. 50, pp. 159–165, 2016.
- [48] A. Haukioja, "Probiotics and oral health," *European Journal of Dentistry*, vol. 4, p. 348, 2010.

Research Article

The Associated Regulatory Mechanisms of Zinc Lactate in Redox Balance and Mitochondrial Function of Intestinal Porcine Epithelial Cells

Wenjie Tang,^{1,2,3} Jing Long,¹ Tiejun Li,⁴ Lingyuan Yang,³ Jianzhong Li ¹, Liuqin He ^{1,4},
Shuwei Li,² Shengyao Kuang ², Yanzhong Feng,⁵ Heshu Chen,⁵ Fenglan Li,⁶ Zhiliang Du,⁷
and Yulong Yin ^{3,4}

¹Hunan Provincial Key Laboratory of Animal Intestinal Function and Regulation, College of Life Sciences, Hunan Normal University, Changsha 410081, China

²Sichuan Academy of Animal Sciences, Animal Breeding and Genetics key Laboratory of Sichuan Province, Chengdu 610066, China

³College of Animal Science and Technology, Hunan Agricultural University, Changsha, Hunan 410128, China

⁴CAS Key Laboratory of Agro-ecological Processes in Subtropical Region, Institute of Subtropical Agriculture, Hunan Provincial Key Laboratory of Animal Nutritional Physiology and Metabolic Process, National Engineering Laboratory for Pollution Control and Waste Utilization in Livestock and Poultry Production, Changsha 410125, China

⁵Heilongjiang Academy of Agricultural Sciences, Harbin 150086, China

⁶College of Life Sciences, Northeast Agricultural University, Harbin 150030, China

⁷Cloud Computing Center, Chinese Academy of Sciences, Dongguan 523808, China

Correspondence should be addressed to Jianzhong Li; ljzhong@hunnu.edu.cn, Liuqin He; 285687180@qq.com, Shengyao Kuang; ksy_cd@163.com, and Yulong Yin; yinyulong@isa.ac.cn

Received 16 August 2020; Revised 18 September 2020; Accepted 30 November 2020; Published 18 December 2020

Academic Editor: Ana Cipak Gasparovic

Copyright © 2020 Wenjie Tang et al. This is an open access article distributed under the Creative Commons Attribution License, which permits unrestricted use, distribution, and reproduction in any medium, provided the original work is properly cited.

Zinc lactate (ZnLA) is a new organic zinc salt which has antioxidant properties in mammals and can improve intestinal function. This study explored the effects of ZnLA and ZnSO₄ on cell proliferation, Zn transport, antioxidant capacity, mitochondrial function, and their underlying molecular mechanisms in intestinal porcine epithelial cells (IPEC-J2). The results showed that addition of ZnLA promoted cell proliferation, inhibited cell apoptosis and IL-6 secretion, and upregulated the mRNA expression and concentration of MT-2B, ZNT-1, and CRIP, as well as affected the gene expression and activity of oxidation or antioxidant enzymes (e.g., CuZnSOD, CAT, and Gpx1, GSH-PX, LDH, and MDA), compared to ZnSO₄ or control. Compared with the control, ZnLA treatment had no significant effect on mitochondrial membrane potential, whereas it markedly increased the mitochondrial basal OCR, nonmitochondrial respiratory capacity, and mitochondrial proton leakage and reduced spare respiratory capacity and mitochondrial reactive oxygen (ROS) production in IPEC-J2 cells. Furthermore, ZnLA treatment increased the protein expression of Nrf2 and phosphorylated AMPK, but reduced Keap1 and p62 protein expression and autophagy-related genes LC3B-1 and Beclin mRNA abundance. Under H₂O₂-induced oxidative stress conditions, ZnLA supplementation markedly reduced cell apoptosis and mitochondrial ROS levels in IPEC-J2 cells. Moreover, ZnLA administration increased the protein expression of Nrf2 and decreased the protein expression of caspase-3, Keap1, and p62 in H₂O₂-induced IPEC-J2 cells. In addition, when the activity of AMPK was inhibited by Compound C, ZnLA supplementation did not increase the protein expression of nuclear Nrf2, but when Compound C was removed, the activities of AMPK and Nrf2 were both increased by ZnLA treatment. Our results indicated that ZnLA could improve the antioxidant capacity and mitochondrial function in IPEC-J2 cells by activating the AMPK-Nrf2-p62 pathway under normal or oxidative stress conditions. Our novel finding also suggested that ZnLA, as a new feed additive for piglets, has the potential to be an alternative for ZnSO₄.

1. Introduction

Zinc (Zn), one of the most important trace elements in mammals, has been reported to reduce the incidence of diarrhea and improve the structure and function of the intestinal barrier in postweaning piglets [1–4]. Extracellular and intracellular Zn²⁺ in mammalian cells play a key role in physiological or pathological processes, including growth, immunity, and nutrient metabolism [5]. Previous reports have confirmed that Zn deficiency in animals led to a decrease in the number of T cells [6], oxidative stress, intestinal dysfunction, and inflammatory cell infiltration [4, 7, 8]. Traditionally, inorganic Zn (oxides and sulfates) has served as a feed additive to promote growth performance in livestock. To date, Zn additives in the market are in various types, such as zinc oxide, zinc sulfate, and nanozinc, all of which have a benefit in Zn absorption and combating diarrhea [9–13]. However, the excessive use and low absorption efficiency of inorganic Zn in livestock and poultry breeding resulted in the deposition of heavy metals in animal products and the high production of excrement, which inevitably caused concerns in meat safety and environmental pollution [14, 15].

Zinc lactate (ZnLA) is chemically synthesized from feed-grade zinc oxide and DL-lactic acid and can easily bind with ligands or metal carriers in enterocytes, which plays a key role in antioxidant function and immune response in animals. Previous studies have reported that the relative bioavailability of ZnLA in animal production is higher than that of inorganic Zn and can improve the growth performance of animals [16]. For example, the addition of ZnLA to animal feed improved the utilization of serum free amino acids and meat quality (e.g., average shell strength and shell thickness) and reduced the shell-breaking rate in chickens [17, 18]. Dietary ZnLA supplementation could also increase the birth weight and weaning survival rate in rabbits, as well as enhance fur elasticity and brightness [19]. Recent reports have indicated that organic Zn in pigs is more helpful in adjusting the adaptive response to piglets' oxidative stress compared with inorganic Zn [20]. However, the effect mechanisms of ZnLA on the antioxidant and anti-inflammatory ability in pigs have not been well-studied.

It is known that nuclear factor erythroid 2-related factor 2 (Nrf2), a principal key transcription factor, has been considered as the main stress regulator that activates the antioxidant system. Upon exposure to various stressors, the release of Nrf2 from Kelch-like ECH-associated protein 1 (Keap1) translocates into the nucleus, resulting in the expression of various cytoprotective genes [21]. Recent studies have reported that Nrf2 could be activated by AMP-activated protein kinase (AMPK) and modulate autophagy-related genes (e.g., p62, Beclin, and LC3B-1/2) to participate in the alleviation of oxidative stress in mammalian cells [22]. Autophagy-related protein p62 can inhibit Nrf2 degradation and promote Nrf2 stability and nuclear translocation by interfering with Keap1-Nrf2 interaction to participate in the cellular antioxidative stress response [23]. However, whether ZnLA could protect against oxidative stress by modulating AMPK-Nrf2 activation and autophagy signals is still poorly understood. Moreover, mitochondria are the main energy source of cells, where they play an important role in cell pro-

cesses such as apoptosis, reactive oxygen species (ROS) generation, cell cycle, and thermogenesis. Oxidative damage leads to ROS production and mitochondrial dysfunction [24]. A previous study showed that the combination of Zn and selenium improved mitochondrial function and alleviated oxidative stress caused by Alzheimer's disease [24]. Therefore, the purpose of this study was to compare the effects of ZnLA and ZnSO₄ on cell proliferation and autophagy, Zn transport, antioxidant capacity, and mitochondrial function in intestinal porcine epithelial cells (IPEC-J2) and to reveal the associated regulatory mechanism of ZnLA in H₂O₂-induced oxidative stress in IPEC-J2 cells.

2. Materials and Methods

2.1. Cell Culture. The IPEC-J2 cells derived from the jejunal epithelia of the neonatal piglets were used in all studies to assess the related mechanisms *in vitro*. IPEC-J2 cells were grown in uncoated plastic culture flasks in Dulbecco's Modified Eagle Medium (DMEM), 10% fetal calf serum (FBS; Hyclone, UT, USA), 5 mM L-glutamine, and 1% antibiotics (100 U/mL penicillin and 100 U/mL streptomycin) and cultured at 37°C with 5% CO₂. The media was changed every two days, and the pH of all cell culture media was maintained at 7.4. The cells covered the bottom of the culture bottle and were trypsinized into a six-well plate and cultured at 37°C with 5% CO₂. When cells were grown to 70–80% confluence, the cells were cultured in treatment mediums. The cells were then collected to determine the relevant indicators.

2.2. Cell Viability Assays. IPEC-J2 cells were seeded in a 96-well plate at a density of 8×10^3 cells/well and grown to 80% confluence. Cells were treated with DMEM containing ZnLA (99%; Sichuan Zoology Feed Co. Ltd.) and ZnSO₄ with final Zn concentrations of 0, 0.1, 0.5, 1, 2.5, 5, 7.5, 10, 15, and 20 mg/L. After incubation for 6, 12, 24, 36, 48, and 60 h, cell viability was evaluated by cell counting kits (CKK-8) (Dojindo, Kumamoto, Japan) using a microplate reader at 450 nm according to the manufacturer's instructions.

2.3. Cell Treatment. At ~70–80% confluence, ZnLA or ZnSO₄ was added to fresh medium without FBS, which contained the same amount of Zn (7.5 mg/L). In order to eliminate the interference of lactic acid, equal amounts of lactic acid and Zn compared with the ZnLA group were used. To induce oxidative stress, 200 μM H₂O₂ (Sigma-Aldrich, MO, USA) was used as previously reported [25]. Compound C (5 μM) (Selleck, Shanghai, China), an AMPK inhibitor, was added to the medium to inhibit AMPK activity.

2.4. Intracellular Enzymes and Inflammatory Cytokines. Harvested cells were extracted total proteins; then, cellular malondialdehyde (MDA), superoxide dismutase (SOD), lactic dehydrogenase (LDH), glutathione peroxidase (GSH-PX), interleukin-6 (IL-6), tumor necrosis factor alpha (TNF-α), cysteine-rich intestinal protein 1 (CRIP1), cysteine-rich intestinal protein 2 (CRIP2), and metallothionein 1A (MT1A) activities or levels were determined using ELISA kits (Wuhan Huamei Biotechnology Co. LTD) in accordance with the manufacturer's protocols.

2.5. Cell Apoptosis Assay. Apoptosis analysis was performed with the Annexin V-FITC/PI (propidium iodide) flow cytometry kit. IPEC-J2 cells were seeded into 6-well plates at a density of 1×10^6 cells/well. After treatment, $5 \mu\text{L}$ Annexin V-FITC for 15 min and $5 \mu\text{L}$ PI for 5 min at room according to the manufacturer's instructions [26].

2.6. Cell Cycle Assay. Cell cycle progression was examined with a flow cytometer using propidium iodide (PI) staining. Briefly, IPEC-J2 cells were seeded into 6-well culture plates. After treatment, the cells were trypsinized and fixed with cold 70% ethanol at 4°C overnight. The cells were then rehydrated, washed twice with ice-cold PBS, and analyzed by PI staining. PI absorbance was determined by fluorescence-activated cell sorting on a flow cytometer (Beckman Coulter Inc., USA).

2.7. Mitochondrial ROS Measurement. Intracellular mitochondrial reactive oxygen (ROS) generation was evaluated using MitoSOX Red reagent (Invitrogen, Shanghai, China). IPEC-J2 cells were seeded into 6-well plates and then cultured in different treatments. Cells were treated with $5 \mu\text{M}$ MitoSOX Red reagent at 37°C for 10 min in the dark. Then, the fluorescence intensity of 12,000 cells was assayed using a Beckman MoFlo XDP flow cytometer (Beckman Coulter Inc., CA, USA).

2.8. Mitochondrial Membrane Potential (MMP) Measurement. Mitochondrial depolarization in the early stages of apoptosis was evaluated using JC-1 reagent (Invitrogen) by double fluorescence staining. The loss of MMP was indicated by a decrease in the red/green mean fluorescence intensity ratio. IPEC-J2 cells were seeded into confocal dishes and then treated under different conditions. JC-1 ($10 \mu\text{g}/\text{mL}$) was added to the medium for 30 min in the dark and then the cells were washed twice with PBS. Cells in the confocal dishes were treated with an anti-fluorescence quenching agent and observed using a Zeiss LSM880 confocal microscope as previously described [26].

2.9. Mitochondrial Respiration Metabolism Assays. Mitochondrial respiration was measured using the XF-24 Extracellular Flux Analyzer and a Cell Mito Stress Test Kit (Agilent Technologies, Inc., CA, USA) in accordance with the manufacturer's instructions. Non-ATP-linked oxygen consumption (proton leak), ATP-linked mitochondrial oxygen consumption (ATP production), and maximal respiration capacity were estimated. Baseline oxygen consumption rate (OCR) minus the maximal respiratory capacity represented the spare respiratory capacity. Residual oxygen consumption after the addition of rotenone and antimycin A was due to nonmitochondrial respiration and was subtracted from all measured values in the analysis. Total cellular protein concentration was determined with a BCA assay kit to normalize mitochondrial respiration rates [27].

2.10. Real-Time Quantitative Polymerase Chain Reaction. The expression of mRNA was measured by real-time quantitative PCR. Total RNA was extracted from samples of IPEC-J2 cells using TRIzol reagent (Invitrogen) and reverse transcribed into cDNA using the Prime Script RT reagent kit

(TaKaRa Bio, Otsu, Japan). Quantitative PCR was performed using SYBR Premix Ex Taq (TaKaRa Bio, Japan). The reaction was performed at a total volume of $10 \mu\text{L}$, with the assay solution containing $5 \mu\text{L}$ SYBR Green mix (TaKaRa Bio, Japan), $0.2 \mu\text{L}$ ROX internal reference dye, $3.4 \mu\text{L}$ deionized H_2O , $1 \mu\text{L}$ cDNA template, and $0.2 \mu\text{L}$ each of the forward and reverse primers. The expression of the housekeeping gene β -actin was used to normalize the expression levels. The primers were designed to flank introns using the Primer 5 software. The primer sequences are listed in the supplemental Table 1.

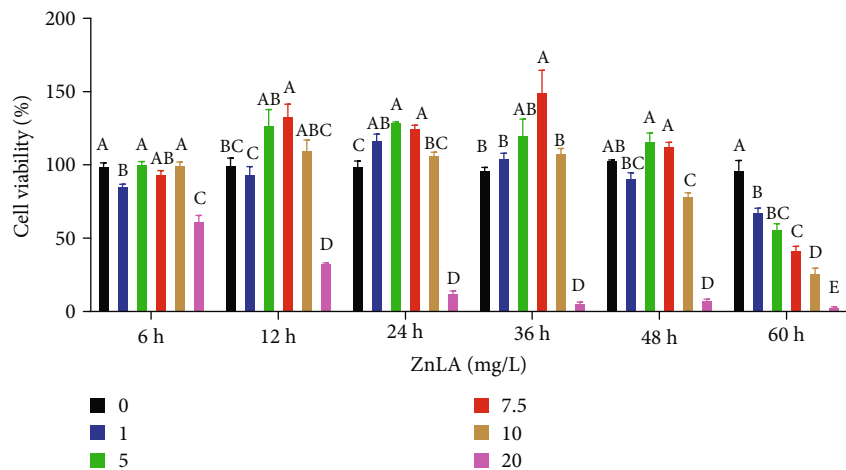
2.11. Protein Qualification by the Wes Simple Western System and Western Blot. The process of protein quantification was performed using the Wes Simple Western System (ProteinSimple, San Jose, CA, USA) or the Western Blot technique as previous described [25, 26]. The antibodies used in the study included nuclear factor erythroid 2-related factor 2 (Nrf2) (Abcam, Cambridge, MA, USA), β -actin (Abcam), Kelch-like ECH-associated protein 1 (Keap1) (Abcam), AMP-activated protein kinase (AMPK) (Abcam), phosphorylated AMPK (Abcam), lamin B (Abcam), and p62 (Abcam). The mouse β -actin antibody was used as a loading control for total protein, while nuclear Nrf2 protein expression was normalized to lamin B. All protein concentrations were determined using a standard BCA protein assay. Results of Wes Simple Western System were obtained using the "gel view" function of the Protein Simple software (ProteinSimple). Western blot data were quantified using the ImageJ software.

2.12. Immunofluorescence Assay. IPEC-J2 cells (1×10^5 cells per well) were seeded into confocal dishes and treated with different conditions. Cells were fixed with 4% paraformaldehyde for 20 min and permeabilized with Triton X-100 (0.3%) for 10 min. Then, cells were blocked with bovine serum albumin (1%) for 30 min and were incubated overnight with Nrf2, caspase-3, or Keap1 antibodies diluted at 1:100 at 4°C . Cells were washed with cold PBS three times, and then incubated with secondary antibody for 1 h. Nuclear DNA was labeled with 4',6-diamidino-2-phenylindole (DAPI) for 2 minutes. The fluorescence images were captured using a Zeiss LSM880 confocal microscope and analyzed with the ZEN software.

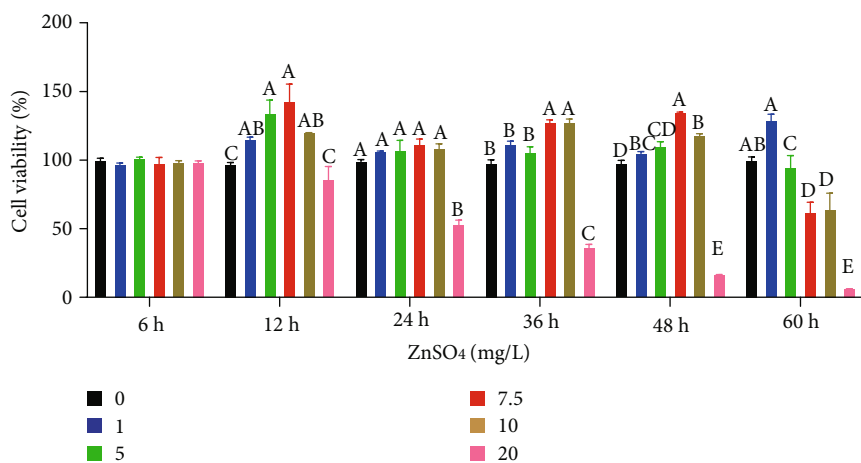
2.13. Statistical Analysis. Statistical analysis was analyzed through one-way ANOVA or *t*-test using the SPSS 19.0 software. All the data were presented as means \pm standard error of the mean (SEM). *P* values below 0.05 were considered statistically significant.

3. Results

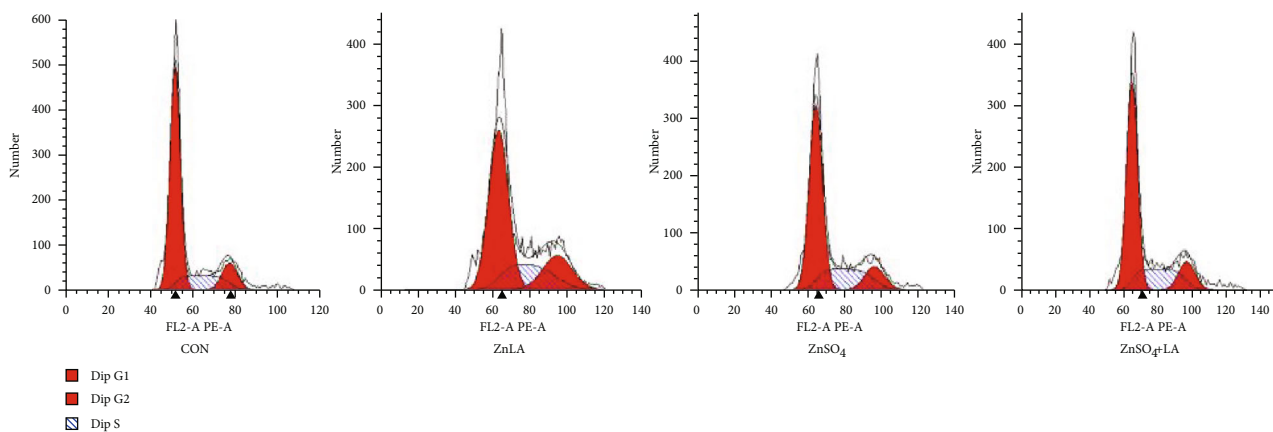
3.1. Effects of ZnLA Supplementation on Cell Viability, Cell Cycle, and Apoptosis. To determine the effects of different Zn sources on cell proliferation in IPEC-J2 cells, we exposed IPEC-J2 cells to increasing concentrations of ZnLA or ZnSO_4 for 6, 12, 24, 36, 48, or 60 h, respectively (Figures 1(a) and 1(b)). We found that exposure to 7.5 mg/L Zn for 12 h significantly increased cell viability compared with other treatments ($P < 0.05$). Thus, the concentrations of 7.5 mg/L Zn



(a)



(b)



(c)

FIGURE 1: Continued.

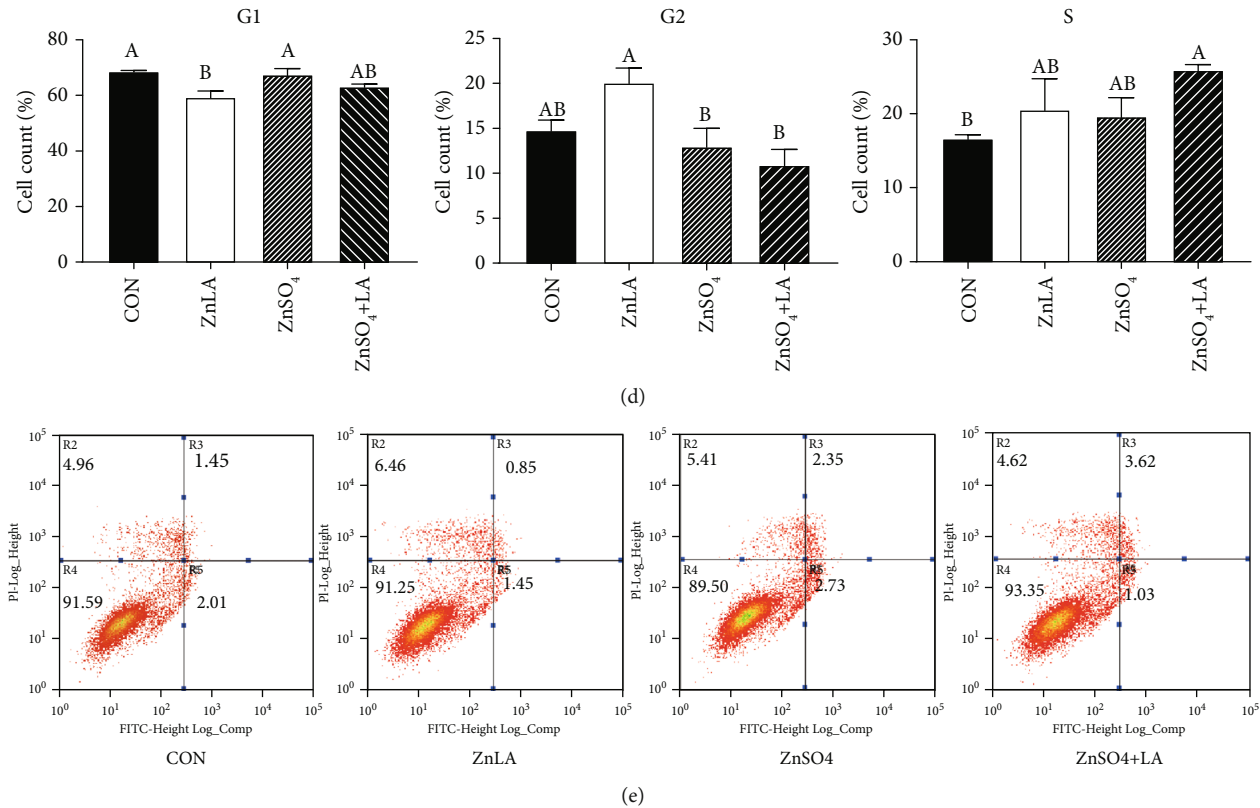


FIGURE 1: Effects of zinc lactate on cell viability, cell cycle, and apoptosis in IPEC-J2 cells. Values are expressed as means \pm SEM ($n = 4$). (a, b) Cell viability under different levels of Zn sources; (c, d) cell cycle in each phase; (e) cell apoptosis ratio. ^{a,b,c}Means of bars with different letters were significantly different ($P < 0.05$).

from ZnLA or ZnSO₄ for 12 h were selected as suitable conditions for the subsequent experiments. As shown in Figures 1(c) and 1(d), the G1 phase of the cell cycle was markedly decreased in the ZnLA group compared with the control group ($P < 0.05$). However, ZnLA administration was increased in the S phase ($P < 0.05$) and G2/M phase ($P < 0.05$). In addition, we found that the proportion of early and late apoptotic cells treated with ZnLA was the lowest compared to the other three groups (Figure 1(e)). These results suggested that ZnLA could reduce cell apoptosis and promote cell proliferation.

3.2. Effects of ZnLA Supplementation on Mitochondrial ROS, MMP, and Mitochondrial Respiration Metabolism. Our results showed that Zn treatment decreased the levels of mitochondrial ROS production ($P < 0.05$) but did not differ between the ZnLA and ZnSO₄ groups (Figures 2(a) and 2(b)). There was no difference in the ratio of JC-1 red fluorescence to green fluorescence ($P > 0.05$) (Figure 2(n)). Compared with the control group, ZnLA treatment remarkably increased the mitochondrial basal OCR, nonmitochondrial respiratory capacity, and proton leak ($P < 0.05$) (Figures 2(c)–2(i)). Compared with the ZnSO₄ group, ZnLA administration increased the mitochondrial basal OCR, nonmitochondrial respiratory capacity, and maximal respiration in IPEC-J2 cells ($P < 0.05$). ZnSO₄+LA administration increased the basal OCR rate, ATP production, and maximal respiration compared with the ZnSO₄ group ($P < 0.05$). As

for mitochondrial-related gene expression, ZnLA supplementation increased the mRNA expression of uncoupling protein 2 (UCP2) and pyruvate dehydrogenase A1 (PDHA1) (Figures 2(j) and 2(m)) compared with the control group, but the mRNA expression of mitochondrial transcription factor A (Tfam) and cytochrome c oxidase (Cycs) was not affected by ZnLA administration (Figures 2(k) and 2(l)). Meanwhile, ZnSO₄ treatment increased UCP2 mRNA abundance but did not affect the expression of Tfam, Cycs, and PDHA1.

3.3. Effects of ZnLA Supplementation on Antioxidant Function, Inflammation, and Zn Transport. For critical validation of the *in vitro* experiment demonstrating the effects of ZnLA on intestinal Zn transport, inflammation, and antioxidant function, we determined the levels or activities of intracellular antioxidant enzymes, inflammatory cytokines, and zinc transporter proteins (Figures 3(a)–3(i)). Compared with the control group, LDH activity was decreased with ZnLA or ZnSO₄ treatment ($P < 0.05$), and the activity of LDH in the ZnLA treatment was lower than that in ZnSO₄ treatment. Compared with the control group, ZnLA treatment significantly increased the activity of GSH-PX ($P < 0.05$), while decreasing the MDA concentration ($P > 0.05$). SOD activity in the ZnSO₄+LA group was the lowest ($P < 0.05$). Compared with the control group, the concentration of intracellular IL-6 in the other three treatments was significantly decreased ($P < 0.05$), but there was no difference in TNF- α concentration among these groups. ZnLA

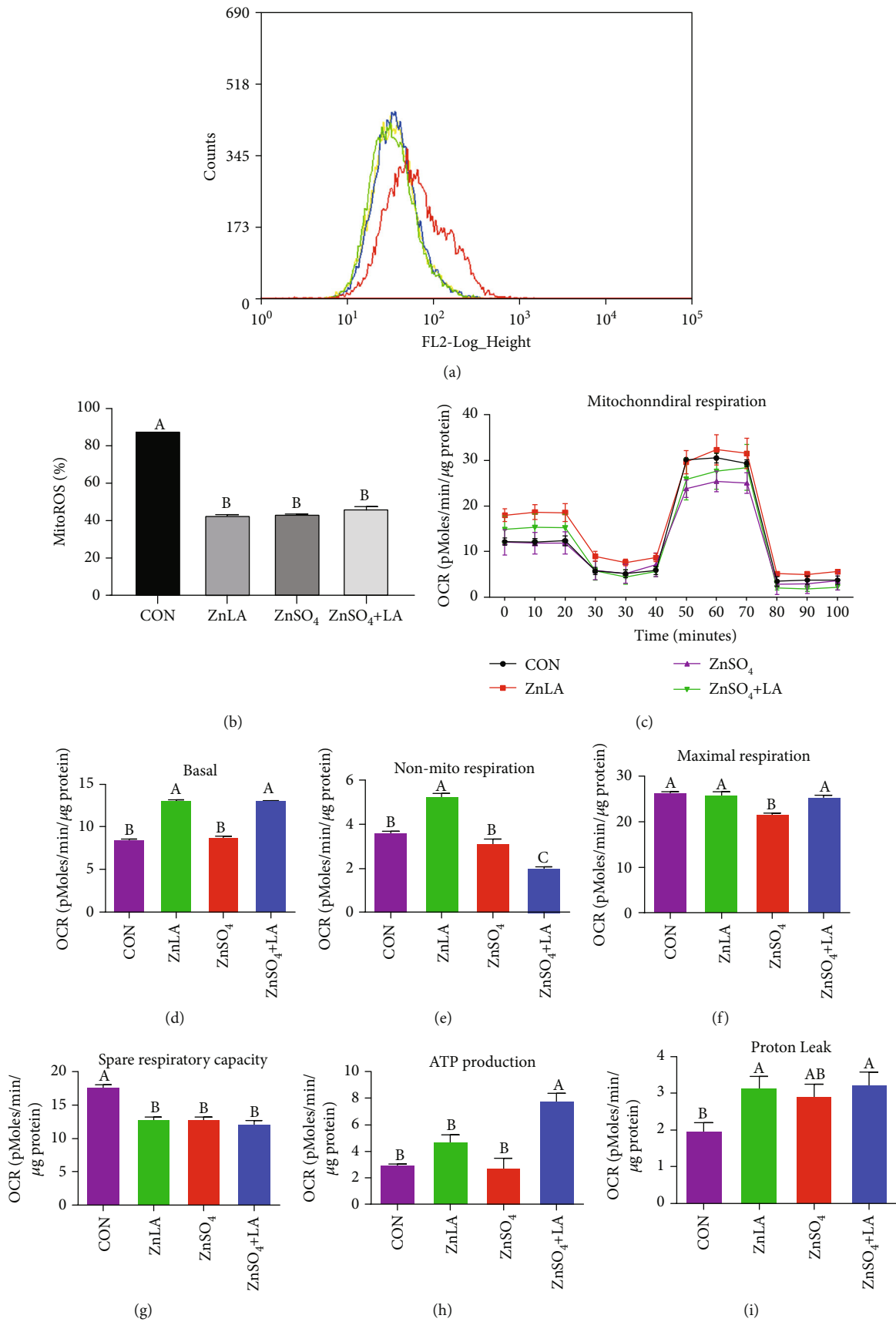


FIGURE 2: Continued.

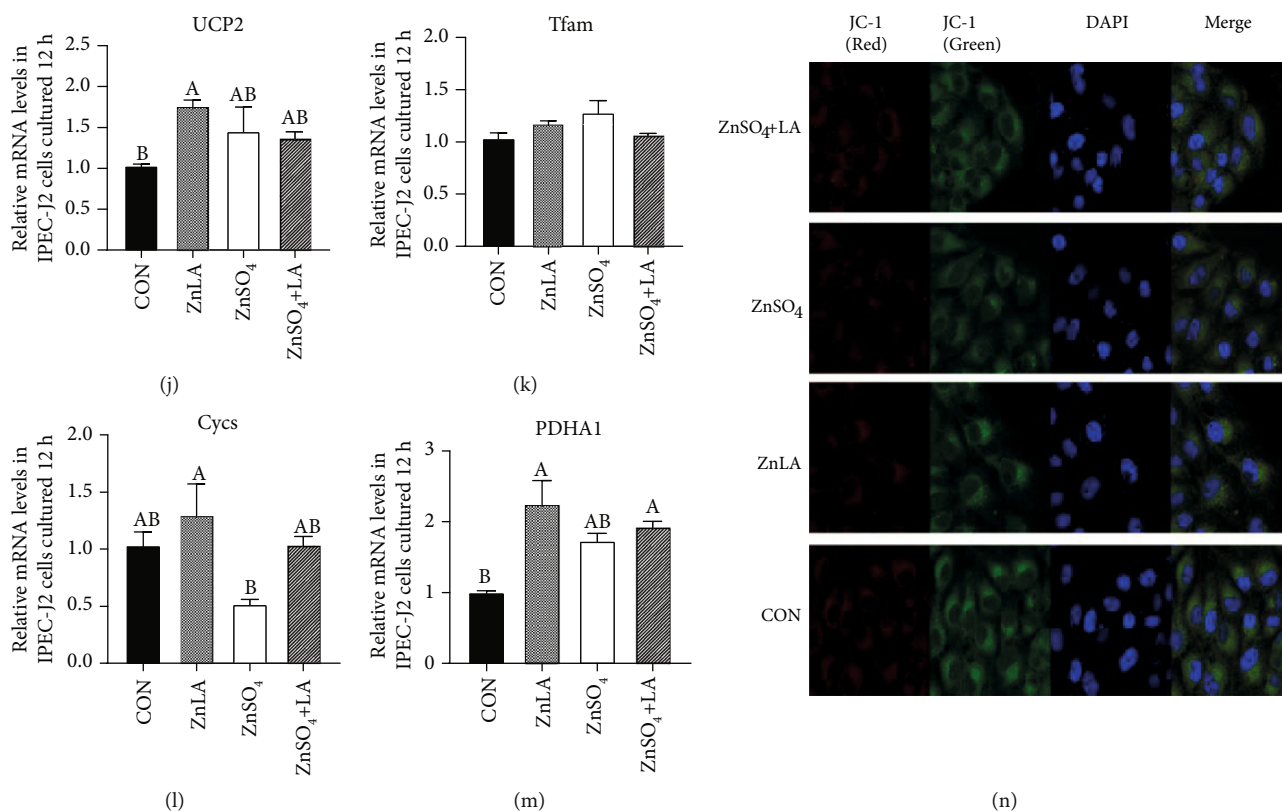


FIGURE 2: Effect of zinc lactate on mitochondrial ROS, mitochondrial membrane potential, and cellular respiration metabolism in IPEC-J2 cells. Values are expressed as means \pm SEM ($n = 4$). (a, b) Mitochondrial ROS level: red line, CON; green line, ZnLA; blue line, ZnSO₄; yellow line, ZnSO₄+LA; (c) oxygen consumption rate; (d) basal respiration; (e) non-mito respiratory; (f) maximal respiration; (g) spare respiratory; (h) ATP production; (i) proton leak; (j) the relative expression of UCP2; (k) the relative expression of Tfam; (l) the relative expression of Cysc; (m) the relative expression of PDHA1; (n) mitochondrial membrane potential: red, aggregate; green, monomer. ^{a,b,c}Means of bars with different letters were significantly different ($P < 0.05$).

supplementation increased the levels of Zn transporter proteins CRIP1 and CRIP2 ($P < 0.05$), but had no effect on MT1A levels compared with that in the CON group. Furthermore, we also determined the mRNA expression levels of Zn transporters and antioxidant-related genes (Figures 3(j)–3(q)). Compared with the control group, ZnLA or ZnSO₄ supplementation markedly increased the mRNA expression of ZNT-1 and MT-2B in IPEC-J2 cells ($P < 0.05$). The mRNA expression of CRIP2 and MT1A in the ZnSO₄ group was also increased in comparison with the other three groups ($P < 0.05$), while there was no difference in the expression of CRIP1 among the four groups. The mRNA expression levels of CAT and CuZnSOD in the ZnLA group were higher than those in the other groups, but there was no difference in the expression of Gpx1 among these groups.

3.4. Effects of ZnLA Supplementation on the Expression of Nrf2/Keap1, AMPK, and Autophagy-Related Pathways. To further validate whether ZnLA supplementation could alleviate oxidative stress in IPEC-J2 cells via Nrf2/Keap1, AMPK, and autophagy-related pathways, we determined the expression of the key target molecules using Western blotting and immunofluorescence techniques. We found that Nrf2 protein was mostly located in the cytoplasm of IPEC-J2 cells, but ZnLA administration could increase the amount of

Nrf2 transferred to the nucleus (Figures 4(a) and 4(c)). Compared with the control group, the expression of Keap1 was reduced by ZnLA treatment ($P < 0.05$). Furthermore, the protein expression of AMPK in ZnSO₄+LA group was highest ($P < 0.05$), and ZnLA treatment remarkably increased ($P < 0.05$) the protein expression of phosphorylated AMPK (Figures 4(c) and 4(d)). Compared with the ZnSO₄ group, the expression of p62 in the ZnLA group was decreased, but there was no significant difference (Figure 4(e)). Our results also showed that ZnLA treatment markedly reduced the mRNA expression of autophagy-related genes LC3B-1 and Beclin ($P < 0.05$), but it had no effect on the mRNA expression of p62 and LC3B-2 ($P > 0.05$) (Figure 4(f)).

3.5. Effects of ZnLA Supplementation on Mitochondrial ROS, Apoptosis, and the AMPK-Nrf2-p62-Mediated Pathway under Oxidative Stress Conditions. To further define the effect of ZnLA on the alleviation of oxidative stress in enterocytes, we built an oxidative stress model of H₂O₂-induced IPEC-J2 cells. The levels of mitochondrial ROS and apoptosis were determined in the presence or absence of 7.5 mg/L ZnLA. As shown in Figure 5(a), H₂O₂ exposure markedly increased cell apoptosis in IPEC-J2 cells, while ZnLA supplementation decreased the proportion of apoptotic cells (the proportion of early apoptotic cells and late apoptotic cells,

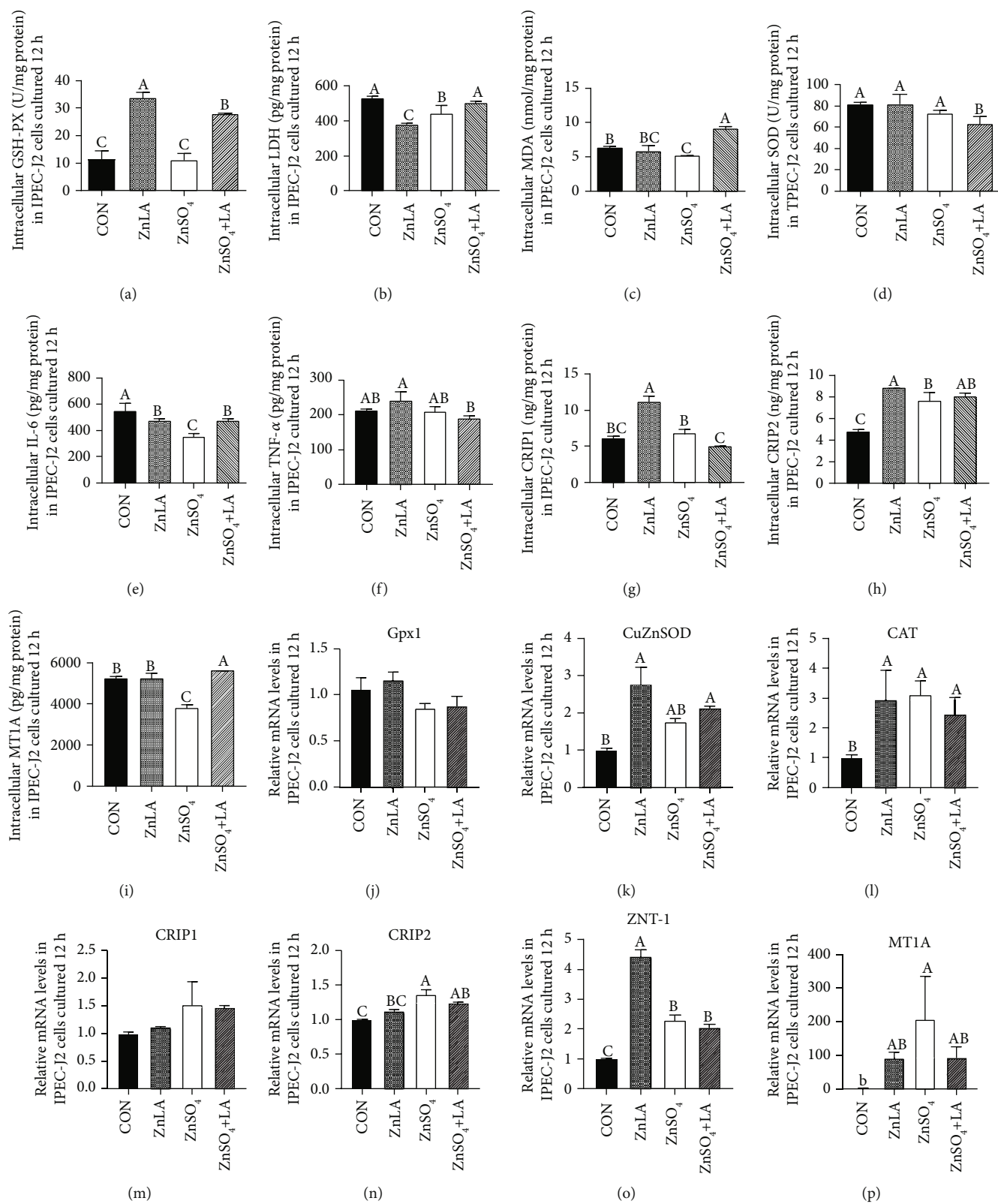


FIGURE 3: Continued.

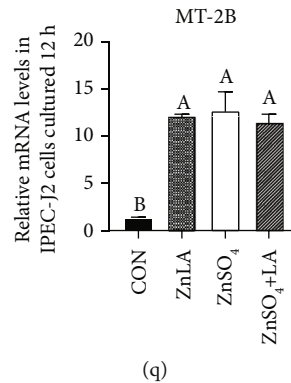


FIGURE 3: Effect of zinc lactate on Zn transport, inflammatory cytokines, and antioxidant enzymes in IPEC-J2 cells. Values are expressed as means \pm SEM ($n = 4$). (a) The activity of GSH-PX; (b) the concentration of LDH; (c) the concentration of MDA; (d) the activity of SOD; (e, f) the concentration of IL-6 and TNF- α ; (g-i) the concentration of CRIP1, CRIP2, and MT1A; (j-q) the mRNA expression of Gpx1, CuZnSOD, CAT, CRIP1, CRIP2, ZNT-1, MT1A, and MT-2B. ^{a,b,c}Means of bars with different letters were significantly different ($P < 0.05$).

6.84%) compared with the H₂O₂ treatment groups (12.24%) ($P < 0.05$). The results of the immunofluorescence assay showed that caspase-3 was located in the cytoplasm of IPEC-J2 cells, and compared with the control group, H₂O₂ exposure significantly increased caspase-3 protein expression ($P < 0.05$) (Figure 5(d)), while ZnLA or ZnSO₄ administration decreased the protein expression of caspase-3.

To test whether ZnLA could protect IPEC-J2 cells from oxidative damage by scavenging intracellular ROS, flow cytometry was used to detect mitochondrial ROS. The results showed that compared with the H₂O₂ group, ZnLA treatment significantly decreased mitochondrial ROS production in the H₂O₂-induced IPEC-J2 cells ($P < 0.05$) (Figures 5(b) and 5(c)). However, ZnSO₄ treatment had no effect on the levels of mitochondrial ROS in H₂O₂-induced IPEC-J2 cells ($P > 0.05$). As shown in Figures 5(e) and 5(f), the protein expression of nuclear Nrf2 in the ZnLA+H₂O₂ group was significantly increased while Keap1 protein expression was decreased compared with the H₂O₂ group. H₂O₂ treatment increased the expression of autophagy-related protein p62, while ZnLA supplementation markedly decreased the expression of p62 in H₂O₂-induced IPEC-J2 cells ($P < 0.05$) (Figure 5(g)). To further explore whether AMPK-Nrf2 signaling could be activated by ZnLA supplementation under oxidative stress conditions, we treated cells with an AMPK inhibitor (Compound C) to inhibit AMPK activity [28]. When AMPK activity was inhibited by Compound C, ZnLA supplementation did not promote the nuclear translocation of Nrf2 and did not decrease the protein expression of Nrf2 and Keap1 in the cytoplasm of IPEC-J2 cells ($P > 0.05$) (Figures 5(h) and 5(i)).

4. Discussion

Dietary Zn supplementation could promote cell proliferation and protect intestinal barrier function in postweaning piglets against diarrhea [29]. In the present study, we found that the addition of ZnLA was more effective in promoting cell proliferation and suppressing cell apoptosis than ZnSO₄ at the same concentration. This is consistent with many reports that Zn supplementation plays an important role in improv-

ing cell proliferation and differentiation [30, 31]. For example, a recent study has reported that ZnLA supplementation improved the growth performance of young grass carp by maintaining intestinal immune and physical barrier functions [32]. The small intestine, as a major site of Zn absorption, can maintain Zn homeostasis by regulating the expression of Zn transport proteins [33]. A number of proteins involved in Zn absorption and transport have also been identified, including metallothionein (MT), SLC30 (ZNT), SLC39 (ZIP), and CRIP [34]. Previous studies reported that downregulation of ZNT-1 protein could cause the release of LDH and the activation of caspase protein following ischemia-reperfusion [35]. MT participates in the storage, transport, and bioutilization of Zn, so a decreased expression of MT reduces the absorption efficiency of Zn in the body [36]. Moreover, MT2 is rich in reduced thiol groups (SH), which have a free radical scavenging capacity 100 times that of GSH, and can inhibit the release of mitochondrial cytochrome c and activate caspase-3 to reduce cell apoptosis and myocardial injury [37, 38]. These were further confirmed by the present study where it was found that ZnLA administration increased the mRNA expression of ZNT-1, MT1A, and MT-2B and intracellular GSH-PX activity, but decreased LDH activity, cell apoptosis, and caspase-3 protein expression levels in IPEC-J2 cells. Further, CRIP and MT regulate physiological balance by competitive transport of Zn [39]. In the current study, we found that ZnLA supplementation promoted the protein expression of CRIP1/2 in IPEC-J2 cells, suggesting the improvement of Zn transport capacity following ZnLA treatment. The results of cell apoptosis and caspase protein expression also indicated that the antiapoptosis effect of ZnLA was better than that of ZnSO₄ in IPEC-J2 cells.

Mitochondria, a site for the major source of intracellular ATP, plays a crucial role in scavenging ROS and is tightly linked to apoptosis and proliferation [40, 41]. Our results showed that ZnLA treatment increased the mRNA expression of PDHA1 and UCP2 in IPEC-J2 cells. PDHA1 can regulate mitochondrial ATP production and control the generation of ROS [42]. This is consistent with the results of present study that ZnLA treatment increased mitochondrial ATP production and decreased the production of

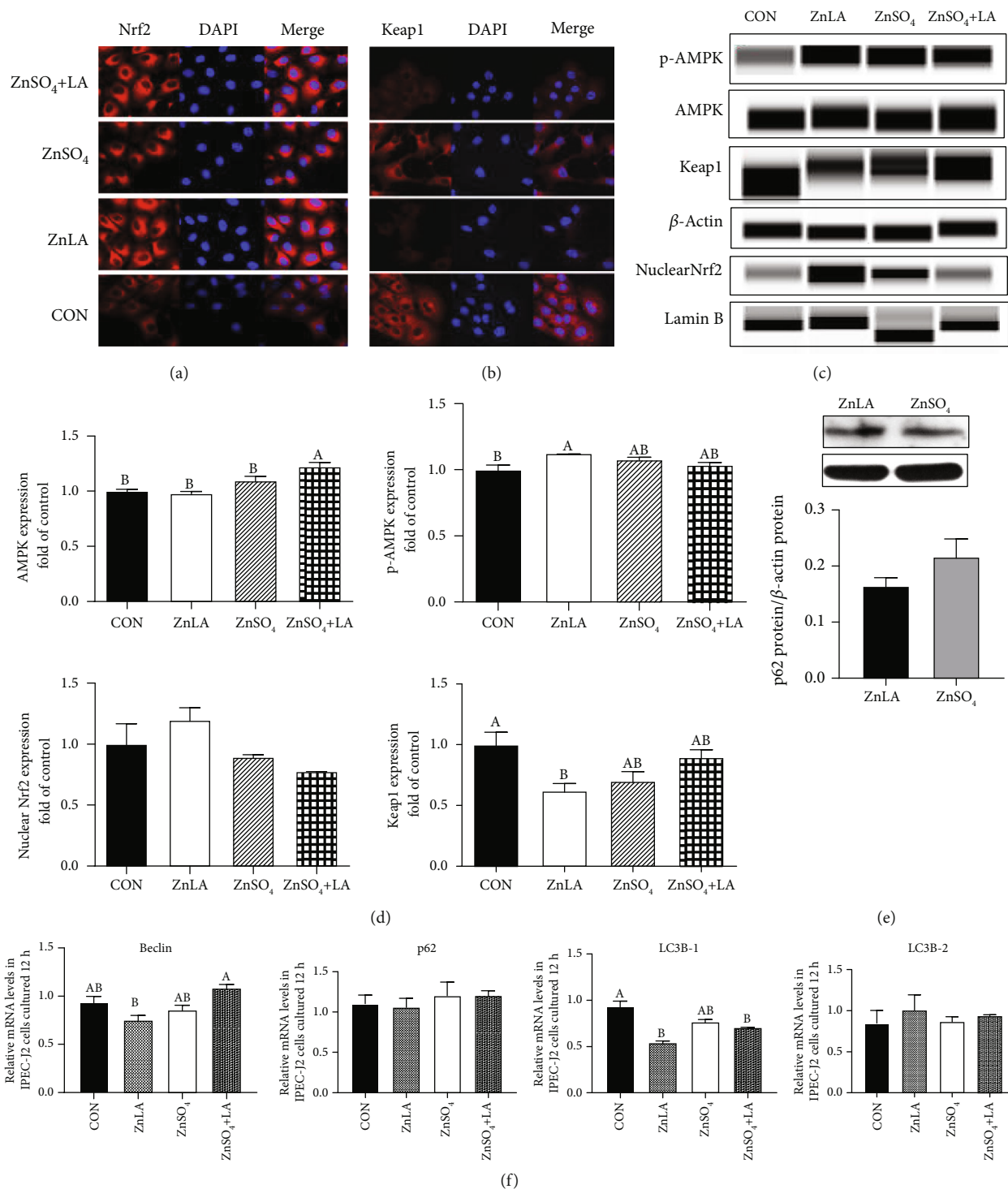
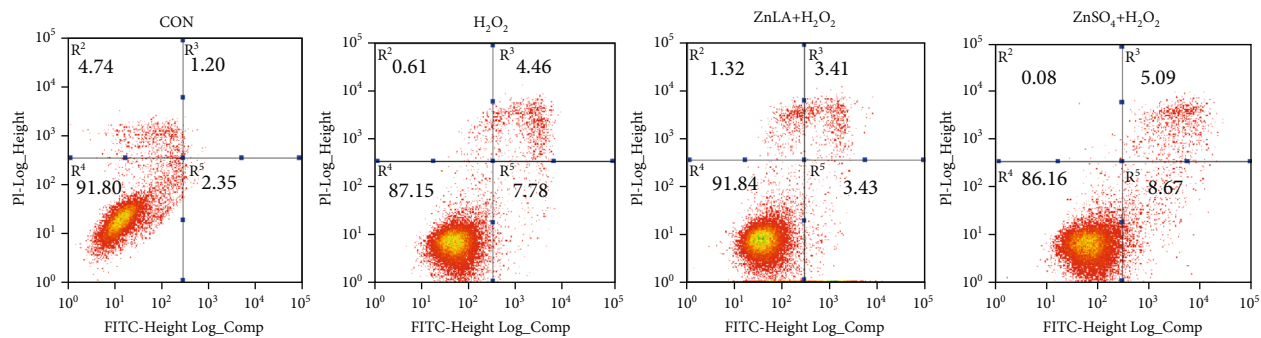


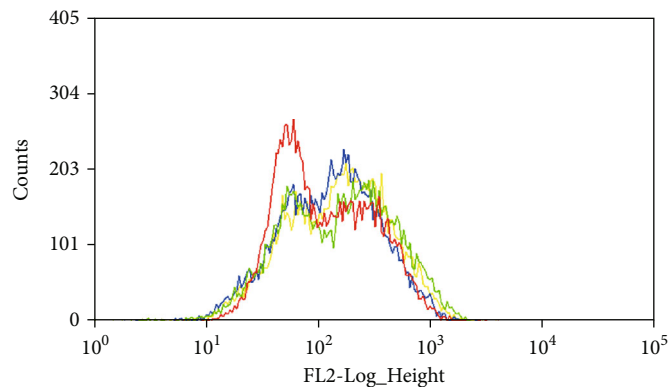
FIGURE 4: Effects of zinc lactate on the AMPK-Nrf2-p62 signaling pathway in IPEC-J2 cells. Values are expressed as means \pm SEM ($n = 4$). (a) Localization of Nrf2 ($\times 63$ magnification): red, Nrf2; blue, DAPI; (b) localization of Keap1 ($\times 63$ magnification): red, Keap1; blue, DAPI; (c, d) protein expression of AMPK-Nrf2 pathway; (e) p62 protein expression; (f) the mRNA expression of Beclin, p62, LC3B-1, and LC3B-2. ^{a,b,c}Means of bars with different letters were significantly different ($P < 0.05$).

mitochondrial ROS. UCP2, a protein on the inner membrane of mitochondria, can inhibit mitochondrial membrane transport pore opening, prevent mitochondrial Ca²⁺ overload, and reduce the formation of ROS, thereby inhibiting cell apoptosis [43]. Diano and Horvath reported that UCP2 activation

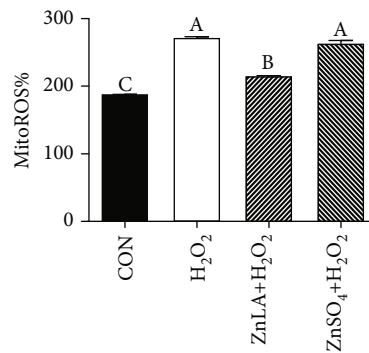
could increase proton leak and then decreased ROS production to defend against oxidative stress [44]. Based on the detection of cell respiration, we also observed that ZnLA administration increased mitochondrial proton leakage, mitochondrial basal OCR, and nonmitochondrial respiratory



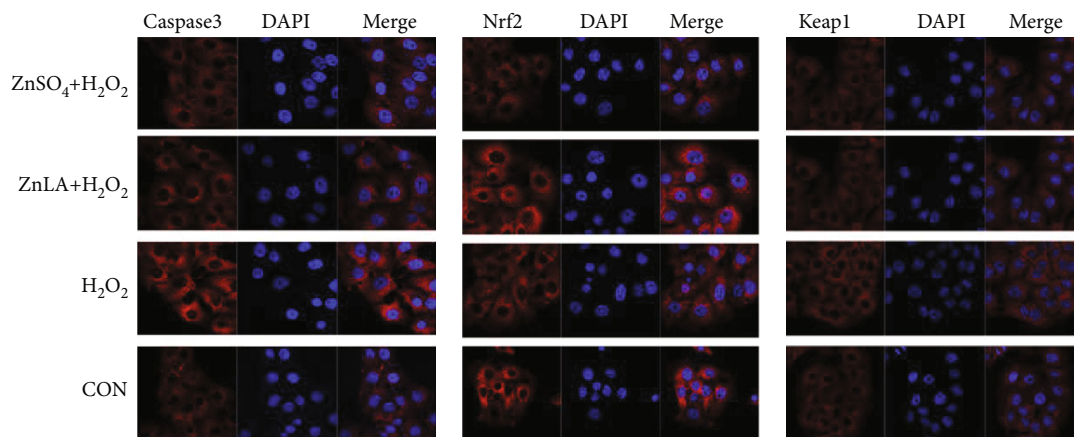
(a)



(b)



(c)



(d)

(e)

(f)

FIGURE 5: Continued.

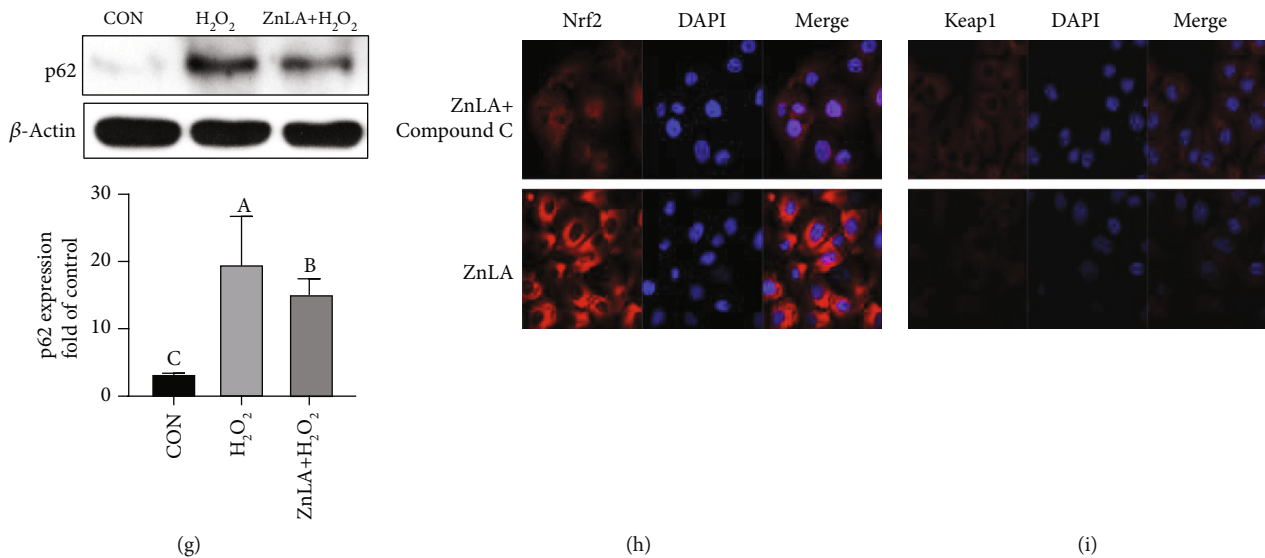


FIGURE 5: Effects of zinc lactate on cell apoptosis, mitochondrial ROS, and AMPK-Nrf2-p62 signaling pathway in H_2O_2 -induced IPEC-J2 cells. Values are expressed as means \pm SEM ($n = 4$). (a) Cell apoptosis; (b, c) mitochondrial ROS level: red line, CON; green line, H_2O_2 ; blue line, ZnLA+ H_2O_2 ; yellow line, ZnSO₄+ H_2O_2 ; (d) caspase-3 expression ($\times 63$ magnification): red, caspase-3; blue, DAPI; (e) localization of Nrf2 ($\times 63$ magnification): red, Nrf2 or Keap1; blue, DAPI; (f) localization of Keap1 ($\times 63$ magnification); (g) p62 protein expression; (h, i) localization of Nrf2 and Keap1 ($\times 63$ magnification): red, Nrf2 or Keap1; blue, DAPI. ^{a,b,c}Means of bars with different letters were significantly different ($P < 0.05$).

capacity, suggesting that ZnLA could improve mitochondrial respiratory metabolism and maintain energy equilibrium in IPEC-J2 cells. Our current results showed that ZnLA had no effect on MMP. It is known that decreased MMP promoted mitochondrial membrane permeability transition pore opening, activated the caspase-mediated apoptosis pathway, and led to cell apoptosis [45]. Increased MMP inhibited oxidative phosphorylation, resulting in an imbalance of energy metabolism [46]. Our results indicated that ZnLA administration could maintain the homeostasis of MMP. In addition, our results also showed that ZnSO₄+LA supplementation increased mitochondrial basal OCR, ATP production, and proton leak. This may be because lactic acid forms pyruvate in the presence of LDH, which then enters the mitochondria to participate in energy metabolism, thereby increasing the production of ATP. These results suggest that ZnLA administration plays important roles in mitochondrial function.

Previous studies reported that dietary Zn deficiency resulted in an increased sensitivity to oxidative stress and increased ROS production in animals [47]. This was evidenced by our findings that treatment with ZnLA improved antioxidant capacity in IPEC-J2 cells by regulating antioxidant-related gene expression and antioxidant enzyme concentrations, as well as reducing mitochondrial ROS levels. GSH-PX, CAT, and SOD are important members of the antioxidant enzyme system [48]. In the present study, ZnLA treatment significantly increased the CAT and CuZnSOD mRNA abundance and the activity of GSH-PX in IPEC-J2 cells, indicating that ZnLA administration may enhance their antioxidant ability by improving the expression and activity of antioxidant-related enzymes. Due to alterations in Zn disposition during the inflammatory response, this makes it

even easier to interpret the relationship between Zn metabolism and immune function in animals [49]. Our results showed that ZnLA administration decreased the secretion of proinflammatory cytokines such as IL-6 and TNF- α in IPEC-J2 cells. This is consistent with a previous study as reported that addition of ZnLA could decrease serum IL-6 concentration of grass carp to improve immunity. Recent reports have proved that Zn plays a role in maintaining the integrity of the intestinal mucosa through its function in T cell generation and regulating inflammatory cytokines [50].

It has been reported that antioxidant enzyme activities were partly related to the gene transcription, which were regulated by Nrf2/Keap1 signaling molecules [51]. In the present study, ZnLA administration promoted Nrf2 nuclear translocation and prevented the formation of the Nrf2/Keap1 complex, which resulted in the upregulation of antioxidant gene expression. Bartolini et al. reported that the aggregation of p62 enhanced its interaction with Keap1 and blocked the degradation of Keap1 by autophagosomes, thus activating the translocation of Nrf2 to the nucleus [52]. However, our results showed that under H_2O_2 induction conditions, ZnLA supplementation decreased the expression of p62 and Keap1, while increasing the expression of Nrf2. It is possible that the activated Nrf2 signaling pathway inhibited cell autophagy by scavenging ROS, thereby forming an antioxidative stress feedback pathway. Furthermore, there is another evidence showing that activation of AMPK could alleviate oxidative stress via the crosstalk between Nrf2 and AMPK signals [28]. In our current study, Compound C, an AMPK inhibitor, was used to inhibit the activity of AMPK and to investigate the interaction between Nrf2 and AMPK. Our results showed that under normal conditions, the protein expression of phosphorylated AMPK was increased by ZnLA

administration, and when the activity of AMPK was inhibited by Compound C, ZnLA treatment still led to a decreased expression of nuclear Nrf2 protein. However, when Compound C was removed, ZnLA administration could significantly increase the expression of Nrf2 and decrease p62 protein expression in H₂O₂-induced IPEC-J2 cells. These suggest that ZnLA might activate the AMPK-Nrf2-p62 signaling pathway to alleviate oxidative stress in IPEC-J2 cells. Zimmermann et al. showed that the activation of AMPK could facilitate the nuclear translocation of Nrf2 and improve mitochondrial respiratory metabolism in response to oxidative stress [53]. This is consistent with our current results as showed that ZnLA administration increased the Nrf2 nuclear translocation and AMPK activity as well as cell respiration, thereby promoting the expression of antioxidant-related genes to eliminate excess mitochondrial ROS. These results indicate that exogenous ZnLA may maintain redox balance and mitochondrial function by activating the AMPK-Nrf2-p62 signaling pathway in enterocytes.

5. Conclusions

This study provided evidence that the administration of ZnLA has a better effect on promoting mitochondrial ROS against oxidative stress, compared to ZnSO₄ treatment. Furthermore, ZnLA supplementation enhanced the activities and expression of antioxidant enzymes, decreased proinflammatory cytokine secretion, and modulated mitochondrial function by activating the AMPK-Nrf2-p62 pathway under normal or oxidative stress conditions. The AMPK-Nrf2-p62 pathway activated by ZnLA could further regulate the restoration of redox balance. The *in vitro* efficacy of ZnLA indicated that it may be used in animal trials for the prevention of oxidative stress. Our novel findings also suggested that ZnLA, as a new feed additive for weaned piglets, has the potential to be an alternative for an equivalent amount of inorganic Zn.

Abbreviations

ZnLA:	Zinc lactate
Zn:	Zinc
Compound C:	AMPK inhibitor
MDA:	Malondialdehyde
SOD:	Superoxide dismutase
LDH:	Lactic dehydrogenase
GSH-PX:	Glutathione peroxidase
ROS:	Reactive oxygen species
MMP:	Mitochondrial membrane potential
Nrf2:	Nuclear factor erythroid 2-related factor 2
Keap1:	Kelch-like ECH-associated protein 1
AMPK:	AMP-activated protein kinase
ZNT-1:	SLC30A1
MT:	Metallothionein
UCP2:	Uncoupling protein 2
CRIP:	Cysteine-rich intestinal protein
CAT:	Catalase
CuZnSOD:	Copper-zinc superoxide dismutase
Tfam:	Mitochondrial transcription factor A

Gpx1:	Glutathione peroxidase 1
PDHA1:	Pyruvate dehydrogenase A1
MTF-1:	Transcription factor.

Data Availability

The data used to support the findings of this study are available from the corresponding author upon request.

Conflicts of Interest

The authors have no conflicts of interest.

Authors' Contributions

Wenjie Tang and Jing Long made equal contributions to this study, so they are joint first authors.

Acknowledgments

This work was supported by the Young Elite Scientists Sponsorship Program by CAST (2019QNRC001), Special Funds for Construction of Innovative Provinces in Hunan Province (2019RS3022), "Huxiang Young Talents" projects of Hunan Province (2020RC3052), Natural Science Foundation of China (31902168 and 31872371), National Science Foundation for Outstanding Young Scholars of Hunan Province (2019JJ30017), Hunan high-level talent gathering project (2018RS3111), Guangdong Basic and Applied Basic Research Fund Project (2019A1515110852), Guangxi Key Research and Development Plan (guike AB19259012), and the Applied Basic Research Grant Project of Sichuan Province (2018JY0641).

Supplementary Materials

Supplemental Table 1 is the primers used for quantitative reverse transcription-PCR. (*Supplementary Materials*)

References

- [1] K. H. Ibs and L. Rink, "Zinc-altered immune function," *Journal of Nutrition*, vol. 133, no. 5, pp. 1452S–1456S, 2003.
- [2] A. Owusu-Asiedu, C. M. Nyachoti, and R. R. Marquardt, "Response of early-weaned pigs to an enterotoxigenic *Escherichia coli* (K88) challenge when fed diets containing spray-dried porcine plasma or pea protein isolate plus egg yolk antibody, zinc oxide, fumaric acid, or antibiotic," *Journal of Animal Science*, vol. 81, no. 7, pp. 1790–1798, 2003.
- [3] C. M. McDonald, K. P. Manji, K. Rodrick et al., "Daily zinc but not multivitamin supplementation reduces diarrhea and upper respiratory infections in Tanzanian infants: a randomized, double-blind, placebo-controlled clinical trial," *Journal of Nutrition*, vol. 145, no. 9, pp. 2153–2160, 2015.
- [4] F. Alberto, M. Mara, C. D. Laura, and M. Elena, "Zinc deficiency induces membrane barrier damage and increases neutrophil transmigration in Caco-2 cells," *Journal of Nutrition*, vol. 138, no. 9, pp. 1664–1670, 2008.
- [5] L. Noam and H. Michal, "How cellular Zn²⁺ signaling drives physiological functions," *Cell Calcium*, vol. 75, pp. 53–63, 2018.

- [6] H. N. Shi, M. E. Scott, M. M. Stevenson, and K. G. Koski, "Energy restriction and zinc deficiency impair the functions of murine T cells and antigen-presenting cells during gastrointestinal nematode infection," *Journal of Nutrition*, vol. 128, no. 1, pp. 20–27, 1998.
- [7] B. Shenying and D. L. Knoell, "Zinc modulates cytokine-induced lung epithelial cell barrier permeability," *American Journal of Physiology Lung Cellular & Molecular Physiology*, vol. 291, pp. L1132–L1141, 2006.
- [8] R. Canali, F. Vignolini, F. Nobili, and E. Mengheri, "Reduction of oxidative stress and cytokine-induced neutrophil chemoattractant (CINC) expression by red wine polyphenols in zinc deficiency induced intestinal damage of rat," *Free Radical Biology & Medicine*, vol. 28, no. 11, pp. 1661–1670, 2000.
- [9] H. Aliarabi, A. Fadayifar, M. M. Tabatabaei et al., "Effect of zinc source on hematological, metabolic parameters and mineral balance in lambs," *Biological Trace Element Research*, vol. 168, no. 1, pp. 82–90, 2015.
- [10] T. C. Huang, W. T. Chang, Y. C. Hu, B. S. Hsieh, and K. L. Chang, "Zinc protects articular chondrocytes through changes in Nrf2-mediated antioxidants," *Cytokines and Matrix Metalloproteinases*, *Nutrients*, vol. 10, p. 471, 2018.
- [11] S. Mwangi, J. Timmons, T. Ao et al., "Effect of zinc imprinting and replacing inorganic zinc with organic zinc on early performance of broiler chicks," *Poultry Science*, vol. 96, no. 4, pp. 861–868, 2017.
- [12] N. W. Shelton, M. D. Tokach, J. L. Nelssen et al., "Effects of copper sulfate, tri-basic copper chloride, and zinc oxide on weanling pig performance," *Journal of Animal Science*, vol. 89, no. 8, pp. 2440–2451, 2011.
- [13] M. M. Bai, H. N. Liu, K. Xu et al., "Use of coated nano zinc oxide as an additive to improve the zinc excretion and intestinal morphology of growing pigs¹," *Journal of Animal Science*, vol. 97, no. 4, pp. 1772–1783, 2019.
- [14] Y. M. Bao, M. Choct, P. A. Iji, and K. Bruerton, "Effect of organically complexed copper, iron, manganese, and zinc on broiler performance, mineral excretion, and accumulation in tissues," *Journal of Applied Poultry Research*, vol. 16, no. 3, pp. 448–455, 2007.
- [15] S. Leeson and L. Caston, "Using minimal supplements of trace minerals as a method of reducing trace mineral content of poultry manure," *Animal Feed Science & Technology*, vol. 142, no. 3-4, pp. 339–347, 2008.
- [16] T. Ao, J. Pierce, R. Power et al., "Effects of feeding different forms of zinc and copper on the performance and tissue mineral content of chicks," *Poultry Science*, vol. 88, no. 10, pp. 2171–2175, 2009.
- [17] J. Yan, C. Zhang, L. Tang, and S. Y. Kuang, "Effects of organic zinc sources on the contents of amino acids and fatty acids in Sichuan chicken," *Nutrition and Feedstuffs*, vol. 53, no. 12, pp. 86–88, 2017.
- [18] B. Zhao, A. Zhou, and X. Li, "Effects of zinc lactate on production performance and shell quality of laying hens," *Science and Technology Outlook*, vol. 17, pp. 28–29, 2012.
- [19] G. Bai, "Research progress of zinc lactate and its application in rabbit nutrition," *Sichuan Animal & Veterinary Sciences*, vol. 8, pp. 34–35, 2007.
- [20] Y. Ma, Q. Huang, M. Lv et al., "Chitosan-Zn chelate increases antioxidant enzyme activity and improves immune function in weaned piglets," *Biological Trace Element Research*, vol. 158, no. 1, pp. 45–50, 2014.
- [21] M. C. Jaramillo and D. D. Zhang, "The emerging role of the Nrf2-Keap1 signaling pathway in cancer," *Genes & Development*, vol. 27, no. 20, pp. 2179–2191, 2013.
- [22] D. Hu, Y. Xu, J. Xie, C. Sun, X. Zheng, and W. Chen, "Systematic evaluation of phenolic compounds and protective capacity of a new mulberry cultivar J33 against palmitic acid-induced lipotoxicity using a simulated digestion method," *Food Chemistry*, vol. 258, pp. 43–50, 2018.
- [23] M. H. Xia, X. Y. Yan, L. Zhou et al., "p62 suppressed VK3-induced oxidative damage through Keap1/Nrf2 pathway in human ovarian cancer cells," *Journal of Cancer*, vol. 11, no. 6, pp. 1299–1307, 2020.
- [24] Y. Farbood, A. Sarkaki, M. Mahdavinia et al., "Protective effects of co-administration of zinc and selenium against streptozotocin-induced Alzheimer's disease: behavioral, mitochondrial oxidative stress, and GPR39 expression alterations in rats," *Neurotoxicity Research*, vol. 38, no. 2, pp. 398–407, 2020.
- [25] L. He, J. Wu, W. Tang et al., "Prevention of oxidative stress by α -ketoglutarate via activation of CAR signaling and modulation of the expression of key antioxidant-associated targets in vivo and in vitro," *Journal of Agricultural and Food Chemistry*, vol. 66, no. 43, pp. 11273–11283, 2018.
- [26] L. Q. He, J. Long, X. H. Zhou, Y. H. Liu, T. J. Li, and X. Wu, "Serine is required for the maintenance of redox balance and proliferation in the intestine under oxidative stress," *The FASEB Journal*, vol. 34, no. 3, pp. 4702–4717, 2020.
- [27] J. Yin, M. Wu, Y. Li et al., "Toxicity assessment of hydrogen peroxide on Toll-like receptor system, apoptosis, and mitochondrial respiration in piglets and IPEC-J2 cells," *Oncotarget*, vol. 8, no. 2, pp. 3124–3131, 2017.
- [28] C. F. Mo, L. Wang, J. Zhang et al., "The crosstalk between Nrf2 and AMPK signal pathways is important for the anti-inflammatory effect of berberine in LPS-stimulated macrophages and endotoxin-shocked mice," *Antioxidants & Redox Signaling*, vol. 20, no. 4, pp. 574–588, 2014.
- [29] W. Chao, L. Zhang, Z. Ying et al., "Effects of dietary zinc oxide nanoparticles on growth, Diarrhea, Mineral Deposition, Intestinal Morphology, and Barrier of Weaned Piglets," *Biological Trace Element Research*, vol. 185, pp. 364–374, 2018.
- [30] Y. Shao, P. G. Wolf, S. Guo, Y. Guo, H. R. Gaskins, and B. Zhang, "Zinc enhances intestinal epithelial barrier function through the PI3K/AKT/mTOR signaling pathway in Caco-2 cells ☆," *Journal of Nutritional Biochemistry*, vol. 43, pp. 18–26, 2017.
- [31] K. Ohashi, Y. Nagata, E. Wada, P. S. Zammit, M. Shiozuka, and R. Matsuda, "Zinc promotes proliferation and activation of myogenic cells via the PI3K/Akt and ERK signaling cascade," *Experimental Cell Research*, vol. 333, no. 2, pp. 228–237, 2015.
- [32] Z. X. Song, W. D. Jiang, Y. Liu et al., "Dietary zinc deficiency reduced growth performance, intestinal immune and physical barrier functions related to NF- κ B, TOR, Nrf2, JNK and MLCK signaling pathway of young grass carp (*Ctenopharyngodon idella*)," *Fish & Shellfish Immunology*, vol. 66, pp. 497–523, 2017.
- [33] T. Kambe, Y. Yamaguchi-Iwai, R. Sasaki, and M. Nagao, "Overview of mammalian zinc transporters," *Cellular & Molecular Life Sciences Cmls*, vol. 61, no. 1, pp. 49–68, 2004.
- [34] L. A. Lichten and R. J. Cousins, "Mammalian zinc transporters: nutritional and physiologic regulation," *Annual Review of Nutrition*, vol. 29, no. 1, pp. 153–176, 2009.

- [35] O. Beharier, S. Dror, S. Levy et al., "ZnT-1 protects HL-1 cells from simulated ischemia-reperfusion through activation of Ras-ERK signaling," *Journal of Molecular Medicine*, vol. 90, no. 2, pp. 127-138, 2012.
- [36] J. S. Kyoung, K. Mi-Kyung, L. Young-Hoon et al., "Lower zinc bioavailability may be related to higher risk of subclinical atherosclerosis in Korean adults," *PLoS One*, vol. 8, article e80115, 2013.
- [37] M. P. Gunderson, B. T. Nguyen, J. C. C. Reyes et al., "Response of phase I and II detoxification enzymes, glutathione, metallothionein and acetylcholine esterase to mercury and dimethoate in signal crayfish (*Pacifastacus leniusculus*)," *Chemosphere*, vol. 208, pp. 749-756, 2018.
- [38] R. María, J. A. Rubiolo, T. Eva, O. P. Thomas, M. R. Vieytes, and L. M. Botana, "Crambescin C1 exerts a cytoprotective effect on HepG2 cells through metallothionein induction," *Marine Drugs*, vol. 13, pp. 4633-4653, 2015.
- [39] O. Escobar, M. Sandoval, A. Vargas, and J. M. Hempe, "Role of metallothionein and cysteine-rich intestinal protein in the regulation of zinc absorption by diabetic rats," *Pediatric Research*, vol. 37, no. 3, pp. 321-327, 1995.
- [40] A. A. Starkov, A. Y. Andreyev, S. F. Zhang et al., "Scavenging of H₂O₂ by mouse brain mitochondria," *Journal of Bioenergetics and Biomembranes*, vol. 46, no. 6, pp. 471-477, 2014.
- [41] G. Lorenzo, K. Oliver, and K. Guido, "Mitochondria: master regulators of danger signalling," *Nature Reviews Molecular Cell Biology*, vol. 13, pp. 780-788, 2012.
- [42] T. Chitoku and D. Sabrina, "Mitochondrial UCP2 in the central regulation of metabolism," *Best Practice & Research Clinical Endocrinology & Metabolism*, vol. 28, pp. 757-764, 2014.
- [43] F. Correa, V. Soto, and C. Zazueta, "Mitochondrial permeability transition relevance for apoptotic triggering in the post-ischemic heart," *The International Journal of Biochemistry & Cell Biology*, vol. 39, no. 4, pp. 787-798, 2007.
- [44] S. Diano and T. L. Horvath, "Mitochondrial uncoupling protein 2 (UCP2) in glucose and lipid metabolism," *Trends in Molecular Medicine*, vol. 18, no. 1, pp. 52-58, 2012.
- [45] J. Yu-Bin and Y. Lei, "N-butanol extract of *Capparis spinosa* L. induces apoptosis primarily through a mitochondrial pathway involving mPTP open, cytochrome C release and caspase activation," *Asian Pacific Journal of Cancer Prevention Apjcp*, vol. 15, pp. 9153-9157, 2014.
- [46] M. Singer, "The role of mitochondrial dysfunction in sepsis-induced multi-organ failure," *Virulence*, vol. 5, pp. 66-72, 2013.
- [47] P. I. Oteiza, K. L. Olin, C. G. Fraga, and C. L. Keen, "Zinc deficiency causes oxidative damage to proteins, lipids and DNA in rat testes," *Journal of Nutrition*, vol. 125, pp. 823-829, 1995.
- [48] X. G. Lei, J. H. Zhu, W. H. Cheng et al., "Paradoxical roles of antioxidant enzymes: basic mechanisms and health implications," *Physiological Reviews*, vol. 96, no. 1, pp. 307-364, 2016.
- [49] S. Hojyo and T. Fukada, "Zinc transporters and signaling in physiology and pathogenesis," *Archives of Biochemistry and Biophysics*, vol. 611, pp. 43-50, 2016.
- [50] Y. M. Song, M. H. Kim, H. N. Kim et al., "Effects of dietary supplementation of lipid-coated zinc oxide on intestinal mucosal morphology and expression of the genes associated with growth and immune function in weanling pigs," *Asian-Australasian Journal of Animal Sciences*, vol. 31, no. 3, pp. 403-409, 2018.
- [51] T. Kensler and N. Wakabayashi, "Cell survival responses to environmental stresses via the Keap1-Nrf2-ARE pathway," *Annual Review of Pharmacology and Toxicology*, vol. 47, no. 1, pp. 89-116, 2007.
- [52] D. Bartolini, K. Dallaglio, P. Torquato, M. Piroddi, and F. Galli, "Nrf2-p62 autophagy pathway and its response to oxidative stress in hepatocellular carcinoma," *Translational Research*, vol. 193, pp. 54-71, 2018.
- [53] K. Zimmermann, J. Baldinger, B. Mayerhofer, A. G. Atanasov, V. M. Dirsch, and E. H. Heiss, "Activated AMPK boosts the Nrf2/HO-1 signaling axis—a role for the unfolded protein response," *Free Radical Biology & Medicine*, vol. 88, pp. 417-426, 2015.

Research Article

Bisphenol A and Its Analogues in Chinese Total Diets: Contaminated Levels and Risk Assessment

Kai Yao,^{1,2} Jing Zhang,² Jie Yin,² Yunfeng Zhao,³ Jianzhong Shen,¹ Haiyang Jiang ¹,
and Bing Shao ^{1,2}

¹College of Veterinary Medicine, China Agricultural University, Beijing 100193, China

²Beijing Key Laboratory of Diagnostic and Traceability Technologies for Food Poisoning, Beijing Center for Disease Prevention and Control, Beijing 100013, China

³NHC Key Laboratory of Food Safety Risk Assessment, China National Center for Food Safety Risk Assessment, Beijing 100021, China

Correspondence should be addressed to Haiyang Jiang; haiyang@cau.edu.cn and Bing Shao; shaobingch@sina.com

Received 30 September 2020; Revised 26 October 2020; Accepted 18 November 2020; Published 17 December 2020

Academic Editor: Si Qin

Copyright © 2020 Kai Yao et al. This is an open access article distributed under the Creative Commons Attribution License, which permits unrestricted use, distribution, and reproduction in any medium, provided the original work is properly cited.

Bisphenol A (BPA) and its analogues (BPs) are suspected posing potential endocrine disrupting properties. They might migrate into foodstuffs through food packaging materials or contaminated water and soil. Dietary exposure is of paramount importance way for human health. European Food Safety Authority (EFSA) lowered the value of tolerable daily intake (TDI) from 50 $\mu\text{g}/\text{kg bw}/\text{day}$ (d) to a temporary (t) TDI (t-TDI) of 4 $\mu\text{g}/\text{kg bw}/\text{d}$. In this study, the Chinese total dietary samples were analyzed for assessing the exposure risk of BPs by diets. BPA, bisphenol F (BPF), bisphenol S (BPS), and bisphenol AF (BPAF) were found in 12 kinds of food samples except for bisphenol B (BPB). A deterministic approach was used to calculate the dietary intakes of 4 kinds of compounds. For different age and gender groups, the exposure levels of BPA (178.440-403.672 $\text{ng}/\text{kg bw}/\text{d}$) was the highest, followed by BPS (21.372-52.112 $\text{ng}/\text{kg bw}/\text{d}$), BPF (20.641-50.507 $\text{ng}/\text{kg bw}/\text{d}$), and BPAF (0.434-1.210 $\text{ng}/\text{kg bw}/\text{d}$). Based on the t-TDI set by EFSA (4 $\mu\text{g}/\text{kg bw}/\text{d}$ for BPA), the BPs through dietary intake pose low risks on the Chinese general population even summarization exposure levels of different BPs. However, human can be exposed to multiple endocrine disrupting chemicals rather than BPs alone; combined exposure risks should be further considered.

1. Introduction

Bisphenol A (BPA) is a high-production and high-volume chemical, which is used to manufacture various commodities, such as inner coatings and contact materials of beverage or food due to its rigidity, transparency, and resistance [1]. However, BPA has been shown to be migrated into food, and the migration can be amplified by exposure to alkaline or acidic conditions. Possible sources of human exposure to BPA has been reported, including personal care products [2], teethers [3], environmental water [4], dust [5], air [6], thermal papers [7], drinks [8], and food [9-13]. Diet is the major source of exposure to BPA [9]. An increasing number of studies have shown that exposure to BPA is associated with a variety of toxicities in the neurological [14], endocrine [15], reproductive [16], metabolic [17], and immune systems

[18]. Regulations on the production and use of BPA have been brought into force in European Union [19], United States [20], South Korea [21], Japan [22], and China [23]. In 2015, the European Food Safety Authority lowered the value of tolerable daily intake (TDI) from 50 $\mu\text{g}/\text{kg bw}/\text{day}$ (d) to a temporary (t) TDI (t-TDI) of 4 $\mu\text{g}/\text{kg bw}/\text{d}$ [19].

Due to the limitation of the BPA use, the bisphenol analogues (BPs), such as BPB, BPS, BPF, and BPAF, were developed as alternatives to BPA and replaced BPA for use in epoxy resins, plastics, thermal papers, and food can linings. As a consequence, BPA analogues were found in several foods (cereals, fruits, meats, etc.) including the commodities from China [24, 25]. However, the endocrine disruptive nature of these analogues seems that they are not less toxic than BPA. Previous reports have shown that the adverse effects of BPs are similar with BPA or more harmful than

BPA [26, 27]. Thus, there is increasing demand for the risk assessment of combined exposure of different BPs. Total diet study (TDS) is considered a most efficient and effective method to evaluate the average daily dietary intake of certain chemical substances through the ready-to-eat diet in populations of different ages or genders. The ready-to-eat diet has the advantage of considering loss or introduction of target chemicals and providing analytical results for realistic estimation of dietary intake [28]. In fact, TDS can be used as a priority-setting tool to enable risk managers to focus their limited resources on target compounds. To date, only dietary intakes of BPA in the composite food samples from the Chinese or Canadian TDS were reported [28, 29]. Dietary intake data from TDS on other BPs was not available by far.

The objectives of this work are (i) to investigate the contamination levels of different BPs in the fifth Chinese TDS (2009-2013) and (ii) estimate exposure risk among different age and gender Chinese populations.

2. Materials and Methods

2.1. Reagents and Chemicals. BPA (CAS 80-05-7, purity 98.5%), BPA- d_4 (purity > 97.8%) BPB (CAS 77-40-7, purity > 98.5%), BPF (CAS 620-92-8, purity > 99.0%), BPAF (CAS 1478-61-1, purity 98.0%), and BPS (CAS 80-09-1, purity > 98%) were supplied by Tokyo Chemical Industry Co. Ltd. (Tokyo, Japan). BPF- d_{10} (purity > 99%) and BPS- $^{13}C_{12}$ (purity > 99%) were purchased from Toronto Research Chemical Inc. (Ontario, Canada), and BPAF- d_4 (purity > 99%) was available from CDN Isotopes Inc. (Quebec, Canada). BPA- d_4 (purity > 99%) and BPB- $^{13}C_{12}$ (purity > 99%) were obtained from Cambridge Isotope Laboratories Inc. (Andover, MA). LC-MS grade methanol (MeOH) and acetonitrile (ACN) were offered by Sigma-Aldrich (St. Louis, MO). Ultrapure water was obtained from a Milli-Q ultrapure system (Millipore, Bedford, MA, USA). Phosphate-buffered saline (PBS, 0.2 M) was purchased from Solarbio Science & Technology Co., Ltd. (Beijing, China). The stock standard solutions (10 μ g/mL) were individually prepared by dissolving in MeOH and were stored at -20°C . Working solutions were prepared by serial dilution of stock solutions with MeOH/water (50:50, v/v).

2.2. Sample Collection. All samples were from the fifth Chinese TDS. The sampling strategy were similar to the fourth Chinese TDS in 2007 [28]. Compared to the fourth Chinese TDS, the sampling sites of the fifth Chinese TDS were enlarged from 12 to 20 provinces (municipalities, autonomous regions), which were geographically divided into four regions. The regions were as follows: North region 1: Heilongjiang (HLJ), Liaoning (LN), Hebei (HB), Jilin (JL) provinces, and Beijing Municipality (BJ); North region 2: Henan (HN), Shanxi (SX), Qinghai (QH) provinces, Ningxia Hui Autonomous Region (NX), and Nei Mongol Autonomous Region (NM); South region 1: Jiangxi (JX), Fujian (FJ), Zhejiang (ZJ) provinces, and Shanghai Municipality (SH); and South region 2: Hubei (HuB), Sichuan (SC), Hunan (HuN), Guangdong (GD) provinces, and Guangxi (GX) Zhuang Autonomous Region. Each region and each province repre-

sent a major market basket and a minor market basket, respectively. In each province (municipality, autonomous region), three survey points (two rural and one urban sites, each site has 30 households) was selected. The selected survey points shall be able to represent the general dietary habits, nutritional pattern, and actual dietary structure of residents of each province. The household-based dietary survey adopted a three-day weighed food record method. The consumption foods were classified into 12 groups: cereals and cereal products, legume and related products, potatoes and potato products, meats and meat products, eggs and egg products, aquatic foods and aquatic food products, milk and dairy products, vegetables and vegetable products, fruits and fruit products, sugar and sugar products, beverages and water, and alcohol beverages. Samples of various groups were purchased from markets, grocery stores, shops, and farms near the survey points and were cooked and mixed to form the composites of different food groups similar to the average daily consumption for the population in the province (municipality, autonomous region) according to the results of dietary survey. All samples were stored at -20°C until use.

2.3. Sample Preparation. All samples were divided into three broad categories: plant-derived foods (including cereals and cereal products, legume and related products, potatoes and potato products, vegetables and vegetable products, fruits and fruit products, and sugar and sugar products), animal-derived foods (including meats and meat products, eggs and egg products, aquatic foods and aquatic food products, and milk and dairy products), and beverages (including beverages and water and alcohol beverages). The sample preparation methods were based on our previous work [30, 31] with some modifications.

For plant-derived foods, 1 g of homogeneous sample were weighed in 15 mL polypropylene centrifuge tubes. After the addition of ACN (5 mL), the tube was vortexed for 30 s. The sample was then ultrasonically extracted for 20 min and centrifuged at 9184 g for 10 min. The supernatant was transferred to another 15 mL polypropylene centrifuge tube. The extraction step was repeated, and the respective extracts were combined and concentrated to dryness by a gentle stream of N_2 at 40°C . The residue was redissolved in MeOH/PBS (10:90, v/v; 10 mL), and the solution was vortexed for 30 s. The resultant solution was subjected to IAC cleanup.

For animal-derived foods, 1 g of sample were weighed in 15 mL polypropylene centrifuge tubes. ACN (5 mL) was added. The mixtures were vortexed for 30 s, ultrasonically extracted for 20 min, and centrifuged at 9184 g for 10 min. The supernatants were transferred to fresh 15 mL polypropylene centrifuge tubes; then, PBS (3 mL) was added, and the mixture was stored at -20°C for 3 h. The upper ACN layer was then collected and concentrated to dryness by a gentle stream of N_2 at 40°C . The residue was redissolved in MeOH/PBS (10:90, v/v; 10 mL), and the solution was vortexed for 30 s. The resultant solution was subjected to IAC cleanup.

For beverage samples were firstly degassed in an ultrasonic bath for 30 min. Degassed samples (4 mL) were diluted with 16 mL PBS and adjusted to pH 8.5 with sodium hydroxide solution (0.2 M). The resultant solution was subjected to IAC cleanup.

The prepared solution was loading onto the IAC, then washed with PBS (9 mL) and water (9 mL). Finally, MeOH (3 mL) was used to desorb BPA and BPs. The MeOH-containing analytes were collected and evaporated under nitrogen at 40°C. The residue was redissolved with MeOH/water (30:70, v/v; 1 mL), and the solution was centrifugated at 9000 rpm and transferred 800 μ L into vial, then analyzed by ultrahigh-performance liquid chromatography tandem mass spectrometry (UHPLC-MS/MS).

2.4. Instrumental Analysis. UHPLC-MS/MS analysis was carried out using a UHPLC system (Nexera X2, Shimadzu, Japan) coupled with a Shimadzu LC-MS 8060 triple quadrupole mass spectrometer (Kyoto, Japan). UHPLC separation was performed on a Waters ACQUITY BEH C18 column (2.1 mm \times 100 mm; 1.7 μ m; MA, USA). The column temperature was set at 40°C with a flow rate of 0.3 mL/min, and the injection volume was 5 μ L. The mobile phases consist of methanol and water. The initial gradient conditions were 30% methanol, followed by a linear increase to 100% methanol in 6 min, and then changed to isocratic conditions with 100% methanol for 2 min. Subsequently, the mobile phase was decreased to 30% methanol in 1 min, held for 3 min before the next injection. The MS/MS detection was operated in the negative ionization mode with multiple reaction monitoring. N₂ was used as the nebulizing gas at flow rate of 3 L/min; heating gas and drying gas flow rate were 10 L/min and 10 L/min, respectively. Interface temperature, desolvation line temperature, and heat block temperature were 300°C, 250°C, and 400°C, respectively. The optimized MS/MS parameters for the target compounds are given in Table S1.

2.5. Quality Assurance and Quality Control (QA/QC). Isotope-labeled internal standards (BPS-¹³C₁₂, BPF-*d*₁₀, BPA-*d*₄, BPB-¹³C₁₂, and BPAF-*d*₄) were used to compensate for the matrix effect and recovery loss during the whole analytical procedure. BPS, BPF, BPA, BPB, and BPAF in the food samples were quantified using calibration curves ($r > 0.999$) that were established with seven different concentrations of target standards (0.05-5.00 ng/mL for BPS and BPAF, 0.50-50.0 ng/mL for BPA and BPB, and 1.00-100 ng/mL for BPF). The limits of quantification (LOQs) of BPS and BPAF were 0.05 μ g/kg for plant-derived foods and animal-derived foods and 0.013 μ g/L for beverages. The LOQs of BPA and BPB were 0.5 μ g/kg for plant-derived foods and animal-derived foods and 0.10 μ g/L for beverages, respectively. The LOQs of BPF were 1.0 μ g/kg for plant-derived foods and animal-derived foods and 0.20 μ g/L for beverages, respectively. The recoveries of BPS, BPF, BPA, BPB, and BPAF standards spiked in the matrix sample ranged from 84.6 to 116.8%, 86.4-113.3%, 87.2-116.3%, 87.3-116.7%, and 87.7-117.5%, respectively. The coefficient of variation of all analytes for spiked samples were both below 13.5%.

Blank contamination is a disturbing problem in the ultra-trace analysis of BPA and should be avoided in order to achieve low detection limit [32]. Several methods were applied to lower the BPA contamination: (i) glassware were used instead of plastics, and glassware was consecutively rinsed with MeOH and ultrapure water, then baked for four hours at 400°C in a muffle

furnace before use (L9/11/B 170, Nabertherm Industrial Furnaces Limited, Lilienthal/Bremen, Germany) [28]; (ii) procedural blanks were analyzed to evaluate background concentration of each analyte, and the concentration was ensured to be below the corresponding LOQ; and (iii) a mid-point calibration standard and methanol were injected every 10 sample injections to check for the instrumental stability, contamination, and the carry-over between samples [33].

2.6. Food Consumption and Bodyweight Data. We combined different age (2-7, 8-12, 13-19, 20-50, 51-65, and >65-year-old) and gender groups to estimate daily dietary intakes (EDI) of seven analytes. The data of food consumption (Table S2) and body weights (Table S3) given by the fifth China total diet study [34] and National Health and Family Planning Commission of the People's Republic of China [35, 36] were used to calculate the dietary doses of different food groups.

2.7. Estimation of Daily Intake. Estimation of daily intake (EDI) represented the individual dietary exposure of specific age and gender groups of the general population by multiplying the detected levels of target foods and by the average daily food intake of the corresponding food items in each age and gender group [9]. EDI for different age and gender groups was assessed and can be expressed using the following equations:

$$EDI = \frac{C/w \times FI}{BW}, \quad (1)$$

where EDI (ng/kg body weight (bw)/day (d)) expresses daily exposure for the different age (2-7, 8-12, 13-19, 20-50, 51-65, and >65-year-old) and gender groups; C (μ g/kg) expresses the measured mean concentrations of seven analytes in the corresponding food item in the current study, and concentrations below the LOD were replaced by 0.5 LOD, and those below the LOQ but above the LOD by 0.5 LOQ [37]; w expresses the water dilution coefficient of the food samples (Table S4); and FI (g/day) expresses the food intake of the corresponding food item by each age and gender group.

3. Results and Discussion

3.1. EDCs in Foodstuffs. Among 240 composite samples involving in 12 different food items, the highest overall detective rate was found to be 76.7% (BPS), followed by 75.8% (BPA), 29.2% (BPF), 20.8% (BPAF), and 0 (BPB). BPB was not detected in any of the 240 food samples; it is unlikely that BPB have been used in food packaging. This was consistent with previous reports [25, 38]. Furthermore, BPB was also not detected in breast milk and urine samples from Chinese residents [39, 40]. This suggested that Chinese people were not exposed to BPB through dietary or environmental conditions. Concentrations of detected 4 EDCs are listed in Table 1. It is noteworthy that all the samples were cooked and then mixed with water. Therefore, we converted the concentrations of detected EDCs in water-diluted samples into original concentrations of EDCs in uncooked samples based on the water dilution coefficient (Table S4). Although BPA was gradually replaced by its analogues, it was demonstrated that BPA and BPS were the predominant contaminants in foodstuffs. Mean BPA

TABLE 1: Concentrations of EDCs in different categories of food items collected from 20 provinces in China.

	BPA	BPS	BPF	BPAF
Cereals ($n = 20$)				
Mean ($\mu\text{g}/\text{kg}$)	4.058	0.314	0.352	0.020
Range ($\mu\text{g}/\text{kg}$)	<LOD-14.773	<LOD-2.203	<LOD-1.743	<LOD – <LOQ
Detective rate (%)	75.0	70.0	40.0	70.0
Legumes and nuts ($n = 20$)				
Mean ($\mu\text{g}/\text{kg}$)	0.815	4.570	5.248	0.032
Range ($\mu\text{g}/\text{kg}$)	<LOD-2.908	<LOD-47.932	<LOD-81.034	<LOD-0.188
Detective rate (%)	45.0	65.0	70.0	80.0
Potatoes ($n = 20$)				
Mean ($\mu\text{g}/\text{kg}$)	7.018	0.618	0.218	0.046
Range ($\mu\text{g}/\text{kg}$)	<LOD-42.945	<LOD-7.619	<LOD-1.160	<LOD-0.753
Detective rate (%)	90.0	85.0	10.0	10.0
Meats ($n = 20$)				
Mean ($\mu\text{g}/\text{kg}$)	2.756	1.774	0.416	0.008
Range ($\mu\text{g}/\text{kg}$)	<LOD-12.088	<LOD-10.121	<LOD-1.535	<LOD
Detective rate (%)	80.0	90.0	25.0	0
Eggs ($n = 20$)				
Mean ($\mu\text{g}/\text{kg}$)	5.531	0.747	4.040	0.013
Range ($\mu\text{g}/\text{kg}$)	<LOD-28.720	<LOD-5.339	<LOD-67.831	<LOD-0.100
Detective rate (%)	90.0	90.0	30.0	10.0
Aquatic foods ($n = 20$)				
Mean ($\mu\text{g}/\text{kg}$)	3.302	1.635	0.653	0.016
Range ($\mu\text{g}/\text{kg}$)	<LOD-19.366	<LOD-9.127	<LOD-5.121	<LOD-0.121
Detective rate (%)	70.0	90.0	30.0	10.0
Milk ($n = 20$)				
Mean ($\mu\text{g}/\text{kg}$)	1.107	0.459	0.281	0.008
Range ($\mu\text{g}/\text{kg}$)	<LOD-4.390	0.324-1.217	<LOD-1.710	<LOD
Detective rate (%)	60.0	100.0	20.0	0
Vegetables ($n = 20$)				
Mean ($\mu\text{g}/\text{kg}$)	15.073	0.738	0.621	0.016
Range ($\mu\text{g}/\text{kg}$)	<LOD-29.966	<LOD-2.437	<LOD-2.997	<LOD – <LOQ
Detective rate (%)	70.0	80.0	40.0	45.0
Fruits ($n = 20$)				
Mean ($\mu\text{g}/\text{kg}$)	14.991	0.795	0.641	0.010
Range ($\mu\text{g}/\text{kg}$)	<LOD-26.420	<LOD-2.006	<LOD-8.572	<LOD – <LOQ
Detective rate (%)	80.0	95.0	25.0	10.0
Sugar ($n = 20$)				
Mean ($\mu\text{g}/\text{kg}$)	12.581	0.553	0.280	0.008
Range ($\mu\text{g}/\text{kg}$)	<LOQ-69.431	<LOD-2.633	<LOD-1.602	<LOD
Detective rate (%)	70.0	70.0	10.0	0
Beverages and water ($n = 20$)				
Mean ($\mu\text{g}/\text{L}$)	1.074	0.439	0.852	0.003
Range ($\mu\text{g}/\text{L}$)	<LOD-3.783	<LOD-8.560	<LOD-11.346	<LOD – <LOQ
Detective rate (%)	80.0	30.0	20.0	15.0
Alcoholic beverages ($n = 20$)				
Mean ($\mu\text{g}/\text{L}$)	1.498	0.006	0.109	0.002
Range ($\mu\text{g}/\text{L}$)	0.285-4.487	<LOD-0.029	<LOD-0.982	<LOD
Detective rate (%)	100.0	55.0	30.0	0

TABLE 2: Dietary exposure of EDCs in different gender and age groups (ng/kg bw/d).

	2-7 (all ^a)	8-12 (all)	13-19 (M ^b)	13-19 (F ^c)	20-50 (M)	20-50 (F)	51-65 (M)	51-65 (F)	>65 (M)	>65 (F)	Mean (>19, all)
BPA	403.672	331.271	321.082	269.759	199.489	218.320	208.380	221.212	178.440	179.890	200.955
BPS	52.112	42.755	40.622	37.975	26.146	27.365	26.159	26.737	22.463	21.372	25.040
BPF	50.507	41.661	39.707	38.501	24.918	26.478	25.144	25.869	21.374	20.641	24.071
BPAF	1.210	0.936	0.868	0.770	0.539	0.544	0.528	0.529	0.453	0.434	0.505
∑BPs	507.501	416.623	402.279	347.005	251.092	272.707	260.211	274.347	222.730	222.337	250.571

^aAll stands for male and female, ^bM stands for male; ^cF stands for female.

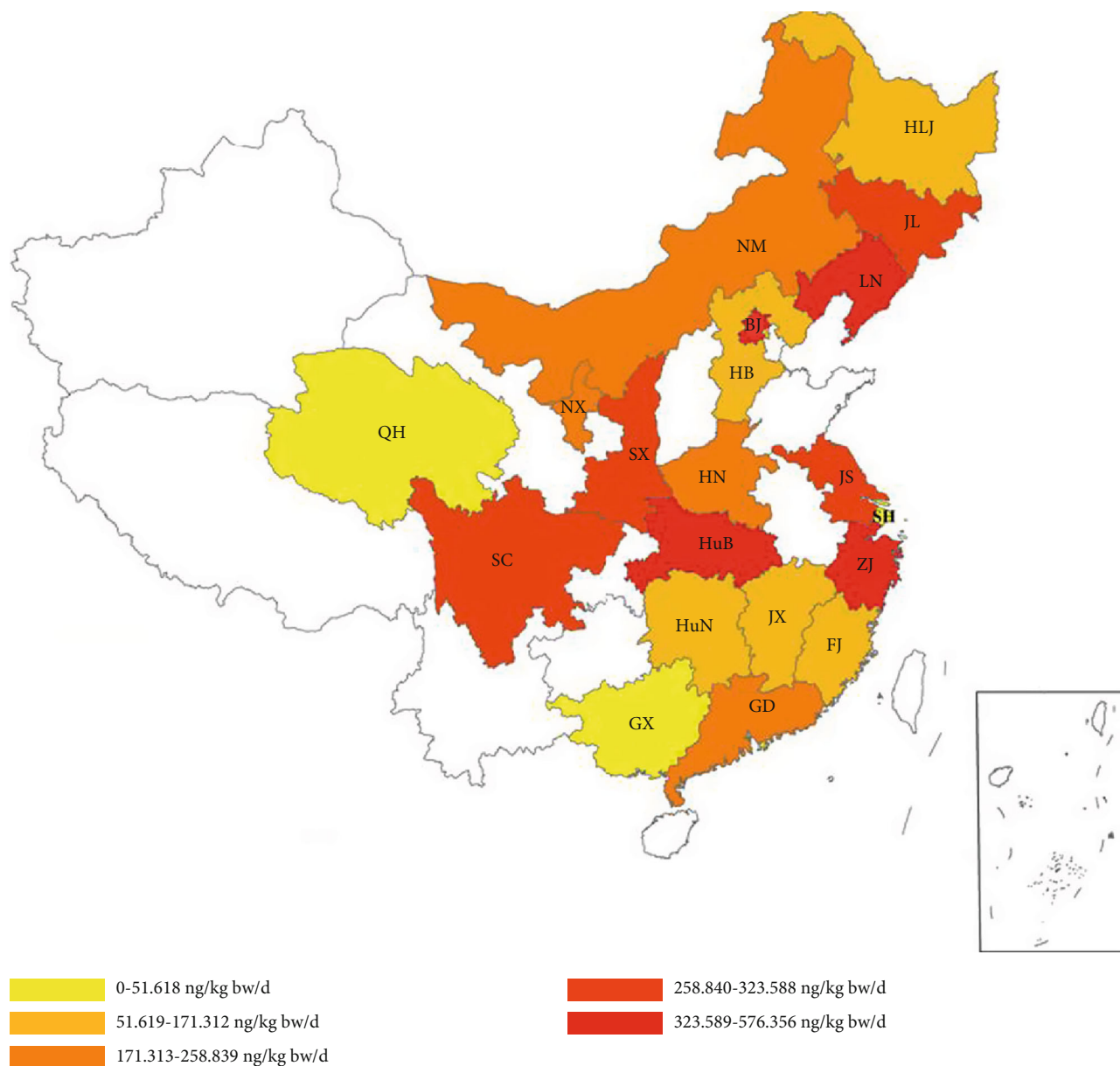
concentrations ranged from 0.815 to 15.073 $\mu\text{g}/\text{kg}$. The BPA concentration of sugar from LN province (69.431 $\mu\text{g}/\text{kg}$) were the highest in all the samples. In China, more than 90% of the sugar production was contributed by sugarcane [41]; the BPA-contaminated sugarcane in LN was extracted and concentrated during the production process leading to the high concentrations of BPA in sugar. Besides, alcoholic beverage samples were all found to be positive; this is due to the migration of BPA from the packaging material (glass bottle or plastic bottle) and the stopper of the glass bottle [42]. Compared to beverages and water, mean concentrations of BPA in alcoholic beverages was higher; it can be interpreted as the higher solubility of BPA in alcohol than in water. Increase levels of BPA was found when comparing with previous Chinese TDS in year 2007 [28]; it can be explained by the fact that growing demand of polycarbonates in consumer goods results in the increase use of BPA. The highest mean concentrations were found in vegetables (mean: 15.073 $\mu\text{g}/\text{kg}$) and fruits (mean: 14.991 $\mu\text{g}/\text{kg}$), followed by sugar (mean: 12.581 $\mu\text{g}/\text{kg}$), which may be due to its widespread presence as environmental contaminants or due to migration from food contact materials. BPA concentrations (1.074 $\mu\text{g}/\text{L}$) in beverages and water in China were consistent with those in Australia [43], French [44], and Portugal [45], but higher than those in Norway [13]. The mean levels of BPA in meat (2.756 $\mu\text{g}/\text{kg}$) and aquatic foods (3.302 $\mu\text{g}/\text{kg}$) are similar to those reported by Zhou et al. [25].

The overall detective rate of BPS was comparable with BPA. The highest BPS concentration (59.915 $\mu\text{g}/\text{kg}$) was detected in legumes and nuts from SX province. The highest mean concentration of BPS was also found in legumes and nuts (4.570 $\mu\text{g}/\text{kg}$), followed by meat (1.774 $\mu\text{g}/\text{kg}$) and aquatic foods (1.635 $\mu\text{g}/\text{kg}$). Compared with nonfat food, concentration of BPS in fat food showed higher levels. The similar trend was found in reports by Zhou et al. [25] and Liao and Kannan [24]. Except for the above three food items, levels of BPS in the rest of food items were significantly higher than those reported by Liao and Kannan [24]. It implies that BPS were increasingly used as a main substitute of BPA in China.

BPF also was detected in various food items (29.2% detective rate). The items of legumes and nuts and eggs contained high concentrations of BPF, and the overall mean concentrations in these two items were 5.248 and 4.040 $\mu\text{g}/\text{kg}$, respectively (Table 1). Mean concentration of BPF in 240 samples ranged from 0.109 to 5.248 $\mu\text{g}/\text{kg}$, which was consistent with those in 289 samples from China [24] and 267 samples from United States [46], respectively. The highest concentration of BPF (94.854 $\mu\text{g}/\text{kg}$) was detected in legumes and nuts from

HLJ province. The detective rate of BPAF was the lowest in 4 EDCs. It should be noticed that BPAF was frequently detected in cereals (70.0%) and legumes and nuts (80.0%). There is a conjecture to explain the high detective rates in these food items: crops may absorb and concentrate the BPF and BPAF from their growing environment, such as water, soil, air, and dust [25].

3.2. Dietary Intakes of EDCs. The previous studies [9, 44] indicated that dietary intakes of EDCs showed a decrease with the growth of the age. This study shows the same trend in Table 2. The highest and the lowest dietary intakes of each EDCs were in 2- to 7-year-old children and over 65-year-old elders, respectively. We found that there was almost no difference in the dietary intakes of BPA between genders. It should be noted that dietary intakes of people aged 2- to 19 year old (critical time of development) were obviously higher than that of aged above 19. When EDCs are present during development, there is now a growing probability that maternal, fetal, and childhood exposure to chemical pollutants play a larger role in the etiology of many endocrine diseases and disorders of the thyroid, immune, digestive, cardiovascular, reproductive, and metabolic systems [47]. These suggested that EDC exposure has greater impact on pre-teens than in adults [9]. Considering the similar structure and endocrine disrupting properties of BPA and other BPs, the exposure levels of all chemicals were summed up to assess the risks through dietary intake (Table 2); the combined exposure levels (222.337-507.501 ng/kg bw/d) were still below the t-TDI of BPA [19], which indicated the safety of BPA exposure. The exposure levels of BPA (178.440-403.672 ng/kg bw/d) was the highest, followed by BPS (21.372-52.112 ng/kg bw/d), BPF (20.641-50.507 ng/kg bw/d), and BPAF (0.434-1.210 ng/kg bw/d). The order was consistent with those of BPs which was conducted by Zhou et al. [25]. Large amounts of sewage sludge were applied as land every year, and plant-derived food could adsorb EDCs through leaves or roots from the land. Concentrations of EDCs in sewage sludge reported by Song et al. [48] in China were BPA (9.4 ng/g), BPS (4.3 ng/g), BPF (1.9 ng/g), and BPAF (0.4 ng/g); the order was the same as the exposure of EDCs in this study. However, the mean exposure of BPF reported by Liao and Kannan [24] was ca 10 times higher than that of BPS. It can be explained by the fact that the samples collected by Liao and Kannan were from nine cities in China; the dietary characteristics of residents in different cities were not fully considered. The intake of BPA in fifth Chinese TDS in this study (200.955 ng/kg bw/d, mean value for male and female above age of 19) was lower than those reported



(a)

FIGURE 1: Continued.

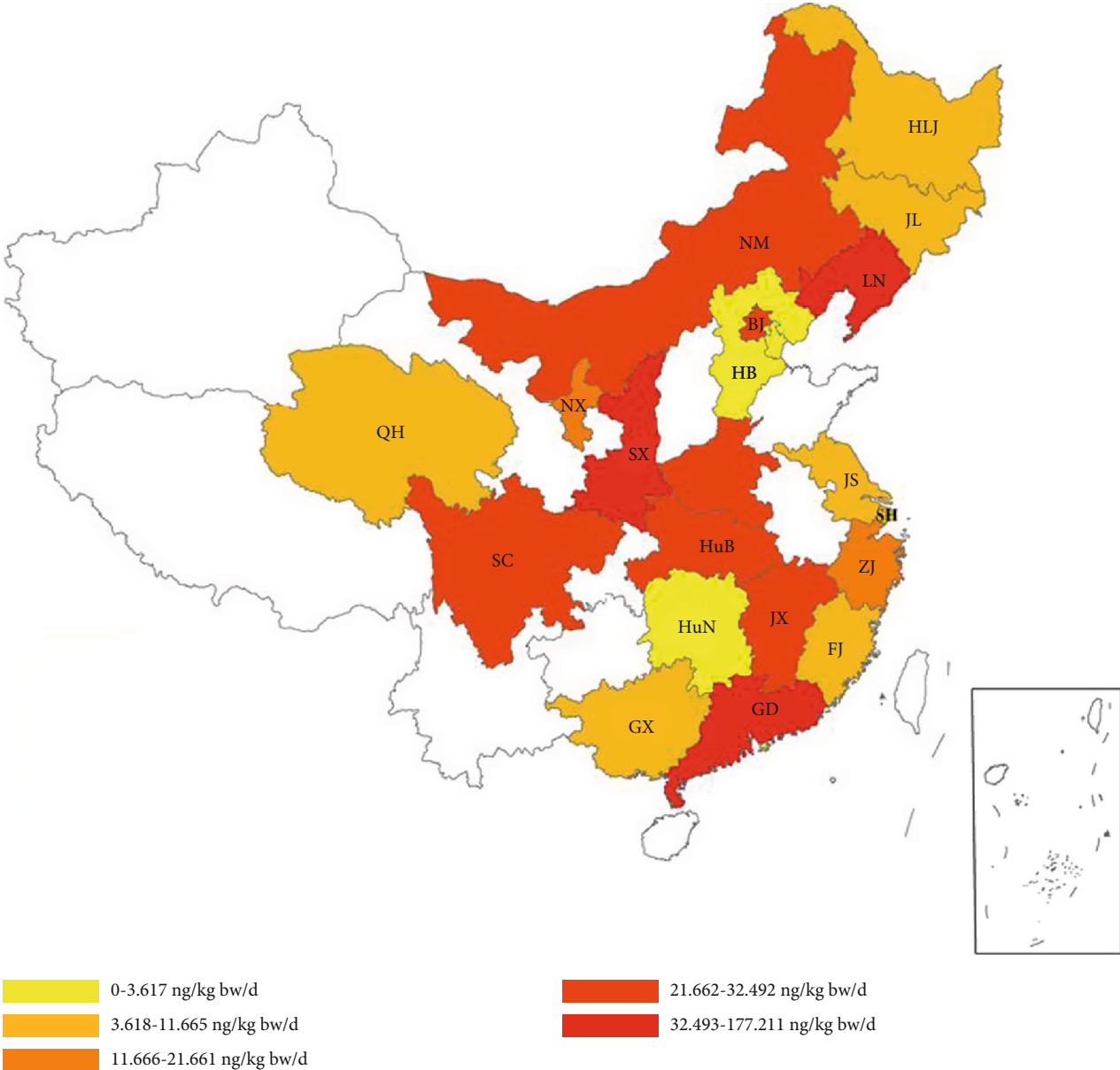
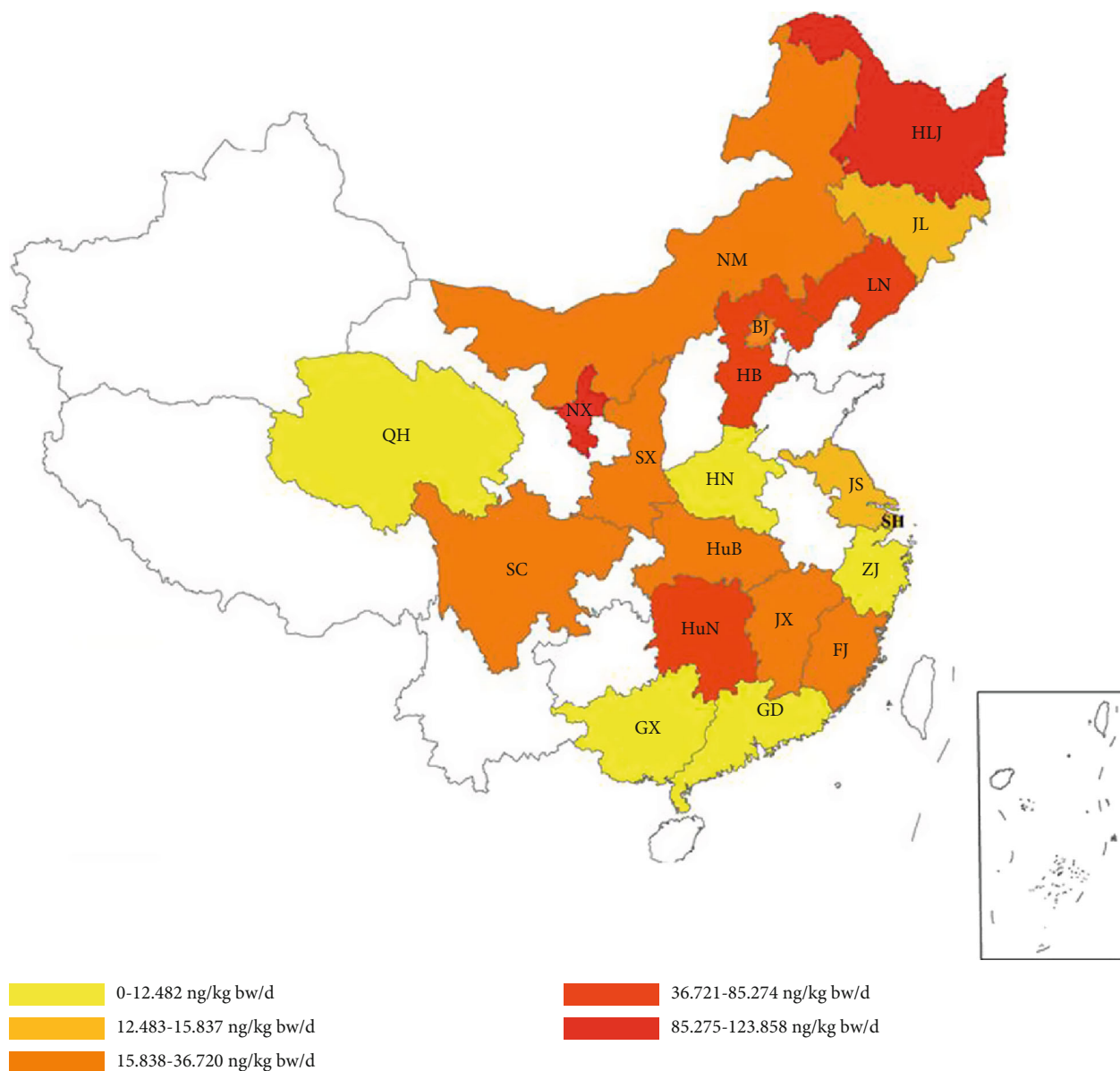


FIGURE 1: Continued.



(c)

FIGURE 1: Continued.

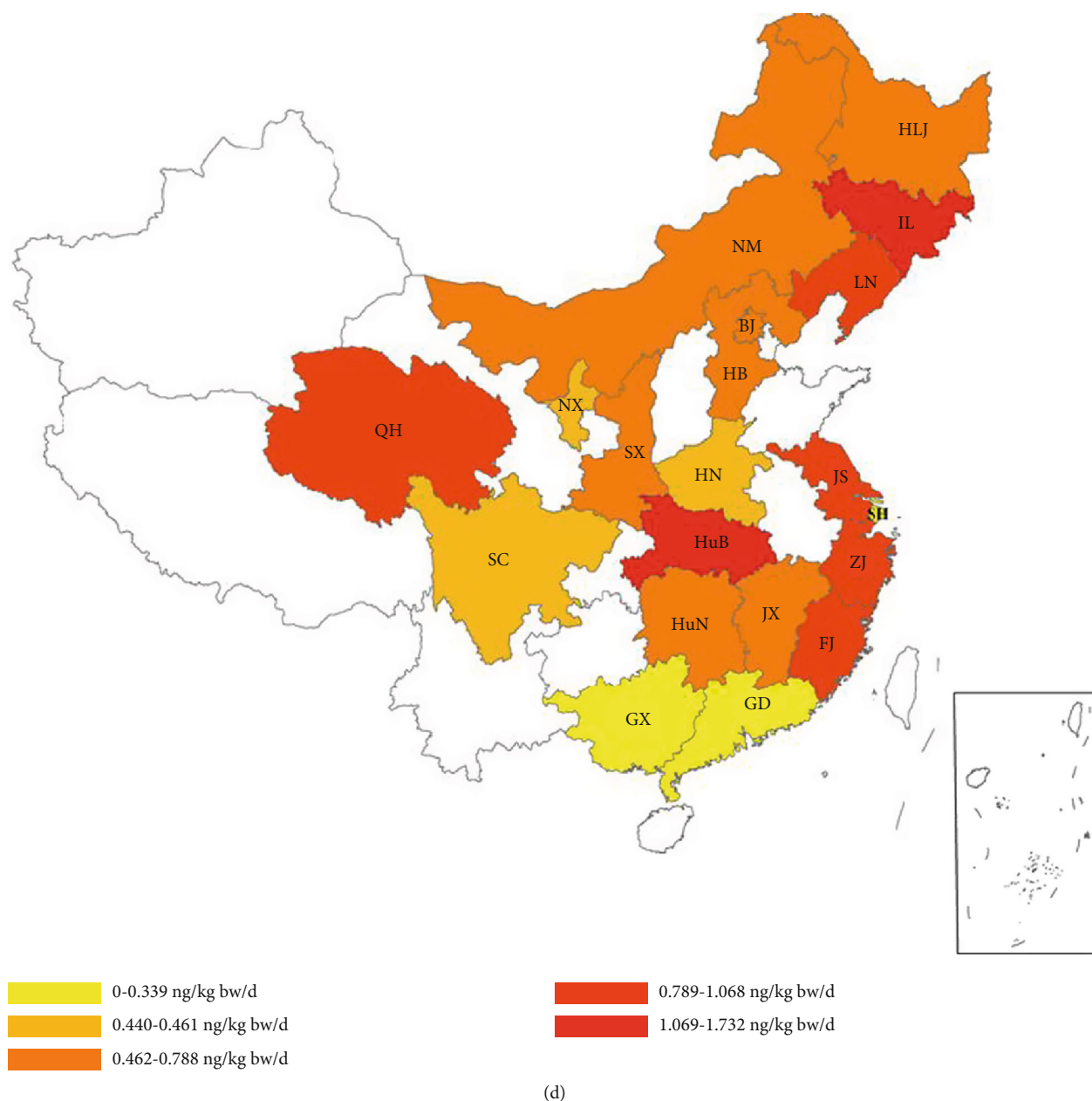
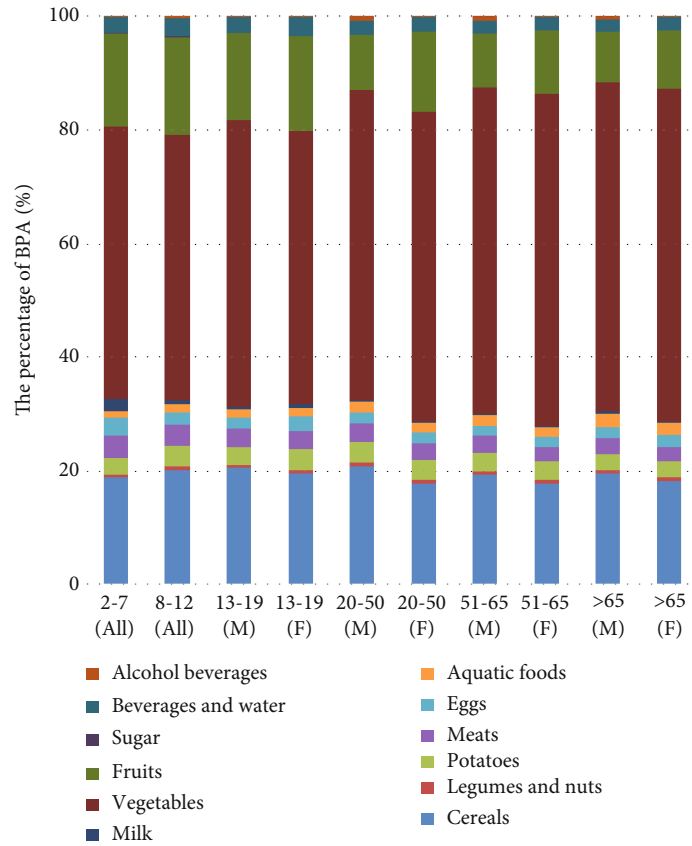


FIGURE 1: Dietary intakes of (a) BPA, (b) BPS, (c) BPF, and (d) BPAF among 20 provinces.

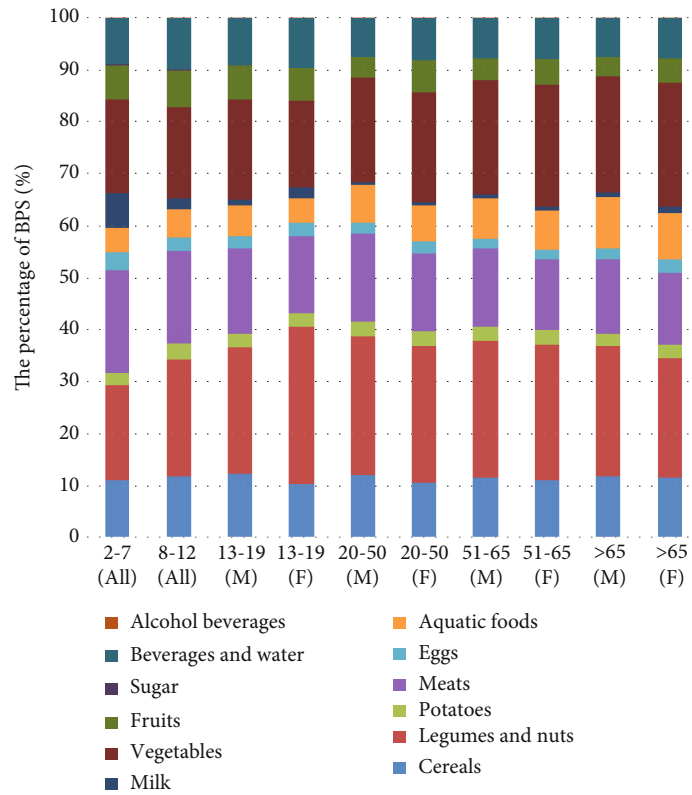
by Liao and Kannan [24], but higher than the fourth Chinese TDS by Niu et al. [28] and 2008 Canadian TDS by Cao et al. [29]. Compared to the TDS in China and Canada, the increase of BPA exposure in fifth Chinese TDS can be interpreted as rising consumption of BPA. It is reported that BPA consumption in China has increased 10-fold for 2000-2014, to ca. 3 million tonnes per year [49]. Intake of BPA in this study was in the range of those reported by the US National Toxicology Program [50] (8–1500 ng/kg bw/d) and was somewhat lower than those reported by the FAO&WHO [51] (400–1400 ng/kg bw/d) and EFSA [52] (1500 ng/kg bw/d). Difference in food habits may contribute to the high intakes of FAO and WHO and EFSA. Migration of BPA often occurs from epoxy can coatings to contents; canned food is largely consumed as the main part of the diet of people from many countries. It was reported that

Chinese ate only 1 kg of canned food per year, but European and American ate 50 and 90 kg per year, respectively [53].

The EDI of EDCs by the adult residents from 20 provinces were shown in Figure 1. The EDI of BPA was higher among the residents of the industrially developed provinces (JL, LN, JS, ZJ, HuB, SC, and SX) than among those of the other regions. The most likely causes of the above is that higher BPA consumptions of industries in these provinces contributes to the dietary intake. The EDI of BPS was higher in the North 2 and South 2 regions due to the high concentrations of BPS and high consumption of meat in these regions. The EDI of BPF in the north regions was higher than that of the south regions. The high dietary intake may be related to the consumption and concentrations of BPF in legumes and nuts and eggs. The EDI of BPAF among the southeast

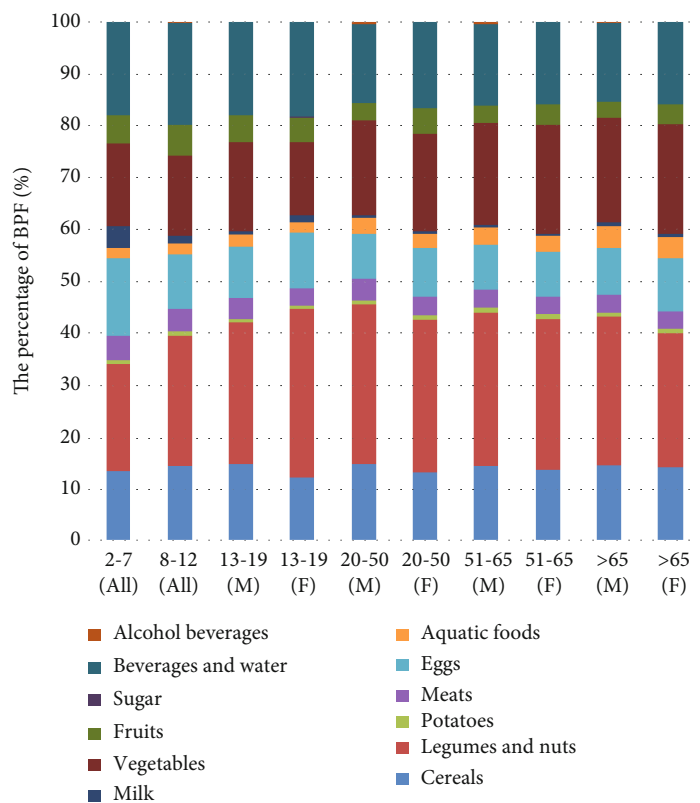


(a)

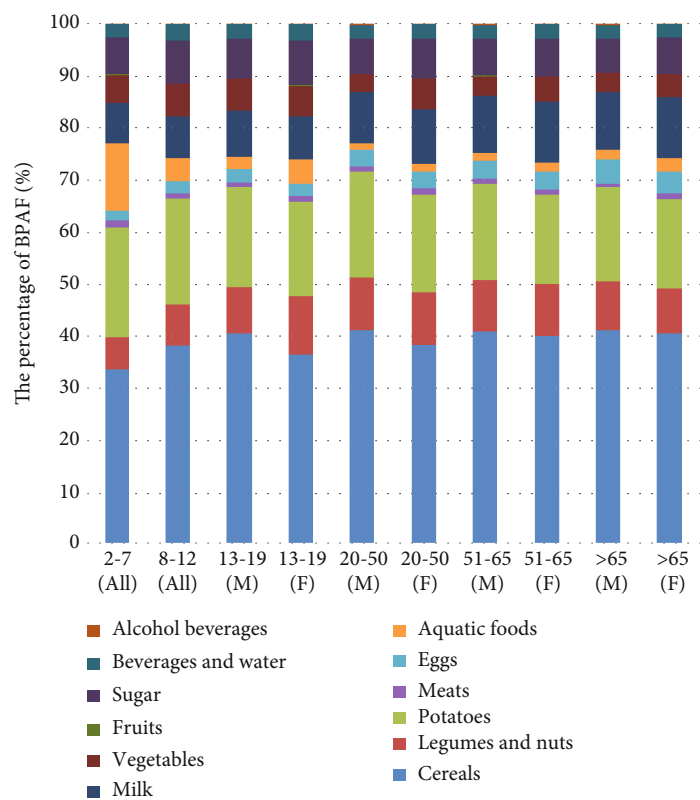


(b)

FIGURE 2: Continued.



(c)



(d)

FIGURE 2: Food items that contribute to total dietary exposure to (a) BPA, (b) BPS, (c) BPF, and (d) BPAF of the different age/gender groups.

of China (JL and LN), South I regions (JS, ZJ, and FJ), QH, and HuB shows high dietary intake; this may be explained by the fact that BPAF was used as important chemical raw materials in these industrial provinces.

BPA contributed to the majority of the total intakes of the EDCs, and the mean dietary exposure to other EDCs was as follows: BPS was 25.040 ng/kg bw/d for adult; this was followed by BPF (24.071 ng/kg bw/d), and BPAF (0.505 ng/kg bw/d), respectively. It was higher than those reported earlier (BPS, 1.310 ng/kg bw/d; BPF, 7.460 ng/kg bw/d; and BPAF, 0.275 ng/kg bw/d) [46]. What deserves our attention is the increasing dietary intakes of BPA, BPS, and BPF, while that of BPAF changed less than other EDCs. Because manufacturers have begun to apply BPS and BPF as BPA substitutes in consumer and commercial use, but BPA are still the predominant chemical used in plastics, food packaging, and other products [27].

The contribution of various food items to total dietary intake of BPA, BPS, BPF, and BPAF are shown in Figure 2 and showed small difference in all age and gender groups. For BPA, the main dietary contributors were vegetables (46.7%-58.4%), cereals (18.1%-21.1%), and fruits (8.9%-17.1%). The results were similar with Niu et al. [28]. For BPS, the main dietary contributors were legumes and nuts (18.4%-30.1%), vegetables (16.5%-23.8%), and meats (13.5%-19.7%). For BPF, the main dietary contributors were legumes and nuts (20.6%-32.3%), beverages and water (15.2%-19.8%), and vegetables (14.0%-21.2%). For BPAF, the main dietary contributors were cereals (33.7%-41.3%) and potatoes (17.1%-21.2%). As shown above, vegetables, cereals, and beverages and water contribute most of the EDC exposure, because these three food items are the major part of people's diet, where the daily consumption are higher than other food. It is important to note that legumes and nuts contribute a lot to the dietary intake of BPS and BPF though its dietary consumption and is not as many as vegetables, cereals, beverages and water. The explanation could be that the BPF is often used in industrial floors and food packaging [27].

4. Conclusion

This report surveyed the contamination levels of 5 kinds of EDCs in food samples from the fifth Chinese TDS and found they were detected with varying degrees. Among all the dietary samples, BPB was not found, and detective rates of BPA and BPS were more than 75.8%. The exposure levels of BPA (178.440-403.672 ng/kg bw/d) was the highest, followed by BPS (21.372-52.112 ng/kg bw/d), BPF (20.641-50.507 ng/kg bw/d), and BPAF (0.434-1.210 ng/kg bw/d). This result implied that though BPF has a low detective rate, BPS and BPF were used as main BPA alternatives. The dietary intake of BPA for Chinese people in different age or gender groups was below the TDI. Especially for the children aged 2-7 years old, dietary intakes of all the EDCs were nearly twice the value of people aged above 19 years old, which posed a potential threat to growth and development of children. Coexistence of BPs often happened in food; a mixture of BPs at lower concentration than BPs alone still had estrogen and antiandrogen activity [54]. Though TDI of BPS, BPF,

and BPAF have not been set by authorities yet, the health risk caused by the coexposure of BPs should not be overlooked.

Data Availability

The data used to support the findings of this study are available from the corresponding author upon request.

Conflicts of Interest

The authors declare that they have no known competing financial interests or personal relationships that could have appeared to influence the work reported in this paper.

Authors' Contributions

Kai Yao did the investigation, validation, writing of original draft, and writing-review and editing. Jing Zhang did the validation, writing of original draft, acquiring of software, and visualization. Jie Yin did the formal analysis and methodology. Yunfeng Zhao did the writing-review and editing and validation. Jianzhong Shen did the conceptualization and validation. Haiyang Jiang did the conceptualization and supervision. Bing Shao did the conceptualization, supervision, and funding acquisition.

Acknowledgments

This work was supported by a Program of the National Natural Science Foundation of China (U1736201) and National Key Research and Development Project of China (2018YFC1602406).

Supplementary Materials

Table S1: MS/MS parameters of the target compounds. Table S2: food consumption data (g/d) in different age and gender groups. Table S3: bodyweight of people in different age and gender groups. Table S4: water dilution coefficient of the food samples in 20 provinces (municipalities, autonomous regions). (*Supplementary Materials*)

References

- [1] S. Almeida, A. Raposo, M. Almeida-González, and C. Carrascosa, "Bisphenol A: food exposure and impact on human health," *Comprehensive Reviews in Food Science and Food Safety*, vol. 17, no. 6, pp. 1503–1517, 2018.
- [2] S. Lu, Y. Yu, L. Ren, X. Zhang, G. Liu, and Y. Yu, "Estimation of intake and uptake of bisphenols and triclosan from personal care products by dermal contact," *Science of The Total Environment*, vol. 621, pp. 1389–1396, 2018.
- [3] A. G. Asimakopoulos, M. Elangovan, and K. Kannan, "Migration of parabens, bisphenols, benzophenone-type UV filters, triclosan, and triclocarban from teethers and its implications for infant exposure," *Environmental Science & Technology*, vol. 50, no. 24, pp. 13539–13547, 2016.
- [4] Y. Liu, D. Wang, F. Du et al., "Dummy-template molecularly imprinted micro-solid-phase extraction coupled with high-performance liquid chromatography for bisphenol a determination in environmental water samples," *Microchemical Journal*, vol. 145, pp. 337–344, 2019.

- [5] X. Fan, C. Kubwabo, F. Wu, and P. E. Rasmussen, "Analysis of bisphenol a, alkylphenols, and alkylphenol ethoxylates in NIST SRM 2585 and indoor house dust by gas chromatography-tandem mass spectrometry (GC/MS/MS)," *Journal of AOAC International*, vol. 102, no. 1, pp. 246–254, 2019.
- [6] C. J. Hines, A. L. Christianson, M. V. Jackson et al., "An evaluation of the relationship among urine, air, and hand measures of exposure to bisphenol A (BPA) in US manufacturing workers," *Annals of Work Exposures and Health*, vol. 62, no. 7, pp. 840–851, 2018.
- [7] D. M. Goldinger, A.-L. Demierre, O. Zoller et al., "Endocrine activity of alternatives to BPA found in thermal paper in Switzerland," *Regulatory Toxicology and Pharmacology*, vol. 71, no. 3, pp. 453–462, 2015.
- [8] P. Gallo, I. di Marco Pisciotano, F. Esposito et al., "Determination of BPA, BPB, BPF, BADGE and BFDGE in canned energy drinks by molecularly imprinted polymer cleaning up and UPLC with fluorescence detection," *Food Chemistry*, vol. 220, pp. 406–412, 2017.
- [9] W. Chang, S. Liu, H. Chen, and C. Lee, "Dietary intake of 4-nonylphenol and bisphenol A in Taiwanese population: integrated risk assessment based on probabilistic and sensitive approach," *Environmental Pollution*, vol. 244, pp. 143–152, 2019.
- [10] W. Chen, Y. Shen, and S. Chen, "Assessing bisphenol A (BPA) exposure risk from long-term dietary intakes in Taiwan," *Science of The Total Environment*, vol. 543, pp. 140–146, 2016.
- [11] D. S. Lim, S. J. Kwack, K. Kim, H. S. Kim, and B. M. Lee, "Risk assessment of bisphenol A migrated from canned foods in Korea," *Journal of Toxicology and Environmental Health, Part A*, vol. 72, no. 21–22, pp. 1327–1335, 2009.
- [12] M. Lorber, A. Schecter, O. Paepke, W. Shropshire, K. Christensen, and L. Birnbaum, "Exposure assessment of adult intake of bisphenol A (BPA) with emphasis on canned food dietary exposures," *Environment International*, vol. 77, pp. 55–62, 2015.
- [13] A. K. Sakhi, I. T. L. Lillegaard, S. Voorspoels et al., "Concentrations of phthalates and bisphenol A in Norwegian foods and beverages and estimated dietary exposure in adults," *Environment International*, vol. 73, pp. 259–269, 2014.
- [14] S. Messinetti, S. Mercurio, and R. Pennati, "Bisphenol A affects neural development of the ascidian *Ciona robusta*," *Journal of Experimental Zoology Part A: Ecological and Integrative Physiology*, vol. 331, no. 1, pp. 5–16, 2019.
- [15] S. Lee, C. Kim, H. Shin, Y. Kho, and K. Choi, "Comparison of thyroid hormone disruption potentials by bisphenols A, S, F, and Z in embryo-larval zebrafish," *Chemosphere*, vol. 221, pp. 115–123, 2019.
- [16] L. V. Laing, J. Viana, E. L. Dempster et al., "Bisphenol A causes reproductive toxicity, decreases dnmt1 transcription, and reduces global DNA methylation in breeding zebrafish (*Danio rerio*)," *Epigenetics*, vol. 11, no. 7, pp. 526–538, 2016.
- [17] Z. Meng, S. Tian, J. Yan et al., "Effects of perinatal exposure to BPA, BPF and BPAF on liver function in male mouse offspring involving in oxidative damage and metabolic disorder," *Environmental Pollution*, vol. 247, pp. 935–943, 2019.
- [18] E. M. Rees Clayton, M. Todd, J. B. Dowd, and A. E. Aiello, "The impact of bisphenol A and triclosan on immune parameters in the U.S. population, NHANES 2003–2006," *Environmental Health Perspectives*, vol. 119, no. 3, pp. 390–396, 2011.
- [19] EFSA Panel on Food Contact Materials, Enzymes Flavourings and Processing, "Scientific opinion on the risks to public health related to the presence of bisphenol A (BPA) in foodstuffs," *EFSA Journal*, vol. 13, no. 1, p. 3978, 2015.
- [20] EPA, "Bisphenol A Action Plan," 2010, (CASRN 80-05-7).
- [21] KFDA, *Standard limits and regulations for utensils, containers, and packing materials*, Korea Food and Drug Administration, 2008, KFDA No. 2008-111.
- [22] K. Masuyama, "The amendment of the specification on plastic packages," *Japanese Food Sanitation Research*, vol. 44, pp. 9–27, 1994.
- [23] NHFPC, "No. 15 Decree of the ministry of health of the People's Republic of China," 2011.
- [24] C. Liao and K. Kannan, "A survey of bisphenol A and other bisphenol analogues in foodstuffs from nine cities in China," *Food Additives & Contaminants: Part A*, vol. 31, no. 2, pp. 319–329, 2014.
- [25] J. Zhou, X. Chen, S. Pan et al., "Contamination status of bisphenol A and its analogues (bisphenol S, F and B) in foodstuffs and the implications for dietary exposure on adult residents in Zhejiang Province," *Food Chemistry*, vol. 294, pp. 160–170, 2019.
- [26] M. Chen, M. Ike, and M. Fujita, "Acute toxicity, mutagenicity, and estrogenicity of bisphenol-A and other bisphenols," *Environmental Toxicology*, vol. 17, no. 1, pp. 80–86, 2002.
- [27] J. R. Rochester and A. L. Bolden, "Bisphenol S and F: a systematic review and comparison of the hormonal activity of bisphenol A substitutes," *Environmental Health Perspectives*, vol. 123, no. 7, pp. 643–650, 2015.
- [28] Y. Niu, J. Zhang, H. Duan, Y. Wuand, and B. Shao, "Bisphenol A and nonylphenol in foodstuffs: Chinese dietary exposure from the 2007 total diet study and infant health risk from formulas," *Food Chemistry*, vol. 167, pp. 320–325, 2015.
- [29] X. L. Cao, C. Perez-Locas, G. Dufresne et al., "Concentrations of bisphenol A in the composite food samples from the 2008 Canadian total diet study in Quebec City and dietary intake estimates," *Food Additives & Contaminants: Part A*, vol. 28, no. 6, pp. 791–798, 2011.
- [30] K. Yao, K. Wen, W. Shan et al., "Development of an immunoaffinity column for the highly sensitive analysis of bisphenol A in 14 kinds of foodstuffs using ultra-high-performance liquid chromatography tandem mass spectrometry," *Journal of Chromatography B*, vol. 1080, pp. 50–58, 2018.
- [31] K. Yao, K. Wen, W. Shan, H. Jiang, and B. Shao, "An immunoaffinity purification method for the simultaneous analysis of triclocarban and triclosan in foodstuffs by liquid chromatography tandem mass spectrometry," *Journal of Agricultural and Food Chemistry*, vol. 67, no. 32, pp. 9088–9095, 2019.
- [32] N. Salgueiro-González, E. Concha-Graña, I. Turnes-Carou, S. Muniategui-Lorenzo, P. López-Mahía, and D. Prada-Rodríguez, "Blank and sample handling troubleshooting in ultra-trace analysis of alkylphenols and bisphenol A by liquid chromatography tandem mass spectrometry," *Talanta*, vol. 101, pp. 413–419, 2012.
- [33] Y. Yang, Y. Yang, J. Zhang, B. Shao, and J. Yin, "Assessment of bisphenol A alternatives in paper products from the Chinese market and their dermal exposure in the general population," *Environmental Pollution*, vol. 244, pp. 238–246, 2019.
- [34] Y. Wu, Y. Zhao, and J. Li, *The Fifth China Total Diet Study*, Beijing: Science Press, 2018.

- [35] NHFPC, “No. 48 Decree of the ministry of health of the People’s Republic of China,” 1996.
- [36] NHFPC, “Report on the nutrition and chronic disease status of Chinese residents,” *Beijing: People’s Medical Publishing House*, pp. 20–21, 2015.
- [37] GEMS-Food, “Report on a workshop in the frame of Gems-Food Euro, EUR/HFA target 22,” in *Second workshop on reliable evaluation of low-level contamination of food*, Federal Republic of Germany, Kulmbach, 1995.
- [38] X. Cao, I. Kosarac, S. Popovic, S. Zhou, D. Smith, and R. Dabeka, “LC-MS/MS analysis of bisphenol S and five other bisphenols in total diet food samples,” *Food Additives & Contaminants: Part A*, vol. 36, no. 11, pp. 1740–1747, 2019.
- [39] Y. Niu, B. Wang, Y. Zhao, J. Zhang, and B. Shao, “Highly sensitive and high-throughput method for the analysis of bisphenol analogues and their halogenated derivatives in breast milk,” *Journal of Agricultural and Food Chemistry*, vol. 65, no. 48, pp. 10452–10463, 2017.
- [40] Y. Yang, J. Guan, J. Yin, B. Shao, and H. Li, “Urinary levels of bisphenol analogues in residents living near a manufacturing plant in South China,” *Chemosphere*, vol. 112, pp. 481–486, 2014.
- [41] M. Zhang and M. Govindaraju, “Sugarcane production in China,” *Sugarcane-Technology and Research*, vol. 49, 2018.
- [42] Z. Brenn-Struckhofova and M. Cichna-Markl, “Determination of bisphenol A in wine by sol-gel immunoaffinity chromatography, HPLC and fluorescence detection,” *Food Additives and Contaminants*, vol. 23, no. 11, pp. 1227–1235, 2006.
- [43] R. Braunrath, D. Podlipna, S. Padlesak, and M. Cichna-Markl, “Determination of bisphenol A in canned foods by immunoaffinity chromatography, HPLC, and fluorescence detection,” *Journal of Agricultural and Food Chemistry*, vol. 53, no. 23, pp. 8911–8917, 2005.
- [44] N. Bemrah, J. Jean, G. Rivière et al., “Assessment of dietary exposure to bisphenol A in the French population with a special focus on risk characterisation for pregnant French women,” *Food and Chemical Toxicology*, vol. 72, pp. 90–97, 2014.
- [45] S. C. Cunha, C. Almeida, E. Mendes, and J. O. Fernandes, “Simultaneous determination of bisphenol A and bisphenol B in beverages and powdered infant formula by dispersive liquid-liquid micro-extraction and heart-cutting multidimensional gas chromatography-mass spectrometry,” *Food Additives & Contaminants: Part A*, vol. 28, no. 4, pp. 513–526, 2011.
- [46] C. Liao and K. Kannan, “Concentrations and profiles of bisphenol A and other bisphenol analogues in foodstuffs from the United States and their implications for human exposure,” *Journal of Agricultural and Food Chemistry*, vol. 61, no. 19, pp. 4655–4662, 2013.
- [47] Å. Bergman, J. Heindel, S. Jobling, K. Kiddand, and R. T. Zoeller, “Chapter 1 what is endocrine disruption all about? State of the science of endocrine disrupting chemicals-2012,” in vol. 23, United Nations Environment Programme and the World Health Organization, 2013.
- [48] S. Song, M. Song, L. Zeng et al., “Occurrence and profiles of bisphenol analogues in municipal sewage sludge in China,” *Environmental Pollution*, vol. 186, pp. 14–19, 2014.
- [49] D. Jiang, W. Chen, X. Zeng, and L. Tang, “Dynamic stocks and flows analysis of bisphenol A (BPA) in China: 2000–2014,” *Environmental Science & Technology*, vol. 52, no. 6, pp. 3706–3715, 2018.
- [50] K. K. Rozman, J. Bhatia, A. M. Calafat et al., “NTP-CERHR expert panel report on the reproductive and developmental toxicity of genistein,” *Birth Defects Research Part B: Developmental and Reproductive Toxicology*, vol. 77, no. 6, pp. 485–638, 2006.
- [51] FAO and WHO, *Joint FAO/WHO expert meeting to review toxicological and health aspects of bisphenol A: final report, including report of stakeholder meeting on bisphenol A*, Ottawa, Canada, 2010.
- [52] EFSA, “Opinion of the scientific panel on food additives, flavourings, processing aids and materials in contact with food (AFC) related to 2,2-bis(4-hydroxyphenyl) propane,” *EFSA Journal*, vol. 5, no. 1, p. 428, 2007.
- [53] X. Yu, “Present status and development countermeasure on canned food industry,” *FOOD MACHINERY*, vol. 1, pp. 4–8, 2002.
- [54] C. Park, H. Song, J. Choi et al., “The mixture effects of bisphenol derivatives on estrogen receptor and androgen receptor,” *Environmental Pollution*, vol. 260, pp. 114036–114045, 2020.

Research Article

Differences in the Hemolytic Behavior of Two Isomers in *Ophiopogon japonicus* *In Vitro* and *In Vivo* and Their Risk Warnings

Huan-Hua Xu ^{1,2}, Zhen-Hong Jiang,³ Yu-Ting Sun,² Li-Zhen Qiu,^{1,2} Long-Long Xu,^{2,4} Xiang-Lin Tang,² Zeng-Chun Ma,² and Yue Gao ^{1,2}

¹Tianjin University of Traditional Chinese Medicine, Tianjin 300193, China

²Department of Pharmaceutical Sciences, Beijing Institute of Radiation Medicine, Beijing 100850, China

³Jiangxi Province Key Laboratory of Molecular Medicine, Nanchang 330006, China

⁴College of Life Science and Bioengineering, Beijing University of Technology, Beijing 100124, China

Correspondence should be addressed to Yue Gao; gaoyue@bmi.ac.cn

Received 21 September 2020; Revised 25 November 2020; Accepted 2 December 2020; Published 15 December 2020

Academic Editor: Si Qin

Copyright © 2020 Huan-Hua Xu et al. This is an open access article distributed under the Creative Commons Attribution License, which permits unrestricted use, distribution, and reproduction in any medium, provided the original work is properly cited.

Ophiopogonin D (OPD) and Ophiopogonin D' (OPD') are two bioactive ingredients in *Ophiopogon japonicus*. Previously published studies have often focused on the therapeutic effects related to OPD's antioxidant capacity but underestimated the cytotoxicity-related side effects of OPD', which may result in unpredictable risks. In this study, we reported another side effect of OPD', hemolysis, and what was unexpected was that this side effect also appeared with OPD. Although hemolysis effects for saponins are familiar to researchers, the hemolytic behavior of OPD or OPD' and the interactions between these two isomers are unique. Therefore, we investigated the effects of OPD and OPD' alone or in combination on the hemolytic behavior *in vitro* and *in vivo* and adopted chemical compatibility and proteomics methods to explain the potential mechanism. Meanwhile, to explain the drug-drug interactions (DDIs), molecular modeling was applied to explore the possible common targets. In this study, we reported that OPD' caused hemolysis both *in vitro* and *in vivo*, while OPD only caused hemolysis *in vivo*. We clarified the differences and DDIs in the hemolytic behavior of the two isomers. An analysis of the underlying mechanism governing this phenomenon showed that hemolysis caused by OPD or OPD' was related to the destruction of the redox balance of erythrocytes. *In vivo*, in addition to the redox imbalance, the proteomics data demonstrated that lipid metabolic disorders and mitochondrial energy metabolism are extensively involved by hemolysis. We provided a comprehensive description of the hemolysis of two isomers in *Ophiopogon japonicus*, and risk warnings related to hemolysis were presented. Our research also provided a positive reference for the development and further research of such bioactive components.

1. Introduction

Hemolysis is the rupturing of erythrocytes and the release of their contents into the surrounding fluid. Hemolysis may occur *in vivo* or *in vitro*. Many factors can cause hemolysis, such as intrinsic causes (i.e., defects in the red blood cell (RBC) membrane, defects in hemoglobin [1], defective erythrocyte metabolism [2], Marchiafava-Micheli syndrome [3], etc.) and extrinsic causes (i.e., immune-mediated causes [4], toxicants or chemical reagents, phys-

ical factors [5], etc.). Regardless of intrinsic or extrinsic causes, disrupted redox balance is one of the common causes of hemolysis. The RBCs, in addition to their primary role as oxygen carriers, function as redox modulators [6]. However, this modulation ability is limited. Instead, mature erythrocytes, with their absence of protein synthesis and high oxygen-carrying capacity, are particularly susceptible to oxidative damage because they are rich in heme iron and oxygen, which can spontaneously generate H₂O₂ and lipid peroxides [7, 8].

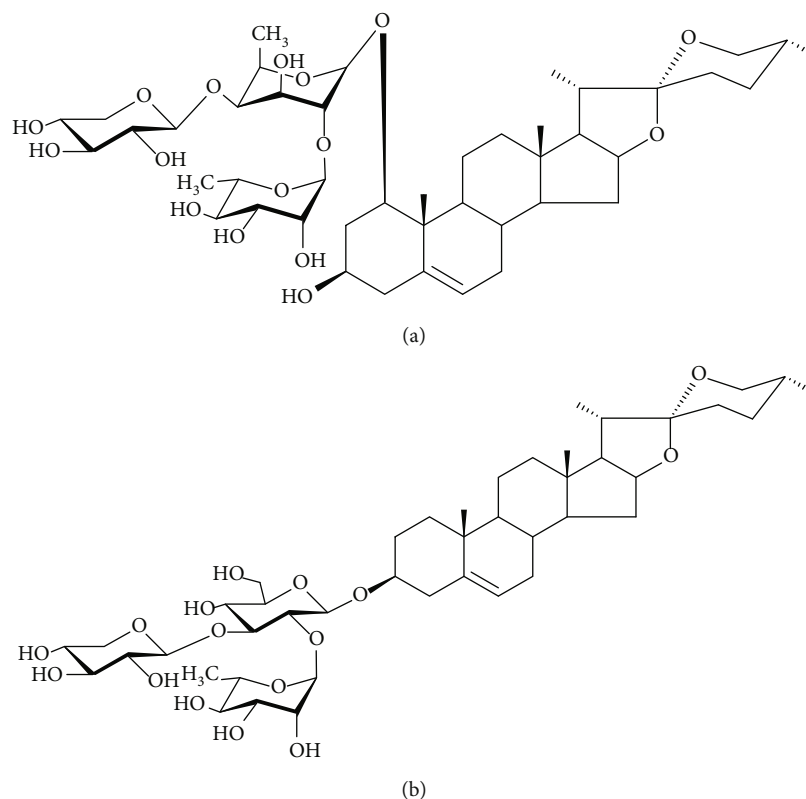


FIGURE 1: The chemical structure of Ophiopogonin D (OPD) and Ophiopogonin D' (OPD'). (a) Ophiopogonin D: ruscogenin 3-O- $\{\alpha$ -L-rhamnopyranosyl (1 \rightarrow 2)- $\{\beta$ -D-xylopyranosyl (1 \rightarrow 3)- β -D-fucopyranoside}. (b) Ophiopogonin D': diosgenin 3-O- $\{\alpha$ -L-rhamnopyranosyl (1 \rightarrow 2)- $\{\beta$ -D-xylopyranosyl (1 \rightarrow 3)- β -D-glucopyranoside}. Chemical formula: $C_{44}H_{70}O_{16}$, MW = 854.

Ophiopogon japonicus (Thunb.) is a well-known traditional Chinese medicine used to treat cardiovascular and chronic inflammatory diseases [9, 10]. Although it is not included in the medicinal and food dual-use list announced by the National Health Commission of the People's Republic of China, it is allowed to be used in functional foods [11], and in southern provinces of China, *Ophiopogon japonicus* is often used in dietary soups [12]. OPD and OPD' are two bioactive ingredients in *Ophiopogon japonicus*, and they are isomers of each other (see Figure 1). Previously, published literature on the active monomers in *Ophiopogon japonicus* mostly focused on OPD and its antioxidant effect [13–16]. Since 2017, the literature related to OPD' has gradually increased and is almost all related to its cytotoxicity [17]. Our mentor's team reported for the first time that OPD' at a concentration greater than $5 \mu\text{mol/L}$ can promote H9C2 cell apoptosis through the endoplasmic reticulum stress pathway [18]. Based on its cytotoxic effect, Zongliang et al. [19, 20] developed it as a potential antiproliferative cancer agent. However, with the deepening of our studies, we found that the cytotoxicity or other properties, such as the hemolytic properties that we discovered and reported in this manuscript, of OPD' limit its druggability. Moreover, in this manuscript, we reported that OPD, as an antioxidant, could also cause hemolysis *in vivo*. Despite extensive studies, a comprehensive analysis of hemolysis and drug-drug interactions (DDIs) between OPD and OPD' is missing, limiting our abil-

ity to assess the risks of medicines, functional foods, and diets containing *Ophiopogon japonicus*. Previous profiling studies lacked hemolysis, which necessarily underestimates its adverse effect and restricts analysis in a hemolysis-biased manner.

In this study, we investigated the effects of OPD and OPD' alone or in combination on the hemolytic behavior *in vitro* and *in vivo*. We identified that there is a huge difference in the hemolysis behavior between OPD and OPD' and clarified the specific manifestations of the behavior. We further adopted chemical compatibility and multiomics (i.e., metabolomics, lipidomics, and proteomics) methods to explain the different hemolytic behaviors *in vitro* and *in vivo*, and we found that both *in vitro* and *in vivo*, redox imbalance and lipid metabolism disorders played an important role in the hemolysis process. We also inferred that the DDIs between OPD and OPD' are not limited to the complementarity of physical and chemical properties, and a competitive target related to hemolysis may also exist. Therefore, molecular modeling technology was used to find the common target of the two isomers.

2. Materials and Methods

2.1. Drugs and Reagents. OPD (F05975, purity: 98% by HPLC) and OPD' (F581298, purity: 98% by HPLC) were purchased from the Shanghai EFE Biotechnology Co., Ltd. (Shanghai, China). Streptavidin PE conjugate (12-4317-87)

was purchased from Thermo Fisher. Biotinamido hexanoic acid N-hydroxysuccinimide ester (B2643, purity $\geq 98\%$, powder) was purchased from Sigma-Aldrich. 1,1-Diphenyl-2-trinitrophenylhydrazine (DPPH) was purchased from the Tokyo Chemical Industry Co., Ltd. (batch number: 217-591-8). Trolox (Lot No.1218C026, purity: not less than 50%) was purchased from the Solarbio Co., Ltd. (Beijing, China). Water was prepared by double distillation. All other reagents were of analytical or HPLC grade. Water, methanol, acetonitrile, and formic acid were purchased from the Sino-pharm Chemical Reagent Co., Ltd. (Beijing, China) and CNW Technologies GmbH (Düsseldorf, Germany).

2.2. Animals, Animal Management, and Experimental Design. The erythrocyte suspensions used in the *in vitro* hemolysis test were collected from New Zealand white rabbits purchased from the Beijing Jinmuyang Laboratory Animal Breeding Co., Ltd. (production license: SCXK (Jing)-2015-0005). An *in vivo* hemolysis study was conducted in apparently healthy adult KM mice (18–20 g, male). Animals were purchased from the Beijing Keyu Animal Breeding Center (production license: SCXK (Jing)-2018-0010). The animals used in the multiomics research were Wistar rats that were purchased from the Beijing Vital River Laboratory Animal Technology Co. Ltd. (production license: SCXK (Jing)-2016-0011). All animals were housed in an environmentally controlled breeding room (temperature: $22 \pm 2^\circ\text{C}$, humidity: $50 \pm 5\%$, dark/light cycle: 12/12 h). The animals were provided with standard laboratory food and water. The rabbits were raised in a single cage, and 3 mice and rats were raised per cage. During the experiment, the animals had free access to food and water [21, 22]. The experimental protocols were approved by the Animal Ethics Committee of Academy of Military Medical Sciences (approval No. IACUC-DWZX-2020-684) and were performed in accordance with the guidelines of the National Institutes of Health for the Care and Use of Laboratory Animals. Prior to each experiment, all animals were kept under laboratory conditions for a period of 4 days or more for acclimatization. Since there are multiple independent animal experiments, the experimental design is described in detail under their respective experimental items, such as in Sections 2.3, 2.6, and 2.7.

2.3. In Vitro Hemolysis Test. The *in vitro* hemolysis test referred to the “Technical Guidelines for the Study of Stimulating and Hemolytic Properties of Traditional Chinese Medicines and Natural Medicines” issued by the State Food and Drug Administration in 2005 (Guideline number: [Z]-GPT4-1). Four groups were designed to investigate whether OPD and OPD' exhibit drug-drug interactions in hemolytic behavior. They were the OPD group, OPD' group, OPD+OPD' group (premixed before administration), and OPD \rightarrow OPD' group (based on the isomers' physical and chemical properties, considering whether preadministration has a protective effect, we set the OPD \rightarrow OPD' group, in which OPD and OPD' were used in sequence, 5 min apart). The concentrations of OPD and OPD' in each group were 0, 5, 10, 20, and 40 $\mu\text{g}/\text{mL}$. After each group of samples were prepared

according to the guidelines, they were immediately placed in a $37 \pm 0.5^\circ\text{C}$ water bath for 3 h, removed, and centrifuged at 3000 rpm for 5 min, and the supernatant was transferred to a 24-well plate. An ultraviolet spectrophotometer was used to measure the absorbance of each group of samples at 570 nm, calculate the hemolysis rate, and draw the hemolysis rate-concentration curve.

One of the difficulties in the study of active monomers of traditional Chinese medicine is poor water solubility, resulting in dose deviation and inaccurate concentration. Both of OPD and OPD' suffered from this problem, and our pilot studies have shown that 25% methanol in saline as the solvent can not only completely dissolve OPD and OPD' but is also safe for RBCs within 4 h of *in vitro* hemolysis experiments. Compared with other solvents, there were no dose deviations, and the results were extrapolated to be more credible clinically.

2.4. Effects of Different Solvents or Compatible Drugs on the Hemolytic Behavior of OPD'. To investigate the effects of commonly used clinical solvents on OPD' hemolytic behavior, saline, glucose (5%), fructose (10%), and mannitol (20%) were selected to dilute the OPD' stock liquid, in which OPD' was completely dissolved in methanol (25%), to the following series of concentrations 5, 10, 20, 40, and 80 $\mu\text{g}/\text{mL}$. The hemolysis rate of each sample was determined according to the guidelines, and the hemolysis rate-concentration curve was drawn.

Trolox is a reductive water-soluble vitamin E that protects RBCs from hemolysis due to its oxidative properties. Investigating the effect of the combined use of Trolox and OPD' on the hemolytic behavior of OPD' was helpful to explore the reasons for the difference in the hemolytic behavior of the two isomers *in vitro*. OPD' (40 $\mu\text{g}/\text{mL}$) was selected as the positive control; at this concentration, the hemolysis rate of RBCs *in vitro* was almost 100%. The concentration of OPD' was fixed and mixed with different concentrations of Trolox solution, and then, the relationship between the change in the hemolysis rate and the concentration of Trolox was revealed. In addition, in the *in vitro* hemolysis test, we discovered that the OPD \rightarrow OPD' group also exhibited drug-drug interactions. Here, we applied the same procedure as with Trolox to further explore the effect of OPD on OPD'-induced hemolysis.

2.5. Reasonable Explanation of the Different Hemolytic Behaviors of OPD' and OPD In Vitro

2.5.1. DPPH Method for the Determination of the Antioxidizability of OPD and OPD'. The DPPH method [23] was first proposed in 1958 and can be used to determine the antioxidant capacity of biological samples *in vitro*. In this study, it was used to investigate whether the difference in the hemolytic behavior between the two isomers is related to the oxidizability and reducibility.

2 mL of 5, 10, 20, and 40 $\mu\text{g}/\text{mL}$ OPD and OPD' samples was added to 5 tubes, followed by the addition of 4 mL of 24 mg/L DPPH ethanol (95%) solution under dark

conditions and shaking. After avoiding light at room temperature for 30 min, UV-visible spectrophotometry was used to measure the absorbance (A_i) at 517 nm. The same amount of DPPH ethanol (95%) without sample extract was used as the control group, and the absorbance (A_0) of the control group was measured by the same method. Equation (1) was used to calculate the inhibition rate, which represents the antioxidant capacity, and the greater the inhibition rate, the stronger the antioxidant capacity.

$$\text{Inhibition rate} = \frac{A_0 - A_i}{A_0} \times 100\%. \quad (1)$$

2.5.2. Effect of OPD' Alone or in Combination with OPD on the SOD, MDA, LDH, GSH, and Na⁺-K⁺-ATPase Content. The experiment was divided into 3 groups: normal control group (NC), OPD' group, and OPD→OPD' group (OPD and OPD' were used in sequence 5 min apart). To a 10 mL test tube, 2.5 mL of RBC suspension (20%) and then 2.5 mL of test drugs in different groups were added in turn, with the same volume of solvent added for the control in the NC group. After careful mixing, the mixture was placed in a 37°C constant temperature water bath and incubated for 4 h. After incubation, the test tubes were carefully removed and centrifuged at 1500 rpm (4°C) for 10 min. The supernatant was discarded with a disposable pipette, and 0.2 mL of the lower layer of the RBC pellet was taken for counting cells, to which 3 mL of prechilled purified water was added, followed by mixing and shaking to fully lyse the RBCs. Then, it was stored at 4°C until use. The ELISA kit instructions were followed to determine lactate dehydrogenase (LDH) enzyme activity and the contents of malondialdehyde (MDA), superoxide dismutase (SOD), glutathione (GSH), and Na⁺-K⁺-ATPase in the cytoplasm of each group of erythrocytes [24, 25].

2.6. In Vivo Hemolysis Test. Biotin labeling, as an alternative nonradioactive approach for the determination of RBC survival, is widely accepted [26, 27]. In this study, 30 mg/kg biotinamido hexanoic acid N-hydroxysuccinimide ester solution was injected via the tail vein to label RBCs. After 1 h, to determine the efficiency of biotin labeling, blood samples were collected from each animal, and streptavidin PE conjugate was used to bind biotin, which was used to label RBCs for flow cytometric analysis. Animals with a labeling efficiency greater than or equal to 95% were selected for RBC lifespan analysis.

Fifteen mice were randomly assigned to 3 groups: normal control group (NC), OPD group, and OPD' group. According to the limit of the clinical hemolysis rate (5%) and the results obtained from the *in vitro* hemolysis test, the plasma concentration of OPD' should not exceed 5 μg/mL. The doses of OPD and OPD' in each group were defined as 0.25 mg/kg; at this dose, the configuration of the drug was free of organic reagents. All drugs were administered by intravascular injection for 30 days. Changes in the percentage of labeled RBCs with the administration time can be used to estimate the RBC lifespan. The first blood sample analysis

should be completed within 3 days after administration, and the subsequent analysis interval was based on the first analysis results, but did not exceed 7 days.

2.7. Proteomics Methods to Explore the Potential Mechanism of OPD- and OPD'-Induced Hemolysis In Vivo. Twenty-two rats were randomly assigned to 3 groups: the normal control group (NC, $n = 6$), OPD group ($n = 8$), and OPD' group ($n = 8$). All drugs were administered by intravascular injection for 14 days. According to the limit of the clinical hemolysis rate (5%) and the results obtained from the *in vitro* hemolysis test, the doses of OPD and OPD' in each group were defined as 0.25 mg/kg. Plasma was prepared by centrifugation for metabolomics and lipidomics analysis. Both metabolomics and lipidomics analyses were performed on a UPLC-MS/MS system tandem with different mass spectrometers and separated under different LC conditions (unpublished manuscript).

At the same time, the nonanticoagulated whole blood of each group was prepared into RBC suspensions according to the guidelines (Guideline number: [Z]-GPT4-1). Subsequently, pure water was added to fully lyse the RBC membrane, followed by centrifugation. The supernatant was discarded, and the precipitate was washed 2-3 times repeatedly. Then, the precipitate was the prepared blood ghost, i.e., the RBC membrane. Fifty microliters of sample lysate was added, and then, protease inhibitor PMSF was added to make the final concentration 1 mM. The solution was then boiled for 10 min and centrifuged at 12000 g for 10 min at room temperature. The supernatant was centrifuged again, and the supernatant is the total protein solution of the sample, with the protein concentration determined by the BCA method. After protein quantification, 100 μg of each sample was placed into a 10 K ultrafiltration tube, and the filter-aided sample preparation (FASP) method [28] was used to enzymatically digest the protein. For tandem mass tag (TMT) labeling, 41 μL of anhydrous acetonitrile was added to a TMT⁶ [29] reagent vial at room temperature. The reagents were dissolved for 5 min and centrifuged. Then, 41 μL of the TMT⁶ label reagent was added to each 100 μL sample for mixing. The tubes were incubated at room temperature for 1 h. Finally, 8 μL of 5% hydroxylamine was added to each sample and incubated for 15 min to terminate the reaction. The prepared sample was first separated by reverse-phase chromatographic separation, and the sample in the period of 8-60 min was collected. Then, the collected samples were further separated by a HPLC system and detected by mass spectrometry. The data were analyzed by Proteome Discoverer™ software (Version 2.2, Thermo, USA), and the databases utilized were UniProt-proteome_UP000002494-Rattus norvegicus (Rat) (Strain Brown Norway). Detailed proteomic analysis methods can be seen in the supplementary materials (see Method S1).

2.8. Molecular Modeling to Find the Common Hemolysis Target of OPD and OPD'. The bioassay of OPD' and OPD indicates that they will result in hemolysis *in vitro* and *in vivo*. To predict the putative targets and conduct pathway enrichment analysis for OPD' and OPD, the targets

associated with hemolysis were collected from famous databases such as UniProt. Putative target prediction was based on the SEA (similarity ensemble approach) [30] approach. This method is based on the molecular fingerprint to calculate the similarity between the query molecule and the corresponding ligand molecule in the target database. ChEMBL17 was used as the target database. RDKit ECFP4 (1024 bits) was used as the molecular fingerprint. Pharmaceutical target seeker (PTS) [31] was used as a shape-based approach. In PTS, the weighted Gaussian algorithm (WEGA) [32], which is based on molecular three-dimensional conformation superposition, was used to calculate the 3D similarity between the query molecule and the corresponding ligand molecule in the target database. The Reactome Pathway Database (<https://reactome.org>) was used for pathway analysis for the predicted potential targets of OPD' and OPD.

2.9. Statistical Analysis. SAS version 9.1 (SAS Inc. USA) was used to perform the statistical analyses. All data are expressed as the mean \pm SD. For comparisons between two groups, Student's *t*-test was used. For comparisons among three or more groups, the data were analyzed using a one-way analysis of variance (ANOVA). For all analyses, a *p* value of <0.05 was considered to indicate statistical significance and a *p* value of <0.01 was considered to indicate extreme statistical significance. GraphPad Prism (version 6.0) was used to draw the statistical figures.

3. Results and Discussion

3.1. In Vitro Hemolytic Behavior of OPD and OPD' Is Inconsistent. The hemolytic behaviors of the 4 test groups (i.e., OPD, OPD', OPD \rightarrow OPD', and OPD+OPD') are presented in Figure 2. The curve shows that OPD has no erythrocyte hemolysis in the concentration range of 0-40 $\mu\text{g}/\text{mL}$. In contrast, the RBCs were rapidly hemolyzed within 15 min after the administration of OPD', and the hemolysis rate was linearly related to the concentration of OPD'. According to the clinical guidelines, the unacceptable hemolysis rate is 5% (Guideline number: [Z]-GPT4-1); therefore, the concentration of OPD' should not exceed 5 $\mu\text{g}/\text{mL}$. More interesting data came from the other two groups, and the hemolytic behavior of OPD' was weak when OPD and OPD' were used in sequence (group OPD \rightarrow OPD'). At a concentration of 20 $\mu\text{g}/\text{mL}$, the hemolysis rate of the OPD' group was approximately 10% lower than that of the OPD+OPD' group. However, the OPD \rightarrow OPD' group's data suggest that OPD plays a role in protecting erythrocytes from being destroyed by OPD'. Obviously, the hemolytic behavior of each group is inconsistent, which provides much evidence for subsequent research.

3.2. Different Solvents or Compatible Drugs Affect the Hemolytic Behavior of OPD' In Vitro. The research results have shown that different solvents or compatible drugs have a significant effect on OPD'-induced hemolysis. As shown in Figure 3(a), compared with saline, glucose (5%), fructose (10%), and mannitol (20%) alleviated hemolysis caused by

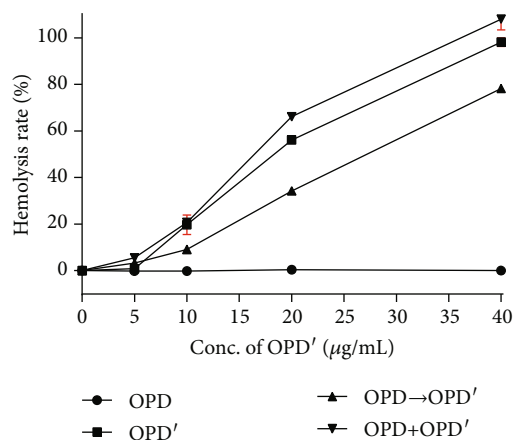


FIGURE 2: *In vitro* hemolytic behavior of OPD and OPD'. The error bars represent the standard deviation of measurements for 4 parallel samples in four separate groups ($n = 4$).

OPD', and mannitol (20%) had the most obvious alleviating effect. For example, when mannitol (20%) was used as the solvent, the hemolysis rate of OPD' (40 $\mu\text{g}/\text{mL}$) was $4.67\% \pm 0.42\%$, and this value was $98.15\% \pm 1.80\%$ when saline was used as the solvent; therefore, the hemolysis rates were reduced by 93.48%. Correspondingly, the hemolysis rates of glucose (5%) and fructose (10%) were $22.53\% \pm 1.26\%$ and $23.36\% \pm 1.07\%$, respectively.

As shown in Figure 3(b), the compatible drug Trolox did not cause hemolysis in a series of concentrations, and 40 $\mu\text{g}/\text{mL}$ OPD' maintained a hemolysis rate close to 100% ($98.15\% \pm 1.80\%$). When a series of concentrations of OPD and Trolox were pretreated with erythrocytes, the high hemolysis rate caused by OPD' (40 $\mu\text{g}/\text{mL}$) was decreased, and the degree of reduction was linearly related to the concentration of OPD and Trolox. In the range of 5-10 $\mu\text{g}/\text{mL}$, the decreasing effect of OPD was better than that of Trolox. However, in the range of 20-40 $\mu\text{g}/\text{mL}$, the decreasing effect of OPD was weakened compared with that of Trolox. The better the decreasing effect, the stronger the ability to protect erythrocytes.

3.3. Relationship between Different Hemolytic Behaviors of OPD and OPD' and the Redox Balance. According to the results of Figures 2 and 3, OPD, Trolox, glucose (5%), and fructose (10%) can all alleviate the hemolysis rate caused by OPD'. Among them, Trolox, glucose (5%), and fructose (10%) are all reductive substances. To explore whether the difference in the hemolysis behavior of OPD and OPD' is related to reductive or oxidative properties, the DPPH method was adopted. As shown in Figure 4, OPD' has almost no DPPH free radical scavenging ability. In contrast, the DPPH free radical scavenging ability of OPD became stronger as the concentration of OPD gradually increased. However, compared with the positive control drug Trolox, OPD is not as good as Trolox in scavenging DPPH free radicals. Therefore, OPD' has almost no reducibility, while OPD has a certain degree of reducibility, which could reasonably

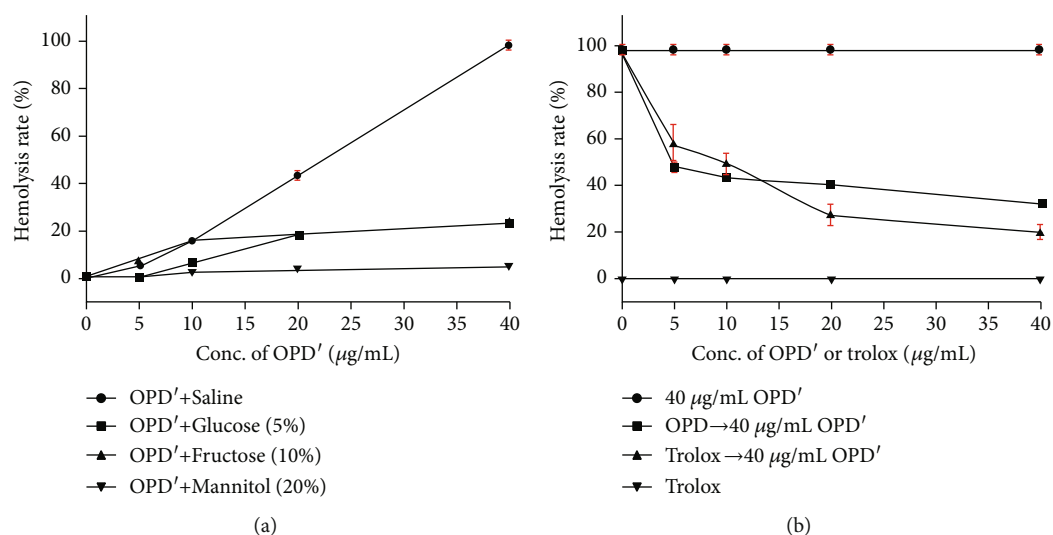


FIGURE 3: Effects of different solvents or compatible drugs on hemolytic behavior of OPD'. (a) The commonly used clinical solvents. (b) The compatible drugs, OPD, and Trolox. The error bars represent the standard deviation of measurements for 4 parallel samples in four separate groups ($n = 4$).

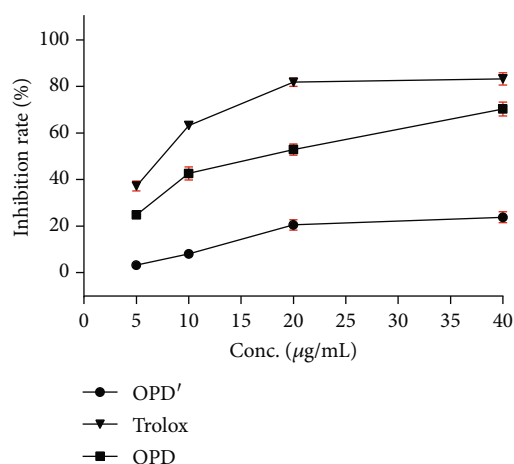


FIGURE 4: The scavenging ability of OPD, OPD', and Trolox in different concentrations on DPPH free radicals. The error bars represent the standard deviation of measurements for 4 parallel samples in three separate groups ($n = 4$).

explain why OPD has the ability to alleviate hemolysis caused by OPD' similar to Trolox, glucose (5%), and fructose (10%).

As shown in Figure 5(a), the LDH content in the erythrocyte cytoplasm gradually decreased as the OPD' concentration increased compared with that in the NC group. At concentrations of 10 µg/mL and 20 µg/mL, the difference was significant ($p < 0.05$), and at a concentration of 40 µg/mL, the difference was very significant ($p < 0.01$). When OPD was used to pretreat erythrocytes at a concentration of 40 µg/mL, the LDH content in the cytoplasm of erythrocytes increased significantly ($p < 0.05$) compared with that in the OPD single-use group. After treatment with OPD', the MDA content in the cytoplasm of RBCs increased, which was positively correlated with the OPD' concentration. Pretreat-

ment with OPD alleviated the increase in the MDA content caused by OPD' (Figure 5(b)). Trends similar to the change in the LDH content also appeared in the SOD, GSH, and Na⁺-K⁺-ATPase content (Figures 5(c)–5(e)). After treatment with OPD', the contents of SOD, GSH, and Na⁺-K⁺-ATPase in the erythrocyte cytoplasm all showed a dose-dependent decrease, and this decrease was reversed or alleviated by pretreatment with OPD to a certain extent.

From the results of the *in vitro* hemolysis test, the effects of solvents and compatible drugs on the hemolysis test, and the detection of redox balance-related factors, it is speculated that the hemolysis caused by OPD' *in vitro* may be related to the destruction of the redox balance. LDH is a marker enzyme that exists in the cytoplasm of cells and can sensitively reflect the degree of cell membrane damage [33]. MDA is a naturally occurring product of lipid peroxidation and prostaglandin biosynthesis that is mutagenic and carcinogenic [34], and the MDA content reflects the degree of lipid peroxidation in erythrocytes. SODs constitute a very important antioxidant defense against oxidative stress in the body [35]. The enzyme acts as a good therapeutic agent against reactive oxygen species-mediated diseases. GSH plays an important role in the body's biochemical defense system. In addition to eliminating free radicals generated by metabolism [36], GSH can also improve the body's immunity. Both SOD and GSH play a very important role in maintaining the redox balance. After treatment with OPD', the erythrocyte membrane was damaged, resulting in increased membrane permeability and the leakage of cell content such as LDH. The MDA content was significantly increased, and both the SOD and the GSH content were significantly decreased. Na⁺-K⁺-ATPase is an important enzyme for erythrocytes to complete energy metabolism [37]. It actively transports K⁺ and Na⁺, thereby maintaining the balance of osmotic pressure on both sides of the cell membrane. In our study, after treatment with OPD', its enzyme activity was suppressed.

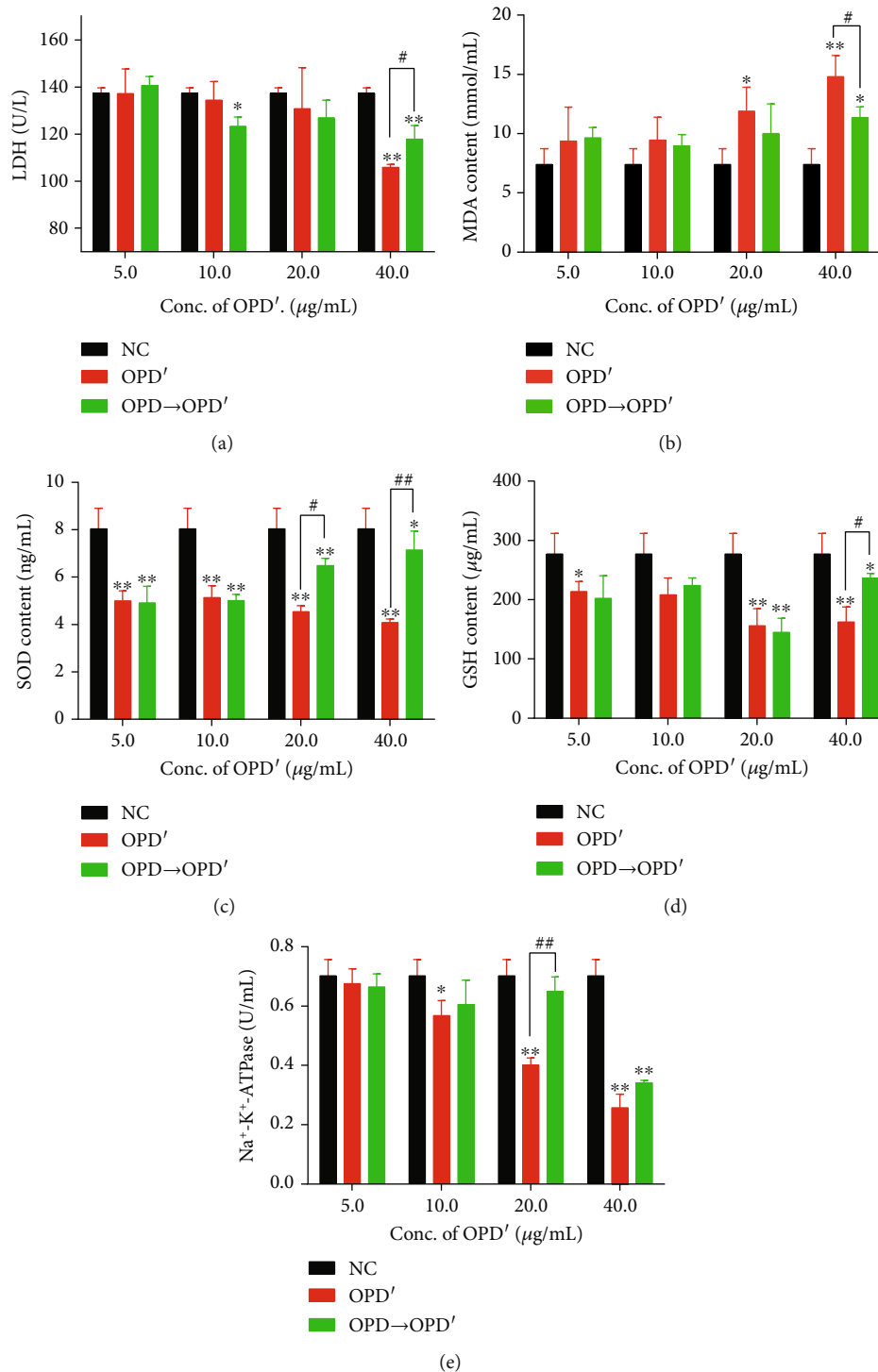


FIGURE 5: Effects of OPD' and OPD pretreated (OPD→OPD') on LDH, MDA, SOD, GSH, and Na⁺-K⁺-ATPase content: (a) LDH content, (b) MDA content, (c) SOD content, (d) GSH content, and (e) Na⁺-K⁺-ATPase content. The error bars represent the standard deviation of measurements for 3 parallel samples in three separate groups ($n = 3$). * Compared with the NC group, the statistical value was significant ($p < 0.05$); ** compared with the NC group, the statistical value was very significant ($p < 0.01$); # compared with the OPD' group, the statistical value was significant ($p < 0.05$); ## compared with the OPD' group, the statistical value was very significant ($p < 0.01$).

Therefore, based on the experimental results, we can infer that the hemolytic behavior of OPD' in RBCs manifests as oxidative damage. By inhibiting the activities of SOD and

GSH, it reduces the ability of RBCs to scavenge superoxide anion free radicals, leading to increased membrane permeability, aggravating the degree of lipid peroxidation of RBC

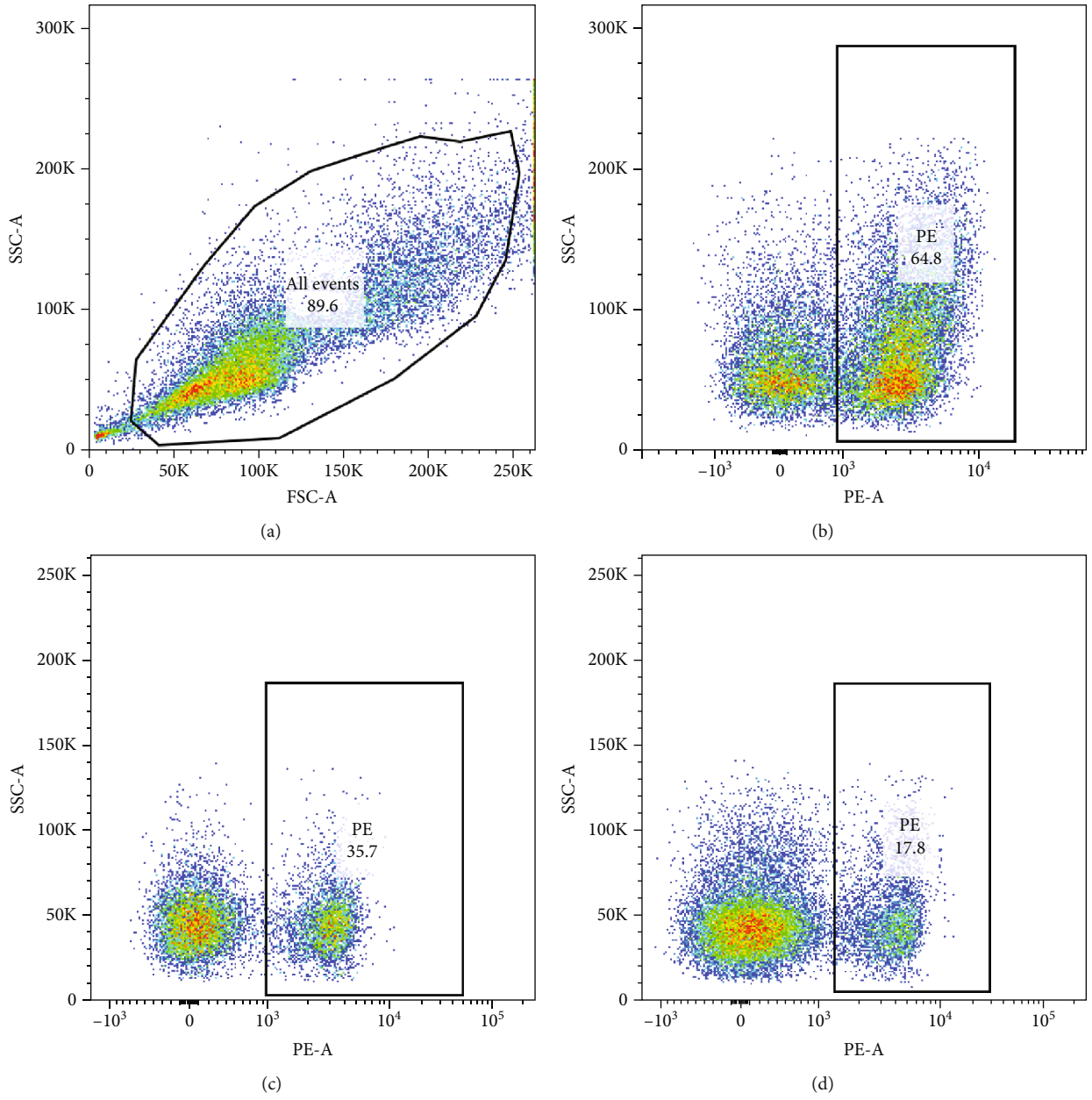


FIGURE 6: Continued.

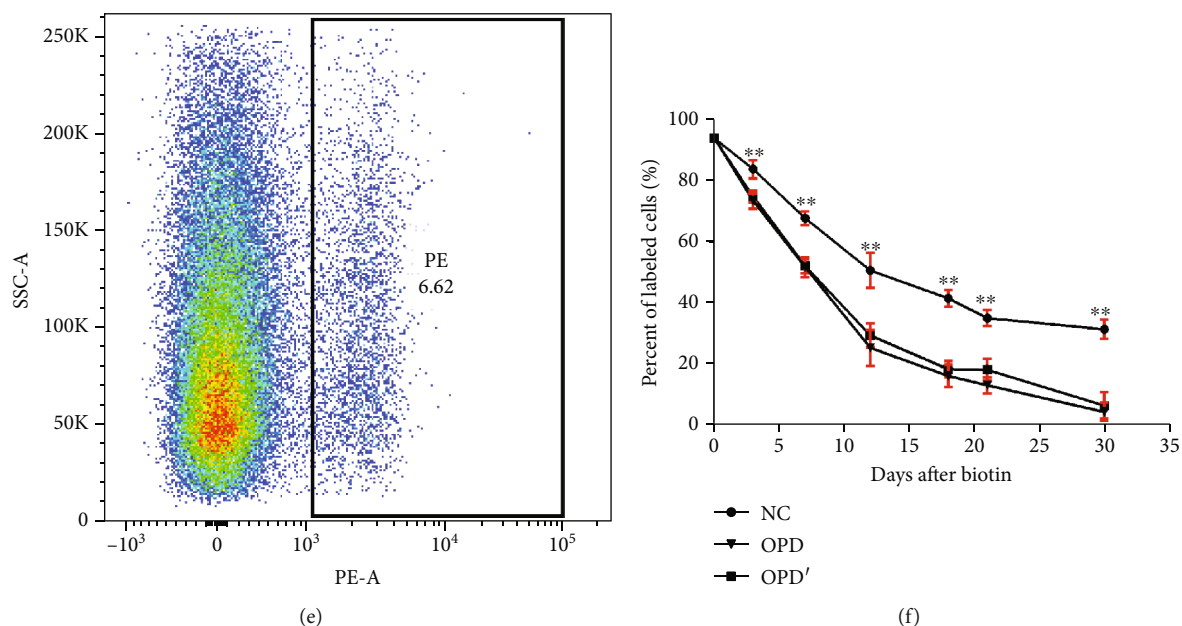


FIGURE 6: Effects of OPD' and OPD on erythrocyte life span. (a) and (b) exhibited the flow cytometry analysis workflow; (b) 7th day, NC group; (c) 12th day, OPD group; (d) 21th day, OPD group; (e) 30th day, OPD' group; (f) relationship between percent of labelled cells and days after biotin. The error bars represent the standard deviation of measurements for 5 parallel samples in three separate groups ($n = 5$). **Compared with the OPD and OPD' group, the statistical value was very significant ($p < 0.01$).

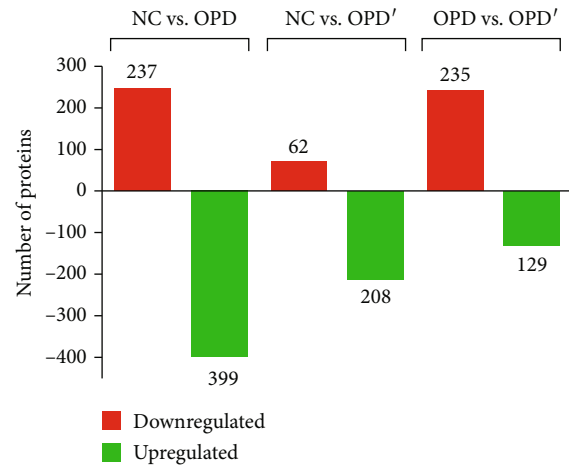
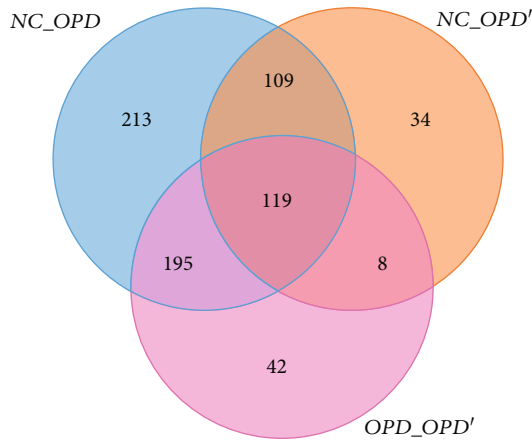
membranes, resulting in increased MDA content, and further aggravating the oxidative damage of cell membranes. Increased membrane permeability also induced LDH leakage, which resulted in a decreased LDH content in the cytoplasm of erythrocytes. OPD' can also inhibit the activity of ATPase on the RBC membrane, affect its material transport and energy metabolism, and lead to changes in the structure and function of the membrane. Eventually, erythrocytes were ruptured, and hemolysis occurred. However, OPD can reverse the hemolysis caused by OPD' to a certain extent because of its reducibility.

3.4. Both OPD and OPD' Caused Hemolysis In Vivo. The differences between the *in vitro* hemolysis behavior of OPD and OPD' and the drug-drug interactions (DDIs) based on the hemolysis behavior of the two isomers were very peculiar, which makes us eager to explore the hemolysis behavior and DDIs of these two isomers *in vivo*. We have used a variety of methods to study the hemolytic behavior of OPD and OPD' *in vivo*, such as single-dose- and multiple-dose-based acute toxicity tests (single-dose or 14 days) and subacute toxicity tests (30 days), and the experimental animals include rats and mice [38]. The data in unpublished manuscripts show that multiple doses of OPD and OPD' both caused hemolysis *in vivo*, which was manifested by a decrease in the HGB content, a decrease in the RBC count, and a significant increase in the absolute value and percentage of RET. Correspondingly, the results related to hemolysis were also observed in the pathological changes of organs and the animal body weight. Urine test results also indicate the occurrence of intravascular hemolysis.

Although these indicators indicate the occurrence of hemolysis, they are not the gold standard examination for the diagnosis of hemolysis. The essential feature of any hemolytic disorder is the shortened RBC lifespan [39, 40]. As shown in Figure 6(f), administering OPD and OPD' through tail vein injection for 30 consecutive days significantly shortens the lifespan of RBCs. At the same time point (i.e., 3rd, 7th, 12th, 18th, 21st, and 30th), compared with the NC group, the percentages of labeled cells in both the OPD and OPD' groups were significantly decreased ($p < 0.05$ or 0.01). These results confirmed that both OPD and OPD' caused hemolysis *in vivo*. Thus far, we not only discovered the hemolysis of OPD' *in vitro* but also found the hemolysis of OPD *in vivo*.

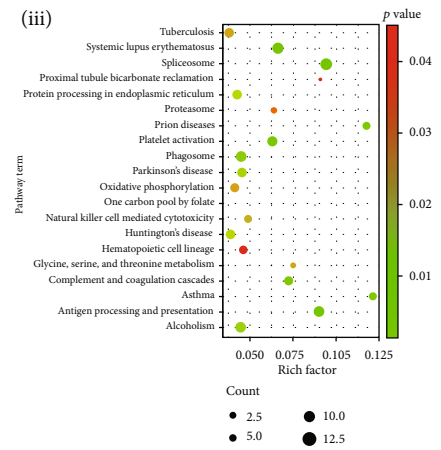
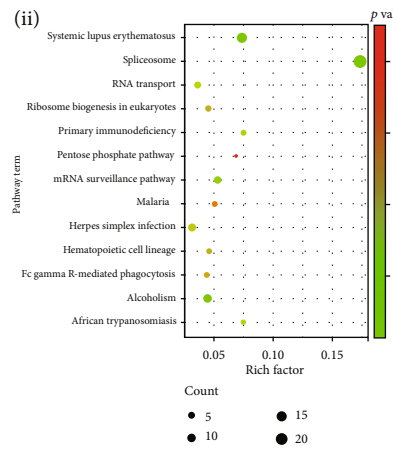
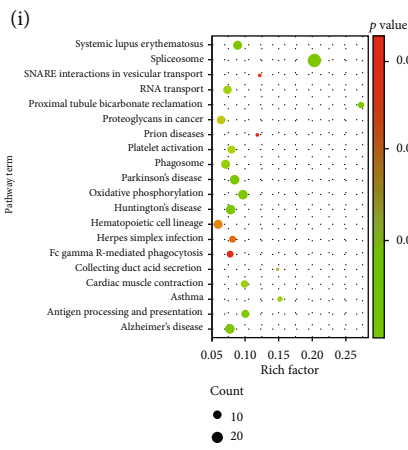
There are some possible speculations for this phenomenon; one is that OPD is biotransformed into OPD' or its analogues in animals, and the other one is that both OPD and OPD' were metabolized into more activated forms for hemolysis, but the speculations lack sufficient data. Based on the speculations, we studied the possibility of the conversion between OPD and OPD' at both the *in vivo* and *in vitro* levels, and the results did not find any signs of such conversion. We hypothesized that the inconsistency of the hemolytic behavior of OPD *in vivo* and *in vitro* may be related to its metabolites, and related research is ongoing.

3.5. Multiomics Studies Reveal the Underlying Mechanism of Hemolysis Caused by OPD and OPD'. Our previous results in an unpublished study demonstrated that changes in endogenous differential metabolites and differential lipids, enrichment of differential metabolic pathways, and



(a)

(b)



(c)

FIGURE 7: Continued.

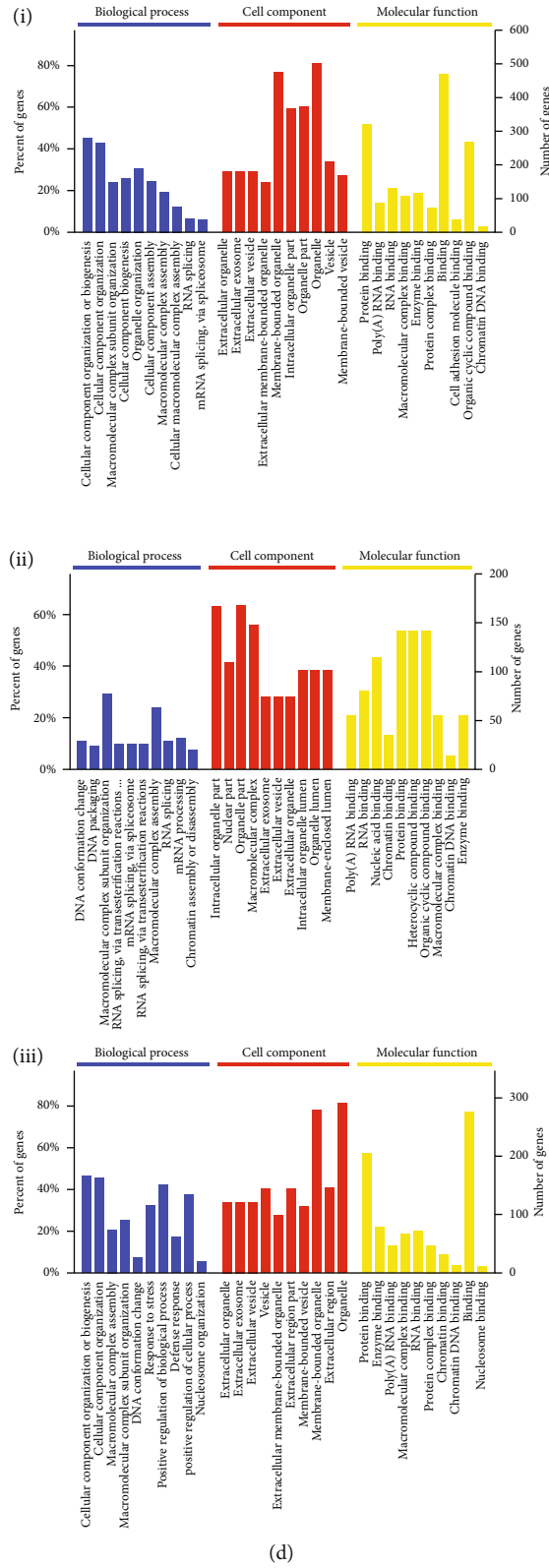


FIGURE 7: Continued.

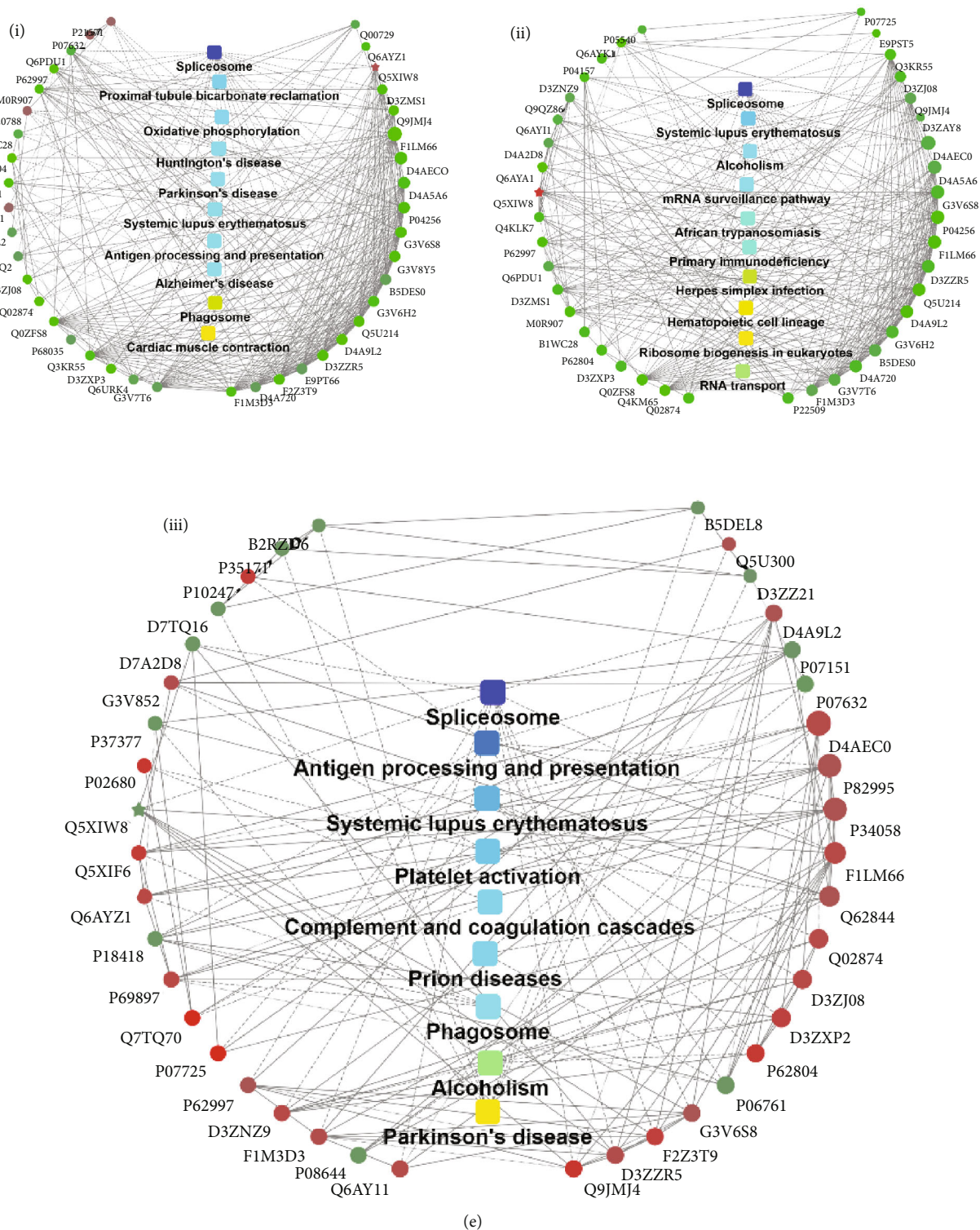


FIGURE 7: Proteomics results of OPD and OPD'. (a) Venn plot of three compared sets. (b) Up- or downregulated differential proteins in three compared sets. (c) KEGG bubble plot of three compared sets. (d) Top 10 biological processes, cell components, and molecular functions of three compared sets. (e) PPI network plots of three compared sets. (i) NC-OPD-compared group, (ii) NC-OPD'-compared group, and (iii) OPD-OPD'-compared group.

correlation analysis all showed that the causes of the hemolysis of OPD and OPD' are closely related to disorders of phospholipid metabolism.

In this study, we focused on the proteomics results of blood ghosts. Based on the screening criteria (i.e., fold-change > 1.5 or < 0.6), 2905 credible proteins were obtained.

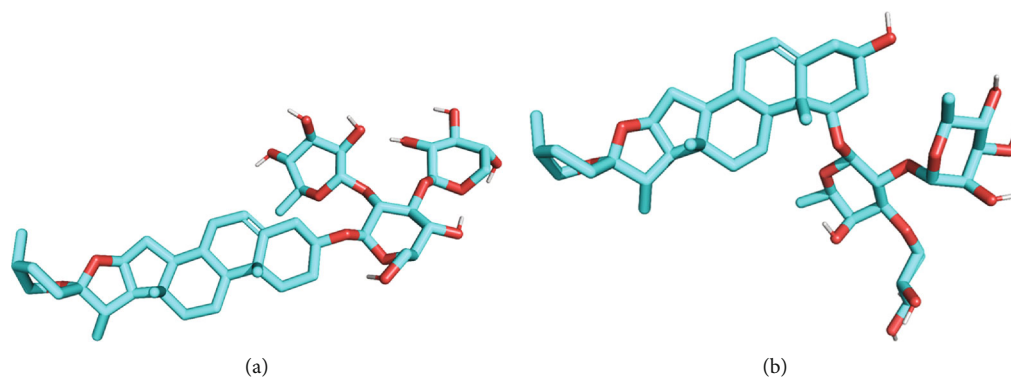


FIGURE 8: Three-dimensional molecular structures of OPD and OPD': (a) OPD'; (b) OPD.

Compared with the NC group, 636 and 270 proteins were differentially expressed between the OPD and OPD' groups, respectively, and 364 proteins were differentially expressed between the OPD and OPD' groups. As shown in Figure 7(a), a Venn plot shows the logical relationships between the three compared sets. In Figure 7(b), the number of up- or downregulated differential proteins is displayed. In Figure 7(c), a bubble plot of KEGG showed that the related enriched significant pathway terms resulted in three compared sets. In Figure 7(d), the top 10 biological processes, cell components, and molecular functions of the three compared sets are displayed. Under OPD intervention, blood ghost proteomics results suggested that biological processes were significantly enriched in the cellular component, subunit or organelle organization, biogenesis, and assembly. However, when treated with OPD', biological processes were different and enriched in DNA conformation changes and packaging, RNA splicing, mRNA splicing, and processing. This provides a new perspective for understanding the interactions of OPD' and OPD with RBCs. Cell component analysis indicated that extracellular organelles, exosomes, extracellular membrane-bound organelles, and vesicles were significantly changed in the NC vs. OPD comparison set. In the NC vs. OPD' comparison set, in addition to extracellular organelles, exosomes, and vesicles, intracellular organelle parts and lumens were significantly changed. At the molecular function level, OPD and OPD' were similar, and they were both enriched in enzyme, protein, and RNA binding. To realize these analyses and visualize the protein interactions between differential proteins and the KEGG pathway, PPI network plots were selected and are shown in Figure 7(e).

Proteomics analysis provided a comprehensive description of protein changes in OPD- and OPD'-treated erythrocytes, but it did not specify the targets for the next step. Differential protein analysis suggested that hemolysis caused by OPD and OPD' may contribute to lipid metabolic disorders (e.g., Q5M872 [41] and Q5XIT9), mitochondrial energy metabolism (e.g., D3ZAQ0 [42] and Q03344), high mobility group protein binding (e.g., P63159 and Q4KLJ0 [43]) and cytoskeletal (e.g., Q6IFU7 [44, 45], Q6IFU9, and A0A0G2JST3). These proteins are very valuable research objects.

3.6. Some Potential Targets Related to Hemolysis Reveal the Difference in Hemolytic Behavior between OPD and OPD'. We first built the three-dimensional molecular structures of OPD and OPD' (see Figure 8) and predicted the putative targets based on the SEA approach and shape-based approach, respectively.

The putative targets of OPD and OPD' predicted by the SEA method are shown in Table 1. Among the 12 targets, the target predicted by the OPD' structure accounted for 100%, while the target predicted by the OPD structure only accounted for 5/12. These 5 targets are indexed as 2, 6, 8, 9, and 10, respectively.

The top 10 targets predicted by the shape similarity method are shown in Table 2.

The putative targets predicted by the shape similarity method were combined with all the putative targets predicted by SEA. These putative targets were then compared with the collected hemolysis-related targets (see Table S1). The results illustrate that the target "solute carrier organic anion transporter family member 1B3" (Q9NPD5) is the potential target for OPD'. Q9NPD5 was submitted to the Reactome Pathway Database for pathway analysis. Detailed pathway information is shown in Table 3.

Q9NPD5, also known as OATP1B3, is an anion transporter. It has been proven that the hepatic uptake of OPD and OPD' is mediated by organic anion-transporting polypeptides (OATPs) [46–48]. This report, on the one hand, confirmed the reliability of the molecular modeling results; on the other hand, it pointed out that OPD and OPD' can affect the transporting activities of OATP1B1 and OATP1B3 in a substrate-dependent manner. Several reports in the literature have shown that the inhibition of organic anion transporting polypeptides OATP1B1 and OATP1B3 might lead to hyperbilirubinemia [49, 50]. This may be one of the reasons why OPD and OPD' cause hemolysis *in vivo*, and it is also a potential hemolysis prevention target worthy of further study.

In addition to Q9NPD5, several other targets that are not directly related to hemolysis are also worthy of attention, such as AT1A1 (Table 1, Index 2), which affects Na⁺-K⁺-ATPase activity, and its effect on hemolysis has been discussed in the previous paragraph. DHCR7 (Table 1,

TABLE 1: The putative targets which predicted by SEA.

Index	Affinity threshold (nM)	<i>p</i> value	Target name	Target description
1	5	5.25E-21	AMYP_HUMAN	Pancreatic alpha-amylase
2	5	1.60E-28	AT1A1_CANLF	Sodium/potassium-transporting ATPase subunit alpha-1
3	5	1.00E-36	CP125_MYCTU	Steroid C26-monooxygenase
4	5	2.85E-09	CP17A_HUMAN	Steroid 17-alpha-hydroxylase/17,20 lyase
5	5	4.51E-06	CP17A_RAT	Steroid 17-alpha-hydroxylase/17,20 lyase
6	5	9.68E-10	DHCR7_RAT	7-Dehydrocholesterol reductase
7	5	3.91E-06	DPOLA_HUMAN	DNA polymerase alpha catalytic subunit
8	5	8.23E-06	EBP_HUMAN	3-Beta-hydroxysteroid-delta(8), delta(7)-isomerase
9	5	1.66E-07	ERG2_YEAST	C-8 sterol isomerase
10	5	7.00E-13	IL2_HUMAN	Interleukin-2
11	5	2.46E-08	MRP4_HUMAN	Multidrug resistance-associated protein 4
12	5	6.15E-29	NPC1_HUMAN	Niemann-Pick C1 protein

TABLE 2: The top 10 predicted targets based on the shape similarity method.

Rank	Entry	Target name	Organism
1	Q11201	CMP-N-acetylneuraminat-beta-galactosamide-alpha-2,3-sialyltransferase 1	Homo sapiens
2	O54939	Testosterone 17-beta-dehydrogenase 3	Rattus
3	Q9UHC9	Niemann-Pick C1-like protein 1	Homo sapiens
4	Q9NPD5	Solute carrier organic anion transporter family member 1B3	Homo sapiens
5	P60568	Interleukin-2	Homo sapiens
6	P08069	Insulin-like growth factor I receptor	Homo sapiens
7	P31749	Serine/threonine-protein kinase AKT	Homo sapiens
8	P04626	Receptor protein-tyrosine kinase erbB-2	Homo sapiens
9	P30304	Dual specificity phosphatase Cdc25A	Homo sapiens
10	P35372	Mu opioid receptor	Homo sapiens

TABLE 3: The pathways details of the target Q9NPD5.

Index	Function	Term
1	Metabolism (Homo sapiens)	Recycling of bile acids and salts
2	Transport of small molecules (Homo sapiens)	Transport of organic anions

Index 6), EBP (Table 1, Index 8), and ERG2 (Table 1, Index 9) proteins encoded by these genes were all involved in the cholesterol biosynthetic pathway, which is part of steroid biosynthesis [51–53]. The interaction between OPD or OPD' and these proteins will further affect the integrity of the cell membrane structure, which may lead to hemolysis. The target predicted by molecular modeling also has limitations, but it provides some references for the study of the potential mechanism of OPD and OPD' hemolysis.

4. Conclusions

In summary, we reported the hemolytic properties of OPD and OPD' and clarified their differences with regard to their hemolytic behavior *in vivo* and *in vitro*. *In vitro*, we established that hemolysis induced by OPD' was related to a redox

imbalance, and OPD has a certain protective effect. We also put forward some reasonable suggestions for safe clinical use. *In vivo*, we confirmed that both OPD and OPD' caused hemolysis, and in addition to redox imbalance, proteomics data revealed that lipid metabolic disorder and mitochondrial energy metabolism have extensive participation in hemolysis. Proteomics and molecular modeling provided a comprehensive description of hemolysis-related protein changes and targets, which may benefit further study of the hemolysis mechanisms of OPD and OPD'.

Data Availability

All data used to support the findings of this study are available from the corresponding author upon request.

Conflicts of Interest

The authors declare that there is no conflict of interest regarding the publication of this paper.

Acknowledgments

The authors would like to thank Xiang-Tao Luo for supporting animal experiments. This research was funded by the National Natural Science Foundation of China (81703669) and National Science and Technology Major Project of “Major New Drug Creation” (2017ZX09301012-007).

Supplementary Materials

See Table S1 in the Supplementary Material for hemolysis-related targets. See Method S1 in the Supplementary Material for detailed proteome analysis conditions. (*Supplementary Materials*)

References

- [1] G. Jacobasch and S. M. Rapoport, “Hemolytic anemias due to erythrocyte enzyme deficiencies,” *Molecular Aspects of Medicine*, vol. 17, no. 2, pp. 143–170, 1996.
- [2] D. Bossi and M. Russo, “Chapter 4 hemolytic anemias due to disorders of red cell membrane skeleton,” *Molecular Aspects of Medicine*, vol. 17, no. 2, pp. 171–188, 1996.
- [3] B. Devalet, F. Mullier, B. Chatelain, J. M. Dogné, and C. Chatelain, “Pathophysiology, diagnosis, and treatment of paroxysmal nocturnal hemoglobinuria: a review,” *European Journal of Haematology*, vol. 95, no. 3, pp. 190–198, 2015.
- [4] W. Barcellini, “Immune hemolysis: diagnosis and treatment recommendations,” *Seminars in Hematology*, vol. 52, no. 4, pp. 304–312, 2015.
- [5] P. Beris and V. Picard, “Non-immune hemolysis: diagnostic considerations,” *Seminars in Hematology*, vol. 52, no. 4, pp. 287–303, 2015.
- [6] E. Fibach and M. Dana, *Red blood cells as redox modulators in hemolytic anemia, Erythrocyte(book)*, intechopen, 2019.
- [7] C. R. Morris, J. H. Suh, W. Hagar et al., “Erythrocyte glutamine depletion, altered redox environment, and pulmonary hypertension in sickle cell disease,” *Blood*, vol. 111, no. 1, pp. 402–410, 2008.
- [8] X. Zhang, G. Campreciós, P. Rimmelé et al., “FOXO3-mTOR metabolic cooperation in the regulation of erythroid cell maturation and homeostasis,” *American Journal of Hematology*, vol. 89, no. 10, pp. 954–963, 2014.
- [9] M. H. Chen, X. J. Chen, M. Wang, L. G. Lin, and Y. T. Wang, “Ophiopogon japonicus—a phytochemical, ethnomedicinal and pharmacological review,” *Journal of Ethnopharmacology*, vol. 181, pp. 193–213, 2016.
- [10] E. Luo, D. Zhang, H. Luo et al., “Treatment efficacy analysis of traditional Chinese medicine for novel coronavirus pneumonia (COVID-19): an empirical study from Wuhan, Hubei Province, China,” *China Chinese Medicine*, vol. 15, no. 1, p. 34, 2020.
- [11] H.-Y. Wang, S.-C. Guo, Z.-T. Peng et al., “Ophiopogon polysaccharide promotes the in vitro metabolism of ophiopogonins by human gut microbiota,” *Molecules*, vol. 24, no. 16, p. 2886, 2019.
- [12] A. Q. Jin, G. Yang, M. Chen et al., “Analysis and evaluation of nutrient composition of Ophiopogonis Radix in Santai area,” *Zhongguo Zhong Yao Za Zhi*, vol. 44, no. 15, pp. 3226–3232, 2019.
- [13] Y.-Y. Zhang, C. Meng, X.-M. Zhang et al., “Ophiopogonin D attenuates doxorubicin-induced autophagic cell death by relieving mitochondrial damage in vitro and in vivo,” *The Journal of Pharmacology and Experimental Therapeutics*, vol. 352, no. 1, pp. 166–174, 2014.
- [14] X. Huang, Y. Wang, Z. Zhang et al., “Ophiopogonin D and EETs ameliorate Ang II-induced inflammatory responses via activating PPAR α in HUVECs,” *Biochemical and Biophysical Research Communications*, vol. 490, no. 2, pp. 123–133, 2017.
- [15] J. H. Lee, C. Kim, and S. G. Lee, “Ophiopogonin D, a steroidal glycoside abrogates STAT3 signaling cascade and exhibits anti-cancer activity by causing GSH/GSSG imbalance in lung carcinoma,” *Cancers*, vol. 10, no. 11, p. 427, 2018.
- [16] J. Qian, F. Jiang, B. Wang et al., “Ophiopogonin D prevents H₂O₂-induced injury in primary human umbilical vein endothelial cells,” *Journal of Ethnopharmacology*, vol. 128, 2010.
- [17] J. Wang, N. N. Wang, Y. X. Ge et al., “Ophiopogonin D protects cardiomyocytes against ophiopogonin D'-induced injury through suppressing endoplasmic reticulum stress,” *Zhongguo Zhong Yao Za Zhi*, vol. 44, no. 9, pp. 1876–1881, 2019.
- [18] S. Ren, X. U. Huanhua, L. I. Ming et al., “Cytotoxicity of ophiopogonin D' for rat H9c2 cardiomyocytes,” *Chinese Journal of Pharmacology and Toxicology*, vol. 31, no. 4, pp. 325–331, 2017.
- [19] Z. Lu, H. Wang, M. Zhu et al., “Ophiopogonin D', a natural product from Radix Ophiopogonis, induces in vitro and in vivo RIPK1-dependent and caspase-independent apoptotic death in androgen-independent human prostate cancer cells,” *Frontiers in Pharmacology*, vol. 9, 2018.
- [20] Z. Lu, C. Wu, M. Zhu et al., “Ophiopogonin D' induces RIPK1-dependent necroptosis in androgen-dependent LNCaP prostate cancer cells,” *International Journal of Oncology*, vol. 56, no. 2, 2020.
- [21] A. Zha, Z. Cui, M. Qi et al., “Dietary baicalin zinc supplementation alleviates oxidative stress and enhances nutrition absorption in deoxynivalenol challenged pigs,” *Current Drug Metabolism*, vol. 10, no. 8, pp. 2174–2625, 2020.
- [22] P. Liao, Y. Li, M. Li et al., “Baicalin alleviates deoxynivalenol-induced intestinal inflammation and oxidative stress damage by inhibiting NF- κ B and increasing mTOR signaling pathways in piglets,” *Food and Chemical Toxicology*, vol. 140, p. 111326, 2020.
- [23] I. Baranowska and S. Bajkacz, “A new UHPLC-MS/MS method for the determination of flavonoids in supplements and DPPH-UHPLC-UV method for the evaluation of the radical scavenging activity of flavonoids,” *Food Chemistry*, vol. 256, pp. 333–341, 2018.
- [24] A. Zha, D. Yuan, Z. Cui et al., “The evaluation of the antioxidant and intestinal protective effects of baicalin-copper in deoxynivalenol-challenged piglets,” *Oxidative Medicine and Cellular Longevity*, vol. 2020, 13 pages, 2020.
- [25] Y. Wu, F. Wang, L. Fan et al., “Baicalin alleviates atherosclerosis by relieving oxidative stress and inflammatory responses via inactivating the NF- κ B and p38 MAPK signaling pathways,” *Biomedicine & Pharmacotherapy*, vol. 97, pp. 1673–1679, 2018.

- [26] S. Wang, G. L. Dale, P. Song, B. Viollet, and M. H. Zou, "AMP-Kalpa1 deletion shortens erythrocyte life span in mice: role of oxidative stress," *The Journal of Biological Chemistry*, vol. 285, no. 26, pp. 19976–19985, 2010.
- [27] S. Wang, G. L. Dale, P. Song, B. Viollet, and M. H. Zou, "Correction: AMPK α 1 deletion shortens erythrocyte life span in mice: role of oxidative stress," *The Journal of Biological Chemistry*, vol. 294, no. 27, p. 10738, 2019.
- [28] J. R. Wiśniewski, A. Zougman, N. Nagaraj, and M. Mann, "Universal sample preparation method for proteome analysis," *Nature Methods*, vol. 6, no. 5, pp. 359–362, 2009.
- [29] Q. Wu, Y. Li, Y. Wang, and H. Lu, "Quantitative mass spectrometry imaging of amino acids with isomer differentiation in brain tissue via exhaustive liquid microjunction surface sampling-tandem mass tags labeling-ultra performance liquid chromatography-mass spectrometry," *Journal of Chromatography. A*, vol. 1621, p. 461086, 2020.
- [30] M. J. Keiser, B. L. Roth, B. N. Armbruster, P. Ernsberger, J. J. Irwin, and B. K. Shoichet, "Relating protein pharmacology by ligand chemistry," *Nature Biotechnology*, vol. 25, no. 2, pp. 197–206, 2007.
- [31] P. Ding, X. Yan, Z. Liu et al., "PTS: a pharmaceutical target seeker," *Database*, vol. 2017, 2017.
- [32] X. Yan, J. Li, Z. Liu, M. Zheng, H. Ge, and J. Xu, "Enhancing molecular shape comparison by weighted Gaussian functions," *Journal of Chemical Information and Modeling*, vol. 53, no. 8, pp. 1967–1978, 2013.
- [33] Z. Feng and H. Wang, "Enzymatic assemblies disrupt the membrane and target endoplasmic reticulum for selective cancer cell death," *Journal of the American Chemical Society*, vol. 140, no. 30, pp. 9566–9573, 2018.
- [34] M. Yang, Y. Li, J. S. Ye, Y. Long, and H. M. Qin, "Effect of PFOA on oxidative stress and membrane damage of *Escherichia coli*," *Huan Jing Ke Xue*, vol. 38, no. 3, pp. 1167–1172, 2017.
- [35] P. C. N. Biapa, H. Matei, Ş. Bălci, J. E. Oben, and J. Y. Ngogang, "Protective effects of stem bark of *Harungana madagascariensis* on the red blood cell membrane," *BMC Complementary and Alternative Medicine*, vol. 13, no. 1, p. 98, 2013.
- [36] A. E. Maciag, R. J. Holland, Y. S. Robert Cheng et al., "Nitric oxide-releasing prodrug triggers cancer cell death through deregulation of cellular redox balance," *Redox Biology*, vol. 1, no. 1, pp. 115–124, 2013.
- [37] P. Iiu, O. V. Simonenko, K. M. Burnysheva et al., "The ability of cells to adjust to the low oxygen content associated with Na,K-ATPase glutathionylation," *Molekuliarnaia Biologiia*, vol. 49, no. 1, pp. 175–183, 2015.
- [38] X. Huan-Hua, Z. H. Jiang, C. S. Huang et al., "Established UPLC-MS / MS method to determinate ophiopogonin D and ophiopogonin D' and clinical risk assessment," *Drug Evaluation Research*, vol. 42, no. 6, pp. 1135–1140, 2019.
- [39] T. Kamesaki, "Diagnosis and treatment of hemolytic anemia," *Rinshō Ketsueki*, vol. 56, no. 10, pp. 1894–1902, 2015.
- [40] H. D. Zhang, Y. J. Ma, Q. F. Liu et al., "Human erythrocyte life-span measured by Levitt's CO breath test with newly developed automatic instrument," *Journal of Breath Research*, vol. 12, no. 3, article 036003, 2018.
- [41] D. E. Moller, "New drug targets for type 2 diabetes and the metabolic syndrome," *Nature*, vol. 414, no. 6865, pp. 821–827, 2001.
- [42] T. M. Decker, I. Forné, T. Straub et al., "Analog-sensitive cell line identifies cellular substrates of CDK9," *Oncotarget*, vol. 10, no. 65, pp. 6934–6943, 2019.
- [43] X. L. Gao, W. J. Tian, B. Liu, J. Wu, W. Xie, and Q. Shen, "High-mobility group nucleosomal binding domain 2 protects against microcephaly by maintaining global chromatin accessibility during corticogenesis," *Journal of Biological Chemistry*, vol. 295, no. 2, pp. 468–480, 2020.
- [44] D. A. Fletcher and R. D. Mullins, "Cell mechanics and the cytoskeleton," *Nature*, vol. 463, no. 7280, pp. 7485–7492, 2010.
- [45] T. Hohmann and F. Dehghani, "The cytoskeleton-a complex interacting meshwork," *Cell*, vol. 8, no. 4, p. 362, 2019.
- [46] X. Liu, L. Chen, M. Liu et al., "Ginsenoside Rb1 and Rd remarkably inhibited the hepatic uptake of Ophiopogonin D in Shenmai injection mediated by OATPs/oatps," *Frontiers in Pharmacology*, vol. 9, p. 957, 2018.
- [47] W. Zhang, X. Xiong, L. Chen et al., "Hepatic uptake mechanism of Ophiopogonin D mediated by organic anion transporting polypeptides," *European Journal of Drug Metabolism and Pharmacokinetics*, vol. 42, no. 4, pp. 669–676, 2017.
- [48] L. Chen, L. Liu, Y. Chen et al., "Modulation of transporter activity of OATP1B1 and OATP1B3 by the major active components of *Radix Ophiopogonis*," *Xenobiotica*, vol. 49, no. 10, pp. 1221–1228, 2019.
- [49] E. Kotsampasakou, S. E. Escher, and G. F. Ecker, "Linking organic anion transporting polypeptide 1B1 and 1B3 (OATP1B1 and OATP1B3) interaction profiles to hepatotoxicity - the hyperbilirubinemia use case," *European Journal of Pharmaceutical Sciences*, vol. 100, pp. 9–16, 2017.
- [50] E. van de Steeg, V. Stránecký, H. Hartmannová et al., "Complete OATP1B1 and OATP1B3 deficiency causes human rotor syndrome by interrupting conjugated bilirubin reuptake into the liver," *The Journal of Clinical Investigation*, vol. 122, no. 2, pp. 519–528, 2012.
- [51] S. Silve, P. H. Dupuy, C. Labit-Lebouteiller et al., "Emopamil-binding protein, a mammalian protein that binds a series of structurally diverse neuroprotective agents, exhibits $\Delta 8$ - $\Delta 7$ sterol isomerase activity in yeast," *The Journal of Biological Chemistry*, vol. 271, no. 37, pp. 22434–22440, 1996.
- [52] F. F. Moebius, K. E. M. Soellner, B. Fiechtner, C. W. Huck, G. Bonn, and H. Glossmann, "Histidine77, glutamic acid81, glutamic acid123, threonine126, asparagine194, and tryptophan197 of the human emopamil binding protein are required for in vivo sterol delta 8-delta 7 isomerization," *Biochemistry*, vol. 38, no. 3, pp. 1119–1127, 1999.
- [53] F. F. Moebius, B. U. Fitzky, G. Wietzorrek, A. Haidekker, A. Eder, and H. Glossmann, "Cloning of an emopamil-binding protein (EBP)-like protein that lacks sterol delta8-delta7 isomerase activity," *The Biochemical Journal*, vol. 374, no. 1, pp. 229–237, 2003.

Research Article

Effects of Fasting-Mimicking Diet and Specific Meal Replacement Foods on Blood Glucose Control in Patients with Type 2 Diabetes: A Randomized Controlled Trial

Fang Tang ¹ and Xuan Lin ²

¹Wuhan University of Science and Technology School of Medicine, Wuhan, 430081 Hubei, China

²Department of Endocrinology, CR & WISCO General Hospital Affiliated to Wuhan University of Science and Technology, Wuhan, 430080 Hubei, China

Correspondence should be addressed to Xuan Lin; 854964946@qq.com

Received 3 October 2020; Revised 16 November 2020; Accepted 24 November 2020; Published 9 December 2020

Academic Editor: Si Qin

Copyright © 2020 Fang Tang and Xuan Lin. This is an open access article distributed under the Creative Commons Attribution License, which permits unrestricted use, distribution, and reproduction in any medium, provided the original work is properly cited.

Type 2 diabetes represents a serious societal health problem due to the vulnerability to cardiovascular events. Diet therapy is the most basic treatment for type 2 diabetes. The present study was conducted to study the effect of a fasting-mimicking diet and specific meal replacement foods on blood glucose control in patients with type 2 diabetes. Our study included 100 patients with type 2 diabetes who underwent a physical examination which were enrolled and randomly assigned as 50 patients each to the test group (with low energy-specific meal replacement meals during a fasting-mimicking diet) and the control group (with specific meal replacement foods given normal adult doses). After 4 months, efficacy indicators which were fasting blood glucose, 2-hour postprandial venous blood glucose, and glycosylated haemoglobin of the experimental group were all lower than those of the control group ($P < 0.05$); observation indicators that include body mass index, waist circumference, blood lipids (triglyceride, cholesterol, and low-density lipoprotein), and blood pressure levels were all lower than the control group, and high-density lipoprotein levels were all higher than the control group (all $P < 0.05$). Both groups of fasting blood glucose, 2-hour postprandial venous blood glucose, and blood pressure had a relatively stable downward trend, but the experimental group had a more significant decline. In conclusion, the study revealed that a fasting-mimicking diet and specific meal replacement foods can safely and effectively reduce weight and improve metabolic syndrome in patients with type 2 diabetes.

1. Introduction

The latest surveys of obesity and metabolic syndrome show that the prevalence of type 2 diabetes in overweight (body mass index (BMI) 25–27.5 kg/m²) and obese (BMI > 27.5 kg/m²) populations in China is 12.8% and 18.5%, respectively. The global prevalence of type 2 diabetes is increasing annually, and the latest data from the International Diabetes Federation (IDF) 2019 showed that approximately 463 million adults worldwide have diabetes. It is estimated that, by 2030 and 2045, the number of individuals with diabetes will reach 578.4 and 700.2 million, respectively. Therefore, the prevention and treatment of type 2 diabetes are particularly important. Diet is presently considered a key factor in the

management of patients with obese type 2 diabetes. The fasting-mimicking diet (FMD) involves alternate fasting and consumption of a calorie-restricted diet wherein only 25% of the normal intake is consumed on fasting days and normal caloric intake is maintained on eating days [1]. A large number of studies have shown that FMD is an emerging dietary intervention that can effectively reduce and control weight in obese patients with type 2 diabetes, improve impaired glucose regulation, and improve the risk factor level of diabetes [2–4]. A study by Cheng et al. at the University of Southern California found that FMD can promote the renewal and growth of pancreatic cells and promote insulin production. Moreover, FMD can reverse the symptoms of type 1 and type 2 diabetes in mouse models and is effective

in insulin in vitro in patients with type 1 diabetes [5]. Furthermore, Stekovic et al. of Graz University of Technology in Austria evaluated the FMD in healthy, nonobese individuals and found that FMD could reduce the body weight, improve the ratio of fat to lean meat, decrease blood lipids, and reduce the levels of the cardiovascular and inflammatory markers related to aging [6]. Several studies have reported that FMD can improve the health of model organisms and prolong their life expectancy, with good physiological regulatory significance in overweight individuals with or without type 2 diabetes as well as in healthy and nonobese participants. However, the determination of 25% of energy intake on a fasting day has not been previously addressed.

To fill this gap, this study developed the Food for Special Medical Purpose (FSMP) protocol, which was quantified and applied to fasting days. The FSMP is a specially formulated food that is developed to meet the special needs of a nutrient or diet for people with restricted eating, digestive and absorption disorders, metabolic disorders, or specific disease states. This study analyzed the effect of FMD combined with specific substitute foods on blood glucose in patients with type 2 diabetes mellitus.

2. Materials and Methods

2.1. Ethics Approval and Consent to Participate. This study conforms to the principles of the Declaration of Helsinki and was conducted with the approval of the Ethics Committee of CR & WISCO General Hospital Affiliated to Wuhan University of Science and Technology and the Chinese Clinical Trial Registry (grant no. ChiCTR2000032968). It was registered on 17 May and 2020-retrospectively registered, <http://www.chictr.org.cn/ChiCTR2000032968>. Permissions were obtained from all the relevant authorities of the hospital before enrollment of the patients, and written informed consent was sought from all the participants before enrollment. Necessary measures were taken to maintain confidentiality of the data and privacy of the participants.

2.2. General Information. From January 2018 to December 2018, 100 patients with type 2 diabetes and $BMI \geq 28 \text{ kg/m}^2$ who underwent a physical examination at the endocrine clinic and physical examination centre of CR & WISCO General Hospital Affiliated to Wuhan University of Science and Technology were selected for a 4-month simulated fasting diet. The random number table method was used to randomly assign 50 patients each to the test and control groups.

2.3. Inclusion and Exclusion Criteria

2.3.1. Inclusion Criteria. The inclusion criteria are as follows: meeting the World Health Organization (WHO) diagnostic criteria for type 2 diabetes, adult male and female participants (age 18–65 years, both inclusive), $BMI \geq 28 \text{ kg/m}^2$, good glycemic control (glycosylated haemoglobin (HbA1c) 7.0–10.0%, both values inclusive), relatively stable weight (weight change $\leq 10\%$ for at least 3 months before study inclusion), and willingness to use a glucometer. The blood glucose was measured and recorded in the participant's diary.

2.3.2. Exclusion Criteria. The exclusion criteria are as follows: participation in other clinical trials within 3 months preceding study enrolment; systolic blood pressure $\geq 180 \text{ mmHg}$ and/or diastolic blood pressure $\geq 110 \text{ mmHg}$ during screening visits; regular use of insulin, oral steroids, or anti-inflammatory drugs; diagnosis of cardiovascular disease; stroke, gastrointestinal disease, chronic nephritis, hepatobiliary disease, or renovascular disease; pregnant and lactating women; relatives of the investigators of the trial, employees of the hospital, or others who were related to the trial personnel; a major illness or physical weakness; and the investigator's judgement that the participant may be unable to complete this study.

2.4. Test Design. The FMD meal replacement food used in the trial was developed by the partner unit Maide Technology Company Limited by Shares (Maide Technology Co., Ltd., Wuhan, China) and had good safety. The meal replacement formula comprised avocado, oatmeal, green food nutrition powder, salt, and bitter melon powder. According to the book *Calories and Protein Intake* published by the WHO, a healthy woman or man needs 1800–1900 and 1980–2340 Kcal per day. This 4-month study included meal replacement intervention for 3 months and normal diet for the last month. The test group consumed FMD meal replacement powder from Monday to Friday in the second week of a month and ate normally for the rest of the month. The energy provision on the first day and the second to fifth days was 1196 and 805 Kcal, respectively (formula for patients weighing 75 kg). The investigator adjusted the meal replacement amount of the patient according to the weight and physical consumption, whereas the control group consumed meal replacement powder from Monday to Friday of the second week of the month (the same composition and different caloric composition as those in the test group; the calories met the abovementioned recommended daily requirement for normal adults) and ate normally for the remainder of the month.

During the test period, all patients received metformin hydrochloride tablets (Gehuazhi, Sino-American Shanghai Bristol-Myers Squibb Pharmaceutical Co., Ltd., Shanghai, China), 0.5 g, once daily as treatment for diabetes, and patient compliance was ascertained. For patients in the test group who had hypoglycemia or other discomforts on FMD meal replacement days, the metformin hydrochloride dosage was adjusted or discontinued after assessment by the endocrinologist.

2.5. Test Indices. The efficacy indicators were fasting plasma glucose (FPG), 2-hour postprandial glucose (2hPG), and HbA1c. The observation indicators included BMI, waist circumference, blood lipids (triglyceride (TG), cholesterol, high-density lipoprotein (HDL), and low-density lipoprotein (LDL)), and blood pressure. The FPG, 2hPG, and blood pressure measurements were obtained every week to evaluate the fluctuation of indicators in the study cycle because of the short-term differences. The remaining indicators are checked before and after the test.

2.6. Statistical Analysis. All data were analyzed in SPSS 21.0 statistical software. The present report is based on the

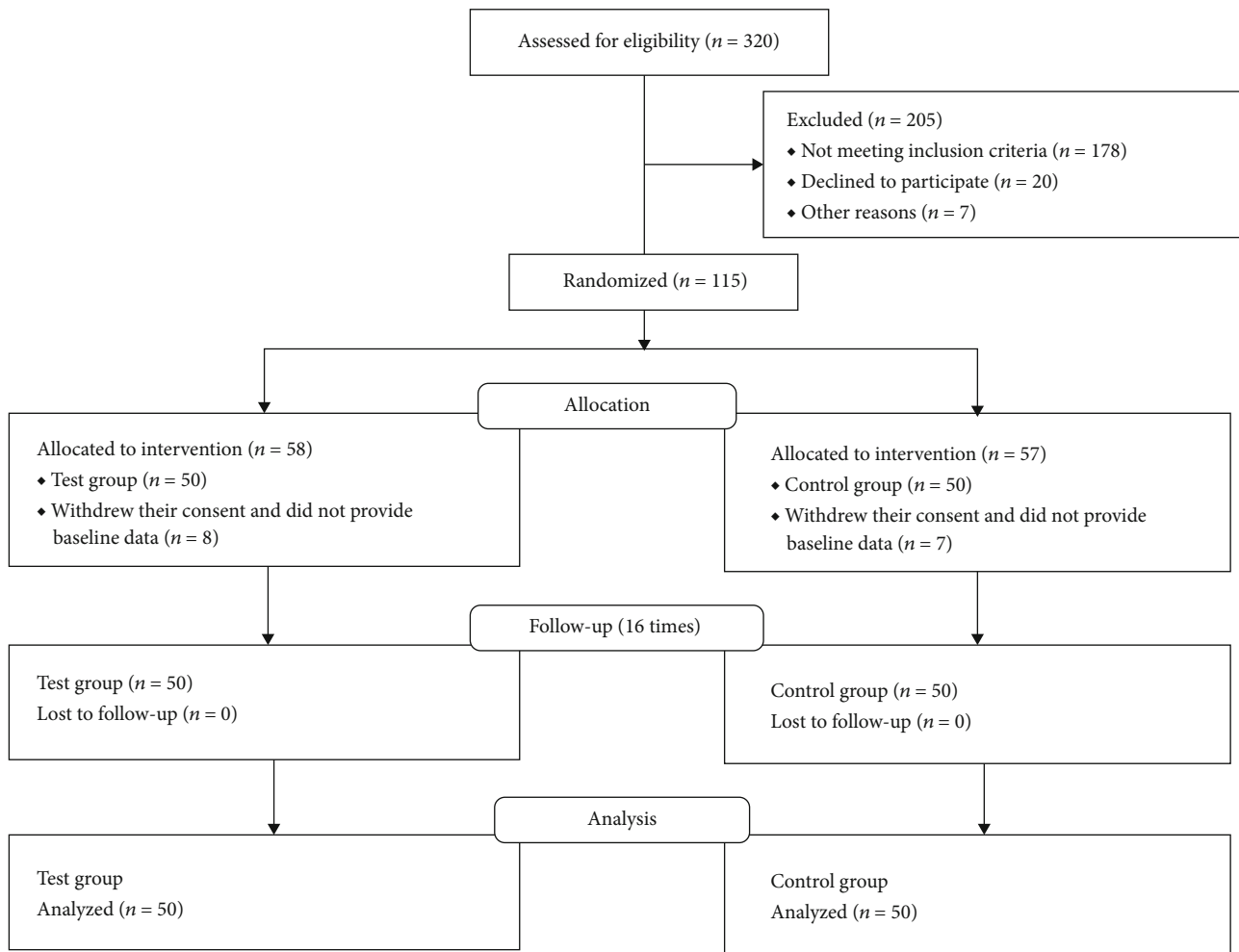


FIGURE 1: CONSORT diagram showing the number of participants at enrollment and follow-ups.

intention-to-treat analysis. Normal distribution of continuous variables was assessed by the Kolmogorov–Smirnov test. Results are expressed as mean \pm standard deviation (SD). Data with normal distribution are expressed as ($\chi \pm s$). Intergroup comparisons were analyzed by the *t*-test. The observation index volatility was measured by repeated measures analysis of variance. Numerical data was expressed as percentages and analyzed with the chi-square test. Differences were statistically significant at $P < 0.05$.

3. Results

We recruited 320 type 2 diabetes patients and selected 115/320 (35.9%) of them to enter this study based on the inclusion and exclusion criteria. Out of 115 participants, 58 (50.4%) were randomized into the test group, and 57 (49.6%) were randomized into the control group. Only 50/58 (86.2%) of the test group received meal replacement diet intervention and also provided baseline data in the test group arm, and only 50/57 (87.7%) of the control group received adult-recommended calorie meal replacement diets and provided baseline data in the control group arm. There were $n = 8$ and $n = 7$ patients in the test group and the control group arm, respectively, who withdrew their consent after

randomization and did not provide baseline data. There was no loss to follow-up in the 16-time visits (see Figure 1).

3.1. Study Participant Characteristics before Experimental Intervention. A total of 100 patients with type 2 diabetes were included in this study, the general information of the two groups of patients was compared, and the difference was not statistically significant (all $P > 0.05$; see Table 1).

3.2. Data Analysis of Efficacy Indicators after Experimental Intervention. Table 2 shows the values after 4 months of experimental intervention. The FPG was 5.25 ± 0.23 mmol/L in the experimental group and 6.27 ± 0.37 mmol/L in the control group, the 2hPG was 7.02 ± 2.27 mmol/L and 8.33 ± 0.89 mmol/L, respectively, and the HbA1c was $6.47 \pm 0.51\%$ and $7.50 \pm 0.50\%$, respectively. All glycemic parameters showed significant statistical intergroup differences ($P < 0.05$; see Table 2).

3.3. Observation Index Data Analysis after Experimental Intervention. After 4 months of experimental intervention, the BMI of the experimental and control groups were 25.04 ± 1.00 and 28.99 ± 0.99 kg/m², respectively, and the waist circumference was 90.82 ± 4.26 and 98.38 ± 4.27 cm,

TABLE 1: Baseline characteristics of the participants in the study subgroups.

Item	Control group	Test group	<i>P</i>
Male (<i>n</i> (%))	24 (48%)	22 (44%)	0.424
Age (y)	49.84 ± 1.94	50.02 ± 1.76	0.628
Course of disease (y)	5.35 ± 1.12	5.37 ± 1.00	0.925
FPG (mmol/L)	7.57 ± 0.52	7.56 ± 0.56	0.956
2hPG (mmol/L)	11.80 ± 1.42	11.97 ± 1.24	0.546
HbA1c (mmol/L)	7.93 ± 0.52	7.83 ± 0.51	0.345
Waist circumference (cm)	104.32 ± 4.84	105.10 ± 5.20	0.439
BMI (kg/m ²)	30.12 ± 1.09	30.15 ± 1.18	0.888
TG (mmol/L)	3.93 ± 0.41	3.80 ± 0.48	0.152
TC (mmol/L)	6.18 ± 0.96	6.41 ± 1.06	0.264
HDL-C (mmol/L)	1.21 ± 0.25	1.23 ± 0.40	0.752
LDL-C (mmol/L)	3.96 ± 0.66	3.83 ± 0.73	0.335
Systolic pressure (mmHg)	155.22 ± 6.21	155.28 ± 5.96	0.960
Diastolic pressure (mmHg)	90.62 ± 6.67	91.48 ± 5.13	0.472

FPG: fasting blood sugar; 2hPG: 2-hour postprandial blood glucose; HbA1c: glycosylated haemoglobin; BMI: body mass index; TG: triglyceride; TC: serum total cholesterol; HDL-C: high-density lipoprotein cholesterol; LDL-C: low-density lipoprotein cholesterol. All values are mean ± standard deviation (SD). *P* values indicated no statistically significant differences (*P* > 0.05) on between-group comparisons.

TABLE 2: Intergroup comparison of blood glucose levels before and after the tests.

Groups	FPG (mmol/L)	2hPG (mmol/L)	HbA1c (%)
	Before the test After the test	Before the test After the test	Before the test After the test
Control	7.57 ± 0.52	11.80 ± 1.42	7.93 ± 0.52
	6.27 ± 0.37	8.33 ± 0.89	7.50 ± 0.50
Test	7.56 ± 0.56	11.97 ± 1.24	7.83 ± 0.51
	5.25 ± 0.23 ^a	7.02 ± 2.27 ^b	6.47 ± 0.51 ^c
<i>t</i> value	-16.75	-9.84	-10.23

n = 50 in each group. All values are mean ± standard deviation (SD). *P* value indicated statistical significance (a, b, and c: *P* ≤ 0.001; all *P* < 0.05).

TABLE 3: Intergroup comparison of the waist circumference and BMI before and after the tests.

Groups	Waist circumference (cm)	BMI (kg/m ²)
	Before the test After the test	Before the test After the test
Control	104.32 ± 4.84	30.12 ± 1.09
	98.38 ± 4.27	28.99 ± 0.99
Test	105.10 ± 5.20	30.15 ± 1.18
	90.82 ± 4.26 ^a	25.04 ± 1.00 ^b
<i>t</i> value	-8.87	-19.84

n = 50 in each group. All values are mean ± standard deviation (SD). *P* value indicated statistical significance (a and b: *P* ≤ 0.001; both *P* < 0.05).

TABLE 4: Intergroup comparison of blood pressure before and after the tests.

Groups	Systolic pressure (mmHg)	Diastolic pressure (mmHg)
	Before the test After the test	Before the test After the test
Control	155.22 ± 6.21	90.62 ± 6.67
	149.08 ± 5.50	85.20 ± 6.12
Test	155.28 ± 5.96	91.48 ± 5.13
	141.10 ± 6.67 ^a	80.50 ± 5.97 ^b
<i>t</i> value	-6.54	-3.89

n = 50 in each group. All values are mean ± standard deviation (SD). *P* value indicates statistical significance (a and b: *P* ≤ 0.001, both *P* < 0.05).

TABLE 5: Intergroup comparison of blood lipids before and after the tests.

Groups	TC (mmol/L)	TG (mmol/L)	HDL-C (mmol/L)	LDL-C (mmol/L)
	Before the test After the test	Before the test After the test	Before the test After the test	Before the test After the test
Control	6.18 ± 0.96	3.93 ± 0.41	1.21 ± 0.25	3.96 ± 0.66
	5.60 ± 0.94	3.51 ± 0.47	1.42 ± 0.27	3.38 ± 0.62
Test	6.41 ± 1.06	3.80 ± 0.48	1.23 ± 0.40	3.83 ± 0.73
	3.63 ± 0.97 ^a	2.05 ± 0.54 ^b	2.28 ± 0.50 ^c	1.97 ± 0.49 ^d
<i>t</i> value	-10.29	-14.51	10.77	-11.96

n = 50 in each group. All values are mean ± standard deviation (SD). *P* value indicates statistical significance (a, b, c, and d: *P* ≤ 0.001; all *P* < 0.05).

respectively, showing significant statistical intergroup differences (all *P* < 0.05; see Table 3).

The systolic blood pressure in the experimental and the control group was 141.10 ± 6.67 and 149.08 ± 5.50 mmHg, respectively, and diastolic blood pressure was 80.50 ± 5.97 and 85.20 ± 6.12 mmHg, respectively, showing significant statistical differences (all *P* < 0.05; see Table 4).

The TC of the experimental group and the control group were 3.63 ± 0.97 and 5.60 ± 0.94 mmol/L, respectively. The TG was 2.05 ± 0.54 and 3.51 ± 0.47 mmol/L, respectively. LDL-C was 1.97 ± 0.49 and 3.38 ± 0.62 mmol/L, respectively. HDL-C was 2.28 ± 0.50 and 1.42 ± 0.27 mmol/L, respectively, showing significant statistical intergroup differences (all *P* < 0.05; see Table 5).

3.4. Overall Trend Analysis of Relevant Data after Test Intervention. The FPG, 2hPG, and blood pressure in the two groups showed a steady decline, and the decline in the test group was more significant. “Some additional figure file shows this in more detail (see Figures 2–5).”

4. Discussion

Diet therapy is the most basic therapy for type 2 diabetes. During the treatment of obesity type 2 diabetes, diet therapy

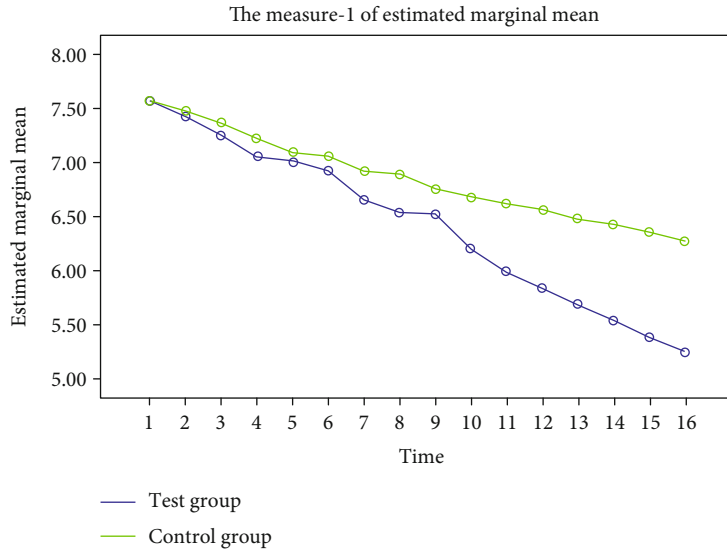


FIGURE 2: Trend of FPG changes during the two groups of experiments. The blue represents the experimental group, and the green represents the control group. After 16 weeks of the experimental cycle, FPG in both groups showed a steady decline, but the decline was more significant in the experimental group.

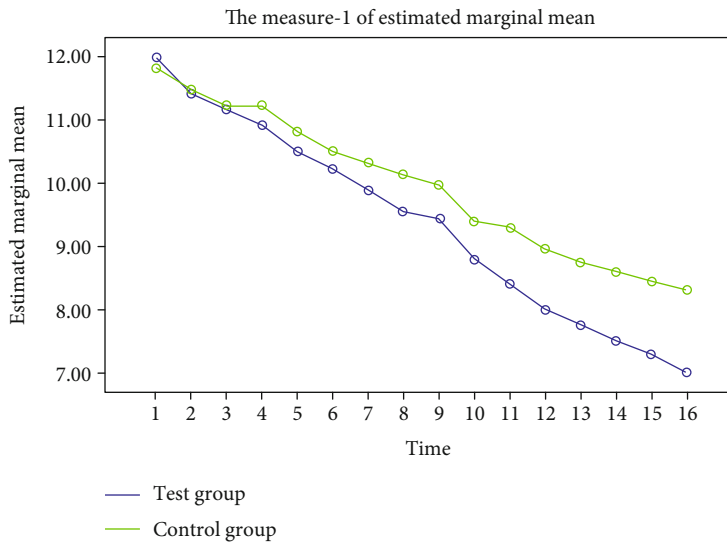


FIGURE 3: Trend of 2hPG changes during the two groups of experiments. The blue represents the experimental group, and the green represents the control group. After 16 weeks of the experiment cycle, both groups showed a steady decline in 2hPG, but the decline was more significant in the experimental group.

is helpful to reduce weight; correct protein, sugar, and lipid metabolism; and improve the metabolic syndrome [7]. As a subclass of diet therapy, FMD has been shown to benefit the reduction of the risks for diabetes and cardiovascular disease and modulate the hormones that regulate hunger and satiety [8]. Whereas all forms of diet therapy exist in patients with long-term adherence to poor compliance, disadvantages such as inaccurate grasp of the value lead to poor dietary treatment, malnutrition, and increased risk of metabolic disorders. However, our study analyzed the effect of specific meal replacement foods during FMD on blood glucose in patients with type 2 diabetes. Specific meal replacement foods were quantified and applied to fasting days. Therefore, this

study not only shows the advantages of FMD in improving blood glucose in patients with type 2 diabetes but also reduces the malnutrition of patients with type 2 diabetes during FMD through the advantages of special medical food.

The result of this study showed that after the 4-month trial, FPG, 2hPG, HbA1c, BMI, waist circumference, blood pressure, and blood lipids (triglycerides, cholesterol, and low-density lipoprotein) in the test group were lower than those in the control group. The density lipoprotein level was higher than the control group, whereas the FPG, 2hPG, and blood pressure in the two groups showed a steady decline, and the decline in the test group was more significant. In addition, the HbA1c in the test group was

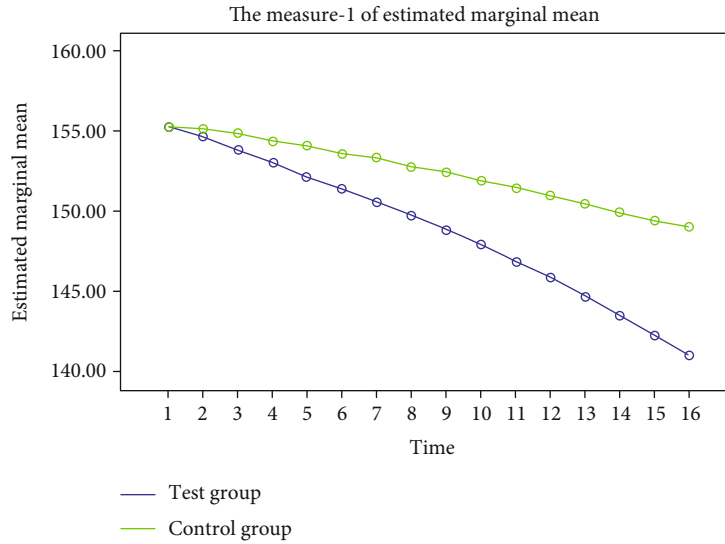


FIGURE 4: Trend of systolic pressure changes during the two groups of experiments. The blue represents the experimental group, and the green represents the control group. After 16 weeks of the experiment cycle, the systolic pressure in both groups showed a stable trend of decline, but the decline in the experimental group was more significant.

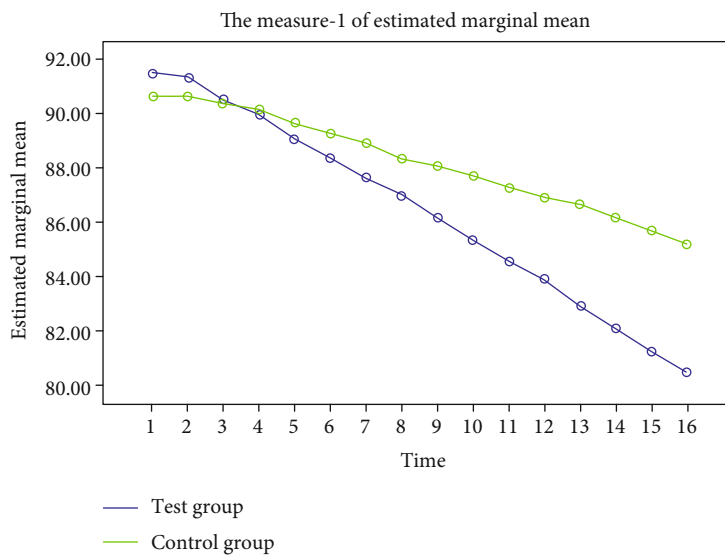


FIGURE 5: Trend of diastolic pressure changes during the two groups of experiments. The blue represents the experimental group, and the green represents the control group. After 16 weeks of the experiment cycle, the diastolic pressure in both groups showed a stable trend of decline, but the decline in the experimental group was more significant.

significantly lower than that of the control group. Thus, specific meal replacement intervention during FMD can safely and effectively improve blood glucose, blood lipids, and blood pressure; reduce weight and improve metabolic parameters in patients with type 2 diabetes; improve patient compliance; achieve stable and lasting blood glucose control. The relevant mechanisms for these findings may be as follows. The pathogenesis of hyperlipidemia, type 2 diabetes mellitus, and metabolic syndrome is modulated by inflammatory cells. Short-term calorie restriction can reduce the metabolism and inflammatory activity of monocytes, thereby significantly reducing the number of inflammation-related monocytes in the blood and tissues and thereby improve

the metabolic parameters [9]. Furthermore, FMD induces prenatal-development gene expression in the adult pancreas. Fasting conditions reduce PKA and mTOR activity and induce Sox2 and Ngn3 expression and insulin production. The effects of the FMD are reversed by IGF-1 treatment and recapitulated by PKA and mTOR inhibition. These results indicate that a FMD promotes the reprogramming of pancreatic cells to restore insulin generation in islets from diabetics [5]. Sutton et al. conducted a 5-week intermittent fasting study on men with prediabetes. The results showed that intermittent fasting could not improve the 24 h blood glucose level and did not affect atherosclerosis, LDL-C, and HDL-C and significantly reduced insulin levels, improved

insulin sensitivity and β -cell reactivity, and lowered blood pressure [10]. The comparison shows that the long-term fasting simulation of decreasing food and giving specific meal replacement food intervention can better benefit the regulation of blood glucose and lipid in patients with type 2 diabetes. Wei et al. conducted a 3-month FMD test on 100 general health participants from the United States. The experimental group showed decreased levels of FPG, insulin-like growth factor 1 (IGF-1), BMI, TG, TC, LDL-C, blood pressure, and C-reactive [11]. The two groups of test subjects are different, but the results of the two groups of experiments are similar, suggesting that the intervention of specific meal replacement foods during FMD in this study is more conducive to the regulation of metabolic indicators in type 2 diabetes patients.

A limitation of this study is that the effect of specific substitute food intervention on patients with type 2 diabetes during FMD was significant. However, the participants of this study were all patients with type 2 diabetes with obesity, hypertension, and high blood lipids. Whether this diet is suitable for type 2 diabetes patients with normal weight and blood pressure needs further investigation. As we use calorie restriction based on its advantages in improving type 2 diabetes, we need to pay attention to avoid potential risks such as hypoglycemia. Exploring the influence of diet therapy on patients with type 2 diabetes for different people is a long-term goal that must be adhered to in the future research.

5. Conclusions

Diet therapy is the most basic treatment for type 2 diabetes. This study found that intervention through specific meal replacement foods for patients with type 2 diabetes during FMD can safely and effectively improve blood glucose, blood pressure, blood lipids, and other metabolic indicators; reduce weight; improve patient compliance; and achieve stable and lasting blood glucose control.

Data Availability

The datasets used and/or analyzed during the current study are available from the corresponding author on reasonable request.

Ethical Approval

This study conforms to the principles of the Declaration of Helsinki and was conducted with the approval of the Ethics Committee of CR & WISCO General Hospital Affiliated to Wuhan University of Science and Technology and the Chinese Clinical Trial Registry (grant no. ChiCTR2000032968). It was registered on 17 May and 2020-retrospectively registered, <http://www.chictr.org.cn/ChiCTR2000032968>. Permissions were obtained from all the relevant authorities of the hospital before enrollment of the patients. Necessary measures were taken to maintain confidentiality of the data and privacy of the participants.

Consent

Written informed consent was sought from all the participants before enrollment.

Conflicts of Interest

The authors declare that there is no conflict of interest regarding the publication of this paper.

Authors' Contributions

XL helped in the study design, data analysis, statistical analysis, and manuscript revising; FT performed the data collection, data analysis, statistical analysis, manuscript writing, and literature search. All authors read and approved the final manuscript.

Acknowledgments

We are thankful to CR & WISCO General Hospital Affiliated to Wuhan University of Science and Technology, Wuhan, Hubei, China. This study was financially supported by the Hubei Province health and family planning scientific research project (grant no. WJ2018H0037).

Supplementary Materials

The study adheres to CONSORT guidelines. "See CONSORT checklist in the Supplementary Material for comprehensive CONSORT analysis." (*Supplementary Materials*)





References

- [1] J. F. Trepanowski, C. M. Kroeger, A. Barnosky et al., "Effect of alternate-day fasting on weight loss, weight maintenance, and cardioprotection among metabolically healthy obese adults: a randomized clinical trial," *JAMA Internal Medicine*, vol. 177, no. 7, pp. 930–960, 2017.
- [2] N. Iqbal, M. L. Vetter, R. H. Moore et al., "Effects of a low-intensity intervention that prescribed a low-carbohydrate vs a low-fat diet in obese diabetic participants," *Obesity*, vol. 18, no. 9, pp. 1733–1738, 2010.
- [3] M. E. Coyle, K. Francis, and Y. Chapman, "Self-management activities in diabetes care: a systematic review," *Australian Health Review*, vol. 37, no. 4, pp. 513–522, 2013.
- [4] E. Brutsaert, M. Carey, and J. Zonszein, "The clinical impact of inpatient hypoglycemia," *Journal of Diabetes and its Complications*, vol. 28, no. 4, pp. 565–572, 2014.
- [5] C. W. Cheng, V. Villani, R. Buono et al., "Fasting-mimicking diet promotes Ngn3-driven β -cell regeneration to reverse diabetes," *Cell*, vol. 168, no. 5, pp. 775–788.e12, 2017.
- [6] S. Stekovic, S. J. Hofer, N. Tripolt et al., "Alternate day fasting improves physiological and molecular markers of aging in healthy, non-obese humans," *Cell Metabolism*, vol. 30, no. 3, pp. 462–476.e6, 2019.
- [7] A. L. Willig, B. S. Richardson, A. Agne, and A. Cherrington, "Intuitive eating practices among African American women living with type 2 diabetes: a qualitative study," *Journal of the Academy of Nutrition and Dietetics*, vol. 114, no. 6, pp. 889–896, 2014.

- [8] V. A. Catenacci, Z. Pan, D. Ostendorf et al., “A randomized pilot study comparing zero-calorie alternate-day fasting to daily caloric restriction in adults with obesity,” *Obesity (Silver Spring)*, vol. 24, no. 9, pp. 1874–1883, 2016.
- [9] S. Jordan, N. Tung, M. Casanova-Acebes et al., “Dietary intake regulates the circulating inflammatory monocyte pool,” *Cell*, vol. 178, no. 5, pp. 1102–1114.e17, 2019.
- [10] E. F. Sutton, R. Beyl, K. S. Early, W. T. Cefalu, E. Ravussin, and C. M. Peterson, “Early time-restricted feeding improves insulin sensitivity blood pressure and oxidative stress even without weight loss in men with prediabetes,” *Cell Metabolism*, vol. 27, no. 6, pp. 1212–1221.e3, 2018.
- [11] M. Wei, S. Brandhorst, M. Shelehchi et al., “Fasting-mimicking diet and markers/ risk factors for aging, diabetes, cancer, and cardiovascular disease,” *Science Translational Medicine*, vol. 9, no. 377, 2017.

Review Article

Mitochondria-Targeted Antioxidants: A Step towards Disease Treatment

Qian Jiang ^{1,2}, Jie Yin ¹, Jiashun Chen,¹ Xiaokang Ma,¹ Miaomiao Wu,¹ Gang Liu ³, Kang Yao,^{1,4} Bie Tan ¹ and Yulong Yin^{1,4}

¹Animal Nutritional Genome and Germplasm Innovation Research Center, College of Animal Science and Technology, Hunan Agricultural University, Changsha, Hunan 410128, China

²Key Laboratory of Feed Biotechnology, The Ministry of Agriculture and Rural Affairs of the People's Republic of China, Beijing 100081, China

³College of Bioscience and Technology, Hunan Agricultural University, Changsha, Hunan 410128, China

⁴Laboratory of Animal Nutritional Physiology and Metabolic Process, Institute of Subtropical Agriculture, Chinese Academy of Sciences, Changsha, Hunan 410125, China

Correspondence should be addressed to Jie Yin; yinjie2014@126.com and Bie Tan; bietan@hunau.edu.cn

Received 21 September 2020; Revised 9 October 2020; Accepted 27 October 2020; Published 7 December 2020

Academic Editor: De-Xing Hou

Copyright © 2020 Qian Jiang et al. This is an open access article distributed under the Creative Commons Attribution License, which permits unrestricted use, distribution, and reproduction in any medium, provided the original work is properly cited.

Mitochondria are the main organelles that produce adenosine 5'-triphosphate (ATP) and reactive oxygen species (ROS) in eukaryotic cells and meanwhile susceptible to oxidative damage. The irreversible oxidative damage in mitochondria has been implicated in various human diseases. Increasing evidence indicates the therapeutic potential of mitochondria-targeted antioxidants (MTAs) for oxidative damage-associated diseases. In this article, we introduce the advantageous properties of MTAs compared with the conventional (nontargeted) ones, review different mitochondria-targeted delivery systems and antioxidants, and summarize their experimental results for various disease treatments in different animal models and clinical trials. The combined evidence demonstrates that mitochondrial redox homeostasis is a potential target for disease treatment. Meanwhile, the limitations and prospects for exploiting MTAs are discussed, which might pave ways for further trial design and drug development.

1. Introduction

Mitochondria, subcellular organelles found in most eukaryotic cells, are responsible for numerous metabolic network processes, including the tricarboxylic acid cycle (TCA cycle), glycolysis, oxidative phosphorylation (OXPHOS), amino acid metabolism, and fatty acid oxidation. Among them, the most important physiological function of mitochondria is to generate ATP by oxidizing nutrients. To participate in adenosine 5'-triphosphate (ATP) production, mitochondria use a complex system interacting with these metabolic network processes, during which free radicals are produced. Generally, mitochondrial ROS production mainly occurs at the site of the electron transport chain located on the mitochondrial inner membrane, and the leakage of electrons from

complex I and complex III leads to oxygen consumption and superoxide formation [1]. The mitochondrial redox homeostasis refers to an equilibrium between ROS production and scavenging, which is the basis for mitochondrial function and cell fate determination [2].

At present, it is recognized that many pathological changes are associated with impaired mitochondrial function [3], such as increased accumulation of ROS and decreased OXPHOS and ATP production. Although the production of intracellular ROS is itself an inevitable process, cells have an adaptive defense system to scavenge ROS [4]. However, under most oxidative stress conditions, the endogenous antioxidant system in the cells is not enough to scavenge excess ROS. In that case, the accumulation of ROS will cause oxidative damage to intracellular lipids, DNA, and proteins,

thereby accelerating the development of related diseases [5]. In the past decade, research has focused on maintaining redox homeostasis and normal function of mitochondria via antioxidants [6]. Current medical projects are aimed at exploiting drugs that restore mitochondrial function and regulate mitochondrial ROS production [7]. To modulate mitochondrial redox homeostasis, the drug should selectively accumulate in the mitochondria and interact with mitochondrial targets, ultimately maintaining normal cellular functions [8]. Although this mitochondrial targeting strategy is attractive, the clinical applications are hampered by some challenges, such as the poor biological availability and the lack of evidence in animal models and clinical research studies [9]. Several drugs have been applied for clinical trials; however, no drug has been approved by the US Food and Drug Administration (FDA) for mitochondria-targeted treatment.

The present review article is aimed at summarizing experimental data on mitochondria-targeted antioxidants (MTAs) for various disease treatments in different models and clinical trials to present the evidence supporting the therapeutic potential of these MTAs. We specifically focused on brain neurological diseases [10, 11], cardiovascular diseases [12–14], and cancer development [15, 16], all of which are closely associated with oxidative damage and signal activation caused by the excess accumulation of ROS in mitochondria. Meanwhile, the potential MTA applications in disease treatment, their limitations, and prospects for exploiting MTAs are discussed.

2. Moving Forward from Nontargeted Antioxidants to MTAs

An increasing number of studies are aimed at developing conventional (nontargeted) antioxidants for restoring physiology conditions during oxidative stress. Although preliminary studies on many cell or animal models showed promising results, the results from clinical trials were sometimes contradictory. A recent review article [17] has summarized the adverse effects of nontargeted antioxidants (NAs) including vitamin A, vitamin C, vitamin E, and β -carotene. These adverse effects of NAs were mainly observed in the treatments of lung cancer and cardiovascular diseases [18]. Redox signaling is an important part of many physiological processes. Excessive or inappropriate use of antioxidants may abolish ROS production and result in compensatory upregulation of mitogen-activated protein kinase (MAPK) pathways [19], which in turn negatively affect the endogenous antioxidant system and normal cell growth [20]. Another concern is whether conventional (nontargeted) antioxidants can be absorbed properly and how they are metabolized in different organs. These uncertainties make it difficult to determine the dose of traditional antioxidants used for disease treatment. The most effective way for an antioxidant stepping forward to disease treatment is to conjugate with a carrier, such as lipophilic cations, liposomes, or peptides, to enable its bioactive ingredient to be targeted for transport into the mitochondria. This targeted delivery enables antioxidants to achieve high concentration accumu-

lation in cells and mitochondria, thereby protecting cells and tissues from oxidative damage through different mechanisms. Ideal antioxidants should be bioavailable and can quickly enter the blood circulation via intestinal absorption or intravenous injection. The MTAs could accumulate in the mitochondria and protect the targeted tissues (brain, liver, kidney, muscle, ear, and heart) from oxidative damage (Figure 1). In the past decade, many studies focusing on the development of mitochondria-targeted antioxidants gave promising results, which we will discuss in detail.

3. Lipophilic Cation-Linked MTAs

The mitochondrial transmembrane potential theory was first proposed by Skulachev et al. in 1969 [21]. The lipophilic cation could easily penetrate cells and mitochondria with the help of $\Delta\Psi_m$, which is positive outside and negative inside. The targeted transport of antioxidants to mitochondria can be achieved by using a lipophilic cation as a transport vehicle. This strategy can be applied for a variety of bioactive substances, especially these hydrophobic ones that are not easily absorbed by cells and mitochondria. In the past decades, triphenylphosphonium (TPP) has been commonly used for the development of MTAs. Presentative studies on the TPP-linked MTAs are summarized in Table 1, and the chemical structures of MitoQ, SkQ1, MitoE, and Mito-TEMPO are shown in Figure 2. Among them, MitoQ and SkQ1 have been extensively studied in various animal models and several human clinical trials [22]. In a clinical trial on twenty healthy older adults (60–79 years) with impaired endothelial function (NCT02597023), oral MitoQ (20 mg/day) supplementation improved brachial artery flow-mediated dilation, decreased aortic stiffness, and lowered the plasma low-density lipoprotein [23]. In a clinical trial on hepatitis C virus- (HCV-) infected patients (NCT00433108), oral MitoQ (40 or 80 mg/day) supplementation decreased serum alanine transaminase (ALT), indicating a decreased necroinflammation in the liver [24]. SkQ1 was documented to relieve the dry eye symptoms in a phase 2 study (NCT02121301) [25]. Meanwhile, a vehicle-controlled study of SkQ1 as a treatment for dry eye syndrome is recruiting (NCT04206020).

Toxicity to mitochondria is a major limiting factor for the application of TPP-linked antioxidants in disease treatment [26]. During the transport of the TPP-linked antioxidants, TPPs increasingly adhere to the surface of the mitochondrial inner membrane. This accumulation of TPPs could destroy the integrity of the mitochondrial membrane and limit aerobic respiration and ATP synthesis [27]. In the toxicity assessment of *in vivo* experiments [28] using a mouse model, the maximum tolerated doses of methyl TPP and MitoE2 are 3.8 and 6.0 mg/(kg * bodyweight), respectively. Evident toxic effects of TPP and MitoE2 were observed at 6.4 and 10.2 mg/(kg * bodyweight), respectively. Intravenous injection of MitoQ was not toxic to the mice at 20 mg/(kg * bodyweight) but significantly toxic at 27.0 mg/(kg * bodyweight). It is noteworthy that long-term and low-dose MitoQ administration did not exhibit any toxic effect to the mouse models [29], which indicates that the toxic effect is caused by the disruption of normal function

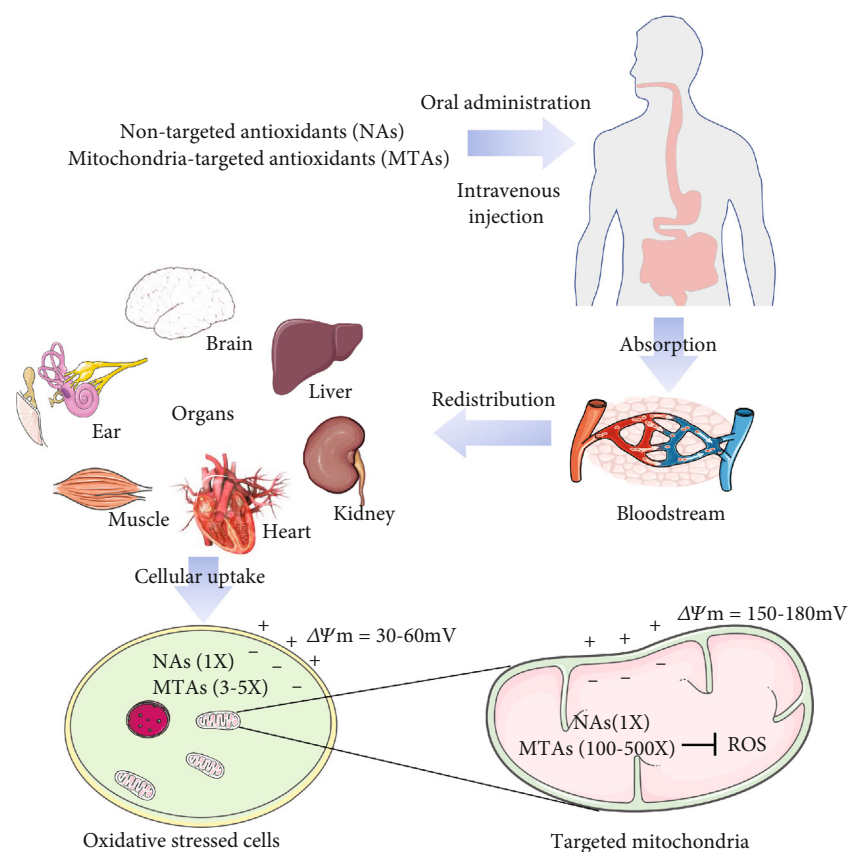


FIGURE 1: Administration and transport of nontargeted antioxidants (NAs) and mitochondria-targeted antioxidants (MTAs). Ideal antioxidants are bioavailable and can be quickly transported into the blood circulation via intestinal absorption or intravenous injection. The NA can hardly be efficiently delivered to the targeted tissues and mitochondria. The MTAs accumulate 100-500 times in the mitochondria and protect the tissues (brain, liver, kidney, muscle, ear, or heart) from oxidative damage.

of mitochondria in response to a concentrated accumulation of TPP, and an oral administration with low-dose TPP compound is feasible. Therefore, in clinical trials testing TPP-linked antioxidants, it is necessary to strictly control the dosage and to ensure the effective concentration of the MTAs is lower than the threshold that destroys the normal function of mitochondria. Although some of these TPP-linked antioxidants such as MitoQ and SkQ1 have been evaluated in a wide range of clinical trials (NCT03166800, NCT02597023, NCT00329056, NCT03764735, and NCT02121301), more studies are required to assess their optimal dosages for different disease phases, their long-term effects on redox signal activation, and their potential side effects.

4. Liposome-Encapsulated Antioxidants

Liposomes are lipid bilayer membrane vesicles first discovered in 1964 and have been commonly used as nanocarriers for pharmaceuticals and bioactive substances [40]. One advantage of the liposomal encapsulation strategy over lipophilic cations is that bioactive molecules can be encapsulated and delivered without altering their molecular structure and bioactivity. The liposome-encapsulated antioxidants are composed of phosphatidylcholine, phosphatidylglycerol, cholesterol, and antioxidant component. The encapsulated

antioxidants such as quercetin, N-acetyl-L-cysteine (NAC), and vitamin E exhibited better therapeutic effects on the models of liver injuries [41] and MCF-7 carcinoma cells [42] when compared with those in nonencapsulated form. For example, only liposomal encapsulated NAC can long-lastingly prevent the cytokine-induced neutrophil chemoattractant expression in the lung, thereby protecting the rats against lipopolysaccharide-induced acute respiratory distress syndrome [43]. It has been reviewed that liposomal encapsulated analogs of vitamin E (α -tocopheryl succinate and α -tocopheryl ether-linked acetic acid) exerted better anticancer effects on various cancer models due to their higher solubility in aqueous solvents [44]. In a clinical study on fatty liver patients, the phospholipid-encapsulated silybin was revealed to protect the liver from oxidative damage via enhancing mitochondrial function and insulin sensitization [45]. Liposome-encapsulated curcumin administration with 100 mg/(kg * bodyweight) increased the parameters of plasma antioxidant activity in the Sprague-Dawley rat [46]. Likewise, astaxanthin encapsulated within liposomes showed a better bioavailability than the nonencapsulated astaxanthin and ameliorated oxidative parameters in the Sprague-Dawley rat model of lipopolysaccharide- (LPS-) induced acute hepatotoxicity [47].

Liposome-based delivery systems can carry conventional antioxidants into the mitochondria of the living cells. The

TABLE 1: TPP-linked MTAs.

Mitochondria-targeted antioxidants	Bioactive component	Linker	Effects	Reference
MitoE	Vitamin E	2-Carbon aliphatic linker	(1) Minimized lipid peroxidation and protected cells from oxidative damage (2) Eliminated H ₂ O ₂ -induced oxidative stress and caspase activation in cells (3) Accumulated in tissues (heart, brain, muscle, liver, and kidney) and protected tissues from oxidative damage	[28, 30]
Mito-vitamin E derivation	Vitamin E	11-Alkyl linker	(1) Inhibited energy metabolism and promote cell death (2) Antitumor properties	[31, 32]
SkQ1 SkQR1	Plastoquinone	10-Alkyl linker	(1) Minimized lipid peroxidation and ROS-induced apoptosis (2) Beneficial roles in many diseases including aging, stroke, myocardial infarction, sarcopenia, dry eye syndrome, vascular inflammation	[33, 34]
MitoQ	Coenzyme Q	10-Alkyl linker	(1) Penetrated the mitochondrial membrane and inhibited lipid peroxidation (2) Beneficial roles in animal models of alcoholic fatty liver, neurodegenerative diseases, ischemia-reperfusion, hypertension, sepsis, and kidney damage in type I diabetes	[35, 36]
MitoC MitoVitC ₁₁	Vitamin C	Thioalkyl linker	(1) Prevented mitochondrial lipid peroxidation and protected mitochondrial aconitase (2) Scavenged O ²⁻ , peroxy radicals, and Fe ³⁺ and could be rapidly recycled to the active ascorbate moiety	[37]
MitoSOD	M40403	Thioalkyl linker	(1) Regulated the mitochondrial redox system to convert ROS (2) Reversed the rapid and progressive inhibition of aconitase through redox cycling (3) Retained Mn ²⁺ under nonacidic conditions	[38, 39]

Notes: $\Delta\Psi_m$: mitochondrial membrane potential; M40403: a macrocyclic Mn SOD mimetic system; ROS: reactive oxygen species; TPP: triphenylphosphonium.

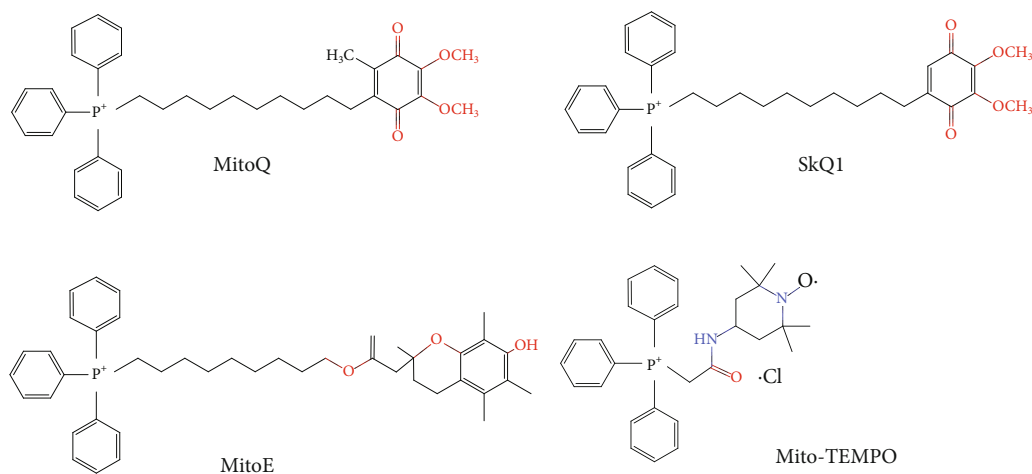


FIGURE 2: Chemical structures of representative TPP-linked mitochondria-targeted antioxidants (MitoQ, SkQ1, MitoE, and Mito-TEMPO are shown).

transport mechanism of liposome-encapsulated MTAs is shown in Figure 3. Liposome-encapsulated antioxidants enter the cells via micropinocytosis; after macropinosome disruption, the liposomal components fuse with the mitochondrial membrane, during which the antioxidant components are delivered into the matrix of targeted mitochondria. The main disadvantage of the liposome system for MTA delivery is the escape of endosome degradation,

which limits the endosomes spontaneously degrading in the cytoplasm and mitochondria. To overcome this limitation, the MITO-Porter that consists of a condensed plasmid DNA and a lipid envelope was developed to deliver bioactive components to mitochondria [48]. The inventors have introduced the characteristics and potential development of MITO-Porter in a specific chapter [49]. Generally, the MITO-Porter-decorated liposomes consist of 1,2-dioleoyl-

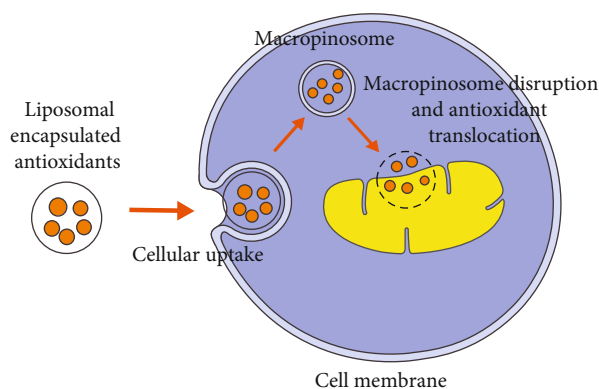


FIGURE 3: The mitochondrial transport of liposome-encapsulated antioxidants. Liposome-encapsulated antioxidants enter cell membranes via micropinocytosis; after macropinosome disruption, the liposomal components fuse with the mitochondrial membrane, during which the antioxidant components are delivered into the matrix of targeted mitochondria.

sn-glycero-3-phosphatidylethanolamine, sphingomyelin, and stearylated octarginine peptide (R8). During a mitochondria-targeted delivery process, the MITO-Porter-decorated liposomes bind to the mitochondria via electrostatic interactions between R8 and negatively charged mitochondria and then fuse with the mitochondrial membrane. This delivery system can achieve efficient cytoplasmic and mitochondria-targeted delivery, which provides a new way for the treatment of mitochondrial disease. Besides, delivery experiments using fluorescent probes have verified MITO-Porter as an effective tool for macromolecule-targeted delivery [50].

In a mouse model of liver ischemia/reperfusion injury, systemic injection of MITO-Porter-encapsulated CoQ10 (CoQ10-MITO-Porter) decreased serum alanine transaminase (ALT) and prevented kidney injury [51]. Recently, the mitochondrial delivery of methylated β -cyclodextrin-threaded polyrotaxanes using a MITO-Porter was revealed to mediate mitochondrial autophagy, which might be useful for mitochondria-associated disease treatment [52]. Moreover, the dual-function MITO-Porter (DF-MITO-Porter) that integrates both R8-modified liposomes and MITO-Porter was developed to effectively deliver exogenous macromolecules into the mitochondria, providing an excellent delivery system for mitochondrial disease treatment [53]. More research studies on the MITO-Porter delivery system are expected to be conducted to shed more light on the mitochondrial therapeutic strategy and targeted antioxidant development.

5. Peptide-Based Mitochondrial Antioxidants

The Szeto-Schiller peptide (SS-peptide) and the mitochondria-penetrating peptide (MPP) are peptide chain-based antioxidant delivery systems. SS-peptides contain different small-molecule lipophilic antioxidant compounds and three positive charges and can be targeted-delivered to the mitochondria with the help of $\Delta\Psi_m$ of the cellular membrane and mitochondrial membrane [54]. The advantageous prop-

erties of SS-peptides include the following: (1) alternating the MPP sequence between the basic and aromatic residues which favor their efficient absorption by cells; (2) unsaturated transport independently from the energy state or a dedicated peptide transporter [55]; (3) small and easily soluble in water, easy to synthesize, and the presence of D-amino acids at specific positions which prevents them from being degraded by aminopeptidases and allows them to be effectively transported into the mitochondria [56]; and (4) 1000-5000 times accumulation in the mitochondria.

Various experiments have confirmed that SS-peptides can be rapidly absorbed by different cell types, such as neurons [57], kidneys [58], epithelial cells, and endothelial cells [59]. It is noteworthy that the mitochondrial uptake speed of SS-peptides is $\Delta\Psi_m$ -independent. The absorption of the SS-peptides does not affect the polarization of the mitochondrial membrane, which makes them ideal antioxidants for disease treatment [60]. For example, SS-02 was revealed to easily penetrate a single layer of intestinal epithelial cells from the basal and apical direction [61]. SS-02 has also been reported to penetrate the blood-brain barrier and thus serve as a neuroprotective agent [62]. The SS-peptides are effective in alleviating oxidative stress both in cell models and isolated mitochondria [63], among them SS-31 was widely validated to be effective. The therapeutic potential of SS-31 has been documented for many conditions including brain microvascular endothelial cell damage [64], lateral line hair cell damage [65], mitochondrial morphogenesis [66], atherosclerosis [67], Friedreich ataxia [68], renal fibrosis [69], limb ischemia-reperfusion injury [70], exercise tolerance [71], type 2 diabetes [72], hearing loss [73], neurovascular coupling responses [74], cardiac arrest [75], traumatic brain injury [76, 77], heart failure [78–81], and acute kidney injury [82]. Of importance, the phase 2a clinical trial of SS-31 (unique identifier: NCT01755858) on the atherosclerotic renal artery stenosis patients (ARASP) showed that supplementing with SS-31 during percutaneous transluminal renal angioplasty alleviated the pathological symptoms and improved kidney function, indicating a positive prospect of SS-31 in clinical application for ARASP [83].

A recent study on aged mice revealed that the disruption of mitochondrial redox homeostasis in muscle resulted in energy defect and exercise intolerance, and SS-31 administration restored redox homeostasis of the aged muscle, thereby increasing the exercise tolerance [71]. Five hours of SS-31 treatment significantly decreased mortality of cardiac arrest rats, during which the blood lactate level in the SS-31-treated rats was significantly decreased, suggesting improved mitochondrial aerobic respiration by SS-31 treatment [75]. The antioxidative roles of SS-31 have been also documented in kidney glomerular mitochondria [84]. SS-31 administration was revealed to prevent negative changes in pathological parameters in chronic kidney disease models [69]. More recently, an acute kidney injury- (AKI-) targeted nanopolyplex was designed for SS-31 delivery, which demonstrates a positive effect of combining the use of nanopolyplexes and SS-31 in the oxidative stressed and inflamed kidney [82]. Similarly, treatment with SS-31 was found to decrease cytoplasmic and mitochondrial O_2^- production by regulating

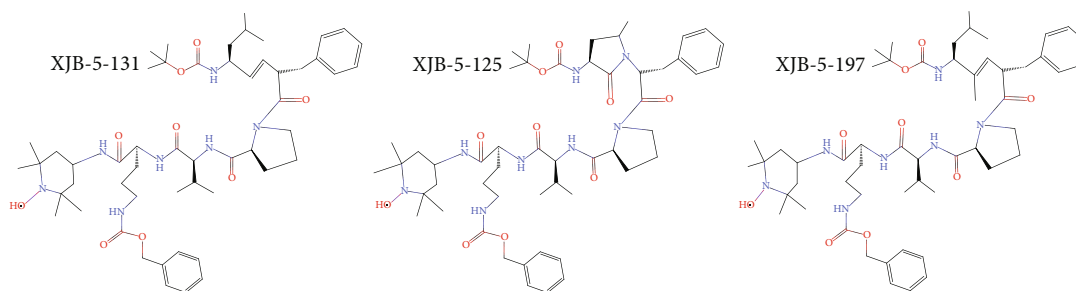


FIGURE 4: Chemical structures of XJB peptide-based mitochondria-targeted antioxidants (XJB-5-131, XJB-5-125, and XJB-5-197 are shown).

the expression of NADPH oxidase subunit NOX4 in a model of traumatic brain injury [76].

Mitochondria-penetrating peptides (MPPs) consist of 4 to 8 alternating positively charged hydrophobically modified amino acids. They have been widely used for the targeted delivery of mitochondrial small molecules with the help of $\Delta\Psi_m$ [85]. A series of XJB peptide-based antioxidants (XJB-5-131, XJB-5-125, and XJB-5-197) have been developed (Figure 4). XJB-5-131, a scavenger for mitochondrial ROS, is the most studied among all the XJB peptide-based antioxidants and has been reported to promote weight gain, prevent neuronal death, and reduce oxidative damage in a mouse model of neurodegeneration [86]. Besides, XJB-5-131 was demonstrated to alleviate oxidative damage of DNA and improve physiology behavior in a Huntington's disease model [87, 88]. Likewise, the compounds of XJB-5-131 and JP4-039 were reported to inhibit ferroptosis via scavenging ROS and altering the subcellular localization of the ferroptosis suppressors [89]. These findings encourage more therapeutic evaluation of XJB peptide-based antioxidants in clinical trials.

6. Potential Applications of MTAs in Disease Treatment

It is noteworthy that MTAs may exert multiple effects, such as alterations in redox status, ETC activity, and ATP synthesis during disease treatments, which could be affected by variations of disease types and phases. Proper dosage of the MTAs used in the trials lowers the ROS production in mitochondria and benefits the disease treatments; however, in some cases, a high dosage of MTAs may inhibit ETC activity and promote oxidative damage. Below, we reviewed the experimental and clinical results in Parkinson's disease (PD), traumatic brain injury (TBI), cardiovascular disorders/cardiovascular diseases (CVDs), or cancers, emphasizing the MTA dosage and potential target mechanisms (Tables 2–5).

6.1. Parkinson's Disease. Parkinson's disease (PD) is a progressive neurodegenerative disease that mainly occurs in the elderly, without any acknowledged therapies. Evidence from *in vitro* cell models, animal models of PD, and genetic analysis has indicated the involvement of oxidative stress and mitochondrial dysfunction during PD development [90]. Thus, the antioxidative strategy shows great potential

for PD therapy. In the past two decades, amounts of studies have been conducted and revealed the beneficial roles of antioxidants in the different cellular and animal models; however, the clinical trials using antioxidants (e.g., NAC (oral 1800, 3600 mg daily; 900 mg effervescent tablet daily), glutathione (100–200 mg daily), and vitamin E (1200 IU/day)+coenzyme Q10 (1200, 2400 mg daily)) to treat PD are mostly disappointing. The experimental factors including inefficient oral administration (NCT01470027, direct oral without any coating or carrier), inadequate patients' replicates (NCT01427517, totally 9 participants were involved; NCT02212678, 8 participants were enrolled), and inappropriate outcome measures (NCT00329056, only UPDRS results were provided; NCT02212678, only GSH levels were provided) may explain these frustrating outcomes from clinical studies. Another possible explanation for this ineffectiveness is that the phase for the antioxidant's treatment is too late for the neurons' rescue. Clinical trial showing high doses of CoQ10 administration benefits the PD patients (NCT01892176), which implies that the traditional antioxidants lack bioavailability, with small scales that can be absorbed into the mitochondria. A systematic review and meta-analysis concluded that CoQ10 cannot provide any symptomatic benefit for PD patients [91]. Consequently, approaches delivering antioxidants to mitochondria for PD treatment have been explored. MitoQ was firstly approved for the clinical trials of PD (NCT00329056) in 2006. A study showed MitoQ (40, 80 mg daily) could slow the progression of PD as measured by the Unified Parkinson's Disease Rating Scale (UPDRS); however, no significant difference between MitoQ and placebo on any measure of PD progression was observed [92]. In regard to dosage, although the experiments *in vitro* (50 nM, 10 μ M) and on mouse models (daily 4 mg/kg * bodyweight) have shown the beneficial effects of MitoQ against mitochondrial dysfunction via preserving striatal dopamine and improving motor functions [93], more study might be conducted to optimize the oral or injection dosage and for the preclinical trials. Besides, the peptide-based mitochondrial antioxidants, such as SS-31 and SS-20 (0.5–5.0 mg/kg * bodyweight), have shown similar neuroprotective effects on cellular and mouse PD models induced by MPTP [94]; however, the clinical trials using peptide-based mitochondrial antioxidants to treat PD have not been approved until now, which might be hampered by the undesirable results of MitoQ in the clinical trials.

TABLE 2: MTAs in PD models and clinical trials.

Mitochondria-targeted antioxidants	Models/clinical trials	Dosage	Effects/mechanism	Reference
MitoQ	Cellular MPP ⁺ model	50 nmol/L in culture medium	(1) Inhibited MPP ⁺ -induced decrease in dopamine levels	[93]
	Mouse MPTP model	4 mg/kg * bodyweight; oral gavage	(1) Protected the nigrostriatal axis against MPTP toxicity (2) Improved locomotor activities in MPTP-treated mice (3) Inhibited mitochondrial aconitase inactivation	[93, 96]
	Cellular 6-OHDA model	10-200 nmol/L in culture medium	(1) Blocked 6-OHDA-induced mitochondrial fragmentation	[97]
	Mouse 6-OHDA model	5 mg/kg * bodyweight; intragastric administration	(1) Rescued dopamine neurons loss in SNc (2) Protected dopamine neurons via activating PGC-1 α and enhance Mfn2-dependent mitochondrial fusion	[97]
	Clinical trial	Daily 40/80 mg; oral administration	(1) Slowed the progression of Parkinson's disease as measured by the UPDRS (2) No difference in the measured parameters between the treatment and the placebo	NCT00329056
SS-20/Phe-D-Arg-Phe-Lys-NH ₂	Cellular MPP ⁺ model	1-10 nmol/L in culture medium	(1) Rescued mitochondrial oxygen consumption and ATP production damaged by MPP ⁺	[94]
	Mouse MPTP model	0.5-5 mg/kg * bodyweight; intraperitoneal injection	(2) SS-20 (4 mg/kg * bodyweight) protected against the loss of dopaminergic neurons in the substantia nigra pars compacta	
SS-31/D-Arg-(2'6'-dimethyltyrosine)-Lys-Phe-NH ₂	Cellular MPP ⁺ model	1-10 nmol/L in culture medium	(1) Improved cell survival and motor performance (2) Decreased cell loss and oxidative stress in the lumbar spinal cord	[94]
	Mouse MPTP model	0.5-10 mg/kg * bodyweight; intraperitoneal injection	(3) SS-31 (10 mg/kg * bodyweight) protected against the loss of dopamine and its metabolites	
P68+DQA nanocarriers NAC	Cellular rotenone PD model	1000 μ mol/L in culture medium	(1) P68+DQA nanocarrier delivery system enhanced the stability, bioavailability, and brain penetrance of NAC (2) Formulation of NAC into P68+DQA nanocarriers rescued cell viability and alleviated oxidative stress	[95]

Notes: 6-OHDA: 6-hydroxydopamine; DQA: dequalinium; Mfn2: mitochondrial GTPase mitofusin-2; MPP⁺: 1-methyl-4-phenylpyridinium; MPTP: 1-methyl-4-phenyl-1,2,3,6-tetrahydropyridine; NAC: N-acetylcysteine; P68: Pluronic F68; PD: Parkinson's disease; PGC-1 α : peroxisome proliferator-activated receptor gamma coactivator 1 alpha; SNc: substantia nigra pars compacta; UPDRS: Unified Parkinson's Disease Rating Scale.

The nanocarrier delivery system that consisted of FDA-approved Pluronic F68 and dequalinium has been revealed to enhance the bioavailability of NAC protecting against the reduced cell viability and oxidative stress in the cellular model of PD, which raises a significant prospect of nanocarrier-based NAC to be transitioned for clinical trials [95]. As indicated by the results from previous clinical trials, the available clinical therapies using antioxidants for PD can only alleviate the symptoms; but none can prevent neuronal degeneration via regulating the dopaminergic system; thus, the combination of MTAs with the traditional drugs (dopamine receptor activator, such as pramipexole) could be a considerable strategy for the further experiments and clinical trials.

6.2. Traumatic Brain Injury (TBI). TBI is a significant cause of death and disability, with an estimated 60-80 million cases per year worldwide, and has been considered an important medical and social problem. TBI can easily damage the cerebral circulatory, which in turn leads to cerebral artery contraction, glutamate poisoning, mitochondrial dysfunction, inflammatory response, and cell death, thereby increasing the severity of the primary damage and causing secondary brain damage [98]. Mechanistically, selective peroxidation of cardiolipin, impaired electron transport, decreased ATP production, and increased formation of ROS during TBI development lead to the final neurodegeneration and brain atrophy [99, 100]. In the past two decades, the beneficial effect of vitamins C and E, progesterone, and NAC to be used

TABLE 3: MTAs in TBI models.

Mitochondria-targeted antioxidants/bioactive component	Models/clinical trials	Dosage	Effects/mechanism	Reference
SkQR1	Rat model by brain surgery	100 nmol/kg; intraperitoneal injection	(1) Decreased the neurological deficit (2) Lowered the volume of the lesion in the brain cortex (3) Decreased mitochondrial ROS and GSK-3 β activity	[106]
	Rat model of focal one-sided TBI	250 nmol/kg; intraperitoneal injection	(1) Rescued the disruptions of limb functions (2) Increased survivability of neurons (3) Decreased astroglial expression and infiltration with segmented neutrophils (4) Beneficial effects are dependent on the reduction of mitochondrial reactive oxygen species	[107]
XJB-5-131	Rat CCI model after TBI	10 mg/kg bodyweight; intravenous injection	(1) Protected brain thiols, GSH and PSH, oxidized by TBI (2) Decreased caspase 3/7 activity and attenuated apoptotic neuronal death (3) Scavenged the electrons leaking from electron carriers	[108]
Mito-TEMPO	Isolated MCAs from rats with traumatic injury	30 nmol in the vessel chamber	(1) Alleviated myogenic constriction (2) Scavenged H ₂ O ₂ (PEG-catalase) by blocking both BKCa channels and TRPV4 channels	[109]
SS-31	Marmarou's weight drop model of TBI	5 mg/kg; intraperitoneal administration	(1) Rescued mitochondrial dysfunction, and alleviated secondary brain injury (2) Decreased ROS, malondialdehyde, and cytochrome c release and prevented the decline of SOD activity (3) Attenuated neurological deficits, brain water content, DNA damage, and neural apoptosis	[77]
MitoQ	Marmarou's weight drop model	4 mg/kg; intraperitoneal administration	(1) Alleviated neurological deficits and brain edema and inhibited cortical neuronal apoptosis (2) Increased the activity of SOD and GPx and decreased MDA level (3) Reduced Bax translocation to mitochondria and cytochrome c release into the cytosol (4) Accelerated the Nrf2 nuclear translocation and upregulated the Nrf2 downstream proteins, including HO-1 and Nqo1	[110]

Notes: Bax: (Bcl-2)-associated X; BKCa: big conductance Ca²⁺-activated K⁺; CCI: chronic constriction injury; GPx: glutathione peroxidase; GSH: glutathione; GSK-3 β : glycogen synthase kinase-3 β ; HO-1: heme oxygenase-1; MCAs: middle cerebral arteries; MDA: malondialdehyde; Nqo1: quinone oxidoreductase 1; Nrf2: nuclear factor erythroid 2; PEG-catalase: polyethylene glycol; PSH: protein thiols; SOD: superoxide dismutase; TBI: traumatic brain injury.

for adjuvant therapy in TBI has been evaluated [101]. Nontargeted antioxidants, commonly in very high concentrations, are used to achieve therapeutic effects. It should be noted that mitochondria are the main source of ROS and determine cell fate [102]; antioxidant delivery to mitochondria is an important target for TBI intervention therapy.

N-Acetylcysteine (NCT00822263), docosahexaenoic acid (NCT01903525), and melatonin (NCT04034771) had been approved for the clinical TBI trials. These clinical results indicated that the NAC (4 grams daily) administration could reduce the sequela of mild TBI [103]. Although the measurements of temperature, mean arterial pressure, intracranial pressure (ICP), use of ICP-directed therapies, surveillance serum brain injury biomarkers, and Glasgow Outcome Scale (GOS) at 3 months were not different between the NAC group and the placebo group [104], the metabolomic results support the antioxidative therapeutic target by the probene-

cid and N-acetylcysteine treatment [105]. Compared with nontargeted antioxidants, relatively low concentrations of MTAs show higher antioxidant activity. The antioxidant activity of SkQR1, XJB-5-131, Mito-TEMPO, SS-31, and MitoQ was revealed in TBI models (Table 3). Although the MTA dosages and mechanisms involved in the therapeutic efficiency are different, data from these different experimental models suggest that MTAs may be a more effective means for mitigating the negative effects of TBI. In terms of mechanism, in addition to antioxidant efficiency, the activation of anti-inflammatory and Nrf2-ARE signaling may also be key indicators for the effectiveness evaluation of MTAs. Until now, the clinical trials using MTAs to treat TBI have not been approved. In future studies, while focusing on the action mechanism and effective dose of various MTAs, the possible toxicological properties of these MTAs also need to be clarified.

TABLE 4: MTAs in cardiovascular disease (CVD) models.

Mitochondria-targeted antioxidants/bioactive component	Models/clinical trials	Dosage	Effects/mechanism	Reference
Mito-TEMPO	THP-1 cell model induced by ox-LDL; high-fat dietary-fed rats	20 $\mu\text{mol/L}$; 0.7 mg/kg * bodyweight; intraperitoneal administration	(1) Attenuated foam cell formation via promoting autophagic flux (2) Increased cholesterol efflux via autophagy-dependent ABCA1 and ABCG1 upregulation (3) Reversed the accumulation of TC and LDL-c	[125]
MitoSNO	Open chest mouse model	100 ng/kg * bodyweight; intravenous injection	(1) Reduced infarct size and troponin release (2) Ineffectiveness on hemodynamics in the heart, dP/dt_{max} or heart rate (3) Alleviated infarction and myocardial fibrosis	[126]
SkQ1	Lifelong treatment of mice	1 or 30 nmol/kg * bodyweight	(1) Prevented spontaneous cardiomyopathy (2) Decreased age-related heart hypertrophy and diffuse fibrosis (3) Affected cell adhesion-related gene expressions, one of which had mitochondrial localization	[127]
	Pressure overload-induced heart failure in rats	100 $\mu\text{mol/L}$ in drinking water	(1) Reduced ventricular hypertrophy and lung congestion (2) Restored membrane potential in IFM (3) Improved retention capacity of mitochondrial calcium in the SSM and IFM	[128]
MitoQ	Pressure overload-induced cardiac fibrosis in rats	2 μmol ; oral gavage	(1) Attenuated apoptosis, hypertrophic remodeling, fibrosis, and left ventricular dysfunction (2) Blunted TGF- β 1 and NOX4 upregulation (3) Prevented Nrf2 downregulation and rescued TGF- β 1 activation (4) Ameliorated the cardiac remodeling dysregulation in phenylephrine and TGF- β 1-induced models	[129]
	Rat model of prenatal hypoxia	125 μmol ; intravenous injection	(1) Improved vasorelaxation (2) Alleviated oxidative stress in placental cells (3) Prevented the decrease in vascular sensitivity to phenylephrine of their offspring	[130]
	Mouse model of aortic stiffening	250 $\mu\text{mol/L}$ in drinking water	(1) Decreased pulse wave velocity in old mice (2) Rescued the decrease of elastin region elastic modulus and elastin expression (3) Reversed <i>in vivo</i> aortic stiffness	[131]
MitoE	Bovine aortic endothelial cells induced by hydrogen peroxide and glucose oxidase	1 $\mu\text{mol/L}$ in culture medium	(1) Abrogated H ₂ O ₂ - and lipid peroxide-induced oxidative protein (2) Inhibited cytochrome c release, caspase 3 activation, and DNA fragmentation (3) Inhibited transferrin receptor-dependent iron uptake and apoptosis	[132]

TABLE 4: Continued.

Mitochondria-targeted antioxidants/bioactive component	Models/clinical trials	Dosage	Effects/mechanism	Reference
SS-20, SS-31	Rat model of myocardial infarction	3 mg/kg * bodyweight; intraperitoneal injection	(1) Reduced lipid peroxidation (2) Decreased the occurrence frequency and severity of arrhythmia	[133]
SS-31/elamipretide/ MTP-131	Clinical trials on heart failure patients	20 mg subcutaneous injection 4 and 40 mg intravenous injection	(1) High-dose SS-31 improved left ventricular volumes (2) Improved super complex-associated oxygen flux, complex (C) I activity	NCT02388464 [78]
	Clinical trials on reperfusion injury patients	Intravenous at 0.05 mg/kg/h	(1) Conjunction SS-31 with standard therapy is superior to placebo for reducing myocardial infarction	NCT01572909 [124]

Notes: CF: cardiac fibroblasts; IFM: interfibrillar mitochondria; LDL-c: high-density lipoprotein cholesterol; lncRNAs: long noncoding RNAs; NOX4: NADPH oxidase subunit 4; Nrf2: nuclear factor erythroid 2; ox-LDL: oxidized high-density lipoprotein; SSM: subsarcolemmal mitochondria; TC: total cholesterol; TEMPO: 4-hydroxy-2,2,6,6-tetramethylpiperidin-N-oxide; TGF- β 1: transforming growth factor β 1.

6.3. Cardiovascular Diseases (CVDs). Cell redox homeostasis maintains a healthy physiological state of cardiomyocytes and vascular endothelial cells. The content of superoxide anions in the failing human myocardium was found to be twice more than that in the healthy myocardium [111]. There are also similar observations in diabetes [112] and hypertensive cardiomyopathy [113]. Besides, the damage parameters of lipid oxidative, nucleic acid, and protein have been observed in the circulation or myocardial tissue of patients with myocardial infarction or heart failure in the animal models of these conditions [113–116]. Moreover, the oxidative damage of the mitochondria and ROS production by endothelial cells were significantly higher compared with the myocardium of young mice, indicating oxidative stress is also involved in age-related CVDs. The depletion of Sod2 (encoding mitochondrial superoxide dismutase) can aggravate the atherosclerotic process in mice, which confirms the detrimental role of ROS overproduction [117]. Interestingly, the absence of a specific cardiomyocyte Txnrd2 (encoding thioredoxin reductase 2) results in fatal dilated cardiomyopathy in the mouse embryo [118]. These observations indicate that overloaded oxidative stress is associated with a variety of cardiovascular diseases, such as atherosclerosis, cardiac hypertrophy, cardiomyopathy, and heart failure [119].

In the cases of overloaded oxidative stress, a timely supplement of antioxidants to maintain the normal function of the cardiovascular system is crucial for the prevention and treatment of cardiovascular diseases. Some conventional antioxidants such as CoQ10 [120], polyphenols [121], vitamin C [122], and vitamin E [123] have been shown to prevent and treat cardiovascular disease in models, with expanded ongoing clinical trials (NCT03133793, NCT01925937, NCT02779634, NCT02847585, NCT02934555, and NCT02218476). However, the majority of these clinical studies are in unknown status which might be attributed to the poor biopharmaceutical properties and the pharmacokinetics of the nontargeted antioxidants. Mitochondria are the main sites for the ROS production and oxidative energy metabolism, implying the MTAs might show better efficacy for the treatment of cardiovascular disease. In recent studies, promising results have

been obtained with the MTAs, including Mito-TEMPO, MitoSNO, SkQ1, MitoQ, MitoE, SS-20, and SS-31, in the cellular and animal models (Table 4), fostering the initiation of clinical trials for CVD treatment. These promising results from preclinical experiments of MitoQ have fostered ongoing clinical trials for diastolic dysfunction (NCT03586414, suspended due to COVID-19 outbreak) and peripheral artery disease (NCT03506633, under recruiting). Clinical trials of SS-31 (formerly named as Bendavia or MTP-131) on the treatment of reperfusion injury (NCT01572909) and heart failure (NCT02388464, NCT02788747, NCT02245620, and NCT02814097) have been completed. The clinical results on reperfusion injury patients indicated that SS-31 combination therapy is superior to placebo [124]. These clinical trials on heart failure patients revealed that SS-31 brings favorable changes in left ventricular volumes in a dose-dependent manner. Recently, one study using an explanted human heart tissue model extended these clinical trials and revealed the beneficial effects of SS-31 on mitochondrial function in heart failure [78]. For further application, the clinical dosage and therapeutic effects of MTAs on the treatment of CVDs need to be further explored.

6.4. Cancer. The mitochondria-derived ROS are crucial in cancer development, which makes mitochondria-targeted antioxidants promising anticancer agents. The relationship between mitochondrial ROS and cancer development has been reviewed in recent publications [134, 135]. Generally, changes in the mitochondrial function of tumor cells (“aerobic glycolysis,” also known as “Warburg effect”) lead to further mitochondrial ROS production and nuclear DNA mutations that impair OXPHOS. As a consequence, oncogenic ROS promote the occurrence and development of tumors via inducing DNA damage and regulating various signaling pathways. For example, the production of H₂O₂ mediated by endogenous oncogenes can improve the proliferation rate of tumor cells via regulating MAPK signals and stimulating extracellular ERK pathway kinase. Mitochondrial production of O²⁻ stimulates the growth of KRAS lung cancer cells through MAPK/ERK signaling [136]. The upregulation

TABLE 5: MTAs in cancer models.

Mitochondria-targeted antioxidants/bioactive component	Models/clinical trials	Dosage	Effects/mechanism	Reference
SkQ1	HT1080 cells	40 nmol/L in culture medium	(1) Suppressed cell growth and prolonged cell mitosis (2) Induced distribution and activation of Aurora family kinases	[132]
	Tumor cells in culture or mouse models	40 nmol/L in culture medium; 250 nmol/kg * bodyweight	(1) Decreased cell growth and the weight of subcutaneous tumors (2) Prolonged cell mitosis and apoptosis	[132]
	p53(-/-) mice	5 nmol/kg * bodyweight per day	(1) Delayed appearance of tumors (2) Inhibited the growth of xenografts tumors and angiogenesis	[133]
	BALB/c mice in SPF environment	1 and 30 nmol/kg * bodyweight per day	(1) Decreased the incidence of spontaneous cancers at the dosage of 30 nmol/kg * bodyweight (2) Suppressed the cancer dissemination at 1 nmol/kg * bodyweight dosage	[134]
	Benzopyrene-induced carcinogenesis in SHR mice	5 and 50 nmol/kg * bodyweight per day	(1) Inhibited tumor growth (2) Dose-dependent effects were observed	[135]
KRSH	HeLa and MCF-7 cells	50 nmol/L in culture medium	(1) Inhibited greater tumor cell growth than the normal cells (2) Increased apoptosis of HeLa and MCF-7 cells, but not of MCF10A cells (3) Accumulated in mitochondria and increased mitochondrial depolarization	[136]
Mito-TEMPO	N-Nitrosodiethylamine-induced hepatocarcinogenesis in BALB/c mice	0.1 mg/kg * bodyweight weekly	(1) Increased animal survival ratio and decreased tumor incidence and tumor multiplicity (2) Rescued the gap junctions and gap junctional intercellular communication of tumor cells	[137]

Notes: HeLa cells: cervical cancer cell line taken from Henrietta Lacks; HT1080: human sarcoma cell line; MCF-7: breast cancer cell line that consisted of the acronym of Michigan Cancer Foundation-7; p53: tumor protein p53; SPF; specific pathogen free.

of ROS also activates transcription factors such as nuclear factor- κ B (NF- κ B), which increases the proliferation of cancer cells [137].

In the past two decades, several studies focused on targeting mitochondria for anticancer therapy. The anticancer mechanism of these agents includes the following: (1) increasing the conductivity of mitochondrial transition pore complex (PTPC), thereby promoting the rupture of mitochondrial membrane and the release of mitochondrial apoptotic factors [138]; (2) targeting proapoptotic Bcl-2 homology domain 3 (BH3) protein mimetics, during which the apoptotic factors are released [139]; (3) sensitizing the cancer cells to conventional treatments via inhibiting glycolysis of cancer cells [140]; and (4) interrupting glutamine catabolism, pyruvate dehydrogenase, and lactate dehydrogenase [138]. Comparatively, the MTAs with the properties of scavenging the mitochondrial ROS or inhibiting the ROS production could only inhibit the proliferation of cancer cells

instead of triggering apoptosis. Several preclinical studies have shown the antigrowth effects of MTAs on cancer models (Table 5). Among the MTAs used for the preclinical experiments, the SkQ1 was the most promising and extensively studied one showing anticancer effects at a nanomole dosage in various models. For example, 40 nmol/L SkQ1 treatment suppressed the proliferation of HT1080 and RD tumor cells in culture via inhibiting mitosis [141]. Daily 5, 30, or 50 nmol/kg * bodyweight SkQ1-supplemented diet decreased the incidence of spontaneous cancers in p53 knockout mice, BALB/c mice, and benzopyrene-induced mice, respectively [142–144]. Recently, a mitochondria-targeted peptide KRSH that consisted of lysine, arginine, tyrosine, and cysteine (Figure 5) was revealed to inhibit cell proliferation and increase apoptosis of HeLa and MCF-7 cell lines [145]. Mechanically, the positively charged lysine and arginine help the KRSH mitochondria-targeted delivery, meanwhile, the tyrosine and cysteine play antioxidative roles

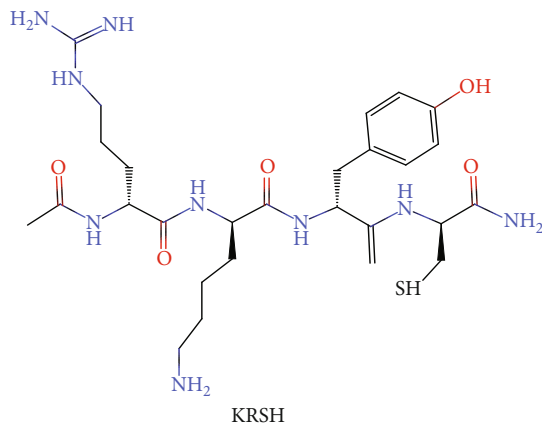


FIGURE 5: Chemical structure of KRSH.

for scavenging mitochondrial ROS. The possible proapoptotic effects of KRSH on HeLa and MCF-7 cells might be attributed to the increased mitochondrial depolarization, but not the antioxidative effects, although the definite mechanism is unknown. The Mito-TEMPO, a TPP-linked MTA whose chemical structure is shown in Figure 2, was revealed to increase the survival ratio and decrease the tumor incidence and tumor multiplicity in the N-nitrosodiethylamine-induced hepatocarcinogenesis mice [146]; however, no *in vitro* evidence attributes its anticancer effect to the ROS scavenging.

MTAs have yielded promising results in several *in vitro* and animal models for cancer studies; however, it is noteworthy that some subsets of cancer cells, such as melanoma tumor cells, exhibit metabolic reprogramming heterogeneity, showing different bioenergy and ROS detoxification capabilities [147]. Besides, a study comparing the effects of MTAs and NAs on the hepatocarcinogenesis indicates contradictory results; that is, nontargeted antioxidants (NAC and vitamin E analog Trolox) prevented tumorigenesis, whereas MTAs (SS-31 and Mito-Q) aggravated tumorigenesis [148]. Therefore, it is critical to clarify the metabolic patterns of different cancer cells in a specific stage and to carefully adopt appropriate therapeutic strategies before clinical intervention with MTAs.

7. Conclusion

Mitochondria produce most of the energy and ROS in cells. Mitochondrial ROS are important signaling molecules involved in many cellular adaptative oxidative defense systems. However, excessive ROS accumulation or insufficient clearance results in damaged mitochondrial DNA and protein, both of which are pathophysiological features of a variety of diseases. In the past decades, many studies focused on developing NAs to restore the normal physiological function of oxidative stressed mitochondria. Research studies on various models were promising, but clinical trials sometimes showed contradictory results. Redox signaling is an important part of many physiological processes. Excessive or inappropriate use of antioxidants may abolish ROS production and result in compensatory upregulation of MAPK path-

ways, which in turn break down the endogenous antioxidant system. Thus, applying the appropriate dosage and delivery method of these antioxidants to balance ROS production and antioxidation is crucial for the clinical trials. Recently, a variety of mitochondria-targeted delivery systems and antioxidants have been exploited to recover mitochondrial function from the pathological conditions in different mechanisms. The outstanding advantages of MTAs over the nontargeted ones include (1) efficient pharmacokinetics and absorption and (2) specific accumulation at cells and mitochondria, avoiding nonspecific high concentration-induced side effects.

This article reviews the characteristics and applications of different mitochondria-targeting tools, including lipophilic cations, liposome vectors, peptide-based targeting, and their recent research reports. Overall, most of these tools have shown beneficial roles for mitochondria-targeting delivery. Based on these delivery tools, an increasing number of MTAs are currently being evaluated, some of which have been validated as effective agents in stage 2 clinical trials, providing unlimited possibilities for mitochondria-targeted therapies. Although the results from current studies are very promising, the human clinical trials on different disease stages should be firstly standardized to effectively translate these research results into usable medicines. Besides, these noteworthy questions should be preferentially considered to exploit more MTAs for disease treatment in the future (refer to noteworthy questions).

Data Availability

No data were used to support this review article.

Additional Points

Noteworthy Questions. (1) What is the decisive mechanism in the development of mitochondria-targeted disease? (2) What is the most effective antioxidant for regulating the decisive mechanism (according to the experiment on separated mitochondria)? (3) Which delivery system will be the best choice for the mitochondria-targeted delivery of antioxidants? (4) How to optimize the effective MTA dosage in different administration approaches (e.g., oral, intravenous, or subcutaneous) for disease treatment? (5) How to standardize a clinical trial (e.g., how many patients to get involved, how long for patient tracking, and what parameters to assess side effects) for the evaluation of MTAs in disease treatment?

Conflicts of Interest

The authors declare no competing financial interest.

Authors' Contributions

Q. J., J. Y., JS. C., XK. M., MM. W., G. L., K. Y., BE. T., and YL. Y. cowrote the manuscript.

Acknowledgments

The authors apologize to scientists in this field whose papers are not cited due to space limitations. The authors are grateful to Emily Ammeter, who is one of the summer undergraduate students in the Department of Animal Science at the University of Manitoba, for her help in the manuscript preparation. This research was funded by the Young Elite Scientists Sponsorship Program by CAST (2019QNRC001), the Human Science Foundation for Outstanding Young Scholars (2020JJ3023), and the Open Project Program of Key Laboratory of Feed Biotechnology, the Ministry of Agriculture and Rural Affairs of the People's Republic of China.

References

- [1] E. Cadenas and K. J. Davies, "Mitochondrial free radical generation, oxidative stress, and aging," *Free Radical Biology & Medicine*, vol. 29, no. 3-4, pp. 222-230, 2000.
- [2] D. R. Green, L. Galluzzi, and G. Kroemer, "Metabolic control of cell death," *Science*, vol. 345, no. 6203, article e1250256, 2014.
- [3] Q. Cai and P. Tammineni, "Alterations in mitochondrial quality control in Alzheimer's disease," *Frontiers in Cellular Neuroscience*, vol. 10, 2016.
- [4] Y. Miura, "Oxidative stress, radiation-adaptive responses, and aging," *Journal of Radiation Research*, vol. 45, no. 3, pp. 357-372, 2004.
- [5] J. P. Kamat, A. Ghosh, and T. P. A. Devasagayam, "Vanillin as an antioxidant in rat liver mitochondria: inhibition of protein oxidation and lipid peroxidation induced by photosensitization," *Molecular and Cellular Biochemistry*, vol. 209, no. 1/2, pp. 47-53, 2000.
- [6] A. Picca, R. T. Mankowski, J. L. Burman et al., "Mitochondrial quality control mechanisms as molecular targets in cardiac ageing," *Nature Reviews Cardiology*, vol. 15, no. 9, pp. 543-554, 2018.
- [7] M. Picard, D. C. Wallace, and Y. Burrelle, "The rise of mitochondria in medicine," *Mitochondrion*, vol. 30, pp. 105-116, 2016.
- [8] H. H. Szeto, "Cell-permeable, mitochondrial-targeted, peptide antioxidants," *The AAPS Journal*, vol. 8, no. 2, pp. E277-E283, 2006.
- [9] W. J. Zhang, X. L. Hu, Q. Shen, and D. Xing, "Mitochondria-specific drug release and reactive oxygen species burst induced by polyprodrug nanoreactors can enhance chemotherapy," *Nature Communications*, vol. 10, no. 1, p. 1704, 2019.
- [10] M. Takahashi and K. Takahashi, "Water-soluble CoQ10 as a promising anti-aging agent for neurological dysfunction in brain mitochondria," *Antioxidants*, vol. 8, no. 3, p. 61, 2019.
- [11] B. G. Trist, D. J. Hare, and K. L. Double, "Oxidative stress in the aging substantia nigra and the etiology of Parkinson's disease," *Aging Cell*, vol. 18, no. 6, 2019.
- [12] V. Ravarotto, F. Simioni, G. Carraro, G. Bertoldi, E. Pagnin, and L. Calò, "Oxidative stress and cardiovascular-renal damage in Fabry disease: is there room for a pathophysiological involvement?," *Journal of Clinical Medicine*, vol. 7, no. 11, p. 409, 2018.
- [13] P. Y. Zhang, X. Xu, and X. C. Li, "Cardiovascular diseases: oxidative damage and antioxidant protection," *European Review for Medical and Pharmacological Sciences*, vol. 18, no. 20, pp. 3091-3096, 2014.
- [14] H. Hadi, R. Vettor, and M. Rossato, "Vitamin E as a treatment for nonalcoholic fatty liver disease: reality or myth?," *Antioxidants*, vol. 7, no. 1, p. 12, 2018.
- [15] U. Ho, J. Luff, A. James et al., "SMG1 heterozygosity exacerbates haematopoietic cancer development in Atm null mice by increasing persistent DNA damage and oxidative stress," *Journal of Cellular and Molecular Medicine*, vol. 23, no. 12, pp. 8151-8160, 2019.
- [16] P. Reberio, A. James, S. Ling et al., "ATM and SMG1 are tumour suppressors which co-regulate blood cancer development and cellular responses to DNA damage and oxidative stress," *Leukemia & Lymphoma*, vol. 56, pp. 78-78, 2015.
- [17] B. Salehi, M. Martorell, J. L. Arbiser et al., "Antioxidants: positive or negative actors?," *Biomolecules*, vol. 8, no. 4, p. 124, 2018.
- [18] Y. Park, D. Spiegelman, D. J. Hunter et al., "Intakes of vitamins A, C, and E and use of multiple vitamin supplements and risk of colon cancer: a pooled analysis of prospective cohort studies," *Cancer Causes & Control*, vol. 21, no. 11, pp. 1745-1757, 2010.
- [19] F. Cerimele, T. Battle, R. Lynch et al., "Reactive oxygen signaling and MAPK activation distinguish Epstein-Barr virus (EBV)-positive versus EBV-negative Burkitt's lymphoma," *Proceedings of the National Academy of Sciences of the United States of America*, vol. 102, no. 1, pp. 175-179, 2005.
- [20] J. R. Burgoyne, H. Mongue-Din, P. Eaton, and A. M. Shah, "Redox signaling in cardiac physiology and pathology," *Circulation Research*, vol. 111, no. 8, pp. 1091-1106, 2012.
- [21] E. A. Liberman and V. P. Topaly, "Permeability of bimolecular phospholipid membranes for fat-soluble ions," *Biofizika*, vol. 14, no. 3, pp. 452-461, 1969.
- [22] R. A. Zinovkin and A. A. Zamyatnin, "Mitochondria-targeted drugs," *Current Molecular Pharmacology*, vol. 12, no. 3, pp. 202-214, 2019.
- [23] M. J. Rossman, J. R. Santos-Parker, C. A. C. Steward et al., "Chronic supplementation with a mitochondrial antioxidant (MitoQ) improves vascular function in healthy older adults," *Hypertension*, vol. 71, no. 6, pp. 1056-1063, 2018.
- [24] E. J. Gane, F. Weilert, D. W. Orr et al., "The mitochondria-targeted anti-oxidant mitoquinone decreases liver damage in a phase II study of hepatitis C patients," *Liver International*, vol. 30, no. 7, pp. 1019-1026, 2010.
- [25] A. Petrov, N. Perekhvatovala, M. Skulachev, L. Stein, and G. Ousler, "SkQ1 ophthalmic solution for dry eye treatment: results of a phase 2 safety and efficacy clinical study in the environment and during challenge in the controlled adverse environment model," *Advances in Therapy*, vol. 33, no. 1, pp. 96-115, 2016.
- [26] N. Apostolova and V. M. Victor, "Molecular strategies for targeting antioxidants to mitochondria: therapeutic implications," *Antioxidants & Redox Signaling*, vol. 22, no. 8, pp. 686-729, 2015.
- [27] M. F. Ross, G. F. Kelso, F. H. Blaikie et al., "Lipophilic triphenylphosphonium cations as tools in mitochondrial bioenergetics and free radical biology," *Biochemistry-Moscow*, vol. 70, no. 2, pp. 222-230, 2005.
- [28] R. A. Smith, C. M. Porteous, A. M. Gane, and M. P. Murphy, "Delivery of bioactive molecules to mitochondria in vivo,"

- Proceedings of the National Academy of Sciences of the United States of America*, vol. 100, no. 9, pp. 5407–5412, 2003.
- [29] V. J. Adlam, J. C. Harrison, C. M. Porteous et al., “Targeting an antioxidant to mitochondria decreases cardiac ischemia-reperfusion injury,” *FASEB Journal*, vol. 19, no. 9, pp. 1088–1095, 2005.
- [30] J. Zielonka, J. Joseph, A. Sikora et al., “Mitochondria-targeted triphenylphosphonium-based compounds: syntheses, mechanisms of action, and therapeutic and diagnostic applications,” *Chemical Reviews*, vol. 117, no. 15, pp. 10043–10120, 2017.
- [31] L. F. Dong, V. J. Jameson, D. Tilly et al., “Mitochondrial targeting of vitamin E succinate enhances its pro-apoptotic and anti-cancer activity via mitochondrial complex II,” *Journal of Biological Chemistry*, vol. 286, no. 5, pp. 3717–3728, 2011.
- [32] V. J. A. Jameson, H. M. Cochemé, A. Logan, L. R. Hanton, R. A. J. Smith, and M. P. Murphy, “Synthesis of triphenylphosphonium vitamin E derivatives as mitochondria-targeted antioxidants,” *Tetrahedron*, vol. 71, no. 44, pp. 8444–8453, 2015.
- [33] L. E. Bakeeva, I. V. Barskov, M. V. Egorov et al., “Mitochondria-targeted plastoquinone derivatives as tools to interrupt execution of the aging program. 2. Treatment of some ROS- and age-related diseases (heart arrhythmia, heart infarctions, kidney ischemia, and stroke),” *Biochemistry-Moscow*, vol. 73, no. 12, pp. 1288–1299, 2008.
- [34] V. P. Skulachev, Y. N. Antonenko, D. A. Cherepanov et al., “Prevention of cardiolipin oxidation and fatty acid cycling as two antioxidant mechanisms of cationic derivatives of plastoquinone (SkQs),” *Biochimica et Biophysica Acta-Bioenergetics*, vol. 1797, no. 6-7, pp. 878–889, 2010.
- [35] M. P. Murphy, “Understanding and preventing mitochondrial oxidative damage,” *Biochemical Society Transactions*, vol. 44, no. 5, pp. 1219–1226, 2016.
- [36] J. S. Tauskela, “MitoQ—a mitochondria-targeted antioxidant,” *IDrugs: the investigational drugs journal*, vol. 10, no. 6, pp. 399–412, 2007.
- [37] P. G. Finichiu, D. S. Larsen, C. Evans et al., “A mitochondria-targeted derivative of ascorbate: MitoC,” *Free Radical Biology and Medicine*, vol. 89, pp. 668–678, 2015.
- [38] G. F. Kelso, A. Maroz, H. M. Cochemé et al., “A mitochondria-targeted macrocyclic Mn(II) superoxide dismutase mimetic,” *Chemistry & Biology*, vol. 19, no. 10, pp. 1237–1246, 2012.
- [39] A. Maroz, G. F. Kelso, R. A. J. Smith, D. C. Ware, and R. F. Anderson, “Pulse radiolysis investigation on the mechanism of the catalytic action of Mn(II) - Pentazamacrocycle compounds as superoxide dismutase mimetics,” *Journal of Physical Chemistry A*, vol. 112, no. 22, pp. 4929–4935, 2008.
- [40] A. D. Bangham and R. W. Horne, “Negative staining of phospholipids and their structural modification by surface-active agents as observed in the electron microscope,” *Journal of Molecular Biology*, vol. 8, no. 5, pp. 660–IN10, 1964.
- [41] M. Alipour, A. Omri, M. G. Smith, and Z. E. Suntres, “Prophylactic effect of liposomal N-acetylcysteine against LPS-induced liver injuries,” *Journal of Endotoxin Research*, vol. 13, no. 5, pp. 297–304, 2016.
- [42] R. Rezaei-Sadabady, A. Eidi, N. Zarghami, and A. Barzegar, “Intracellular ROS protection efficiency and free radical-scavenging activity of quercetin and quercetin-encapsulated liposomes,” *Artificial Cells Nanomedicine and Biotechnology*, vol. 44, no. 1, pp. 128–134, 2014.
- [43] J. Fan, P. N. Shek, Z. E. Suntres, Y. H. Li, G. D. Oreopoulos, and O. D. Rotstein, “Liposomal antioxidants provide prolonged protection against acute respiratory distress syndrome,” *Surgery*, vol. 128, no. 2, pp. 332–338, 2000.
- [44] S. Koudelka, P. Turanek Knotigova, J. Masek et al., “Liposomal delivery systems for anti-cancer analogues of vitamin E,” *Journal of Controlled Release*, vol. 207, pp. 59–69, 2015.
- [45] C. Loguercio, A. Federico, M. Trappolieri et al., “The effect of a silybin-vitamin E-phospholipid complex on nonalcoholic fatty liver disease: a pilot study,” *Digestive Diseases and Sciences*, vol. 52, no. 9, pp. 2387–2395, 2007.
- [46] M. Takahashi, S. Uechi, K. Takara, Y. Asikin, and K. Wada, “Evaluation of an oral carrier system in rats: bioavailability and antioxidant properties of liposome-encapsulated curcumin,” *Journal of Agricultural and Food Chemistry*, vol. 57, no. 19, pp. 9141–9146, 2009.
- [47] C. H. Chiu, C. C. Chang, S. T. Lin, C. C. Chyau, and R. Y. Peng, “Improved hepatoprotective effect of liposome-encapsulated astaxanthin in lipopolysaccharide-induced acute hepatotoxicity,” *International Journal of Molecular Sciences*, vol. 17, no. 7, p. 1128, 2016.
- [48] Y. Yasuzaki, Y. Yamada, and H. Harashima, “Mitochondrial matrix delivery using MITO-Porter, a liposome-based carrier that specifies fusion with mitochondrial membranes,” *Biochemical and Biophysical Research Communications*, vol. 397, no. 2, pp. 181–186, 2010.
- [49] Y. Yamada and H. Harashima, “MITO-Porter for mitochondrial delivery and mitochondrial functional analysis,” in *Pharmacology of Mitochondria*, H. Singh and S.-S. Sheu, Eds., pp. 457–472, Springer International Publishing, Cham, 2017.
- [50] Y. Yamada, H. Akita, H. Kamiya et al., “MITO-Porter: a liposome-based carrier system for delivery of macromolecules into mitochondria via membrane fusion,” *Biochimica et Biophysica Acta-Biomembranes*, vol. 1778, no. 2, pp. 423–432, 2008.
- [51] Y. Yamada, K. Nakamura, J. Abe et al., “Mitochondrial delivery of coenzyme Q10 via systemic administration using a MITO-Porter prevents ischemia/reperfusion injury in the mouse liver,” *Journal of Controlled Release*, vol. 213, pp. 86–95, 2015.
- [52] Y. Yamada, S. Daikuhara, A. Tamura, K. Nishida, N. Yui, and H. Harashima, “Enhanced autophagy induction via the mitochondrial delivery of methylated β -cyclodextrin-threaded polyrotaxanes using a MITO-Porter,” *Chemical Communications*, vol. 55, no. 50, pp. 7203–7206, 2019.
- [53] Y. Yamada, R. Furukawa, Y. Yasuzaki, and H. Harashima, “Dual function MITO-Porter, a nano carrier integrating both efficient cytoplasmic delivery and mitochondrial macromolecule delivery,” *Molecular Therapy*, vol. 19, no. 8, pp. 1449–1456, 2011.
- [54] C. P. Cerrato, M. Pirisinu, E. N. Vlachos, and Ü. Langel, “Novel cell-penetrating peptide targeting mitochondria,” *FASEB Journal*, vol. 29, no. 11, pp. 4589–4599, 2015.
- [55] S. Toyama, N. Shimoyama, H. H. Szeto, P. W. Schiller, and M. Shimoyama, “Protective effect of a mitochondria-targeted peptide against the development of chemotherapy-induced peripheral neuropathy in mice,” *ACS Chemical Neuroscience*, vol. 9, no. 7, pp. 1566–1571, 2018.

- [56] N. Qvit, S. J. S. Rubin, T. J. Urban, D. Mochly-Rosen, and E. R. Gross, "Peptidomimetic therapeutics: scientific approaches and opportunities," *Drug Discovery Today*, vol. 22, no. 2, pp. 454–462, 2017.
- [57] D. M. A. Oliver and P. H. Reddy, "Small molecules as therapeutic drugs for Alzheimer's disease," *Molecular and Cellular Neuroscience*, vol. 96, pp. 47–62, 2019.
- [58] A. Kezic, I. Spasojevic, V. Lezaic, and M. Bajcetic, "Mitochondria-targeted antioxidants: future perspectives in kidney ischemia reperfusion injury," *Oxidative Medicine and Cellular Longevity*, vol. 2016, Article ID 2950503, 12 pages, 2016.
- [59] E. BÖHMOVÁ, D. MACHOVÁ, M. PECHAR et al., "Cell-penetrating peptides: a useful tool for the delivery of various cargoes into cells," *Physiological Research*, vol. 67, Suppl 2, pp. S267–S279, 2018.
- [60] N. N. Alder, W. Mitchell, E. Ng et al., "Biophysical approaches toward understanding the molecular mechanism of action of the mitochondrial therapeutic SS-31 (elamipretide)," *Biophysical Journal*, vol. 116, no. 3, pp. 511a–512a, 2019.
- [61] S. Galdiero and P. Gomes, "Peptide-based drugs and drug delivery systems," *Molecules*, vol. 22, no. 12, p. 2185, 2017.
- [62] H. H. Szeto, "Stealth peptides target cellular powerhouses to fight rare and common age-related diseases," *Protein & Peptide Letters*, vol. 25, no. 12, pp. 1108–1123, 2018.
- [63] G. Serviddio, F. Bellanti, J. Sastre, G. Vendemiale, and E. Altomare, "Targeting mitochondria: a new promising approach for the treatment of liver diseases," *Current Medicinal Chemistry*, vol. 17, no. 22, pp. 2325–2337, 2010.
- [64] T. Imai, K. Mishiho, T. Takagi et al., "Protective effect of Bendavia (SS-31) against oxygen/glucose-deprivation stress-induced mitochondrial damage in human brain microvascular endothelial cells," *Current Neurovascular Research*, vol. 14, no. 1, pp. 53–59, 2017.
- [65] X. Kuang, S. Zhou, W. Guo, Z. Wang, Y. Sun, and H. Liu, "SS-31 peptide enables mitochondrial targeting drug delivery: a promising therapeutic alteration to prevent hair cell damage from aminoglycosides," *Drug Delivery*, vol. 24, no. 1, pp. 1750–1761, 2017.
- [66] J. Wu, S. Hao, X. R. Sun et al., "Elamipretide (SS-31) ameliorates isoflurane-induced long-term impairments of mitochondrial morphogenesis and cognition in developing rats," *Frontiers in Cellular Neuroscience*, vol. 11, p. 119, 2017.
- [67] M. Zhang, H. Zhao, J. Cai et al., "Chronic administration of mitochondrion-targeted peptide SS-31 prevents atherosclerotic development in ApoE knockout mice fed Western diet," *PLoS One*, vol. 12, no. 9, article e0185688, 2017.
- [68] H. Zhao, H. Li, S. Hao et al., "Peptide SS-31 upregulates fractaxin expression and improves the quality of mitochondria: implications in the treatment of Friedreich ataxia," *Scientific Reports*, vol. 7, no. 1, p. 9840, 2017.
- [69] H. Zhao, Y. J. Liu, Z. R. Liu et al., "Role of mitochondrial dysfunction in renal fibrosis promoted by hypochlorite-modified albumin in a remnant kidney model and protective effects of antioxidant peptide SS-31," *European Journal of Pharmacology*, vol. 804, pp. 57–67, 2017.
- [70] J. Cai, Y. Jiang, M. Zhang et al., "Protective effects of mitochondrion-targeted peptide SS-31 against hind limb ischemia-reperfusion injury," *Journal of Physiology and Biochemistry*, vol. 74, no. 2, pp. 335–343, 2018.
- [71] M. D. Campbell, J. Duan, A. T. Samuelson et al., "Improving mitochondrial function with SS-31 reverses age-related redox stress and improves exercise tolerance in aged mice," *Free Radical Biology and Medicine*, vol. 134, pp. 268–281, 2019.
- [72] I. Escribano-Lopez, N. Diaz-Morales, F. Iannantuoni et al., "The mitochondrial antioxidant SS-31 increases SIRT1 levels and ameliorates inflammation, oxidative stress and leukocyte-endothelium interactions in type 2 diabetes," *Scientific Reports*, vol. 8, no. 1, p. 15862, 2018.
- [73] S. Hou, Y. Yang, S. Zhou et al., "Novel SS-31 modified liposomes for improved protective efficacy of minocycline against drug-induced hearing loss," *Biomaterials Science*, vol. 6, no. 6, pp. 1627–1635, 2018.
- [74] S. Tarantini, N. M. Valcarcel-Ares, A. Yabluchanskiy et al., "Treatment with the mitochondrial-targeted antioxidant peptide SS-31 rescues neurovascular coupling responses and cerebrovascular endothelial function and improves cognition in aged mice," *Aging Cell*, vol. 17, no. 2, article e12731, 2018.
- [75] W. Zhang, J. Tam, K. Shinozaki et al., "Increased survival time with SS-31 after prolonged cardiac arrest in rats," *Heart Lung and Circulation*, vol. 28, no. 3, pp. 505–508, 2019.
- [76] A. Czigler, L. Toth, N. Szarka et al., "Hypertension exacerbates cerebrovascular oxidative stress induced by mild traumatic brain injury: protective effects of the mitochondria-targeted antioxidative peptide SS-31," *Journal of Neurotrauma*, vol. 36, no. 23, pp. 3309–3315, 2019.
- [77] Y. Zhu, H. Wang, J. Fang et al., "SS-31 provides neuroprotection by reversing mitochondrial dysfunction after traumatic brain injury," *Oxidative Medicine and Cellular Longevity*, vol. 2018, Article ID 4783602, 12 pages, 2018.
- [78] K. C. Chatfield, G. C. Sparagna, S. Chau et al., "Elamipretide improves mitochondrial function in the failing human heart," *JACC: Basic to Translational Science*, vol. 4, no. 2, pp. 147–157, 2019.
- [79] M. A. Daubert, E. Yow, G. Dunn et al., "Novel mitochondria-targeting peptide in heart failure Treatment," *Circulation-Heart Failure*, vol. 10, no. 12, article e004389, 2017.
- [80] H. N. Sabbah, R. C. Gupta, V. Singh-Gupta, and K. Zhang, "Effects of elamipretide on skeletal muscle in dogs with experimentally induced heart failure," *ESC Heart Failure*, vol. 6, no. 2, pp. 328–335, 2019.
- [81] H. N. Sabbah, R. C. Gupta, V. Singh-Gupta, K. Zhang, and D. E. Lanfear, "Abnormalities of mitochondrial dynamics in the failing heart: normalization following long-term therapy with elamipretide," *Cardiovascular Drugs and Therapy*, vol. 32, no. 4, pp. 319–328, 2018.
- [82] D. Liu, F. Jin, G. Shu et al., "Enhanced efficiency of mitochondria-targeted peptide SS-31 for acute kidney injury by pH-responsive and AKI-kidney targeted nanopolyplexes," *Biomaterials*, vol. 211, pp. 57–67, 2019.
- [83] A. Saad, S. M. S. Herrmann, A. Eirin et al., "Phase 2a clinical trial of mitochondrial protection (elamipretide) during stent revascularization in patients with atherosclerotic renal artery stenosis," *Circulation-Cardiovascular Interventions*, vol. 10, no. 9, article e005487, 2017.
- [84] M. T. Sweetwyne, J. W. Pippin, D. G. Eng et al., "The mitochondrial-targeted peptide, SS-31, improves glomerular architecture in mice of advanced age," *Kidney International*, vol. 91, no. 5, pp. 1126–1145, 2017.
- [85] L. F. Yousif, K. M. Stewart, K. L. Horton, and S. O. Kelley, "Mitochondria-penetrating peptides: sequence effects and

- model cargo transport,” *Chembiochem*, vol. 10, no. 12, pp. 2081–2088, 2009.
- [86] A. Polyzos, A. Holt, C. Brown et al., “Mitochondrial targeting of XJB-5-131 attenuates or improves pathophysiology in HdhQ150 animals with well-developed disease phenotypes,” *Human Molecular Genetics*, vol. 25, no. 9, pp. 1792–1802, 2016.
- [87] A. A. Polyzos, N. I. Wood, P. Williams, P. Wipf, A. J. Morton, and C. T. McMurray, “XJB-5-131-mediated improvement in physiology and behaviour of the R6/2 mouse model of Huntington's disease is age- and sex- dependent,” *PLoS One*, vol. 13, no. 4, article e0194580, 2018.
- [88] Z. Xun, S. Rivera-Sánchez, S. Ayala-Peña et al., “Targeting of XJB-5-131 to mitochondria suppresses oxidative DNA damage and motor decline in a mouse model of Huntington's disease,” *Cell Reports*, vol. 2, no. 5, pp. 1137–1142, 2012.
- [89] T. Krainz, M. M. Gaschler, C. Lim, J. R. Sacher, B. R. Stockwell, and P. Wipf, “A mitochondrial-targeted nitroxide is a potent inhibitor of ferroptosis,” *ACS Central Science*, vol. 2, no. 9, pp. 653–659, 2016.
- [90] S. R. Subramaniam and M. F. Chesselet, “Mitochondrial dysfunction and oxidative stress in Parkinson's disease,” *Progress in Neurobiology*, vol. 106–107, pp. 17–32, 2013.
- [91] A. Negida, A. Menshawy, G. el Ashal et al., “Coenzyme Q10 for patients with Parkinson's disease: a systematic review and meta-analysis,” *CNS & Neurological Disorders-Drug Targets*, vol. 15, no. 1, pp. 45–53, 2016.
- [92] B. J. Snow, F. L. Rolfe, M. M. Lockhart et al., “A double-blind, placebo-controlled study to assess the mitochondria-targeted antioxidant MitoQ as a disease-modifying therapy in Parkinson's disease,” *Movement Disorders*, vol. 25, no. 11, pp. 1670–1674, 2010.
- [93] A. Ghosh, K. Chandran, S. V. Kalivendi et al., “Neuroprotection by a mitochondria-targeted drug in a Parkinson's disease model,” *Free Radical Biology and Medicine*, vol. 49, no. 11, pp. 1674–1684, 2010.
- [94] L. Yang, K. Zhao, N. Y. Calingasan, G. Luo, H. H. Szeto, and M. F. Beal, “Mitochondria targeted peptides protect against 1-methyl-4-phenyl-1,2,3,6-tetrahydropyridine neurotoxicity,” *Antioxidants & Redox Signaling*, vol. 11, no. 9, pp. 2095–2104, 2009.
- [95] L. Mursaleen, B. Noble, S. H. Y. Chan, S. Somavarapu, and M. G. Zariwala, “N-Acetylcysteine nanocarriers protect against oxidative stress in a cellular model of Parkinson's disease,” *Antioxidants*, vol. 9, no. 7, p. 600, 2020.
- [96] H. Jin, A. Kanthasamy, A. Ghosh, V. Anantharam, B. Kalyanaraman, and A. G. Kanthasamy, “Mitochondria-targeted antioxidants for treatment of Parkinson's disease: preclinical and clinical outcomes,” *Biochimica et Biophysica Acta*, vol. 1842, no. 8, pp. 1282–1294, 2014.
- [97] Y. Xi, D. Feng, K. Tao et al., “MitoQ protects dopaminergic neurons in a 6-OHDA induced PD model by enhancing Mfn2-dependent mitochondrial fusion via activation of PGC-1 α ,” *Biochimica et Biophysica Acta (BBA) - Molecular Basis of Disease*, vol. 1864, no. 9, pp. 2859–2870, 2018.
- [98] R. Fernández-Gajardo, J. M. Matamala, R. Carrasco, R. Gutiérrez, R. Melo, and R. Rodrigo, “Novel therapeutic strategies for traumatic brain injury: acute antioxidant reinforcement,” *CNS Drugs*, vol. 28, no. 3, pp. 229–248, 2014.
- [99] V. Calabrese, R. Lodi, C. Tonon et al., “Oxidative stress, mitochondrial dysfunction and cellular stress response in Friedreich's ataxia,” *Journal of Neurological Sciences*, vol. 233, no. 1–2, pp. 145–162, 2005.
- [100] C. B. Pointer and A. Klegeris, “Cardiolipin in central nervous system physiology and pathology,” *Cellular and Molecular Neurobiology*, vol. 37, no. 7, pp. 1161–1172, 2017.
- [101] Q. Shen, J. B. Hiebert, J. Hartwell, A. R. Thimmesch, and J. D. Pierce, “Systematic review of traumatic brain injury and the impact of antioxidant therapy on clinical outcomes,” *Worldviews on Evidence-Based Nursing*, vol. 13, no. 5, pp. 380–389, 2016.
- [102] A. Singh, R. Kukreti, L. Saso, and S. Kukreti, “Oxidative stress: a key modulator in neurodegenerative diseases,” *Molecules*, vol. 24, no. 8, p. 1583, 2019.
- [103] M. E. Hoffer, C. Balaban, M. D. Slade, J. W. Tsao, and B. Hoffer, “Amelioration of acute sequelae of blast induced mild traumatic brain injury by N-acetyl cysteine: a double-blind, placebo controlled study,” *PLoS One*, vol. 8, no. 1, article e54163, 2013.
- [104] R. S. B. Clark, P. E. Empey, H. Bayir et al., “Phase I randomized clinical trial of N-acetylcysteine in combination with an adjuvant probenecid for treatment of severe traumatic brain injury in children,” *PLoS One*, vol. 12, no. 7, article e0180280, 2017.
- [105] F. T. Hagos, P. E. Empey, P. Wang et al., “Exploratory application of neuropharmacometabolomics in severe childhood traumatic brain injury,” *Critical Care Medicine*, vol. 46, no. 9, pp. 1471–1479, 2018.
- [106] N. K. Isaev, S. V. Novikova, E. V. Stelmashook et al., “Mitochondria-targeted plastoquinone antioxidant SkQR1 decreases trauma-induced neurological deficit in rat,” *Biochemistry (Mosc)*, vol. 77, no. 9, pp. 996–999, 2012.
- [107] E. E. Genrikhs, E. V. Stelmashook, O. P. Alexandrova et al., “The single intravenous administration of mitochondria-targeted antioxidant SkQR1 after traumatic brain injury attenuates neurological deficit in rats,” *Brain Research Bulletin*, vol. 148, pp. 100–108, 2019.
- [108] J. Ji, A. E. Kline, A. Amoscato et al., “Lipidomics identifies cardiolipin oxidation as a mitochondrial target for redox therapy of brain injury,” *Nature Neuroscience*, vol. 15, no. 10, pp. 1407–1413, 2012.
- [109] N. Szarka, M. R. Pabbidi, K. Amrein et al., “Traumatic brain injury impairs myogenic constriction of cerebral arteries: role of mitochondria-derived H₂O₂ and TRPV4-dependent activation of BKCa channels,” *Journal of Neurotrauma*, vol. 35, no. 7, pp. 930–939, 2018.
- [110] J. Zhou, H. Wang, R. Shen et al., “Mitochondrial-targeted antioxidant MitoQ provides neuroprotection and reduces neuronal apoptosis in experimental traumatic brain injury possibly via the Nrf2-ARE pathway,” *American Journal of Translational Research*, vol. 10, no. 6, pp. 1887–1899, 2018.
- [111] F. Sam, D. L. Kerstetter, D. R. Pimental et al., “Increased reactive oxygen species production and functional alterations in antioxidant enzymes in human failing myocardium,” *Journal of Cardiac Failure*, vol. 11, no. 6, pp. 473–480, 2005.
- [112] D. Montaigne, X. Marechal, A. Coisne et al., “Myocardial contractile dysfunction is associated with impaired mitochondrial function and dynamics in type 2 diabetic but not in obese patients,” *Circulation*, vol. 130, no. 7, pp. 554–564, 2014.
- [113] D. F. Dai, T. Chen, H. Szeto et al., “Mitochondrial targeted antioxidant peptide ameliorates hypertensive cardiomyopathy,” *Journal of the American College of Cardiology*, vol. 58, no. 1, pp. 73–82, 2011.

- [114] M. Canton, S. Menazza, F. L. Sheeran, P. Polverino de Laurito, F. di Lisa, and S. Pepe, "Oxidation of myofibrillar proteins in human heart failure," *Journal of the American College of Cardiology*, vol. 57, no. 3, pp. 300–309, 2011.
- [115] Y. Kono, K. Nakamura, H. Kimura et al., "Elevated levels of oxidative DNA damage in serum and myocardium of patients with heart failure," *Circulation Journal*, vol. 70, no. 8, pp. 1001–1005, 2006.
- [116] Z. Mallat, I. Philip, M. Lebret, D. Chatel, J. Maclouf, and A. Tedgui, "Elevated levels of 8-iso-prostaglandin F₂α in pericardial fluid of patients with heart failure," *Circulation*, vol. 97, no. 16, pp. 1536–1539, 1998.
- [117] A. E. Vendrov, M. D. Stevenson, S. Alahari et al., "Attenuated superoxide dismutase 2 activity induces atherosclerotic plaque instability during aging in hyperlipidemic mice," *Journal of the American Heart Association*, vol. 6, no. 11, 2017.
- [118] M. Conrad, C. Jakupoglu, S. G. Moreno et al., "Essential role for mitochondrial thioredoxin reductase in hematopoiesis, heart development, and heart function," *Molecular and Cell Biology*, vol. 24, no. 21, pp. 9414–9423, 2004.
- [119] B. K. Ooi, B. H. Goh, and W. H. Yap, "Oxidative stress in cardiovascular diseases: involvement of Nrf2 antioxidant redox signaling in macrophage foam cells formation," *International Journal of Molecular Sciences*, vol. 18, no. 11, p. 2336, 2017.
- [120] V. I. Zozina, S. Covantev, O. A. Goroshko, L. M. Krasnykh, and V. G. Kukes, "Coenzyme Q10 in cardiovascular and metabolic diseases: current state of the problem," *Current Cardiology Reviews*, vol. 14, no. 3, pp. 164–174, 2018.
- [121] Q. Jiang, H. Zhang, R. Yang et al., "Red-osier dogwood extracts prevent inflammatory responses in Caco-2 cells and a Caco-2 BBe1/EA.hy926 cell co-culture model," *Antioxidants*, vol. 8, no. 10, p. 428, 2019.
- [122] A. W. Ashor, R. Brown, P. D. Keenan, N. D. Willis, M. Siervo, and J. C. Mathers, "Limited evidence for a beneficial effect of vitamin C supplementation on biomarkers of cardiovascular diseases: an umbrella review of systematic reviews and meta-analyses," *Nutrition Research*, vol. 61, pp. 1–12, 2019.
- [123] E. Sozen, T. Demirel, and N. K. Ozer, "Vitamin E: regulatory role in the cardiovascular system," *IUBMB Life*, vol. 71, no. 4, pp. 507–515, 2019.
- [124] A. K. Chakrabarti, K. Feeney, C. Abueg et al., "Rationale and design of the EMBRACE STEMI study: a phase 2a, randomized, double-blind, placebo-controlled trial to evaluate the safety, tolerability and efficacy of intravenous Bendavia on reperfusion injury in patients treated with standard therapy including primary percutaneous coronary intervention and stenting for ST-segment elevation myocardial infarction," *American Heart Journal*, vol. 165, no. 4, pp. 509–514.e7, 2013.
- [125] Y. Ma, Z. Y. Huang, Z. L. Zhou et al., "A novel antioxidant Mito-Tempol inhibits ox-LDL-induced foam cell formation through restoration of autophagy flux," *Free Radical Biology and Medicine*, vol. 129, pp. 463–472, 2018.
- [126] C. Methner, E. T. Chouchani, G. Buonincontri et al., "Mitochondria selective S-nitrosation by mitochondria-targeted S-nitrosothiol protects against post-infarct heart failure in mouse hearts," *European Journal of Heart Failure*, vol. 16, no. 7, pp. 712–717, 2014.
- [127] V. N. Manskikh, O. S. Gancharova, A. I. Nikiforova et al., "Age-associated murine cardiac lesions are attenuated by the mitochondria-targeted antioxidant SkQ1," *Histology and Histopathology*, vol. 30, no. 3, pp. 353–360, 2015.
- [128] R. F. Ribeiro Junior, E. R. Dabkowski, K. C. Shekar, K. A. O'Connell, P. A. Hecker, and M. P. Murphy, "MitoQ improves mitochondrial dysfunction in heart failure induced by pressure overload," *Free Radical Biology and Medicine*, vol. 117, pp. 18–29, 2018.
- [129] K. Y. Goh, L. He, J. Song et al., "Mitoquinone ameliorates pressure overload-induced cardiac fibrosis and left ventricular dysfunction in mice," *Redox Biology*, vol. 21, article 101100, 2019.
- [130] M. M. Aljunaidy, J. S. Morton, R. Kirschenman et al., "Maternal treatment with a placental-targeted antioxidant (MitoQ) impacts offspring cardiovascular function in a rat model of prenatal hypoxia," *Pharmaceutical Research*, vol. 134, pp. 332–342, 2018.
- [131] R. A. Gioscia-Ryan, M. L. Battson, L. M. Cuevas, J. S. Eng, M. P. Murphy, and D. R. Seals, "Mitochondria-targeted antioxidant therapy with MitoQ ameliorates aortic stiffening in old mice," *Journal of applied physiology: respiratory, environmental and exercise physiology*, vol. 124, no. 5, pp. 1194–1202, 2018.
- [132] A. Dhanasekaran, S. Kotamraju, S. V. Kalivendi et al., "Supplementation of endothelial cells with mitochondria-targeted antioxidants inhibit peroxide-induced mitochondrial iron uptake, oxidative damage, and apoptosis," *The Journal of Biological Chemistry*, vol. 279, no. 36, pp. 37575–37587, 2004.
- [133] J. Cho, K. Won, D. Wu et al., "Potent mitochondria-targeted peptides reduce myocardial infarction in rats," *Coronary Artery Disease*, vol. 18, no. 3, pp. 215–220, 2007.
- [134] B. Kalyanaraman, G. Cheng, M. Hardy, O. Ouari, B. Bennett, and J. Zielonka, "Teaching the basics of reactive oxygen species and their relevance to cancer biology: mitochondrial reactive oxygen species detection, redox signaling, and targeted therapies," *Redox Biology*, vol. 15, pp. 347–362, 2018.
- [135] Y. H. Yang, S. Karakhanova, W. Hartwig et al., "Mitochondria and mitochondrial ROS in cancer: novel targets for anti-cancer therapy," *Journal of Cellular Physiology*, vol. 231, no. 12, pp. 2570–2581, 2016.
- [136] F. Weinberg, R. Hamanaka, W. W. Wheaton et al., "Mitochondrial metabolism and ROS generation are essential for Kras-mediated tumorigenicity," *Proceedings of the National Academy of Sciences of the United States of America*, vol. 107, no. 19, pp. 8788–8793, 2010.
- [137] M. J. Morgan and Z. G. Liu, "Crosstalk of reactive oxygen species and NF-κB signaling," *Cell Research*, vol. 21, no. 1, pp. 103–115, 2011.
- [138] S. Fulda, L. Galluzzi, and G. Kroemer, "Targeting mitochondria for cancer therapy," *Nature Reviews Drug Discovery*, vol. 9, no. 6, pp. 447–464, 2010.
- [139] E. L. Zhang, C. Zhang, Y. P. Su, T. Cheng, and C. Shi, "Newly developed strategies for multifunctional mitochondria-targeted agents in cancer therapy," *Drug Discovery Today*, vol. 16, no. 3–4, pp. 140–146, 2011.
- [140] X. H. Cao, L. Y. Fang, S. Gibbs et al., "Glucose uptake inhibitor sensitizes cancer cells to daunorubicin and overcomes drug resistance in hypoxia," *Cancer Chemotherapy and Pharmacology*, vol. 59, no. 4, pp. 495–505, 2007.
- [141] E. Titova, G. Shagieva, O. Ivanova et al., "Mitochondria-targeted antioxidant SkQ1 suppresses fibrosarcoma and rhabdomyosarcoma tumour cell growth," *Cell Cycle*, vol. 17, no. 14, pp. 1797–1811, 2018.

- [142] L. S. Agapova, B. V. Chernyak, L. V. Domnina et al., "Mitochondria-targeted plastoquinone derivatives as tools to interrupt execution of the aging program. 3. Inhibitory effect of SkQ1 on tumor development from p53-deficient cells," *Biochemistry-Moscow*, vol. 73, no. 12, pp. 1300–1316, 2008.
- [143] E. K. Fetisova, M. S. Muntyan, K. G. Lyamzaev, and B. V. Chernyak, "Therapeutic effect of the mitochondria-targeted antioxidant SkQ1 on the culture model of multiple sclerosis," *Oxidative Medicine and Cellular Longevity*, vol. 2019, 10 pages, 2019.
- [144] I. V. Anikin, I. G. Popovich, M. L. Tyndyk et al., "Effect of plastoquinone derivative SkQ1 on benzo(a)pyrene-induced soft tissue carcinogenesis," *Voprosy Onkologii*, vol. 59, no. 1, pp. 89–93, 2013.
- [145] W. Zhan, X. Liao, L. H. Li et al., "In vitro mitochondrial-targeted antioxidant peptide induces apoptosis in cancer cells," *Oncotargets and Therapy*, vol. Volume 12, pp. 7297–7306, 2019.
- [146] S. Shetty, R. Kumar, and S. Bharati, "Mito-TEMPO, a mitochondria-targeted antioxidant, prevents N-nitrosodiethylamine-induced hepatocarcinogenesis in mice," *Free Radical Biology and Medicine*, vol. 136, pp. 76–86, 2019.
- [147] F. Vazquez, J. H. Lim, H. Chim et al., "PGC1 α expression defines a subset of human melanoma tumors with increased mitochondrial capacity and resistance to oxidative stress," *Cancer Cell*, vol. 23, no. 3, pp. 287–301, 2013.
- [148] B. B. Wang, J. Fu, T. Yu et al., "Contradictory effects of mitochondria- and non-mitochondria-targeted antioxidants on hepatocarcinogenesis by altering DNA repair in mice," *Hepatology*, vol. 67, no. 2, pp. 623–635, 2017.

Research Article

Protective Effect of Quercetin against H₂O₂-Induced Oxidative Damage in PC-12 Cells: Comprehensive Analysis of a lncRNA-Associated ceRNA Network

Zheyu Zhang,^{1,2,3} Pengji Yi,¹ Min Yi,¹ Xiaoliang Tong,⁴ Xin Cheng,¹ Jingjing Yang,⁵ Yang Hu,¹ and Weijun Peng¹

¹Department of Integrated Traditional Chinese & Western Medicine, The Second Xiangya Hospital, Central South University, Changsha, Hunan 410011, China

²Department of Gastroenterology, Xiangya Hospital, Central South University, Changsha, Hunan 410008, China

³Department of Gastroenterology, Affiliated Hospital of Guilin Medical University, Guilin, Guangxi 541001, China

⁴Department of Dermatology, Third Xiangya Hospital, Central South University, Changsha 410013, China

⁵Department of Integrated Traditional Chinese and Western Medicine, Xiangya Hospital, Central South University, Changsha, Hunan 410008, China

Correspondence should be addressed to Weijun Peng; pengweijun87@csu.edu.cn

Received 4 June 2020; Revised 28 September 2020; Accepted 21 October 2020; Published 2 December 2020

Academic Editor: Wuquan Deng

Copyright © 2020 Zheyu Zhang et al. This is an open access article distributed under the Creative Commons Attribution License, which permits unrestricted use, distribution, and reproduction in any medium, provided the original work is properly cited.

Quercetin is a bioflavonoid with potential antioxidant properties. However, the mechanisms underlying its effects remain unclear. Herein, we focused on integrating long noncoding RNA (lncRNA), microRNA (miRNA), and messenger RNA (mRNA) sequencing of PC-12 cells treated with quercetin. We treated PC-12 cells with hydrogen peroxide to generate a validated oxidative damage model. We evaluated the effects of quercetin on PC-12 cells and established the lncRNA, miRNA, and mRNA profiles of these cells. Gene Ontology and Kyoto Encyclopedia of Genes and Genomes analyses of these RNAs were conducted to identify the key pathways. Quercetin significantly protected PC-12 neuronal cells from hydrogen peroxide-induced death. We identified 297, 194, and 14 significantly dysregulated lncRNAs, miRNAs, and mRNAs, respectively, associated with the antioxidant effect of quercetin. Furthermore, the phosphatidylinositol-3-kinase/protein kinase B pathway was identified as the crucial signalling pathway. Finally, we constructed a lncRNA-associated competing endogenous RNA (ceRNA) network by utilizing oxidative damage mechanism-matched miRNA, lncRNA, and mRNA expression profiles and those changed by quercetin. In conclusion, quercetin exerted a protective effect against oxidative stress-induced damage in PC-12 cells. Our study provides novel insight into ceRNA-mediated gene regulation in the progression of oxidative damage and the action mechanisms of quercetin.

1. Introduction

The maintenance of normal physiological functions depends on the balance between reactive oxygen species (ROS) and intracellular antioxidant factors. Oxidative stress (OS), caused by the imbalanced regulation of oxidant and antioxidant systems in cells, is deleterious to cells through DNA damage, cellular dysfunction, and apoptosis [1, 2]. OS has been implicated in the pathogenesis of numerous disorders by affecting the normal functions of several tissues [3–5].

Furthermore, numerous age-related and neurodegenerative diseases, such as Alzheimer's disease (AD), Parkinson's disease (PD), and inherited mitochondrial disorders, are also directly associated with OS [6–8]. Considering this relationship, extensive research is focused on uncovering the underlying mechanisms and role of OS in the onset and development of disease. It is thought that the discovery of new therapeutic strategies for alleviating OS may be helpful for the treatment of many diseases, especially neurodegenerative diseases.

Quercetin (QUE) is a natural flavonoid widely distributed in many fruits and vegetables. It has numerous biological activities, including antitumour effects, anti-inflammatory properties, cardiovascular protection, and regulation of blood sugar levels [9]. An increasing body of evidence indicates that QUE has the ability to scavenge ROS, such as superoxide radical anion and hydroxyl radical, and can act as an antioxidant agent. Previous *in vitro* research studies suggested that QUE has the ability to quench oxygen free radicals [10–12]. Recent findings indicated that QUE can provide protection against OS when administered *in vivo* [13, 14]. In addition, several studies revealed signal transduction pathways associated with the ability of QUE to counteract oxidative damage, such as activation of the nuclear factor erythroid 2-related factor 2-antioxidant response element (Nrf2-ARE) pathway, induction of Nrf2 nuclear translocation, and an increase in glutathione levels [15–17]. To date, research studies on the antioxidant mechanism of QUE are insufficient.

Recently, noncoding RNAs (ncRNAs), including long ncRNAs (lncRNAs; with lengths > 200 bp) and microRNAs (miRNAs; measuring < 200 nucleotides long), have attracted considerable attention. Dysregulation of lncRNAs and miRNAs has been strongly associated with the pathogenesis of OS [18–20]. Researchers have theorized that lncRNAs harbouring miRNA response elements could compete with each other for binding to a common miRNA, thereby regulating the levels and downstream functions of miRNAs. This hypothesis is termed “competing endogenous RNA (ceRNA)” [21]. Previous evidence demonstrated that OS is strongly correlated with ceRNA. lncRNA LINC01619, as the endogenous competitor, has been shown to regulate miR-27a/forkhead box protein O1 (miR-27a/FOXO1) for the induction of endoplasmic reticulum stress and podocyte damage and subsequently trigger OS [22]. Likewise, by competing to bind to miRNA-150, lncRNA FOXD3-AS1 blocked its protective effect, thereby contributing to the OS-induced apoptosis of lung epithelial cells [23]. Overall, these studies indicated that the link between ncRNAs and OS is stronger than previously thought. However, there is limited knowledge on the role of functional RNA molecules and RNA-mediated regulation networks in the antioxidant mechanism of QUE. Thus, further efforts (*i.e.*, analysis of lncRNA and miRNA) to elucidate the antioxidant mechanisms of QUE are warranted.

The cell line rat pheochromocytoma PC-12 has been commonly used in the investigation of neurological diseases, such as AD and PD [24]. In the present study, a model of oxidative injury was established by hydrogen peroxide- (H_2O_2 -) induced damage in PC-12 cells [25] and used to identify the antioxidant function of QUE. Furthermore, transcriptomics and bioinformatics analyses were conducted to further investigate the regulatory mechanisms of QUE in protecting neuronal cells from oxidative damage.

2. Materials and Methods

2.1. Cell Culture and Treatment. PC-12 cells derived from a transplantable rat pheochromocytoma were cultured in Dulbecco's modified Eagle's medium containing 10% foetal calf

serum, 100 U/mL penicillin, and 100 μ g/mL streptomycin at a density of 1×10^4 cells per well (5% CO_2 at 37°C). Experiments were performed 24 h after cells were seeded. The PC-12 cells were pretreated with various concentrations (6.25, 12.5, or 25 μ M) of QUE in serum-free Dulbecco's modified Eagle's medium for 2 h. Subsequently, the pretreated cells were cultured for an additional 6 h with 500 μ M H_2O_2 to stimulate oxidative damage, as previously described [24]. Untreated cells and cells treated with H_2O_2 alone were used as normal and model control, respectively. H_2O_2 was purchased from Sigma-Aldrich (St. Louis, MO, USA).

2.2. Cell Viability Assay. Cellular toxicities of H_2O_2 and the protective effect of QUE were measured in PC-12 cells using the MTS assay (Promega Corporation, Madison, WI, USA). After treatment with the indicated concentrations of H_2O_2 or QUE, 10 μ L MTS kit solution was added, and the cells were incubated for 1 h at 37°C. Subsequently, the absorbance was measured using a Microplate Reader (BioTek Instruments, Winooski, VT, USA).

2.3. Biochemical Analysis. Cold phosphate-buffered saline was used to collect treated and untreated PC-12 cell samples through centrifugation according to the instructions provided in each enzyme kit. The cells were homogenized with cold phosphate-buffered saline, and commercial kits (Jiangsu Feiya Biological Technology Co., Ltd.) were used to obtain the supernatant for the measurement of malondialdehyde (MDA), glutathione (GSH), and superoxide dismutase (SOD) activity.

2.4. Cell Apoptosis Assay. The protective effect of QUE on apoptosis in PC-12 cells was determined using the Hoechst assay. The cells pretreated with 25 μ M QUE were used as the protection group. After treatment of the cells, 5 μ g/mL Hoechst staining solution was added to avoid light staining, and the cells were placed under an Olympus fluorescence microscope for imaging. This experiment was repeated thrice.

2.5. Western Blotting Analysis. Total protein was extracted from PC-12 cells according to the instructions provided by the manufacturer for the radioimmunoprecipitation assay lysis buffer. The protein assay reagent kit was used to measure the concentrations of the extracted protein. The western blotting protocol was described in detail in our previous study [26]. The glyceraldehyde-3-phosphate dehydrogenase antibody (GAPDH) and β -actin were used as the internal reference, and the grey value was analyzed using the ImageJ software.

2.6. RNA Extraction and Monitoring of Quality. We selected three groups of PC-12 cells, H_2O_2 -induced PC-12 cells, and H_2O_2 -induced PC-12 cells pretreated with 25 μ M QUE for RNA sequencing. For the extraction of total cell RNA from PC-12 cells, the Trizol reagent (Invitrogen, Carlsbad, CA, USA) was used in accordance with the protocol provided by the manufacturer. The detection of RNA quality was performed using the following methods: NanoDrop detection, Qubit 2.0 detection, and Agilent 2100 bioanalyzer test.

2.7. Small RNA Library Construction, High-Throughput Sequencing, and Data Processing. After passing the sample test, 1.5 μg was used as the starting amount of the RNA sample. The volume was adjusted to 6 μL with water, and the small RNA Sample Prep Kit was used for the construction of the library. Next, the concentration and insert size of the library were determined using Qubit 2.0 and Agilent 2100 bioanalyzer test, respectively. The effective concentration of the library was accurately quantified using quantitative polymerase chain reaction (qPCR). Subsequently, the Illumina NovaSeq platform was used for high-throughput sequencing with a single-end 50-nucleotide read length. The raw image data files obtained by Illumina NovaSeq platform sequencing were converted into raw sequencing sequences (Raw Reads) in a FASTQ file format. The following quality control was performed on the Raw Reads to obtain the high-quality sequences (Clean Reads) by removing the following: (1) for each sample, the series with low-quality values; (2) reads with unknown base N (N is an unrecognizable base) with content $\geq 10\%$; (3) reads without 3' linker sequence and inserts; (4) reads contaminated with 5' joints; (5) the 3' linker sequence; (6) reads from ploy A/T/C/G; and (7) sequences < 18 or > 30 nucleotides.

2.8. lncRNA Library Construction, High-Throughput Sequencing, and Data Processing. After the qualification of the samples, library construction was performed. Firstly, the ribosomal RNA (rRNA) of the sample was removed using the epicentre Ribo-Zero™ kit; rRNA-depleted RNA was randomly interrupted by adding fragmentation buffer; rRNA-depleted RNA was used as a template, and random hexamers were used to synthesize the first one cDNA strand. Subsequently, we added buffer, deoxyadenosine triphosphate, deoxyuridine triphosphate, deoxycytidine triphosphate, deoxyguanosine triphosphate, RNase H, and DNA polymerase I to synthesize a second cDNA strand and used AMPure XP beads to purify the cDNA. The purified double-stranded cDNA was then subjected to end repair, and a sequencing adapter was connected. AMPure XP beads were used to select the fragment size. Finally, the U-chain was degraded, and the cDNA library was enriched by PCR. The original sequence (measured by the deribosomal library) was quality controlled, and the method was based on previous studies [27].

2.9. Validation through Real-Time qPCR. Real-time qPCR analysis was used to validate the results of RNA-Seq. The ViiA 7 Real-Time PCR System (Applied Biosystems) and 2X PCR master mix (Arraystar, USA) were selected according to the instructions provided by the manufacturer. The lncRNA, mRNA, and miRNA expression levels were normalized to those of β -actin, ACTB, and U6, respectively. The details of the primers are shown in Table 1. The data represent the average of three experiments.

2.10. Gene Ontology (GO) and Kyoto Gene and Genomic Encyclopedia (KEGG) Pathway Analyses. Furthermore, transcriptional changes were determined at the overall level by GO and KEGG pathway enrichment analyses on mRNAs,

target genes of miRNAs, and target genes of lncRNAs related to QUE treatment. Both analyses were conducted using the R language (version 3.5.3).

2.11. Construction of the lncRNA-Associated ceRNA Network. The ceRNA hypothesis reveals a novel regulatory mechanism between ncRNAs and coding RNAs [27]. The lncRNA-associated ceRNA network was established following these three steps: (1) lncRNA, mRNA, and miRNA related to OS and those altered by QUE were selected; (2) miRanda and TargetScan were applied to predict the correlation of miRNA with ceRNA (herein, lncRNA and mRNA); and (3) a lncRNA-miRNA-mRNA network was constructed using the Cytoscape v3.01 software.

2.12. Statistical Analysis. The SPSS version 22.0 (IBM Corp., Armonk, NY, USA) software was used for statistical analysis in our study. p values < 0.05 denoted statistically significant differences. The DEseq software was utilized to process the sequencing data. Using $p < 0.01$ and $|\log_2(\text{fold change})| > 2$ as the criteria, the differentially expressed (DE) lncRNAs, DE miRNAs, and DE mRNAs were identified.

3. Results

3.1. QUE Protected PC-12 Cells from H_2O_2 -Triggered Injury. The protective effect of QUE on PC-12 cell viability rate induced by H_2O_2 was detected by the MTS assay. As shown in Figure 1(a), the cell survival rate in the model group was significantly reduced compared with that noted in the control group, indicating that H_2O_2 induced cytotoxic damage to PC-12 cells ($p < 0.05$). Through treatment with QUE, the survival rate of PC-12 cells was significantly increased in a dose-dependent manner ($p < 0.05$).

The protective effect of QUE on the activities of SOD and GSH and the content of MDA in PC 12 cells injured by H_2O_2 were detected. As shown in Figure 1(b), the expression levels of MDA in the model group were higher than those recorded in the control group. Compared with the model group, the levels of MDA enzymes in the samples pretreated with QUE were significantly lower. As shown in Figures 1(c) and 1(d), the expression levels of SOD and GSH in the model group were significantly reduced compared with those noted in the control group. Through treatment with QUE, their expression levels were significantly increased in a dose-dependent manner. These results indicate that QUE pretreatment can significantly reduce the inhibitory effect of H_2O_2 on antioxidant enzymes.

3.2. QUE Protected PC-12 Cells from H_2O_2 -Induced Cell Apoptosis. To investigate the effects of QUE on the H_2O_2 -induced apoptosis of PC-12 cells, the Hoechst 33342 staining method was used to detect cell apoptosis, as shown in Figure 2(a). The cells in the control group were dark blue. In the model group, the apoptosis of stained cells was significantly increased after induction treatment and appeared blue-white, while the nuclei showed irregular marginalization. In the protective group pretreated with QUE, the phenomenon of cell apoptosis was obviously alleviated.

TABLE 1: Primers designed for qRT-PCR validation of candidate miRNAs, mRNAs, and lncRNAs.

Names	Forward primer and reverse primer	T _m (°C)	Product length (bp)
ACTB	F: 5' CGAGTACAACCTTCTTGCAGC3' R: 5' ACCCATACCCACCATCACAC3'	60	202
β -Actin (R)	F: 5' CGAGTACAACCTTCTTGCAGC3' R: 5' ACCCATACCCACCATCACAC3'	60	202
U6	F: 5' GCTTCGGCAGCACATATACTAAAAT3' R: 5' CGCTTACGAATTTGCGTGTCAT3'	60	89
IL6	F: 5' TCAGAGCAATACTGAAACCCTA3' R: 5' TCCTTAGCCACTCCTTCTGT3'	60	134
PLK2	F: 5' ATGGTGGCGATCTCCCTAGT3' R: 5' AGCGAACAGCCAGACATCAA3'	60	247
MDM2	F: 5' TGAGGTCTATCGGGTCACAGTC3' R: 5' CAGGCACATCTAAGCCTTCTTCT3'	60	263
CDKN1A	F: 5' TCTTGTGATATGTACCAGCCACAG 3' R: 5' GTCAAAGTTCACCGTTCTCG 3'	60	182
GADD45G	F: 5' GTCTACGAGTCCGCCAAAGTC3' R: 5' CTATGTCGCCCTCATCTTCT3'	60	92
MSTRG.89940.1	F: 5' GTCACCTTACCGTAGGCACA 3' R: 5' CCAAATTCCTCCAGCTTCACT 3'	60	157
MSTRG.4076.1	F: 5' AGTGCTCCCGACATTCACTT 3' R: 5' TCCTTACGCTCAATCTATCCC 3'	60	103
MSTRG.48686.2	F: 5' GCAGTACAACAATTATCGCCAA 3' R: 5' AGGTCCTTAGAGTGAGCAACG 3'	60	197
MSTRG.34031.1	F: 5' TTTCCACAGCCTTCCACG 3' R: 5' CACTTCCACATTGCTCTTCATC 3'	60	196
Novel_miR_1502	GSP: 5' GGGGAATACTGGGTGCTGT 3' R: 5' GTGCGTGTCGTGGAGTCG3'	60	64
Novel_miR_2218	GSP: 5' GGGTTCTGGGTGCTGTA3' R: 5' GTGCGTGTCGTGGAGTCG3'	60	62
Novel_miR_298	GSP: 5' GAAACGGCGCGGATG3' R: 5' GTGCGTGTCGTGGAGTCG3'	60	59
Novel_miR_345	GSP: 5' GGAGGAGGGAACGCAGTCT3' R: 5' GTGCGTGTCGTGGAGTCG3'	60	64
Novel_miR_97	GSP: 5' GGGGTGTCGTCTGAGTG3' R: 5' GTGCGTGTCGTGGAGTCG3'	60	62

Furthermore, western blotting was performed to detect the expression of apoptosis-related proteins, including Bax, procaspase-9, cleaved caspase-9, and procaspase-3. As shown in Figure 2(b), compared with the control group, H₂O₂ induced an obvious increase in the expression of Bax and cleaved caspase-9, whereas it decreased the expression of procaspase-3 and procaspase-9. Pretreatment with QUE enhanced the expression of procaspase-3 and procaspase-9, whereas it reduced that of Bax and cleaved caspase-9 compared with the H₂O₂ group. These results indicate that pretreatment with QUE can significantly protect PC-12 cells from H₂O₂-induced apoptosis.

3.3. DE mRNA and Functional Enrichment Analysis. We firstly focused on changes in the expression of the coding genes. Using the criterion of $p < 0.01$ and $|\log_2(\text{fold change})| > 2$, 966 DE genes (i.e., 823 upregulated and 143 downregulated) between the model and control groups and 495 DE genes (i.e., 130 upregulated and 365 downregulated) between the model and QUE groups were detected. The MA plot (Figures 3(a) and 3(b)) and volcano plot (Figures 3(c) and 3(d)) were applied to exhibit differential gene expression in the above two pairs. The expression profiles of the top 20 upregulated and downregulated DE mRNAs are shown in Figures 3(e) and 3(f), using unsupervised clustering

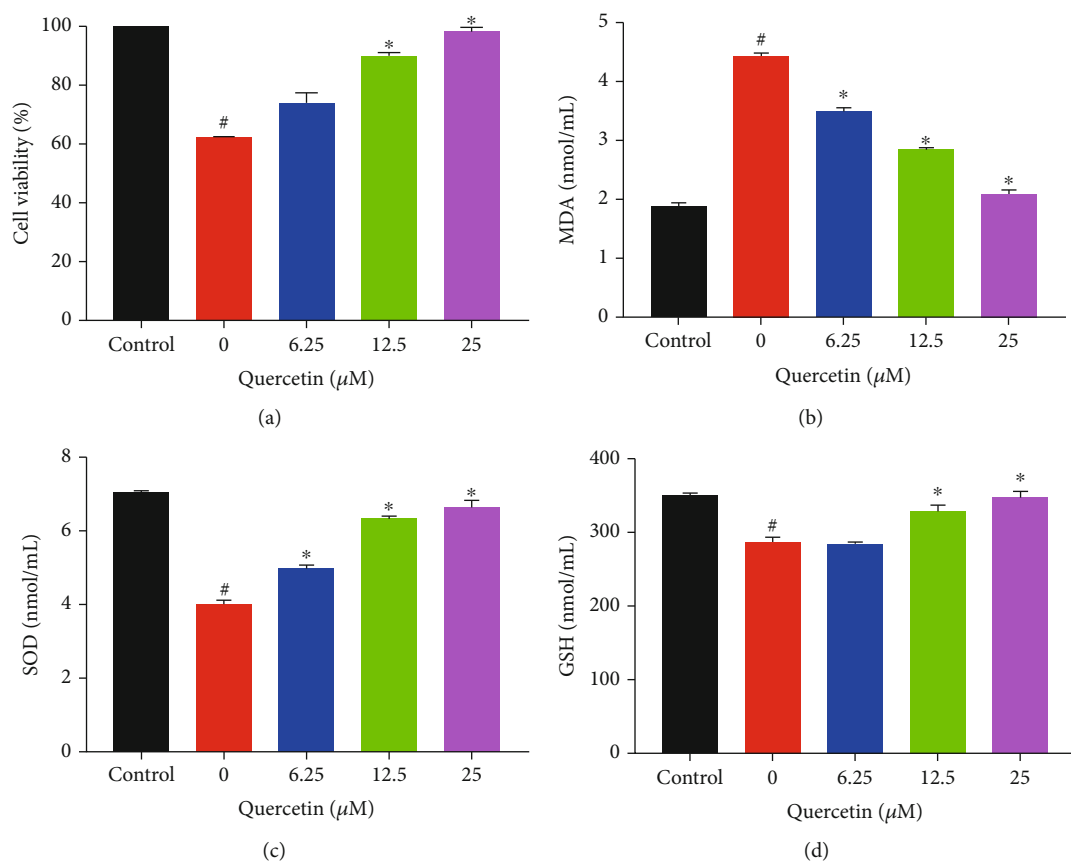


FIGURE 1: Protective effect of QUE on H_2O_2 -induced cytotoxicity in PC-12 cells. (a) Effect of QUE on PC-12 cell viability rate induced by H_2O_2 . The percentage of cell viability was relative to that of untreated control cells. Effect of QUE on (b) MDA, (c) SOD, and (d) GSH in PC-12 cells induced by H_2O_2 . In the protected group, PC-12 cells were pretreated with different concentrations of QUE for 2 h and subsequently incubated with 500 μM H_2O_2 for an additional 6 h. Values represent mean \pm SEM of three independent experiments. # $p < 0.05$ versus control; * $p < 0.05$ versus H_2O_2 -treated cells. H_2O_2 : hydrogen peroxide; QUE: quercetin; SEM: standard error of the mean.

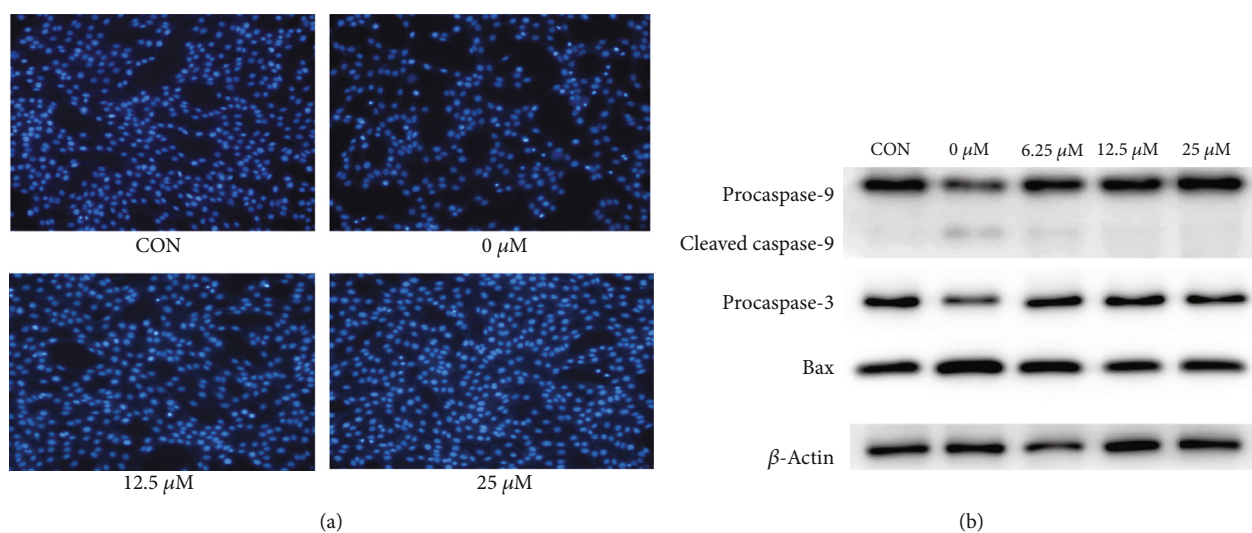


FIGURE 2: Protective effect of QUE against H_2O_2 -induced apoptosis in PC-12 cells. (a) The effect of QUE on H_2O_2 -induced apoptosis detected by Hoechst 33342 staining. (b) Western blotting analysis of the expression of apoptotic proteins. The expression levels of Bax, procaspase-9, cleaved caspase-9, and procaspase-3 were detected. In the protected group, PC-12 cells were pretreated with different concentrations of QUE for 2 h and subsequently incubated with 500 μM H_2O_2 for an additional 6 h. H_2O_2 : hydrogen peroxide; QUE: quercetin.

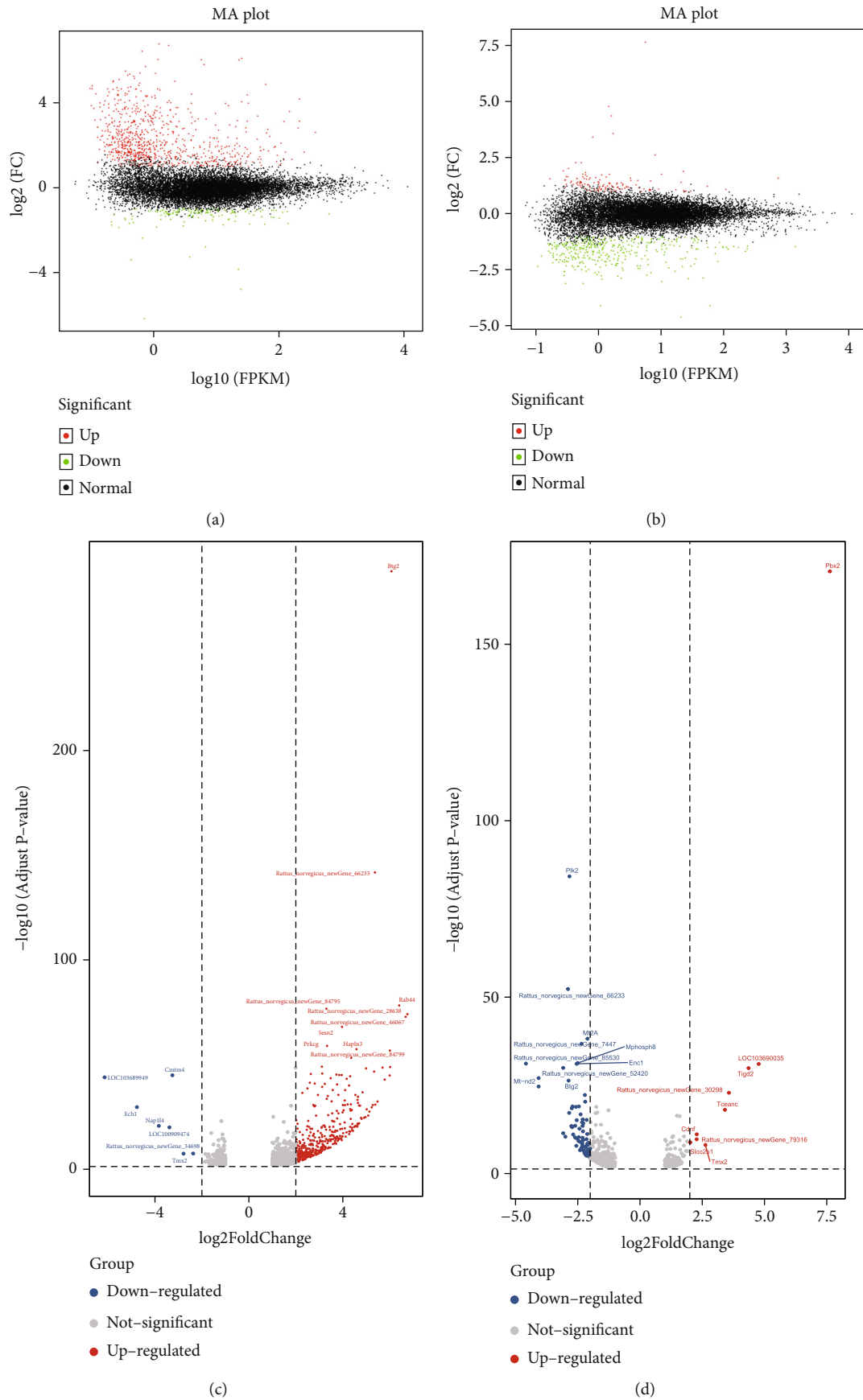
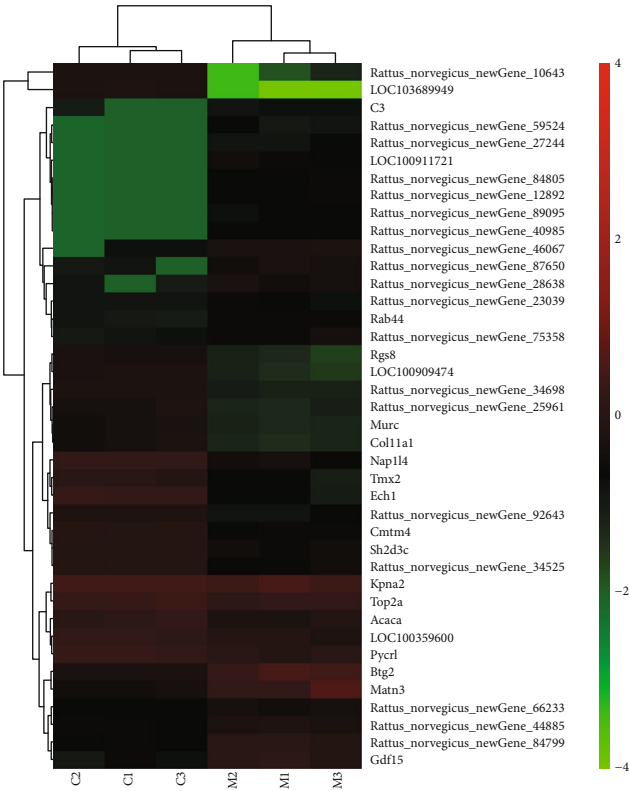
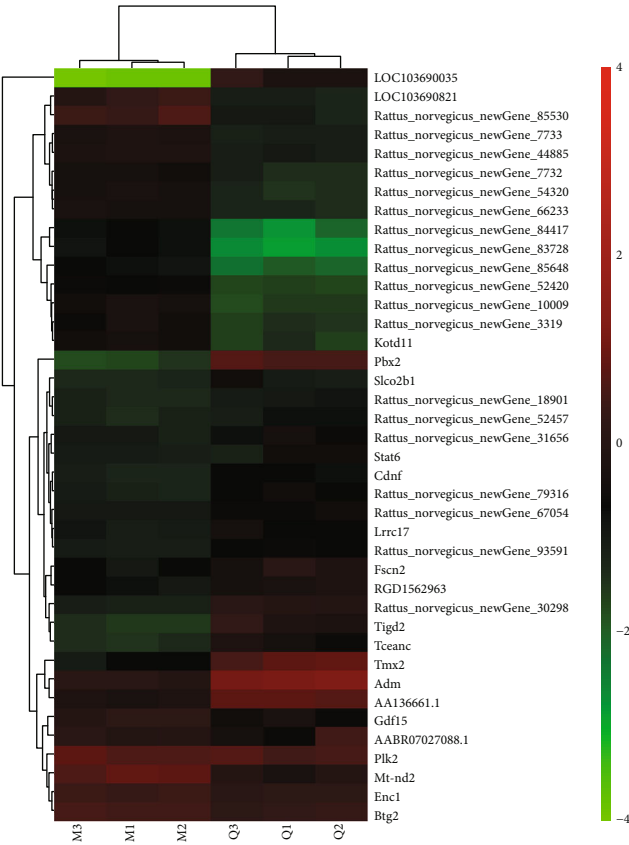


FIGURE 3: Continued.

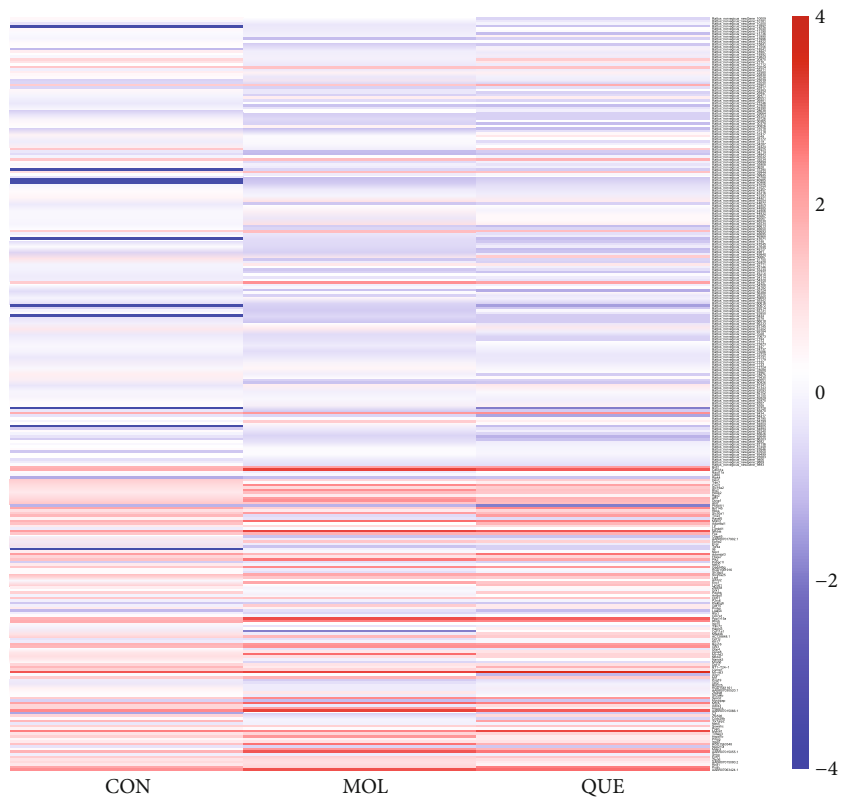


(e)

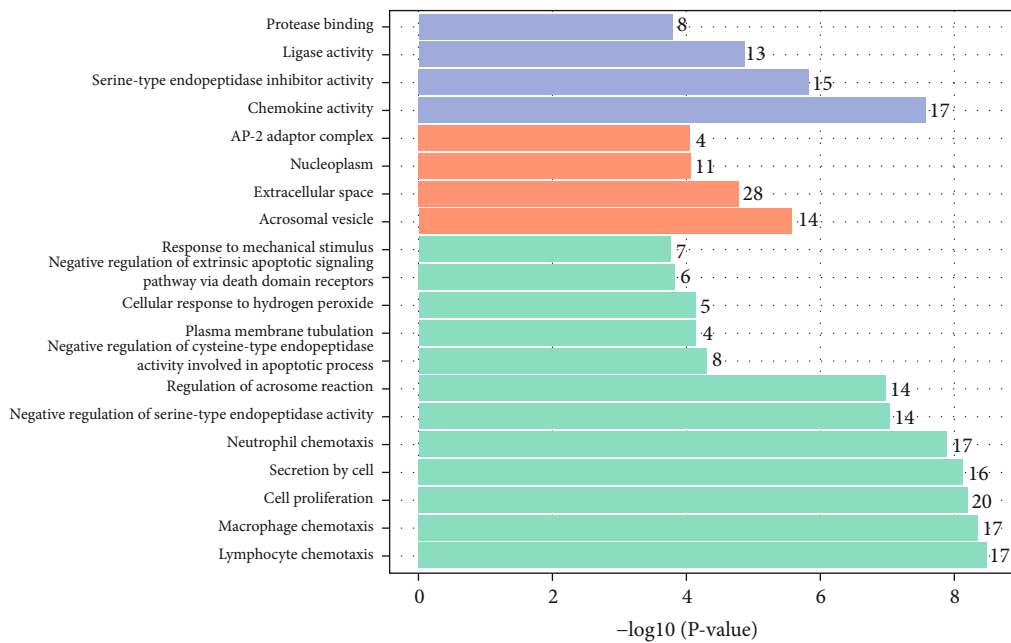


(f)

FIGURE 3: Continued.



(g)



(h)

FIGURE 3: Continued.

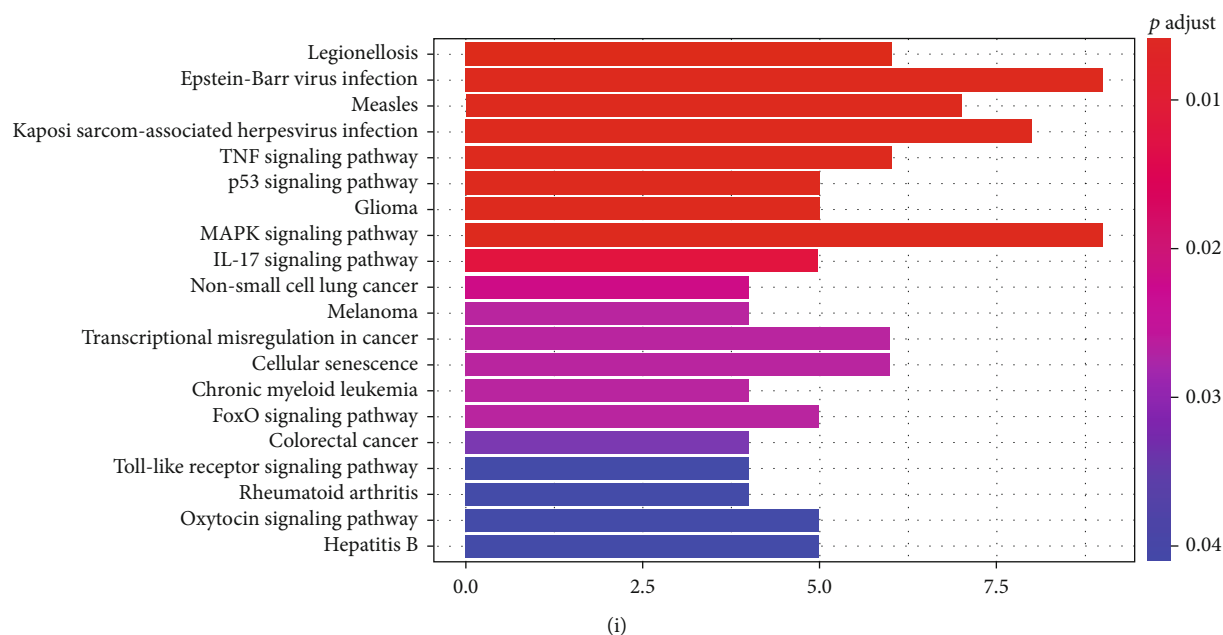


FIGURE 3: Distinct expression pattern of mRNAs and functional enrichment analysis. The MA plot of DE mRNA expression profiles (a) between the CON group and the model group and (b) between the model group and the QUE group. The volcano plot of DE mRNA expression profiles (c) between the CON group and the model group and (d) between the model group and the QUE group. Unsupervised clustering analysis showing the expression profiles of the top 20 upregulated and downregulated mRNAs (e) between the CON group and the model group and (f) between the model group and the QUE group. (g) Heat map showing 294 mRNAs that were changed when PC-12 cells were subjected to oxidative damage; pretreatment with QUE reversed these alterations. (h) GO enrichment analysis of mRNAs altered by QUE. The superscripted number represents the number of genes annotated in the GO term, the ordinate represents the GO term, and the abscissa represents the $-\log_{10}(p \text{ value})$. (i) KEGG enrichment analysis of mRNA altered by QUE. The ordinate represents the KEGG pathway, and the abscissa represents the adjusted p value. CON: control; DE: differentially expressed; GO: Gene Ontology; H_2O_2 : hydrogen peroxide; KEGG: Kyoto Gene and Genomic Encyclopedia; MOL: model; mRNA: messenger RNA; QUE: quercetin.

analysis. Furthermore, a total of 294 mRNAs related to the protection of neuronal cells from OS through treatment with QUE were identified by comparing gene expression in the three groups (Figure 3(g)). Notably, 278 mRNAs were upregulated in the H_2O_2 group compared with the control group. Interestingly, intervention with QUE could reverse these H_2O_2 -induced alterations, producing expression levels similar to those observed in the control group. Likewise, 16 mRNAs were downregulated in the model group compared with the control group; these changes were also reversed after treatment with QUE. Collectively, these results suggested that OS induced transcriptome alterations in neuronal cells, whereas treatment with QUE could reverse these changes to a large extent.

GO and KEGG analyses were performed to investigate the function of QUE-targeted mRNAs. As shown in Figure 3(h), the most enriched biological process (BP) in GO terms were lymphocyte chemotaxis, macrophage chemotaxis, cell proliferation, etc. The most enriched cellular component (CC) terms were acrosomal vesicle, extracellular space, nucleoplasm, etc., while the most enriched molecular function (MF) terms were chemokine activity, serine-type endopeptidase, ligase activity, etc. The top significantly enriched KEGG pathways are shown in Figure 3(i). The tumour necrosis factor signalling pathway, FOXO signalling pathway, and mitogen-activated protein kinase signalling

pathway may be closely involved in the protective effect to neuronal cells against OS.

3.4. DE lncRNAs and Functional Enrichment Analysis. Likewise, the MA plot (Figures 4(a) and 4(b)) and volcano plot (Figures 4(c) and 4(d)) were applied to compare the DE lncRNA expression profiles of “model group vs. control group” and “QUE group vs. model group.” Like mRNA, the expression profiles of the top 20 upregulated and downregulated DE lncRNAs are exhibited in Figures 4(e) and 4(f). Using the same criterion (fold change ≥ 2 and $p < 0.01$), 1,186 DE lncRNAs (i.e., 1,051 upregulated and 135 downregulated) in the control group compared with the model group and 489 DE lncRNAs (i.e., 228 upregulated and 261 downregulated) in the model group compared with the QUE treatment group were detected. In comparison with the control group, 197 lncRNAs were clearly dysregulated in the model group (i.e., 184 upregulated and 13 downregulated) (Figure 4(g)). Moreover, after treatment with QUE, these H_2O_2 -induced lncRNA alterations were reversed, producing expression levels similar to those noted in the control group. We subsequently performed a functional enrichment analysis using these 197 lncRNAs.

As shown in Figure 4(h), GO analysis regarding QUE-targeted lncRNA potential target genes indicated that the most enriched GO terms included neutrophil chemotaxis,

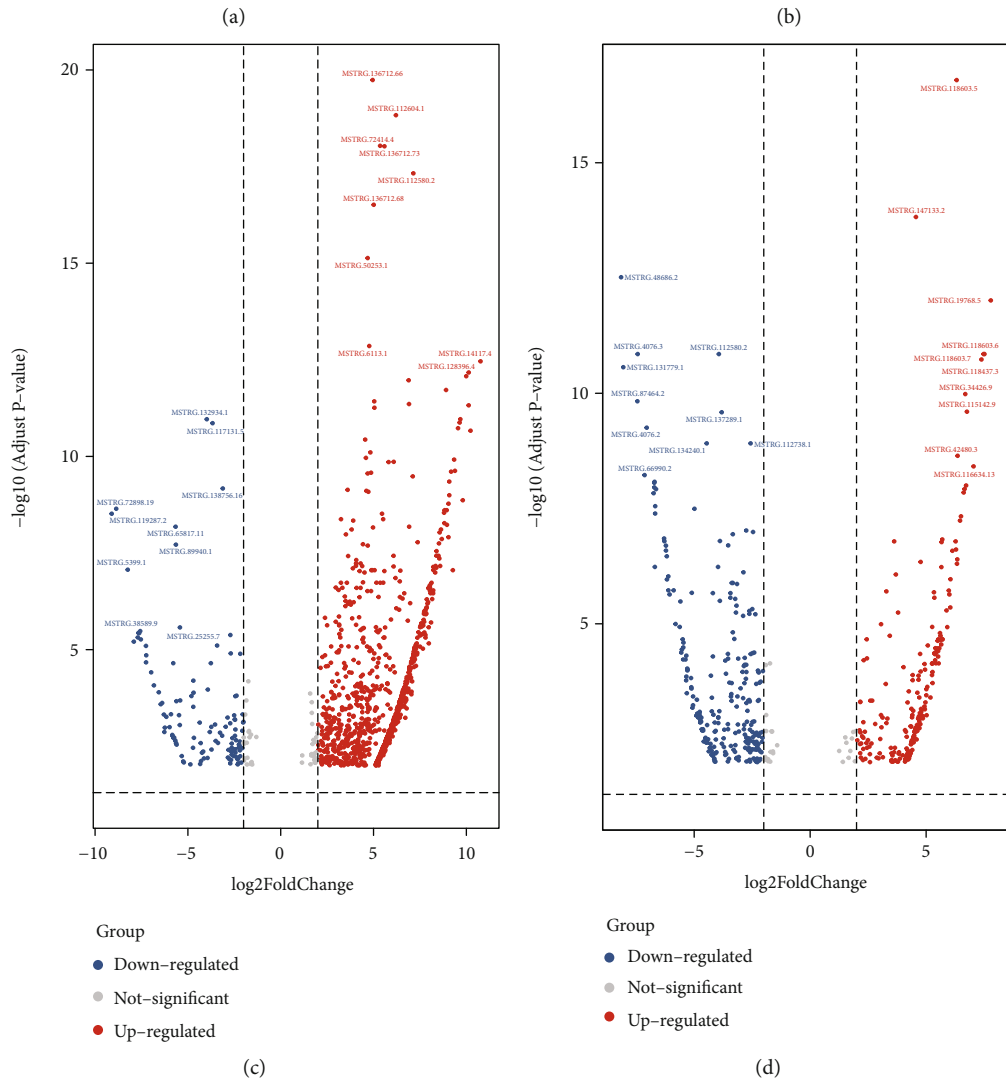
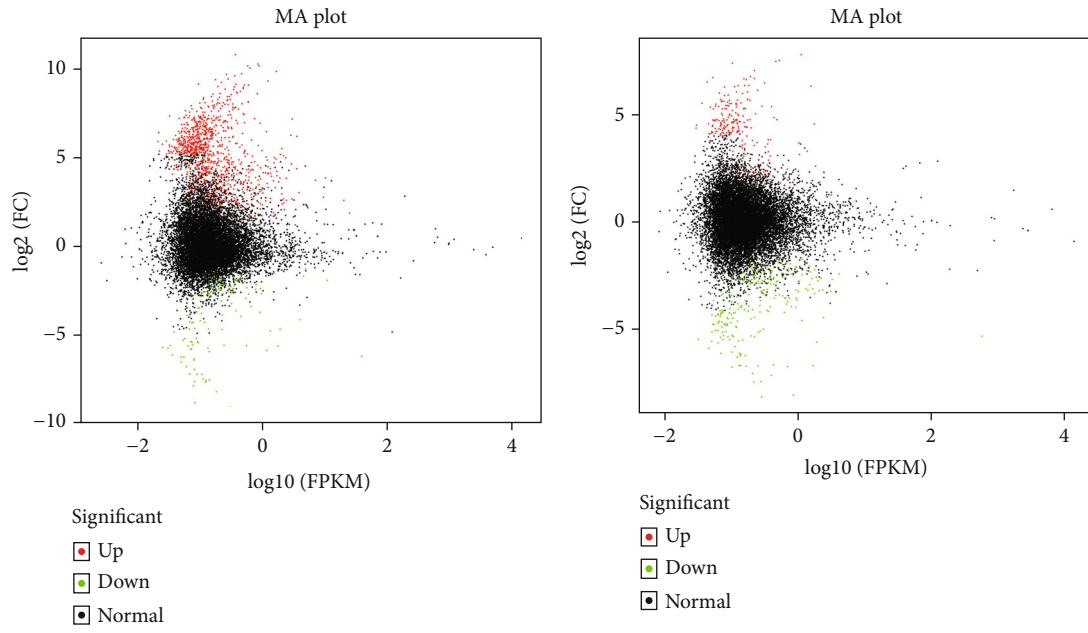
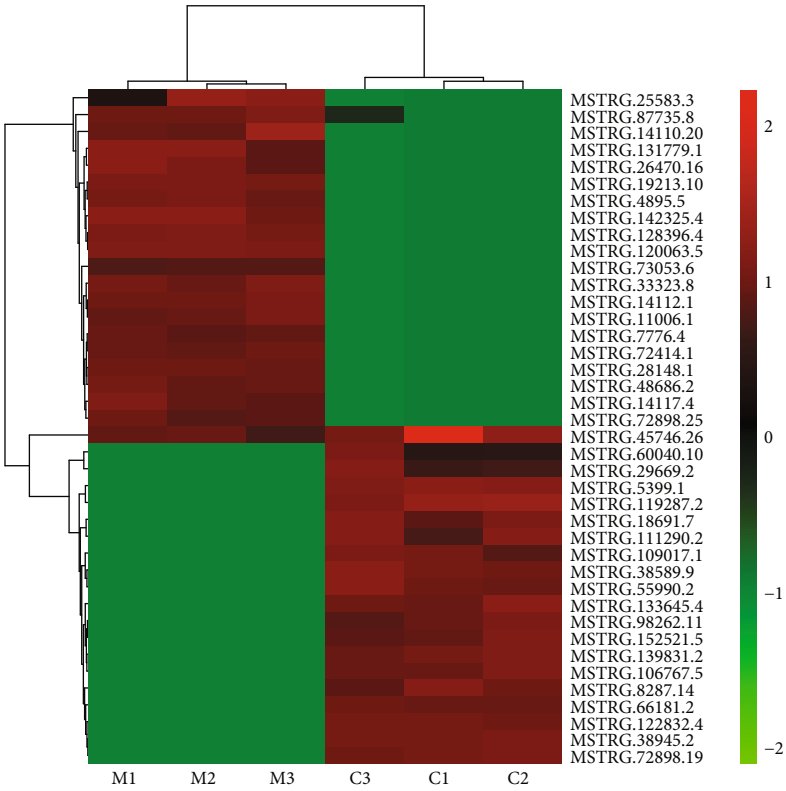
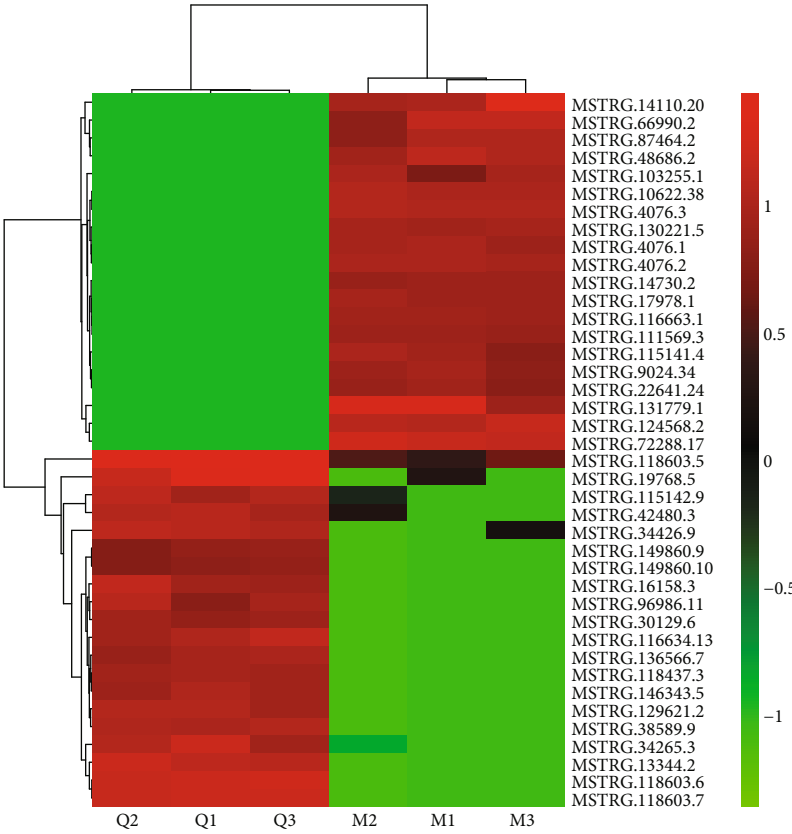


FIGURE 4: Continued.

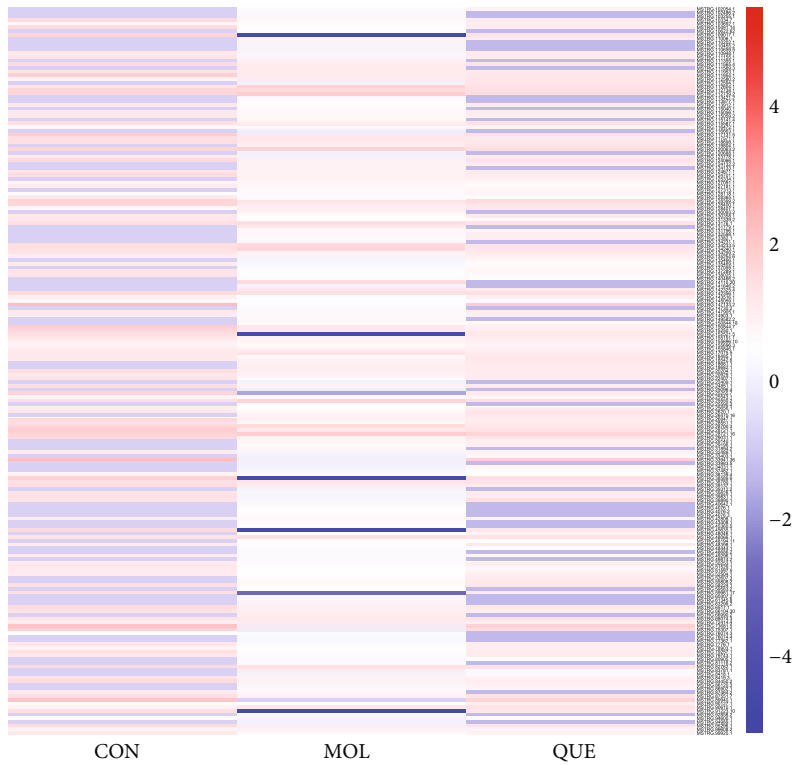


(e)

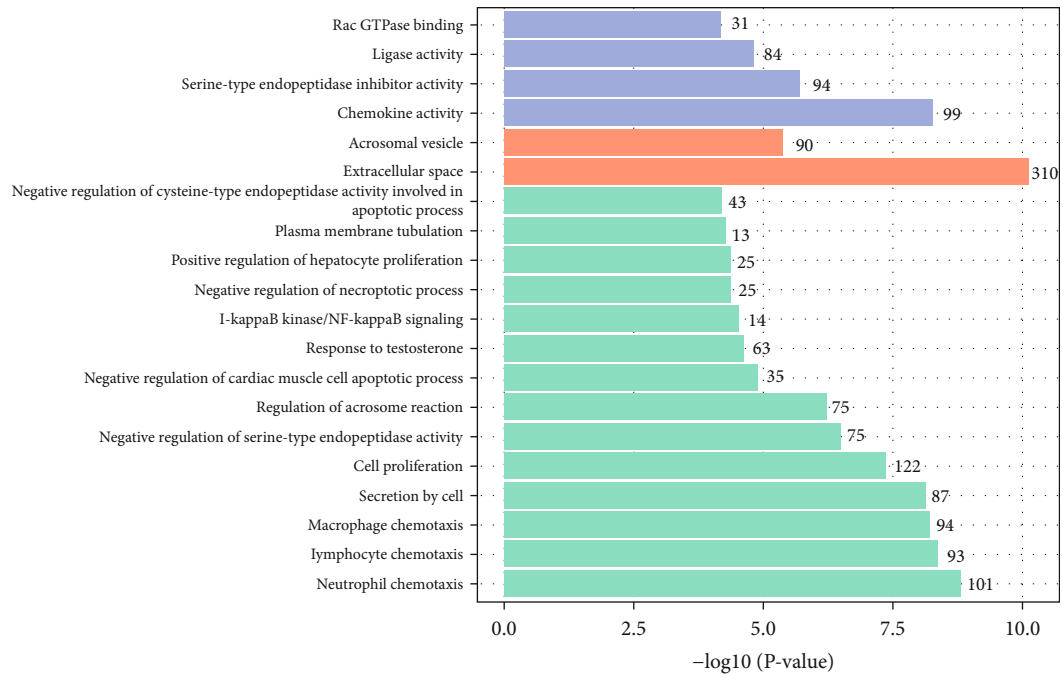


(f)

FIGURE 4: Continued.



(g)



(h)

FIGURE 4: Continued.

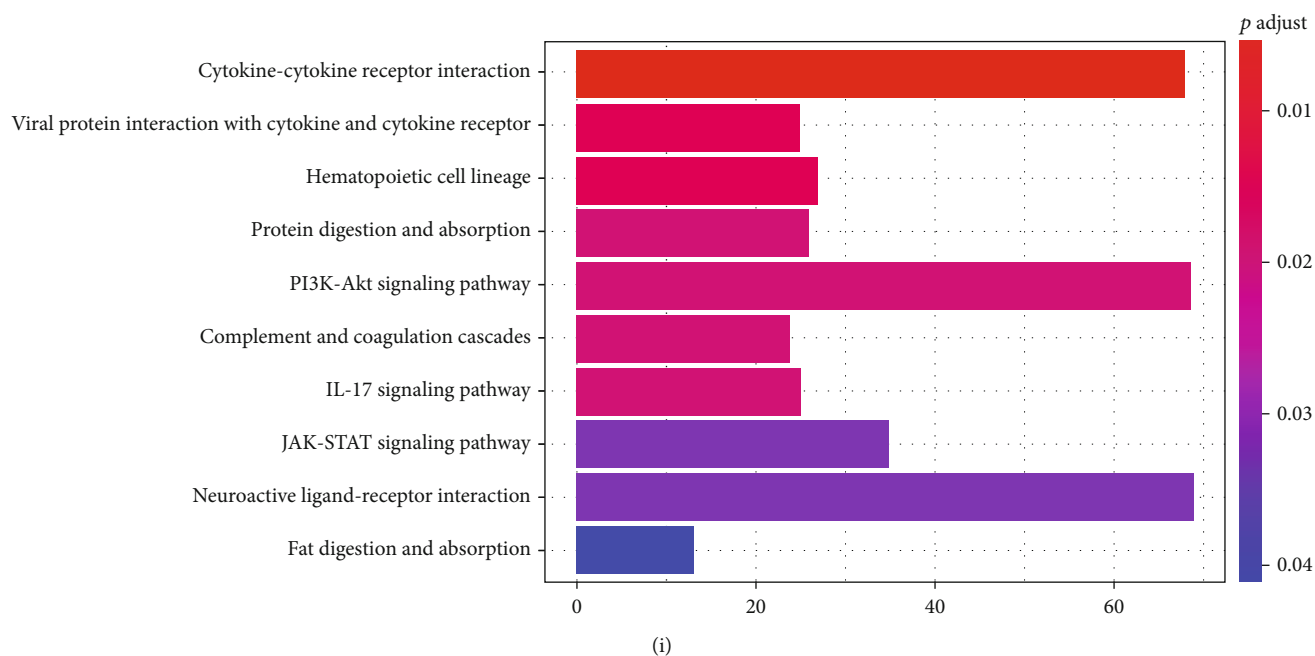


FIGURE 4: Distinct expression pattern of lncRNAs and functional enrichment analysis. The MA plot of the expression profiles of DE lncRNAs (a) between the CON group and the model group and (b) between the model group and the QUE group. The volcano plot of the expression profiles of DE lncRNAs (c) between the CON and model groups and (d) between the model and QUE groups. Unsupervised clustering analysis showing the expression profiles of the top 20 upregulated and downregulated lncRNAs (e) between the CON and model groups and (f) between the model and QUE groups (f). (g) Heat map showing 197 lncRNAs that were altered when PC-12 cells were subjected to oxidative damage; pretreatment with QUE reversed these alterations. (h) GO enrichment analysis of targeted genes for lncRNAs altered by QUE. The superscripted number represents the number of genes annotated in the GO term, the ordinate represents the GO term, and the abscissa represents the $-\log_{10}(p)$ value. (i) KEGG enrichment analysis of targeted genes for lncRNAs altered by QUE. The ordinate represents the KEGG pathway, and the abscissa represents the adjusted p value. CON: control; DE: differentially expressed; GO: Gene Ontology; H_2O_2 : hydrogen peroxide; KEGG: Kyoto Gene and Genomic Encyclopedia; lncRNA: long noncoding RNA; MOL: model; QUE: quercetin.

lymphocyte chemotaxis, and macrophage chemotaxis (BP); extracellular space and acrosomal vesicle (CC); and chemokine activity, serine-type endopeptidase inhibitor activity, and ligase activity (MF). As shown in Figure 4(i), the PI3K-AKT signalling pathway, interleukin 17 (IL17) signalling pathway, and neuroactive ligand-receptor interaction were enriched in the KEGG analysis of lncRNA potential target genes.

3.5. DE miRNAs and Functional Enrichment Analysis. By comparing the miRNA transcriptomes from different groups, 135 H_2O_2 -responsive miRNAs (i.e., 122 upregulated and 13 downregulated in the H_2O_2 intervention group) and 34 QUE-responsive miRNAs (i.e., five upregulated and 29 downregulated after treatment with QUE) were identified. The MA plot (Figures 5(a) and 5(b)) and volcano plot (Figures 5(c) and 5(d)) were applied to detect H_2O_2 -responsive miRNAs and QUE-responsive miRNAs. The results of the unsupervised clustering analysis, indicating the top 20 upregulated and downregulated DE miRNAs, are shown in Figures 5(e) and 5(f). Compared with the control group, 14 miRNAs in the model group were upregulated, and this effect was reversed after treatment with QUE. Of note, all those miRNAs were newly discovered. This effect was reversed after treatment with QUE (Figure 5(g)). Functional enrichment analysis was subsequently performed to investigate

the functions of these dysregulated miRNAs based on their target genes.

In the GO analysis (Figure 5(h)), the top two terms in BP were negative regulation of transcription from the RNA polymerase II promoter and positive regulation of transcription from the RNA polymerase II promoter. MFs were mainly enriched in the transcription factor complex and transcription repressor complex. Regarding CCs, the enriched terms included sequence-specific DNA binding and transcription factor activity, and sequence-specific DNA binding. The most enriched KEGG pathways are shown in Figure 5(i). Major genes were enriched in the following pathways: Hippo signalling pathway, Wnt signalling pathway, etc. These results suggest that miRNA-regulated target mRNAs may participate in the protective function of QUE through these pathways. The PI3K-AKT signalling pathway has also been found to be closely related to this process.

3.6. Expression Profile Validation. We conducted real-time qPCR analysis to verify the findings obtained from RNA-Seq. Of the DE mRNAs most relevant to the antioxidant stress mechanism of QUE, five mRNAs enriched in the FOXO signalling pathway were selected for real-time qPCR: polo-like kinase 2 (PLK2), MDM2, IL6, growth arrest and DNA damage-inducible gamma (GADD45G), and cyclin-dependent kinase inhibitor 1A (CDKN1A). Furthermore,

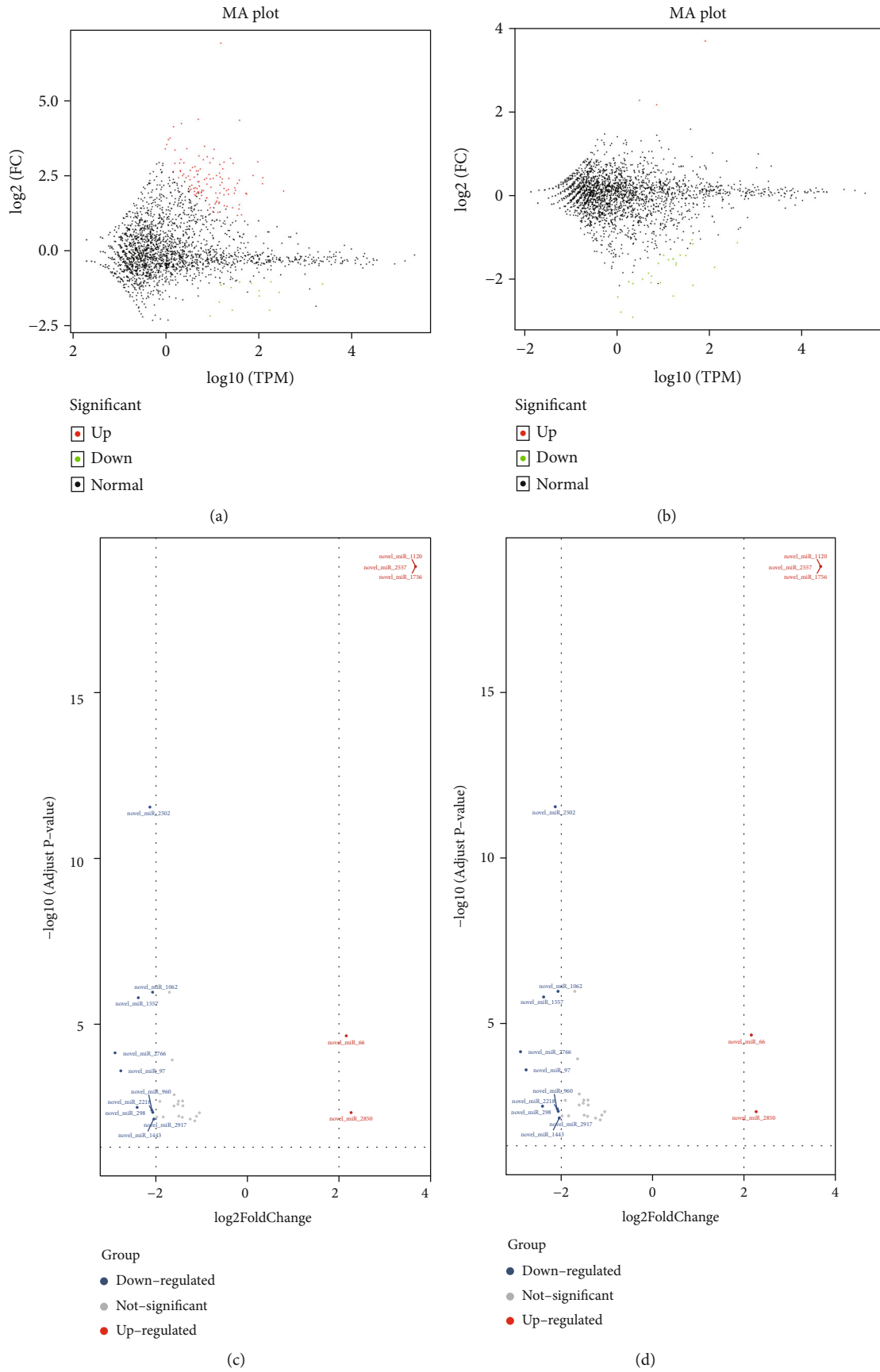
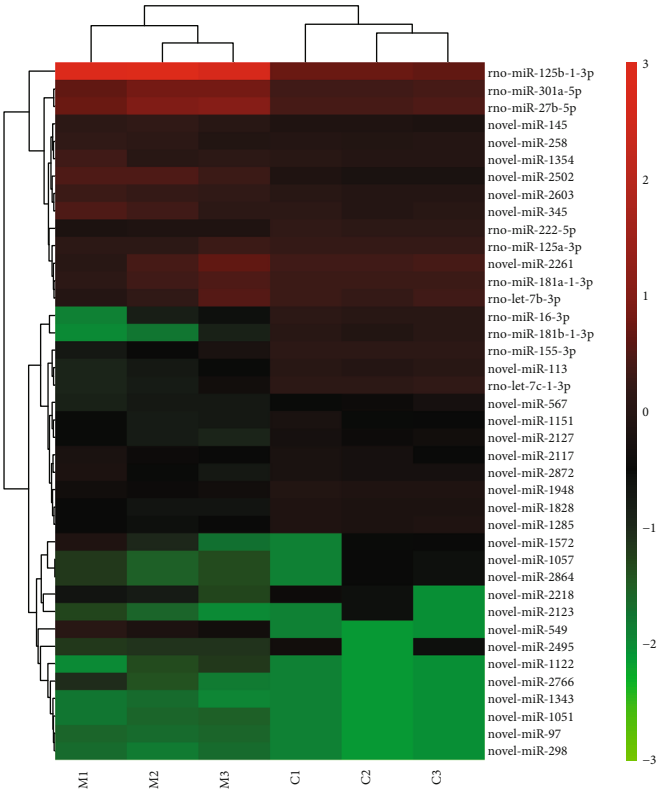
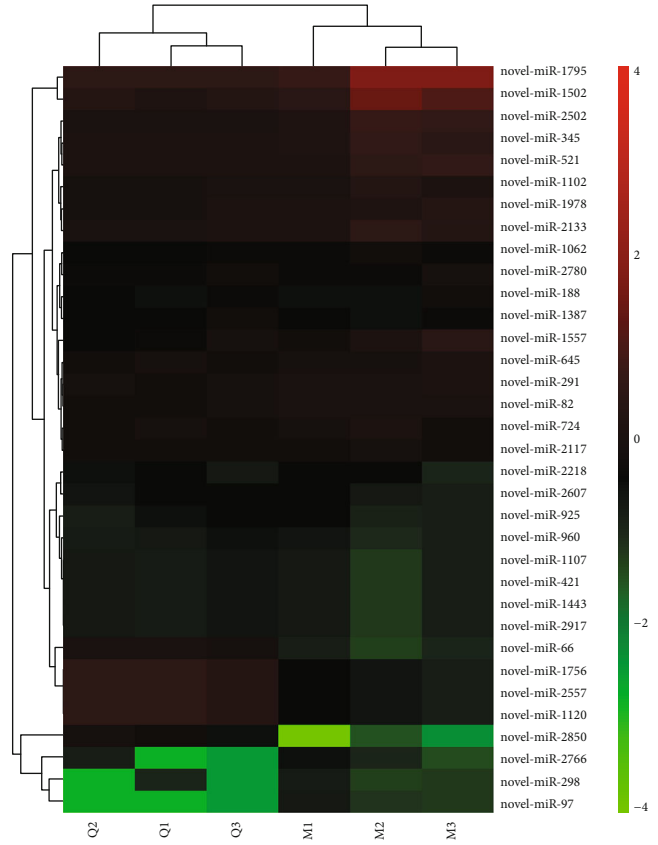


FIGURE 5: Continued.

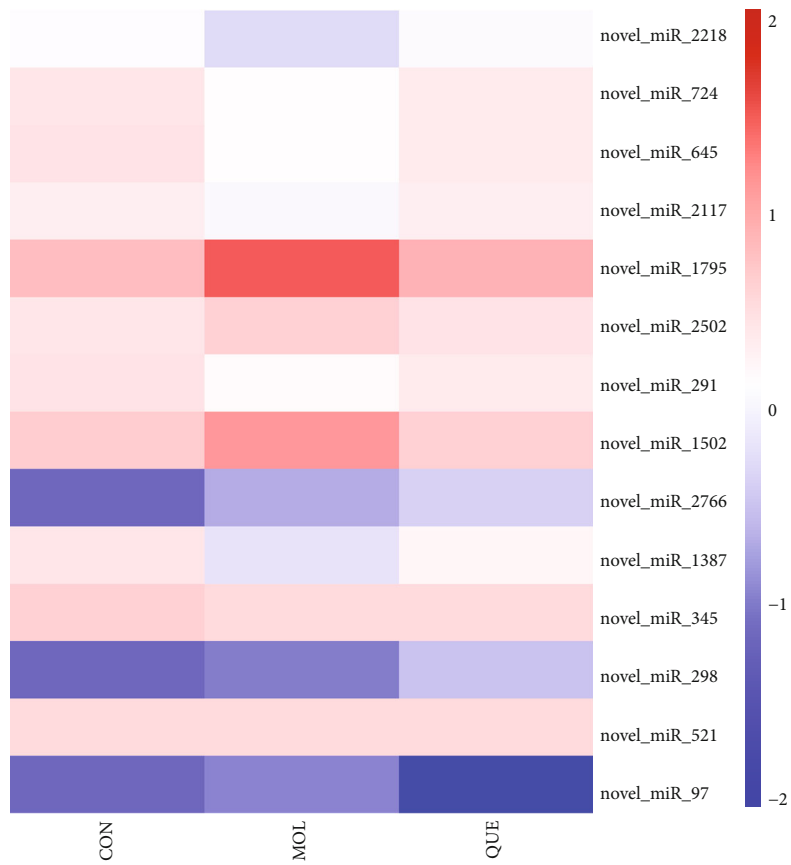


(e)

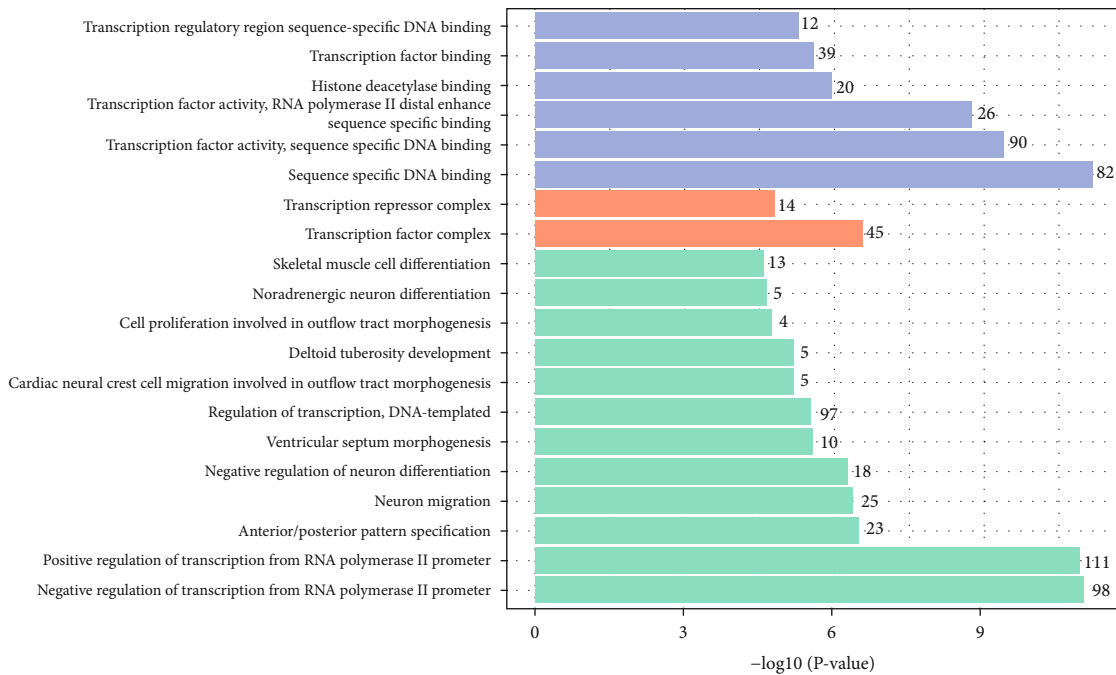


(f)

FIGURE 5: Continued.



(g)



(h)

FIGURE 5: Continued.

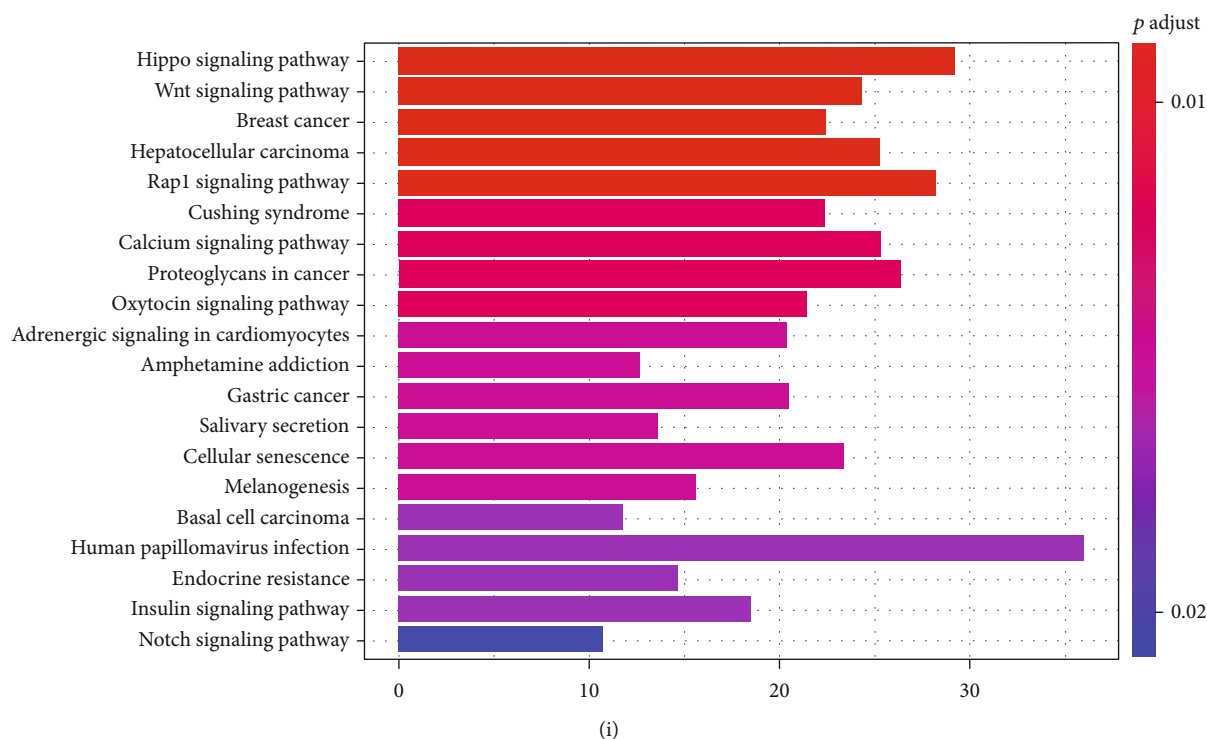


FIGURE 5: Distinct expression pattern of miRNAs and functional enrichment analysis. The MA plot of the expression profiles of DE miRNAs (a) between the CON and model groups and (b) between the model and QUE groups. The volcano plot of the expression profiles of DE miRNAs (c) between the CON and model groups and (d) between the model and QUE groups. Unsupervised clustering analysis showing the expression profiles of the top 20 upregulated and downregulated miRNAs (e) between the CON and model groups and (f) between the model and QUE groups. (g) Heat map showing 14 miRNAs that were altered when PC-12 cells were subjected to oxidative damage; pretreatment with QUE reversed these alterations). (h) GO enrichment analysis of targeted genes for miRNAs altered by QUE. The superscripted number represents the number of genes annotated in the GO term, the ordinate represents the GO term, and the abscissa represents the $-\log_{10}(p \text{ value})$. (i) KEGG enrichment analysis of targeted genes for miRNAs altered by QUE. The ordinate represents the KEGG pathway, and the abscissa represents the adjusted p value. CON: control; DE: differentially expressed; GO: Gene Ontology; H_2O_2 : hydrogen peroxide; KEGG: Kyoto Gene and Genomic Encyclopedia; miRNA: microRNA; MOL: model; QUE: quercetin.

nine dysregulated ncRNAs were selected for real-time qPCR analysis, including five miRNAs (i.e., novel_miR_97, novel_miR_298, novel_miR_2218, novel_miR_1502, and novel_miR_2117) and four lncRNAs (i.e., MSTRG.89940.1, MSTRG.4076.1, MSTRG.48686.2, and MSTRG.34031.1). As shown in Figure 6, the expression levels determined by real-time qPCR were in agreement with the results of RNA-Seq. Thus, all lncRNAs, miRNAs, and mRNAs were affirmed as targets closely related to treatment with QUE and included in further analyses.

3.7. QUE Activates the PI3K-AKT Pathway in Oxidatively Damaged PC-12 Cells. By combining our findings of the KEGG analysis and those of previous studies, we hypothesized that the PI3K-AKT pathway may be a key pathway for the antioxidant mechanism of QUE. As shown in Figure 7, the protein levels of p-PI3K, p-AKT, PI3K, and AKT were increased in the QUE group, in a concentration-dependent manner, compared with those recorded in the model group. This result suggested that the protein levels of p-PI3K, p-AKT, PI3K, and AKT were increased in response to QUE. The above results confirm that QUE may protect PC-12 cells from H_2O_2 -induced oxidative damage by activating the PI3K-AKT signalling pathway.

3.8. Integrated Analysis of the lncRNA-Associated ceRNA Network. In this study, LncBase v.2 available in DIANA Tools was used to retrieve information on miRNA binding to specific lncRNAs, and Ingenuity Pathway Analysis was applied to ascertain the experimentally validated miRNA-to-mRNA interactions. Based on the DE RNAs identified between the control group and the model group, the lncRNA-associated ceRNA network related to OS (containing 65 mRNAs, 77 lncRNAs, and nine miRNAs) was constructed (Figure 8). Furthermore, treatment with QUE can act on the expression of 18 lncRNAs and subsequently regulate that of 27 mRNAs, by competitively binding with novel_miR_345 and novel_miR_298. The arrows in this lncRNA-miRNA-mRNA network represent RNAs that QUE acted on. Overall, the evidence obtained from our bioinformatics analysis suggests that lncRNAs harbour miRNA response elements and play pivotal regulatory roles in the antioxidant stress mechanism of QUE.

4. Discussion

To the best of our knowledge, this is the first comprehensive study of a lncRNA-associated ceRNA network to reveal regulator pathways with regard to the protective effect of QUE

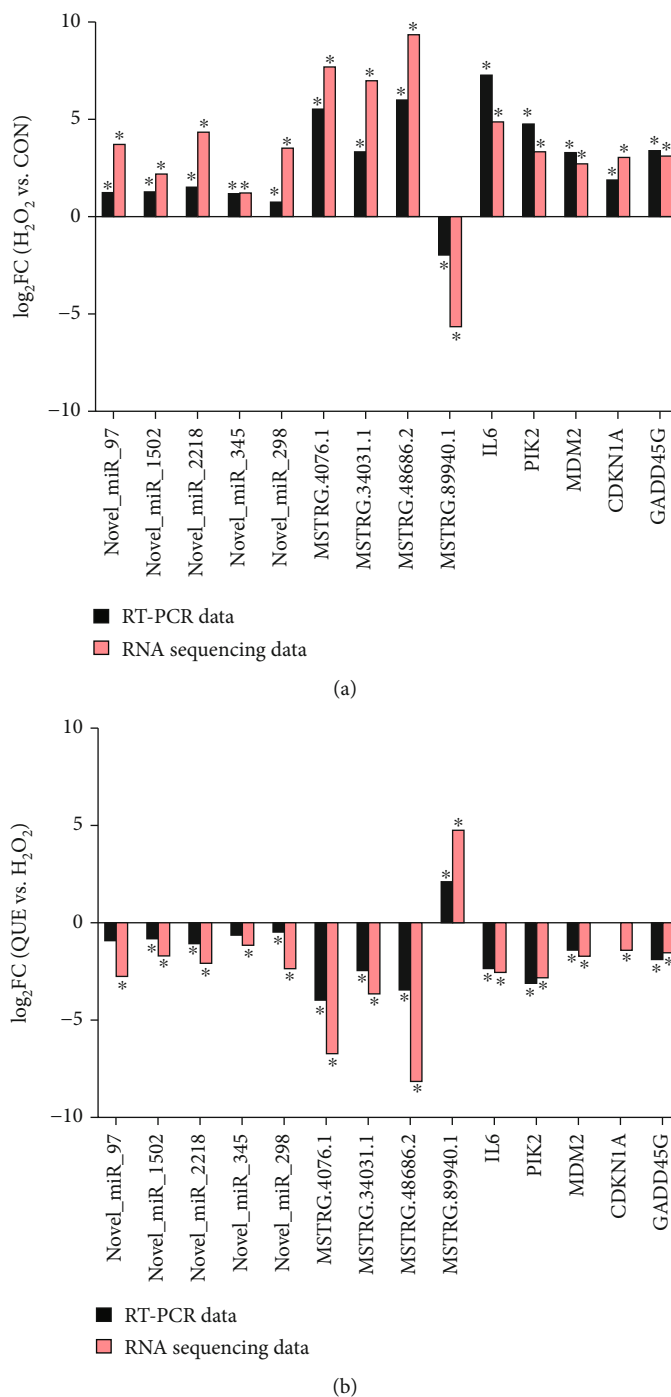


FIGURE 6: Differential expression of ncrRNAs and mRNAs validated by real-time quantitative polymerase chain reaction (qPCR). The data showed that the expression levels of the lncRNAs (MSTRG.4076.1, MSTRG.48686.2, and MSTRG.34031.1), miRNAs (novel_miR_97, novel_miR_298, novel_miR_2218, novel_miR_1502, and novel_miR_2117), and mRNA (PLK2, MDM2, IL6, GADD45G, and CDKN1A) were upregulated in H₂O₂-induced PC-12 cells and downregulated when pretreated with QUE. The expression levels of MSTRG.89940.1 were downregulated in H₂O₂-induced PC-12 cells and upregulated when pretreated with QUE. The real-time qPCR results were consistent with the RNA sequencing data. **p* < 0.05, (a) H₂O₂ vs. CON; (b) QUE vs. H₂O₂. QUE represents H₂O₂-induced PC-12 cells pretreated with QUE. CON represents untreated PC-12 cells. H₂O₂ represents H₂O₂-induced PC-12 cells. CON: control; H₂O₂: hydrogen peroxide; lncRNA: long noncoding RNA; mRNA: messenger RNA; miRNA: microRNA; ncrRNA: noncoding RNA; QUE: quercetin.

on neural cells from OS-induced damages. Our findings indicated that pretreatment with QUE markedly increased cell viability in a dose-dependent manner versus that observed for cells treated with H₂O₂ alone. In addition, we found that

pretreatment with QUE induced the production of antioxidant enzymes and inhibited apoptosis in H₂O₂-induced PC-12 cells. Moreover, 197 DE lncRNAs, 14 DE miRNAs, and 294 DE mRNAs were identified as related to the

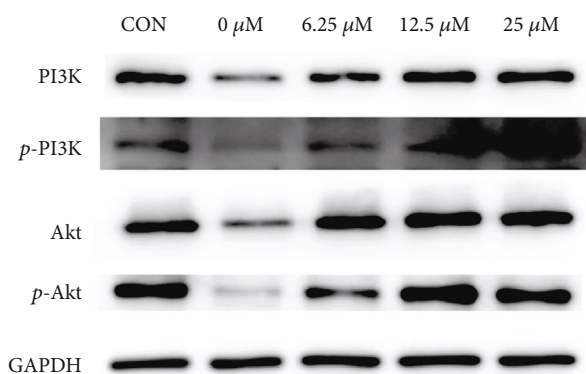


FIGURE 7: QUE activates the PI3K-AKT pathway in oxidatively damaged PC-12 cells. PC-12 cells were pretreated with different concentrations of QUE for 2 h, and the expression of proteins in the PI3K-AKT signalling pathway was detected through western blotting analysis. GAPDH was used as a loading control. GAPDH: glyceraldehyde-3-phosphate dehydrogenase; QUE: quercetin.

antioxidant activities of QUE, and the results of sequencing were validated by real-time qPCR. The evidence obtained from the KEGG enrichment function analysis suggests that the protective effect of QUE may be related to the PI3K/AKT signalling pathway, which was further verified by western blotting. Based on authoritative databases, the lncRNA-associated ceRNA network was visualized for the comprehensive analysis of miRNAs, lncRNAs, and mRNAs. This approach could shed new light on the prevention of neurodegenerative disorders.

Firstly, we focused on the DE coding genes. A total of 966 H_2O_2 -responsive genes (i.e., 823 upregulated and 143 downregulated) were detected. In addition, 495 QUE-responsive genes (i.e., 130 upregulated and 365 downregulated) were identified. By comparing the gene expression of the three groups, we finally determined that 294 mRNAs were potentially related to the protective effect of QUE against OS in PC-12 cells. Of those, 175 genes were newly discovered genes, and further follow-up studies are warranted for their functional annotation. Regarding other genes that have been previously annotated, some are involved in the mechanism of OS: hes family bHLH transcription factor 1 (HES1), dual specificity phosphatase 1 (DUSP1), BTG antiproliferation factor 2 (BTG2), regulator of G protein signalling 2 (RGS2), and activating transcription factor 3 (ATF3). HES1-mediated promotion of the extracellular matrix protein expression inhibits the proliferative and migratory functions of trabecular meshwork cells under OS [28]. Overexpression of DUSP1 increases cellular susceptibility to oxidative injury [29]. It has been suggested that the upregulation of BTG2 expression in response to OS may involve the ROS-protein kinase C-nuclear factor κB cascade [30]. Similarly, RGS2 has been implicated in OS, and a time- and concentration-dependent upregulation in RGS2 mRNA has been observed in human astrocytoma 1321N1 cells treated with H_2O_2 [31, 32]. Upregulation of ATF3 has been observed in H_2O_2 -stimulated NP31 cells, as well as endothelial cells of the glomerulus and aorta of diabetic model rats [33]. Similar results were found in the present study. Elevated levels of HES1, DUSP1, BTG2,

RGS2, and ATF3 were identified in the H_2O_2 -treated group compared with the control group. Interestingly, the expression of these genes declined to control levels after pretreatment with QUE. The specific roles of these mRNAs associated with the antioxidative effect of QUE in neurodegenerative disease warrant further investigation.

The negative or positive role of lncRNAs is observed in the oxidation/antioxidant system [34, 35]. Therefore, studies aiming to explore the lncRNAs in the OS field may be helpful for the further investigation of specific biomarkers of OS-related diseases [18]. Antioxidant drugs that target lncRNA potentially provide a novel strategy for the treatment of neurodegenerative diseases. In our findings, a total of 1,186 lncRNAs were identified to be related to H_2O_2 -induced OS, and a large number of lncRNAs were previously functionally characterized. Furthermore, a total of 197 lncRNAs were found to play critical roles in the protective effects of QUE on H_2O_2 -induced oxidative injury. However, there is limited knowledge regarding the potential functions of these dysregulated lncRNAs. Future studies will contribute to the precise mechanism of lncRNAs in the protective effects of QUE against oxidative injury.

ROS are upstream regulators or downstream effectors of miRNAs, and both are inextricably linked to neurodegenerative processes [19]. Previous studies demonstrated that free radicals may be one of the signals that change the levels of miRNAs and their target proteins, leading to neurodegeneration in neurodegenerative diseases. Moreover, antioxidants that reduce OS may be affecting the levels of miRNAs [36, 37]. In the present study, a total of 135 miRNAs were observed in response to OS, and a limited number of miRNAs were found to play important roles in the antioxidant effects of QUE. Interestingly, all these miRNAs associated with the antioxidant properties of QUE were newly discovered. Further observations are needed to reveal the annotations of these miRNAs in neurodegenerative disease and their specific role in the antioxidant mechanism of QUE.

KEGG pathway analysis was performed to further predict the potential functions of the DE mRNAs and ncRNAs identified in this study. The pathway analysis on mRNAs indicated the crucial role of the FOXO signalling pathway related to the antioxidant mechanism of QUE. Furthermore, PLK2, MDM2, IL6, GADD45G, and CDKN1A in the FOXO signalling pathway were validated using real-time qPCR. In addition, pathway analysis of the miRNA target genes and lncRNA target genes related to QUE revealed that both are involved in the PI3K/AKT signalling pathway. Western blotting demonstrated that the levels of p-PI3K, p-AKT, PI3K, and AKT were increased in a dose-dependent manner by treatment with QUE. Manipulation of PI3K/AKT/FOXO3a signalling modulates OS, which may potentially provide novel therapeutic avenues for PD and AD [38]. It has been documented that actions on the PI3K/AKT pathway may be an important strategy associated with protecting cortical neurons against 4-hydroxynonenal-induced protein oxidation, lipid peroxidation, and mitochondrial dysfunction [39]. FOXO3a, an important downstream target of PI3K/AKT, was recognized as a protective factor that participates in controlling cell fate. OS has been found to trigger FOXO3a

Data Availability

The data that support the findings of this study are available from the corresponding author upon reasonable request.

Conflicts of Interest

The authors declare that there are no conflicts of interest in relation to this work.

Authors' Contributions

Weijun Peng conceived the study. Zheyu Zhang, Pengji Yi, and Weijun Peng drafted the manuscript and performed the analysis. Xiaoliang Tong, Min Yi, Xin Cheng, Jingjing Yang, and Yang Hu contributed to drafting the manuscript and interpreting data. All authors read and approved the final manuscript. Zheyu Zhang and Pengji Yi contributed equally to this work.

Acknowledgments

This work was financially supported by the National Natural Science Foundation of China (Nos. 81603670 and 81873169) and the Hunan Provincial Natural Science Foundation of China (Nos. 2017JJ3459 and 2020JJ4803).

References

- [1] H. Sies, C. Berndt, and D. P. Jones, "Oxidative stress," *Annual Review of Biochemistry*, vol. 86, pp. 715–748, 2017.
- [2] J. Nordberg and E. S. J. Arnér, "Reactive oxygen species, antioxidants, and the mammalian thioredoxin system," *Free Radical Biology and Medicine*, vol. 31, no. 11, pp. 1287–1312, 2001.
- [3] J. L. dos Santos, A. S. de Quadros, C. Weschenfelder, S. B. Garofalo, and A. Marcadenti, "Oxidative stress biomarkers, nutrient-related antioxidants, and cardiovascular disease," *Nutrients*, vol. 12, no. 3, p. 682, 2020.
- [4] O.-M. Zahan, O. Serban, C. Gherman, and D. Fodor, "The evaluation of oxidative stress in osteoarthritis," *Medicine and Pharmacy Reports*, vol. 93, no. 1, pp. 12–22, 2020.
- [5] C. Gorrini, I. S. Harris, and T. W. Mak, "Modulation of oxidative stress as an anticancer strategy," *Nature Reviews Drug Discovery*, vol. 12, no. 12, pp. 931–947, 2013.
- [6] Z. Chen and C. Zhong, "Oxidative stress in Alzheimer's disease," *Neuroscience Bulletin*, vol. 30, no. 2, pp. 271–281, 2014.
- [7] C. Cabello-Verrugio, M. Ruiz-Ortega, M. Mosqueira, and F. Simon, "Oxidative stress in disease and aging: mechanisms and therapies," *Oxidative Medicine and Cellular Longevity*, vol. 2016, Article ID 8786564, 2 pages, 2016.
- [8] M. Al Shahrani, S. Heales, I. Hargreaves, and M. Orford, "Oxidative stress: mechanistic insights into inherited mitochondrial disorders and Parkinson's disease," *Journal of Clinical Medicine*, vol. 6, no. 11, p. 100, 2017.
- [9] G. S. Kelly, "Quercetin. Monograph," *Alternative Medicine Review*, vol. 16, no. 2, pp. 172–194, 2011.
- [10] A. V. A. David, R. Arulmoli, and S. Parasuraman, "Overviews of biological importance of quercetin: a bioactive flavonoid," *Pharmacognosy Reviews*, vol. 10, no. 20, pp. 84–89, 2016.
- [11] K. J. Meyers, J. L. Rudolf, and A. E. Mitchell, "Influence of dietary quercetin on glutathione redox status in mice," *Journal of Agricultural and Food Chemistry*, vol. 56, no. 3, pp. 830–836, 2008.
- [12] L. Rivera, R. Morón, M. Sánchez, A. Zarzuelo, and M. Galisteo, "Quercetin ameliorates metabolic syndrome and improves the inflammatory status in obese Zucker rats," *Obesity (Silver Spring)*, vol. 16, no. 9, pp. 2081–2087, 2008.
- [13] A. Ishisaka, S. Ichikawa, H. Sakakibara et al., "Accumulation of orally administered quercetin in brain tissue and its antioxidant effects in rats," *Free Radical Biology & Medicine*, vol. 51, no. 7, pp. 1329–1336, 2011.
- [14] S. Das, A. Mandal, A. Ghosh, S. Panda, N. Das, and S. Sarkar, "Nanoparticulated quercetin in combating age related cerebral oxidative injury," *Current Aging Science*, vol. 1, no. 3, pp. 169–174, 2008.
- [15] F. Arredondo, C. Echeverry, J. A. Abin-Carriquiry et al., "After cellular internalization, quercetin causes Nrf2 nuclear translocation, increases glutathione levels, and prevents neuronal death against an oxidative insult," *Free Radical Biology and Medicine*, vol. 49, no. 5, pp. 738–747, 2010.
- [16] C. L. L. Saw, Y. Guo, A. Y. Yang et al., "The berry constituents quercetin, kaempferol, and pterostilbene synergistically attenuate reactive oxygen species: involvement of the Nrf2-ARE signaling pathway," *Food and Chemical Toxicology*, vol. 72, pp. 303–311, 2014.
- [17] M. P. Mattson and A. Cheng, "Neurohormetic phytochemicals: low-dose toxins that induce adaptive neuronal stress responses," *Trends in Neurosciences*, vol. 29, no. 11, pp. 632–639, 2006.
- [18] X. Wang, C. Shen, J. Zhu, G. Shen, Z. Li, and J. Dong, "Long noncoding RNAs in the regulation of oxidative stress," *Oxidative Medicine and Cellular Longevity*, vol. 2019, Article ID 1318795, 7 pages, 2019.
- [19] J. Konovalova, D. Gerasymchuk, I. Parkkinen, P. Chmielarz, and A. Domanskyi, "Interplay between microRNAs and oxidative stress in neurodegenerative diseases," *International Journal of Molecular Sciences*, vol. 20, no. 23, article 6055, 2019.
- [20] Y. H. Lin, "MicroRNA networks modulate oxidative stress in cancer," *International Journal of Molecular Sciences*, vol. 20, no. 18, p. 4497, 2019.
- [21] L. Salmena, L. Poliseno, Y. Tay, L. Kats, and P. P. Pandolfi, "A ceRNA hypothesis: the Rosetta Stone of a hidden RNA language?," *Cell*, vol. 146, no. 3, pp. 353–358, 2011.
- [22] X. Bai, J. Geng, X. Li et al., "Long noncoding RNA LINC01619 regulates microRNA-27a/forkhead box protein O1 and endoplasmic reticulum stress-mediated podocyte injury in diabetic nephropathy," *Antioxidants & Redox Signaling*, vol. 29, no. 4, pp. 355–376, 2018.
- [23] D. Zhang, H. Lee, J. A. Haspel, and Y. Jin, "Long noncoding RNA FOXD3-AS1 regulates oxidative stress-induced apoptosis via sponging microRNA-150," *The FASEB Journal*, vol. 31, no. 10, pp. 4472–4481, 2017.
- [24] Z. Zhang, P. Xu, H. Yu, and L. Shi, "Luteolin protects PC-12 cells from H₂O₂-induced injury by up-regulation of microRNA-21," *Biomedicine & Pharmacotherapy*, vol. 112, article 108698, 2019.
- [25] D. Bao, J. Wang, X. Pang, and H. Liu, "Protective effect of quercetin against oxidative stress-induced cytotoxicity in rat pheochromocytoma (PC-12) cells," *Molecules*, vol. 22, no. 7, article 1122, 2017.
- [26] W. Peng, S. Zhang, Z. Zhang et al., "Jianpi Jiedu decoction, a traditional Chinese medicine formula, inhibits tumorigenesis,

- metastasis, and angiogenesis through the mTOR/HIF-1 α /VEGF pathway," *Journal of Ethnopharmacology*, vol. 224, pp. 140–148, 2018.
- [27] Z. Zhang, B. Li, P. Xu, and B. Yang, "Integrated whole transcriptome profiling and bioinformatics analysis for revealing regulatory pathways associated with quercetin-induced apoptosis in HCT-116 cells," *Frontiers in Pharmacology*, vol. 10, p. 798, 2019.
- [28] L. Xu, Y. Zhang, R. Guo et al., "HES1 promotes extracellular matrix protein expression and inhibits proliferation and migration in human trabecular meshwork cells under oxidative stress," *Oncotarget*, vol. 8, no. 13, pp. 21818–21833, 2017.
- [29] Y. X. Liu, J. Wang, J. Guo, J. Wu, H. B. Lieberman, and Y. Yin, "DUSP1 is controlled by p53 during the cellular response to oxidative stress," *Molecular Cancer Research*, vol. 6, no. 4, pp. 624–633, 2008.
- [30] M. Imran and I. K. Lim, "Regulation of Btg2(/TIS21/PC3) expression via reactive oxygen species-protein kinase C-NF κ B pathway under stress conditions," *Cellular Signalling*, vol. 25, no. 12, pp. 2400–2412, 2013.
- [31] J. W. Zmijewski, L. Song, L. Harkins, C. S. Cobbs, and R. S. Jope, "Oxidative stress and heat shock stimulate RGS2 expression in 1321N1 astrocytoma cells," *Archives of Biochemistry and Biophysics*, vol. 392, no. 2, pp. 192–196, 2001.
- [32] S. Salim, M. Asghar, M. Taneja et al., "Novel role of RGS2 in regulation of antioxidant homeostasis in neuronal cells," *FEBS Letters*, vol. 585, no. 9, pp. 1375–1381, 2011.
- [33] A. Okamoto, Y. Iwamoto, and Y. Maru, "Oxidative stress-responsive transcription factor ATF3 potentially mediates diabetic angiopathy," *Molecular and Cellular Biology*, vol. 26, no. 3, pp. 1087–1097, 2006.
- [34] P. Fuschi, M. Carrara, C. Voellenkle et al., "Central role of the p53 pathway in the noncoding-RNA response to oxidative stress," *Aging*, vol. 9, no. 12, pp. 2559–2586, 2017.
- [35] C. Kim, D. Kang, E. K. Lee, and J. S. Lee, "Long noncoding RNAs and RNA-binding proteins in oxidative stress, cellular senescence, and age-related diseases," *Oxidative Medicine and Cellular Longevity*, vol. 2017, Article ID 2062384, 21 pages, 2017.
- [36] K. N. Prasad, "Oxidative stress and pro-inflammatory cytokines may act as one of the signals for regulating microRNAs expression in Alzheimer's disease," *Mechanisms of Ageing and Development*, vol. 162, pp. 63–71, 2017.
- [37] K. N. Prasad, "Oxidative stress, pro-inflammatory cytokines, and antioxidants regulate expression levels of microRNAs in Parkinson's disease," *Current Aging Science*, vol. 10, no. 3, pp. 177–184, 2017.
- [38] T. Jiang, Q. Sun, and S. Chen, "Oxidative stress: a major pathogenesis and potential therapeutic target of antioxidative agents in Parkinson's disease and Alzheimer's disease," *Progress in Neurobiology*, vol. 147, pp. 1–19, 2016.
- [39] H. M. Abdul and D. A. Butterfield, "Involvement of PI3K/PK-G/ERK1/2 signaling pathways in cortical neurons to trigger protection by cotreatment of acetyl-L-carnitine and α -lipoic acid against HNE-mediated oxidative stress and neurotoxicity: implications for Alzheimer's disease," *Free Radical Biology and Medicine*, vol. 42, no. 3, pp. 371–384, 2007.
- [40] M. H. Liu, C. Yuan, J. He et al., "Resveratrol protects PC12 cells from high glucose-induced neurotoxicity via PI3K/Akt/FoxO3a pathway," *Cellular and Molecular Neurobiology*, vol. 35, no. 4, pp. 513–522, 2015.
- [41] F. Safarian, B. Khallaghi, A. Ahmadiani, and L. Dargahi, "Activation of S1P1 receptor regulates PI3K/Akt/FoxO3a pathway in response to oxidative stress in PC12 cells," *Journal of Molecular Neuroscience*, vol. 56, no. 1, pp. 177–187, 2015.
- [42] E. Zeldich, C. D. Chen, T. A. Colvin et al., "The neuroprotective effect of klotho is mediated via regulation of members of the redox system," *The Journal of Biological Chemistry*, vol. 289, no. 35, pp. 24700–24715, 2014.

Research Article

Diazepam and Its Disinfection Byproduct Promote the Early Development of Nervous System in Zebrafish Embryos

Xiaole Zhao,¹ Xiaoyong Huang,^{1,2} Jiachen Shi,² Kui Zhu,¹ and Bing Shao ^{1,2}

¹College of Veterinary Medicine, China Agricultural University, No. 2 Yuanmingyuan West Road, Beijing 100193, China

²Beijing Key Laboratory of Diagnostic and Traceability Technologies for Food Poisoning, Beijing Center for Disease Prevention and Control, Beijing 100013, China

Correspondence should be addressed to Bing Shao; shaobingch@sina.com

Received 1 October 2020; Revised 3 November 2020; Accepted 18 November 2020; Published 30 November 2020

Academic Editor: Si Qin

Copyright © 2020 Xiaole Zhao et al. This is an open access article distributed under the Creative Commons Attribution License, which permits unrestricted use, distribution, and reproduction in any medium, provided the original work is properly cited.

The widely used diazepam, as central nervous system inhibitor, has found to be ubiquitous in surface water and drinking water. Moreover, a series of byproducts such as 2-methylamino-5-chlorobenzophenone (MACB) were generated after the chlorine disinfection process. However, little information is available about the neurobiological effects of these emerging chemicals at low doses, especially on infants and children. Here, we exposed zebrafish (*Danio rerio*) embryos to diazepam and MACB at 0.05, 0.5, and 5 nM, which were equivalent to environmental levels. Both diazepam and MACB increased the somite number and promoted nervous development of transgenic zebrafish [Tg (elavl3: EGFP) larvae] at 72 hours postfertilization (hpf). Both diazepam and MACB also disrupted the homeostasis of adenosine monophosphate, valine, methionine, and fumaric acid in zebrafish embryos at 12 hpf. Additionally, the locomotor behavior activity of zebrafish was significantly enhanced after 120-hour sustained exposure to diazepam or MACB. Moreover, the mRNA expression levels of *oct4*, *sox2*, and *nanog*, modulating the pluripotency and self-renewal, were upregulated by diazepam and MACB in zebrafish embryo. Altogether, diazepam and MACB stimulate developmental neurogenesis and may induce neuronal excitotoxicity at quite low doses. These results indicated that the chronic exposure to psychoactive drugs may pose a potential risk to the development of the nervous system in infancy.

1. Introduction

Drinking water pollution by pharmaceuticals and personal care products (PPCPs) poses global concerns since it exhibit pharmacological action potencies even at low concentrations [1–3]. Psychoactive drugs are one kind of PPCPs and ubiquitously found in the environment [4, 5]. Diazepam (DZP), as one of the mostly prescribed psychoactive drug, was routinely used to treat anxiety disorders [6] which troubled about 14% people worldwide [7]. With the widespread application or abuse [8], a large amount of DZP was released into environment by excretion and discard. Thus, DZP has been detected in wastewater, surface water, and drinking water and persists at levels as high as hundreds nanograms per liter [9–11].

As an antianxiety and sedative drug, DZP can inhibit different parts of the central nervous system (CNS) by enhancing the postsynaptic inhibition of gamma-aminobutyric acid type A (GABAA) [12]. However, there have been concerns

that the drug causes adverse effects on fetal development because of its fast oral absorption, high bioavailability, long half-life, and easy penetration of the blood-brain barrier and blood-fetal barrier [13]. The offspring of Wistar rats presented neurobehavioral toxicity after prenatal exposure to different doses of DZP, manifesting as early physiological development and delayed neurobehavioral development [14], although the malformation evidences for newborns when maternal exposed to diazepam are of contradictory [13]. The floppy infant syndrome of newborn was well documented after prenatal exposure to diazepam during the last trimester of pregnancy, the newborns characterized as hypotonia, hypothermia, lethargy, respiratory distress, suckling difficulties, lower self-regulation, and more CNS stress signs across the first postnatal month [15, 16]. A survey study in 2016 showed that prenatal exposure to benzodiazepine would cause severe damage to the hearing and visual cognition of newborns [17]. All above-mentioned evidences are

based on prescribed dose exposure to DZP. Few information is available on adverse effects of DZP at low-dose exposure. As the same family drug of DZP, oxazepam was found to alter behavior and the feeding rate of wild European perch (*Perca fluviatilis*) at concentrations encountered in effluent-influenced surface waters [1], while wild-caught zebrafish exposed to concentrations of the anxiolytic drug oxazepam as low as 0.57 $\mu\text{g/L}$ showed a reduction in the response to conspecific alarm pheromone [18]. The brain neurochemistry for wild-type zebrafish was also altered after 28 days of exposure to oxazepam at 0.57 $\mu\text{g/L}$ level, and the serotonin turnover (ratio 5-HIAA/5-HT) was reduced [19]. As an important source of drinking water, PPCPs can transfer to tap water since the treatment techniques are not specifically aimed to trace drugs. It is particularly worrying that chlorination of these drugs can produce a series of byproducts that were more serious toxic effects than their precursors [20–22]. 2-Methylamino-5-chlorobenzophenone (MACB) was identified as predominate chlorinated chemical of DZP after chlorination disinfection process [5, 23] and ubiquitously found in tap water of Beijing. Even so, there is little information on the developmental and ethological effects of the DZP and MACB at low-dose exposure for newborn and infant, although MACB was predicted to be more likely to accumulate in nervous system and toxic/mutagenic than the precursor drug base on quantitative structure-activity relationship [24].

Here, we utilized zebrafish as a neonatal model to determine the potential effects of DZP and MACB at environmental concentration. We show that DZP and MACB increased the somite number of zebrafish embryos after 10-hour exposure. Peripheral and central neurons were quantified in embryo of HuC-GFP line. The enhancement of neuronal proliferation was verified in DZP- and MACB-treated zebrafish larvae. Moreover, zebrafish larvae exhibited hyperactivity after sustained exposure to DZP and MACB. The transcription factors in the pluripotency regulatory network were also upregulated in the treated zebrafish embryo. These findings supported the notion that psychoactive drugs at environmental concentration posed a serious risk to the neurodevelopment of infancy.

2. Materials and Methods

2.1. Chemicals and Reagents. DZP with purity > 98% was purchased from the National Institutes for Food and Drug Control (Beijing, China). MACB with purity > 98% was synthesized in laboratory. Dimethyl sulfoxide (DMSO) was supplied by Sigma-Aldrich (purity > 99.7%, St. Louis, USA). The stock solution of DZP and MACB (10 mg/mL) was prepared in DMSO and stored at -20°C .

2.2. Zebrafish and Treatment. Wild-type (WT) and transgenic (TG) line CZ160 [Tg (elavl3: EGFP)] zebrafish were purchased from China Zebrafish Research Centre (Wuhan, China) at 3 months old and maintained on aquatic habitat recirculation systems (Pentair Aquatic Habitats, Apopka, FL). The neuronal Elav-like (nElavl or neuronal Hu) proteins are RNA-binding proteins, which are early neuronal markers in the early development and are crucial for the maintenance

of axonal homeostasis in mature neurons [25, 26]. In transgenic HuC-GFP [Tg (elavl3: EGFP)] line, GFP was expressed in all neurons [27]. HuC-GFP expression could be occurred in all neuronal process and is important marker in early development of brain and spinal cord [28]. Water was maintained at 28.5°C , with a pH of 7.5, and a conductivity of 500–780 μS . Zebrafish were held at a light cycle of 14:10 light-dark, fed with *Artemia nauplii* twice daily.

To fertilize embryos, adult zebrafish were separated with 2 males to 1 female in spawning boxes overnight. The division plate was removed at the next beginning of light cycle. Then, incubation ended in 30 minutes, and the embryos were collected and washed three times with embryo medium. Subsequently, embryos were selected for exposure experiments at 1 hour postfertilization (hpf) in 6 cm high borosilicate glass dish with DZP and MACB. Our study had indicated that the concentration of DZP or MACB was about 0.05 nM in drinking water [5]. Zebrafish embryos ($n = 45 \pm 5$) were exposed to MACB at 0.05 nM, 0.5 nM, and 5 nM with three replicates. The vehicle group is 0.01% DMSO. During the experiment periods, fifty percent of EM was renewed to keep optimum and equal concentrations of tested material. The embryos incubated in a thermostatic climate incubator at 28°C (Jiangnan Instrument Co., Ltd., Ningbo, China). At 12 hpf, 60 embryos were taken to detect adenosine monophosphate, valine, methionine, and fumaric acid. Embryos were extracted with acetonitrile and analyzed by LCMS-8045 (Shimadzu Corporation, Japan).

2.3. Developmental Assessment. Embryos were viewed under the stereomicroscope (SZM76, UOP, China), and photographs were taken in 1280×1024 image resolution for counting somites at 10, 12, and 16 hpf, respectively. The key components of the HuC promoter drive expression of green fluorescent protein (GFP) expressed specifically in neurons. The impact of DZP and MACB on neuronal development was assessed at low concentration using the TG embryos [Tg (elavl3: EGFP)]. Adult male (or female) WT and female (or male) TG were separated in spawning boxes overnight. The TG larvae were collected at 72 hpf and imaged using laser confocal fluorescence (TCS SP8, Leica, Germany) with the excitation wavelength at 425 nm and emission at 600 nm. The length of HuC-GFP was measured accurately.

2.4. Locomotor Behavior Assays. Embryo was exposed to embryo medium with different DZP or MACB concentrations at 1 hpf. Zebrafish (120 hpf) behavior was assessed using either a light/dark cycle. Briefly, at 104 hpf, zebrafish larvae were loaded into 96-well plates in 300 μL of embryo media and allowed to acclimate overnight at 28.5°C . At 120 hpf, zebrafish were placed into a box tracking system and allowed to acclimate for 10 min, following which they were exposed to alternating 10 min cycles of dark and light for an hour. The speed per minute of larva moved in the well was calculated for each individual larva ($n = 24$ larvae).

2.5. Total RNA Extraction and Quantitative Real-Time PCR (qRT-PCR). In order to investigate whether *oct4* expression was associated with high hatch rate before 50 hpf, RT-qPCR

TABLE 1: Primers used in real-time PCR analyses of mRNA expression.

Gene name	Sequence of the primers (5'-3')	
	Forward	Reverse
<i>rpl13</i>	TCTGTCCCATGCCAACCAT	TCAGACGCACAATCTTGAGAGCAG
<i>oct4</i>	TGTAGTGCCTGTATGGTTCTGC	GGTGGTGGACTCTGCTCGTAA
<i>sox2</i>	TGAACGCCCTTCATGGTGTGGTC	TGAATGGTCGCTTCTCGCTCTC
<i>Nanog</i>	AAGACTGAGCCCGACCAAAA	GTCAGAGGAACCCCTTCTCG

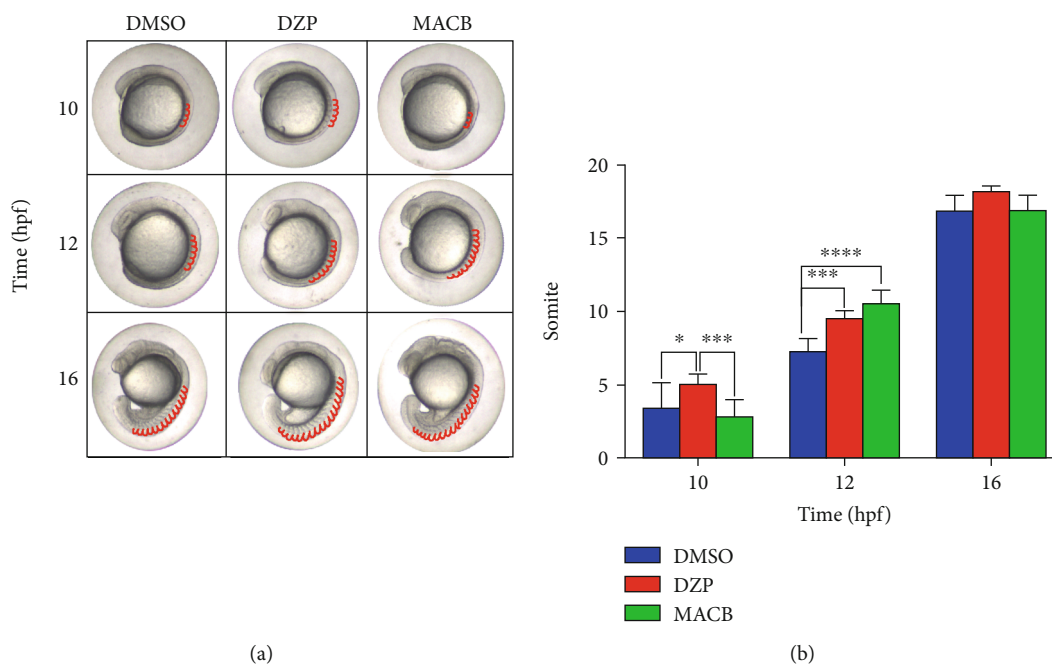


FIGURE 1: DZP and MACB accelerated the development of embryo somite. (a) Early somite development of zebrafish embryos. (b) Total somite of embryo treated with DZP and MACB at 5 nM for 10 hpf, 12 hpf, and 16 hpf. Data was analyzed by nonparametric, one-way analysis of variance (ANOVA) test, $n = 7 \sim 10$ larvae per group, followed with Tukey's multiple comparisons test, expressed as mean \pm SEM. * $P < 0.05$; ** $P < 0.01$; **** $P < 0.0001$; NS: not significant.

was used to detect the gene expression of *oct4*, *sox2*, and *nanog* in zebrafish embryos. A total of 30 embryos (treated with 5 nM) or larvae were collected at 24, 48, and 72 hpf, respectively. Total RNA of zebrafish larvae was extracted using Trizol reagents (Thermo Fisher Science, USA) following the manufacturer's instruction. The concentrations of RNA samples were measured by Nano Drop, and genomic DNA was removed by RNase-free DNase I. 1 μ g RNA of each sample was used to synthesize first-strand cDNA using cDNA Synthesis kit (Takara, Japan). qRT-PCR was performed using SYBR Green qPCR Master Mix (BioRad, USA) in real-time PCR system (Applied Biosystem, Roche Life Science, USA). In 20 μ L of PCR reaction system, 1 μ L of cDNA template, 0.8 μ L of forward primer, 0.8 μ L of reverse primer, 7.4 μ L of nuclease-free water, and 10 μ L of SYBR Green qPCR Master Mix were mixed. The PCR reaction condition was set at 50°C for 2 min, 95°C for 3 min, followed by 40 cycles of 95°C for 15 s, 60°C for 1 min, and 72°C for 2 min. The corresponding pair primer sequences were designed by NCBI (Table 1). Quantitative polymerase chain reaction (qPCR) was performed to evaluate the expression

level of *oct4*, *sox2*, and *nanog* genes in real-time PCR system for three times.

2.6. Statistical Analysis. Prism 7.0 (Graphpad Prism Software, CA) was used for statistical analysis. The data analysis was carried out using one-way analysis of variance (ANOVA) with Tukey's multiple comparisons test to compare significance. All data were shown as mean \pm SEM, and $P < 0.05$ was defined as statistically significant.

3. Results

3.1. DZP and MACB Promote Somite Development in Zebrafish. To determine the developmental effects of DZP and MACB, we exposed zebrafish embryos to these two chemicals at 5 nM and then monitored the growth from 1 hpf (hour postfertilization) to end of the experiment. We found that developmental rates of somite were different among groups (Figure 1(a)). DZP significantly ($P < 0.05$) increased the number of embryonic segments from 4 to 5 compared with DMSO-treated zebrafish embryos at 10 hpf (Figure 1(b)).

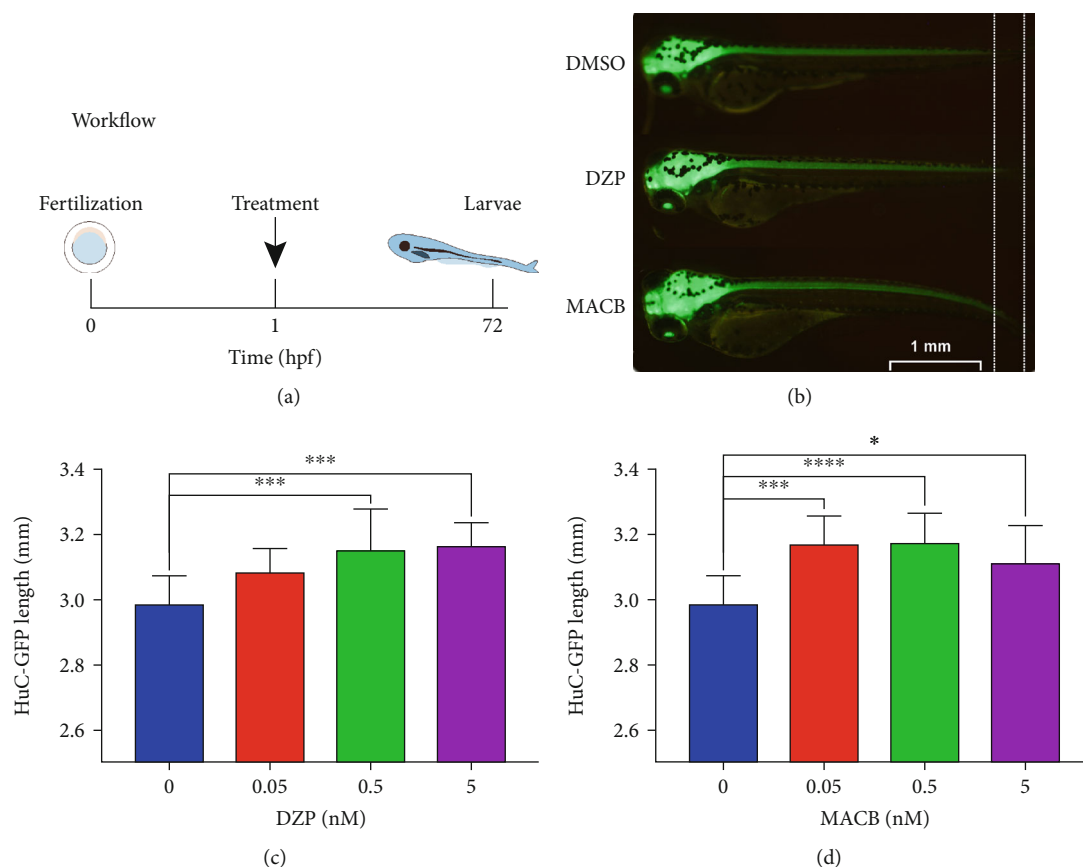


FIGURE 2: DZP and MACB stimulate neurogenesis. (a) Treatment flowchart for DZP and MACB exposure in embryonic zebrafish. (b) Representative images for the protein expression of HuC-GFP in the transgenic (TG) zebrafish treated with 0.05 nM DZP or MACB. The intensity of HuC was the indicator of neurogenesis and quantified by measuring the fluorescence length. The zebrafish larvae of HuC-GFP line treated with (c) DZP or (d) MACB for 72 hpf. Data was analyzed by nonparametric, one-way analysis of variance (ANOVA) test, $n = 12$ larvae per group, followed with Tukey's multiple comparisons test, expressed as mean \pm SEM. * $P < 0.05$; *** $P < 0.001$; **** $P < 0.0001$; NS: not significant.

Somite increased to 7 in DMSO-treated zebrafish at 12 hpf. DZP and MACB further accelerated the embryonic segment development at this stage. However, no differences were observed at 16 hpf for the embryonic somites among groups (Figure 1(b)). Thus, zebrafish were sensitive to DZP and MACB in somite development at early stage.

3.2. Assessment of Impact on Nervous Development. For somitic organization underlies the segmental organization of nerves [29], we further determined neural effects of DZP and MACB in GFP zebrafish embryos labeled the neural RNA-binding protein HuC. Embryos were incubated in DZP or MACB solutions during the period of neural development from 1 hpf to 72 hpf (Figure 2(a)) [30, 31]. The expression levels of the HuC-GFP were measured by the length of body with green fluorescence at 72 hpf (Figure 2(b)). DZP significantly ($P < 0.001$) promoted neuron proliferation at 0.5 and 5 nM (Figure 2(c)). The nervous system was more sensitive to MACB, and the body length significantly increased at 0.05 nM exposure. These results indicated that DZP and MACB could speed up the neurodevelopmental process at low concentration.

3.3. The Locomotor Behavior of Larvae. Previous studies have shown that DZP and MACB at drinking water pollution level interfere with the neurodevelopment of juvenile fish; we further explored the behavioral effect of DZP and MACB on the larval fish using the dark-light test [32, 33]. The eyes of larvae could detect light signals and made a judgement [34]. For example, the larval locomotion was high in dark and low in light when exposed a dark-light cycle [35]. The movement distance of larvae treated with DZP and MACB was presented in the dark-light cycles (Figures 3(a) and 3(c)). Our results showed that DZP and MACB treatment significantly excited the activity level of larvae in the light (Figures 3(b) and 3(d)), and the excitatory effect of MACB on motor neurons was obvious over time (Figure 3(c)). There were no behavioral differences among all groups in dark periods (Figures 3(e) and 3(f)). Therefore, DZP and MACB stimulated hyperactivity for zebrafish larvae at environmental doses.

3.4. The Level of Nutrients in Embryos. To further study the effects of DZP and MACB on neurometabolic, we analyzed embryonic endogenous substances in the embryo treated

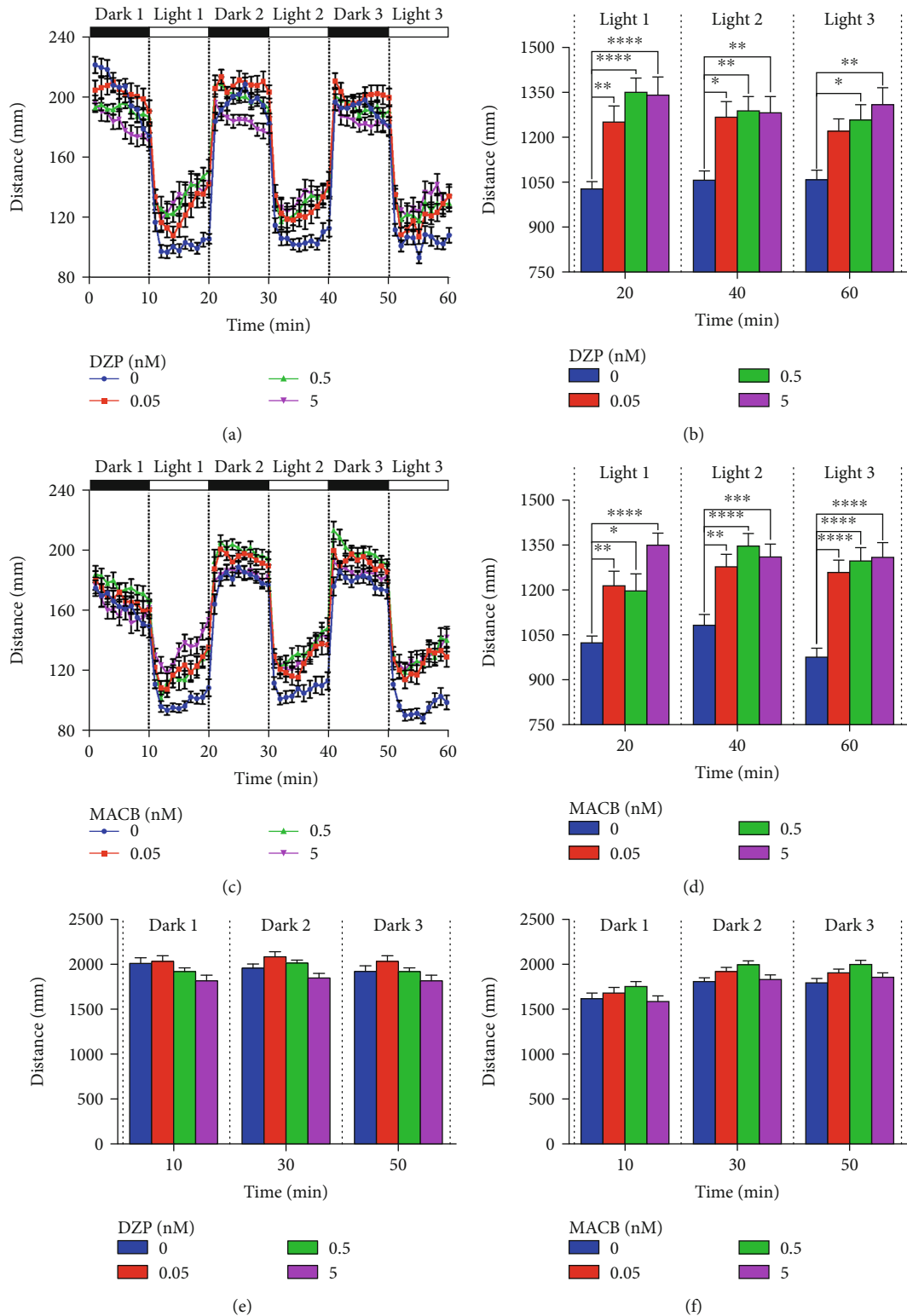


FIGURE 3: DZP and MACB enhance the locomotor behavior activity of larvae. (a) The distance of zebrafish larvae treated with DZP. Larvae moved every 1 min at 120 hpf exposed to alternating cycles of light and dark for 60 min each. (b) Total distance moved in each light period by larvae treated with DZP. (c) The distance of zebrafish larvae treated with MACB. Larvae moved every 1 min at 120 hpf exposed to alternating cycles of light and dark for 60 min each. (d) Total distance moved in each light period by larvae treated with MACB. Total distance moved in each dark period by larvae treated with (e) DZP and (f) MACB. Data was analyzed by nonparametric, one-way analysis of variance (ANOVA) test, $n = 20 \sim 24$ larvae per group, followed with Tukey's multiple comparisons test, expressed as mean \pm SEM. * $P < 0.05$; ** $P < 0.01$; **** $P < 0.0001$; NS: not significant.

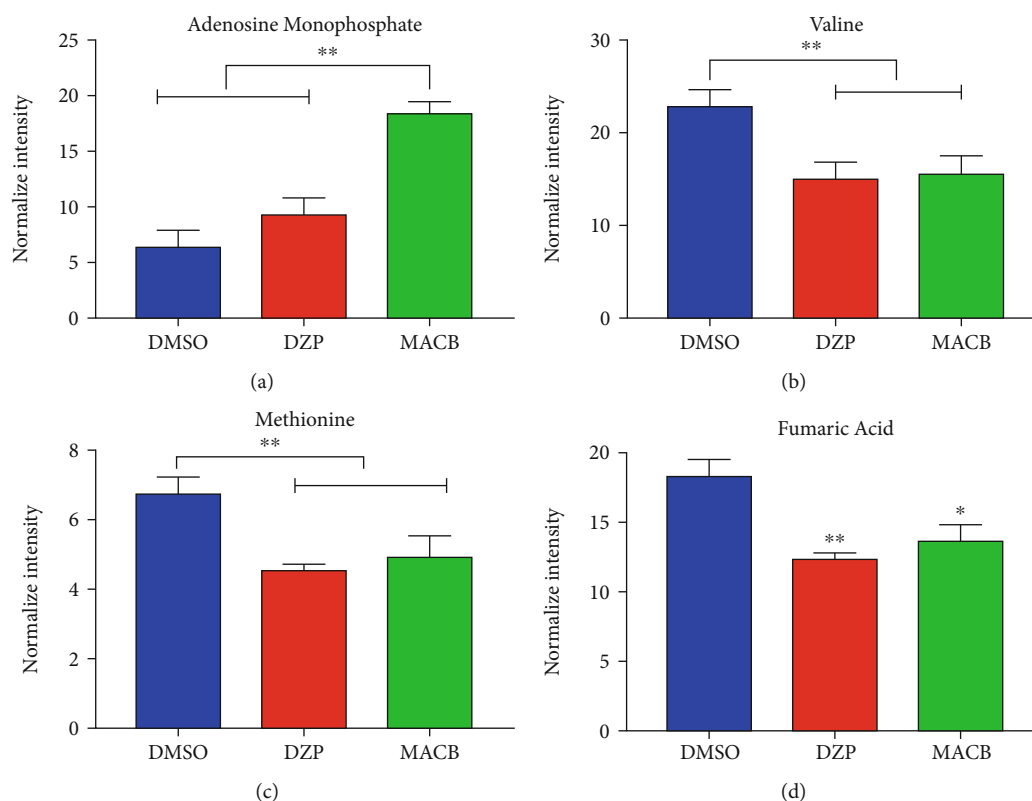


FIGURE 4: DZP and MACB affected the levels of nutrients in embryos. (a) MACB upregulated adenosine monophosphate. (b) DZP and MACB downregulated (b) valine, (c) methionine, and (d) fumaric acid. Data was analyzed by nonparametric, one-way analysis of variance (ANOVA) test, with 3 replicates ($n = 50$ larvae per group) followed with Tukey's multiple comparisons test, expressed as mean \pm SEM. * $P < 0.05$; ** $P < 0.01$.

with DZP or MACB at 5 nM. Zebrafish embryo was entirely dependent on their own nutrients in yolk sac to sustain growth and development [36]. The results showed that MACB increased the level of adenosine monophosphate (AMP) (Figure 4(a)), which generated the cyclic adenosine 3',5'-monophosphate (cAMP). The cAMP was an important signalling molecular improving axonal regeneration [37]. The valine promoted cellular sensitization [38] and was downregulated by DZP and MACB (Figure 4(b)). Moreover, the levels of methionine were also decreased by DZP and MACB (Figure 4(c)). The valine and methionine could affect the activity of brain-derived neurotrophic factor (BDNF) [39]. In addition, the fumaric acid has neuroprotection role in multiple sclerosis (MS) therapy [40]. The metabolic of fumaric acid was disrupted (Figure 4(d)), indicating neural developmental disorders in DZP- and MACB-treated zebrafish embryos. These results indicated that DZP and MACB could disrupt neural metabolism at low doses.

3.5. Detection of Gene Expression Related with *oct4*, *sox2*, and *Nanog*. To explore molecular mechanism regulating the proliferation and differentiation, we analyzed the expression of transcription-related factors in 10 hpf zebrafish embryos. Octamer-binding transcription factor 4 (*oct4*), SRY- (sex-determining region Y-) box 2 (*sox2*), and homeobox protein *nanog* regulate the differentiation of embryonic stem cells into specific cells. Our results showed that DZP and MACB

upregulated expression levels of *oct4* and *sox2* at 5 nM (Figures 5(a) and 5(b)). This trend was consistent with the accelerated somite growth at 12 hpf and the enhanced sport ability at 120 hpf. In addition, the risk of MACB was higher than DZP, because MACB also upregulated the expression level of *nanog* (Figure 5(c)). Therefore, both DZP and MACB promoted the early development of nervous system in zebrafish embryos through increasing pluripotency and self-renewal rates (Figure 5(d)).

4. Discussion

The pharmaceutical pollution in drinking water posing a risk to human health has attracted great concern. A diverse set of chemical exposure has been shown to affect infant nervous development at low concentration due to the immature development of the blood-brain barrier (BBB) [30, 41]. In our previous study, we found that the widely used DZP has contaminated drinking water and generated disinfection byproduct MACB. Thus, we further investigated their neurotoxicology and metabolic effects in zebrafish. We demonstrated that DZP and MACB increased the number of somites and neurons and upregulated the expression of pluripotency and self-renewal transcription factors, promoting the early development of nervous system in zebrafish embryos.

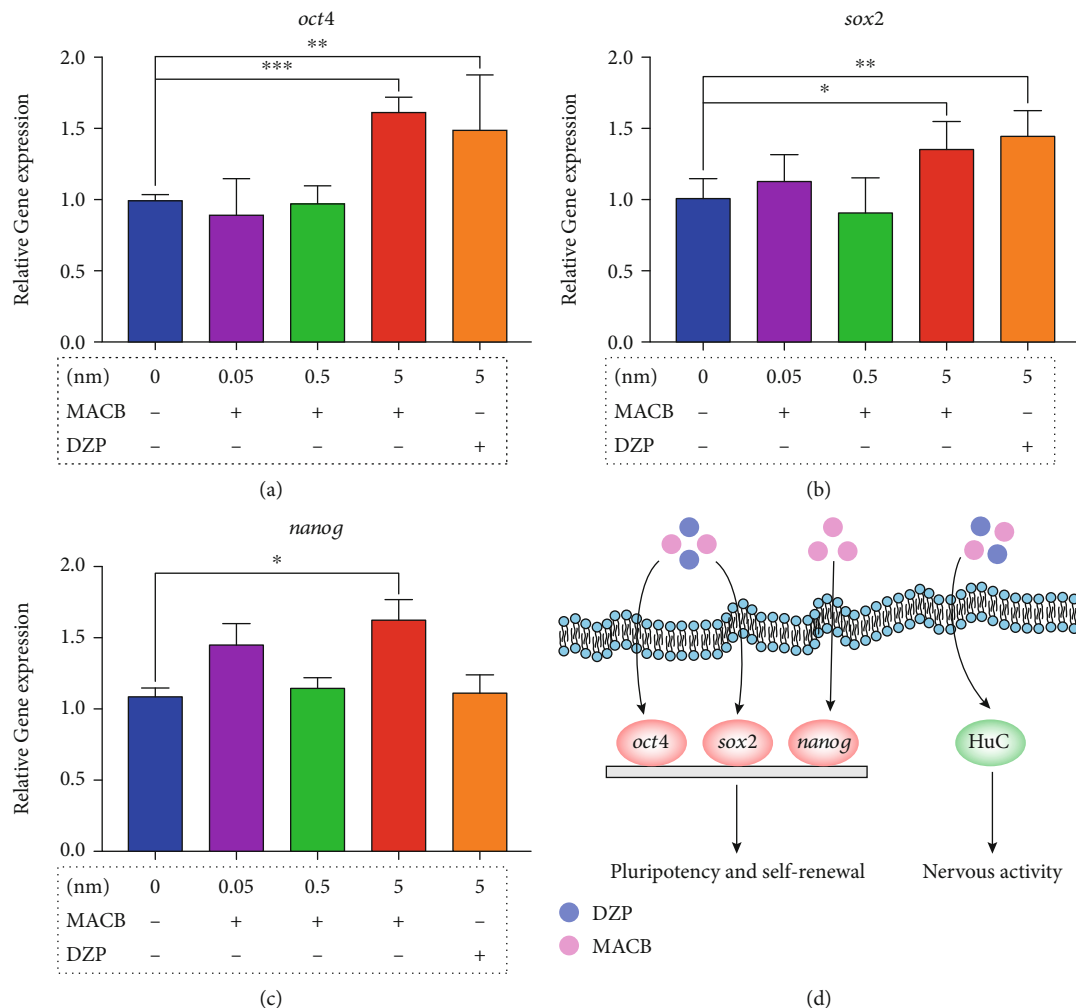


FIGURE 5: Expression level of transcription factors, *oct4*, *sox2*, and *nanog*, were upregulated. (a) The mRNA expression level of (a) *oct4* and (b) *sox2* were upregulated by DZP and MACB at 10 hpf. (c) The mRNA expression level of *nanog* was upregulated by MACB at 10 hpf. Data was analyzed by nonparametric, one-way analysis of variance (ANOVA) test, $n = 30$ larvae per group, followed with Tukey's multiple comparisons test, expressed as mean \pm SEM. * $P < 0.05$; ** $P < 0.01$; **** $P < 0.0001$; NS: not significant. (d) Diagram showing how DZP and MACB affect early proliferation and differentiation and nervous activity.

The total number of somites formed during somitogenesis is tightly fixed within a given species. The somites are derived from the paraxial mesoderm and are located on either side of the neural tube. Somitogenesis is of vital developmental importance and controls the differentiation of peripheral spinal nerves, vertebrae, and skeletal muscle [42]. It suggests that DZP and MACB would affect early embryo development at the micropollutant dose. The rapid onset of somitogenesis in DZP- or MACB-treated group suggests that the nervous inhibitor can accelerate early development at low concentration (nM), which was similar with the effect of antidepressant venlafaxine (10 ng) stimulating neurogenesis in zebrafish embryo [43]. The larval behavioral phenotype observed in response to cycles of dark-light could assess swimming behavior at these early life stages. Although the behavioral test is relatively simple, it can be used to screen the early neurological dysfunction caused by exogenous compounds [44]. DZP and MACB treatment significantly increased the activity of larvae in the dark but not in the light,

which may be corresponded with an increase in primary neurogenesis in larval zebrafish. Therefore, DZP and MACB had neuroexcitatory effects and stimulated the spontaneous movement of juvenile fish at low doses.

AMP facilitates the cAMP level that improves axonal regeneration [37] that explains why DZP and MACB accelerated zebrafish motion. In addition, the AMP strictly controls the activity of AMP-activated protein kinase (AMPK), which maintains metabolic homeostasis of energy and regulates growth and proliferation through nutritional signals [45]. The increased AMP could impair protein balance and decrease the levels of valine and methionine [46]. In addition, fumaric acid could clean ROS during the process of inflammation to protect neurons and glial cells [40]. DZP and MACB decreased the levels of fumaric acid that implied the occurrence of inflammation in early embryos. Thus, DZP and MACB might disturb the energy balance and protein homeostasis.

Many transcription factors can regulate the differentiation of embryonic stem cells into specific cells. The *oct4*, a

member of the family of POU-domain transcription factors, was required for pluripotency and self-renewal in embryonic stem (ES) during embryo development. The *sox2* is a transcription factor that is essential for maintaining self-renewal or pluripotency of undifferentiated embryonic stem cells, including neural stem cells. Homeobox protein *nanog* is a transcriptional factor that helps ESCs maintain pluripotency by suppressing cell determination factors. DZP and MACB promote the expression level of *oct4* and *sox2* accelerating the early neurodevelopment of zebrafish embryo [47, 48]. In addition, MACB upregulated the expression of *oct4* and *nanog*. In previous study, antipsychotic lithium enhanced *oct4* and *nanog* expression to facilitate reprogramming depending on major target GSK3 β [49]. Thus, MACB enhanced proliferation and differentiation of somatic cells which might depend on GABAA receptors or other targets. GABAergic neurons are critical for early development of hippocampus and neocortex [50]. Previous study showed that DZP could downregulate GABAergic synapses which modulated neural behavior with compartmentalized Ca²⁺ dynamics [51]. In addition, intracellular calcium mobilization is required to modulate development and tissue patterning in zebrafish embryos [52]. Therefore, it is possible that MACB accelerated the developing embryos through modulating intracellular calcium.

5. Conclusion

In conclusion, DZP and MACB accelerated the development of embryo somites and neurons through upregulating the transcription factors at drinking water pollution levels. Meanwhile, DZP and MACB promoted energy metabolism and resulted in excited behavior. Our results highlighted that psychiatric drugs stimulated neural genesis at low doses.

Data Availability

The data used to support the findings of this study are included within the article.

Conflicts of Interest

The authors declare no conflicts of interest.

Authors' Contributions

Xiaole Zhao, Xiaoyong Huang, Kui Zhu, and Bing Shao designed the research. Xiaole Zhao and Xiaoyong Huang performed the research. Jiachen Shi and Xiaofei Jia contributed new analytic tools. Xiaole Zhao, Xiaoyong Huang, Kui Zhu, and Bing Shao analyzed and wrote the paper.

Acknowledgments

This study was supported by the National Natural Science Foundation of China (21677019), Capital Foundation of Medicine Research and Development (2018-1-302), and Beijing Postdoctoral Research Foundation.

References

- [1] T. Brodin, J. Fick, M. Jonsson, and J. Klaminder, "Dilute concentrations of a psychiatric drug alter behavior of fish from natural populations," *Science*, vol. 339, no. 6121, pp. 814-815, 2013.
- [2] M. F. Meyer, S. M. Powers, and S. E. Hampton, "An evidence synthesis of pharmaceuticals and personal care products (PPCPs) in the environment: imbalances among compounds, sewage treatment techniques, and ecosystem types," *Environmental Science & Technology*, vol. 53, no. 22, pp. 12961-12973, 2019.
- [3] M. J. S. Chaves, S. C. Barbosa, M. M. Malinowski et al., "Pharmaceuticals and personal care products in a Brazilian wetland of international importance: occurrence and environmental risk assessment," *Science of the Total Environment*, vol. 734, article 139374, 2020.
- [4] D. Muir, D. Simmons, X. Wang et al., "Bioaccumulation of pharmaceuticals and personal care product chemicals in fish exposed to wastewater effluent in an urban wetland," *Scientific Reports*, vol. 7, no. 1, p. 16999, 2017.
- [5] X. Zhang, Y. Yang, J. Zhang et al., "Determination of emerging chlorinated byproducts of diazepam in drinking water," *Chemosphere*, vol. 218, pp. 223-231, 2019.
- [6] N. E. Calcaterra and J. C. Barrow, "Classics in chemical neuroscience: diazepam (valium)," *ACS Chemical Neuroscience*, vol. 5, no. 4, pp. 253-260, 2014.
- [7] M. G. Craske, M. B. Stein, T. C. Eley et al., "Anxiety disorders," *Nature Reviews. Disease Primers*, vol. 3, no. 1, p. 17024, 2017.
- [8] K. Bykov, M. He, and J. J. Gagne, "Trends in utilization of prescribed controlled substances in US commercially insured adults, 2004-2019," *JAMA Internal Medicine*, vol. 180, no. 7, pp. 1006-1008, 2020.
- [9] T. Kosjek, S. Perko, M. Zupanc et al., "Environmental occurrence, fate and transformation of benzodiazepines in water treatment," *Water Research*, vol. 46, no. 2, pp. 355-368, 2012.
- [10] U. Hass, U. Duennbier, and G. Massmann, "Occurrence and distribution of psychoactive compounds and their metabolites in the urban water cycle of Berlin (Germany)," *Water Research*, vol. 46, no. 18, pp. 6013-6022, 2012.
- [11] C. Wang, L. Hou, J. Li et al., "Occurrence of diazepam and its metabolites in wastewater and surface waters in Beijing," *Environmental Science and Pollution Research International*, vol. 24, no. 18, pp. 15379-15389, 2017.
- [12] J. Riss, J. Cloyd, J. Gates, and S. Collins, "Benzodiazepines in epilepsy: pharmacology and pharmacokinetics," *Acta Neurologica Scandinavica*, vol. 118, no. 2, pp. 69-86, 2008.
- [13] P. R. McElhatton, "The effects of benzodiazepine use during pregnancy and lactation," *Reproductive Toxicology*, vol. 8, no. 6, pp. 461-475, 1994.
- [14] P. Liu and L. Shang, "Neurobehavioral toxicity in offspring of Wistar rats after prenatal exposure to different doses of diazepam," *Chinese Journal of Behavioral Medical Science*, vol. 12, pp. 246-248, 2003.
- [15] L. Laegreid, G. Hagberg, and A. Lundberg, "The effect of benzodiazepines on the fetus and the newborn," *Neuropediatrics*, vol. 23, no. 1, pp. 18-23, 1992.
- [16] L. Laegreid, G. Hagberg, and A. Lundberg, "Neurodevelopment in late infancy after prenatal exposure to benzodiazepines—a prospective study," *Neuropediatrics*, vol. 23, no. 2, pp. 60-67, 1992.

- [17] A. L. Salisbury, K. E. O'Grady, C. L. Battle et al., "The roles of maternal depression, serotonin reuptake inhibitor treatment, and concomitant benzodiazepine use on infant neurobehavioral functioning over the first postnatal month," *The American Journal of Psychiatry*, vol. 173, no. 2, pp. 147–157, 2016.
- [18] L. E. Vossen, D. Červený, O. Sen Sarma et al., "Low concentrations of the benzodiazepine drug oxazepam induce anxiolytic effects in wild-caught but not in laboratory zebrafish," *Science of the Total Environment*, vol. 703, article 134701, 2020.
- [19] L. E. Vossen, D. Cervený, M. Österkrans et al., "Chronic exposure to oxazepam pollution produces tolerance to anxiolytic effects in zebrafish (*Danio rerio*)," *Environmental Science & Technology*, vol. 54, no. 3, pp. 1760–1769, 2019.
- [20] M. Bedner and W. A. MacCrehan, "Transformation of acetaminophen by chlorination produces the toxicants 1,4-benzoquinone and N-acetyl-p-benzoquinone imine," *Environmental Science & Technology*, vol. 40, no. 2, pp. 516–522, 2006.
- [21] F. M. Wendel, C. Lütke Eversloh, E. J. Machek et al., "Transformation of iopamidol during chlorination," *Environmental Science & Technology*, vol. 48, no. 21, pp. 12689–12697, 2014.
- [22] J. Y. Hu, T. Aizawa, and S. Ookubo, "Products of aqueous chlorination of bisphenol A and their estrogenic activity," *Environmental Science & Technology*, vol. 36, no. 9, pp. 1980–1987, 2002.
- [23] I. Carpinteiro, R. Rodil, J. B. Quintana, and R. Cela, "Reaction of diazepam and related benzodiazepines with chlorine. Kinetics, transformation products and in-silico toxicological assessment," *Water Research*, vol. 120, pp. 280–289, 2017.
- [24] C. Postigo and S. D. Richardson, "Transformation of pharmaceuticals during oxidation/disinfection processes in drinking water treatment," *Journal of Hazardous Materials*, vol. 279, pp. 461–475, 2014.
- [25] H. C. Park, S. K. Hong, H. S. Kim et al., "Structural comparison of zebrafish *Elav/Hu* and their differential expressions during neurogenesis," *Neuroscience Letters*, vol. 279, no. 2, pp. 81–84, 2000.
- [26] Y. Ogawa, K. Kakumoto, T. Yoshida et al., "Elavl3 is essential for the maintenance of Purkinje neuron axons," *Scientific Reports*, vol. 8, no. 1, p. 2722, 2018.
- [27] H. C. Park, C. H. Kim, Y. K. Bae et al., "Analysis of upstream elements in the *HuC* promoter leads to the establishment of transgenic zebrafish with fluorescent neurons," *Developmental Biology*, vol. 227, no. 2, pp. 279–293, 2000.
- [28] D. A. Lyons, A. T. Guy, and J. D. Clarke, "Monitoring neural progenitor fate through multiple rounds of division in an intact vertebrate brain," *Development*, vol. 130, no. 15, pp. 3427–3436, 2003.
- [29] O. Pourquie, "Vertebrate segmentation: from cyclic gene networks to scoliosis," *Cell*, vol. 145, no. 5, pp. 650–663, 2011.
- [30] C. B. Kimmel, W. W. Ballard, S. R. Kimmel, B. Ullmann, and T. F. Schilling, "Stages of embryonic development of the zebrafish," *Developmental Dynamics*, vol. 203, no. 3, pp. 253–310, 1995.
- [31] C. D. Kinch, K. Ibzhazehiebo, J. H. Jeong, H. R. Habibi, and D. M. Kurrasch, "Low-dose exposure to bisphenol A and replacement bisphenol S induces precocious hypothalamic neurogenesis in embryonic zebrafish," *Proceedings of the National Academy of Sciences of the United States of America*, vol. 112, no. 5, pp. 1475–1480, 2015.
- [32] A. C. Mendes Hacke, E. Miyoshi, J. A. Marques, and R. P. Pereira, "Anxiolytic properties of *Cymbopogon citratus* (DC.) stapf extract, essential oil and its constituents in zebrafish (*Danio rerio*)," *Journal of Ethnopharmacology*, vol. 260, p. 113036, 2020.
- [33] X. Liu, R. Zhang, and Y. Jin, "Differential responses of larval zebrafish to the fungicide propamocarb: endpoints at development, locomotor behavior and oxidative stress," *Science of the Total Environment*, vol. 731, p. 139136, 2020.
- [34] D. Whitmore, N. S. Foulkes, and P. Sassone-Corsi, "Light acts directly on organs and cells in culture to set the vertebrate circadian clock," *Nature*, vol. 404, no. 6773, pp. 87–91, 2000.
- [35] R. C. MacPhail, J. Brooks, D. L. Hunter, B. Padnos, T. D. Irons, and S. Padilla, "Locomotion in larval zebrafish: influence of time of day, lighting and ethanol," *Neurotoxicology*, vol. 30, no. 1, pp. 52–58, 2009.
- [36] J. L. Anderson, J. D. Carten, and S. A. Farber, "Zebrafish lipid metabolism: from mediating early patterning to the metabolism of dietary fat and cholesterol," *Methods in Cell Biology*, vol. 101, pp. 111–141, 2011.
- [37] A. Guijarro-Belmar, D. M. Domanski, X. Bo, D. Shewan, and W. Huang, "The therapeutic potential of targeting exchange protein directly activated by cyclic adenosine 3',5'-monophosphate (Epac) for central nervous system trauma," *Neural Regeneration Research*, vol. 16, no. 3, pp. 460–469, 2021.
- [38] M. G. Mirisola, G. Taormina, P. Fabrizio, M. Wei, J. Hu, and V. D. Longo, "Serine- and threonine/valine-dependent activation of PDK and Tor orthologs converge on Sch9 to promote aging," *PLoS Genetics*, vol. 10, no. 2, article e1004113, 2014.
- [39] M. F. Egan, M. Kojima, J. H. Callicott et al., "The BDNF val66met polymorphism affects activity-dependent secretion of BDNF and human memory and hippocampal function," *Cell*, vol. 112, no. 2, pp. 257–269, 2003.
- [40] U. Schulze-Topphoff, M. Varrin-Doyer, K. Pekarek et al., "Dimethyl fumarate treatment induces adaptive and innate immune modulation independent of Nrf2," *Proceedings of the National Academy of Sciences of the United States of America*, vol. 113, no. 17, pp. 4777–4782, 2016.
- [41] I. Loryan, E. Melander, M. Svensson et al., "In-depth neuropharmacokinetic analysis of antipsychotics based on a novel approach to estimate unbound target-site concentration in CNS regions: link to spatial receptor occupancy," *Molecular Psychiatry*, vol. 21, no. 11, pp. 1527–1536, 2016.
- [42] Y. Saga and H. Takeda, "The making of the somite: molecular events in vertebrate segmentation," *Nature Reviews. Genetics*, vol. 2, no. 11, pp. 835–845, 2001.
- [43] W. A. Thompson, V. I. Arnold, and M. M. Vijayan, "Venlafaxine in embryos stimulates neurogenesis and disrupts larval behavior in zebrafish," *Environmental Science & Technology*, vol. 51, no. 21, pp. 12889–12897, 2017.
- [44] M. B. Orger and G. G. de Polavieja, "Zebrafish behavior: opportunities and challenges," *Annual Review of Neuroscience*, vol. 40, no. 1, pp. 125–147, 2017.
- [45] A. L. de Souza Almeida Matos, J. S. Oakhill, J. Moreira, K. Loh, S. Galic, and J. W. Scott, "Allosteric regulation of AMP-activated protein kinase by adenylate nucleotides and small-molecule drugs," *Biochemical Society Transactions*, vol. 47, no. 2, pp. 733–741, 2019.
- [46] M. Holecek and M. Vodenicarovova, "Effects of low and high doses of fenofibrate on protein, amino acid, and energy metabolism in rat," *International Journal of Experimental Pathology*, vol. 101, no. 5, pp. 171–182, 2020.

- [47] L. A. Boyer, T. I. Lee, M. F. Cole et al., “Core transcriptional regulatory circuitry in human embryonic stem cells,” *Cell*, vol. 122, no. 6, pp. 947–956, 2005.
- [48] X. Wei, J. Guo, Q. Li et al., “Bach1 regulates self-renewal and impedes mesodermal differentiation of human embryonic stem cells,” *Science Advances*, vol. 5, no. 3, p. eaau7887, 2019.
- [49] Q. Wang, X. Xu, J. Li et al., “Lithium, an anti-psychotic drug, greatly enhances the generation of induced pluripotent stem cells,” *Cell Research*, vol. 21, no. 10, pp. 1424–1435, 2011.
- [50] Y. Murata and M. T. Colonnese, “GABAergic interneurons excite neonatal hippocampus in vivo,” *Science Advances*, vol. 6, no. 24, article eaba1430, 2020.
- [51] W. S. Costa, P. Van der Auwera, C. Glock et al., “A GABAergic and peptidergic sleep neuron as a locomotion stop neuron with compartmentalized Ca^{2+} dynamics,” *Nature Communications*, vol. 10, no. 1, article 4095, 2019.
- [52] D. Klatt Shaw, D. Gunther, M. J. Jurynek, A. A. Chagovetz, E. Ritchie, and D. J. Grunwald, “Intracellular calcium mobilization is required for sonic hedgehog signaling,” *Developmental Cell*, vol. 45, no. 4, pp. 512–525.e5, 2018.

Research Article

Inhibitory Effect of Delphinidin on Oxidative Stress Induced by H₂O₂ in HepG2 Cells

Jingjing Xu,^{1,2} Yanwei Zhang,^{1,2} Guofeng Ren ^{1,2} Rengui Yang,³ Jingfang Chen,³ Xiaojing Xiang,⁴ Hong Qin ^{1,2} and Jihua Chen ^{1,2}

¹Xiangya School of Public Health, Central South University, Changsha 410078, China

²Hunan Provincial Key Laboratory of Clinical Epidemiology, Changsha 410078, China

³Changsha Center for Disease Control and Prevention, Changsha 410002, China

⁴Department of Neurology, Changsha Central Hospital, Changsha 410018, China

Correspondence should be addressed to Hong Qin; qinhong@csu.edu.cn and Jihua Chen; chenjh@csu.edu.cn

Received 8 July 2020; Revised 14 October 2020; Accepted 26 October 2020; Published 21 November 2020

Academic Editor: Si Qin

Copyright © 2020 Jingjing Xu et al. This is an open access article distributed under the Creative Commons Attribution License, which permits unrestricted use, distribution, and reproduction in any medium, provided the original work is properly cited.

Chronic liver diseases (CLDs) are correlated with oxidative stress induced by the accumulation of intracellular reactive oxygen species (ROS). In this study, we employed HepG2, a human liver carcinoma cell line containing many antioxidant enzymes, to explore the function of delphinidin against oxidative stress induced by H₂O₂ and to provide scientific data of the molecular mechanism. Cells were pretreated with different concentrations of delphinidin (10 μmol/L, 20 μmol/L, and 40 μmol/L) for 2 h before treatment with 750 μM H₂O₂ for 1 h. The results showed that H₂O₂ decreased the survival rate of HepG2 cells and increased the level of ROS, but delphinidin pretreatment could possess the opposite result. At the same time, the expression of Nrf2 was enhanced by the delphinidin pretreatment. This was because delphinidin promoted Nrf2 nuclear translocation and inhibited its degradation, which led to the increase expression of antioxidant protein HO-1 (Nrf2-related phase II enzyme heme oxygenase-1). Besides, we found that delphinidin could significantly alleviate the reduction of Nrf2 protein levels and the accumulation of intracellular ROS levels in Nrf2 knockdown HepG2 cells. In conclusion, our study suggested that delphinidin, as an effective antioxidant, protected HepG2 cells from oxidative stress by regulating the expression of Nrf2/HO-1.

1. Introduction

The death toll of chronic liver disease (CLDs) associated with cirrhosis, liver cancer, hepatitis, etc. is on the rise worldwide [1]. Increasing evidences confirmed the contributory role of oxidative stress in the pathogenesis of CLDs. As the common cause of oxidative stress [2, 3], reactive oxygen species (ROS) are a collective name for molecules containing oxidative reactions, including superoxide anions (O₂⁻), hydroxyl radicals (OH), hypochlorous acid (HOCl), ozone (O₃), and hydrogen peroxide (H₂O₂) [4].

There is an adaptive and dynamic antioxidant defense system to eliminate excessive ROS and protect cells against oxidative stress in human body. Antioxidants, antioxidant enzymes, and phase II detoxifying enzymes are included in this system. Previous studies have shown that the phase II

detoxification enzymes consisted of glutathione S-transferase (GST), NAD(P)H quinone oxidoreductase-1 (NQO1), and heme oxygenase-1 (HO-1) which could scavenge free radicals and electrophiles [5]. In addition, the antioxidant response element (ARE), a common nucleotide sequence in the promoter regions of phase II detoxifying enzymes, could be effectively activated by nuclear factor erythroid 2-related factor 2 (Nrf2) and could regulate the expression of its downstream genes [6].

As a key transcription factor, Nrf2 regulates the response of intracellular antioxidant and plays a crucial role in homeostasis maintenance [7]. Under normal conditions, Nrf2 is stored in the cytoplasm in an inactive state until it is coupled with Kelch-like ECH-associated protein 1 (Keap1) and rapidly degraded by the ubiquitin-protease system. Thereby the expression of Nrf2 is stable and the transcriptional activity is

low at this time. While under oxidative stress conditions, Nrf2 is responsible for its separation with Keap1 and transfers into the nucleus before recognizing and binding with the ARE which regulates the transcription of downstream biphasic detoxification enzymes and antioxidant protein genes, such as GST, NQO1, and HO-1. Previous studies demonstrated that Nrf2 had protective effects against oxidative stress-induced diseases such as cancer [8], diabetes [9], respiratory diseases [10], chronic inflammation [11], cardiovascular diseases [12], and neurodegenerative diseases [13]. Other than that, several studies previously revealed that polyphenols activated the Nrf2/Keap1 pathway through different mechanisms to exert antioxidant activity such as quercetin [14, 15], epigallocatechin gallate [16], baicalein [17], and resveratrol [18].

Anthocyanins, which are widely distributed in edible plants, are a benefit to health [19–21]. For instance, anthocyanins have an effective function in neurological diseases, hypoglycemia, cardiotoxicity, and anti-inflammation [22–24]. Delphinidin, a natural anthocyanin, is one of the most valuable polyphenols due to its high antioxidant activity. Kim et al. previously revealed that delphinidin possessed antiangiogenic function potential [25]. Moreover, delphinidin could inhibit the proliferation of SKOV3 cells (ovarian cancer cells) [26] and it could prevent prostate cancer via inhibiting the apoptosis mediated by p53 [27]. Lee et al. reported that delphinidin could protect chondrocytes against H₂O₂-mediated oxidative stress by activating NF- κ B and Nrf2 [28]. However, there is a lack of data on how delphinidin regulates Nrf2 to exert the function of antioxidant stress. In this study, we intend to use H₂O₂ to construct a cell model of oxidative damage and evaluate the antioxidant activity of delphinidin. The purpose of this study is to investigate whether delphinidin exerts antioxidant protection on cells by regulating the Nrf2 pathway.

2. Materials and Methods

2.1. Cells and Reagents. HepG2 cells were obtained from Cancer Research Institute of Central South University (Changsha, China). Delphinidin was purchased from Cayman company (Michigan, USA). Hydrogen peroxide solution (H₂O₂) was purchased from HengXing Chemical Reagent (Tianjin, China). RPMI 1640 medium and fetal bovine serum (FBS) were purchased from Gibco (Grand Island, NY, USA). Penicillin–streptomycin solution and 3-(4,5-dimethylthiazol-2-yl)-2,5-diphenyltetrazolium bromide (MTT) reagent were obtained from Gen-View (Calimesa, CA, USA). The formation of intracellular ROS was determined using DCFH-DA (Sigma-Aldrich, St. Louis, MO, USA). The Nuclear and Cytoplasmic Protein Extraction Kit and protease inhibitor phenylmethylsulfonyl fluoride (PMSF) were bought from Beyotime (Shanghai, China). The primary antibodies, such as anti-Keap1, anti-HO-1, and anti-Lamin B were bought from Santa Cruz Biotechnology (CA, USA). The Nrf2 antibody was purchased from Abcam (Cambridge, UK). Antibodies against β -actin antibody and α -tubulin were obtained from ABclonal (Boston, MA, USA). Paraformaldehyde was purchased from Dingguo (Beijing, China). Triton-X was obtained from Solarbio (Beijing, China). Goat Serum

and DAPI were purchased from Boster (Wuhan, China). Trizol reagent was obtained from Ambion (Austin, USA). qPCR SYBR Green Master Mix was bought from Vazyme (Nanjing, China). Reverse transcription kit instructions and Lipofectamine 3000 were purchased from Thermo Fisher Scientific (Wilmington, USA).

2.2. Cell Culture. HepG2 cells were cultured in RPMI 1640 medium, supplemented with 10% FBS and 1% penicillin–streptomycin solution at 37°C in a 5% CO₂ atmosphere.

2.3. MTT Assay. MTT assay was performed to detect the effect of delphinidin on cell viability. HepG2 cells ($\sim 5 \times 10^3$ cells/well) were seeded in 96-well plates for 24 h and then treated with different concentrations of delphinidin for 24 h. After changing the culture medium, 5 mg/mL MTT reagent was added and the cells were incubated for 4 h. Cell viability was calculated by measuring absorbance at 490 nm using a microplate reader. 10 μ M, 20 μ M, and 40 μ M delphinidin with the treatment of H₂O₂ were pretreated to assess the impact on cell viability based on the results of the above experiment.

2.4. ROS Assay. HepG2 cells ($\sim 5 \times 10^3$ cells/well) were seeded in 96-well plates for 24 h. After refreshing the culture medium, cells were treated with delphinidin (10 μ mol/L, 20 μ mol/L, and 40 μ mol/L) for 2 h. And then the cells were exposed with H₂O₂ (750 μ mol/L) for 1 h. Cells were washed once with warm phosphate buffer saline (PBS) and a serum-free culture medium containing 5 μ M ROS probe was added and reacted for 30 min. The fluorescence was read with a spectrofluorimeter (PerkinElmer, Waltham, MA, USA) at excitation wavelength of 485 nm.

2.5. Western Blot Analysis. Cytoplasm and nuclear protein extraction was prepared by using the Nuclear and Cytoplasmic Protein Extraction Kit. Cells were washed 3 times with ice-cold 1 \times PBS and lysed in 140 μ L 1 \times SDS. Proteins were separated in a 10% sodium dodecyl sulfate-polyacrylamide gel electrophoresis (SDS-PAGE) and subsequently transferred to polyvinylidene difluoride (PVDF) membranes for 1.5 h before blocking in a 5% skimmed milk for 1 h. Then, the PVDF membranes were incubated into the specific primary antibody (Nrf2, Keap1, HO-1, β -actin, Lamin B, and α -tubulin) at 4°C overnight. After washing 3 times with Tris-Buffered Saline Tween20 (TBS-T) solution, the PVDF membranes were incubated with the corresponding secondary antibody at room temperature. Finally, the membranes were scanned in a chemiluminescence imaging system (Tanon 5500, Shanghai, China).

2.6. Immunofluorescence Assay. HepG2 cells ($\sim 3 \times 10^4$ cells/well) were cultured for 24 h on coverslips in 24-well plates. Cells were treated with delphinidin (20 μ mol/L) for 3 h and then H₂O₂ (750 μ mol/L) for 1 h. The cells were subsequently washed twice with warm PBS and fixed with 4% paraformaldehyde at room temperature for 30 min. After permeation with 0.1% Triton-X at room temperature for 20 min, cells were blocked with Goat Serum for 1 h. Then, cells were incubated with Nrf2 primary antibody at 4°C overnight. After washing 3 times with cold PBS, cells were incubated with

fluorescent secondary antibody for 1.5 h and stained with DAPI for 5 min in the dark at room temperature. Finally, coverslips were mounted onto glass slides, and the images were taken by fluorescence microscope (Thermo Scientific, Wilmington, USA).

2.7. Immunoprecipitation. HepG2 cells ($\sim 5 \times 10^6$ cells/dish) were seeded in 10 cm petri dish for 24 h. Then, cells were treated with delphinidin (20 $\mu\text{mol/L}$) for 2 h and H_2O_2 (750 $\mu\text{mol/L}$) for 1 h. After washing twice with cold PBS, cells were lysed with cell lysis buffer containing 1 mM PMSF. The lysates were stirred for 1 h at 4°C and then centrifuged at 12,000 $\times g$ in a high-speed refrigerated centrifuge at 4°C for 15 min. After determining the protein concentrations of supernatants, the cell extracts were preincubated with 2 μg normal rabbit immunoglobulin G (IgG) and 20 μL Protein A agarose beads (Beyotime, Shanghai, China) for 2 h. The mixture was centrifuged at 2,500 rpm in a high-speed refrigerated centrifuge at 4°C for 5 min. The supernatants were added with anti-Nrf2 antibody (2 μg) and stirred at 4°C overnight and then the supernatants were mixed with 30 μL Protein A agarose beads for 2 h at 4°C. Subsequently, the mixture was centrifuged at 2,500 rpm in a high-speed refrigerated centrifuge at 4°C for 5 min to collect the beads. After washing once with cell lysis buffer, the beads were added into 1 \times SDS loading buffer and then heated at 100°C for 5 minutes for subsequent Western blotting experiments.

2.8. Quantitative Real-Time PCR. Total RNA was extracted from cells with trizol reagent, and 1% agarose gel was used to assess RNA integrity by using a UV gel imaging system. Total RNA was reverse transcribed into cDNA according to the reverse transcription kit instructions. Moreover, real-time PCR analysis was performed using a qPCR SYBR Green Master Mix and a LightCycler 96 Instrument (Roche, Basel, Switzerland). The primers used in the study were synthesized by Sangon Biotech (Sangon Biotech Co, Shanghai, China) and shown in Table 1. Finally, the data were calculated using the $2^{-\Delta\Delta Cq}$ method.

2.9. Transfection of shRNA. The design of knockdown short hairpin ribonucleic acid (shRNA) (ccggacTGACAGAAGTTGACAATTactcgagTAATTGTCAACTTCTGTCAggtttt-tg) targeting Nrf2 was commissioned by GeneChem (Shanghai, China), and subsequently, the shRNA was cloned into double-marked lentiviral vector GV248 (GeneChem, Shanghai, China). Lipofectamine 3000 was used to transfect sh-con (negative control) and sh-Nrf2 plasmids into HepG2 cells. After puromycin treatment, nonspecific cells were eliminated and cells with green fluorescence were sorted using flow cytometry. Transfection cells were cultured and detected using Western blot and ROS methods.

2.10. Statistical Analysis. The SPSS18.0 statistical (Chicago, IL, USA) software was used for statistical analysis. All the data was repeated at least 3 times, and the results were expressed as the mean \pm SD. The data was estimated the normality distribution and homogeneity of variance. Statistical differences between two groups were assessed using a two-tailed Student's *t*-test. The one-way analysis of variance was

used between the multiple sample means (the pairwise comparison used the LSD test). Otherwise, the Kruskal-Wallis H test was used for data analysis (Student-Newman-Keuls test was used for pairwise comparison). Statistical significance was considered at $P < 0.05$.

3. Results

3.1. Delphinidin Protects HepG2 Cells against H_2O_2 -Induced Oxidative Stress. HepG2 cells were treated with different concentrations (0~200 μM) of delphinidin for 24 h to test the cytotoxicity, and the growth inhibition rate was measured by MTT assays. As shown in Figure 1(b), the IC50 value of HepG2 cells treated with delphinidin was 65.58 μM . Compared with the control group, cells treated with delphinidin at different concentrations (10 μM , 20 μM , and 40 μM) showed normal growth, polygonal shape, and well-defined boundaries (Figure 1(c)). According to the results of the above MTT experiments, 10 μM , 20 μM , and 40 μM delphinidin were used to pretreat the cells and then the cell viability of HepG2 cells treated with H_2O_2 (750 μM) was examined. On the one hand, the cell viability of the H_2O_2 -treated group decreased significantly (100% and $50.84\% \pm 1.26\%$, $P < 0.05$). On the other hand, the delphinidin intervention group increased significantly. ($50.84\% \pm 1.26\%$ and $53.59\% \pm 0.51\%$, $55.58\% \pm 0.28\%$, and $59.52\% \pm 1.08\%$, respectively, $P < 0.05$) (Figure 1(d)).

Moreover, the 2',7'-dichlorofluorescein diacetate (DCFH-DA) probe was used to detect intracellular ROS levels. Compared with the control group, the level of ROS in the H_2O_2 -treated group increased by 60% ($P < 0.05$). On the contrary, compared with the H_2O_2 -treated group, the level of ROS in the delphinidin intervention group (10 μM , 20 μM , and 40 μM) decreased by 9.4%, 28.7%, and 21.1%, respectively ($P < 0.05$) (Figure 1(f)).

3.2. Activation of Nrf2-Related Proteins Regulated by Delphinidin. Compared with the control group, the protein expression of Nrf2 increased 1.2-fold at 3 h ($P < 0.05$) and that of HO-1 promoted at 3 h, 6 h, and 9 h ($P < 0.05$) after treatment with 20 μM of HepG2 cells (Figures 2(a) and 2(b)). The results showed that cells treated with 20 μM delphinidin had upregulated the level of Nrf2 and HO-1 protein at 3 h. Besides, the protein expression of Nrf2 and HO-1 was upregulated after 20 μM and 40 μM delphinidin treatment ($P < 0.05$). On the other hand, delphinidin did not affect the protein expression of Keap1 (Figures 2(c) and 2(d)). Therefore, 3 h processing time and 20 μM delphinidin were chosen for the following experiment.

3.3. Activation of Nrf2/HO-1 Pathway by Delphinidin under Oxidative Stress. In order to investigate whether delphinidin could regulate the Nrf2/HO-1 pathway, HepG2 cells were treated with different concentrations (10 μM , 20 μM , and 40 μM) of delphinidin for 2 h and subsequently treated with H_2O_2 (750 μM) for 1 h (the total treatment time was 3 h). Then, the expression of Nrf2-related mRNA and protein was detected by qPCR and Western blot. Compared with the H_2O_2 -treated group, the level of Nrf2 mRNA was

TABLE 1: The primer sequences for real-time PCR.

Gene	Forward primer	Reverse primer
Nrf2	5'-TACTCCCAGTTGCCACA-3'	5'-CATCTACAAACGGGAATGTCTGC-3'
HO-1	5'-CTGACCCATGACACCAAGGAC-3'	5'-AAAGCCCTACAGCAACTGTGC-3'
NQO1	5'-GGCAGAAGAGCACTGATCGTA-3'	5'-TGATGGGATTGAAGTTCATGGC-3'
β -Actin	5'-ATCATGTTTGAGACCTTCAACA-3'	5'-CATCTCTTGCTCGAAGTCCA-3'

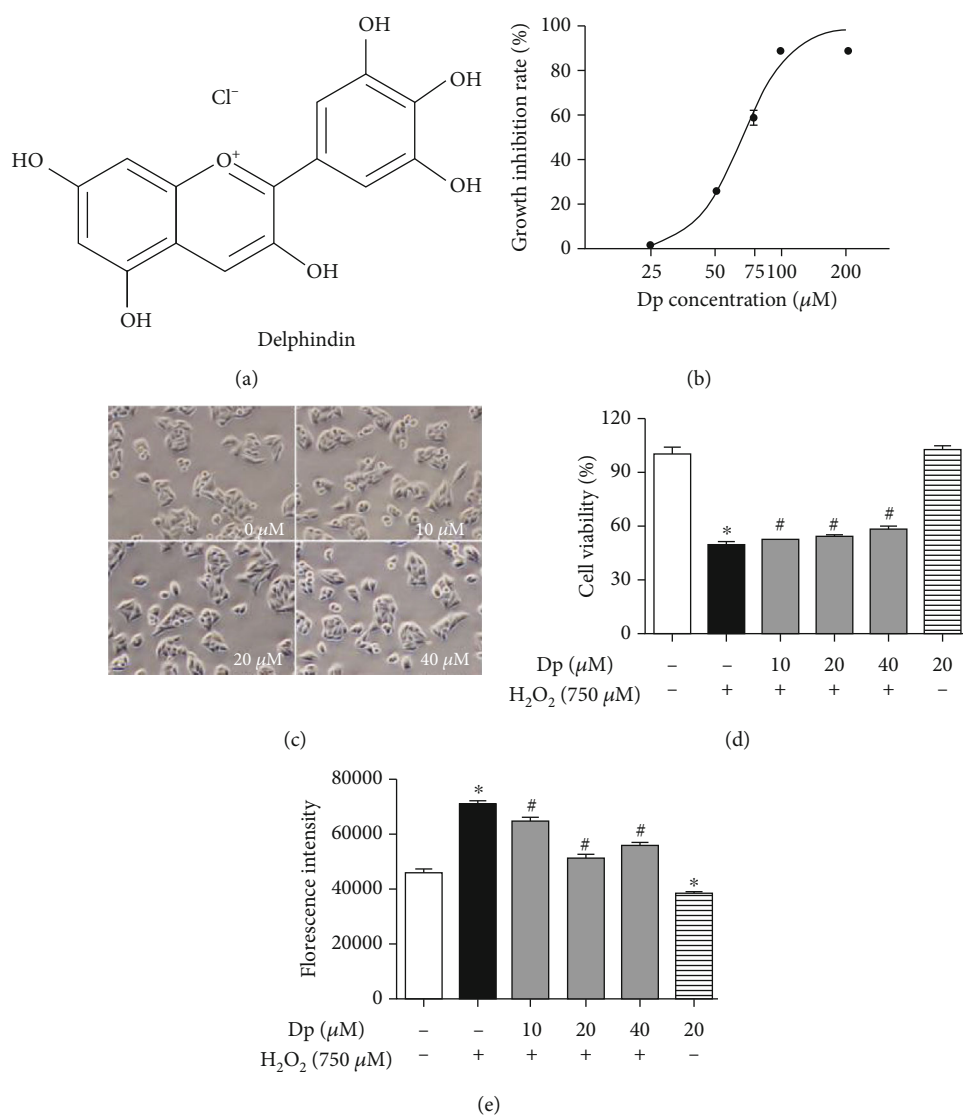


FIGURE 1: Effect of delphinidin on cell viability and the generation of ROS level induced by H_2O_2 : (a) a chemical structure of delphinidin; (b) growth inhibition rate of HepG2 cells treated with different concentrations of delphinidin; (c) morphological observation of HepG2 cells treated with different concentrations of delphinidin; (d) cell viability of HepG2 cells treated with delphinidin and H_2O_2 ; (e) effects of delphinidin (10 μ M, 20 μ M, and 40 μ M) on intracellular ROS levels induced by H_2O_2 . Values were presented as mean \pm SD. * $P < 0.05$ vs. the control group and # $P < 0.05$ vs. the H_2O_2 -treated group.

significantly increased in delphinidin intervention groups (10 μ M, 20 μ M, and 40 μ M). Other than that, delphinidin resulted in a significant upregulation of HO-1 mRNA in 20 μ M and 40 μ M delphinidin groups. There was no significant difference in the expression of Keap1 mRNA (Figure 3(a)). As shown in Figures 3(b) and 3(c), we found

that at concentrations of 20 μ M and 40 μ M also upregulated the protein expression of Nrf2 and HO-1. However, the level of Keap1 protein remained unchanged in each group ($P > 0.05$). This result showed that delphinidin could increase Nrf2 and HO-1 mRNA and protein levels, but had no effect on Keap1.

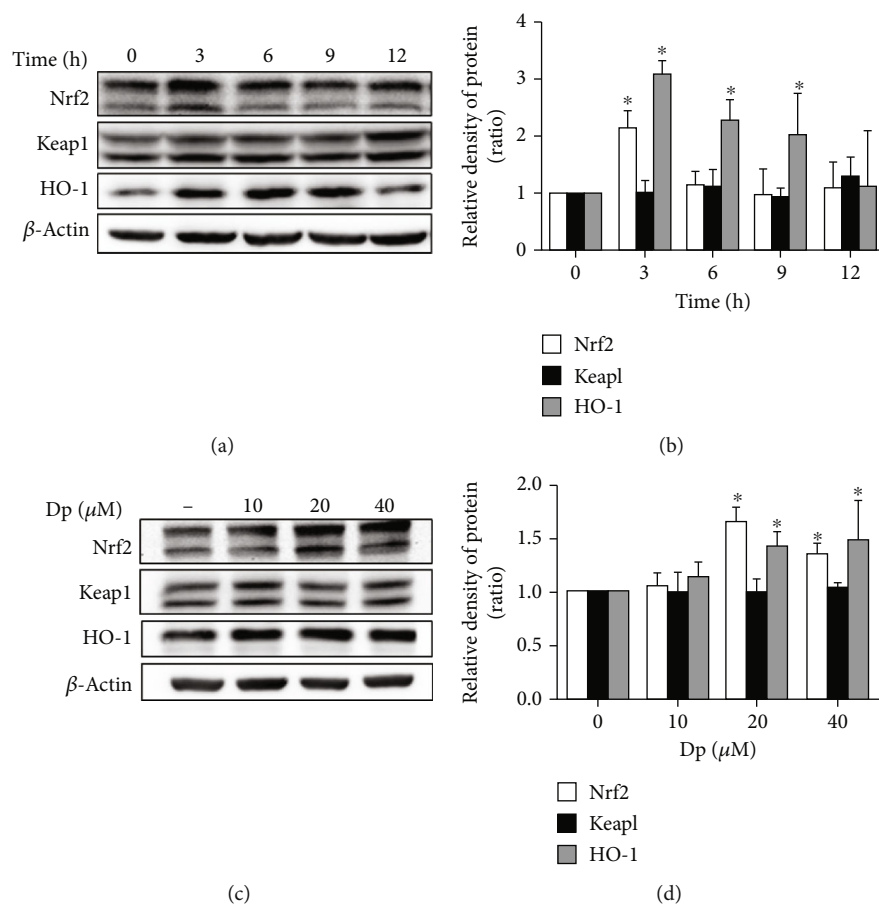


FIGURE 2: Nrf2-related protein expression was regulated by delphinidin in time and concentration dependence. The (a) protein bands and (b) relative protein expression of total Nrf2, Keap1, and HO-1 were reregulated by delphinidin (20 μM) in time dependence. The (c) protein bands (d) and relative protein expression of total Nrf2, Keap1, and HO-1 were regulated by delphinidin (3 h) in different concentrations. β-Actin was used as a loading control for the total protein. Values were presented as mean ± SD. * $P < 0.05$ vs. the control group.

3.4. Delphinidin Promoted the Nuclear Translocation of Nrf2.

To further investigate whether delphinidin could regulate the nuclear translocation of Nrf2, immunofluorescence experiment was performed to locate Nrf2 in HepG2 cells treated with delphinidin (20 μM) and H₂O₂ (750 μM). Moreover, Western blot was used to detect the level of Nrf2 in the cytoplasm and nucleus. Compared with the H₂O₂-treated group, the green fluorescence expression in the nucleus of HepG2 cells was enhanced after treating with delphinidin (Figure 4(a)). In Figure 4(b), the results showed that few Nrf2 could be detected in the cytoplasm of the control group. Conversely, compared with the H₂O₂-treated group, Nrf2 protein expression was increased in the nucleus of the delphinidin intervention group (10 μM, 20 μM, and 40 μM) ($P < 0.05$). These data indicated that delphinidin could promote Nrf2 to enter and accumulate in the nucleus.

3.5. Inhibition of Nrf2 Degradation by Delphinidin and H₂O₂.

Nrf2 in the cytoplasm was degraded by the 26S proteasome. The 26S proteasome inhibitor MG132 was employed to pre-treat cells and then the ubiquitination of Nrf2 was detected by coimmunoprecipitation and Western blot. After treatment with MG132, the levels of ubiquitinated protein and

Nrf2 protein were higher in each group than those without MG132 (Figure 5(a)). In the IP experiment, whether MG132 (10 μM) was added or not, the expression of ubiquitinated Nrf2 was higher in cells supplemented with delphinidin (20 μM) and H₂O₂ (750 μM) than other groups (Figure 5(b)). The above results might indicate that delphinidin could attenuate the degradation of Nrf2 by inhibiting the function of the 26S proteasome.

3.6. Effect of Delphinidin and H₂O₂ on Nrf2 Knockdown Cells.

In order to further verify the cytoprotective effect of Nrf2 and delphinidin on oxidative stress, HepG2 cells were transfected with sh-Nrf2 plasmid and subsequently pretreated with 20 μM delphinidin before adding 750 μM H₂O₂. The expression of Nrf2 in the control group was significantly reduced after transfecting with sh-Nrf2 plasmid, indicating that the transfection was effective. In addition, the expression of Nrf2 in HepG2 cells treated with delphinidin alone increased in both sh-con and sh-Nrf2 cells, which indicated that delphinidin could upregulate the expression of Nrf2 (Figures 6(a) and 6(b)). Compared with the control group, the results of ROS assay showed that H₂O₂ treatment significantly increased the fluorescence intensity of sh-con cells by

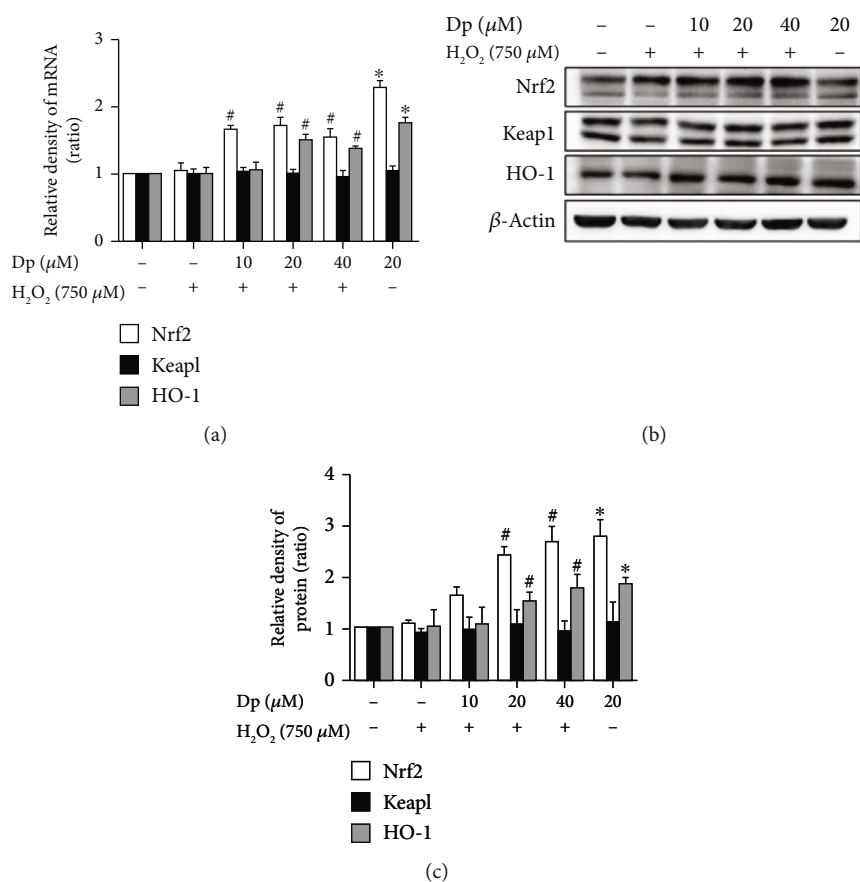


FIGURE 3: Delphinidin affected the level of Nrf2-related mRNA and protein in HepG2 cells under oxidative stress. (a) Effects of delphinidin (10 μM , 20 μM , and 40 μM) and H_2O_2 (750 μM) on Nrf2-related mRNA expression. The (b) protein bands and (c) relative protein expression of total Nrf2, Keap1, and HO-1 proteins were regulated by delphinidin (10 μM , 20 μM , and 40 μM) under oxidative stress. β -Actin was used as a loading control for the total protein. Values were presented as mean \pm SD. * $P < 0.05$ vs. the control group and # $P < 0.05$ vs. the H_2O_2 -treated group.

0.77 times, while that of sh-Nrf2 cells increased by 1.55 times ($P < 0.05$). Furthermore, the fluorescence intensity of sh-con cells and sh-Nrf2 cells in the delphinidin intervention group was significantly reduced by 32.5% and 64.9%, respectively, compared with that in the H_2O_2 -treated group (Figure 6(c)). These results indicated that silencing Nrf2 gene enhanced H_2O_2 -induced oxidative stress in HepG2 cells, while delphinidin reduced oxidative stress back to normal.

4. Discussion

According to several reports [29], anthocyanins are water-soluble flavonoids, and their skeleton is a 2-phenylbenzopyran ring structure (Figure 1(a)). They have an antioxidant activity which is associated with the diortho-hydroxyl functional moiety. Among various kinds of anthocyanins, delphinidin (Dp) has attracted much attention due to its largest number of hydroxyl groups on the B ring and high antioxidant activity [30, 31]. In this study, the HepG2 cells, which possessed many biological characteristics of hepatocytes and the activity of many phases I and II antioxidant enzymes, were selected to evaluate the antioxidative property effect of delphinidin treatment [32, 33]. So far, there are few reports on the antioxidant activity of delphinidin in HepG2 cells. As a small molecule

that easily crosses the cell membrane, H_2O_2 is the main component of intracellular ROS produced in many physiological and pathological processes, and it can cause oxidative damage to cells [34, 35]. Therefore, H_2O_2 is often used to investigate the mechanism of oxidative stress [34, 36]. In our previous experiments, we treated HepG2 cells with 500 μM H_2O_2 and found that although the intracellular ROS level increased, it could not meet the requirements for a stable oxidative stress environment. In this experiment, we selected 750 μM H_2O_2 to treat HepG2 cells for 1h, based on the results of our previous experiments and others' studies [37–39]. In our study, the treatment with 750 μM H_2O_2 resulted in decreased cell viability and accumulated ROS in HepG2 cells. Similarly, our study also showed that 750 μM H_2O_2 could cause the changes of cells morphology (Figure S1). It was significantly alleviated after pretreatment with delphinidin, which was consistent with the researches of NI [40] and Lee et al. [28]. At present, the toxicity of delphinidin to HepG2 cells has not been studied. In our study, we obtained that the IC50 value of delphinidin was 65.58 μM by using MTT assays (Figure 1(b)). The cells treated with different concentrations (10 μM , 20 μM , and 40 μM) of delphinidin did not cause any damage to the cells (Figure 1(c)). In some other studies, varied concentrations of delphinidin were used to treat with

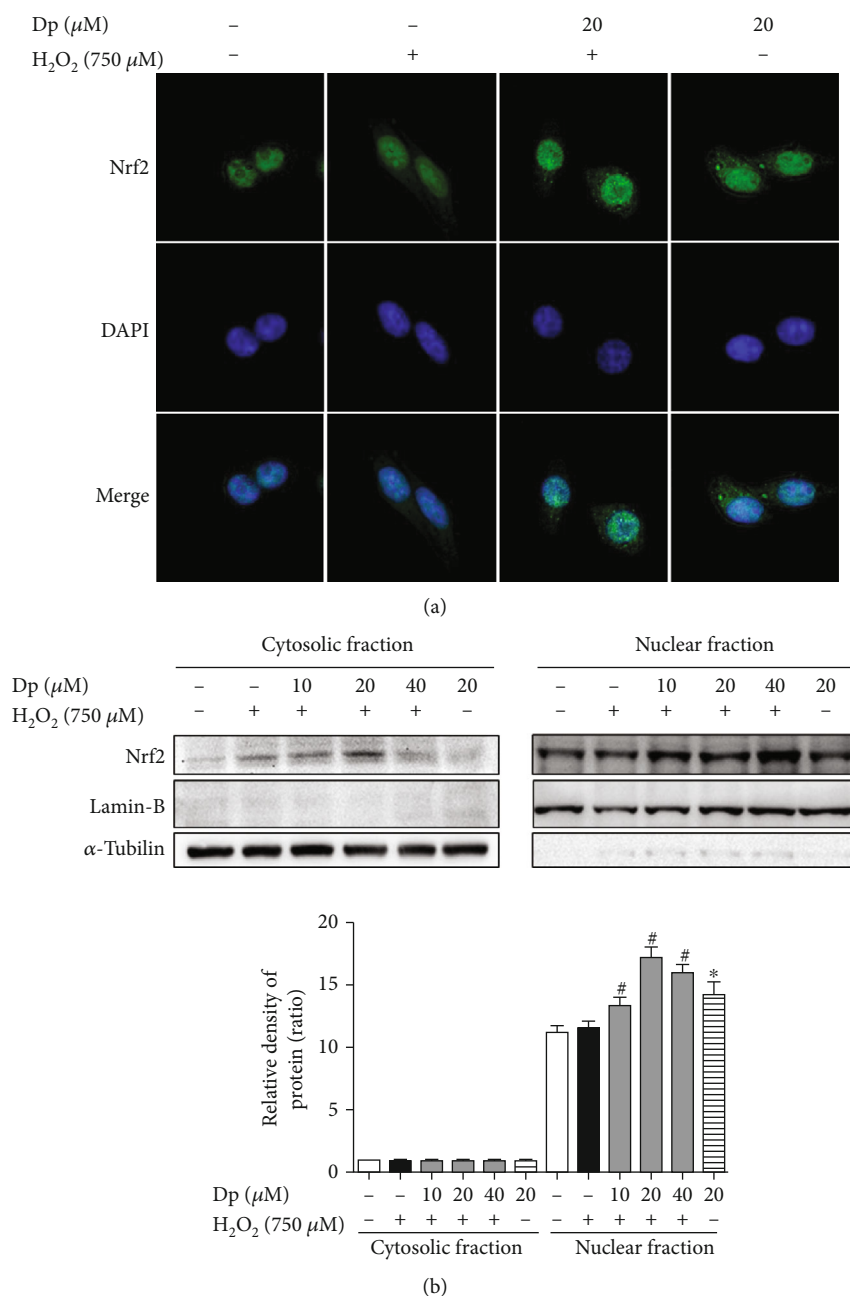


FIGURE 4: Effects of delphinidin on Nrf2 nuclear translocation in HepG2 cells under H_2O_2 -induced oxidative stress. (a) Localization of Nrf2 in cells after treating with delphinidin and H_2O_2 . (b) The expression of Nrf2 protein in cytoplasm and nucleus after treating with delphinidin and H_2O_2 . α -Tubulin was used as a loading control for the total protein. Values were presented as mean \pm SD. * $P < 0.05$ vs. the control group and # $P < 0.05$ vs. the H_2O_2 -treated group.

different cells, but it was generally believed that the dose of delphinidin under of $40 \mu\text{M}$ had no impact to cell proliferation [28, 41]. Compared with the delphinidin intervention group ($40 \mu\text{M}$), the delphinidin intervention group ($20 \mu\text{M}$) had a stronger antioxidant capacity (Figures 1(d) and 1(e)). It was suggested that the antioxidant activity of delphinidin in HepG2 cells might be associated with the dose dependence. As we all known, delphinidin has a strong antioxidant capacity, but the molecular mechanism by which delphinidin exerts its antioxidant activity remains elusive.

Polyphenols, such as delphinidin, quercetin, and kaempferol, could exert its cytoprotective properties due to its ability to increase the activity of phase II detoxification enzymes and the ability to directly clear ROS [42–44]. Among multiple phase II detoxification enzymes, HO-1 and NQO1 are considered to produce beneficial responses to oxidative stress in a variety of cells [16, 45]. In fact, that is because heme-derived metabolites produced by HO-1 have powerful antioxidant and cytoprotective activities [46, 47]. In addition, according to the related researches, it has been found that HO-1 and NQO1 could be effectively activated

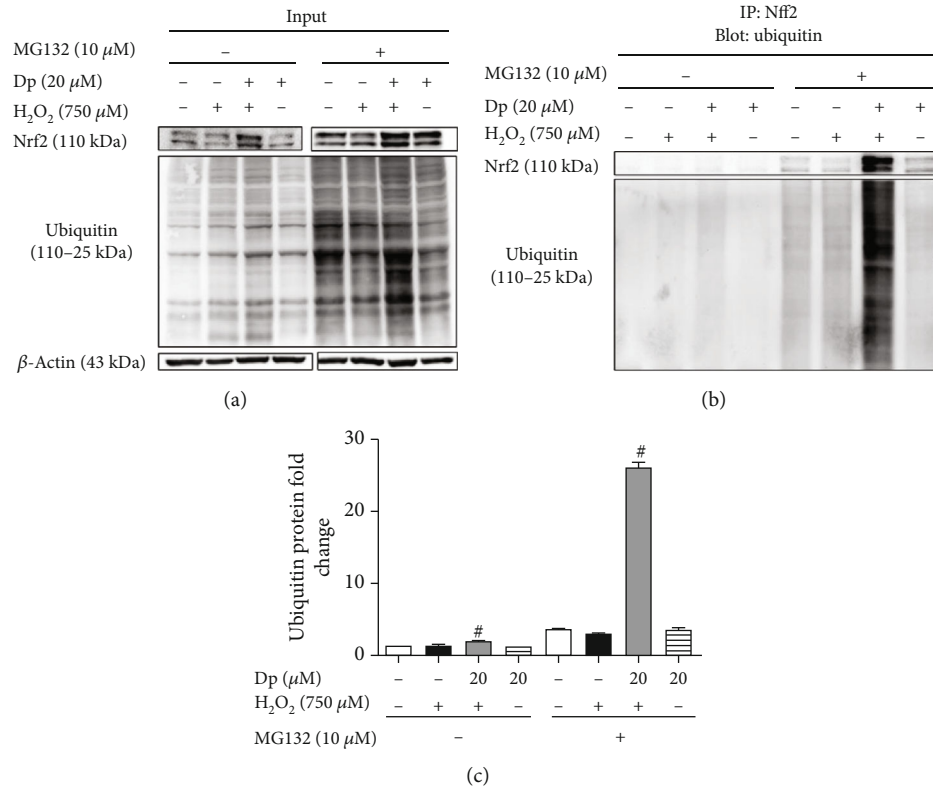


FIGURE 5: Delphinidin inhibited the degradation of Nrf2 protein in H_2O_2 -mediated oxidative stress. (a) The total Nrf2 and ubiquitin protein were detected and used as a control. (b) The Nrf2 and ubiquitin protein were detected after immunoprecipitation with Nrf2. (c) The relative protein expression of ubiquitin protein bands. β -Actin was used as a loading control for the total protein. Values were presented as mean \pm SD. [#] $P < 0.05$ vs. the H_2O_2 -treated group.

by Nrf2 [30]. In our study, delphinidin treatment significantly upregulated the protein expression of Nrf2 and HO-1 (Figure 3). Unlike the petunidin [48], delphinidin also increased the mRNA level of Nrf2. Moreover, according to several previous reports, we found that polyphenols might activate the Nrf2 pathway by applying slightly oxidative stress [49]. However, in our study, compared with the control group, there were no significant differences in ROS levels when cells were treated with delphinidin (20 μ M) alone (Figure 1(e)). Thus, delphinidin did not promote Nrf2 activation in a way that increased slightly ROS levels.

In physiological conditions, Nrf2 binds to Keap1 in the cytoplasm and it is continuously ubiquitinated under the synergistic effect of ub-activating enzyme E1, ub-conjugating enzyme E2, and ub-ligating enzyme E3. After that, the ubiquitinated Nrf2 is rapidly degraded by the 26S proteasome. However, if the body is exposed to poisons, drugs, carcinogens, or other electrophiles, Nrf2 will be isolated from Keap1 and transferred into nucleus, where Nrf2 combines with small Maf proteins to form heterodimers before binding to the ARE; finally, the downstream phase II detoxification enzyme is activated [7, 50] (Figure 7). In this study, the immunofluorescence and ubiquitination experiments were used to investigate whether delphinidin exerted an antioxidant effect through this mechanism. The results showed that after delphinidin treatment, the expression of green fluorescence in the nucleus of HepG2 cells was enhanced (Figure 4(a)). In addition, according to the results of Nrf2 protein expression in cytoplasm and

nucleus, we could see that delphinidin promoted the nuclear translocation of Nrf2 (Figure 4(b)). Recently, it has been reported that polyphenols such as geraniin [51] and hyperoside [49] could stimulate the expression of Nrf2 in the nucleus, and our results were consistent with these compounds, but different from the quercetin in NB4 leukemia cells [52]. Especially after the pretreatment of MG132, we found that the expression of Nrf2 and ub-Nrf2 was higher in the group which treated with delphinidin (20 μ M) and H_2O_2 (750 μ M) than in other groups (Figure 5). Zhang et al. previously demonstrated that the fisetin, a dietary flavonoid that had the same function as delphinidin in upregulating the expression of Nrf2, prolonged the half-life of Nrf2 protein [2]. These results suggested that delphinidin might reduce the degradation of Nrf2 by inhibiting the function of the 26S proteasome, resulting in a higher expression of the total Nrf2 protein. Actually, Chen et al. previously revealed that the dietary flavonoids with OH groups on the B ring and/or unsaturated C ring could act as proteasome inhibitors [53], which was further supported by our finding. In addition, Qin et al. previously revealed that myricetin [54] and baicalein [17] could inhibit the ubiquitination of Nrf2 and downregulate the expression of Keap1, but this change was not observed after delphinidin intervention. After analyzing the structures of those compounds, we speculated that it might be associated with a 4-carbonyl group on the C ring, which needed further experimental verification. Based on the above results, we considered that delphinidin elevated Nrf2 activation probably by upregulating Nrf2 mRNA

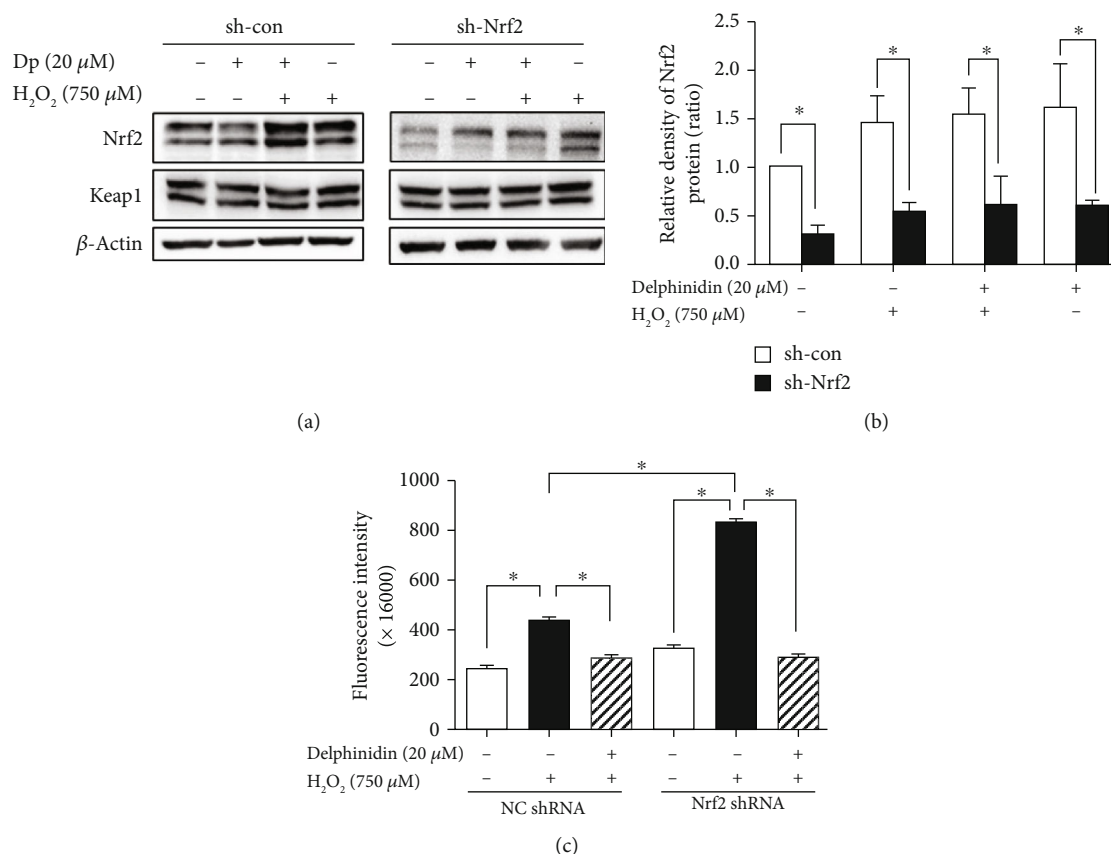


FIGURE 6: Delphinidin played an important role in Nrf2 elimination of intracellular ROS. The (a) protein bands and (b) relative protein expression of Nrf2 were regulated by delphinidin in Nrf2 knockdown HepG2 cells. (c) Effects of delphinidin (20 μ M) on intracellular ROS level induced by H₂O₂ in Nrf2 knockdown HepG2 cells. β -Actin was used as a loading control for the total protein. Values were presented as mean \pm SD. * $P < 0.05$.

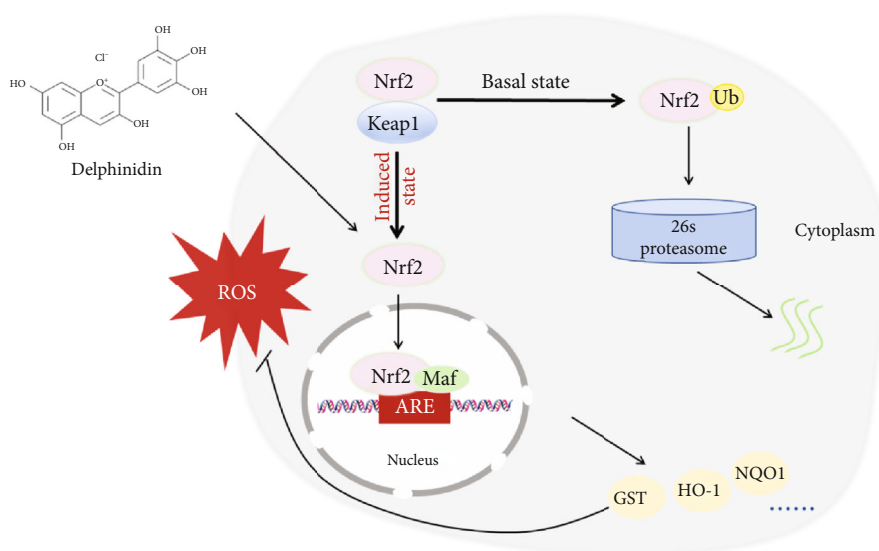


FIGURE 7: Schematic representation of the process by which Nrf2 exerts its antioxidant effect in cells treated with delphinidin.

expression and promoting Nrf2 nuclear translocation, rather than by inducing Keap1 degradation.

According to the above study, we must consider whether delphinidin could still protect cells from oxidative stress

when Nrf2 was knocked down. Although the ROS level of the H₂O₂-treated group in the sh-Nrf2 cells was higher than that of the sh-con cells, delphinidin could still decrease the ROS in the sh-Nrf2 cells back to normal level (Figure 6(c)),

and we also found that the delphinidin could promote the expression of Nrf2 protein after knocking down Nrf2. The above results indicated the important role of delphinidin in alleviating intracellular oxidative damage in Nrf2 knock-down cells (Figures 6(a) and 6(b)). Considering that there were no significant differences in ROS levels which treated with delphinidin (20 μM) among the sh-con and sh-Nrf2 cells, and the fluorescence intensity of the delphinidin intervention group was lower than that of the control group in sh-Nrf2 cells, we speculated that delphinidin might also play a role in cytoprotective effect by activating other antioxidant pathways, such as phosphatidylinositol-3-kinase (PI3K)/Akt signaling pathway [55] or inhibiting phosphorylation of ERK, JNK, and p38 [56], which needed further experimental verification.

5. Conclusion

As an antagonist of the 26S proteasome, delphinidin could upregulate the expression of Nrf2 mRNA, promote the accumulation of Nrf2 in the nucleus, and inhibit the degradation of ub-Nrf2, which activated the expression of the downstream HO-1. In summary, this study demonstrated that delphinidin proposed an antioxidant protective effect of alleviating the toxic effect induced by H_2O_2 in HepG2 cells, and the mechanism was through the Nrf2 signaling pathway. It was suggested that delphinidin could be used as a new type of antioxidant to prevent diseases related to oxidative stress.

Data Availability

The data used to support the findings of this study are available from the corresponding author upon request.

Conflicts of Interest

The authors declare no conflict of interest.

Authors' Contributions

Jingjing Xu and Yanwei Zhang conceived and designed the study. Jingjing Xu, Yanwei Zhang, Jihua Chen, Hong Qin, Rengui Yang, Guofeng Ren, Jingfang Chen, and Xiaojing Xiang performed the experiments. Jingjing Xu wrote the paper. Yanwei Zhang, Jihua Chen, and Hong Qin reviewed and edited the manuscript. All authors read and approved the manuscript. Jingjing Xu and Yanwei Zhang contributed equally to this work.

Acknowledgments

This research was funded by the National Natural Science Foundation of China (No. 81472972) and the Innovative research program for graduates of Central South University (2020zzts808). Jihua Chen and Hong Qin were the cocorresponding author of this article.

Supplementary Materials

Figure S1: the morphology observation of the different concentrations (10 μM , 20 μM , and 40 μM) of delphinidin with H_2O_2 (750 μM) (*Supplementary Materials*)

References

- [1] N. Embade and O. Millet, "Molecular determinants of chronic liver disease as studied by NMR-metabolomics," *Current Topics in Medicinal Chemistry*, vol. 17, no. 24, pp. 2752–2766, 2017.
- [2] H. Zhang, W. Zheng, X. Feng et al., "Nrf2(-)ARE signaling acts as master pathway for the cellular antioxidant activity of fisetin," *Molecules*, vol. 24, no. 4, p. 708, 2019.
- [3] W. Ahmad, B. Ijaz, K. Shabbiri, F. Ahmed, and S. Rehman, "Oxidative toxicity in diabetes and Alzheimer's disease: mechanisms behind ROS/RNS generation," *Journal of Biomedical Science*, vol. 24, no. 1, p. 76, 2017.
- [4] D. B. Zorov, M. Juhaszova, and S. J. Sollott, "Mitochondrial reactive oxygen species (ROS) and ROS-induced ROS release," *Physiological Reviews*, vol. 94, no. 3, pp. 909–950, 2014.
- [5] L. Qi, J. Jiang, J. Zhang, L. Zhang, and T. Wang, "Curcumin protects human trophoblast HTR8/SVneo cells from H_2O_2 -induced oxidative stress by activating Nrf2 signaling pathway," *Antioxidants*, vol. 9, no. 2, p. 121, 2020.
- [6] G.-H. Li, Y.-R. Li, P. Jiao et al., "Therapeutic potential of *Salviae miltiorrhizae Radix et Rhizoma* against human diseases based on activation of Nrf2-mediated antioxidant defense system: bioactive constituents and mechanism of action," *Oxidative Medicine and Cellular Longevity*, vol. 2018, Article ID 7309073, 13 pages, 2018.
- [7] S. Qin and D. X. Hou, "Multiple regulations of Keap1/Nrf2 system by dietary phytochemicals," *Molecular Nutrition & Food Research*, vol. 60, no. 8, pp. 1731–1755, 2016.
- [8] T. O. Khor, M. T. Huang, A. Prawan et al., "Increased susceptibility of Nrf2 knockout mice to colitis-associated colorectal cancer," *Cancer Prevention Research (Philadelphia, Pa.)*, vol. 1, no. 3, pp. 187–191, 2008.
- [9] E. Bhakkiyalakshmi, D. Sireesh, P. Rajaguru, R. Paulmurugan, and K. M. Ramkumar, "The emerging role of redox-sensitive Nrf2-Keap1 pathway in diabetes," *Pharmacological Research*, vol. 91, no. 91, pp. 104–114, 2015.
- [10] H. Y. Cho and S. R. Kleeberger, "Nrf2 protects against airway disorders," *Toxicology and Applied Pharmacology*, vol. 244, no. 1, pp. 43–56, 2010.
- [11] J. Kim, Y. N. Cha, and Y. J. Surh, "A protective role of nuclear factor-erythroid 2-related factor-2 (Nrf2) in inflammatory disorders," *Mutation Research/Fundamental and Molecular Mechanisms of Mutagenesis*, vol. 690, no. 1-2, pp. 12–23, 2010.
- [12] R. Howden, "Nrf2 and cardiovascular defense," *Oxidative Medicine and Cellular Longevity*, vol. 2013, Article ID 104308, 10 pages, 2013.
- [13] I. Buendia, P. Michalska, E. Navarro, I. Gameiro, J. Egea, and R. León, "Nrf2-ARE pathway: an emerging target against oxidative stress and neuroinflammation in neurodegenerative diseases," *Pharmacology & Therapeutics*, vol. 157, no. 157, pp. 84–104, 2016.
- [14] S. Tanigawa, M. Fujii, and D. Hou, "Action of Nrf2 and Keap1 in ARE-mediated NQO1 expression by quercetin," *Free Radical Biology & Medicine*, vol. 42, no. 11, pp. 1690–1703, 2007.

- [15] P. Yao, A. Nussler, L. Liu et al., "Quercetin protects human hepatocytes from ethanol-derived oxidative stress by inducing heme oxygenase-1 via the MAPK/Nrf2 pathways," *Journal of Hepatology*, vol. 47, no. 2, pp. 253–261, 2007.
- [16] H. K. Na, E. H. Kim, J. H. Jung, H. H. Lee, J. W. Hyun, and Y. J. Surh, "(-)-Epigallocatechin gallate induces Nrf2-mediated antioxidant enzyme expression via activation of PI3K and ERK in human mammary epithelial cells," *Archives of Biochemistry and Biophysics*, vol. 476, no. 2, pp. 171–177, 2008.
- [17] S. Qin, F. Deng, W. Wu et al., "Baicalein modulates Nrf2/Keap1 system in both Keap1-dependent and Keap1-independent mechanisms," *Archives of Biochemistry and Biophysics*, vol. 559, no. 559, pp. 53–61, 2014.
- [18] B. Singh, R. Shoulson, A. Chatterjee et al., "Resveratrol inhibits estrogen-induced breast carcinogenesis through induction of NRF2-mediated protective pathways," *Carcinogenesis*, vol. 35, no. 8, pp. 1872–1880, 2014.
- [19] M. Garcia-Alonso, G. Rimbach, M. Sasai et al., "Electron spin resonance spectroscopy studies on the free radical scavenging activity of wine anthocyanins and pyranoanthocyanins," *Molecular Nutrition & Food Research*, vol. 49, no. 12, pp. 1112–1119, 2005.
- [20] M. Kolehmainen, O. Mykkänen, P. V. Kirjavainen et al., "Bilberries reduce low-grade inflammation in individuals with features of metabolic syndrome," *Molecular Nutrition & Food Research*, vol. 56, no. 10, pp. 1501–1510, 2012.
- [21] X. Wang, D.-Y. Yang, L.-Q. Yang, W.-Z. Zhao, L.-Y. Cai, and H.-P. Shi, "Anthocyanin consumption and risk of colorectal cancer: a meta-analysis of observational studies," *Journal of the American College of Nutrition*, vol. 5, no. 38, pp. 470–477, 2018.
- [22] M. Suárez, N. Boqué, J. del Bas, J. Mayneris-Perxachs, L. Arola, and A. Caimari, "Mediterranean diet and multi-ingredient-based interventions for the management of non-alcoholic fatty liver disease," *Nutrients*, vol. 9, no. 10, p. 1052, 2017.
- [23] T. Ali, M. J. Kim, S. U. Rehman, A. Ahmad, and M. O. Kim, "Anthocyanin-Loaded PEG-Gold Nanoparticles Enhanced the Neuroprotection of Anthocyanins in an A β 1–42 Mouse Model of Alzheimer's Disease," *Molecular Neurobiology*, vol. 54, no. 8, pp. 6490–6506, 2017.
- [24] I. Fernandes, R. Perez-Gregorio, S. Soares, N. Mateus, and V. de Freitas, "Wine flavonoids in health and disease prevention," *Molecules*, vol. 22, no. 2, p. 292, 2017.
- [25] M. H. Kim, Y. J. Jeong, H. J. Cho et al., "Delphinidin inhibits angiogenesis through the suppression of HIF-1 α and VEGF expression in A549 lung cancer cells," *Oncology Reports*, vol. 37, no. 2, pp. 777–784, 2017.
- [26] W. Lim and G. Song, "Inhibitory effects of delphinidin on the proliferation of ovarian cancer cells via PI3K/AKT and ERK 1/2 MAPK signal transduction," *Oncology Letters*, vol. 14, no. 1, pp. 810–818, 2017.
- [27] D. N. Syed, Y. Suh, F. Afaq, and H. Mukhtar, "Dietary agents for chemoprevention of prostate cancer," *Cancer Letters*, vol. 265, no. 2, pp. 167–176, 2008.
- [28] D. Y. Lee, Y. J. Park, M. G. Song, D. R. Kim, S. Zada, and D. H. Kim, "Cytoprotective effects of delphinidin for human chondrocytes against oxidative stress through activation of autophagy," *Antioxidants*, vol. 9, no. 1, p. 83, 2020.
- [29] S. Habtemariam, "The Nrf2/HO-1 axis as targets for flavanones: neuroprotection by pinocembrin, naringenin, and eriodictyol," *Oxidative Medicine and Cellular Longevity*, vol. 2019, Article ID 4724920, 15 pages, 2019.
- [30] H.-C. D. Kuo, R. Wu, S. Li, A. Y. Yang, and A.-N. Kong, "Anthocyanin delphinidin prevents neoplastic transformation of mouse skin JB6 P⁺ cells: epigenetic re-activation of Nrf2-ARE pathway," *The AAPS Journal*, vol. 21, no. 5, p. 83, 2019.
- [31] M. Parra-Vargas, A. Sandoval-Rodriguez, R. Rodriguez-Echevarria, J. Dominguez-Rosales, A. Santos-Garcia, and J. Armendariz-Borunda, "Delphinidin ameliorates hepatic triglyceride accumulation in human HepG2 cells, but not in diet-induced obese mice," *Nutrients*, vol. 10, no. 8, p. 1060, 2018.
- [32] L. Deferme, J. J. Briedé, S. M. H. Claessen, D. G. J. Jennen, R. Cavill, and J. C. S. Kleinjans, "Time series analysis of oxidative stress response patterns in HepG2: a toxicogenomics approach," *Toxicology*, vol. 306, no. 306, pp. 24–34, 2013.
- [33] A. Iriondo-DeHond, A. I. Haza, A. Ávalos, M. D. del Castillo, and P. Morales, "Validation of coffee silverskin extract as a food ingredient by the analysis of cytotoxicity and genotoxicity," *Food Research International*, vol. 100, no. 1, pp. 791–797, 2017.
- [34] H. Wang, Z. Xue, Q. Wang, X. Feng, and Z. Shen, "Propofol protects hepatic L02 cells from hydrogen peroxide-induced apoptosis via activation of extracellular signal-regulated kinases pathway," *Anesthesia and Analgesia*, vol. 107, no. 2, pp. 534–540, 2008.
- [35] Y. Pan, D. Chen, Q. Lu, L. Liu, X. Li, and Z. Li, "Baicalin prevents the apoptosis of endplate chondrocytes by inhibiting the oxidative stress induced by H₂O₂," *Molecular Medicine Reports*, vol. 16, no. 3, pp. 2985–2991, 2017.
- [36] J. Ma, M. Li, P. K. Kalavagunta et al., "Protective effects of cichoric acid on H₂O₂-induced oxidative injury in hepatocytes and larval zebrafish models," *Biomedicine & Pharmacotherapy*, vol. 104, no. 104, pp. 679–685, 2018.
- [37] B. Zou, G. Xiao, Y. Xu, J. Wu, Y. Yu, and M. Fu, "Persimmon vinegar polyphenols protect against hydrogen peroxide-induced cellular oxidative stress via Nrf2 signalling pathway," *Food Chemistry*, vol. 255, no. 255, pp. 23–30, 2018.
- [38] S. Emami, Z. Esmaili, G. Dehghan et al., "Acetophenone benzoylhydrazones as antioxidant agents: synthesis, in vitro evaluation and structure-activity relationship studies," *Food Chemistry*, vol. 268, no. 268, pp. 292–299, 2018.
- [39] M. A. Siddiqui, Z. Ali, A. G. Chittiboyina, and I. A. Khan, "Hepatoprotective effect of steroidal glycosides from *Dioscorea villosa* on hydrogen peroxide-induced hepatotoxicity in HepG2 cells," *Frontiers in Pharmacology*, vol. 9, p. 797, 2018.
- [40] T. Ni, W. Yang, and Y. Xing, "Protective effects of delphinidin against H₂O₂-induced oxidative injuries in human retinal pigment epithelial cells," *Bioscience Reports*, vol. 39, no. 8, 2019.
- [41] C. C. Huang, C. H. Hung, T. W. Hung, Y. C. Lin, C. J. Wang, and S. H. Kao, "Dietary delphinidin inhibits human colorectal cancer metastasis associating with upregulation of miR-204-3p and suppression of the integrin/FAK axis," *Scientific Reports*, vol. 9, no. 1, p. 18954, 2019.
- [42] M. S. Lee, B. Lee, K. E. Park et al., "Dieckol enhances the expression of antioxidant and detoxifying enzymes by the activation of Nrf2-MAPK signalling pathway in HepG2 cells," *Food Chemistry*, vol. 174, no. 174, pp. 538–546, 2015.
- [43] H. Y. Choi, J. H. Lee, K. H. Jegal, I. J. Cho, Y. W. Kim, and S. C. Kim, "Oxyresveratrol abrogates oxidative stress by activating ERK-Nrf2 pathway in the liver," *Chemico-Biological Interactions*, vol. 245, no. 245, pp. 110–121, 2016.
- [44] C. L. L. Saw, Y. Guo, A. Y. Yang et al., "The berry constituents quercetin, kaempferol, and pterostilbene synergistically

- attenuate reactive oxygen species: involvement of the Nrf2-ARE signaling pathway,” *Food and Chemical Toxicology*, vol. 72, pp. 303–311, 2014.
- [45] C. Y. Chen, J. H. Jang, M. H. Li, and Y. J. Surh, “Resveratrol upregulates heme oxygenase-1 expression via activation of NF-E2-related factor 2 in PC12 cells,” *Biochemical and Biophysical Research Communications*, vol. 331, no. 4, pp. 993–1000, 2005.
- [46] R. Garg, S. Gupta, and G. B. Maru, “Dietary curcumin modulates transcriptional regulators of phase I and phase II enzymes in benzo[a]pyrene-treated mice: mechanism of its anti-initiating action,” *Carcinogenesis*, vol. 29, no. 5, pp. 1022–1032, 2008.
- [47] K. C. Kim, K. A. Kang, R. Zhang et al., “Up-regulation of Nrf2-mediated heme oxygenase-1 expression by eckol, a phlorotannin compound, through activation of Erk and PI3K/Akt,” *The International Journal of Biochemistry & Cell Biology*, vol. 42, no. 2, pp. 297–305, 2010.
- [48] S. Zheng, Z. Deng, F. Chen et al., “Synergistic antioxidant effects of pectinidin and lycopene in H9c2 cells submitted to hydrogen peroxide: role of Akt/Nrf2 pathway,” *Journal of Food Science*, vol. 85, no. 6, pp. 1752–1763, 2020.
- [49] H. Y. Xing, Y. Liu, J. H. Chen, F. J. Sun, H. Q. Shi, and P. Y. Xia, “Hyperoside attenuates hydrogen peroxide-induced L02 cell damage via MAPK-dependent Keap1-Nrf2-ARE signaling pathway,” *Biochemical and Biophysical Research Communications*, vol. 410, no. 4, pp. 759–765, 2011.
- [50] J. Chen, Y. Li, F. Liu et al., “Prodigiosin promotes Nrf2 activation to inhibit oxidative stress induced by microcystin-LR in HepG2 cells,” *Toxins*, vol. 11, no. 7, p. 403, 2019.
- [51] P. Wang, X. Peng, Z. F. Wei et al., “Geraniin exerts cytoprotective effect against cellular oxidative stress by upregulation of Nrf2-mediated antioxidant enzyme expression via PI3K/AKT and ERK1/2 pathway,” *Biochimica et Biophysica Acta*, vol. 1850, no. 9, pp. 1751–1761, 2015.
- [52] V. Rubio, A. I. García-Pérez, A. Herráez, and J. C. Diez, “Different roles of Nrf2 and NFKB in the antioxidant imbalance produced by esculetin or quercetin on NB4 leukemia cells,” *Chemico-Biological Interactions*, vol. 294, pp. 158–166, 2018.
- [53] D. Chen, “Structure-proteasome-inhibitory activity relationships of dietary flavonoids in human cancer cells,” *Frontiers in Bioscience*, vol. 12, no. 1, pp. 1935–1945, 2007.
- [54] S. Qin, J. Chen, S. Tanigawa, and D. X. Hou, “Microarray and pathway analysis highlight Nrf2/ARE-mediated expression profiling by polyphenolic myricetin,” *Molecular Nutrition & Food Research*, vol. 57, no. 3, pp. 435–446, 2013.
- [55] J. Chen, H. Y. Li, D. Wang, and X. Z. Guo, “Delphinidin protects β 2m-/Thy1+ bone marrow-derived hepatocyte stem cells against TGF- β 1-induced oxidative stress and apoptosis through the PI3K/Akt pathway in vitro,” *Chemico-Biological Interactions*, vol. 297, pp. 109–118, 2019.
- [56] D. C. Nam, Y. S. Hah, J. B. Nam, R. J. Kim, and H. B. Park, “Cytoprotective mechanism of cyanidin and delphinidin against oxidative stress-induced tenofibroblast death,” *Biomolecules & Therapeutics*, vol. 24, no. 4, pp. 426–432, 2016.